# AD A 124264

AFWAL-TR-82-3059

PROCEEDINGS: EJECTOR WORKSHOP
FOR AEROSPACE APPLICATIONS

R. P. BRADEN
K. S. NAGARAJA
H. J. P. VON OHAIN

UNIVERSITY OF DAYTON RESEARCH INSTITUTE
300 COLLEGE PARK AVENUE
DAYTON, OHIO 45469
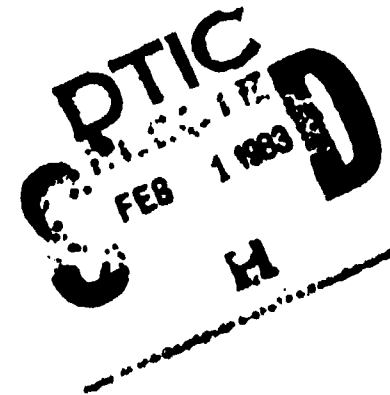
JUNE 1982

FINAL REPORT FOR PERIOD AUGUST 1981 - JANUARY 1982

APPROVED FOR PUBLIC RELEASE; DISTRIBUTION UNLIMITED

FLIGHT DYNAMICS LABORATORY
AIR FORCE WRIGHT AERONAUTICAL LABORATORIES
AIR FORCE SYSTEMS COMMAND
WRIGHT-PATTERSON AIR FORCE BASE, OHIO 45433

83 02 01 045

K.S. NAGARAJA
Project Engineer

LOWELL C. KEEL, Lt, Col., USAF
Chief, Aerodynamics and Airframe Branch

FOR THE COMMANDER

JOHN R. CHEVALIER
Colonel, USAF
Chief, Aeromechanics Division

# COMPONENT PART NOTICE

THIS PAPER IS A COMPONENT PART OF THE FOLLOWING COMPILATION REPORT:

(TITLE): Proceedings: Ejector Workshop for Aerospace Applications Held at

Bergamo Center, Dayton, Ohio on 2-5 August 1981.

(SOURCE): Dayton Univ., OH  Research Inst.

TO ORDER THE COMPLETE COMPILATION REPORT USE __AD-A124 264__.

THE COMPONENT PART IS PROVIDED HERE TO ALLOW USERS ACCESS TO INDIVIDUALLY
AUTHORED SECTIONS OF PROCEEDINGS, ANNALS, SYMPOSIA, ETC. HOWEVER, THE
COMPONENT SHOULD BE CONSIDERED WITHIN THE CONTEXT OF THE OVERALL COMPILATION
REPORT AND NOT AS A STAND-ALONE TECHNICAL REPORT.

THE FOLLOWING COMPONENT PART NUMBERS COMPRISE THE COMPILATION REPORT:

# COMPONENT PART NOTICE (CON'T)

AD#: P000 534 TITLE: Some Applications of Ejector Technology to STOL
and V/STOL Aircraft Projects.

AD-P000 535  Ejector Ram Dras.
AD-P000 536  Supersonic Ejector-Diffuser Theory and Experiments.
AD-P000 537  A Reduced Ejector Equation.

| Accession For | | |
|---|---|---|
| NTIS GRA&I | ☑ | |
| DTIC TAB | ☐ | |
| Unannounced | ☐ | |
| Justification | | |
| By | | |
| Distribution/ | | |
| Availability Codes | | |
| Dist | Avail and/or Special | |
| A | | |

DTIC
ELECTE
FEB 1 7 1983
A

| REPORT DOCUMENTATION PAGE | | READ INSTRUCTIONS BEFORE COMPLETING FORM |
|---|---|---|
| 1. REPORT NUMBER<br>AFWAL-TR-82-3059 | 2. GOVT ACCESSION NO.<br>AD·A124264 | 3. RECIPIENT'S CATALOG NUMBER |
| 4. TITLE (and Subtitle)<br>PROCEEDINGS: EJECTOR WORKSHOP FOR AEROSPACE APPLICATIONS | | 5. TYPE OF REPORT & PERIOD COVERED<br>Final - August 1981 - January 1982 |
| | | 6. PERFORMING ORG. REPORT NUMBER<br>UDR-TR-82-64 |
| 7. AUTHOR(s)<br>R. P. Braden<br>K. S. Nagaraja<br>H. J. P. von Ohain | | 8. CONTRACT OR GRANT NUMBER(s)<br>F33615-81-K-3032 |
| 9. PERFORMING ORGANIZATION NAME AND ADDRESS<br>University of Dayton Research Institute<br>300 College Park Avenue<br>Dayton, Ohio 45469 | | 10. PROGRAM ELEMENT, PROJECT, TASK AREA & WORK UNIT NUMBERS<br>2307-N4-17 |
| 11. CONTROLLING OFFICE NAME AND ADDRESS<br>Air Force Wright Aeronautical Laboratories<br>Flight Dynamics Laboratory (AFWAL/FIM)<br>Wright-Patterson AFB, Ohio 45433 | | 12. REPORT DATE<br>June 1982 |
| | | 13. NUMBER OF PAGES<br>1081 |
| 14. MONITORING AGENCY NAME & ADDRESS(if different from Controlling Office) | | 15. SECURITY CLASS. (of this report)<br>Unclassified |
| | | 15a. DECLASSIFICATION/DOWNGRADING SCHEDULE |

16. DISTRIBUTION STATEMENT (of this Report)

Approved for public release; distribution unlimited.

17. DISTRIBUTION STATEMENT (of the abstract entered in Block 20, if different from Report)

18. SUPPLEMENTARY NOTES

Funding was provided from program element 2307.

19. KEY WORDS (Continue on reverse side if necessary and identify by block number)

Ejectors      VTOL aircraft
Thrust augmentation      STOL aircraft
Workshops
Aerospace ejectors

20. ABSTRACT (Continue on reverse side if necessary and identify by block number)

These are the Proceedings of the Ejector Workshop for Aerospace Applications, which was conducted 2-5 August 1981 at the Bergamo Conference Center, Dayton, Ohio. The Workshop was hosted by the Air Force Office of Scientific Research and the Flight Dynamics and Aeropropulsion Laboratories of the Air Force Wright Aeronautical Laboratories.

DD FORM 1473   1 JAN 73    EDITION OF 1 NOV 65 IS OBSOLETE

# FOREWORD

The Ejector Workshop for Aerospace Applications was conducted August 2-5, 1981, at the Bergamo Center, Dayton, Ohio, hosted by the Air Force Office of Scientific Research, Bolling Air Force Base (Bolling AFB), Washington, D.C., and the Flight Dynamics and Aeropropulsion Laboratories of the Air Force Wright Aeronautical Laboratories, Wright-Patterson Air Force Base, (W-PAFB), Dayton, Ohio.

The Flight Dynamics Laboratory Technical Monitor was Dr. K. S. Nagaraja. The Aerodynamics/Energy Conversion Group, Aerospace Mechanics Division, University of Dayton Research Institute (UDRI), Dayton, Ohio, conducted the workshop under Contract Number F33615-81-K-3032, Project Number 2307, Task Number N4, Work Unit 17. The senior administrator and proceedings editor for the workshop was Dr. Richard P. Braden, Research Engineer.

Government, industrial, and private groups in the United States, Canada, Europe, and India participated in the workshop. The list of attendees is included. Also included are the meeting agenda, a short summary of and recommendations by the workshop, and the results of the daily wrap-up sessions which were conducted on August 3, 4, and 5.

Also included are the papers which were presented at the workshop, plus some additional papers which were in preparation at that time. The additional papers are presented in the interest of completeness since they add to the state of the art. The papers were regrouped according to topic for publication; in some cases they were presented in a different order.

The editors of the proceedings, Dr. R. P. Braden, Dr. K. S. Nagaraja, and Dr. Hans J. P. von Ohain, wish to acknowledge the special assistance of approximately 50 attendees who read and corrected the preliminary drafts of the proceedings.

# TABLE OF CONTENTS

DTIC
COPY
INSPECTED
3

v

TABLE OF CONTENTS (Continued)

## TABLE OF CONTENTS (Concluded)

# LIST OF ILLUSTRATIONS

# INTRODUCTION

The following is an excerpt of the "Welcome" presented by Colonel Robert R. Rankine, Commander, Air Force Wright Aeronautical Laboratories (AFWAL).

"It is a pleasure for me to be here this morning, and it is a pleasure to welcome you to this Workshop on Ejector Technology for Aircraft Applications. . ."

"Although ejector technology is perceived to offer signifi-cant advantages, the fact that we do not yet have an operational ejector thrust augmented or ejector integrated aircraft indicates we have yet to reach the level of acceptance and maturity required for practical applications.

"Many milestones must be satisfied before we can venture into fabricating the ejector. We at AFWAL are committed to advancing innovative technology promising potential. The workshop has been organized to assist us in defining such a course in the ejector technology goals. As a result of some of these studies, some areas of high potential have been revealed. Among these are the prospects for supersonic mixing. AFWAL would like to see this body of technical experts consider all the aspects of technology and come up with a better definition of potential and related problems, as well as clear recommendations for futher development.

"The results of the deliberations of this workshop are desired to insure that support is focused with results to date, or continuation of specific efforts.

"It is advisable, and we are still looking at some fun-damental problems, that all of the interested organizations work in coordination fashion. I am reassured with the fact that AFWAL is maintaining close liaison with both the Navy and NASA, and will continue to maintain such as useful cooperative approach to con-tinued development in this technology area.

"Ejector technology has interesting possibilities for STOL and VTOL aircraft applications, primarily because of the characteristically benign exhaust. However, questions of the aircraft volume required and its distribution, as well as the mechanical complexity, must be addressed if ejector systems are to be competitive with other approaches to high performance aircraft design.

"The challenge, then, is to obtain a high level of thrust augmentation in very compact form, without creating a maintenance catastrophe when placed in service. Payofts which ejectors can impose upon performance of the total system have to be carefully assessed. Although fundamental investigations are very intriguing and challenging, ultimately it is the integrated system which will provide the level of performance gained, which is anticipated.

"Questions relating to thermodynamic capabilities, scale effect, lightweight hardware, and other significant parameters have to be determined so that what is achieved in the laboratory will still meet the performance goals under the constraints of flight hardware performance.

"AFWAL encourages you to fully deliberate on all the issues of technology, both pro and con.

"My best wishes for a successful conference."

# SUMMARY

The first day's presentations included papers on the more fundamental aspects of ejector technology: an overview of current research; jet mixing phenomena; entrainment; pulsating flows; swirling flows; ejector scaling; and inlet and diffuser effects. The wrap-up session which followed late in the afternoon centered on these issues:

(1) The lack of both analytical and experimental data for the same identical one- or two-dimensional ejector configurations subjected to pressure ratios and primary/secondary flow temperatures common to turbine engine exhausts and aerospace vehicles.

(2) The conflicting reports on the effects of temperature scaling (from a cold flow laboratory model to hot flow, airworthy hardware).

(3) A conflict in reported scaling effects (laboratory models to full-scale demonstration hardware).

(4) The utility of one- and two-dimensional integrated continuity, momentum, energy equation models versus finite difference models.

(5) The nature of the basic mixing/entrainment phenomena, and the effect of large scale turbulence on the mixing process.

The second day's presentations included: an overview of the Navy's interests in VTOL/STOL aircraft; systematic approaches to determining theoretical upper bounds of ejector performance; the supersonic primary/supersonic secondary ejector; jet flaps; ejector wings; and the disparity between laboratory and full-scale experimental results with ejectors. The wrap-up session in the evening centered on these issues:

(1) The existence of the supersonic "second solution" with supersonic primary inlet flow, subsonic or supersonic secondary inlet flow, and supersonic mixed flow at the ejector outlet.

(2) The advisability of further full-scale demonstration work versus continued small-scale laboratory studies and experiments.

(3) Continued discussions on scaling effects and temperature effects (laboratory model versus full-scale hardware results).

The third day's presentations began with an overview of NASA sponsored ejector research. This was followed by reports on experimental and analytical work on ejector applications for VTOL and STOL, and supersonic aircraft/missiles. The wrap-up session was conducted at noon on August 5, and invited discussion on all of the three days' presentations. The discussion centered on these issues:

(1) Positive and negative ground effect with VTOL/STOL aircraft.

(2) Problems in "packaging" ejectors on high performance aircraft.

(3) Lessons learned from the XVF-12A program.

(4) The need for higher pressure ratio propulsion engines for VTOL and STOL.

(5) The need for a flying demonstration VTOL/STOL high performance aircraft.

Major Keel, AFWAL/FIMM, whose group hosted the workshop, closed the meeting with a short discussion of the avenues open to the participants to insure a coordinated VTOL/STOL research effort in the coming years.

# RECOMMENDATIONS

Based upon the papers presented at the Ejector Workshop, the discussions at the end of each paper, the comments offered at the daily wrap-up sessions, and the written comments by the participants after the workshop, the group recommends that:

(1) Futher basic research be conducted to determine the limits of the "second solution ejectors," since the supersonic mixed flow should result in higher thrust augmentation than that achieved with subsonic mixed flow. Applications of such ejectors for V/STOL, as well as for in-flight regimes such as cruise and manuvering, need to be explored.

(2) Basic studies should be conducted to develop methods of achieving higher thrust augmentation ratios either with or without complete mixing of the primary and secondary flows with minimum length ejectors. Higher thrust augmentation must be the goal, not necessarily better mixing techniques.

(3) Basic understanding of ejectors through continued fundamental research efforts are required, since they are the key to the advancement of aerospace application of ejectors.

(4) Although fundamental research in the field of ejectors is still recommended, the knowledge of ejectors is sufficiently advanced that meaningful ejector application efforts can be undertaken. These efforts should include analytical and experimental techniques for modeling the flow through the ejector as design aids for aerospace ejector applications, some of the goals being to develop ejectors applicable for a wide range of flight speeds and angles of attack. Also, ejectors must become a part of the aircraft structure, not appendages to the existing airframe.

(5) Small-scale laboratory tests should be conducted to optimize those parameters which contribute most directly to overall ejector performance. Emphasis should be applied to

ejector concepts that currently show the most promise for aircraft integration. Temperature, scaling, and pressure ratio effects on ejector performance must be determined through both analysis and long-term laboratory testing.

(6) The laboratory test results should be validated with large or full-scale boilerplate models incorporating aircraft propulsive systems which show promise for tactical aircraft. Both fluid dynamic and mechanical problems in the particular aircraft installation should be addressed, both in hover and throughout transition flight.

(7) Many questions on the suitability of particular ejector configurations for particular portions of the flight envelope can only be adequately resolved by large-scale wind tunnel and flight tests. Because of the many potential advantages available with ejectors (e.g., benign footprint, fuel savings, synergistic effects such as supercirculation, etc.), at least one large-scale test and evaluation program should be maintained in the future.

(8) Ejector applications should not be limited to VTOL aircraft, but should be equally considered for STOL as well as forward flight applications.

(9) Engine manufacturers must be encouraged to develop variable cycle, high pressure ratio propulsion engines suitable for V/STOL aircraft.

(10) Systematic studies on ejector packaging, ejector integrated aircraft structural problems, as well as relevant problems relating to the use of metals, composites, and ducting systems, need to be made. Problem areas should be defined and methodologies for resolving the problems should be explored and established.

# EJECTOR WORKSHOP

First day's wrap-up session, Monday, 3 August 1981,
6-7 P.M.  Dr. James Wilson, Chairman.

DR. J. WILSON:  When the idea for this workshop was born,
the meeting was expected to have more of a workshop format:
fewer papers and more informal discussions.  We have gone the
other way.  Nevertheless, it is probably a good thing to take
some time at selected points in the proceedings to take stock of
where we are.

One of the points of the meeting was to give the research
sponsors some insights into what the community of researchers
feels are some of the key issues which require more work -- areas,
perhaps, that are being overlooked, or approaches to ongoing
research about which there may be reservations.

It was hoped that there would be fairly free interaction.
This evening there is not a lot of time for discussion.  So the
first thing I would like to do is reopen any of the papers that
we have seen so far to further discussion.  There are, in partic-
ular, two papers in which there are unanswered questions.  The
discussions started and were terminated for lack of time.  They
both fall into the overall subject of this phase of the workshop
and that is the basic research issues associated with energy
exchange and thrust augmenting ejectors of a class that would be
of interest in V/STOL applications.

If you look again at the sheet that you have in your
handouts, this would be Roman numeral I, questions of a fundamen-
tal nature relating to mixing and entrainment, and their signifi-
cance to ejector performance.

DR. J. FABRI:  I was very much impressed with the amount of
work that is going on in the area of thrust augmenting ejectors;
both sides, fundamental and experimental work going on; but was
quite surprised by the fact that these are treated as two

different things. Some people make computations, some people make experimental tests, and very seldom can you see both of them on the same problem. You can see in some fundamental cases, when you have constant cross-section for example, then you have both tests and fundamental calculations. But when you have more complex ejectors, which fit better in the subject of thrust augmentation, then we did not see much calculations. Nobody tries to make these calculations.

Perhaps you have had a chance to see the paper Chinese scientists presented at the last meeting in Bangalore. It is finite computation for ejectors. A friend of mine who attended the meeting claims they get easily good results, and the method seems to be suited to the geometries you have discussed here.

DR. V. SAROHIA: In most analyses, assumptions are made at the very start which produce beautiful profiles. But they go away from what happens in real life. We have a problem here; we don't understand how turbulent air flows under adverse pressure gradients. These effects are absent, and we are making some gross assumptions which are so strong that the real physics of the problem is eliminated right at the very first step you make in your computational technique.

DR. G. OATES: I would make a comment that I agree with you. It would seem to me that to conduct a full numerical investigation of thrust augmenting ejectors, you must know the transport properties rather well, because that is what is governing the driving mechanism. And it would also seem to me that quite a few of the papers today have no relevant techniques to enhance the transport mechanisms. Certainly, it would be hard to simulate them even to get the differences between the various approaches that have been advanced here, because they are very novel approaches, and there isn't a bank of experimental data to draw from.

DR. SAROHIA: At least we are trying to document this and see how the realistic profile evolves in connection with inlet

8

flow, pressure gradient, jet flow, and mixing. But I think it is crucial that this information should be available to analytical personnel.

DR. WILSON: I think one of the things that has slowed the development of computational methods is just that. We haven't had much information about what is going on inside the shrouds. Traditionally, you take a few outlet profiles and measure the forces, and that is all that the modelers have to go on.

DR. P. BEVILAQUA: The first two papers tomorrow morning are going to be presentations of the computation methods we at Rockwell International have developed. The first paper, on ejector shroud aerodynamics, is an application of potential flow theory to calculate pressure distributions on an ejector shroud. This analysis also gives the inlet velocity distribution, distortion factor, and so forth.

The second paper is a discussion of ejector nozzle design. A finite difference analysis which uses a two equation model for turbulence closure has been developed. We use this program to analyze the mixing of deflected jets in order to trade off the loss in primary thrust due to jet deflection for the gain in augmenting thrust due to increased mixing.

There will be a third paper in the afternoon on viscid/inviscid interaction analysis, in which we iterate between the two programs. We use the viscous program to calculate the jet entrainment, which defines an equivalent sink strength; we use the sink strengths in the inviscid programs to calculate the secondary flow field. This is fed back into the viscous program to update the velocity effect on the entrainment.

So, in summary, there are three or four different ways you can analyze the ejector. The one-dimensional methods we have seen today have their place, because they allow you to arbitrarily vary one of the parameters, like the exit velocity distribution, and see what the effect on performance is.

9

However, more sophisticated methods are also available to analyze methods of obtaining a particular exit velocity distribution. Thus each method has its place.

DR. WILSON: What is the generality of the most detailed method?

DR. BEVILAQUA: The only real limitation is that the ejector shroud is assumed to be two-dimensional (the ejector isn't tapered). The nozzle is completely general.

DR. WILSON: Compressible flow?

DR. BEVILAQUA: Yes, compressible, hot flow. This was mentioned briefly in the scaling study in which we calculated temperature effects. That was done by solving the energy equation, in addition to the mass and momentum equations.

DR. SAROHIA: The secondary fluid velocities shown in the scaling paper are very low. How can we be sure the results are correct?

DR. BEVILAQUA: They are to scale.

DR. SAROHIA: You are not clearly scaling up when you go from small scale to full scale.

UNIDENTIFIED: But the area of full scale in that area is also up.

DR. SAROHIA: You cannot scale the results. It's alright if you transfer from low condition one to low condition two. But it cannot be scaled with the data you get on a lab scale.

DR. BEVILAQUA: I think it can. We have experimental results to show you can do good scaling between the models.

DR. K. GREEN: Concerning some of those issues with respect to temperature scaling: my understanding is that the Rockwell work was done with a small-scale cold flow test, and it was compared to a large-scale hot test. There is also some data that was published several years ago by Rockwell showing that if you

10

maintain the temperature, and look at geometry scale changes, there was an effect. The augmentation ratio did not scale, so I am wondering about the issues that have been raised in the past about the geometric scale and the temperature scale compensating each other as you go from small-scale cold to large-scale hot; perhaps we are missing something.

DR. BEVILAQUA: Those "scaling tests" were not truly scaling tests. We did not build three ejectors and run each of them to compare performance. It was actually the same ejector with the throat opened up, and the flaps extended to try to simulate a scale change. That was the point of the second part of the paper we presented today: about the necessity for scaling, the internal geometry, keeping the nozzle gaps scaled, and so forth.

We believe the results of the older study are suspect, due to configuration changes. It was not a pure geometric scaling study; it was actually one ejector that was patched up to simulate three different scales. Some of the things that remained the "same" actually had detail changes and that is what introduced the difference in cold flow performance.

UNIDENTIFIED: Did you scale the inlet?

DR. BEVILAQUA: We scaled geometric parameters -- inlet area ratios.

UNIDENTIFIED: They were maintained fixed?

DR. BEVILAQUA: They were fixed, but in fact we used the same nozzles and the same Coanda surface. We opened the gap, which meant we didn't have the same ratio of gap to surface radius. There were other detail changes in the models which probably clouded the results of this study.

In the more recent study, the scale model was an exact copy of the full size ejector. In this case, the correlation was very good. In fact, if you go back to the old Boeing and De Havilland data where the full scale performance seemed to be less than the

11

scale model, we are always comparing airplane hardware to an idealized model. I believe the detail changes, the addition of brackets, and braces, and hinges etc., which were necessary on the airplane, reduced performance.

If the model had included scale brackets, and so forth, we would have probably gotten the same poor performance.

DR. K. NAGARAJA: I have a few questions. First, I would like to bring up this question of temperature effect. I was intrigued from the compressible analyses that were done some time ago that even in the ideal case there was very significant temperature effect on the performance of ejectors in which mixed flows are subsonic.

However, looking at the Rockwell plot that was presented this morning, I am confused. In addition to what Dr. Green brought up that perhaps you are trying to compare results from two different types of tests, there is still the fundamental question of the temperature effect. One may have to consider the pressure effects too, simultaneously.

Now, here you have the Rockwell analytical data and Rockwell experimental data, and there is a discrepancy between the two. This has to be looked at more critically.

DR. BEVILAQUA: The data shown by RI today are for different ejector configurations. The Rockwell data represents a test that was performed on a hot full-scale ejector. The methods used to cool down the primary flow (water injection) also changed the properties of the primary jet. That test was a pure temperature change; it was a way to get a handle on the temperature effect.

The analysis was not performed for that ejector configuration. It was performed for the XV-12 airplane configuration. It shows that when you increase the temperature, there is a small decrease in performance.

12

We don't propose in this paper that we have answered all the questions on scale effects. We don't even know what the effect of Mach number is. We say that if you run a model, run at the same Mach number as full size.

DR. NAGARAJA: Maybe the question is still not completely answered. I would still like again to go back to what was brought out this morning and what other people have shown, that there may be some coupling effects because the flow is unsteady, and we know in the unsteady case the temperature has opposite effect of what you have in the steady flow. Maybe there is some compensating effect.

DR. BEVILAQUA: Entirely possible.

DR. NAGARAJA: So we do not have that kind of analysis. This is still an open question, perhaps, that will have to be looked at.

Now, the other question that I have is the question of one-dimensional approach that was brought up a little while ago. In the absence of a knowledge of detailed flow phenomena in ejectors we have no recourse other than to take a one-dimensional approach where we can assign some average values to the flow properties. Some experiments done at W-PAFB some years ago by Colonel Nelson, who is still at Wright-Patterson, shows that when you have super-sonic mixed flow there are some significant two-dimensional effects. But we don't know what they are at this point. Maybe we have to explore in some way how to take account of other effects due to two- or even three-dimensional aspects.

The question of the approach that the Chinese scientists presented at a meeting in Bangalore has been brought up. I've seen that paper in a very cursory fashion. I didn't go through it in detail. I still don't know how a complete 3-D approach can be developed, and in fact, Dr. Ken Green may be able to make some comments on that, because he has seen a more complex computation 3-D computational methodology developed some years ago. Perhaps

13

he would like to make some comment on how difficult or how practical the method is.

In regard to the total flow structure problem, there are some questions about energy dissipation and sources of energy. Dr. Foa has discussed the energy exchange processes in a crypto-steady mixing device. Some have said it is not realistic because it dissipates energy. We also want to know the structure of the mixing process in different flow conditions. Unfortunately, a lot of research is being done in fundamental fashion, but because of the limitation of the facilities, experiments are done which may not have any relation to realistic problems that we have.

One group is concerned with the design of an airplane, another is involved only with ejector design. It is necessary, I think, that we develop a systematic approach to do the right type of research which includes both airplane and ejector design. Rockwell will probably have some comments to make on that later on.

DR. GREEN: Concerning 3-D solutions to ejector problems: we have looked at a finite element code that was developed at Bell Aerospace which has a number of modes of operation. One of these modes handles ejectors. It is rather complex to use, and very expensive to run for any kind of a reasonable ejector configuration. If you are talking slot nozzles with no BLC control, things like that, then you can use it.

As soon as you introduce boundary layer control nozzles into the problem and you are modeling a relatively complex primary nozzle, the number of finite elements jump up greatly. It gets very expensive to run, so we did not pursue it.

DR. WILSON: Thank you.

****

A lengthy discussion on the merits of 2-D and 3-D solutions over the currently available 1-D solutions followed. Then Dr. Bevilaqua was asked to discuss Rockwell's modeling techniques.

14

****

DR. BEVILAQUA: What I have sketched on the board is the very simplest kind of ejector. We have a center-body nozzle ejecting air through a very simple shroud. In order to compute the performance, we needed to take a look at what the mixing mechanisms are, and where the thrust augmentation comes from.

The basic mechanism is entrainment by the primary jet, which draws the secondary flow through the ejector inlet. If we represent the entrainment by a sink, which is the effect of the jet on the external flow, we can compute the streamlines which are set up by the jet. There is a stagnation point near the ejector inlet which separates the flow drawn through the ejector from the flow that goes around it. The ejector shroud is very similar to an airfoil. If you rotate your view 90 degrees, the ejector shroud looks like an airfoil. The force on the ejector, the augmenting force, is just like the lift that develops on a wing. To compute the force, you need to combine a potential flow analysis (which determines the external flow) with a viscous analysis which gives the entrainment of the jet. Since it is not practical to solve the complete Navier-Stokes equations for the entire flow field, it is necessary to treat each region of the flow separately. An inviscid analysis is used to determine the force on the shroud, and a viscous analysis is used to determine the thrust of the jet. A solution is obtained when these forces are equal but opposite. The iteration is begun by guessing a value for the secondary velocity at the ejector inlet. The viscous program is then used to compute the jet entrainment, from which the equivalent sink strength is defined.

A potential flow panel method is then used to compute the secondary velocity field for the given sink strength. The inviscid solution satisfies the Kutta condition for the shroud section. This yields an estimate for the inlet velocity which is used to update the jet entrainment calculation. The solution is

15

thus determined by satisfying the Kutta condition on the shroud for given jet mixing characteristics.

In simpler solutions, the inviscid solution and Kutta condition are replaced by some simple requirement on the exit pressure. For example, the approximation that the exit pressure is equal to atmospheric pressure.

DR. WILSON: You are using physical reasoning to put together a model?

DR. BEVILAQUA: The basic question we are trying to answer is: where did the augmentation come from? As you answer that question, you move toward a proper model of the ejector. It is necessary to have a physical model of the augmentation process, an ejector theory, in order to put together a mathematical model. However, the predictions of the model may lead to better understanding of how the ejector works, and then to a better theory.

DR. H. VIETS: Having done that, we still have to ask the question, is the problem properly specified? What is it we should do from the empirical point of view to enhance our understanding? Are the solutions close to that achieved by experiment?

DR. BEVILAQUA: The answer to a question like that is a philosophical one. The theory is correct when it is useful for you. If one-dimensional analysis can answer a question like "what is the effect of inlet distortion?" then it is a satisfactory model. You go to experiment, and what the model says should happen, does happen. Newtonian mechanics is not adequate for atomic physics, but is a perfectly good theory for calculating the flight of an airplane. I am not suggesting that we understand everything about the ejector. I am saying this is a useful theory for developing the ejector.

If you work hard to increase the mixing in an ejector, but don't understand that the augmenting thrust has to appear on the shroud and that the shroud has to have sufficient inlet radius to

16

carry the load, you may not see the increase in performance which a simple analysis leads you to expect.

DR. VIETS: Don't misunderstand me. I am not criticizing. You answered me.

DR. BEVILAQUA: It is similar to the Kutta condition. You need the viscosity to set the rear stagnation point at the trailing edge, but then once you establish that condition, you can do an inviscid analysis of the whole problem.

With the ejector, you need the viscosity and the mixing to start the entrainment. Something has to draw that secondary fluid into the ejector.

DR. FABRI: The primary flow span gives you enough low pressure to suck the flow in.

DR. BEVILAQUA: Is that not the tail wagging the dog?

DR. FABRI: No.

DR. BEVILAQUA: The jets tend to be thin and the pressure in the jet is imposed by the external stream rather than the pressure in the external stream adjusting to the jet pressure.

DR. FABRI: That may be true. That may be during the transient condition at the start of the process. It is necessary to have the viscous effects, but once you have the pressure viscous condition the main effect is distribution effect.

DR. BEVILAQUA: Something has to draw the secondary fluid in.

DR. FABRI: When the sinks are already fixed, the inlet part of the ejector is enough to fix all the conditions in that case. I don't talk of any other than that case -- in the case of constant area, you have no change in impulse between the inlet and outlet.

DR. BEVILAQUA: Supposing you had a convergent supersonic nozzle. The pressure inside the jet in that case will certainly

17

be different than in the secondary flow, and your pressure condition is not matched.

DR. FABRI:  No  you have pressures compatible with the two flows, and the advance pressure is enough to drive the flow in.

DR. BEVILAQUA:  But you don't have the same pressures in the choked jet and the secondary flow, and yet the flow is still drawn into the ejector.

DR. FABRI:  You still have compatibility between the primary and secondary flows.

DR. BEVILAQUA:  If you replace the jet boundary by a solid body, would you get an ejector?

DR. FABRI:  This is not the case.

DR. BEVILAQUA:  Once you have a solution, you should be able to replace a streamline by a solid body, and not change the flow. In an inviscid analysis, you can replace any streamline by a solid surface.

DR. WILSON:  Are there other points of view?

DR. SAROHIA:  I think what everybody is saying is that this should be a very simple analytical problem, but I think it is a very complex fluid mechanics problem.  Physically the geometry is very simple, but the interactions are very complex.  We are going to have this confusion for a long time.

DR. N. MALMUTH:  I think it is a question of relative worth. If you work the one dimensional problem that Dr. Bevilaqua wants to do, I think that is very useful.  But if you want to get a certain resolution of the flow and have consistency of all the conservation laws, you really should be working with something like the two-dimensional model with viscous interactions with it, rather than the one-dimensional model.  If you really want to get into the nitty-gritty of what is going on, trying to explain some of the experiments, I think we have to get more sophisticated in our modeling.

18

DR. WILSON: Thank you. There is one other topic, one other area that I wanted to bring up, but hasn't come up. Dr. Nagaraja mentioned it. It was the business of energy exchange that Dr. Foa was talking about earlier today. There was some discussion at that point that wasn't finished, and why don't we take ten minutes, if there is anyone else that would like to comment on it. In the energy exchange process with large scale vortical structures present, is work done on the entrained fluid by both normal stresses and shear stresses? Is this a helpful viewpoint in trying to understand the process?

DR. BEVILAQUA: Are you asking a big eddy versus little eddy question?

DR. WILSON: I am referring to the role of the large structure.

DR. BEVILAQUA: I think it is pretty well agreed the large eddies are responsible for energy extraction from the mean flow, and it is the large eddies that pass the energy down to the small scale eddies where they are dissipated. There is disagreement about how the large eddies extract the energy, what the mechanisms are.

DR. WILSON: Yes, but in ejectors we have seen 'large scale eddies; they exist. A lot of people go to a lot of trouble to generate them. A lot of the unsteady flow devices seem to generate them. Dr. Viets shows in his paper that they do exist. Is that what you are getting from the introduction of unsteadiness?

DR. VIETS: I have an opinion, too. I think there are two different kinds of mechanisms that perhaps fall under that general heading. One is the one you alluded to with the large eddies, where you get some mass transfer from one position in the flow to another in terms of gulping. I think that you can call the other pressure transfer, although I would tend to call it more entrainment, and I would treat it as a quasi-viscous kind of thing, although it is a large-scale.

19

The other possibility is, if you do have a moving mass of fluid moving more or less as a lump by itself, at least for a short interval of time, I think that this mass of fluid has the possibility, under the right circumstances, to transfer energy through a more normal force kind of arrangement. For some time it may exist as an entity, and transfer energy to the flow in front of itself.

Now the scales involved are quite another thing. You can do it with a vortex ring that fills a duct entirely, and it will work very well. That has been shown by Lockwood's experiments.

If you don't fill the entire flow, then the question arises whether or not the transfer is really a question of normal force energy transfer or whether it is just simply the fact that you have enhanced the mixing.

Then it gets back to the question: Is it a large eddy that is dragging this material in, or is there really some pressure transfer of energy? Conceptually it would be a lot more efficient to transfer energy by this pressure method than it is by the viscous method. It is not only more efficient, but it can be accomplished in a shorter distance.

So if we can generate flows that produce large energy transfer, they offer lots of advantages.

There is also the possibility that this kind of transfer is caused by acoustics. That is, if you can find a method by which the acoustics can be generated to produce a normal force directed in the way that you want the stream to go, you may have another chance of transferring the energy that way.

DR. WILSON: Dr. Foa.

DR. J. FOA: Dr. Viets is absolutely correct in what he said. However, I find it very difficult to accept that you have pressure exchange when the eddies fill the entire interaction space and not when they don't.

20

A discontinuous transition from full pressure exchange when the eddy spans the interaction space, to no pressure change when the eddy is any smaller, seems physically implausible. My hypothesis is that eddies, and particularly large ones, exert surface pressure forces on the surrounding medium and that since the eddies move, these pressure forces do work. The transfer of energy will, therefore, consist in part of the work of surface pressure forces, which is an efficient mode.

DR. WILSON: Dr. Viets, can you respond?

DR. VIETS: I am sure if you look back in the transcript you will find I did not say it is not possible. I say it is a lot easier for it to occur if you fill out the entire duct. I do not mean to say it is not possible if you do not fill out the entire duct. It is just a lot less clear how efficiently one can do it or whether or not it happens at all.

I believe it happens, but on a much more limited scale, if you don't fill out the entire duct and allow no pressure around the formation of the flow.

DR. A. KROTHAPALLI: I think there were two cases which I showed this afternoon, one in which the object is completely expanded in a very small distance, and mixing is quite enhanced. You can see large-scale motions. In the second case you don't see large-scale motions.

The question is: is the first case, which fills the duct so fast, is that better than a case where we have a jet which goes straight out without spreading until much further down the mixing tube? Which one is most efficient? I don't know the answer between the two right now.

DR. VIETS: I think the question is one that has been looked at by several people, and it is a question of whether or not you want the mixing to be relatively complete by the end of the duct. You don't want the mixing to be complete one-fourth of the way down, and suffer all the wall losses from there on. You want the

21

duct to be only as long as it needs to be for the mixing to be complete.

If it is any longer, from there on you are going to suffer losses and those losses will make it worse, not better. So a duct that is longer than it has to be is bad.

DR. L. BERNAL: I have a question, perhaps, of semantics here. I think there are only two types of forces. We are talking about either pressure forces or viscous forces, as I understand, and the question is really a question of organization.

Highest order viscous forces are negligible for our purposes, but there is always going to be an effect on pressure forces. I don't think viscous forces are going to have any effect.

DR. KROTHAPALLI: Yes, if the jet is not completely filling the channel.

DR. BEVILAQUA: If we look more deeply into the basic energy transfer process there isn't a difference between the unsteady pressure mechanism and the steady viscous mechanism. We are really talking about a collision between the jet and the secondary stream. It is similar to shooting a bullet into either a block of wook or a bale of straw, both of which have the same mass. The energy gets dissipated in different ways. When a wooden target is used the bullet gets smashed up, whereas with a straw target, the bullet hardly gets damaged at all, but the same amount of energy is dissipated because the velocity is the same. It is the mass ratio between the target and bullet that determines the energy loss and momentum transfer. The details of the transfer mechanism, whether the bullet is deformed or the target is deformed, or some combination of the two, does not affect the net energy loss.

The same is true of jet mixing within the ejector. Whether there are pressure forces or only viscous forces, the net energy transfer is the same if the same degree of mixing is achieved.

22

How long it takes might depend on how you do it, but if you transfer so much energy from the primary jet to the secondary flow, you are going to end up with so much augmentation, and there is nothing you can do to increase it (beyond that limit).

DR. OATES: I am not sure I completely understand the comments made here, but I would like to remind myself, anyway, that these are momentum devices, not energy devices, and I feel that when one deals with the pulsating device, there is energy tied up with the pulsation mechanism, and if you get pulses out the back, that to me represents wasted energy. I think there will be a penalty that will come with that. It may be true that you get the other benefits -- enhanced mixing, (for example); and consequently, better mass to the flowrate, and so on, but we have to be a little careful talking about energy transfer when it is really the momentum generated that results in thrust.

DR. BEVILAQUA: The momentum is always conserved. Some of the energy is dissipated, but in the end, what you need to do is transfer momentum. Energy is transferred as a "by product".

DR. OATES: The device is going to feel the result of the momentum transfer, so you want to have the energy shared by the streams in a way that enhances the momentum.

DR. BEVILAQUA: My point was that the momentum is conserved, and in the process a certain amount of energy is dissipated. How much is determined by the conservation of momentum and the mass ratio. It doesn't matter how the transfer occurs.

DR. FOA: It does, because the collision velocity itself depends on the mode of energy transfer.

DR. OATES: I don't agree with the comment the momentum is conserved. If we make the problem simple and shut the front, so that we have the internal flow prescribed, we have two streams with a nozzle at the back of all of this. Then you will get more

23

thrust, (assuming appropriate conditions, that is higher temperature in one stream than the other) and you will get more thrust if mixing occurs because the momentum of the departing mixed streams is larger.

DR. BEVILAQUA: We are talking of thrust augmenting ejectors which draw air from the atmosphere and eject it back into the atmosphere; in that case momentum must be conserved. The thrust of the jet at the ejector exit equals the thrust of the jet at the inlet plus the secondary stream thrust. But the kinetic energy at the exit is less than the kinetic energy at the inlet, because some is dissipated as turbulence and heat during the mixing process.

DR. M. ALPERIN: The forces are equal to the change of momentum. Looking at this from an engineering point of view, what you really want to do is increase the stagnation pressure so that you can get the thrust. That can't be done by pressure; it can only be done by some viscous interaction.

DR. R. BRADEN: Professor von Ohain, did you have a comment?

DR. H. VON OHAIN: I say the impulse function is conserved in the constant mixing duct, and if you take the control volume, including the inlet and exit nozzle, then the impulse function is increased because you have thrust augmentation. So you have to be careful where you put your control volume.

UNIDENTIFIED: I feel that the purpose of our discussion this evening is to map some plans for where one should go in this ejector business. I would have to say I think that the ejector designer analyst needs every possible tool that he can get his hands on, and I don't think that we want to consider eliminating one-dimensional analyses. Perhaps two-dimensional analyses are required where you have short ejector shrouds, nonconstant area, or similar non-uniform effects. But the one-dimensional model has its place.

These are all attempts at modeling, and I think the ultimate goal should also be to have a multi-dimensional finite difference model, at least starting with simple configurations, not these really complex cases that I think you encounter in thrust augmentation devices. But I think we should at least get started, for example, analyzing the constant area ejector by finite difference techniques.

We shouldn't eliminate other modeling techniques; for a long time they will be the only way we will get reasonable engineering answers. There are problems where you have higher compression ratios, or a smaller induced flow rate. Here you enter domains where mixing is a dominant factor; for example, in supersonic jet entering a mixing shroud. Empirical solutions have done a terrific job in looking at this problem.

I believe as an objective one should have finite difference analysis of simple configurations. I think one should have a systematic approach in trying to model the various other configurations, and of course, always keeping in mind that in many cases one-dimensional analysis will give you a quick and very good idea of what might happen. But one must not place total faith in these quick analyses.

DR. GREEN: I would like comments from the group with respect to having modeling going on simultaneously with fundamental experimental work. Sometimes I get very concerned that after your experimental work is done, somebody goes back and tries modeling, and the experimental work never really measured some of the upstream conditions, so these things are guessed at, and because of that, it adds one other dimension of unknown to the solution.

So I would be very interested in the comment of the group as to the need of coupling both an experimental and analytical approach together in one program.

DR. J. C. DUTTON: I would like to address that question, or that request. I think Professor Addy from the University of

25

Illinois has made, for the higher pressure-ratio ejectors, both systematic analytical and experimental investigations of supersonic ejector systems. He has shown that for the higher compression type ejectors, one-dimensional analysis works very well if the secondary flow rate is reasonably high. If the secondary flow rate is low, viscous effects are very dominant and you have to couple the viscous and inviscid flows. Perhaps he will tell us more about this tomorrow.

DR. WILSON: We have come to the end of this discussion. One more comment.

UNIDENTIFIED: One final comment about modeling and experiments. I think it would be ideal if we could have some experiments planned that would be very closely coordinated with theoretical analyses which are fundamental in nature, and also the more technological hardware type development where you might want to put this practical application. Many times, when you encounter experimental data, the experimentalist does not measure all of the stated variables which the analyst must include in his model. Consequently there can be no comparison between the experiment and the supposed "model" of the physical phenomena.

DR. GREEN: Maybe someone would comment on the need for having both analytical work and experimental work done at the same facility, or can they be done at separate facilities as long as there is communication. Or does that get to be a problem?

UNIDENTIFIED: At the same laboratories, you can communicate rapidly and observe the results and compare it.

DR. K. KARAMCHETI: I would like to comment on that. That was one of the objects of the program at Stanford. We want to compare the analytical with the experimental. We have just started working on it.

DR. SAROHIA: I would like to make a comment. If the same group is doing both the analytical and experimental work, it is very possible for them to reach agreement even when the data is bad.

DR. OATES: Perhaps I could quote a rather well known person, but not give his name, who had established an unimpeachable reputation as an experimentalist. He said before he died that he wanted to publish a lot of absolutely nonsensical data and wait for the theoreticians to match it.

DR. WILSON: I know in the 1968 Stanford conference on turbulent flows, they had a few blind cases; they didn't give anyone the results until the computations had been made. There is something to be said for that.

Further comments?

UNIDENTIFIED: Since we are talking experiments, didn't you mention in the preliminary comments a little while ago about the role of so-called large-scale structures?

DR. WILSON: I mentioned that, yes.

UNIDENTIFIED: I would like to make a comment, if I may. I think, first of all, the question has been repeatedly asked to what extent large-scale structures are important to enable us to model turbulent flows, to what extent large-scale structures play a part in the generation of aerodynamic flows, and perhaps we can ask the same question here in respect to energy. Do we spend a lot of time and money trying to study large-scale structures because it is fashionable, or because they play a part in the understanding of ejectors?

I would suggest a simple program to determine the role of large-scale structures before we spend a lot of time and money on their analysis.

DR. NAGARAJA: Perhaps what we need is an ejector tomography to really understand what is happening internally, to decide

27

whether we are looking at the large-scale structure, whether they do exist under the stream aerothermodynamic conditions, and then say if the tomography gives any reasonable result. Then we can probably undertake a more systematic study of the problem.

DR. WILSON: Under adverse experimental conditions or in compressible flows, can you even find them?

DR. NAGARAJA: Not if you simplify the problem. To see realistic operating conditions, we probably need a test airplane.

DR. WILSON: I understand that, but I don't think that is a simple thing to do.

DR. NAGARAJA: It is not simple.

DR. K. AHUJA: I have a few slides showing results that shed considerable light on the role of large-scale structure on jet mixing, and if the audience is interested, I would like to show these.

(The group gave its consent.)

DR. AHUJA: I think this session can be concluded by four slides I am going to show. In relation to large-scale turbulence structures, what we have been doing at the Lockheed-Georgia Company has little to do directly with ejectors, but has something to do with exciting a jet with upstream sound at discrete frequencies.

First of all, we have conducted a flow visualization study to determine what is the shape of the so-called large-scale tur-bulence structure.

Most shadowgraphs and schlieren photographs, particularly those for axisymmetric flows, display a certain degree of con-fused detail resulting from small-scale turbulence in the jet, and from thermal convection in the ambient air. A method of removing these sometimes unwanted details, and thereby high-lighting essential characteristics, is the application of a pho-tographic averaging technique. This is an effective method for

revealing orderly turbulence structure in a jet. The method involves repeated triggering of a light source and superposition of all the schlieren images on a single photographic film. By this means, the images of the coherent structure associated with the trigger signal are reinforced and those from the random turbulence tend to cancel.

This method was used in our experiments but a new and very simple method of synchronizing the source of light was used. The laser beam passing through a Bragg cell was the source of light. The Bragg-cell shutter was synchronized with the excitation signal itself, thus the strobe frequency was the same frequency as that of the acoustic signal used to excite the jet. Some optical schlieren pictures obtained in this way will be seen in the next three slides.

The first slide here (Figure 1a) shows typical schlieren pictures of an unexcited jet and an excited jet. Here the light source was synchronized with the acoustic signal but the film plate was exposed only once. These pictures show quite clearly how the jet plume has widened considerably as a result of upstream excitation. Besides a general disruption in the movement of the small-scale turbulence, new large-scale vortices appear to be formed some distance downstream of the exit. These vortices travel downstream, and, where they appear in the schlieren photographs, depends upon the phase relationship between this orderly vortex structure and the strobe signal.

To prove that these vortices are indeed orderly, the film plate was exposed 30 times using the technique of photographic averaging I just talked about, and the resulting photograph is shown in the second slide (Figure 1b).

The vortex structure seen here is the so-called large-scale structure, also called by some researchers the "instability wave."

The third slide here (Figure 2) shows the motion of the same large-scale structure at different times.
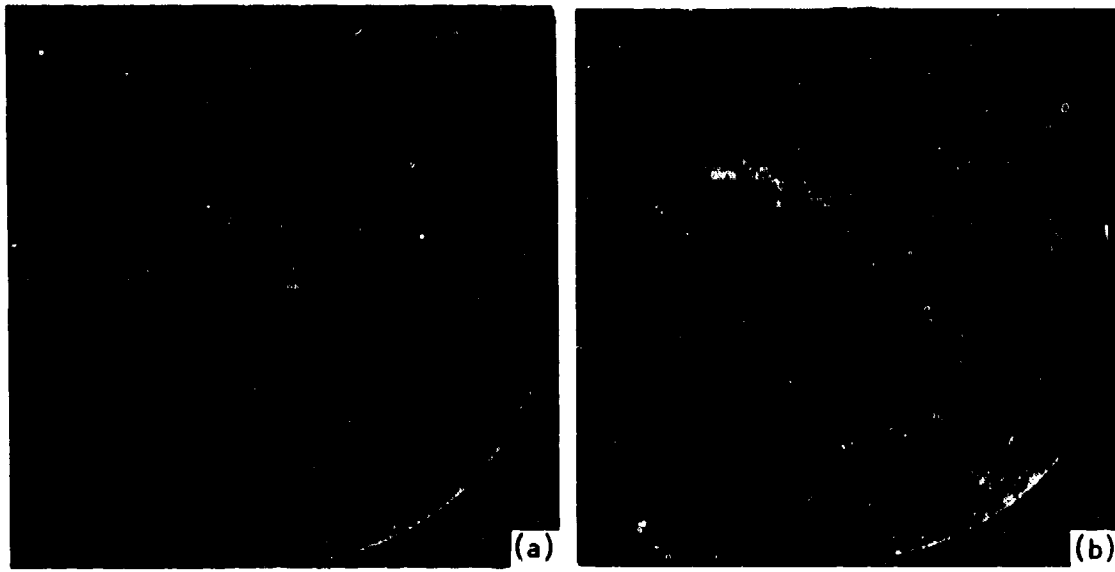
Figure 1a.  Schlieren Pictures of an (a) Unexcited and
(b) Excited Jet.



Figure 1b.  Photographic Averaging of Excited Jet.

30

Figure 2. Large-scale Structures at Different Times.

31

The last slide (Figure 3) shows the variation of the large-scale turbulence pressure magnitude with distance (x/D), along the axis. Here the jet was excited with a discrete tone at Strouhal number, $S_e$ = 0.5. The topmost curve was obtained at a excitation level of 141 dB. On the same figure is shown the pressure variation with the flow turned off but with the excitation level kept at 141 dB. It is clear from this figure that, in the presence of the jet flow, the acoustic signal is dominant close to the nozzle exit up to about 1/2 diameter. Thereafter, the hydrodynamic wave magnitude starts rising very rapidly, reaches a peak, and is then followed by a gradual decrease in level. The fluctuating pressure due to the large-scale structure is about 35 decibels higher than that due to the acoustic signal.

Curves of the large-scale instability wave are not necessarily parallel to each other for various excitation levels as seen here (Figure 3) for three different excitation levels, namely, 141 dB, 136 dB and 128 dB. Close to the nozzle exit the behavior is linear, but further downstream there is considerably less amplification at the higher excitation levels. At large distances downstream, in fact, there is even a decrease in the measured pressures for an increase in excitation level.

These results can be explained as follows. When the jet is excited by a low-level acoustic source, the large-scale instability wave tends to lock onto it, and produces a response which is in agreement with the linear shear-layer instability theory. It extracts energy from the mean flow in the initial region of the jet, indicated by the initial rise of the curve here (Figure 3). However, further downstream, due to large jet width, the growth rate of the instability wave is decreased, and as the wave decays, part of its energy is transferred back to the mean flow. Thus, at low excitation levels there is basically a back-and-forth exchange of energy between the instability wave and mean flow. At higher excitation levels, however, the wave extracts considerable energy from the jet mean flow, and the response

32
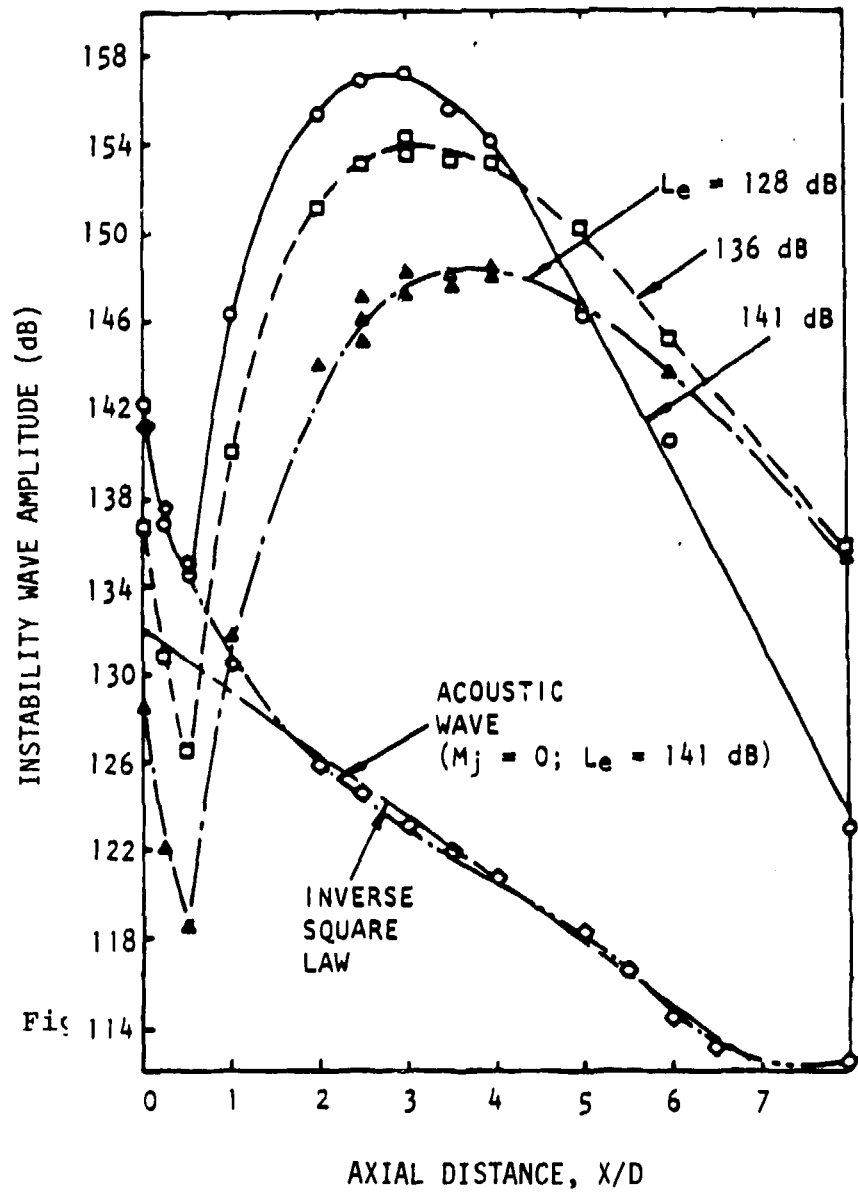
Figure 3.  Centerline Variation of Instability-Wave
Amplitude at Various Excitation Levels
$(M_j = 0.58; S_e = 0.5)$.

33

becomes nonlinear as some of this energy is converted into tur-
bulent energy. This interaction involves both the generation of
random turbulence and its transport.

The increase in the level of the random turbulent kinetic
energy causes a more rapid spreading of the jet flow through an
increase in turbulent stresses. Thus, for high-level excitation,
some distance downstream of the nozzle exit (e.g. beyond the peak
of the upper curve in Figure 3), the wave transfers more energy
to the random turbulence than it gains from the mean flow, and it
begins to decay rapidly.

I think that's about it on large-scale structures. Thank
you.

***

(Workshop recessed at 7:00 o'clock, P.M. to reconvene at
8:30 A.M. August 4, 1981.

***

# EJECTOR WORKSHOP

Second day's wrap-up session, Tuesday, 4 August 1981, 6-7 P.M. Dr. Ken Green, Chairman.

DR. VON OHAIN: Many people have suggested that Professor Sears should discuss any impressions he may have had in this meeting.

DR. NAGARAJA: Because of Professor Sears' background and noted experience, and his association with the Rockwell VTOL program, I think any comments he might make may be very worthwhile. His observations on specific developments, and comments as to what needs to be done, will be useful.

DR. W. SEARS: It seems to me that ejector technology is quite an old subject, but one that was never carried through in the past to the kind of application that we are thinking of. I guess the mechanical engineers and various other people tried some applications in the past, but now we have modern ideas of using the jet exhaust to produce vertical or nearly vertical flight through thrust augmentation. We went into new areas, and as could be anticipated, since it was a rather old technology, it was considered to be fairly well understood. But it really wasn't that well understood. We've all heard many new things in the last two days at this workshop, things that were in the literature but they weren't in everybody's minds just because they were in the literature.

The Wright Field people did a lot of good work when they got interested in ejectors a few years ago, specifically Hans von Ohain's group at ARL, and some of the best experts in this subject were working developing those cruciform nozzles, hypermix nozzles, and things like that. It all looked so attractive to put these devices to work in high performance airplanes. Well, we saw the history of what happened. It was very interesting to hear Dr. Green go over the history of VTOL the way he did, because we all get very smart looking at it in retrospect. It

turns out, as Dr. Green pointed out to us, that it was supposed to be a program with big payoffs and high risks. That is what it turned out to be -- high risk. A lot of good work has been done in these last few years. Mistakes have been made, a lot of good inventions have been made, and our understanding of ejectors has been increased. The thermodynamics of the problem is quite clearly understood.

We've seen today and yesterday that a number of people have some very strong feelings on how to analyze ejectors. I tend to agree with the person that objected to the last line on one chart that said "we need a new fundamental program of research and development," or something like that. While no one in this room would claim we've got all the answers, but compared with other technologies that are useful in our field, and where we were when we started putting them to work and cutting hardware, it seems to me that the subject has progressed to the point where what is badly needed is to solve these practical problems of application, the hardware problems.

It was mentioned that I was one of the people that looked at the Rockwell VTOL technology for the last couple of years. It was four years, really, at the request of the Navy, and it is very interesting how much progress they made at Rockwell during those four years. As you have seen, they are able now to make some very impressive flow field calculations, and they will do better as time goes on.

What needs to be done, probably, is to be sure that the applications are made where there will be really big payoffs. The problems are largely practical problems, like packaging, and getting something flying that we can use to learn about flight qualities of this type of aircraft in cross winds, in gusty weather, and rolling ship carrier decks, and such things.

The science of the subject will go along faster under the impetus of the application programs. One of the new things I

36

have learned about at this workshop is the development concerning the second solution, the supersonic solution. Surely this is very exciting and must be looked at very seriously from the standpoint of applications.

Thank you very much.

DR. GREEN: There were a number of papers presented today where there was very little chance for questions and answers, so I would like to go through each of the papers and ask if anyone would like to raise any additional questions or make any additional comments. I will ask for questions on the papers in the order they were presented today. "Ejector Shroud Aerodynamics." Are there any additional questions or comments? "Ejector Nozzle Development," Gene Schum. "Ejector Performance." We will skip my paper and go on to the next one.

"Considerations of the Control Volume Approach to Ejectors as Applied to Thrust Augmentation," by Dr. Minardi. He had very few questions because of the time constraints. Is there anyone that would like to raise any questions with Dr. Minardi?

DR. SEARS: Just a remark. I really enjoyed those engines, those ghost machines which Dr. Minardi showed because it seems to me that they are very revealing as to what is going on inside an ejector. Those funny curves and negative entropies and all kinds of nonsense that we don't understand have all got to mean something, and I can understand the basic processes better. I thank you very much for that.

DR. J. MINARDI: That was my intent. I was not trying to suggest that we build such machines, but merely that we explain by this kind of machinery the equations that we are using to analyze the ejector problem. The equations for the ghost machine network are identical to the ones you would write for an ejector. That was my point.

DR. ALPERIN: My only objection was that among all the machines shown there was one called a ghost machine, which can be

37

replaced by a constant area mixing ejector. The equations apply to those machines as well as to a constant area mixing ejector, and I think that a constant area mixing ejector can't be termed a ghost machine.

DR. MINARDI: The ghost machine is one that cheats a little bit because it acts uniquely with the environment, exchanging heat and work with the environment. It obviously can't be in an ejector, and it is the one machine that allows you to get performance in excess of a hundred percent. It is required if you are going to get the second solution efficiencies.

DR. ALPERIN: I apparently misinterpreted your materials in which you showed something which had a value of one which you indicated was the limit of the second law of thermodynamics. I assumed it was the same curve that I had plotted, which was the ratio of the mechanical energy. If I assumed wrong, I apologize.

DR. MINARDI: What I had plotted was the efficiency based on availability and not the mechanical and kinetic energy. When the efficiency is one, the entropy increase is zero, so it was exactly the same.

DR. ALPERIN: I think we all admit you can't achieve the entropy change of zero in a real case, but I think you can come pretty close to it with the constant area mixing ejector. How close is something that we have yet to determine.

DR. VON OHAIN: No, Minardi's paper does actually show the best that an ejector can do. His paper has an analysis of the constant area ejector and the limits of its use. If you want to go further, then you have to have extensive machinery. That is what his paper says.

DR. GREEN: Any response to that, Dr. Alperin?

DR. ALPERIN: I guess I don't know where that limit is. The difference in semantics makes it very hard to determine.

DR. GREEN: There is a question in the back.

UNIDENTIFIED: Isn't there a way, instead of using zero entropy change, to calculate the minimum entropy arrived at the mixing, and use that as a limit?

DR. MINARDI: If I knew how to do that, I would like to do it, but I don't know how to do it. But the point is that using the analysis that Dr. Fabri had presented in his '58 paper allows you to determine for the supersonic case where that ejector is actually going to perform. So you end up with only one point on the curve that you are actually going to achieve. There is already a theory in place. That has been verified by experimental evidence that will allow you to predict what a given constant area ejector with subsonic flow inlet will do.

The last two slides I tried to present, which I really didn't have time to explain, tried to predict the expected performance of a given constant area ejector.

DR. GREEN: Any other comments? The next paper was "Thrust Augmenting Ejectors," by Dr. Alperin. Any questions or comments to Dr. Alperin.

DR. M. PLATZER: I don't recall whether you showed it in your presentation, but in your paper on "Mixing of Compressible Flows with Application to Ejector Thrusters" by M. Alperin and J.J. Wu you showed for static operation (M = 0) a thrust augmentation ratio of close to 8 to 1. Can you describe the exact flow conditions a little more?

DR. ALPERIN: That is under the second solution.

DR. PLATZER: Yes, the second solution.

DR. ALPERIN: That was, as I recall, and I don't have my paper in front of me, it was utilizing a ram jet ejector, again, low pressure and high temperature injected gas with alpha infinity of 20, and under stationary conditions. That is an ideal case, under the conditions when entropy change is zero. It is a limiting point.

39

DR. PLATZER: What is the outflow velocity?

DR. ALPERIN: The outflow velocity in subsonic, I don't know exactly what they are. We have all of that on computer printout, but I don't have that with me. I have all of the flow properties.

DR. PLATZER. Is the ratio of 8 to 1 physically possible?

DR. ALPERIN: No. That is the limit. That is an ideal case without losses, and at the limit when the entropy change is zero. It is a limiting case. Why would it be impossible as an ideal case?

DR. PLATZER: Well, I am searching for what is physically possible. How idealistic are the other cases which you showed?

DR. ALPERIN: All of the maps where I showed iso-augmentation lines are all ideal flow at the optimal performance point. There were three optimal performance points, and the best ones were at the delta S equals zero point. They are all ideal flow, no losses, isentropic inlet, isentropic outlet, and the delta S equals zero point means the total entropy change is zero. That is, the entropy at the end of mixing is equal to the sum of the entropies at the start of mixing.

DR. PLATZER: Have you attempted to estimate more realistic flow conditions?

DR. ALPERIN: Yes, I did show some effects of losses at the end of my paper, but not for that condition.

DR. PLATZER: Did you also do that for the static case?

DR. ALPERIN: The ones calculated were for a flight Mach number of 0.65 under the second solution with the shock waves in the outlet. That was the last slide I presented, I think.

DR. GREEN: If I may say something here, I think Dr. Platzer is referring to one other paper that you had written some time ago where you showed augmentation ratio versus temperature ratio

40

(stagnation primary to secondary), for various secondary stream Mach numbers using both the positive and negative solutions. The freestream Mach number was zero. I believe the peak augmentation ratio showed up at a secondary stream Mach number about 0.4, and was giving computed augmentation ratios about 8, for the positive solution.

DR. ALPERIN: No, that was in the region where the entropy change is negative. That part of the curve was in a dashed line.

DR. PLATZER: But then it is a solid line which I believe, means that the entropy change is positive.

DR. ALPERIN: Yes, the solid line ends at the point where the entropy change is zero. That is also an ideal situation.

DR. PLATZER: Could it become realistic?

DR. ALPERIN: Well, not that way, no. Obviously, losses involved will reduce that. Now, I hav not calculated the stationary case, the stationary ejector second solution with losses, because I have had no reason to do so. I did calculate the stationary case with losses under the first solution, which we did in connection with the work we did for NASA on the E205 airplane, but we didn't do the second solution, because that ejector was not designed that way. It was just a jet diffuser ejector, and I have never put losses into that case. I can do it. We have the computer program.

DR. PLATZER: If viscous losses are included, could the augmentation ratio decrease from 8 to 6 or so?

DR. ALPERIN: I think that might be in the ball park, although in the stationary case under the second solution you need -- you need a normal shock, because the exit flows are subsonic, and it would be a matter of designing the outlet so that the losses in the shock wave system would be small. Now how much that would reduce the augmentation from the ideal case, I don't know, but I think it would still be very high.

41

DR. PLATZER: But you could still obtain, let's say, a factor of three improvement over the present technology?

DR. ALPERIN: I think you could, yes. I think it would not be easy to do. It might require an adjustable outlet. And whether the adjustable outlet would be a simple adjustable outlet or something like you have on supersonic wind tunnel, I don't know.

DR. PLATZER: What about the efficiency, then? Doesn't one normally say that, in order to get good hovering efficiency, you have to impact a small velocity increase to a large mass? However, it seems that in your case you would have relatively high outlet flows. Is mass flow in your second solution much larger than in the subsonic solution?

DR. ALPERIN: I think it is 60 to 1, at those high temperatures.

DR. PLATZER: And what is the exit velocity?

DR. ALPERIN: The area ratio is small. You have a high temperature primary jet, in which the mass flow is small, and the alpha infinity is 20.

DR. BEVILAQUA: I am trying to understand the nature of some of the losses that Dr. Alperin is assuming. If you are getting high augmentation but you require a large secondary mass flow that means you can't use all of the engine outflow. If 60 times the primary mass, you will need an ejector bigger than the airplane. You couldn't get that mass flow in a practical ejector.

DR. ALPERIN: Not necessarily. It depends on the primary stagnation pressure and temperature.

DR. BEVILAQUA: I don't understand. Correct me if I misunderstood you, you said in response to Professor Platzer's point, that obtaining very large augmentation required something like 60 times the primary mass flow.

42

DR. ALPERIN:  I think that is it.

DR. BEVILAQUA:  How will it be possible to get 60 times the mass flow of the subsonic solution through an aircraft ejector?

DR. ALPERIN:  I didn't say 60 times the subsonic solution. It is 60 times the primary jet mass flow.

DR. PLATZER:  In the subsonic or in the supersonic solution?

DR. ALPERIN:  Both.

DR. GREEN:  Dr. Addy?

PROF. A. ADDY:  I had several questions this morning.  One question that came to my mind was "what determines whether you get the first or second solution in your analysis?"

DR. ALPERIN:  The geometry of the inlet and outlet, primarily.

PROF. ADDY:  What about the back pressure, boundary condition?

DR. ALPERIN:  Back pressure?  All thrust augmenting ejectors exhaust to ambient pressure, and ingest from ambient pressure. They are blowers in a sense.

PROF. ADDY:  That was my next question you anticipated. How do you get this pressure rise?

DR. ALPERIN:  Which pressure rise?

PROF. ADDY:  If you are taking air from the atmosphere, putting it through this device and producing supersonic mixed flow at the exit, you are discharging at essentially the same pressure.

DR. ALPERIN:  The stagnation pressure rise is obtained from the mixing process, by mixing in a constant area duct.

PROF. ADDY:  I've done lots of experiments like that.  I can only get supersonic exit flow in short ducts if I have a high primary stagnation pressure and low back pressure.

43

DR. ALPERIN:  That is what we have.

PROF. ADDY:  But the problem is, we must take that flow at ambient conditions, put it through the ejector, and discharge it at the ambient conditions.

DR. ALPERIN:  Why is that a problem?

PROF. ADDY:  Well, to get the kind of flow rates you want, you must have high compression ratios.  You do not have a high compression ratio.  I don't understand how this works.

DR. ALPERIN:  The stagnation pressure after mixing is higher than ambient.

PROF. ADDY:  Higher than ambient?

DR. OATES:  I think this is a trivial question, but I hope it isn't too trivial.  Do I understand, in essence, you've got a high pressure primary, ambient secondary, and then enormous acceleration up to the mixer because you have compound supersonic flow going in, and also supersonic flow departing.  Therefore you have a very large diffusion requirement to get back to ambient, so your whole system, the operational part of your system is operating at a very, very suppressed pressure compared to the ambient static pressure?

DR. ALPERIN:  Yes.

PROF. ADDY:  I guess I don't understand it.  I am just trying to relate this to my experiences.

DR. OATES:  Did you see what I meant?

DR. ALPERIN:  Most of your experience, I assume, is with jet pumps, Dr. Addy?

PROF. ADDY:  No, as a matter of fact, we wrote a paper about matching intakes and ejectors for thrust augmentation purposes, and we found when we did this work that the three-dimensional surface that represents the performance characteristic of an ejector had to be intersected by a surface that stated the

44

boundary condition that the entrance stagnation pressure was equal to the exit static pressure. In other words, we were drawing from atmosphere, we were discharging to atmosphere, and we had the ejector choking phenomenon. I think the only way we would get supersonic flow at the exit is if we dramatically reduced the back pressure.

DR. GREEN: Dr. Oates, did you want to say something?

DR. OATES. I just wanted to make a small comment. I am wondering if your concept of "what the exit is," is part of the problem. There is an exit from the ejector, but then there is an exit up to atmospheric pressure. In this case it is going to require a very large diffuser following the ejector.

PROF. ADDY: If you take off the diffuser, the ejector will do its own diffusion right in the mixer tube.

DR. ALPERIN: It will not diffuse back to ambient pressure without a shock wave. If the normal shock occurs in the mixing section, then you are back to the first solution. The trick is to design the outlet so that the normal shock, if it exists, exists at much lower Mach number than that which is at the end of mixing, so the losses are less.

DR. GREEN: Dr. Fabri.

DR. FABRI: I'm sorry, I don't understand. You have a constant section channel, and a normal shock, which does not change the momentum. You have the same thrust if you have the separate thrust or separate --

DR. ALPERIN: It is not true.

DR. FABRI: Yes, it is true. You have one.

DR. ALPERIN: I agree with you in the outlet, where you have subsonic flow, the pressure distribution on the outlet shape will reduce the thrust because you are getting pressure forces on the outlet, which you have to design to return to ambient pressure.

45

DR. FABRI:  No.  You see, it is a constant section there; then you have constant momentum, right, constant egress.

DR. ALPERIN:  But you are not to ambient pressure.

PROF. ADDY:  That is why the shock wave is there.

DR. FABRI:  That is the ambient pressure.

DR. ALPERIN:  Your normal shock occurs, let's say in a constant area section, at a certain Mach number, and a certain pressure after mixing.  A normal shock usually does not get you back to ambient pressure, and what you may need is a subsonic diffuser, or a nozzle after that shock to get back to ambient pressure.

PROF. ADDY:  That involves a good gas dynamics question.  If you have a normal shock in the constant area duct, the flow has to discharge at the same pressure as the exit or back pressure.

DR. ALPERIN:  Not without further changes in the stream, because the pressure drop across the normal shock is a function of the Mach number upsteam of the shock.

Now, pressure upstream of that shock is also determined by the mixing process, so if the Mach number and the pressure upstream of the shock is such that the shock does not return you to ambient pressure, then you have to have some more hardware. You have to have a nozzle or diffuser.

PROF. ADDY:  That is the whole reason that the shock, the normal shock occurs, is to match the downstream boundary conditions.

DR. ALPERIN:  You don't match with just a normal shock.

PROF. ADDY:  It has to, because the flow is discharging subsonically.  You can't have any significant normal pressure gradient at the exit.

DR. ALPERIN:  You can have flow separation behind the shock, and you can have a change in the end tube flow configuration.

46

PROF. ADDY: These are additional factors that we are introducing into this constant area problem, because the idealized normal shock doesn't occur, anyway.

I think we all agree the recompression is a series of oblique normal shocks that have almost the effect of normal shock.

DR. ALPERIN: Whatever it is, once you get the subsonic flow, you may not be at ambient pressure.

DR. BEVILAQUA: That is the purpose of the shock, why the shock occurs.

DR. ALPERIN: No, sir. A normal shock may not be able to do that, depending on the conditions upstream of the shock. It determines the conditions downstream of the shock, and it may not be ambient.

DR. BEVILAQUA: Shall we agree to disagree?

DR. GREEN: Did you have a comment you wanted to make?

DR. D. DOSANJH: The normal shock occurs to match the flow conditions downstream of it. The strength of the shock or the change of pressure across it is a function of the upstream flow Mach number. The location of the shock front however varies with the back pressure. If strictly a constant area duct flow is assumed, then the static pressure of the subsonic flow behind the normal shock will be equal to the exit or the back pressure. However, if additional factors such as the boundary layer growth in the constant area ejector-duct and/or the presence of any additional nozzle or diffuser configuration as a continuation of the constant area ejector-duct are considered, then the static pressure of the subsonic flow just behind the normal shock fronts may not be equal to the static pressure at the exit.

DR. ALPERIN: You are inventing a new kind of shock wave, because pressure change across the shock wave is determined by the Mach number in front of it, not the downstream conditions. The pressure does not have to be ambient.

47

DR. GREEN:  Dr. Oates.

DR. OATES:  I need to make some simple drawings on the board, to represent the ejector.

There would be a very large contraction with some kind of device at the inlet with very high pressure injectants.  At the inlet there is ambient flow up to high Mach number.  At entrance to the mixer you have combined Mach number that is in the compound sense supersonic, after mixing the flow is still supersonic.  You have your secondary solution here after mixing, with no shock waves.  From there the flow passes into an excellently-designed subsonic, supersonic diffuser.  A shock wave occurs right there, (at the throat) and then the flow diffuses back up to the ambient pressure.

DR. ALPERIN:  That would do it if you could design such a thing.

DR. OATES:  This is the limit concept, and if we got absurd, we could take the throat Mach number to be Mach 1, which we know is unstable, but it is from this ideal behavior chat you argue real diffusers and real mixer losses.

DR. ALPERIN:  Yes, but you still have to return to ambient pressure.

DR. OATES:  This is the technique to do it, and conceptually you can do it, after all the Boeing Mach 2.8 inlet has 88 percent efficiency.  That is the point.  I think that the diffusion process is anything but constant area.  It is not a constant area diffuser.  I am not taking sides; I am just trying to understand.

PROF. ADDY:  I don't think there are any sides.  I think there are only physical laws that are involved, and I am not persuaded.  I would like to buy one of these devices when Dr. Alperin gets it made.

DR. ALPERIN:  Let me say one thing.  The stationary problem is a more difficult one than when the ejector is in motion, for

48

the simple reason in the stationary case all of the conditions with reasonable pressure and temperature primary jets end up with subsonic exhaust flow, so that you do need an ideal diffuser or a normal shock. We are designing one, and I will be glad to sell it to you. We are going to build it. It is going to be one that will operate at a flight Mach of 0.65, where the exit conditions are still subsonic, but high subsonic.

PROF. ADDY: Yes. That brings up my last question. Do you constrain the selection of your entering secondary Mach number, based on the aerodynamic choking phenomena that we know occurs in ejectors?

DR. ALPERIN: No.

PROF. ADDY: You see, that constraint eliminates possible solutions.

DR. ALPERIN: I agree that constraint does eliminate a lot of solutions, providing the primary nozzle is in the constant area section.

PROF. ADDY: Are you going to pull it (primary nozzle) out and make it a nonconstant area problem?

DR. ALPERIN: Right. Because that is the only way we can control M-1, and the only other way would be to design a primary nozzle which has exactly the right pressure at the start, at its exit at the start of mixing to correspond to the M-1, this will only operate under the one condition, if you could achieve it.

PROF. ADDY: So the constant area ejector that you refer to actually has additional features. It has a converging section at the start where you can displace the nozzle, which can have a significant effect on ejector operation, and then it has a diffuser at the end.

DR. ALPERIN: Just like any ejector, they all differ from the mathematical model. If you do the mathematics, one has to assume constant area or constant pressure mixing, and has to

49

assume that the primary flow has the optimal Mach number at the start of mixing, and when you build an ejector, you can't achieve that. If you do, it would only operate at one particular design point. So we put the primary nozzle up front of the ejector, which allows us, by moving them around and optimizing the performance, to find the right position, which is the corresponding thing in real life to achieving the desired M-1.

PROF. ADDY: How can you operate the short ejectors with a supersonic exit? I've had to have high pressure ratios to produce supersonic flows.

DR. GREEN: I would like to terminate this particular discussion at this time, and you can continue the conversation individually afterwards. Let's go on to the next paper, "Investigation of the Supersonic-Supersonic Ejector," by Dutton. Are there any comments or questions that remain unasked?

The next one, "Analytical Investigation of High Performance, Short, Thrust Augmenting Ejectors," by Tahteh Yang. Any comments or questions that were unsaid there?

DR. T. YANG: Presently, the method we use in designing a short curved-wall diffuser is based on inverse method of solution for irrotational flow. After the diffuser geometry is established, we use a rotational flow analysis to examine the pressure distribution along the curved wall. In ejector application, there is a shear flow at the diffuser inlet in most cases. However, if the rotational flow analysis shows there is an adverse pressure gradient either upstream of the suction slot, or downstream of the suction slot, we have to repeat the design iteratively, until there is no adverse pressure gradient over the solid surface of the diffuser wall. We have made preliminary study for an inverse method of solution for axisymmetric tional flow. It would be desirable if the rotational flow inverse solution and its computer code be established. Also, I would like to see that a general 3-D inverse method for

rotational flow be developed. For irrotational 3-D inverse method, John D. Stanitz has completed an analysis and is reported in NASA Contractor report number 3288.

DR. OATES: Just a question for clarification. Your investigation is restricted to incompressible flows?

DR. YANG: Incompressible, yes. It can be extended to compressible subsonic flows, however.

DR. OATES: But your vorticity does change?

DR. YANG: That is right.

DR. GREEN: Thank you. Any other comments? "An Overview of Supersonic Ejector Performance Analyses," by Professor Addy. Any comments on that?

DR. ALPERIN: I would like to know what criteria are used to determine when you have a good jet pump? What do you use in a jet pump?

PROF. ADDY: In most of the cases we have considered we were primarily interested in being able to achieve a certain compression ratio.

DR. ALPERIN: At a certain mass flow ratio?

PROF. ADDY: If possible, a minimized primary mass flow rate.

DR. ALPERIN: You want the highest curve you can get, mass flow ratio versus compression ratio?

PROF. ADDY: Yes, that is correct (i.e., highest compression ratio for the least primary mass flow rate).

DR. ALPERIN: Professor Keenan wrote a paper in which he used the criterion of the work done on the secondary flow. The more work you can do on the secondary flow, the better, and that I thought was very interesting, but nobody else seems to use it. It may be that it just doesn't show the mass flow ratio.

PROF. ADDY: There have been other attempts to show things like that. There have been attempts to show the desirability of certain entropy changes. Oftentimes, one encounters a problem incorrectly evaluating the entropy changes for an ejector.

DR. ALPERIN: That may be a good criterion for constant pressure mixing, but there again, it may not. I'm not sure. But there was a paper written by Dr. Petty of the Air Force Propulsion Lab, in which he shows that the minimum entropy change is the best condition, and then he went along to differentiate the entropy to find where the minima are. I wondered if that was the correct minimum, or if there was some case where there was no zero derivative, where the entropy change went from positive to negative, which might give him better performance. He didn't prove there was also a minimum in the sense of zero derivative.

PROF. ADDY: It would be useful if we had a general physical law to correspond to the minimum entropy case. Unfortunately, it does not exist.

DR. GREEN: Are there any other comments? Let's go onto the ejector aircraft integration, "Progress Towards a Theory of Jet Flap Thrust Recovery," by Paul Bevilaqua. Any additional questions to Paul? Next paper: "Viscid-Inviscid Interaction Analysis of Ejector Wings," by Bevilaqua, Woan and Schum. Any comments there?

Next, "Transitioning Ejector Augmentor Laboratory Experiments to Flight System Applications: The Technical Challenges," by John Porter. Any comments to John? Everybody agreed with your conclusions.

DR. GREEN: Major Keel.

MAJ. KEEL: I have a question for Paul Bevilaqua about his earlier comments on Dr. Porter's paper. You said you agreed with all of John's conclusions except one, and that was on scaling effects.

DR. BEVILAQUA:  I agreed with what Dr. Porter said on his conclusion chart.  We can discuss statements he made in the paper; for example, eddy effects.  I believe that the large eddies do scale with the width of the jet.  Since I believe the larger eddies dominate the entrainment mechanism I feel the jet entrainment will also scale with the jet.  I think we disagree on this point.

DR. GREEN:  Paul, what about the scaling of the temperature? Yesterday you indicated that the effect of temperature was pretty minimum, and yet John has shown pretty significant effects due to change of temperature.

DR. BEVILAQUA:  I don't believe he was showing significant effects.  He used the same data as we did, but chose to call the measured differences "significant."

MR. C. COMBS:  Dr. Porter came to a totally different conclusion.  He shows that a three, four, or five point change in augmentation is significant.  I don't know that it is.  (EDITOR'S NOTE:  1 Point = a one percent increase in thrust augmentation.) We need 20 counts, not one or two.  I think that the data shows the temperature effects over the range we were discussing yester- day were relatively small.

DR. GREEN:  Some of those temperature effects that we saw in Roman Dejneka's work at the Naval Air Propulsion Center were pretty significant, I thought.  He was going from ambient to 800 degrees fahrenheit, dropping in augmentation from about 1.86, to about 1.65.

MR. COMBS:  He had other changes.

DR. BEVILAQUA:  The nozzle gap was opening as the tempera- ture was increased.

DR. ALPERIN:  That ejector was designed before we had a good compressible flow theory to design ejectors for higher temperatures.  We didn't know how to do it then, and I think if

53

we had a chance to modify that, we could make it look at lot better.

MR. COMBS:  He had some experimental problems, too, that he pointed out on his paper.

DR. GREEN:  Any other comments?

DR. NAGARAJA:  I have one comment.  I gather from the discussion that there are no pressure or temperature effects in ejectors.

MR. COMBS:  We are not saying no temperature effect.

DR. NAGARAJA:  Have you taken one model and used both cold and hot flow?

DR. BEVILAQUA:  We tried to do that with water injection, and we obtained similar results.  None of the tests are defini-tive regarding temperature effects, but the experimental trends seem to be consistent and the analysis is consistent with experiment, so the indication is that a 1000° temperature change is not significant.  That doesn't say what the effect is going to be (if you make a 2000° temperature change).  We say we should match Mach numbers.  We don't know what the Mach number effect is.  We are not saying we understand the dependence on Mach number or the dependence on temperature.  We are saying what parameters we must match with a cold flow model.

DR. NAGARAJA:  Is there some way that we can develop some modeling to predict the temperature effect?

DR. BEVILAQUA:  We did that, and we presented those results. That was the turbulence kinetic energy analysis.  That is where the predictions came from.

DR. NAGARAJA:  I thought your predicted curve was different from what you had discussed earlier.

DR. BEVILAQUA:  The levels of thrust augmentation were different, because we analyzed the XFV-12A ejector configuration, but the data was from tests run by others several years ago.

DR. NAGARAJA: Was there empiricism in turbulence model?

DR. BEVILAQUA: There is empiricism in all turbulence models. However, we did not adjust the constants to fit out test results.

DR. J. LOTH: Back in 1974, West Virginia University built a circulation controlled aircraft. This STOL Technology Demonstrator generated high lift by blowing compressor air over a rounded trailing edge of the wing flap. The Coanda effect maintains the walljet attached to the rounded trailing edge and creates the high circulation and associated high lift. Using the high pressure from the compressor we obtained a supersonic wall jet which did not COANDA very well. We needed a subsonic walljet to get a good turning wall jet. Therefore we built an ejector inside the blowing jet slot which doubled the mass flow and lowered the jet velocity to half without loss in blowing coefficient. The resulting subsonic walljet worked very well.

DR. GREEN: Certainly.

DR. LOTH: Our problem was basically a wing like this, with a flap with a 40 psi compressed air supply pipe serving the dual function of also being the rounded trailing edge for circulation control. The high pressure air was expanded in a converging-diverging 0.012" throat nozzle into a constant area ejector of 0.048" in height. The secondary flow for the ejector was provided through the hollow flap. The ejector outlet formed the circulation control walljet.

Has anyone worked on this?

DR. BEVILAQUA: Yes, we have. I would like to make a couple comments. First, we tried what we call inlet vanes in the location where you showed something similar but they haven't proven out yet.

Secondly, I suppose you had a convergent nozzle for the Coanda jets?

55

DR. LOTH: We used sonic nozzle at this point.

DR. BEVILAQUA: Yes, when you use a convergent/divergent nozzle, the supersonic Coanda jet is easier to attach to the Coanda surface and is deflected through a larger angle. The difficulty with deflecting a supersonic jet is the shock/boundary layer interaction which can occur. If a convergent nozzle is used, there are expansion shocks, which caused the jet boundary layer to separate. Using a C/D nozzle solves this problem, but even in this case there are turning waves which are set up as the jet deflects over the surface and these can also cause boundary layer separation. A possible solution is to design the nozzle to produce a jet with a skewed, rather than a uniform, exit velocity distribution. With the high speed, low pressure region of the jet on the wall, the jet turns without creating shock waves. This idea is being used to form the "aerodynamic window" on some gas laser systems.

DR. LOTH: Ours, when you stand on the runway, this jet hits you right in the face, across the cheek, so we get excellent turning with low-speed jet. I know it is just a thought. People working with these ejectors might as well use it.

DR. BEVILAQUA: Have you published any of that?

DR. LOTH: Yes, in the Journal Aircraft of '76, we test-proved the aircraft.

DR. BEVILAQUA: With a description of the vane?

DR. LOTH: The double ejector pictures are in the paper. The paper was March of '76.

MR. COMBS: We should note, Paul mentioned we tried the inlet vanes. All of the data is not in on that yet, and even though we can't say it works, we are seeing some interesing results. Dr. von Ohain is probably familiar with what we are trying to do there.

DR. GREEN: Any additional comments with respect to this paper?

DR. J. PORTER: My last conclusion drew a little bit of fire, and I would like to point out that the conclusion was that a systematic R&D program is needed in ejector technology, not that a flight development program is not needed.

So I hope that that is clear, that although a flight development program is still a desperate need, most of us have also tried to get funding for a systematic research and development program.

DR. GREEN: Could you be more specific? Would you refer to the recent report that you put out as indicating these specific things? EDITOR'S NOTE: Dr. Porter's recent report is entitled "A Summary/Overview of Ejector Augmentor Theory and Performance," USAF Technical Report No. R-91100-9CR-47, April 1981, Volumes I and II.

DR. PORTER: Yes. I think some of those things are definitely required.

DR. OATES: This is a thought that has caught me by surprise, but far better than to think it over, I will just state it.

As a newcomer to this group, working on ejectors, I am somewhat impressed at the very wide breadth of experience, and yet the number of legitimate questions that seem to be at least still debatable, if not in actual disagreement.

Quite a few years ago I ended up being an editor of a book, funded by both AFAPL and AFOSR that was on gas turbine engines, and I am, if anything, not volunteering to be an editor, because I learned what it is like! As a suggestion however it might be a very appropriate point in time to try to have a similar exercise on the subject matter of this meeting, an overview write-up by some of the experts, probably from here, attempting to get some kind of a consensus on the more fundamental aspects, because it seems to be there has been an awful lot of fundamental work done.

Again, it is the first time I've been here, and yet there are still very many debatable points, and surely they can be resolved by a smaller sub-group having longer time.

I would like to suggest that for consideration.

DR. GREEN: Any other suggestions?

MR. C. CLINE: Dr. Green, I just want to make a comment relative to Dr. Porter's overview. From Rockwell's experience, the fundamental fluid mechanics is not always well understood, as we have seen here the last couple of days. However, I think we should also recognize the problems associated with integration of ejectors into an aircraft. Most of the difficult problems occur when you go to integrate/install an ejector into an aircraft.

A lot of problems that we have addressed in the last two and a half to three years have been involved with just that. Even though you can optimize a section in the laboratory, to put that into an actual flyable article is a task that is even greater than some of the fluid mechanics problems we have experienced. I just want to make sure that people realize that even though we may have trouble defining the fluid mechanics limits of an ejector, you haven't seen any real problems until you go to put it in an airplane.

Even though you may have developed a good R&D program for an ejector in the laboratory, you still have to address the integration problems, which themselves create additional problems that must be resolved.

DR. GREEN: Can I reword that a little bit, and say any kind of a program that is established should be built around a con-figuration of some type?

MR. CLINE: Yes sir, absolutely.

DR. GREEN: So even if you are doing more basic kinds of studies, if it is related to a configuration, you can see the next step as to where it is going to go as far as usefulness.

58

DR. ALPERIN: Isn't that sort of what we did in this program that we had, Ken?

DR. GREEN: That was its whole purpose.

DR. ALPERIN: We modified the ejector to fit into the airplane and modified the airplane to go around the ejector, and finally got something that might work.

DR. GREEN: Any other comments on that? Any other suggestions as to program direction?

MR. R. CLARK: It seems to me that we have a lot of existing hardware that could be put into a wind tunnel together with an existing engine. If we could put it in a 40 by 80 wind tunnel the full-scale concepts could be tested.

DR. GREEN: You are speaking specifically of the Rockwell ejectors?

MR. CLARK: Right, the rectangular configuration. It seems like a lot of equipment has already been purchased for the program; all we need are some more pieces, and we can put it in a wind tunnel to get some data, as opposed to starting over at zero.

MR. CLINE: A proposal to do just that has been submitted to the Navy, where we were taking the rectangular configuration developed in the laboratory to full scale hardware for concept validation of the augmentor and also putting together the assets from the XFV-12A program, a wind tunnel model for test in the NASA Ames 80x120 tunnel. That proposal is in that area already.

DR. GREEN: If I may comment on that, I would imagine that this proposal is probably going to get caught up in the latest Navy V/STOL program. What is going to eventually happen, I have no idea.

MR. CLARK: I would like to see a recommendation from this workshop that that be done. Let's don't throw all of that away.

MR. CLINE:  Are there other agencies that should be involved?

DR. GREEN:  We are working very closely with NASA Ames on that.

MR. CLARK:  How about the Air Force?

DR. GREEN:  As far as I know, the Air Force is only interested in STOL, not VTOL.  But certainly, the XFV-12A could be tested in the 40 by 80, in the STOL configuration, and see what the characteristics are.  So it is a possibility.

Any other comments?  Let's go on to the last two papers here.  I believe the next one was "Turbulence in an Ejector Wing Flow Field," by Catalano.

Any comments on that?  The last paper was "Integration of Ejector Thrust Augmentation Lift Systems into a Supersonic V/STOL Research Aircraft," by Farley and Murphy, and I will entertain any questions on that paper.

Thank you very much for your attention and your comments.

***

(Workshop adjourned at 6:20 P.M., to reconvene at 8:30 A.M., August 5, 1981.)

***

# EJECTOR WORKSHOP

Third day's wrap-up session, Wednesday, 5 August 1981,
11:30 A.M. - 12:30 P.M., Mr. David Koenig, Chairman.

MR. D. KOENIG: Since we have time now, we should go through
the papers again and see if there are some questions that we
didn't have time for earlier. Starting with the first paper,
"Flow Structures Associated with Upper Surface Blown Airfoils,"
are there any questions?

How about mine?

MR. D. GARLAND: I have one. That gem of a model, the small
model that you are putting in the 40 by 80 tunnel, are you
bothered by Reynolds number?

MR. KOENIG: I am, yes. That is one of the big questions.
That is the reason it is instrumented to the hilt with pressures
all over the model, to document where the separation effects are
going to be. That is one of the reasons we have two or three
balances in it, to separate duct and propulsion forces. I
believe they are able to separate the wing forces on that, also.

DR. MALMUTH: Are you thinking about using moving belt
arrangements in the wind tunnel?

MR. KOENIG: For ground effect?

DR. MALMUTH: Yes. Langley uses them for vortex formation
and ground effect. There certainly are scale effects associated
with that.

MR. KOENIG: Yes, there has to be. So far, we don't have
plans to look at ground effect on the model very much, because we
think it doesn't have any. If anything, it is negative, and
major effects just counterbalance themselves.

We have done some ground effect testing in hover on the
large-scale model. There is some adverse effect due to the
ground, but what we really want to do is put the large-scale

61

model out on a static testing rig again, and do some differential thrust control. One interesting point on that large-scale test was the oscillating flow underneath the model.

We had a hard time getting steady state data. Everybody looked at the ground effect, but in this case, with the two-poster, you would think it would be a little more stable, but it wasn't. You got the oscillating flow.

In forward speed, we will have the small model in the 40 by 80 wind tunnel. I think we will stick a piece of flat wood or something under it for that. But that would probably be at a low priority -- we have had a hard time getting scheduled in the V/STOL tunnel at Langley, which would be the next step, with their moving belt arrangement.

DR. MALMUTH. I guess I didn't get that out of the movie that was shown. It wasn't clear to me whether there was suck-down effect or not, on that. Are you concerned with the suck-down, or if so, is it going to do experimental work?

MR. KOENIG: You are talking about the augmentor wing?

DR. MALMUTH: Right.

MR. KOENIG: No. On the augmentor wing model, the DeHavil-land Buffalo, there was fairly light wing loading. That wasn't mentioned. I think it was 45 or 50 lbs/ft$^2$, and the aircraft actually floated quite a bit. It was very stable.

I thought you were talking about the two poster. I got the wrong model.

DR. MALMUTH: My question was a little more generic. In the test program is there going to be any consideration of these kinds of phenomena in terms of configurations you are looking at, and how are you going to implement those considerations in your test plan?

MR. KOENIG: That is going to be a very significant part of our test. With the ejector wing, as Mr. Garland mentioned, we

got favorable ground effect, but there were compensating factors there, and I think we were getting into some oscillating flow on that model.

MR. GARLAND: I wasn't aware of it.

MR. KOENIG: There was some, but I think that was the most stable of the models I've ever seen.

UNIDENTIFIED: Is that scale effect, then?

DR. MALMUTH. Yes.

MR. KOENIG: That is a good question. I think we will be able to determine that on the small two-poster tilt-nacelle model that we have.

DR. MALMUTH: Is there enough control authority to cover it, to handle those unsteady effects, you think?

MR. KOENIG: We think so at this time, using the existing control system and the T34 engine. If they go to another power plant, the response may be another thing. On the response, I think we could have another workshop on that, and I wouldn't want to go into that right now.

Any other questions on my paper? Are there questions on Mr. Garland's paper? We discussed Dr. Foley's paper on "Ejector Ram Drag" at great lengths when he presented it earlier. Are there further questions.

DR. ALPERIN: I have argued with many people about this matter. I think we can design a VTOL ejector so the effluent flow isn't necessarily vertical, but you can have the ejector inlet and outlet design so that the flow goes through it without much net momentum change in the flight direction.

MR. KOENIG: But the physics may be against you unless ram drag is counteracted.

DR. ALPERIN: The physics are not against you. That is the point.

63

MR. B. LINDENBAUM, University of Dayton: I have one question. You show a positive ground effect for the two ejectors which decreases with aircraft height. If you go high enough, do you have a suck-down effect in the hover mode?

Go back to the Avrocar, which had a very positive ground effect. When it got out of the ground effect, it had a tremendous suck-down and caused all kinds of problems.

MR. GARLAND: When you get into free air with two augmentors on the one fuselage, the fuselage base pressure becomes negative. An interesting thing there, is that the exit static pressure of the augmentor diffuser, of course, sees that negative base pressure, and the effective thrust augmentation rises to the point where it almost, but not quite, offsets the negative base pressure, so the loss in free air is really quite small.

MR. LINDENBAUM: But the Avrocar did have a substantial negative pressure near the ground.

MR. KOENIG: That is true. As the aircraft got off the ground it had quite a suck-down effect. We measured that. But when you got further out, with a little bit of forward flight, that disappeared very quickly. So in operations you might not notice it.

MR. LINDENBAUM: One other comment about the fact that the flow is very directional sidewise: there is a region on each side which has very little flow. If you move forward, that flow may change completely. You get a roll-up of the exhaust that is going forward; you don't know what is going to happen to that, and it may roll-up in the intake. We've had that on V/STOL aircraft.

MR. GARLAND: There fortunately wasn't very much forward moving flow and there will certainly be some ingestion from that, but it is very small.

MR. LINDENBAUM: And the ejector exhaust is also cold.

MR. GARLAND:  Very cold.  You can walk through it quite easily.

MR. LINDENBAUM:  The other aspect is the debris raised by the exhaust.  I am not talking about hot gas now, but the debris.

MR. GARLAND:  The exhaust has very low velocity, fortunately.

MR. KOENIG:  The inlet was south for the tests and there was running with heavy north winds coming in sometime.  At times we shut down because of wind, but we were wondering about this and somebody got out there again, trying to see where this pattern was changed.  We must have had 20 to 25 knots coming in before we shut down.

We had the tailpipe right into the wind, and you have to idle a little bit before you shut the engine off, but they held it up just enough so we could go out and see where the flow was going.  We didn't notice too much change, but that was 20 to 25 knots.  I would imagine in takeoff you probably, would get out of that region pretty rapidly.  It would be interesting academically, but operationally, you probably wouldn't be worrying about it too much.

MR. LINDENBAUM:  Unless you used ground effect.

MR. KOENIG:  Possibly, if you use it for STOL, like General Dynamics.  Any more?

DR. GREEN:  Just a comment.  Most of what you have been talking about has been in the ground plane, and the direction of momentum flux coming out of the rectangular nozzles.  Kotansky at MCAIR has recently demonstrated that the momentum flux in the ground plane is very directional with 2-D nozzles, depending on the aspect ratio.

Most of the flow definitely goes off to the side.  The problem is that you are talking about far-field reingestion, and you are not talking about near-field reingestion.  You've got all

65

of the flow from the center coming up, hitting the under surface, and then the only place it can go is fore and aft. If you've got inlets sitting right on the side of the fuselage, in front of the wings, it is a very high probability that near-field up-wash flow going forward is going to be sucked into the inlets.

MR. KOENIG: That is where the fences come in and our inlet was pretty far forward. We weren't getting too much reheat from that.

MR. GARLAND: I would like to make a comment on that. Of the total flow coming from the two ejectors, only a small percentage is directed inward into the cavity under the fuselage. Most of the flow is bent coanda style, or due to a positive pressure under the fuselage, and flows outward.

What does flow in (and obviously there has to be some) goes out, as you said, forward and aft, but it is a very small percentage of the total flow.

DR. GREEN: That is probably a function of the spacing between the nozzles, put them further apart and it will make the upwash a lot stronger.

DR. BEVILAQUA: I would just like to add something, Ken. The gradient's advanced area tried to solve the problem by putting the jets inward so they combine under the airplane and they go down as one jet and don't form the fountain. You have to make a trade against the direct thrust loss and re-entrance temperature loss, and come out ahead. But that is another solution to that.

MR. KOENIG: Are there any more comments on the papers? I think that at least two or three of the papers addressed the application of the ejector to an aircraft, so I think the rest of this session should take up possible packaging problems.

First, I would like someone to define what packaging is, what do we mean by it. Someone might also address, and

66

especially the people working on the XV-12 project, what is a good approach to develop an aircraft, if someone wanted to go in with a given propulsion and ejector unit now and do it. What is the next step?

Another, of course, are the weight penalties involved. In the XV-12 case I think, the cart came before the horse, to a certain extent, but that was quickly reversed to the point where now the technology is up and very advanced.

What would you do over again, if there is any way? Commence with that.

I would like to now open it with any comments, and, I would hope, from the XV-12 people on general philosophy and approach.

MR. CLINE: Let me say the XFV-12 packaging problem has been very difficult in trying to package a very short high-performance diffuser in a very thin supersonic airfoil.

We had toyed with the idea of presenting a paper here today, but we just ran out of people and time, regarding the development of the Coanda surface in a thin airfoil to maximize performance. However, we do have that capability and it works very well.

To answer the question of what would we do if we had a propulsion system and ejector, how would we package it, I guess you have to start with the question, what is the ejector? If it is a spanwise augmentor, I think we could handle that very easily. We have developed the structural techniques, the lightweight structures involved, and the configuration sensitivities.

The high temperature titanium alloys, developed specifically for this program, even though it existed and had never been put into usage in structural parts, had been primarily used in engine application. We developed on this program, not by the program, but separately, a super plastic-forming technique where we formed the titanium alloys at very high temperatures, and therefore can very readily develop complex parts.

67

Let me say again, the only studies that we can readily answer right away, what are the packaging restraints, et cetera, are for the spanwise augmentor. We are currently doing the studies for the chordwise augmentor. We are not far enough along to answer those type questions.

I am not sure whether all of you are familiar with the concept of the XFV-12A, but basically the engine nozzle is plugged, and all of the engine exhaust is diverted through internal ducting into both the wing and canard and exits into the augmentor. That internal ducting has been optimized from a weight and configuration standpoint to where we have been able to minimize the losses.

A special titanium large diameter duct, 17-inch diameter duct, made from titanium alloy, was made specifically for this program, and it is very, very efficient, very lightweight.

The primary construction of the surface panels on the augmentors themselves are titanium honeycomb panels. That, in itself, makes for a very lightweight structure. The primary weight in each of the surfaces is comprised of the nozzle.

We have investigated various construction techniques for the nozzle. However, for the prototype airplane, it was made from flat sheet. That in itself was a manufacturing nightmare, and that is putting it politely.

I think if anyone has specific questions I can answer, but to go into detailed construction of the aircraft, it would get rather lengthy.

DR. BEVILAQUA: Let me make a few comments, too, before we get to the questions. One of the things we would probably try to do differently, would be to go to a higher pressure ratio engine. The higher you drive the pressures, the smaller the duct losses become.

68

Another one of the things we probably try to do is to reduce the taper of the ejector. The taper effects still contribute significant losses.

We would probably try to split the load more equally between the wing and the canard. In a sense our configuration is canard limited; that is, we can develop more lift on the wing than we can really use because the canard doesn't develop enough lift to balance the airplane with full wing lift.

MR. KOENIG: Excuse me for interrupting. This might be affected by the planform. If you go to the delta, then you get more space for the ejector.

DR. BEVILAQUA: Yes, that's right.

DR. VON OHAIN: And hot ducts help also.

DR. BEVILAQUA: Right. The big advantage of the XFV ducting system over the Hummingbird -- I don't know if you are familiar with the Hummingbird ducts which were made of a metal foil -- but the mechanics could drop a nut through an access panel and it would go through the ducts, and you would have to patch them. The patches would leak.

The titanium honeycomb ducts on the XFV-12A were a big advantage, and that should be incorporated in any concept. You might also try sweeping the wings forward on the airplane, because that would move the center of lift of the wings up towards the CG, and help the balance problem.

MR. KOENIG: What I am getting from you is that there is a keen relationship, then, between ejector configuration and the planform of course, and a lot of materials that are available to put the aircraft together.

Now what we are asking in this section probably has no simple answer, but I think that what is facing the ejector technology right now is looking at some of these other concepts. Where do you go from where we are right now in a wind tunnel

69

model, even a large-scale boilerplate model. What next would you try? Would you really simulate the ducting, and go back to large-scale testing? Would you study more ground effect, very similar to what Rockwell has done? Is that a good procedure?

MR. CLINE: I think it has to be a combination of both. You have to prove to yourself and the aircraft community that you do have the performance in a full-scale ejector. It has to be hot, and it has to be the correct pressure ratio, et cetera, before you go into a wind tunnel model. I think the scale models can be used quite effectively in the generation or the initiation of some of your data base for both the augmentor as well as wind tunnel models. For example, work still has to be done in the transitioning phase of augmentors. What is the performance, how do you gear it to minimize the thrust loss, the ram effects and reingestion?

Although we feel that with the spanwise augmentor configurations ground effect is positive and reingestion can be controlled, I think the answer to your question is that it has to be a procedural step utilizing all of the facilities available.

The program has to be laid out to use all of those capabilities in the most efficient way possible. So to reiterate, I think you need the full concept single-ejector test as a validation prior to proceeding to a full-scale wind tunnel boilerplate model.

DR. MALMUTH: I would also like to say, with respect to the plumbing business and the losses, that there is a real need to do flow modeling of complex flow passages to pin down some of these losses, and I think that can be handled now with some of our modern tools, computational tools, to get a good idea what those things are.

DR. SEARS: In retrospect, you can't help looking at the XFV-12 program; you can't help concluding that you could very easily have made from the existing XFV-12 a test airplane that

70

would have flown and would have demonstrated this concept. It would have permitted the study of handling qualities and pilot loads, and a lot of these practical questions that are important to answer.

There was always the question in everyone's minds of how far Rockwell should be told to go in that direction, violating some of the packaging requirements and giving up perhaps the idea that the airplane was a supersonic fighter when it was finished.

For example, you could imagine that you could start out, as they did, with a concept of a supersonic fighter, with ejector augmented lift. But some things had to stick out the top of the planform, and that, obviously, wouldn't be satisfactory for supersonic operation. So one could take the view that we didn't quite have a supersonic airplane, but we have one that is close to it, and it does other things, that should be done. But the program didn't permit that.

It was an expensive program. It was felt by most of the people concerned, that the program had to produce a supersonic fighter aircraft. Maybe in retrospect, as we look at it now, especially since the Navy isn't very much interested in that particular supersonic sea control concept any more, wouldn't it have been wonderful if we had relaxed some of the constraints, made the wing a bit thicker, etc. I don't know. Several things that could have been done that would have produced a flying airplane today.

I don't know what the conclusions of my remarks are. I leave it up in the air. It means that we could have had a research airplane, but it would have been a very expensive one, and it still would leave the military people unsatisfied, because they wouldn't have something they could immediately turn into a production fighter.

MR. KOENIG: Well, if you look over the years, we've had a lot of these flight demonstrators. Every design has come along with deflected thrust, lower surface blowing, or upper surface

71

blowing. We've had an airplane flying, but we haven't had a fighter. We certainly have the Buffalo, but we haven't had something operational that would --

DR. SEARS: If you want to be real mean, you can accuse the Navy and Rockwell of what Dr. Von Karmen used to say: "Imagine what would happen if the Wright Brothers had not been willing to fly until they had the 747."

(Laughter)

MR. KOENIG: I can't top that.

DR. FOLEY: I fully agree with what has been said so far, but to defend the XFV-12A for a little bit (which is kind of unusual, coming from someone at General Dynamics) remember how the program started.

Admiral Davies wanted to bypass the entire research organization of the Navy and NASA and to go straight from concept to fighter. He admitted it was high risk. It was very high risk, and it didn't pay off, but that should be borne in mind when pointing the finger at Rockwell on the 12A. That was the stumbling block on the program. If it had worked, everyone would have been a hero.

MAJ. KEEL: Perhaps the XFV-12A program was more successful than we give it credit for. I know of very few problems that we have solved in this business, until they have been defined. I've seen a lot here in the last couple of days that has been done in the last two and a half years because we defined problems specific enough to get people to work on them and got the resources to accomplish them.

As I look back over my short career in the aircraft business, I can identify the major advances we have made almost one for one with major problems that have been defined by somebody's system or another, and until we get the courage and the strength of our convictions to step out and build something,

72

find out what part of it does work and what part doesn't work, we are probably not going to define problems clearly enough for us to solve them, and go work on them.

I think the real advantage of what I heard Professor Sears say here is if we had compromised a little bit, we might have defined some other problems further downstream that would have allowed other people to get busy, like the handling qualities problem, some structural problems, and so forth.

I heard Dr. Sears say the other day that we started in the VTOL business by going directly to the full-scale hardware phase. There are a lot of questions that are running around in my head that I haven't heard anybody here address yet.

DR. VON OHAIN: Name some.

MAJ. KEEL: Questions like flight worthy hardware, how flexible it gets, how we hold the tolerance on the geometry, and all of these kinds of things. I've heard a lot about temperature effects here, but only about laboratory and theoretical models. Anytime I've messed with temperatures, it makes parts change size, and they don't fit together right, and that is going to affect the performance more directly than is the temperature effects on the gas theory.

The aircraft just isn't going to work the way we think it is, unless we put it together. You don't have our two-stripers working on it yet. After they get through putting it together and taking it apart a couple of times, it is not going to look like what we designed.

That is going to be a very real part of whether it really works or not. Military machinery has to be tolerant if it is going to be successful. If I've got a major concern about ejector technology, it is the fact that most of what I've seen to date indicates to me that it is not extremely tolerant, at least at its current level of maturity. If we are going to make it work for a real, live airplane, we've got to work at building

73

some tolerance into it so that when the loads change a little bit, there will be enough performance to get the aircraft off the ground. I see those as some of the full-scale requirements that we haven't even started discussing, and I think that is what could have been done with your XFV-12A, Professor Sears, if we had built one.

DR. SAM WILSON: I think one of the recommendations that ought to come out of this workshop is that the work that has been done on the XFV-12, should be preserved if the Navy doesn't have funds to keep it going. If, a few years down the road, we decided some STOL potential exists, then we can go back and take this hardware out of storage and use it. I would hate to see a valuable asset like this, with so much money put into it, lost because it is forgotten about.

DR. GREEN: Let me respond to that. I don't think you should conclude that the Navy is going to drop the program at this point. In its present form, that is true. My understanding is that it is going to have to compete with a lot of other concepts within the Navy V/STOL program. To say it has been ruled out, that it is going to be set aside and the Navy will not conduct full-scale tests on its various components, I don't think you can conclude that at this point.

So I would say it is still a viable competitor in the whole scheme of things.

MR. KOENIG: Glad to hear that.

DR. GREEN: With respect to the comments that Bill Sears made, I happen to agree with him, that that is the kind of thing that should have been done.

..he point that I would like to get across is that there are a lot of people in the Navy that are looking at total systems. How is it going to be used? Where are you going to hang your external fuel tanks? Where are you going to hang your weapons systems? These are the kinds of things they get very concerned

about. You start modifying the geometry of the airplane,
violating the mold lines, and everything else, then they kind of
lose interest. Plus the fact that if the augmentors are so sen-
sitive to their design, once you've designed something that
violates the mold lines and you've got it flying around, who is
to say that you can ever get it inside that wing. So a major
concern is the packaging problem.

MR. KOENIG: I haven't been in the aircraft design business
for a number of years, but I remember when I was, you acquire a
lot of empirical data, and what they've got here is data based on
how to do this for different duct sizes, etc. They probably have
been through these exercises, and should be able to continue with
data acquisition even though they don't have a viable configura-
tion for a particular tactical mission.

If someone comes along and has a mission, finally, in the
nineties, he can use this data then and look at the ejector and
see whether it can be worked into his weapon system.

I wouldn't be too concerned as to what the thing looks like
as long as it flies, maybe eventually supersonic, if you can get
the cross-sectional area down and house the ejector in something,
the storage might come some place else.

Then you could be able to predict what would happen if ejec-
tors moved or the payload changed and to a certain extent, the
range might be varying, too.

What you want right now is to continue this technology,
advancement in structures, in the fluid dynamics area, and hope-
fully fly something, and say, you have flown something of a cer-
tain weight empty. You are able to design it now, you can
control it, you can put ducts out to the tips and control it.

I think the basic technology should be here.

DR. MALMUTH: I concur heartily with you. I think there is
a high risk aspect to the thing originally addressed, and I think

if we can get over that hurdle, I think we can address those other issues. I don't mean to make them secondary, but I think the main thing is to get it to work.

DR. VIETS, Wright State: It seems to me what we are talking about is objectives. The Navy has certain objectives to get an airplane that does certain things. But now we are hearing opinions from various other organizations that would like to see a vertical take-off plane actually get off the ground. It seems to me the only way you are going to do that is to have funding coming from various sources and make it a demonstrator rather than making it a supersonic fighter.

MR. KOENIG: The money has to come from somewhere.

DR. VIETS: It is not going to come entirely from the Navy, is what I am saying. I don't think it will, anyway.

MAJ. KEEL: It's got to be a little more than that, in what we want to get flying. Some of this business of it being a supersonic fighter or with supersonic capability has to fit in there. We've seen airplanes fly, like our V/STOL airplane. We need to demonstrate more than that.

By most people's definitions, the Cessna 150 is a STOL air-plane. We may have not set our objectives broad enough to really demonstrate what we wanted to, or at least convince the people that need to be convinced, and that may be part of our problem.

MR. KOENIG: That means you have to be pretty careful in what you fly to demonstrate.

MAJ. KEEL: That is right.

MR. KOENIG: It has to have V as well as STOL. If you ever say you want to go V again, we've got the technology here, allowing you to go straight up, but you can also take this thing off heavy for STOL, and you could add weights as needed for the flight demonstrator, to look at the performance at various gross weights.

76

DR. ALPERIN:  We've got the laboratory technology, but we don't have the practical technology.

MR. KOENIG:  Right.

MR. DIETZLER, Flight Dynamics:  I haven't been in this business very long, but I am getting a picture of something about this ejector technology I would like to get a comment on.

We have demonstration aircraft that work with thrust vectoring in pretty much the mode you are talking about except they are not supersonic, but it looks like something could be made from that.  One speaker today pointed out the main reason the Navy is interested in the ejector technology is the benign footprint.  The Navy doesn't want a hole in the carrier deck.

Does the Air Force, does the Army, do the Marines, unless they are on a carrier, need that benign footprint bad enough to make the effort to demand this requirement from the ejector technology?  In other words, can't we do most of what we would want to do with this type of already existing demonstration airplane, both V and STOL, the way the carrier did?  That is my question.

DR. W. FOLEY:  I want to respond to two statements.  First, Major Keel's:  if I may paraphrase what you were saying, we have built a lot of machines, the Pogos, and so forth and none have been able to do anything once they got up into the air.  The Harrier is the only exception I can think of.

DR. ALPERIN:  The Harrier couldn't do anything either.

DR. FOLEY:  It took 14 years.  Now it is getting up to the point where it is a useful machine.

MR. LINDENBAUM:  There are a number of other concepts.

DR. FOLEY:  It must be admitted that a demonstrator has to do something, or at least have the potential to do something. If it is worth the effort.  I would think the benign footprint is

more important to the Air Force and Marines than the Navy. The Navy has sea water to cool the flight deck.

The next logical step in the Harrier is something like the PCB configuration, which now puts temperatures on the order of 2,800 degrees Fahrenheit on the deck or a concrete surface. I think when you are talking that kind of environment, you are asking for trouble.

Every piece of data we have indicates there are serious problems because of this environment. I am not saying you cannot work around it with deflection grids, or that sort of thing. It is that everything we've come up with to get around that problem impacts flexibility, so we've just backed off and gone to ejectors for that reason.

MR. KOENIG: Is there anyone else?

DR. GREEN: I would like to change the subject slightly.

MR. KOENIG: All right.

DR. GREEN: I would like to go back to a comment that Dr. Bevilaqua made with respect to tapering ejectors and his suggestions of things that he would have liked to have seen done differently, had he a chance to do them over again. He said he would like to make them less tapered.

My understanding at this point is that most of the work has been done with rectangular augmentors, because it is much easier to develop an understanding there, but you still imply that work in tapered ejectors would be worthwhile. Could you elaborate on why that is true? Is it just the installation problem?

DR. BEVILAQUA: We have asked the designers to come up with rectangular ejectors, given them complete freedom, but they always say: "Couldn't I just taper this a little bit, couldn't I taper the Coanda surface?" Something always ends up tapered because the wing is tapered, so, yes, I think eventually you are going to need the technology and capability to put some kind of

78

taper in the ejector. You need to know what is important and what you can taper without a lot of thrust loss.

DR. GREEN: Hasn't Rockwell done a fair amount of that kind of work; determining important parameters with taper?

DR. BEVILAQUA: We know what some of the important parameters are, but we haven't really pursued solutions.

The important parameter is diffuser taper. If you taper everything else but have a rectangular diffuser, you are going to see a very small loss in augmentation ratio.

But suppose you are forced to taper the diffuser, what can you do to minimize losses? You might try a jet flap diffuser to untaper the solid diffuser. That needs to be explored and studied, and the technology developed.

DR. GREEN: I would like to refer the same kind of question to Bill Foley, or Doug Garland. Is there any reason you might want to taper the wing root augmentor?

DR. FOLEY: Yes. However, in our design work, based around the de Havilland ejector, we put the designers' feet to the fire: they shall not change the ejector from what was tested at Ames because of the trouble the taper caused on the XFV-12A.

MR. GARLAND: We have certainly drawn airplanes, with tapered ejectors, and there are some packaging benefits from drawing the tapered one, but we too are aware of the loss of augmentation which occurs due to the nonorthogonal-sided-box, I guess you would call it. We've measured this on the swept wing augmentor wing model, tested in the Ames tunnel and the loss is something like five counts due to the tapered, swept augmentor.

We don't like to throw that amount away We don't know any way around it at the moment.

MR. KOENIG: A count being what?

MR. GARLAND: 0.01 in augmentation ratio.

79

MR. KOENIG: Anybody else?

If not, I think we have adressed the primary question. I think we are probably ready for summary on this.

Do you want to wind it up, Major Keel?

DR. BRADEN: Either Major Keel or Dr. Nagaraja is going to do that.

MAJ. KEEL: I guess I will ask if anybody else has any summary comments they would like to make, or any general recommendations that they would like to make, either government to industry or industry to government.

DR. GREEN: I would like to reopen something that was discussed yesterday with respect to the forward flight ejectors. A lot of the discussion that went on, I think, led to some confusion as to the exact position people were taking with respect to the viability of the concept. In particular, I would like to ask Dr. Minardi and Dr. Addy to comment on whether they think, first of all, that the forward flight ejector is a feasible concept, and whether or not the supersonic solution can ever be achieved.

DR. MINARDI: Well, as far as whether the supersonic solution can be achieved or not, it has been experimentally verified by Fabri's work, and possibly by Dr. Addy's work. When I say it has been verified, the way Fabri's ejector worked was that he throttled ambient air in as the secondary fluid, so he was starting out with air that was at a stagnation pressure lower than ambient pressure. He ran ejectors with and without diffusers.

He could then eject that air with supersonic mixed flow into the ambient. So there isn't, in my mind, any question whether you could do that. It has already been experimentally verified.

The questions, obviously, are if one does a study of what really can be achieved, what kind of advantages and thrust augmentation might then result from that knowledge.

80

So I don't know at this point in time, not having yet performed any real parametric studies on what kind of thrust augmentations one could achieve, what the actual performance will be. I haven't performed these studies yet, so I don't know whether there is a payoff or not at this point in time.

PROF. ADDY: Dr. Minardi talked to me yesterday, and he indicated that I had apparently given the impression to him, anyway, and maybe to some of the other people, that you couldn't get supersonic flow at the exit of the ejector. Correct?

DR. MINARDI: Yes.

PROF. ADDY: I didn't want to give that impression, because I have run experiments where we did have supersonic flow at the exit of the ejector. I simply pointed out to him a simple example of how you might accomplish this.

You could have, say, a converging-diverging nozzle, the primary nozzle of your ejector flowing into a constant area mixing tube. If you close off the mixing tube, so that you have no secondary flow and if you have a sufficiently high primary flow and a sufficiently low back pressure, you can maintain supersonic flow down that duct (i.e., a sudden-enlargement supersonic nozzle is formed by the combination of the primary nozzle and the mixing duct).

This is with no secondary flow. If you then just start to open the secondary valve a little bit, you will induce some secondary flow; you will still maintain essentially the supersonic conditions at the ejector exit. (Supersonic flow conditions can be maintained in the ejector duct at higher secondary flow rates. The ejector exit conditions must be in accord with the imposed back pressure conditions).

My point yesterday was that I think one has to apply all the constraints that ejectors have to operate under when you are

considering them. Generally when you have a supersonic ejector, aerodynamic choking naturally occurs in the ejector, this does constrain the mass flow rate.

In other words, if you have a small primary nozzle and a large mixing tube, then I would say only under very special conditions could you produce supersonic flow at the ejector exit. But then, you have all sorts of other practical problems; the type of configuration, geometrically induced flow separation, flow being induced by mixing along the jet boundary, and then flow separation at the wall in the recompression region. Thus, you probably don't have one-dimensional flow.

So, there are many factors that one has to consider. The best way to do it, in my opinion, is to apply all the correct constraints to the ejector to match the ejector with the inlet, and to apply the downstream boundary conditions. This problem is further constrained by the fact that the inlet takes in ambient air and the ejector discharges it back to ambient conditions.

DR. MINARDI: Of course, in flight, obviously, the stagnation pressure is higher than the ambient pressure, and this is an advantage to the ejector that you don't have, probably, in some of the cases you are talking about.

PROF. ADDY: Well, I think that there are advantages and disadvantages because of the ram effect. You have inlet and associated effects.

DR. MINARDI: I agree. We don't know the answers at this point in time.

DR. GREEN: I just wanted to clarify the general feeling that was left with my group. My feeling, and some of the comments that I got, indicated there was confusion as to what you were really saying. That is really what I wanted.

MAJ. KEEL: Dr. Green, what if it took a higher pressure ratio engine to make this possible? Are these things coming down

82

the track? Are you going to see engines that are putting out higher pressure ratio exhaust on the order of six or eight? Are we going to see that?

DR. GREEN: Well, there is certainly technology being developed for higher overall pressure ratio engines, primarily for fuel efficiency, but I don't know of any engine development program that is currently under way aimed at high exhaust pressure ratios.

PROF. ADDY: One other comment about ejectors. Pressure ratio is, of course, another very strong constraint in the problem. If you have a primary pressure ratio available of maybe three, then you are immediately limited on the expansion Mach number entering the ejector section. This, of course, limits the potential ejector performance, because typically, in many ejectors, you might be talking about primary pressure ratios of 6, 10, etc., which I don't think are going to be readily available.

DR. SAROHIA: I think supersonic ejectors would be even more sensitive to changes in operating point, and as you mentioned, in the system, too sensitive to get ambience in that technology. We will have more problems than even we have in existing ejectors.

PROF. ADDY: May I make a comment on that? That is one of the things that we found in looking at supersonic-supersonic and subsonic-supersonic ejectors for laser applications. Our conclusion was that when you have all supersonic flow, there are strong interactions, also, that come into play, and the ejector was not very forgiving if you changed the operating point; whereas with the subsonic-supersonic ejector, it was more forgiving. The subsonic-supersonic ejector would adjust itself aerodynamically; The supersonic-supersonic ejector would oftentimes result in shock waves and flow separation which significantly alter the ejector flow field. It is relatively sensitive.

DR. MINARDI: To just answer your question, what I know about it, I think the engine's coming along, the pressure inlets

83

are probably around 4. Much more than that, I don't think you are going to see for quite some time. There is probably a bleed on the compressor. You can get tremendous pressure ratios there, but you cannot get too much flow, as a rule.

PROF. ADDY: I think that all factors must be incorporated into a careful study of all these constraints.

DR. FOLEY: This is not to say you couldn't put together an engine of pressure ratio of 8 if you needed it. I am saying over the shelf today I don't see anything that would fill that.

PROF. ADDY: I think that would have to be a result of providing some beneficial effects that would be worthwhile to take if off the compressor at a higher pressure.

DR. FOLEY: You get a fan that gets up to a pressure ratio of 8, for instance, but it is heavy, very heavy.

DR. ALPERIN: What I want to say is that getting supersonic flow out of the end of an ejector does not necessarily mean that it is an effective second solution thrust augmentor.

As a matter of fact, in the stationary case, to get a good second solution ejector, the exit flow is generally subsonic, in most practical situations and I think the whole key to the thing is to produce the kind of flows that are dictated by the theory as being optimal. This requires very careful consideration of the outlet design with minimal losses. You have to go from a supersonic flow at the end of the mixing to a subsonic flow at the exit for a stationary ejector, when the primary nozzle pressure ratios are within the bounds of modern technology.

If you are flying at high speed, high subsonic, or supersonic speed, then the exit flow will optimally be supersonic.

But just the fact that you can get a supersonic flow coming out of the end does not mean that you have an effective second solution ejector.

84

MR. KOENIG: Maybe we can get a little summary into this part of our session, and that was what we just touched on in engine technology. I think one of the recommendations here, of course, should be to the engine manufacturer to look at the engine technology as required for the ejectors in the future, which includes the second solution, if that becomes practical, and get some good basic experimental data on it.

And the other thing, of course, is for the airplane manufacturers. I think all the airplane manufacturers ought to be put to work, not just Rockwell, all of them, work on structures, metals, composites, if you need more ducts, not just hot ducts, but ducts used for cold and high pressure ratio flow.

So in that respect, I think there ought to be some recommendations from this workshop to the manufacturers of all aircraft suppliers.

MAJ. KEEL: Yes, sir.

MR. P. COPAS: Pete Copas, formerly General Electric. I am retired now. About the question about supersonic ejectors, if you limit your concentration to operations at supersonic flight speeds, of course, you have much higher primary nozzle pressure ratios available, simply due to the higher ram pressure, so the question of engines being limited to pressure ratios of four, five, or eight, it applies only under stationary conditions. Under flight conditions, I am sure you have much higher pressures.

PROF. ADDY: It is too difficult a subject to sit here and try to toss back and forth the various ideas. I think the only way we can do it is systematically to look at all the problems. It is the whole package. We did this in a sample problem for an ejector, a supersonic ejector, which was a short one. We showed at that time, in that particular paper, that approximately a 10 percent thrust augmentation could be achieved.

This analysis matched the flow characteristics of the intake with the mass flow characteristics of the ejector, and it imposed all the proper conditions in the flow-through device.

85

I think that is the only way you really can tell. We just can't pick out and isolate all the different effects and interactions and say, well, we would like this to be the case, or if this happens, etc. because the flow oftentimes will not cooperate with that approach.

DR. J. LOTH: The advantage of running this primary jet at a pressure ratio of 3, of course, keep the ducts small so you can duct it through where you need it and keep the temperature reasonable.

From the thrust power ratio, it also decreases the augmentation ratio. I can't see any advantage of going to six. Power ratio really decreases rapidly, your problem becomes enormous, and I think the pressure ratio 3 seems to be a good workable limit.

DR. BEVILAQUA: We are talking about a supersonic fighter incorporating an ejector, but there is one other possibility; that is, to leave the ejectors open at high speed and inject fuel and ignite it. You can actually get a ram jet on what is left of the ejector, and talk about a hypersonic fighter. That is a little further in the future, but it is an alternative way of using the ejector supersonically. Turn it into a ram jet.

DR. ALPERIN: It is a ram jet.

DR. BEVILAQUA: With fuel injection.

DR. ALPERIN: It has the heat of the exhaust jet, and you can add fuel. How much heat do you want? If you use the heat from the jet of the primary jet, you have a ram jet. It doesn't matter how you heat it.

DR. SAROHIA: It is very advantageous to add heat. The velocities are pretty large.

DR. ALPERIN: Velocities are low at the inlet.

MR. CLINE: I would like to reiterate the statement I made yesterday in light of what discussion we've had here today. When

86

we talk about incoporation of ejectors into an airplane, you have to evaluate all of the construction techniques, and you've got to do it on flight weight hardware.

That means new materials, new fabrication techniques, to keep the weight down. Otherwise, you are not going to be able to evaluate in a demonstrator what you can or cannot do. Now there are various technologies going on within the industry, types of material construction, V/STOL study for fabrication of light-weight fuselage, et cetera, et cetera.

However, the ejector techniques are dictated very largely by incorporation into some aircraft. That aircraft has to be configured to allow you to get supersonic, if necessary.

This prototype program is not a cheap program. You are talking about a very expensive program to go through a good demonstrator evaluation. You are going to evaluate not only the ejector, but the materials, the technology, the aerodynamics of the configuration (which is different than the conventional airplane) so we are not talking about something that you can put a few bucks into a get a quick demonstrator and evaluate.

MR. FINCH, General Electric: Being an engine manufacturer, and loving to sell engines, I started thinking about the source of air, and generally, the high pressure ratio engines required to fly an airplane with an ejector like that. I think you run into a problem with the ejector yielding low specific thrust, and the ram drag maintains itself up there, so you match the engine to an airplaen that has a high speed flight regime, and you are probably going to have less efficient use of an ejector.

Perhaps the engine manufacturers should look at some kind of compound engine for a source of air that is readily ducted away to support an aircraft with ejectors.

MAJ. KEEL: Do we have any other general comments or questions at this point? Recommendations?

87

Perhaps it is time for me to make a couple of general comments that I have in the way of closing, and then say a final thank you.

One, I think we heard from David Koenig this morning that NASA has an interest in the powerlift area, and I am hoping that they will continue to help develop some of the things we are talking about here, and help draw it to a focus.

We also heard from Dr. Green yesterday that the Navy is developing, and we are seeing it take on more shape and form, a program in the area of VTOL technology. I would feel much better if I could stand in front of you this morning and say that I honestly thought the Air Force had its act together nearly so well in this area.

I've also heard some comments here today, though, about what the NASA position is, and what the Navy position is, and so forth, and I guess I was reflecting that most of these things are institutions and very rarely do institutions really have positions. I think it is people that do that.

I as an individual have a very strong opinion in this area that right now the Air Forces R&D program is sort of short-sighted. We've got a management approach that limits us to only those systems that are in detail defined, and that makes it very difficult to work on new concepts, new visions.

We also are living in an environment where we hear consistently that aeronautics is a mature science, and has very little to offer on R&D investment. I would like to throw out a little bit of a challenge, and maybe I am leaning on you people a bit, but I am not above that, that we need to dream a little bit. We need to think a little bit about what we can do. We need to take the kind of risks that get us the kind of problems defined that we can work on and identify. I need some of your ideas, and some of your estimates about what we can do for aeronautics, and

I will fight to make sure we can have a piece of the program to help Ken Greene and Dave Koenig complete what they have started to do in ejector technology, I will try to take that on as part of my objective in this area.

I've already said this morning that my personal conviction is that we need to build hardware. I think we learned from hardware. I think it is from hardware that we get the definition of the problems that we can solve with theory, and that we can solve in our laboratories.

I've spent a good equal amount of my career in the laboratory and in large scale hardware, but what we are really missing at this point, to me, is the focus that large scale hardware can put on our problems.

If people have different opinions on this matter, please feel free to speak. I was encouraged by what I saw in the scaling effects paper; that things are the same in ejectors that they are in all other experimental work I was ever part of.

I talked a little bit about some of the full scale problems. There are a couple of others I would like to mention, and I think they fit in with your last comments here Tuesday. I was at Edwards during some of the YC-14 and YC-15 days. I saw a lot of trailing edge flaps being changed early in the program, and I think we are probably going to end up with some sonic fatigue problems, and those kinds of things.

I do think that the real estate problem on the airplane is a very real one, and somehow, even in our paper studies, we have to think about those to a point that we can get some of the operations people at least a little excited about what we might do with these airplanes if we are going to keep them on board.

My only final comment is that we have all learned a lot here, but I think what is important is what we do with it once we leave here. I think we have some technologies here that we can all still contribute more to.

89

I personally think the conference has not done everything I would have liked for it to, but most of our endeavors don't. That leaves us some room to improve and some room to dream and some room to try to do better next time. But it has certainly accomplished a lot of things that I didn't have in mind. I am very happy with what we have accomplished.

I would like to thank each of you for coming, for contributing, and for what I think you are going to do for us in the future. Please take time to go through these packets and sheets and scratch out some comments; try to do that for us.

If you don't leave them with us today, try to do it before you get too involved in what you are going to do when you get back home. Do it while you are sitting in the terminal waiting on the airplane.

I personally would like to thank Dr. Braden and the staff he put together, the U. D. folks, because I think they did a fine job.

***

(Workshop concluded and adjourned at 12:30 o'clock, P.M., August 5, 1981.)

***

APPENDIX A

WORKSHOP AGENDA

EJECTOR WORKSHOP FOR AEROSPACE APPLICATIONS

(All meetings will be held in the South Conference Room)

Monday, August 3, 1981

Hours

| | |
|---|---|
| 0730-0820 | Breakfast |
| 0830-0900 | Welcome by Colonel Robert Rankine, Commander, Air Force Wright Aeronautical Laboratories |
| 0900-0940 | "Overview of Air Force Activity in the Ejector Field," Dr. K. Nagaraja, Flight Dynamics Laboratory |

Part I:   Ejector Aerodynamics

| | |
|---|---|
| 0940-1020 | "Ejector Nozzle Development," by E. F. Schum and J. H. DeHart, Rockwell International, North American Aircraft Division, Columbus, Ohio |
| 1020-1040 | Break |
| 1040-1120 | "Theory and Practice of Ejector Scaling," by P. M. Bevilaqua and C. P. Combs, Rockwell International, North American Aircraft Division, Columbus, Ohio |
| 1120-1200 | "Ejector Shroud Aerodynamics," by J. H. DeHart and S. J. Smrdel, Rockwell International, North American Aircraft Division |
| 1200-1300 | Lunch |
| 1300-1340 | "An Investigation of Planar, Two-Dimensional Ejectors with Periodic or Steady Supersonic Driver Flow," by H. L. Petrie and A. L. Addy, Department of Mechanical and Industrial Engineering, University of Illinois |
| 1340-1420 | "Some Observations on Mixing of Free and Confined Underexpanded Rectangular Jets," by A. Krothapalli, Y. Hsia, D. Baganoff, and K. Karamcheti, Standford University |
| 1420-1500 | "The Mixing of Swirling Flows," by G. C. Oates, Department of Aeronautics and Astronautics, University of Washington |
| 1500-1540 | "Mixing of Jets and the Effect of Velocity Ratio on Entrainment," M. A. B. Narayanan, Indian Institute of Science, Bangalore, India |
| 1540-1600 | Break |

| | |
|---|---|
| 1600-1640 | "Fundamental Studies in Thrust Augmenting Ejector Flows," by L. P. Bernal and V. Sarohia, California Institute of Technology, Pasadena, California |
| 1640-1740 | "Considerations on Steady- and Nonsteady-Flow Ejectors," by J. V. Foa and Charles Garris, George Washington University, Washington, D.C. |
| 1740-1820 | "Some Interesting Flow Features of Supersonic Co-axial Jets," by D. Dosanjh, Department of Mechanical and Aerospace Engineering, University of Syracuse, New York |
| 1930-2000 | Dinner |
| 2000-2200 | Evening Discussions |

## Tuesday, August 4, 1981

| | |
|---|---|
| 0730-0820 | Breakfast |

Part I (continued): Ejector Aerodynamics

| | |
|---|---|
| 0830-0910 | "Jet Mixing and Entrainment Using an Oscillating Vane," by D. J. Collins and M. F. Platzer, Naval Postgraduate School and J. C. S. Lai and J. M. Simmons, University of Queensland |
| 0910-0950 | "Unsteady Flows Applicable to Ejector Mechanics," by H. Viets, M. Piatt, M. Ball, R. Bethke, D. Bougine, Wright State University, Dayton, Ohio |

Part II: Ejector Performance

| | |
|---|---|
| 0950-1030 | "Considerations of the Control Volume Approach to Ejectors as Applied to Thrust Augmentation," by J. E. Minardi, University of Dayton Research Institute, Dayton, Ohio |
| 1030-1040 | Break |
| 1040-1120 | "An Overview of Supersonic Ejector Performance Analyses," by A. L. Addy, Department of Mechanical and Industrial Engineering, University of Illinois |
| 1120-1200 | "Thrust Augmenting Ejectors," by M. Alperin, Flight Dynamics Research Corporation, Van Nuys, California |
| 1200-1300 | Lunch |
| 1300-1340 | "Investigation of the Supersonic-Supersonic Ejector," by J. C. Dutton, Texas A & M University |

| 1340-1420 | "Analytical Investigation of High Performance Short, Thrust Augmenting Ejectors," by T. Yang and Francois Ntone, Mechanical Engineering Department, Clemson University |
| --- | --- |
| 1420-1500 | "Recent Ejector Technology Programs at the Naval Air Development Center," by K. A. Green, Naval Air Development Center, Warminster, Pennsylvania |
| 1500-1520 | Break |

Part III:  Ejector-Aircraft Integration

| 1520-1600 | "Progress Towards a Theory of Jet Flap Thrust Recovery," by P. M. Bevilaqua, E. F. Schum, and C. J. Woan, Rockwell International, North American Aircraft Division, Columbus, Ohio |
| --- | --- |
| 1600-1640 | "Viscid/Inviscid Interaction Analysis of Ejector Wings," by P. M. Bevilaqua, C. J. Woan, and E. F. Schum, Rockwell International, North American Aircraft Division, Columbus, Ohio |
| 1640-1720 | "Transitioning Ejector Augmentor Laboratory Experiments to Flight System Applications: The Technical Challenges," by John Porter, Vought Corporation, Dallas, Texas |
| 1720-1800 | "Turbulence in an Ejector Wing Flow Field," by G. D. Catalano, Mechanical Engineering Department, Louisiana State University |
| 1800-1840 | "Integration of Ejector Thrust Augmentation Lift Systems into a Supersonic V-STOL Research Aircraft," by J. M. Farley and R. D. Murphy, Naval Air Systems Command Headquarters, Washington, D.C. |
| 1930-2000 | Dinner |
| 2000-2200 | Evening Discussions |

## Wednesday, August 5, 1981

| 0730-0820 | Breakfast |
| --- | --- |

Part III (continued):  Aircraft-Ejector Integration

| 0830-0910 | "Studies of Lift Enhancement and Separation Control for Transonic Upper Surface Blowing," by N. D. Malmuth and W. D. Murphy, Rockwell International Science Center, Thousand Oaks, California, and J. D. Cole, University of California |
| --- | --- |

95

| 0910-0950 | "Investigation at Large Scale of Thrusting Ejector Applications to V/STOL Aircraft," by D. Koenig, NASA Ames Research Center, Moffett Field, California |
| 0950-1030 | "Some Applications of Ejector Technology to STOL and V/STOL Aircraft Projects," by D. Garland, DeHavilland Aircraft of Canada, Ltd., Ontario, Canada |
| 1030-1040 | Break |
| 1040-1120 | "Ejector Ram Drag," by B. B. Beard and W. R. Foley, General Dynamics Corporation, Fort Worth, Texas |

Part IV:   Prioritization and Implementation of Advanced Ejector Research Programs

| 1120-1200 | Navy, Air Force, NASA Overview |
| 1200-1300 | Lunch |
| 1300-1600 | Continuation of Part IV |

APPENDIX B

LIST OF ATTENDEES

ATTENDEES

Prof. A.L. Addy
144 MEB
University of Illinois at U-C
1206 W. Green St.
Urbana, Illinois 61801
217-333-1126

Dr. R. Agarwal
McDonnmell Douglas Research Laboratory
Bldg. 110
P.O. Box 516
St. Louis, Missouri 63017
314-233-2528

Dr. Krish Ahuja
Lockheed Georgia Co.
Dept. 72-74 Z403
Marietta, Georgia 30342
404-424-5990

Dr. Morton Alperin
Flight Dynamics Research Corporation
15809 Stagg St.
Van Nuys, California 91406
213-988-8000

Dr. M.A. Badri Narayanan
Department of Aeronautical Engineering
Indian Institute of Science
Bangalore 560012 INDIA
(local #) 513-878-6773

Dr. Luis P. Bernal
Jet Propulsion Laboratory (MC-67/201)
4800 Oak Grove Drive
Pasadena, California 91103
213-354-7449

Dr. Paul Bevilaqua
Rockwell International Corporation
4300 E. Fifth Avenue
Columbus, Ohio 43216
614-239-3242

Dr. Louis Boehman
University of Dayton Research Institute, KL121E
300 College Park
Dayton, Ohio   45469
229-2835

Dr. R.J. Boray
AFWAL/PORT
Wright-Patterson Air Force Base
Dayton, Ohio   45433
513-255-7119

Dr. Richard P. Braden
1875 Campus Drive
Fairborn, Ohio   45406
513-229-3845

Mr. William T. Carter
Systems Research Labs
1905 Woods Drive
Dayton, Ohio   45432
513-426-4051

Dr. George Catalano
Department of Mechanical Engineering
Louisiana State University
Baton Rouge, Louisiana   70803
504-388-5792

Mr. Y.T. Chin
Lockheed California Corporation
P.O. Box 551
Burbank, California   91520
213-847-5608

Mr. Rodney L. Clark
AFWAL/FIMM
Wright-Patterson Air Force Base
Dayton, Ohio   45433
513-255-3788

Mr. Cecil Cline
Rockwell International Corporation
4300 E. Fifth Avenue.
Columbus, Ohio   43216
614-239-3274

Mr. C.P. Combs
Rockwell International Corporation, NAAD
4300 E. Fifth Avenue.
Columbus, Ohio   43216
614-239-2174

Maj. Michael Dauth
Hq, AFSC/XRLA
Andrews Air Force Base, MD.   20334
301-981-5646

Mr. John H. DeHart
Rockwell International Corporation
4300 E. Fifth Avenue.
Columbus, Ohio   43216
614-239-2342

Mr. Carl Dienstberger
AFWAL/POTA
Wright-Patterson Air Force Base
Dayton, Ohio   45433
513-255-4830

Dr. Darshan Dosanjh
University of Syracuse
Dept. of Mechanical and Aerospace Engineering
Syracuse, New York   13210
315-423-2618

Dr. J. Craig Dutton
Mechanical Engineering Dept.
Texas A&M University
College Station, Texas   77843
713-845-5011

Dr. J. Fabri
Office National d'Etudes
  et de Recherches Aeronautique
92320 Chatillons/Bagneux
Paris, FRANCE

Dr. Joseph Foa
School of Engineering and Applied Science
George Washington University
Washington, D.C.   20052
202-676-6149

Dr. William Foley
General Dynamics Corporation
P.O. Box 748
Fort Worth, Texas   76101
817-732-4418

Dr. Milton Franke
Air Force Institute of Technology
AFIT/ENY
Wright-Patterson Air Force Base
Dayton, Ohio   45433
513-255-2362

Mr. Douglas Garland
DeHavilland Aircraft of Canada, Ltd.
Garratt Blvd.
Downsview, Ontario, CANADA   M3K1Y5
416-633-7310

Mr. Charles A. Garris
Dept. CMEE
George Washington University
Washington, D.C.   20052
202-676-3646

Mr. Kenneth Green
Code 6052
Naval Air Development Center
Warminster, Pennyslvania   18974
215-441-2125

Mr. Siegfried Hasinger
AFWAL/FIMM
Wright-Patterson Air Force Base
Dayton, Ohio   45433
513-255-4052

Mr. Franz J.A. Huber
2725 Big Woods Trail
Fairborn, Ohio   45321
513-426-2498

Mr. Richard Johnson
ASD/ENFTA
Wright-Patterson Air Force Base
Dayton, Ohio   45433
513-255-5503

Dr. K. Karamcheti
Joint Institute for Aeronautics and Acoustics
Department of Aeronautics and Astronautics
Stanford University
Stanford, California   94305
415-497-9489

Maj. Lowell Keel
Chief, Airframe and Aerodynamics Branch
AFWAL/FIMM, Bldg. 450
Wright-Patterson Air Force Base
Dayton, Ohio   45433
513-255-4579

Dr. David Koenig
M/S 247-1
NASA Ames Research Center
Moffett Field, California   94035
415-965-5047

Mr. Mike Konarski
General Electric Co. E198
Evendale, Ohio
513-243-4881

Dr. A. Krothapalli
Department of Aeronautics and Astronautics
Stanford University
Stanford, California   94305
415-497-9489

Mr. Al Laughrey
AFWAL/FIMM, Bldg. 450
Wright-Patterson Air Force Base
Dayton, Ohio   45433
513-255-6207

Mr. Maurice Lawson
University of Dayton Research Institute
KL-473
300 College Park
Dayton, Ohio   45469
513-229-3845

Dr. John Lee
Ohio State University
Aero Astro Research Labs
2300 West Case Road
Columbus, Ohio   43220
614-422-1241

Mr. Bernard Lindenbaum
4929 Thorain Ct.
Dayton, Ohio   45416
513-275-6723

Dr. John Loth
Department of Aerospace Engineering
West Virginia University
Morgantown, West Virginia  26506
304-293-4111

Dr. N. Malmuth
Rockwell International
Science Center
P.O. Box 1085
Thousand Oaks, California  91360
805-498-4545, ext. 154

Dr. John E. Minardi
University of Dayton Research Institute
KL-473
300 College Park
Dayton, Ohio  45469
513-229-3845

Dr. K. S. Nagaraja
Air Force Wright Aeronautical Laboratories
AFWAL/FIMM, Bldg. 450
Wright-Patterson Air Force Base
Dayton, Ohio  45433
513-255-6207

Mr. Ronald K. Newman
University of Dayton Research Institute
KL-473
300 College Park
Dayton, Ohio  45469

Dr. Gordon Oates
University of Washington
Dept. of Aeronautics and Astronautics
Seattle, Washington  98195
206-543-6061

Mr. Ronald Petsch
General Electric
Mail Drop E198
Evendale, Ohio
513-243-5168

Dr. James Petty
AFWAL/POTC, Bldg. 18
Wright-Patterson Air Force Base
Dayton, Ohio  45433
513-255-5308, 255-2744

Dr. Max Platzer
Aerospace Engineering Department
Naval Post Graudate School
Monterey, California
408-646-2311

Capt. Steven G. Reznick
AFWAL/FIMM
Wright-Patterson Air Force Base
Dayton, Ohio   45433
513-255-4052

Dr. Virender Sarohia
Jet Propulsion Laboratory
California Institute of Technology
4800 Oak Drive
Pasadena, California   91103
213-354-6758

Mr. E.F. Schum
Rockwell International Corporation
Building 6/Engineering
4300 E. Fifth Avenue.
Columbus, Ohio   43216
614-239-3242

Dr. James Scott
University of Dayton Research Institute
KL-473
300 College Park
Dayton, Ohio
513-229-3845

Dr. William Sears
6560 Skyway Road
Tucson, Arizona   85718
602-626-1315

Mr. George L. Seibert
AFWAL/FIMM
Wright-Patterson Air Force Base
Dayton, Ohio   45433
513-255-6207

Mr. Vajaya Shankar
Rockwell International
Science Center
P.O. Box 1085
Thousand Oaks, California   91360
805-498-4545, ext. 154

Mr. S. J. Smrdel
Rockwell International Corporation
4300 E. Fifth Avenue.
Columbus, Ohio   43216
614-239-2174

Dr. Frank D. Stull
Wright Aeronautical Laboratories
AFWAL/PORT, Bldg. 18
Wright-Patterson Air Force Base
Dayton, Ohio   45433
513-255-5210

Mr. Edward B. Thayer
Mail Location R-132
P.O. Box 2891
West Palm Beach, Florida
305-840-6654

Mr. Gregory Unnever
AFIT/EN
Wright-Patterson Air Force Base
Dayton, Ohio   45433
513-255-5533

Dr. Hans von Ohain
5598 Folkestone Drive
Dayton, Ohio   45459
513-434-1120

Dr. Hermann Viets
Wright State University
7751 Col. Glenn Hwy.
Dayton, Ohio   45431
513-873-2501

Dr. James Wilson
Directorate of Aerospace Sciences
AFOSR/NA, Bldg. 410
Bolling Air Force Base
Washington, D.C.   20332
202-767-4935

Dr. Sam Wilson III
NASA Ames Research Center
MS 237-11
Moffett Field, California   94035
415-965-5903

Mr. Chung-Jin Woan
Rockwell International Corporation
4300 E. Fifth Avenue.
Columbus, Ohio   43216
614-239-2342

Dr. Henry Woolard
AFWAL/FIGC, Bldg. 45
Wright-Patterson Air Force Base
Dayton, Ohio   45433
513-255-4315

Dr. T. Yang
Mechanical Engineering Department
315 Riggs Hall
Clemson University
Clemson, South Carolina   29631
803-656-3470, 3471

APPENDIX C

SESSION PAPERS

# AN OVERVIEW OF EJECTOR TECHNOLOGY DEVELOPMENT
## IN THE AIR FORCE

K. S. Nagaraja
Air Force Wright Aeronautical Laboratories
Wright Patterson Air Force Base, Dayton, Ohio

In the last two decades, Air Force has made significant contributions to the development of the ejector technology for thrust augmentation purposes. Initially, Aerospace Research Laboratories at WPAFB undertook a major task of demonstrating that compact, thrust augmenting ejectors could be designed. After ARL successfully demonstrated that by utilizing hypermixing nozzles, thrust augmentation ratio of the order of two could be achieved, Flight Dynamics Laboratory launched a program of conducting preliminary design of an ejector thrust augmented demonstrator aircraft. FDL accomplished the objective of doing a design study. However, no demonstration fabrication was performed. Subsequently, over the years in seventies, FDL continued to support some efforts in the technology area. In the following, a brief outline of those developments will be presented.

An outline of what is going to be discussed is briefly presented in Figure(1). As can be seen in Figure(2), ARL's work laid the foundation for a systematic study of the ejector application for V/STOL aircraft.

By utilizing hypermixing nozzles, ARL achieved an augmentation ratio of 2 in an ejector of inlet area ratio of 23. In these tests, primary air was not heated, and the stagnation pressure of the primary air was about 1.3. Further, a trailing edge ejector wing was also built by Bell Aerospace for ARL, and supercirculation effects were shown in low speed. As the forward velocity increased, the ram drag penalty degraded the performance of the ejector. Further, Vought corporation under ARL contract designed a more compact ejector by using trapped vortex cavity than what ARL had done with the same inlet area ratio ejector and achieved slightly improved thrust augmentation ratio.

# INTRODUCTION

- BRIEF HISTORY
    - ARL AND AFFDL STUDIES

- RECENT AIR FORCE RESULTS
    - HIGH SPEED EJECTORS
    - HIGH PERFORMANCE EJECTORS
        - SECOND SOLUTION DEMONSTRATION
    - EJECTOR INDUCED LIFT AUGMENTATION
    - FUNDAMENTAL TURBULENT MIXING AND
        ENTRAINMENT STUDIES
    - OBSERVATIONS
    - SUMMARY

Figure 1

## ARL'S INVESTIGATIONS IN THE SIXTIES ACCOMPLISHED THE FOLLOWING:

1. DEVELOPMENT OF HYPERMIXING NOZZLES FOR MIXING ENHANCEMENT FOR COMPACT EJECTOR DESIGNS.

2. THRUST AUGMENTATION OF THE ORDER OF 2 IN AN EJECTOR OF INLET AREA RATIO 23.

3. MULTI CHANNEL EJECTORS UTILIZING FAN BY-PASS AIR ALSO TESTED. THRUST AUGMENTATION WAS REALIZED.

4. BELL AEROSPACE UNDER ARL CONTRACT TESTED A T.E. EJECTOR WING AND DEMONSTRATED TRANSITIONING CAPABILITY DUE TO SUPERCIRCULATION EFFECTS.

5. FURTHER COMPACTNESS WAS REALIZED BY USING A TRAPPED VORTEX CAVITY FOR BOUNDARY LAYER ENERGIZATION.

Figure 2

In the early seventies, FDL began work on integrating an ejector in a demonstrator vehicle design. In the course of this effort, an analytical method was developed for predicting the ejector performance characteristics. The method was based on one-dimensional compressible flows, and the losses were incorporated in the analysis by correlation with ARL experimental data. The results showed the effects of primary gas temperature as well as forward flight condition. A schematic of the ejector for the analysis purposes is shown in Figure(3). In the analysis, it was assumed that the mixed flow at station (2) was subsonic, although it was shown that supersonic mixed flows could be realized. It is the latter possibility that has spurred renewed interest presently in the ejector technology development.

Figure (4) shows an outline of what was accomplished in FDL. Figures (5), (6), and (7) show some of the salient results of the analysis. It can be noticed that even in an ideal situation, the results interestingly showed that as the primary gas gets hotter, the thrust augmentation ratio $\phi$ decreases. Also, as the forward flight velocity increases $\phi$ decreases up to a point, and begins to go up around Mach number one. However, this particular aspect was not investigated further when FDL's analytical work was accomplished in 1973. References 1 and 2 can be seen for further details of these efforts both at ARL and FDL. Figure(7) shows that the design of the inlet plays an important role in gaining the full benefit of an ejector. The ejector performance can be very sensitive to the inlet efficiency.

It was realized in the course of an examination of the results that in an efficient ejector design, geometric as well as thermodynamic parameters have to be properly selected. Figure (8) which was derived from incompressible flow equations illustrated the significance of the coupling effects of the parameters on the performance. It was then decided to embark on a systematic study of the ejector performance characteristics with no restriction that the mixed flow would have to be subsonic as was done in Reference 2.

114

# EJECTOR DIAGRAM

PRIMARY
AIR
CHAMBER

SECONDARY FLOW

$T_{OP}$
$P_{OP}$

PRIMARY AIR

ATMOSPHERE

MIXING DUCT

STATION 1
(INJECTION PLANE)

STATION 2
(END OF THE MIXING
DUCT OR DIFFUSER
ENTRANCE)

DIFFUSER

STATION 3
(DIFFUSER EXIT)
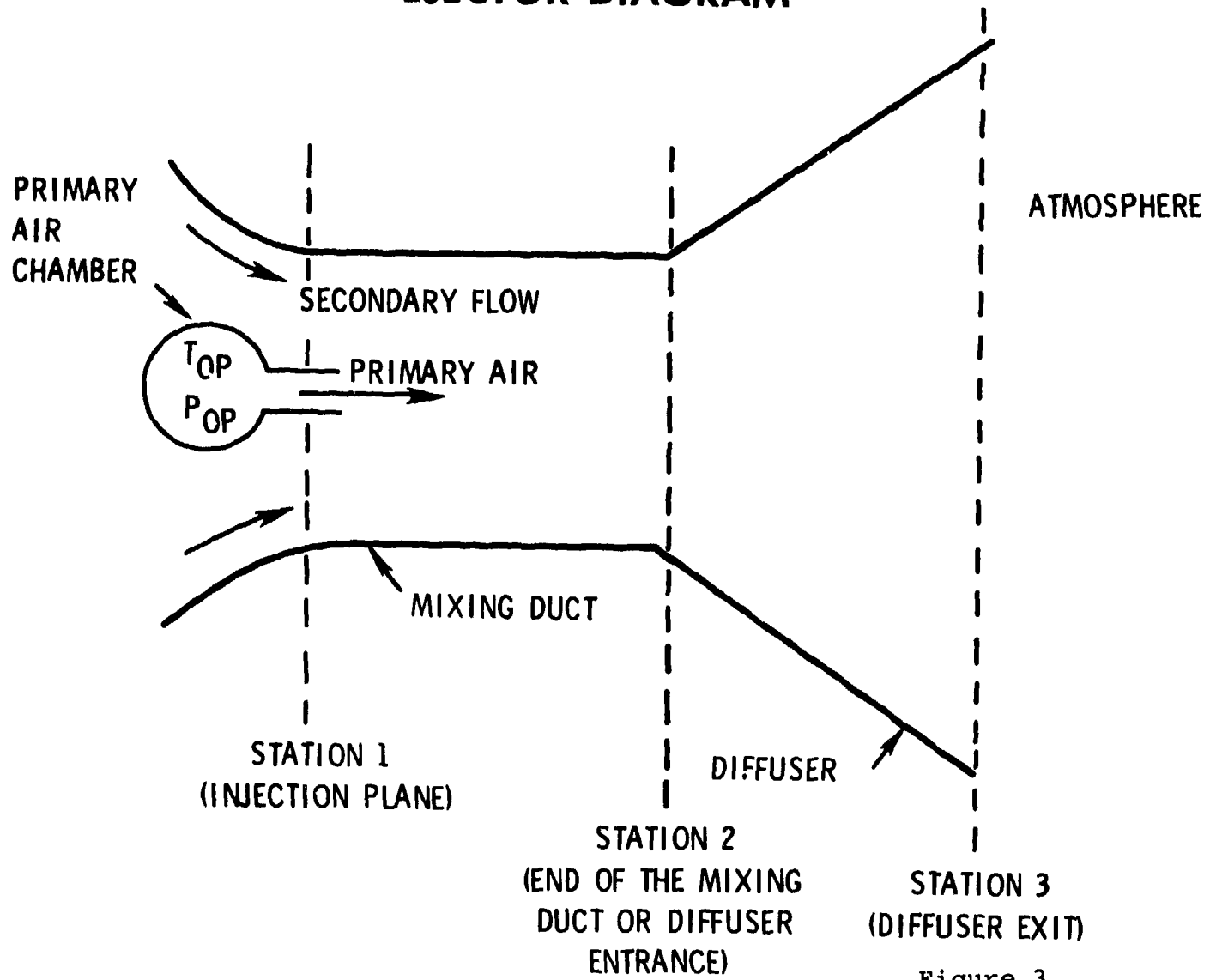
Figure 3

# AIR FORCE FLIGHT DYNAMICS LABORATORY (AFWAL/FI) SUPPORTED A PRELIMARY DESIGN STUDY OF A V/STOL DEMONSTRATOR AIRCRAFT

- AN EJECTOR-WING (2D) MODEL WAS BUILT AND TESTED IN NASA AMES

- COMPRESSIBLE FLOW ANALYSIS WAS DEVELOPED

- AN RPV VEHICLE HAVING A CANARD WING ARRANGEMENT WITH A T.E. EJECTOR WAS DESIGNED

- HIGH LIFT CHARACTERISTICS OF AN EJECTOR-FLAPPED WING WAS THEORETICALLY EVALUATED

- A 3D CALCULATION METHOD FOR DETERMINING THE AERO CHARACTERISTICS OF ARBITRARY EJECTOR JET FLAPPED WINGS WAS DEVELOPED BY McDONNELL DOUGLAS

- TESTS PERFORMED AT AFFDL FACILITY ALSO DEMONSTRATED THAT THE EJECTOR POWERED WING STALL ANGLE WAS LARGER COMPARED TO THE UNAUGMENTED WING

Figure 4

THRUST AUGMENTATION RATIO VS. DIFFUSER AREA RATIO

Figure 5

DISTRIBUTION OF $\phi_N$(MAX) VS. $V_a$

$AR_{SP} = 15.0$

$P_r = 2.5$

$T_{op}$ — $800^\circ R$ (III)

$T_{op}$ — $1400^\circ R$ (II)

$T_{op}$ — $1800^\circ R$ (I)

— — — NO LOSS CASE

——— LOSS CASE

$\phi_N$(MAX) →

$V_a$ (FT/SEC) →

118
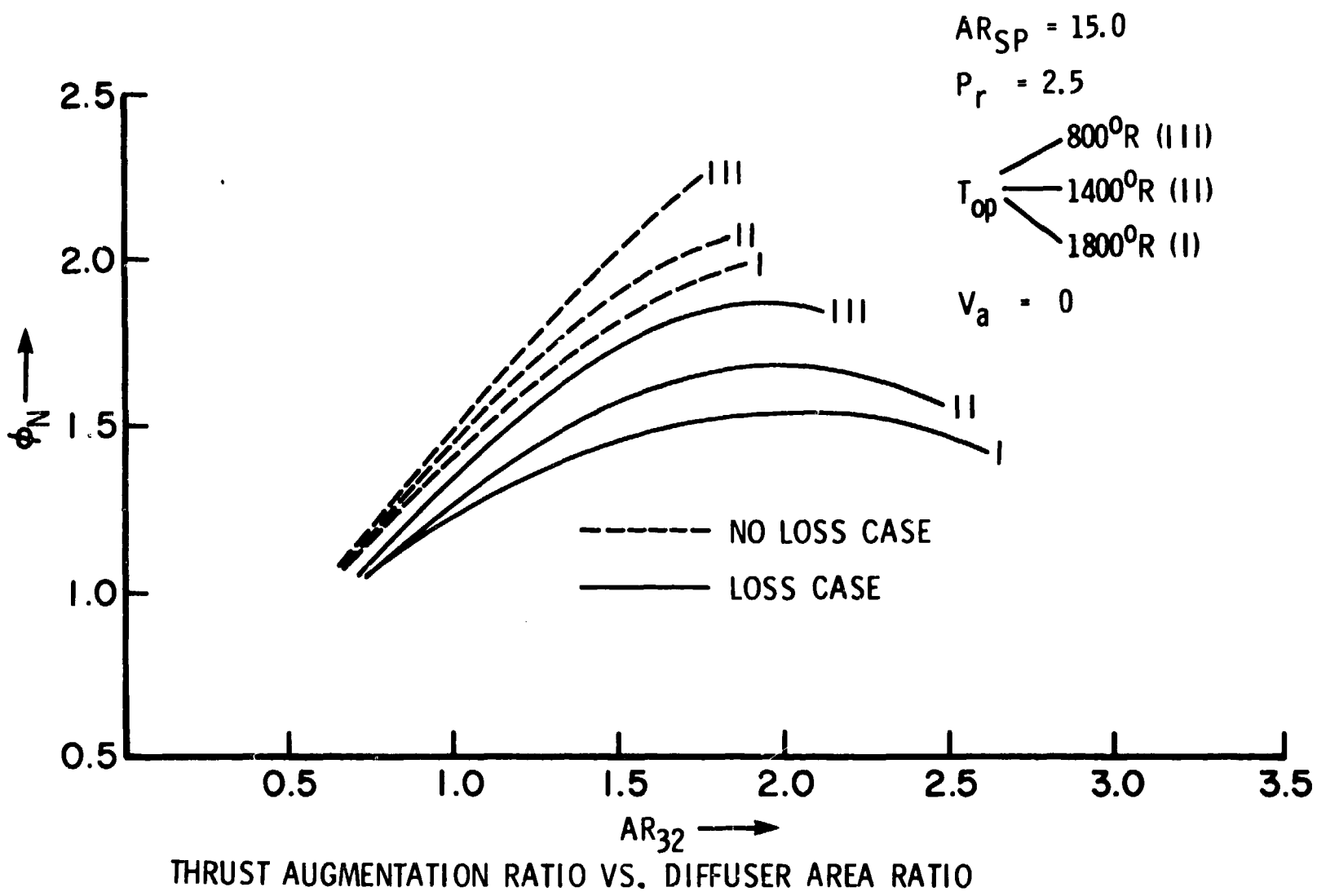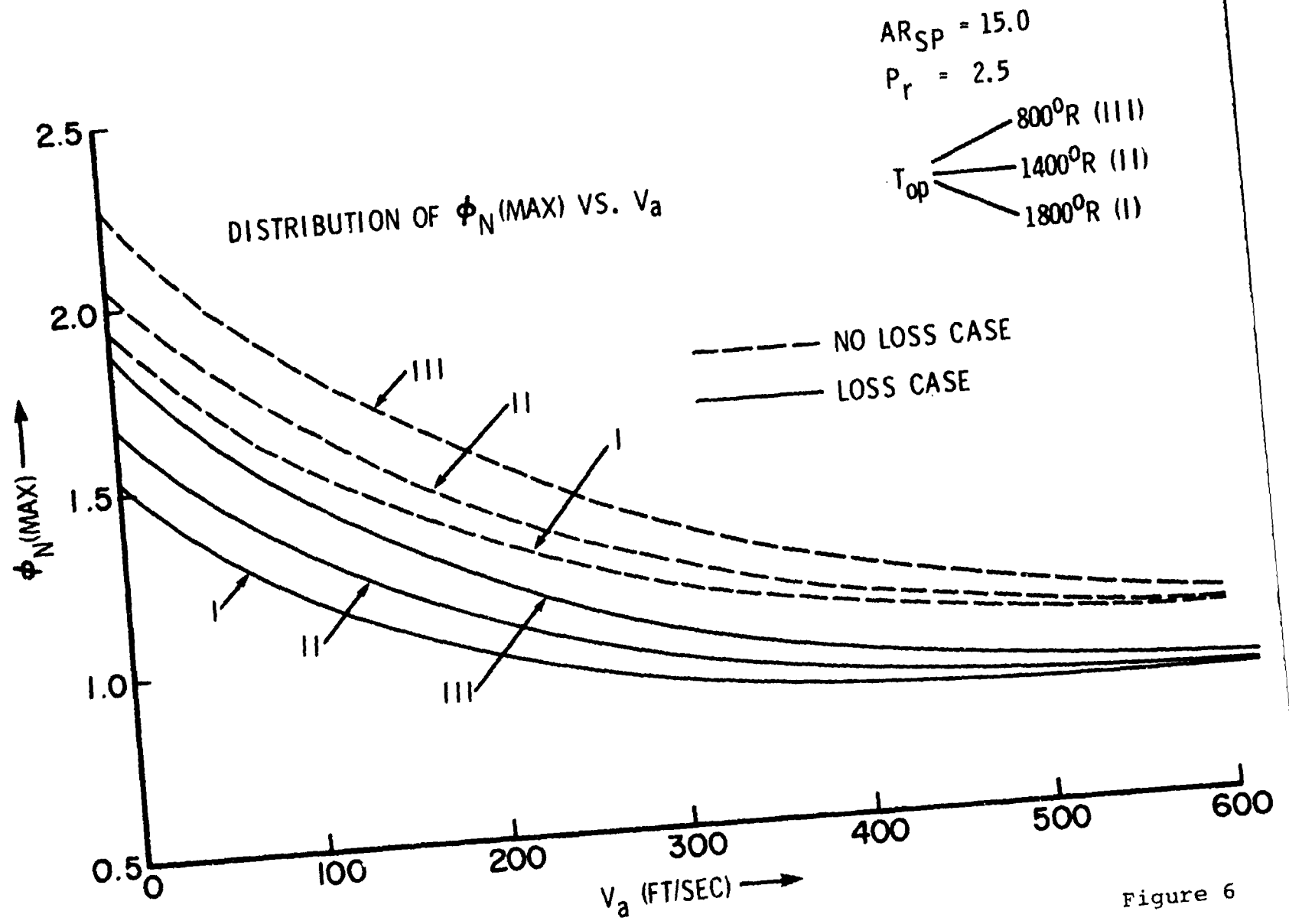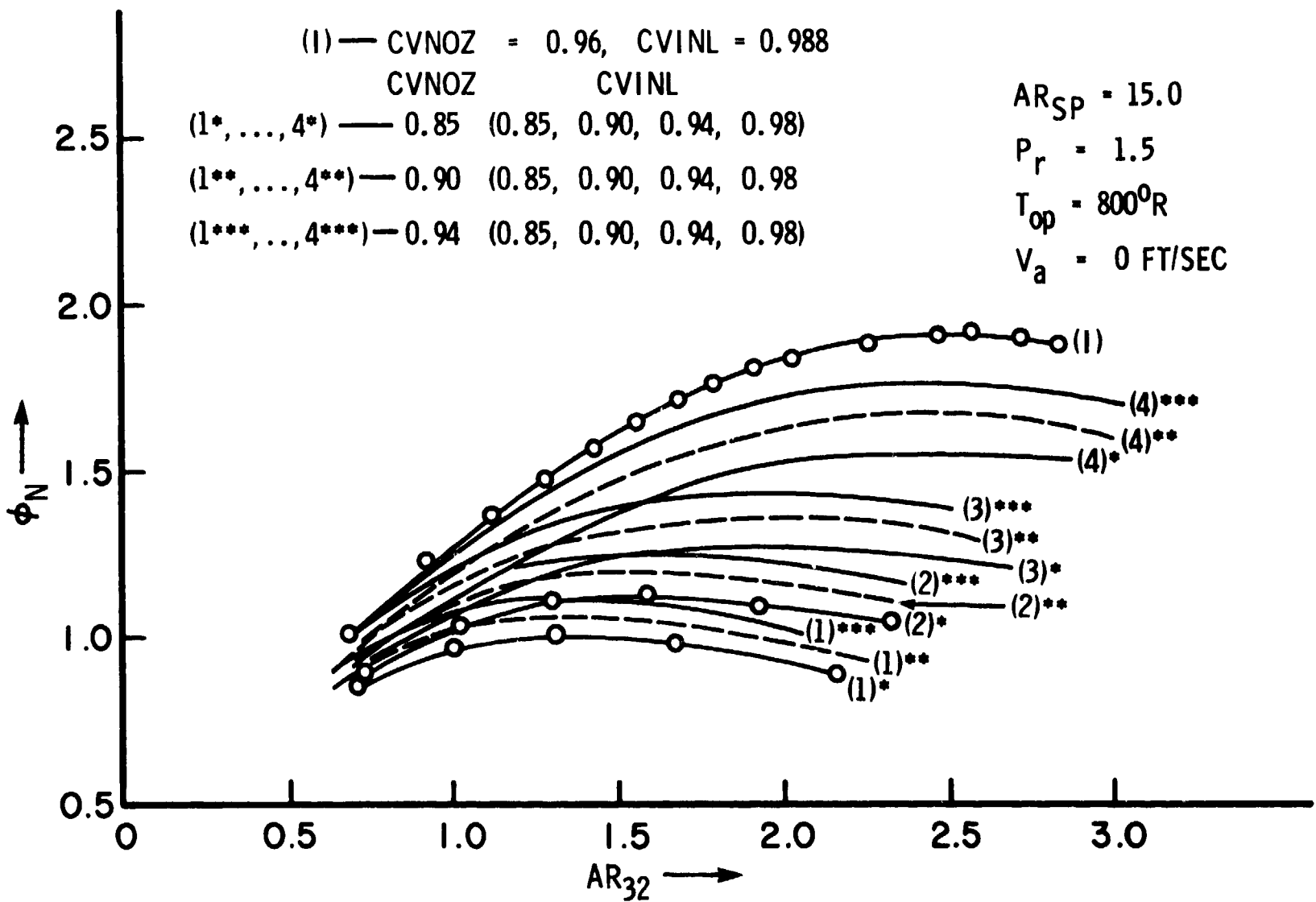
Figure 6

THRUST AUGMENTATION CHARACTERISTICS FOR SEVERAL NOZZLE AND INLET LOSSES

Figure 7

q – DYNAMIC PRESSURE
Δp – INCREMENTAL STAGNATION PRESSURE = $P_{op} - P\infty$
α – INLET AREA RATIO
δ – DIFFUSER AREA RATIO
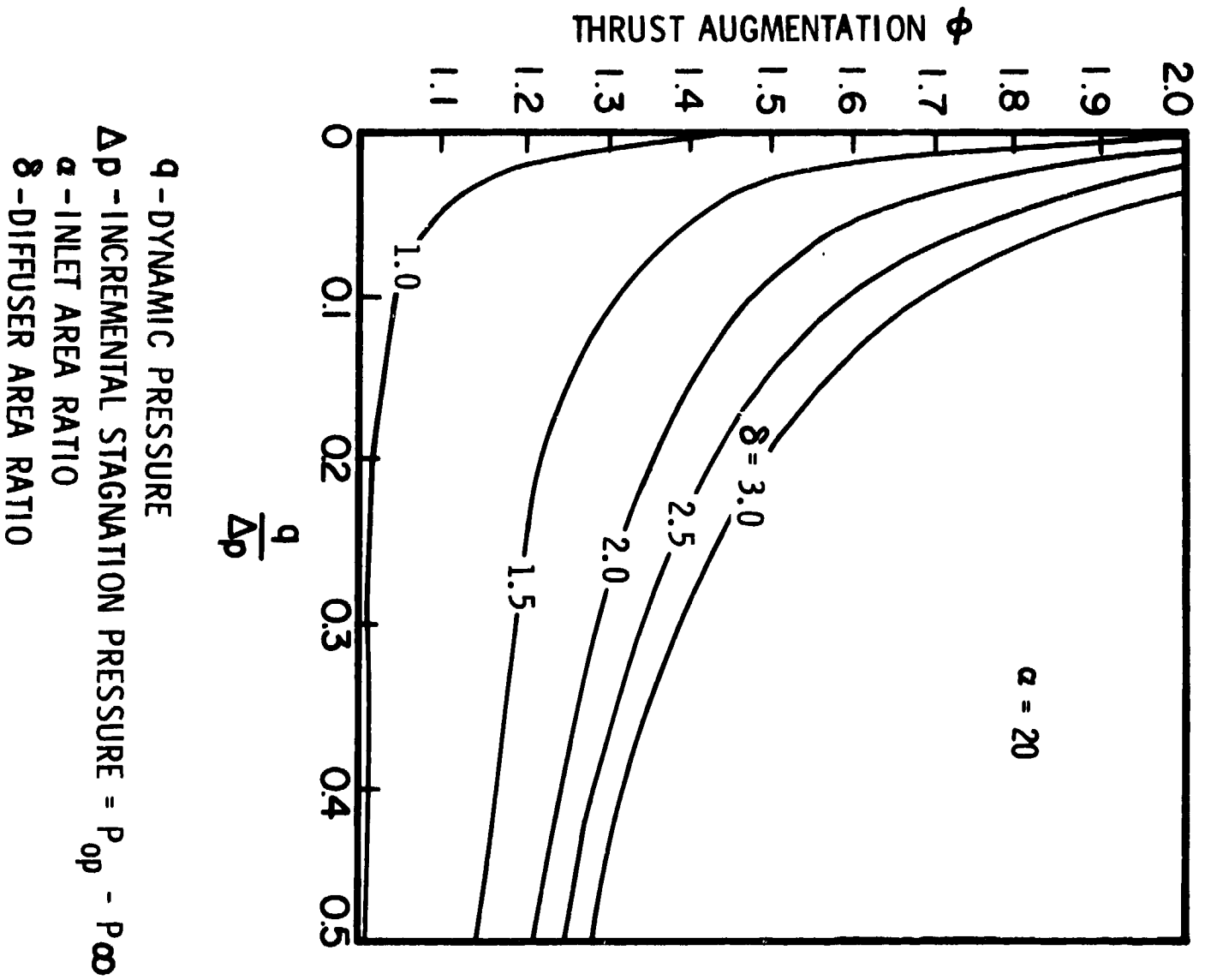
Figure 8

Flight Dynamics Research Corporation under the direction of
Morton Alperin performed these studies (Reference 3) and the
results of that study have greatly stimulated a reevaluation of
the potential that ejectors have for thrust augmentation purposes
in flight (Figure 9). Figures (10) to (14) typically illustrate
the types of performance characteristics that one realizes under
mixed subsonic and supersonic flow conditions. In the latter
flow condition, there can be forbidden zones where the equations
will not yield physically correct results. Outside of those for-
bidden zones, real solutions are possible. It is shown that
whenever the inlet Mach number of the secondary flow is subsonic,
the ejector performance is very high. These were also indepen-
dently verified by the University of Dayton Research Institute
(Ref. 4). Based on the thermodynamic availability, the results
show that the efficiency of an ejector under the second solution
(i.e. mixed flow being supersonic) is much higher at subsonic
inlet Mach numbers (for the secondary flow).

Figures (15) and (16) are drawn so that a map of the perfor-
mance for all possible inlet Mach numbers can be shown for both
branches of the solution. Lines of constant efficiency based on
availability are drawn in the $M_p^*$ - $M_s^*$ plane. The cross-hatched
region (or the egg-shaped regions) are forbidden zones on the
boundary of which the mixed flow Mach number is one. The line
labeled $p_{1p}$ = $p_{1s}$ on the figures refer to inlet pressures being
equal. Plots such as those drawn in the figures are informative
for they show regions where high efficiencies are attainable
under both branches of the solution for mixed flow. They also
indicate where ejector type flows can be realized.

The data plotted in Figures (17) through (20) show that the
second solution with inlet secondary Mach number less than one
can be achieved. These figures are drawn for constant area
ejectors. Figure (19) shows high values of efficiency at the
subsonic inlet Mach numbers of the secondary flow on the second
solution branch. Figure (18) presents the static pressure on the

121

# ANALYSIS OF HIGH SPEED EJECTORS

1. COMPRESSIBLE FLOW ANALYSES

2. LOSSES ARE PRESENTLY NOT INCLUDED

3. SUPERSONIC SOLUTION AT STATION "2" CONSIDERED

4. ENTROPY CHANGE REQUIREMENT USED FOR MAINTAINING
   CORRECTNESS OF THE SOLUTIONS

Figure 9

CONDITION: (RAM-JET)

$M_\infty = 2$; $\Delta P/P_\infty = 0$; $\Delta T/T_\infty = 10$; $\alpha = 20$
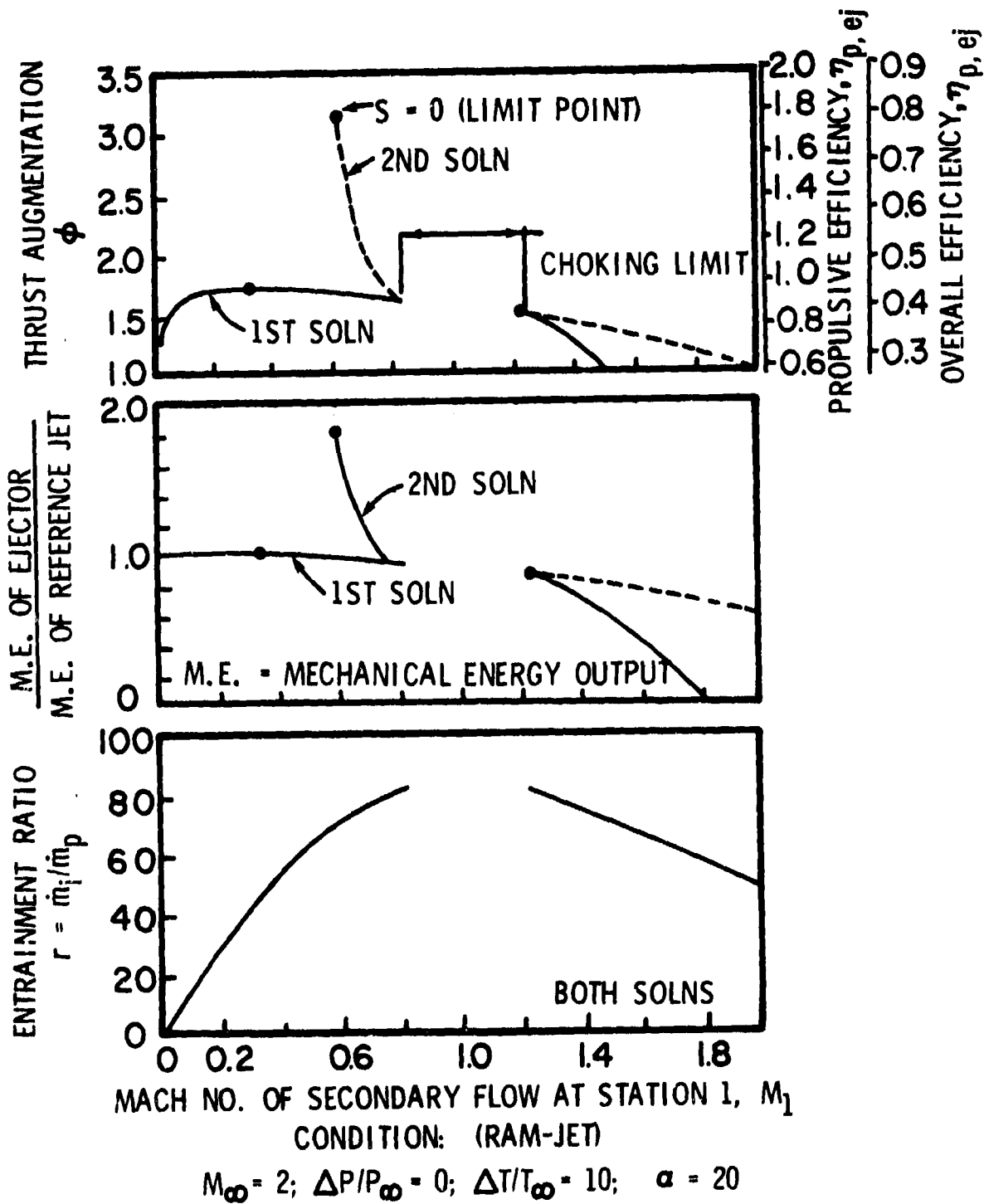
Figure 10

EJECTOR PERFORMANCE CHARACTERISTICS
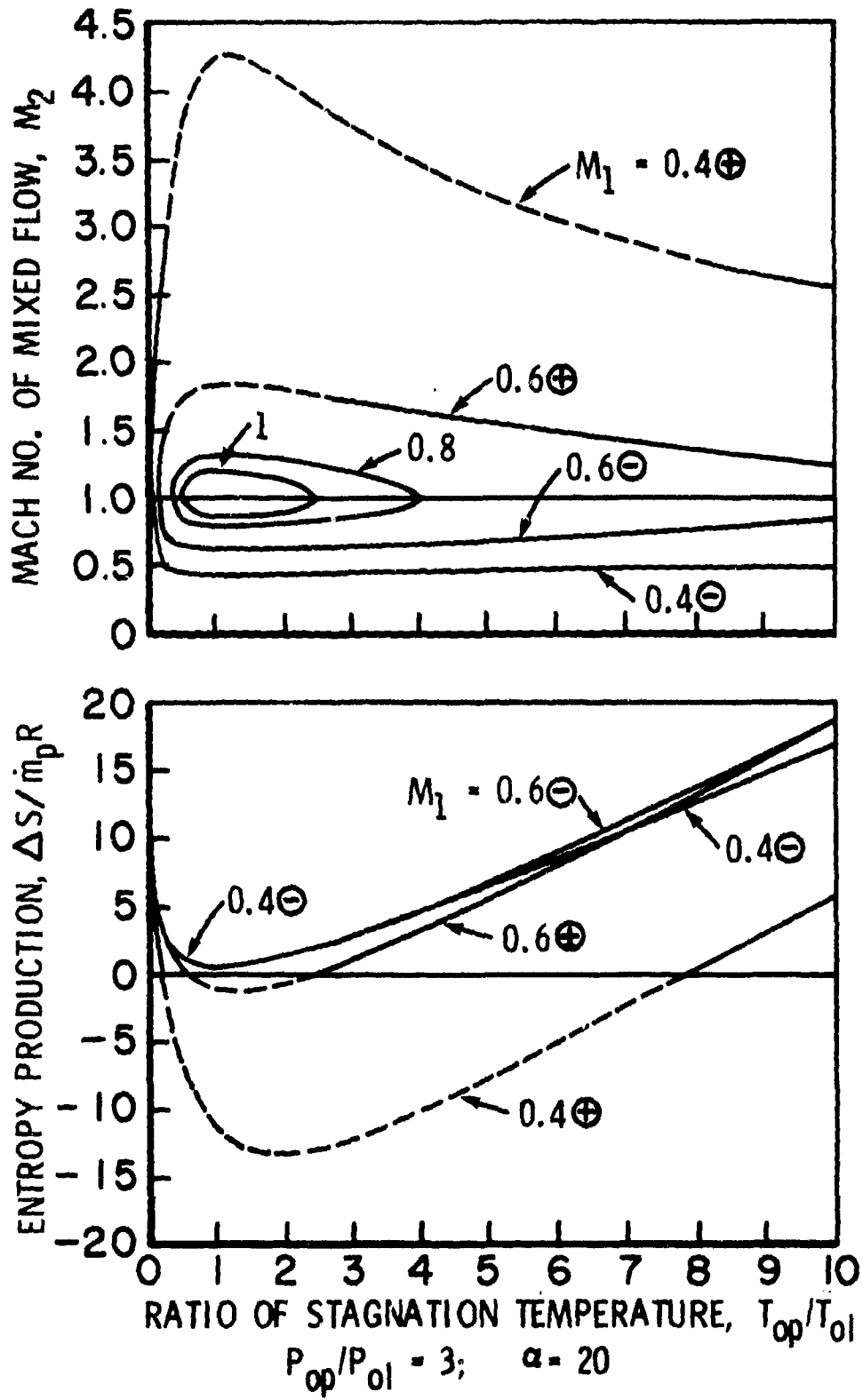


Figure 11

# EJECTOR PERFORMANCE CHARACTERISTIC
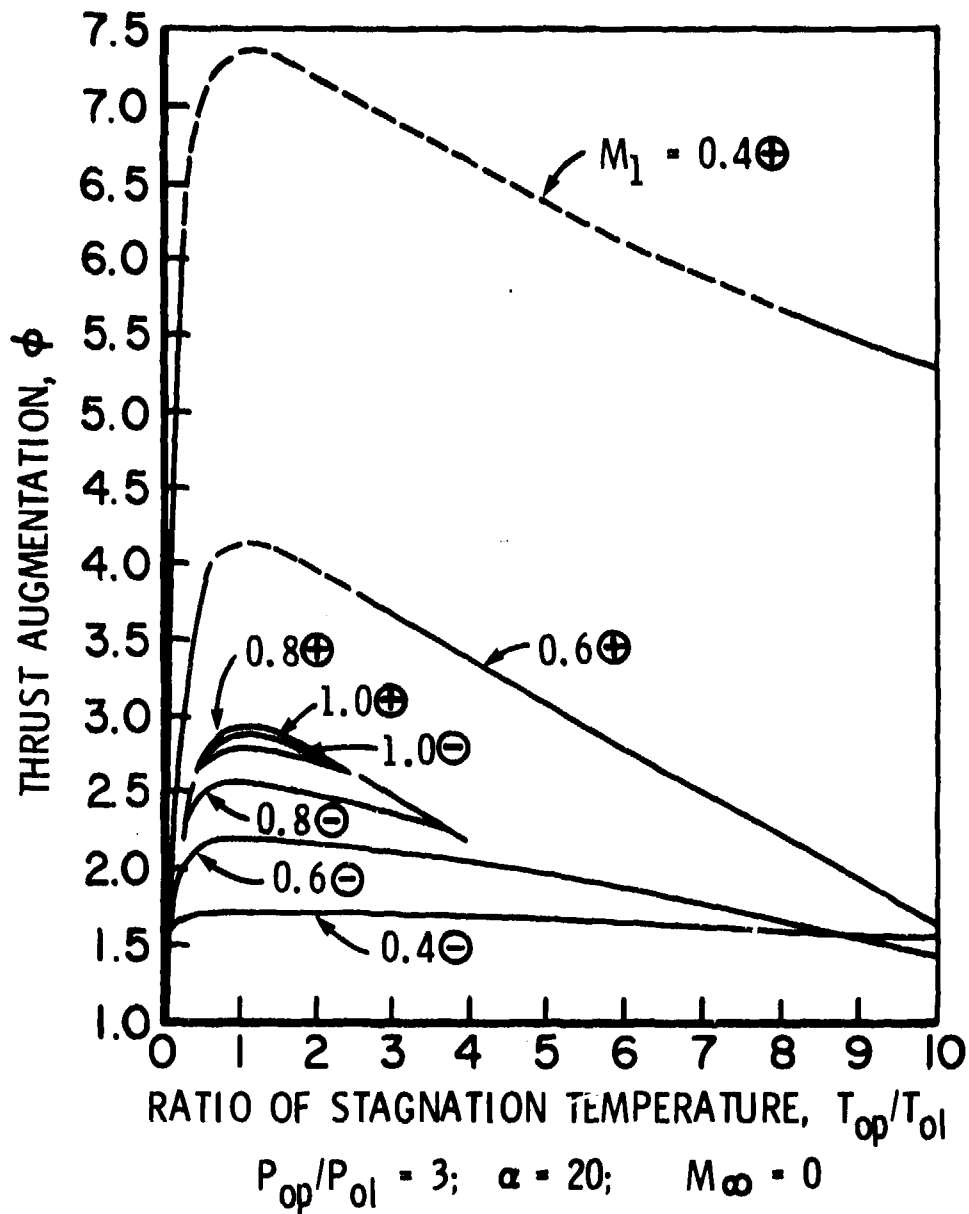


Figure 12

EJECTOR PERFORMANCE CHARACTERISTICS



$P_{op}/P_{ol} = 3; \quad \alpha = 20$
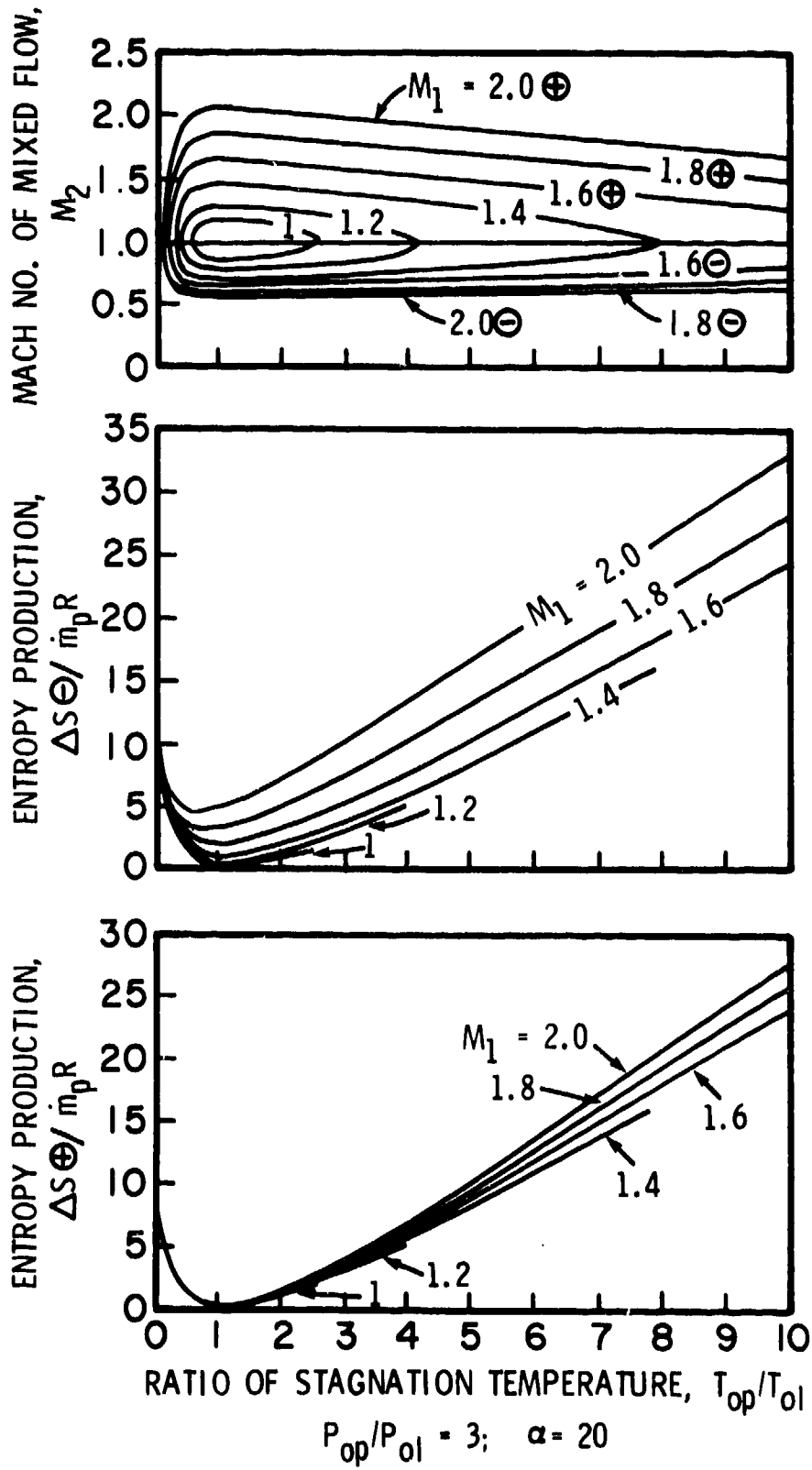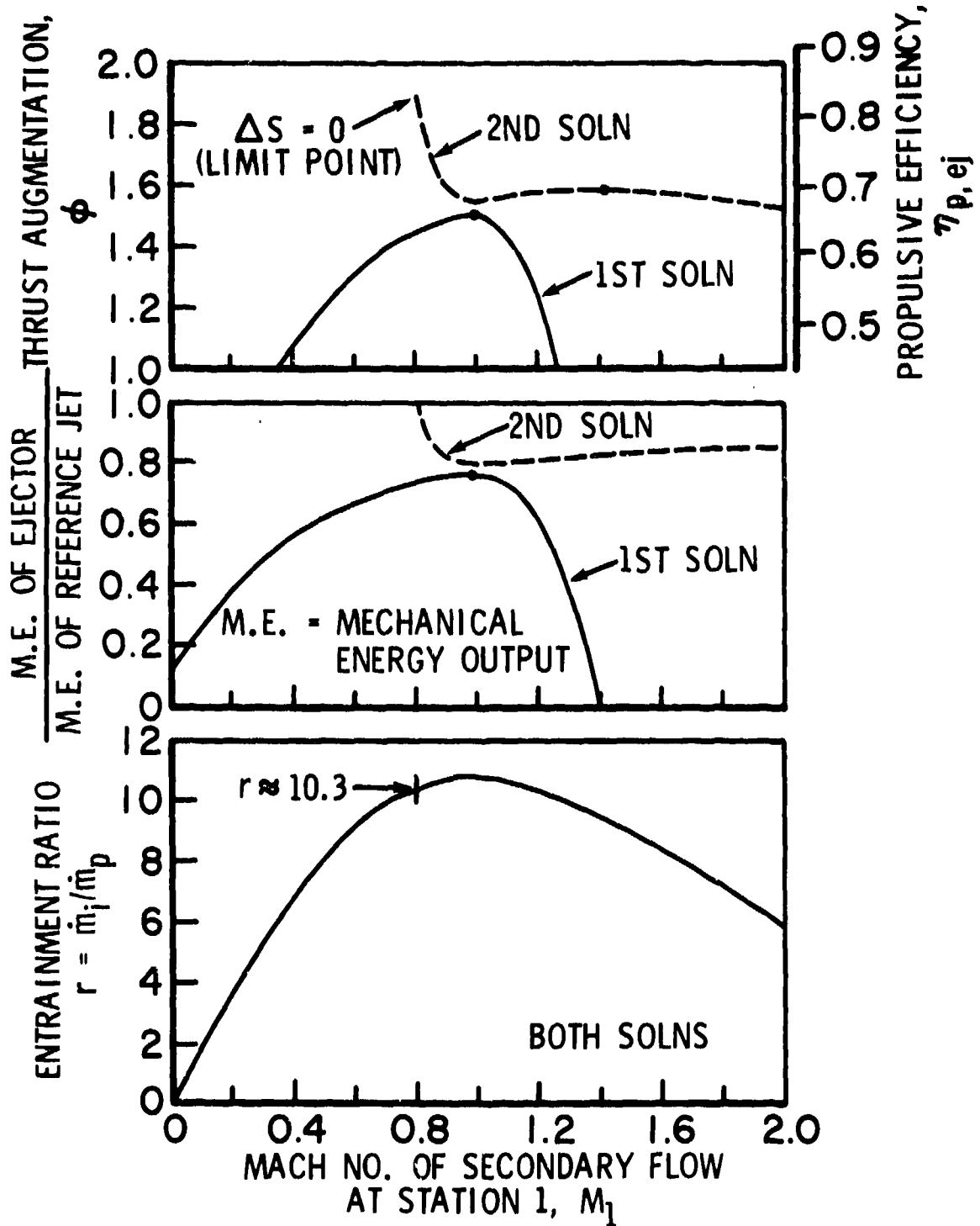
Figure 13

CONDITION: (FAN-JET)

$M_\infty = 0.3$; $\Delta P/p_\infty = 1$; $\alpha_\infty = 20$

Figure 14

SUBSONIC BRANCH EFFICIENCY
MR = 0.10   PR = 6.0   TR = 3.7

Figure 15

128
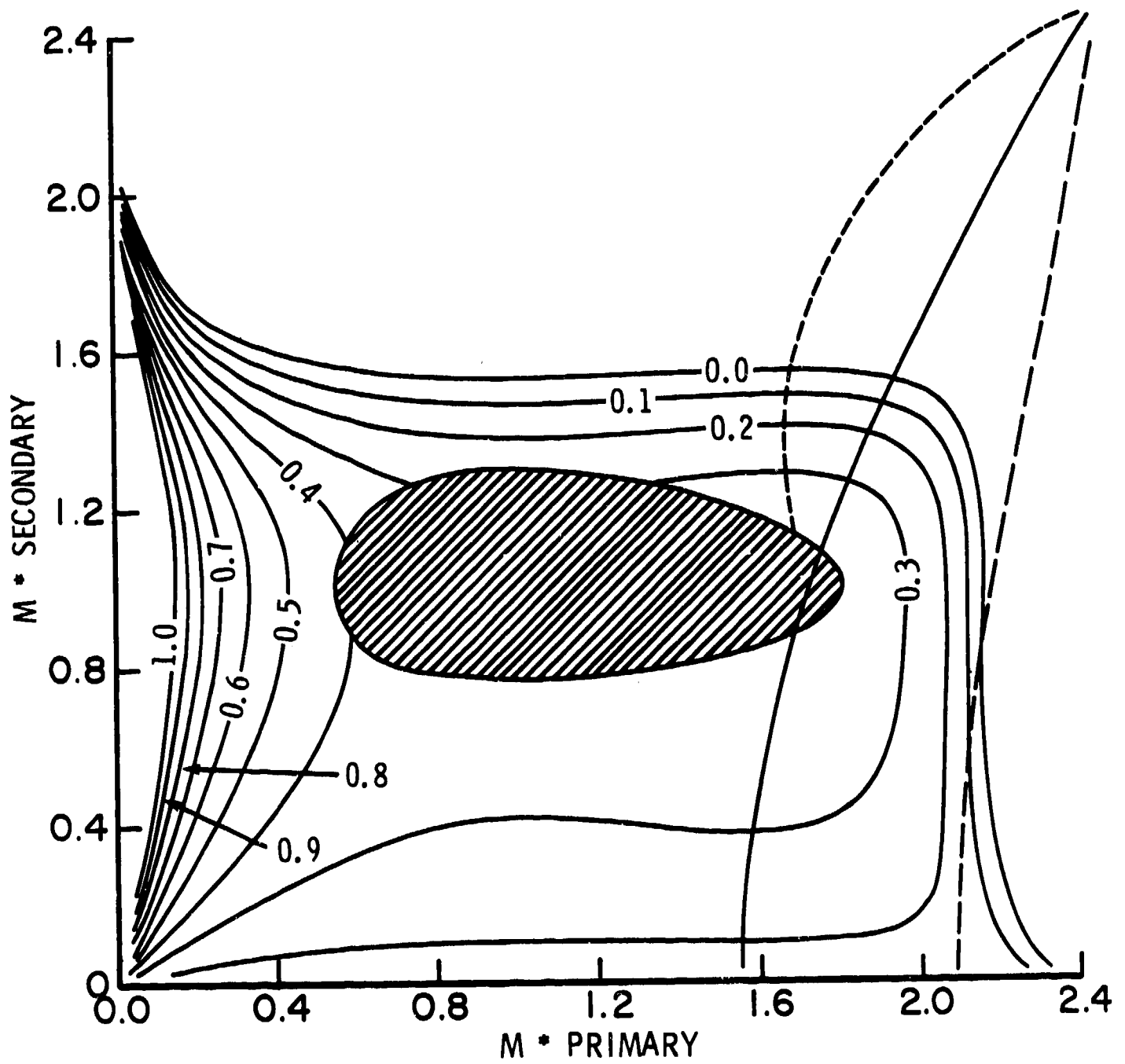
SUPERSONIC BRANCH EFFICIENCY
MR = 0.10    PR = 6.0    TR = 3.7
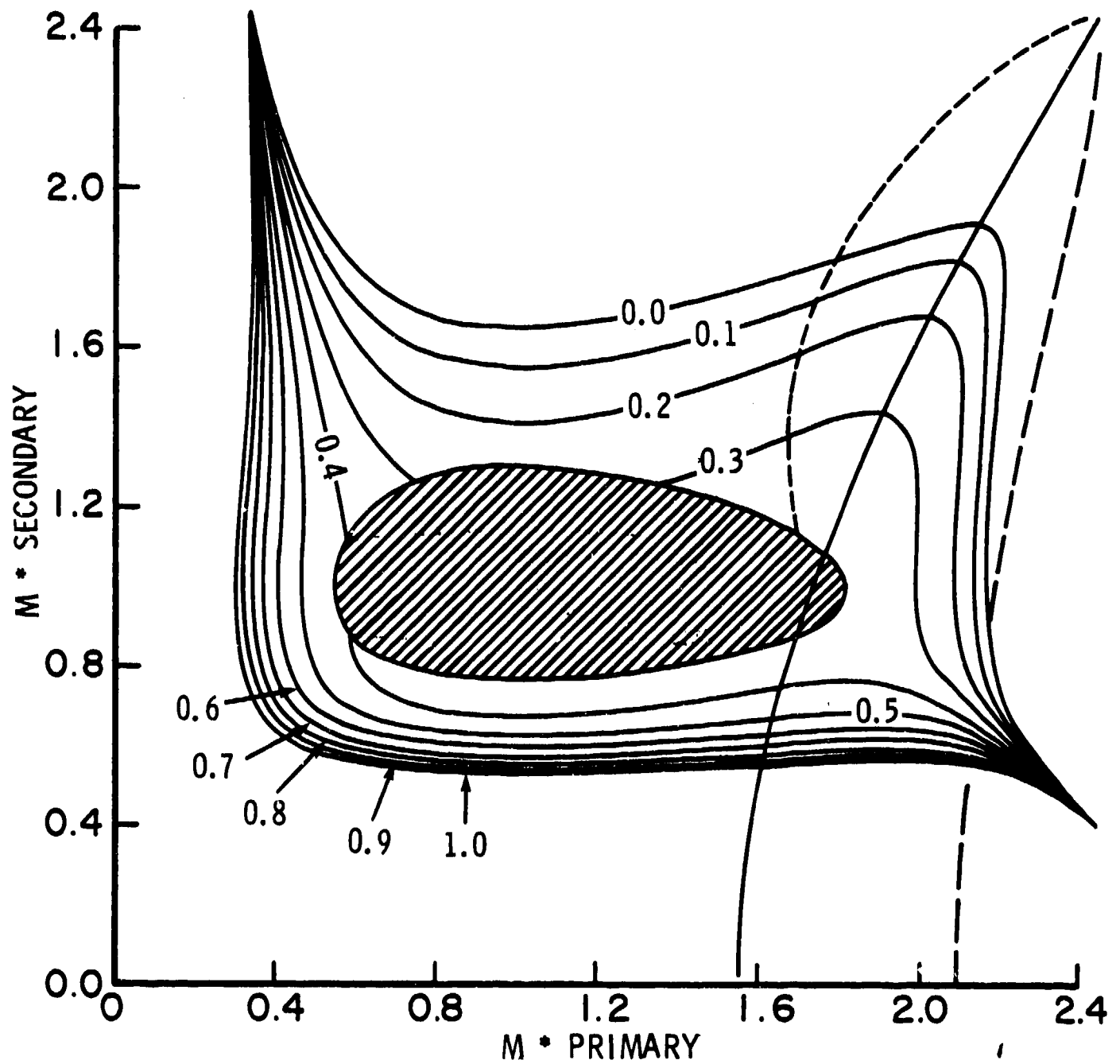
Figure 16
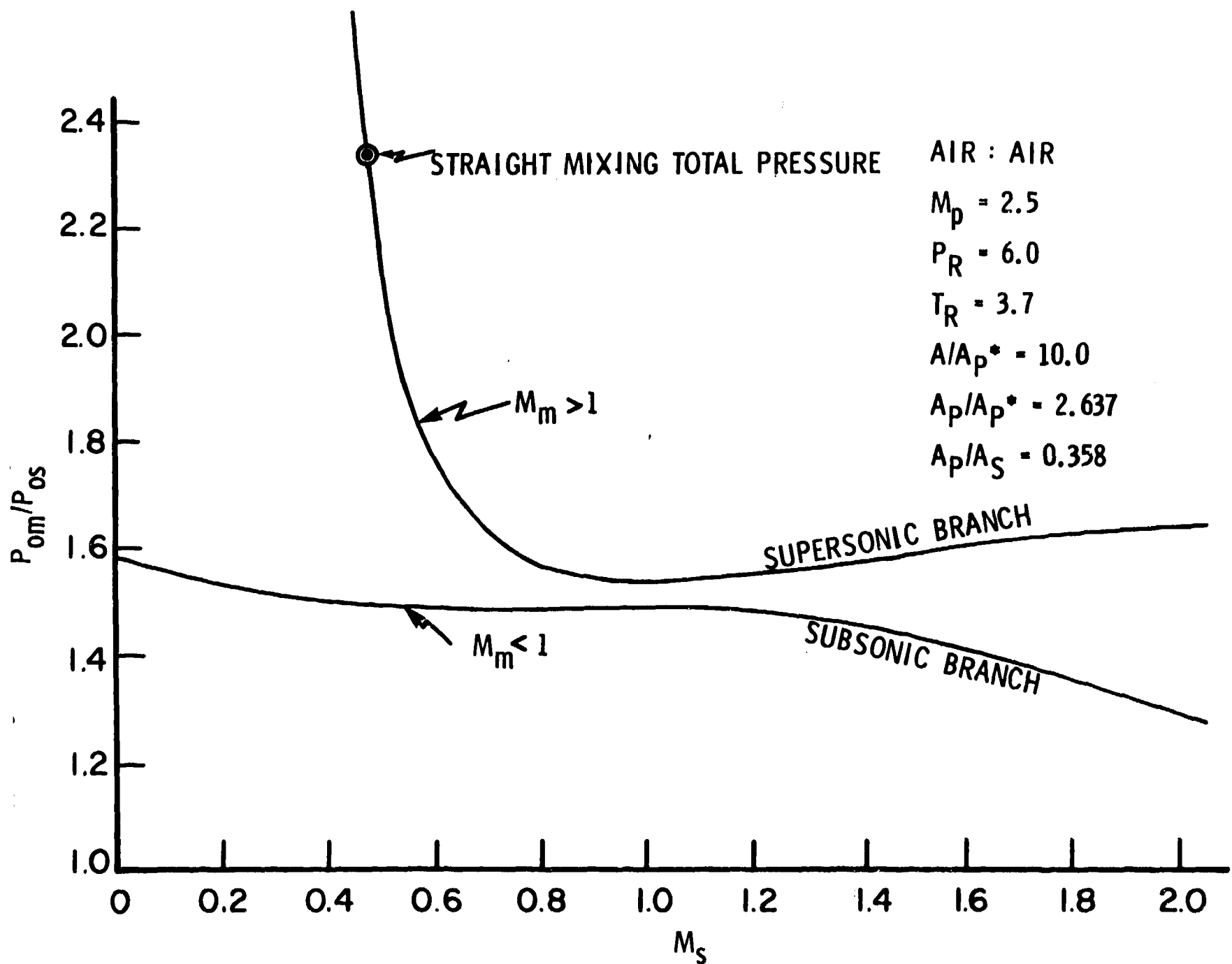
Figure 17.   Mixed Flow Total Pressure Distribution.
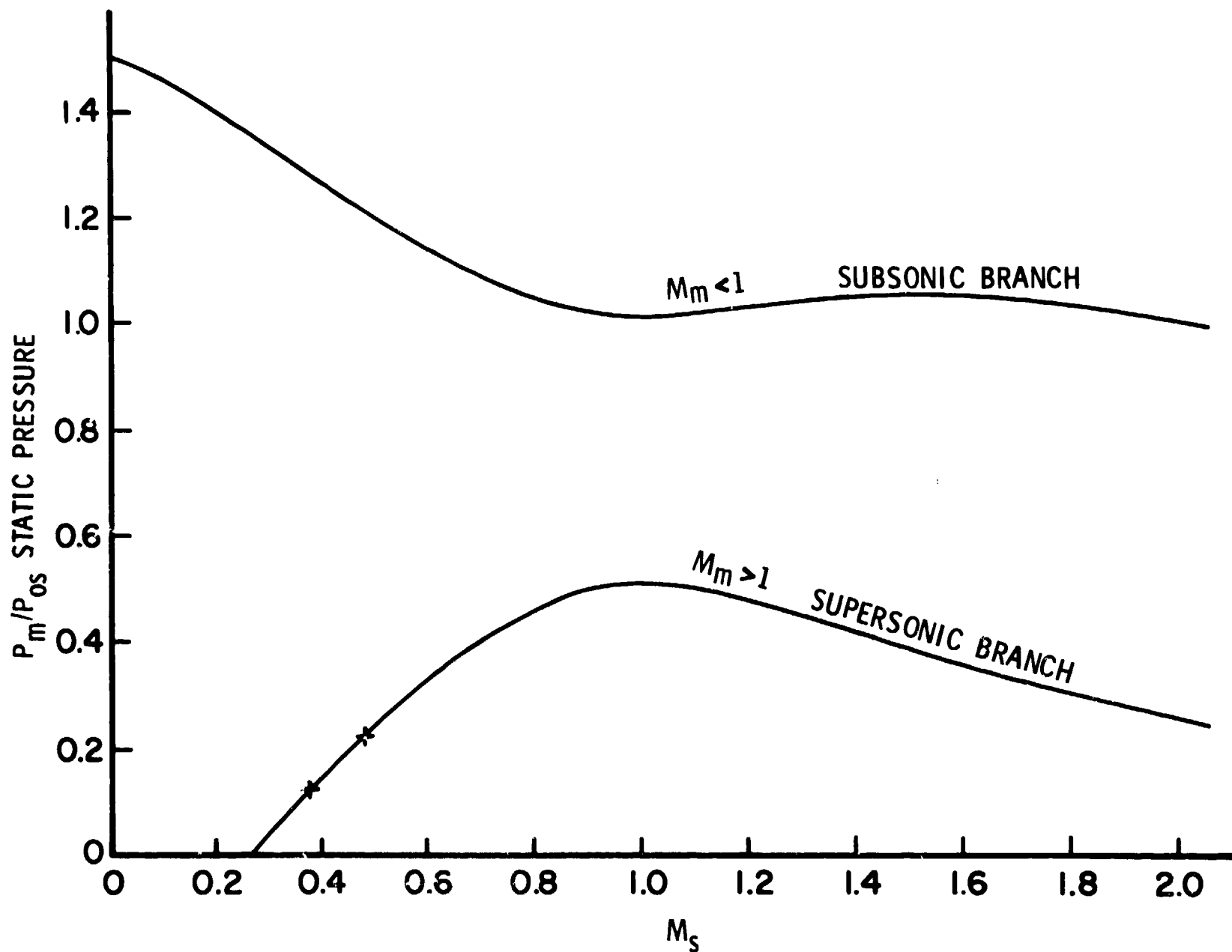
Figure 18. Mixed Flow Static Pressure Distribution.
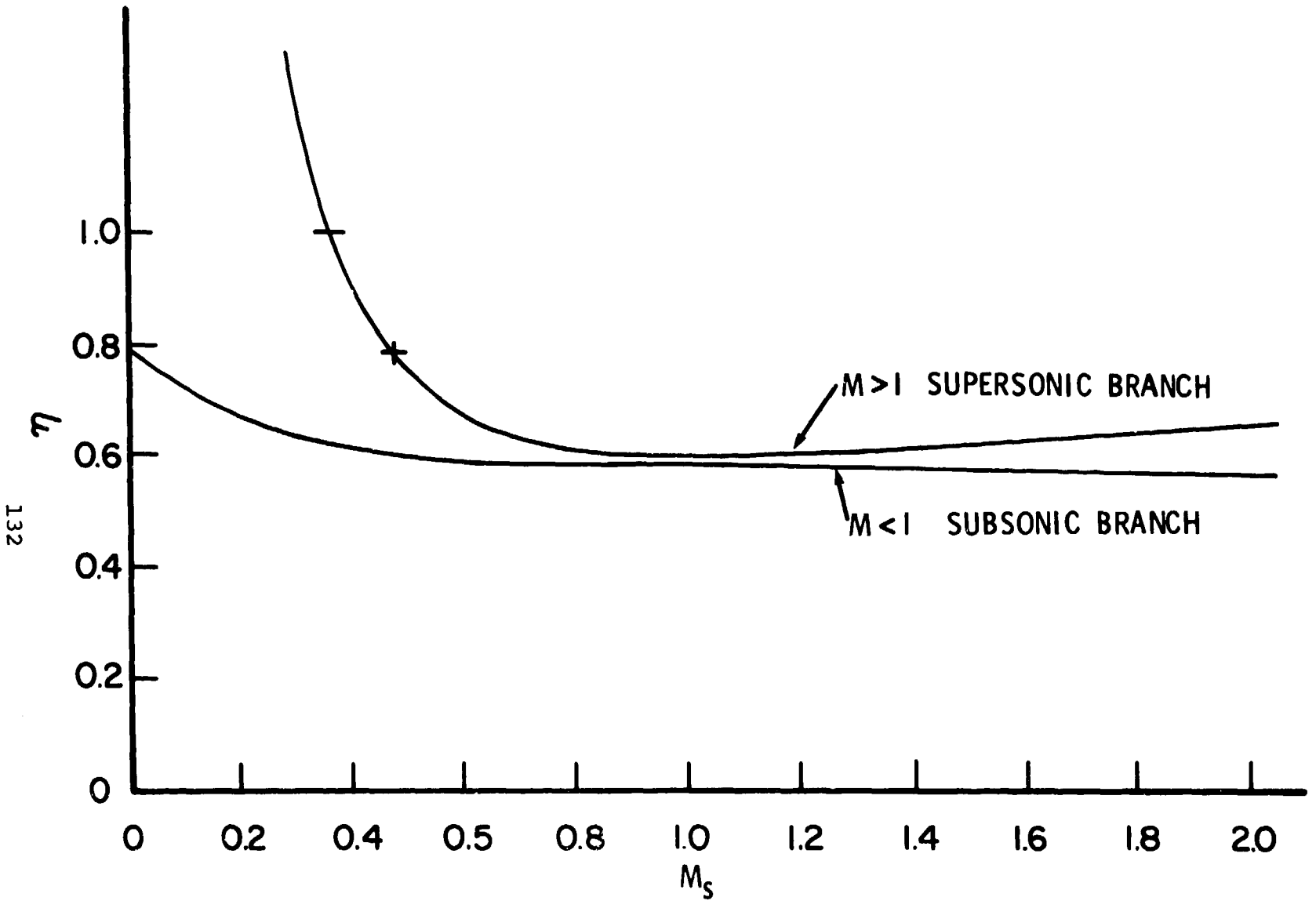
Figure 19.   Ejector Efficiency Distribution.
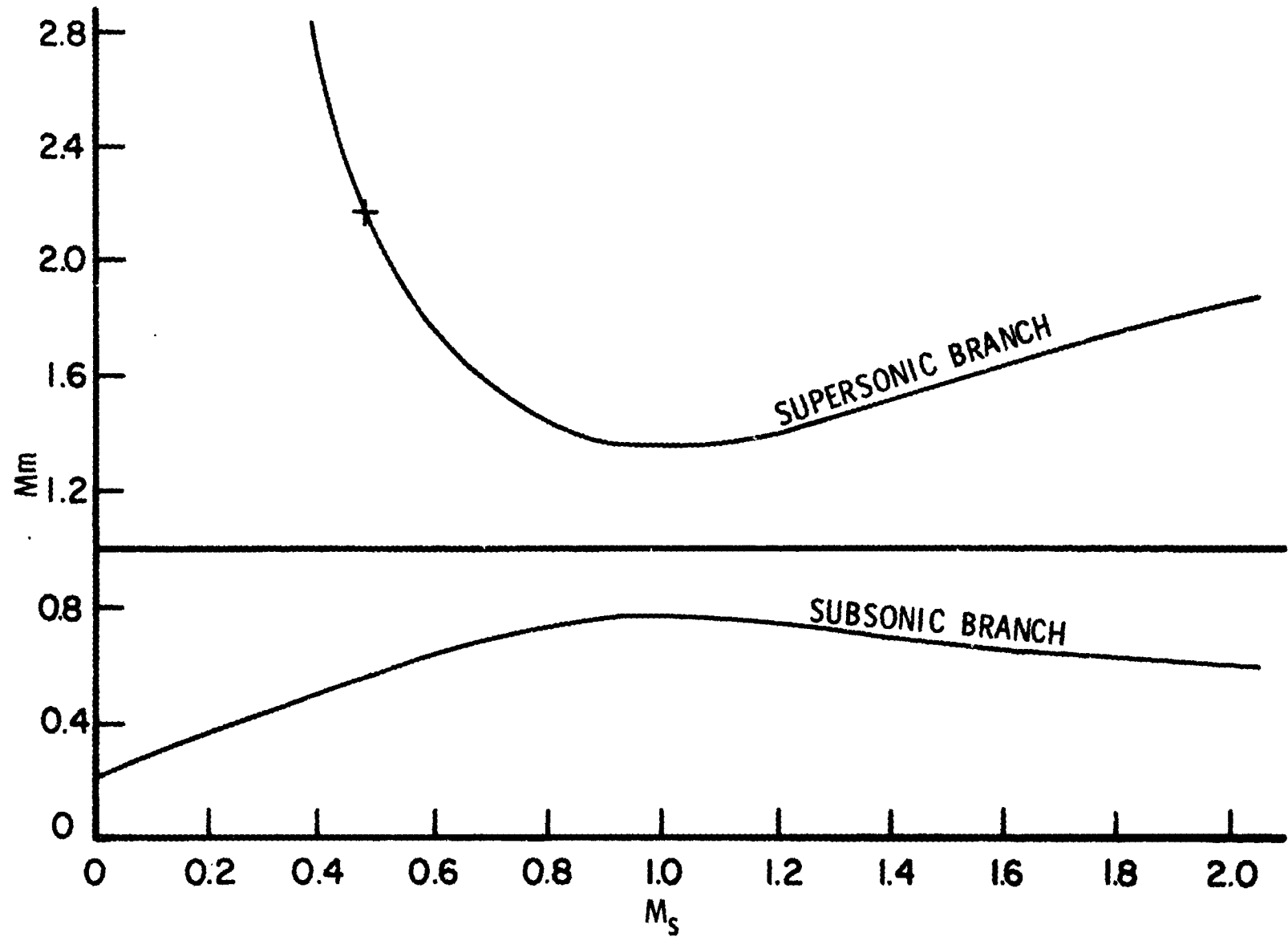
Figure 20. Mixed Flow Mach Number Distribution.

subsonic branch is higher than on the supersonic branch. By
setting the back pressure (in the region where the mixed flow
exhausts into) at appropriate levels, the types of data points
shown in the figures are achieved. Since no throat is provided
for the secondary flow at the inlet, $M_s$ will stay below 1.0, and
if the back pressure is further reduced, then the flow will jump
into the second solution branch. Once the back pressure is low
enough so that the supersonic branch is achieved, the operation
of the ejector is independent of the back pressure. The ejector
will operate at one point on the supersonic branch irrespective
of the value of the back pressure. UDRI has further discussed
the condition which determines where the ejector operating point
is on the supersonic branch. Figure (20) shows the distribution
of the mixed flow Mach number.

The results of the high performance of high speed ejectors
have shown that we need to arrive at geometric and thermodynamic
conditions at the ejector inlet as well as the outlet which will
allow the ejector to operate at certain points on the supersonic
solution branch. Computer programs which will define optimal
ejector characteristics are being developed and investigated, and
experiments are being planned to verify the theoretical results.

Another ejector related project which FDL has performed is
the ejector wing design study. NASA Ames Research Center has
also supported this study. FDL proposed a concept of an ejector
integrated wing which can demonstrate high lift (augmented due to
supercirculation effects of the ejector flows) characteristics
over a wide range of angles of attack in a Mach number range up
to 0.3. After some analytical studies involving 3-D vortex lat-
tice code coupled with ejector flow prediction methodology, an
ejector wing configuration in which the ejector inlet is located
on the underside of the wing near the leading edge, and the ejec-
tor exhaust flow outlet located on the upperside of the wing near
the trailing edge was chosen.

Advanced Technology center of Vought Corporation, Dallas,

134

Texas, performed the tests under contract. Electric analog
experiments were performed to map out potential flow solutions.
A four-foot span wing model with a swept leading edge and an
aspect ratio of about 4 was fabricated for test purposes. The
ejector itself was designed to be a constant pressure mixing type
ejector. The model was tested in the 7' x 10' Army tunnel
located in NASA Ames Research Center. The primary flow was
injected supersonically into the ejector, and the model was
tested over a range of angles of attack, $\alpha$ , going from -15° to
+25° in increments of 5°, and at two flow Mach numbers 0.15 and
0.28. Details of these tests are going to be published in a
forthcoming report. (Ref. 5). Figures (21) and (22) show the
model that was tested in the 7' x 10' subsonic tunnel. The
results of the tests are shown in Figures (23) and (24).

Significant improvements realized in the aerodynamic charac-
teristics due to ejector integrated effects are shown in Figure
(24). Clearly, such a high lift technology wing concept which
has demonstrated both lift and thrust augmentation characteris-
tics can conceivably impact on maneuvering capability at low
speeds. The tests have also demonstrated that further useful
investigations need to be performed with such a concept for eval-
uating the benefit of such an ejector wing configuration.

Flight Dynamics Laboratory has given support to another area
of investigation which involve questions of mixing and entrain-
ment, and the relative roles they play in determining ejector
performance characteristics. A project supported by the Air
Force, the Navy, and NASA has been initiated and Jet Propulsion
Laboratory of the California Institute of Technology has been
tasked to perform detailed flow studies using laser velocimeter
as well as hot wire instrumentation techniques. Figure (25)
outlines JPL test objectives. Subsonic and supersonic primary
flows, both hot and cold, will be injected into ejector shrouds,
and detailed flow measurements as well as thrust levels will be
determined. Correlation of measured data will be made with a

135
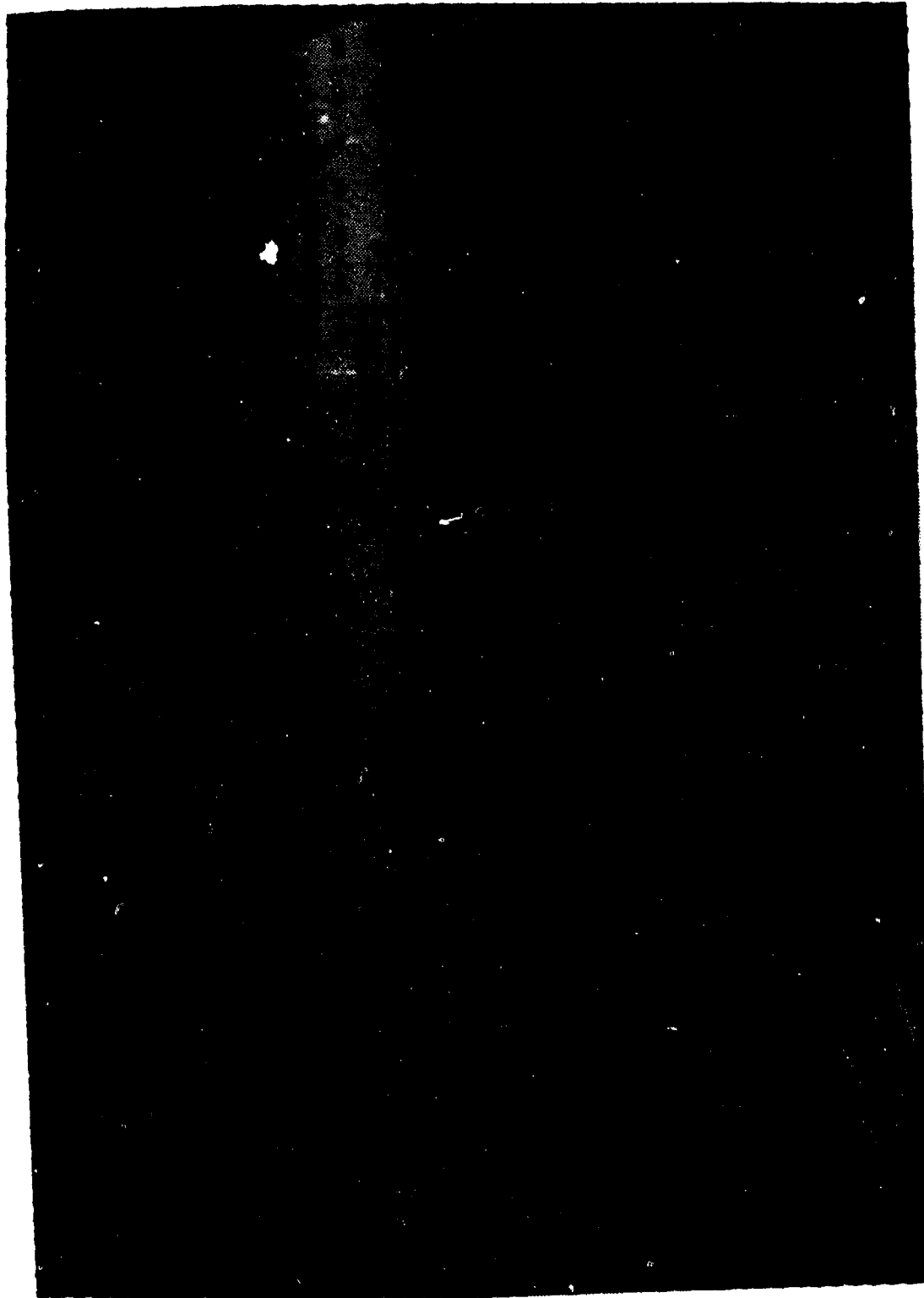
Figure 21.   Ejector Wind Model Looking at the Upper Surface.

Figure 22.  Ejector Wing Model Looking at the Bottom Side.

# BASELINE WING PERFORMANCE

$M_0 = 0.10$
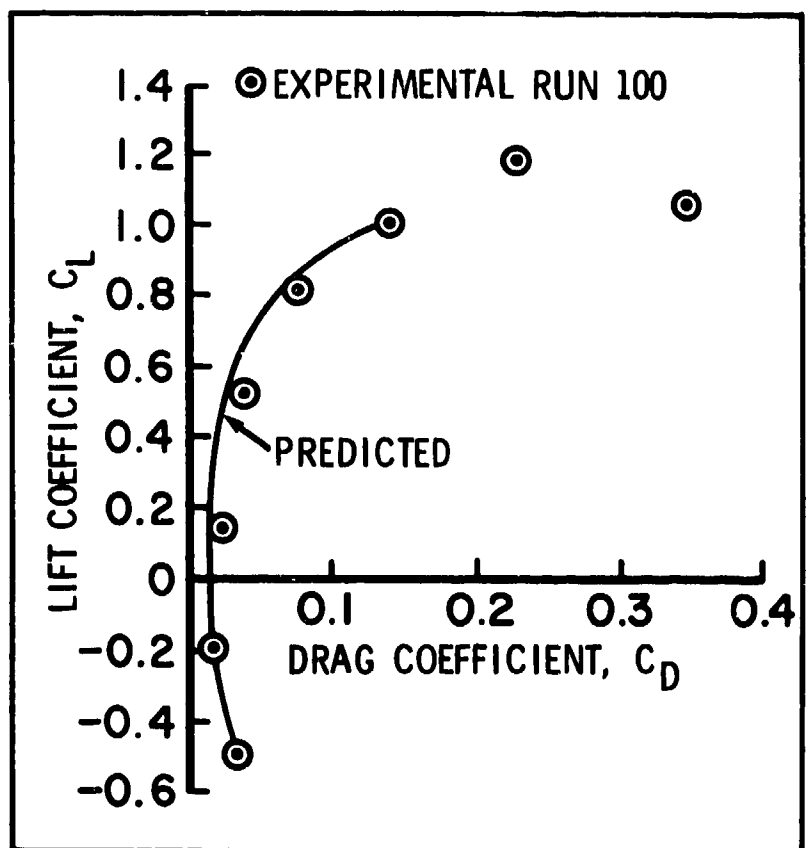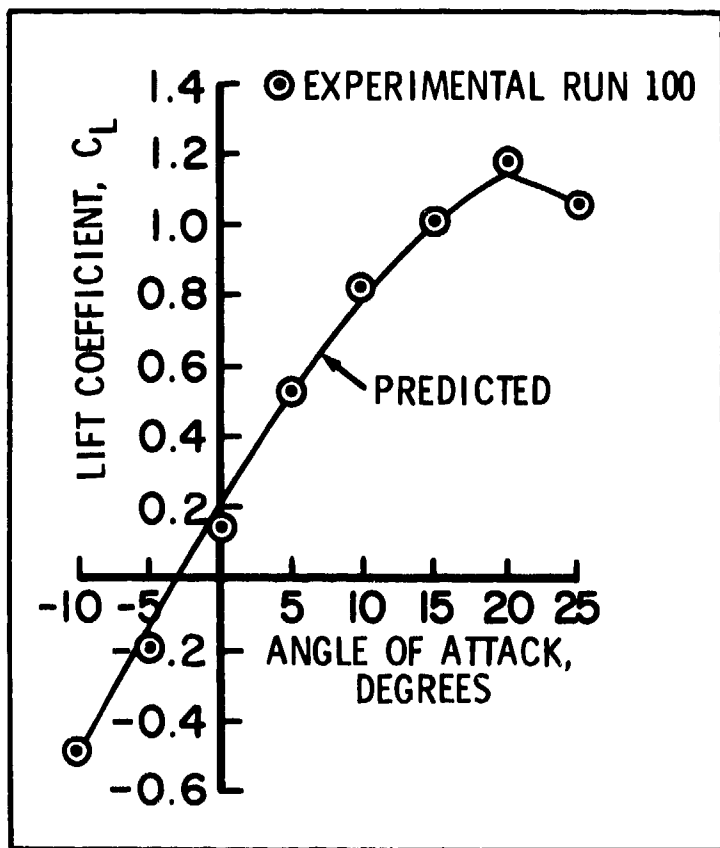


Figure 23
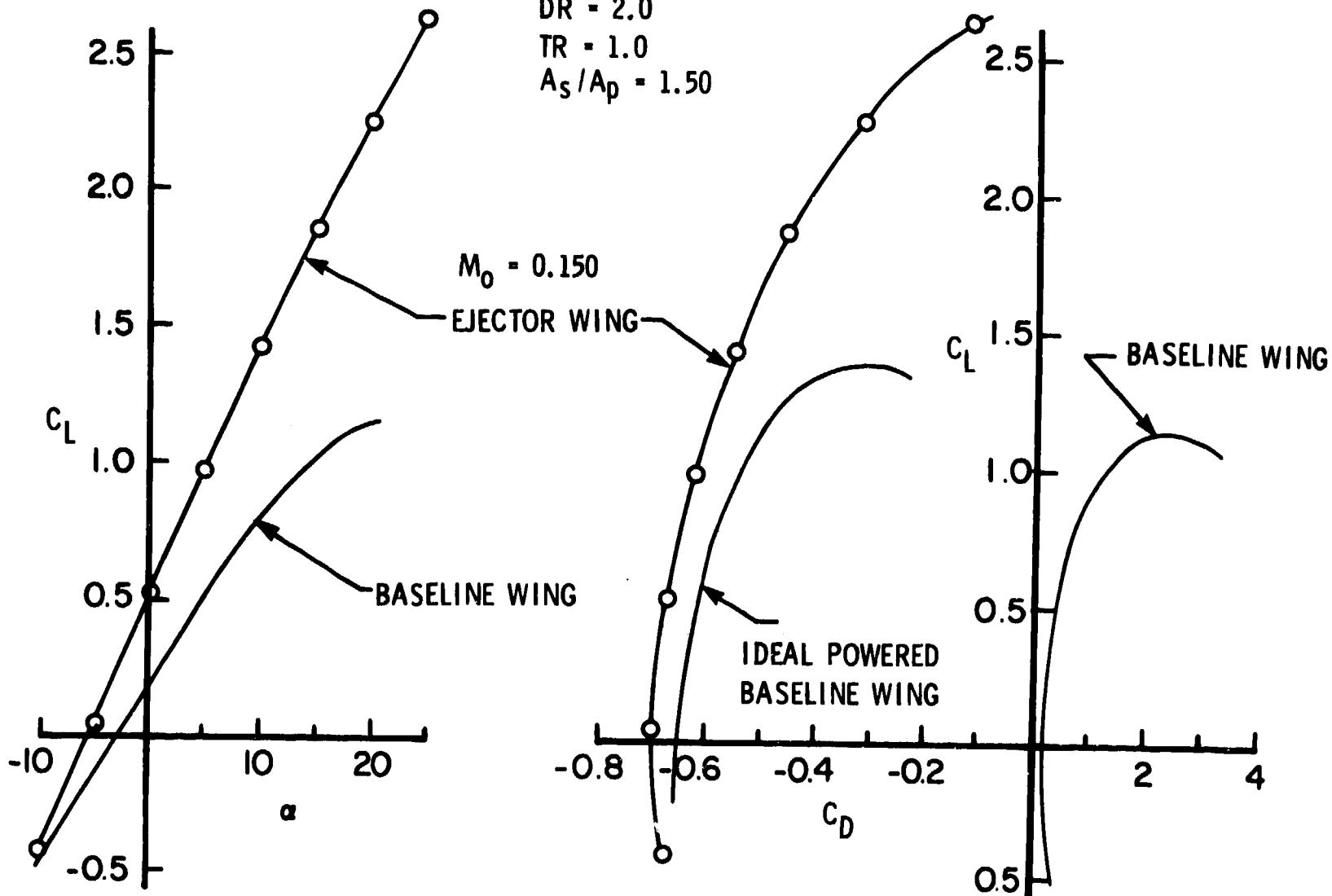
Figure 24.   Wind Tunnel Data of the Ejector Wing Characteristics.

# OBJECTIVES/PLANS

- CONCENTRATE ON FLUID-DYNAMICS OF THE EJECTOR FLOW

- DETERMINE ROLE OF THE ENTRAINED FLUID AND ITS MIXING WITH PRIMARY JET ON EJECTOR PERFORMANCE

- DETERMINE HOW THE VARIOUS PROFILES EVOLVE AND THEIR RELATIONSHIP TO THE THRUST AUGMENTATION

- SEARCH FOR TURBULENT STRUCTURE OF EJECTOR FLOW FOR ACTIVE INTERACTIONS TO ENHANCE EJECTOR PERFORMANCE

140

Figure 25

view to understand the basic flow processes. The effort is underway presently, and substantial data from this study will be available in the latter part of 1982. Figures (26) and (27) show the LDV set up at JPL. The LDV is a 2-component system, and it is expected that measured data can provide appropriate turbulence models in the ejector mixing region.

It is evident from the above discussions that though modest, but significant basic understanding has been realized by various efforts performed in or supported by the Air Force. Some of the significant observations on what has been accomplished are shown in Figure (28). Two workshops were conducted to assess the progress made and to recognize the problems in the technology area (Fig. 29). Figure (30) gives a summary of the Air Force's effort. Further progress will be made in the coming years in gaining a better understanding of the potential of ejectors in aerospace technology development, and the Air Force will play its due role.

## REFERENCES

1. "Workshop on Thrust Augmenting Ejectors" Cosponsored by NASA-Ames Research Center, Naval Air Development Center and Air Force Flight Dynamics Laboratory. Held at Ames Research Center, Moffett Field, California, June 1978. NASA CP-2093.

2. "One-Dimensional Compressible Ejector Flows". K.S. Nagaraja, David L. Hammond and J.E. Hammond and J.E. Graetch, AIAA Paper 73-1184, Nov. 1973.

3. "High Speed Ejectors", Morton Alperin and Jiumm-Jeng Wu, AFFDL TR-79-3048, May 1979.

4. "Characteristics of High Performance Ejectors", University of Dayton Research Institute (to be published).

5. "Ejector-wing Design", Advanced Technoloy Center, Vought Corporation, Dalas, Texas, (to be published).
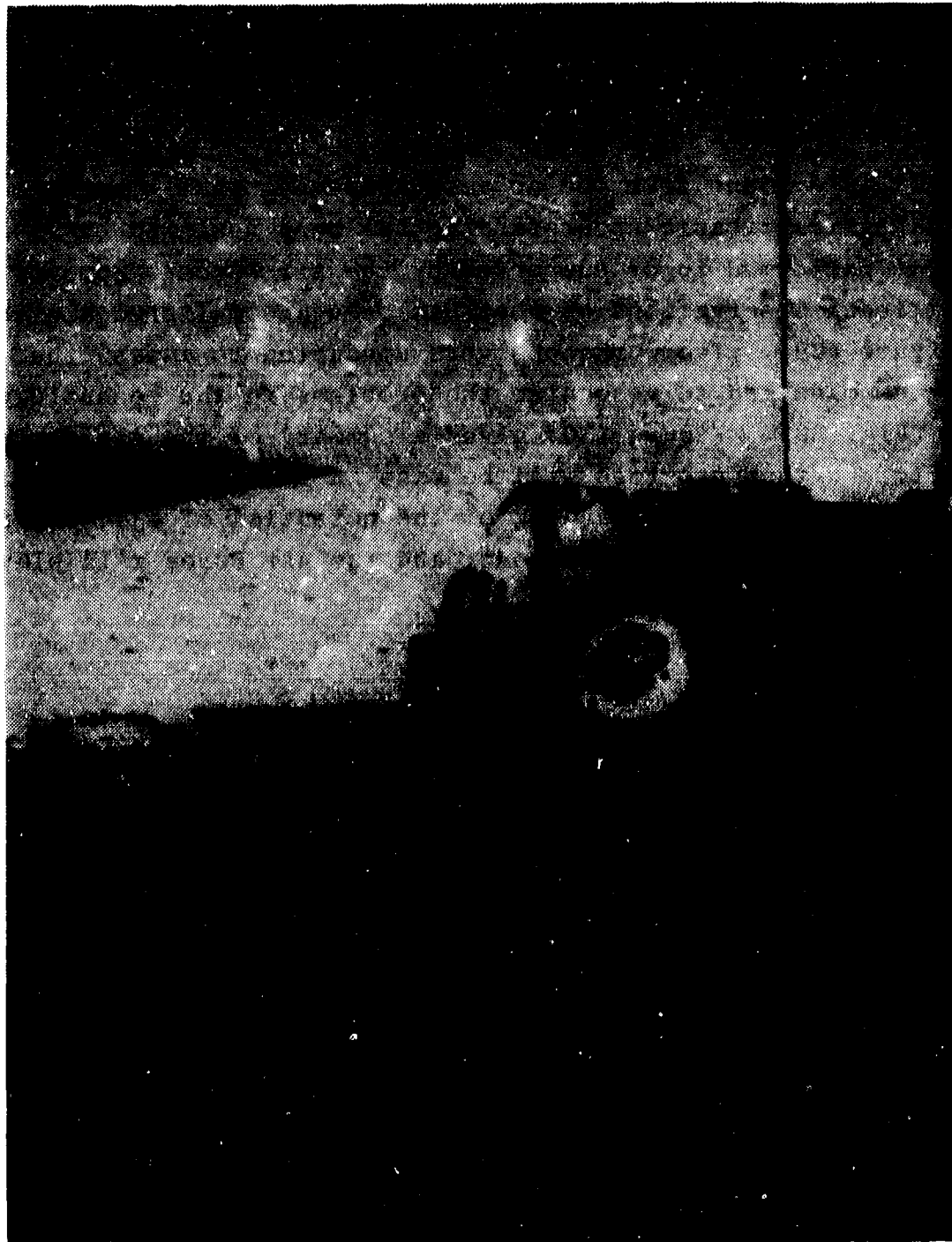
Figure 26.   LDV Set-up at JPL.
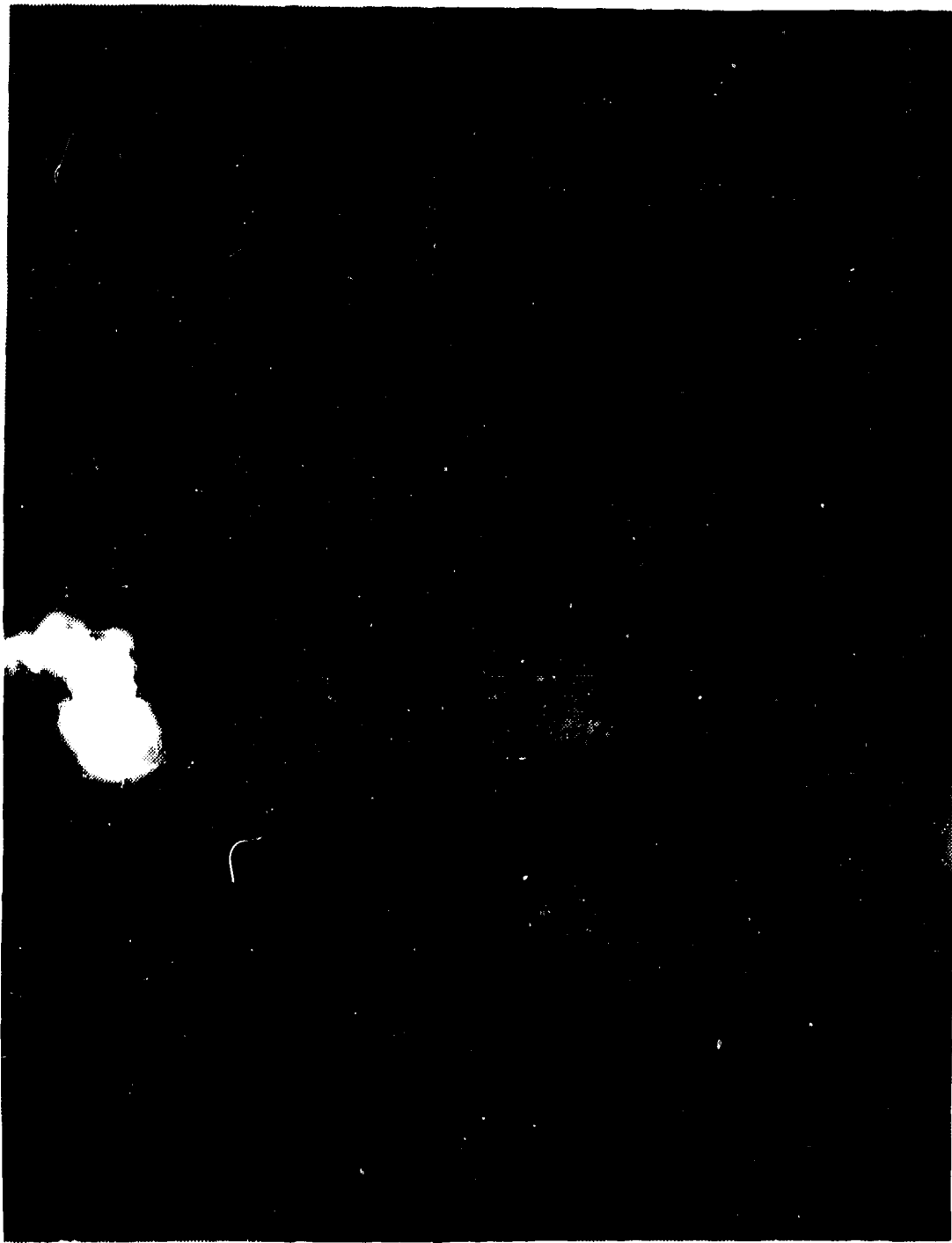
Figure 27. LDV Set-up at JPL.

143

# OBSERVATIONS

- PRIMARY TEMPERATURE EFFECTS PLAY AN IMPORTANT ROLE

- CROSS FLOW VELOCITY EFFECTS

- INLET DESIGN

- SECOND SOLUTION IF REALIZED IS EXPECTED TO PROVIDE
  LARGE INCREASES IN AUGMENTATION

- MATCHING OF AEROTHERMODYNAMIC CONSIDERATIONS IN
  OPTIMAL EJECTOR DESIGNS

- SELECTION OF PRACTICAL CONFIGURATIONS AND ITERATIONS
  TOWARD OPTIMIZATION

144

Figure 28

# CONFERENCES AND MEETINGS

●WORKSHOP ON THRUST-AUGMENTING EJECTORS

- •JOINT SPONSORSHIP BY NASA/NAVY/AIR FORCE.
  FULLY FUNDED BY NASA-AMES. JUNE 28-29, 1978
  AT AMES R.C.

- •TECHNICAL MEETING PRIMARILY PROVIDING A FORUM
  FOR PRESENTATION OF VARIOUS RESULTS.
  (NASA CP-2093, SEP 1979)

●WORKSHOP ON EJECTOR TECHNOLOGY

- •JOINT SPONSORSHIP BY AFOSR AND AFWAL (44K AFWAL)
  DAYTON, OHIO - AUGUST 3-5, 1981

Figure 29

# SUMMARY

- THEORETICAL POSSIBILITY OF HIGH PERFORMANCE EJECTORS DEMONSTRATED

- GOOD PERFORMANCE FROM EJECTOR WING IS REALIZED AND THE TESTS ARE CONTINUING

- JPL EFFORT WILL SEEK TO RESOLVE SOME QUESTIONS ON MIXING AND ENTRAINMENT CHARACTERISTICS

- FDRC AND UDRI WILL MAP OUT AREAS FOR REALIZING "SECOND SOLUTION" EJECTORS

- WORKSHOP IN AUGUST WILL ADDRESS QUESTIONS AND PREPARE ROADMAPS PERTAINING TO HIGH PERFORMANCE EJECTORS

Figure 30

RECENT EJECTOR TECHNOLOGY PROGRAMS AT THE
NAVAL AIR DEVELOPMENT CENTER

K. A. GREEN
Naval Air Development Center
Warminster, PA   18974

During the past several years, the major ejector activity within the
Navy has concentrated on the Thrust Augmenter Wing (TAW) concept and its
application to the Rockwell XFV-12A technology demonstrator.  Other papers
to be presented in this workshop will discuss in detail the work that was
accomplished during this program.  The purpose of this paper is to outline
some of the recent ejector technology work supported by the Naval Air
Development Center jointly with the Air Force and/or NASA AMES and the
rationale behind the programs.

Following the 1978 Ejector Workshop, held at NASA AMES, several follow-
up meetings were conducted with NASA, Navy and Air Force representatives to
determine, based on the presentations and discussions at the conference,
what areas should be pursued to improve the technology data base.  Although
many specific areas of work were recognized, two areas in particular contin-
ually surfaced.  The first concern was to obtain a better fundamental under-
standing of the important flow mechanisms taking place within an ejector,
e.g., turbulent mixing and entrainment, and how these parameters were influ-
enced by such things as pressure ratio, temperature effects, supersonic primary
flows, inlet configuration, primary nozzle design and diffuser characteristics.
There was by no means a general consensus of opinion during the last workshop
in many of these areas and some type of study to better understand and eluci-
date these mechanisms appeared to be a worthwhile research direction.  The
purpose of the study would not be to design an improved ejector but rather
probe the flows using laser doppler velocimeters, hot wire anomometers and
photographic techniques such as Schlieren and shadowgraphs.

As a result of these discussions, a program was established at the Jet
Propulsion Laboratory (Reference a) to accomplish the above objectives and is
currently being jointly supported by the Naval Air Development Center, NASA
AMES and the Air Force (See Figure 1).  Specific details of this program, such
as measuring techniques, data reduction methods and results to date, will be
presented as a separate paper by the principal investigator  during this work-
shop.

The second area that was repeatedly mentioned, during the 1978 workshop,
was the practical difficulties of taking a high performance laboratory ejector
and integrating it into an aircraft configuration.  This involves not only
compressing the size of the ejector but carefully studying how engine exhaust
gases can be reasonably ducted to the primary nozzles, to what extent aircraft
surfaces surrounding the ejector will influence inlet and exhaust flow and how
well the ejector/aircraft can pass through transition from VTOL to conventional
flight.

Currently there are two generic configurations for ejector aircraft.

The first is the Thrust Augmenter Wing or TAW concept characterized by the XFV-12A program. In this case the ejectors are mounted in the wings which fold up for the conventional flight mode. The ability to deflect the augmenter flow in a jet-flap fashion would appear to provide an advantage during the transition phase because of the supercirculation and increased lift generated. The second concept involves the use of ejectors mounted fore and aft in the aircraft fuselage or strake areas close to the fuselage. Although the concept seems to offer some practical advantages in packaging and ducting of primary flows, concern remains with the ability of the configuration to pass through transition. This concept has been extensively pursued by NASA AMES with a DeHavilland ejector design and more recently by General Dynamics.

Looking at other ejector concepts being developed, that had high performance, the Alperin Jet Diffuser Ejector seemed to offer good performance in a relatively compact design. This ejector was originally developed for the Navy as part of a propulsion system for a Small Tactical Air Mobile Platform (STAMP). Although it appeared that this device might be suitable for the fore-aft fuselage mounted approach, it was felt that significant gains in compactness could be made by redesigning the diffuser and attaching the primary nozzles at the inlet of the shroud. The Naval Air Development Center supported these modifications and in the case of the attached primary nozzles the work was supported jointly with NASA AMES (Figure 2). The results of these changes are shown in (Figure 3).

From this figure it can be seen that the large end-plates existing on the original "STAMP" ejector have been eliminated. The approach used (Reference b) was a combination of analytical prediction and experimental verification. Since the "STAMP" ejector worked well in the middle plane but poorly at its ends, the analysis involved a closed, rectangular distribution of vortices of constant strength with their position and size chosen such that the resulting streamline at the middle plane closely matched the "STAMP" ejector's geometric requirement. A series of vortex distributions were developed such that the maximum pressure gradients at the corners and end walls did not exceed that of the "STAMP" ejector in the middle plane. This device produced an augmentation ratio of 2.13 when the diffuser area ratio was 3.0.

The next step was to attach the primary nozzles on the inlet shroud. This was done by experimentally mapping augmentation ratio as a function of the position and injection angles of the primary nozzles (Reference c). This again reduced the overall length of the ejector with a slight reduction in augmentation ratio. From Figure 3, it can be seen that the attached primary nozzle No. 4A produced an augmentation ratio of 2.02. Having now significantly compressed the overall length of the ejector while maintaining the high augmentation ratios previously achieved, both NASA AMES and the Naval Air Development Center agreed that it would be worthwhile to attempt to integrate the ejector into an aircraft configuration, look at methods of enhancing the transition characteristics, design and build a semi-span model and test in the NASA 7 x 10 wind tunnel. The aircraft configuration chosen was a General Dynamics V/STOL "B" Fighter design that NASA has been looking at for some time and currently has a 70% model that is being considered for modifications with the DeHavilland ejector. The design of the semi-span model with the integrated jet diffuser ejector and some limited in-house testing by the contractor

148

(Reference d) was jointly supported by NASA AMES and the Naval Air Development Center (Figure 4-5).

In order to minimize the strake thickness, it was necessary to further compress the location of the primary nozzles. The result of this modification is shown in Figure 3 as attached primary nozzle No. 5. In this case the maximum augmentation ratio attained was 1.95. This was reduced even further when installed in the model. In this case a maximum value of 1.93 was realized.

In order to assist the ejector in passing through transition from a VTOL to a conventional flight mode, two features were added (See Figure 5). The first is an asymmetric extension of the diffuser (diffuser flap) which, due to an unbalanced pressure distribution produces a thrust in the forward direction. The second feature was a vector control jet mounted within the throat of the ejector. By changing the angle of the vector control jet up to 30° a thrust component in the forward direction of 11% of the total thrust was realized. Thrust augmentation, however, again dropped to a value of 1.91. Currently, construction of the semi-span model is underway at NASA AMES and it is hoped that tunnel testing of the concept will take place next summer. Although pressure ratios up to a value of three for the primary nozzles will be possible with the semi-span model, it will only have limited temperature capability. If the ejector characteristics during transition are encouraging, further testing and development would be to consider a large scale hot model to be tested statically and, with continued success, incorporated into a large scale configuration for use in the 40 x 80 wind tunnel.

Current in-house efforts have been looking at the application of ejectors to forward flight conditions for energy efficient aircraft, based on the recent Air Force report entitled "High Speed Ejectors" (Reference e). The intention of this effort is to convert the analysis to a subroutine suitable for use in the Navy Engine Performance Computer Program. This will then permit the simulation of complete propulsion systems with and without the ejector operating for both the subsonic and supersonic mixed flow conditions as outlined in Reference e. These modified propulsion systems can then be applied to a conceptual design aircraft to determine performance, fuel savings and possible trade-offs (Figures 6 & 7).

# REFERENCES

a) "Fundamental Studies in Thrust Augmenting Ejector Flows" NASA
Contract No. NAS7-100 with the Jet Propulsion Laboratory.

b) Alperin, M., Wu, J.J., "End Wall and Corner Flow Improvements of the
Rectangular Alperin Jet-Diffuser Ejector," NADC-77050-30, May 1978.

c) Alperin, M., Wu, J.J., "Jet-Diffuser Ejector - Attached Nozzle Design,"
NASA CR-152361, May 1980.

d) Alperin, M., Wu, J.J. "A Jet-Diffuser Ejector for a V/STOL Fighter,"
NASA CR-166-161, February 1981.

e) Alperin, M. Wu, J.J., "High Speed Ejectors," AFFDL-TR-79-3048, May 1979.

- JOINT PROGRAM WITH NASA, AIR FORCE AND NAVY

- WORK BEING DONE BY JET PROPULSION LABORATORY

- OBJECTIVE

  - EVALUATION OF MIXING, ENTRAINMENT, SCALING AND THERMO-
    DYNAMIC EFFECTS ASSOCIATED WITH COLD AND HIGH TEMPERATURE
    SUBSONIC AND SUPERSONIC PRIMARY JET FLOWS IN EJECTORS

- APPROACH

  - EXPERIMENTAL PROGRAM TO CHARACTERIZE FLOWS WITH LDV AND
    HOT WIRE PROBES AS WELL AS SHADOWGRAPH/SCHLIEREN PICTURES

  - DETERMINE HOW VARIOUS PROFILES EVOLVE AND SEARCH FOR ACTIVE
    FLUID INTERACTIONS TO ENHANCE EJECTOR PERFORMANCE

Figure 1.  Fundamental Ejector Study

- ALPERIN JET DIFFUSER EJECTOR

- JOINT PROGRAMS WITH NASA AMES

- REDUCE SIZE OF DIFFUSER AND IMPROVE END WALL AND CORNER FLOW

- ATTACH PRIMARY NOZZLES TO EJECTOR SHROUD

- INTEGRATE EJECTOR DESIGN INTO GENERAL DYNAMICS E-205 TWO ENGINE
  V/STOL FIGHTER AIRCRAFT

- CONSTRUCT SEMI-SPAN MODEL TO STUDY EJECTOR TRANSITION CHARACTER-
  ISTICS IN NASA AMES 7 X 10 WIND TUNNEL

Figure 2.   Integration of High Performance Ejector
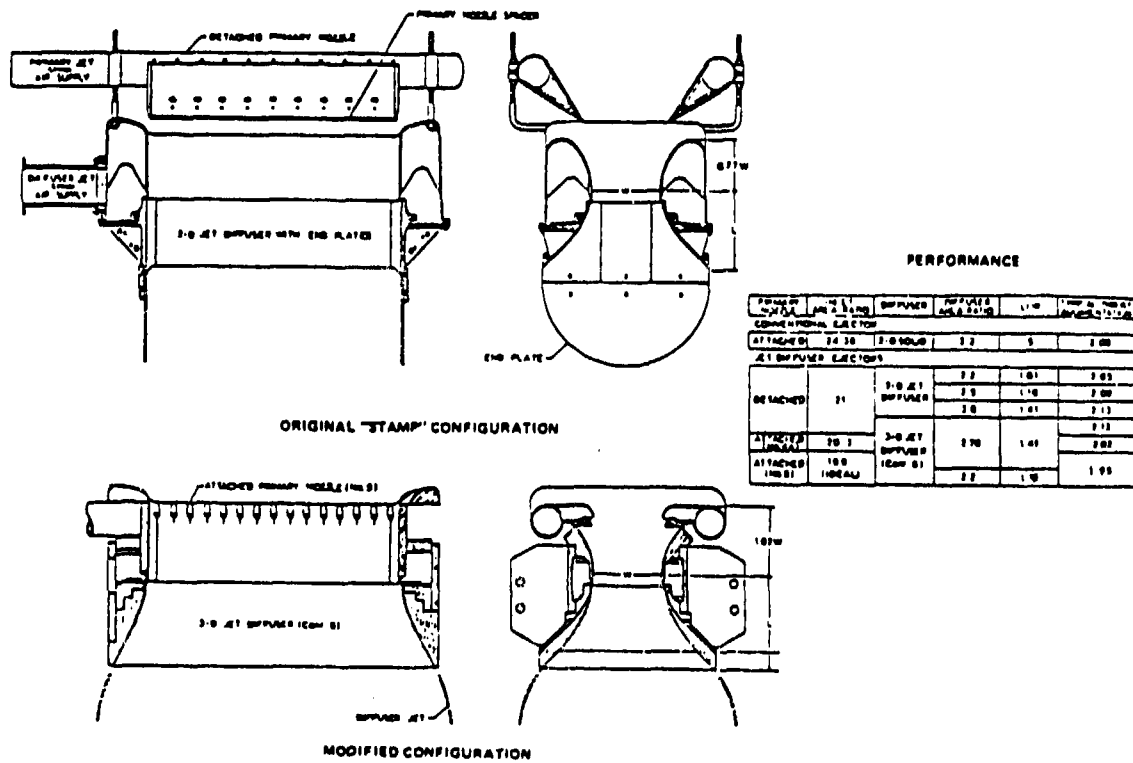


Figure 3.   Development of Jet Diffuser Ejector
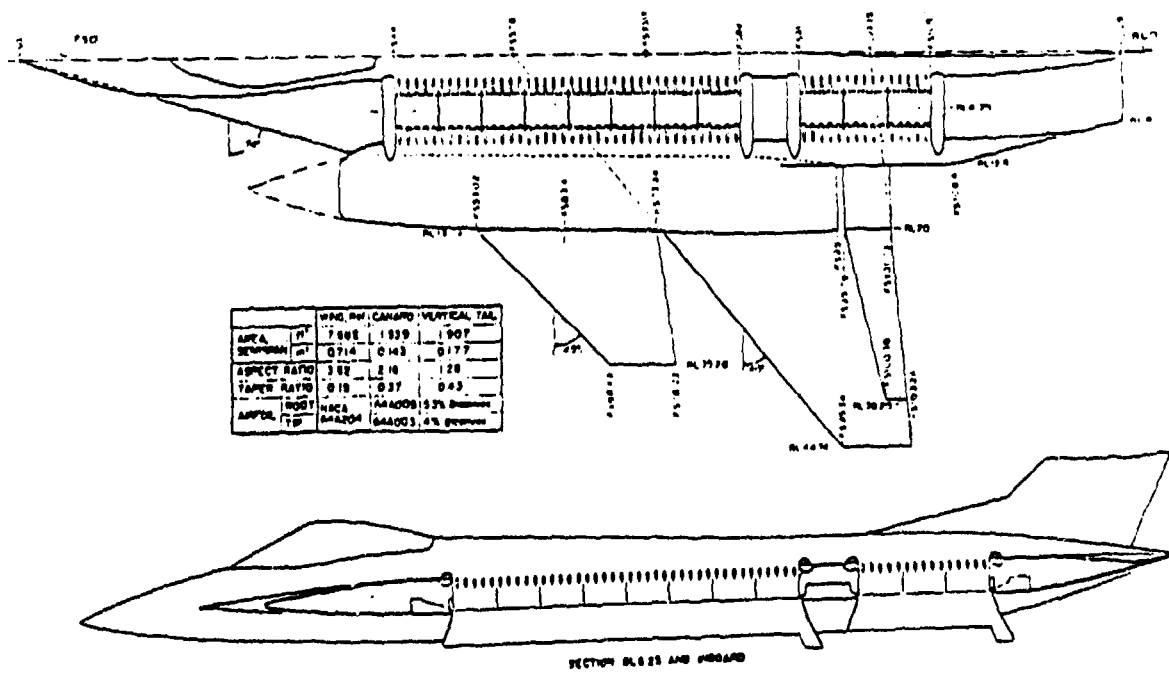
Figure 4. Ejector Integrated in V/STOL Fighter
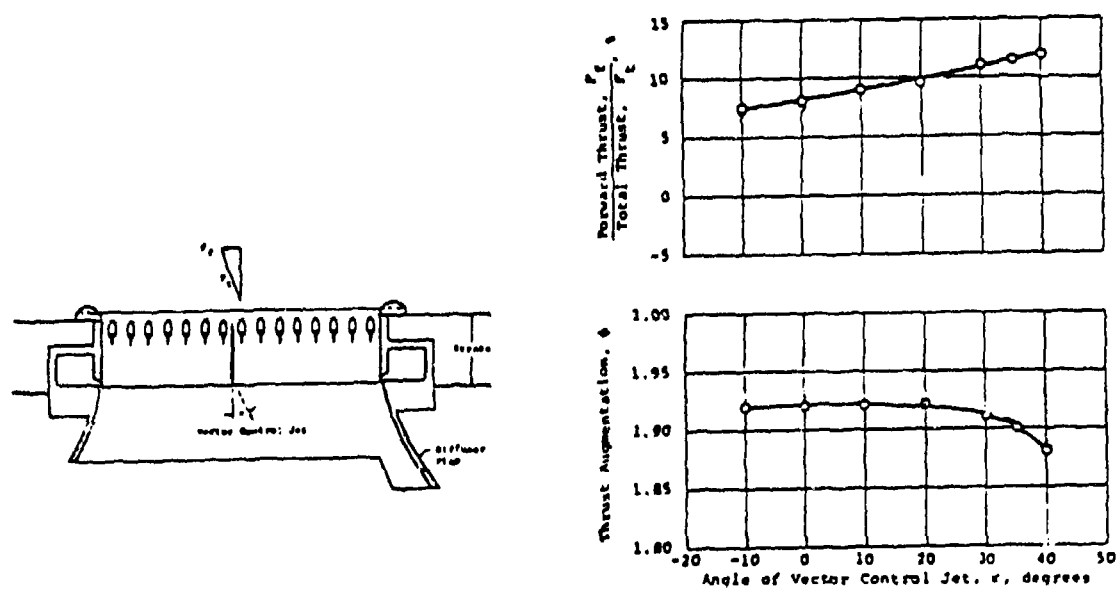


Figure 5. Thrust Vector Control System

152

- OBJECTIVE

  - EXAMINE POTENTIAL OF USING EJECTOR TECHNOLOGY IN FORWARD
    FLIGHT FOR APPLICATION TO ENERGY EFFICIENT AIRCRAFT

- APPROACH

  - CONVERT ANALYSIS IN RECENT AIR FORCE REPORT TO SUBROUTINE
    SUITABLE FOR INCORPORATION INTO NAVY ENGINE PERFORMANCE
    COMPUTER PROGRAM

  - SIMULATE COMPLETE PROPULSION SYSTEMS WITH AND WITHOUT
    EJECTOR OPERATING

  - APPLY PROPULSION SYSTEM TO CONCEPTUAL DESIGN AIRCRAFT AND
    DETERMINE PERFORMANCE, FUEL SAVINGS AND POSSIBLE TRADE-OFFS

Figure 6.   Current In-House Ejector Work
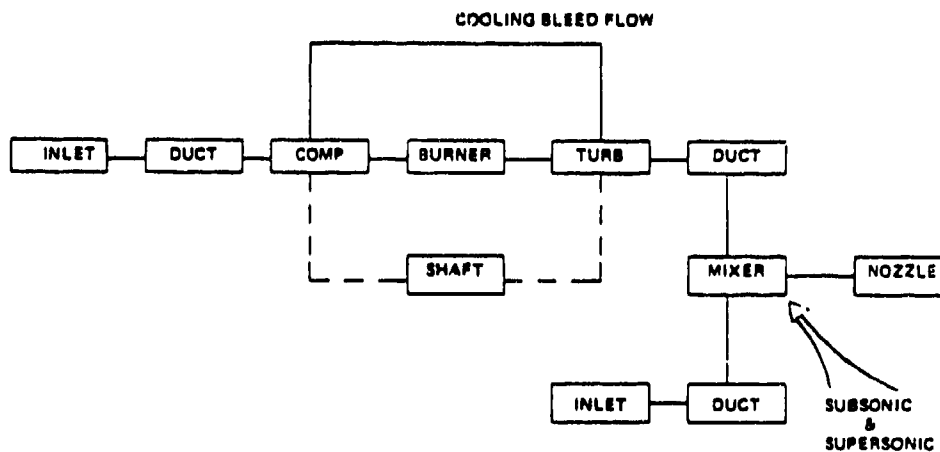


Figure 7.   Combine Mixing Analysis with Navy
            Engine Performance Computer Code
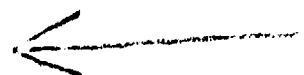
153

# INVESTIGATION AT LARGE SCALE OF THRUSTING EJECTOR APPLICATIONS TO V/STOL AIRCRAFT

David G. Koenig

## Summary

Ames Research Center, NASA, has been active in several programs which have the objectives of learning to both predict thrusting ejector performance and to package the ejector in tactical aircraft. The Ames 40-by 80-foot Wind Tunnel has been used to evaluate the deHavilland fuselage ejector at large-scale and this wind tunnel and the newer 80- by 120-foot will be used in future programs. These programs will include: (a) the improvement of the fuselage ejector performance; (b) its application to tactical aircraft design through full-scale testing; (c) possibly, the application of the short (Alperin) diffuser to tactical aircraft; (d) evaluation of new ejector concepts. To take advantage of the size, the objectives of these investigations will focus on the establishment of a well documented data base and evaluating packaging problems - from seal door design to duct losses. The advantage of the new 80- by 120-foot Wind Tunnel will be to allow the use of 15,000 lb (+) engines for propulsion, for singe or two engine configurations, at moderate airspeeds, for larger aircraft. The ejector designs tested will be continually compared with that of other V/STOL designs in the large-scale testing phase.

## Notation

AL      Lifting element area

AM     Wing momentum area

AN     Nozzle area

$A_T$     Wind tunnel test section area

$C_d$     Discharge coefficient

$C_v$     Velocity coefficient

F      Total ejector thrust

$F_I$     "Isentropic" thrust of primary nozzles

$\ell$     Distance from primary nozzles to the end of the diffuser

$\bar{t}$     AN / (length of throat)

$V_j$     "Isentropic" jet velocity

$P_N$     Density of fully expanded jet

## Introduction

Ames Research Center, NASA, has been active in developing the thrusting ejector for use in STOL and VTOL aircraft designs since the advent of the "Augmentor Wing" in the early 60's. Following these studies of the use of ejector systems on STOL transports, it became evident that ejectors should be considered seriously in the design of and planning of future high performance tactical aircraft. As a result, Ames has supported the development of the ejector concepts which seemed to have the most promise in both installed thrusting performance and the "packaging" in the aircraft for minimizing penalties in aircraft cost and airframe weight.

This effort involving both large and small scale testing has involved, essentially, all of the ejectors shown in Figure 1. This plot is an updated one from the Ames Ejector Conference 4 years ago and ratios the thrust to an isentropic value based on duct or nozzle conditions.

Since the mixing length $\ell$ must be subject to aircraft external geometry restriction for a given primary slot value, $\bar{t}$, more favorable integration into an aircraft moves up and to the left on the plot. At the present time, the XFV-12A is the only design having any significant hardware development and this as well as the fuselage ejector (de Havilland) are the only ejectors undergoing large scale testing. Although hardware development must be a factor in assessing the viable ejector concepts, of equal importance, is the verification of ejector performance through large scale testing. This paper describes Ames participation in large scale testing of ejector equipped aircraft configuration, with the combined use of the 40- by 80-/80- by 120-Foot Wind Tunnel and the Ames Static Test Facility.

It should be emphasized that part of the program structure presented does not represent, necessarily, the views of Ames Management, at this point, and certainly depends on budgeting constraints.

## Ejector Configurations

Thrusting ejector concepts now being considered for use in fighter aircraft designs with "V" capability are sketched in Figure 2. These designs may not be the only ones being studied for this but have lately received considerable attention. The fuselage ejector was and is being developed by de Havilland and has been carried through large scale testing. This concept takes a significant roll in Ames planning. The short diffuser ejector, developed by Dr. Alperin of Flight Dynamics is now planned for 7- by 10- tests and will be discussed below. The spanwise ejector or "wing augmenter" is that of the XV-12A ejector and could go to large scale wind tunnel testing if parts of the program continue. All three of these concepts have been studied extensively, both theoretically and through small scale testing. The fuselage and spanwise ejector have proceeded to large or full scale (for the XFV-12A) testing phase.

The ejector designs which have been considered for powered lift STOL applications are summarized in Figure 3. The external ejector was considered

157

in several types of designs with one or two having been tested at small scale. The Cruise Augmentor have been studied extensively by de Havilland. The spanwise ejector of Rockwell is that of Figure 2(c) but in the "STOL mode" is effective in producing circulatory lift needed for this application. Another design could evolve from work from Flight Dynamics on the "High Speed Ejector". Only the Spanwise Ejector has been carried through large scale testing (but, it is hoped, others will evolve as specific aircraft designs evolve).

Programs involving NASA-Ames funding have and will involve the so called chordwise ejectors (fuselage and short diffuser) of Figure 2(a) and 2(b). This does not reflect a lack of interest in the other concepts but is consistant with the objective of studying the application of ejectors to tactical fighter designs both in performance and installation techniques. It is also realized that the spanwise ejectors such as the XFV-12A type or the cruise augmentor should be considered seriously for powered trailing edge devices needed for effective STOL capability. Furthermore, of equal importance to Ames large scale investigations is the need for theoretical and small scale testing effort of new and advanced designs. NASA intends to continue to contribute to this research.

## Fuselage Ejector

The fuselage ejector was initially proposed for use on a single engine supersonic fighter design having a double delta wing. The studies which were started by de Havilland indicated that there was promise of integrating the ejector with the wing root design using a side of the fuselage for the diffuser. In the laboratory, several aspects of design were initially studied and cold flow static tests at moderate scale were encouraging. In a jointly funded program (NASA and Canadian DRB), a large scale "boiler plate" model was designed and built at de Havilland and tested at Ames. It is shown mounted in the Ames 40- by 80- in Figure 4. The model went through three wind tunnel tests as well as a test on the Ames static test stand. The result of these tests are well published, Reference 2 through 5, and have been used in recent aircraft design studies.

People who have examined the functioning of and possible applications of the fuselage ejector have done so primarily because of its mechanical simplicity combined with the performance attained. The large scale model, even though it was powered by a J97 turbojet engine, was conceptual in the respect that no seals, door hinges, or actuator brackets were simulated. Even with some lack of detail of a "flying ejector" installation, the program showed that a large scale, engine powered, thrusting ejector could be built with good static performance and little adverse effect of forward speed on the performance. In addition, there was no reduction in lift due to ground and as was described in Reference 5, if powered "hot" the inlet injestion for a forward facing inlet might be small.

Future plans involve the further evaluation of vectoring by swiveling the primary nozzles. The mixing of each lobe will be improved allowing reduction of the number of lobes for a given thrust loading. Other objectives of another large scale test program in late 1982 will be the evaluation of methods of lateral and directional control. The model will be

158

instrumented to improve the evaluation of the effect of airspeed on ejector performance. Results of the test will be used to plan advanced work on the full scale model of the fuselage ejector-thrust deflector to be described next.

## Full Scale Testing of Fuselage Ejector

In view of the success with the performance of the fuselage ejector, to date, it is felt that a more detailed study of the concept is warranted in a viable aircraft installation, or in a close simulation of that installation. The next stage will involve the use of a fullscale "boiler plated" model powered by an engine close to that which could be used in the aircraft. Two likely candidates are those in Figures 5 and 6. The design in Figure 5 has been studied by both de Havilland and Ames with a likely engine candidate of a modified Rolls-Spey. The design in Figure 6 is being studied by General Dynamics and no engine has yet been chosen. When an engine is finally adopted, a complication for the boiler-plated version will be the acquisition of the engine or an equivalent propulsion system by a projected early 1984 test date.

Design objectives for the model will be to simulate, economically, all mechanical systems, internal aerodynamics as well as ejector itself, which could have any influence on the installed performance of the ejector. The current thinking is that the mechanical simulations are as vital as the ejector itself due to projected weight penalties of the components simulated. Because of the boiler plating technique, it will be feasible to instrument all internal and external aerodynamic surfaces and the information obtained from this instrumentation will project a significant data base for evaluating the fuselage ejector as well as other ejector concepts for V/STOL aircraft.

## Short Diffuser Ejector

Programs sponsored jointly by the Navy and NASA have refined what was the "STAMP" ejector into a design which may have potential for installation in a two engine fighter configuration.

The results of an initial attempt at this, shown in Figure 7 and reported on in Reference 6 were less than encouraging due to several factors. A major one was the problem of stowing the upper primary nozzles. Others included loadpaths needed for structure and seal plates on the upper surface. In the NASA-Navy program, the upper "STAMP" nozzles were retracted in favor of short lobed nozzles at the inlet. The contractor, Flight Dynamic Research Corporation, incorporated the result into the proposed adaption of the General Dynamics GD 205 shown in Figure 8 and reported on in References 7 and 8. A .2 scale semispan model is being designed and built for testing in the Ames 7- by 10-Foot Wind Tunnel. To date, this ejector has been shown to have a high augmentation ratio, 1.95 but at low pressures and temperatures. We still have to extend these values and show airspeed effects. If all is still promising, a full span or large scale model will warranted; but this will not be designed and built before additional static testing at large scale is completed.

## Concurrent Large Scale Testing Programs

The foregoing projects will proceed at the same time other V/STOL concepts are being investigated. A major program at Ames is continuing with the application of RALS and thrust deflectors to supersonic fighter configuration. A simulated RALS combined with an aft mounted VEO-thrust deflector will be incorporated into a configuration identical to that of the large scale 2 engine fighter model shown in Figure 9 (see Reference 9). This model is similar to the configuration of Figure 7 studied by General Dynamics of application of the short diffuser ejector. The low speed, high lift aerodynamics of the forward swept wing will be studied by removing the strake of the original 2 engine fighter model, moving the nacelles together and replacing the wing. For medium speed aircraft, the Grumman 698 tilt nacelle model will be tested both in the 40- by 80- and 80- by 120-. The model is shown mounted on the Ames Static Test Stand in Figure 10.

A significant objective of all this testing, as with the ejector programs, is to take full advantage of the size of models and advancements in instrumentation and data acquisition techniques in order to obtain information on component loads, engine performance, and characteristic of the flow around the model as well as the six component force and moment data. These factors are illustrated in Figure 11. This information will contribute directly to the development and verification of prediction techniques. The instrumentation must then provide data for such things as modeling separated or unsteady flow or simulating the conditions that propulsion jets can impinge on a curved surface near the wing root.

## Large Scale Test Facilities

Since it has been emphasized above that large scale testing should take a major part in developing the thrusting ejector, as well as other V/STOL lifting concepts, it is appropriate that the facilities themselves and testing techniques must be addressed. Reference 10 described some of the advantage and factors to consider in planning large scale tests. The following is a brief update of some of those conclusions and a description of the new Ames 40- by 80- by 120- system.

Since July 1980, the Ames 40- by 80- has been undergoing a modification to increase its own maximum test section velocity to 300K and to add an open throat 80- by 120-Foot test section. A schematic of the wind tunnel systems is shown in Figure 12. The new test section will take an aircraft installation of 100,000 lbs. and the scale system has the capacity of 150,000 lift and 50,000 drag. Even with this larger capacity, the scale system has least counts close to that of the original 40- by 80- ±5 lift and ±2 lb. drag. In addition, the 40- by 80- scale system data acquisition systems are being improved. The 40- by 80- is scheduled for start-up in April 1982, with the 80- by 120- starting in September 1982.

Figure 13.a & b is a classical size plot for the 40- by 80-. It should be worthy of note that the 80- by 120-Foot Wind Tunnel will help reduce these ratios by a factor of 4. An important impact of this will be the

ability to reduce the airspeed in the wind tunnel to values where flight conditions for steep landing approaches can be simulated without inducing recirculation of the lift jets. Note, another practical advantage of the design itself for jet turbine powered aircraft operations will be the ability to run continually without having to stop to purge and cool the tunnel air as was the case, and may be still a problem with the 40- by 80-.

If we want to push the size limit again, the 80- by 120- will enable us to use full scale and, therefore be more able to take advantage of the combination of a viable power plant and a "boiler plated" aircraft. The advantage of this can be seen by noting the characteristics of the intermediate sized engines of Figure 14 where it can be seen that there is a lack of low bypass ratio engines available for use with large scale models of high speed aircraft designs. For reference, the physical size of these engines are compared in Figure 15 and it should be mentioned that the accessory locations on some of the turbojet engines has made actual scaling of intermediate scaled nacelles difficult. The ability to use the actual full scale propulsion systems will help this problem.

And, not to be over looked, will be the ability to test a light transport aircraft, which could have complicated systems of powered lift as shown in Figure 16 and evaluate full, and safely, the functioning of flaps, controls, and propulsion systems. The aircraft tested could take advantage of all the flight instrumentation, as has been done in previous 40- by 80-tests as well as other measurements not possible in flight testing.

## Concluding Remarks

The Ames programs for testing, at large scale, ejector powered aircraft configurations have been outlined. The advantages of testing at large scale, particularly in the case of ejectors, are evident and should be considered in planning all future development programs. The new Ames Large Scale Wind Tunnel system will increase the scope of the tests.

161

# References

1. Workshop on Thrust Augmenting Ejectors, Ames Research Center, Moffett Field, California, June 28-29, 1978, NASA CP-2093.

2. Garland, D.B., and Whittley, D.C.; "Phase 1 Wind Tunnel Tests of the J-97 Powered, External Augmentor V/STOL Model", Report prepared for NASA/Ames Research Center and Canadian Dept. of National Defense, NASA CR-152255.

3. Garland, D.B., and Harris, J.L.; "Phase 2 and 3 Wind Tunnel Tests of the J-97 Powered, External Augmentor V/STOL Model", Report prepared for NASA/Ames Research Center and Canadian Dept. of National Defense.

4. Gilbertson, F.F., and Garland D.B.; "Static Test of the J-97 Powered External Augmentor V/STOL Model at the NASA/Ames and Canadian Dept. of National Defense, NASA CR-152404.

5. Whittley, D.C. and Koenig, D.G.; "Large-Scale Model Tests of a New Technology V/STOL Concept", AIAA Paper No. 80-0233, AIAA 18th Aerospace Sciences Meeting, Pasadena, CA. January 45-16, 1980.

6. Lummus, J.R.; "Study of Aerodynamic for a V/STOL Fighter/Attack Aircraft" May 1978, NASA CR-152128, General Dynamics.

7. Alperin, Morton and Wu, J.J.; "Recent Development of a Jet Diffuser Ejector", AIAA Paper No. 80-0231, AIAA 18th Aerospace Sciences Meeting, January 14-15, 1980, Pasadena, CA.

8. Alperin, Morton, and Wu, Jiunn-Jeng Wu; "A Jet-Diffuser Ejector for a V/STOL Fighter", Flight Dynamics Research Corporation, Final Report prepared for NASA/Ames Research Center annd Naval Air Development Center, NASA CR-166161, February 1981.

9. Falarski, M.D. and Whitten, P.D.; "Aerodynamic Characterisitcs of a Large Scale Model of a Highly Maneuverable Supersonic V/STOL Fighter: STOL Configuration", AIAA Paper 80-0234, January 14-16, 1980 Pasadena, CA, AIAA 18th Aerospace Sciences Meeting.

10. Koenig, David G., Aiken, Thomas N. and Aoyagi, Kiyoshi, Large Scale V/STOL Testing, AIAA Paper 77-586 and NASA TMX 73,231.
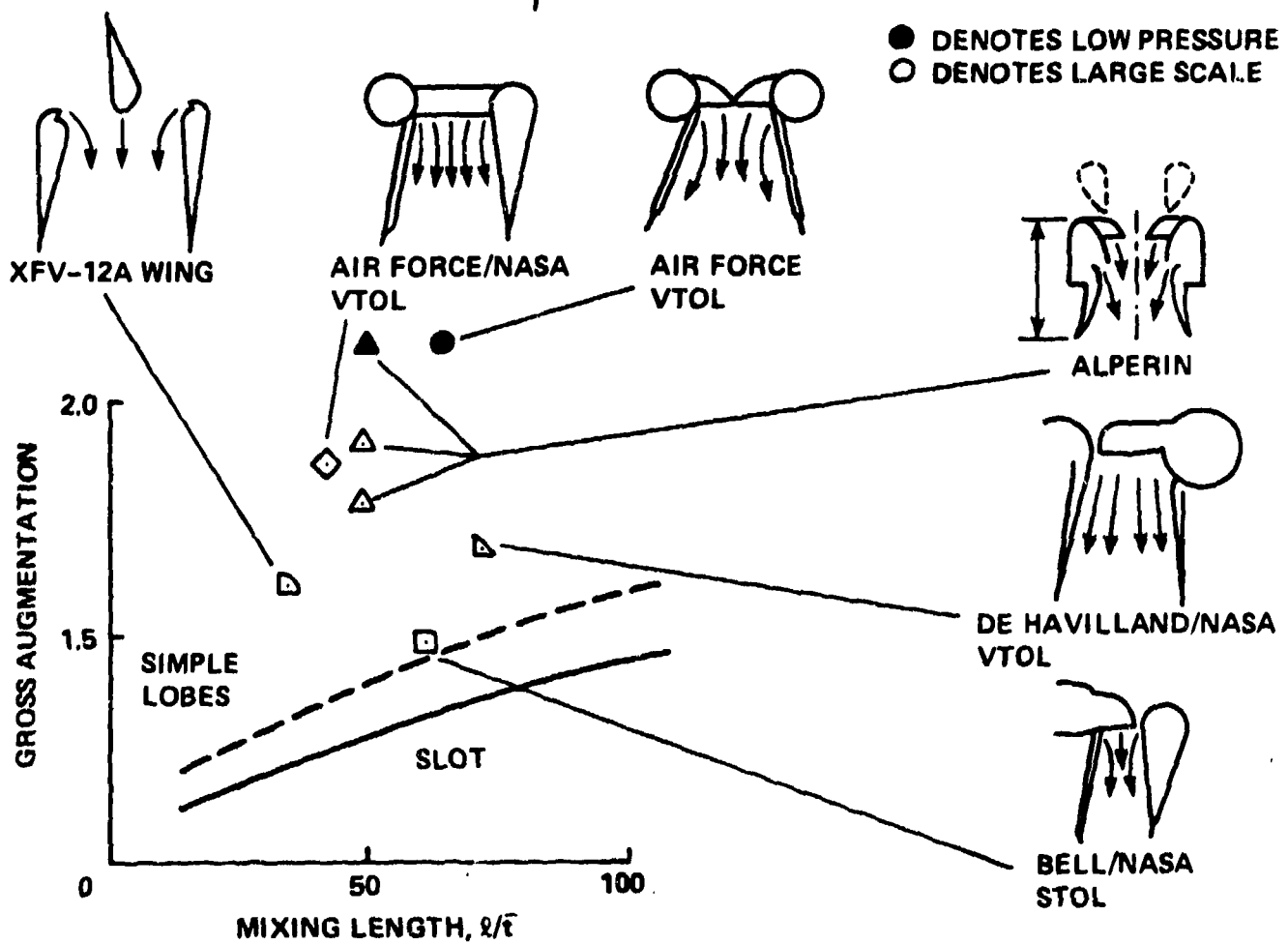
Figure 1. Thrust Augmentor Performance

# THRUSTING EJECTOR CONCEPTS FOR V/STOL AIRCRAFT



(a) FUSELAGE EJECTOR

(b) SHORT DIFFUSER EJECTOR

(c) SPANWISE EJECTOR
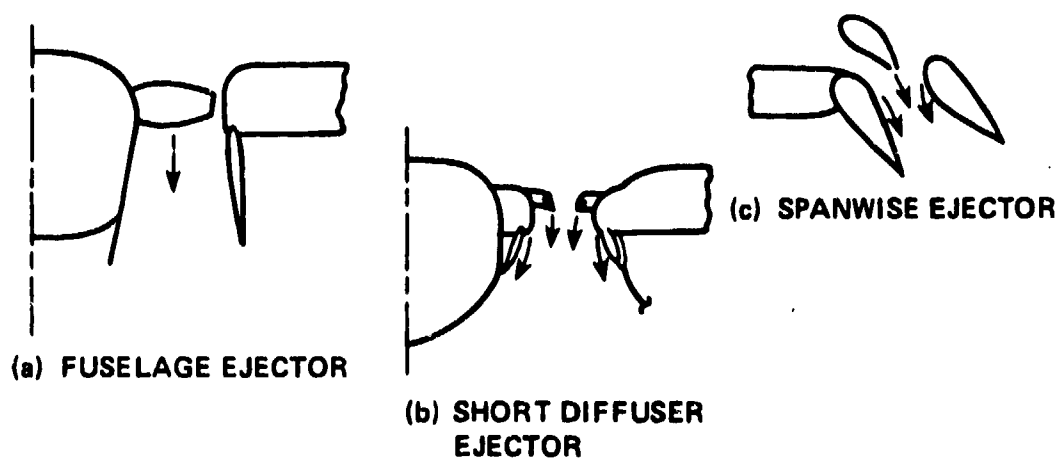
Figure 2. Thrusting Ejector Concepts for V/STOL Aircraft

# THRUSTING EJECTOR CONCEPTS FOR STOL AIRCRAFT



| (a) EXTERNAL EJECTOR | (b) CRUISE AUGMENTOR | (c) SPANWISE EJECTOR |
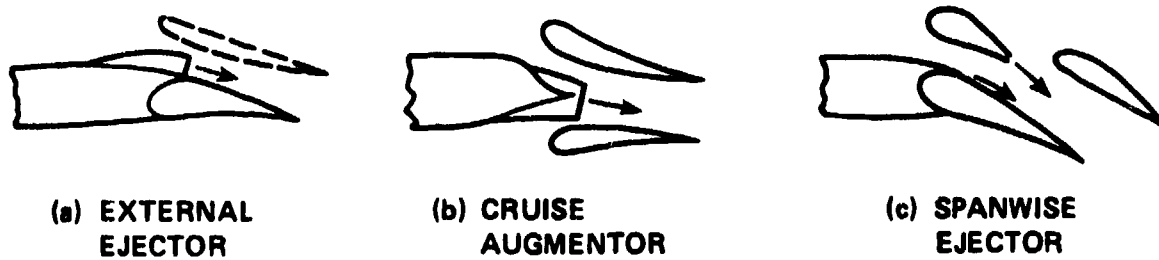
Figure 3.  Thrusting Ejector Concepts for STOL Aircraft

**FIGURE 4 FUSELAGE EJECTOR MODEL MOUNTED IN THE AMES 40-80 FOOT WIND TUNNEL**

**Figure 5. Single Engine V/STOL Ejector Fighter Conceptual Design**

# GENERAL DYNAMICS GD E-3 DESIGN OF EJECTOR FIGHTER



**32 ft 4.8 in.**
**— OVERALL SPAN →**

**50.5 ft OVERALL LENGTH**

**16 ft 8 in.**
**OVERALL HEIGI**
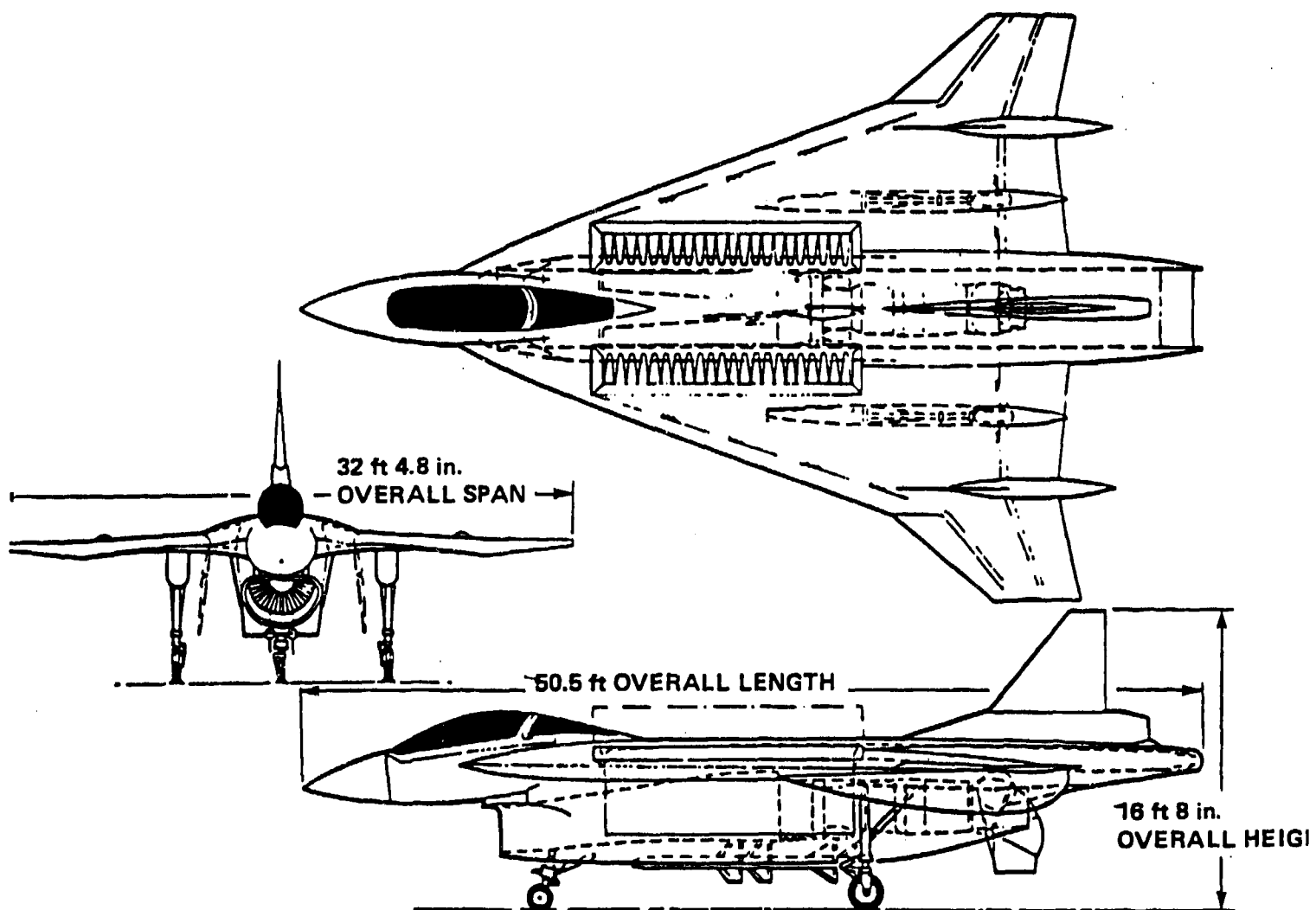
Figure 6.  General Dynamics GD E-3 Design of Ejector Fighter

168

# GENERAL DYNAMICS CONFIGURATION E205,

FUEL

EJECTOR AREA  FUEL  EJECTOR AREA  FUEL

FLAPS

FUEL

AVIONICS BAY

FUEL BAY

JET FLAP

SPANWISE BLOWING PORT

0    100    200    300    400    500
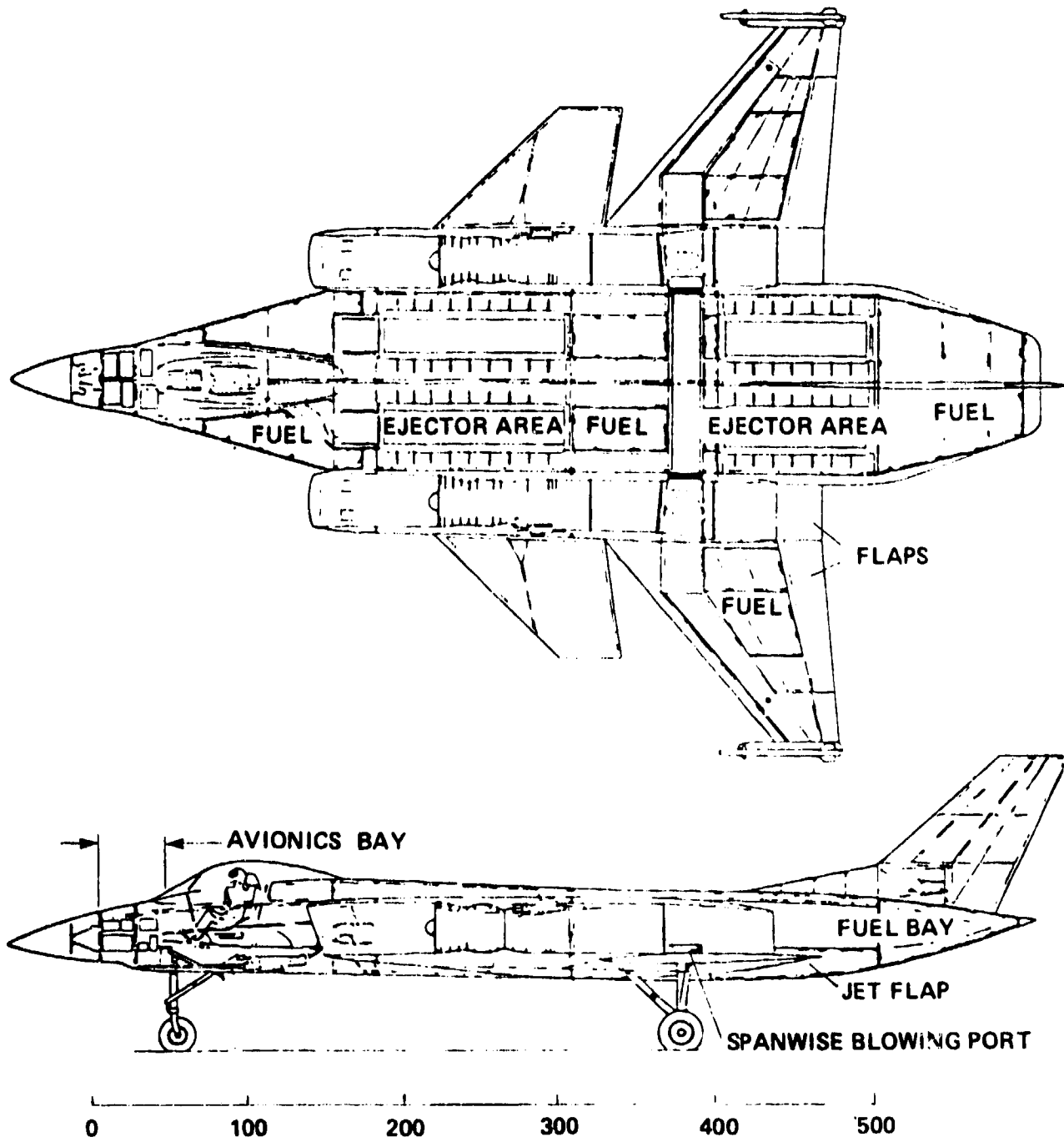
Figure 7.  General Dynamics Configuration E205,

# REVISED GD 205 DESIGN WITH A SHORT
# DIFFUSER EJECTOR



F30

FS106

FS101.09

45°

40°

WL 332

WL 26.74

SECTION BL 6.25 AND INBOARD
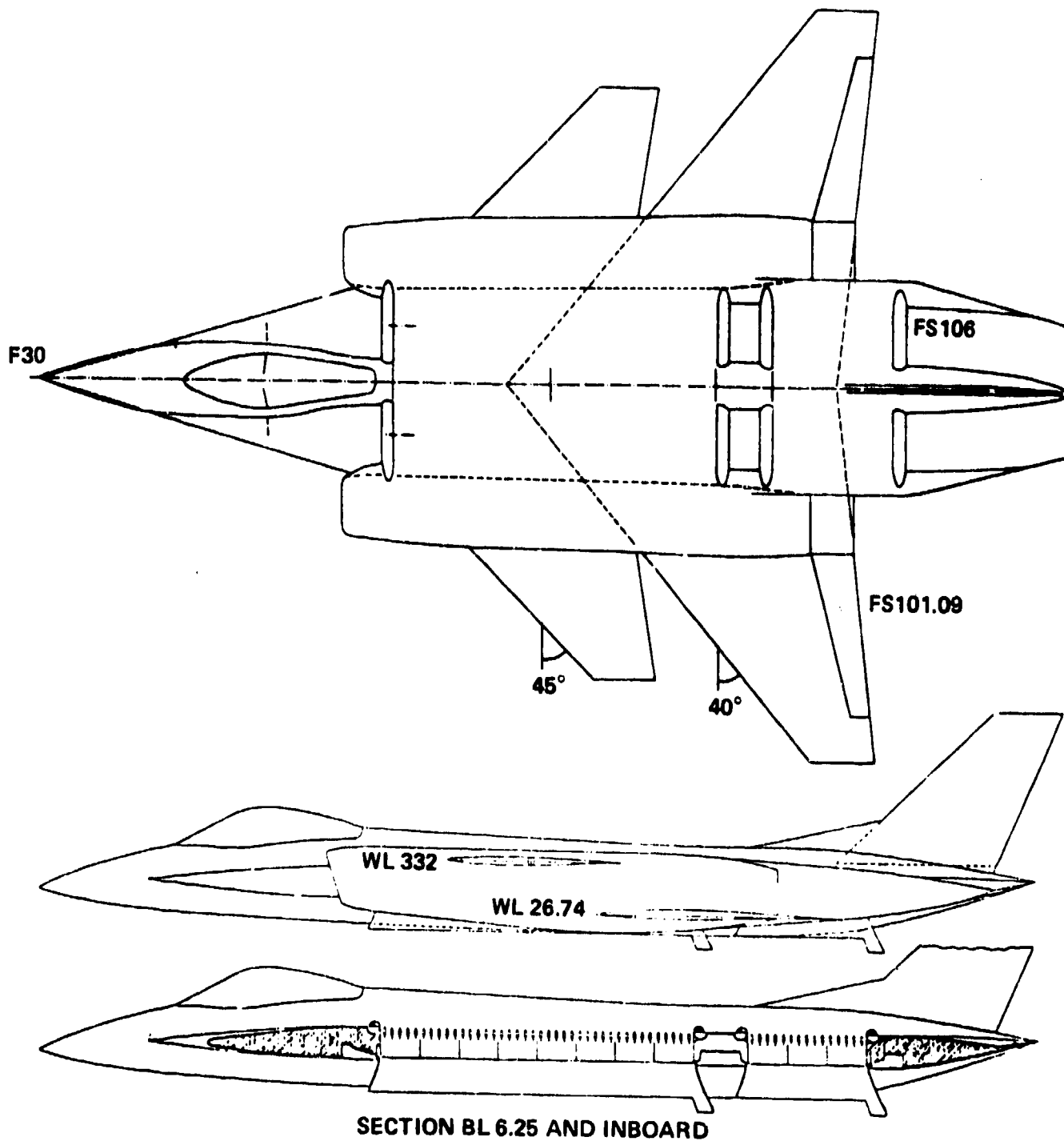
Figure 8. Revised GD 205 Design with a Short Diffuser Ejector
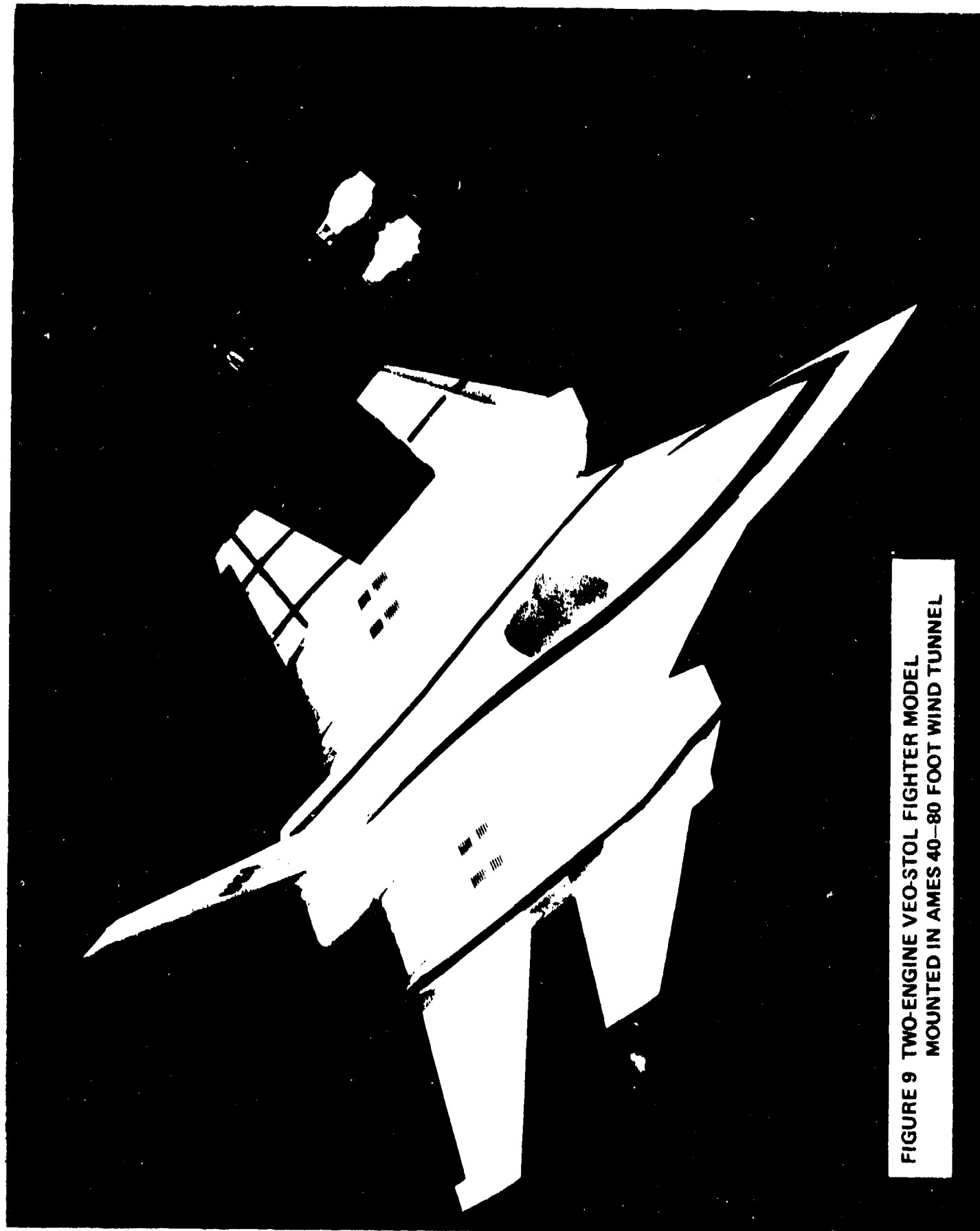
FIGURE 9  TWO-ENGINE VEO-STOL FIGHTER MODEL
MOUNTED IN AMES 40–80 FOOT WIND TUNNEL
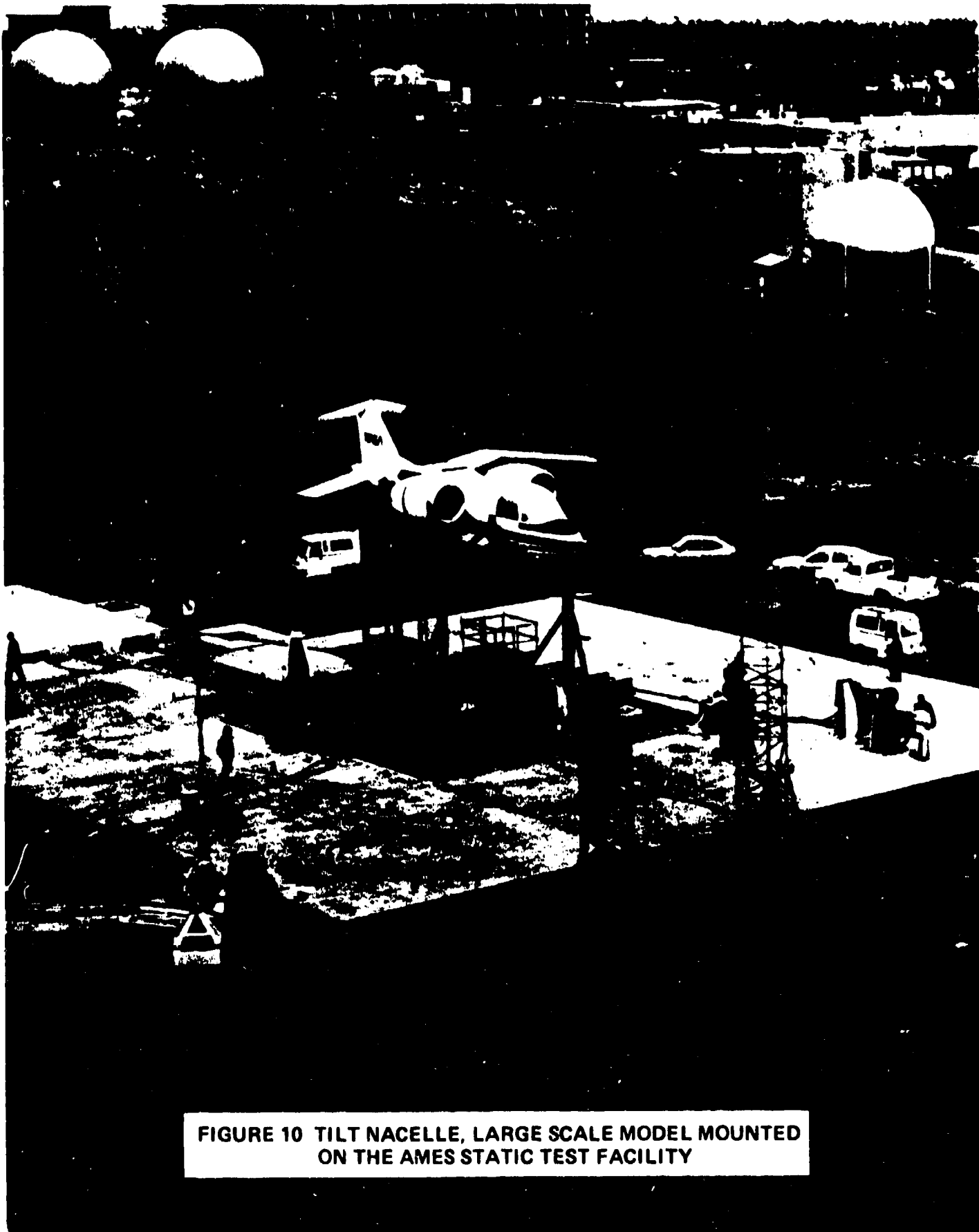
FIGURE 10 TILT NACELLE, LARGE SCALE MODEL MOUNTED
ON THE AMES STATIC TEST FACILITY

# MEASUREMENTS USING LARGE AND SMALL SCALE MODELS

**LARGE SCALE**

- **AERODYNAMIC PERFORMANCE**
- **STABILITY AND CONTROL**
- **INLET**
- **EXHAUST GAS INGESTION**
- **DEFLECTOR PERFORMANCE**
- **PRESSURE DISTRIBUTION**

- **NOISE → FARFIELD ↘ NEARFIELD**
- **FLOW SURVEYS**
- **STEADY AND FLUCTUATING LOADS**
- **GROUND EFFECT**

**SMALL SCALE**
**COMPONENT TESTS**
- **INLET**
- **INGESTION**
- **DEFLECTOR PERFORMANCE**
- **LOADS**

**COMPLETE MODEL TESTS**
- **PERFORMANCE**
- **STABILITY AND CONTROL**
- **PRESSURE DISTRIBUTION**
- **INGESTION**

Figure 11.—

# AMES LARGE SCALE WIND TUNNEL SYSTEM

**12 X 24-m
(40 X 80-ft)
TEST SECTION
100 m/s → 150 m/s
(200 knots → 300 knots)**

**24 X 37-m
(80 X 120-ft)
TEST SECTION
50 m/s
(100 knots)**

**DRIVE
27 MW → 100 MW
(36,000 hp → 135,000 hp)**
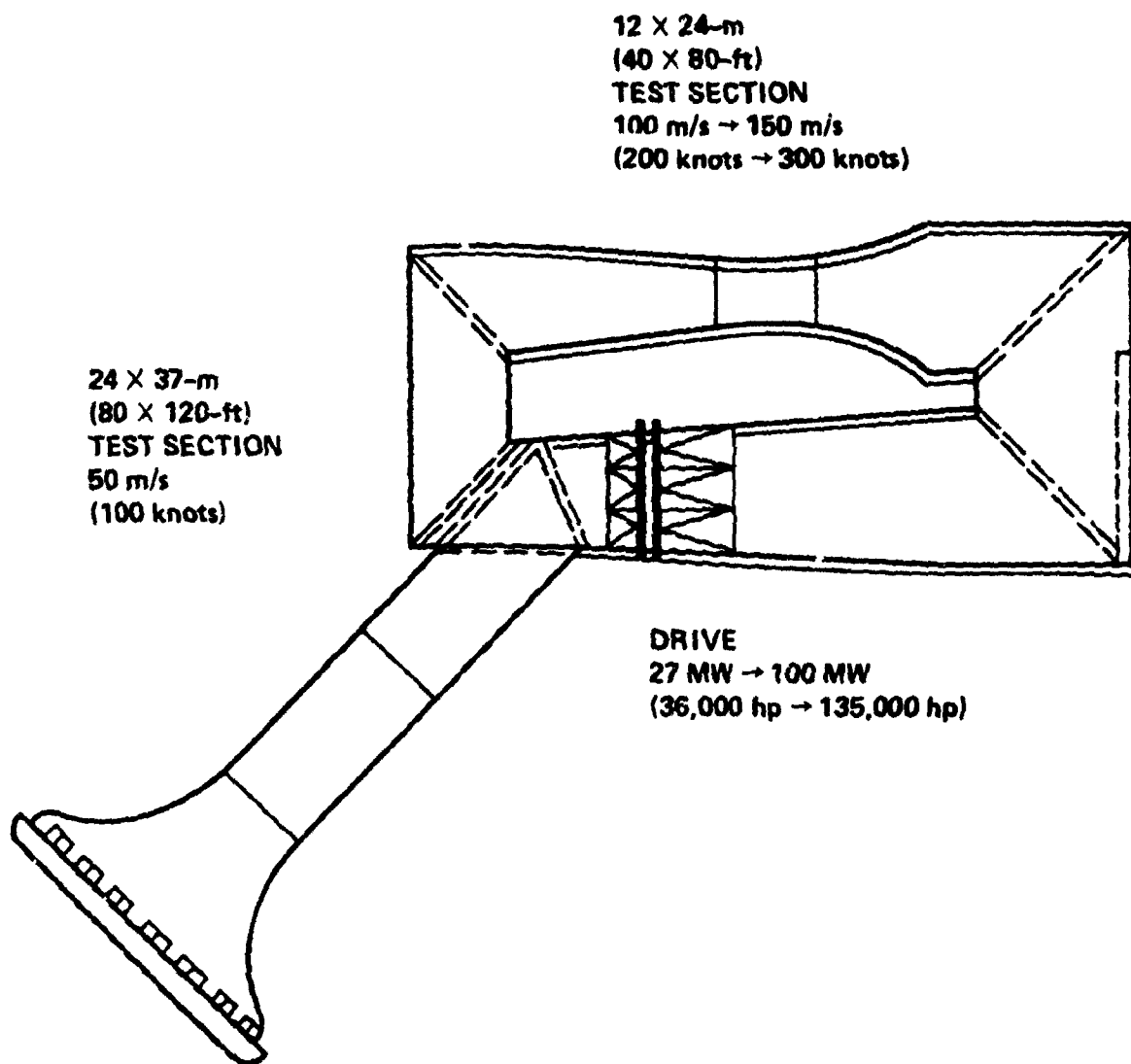
Figure 12. Ames Large Scale Wind Tunnel System

174

# MOMENTUM AREA SIZING FOR THE 40 x 80
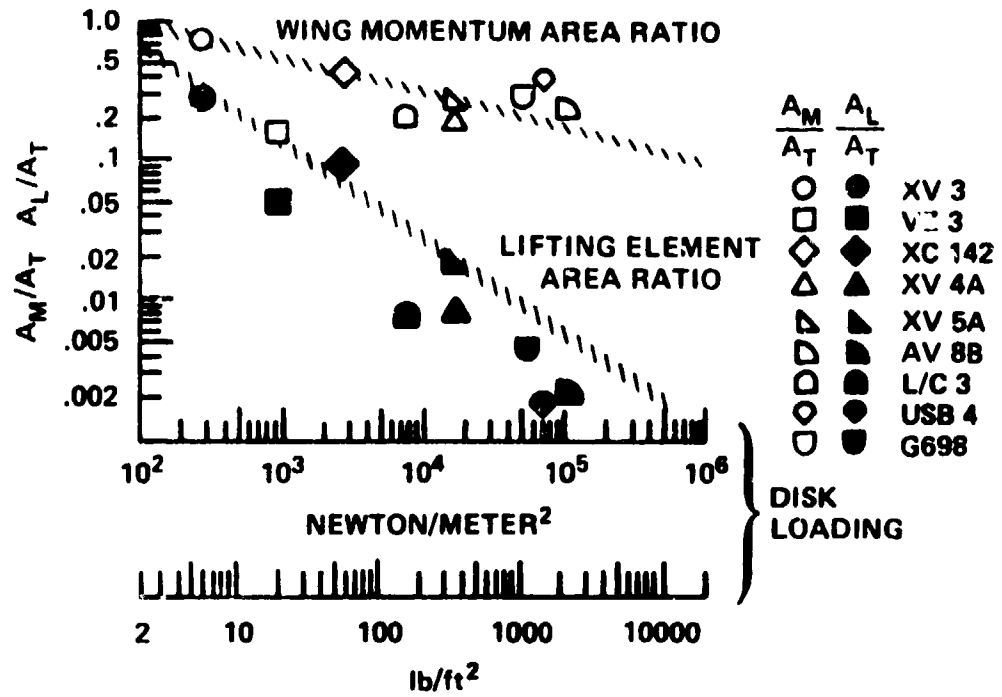


Figure 13. Momentum Area Sizing for the 40 x 80

# SUMMARY OF POSSIBLE GAS ENERGY SOURCES FOR SCALED MODELS.
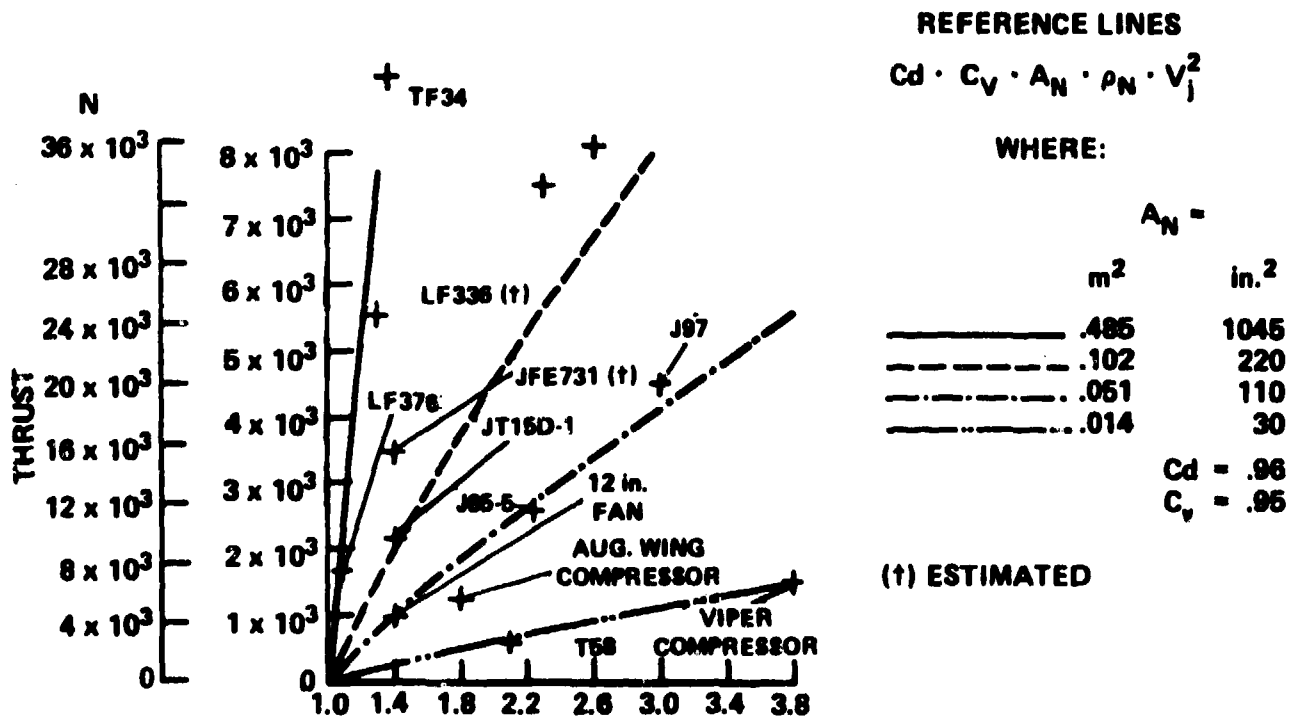


Figure 14. Summary of Possible Gas Energy Sources for Scaled Models

# TURBOFAN OR TURBOJET ENGINES AVAILABLE FOR USE IN LARGE SCALE V/STOL TESTING

| | THRUST | | W | | $P_T/P_O$ | $A_e$ | |
|---|---|---|---|---|---|---|---|
| | N | (lb) | kg/sec | (lb/sec) | | $m^2$ | $in.^2$ |
| J85-5 | 11,560 | (2600) | 19.3 | (42.5) | 2.24 | .074 | (115) |
| T58 | 2,670 | (600) | 5.7 | (12.5) | 2.1 | .019 | (29.2) |
| J97 | 20,020 | (4500) | 31.8 | (70) | 3.0 | .084 | (130) |
| JT15-D | 8,450 | (1900) | 34.0 | (75) | 1.35 | .142 | (220) |
| TF-34 | 40,030 | (9000) | 145.2 | (320) | 1.48 | .581 | (900) |



|  |  |
|---|---|
| ——— | J85-5 |
| — — | T58 |
| ········ | J97 |
| —·— | JT15-D |
| — —· | TF-34 |
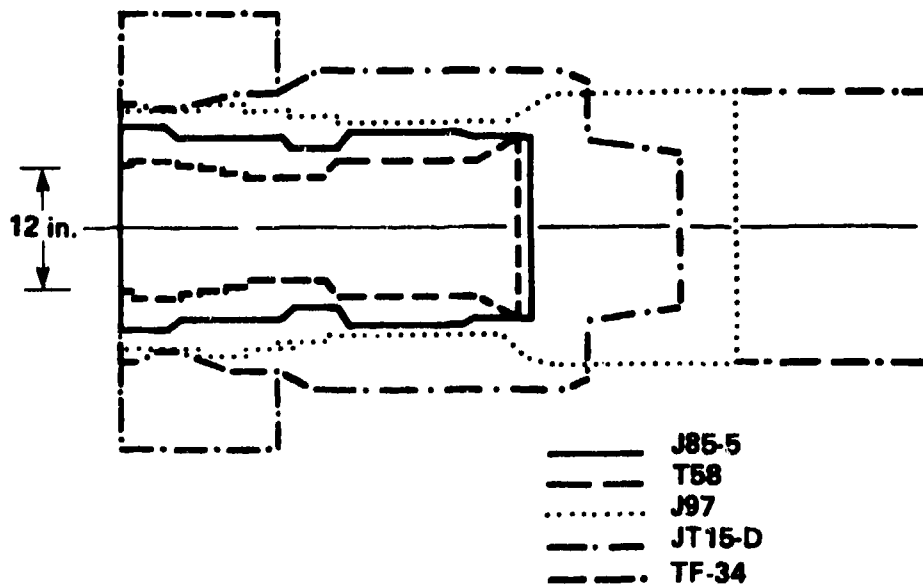
Figure 15. Turbofan or Turbojet Engines Available for Use in Large Scale V/STOL Testing

# POWERED LIFT TRANSPORT AIRCRAFT
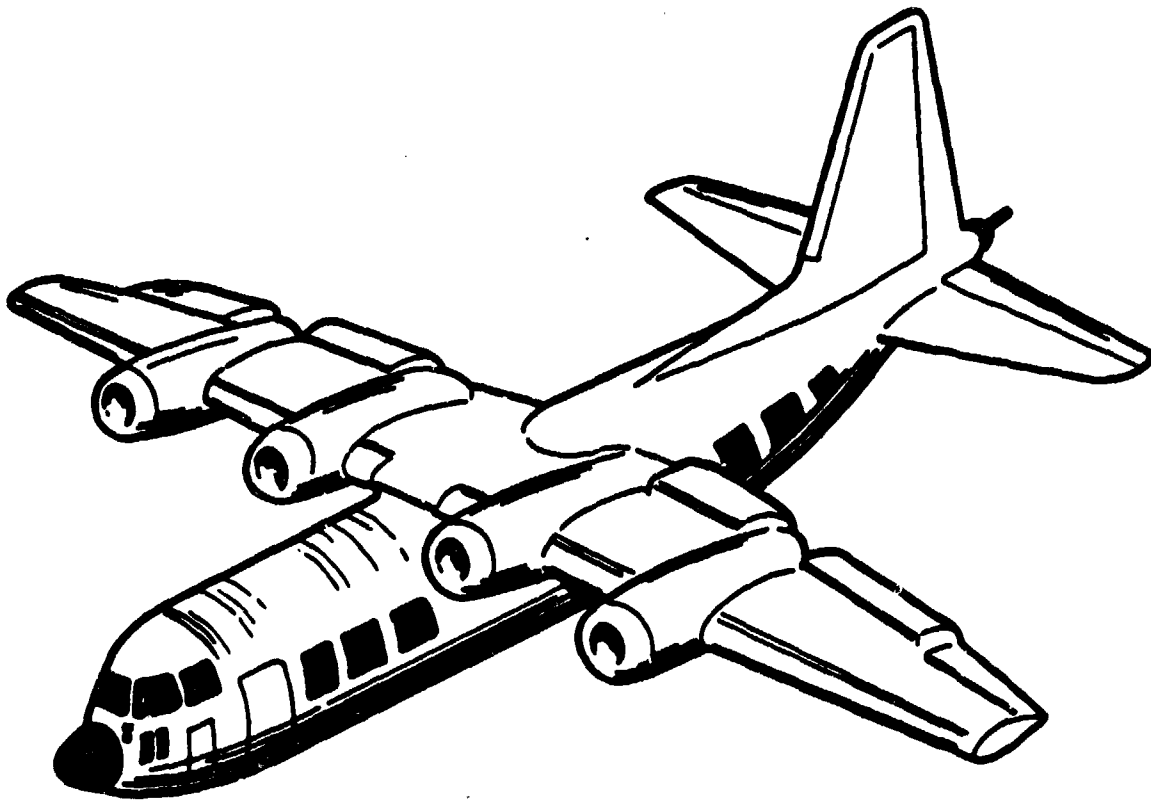


Figure 16. Powered Lift Transport Aircraft
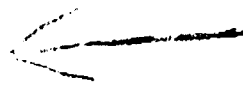
# CHARACTERISTICS OF HIGH PERFORMANCE EJECTORS

J. E. Minardi
University of Dayton
Research Institute
300 College Park Avenue
Dayton, Ohio 45469

## FOREWORD

The paper which was presented in the workshop reports the results of an effort performed under AFWAL/FDL Contract No. F33615-81-K-3017. The results have also been published as an AFWAL Technical Report bearing the number TR-81-3170. For completeness of the workshop purpose, as the effort breaks new ideas and extends the state-of-the-art of ejector technology, the paper is included in the workshop proceedings.

## ABSTRACT

The use of ejectors in energy conversion processes and thrust augmentation requires that the mixed flow be produced at a high efficiency. Although many definitions of efficiency have been used to describe the efficiency of an ejector, we have used an efficiency based on thermodynamic availability which is referenced to the stagnation properties of the secondary flow (the flow being "pumped"). As is well known, a compressible-flow, control-volume approach to analyzing a constant area ejector yields two solutions: one with a subsonic mixed flow and one with a super-sonic mixed flow. The supersonic mixed flow produces the best efficiencies and highest total pressures. The properties of the supersonic mixed flow are of necessity related to the properties of the subsonic mixed flow by the normal shock relations. None-theless, in practice, the subsonic mixed flow is, in general, not achieved through a normal shock (or pseudo-normal shock) from the supersonic mixed flow solution.

If the ejector has a supersonic primary flow at the inlet and if the resulting mixed flow is supersonic, then the highest effi-ciencies are achieved with a subsonic secondary flow at the inlet. Thus, this is the most favorable condition to operate an ejector. Other regions of the solution with supersonic mixed flow do not violate the second law but produce mixed flows that have higher kinetic energies when expanded to ambient pressure than the kinetic energy in the primary flow when expanded to the same pressure.

In this paper, these conditions are investigated and thermo-dynamic processes and associated devices are identified which would be able to achieve this performance, consistent with the control volume requirements upon which the ejector analysis is based. It is important to determine the conditions and range of operation that can actually be achieved in an ejector. This is accomplished in this paper.

If the exit flow from the ejector is subsonic, the back pressure (or the effective back pressure if there is a diffuser) determines where the ejector will operate: that is, the inlet secondary flow Mach number is determined by the pressure boundary condition at the exit for a given geometry and given stanation conditions of the primary and secondary fluids. However, if the back pressure is low enough, then the mixed flow at the exit is supersonic and the operating condition is independent of the back pressure at lower values. Thus, for a supersonic mixed flow at the exit, some other condition is required to determine the operating point. This condition is given in the paper and incorporated in the analysis.

A model is presented that gives a physical interpretation to the various solutions obtained from the mathematics, and more importantly, some fundamental limits are presented and a procedure is developed for determining the efficiency that can be achieved in a constant area ejector when the mixed flow is supersonic.

# TABLE OF CONTENTS

# LIST OF ILLUSTRATIONS

## LIST OF ILLUSTRATIONS (Continued)

# SECTION 1
## INTRODUCTION

For many years ejectors have found wide applications in jet pumps, steam-jet refrigeration, mercury diffusion pumps, etc. More recently ejectors have been investigated for flight applications especially as a method of thrust augmentation and their potential usefulness has been demonstrated in experimental aircraft.

The topic of ejectors has been extensively studied over the years: a recent publication by Porter and Squyers[1] lists over 1,600 references concerning ejector systems and related topics. Analyses of the mixing problem can be divided into two general types: detailed mixing models using the Navier-Stokes equations or the control volume approaches which use integrated forms of the conservation equations of mass, momentum, and energy. The one-dimensional control-volume approach using a compressible fluid was chosen for this study since it affords the best vehicle for the parametric studies required to understand the potential of ejectors for a given application.

It has been known for some time (see for example references 2 through 5) that the analyses of a constant area ejector lead to a double valued solution: one where the mixed flow is subsonic and the other where the mixed flow is supersonic. Further, it is well known that these two solutions are related by the normal shock relations.

Recently, Alperin and Wu[6] have pointed out the potential advantages of the supersonic branch for applications to thrust augmentation. Minardi, et al,[7] who were recently studying two fluid ejectors for applications in turbines at the University of Dayton Research Institute (UDRI), found results for their applications that were consistent with those of Alperin and Wu. Both studies indicated that extremely high efficiencies could be

189

obtained on the supersonic branch. It was the purpose of this
study to determine fundamental performance characteristics and
limitations of these high performance ejectors to establish a
basis for their application to thrust augmentation.

# SECTION 2
## CONTROL VOLUME ANALYSIS

Two types of ejectors are widely considered: the constant area ejector and the constant pressure ejector. We will concern ourselves mainly with the constant area ejector, a schematic of which is shown on Figure 1. Of course, a flightworthy ejector used for thrust augmentation would have many essential elements that must be properly integrated. A good discussion of such an integration is given by Alperin and Wu.[6]. The major elements are the flight inlet diffusers for the engine and bypass air, the jet engine itself, the inlet nozzle geometry for the secondary air (bypass air) to the ejector, the inlet geometry for the primary gas (engine gas le.ving the turbine) the ejector mixing tube and finally, the diffusor (or nozzle) where the mixed flow exits to the atmosphere. We are going to concentrate only on the ejector since the other elements, although not simple, are well understood and have found wide application in flight vehicles.

For example, a better bypass air inlet would simply produce a higher value of secondary inlet air total pressure $P_{os}$. (See Figure 1) The ideal inlet would produce a value of $P_{os}$ equal to the isentropic stagnation pressure determined by the flight Mach number. A better exit diffusor would allow the ejector to exhaust to a higher back pressure, $P_{back}$ (see Figure 1). An ideal isentropic diffusor would allow the ejector to exhaust the flow into a back pressure equal to the total pressure of the mixed flow at the exit, $P_{om}$ (the mixed flow at station m of Figure 1).

However, to understand the essential features of an ejector it is best to first consider only the simple schematic of Figure 1 where the stagnation conditions of the primary and secondary gasses are considered given and that the back pressure, $P_{back}$, can be adjusted to any designed value. In this way, the essential features of the ejector will not be masked by the

191
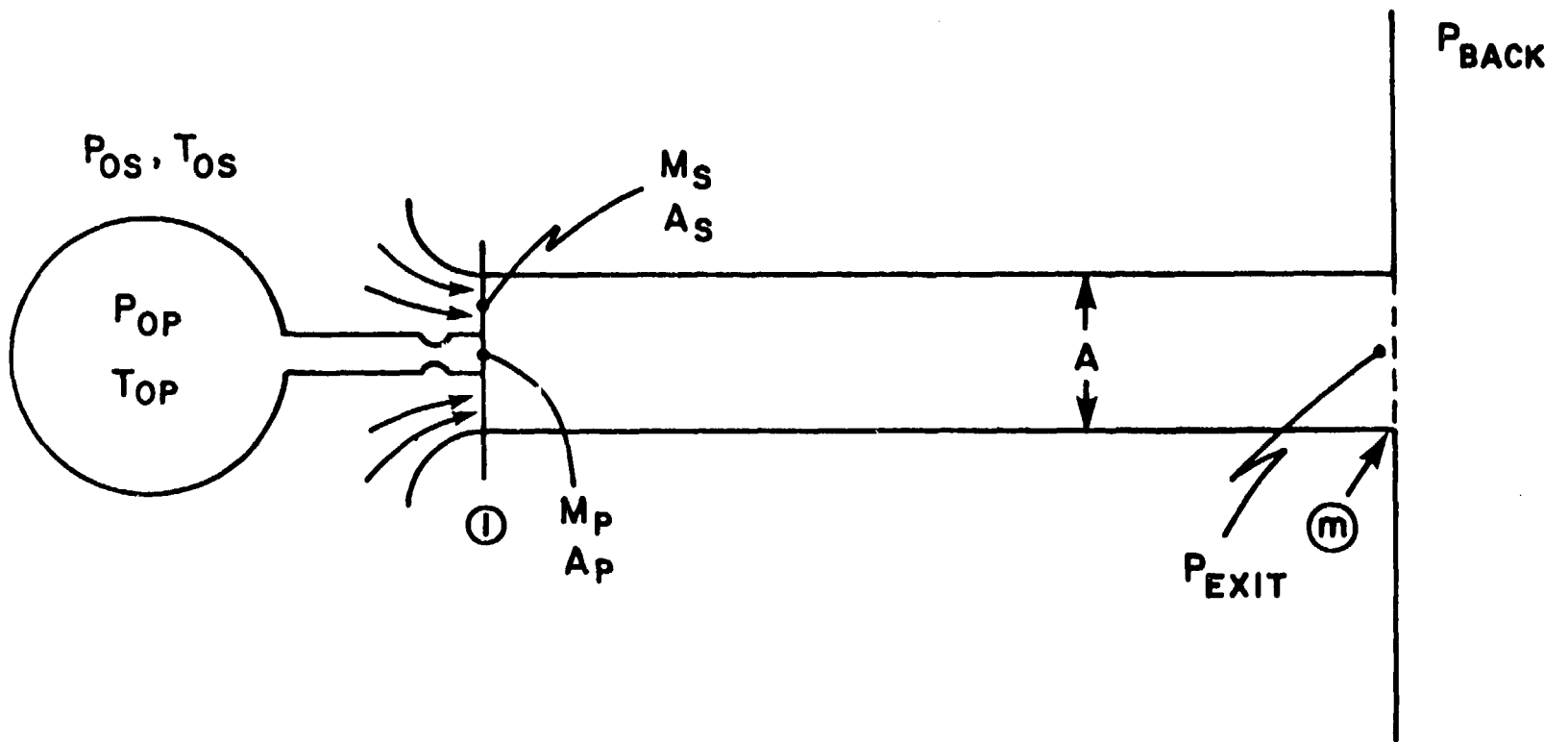
Figure 1. Constant Area Ejector.

features of the other elements, especially the exit diffusor. However, a word of warning may be in order: a poor diffusor can completely obviate the value of a good ejector.

The usual conditions that are applied to constant area mixing are as follows:

1) The flow is steady and the enthalpy is constant,

2) The exit area (A in Figure 1) is equal to the sum of the inlet areas of the primary flow $A_P$ and the secondary flow $A_s$, and

3) No net pressure forces are acting on the ejector walls (friction forces are frequently accounted for).

Condition 1 is an obvious, reasonable assumption. Conditions 2 and 3 follow directly from the constant area geometry. However, condition 2 could also be valid for a nonconstant area geometry and it is conceivable that condition 3 might also hold for some nonconstant area geometry where the exit area equals the inlet areas. Thus, the constant area geometry is a sufficient condition to yield the three conditions stated above but not a necessary condition. This will be discussed in greater detail later in this report.

In view of Figure 1 and the conditions stated above, we can write the following equations for one-dimensional flow that is completely mixed at station m.

Continuity:

$$\rho_{1s} A_s V_s + \rho_{1P} A_P V_P = \rho_m A V_m \tag{1}$$

or

$$\dot{m}_s + \dot{m}_p = \dot{m}_m \tag{1'}$$

Energy:

$$\dot{m}_s h_{os} + \dot{m}_p h_{op} = \dot{m}_m h_{om} \tag{2}$$

Momentum:

$$P_{1p}A_p + \dot{m}_p V_p + P_{1s}A_s + \dot{m}_s V_s = P_m A + \dot{m}_m V_m \qquad (3)$$

also from condition 2

$$A = A_s + A_p \qquad (4)$$

If we assume that we have ideal gases then we can solve the above system of equations in a straightforward, though somewhat tedious manner. Our approach to this is given in Reference 7 and in Appendix I. Other equally valid approaches are given in References 2 through 6 and in many of the 1,600 references of Reference 1. It is not our purpose here to review the details of these solutions but rather to discuss some of the results obtained from computer programs based on these solutions.

Figure 2 presents the results for both branches for the solution of the equations for a constant-area ejector with a constant mass flow ratio. The two solution branches are marked subsonic and supersonic on Figure 2. The branch with supersonic mixed flow is referred to by Alperin and Wu[6] as the "second solution." We have also shown the results for a constant pressure solution on Figure 2. The solutions presented are for air driving air with a pressure ratio, $P_r$, of 6 ($P_r \equiv P_{op}/P_{os}$) and a temperature ratio, $T_r$, of 3.7 ($T_r \equiv T_{op}/T_{os}$). These ratios are representative of what might be possible with a modern jet engine. The mass flow ratio (MR $= \dot{m}_p/\dot{m}_s$) was taken as 0.1 (or a bypass ratio of 10). The efficiency based on availability is plotted as a function of the secondary inlet Mach number $M_s$. The primary inlet Mach number, $M_p$ is adjusted to match the pressure at the inlet (i.e., $P_{1p} = P_{1s}$).

The efficiency based on availability is the ratio of the thermodynamic availability in the mixed flow divided by the availability in the incoming primary flow. The availability for both flows is referenced to the stagnation conditions of the secondary flow. The second law requires that the efficiency

194
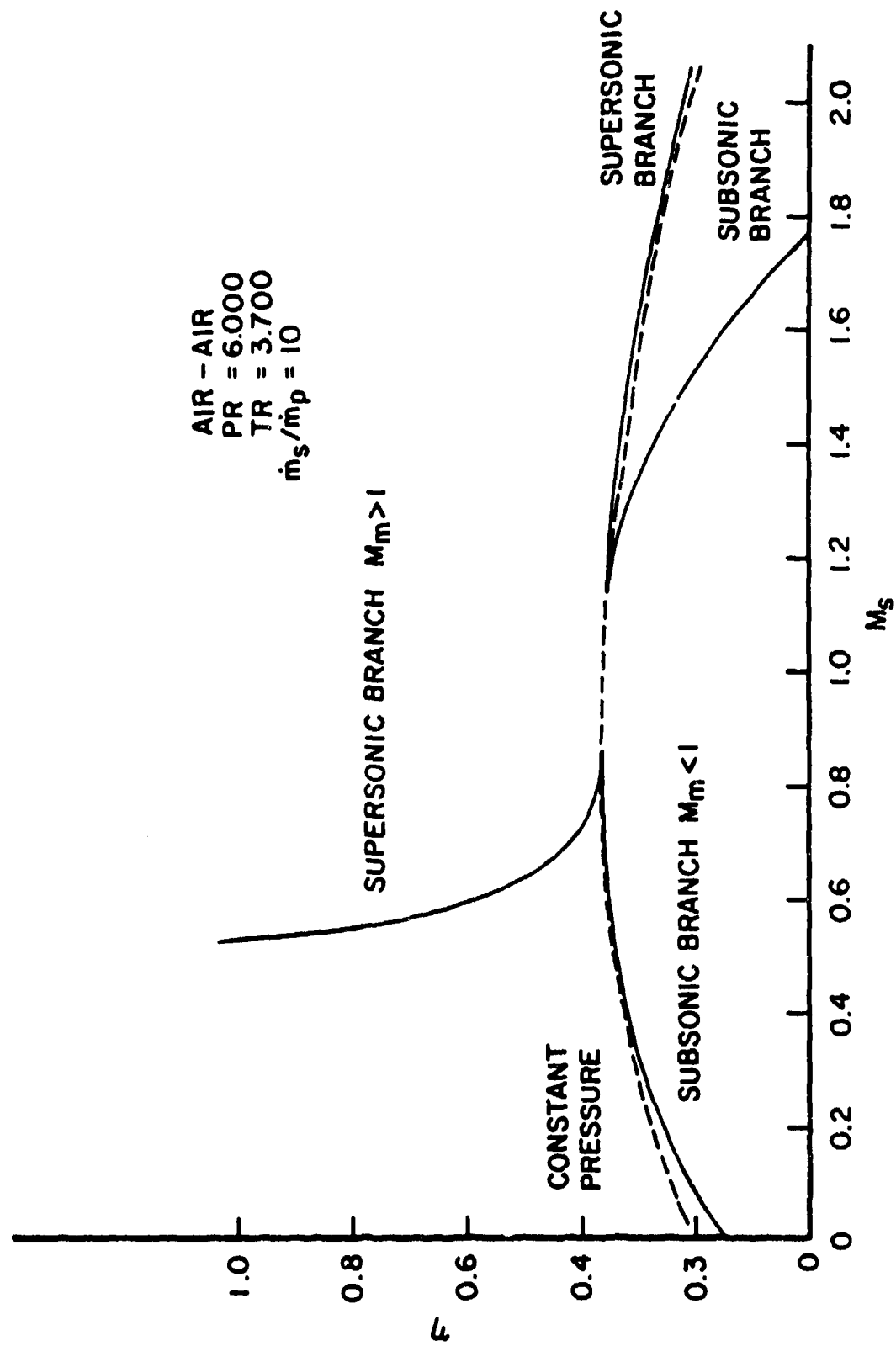
Figure 2. Efficiency Based on Availability versus Secondary Inlet Mach Number for a Bypass Ratio of 10.

195

based on this concept be less than or equal to one for an adiabatic system.

As seen in Figure 2, the value of the efficiency, $\eta$, exceeds one on the supersonic branch at subsonic inlet Mach numbers, $M_s$, less than 1. Also note that a choking of the flow takes place in the constant area case and no real solution exists for a range of secondary inlet Mach numbers, $M_s$. This condition disappears at lower bypass ratios as seen in Figure 3 where all the conditions are the same except that the bypass ratio is 2 instead of 10. Complete tables of data for Figures 2 and 3 are given in Appendix A.

In calculating the data for Figures 2 and 3, we assumed that the inlet pressures of the primary and secondary flows were the same. However, if one of the inlet flows is supersonic then this condition need not be true. In fact, a map of the performance for all combinations of inlet Mach numbers can be developed for both branches of the solution. We developed a computer program based on the work of Hoge[4] to construct such maps. Results of these calculations are shown in Figures 4 and 5 where lines of constant efficiency, based on availability, are drawn in the $M_p^*$-$M_s^*$ plane. (M,* the ratio of velocity to the speed of sound at Mach one, was used since it has a finite maximum value). For Figures 4 and 5 the pressure ratio and temperature ratio are the same as used for Figures 2 and 3. The mass flow ratio MR is 0.1 (bypass ratio of 10) which is the same as for Figure 2. The region of imaginary solutions, called the forbidden region, is a large, egg-shaped region which is cross hatched on Figures 4 and 5. The value of the mixed Mach number on the boundary of this region is one.

The locus of points in the plane where the inlet pressures are equal is the solid line labeled $P_{1p} = P_{1s}$ on Figures 4 and 5. If we took a cut through the two surfaces along this line and plotted the efficiencies versus $M_s$ (instead of $M_s^*$) we would obtain the same results as plotted on Figure 2 for the constant area solutions. The part within the forbidden region, of course,
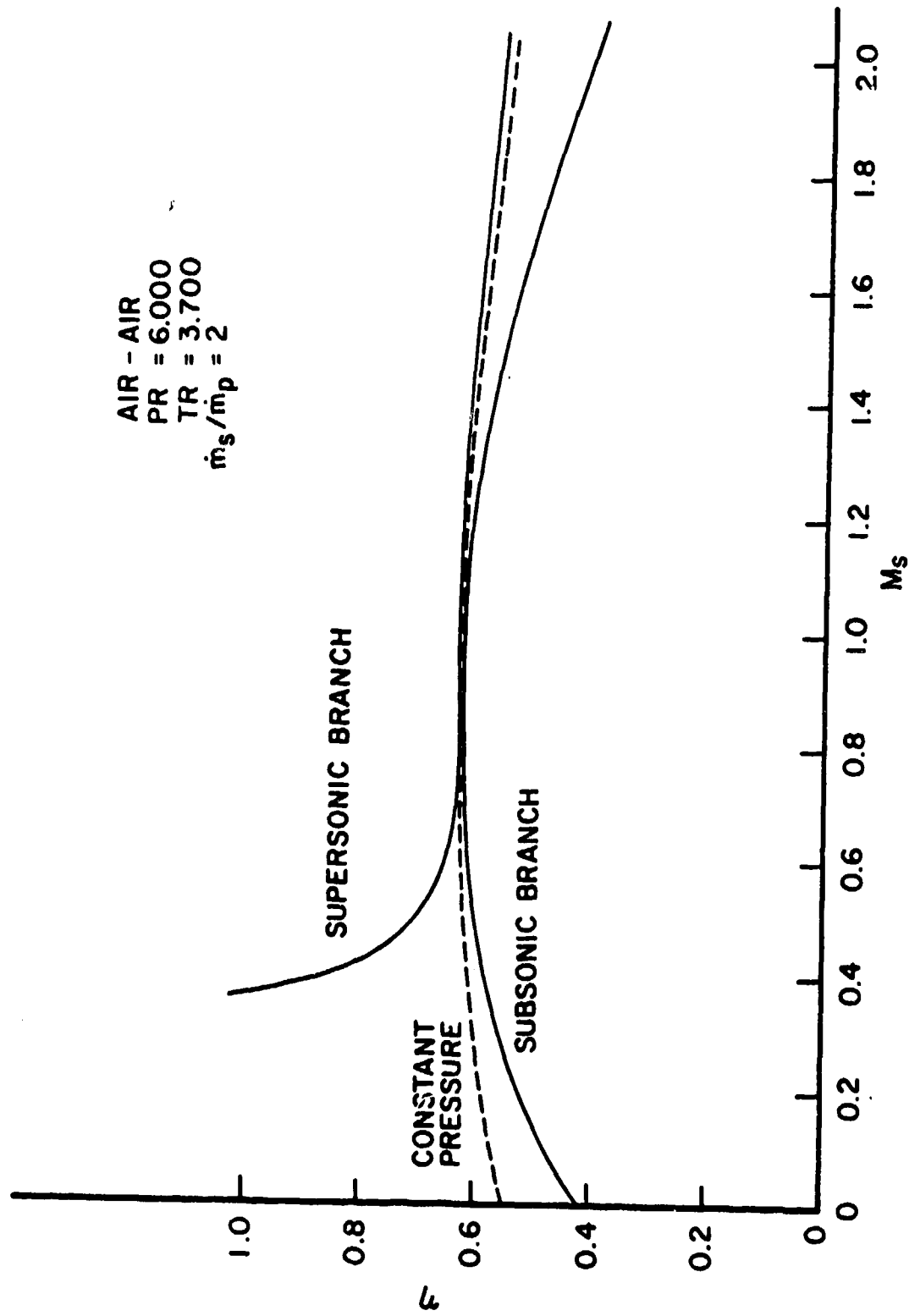
Figure 3. Efficiency Based on Availability versus Secondary Inlet Mach Number for a Bypass Ratio of. 2.
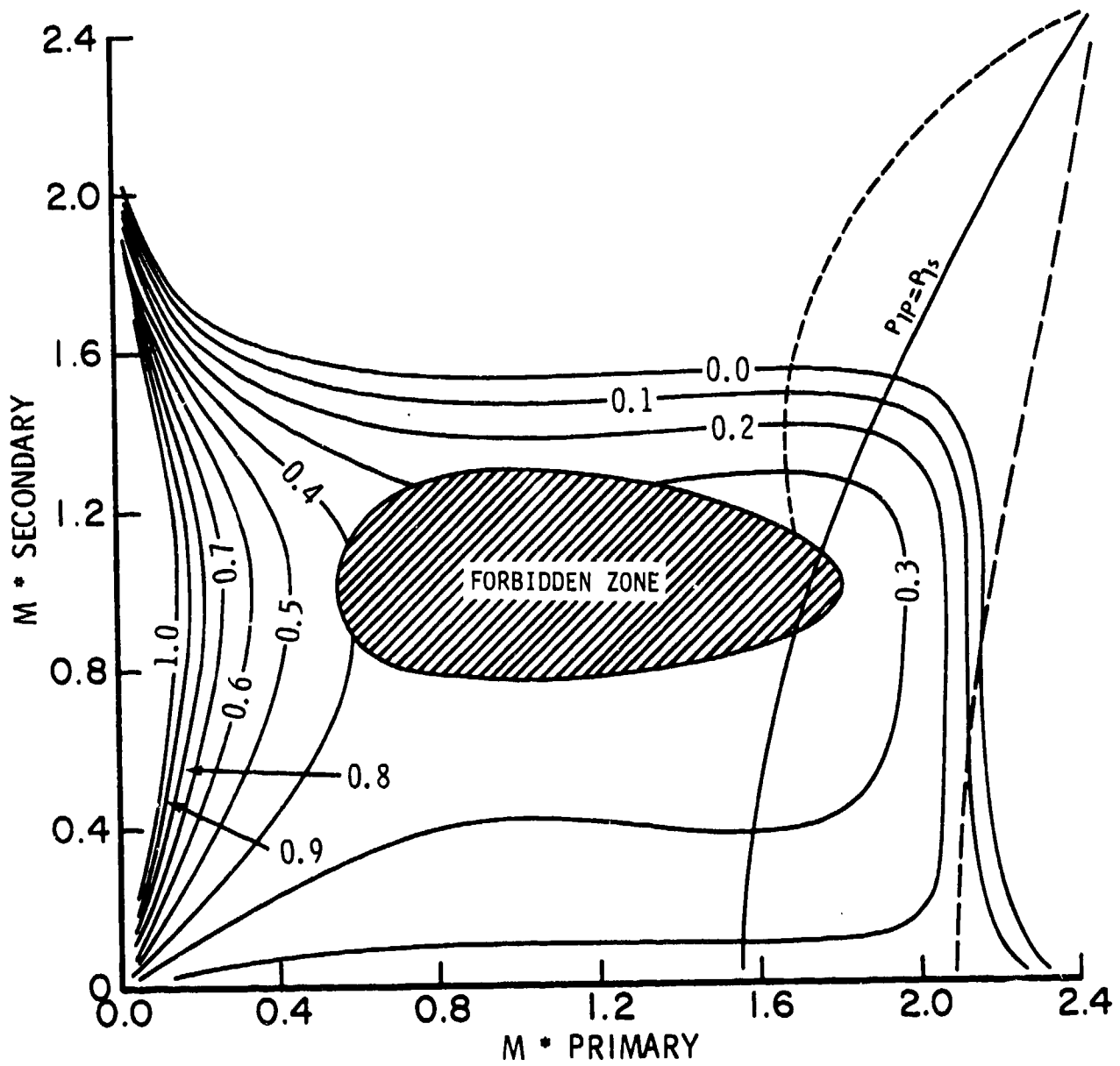
Figure 4. Subsonic Branch Efficiency Map.
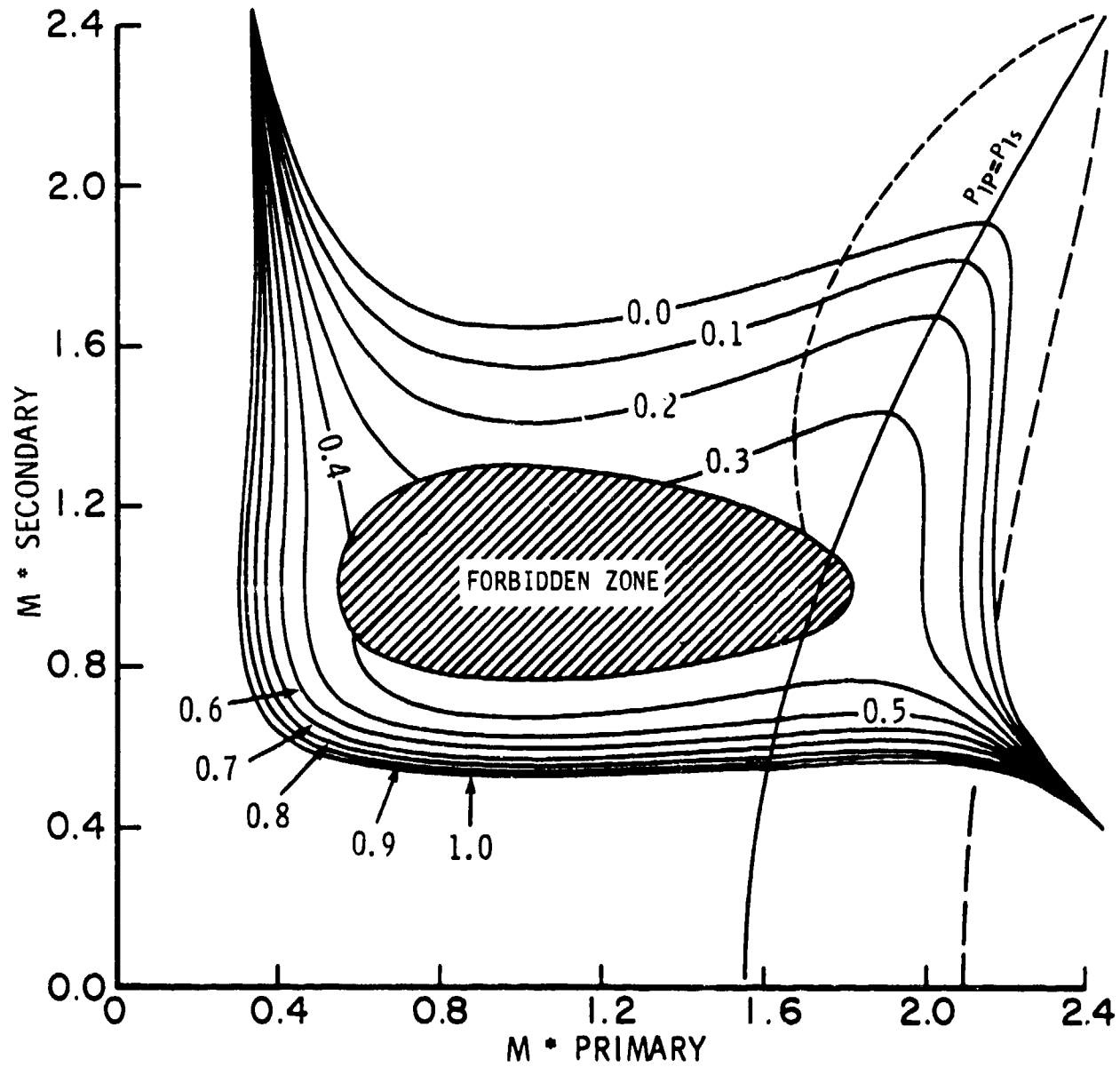
Figure 5.    Supersonic Branch Efficiency Map.

has only imaginary solutions and neither branch is shown on Figure 2 for that range of Mach numbers, $M_s$, that lie within the forbidden region.

It is of interest to note that extremely high efficiencies, equal to or greater than one, are achieved on the subsonic branch (at low $M_p^*$ values of Figure 4) as well as the supersonic branch (see Figure 5). Thus, the high efficiencies are not just a property of the second solution, but can occur on either branch. However, if the condition of equal pressure at the inlet is used, then only the supersonic branch exhibits the extremely high efficiencies.

Figures 4 and 5 illustrate all of the possible solutions that satisfy the equations listed earlier for the given set of conditions. It is quite clear, however, that many of them could not possibly be achieved in an ejector. For example, if both $M_s^*$ and $M_p^*$ are subsonic, then $P_{1p}$ must be equal to $P_{1s}$ is the flows were to enter an ejector. But the locus of points along which this pressure condition holds does not enter the part of the plane where both $M_s^*$ and $M_p^*$ are subsonic. Thus, none of these solutions could occur in an ordinary ejector.

It was considerations such as these that lead to the following set of questions.

1.  Can the supersonic solution be achieved at a subsonic value of secondary inlet mach number $M_s$?

2.  How does one understand the exceptional solutions exemplified by the values at subsonic inlet mach numbers of the second solution?

3.  What are some fundamental limits of performance of mixers?

4.  What are the limits of performance that can actually be achieved on the second solution branch?

In the remainder of the report we will attempt to answer these questions.

# SECTION 3
## ON THE EXISTENCE OF THE SECOND SOLUTION

From the theoretical perspective given below, it will become obvious that the second solution can be achieved in the region where the inlet secondary Mach number is one or less. This is most easily seen if we consider the results for the solution of a constant geometry case in response to operation with different back pressures, $P_b$ of Figure 1. Figures 6 through 9 were obtained for constant geometry. The curves shown on Figure 6 are fundamentally different from those of Figure 2 and 3. All three figures are drawn for constant area ejectors but the geometry of the ejector is different at each value of $M_s$ in either Figure 2 or Figure 3 while the geometry within the control volume is constant for all values of $M_s$ in Figure 6 through 9. In calculating the data for Figures 2 and 3 the mass flow ratio was held constant and a side condition was set: the inlet pressures of the primary and secondary stream were made equal. Thus, the geometry required to produce the same pressure at the inlet and the constant mass flow ratio changes at each value of $M_s$ in either Figure 2 or 3.

Nonetheless, we see that Figure 6 still exhibits the extremely high values of efficiency at the subsonic inlet Mach numbers of the secondary flow on the supersonic branch of the solution (i.e., second solution). The conditions used for calculating the data for Figures 6 through 9 are given on the figures. Figure 7 presents the total pressure of the mixed flow at the exit divided by the total pressure of the secondary gas. Since the total temperature is fixed by the ratio of the mass flow rates only one other thermodynamic property from the stagnation state is required to fix the stagnation state of the mixed flow. Therefore, knowledge of either the total pressure, (from Figure 7) or the availability (from Figure 6) is adequate to fix the stagnation state of the mixed flow. Thus, either Figure 6 or 7 could be obtained from information on the other.

201
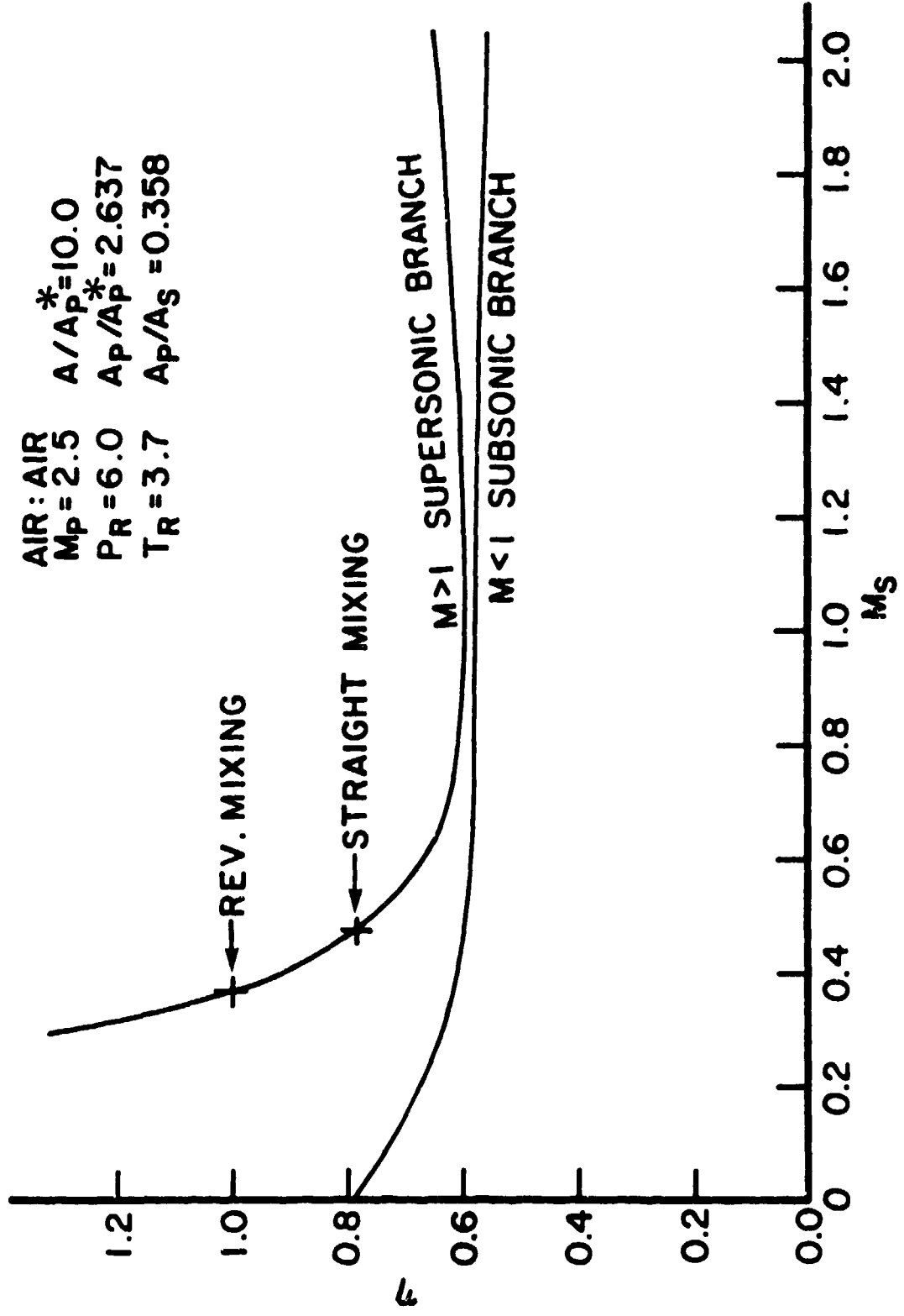
Figure 6. Efficiency Based on Availability for a Constant Geometry Solution for the Indicated Conditions.
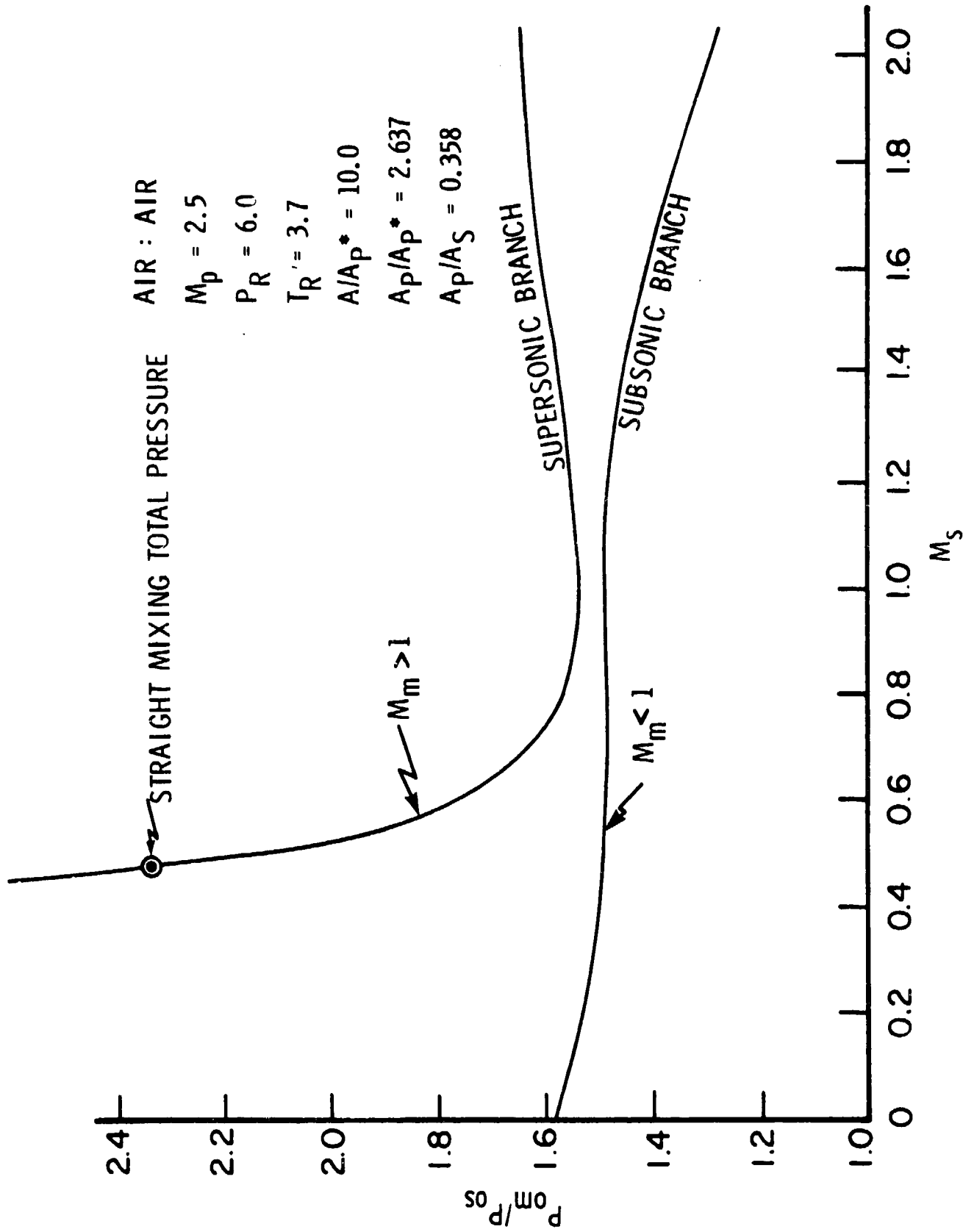
Figure 7. Total Pressure of the Mixed Flow for the Constant Geometry Solution for the Indicated Conditions.

203
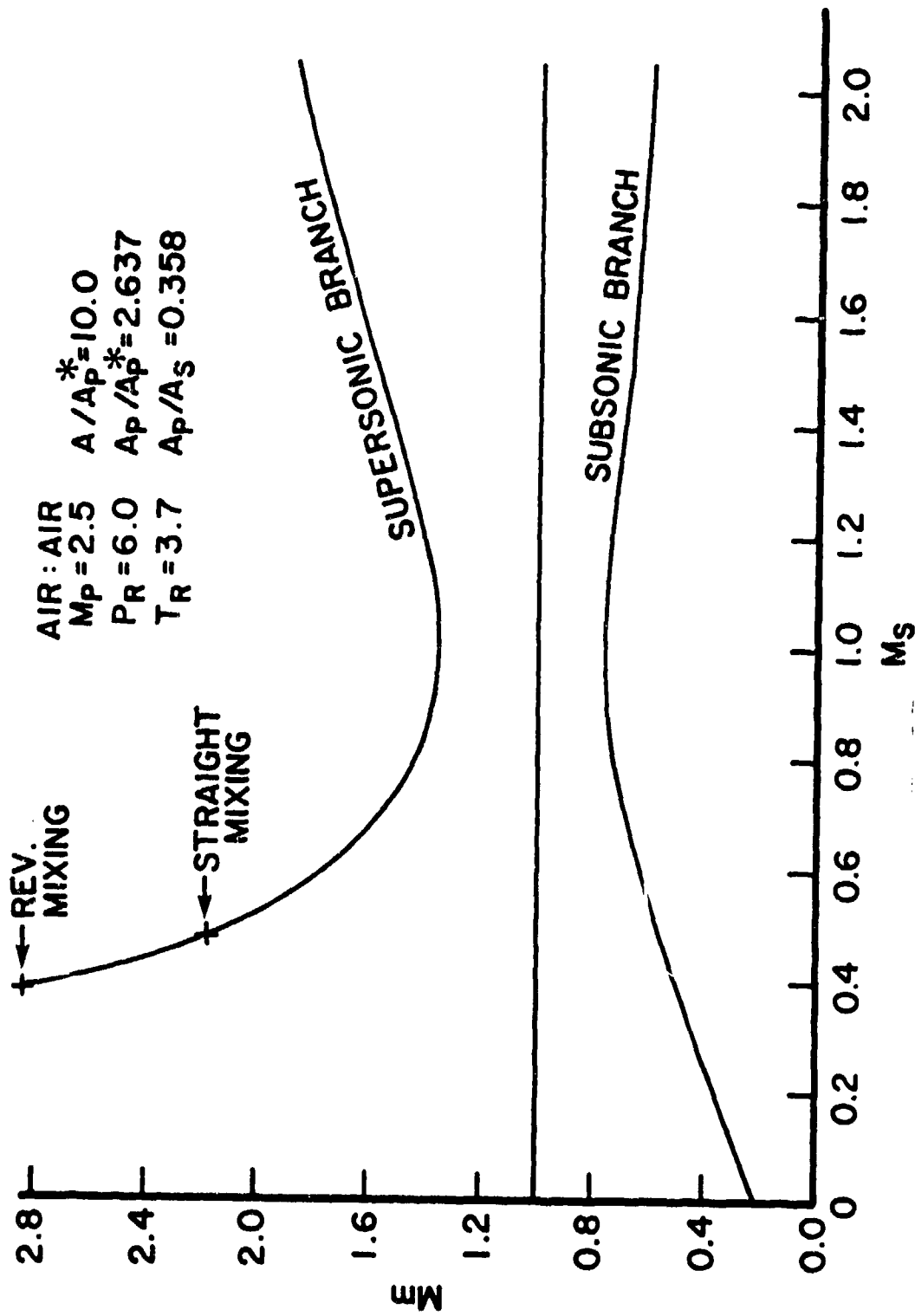
Figure 8. Mixed Flow Mach Number, Mm, for the Constant Geometry Solution for the Indicated Conditions.
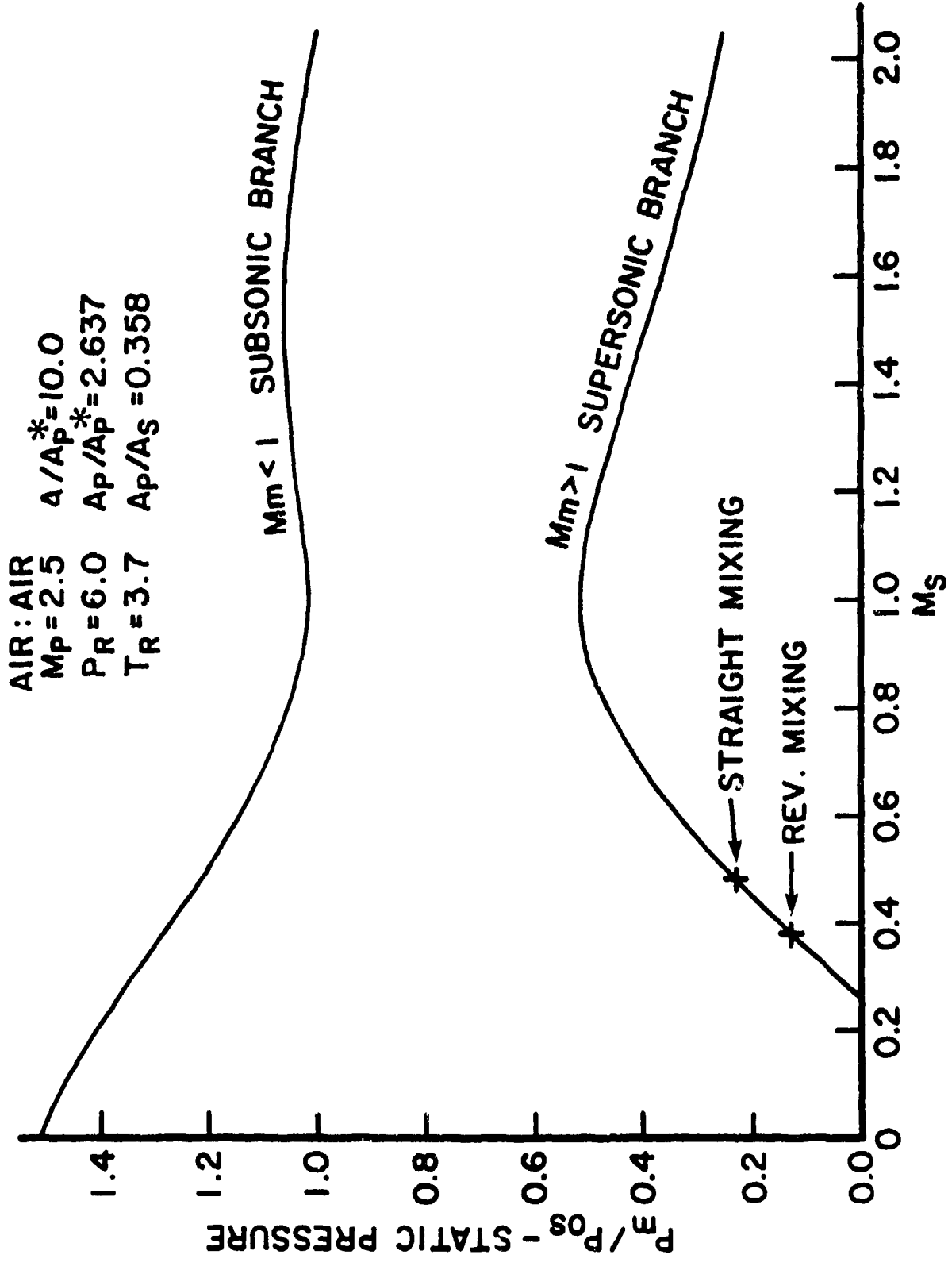
Figure 9. Exit Values of Static Pressure of the Mixed Flow for the Constant Geometry Solution for the Indicated Conditions.

205

Figure 8 presents the mixed flow Mach number for both solution branches. From Figure 8 it is clear that the mixed flow Mach number on the subsonic branch is well subsonic; less than 0.8, while the supersonic mixed flow Mach number is greater than 1.3.

Figure 9 presents the static pressure in the mixed flow for both branches. Note that the static pressure on the subsonic branch is higher than on the supersonic branch. It is instructive to do a thought experiment with Figure 9 and Figure 1 in view. A particular solution from those presented on Figures 6 through 9 results by setting the back pressure, $P_{back}$ of Figure 1. The setting of this boundary condition actually determines where the ejector will operate. From the geometry of Figure 1 it is clear that $M_s$ must be 1 or less since there is no throat in the secondary flow ahead of the inlet. Therefore, we are only concerned with the solutions where $M_s$ is one or less on Figures 6 through 9.

If the mixed flow Mach number, $M_m$, is subsonic, then the exit static pressure must be equal to the back pressure. Consequently, in view of Figure 9, the subsonic solution is possible only if the back pressure is in the range of 1.01 to 1.51. If the back pressure is set below 1.01, say 0.8, then the supersonic solution must be achieved at some secondary inlet Mach number of one or less. Of course once the back pressure is low enough so that the supersonic branch is achieved, the operation of the ejector is independent of the back pressure since signals cannot be transmitted upstream. Thus, the ejector will operate at only one point on the supersonic branch, irrespective of the value of the back pressure. Since the ejector operation is independent of the back pressure on the supersonic branch, another condition is required to determine the operating point. This condition will be discussed in detail later in the report. In any event, from our theoretical arguments, it is clear at this time that the

206

supersonic branch can be achieved.  Furthermore, there is sub-
stantial data in the literature to support this conclusion (e.g.,
see Reference 3).

It is still important to understand the physical significance
of the extremely high efficiencies that we have seen on both the
subsonic and supersonic branches as indicated on Figures 2 through
6.  We will consider this in the next section.

# SECTION 4

## CONSIDERATIONS OF THE CONTROL VOLUME ANALYSIS

As discussed previously the constant area geometry is a suf-
ficient condition to derive the control volume equations used to
obtain the solutions we have discussed. The geometry shown in
Figure 10 might also give the same set of equations.

In the geometry of Figure 10 the exit area, $A_m$, equals the
sum of the inlet areas, therefore, the continuity and energy
equations are the same as for the constant area geometry. If a
turbine-fan combination was included in the control volume it
would exchange energy between the primary and secondary flows,
but no heat or work would cross the control volume boundaries.
Consequently the energy equation would not change.

Finally, if the wall shapes were properly chosen the momen-
tum equation could also be the same. Clearly we could get some
results with this device that we could not obtain with the ejec-
tor and vice-versa.

Considerations such as these lead to the conclusion that the
constant area geometry is a sufficient condition to derive the
set of equations used for its analysis but it is not a necessary
condition. Since it is not a necessary condition some of the
solutions to the equations may not be possible with an ejector.
On the other hand, since it is a sufficient condition all of the
solutions possible with an ejector will be found using the
equations.

In order to understand how all of the solutions could be
achieved and determine fundamental limits of mixers we have deve-
loped, for thought experiments, a set of machinery within our
control volume for which the equations are still valid. We will
look at some of the fundamental limits in the next section.
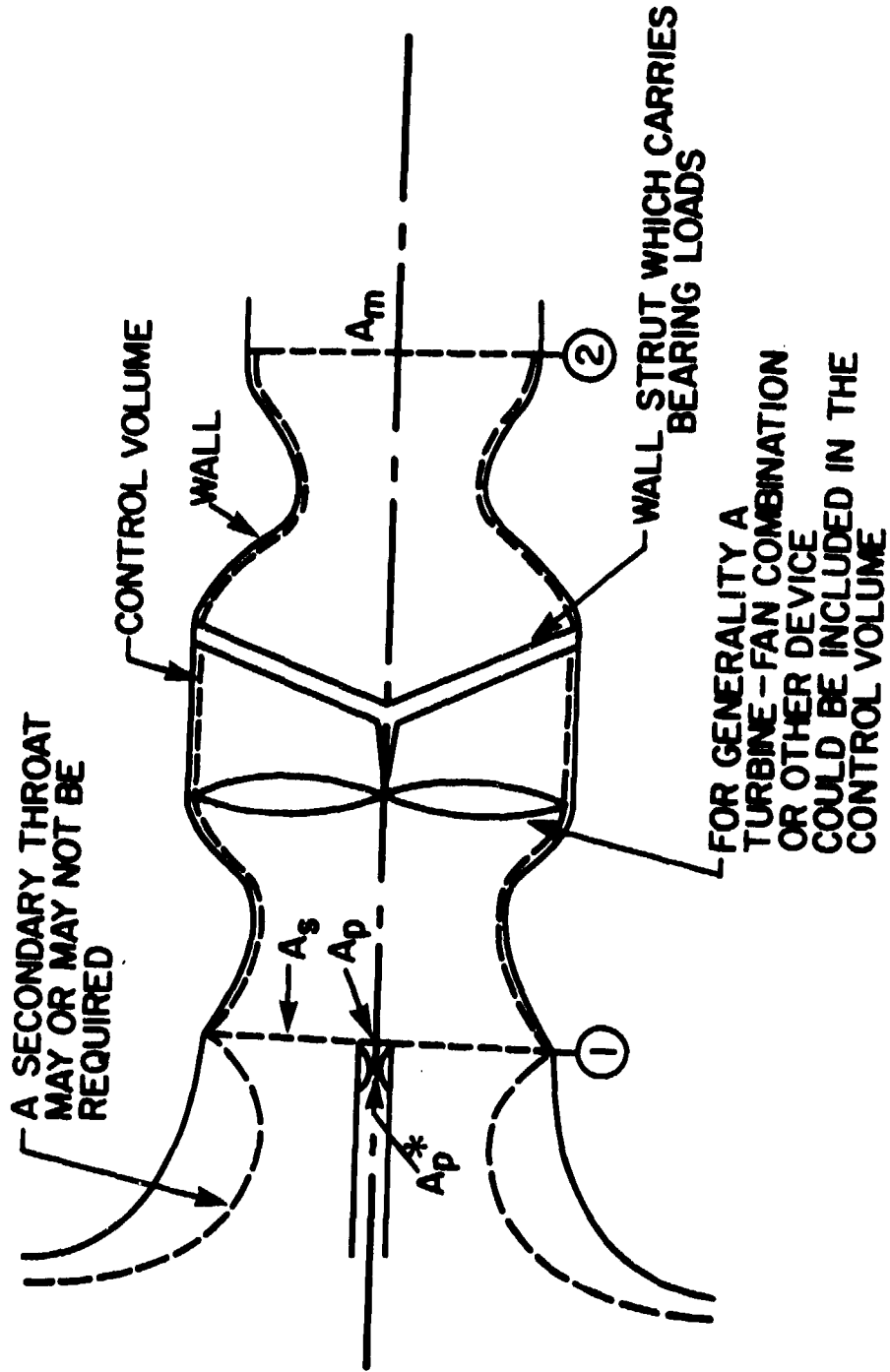
Figure 10. A Geometry Which May Give the Same Set of Equations as a Constant Area Geometry. The Exit Area Equals the Sum of the Inlet Areas: $A_m = A_s + A_p$.

## SECTION 5

## FUNDAMENTAL LIMITS OF MIXERS

For purpose of a thought experiment consider Figure 11 which contains a set of machinery within a control volume. The machinery of Figure 11 is described in detail in Appendix B. We show a jet engine as the source of the primary fluid while the secondary fluid is supplied by the atmosphere.

The first thing we wish to consider is reversible mixing of the two streams.

### 5.1 REVERSIBLE MIXING

As an aid in understanding reversible mixing and other concepts discussed later, we want to consider the processes shown on the T-s diagrams of Figures 12 and 13. The T-s diagram being used was normalized with the properties of the secondary flow: $T_{os}$ and $P_{os}$. Further, the entropy is reference to the secondary flow and then normalized with the gas constant, R. The $\Delta s/R$ on the T-s diagram is $(s-s_{os})/R$.

In the case of reversible mixing, the primary fluid expands in the reversible isentropic turbine to state 2P (see Figures 11 and 12). The work from the turbine is used to compress the secondary gas in the reversible isentropic compressor C4 to the state 2s. The stagnation temperature of the two fluid streams are the same in states 2P and 2s, and we will call this temperature $T_{om}$.

Equating the work of the turbine to the work of a compressor for arbitrary flow rates yields:

$$\dot{m}_p c_p (T_{op} - T_{om}) = \dot{m}_s c_p (T_{om} - T_{os}) \qquad (5)$$
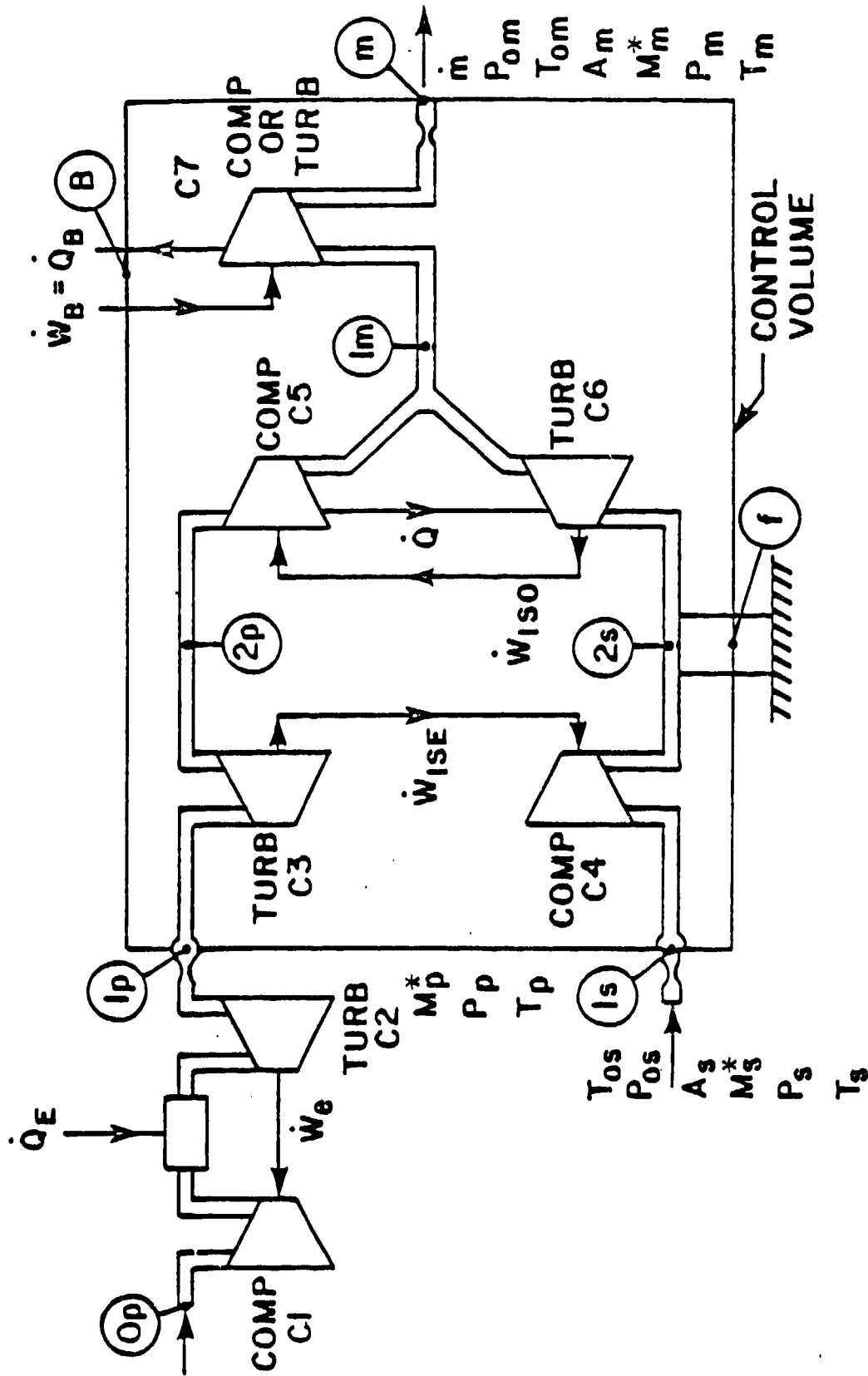
Figure 11. Machinery for Producing Any Desired Total Pressure for Constant Enthalpy Steady Flows.

212
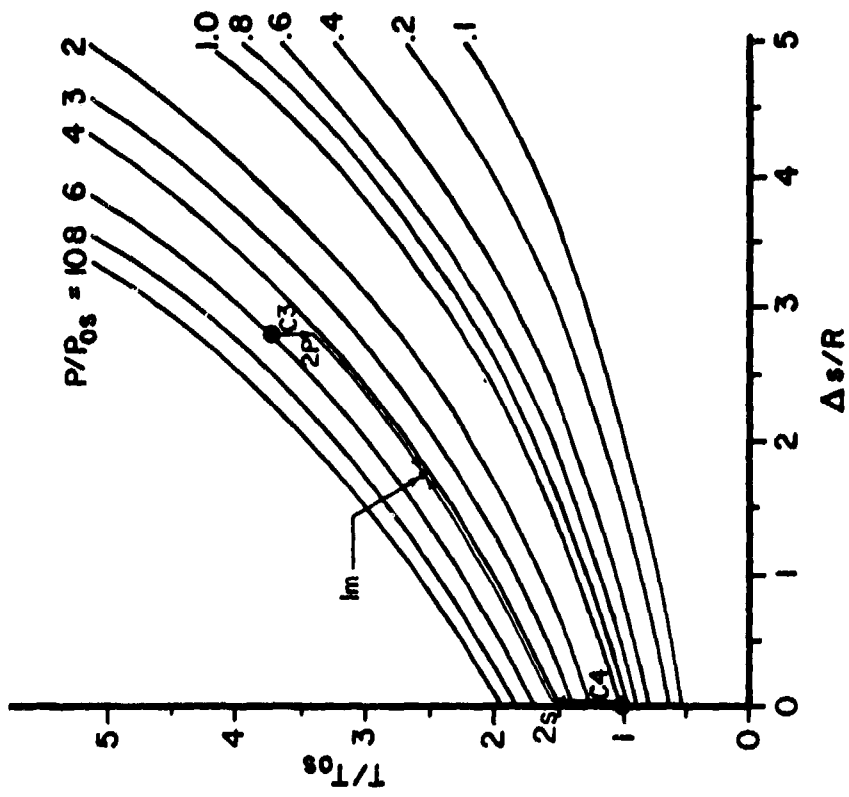
Figure 12. Reversible Mixing of the Primary and Secondary Streams: Since the work from process C3 drives process C4, the length of C3 is to the length of C4 as $\dot{m}_s$ is to $\dot{m}_p$. A single relation holds for the lengths of C5 and C6 since the heat transferred from C5 goes to C6. Thus, 1M lies on the straight line joining p to s.
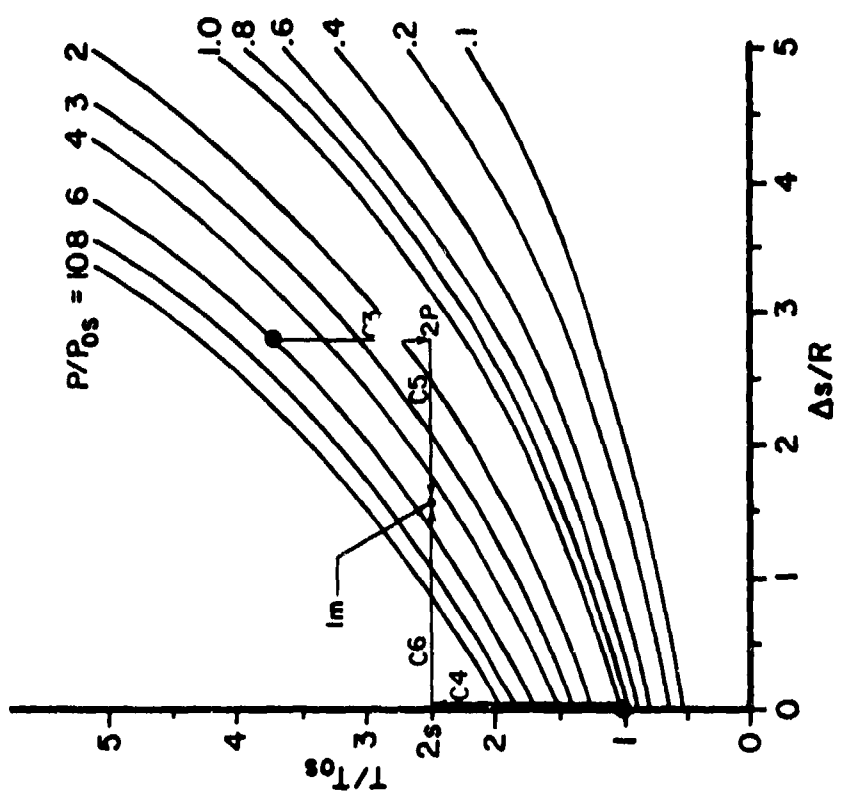
Figure 13. Constant kinetic energy mixing. Processes C3 and C4 equalizes the pressure and then the streams are mixed at constant pressure.

213

or,

$$\dot{m}_p h_{op} + \dot{m}_s h_{os} = (\dot{m}_p + \dot{m}_s) h_{om}. \qquad (5')$$

In view of Equations 1 and 2 we see that the temperature $T_{om}$ is the mixed flow stagnation temperature which depends only on the mass flow ratio or by-pass ratio and the total temperature of the two streams.

The secondary flow then enters the isothermal turbine C6 (see Figures 11 and 12) and the work from the turbine drives the isothermal compressor C5 which compresses the primary gas. The heat transfer from the primary gas required for the isothermal processes is transferred to the turbine C6 to maintain the temperature of the secondary gas. Since we are assuming that the processes are reversible we have for the heat transfers:

$$\dot{m}_p T_{om}(s_{op} - s_{om}) = \dot{m}_s T_{om}(s_{om} - s_{os}) \qquad (6)$$

In view of Equations 5 and 6 we have

$$\frac{T_{op} - T_{om}}{T_{om} - T_{os}} = \frac{s_{op} - s_{om}}{s_{om} - s_{os}} \qquad (7)$$

From Equation (7) we see that the mixed state in reversible mixing lies on the straight line joining the point s to the point p. Equation (7) can be rearranged to show this more clearly:

214

$$\frac{T_{om}}{T_{os}} = 1 + \left(\frac{T_{op}}{T_{os}} - 1\right)\frac{\Delta s_{om}/R}{\Delta s_{op}/R} \tag{8}$$

where $\Delta s = s - s_{os}$.

In order to determine the value of the total pressure, $P_{om}$ for the reversible mixing we need to use Equation (6) and the equation for the entropy change for an ideal gas:

$$\frac{\Delta s}{R} = \frac{\gamma}{\gamma-1} \ln \frac{T}{T_{os}} - \ln \frac{P}{P_{os}} \tag{9}$$

In view of (6) we can obtain

$$\dot{m}_p \Delta s_{op} = \dot{m}_m \Delta s_{om} \tag{10}$$

Therefore:

$$\frac{\dot{m}_p}{\dot{m}_m} \frac{\gamma}{\gamma-1} \ln\left(\frac{T_{op}}{T_{os}}\right) - \frac{\dot{m}_p}{\dot{m}_m} \ln\left(\frac{P_{op}}{P_{os}}\right) = \frac{\gamma}{\gamma-1} \ln\left(\frac{T_{om}}{T_{os}}\right) - \ln\left(\frac{P_{om}}{P_{os}}\right) \tag{11}$$

From Equation (11) and the energy equation we can show:

$$\frac{P_{om}}{P_{os}} = \left(\frac{P_{op}}{P_{os}}\right)^{\frac{\dot{m}_p}{\dot{m}_m}} \left[\frac{\frac{\dot{m}_p}{\dot{m}_m}\frac{T_{op}}{T_{os}} + \frac{\dot{m}_s}{\dot{m}_m}}{\left(\frac{T_{op}}{T_{os}}\right)^{\frac{\dot{m}_p}{\dot{m}_m}}}\right]^{\frac{\gamma}{\gamma-1}} \tag{12}$$

Equation (12) gives the total pressure of the mixed flow

that can be achieved in reversible mixing at the station lm and agrees with a similar result obtained by Kennedy.[2] This is the highest value of total pressure that can be obtained without the aid of heat transfer out of the control volume. With the use of the isothermal machine, C7 (see Figure 11) still higher total pressures would be possible. It is very important to realize that the presence of C7 is consistent with the energy equation, Equation (2).

Of course, if the final total pressure exceeds that given by Equation 12 one can say that the second law is violated for an adiabatic control volume (or, we need C7). However, in the cases when the machines C3 through C6 (see Figure 11) are real, the situation is different: the total pressure at lm would be less than that given by Equation 12. But, the isothermal machine, C7, could bring it closer to the value for reversible mixing without it being an obvious violation of the second law. For this reason we have called the machine, C7, the "ghost machine" since its effect may be totally masked.

For the thought experiments for the machinery of Figure 11 this ghost machine is not too important, but, for an ejector there must be intrinsic loss mechanisms because we have in general differences in velocity, temperature, pressure, and sometimes species at the entrance to the ejector.

However, the ghost machine, which is consistent with our equations, can completely mask these intrinsic losses without an apparent violation of the second law. The second law, therefore, may not give us a realistic estimate of the maximum performance of an ejector. Some other condition is needed to more realistically estimate the maximum performance; such a condition is available and will be discussed in detail later.

Another interesting point about Equation 12 is the fact that in general more kinetic energy can be obtained from an expansion of the mixed flow to any pressure than could be obtained from

separate expansion of primary and secondary flows to the same
pressure. The total pressure that yields the same kinetic energy
is derived in the next section.

## 5.2 CONSTANT KINETIC ENERGY MIXING

If the flow mixes such that the gross exit kinetic energy is
constant we can write the following equation:

$$
\dot{m}_s T_{os} \left[ 1 - \left( \frac{P_f}{P_{os}} \right)^{\frac{\gamma-1}{\gamma}} \right] + \dot{m}_p T_{op} \left[ 1 - \left( \frac{P_f}{P_{op}} \right)^{\frac{\gamma-1}{\gamma}} \right] \\
= \dot{m}_m T_{om} \left[ 1 - \left( \frac{P_f}{P_{om}} \right)^{\frac{\gamma-1}{\gamma}} \right] \tag{13}
$$

In Equation (13) $P_f$ is an arbitrary final pressure to which the
flows expand. In view of the energy equation for an ideal gas,
Equation (13) becomes

$$
- \dot{m}_s T_{os} \left( \frac{P_f}{P_{os}} \right)^{\frac{\gamma-1}{\gamma}} - \dot{m}_p T_{op} \left( \frac{P_f}{P_{op}} \right)^{\frac{\gamma-1}{\gamma}} = - \dot{m}_m T_{om} \left( \frac{P_f}{P_{om}} \right)^{\frac{\gamma-1}{\gamma}} \tag{14}
$$

Clearly, since $P_f$ cancels out of Equation (14), the result is
independent of the final pressure to which we can expand the
flows. In particular, this means the result is independent of
the ambient pressure except for its influence on $P_{os}$. In that
case, $P_{os}$ would be the stagnation pressure due to the flight Mach
number and $P_f$ would be the ambient pressure. In view of the
energy equation, we can solve Equation (14) and obtain:

217

$$
\frac{P_{om}}{P_{os}} = \frac{P_{op}}{P_{os}} \left[ \frac{\dfrac{\dot{m}_p}{\dot{m}_s} \dfrac{T_{op}}{T_{os}} + 1}{\left(\dfrac{P_{op}}{P_{os}}\right)^{\frac{\gamma-1}{\gamma}} + \dfrac{\dot{m}_p}{\dot{m}_s} \dfrac{T_{op}}{T_{os}}} \right]^{\frac{\gamma}{\gamma-1}}
\tag{15}
$$

Equation (15) determines the total pressure of the mixed flow that will yield the same kinetic energy as was available in the primary and secondary flows before mixing.

This pressure can be obtained by the machinery of Figure 11 in the following way.  The primary flow expands through the reversible adiabatic turbine C3 and compresses the secondary flow to the same value of pressure in the reversible adiabatic compressor C4.  The processes are shown on the T-s diagram of Figure 13.  The two flows are then mixed and come to the final temperature $T_{om}$.  The processes just described also represent the ideal mixing turbofan.

Since the work of the turbine equals the work of the compressor we have in view of the T-s diagram of Figure 13

$$
\dot{m}_s (T_{2s} - T_{os}) = \dot{m}_p (T_{op} - T_{2p})
\tag{16}
$$

or

$$
\dot{m}_s T_{os} \left( \frac{T_{2s}}{T_{os}} - 1 \right) = \dot{m}_p T_{op} \left( 1 - \frac{T_{2p}}{T_{op}} \right)
\tag{17}
$$

Because of the isentropic processes we have:

$$\dot{m}_s T_{os} \left[ \left( \frac{P_{om}}{P_{os}} \right)^{\frac{\gamma-1}{\gamma}} - 1 \right] = \dot{m}_p T_{op} \left[ 1 - \left( \frac{P_{om}}{P_{op}} \right)^{\frac{\gamma-1}{\gamma}} \right] \qquad (18)$$

Equation (18) can easily be rearranged to obtain Equation (15). Hence, the total pressure given by equation (15), which conserves kinetic energy, can also be considered as the total pressure which is obtained from an ideal mixing turbofan.

In deriving equation (15) we assumed that the gross exit kinetic energy in the mixed flow was equal to that of the two separated flows before mixing. It can be shown, however, that exactly the same result is obtained if we equate the increase in kinetic energy across the core engine by itself to that of the engine-mixer combination. (i.e. $\dot{m}_p(V_{jp}^2 - V_f^2) = \dot{m}_m(V_{jm}^2 - V_f^2)$ from which we can show that $\dot{m}_p V_{jp}^2 + \dot{m}_s V_f^2 = \dot{m}_m V_{jm}^2$. In these equations we have assumed expansion to atmospheric pressure. The exit-jet, primary velocity is $V_{jp}$ and mixed-flow, exit-jet velocity is $V_{jm}$. The loss-free, exit-jet velocity of the secondary flow is equal to the flight speed, $V_f$.) Thus, the thermodynamic efficiency of the engine with mixer is the same as that of the core engine. Again this represents an ideal turbofan.

## 5.3 SIMPLE MIXING OR STRAIGHT MIXING

Still another pressure of interest is the final pressure that results from mixing two quantities of gas in a nonflow system with mass ratios equal to the bypass ratio. We have referred to this as simple mixing or straight mixing. We can think of having two cylinders of gas: one with a mass equal to $\dot{m}_p$ and total temperature and pressure of the primary; the other with a mass equal to $\dot{m}_s$ and total temperature and pressure of the secondary. We then allow the two cylinders to communicate and mix adiabatically. Since the total volume remains unchanged we have in view of the energy equation and ideal gas relations

$$\dot{m}_s T_{os} + \dot{m}_p T_{op} = \dot{m}_m T_{om} = P_{om}(V_s + V_p) \qquad (19)$$

where $V_s$ and $V_p$ are the total volumes of secondary and primary gas respectively. Eliminating the volumes yields

$$\dot{m}_s T_{os} + \dot{m}_p T_{op} = P_{om}\left(\frac{\dot{m}_p T_{op}}{P_{os}} + \frac{\dot{m}_s T_{os}}{P_{op}}\right) \qquad (20)$$

Solving for $P_{om}/P_{os}$ yields:

$$\frac{P_{om}}{P_{os}} = \frac{P_{op}}{P_{os}}\left[\frac{\dfrac{\dot{m}_p}{\dot{m}_s}\dfrac{T_{op}}{T_{os}} + 1}{\dfrac{P_{op}}{P_{os}} + \dfrac{\dot{m}_p}{\dot{m}_s}\dfrac{T_{op}}{T_{os}}}\right] \qquad (21)$$

Equation (21) gives the pressure that can be achieved in a simple mixing of the two gases in a nonflow process. However, a cyclic, quasi-steady-flow device can be envisioned that would mix two quantities of gases according to Equation (21). Thus, it is resonable to compare the performance of an ejector to the simple mixing case.

It can be formally shown that if one expands the primary fluid in a reversible adiabatic process and uses the work to compress the secondary fluid in a reversible adiabatic process and then mixes the two fluids by simple mixing, then a maximum value of $P_{om}$ is achieved if the pressures are equalized before mixing. The value of this maximum pressure, $P_{om}$, is again given by Equation (15) and shows that conserving kinetic energy is the optimum that can be achieved by the use of isentropic machines in the nonflow case.

220

Having determined a number of limiting pressures it is of interest to determine the minimum total pressure of the mixed flow which gives a thrust augmentation of one for various conditions.

## 5.4 TOTAL PRESSURE NEEDED FOR THRUST AUGMENTATION

The overall efficiency of an aircraft engine is defined as the power out (thrust, $\tau$, of the engine times the flight velocity, $V_f$) divided by the heat rate, $\dot{Q}$, supplied to the engine:

$$\eta_{OA} = \frac{\tau V_f}{\dot{Q}} = \frac{\Delta KE_j}{\dot{Q}} \cdot \frac{\tau V_f}{\Delta KE_j} = \eta_{th} \cdot \eta_{PR} \qquad (22)$$

As shown in Equation (22) the overall efficiency, $\eta_{OA}$, is the product of the engine efficiency, $\eta_{th}$, and the propulsion efficiency, $\eta_{PR}$. ($\eta_{th} = \Delta KE_j/\dot{Q}$ and $\eta_{PR} = \tau V_f/\Delta KE_j$ where $\Delta KE_j$ is the increase in jet kinetic power, $1/2\dot{m}_p(V_{Jp}^2 - V_f^2)$). If the thrust of an engine is augmented while holding the flight speed constant and engine heat rate fixed (which is the case of the mixer) we see from Equation (22) that

$$\frac{\eta_{OA2}}{\eta_{OA1}} = \frac{\tau_2}{\tau_1} \equiv \phi \qquad (23)$$

where subscripts 2 and 1 refer to augmented and unaugmented values, respectively.

Hence, the ratio of overall efficiencies is equal to the ratio of thrust (the thrust augmentation, $\phi$). Equation (23) is valid even if $\eta_{PR}$ is unchanged but $\eta_{th}$ is changed. This can happen, for example, if the jet velocity and $\dot{Q}$ are fixed but the mass flow is increased (decreased) because $\eta_{th}$ is increased

221

(decreased). (Note that we are concerned with a given engine in combination with a mixer and, therefore, the heat rate, $\dot{Q}$, is fixed.) From Equation (22) we see that $\eta_{OA}$ can increase because, either $\eta_{th}$ increases or $\eta_{PR}$ increases or both increase. If the kinetic energy decreases, $\eta_{th}$ will decrease but $\eta_{OA}$ can still increase if $\eta_{PR}$ is sufficiently increased (e.g. as happens with a turbofan).

For the case of a mixer we have for complete expansion to atmospheric pressure:

$$\phi = \frac{\tau_2}{\tau_1} = \frac{\dot{m}_m (V_{JM} - V_f)}{\dot{m}_p (V_{JP} - V_f)} \qquad (24)$$

where $V_{JM}$ is the jet velocity of the mixed flow, $V_{JP}$ is the jet velocity of primary flow without the mixer and $V_f$ is the flight velocity.

If we set the thrust augmentation to one we can solve Equation (24) for the jet velocity ratio:

$$\frac{V_{JM}}{V_{JP}} = \frac{\dot{m}_s}{\dot{m}_m} \frac{V_f}{V_{JP}} + \frac{\dot{m}_p}{\dot{m}_m} \qquad (25)$$

Now for an ideal gas with constant specific heats we have for the jet velocity ratio:

$$\left(\frac{V_{JM}}{V_{JF}}\right)^2 = \frac{T_{om}}{T_{op}} \left[ \frac{1 - \left(\frac{P_{amb}}{P_{om}}\right)^{\frac{\gamma-1}{\gamma}}}{1 - \left(\frac{P_{amb}}{P_{op}}\right)^{\frac{\gamma-1}{\gamma}}} \right] \qquad (26)$$

222

If we combine Equations (25) and (26) we can solve for $P_{om}/P_{os}$:

$$\frac{P_{om}}{P_{os}} = \frac{P_{amb}}{P_{os}} \left\{ 1 - \frac{T_{op}}{T_{om}} \left( \frac{\dot{m}_s}{\dot{m}_m} \frac{V_f}{V_{JP}} + \frac{\dot{m}_p}{\dot{m}_m} \right)^2 \; x \right.$$

$$\left. \left[ 1 - \left( \frac{P_{amb}}{P_{os}} \cdot \frac{P_{os}}{P_{op}} \right)^{\frac{\gamma-1}{\gamma}} \right]^{\frac{-\gamma}{\gamma-1}} \right\} \tag{27}$$

If we assume that $P_{os}$ is the isentropic stagnation pressure resulting from the flight velocity then:

$$\left( \frac{V_f}{V_{JP}} \right)^2 = \frac{T_{os}}{T_{op}} \frac{1 - \left( \frac{P_{amb}}{P_{os}} \right)^{\frac{\gamma-1}{\gamma}}}{1 - \left( \frac{P_{amb}}{P_{os}} \cdot \frac{P_{os}}{P_{op}} \right)^{\frac{\gamma-1}{\gamma}}} \tag{28}$$

and

$$\frac{P_{amb}}{P_{os}} = \left( 1 + \frac{\gamma-1}{2} M_\infty^2 \right)^{-\frac{\gamma}{\gamma-1}} \tag{29}$$

Clearly, in view of Equations (27), (28) and (29) we see that

$$\frac{P_{om}}{P_{os}} = f \left( M_\infty, \; \frac{T_{op}}{T_{os}}, \; \frac{P_{op}}{P_{os}}, \; \frac{\dot{m}_p}{\dot{m}_m} \right) \tag{30}$$

223

An explicit expression will be derived in the next section. Equations (27) through (29) were solved and $P_{om}/P_{os}$ was plotted versus $M_{\infty}$ on Figure 14 for $P_{op}/P_{os}$ 6 and $T_{op}/T_{os} = 3.7$. The curve parameter is $\dot{m}_p/\dot{m}_m$. If the mixed total pressure is greater than the value read off the appropriate curve of Figure 14 then the thrust augmentation would be greater than one.

The data from Figure 14 can be used to draw lines on a T-s diagram where $\phi = 1$ as shown on Figure 15. We have also shown the locus of states for reversible mixing (Equation 12), constant kinetic energy (Equation 15) simple mixing (Equation 21) along with the values for $\phi = 1$ at the indicated Mach numbers. We have only shown supersonic flight Mach numbers but the subsonic curves would lie between the $M = 1$ and $M = 2$ curves or just slightly to the left of the Mach one curve. The peaks of the curves of Figure 14 are just slightly subsonic, like $M = 0.85$.

Since $T_{om}/T_{os}$ is fixed for a given mass flow we have shown lines of constant $\dot{m}_p/\dot{m}_m$ on Figure 15, which are, of course, horizontal lines on the T-s diagram. If the total pressure out of a given mixer lies between the reversible mixing curve and the constant kinetic energy curve both $\eta_{th}$ and $\eta_{PR}$ would be increased in Equation (22). If the total pressure lies between the constant kinetic energy curve and the appropriate $\phi$ curve for the flight Mach number then $\eta_{th}$ decreases but $\eta_{PR}$ increases sufficiently to give a thrust augmentation greater than one. If the total pressure lies to the right of the appropriate $\phi$ curve for the flight Mach number then the thrust augmentation is less than one and the overall efficiency will have decreased.

In the next section we will generalize the thrust augment-ation curves for any mixer in terms of the efficiency of the mixing process.

5.5   THRUST AUGMENTATION AS A FUNCTION OF MIXER EFFICIENCY

When the velocity of a fluid is achieved in an isentropic

224
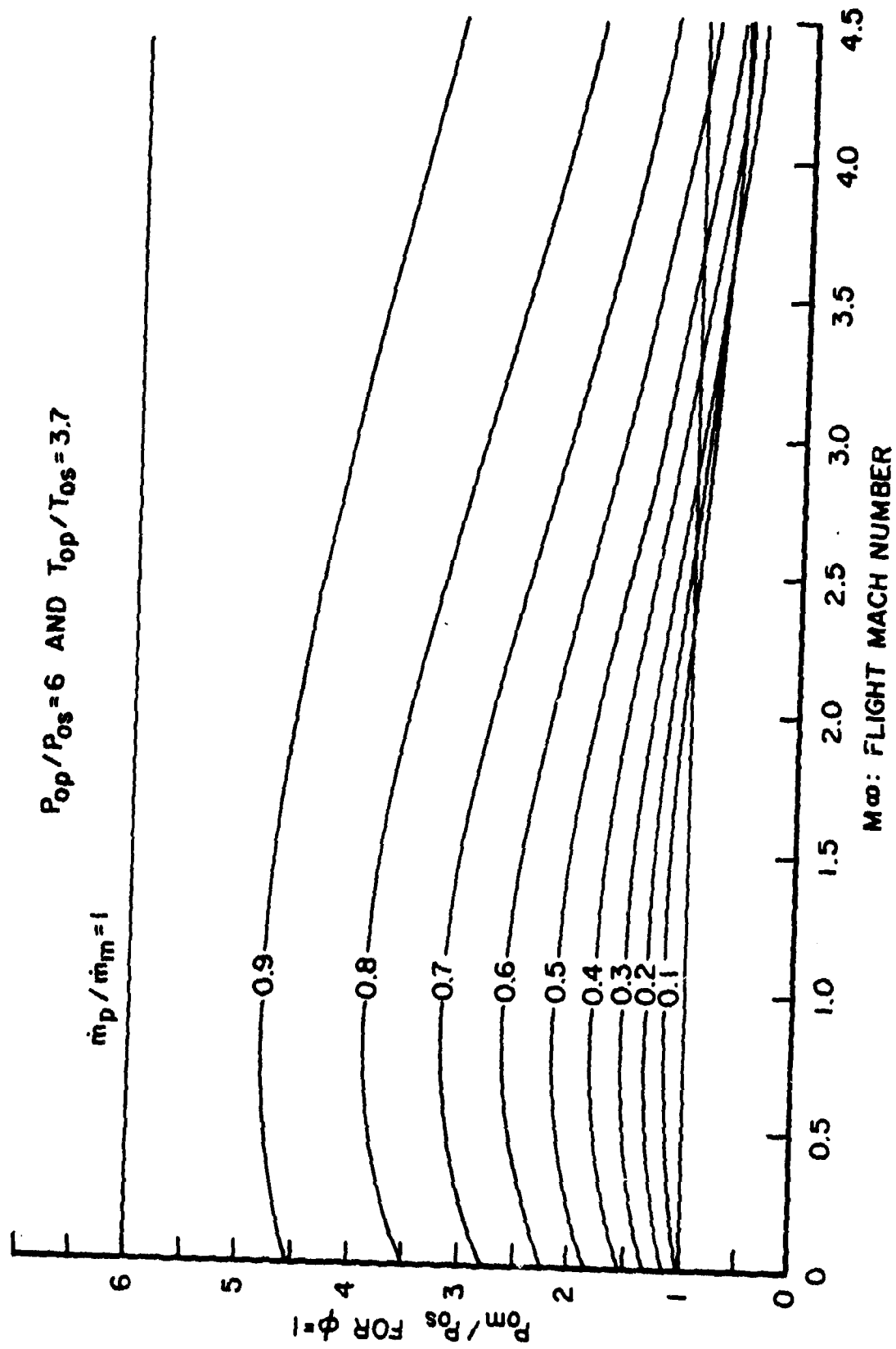
Figure 14. Total Pressure that Gives a Thrust Augmentation of 1.
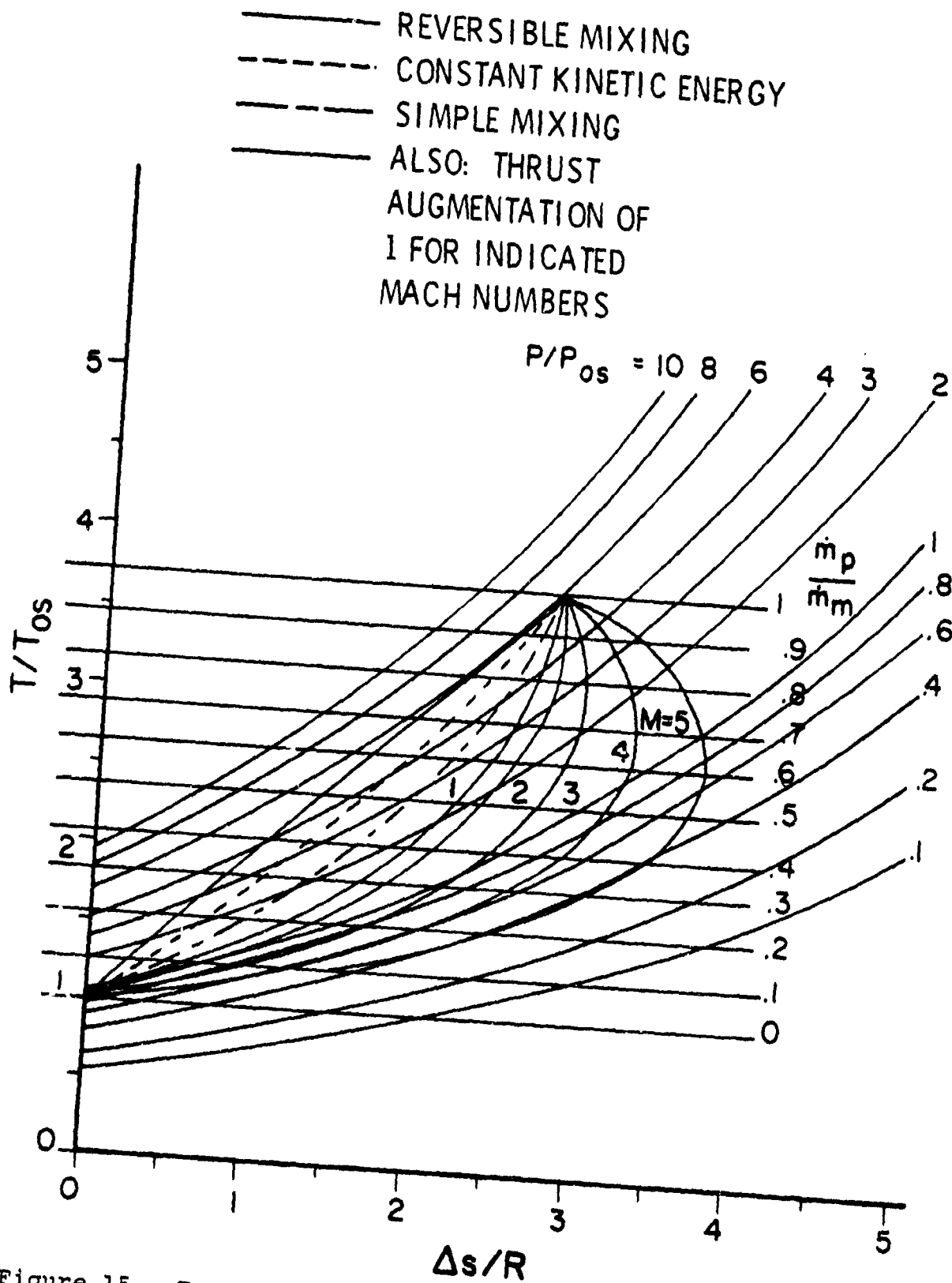
Figure 15. T-s Diagram for $P/P_{os} = 6$ and $T/T_{op} = 3.7$, Showing States for Reversible Mixing, Constant Kinetic Energy, Simple Mixing, and Thrust Augmentation of 1.

flow we can relate the velocity to the temperature as

$$V = \sqrt{2C_p T_o \left(1 - \frac{T}{T_o}\right)}$$ (31)

In view of Equation (31) and (24) we have for the thrust augmentation.

$$\phi = \frac{\dot{m}_m}{\dot{m}_p} \frac{\sqrt{\frac{T_{om}}{T_{os}}} \sqrt{1 - \frac{T_m}{T_{om}}} - \sqrt{1 - \frac{T_{amb}}{T_{os}}}}{\sqrt{\frac{T_{op}}{T_{os}}} \sqrt{1 - \frac{T_p}{T_{op}}} - \sqrt{1 - \frac{T_{amb}}{T_{os}}}}$$ (32)

Using the energy equation and the well-known isentropic relationships we can show:

$$\phi = \frac{\dot{m}_m}{\dot{m}_p} \frac{\sqrt{\frac{\dot{m}_p}{\dot{m}_m} \frac{T_{op}}{T_{os}} + \frac{\dot{m}_s}{\dot{m}_m}} \sqrt{\left(1 + \frac{\gamma-1}{2} M_\infty^2\right) - \left(\frac{P_{om}}{P_{os}}\right)^{-\frac{\gamma-1}{\gamma}}} - \sqrt{\frac{\gamma-1}{2}} M_\infty}{\sqrt{\frac{T_{op}}{T_{os}}} \sqrt{\left(1 + \frac{\gamma-1}{2} M_\infty^2\right) - \left(\frac{P_{op}}{P_{os}}\right)^{-\frac{\gamma-1}{\gamma}}} - \sqrt{\frac{\gamma-1}{2}} M_\infty}$$

(33)

We can relate the total pressure to the efficiency based on availability by using Equation (A-34) of Appendix A and the energy equation:

$$\frac{P_{om}}{P_{os}} = \text{Exp}(D\eta - N) \tag{34}$$

where

$$D = \frac{\gamma}{\gamma-1} \; \frac{\dot{m}_p}{\dot{m}_m} \left[ \frac{T_{op}}{T_{os}} - 1 - \ln\left(\frac{T_{op}}{T_{os}}\right) \right] + \frac{\dot{m}_p}{\dot{m}_m} \ln\left(\frac{P_{op}}{P_{os}}\right) \tag{35}$$

and

$$N = \frac{\gamma}{\gamma-1} \left[ \frac{\dot{m}_p}{\dot{m}_m} \left( \frac{T_{op}}{T_{os}} - 1 \right) - \ln\left( \frac{\dot{m}_p}{\dot{m}_m} \frac{T_{op}}{T_{os}} - \frac{\dot{m}_s}{\dot{m}_m} \right) \right] \tag{36}$$

Of course the bypass ratio, $\dot{m}_s/\dot{m}_p$, is easily determined from either of the other mass flow ratios.

We have used Equations (33) through (36) to construct Figures 17 and 18 which show thrust augmentation versus Mach number. In all of the three figures $P_{op}/P_{os}$ is 6 and $T_{op}/T_{os}$ is 3.7. The page parameter is the bypass ratio, $\dot{m}_s/\dot{m}_p$, which is 14.9, 5 and 2 on Figures 16, 17 and 18 respectively. Each of the figures has the efficiency as the curve parameter, 100% efficiency is, of course, reversible mixing. We have also shown the thrust augmentation for constant kinetic energy mixing (labeled ideal turbo-fan) and straight mixing. Since both of these pressures are independent of the flight Mach number they correspond to only one value of efficiency on a given figure: e.g., the ideal turbo-fan corresponds to about 80% efficiency on Figure 16.

From the figures we see that the highest thrust augmentation occurs at subsonic flight Mach numbers for the higher

228

efficiencies. The lower efficiencies, however, have higher
thrust augmentations at the higher Mach numbers. In Figures 16,
17 and 18 the pressure ratios and temperature ratios are held
constant and no attempt was made to model these parameters to fit
actual engine performance as a function of flight Mach number.
We plan to do this as part of our future work.

There is still one limit value of pressure that can be
determined with the aid of Fanno lines generated for the mixed
flow.

## 5.6 MINIMUM TOTAL PRESSURE FOR A GIVEN BYPASS RATIO

If the exit flow is completely mixed, as we have assumed,
then we can evaluate a minimum total pressure that is consistent
with the mass flow ratio or bypass ratio. Fanno line flow is
developed from considerations of only the continuity and energy
equations for a constant area channel. The mass flow parameter,
G (the mass velocity) is defined as,

$$G \equiv \frac{\dot{m}_m}{A} .$$  (37)

For a given geometry and given states of primary and secon-
dary fluids the value of G is fixed as soon as the total mass
flow, $\dot{m}_m$, is known. Of course, the total temperature is deter-
mined by knowledge of the mass flow. Thus, we can immediately
construct a T-s diagram for the given conditions. Such a T-s
diagram is sketched on Figure 19 for values of $T_{op}/T_{os}$ of 3.7
and $P_{op}/P_{os}$ of 6. If we know the geometry (e.g., as in the case
of the ejector of Figure 1) we could also determine a value of
$M_s$ (inlet secondary Mach number) required to give the mass flow
ratio under consideration. Thus, we have indicated values of
$M_s$ on Figure 19 that might be valid for a particular geometry of
the type shown on Figure 1. For any given flow rate two values

229
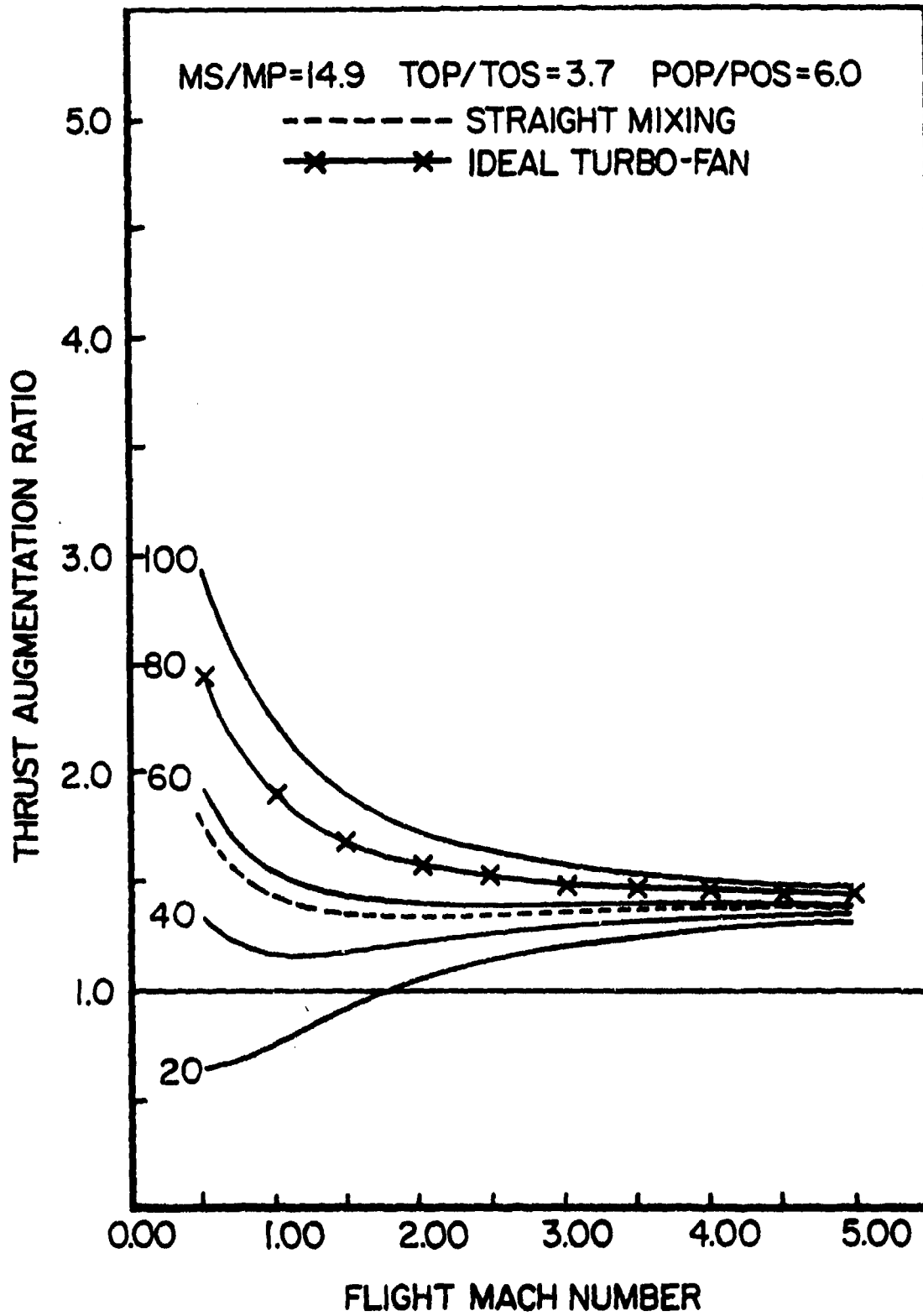
Figure 16. Thrust Augmentation as a Function of Flight Mach Number for a By-Pass Ratio of 14.9. Curve parameter is efficiency.
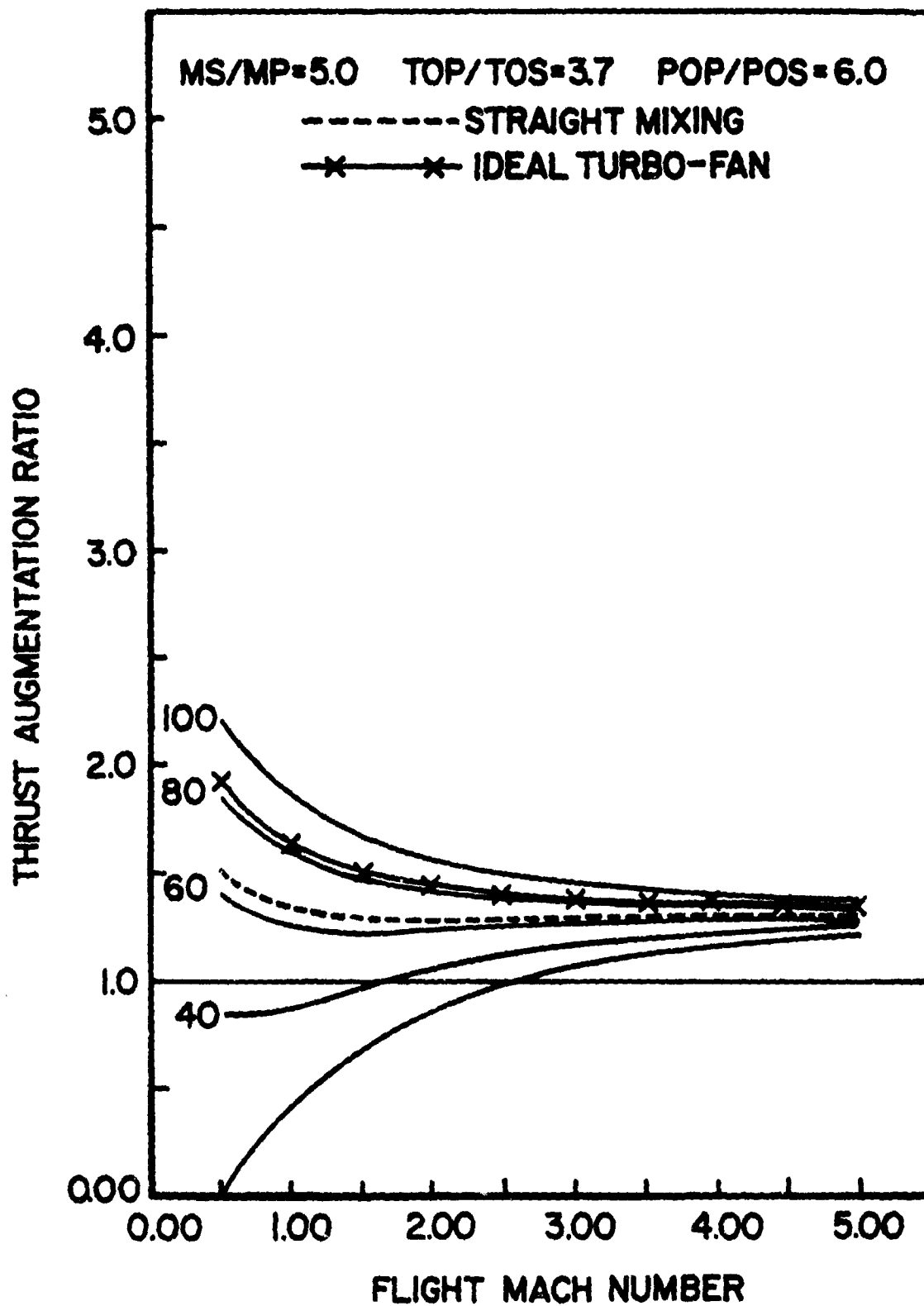
Figure 17. Thrust Augmentation as a Function of Flight Mach Number for a By-Pass Ratio of 5.0; Curve Parameter is Efficiency.
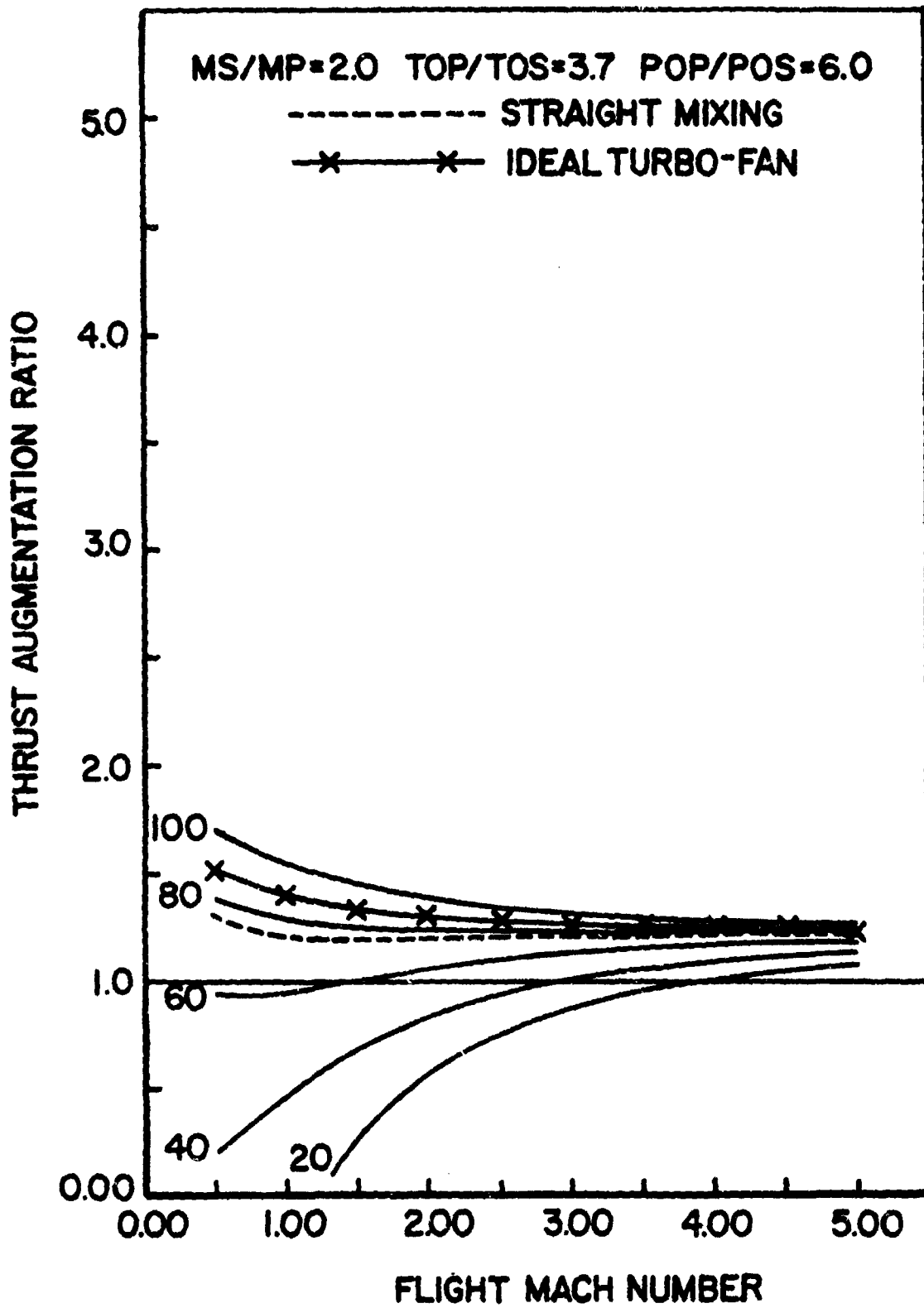
Figure 18. Thrust Augmentation as a Function of Flight Mach Number for a By-Pass Ratio of 2.0; Curve Parameter is Efficiency.

232

of $M_s$ are valid: one subsonic and the other supersonic.

As an example on Figure 19 we have labeled a value of $T_{om}/T_{os}$ that corresponds to a value of $M_s = 0.6$ (or $M_s = 1.52$). The intersecti of this particular temperature line and the straight line in the primary and secondary stagnation conditions gives e state for reversible mixing.

If we drop an isentropic (vertical) line from this stagnation state for reversible mixing we can find the two intersections with the appropriate Fanno line. We have shown these intersections as small circles on the T-s diagram of Figure 19. The intersections represent the static properties of the flow that correspond to the given flow rate and the stagnation conditions of the mixed flow. Of course, the flow on the upper branch is subsonic and that along the lower branch is supersonic.

We have also indicated a pair of points connected by a dashed line which represents a normal shock. These points represent the pair of solutions that can be obtained for the ejector. Isentropic lines connecting these points to the appropriate total temperature gives the stagnation states which correspond to the two solutions.

Additional dissipative mechanisms (such as friction) would move the resulting solutions to the right (increasing the entropy) on the T-s diagram. As is well known there is a limit to the dissipation that can take place without decreasing the mass flow. At this limit point the mixed flow Mach number is one. The intersection of the isentropic line drawn from the limit point to the appropriate total temperature gives the minimum value of the total pressure that is consistent with the exit area and the mixed flow mass-flow rate.

The value of this minimum total pressure can be found in a straightforward manner. The value of the mass velocity can be written in terms of Mach number and stagnation conditions:
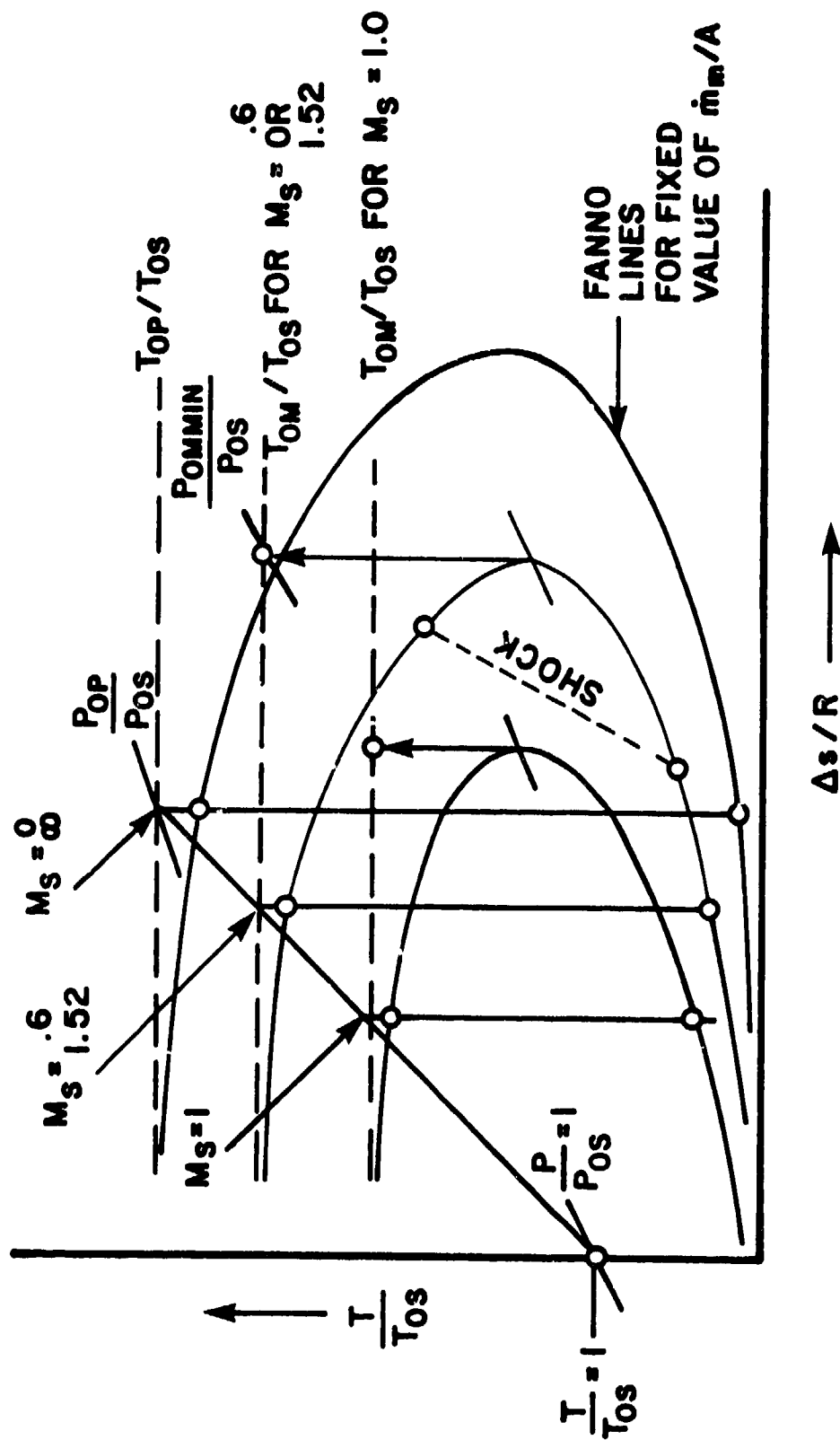
Figure 19. Fanno Lines for the Mixed Flow on a T-s Diagram. Reversible Mixing Would Occur on the Straight Line Joing the Primary and Secondary Total Condition.

$$G = \sqrt{\frac{\gamma}{R}} \cdot \frac{P_o}{\sqrt{T_o}} \frac{M}{\left(1 + \frac{\gamma-1}{2}M^2\right)^{\frac{\gamma+1}{2(\gamma-1)}}} \tag{38}$$

Thus, for the mixed flow at the point where the Mach number is one:

$$G_m = \frac{P_{om_{min}}}{\sqrt{T_{om}}} \sqrt{\frac{\gamma}{R}} \left(\frac{2}{\gamma+1}\right)^{\frac{\gamma+1}{2(\gamma-1)}} \tag{39}$$

or

$$G = f(\gamma,R) \cdot \frac{P_{om_{min}}}{\sqrt{T_{om}}} \tag{40}$$

Now

$$f(\gamma,R) \cdot \frac{P_{om_{min}}}{\sqrt{T_{om}}} = \frac{\dot{m}_m}{A} \cdot \frac{A_p^*}{\dot{m}_p} \cdot \frac{\dot{m}_p}{A_p^*} = \frac{\dot{m}_m}{\dot{m}_p} \cdot \frac{A_p^*}{A} \cdot G_p \tag{41}$$

We have assumed the $P_{op}$ is high enough that the primary nozzle flows full. Therefore, an equation similar to Equation (40) is also valid for the primary flow when the Mach number is one at the nozzle throat. Using this condition we can easily obtain:

$$\frac{P_{om_{min}}}{P_{os}} = \frac{\dot{m}_m}{\dot{m}_p} \cdot \frac{A_p^*}{A} \frac{P_{op}}{P_{os}} \frac{\sqrt{T_{om}/T_{os}}}{\sqrt{T_{op}/T_{os}}} \tag{42}$$

235

In view of the energy equation

$$\frac{P_{om_{min}}}{P_{os}} = \frac{\dot{m}_m}{\dot{m}_p} \frac{A_p^*}{A} \frac{P_{op}}{P_{os}} \sqrt{\frac{\dot{m}_p}{\dot{m}_m} + \left(1 - \frac{\dot{m}_p}{\dot{m}_m}\right) \frac{T_{os}}{T_{op}}} \qquad (43)$$

Thus, the minimum pressure can be determined immediately from the geometry and the stagnation conditions once the mass flow ratio is given. If the dissipative processes required a lower pressure than the value given by Equation (43) the flow would choke and the mass flow ratio would be reduced. For the case of a constant area ejector the inlet Mach number of the secondary flow would be reduced.

Figure 20 shows the results of calculations for a constant geometry ejector. The conditions are shown on Figure 20 for which the curve was constructed. We show the total pressure resulting from reversible mixing, Equation (12), constant kinetic energy, Equation (15), straight mixing, Equation (21) and the minimum possible total pressure Equations (43) for the indicated secondary Mach number.

We have also shown results from our computer program for constant area ejectors with friction. We have shown both solutions for two values of $f(L/D)$: 0 and 0.1.

The significance of the minimum pressure curve is apparent for the value of $f(L/D) = 0.1$: both branches terminate on this limit curve where the mixed flow is Mach one. The same is true for each of the other supersonic branches that terminate on the minimum pressure curve: the subsonic branch also terminates at the same point. Each value of $M_s$ represents one Fanno line for the mixed flow. Thus, if a value of $P_{om}$ greater that $P_{om_{min}}$ is achieved at some value of $M_s$ we could increase the length of the mixing tube, thereby causing the value of $f(L/D)$ to increase, until the minimum pressure is reached, at which point the flow

236
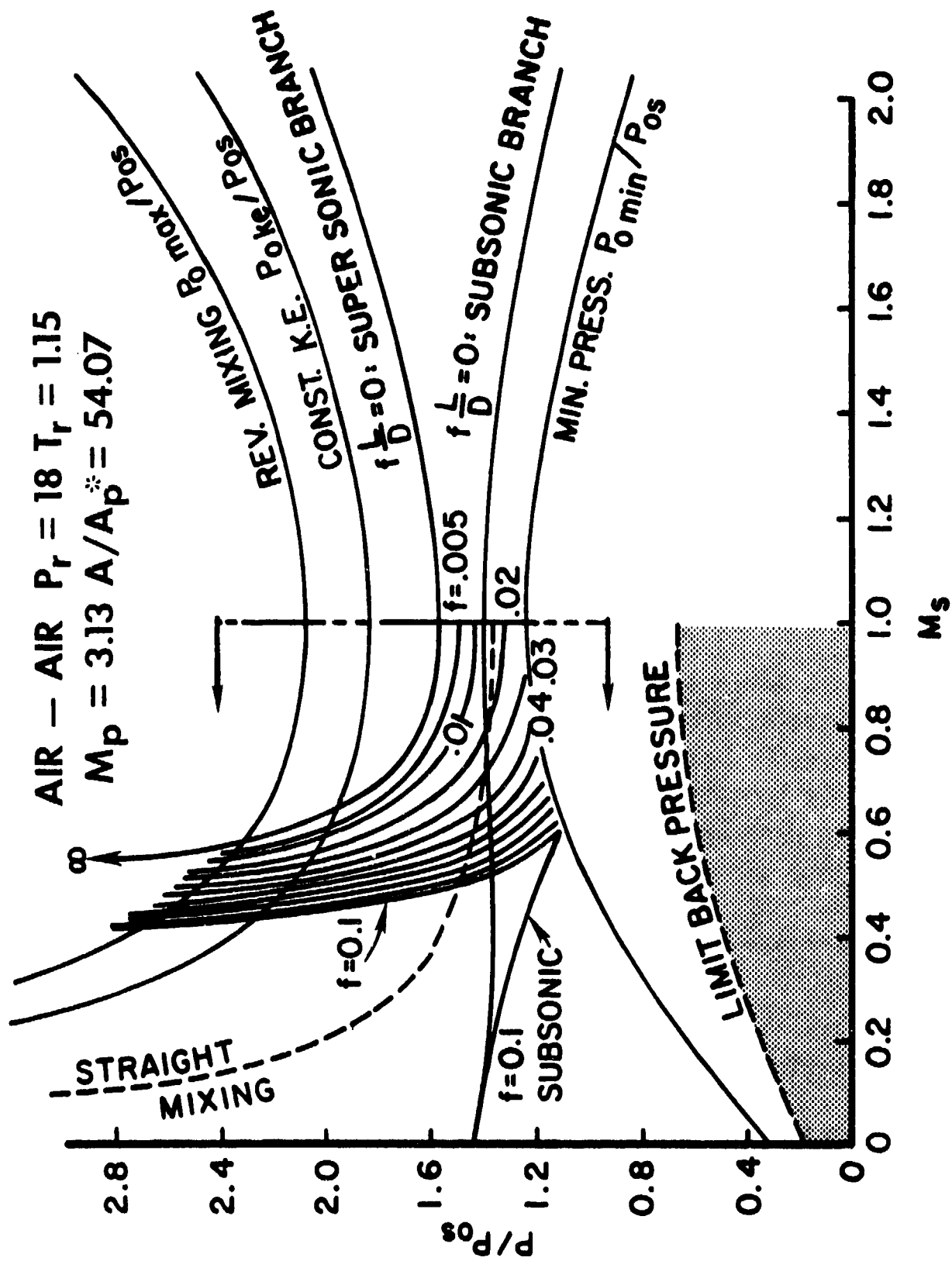
Figure 20.  Composite Curve Showing Various Limit Lines and Ejector Curves for Various Value of Friction.

would be choked. On the other hand, if we could reduce the length and still have the flow completely mixed we could increase the total pressure. This increase would terminate on one of the two branches for which $f(L/D) = 0$.

If the mixed flow is subsonic the operating point is uniquely determined by the back pressure for the appropriate $f(L/D)$.

Referring again to Figure 19 we can determine a value of the back pressure for which the flow must be supersonic. Since the Fanno line represents the locus of all possible static states that are consistant with the area and $M_S$ (or mass flow ratio) we can determine the minimum static pressure that is consistent with subsonic flow at the point where the Mach number approaches one. This limiting back pressure is also indicated on Figure 20. If the back pressure is below this curve in the shaded region the exit flow must be supersonic. Since we are concerned at this time only with a configuration like Figure 1 the inlet secondary Mach number must be equal to or less than one.

Clearly, in an experiment we could set the back pressure low enough to insure supersonic operation. However, as stated earlier, this boundary condition can not by itself enable us to determine the operating point since the mixed flow is supersonic and the exit pressure does not have to match the back pressure. Of course in a flying ejector we would want to adjust the flow through a suitably designed diffusor or nozzle in order to match the back pressure since this would optimize the thrust.

However, no matter how well we design the exit diffusor or nozzle we can not improve the performance of the ejector: we can in fact only lower the value of the exit total pressure. The operating point on the supersonic branch is not determined by either the back pressure or the exit diffusor (or nozzle design). It is in fact uniquely determined by the inlet conditions as discussed in the next section.

238

# SECTION 6

## DETERMINATION OF THE SUPERSONIC OPERATING POINT

Fabri and Siestrunck[3] in 1958 presented the results of an
extensive study of air-to-air ejectors with high pressure ratios
in which the primary air flow is supersonic. Although they were
primarily concerned with jet pumps they presented a theory that
was in good agreement with their experimental results for the
predicted rates of induced mass flows if the mixing tube is long
enough and the geometric configuration of the set up is similar
to the theoretical one. Thus, even though our application is
vastly diferent we can use their approach to determine the
operating point on the supersonic branch.

For the case of supersonic mixed flows and a supersonic
primary flow Fabri and Siestrunck[3] state that the inlet flow pat-
tern is similar to that shown on Figure 21. This flow pattern
represents the case where the inlet pressure in the primary flow
exceeds the inlet pressure of the secondary flow. Therefore, the
primary flow must undergo an additional expansion in the entrance
region of the mixing tube. The case where the two inlet
pressures match is a limiting case and therefore can be deter-
mined from this analysis. Since the expansion takes place very
quickly in the entrance region the flows will remain unmixed and
the slip line between the the primary and secondary flow is shown
as a double line eminating from the primary nozzle. (The double
line was originally drawn by Fabri and Siestrunck[3] to account for
the wake effect due to the wall thickness of the primary nozzle
which they could not neglect since they were working with very
small ejectors. We will neglect the effect in our analysis since
it can be accounted for in a simple adjustment of the area ratio.)

If one considers the case where the primary inlet pressure
is less than the secondary inlet pressure, there would be a shock
in the primary fluid immediately at the entrance that increases the
pressure in the primary fluid. This requires the slip line at

239

Figure 21. Inlet Flow Pattern for an Ejector Operating with a Supersonic Mixed Flow and Having a Supersonic Primary Flow and a Subsonic Secondary Flow.

the nozzle lip to turn inward. Thus, the secondary flow sees a minimum area at the inlet and the inlet secondary Mach number will be Mach one for the supersonic mixed flow case because of the flow pressure in the mixing tube required for the supersonic branch. (If this were not the case the pressure in the secondary flow would increase after the flow entered the mixing tube and this requires a still further shock compression in the primary flow which eventually would lead to a breakdown of the supersonic flow in the primary jet. This breakdown would lead to a subsonic mixed flow.) The case where the pressures are equal is again a limiting case. But the inlet Mach number is always one, including the limiting case.

These arguments do not hold if a throat is placed in the secondary stream ahead of the inlet since the secondary flow could then be supersonic when the pressures were matched at the inlet.

The continuity and momentum equations can be written for the control volume shown on Figure 21. The supersonic primary flow expands and the Mach number increases to station e. The subsonic secondary flow also undergoes an expansion and the Mach number increases until it reaches Mach one at the station e; in fact, this is the criteria by which we select the station e. The method of characteristics would be required to study the supersonic primary flow. However, the good agreement with experiment obtained by Fabri and Siestrunck show that it is adequate to treat both flows by simple one-dimensional isentropic equations.

Since the secondary Mach number is one at station e we can write for the constant area channel.

$$\frac{A_{p_e} + A_s^*}{A_p^*} = \frac{A}{A_p^*} \qquad (44)$$

241

or

$$\frac{A_{p_e}}{A_p^*} = \frac{A}{A_p^*} - \frac{A_s}{A_p^*} \cdot \frac{A_s^*}{A_s} \tag{45}$$

Using the well known isentropic flow equations for the area ratios we have

$$\frac{1}{M_{ep}^*}\left(\frac{\gamma+1}{2} - \frac{\gamma-1}{2} M_{ep}^{*2}\right)^{-\frac{1}{\gamma-1}} = \frac{A}{A_p^*} - \frac{A_s}{A_p^*} M_s^*\left(\frac{\gamma+1}{2} - \frac{\gamma-1}{2} M_s^{*2}\right)^{\frac{1}{\gamma-1}} \tag{46}$$

The isentropic relationships for the pressures can also be used.

$$P_{ep} = P_{op}\left(1 - \frac{\gamma-1}{\gamma+1} M_{ep}^{*2}\right)^{\frac{\gamma}{\gamma-1}} \tag{47}$$

and since $M_{es}^* = 1$

$$P_{es} = P_{os}\left(\frac{2}{\gamma+1}\right)^{\frac{\gamma}{\gamma-1}} \tag{48}$$

using the momentum equation along with the isentropic relations and the fact that $M_{es}^* = 1$ enables one to derive the following equation.

242

$$\frac{1 + M_{ep}^{*2}}{M_{ep}^{*}} = \frac{1 + M_{p}^{*2}}{M_{p}^{*}} + \frac{A_s}{A_p^{*}} \frac{P_{os}}{P_{op}} \left( \frac{\gamma+1}{2} - \frac{\gamma-1}{2} M_s^{*2} \right)^{\frac{1}{\gamma-1}} \left( 1 - M_s^{*} \right)^2$$

(49)

A computer program was written to solve these equations for a given geometry which fixes $M_p^{*}$. The continuity equation, Equation (46), was solved for $M_{ep}^{*}$ for given choice of $M_s^{*}$. These values were then used in Equation (49) to determine the value of $P_{os}/P_{op}$ that was consistant with the choice of $M_s^{*}$. In this way the curve shown on Figure 22 was constructed for the geometric values (including $M_p$) shown on Figure 22.

In Figure 22 we show the total pressure required to achieve the value of $M_s^{*}$. Since the geometry is fixed the value of the mass flow ratio is determined by $M_s^{*}$ and we can use the mass flow ratio and the values of $P_{op}/P_{os}$ to determine the various limit lines that we have previously discussed and they are also shown on Figure 22. Finally, we have also shown the total pressure achieved by the mixed flow on the supersonic branch.

When $M_s^{*} = 1$, it is clear from Equation (46) that $M_{ep}^{*} = M_p^{*}$ since the right side of Equation (46) is simply $A_p/A_p^{*}$ (note $A_p = A - A_s$).

If we solve Equation (49) for $P_{op}/P_{os}$ for the conditions where $M_s^{*} = 1$ and $M_{pe}^{*} = M_p^{*}$, we obtain the indeterminate form of zero over zero. However, using Y'Hospital's rule, we can show that the value of $P_{op}/P_{os}$ is related to $M_p^{*}$:

$$\frac{P_{op}}{P_{os}} = \left( \frac{\gamma+1}{2} - \frac{\gamma-1}{2} M_p^{*2} \right)^{-\frac{\gamma}{\gamma-1}}$$

(50)

Since $M_s^{*} = 1$ when equation (50) is valid, it can be shown, using the isentropic relations for pressure, that $P_{1p} = P_{1s}$ at this condition also. This is indicated on Figure 22. Fabri and Siestrunck refer to this condition as saturated flow.
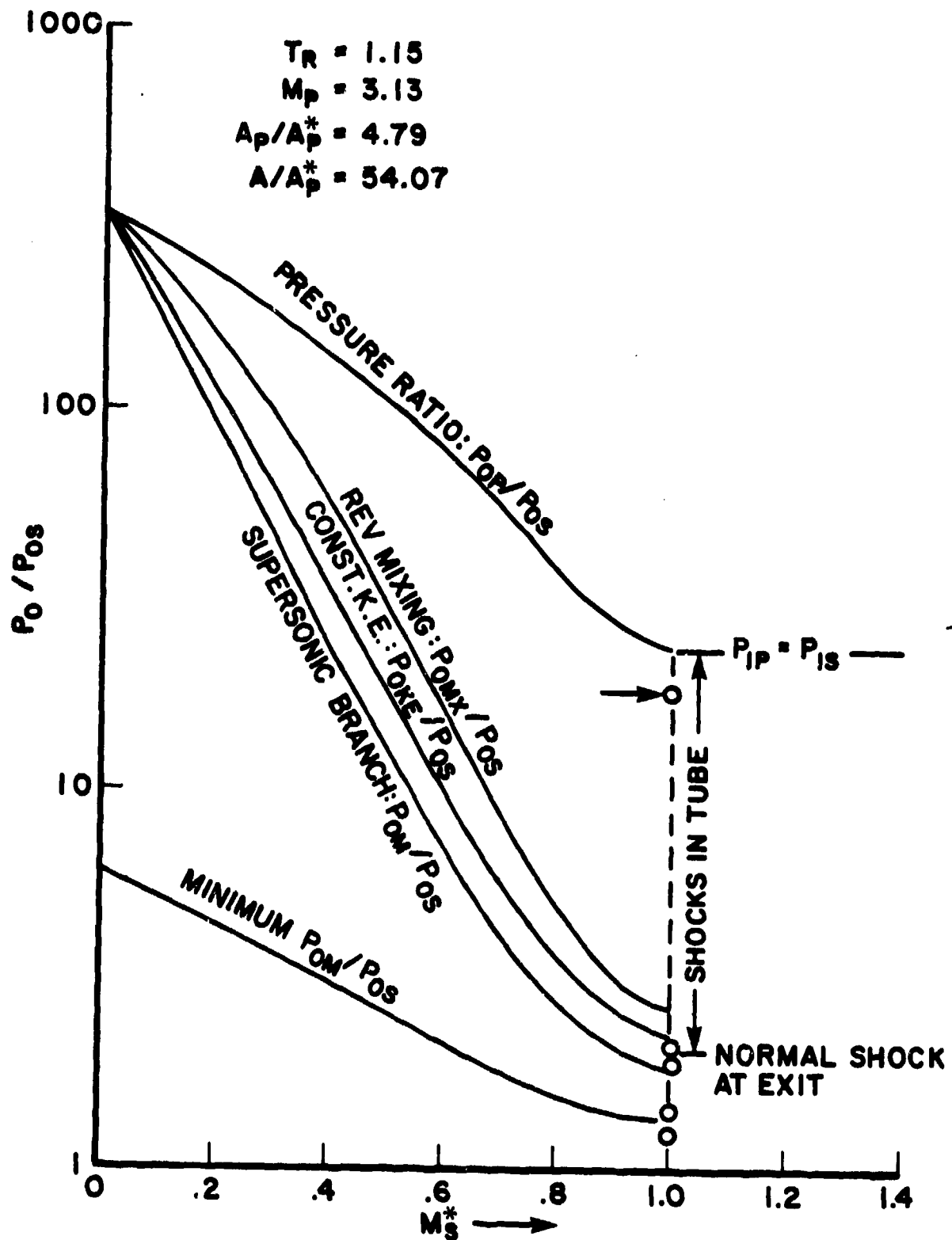
Figure 22. Pressure Ratio Required to Achieve a Given Value of $M_s^*$ Along with Limit Lines and the Supersonic Branch Solution.

244

Dr. Morton Alprin has pointed out[8] that there may also be a point where $M_s^*$ is less than 1 and $P_{1p} = P_{1s}$. The value of $M_s^*$ at which this occurs depends upon $M_p^*$ and the geometry.

For still lower values of the pressure ratio the inlet static pressure of the primary flow is lower than the static pressure in the secondary flow. Thus, the primary fluid experiences shocks within the mixing tube as indicated on Figure 22. Finally, we reach the point where a normal shock stands in the exit of the primary nozzle and for lower pressures we would have subsonic primary exit flow into the mixing tube.

It is of value to consider the following thought experiment. If we assumed that we have value of $P_{op}/P_{os} = 100$ for the ejector of Figure 22, we see that $M_s^* = 0.55$. With this value of $P_{op}/P_{os}$ suppose that we set the value of the back pressure such that the value of $M_s^*$ is 0.1 and the mixed flow is subsonic. As we lower the back pressure the value of $M_s^*$ increases toward 0.55. (For an example of how back pressure affects $M_s^*$, see Figure 9). When we reach $M_s^* = 0.55$, a further reduction in back pressure would require a higher value of $M_s^*$ and consequently a higher value of $\dot{m}_s/\dot{m}_p$. The experimental work of Fabri and Siestrunck[3] show definitely that this will not happen. Rather, the flow will make a transition to the supersonic branch and from then on it will be independent of the back pressure. Thus, we can determine the value of the transition back pressure from the subsonic branch by evaluating the back pressure at the same value of $M_s^*$ at which the supersonic branch will operate.

We can use the kinds of information shown on Figure 22 to construct a graph like that shown on Figure 23. We have chosen various area ratios and plotted the efficiency versus the mass flow ratio achieved for values of other parameters shown on the figure. Each curve terminates at the point where the value of $M_s^*$ first reaches Mach one. The points are indicated by the hack marks on Figure 23 along each area ratio curve. Now it is clear from Figure 23 that the maximum efficiency is achieved for a given mass flow ratio with the smallest diameter tube operating at a value of $M_s^* = 1$.
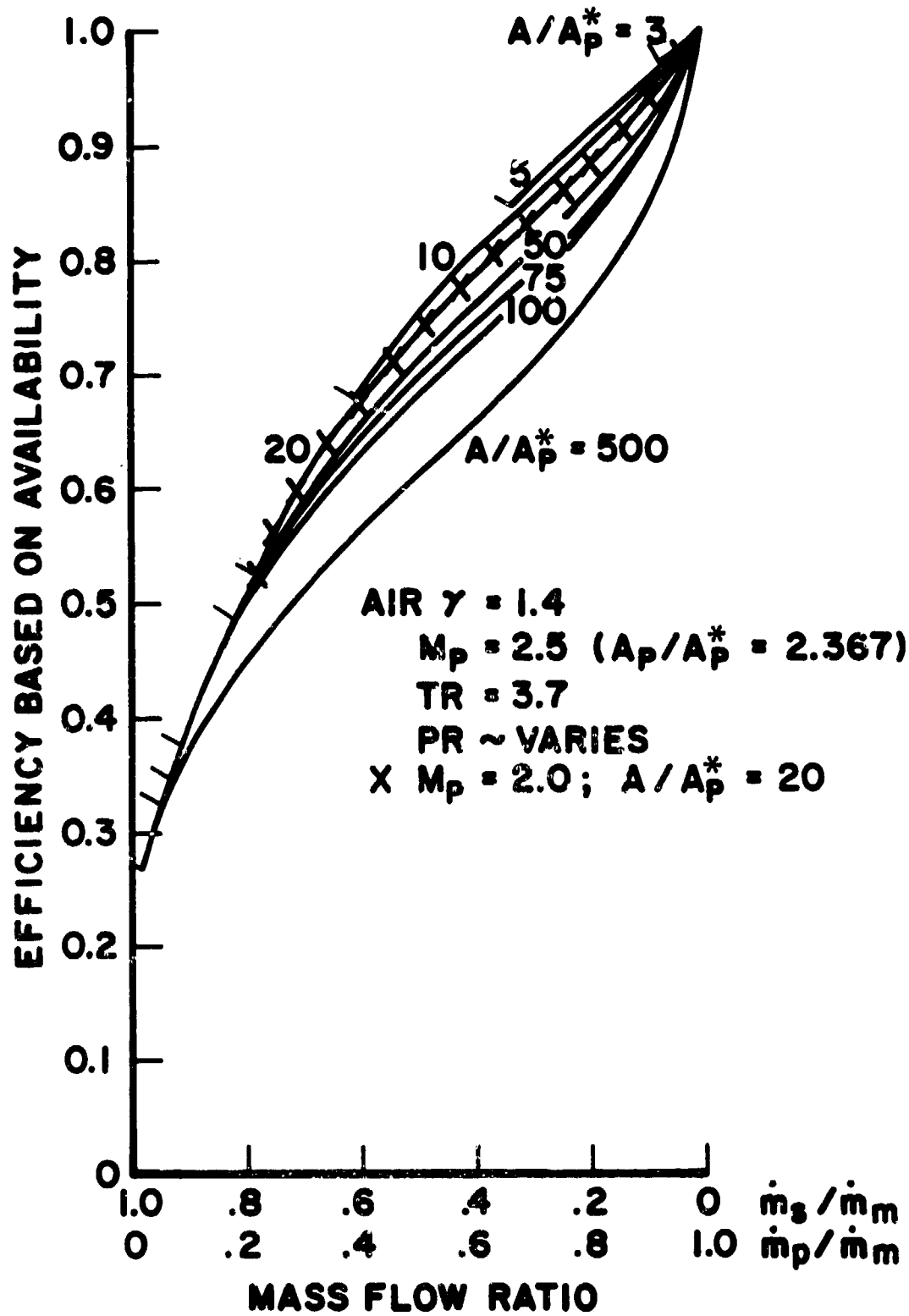
Figure 23.   Efficiency Versus Mass:   Flow Ratio for
Different Geometry Mixing Tubes.

## SECTION 7
## SUMMARY AND RECOMMENDATION

The results of our study have shown:

1) The supersonic branch can be achieved at subsonic, secondary inlet Mach numbers.

2) The extremely high values of efficiency obtained on both solution branches can be explained by the observation that the constant area geometry is a sufficient conditon but not a necessary condition for deriving the set of equations used for analyzing an ejector.

3) Since the constant area condition is not a necessary condition, it explains why some of the solutions obtained with the equations could not be achieved in an ejector.

4) Since the constant area condition is a sufficient condition for deriving the set of equations, all of the physically possible operating points (which conform to the assumptions) for an ejector will be included in the set of solutions.

5) The Fabri and Siestrunck[3] inlet condition uniquely determines the __single__ operating point for a given ejector that can be obtained on the supersonic branch with $M_s \leq 1$.

6) The back pressure at which the supersonic solution is acquired can also be determined.

7) Operation at values of $M_s \geq 1$ can be forced by the presence of a throat in the secondary flow before the inlet.

8) The optimum efficiency for a given mass flow ratio occurs when $M_s = 1$ and the mixing tube has the smallest area consistent with the mass flow requirements.

9) Limit lines were established for generalized mixers. These limit lines include:

Reversible mixing;

Constant kinetic energy;

Simple mixing;

Minimum total pressure.

10) Methods were shown for constructing T-s diagrams which show the limit lines and the stagnation states required for thrust augmentation at given flight Mach numbers.

11) Generalized thrust augmentation curves were constructed using the efficiency, based on availability, as a parameter.

12) The analysis presented will enable the complete determination of performance of an ejector when used for thrust augmentation. Thus, we are now in a position to determine realistic estimates of the upper performance limits of ejectors for thrust augmentation over a wide range of flight conditions.

We therefore make the following recommendations for future work:

1) The current ejector investigation be extended toward establishing a theory and analysis of the upper bound of ejector performance obtainable with the "second solution." Obtain upper limits of ejector thrust augmentation characteristics over various flight, altitude regimes and bypass ratios, and compare them with turbofan engine performance characteristics.

2) Based on the analytical results achieved in 1), we would:

a) Conduct theoretical studies of new methods of achieving high performance ejector devices that are characterized by compactness, light weight, and high efficiency; and

b) Outline the methods to be used in an experimental verification of the theory that would define the fundamental limitations of constant area ejectors operating with supersonic mixed flow.

248

# REFERENCES

1.  J. L. Porter, R. A. Squyers, A Summary/Overview of Ejector Augmentor Theory and Performance, USAF Technical Report No. R-91100-9CR-47, April 1981, Volumes I and II.

2.  E. D. Kennedy, "The Ejector Flow Process," Master of Science Thesis, University of Minnesota, Minneapolis, Minn., 1955.

3.  J. Fabria dn R. Siestrunck, Supersonic Air Ejectors, Advances in Applied Mechanics, Vol. 5, Academic Press, Inc., New York, NY, 1958.

4.  H. J. Hoge, On the Theory of Mixing of Fluid Streams, Quartermaster Research and Engineering Center, Pioneering Research Division, Technical Report PR-2, February 1959.

5.  B. Kiselev, Calculation on One-Dimensional Gas Flows, USAF Technical Report No. F-TS-1209-1A, January 1949, (translated from the Russian by Brown University).

6.  M. Alperin and J. Wu, High Speed Ejectors, AFFDL-TR-79-3048, May 1979.

7.  J. E. Minardi, et al., Rankine Cycle Augmented Light Gas Turbine, UDR-TR-80-53, May 1980.

8.  M. Alperin, personal communication, 1982.

# APPENDIX A

## COMPRESSIBLE FLOW EJECTOR ANALYSES FROM REFERENCE 7

## COMPRESSIBLE FLOW EJECTOR ANALYSIS

In this section we present a compressible flow analysis of an ejector for both constant area and constant pressure. Both problems can be solved in closed form if the fluids are assumed to be ideal gases. However, the solutions are somewhat complex and, therefore, computer programs were developed to obtain solutions over a wide range of parameters for a number of combinations of fluids.

We will first present the constant area analysis, then the constant pressure analysis and finally some results from the computer runs.

## Constant Area Analysis

A schematic of a constant area ejector is shown on Figure A-1. Also shown is the control volume used in the analysis.

At station 1 the flows are completely unmixed and each flow is assumed to be uniform and parallel. Station 1 is located at the exit plane of the primary nozzle. The exit area of the nozzle is $A_p$ and the area occupied by the secondary flow at station 1 is $A_s$. The exit area, A, at station 2 is the sum of the areas:

$$A = A_p + A_s \qquad (A-1)$$

Station 2 is assumed to be located far enough downstream from station 1 so that complete mixing has taken place and the flow is uniform and parallel.

For the control volume shown we can write the continuity, momentum and energy equations:

$$\dot{m}_p + \dot{m}_s = \dot{m}_m \qquad (A-2)$$

$$P_m A - P_{1p} A_p - P_{1s} A_s + 2\pi r \ell \tau = \dot{m}_p (V_p - V_m) + \dot{m}_s (V_s - V_m) \qquad (A-3)$$

$$\dot{m}_p h_{op} + \dot{m}_s h_{os} = \dot{m}_m (h_m + \frac{V_m^2}{2}) \qquad (A-4)$$
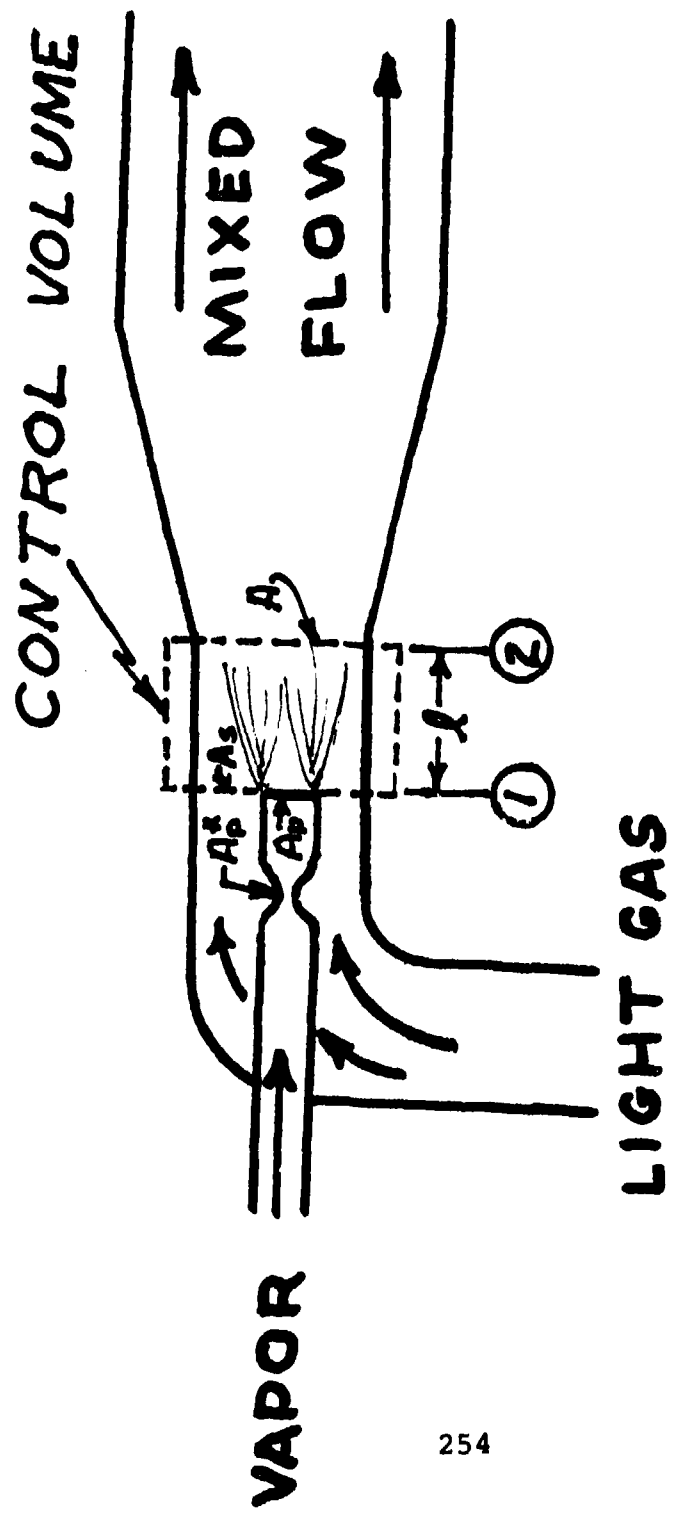
Figure A-1. Constant Area Ejector.

254

In Equations (A-2) to (A-4) $\dot{m}$ is the mass flow rate and the sub-
script designates the primary flow at station 1, s designates the
secondary flow at station 1, and m the mixed flow at station 2.

In the momentum equation, P is the pressure and V the velocity;
r is the radius of the tube at station 2 and ℓ is the distance
between station 1 and 2. The pressure $P_{1p}$ does not have to be
equal to $P_{1s}$ since the primary nozzle will be a supersonic nozzle
in the applications of interest.

In the energy equation $h_{op}$ and $h_{os}$ are the stagnation
enthalpies of the primary and secondary flows, respectively, and
$h_m$ is the static enthalpy of the mixed flow.

The mass flow rates of both the primary and secondary flows
can be adjusted at will by controlling the stagnation conditions.
Thus, in view of (A-2), all mass flow rates are known.

Of course the uniform flow assumption allows us to write:

$$\rho_{1p} A_p V_p = \dot{m}_p \tag{A-5}$$

$$\rho_{1s} A_s V_s = \dot{m}_s \tag{A-6}$$

$$\rho_m A V_m = \dot{m}_m \tag{A-7}$$

Hence, from the known geometry of the nozzle and ejector we
can obtain $V_p$ and $V_s$ if we assume an isentropic expansion from the
known stagnation conditions for the flow in the primary nozzle and
for the secondary fluid.

Consequently, the only unknowns in equations (A-3), (A-4), and
(A-7) are $P_m$, $h_m$, $\rho_m$ and $V_m$. However, we also know an equation of
state:

$$P_m = f(h_m, \rho_m) \tag{A-8}$$

If conditions are such that condensation of the primary
vapor occurs in the ejector, an iterative procedure would be
required to obtain a solution since Equation (A-8) would not be
simple. However, for many cases of interest, it will be

satisfactory to assume ideal gas behavior between station 1 and 2
for both the vapor and the secondary gas. (It is not required
that the primary gas expand as an ideal gas in the nozzle).

In the remainder of this section we will assume that the
gases are ideal gases with constant specific heats. Thus, we
can write:

$$h = C_p T \tag{A-9}$$

and

$$P = \rho RT \tag{A-10}$$

where $C_p$ is the specific heat at constant pressure and R is
the gas constant for the particular gas. For the mixed flow at
station 2 we have:

$$h_m = C_{p_m} T_m \tag{A-11}$$

$$P_m = \rho_m R_m T_m \tag{A-12}$$

Combining (A-12) and (A-7) yields

$$P_m = \frac{\dot{m}_m R_m}{A V_m} T_m \tag{A-13}$$

(note that Equations (A-13) and (A-11) could be combined to form
an equation in the form of Equation (A-8) is desired).

We can obtain the following two equations from the momentum
and energy equations:

$$\frac{\dot{m}_m R_m}{A V_m} T_m A - (P_{1p} A_p + P_{1s} A_s - 2\pi r \ell \tau) = \\ \dot{m}_p (V_p - V_m) + \dot{m}_s (V_s - V_m) \tag{A-14}$$

$$\dot{m}_p h_{op} + \dot{m}_s h_{os} = m_m (C_p T_m + \frac{v_m^2}{2}) \tag{A-15}$$

256

Now $R_m$ can be determined from the following simple mixing formula for an ideal gas.

$$\dot{m}_m R_m = \dot{m}_p R_p + \dot{m}_s R_s \qquad (A-16)$$

Thus, (A-14), (A-15), and (A-16) can be combined to obtain a closed form solution to $V_m$, $T_m$ and $R_m$. From Equation (A-14)

$$T_m = \frac{1}{\dot{m}_m R_m} \; [(P_{1p} A_p + P_{1s} A_s - 2\pi r \ell \tau) V_m$$

$$+ \dot{m}_p (V_p - V_m) V_m + \dot{m}_s (V_s - V_m) V_m] \qquad (A-17)$$

while from Equation (A-15) and (A-9) we have

$$T_m = \frac{C_{p_p} \dot{m}_p}{C_{p_m} \dot{m}_m} \; T_{op} + \frac{C_{p_s} \dot{m}_s}{C_{p_m} \dot{m}_m} \; T_{os} - \frac{V_m^2}{2 C_{p_m}} \qquad (A-18)$$

Substituting for $T_m$ in Equation (A-17) from Equation (A-18) and dividing by $T_{1s}$ yields

$$\left[ \frac{C_{p_p} \dot{m}_p}{C_{pm} \dot{m}_m} \; \frac{T_{op}}{T_{os}} \; \cdot \; \frac{T_{os}}{T_{1s}} \; + \; \frac{C_{ps} \dot{m}_s}{C_{pm} \dot{m}_m} \right] \frac{T_{os}}{T_{1s}} - \frac{V_m^2}{2 C_{pm} T_{os}} \; \frac{T_{os}}{T_{1s}} \; =$$

$$\left[ \left( \frac{P_{1p}}{P_{os}} \right) \left( \frac{P_{os}}{P_{1s}} \right) \frac{A_p}{A} \; + \; \frac{A_s}{A} \; - \; \frac{2\tau \ell}{P_{1s} r} \right] \; \frac{A P_{1s}}{\dot{m}_m R_m T_{1s}} \; V_m$$

$$+ \; \frac{\dot{m}_p V_p}{\dot{m}_m R_m T_{1s}} \; V_m + \frac{\dot{m}_s V_s}{\dot{m}_m R_m T_{1s}} \; V_m - \frac{\dot{m}_p + \dot{m}_s}{\dot{m}_m \; R_m} \; \frac{V_m^2}{T_{1s}} \qquad (A-19)$$

Equation (A-19) is a quadratic equation in $V_m$ and can, therefore, be solved since all the quantities in the equation are known once the geometry and stagnation conditions are known.

Of course, a suitable estimate of the shear stress, $\tau$, needs to be available. However, for our first estimates we have assumed that $\tau = 0$ (Equation A-19).

The formulas of Table A-1 are helpful in obtaining a solution to Equation (A-19). In Table A-1, W is the molecular weight of the fluid.

With the exception of the fluid gas constant, $\bar{R}$, in equation T6 of Table A-1, all of the quantities with a bar over them are ratios of the primary flow value to the secondary flow value. If we cast each of the terms (excluding $V_m$) in Equation (A-19) in terms of these ratios, we obtain the following set of terms which we designate with C's:

$$C1 = \frac{\Gamma \bar{m} \, \bar{T}_o + W}{\Gamma \bar{m} + \bar{W}} \quad (1 + \frac{\gamma_s - 1}{2} \, M_s^2) \tag{A-20}$$

$$C2 = \frac{\bar{W}(\bar{m} + 1)}{\Gamma \bar{m} + \bar{W}} \quad \frac{\gamma_s - 1}{2} \, M_s^2 \tag{A-21}$$

$$C3 = (\bar{P}_1 \, \bar{A} + 1 - \frac{2\tau \ell}{P_{1s} r} (1 + \bar{A})) \, \frac{\bar{W}}{\bar{m} + \bar{w}} \tag{A-22}$$

$$C4 = \frac{\bar{m} \, \bar{W} \, \bar{V}}{\bar{m} + \bar{w}} \, \gamma_s \, M_s^2 \tag{A-23}$$

$$C5 = \frac{\bar{W}}{\bar{m} + \bar{w}} \, \gamma_s M_s^2 \tag{A-24}$$

$$C6 = \frac{\bar{W}(\bar{m} + 1)}{\bar{w} + \bar{m}} \, \gamma_s M_s^2 \tag{A-25}$$

Setting the ratio $V_m / V_{1s} \equiv \bar{V}_m$, we can write Equation (A-19) in terms of the C's as:

$$(C2 - C6) \, V_m^2 + (C3 + C4 + C5) \, \bar{V}_m - C1 = 0 \quad . \tag{A-26}$$

## TABLE A-1

## USEFUL OTHER EQUATIONS FOR AN IDEAL GAS

### ISENTROPIC FLOW

$$\frac{T_o}{T} = 1 + \frac{\gamma - 1}{2} M^2 \tag{A-T1}$$

$$\frac{P_o}{P} = \left(1 + \frac{\gamma - 1}{2} M^2\right)^{\frac{\gamma}{\gamma - 1}} \tag{A-T2}$$

$$\frac{\rho_o}{\rho} = \left(1 + \frac{\gamma - 1}{2} M^2\right)^{\frac{1}{\gamma - 1}} \tag{A-T3}$$

$$\frac{A}{A^*} = \frac{1}{M} \left[\frac{2}{\gamma + 1} \left(1 + \frac{\gamma - 1}{2} M^2\right)\right]^{\frac{\gamma + 1}{2(\gamma - 1)}} \tag{A-T4}$$

$$\frac{T_o}{T} \frac{V^2}{2h_o} = \frac{\gamma - 1}{2} M^2 \tag{A-T5}$$

$$\frac{\dot{m}}{A} = \frac{\gamma W}{R} \frac{P_o}{\sqrt{T_o}} \frac{M}{\left(1 + \frac{\gamma - 1}{2} M^2\right)^{\frac{\gamma + 1}{2(\gamma - 1)}}} \tag{A-T6}$$

### MIXING FORMULA

$$C_{p_m} \dot{m}_m = C_{p_p} \dot{m}_p + C_{ps} \dot{m}_s \tag{A-T7}$$

$$C_{v_m} \dot{m}_m = C_{v_p} \dot{m}_p + C_{v_s} \dot{m}_s \tag{A-T8}$$

$$R_m \dot{m}_m = R_p \dot{m}_p + R_s \dot{m}_s \tag{A-T9}$$

$$\gamma_m = \gamma_p \frac{1 + \frac{W_p}{W_s} \frac{m_s}{m_p} \frac{\gamma_p - 1}{\gamma_p} \cdot \frac{\gamma_s}{\gamma_s - 1}}{1 + \frac{W_p}{W_s} \frac{m_s}{m_p} \cdot \frac{\gamma_p - 1}{\gamma_s - 1}} \tag{A-T10}$$

259

# TABLE A-1 (Concluded)
## USEFUL OTHER EQUATIONS FOR AN IDEAL GAS

$$\Gamma \equiv [\gamma_p/(\gamma_p - 1)]/[\gamma_s/(\gamma_s - 1)] \qquad\qquad\qquad (A\text{-}T11)$$

$$C_{pp}/C_{ps} = \Gamma/\overline{W}$$

$$C_{pm}/C_{ps} = (\Gamma\overline{m} + \overline{W})/[\overline{W}(\overline{m} + 1)] \qquad\qquad (A\text{-}T12)$$

$$R_m/R_s = (\overline{m} + \overline{W})/[\overline{W}(\overline{m} + 1)] \qquad\qquad\qquad (A\text{-}T13)$$

$$C_{pp}\dot{m}_p/C_{pm}\,\dot{m}_m = \Gamma\overline{m}/(\Gamma\overline{m} + \overline{W}) \qquad\qquad (A\text{-}T14)$$

$$R_p\dot{m}_p/R_m\dot{m}_m = \overline{m}/(\overline{m} + \overline{W}) \qquad\qquad\qquad (A\text{-}T15)$$

260

If we evaluate Equation (A-6) for the secondary flow rate and the primary flow rate, we can show that

$$\frac{\bar{m}}{\bar{A}} = \sqrt{\bar{\gamma}\,\bar{W}}\left(\frac{P_o}{\sqrt{T_o}}\right)\left(\frac{2}{\gamma_p+1}\right)^{\frac{\gamma_p+1}{2(\gamma_p-1)}}\left(\frac{A_p^*}{A_p}\right)\frac{\left(1+\frac{\gamma_s-1}{2}M_s^2\right)^{\frac{\gamma_s+1}{2(\gamma_s-1)}}}{M_s} \quad (A-27)$$

In Equation (A-27) we have assumed the primary nozzle is chocked. The value of $M_s$ can be controlled in an experiment by adjusting the back pressure on the ejector at station 2 for a given value of $P_{os}$. Thus, we have used $M_s$ as our independent variable in our computer calculations. A geometry, pair of fluids, and stagnation conditions are chosen and Equation (A-27) is solved for $\bar{m}$ (or we hold $\bar{m}$ fixed and calculate $\bar{A}$) for various values of $M_s$. Equations (A-20) through (A-26) can then be solved for each value of $M_s$. Once $V_m$ is determined, either Equation (A-27) or (A-28) can be used to determine $T_m$. The density and pressure can be determined by Equations (A-7) and (A-13). Therefore, all of the properties at station 2 are completely determined.

## Ejector "Efficiency"

Many definitions of ejector efficiency can be made and found to be useful. Some of them, however, are pseudal efficiencies since they can be greater than one under certain conditions of operation.

For our purposes we have calculated at this time four pseudal efficiencies. Each is briefly discussed below.

The first pseudal efficiency that we have considered is based on the thermodynamic availability, $\psi$, of the primary vapor and the availability of the mixed gas and vapor leaving the ejector. If we neglect potential energy terms we have, in general, for the availability of a fluid in steady flow:

$$\psi = h_o - h_R - T_R(s - s_R) \quad (A-28)$$

where $h_R$ is the reference enthalpy and $s_R$ is the reference entropy and $h_o$ is the stagnation enthalpy of the fluid (therefore, it

261

includes kinetic energy) and s is the static entropy of the fluid. Ordinarily, the reference values would be evaluated at atmospheric pressure and temperature; however, for our purposes we will evaluate the reference values at the stagnation temperature and pressure of the secondary gas. This insures us that the secondary gas will have zero availability before mixing and that all the availability results only from the primary flow.

For an ideal gas with constant specific heats, we have:

$$h_o - h_R = C_P(T_o - T_R) \qquad (A-29)$$

and since the entropy can be found from the isentropic stagnation conditions, we have:

$$s - s_R = C_P \ln\left(\frac{T_o}{T_R}\right) - R \ln\left(\frac{P_o}{P_R}\right) \qquad . \qquad (A-30)$$

Therefore, we can write for the general case

$$\psi = C_P T_R \left( \frac{T_o}{T_R} - 1 - \ln\left[ \frac{T_o}{T_R} \left(\frac{P_R}{P_o}\right)^{\frac{\gamma-1}{\gamma}} \right] \right) \qquad (A-31)$$

Evaluating Equation (A-31) for the primary flow and the secondary stagnation conditions for the reference state, we have

$$\psi_P = C_{PP} T_{os} \left( \frac{T_{op}}{T_{os}} - 1 - \ln\left[ \frac{T_{op}}{T_{os}} \left(\frac{P_{os}}{P_{op}}\right)^{\frac{\gamma_p-1}{\gamma_p}} \right] \right) \qquad (A-32)$$

and for the mixed gas we have

$$\psi_m = C_{P_m^*} T_{os} \left( \frac{T_{om}}{T_{os}} - 1 - \ln\left[ \frac{T_{om}}{T_{os}} \left(\frac{P_{os}}{P_{om}}\right)^{\frac{\gamma_m-1}{\gamma_m}} \right] \right) \qquad . \qquad (A-33)$$

262

Thus, the efficiency based on availability, $\eta_{av}$, is

$$\eta_{av} = \frac{\dot{m}_m C_{pm}}{\dot{m}_p C_{pp}} \; \frac{\dfrac{T_{om}}{T_{os}} - 1 - \ell n \left[ \dfrac{T_{om}}{T_{os}} \left( \dfrac{P_{os}}{P_{om}} \right)^{\frac{\gamma_m - 1}{\gamma_m}} \right]}{\dfrac{T_{op}}{T_{os}} - 1 - \ell n \left[ \dfrac{T_{op}}{T_{os}} \left( \dfrac{P_{os}}{P_{op}} \right)^{\frac{\gamma_p - 1}{\gamma_p}} \right]} \qquad (A-34)$$

Since all the quantities in Equation (A-34) are known from the previous calculations, we can determine $\eta_{av}$, and it is a true efficiency for the ejector if primary and secondary gases are the same, but a pseudal efficiency if not, since we neglected the availability due to disimilare gases.

In the other pseudal efficiencies that we have looked at, we divide the enthalpy change of the mixed flow for an isentropic expansion from the stagnation conditions of the mixed flow to the secondary stagnation pressure, $P_{os}$, by three different changes in enthalpy of the primary.

In the first case, we use the change in the enthalpy of the primary for an isentropic expansion from the primary stagnation conditions to the secondary stagnation pressure.

$$\eta_{pos} = \frac{\dot{m}_m}{\dot{m}_p} \; \frac{(h_{om} - h_{m@Pos})}{(h_{op} - h_{@Pos})} \qquad (A-35)$$

In the second case we use the change in the enthalpy of the primary for an isentropic expansion from the primary stagnation conditions to the static pressure, $P_{1p}$ at the inlet to the ejector.

$$\eta_{p1p} = \frac{\dot{m}_m}{\dot{m}_p} \; \frac{(h_{om} - h_{m@Pos})}{(h_{op} - h_{@P1p})} \qquad (A-36)$$

263

Finally in the third case we use the change in the enthalpy of primary for an isentropic expansion from the primary stagnation conditions to the secondary stagnation temperature.

$$\eta_{Tos} = \frac{\dot{m}_m}{\dot{m}_p} \; \frac{(h_{om} - h_{m@Pos})}{(h_{op} - h_{@Tos})} \tag{A-37}$$

Under certain conditions the "efficiencies" in Equations (A-35) to (A-37) can be greater than one and, therefore, they are not true efficiencies.

## Constant Pressure Analysis

For the constant pressure case, the momentum equation takes a very simple form if we neglect shear stress:

$$\dot{m}_p(V_p - V_m) + \dot{m}_s(V_s - V_m) = 0. \tag{A-38}$$

Equation (A-38) can be immediately solved for $V_m$. Using the same notation as for the constant area case we obtain the result:

$$\bar{V}_m = \frac{\bar{m}\,\bar{V} + 1}{\bar{m} + 1} \tag{A-39}$$

The temperature can be found from the energy equation, Equation (A-18), which is also valid for the constant pressure case. The pressure is, of course, equal to the inlet value, therefore Equation (A-13) can be solved for the exit area. Thus, a complete solution can be found for constant pressure which is simpler than the constant area case. The efficiency definitions can be used for either the constant pressure or constant area case.

## Computer Results of Ejector Studies

A large number of comptuer runs have been made for various combinations of fluids and geometries. Data for the runs presented in the main body are presented in this section.

264

The first set of data is presented for air driving air in the constant area case. The mass flow ratio was set to 0.1. All of the tables present the tabulated comptuer results used to plot Figures 2 and 3 in the main body. The first column contains the secondary Mach number Ms which is taken as the independent variable. The second column is $P_{1s}/P_{0s}$ (because of lack of space, it is labeled (P1S/ and the third column is the temperature ratio $T_{1s}/T_{0s}$. Each of these values are obtained from Ms using isentropic relations. The exit area of the primary nozzle is chosen to match the pressure of the primary to the secondary. This sets the value of the primary Mach number, $M_p$ (located in column 10) and enables one to find $T_{1p}/T_{op}$ and $P_{1p}/P_{op}$ (located in columns 11 and 12).

Column four gives the ratio of the primary velocity to the secondary velocity $V_p/V_s$ and column five gives the ratio of the mixed velocity to the secondary velocity.

Column six gives the mixed flow Mach number. Column seven is the pessure ratio $P_m/P_{os}$ and column eight is the temperature ratio $T_m/T_{os}$. The gamma value of the mixture is given in column nine.

Column thirteen gives the area ratio $A_p/A_s$ required to match the exit pressure and column fourteen gives the value of $A/R_p^*$. The last four columns give the three efficiencies discussed in this Appendix and the entropy increase.

CONSTANT AREA CALCULATIONS
SUBSONIC BRANCH
PRIMARY VAPOR: AIR   SECONDARY GAS:AIR
PR= 6.000 TR= 3.700 GP=1.400 GS=1.400 WR=   1.00 WP= 29.00 WS= 29.00
M.P/M.S=   0.100

| MS | PIS/ | TIS/ | VP/VS | VM/VS | MM | PM/ | TM/ | GM | MP | TIP/TOP | PIP/POP | AP/AS | A/AP* | EFPOS | EFTOS | EFAVL | SR |
|---|---|---|---|---|---|---|---|---|---|---|---|---|---|---|---|---|---|
| 0 3500 | 0.995 | 1.000 | 54.485 | 1.341 | 0.060 | 1.016 | 1.245 | 1.400 | 1.83 | 0.599 | 0.166 | 0.004 | 363.038 | 0.05 | 0.03 | 0.180 | 0.497 |
| 0.1000 | 0.993 | 0.998 | 27.293 | 1.316 | 0.118 | 1.024 | 1.242 | 1.400 | 1.83 | 0.598 | 0.166 | 0.008 | 183.073 | 0.09 | 0.05 | 0.204 | 0.481 |
| 0.1500 | 0.984 | 0.996 | 18.252 | 1.295 | 0.174 | 1.027 | 1.238 | 1.400 | 1.84 | 0.597 | 0.164 | 0.012 | 123.455 | 0.13 | 0.07 | 0.229 | 0.467 |
| 0.2000 | 0.972 | 0.992 | 13.748 | 1.277 | 0.229 | 1.025 | 1.233 | 1.400 | 1.85 | 0.595 | 0.162 | 0.016 | 93.931 | 0.16 | 0.09 | 0.250 | 0.454 |
| 0.2500 | 0.957 | 0.988 | 11.059 | 1.261 | 0.283 | 1.017 | 1.226 | 1.400 | 1.86 | 0.592 | 0.160 | 0.020 | 76.449 | 0.19 | 0.10 | 0.269 | 0.443 |
| 0.3000 | 0.939 | 0.982 | 9.277 | 1.247 | 0.336 | 1.004 | 1.218 | 1.400 | 1.87 | 0.589 | 0.157 | 0.024 | 64.996 | 0.21 | 0.12 | 0.285 | 0.433 |
| 0.3500 | 0.919 | 0.976 | 8.013 | 1.234 | 0.388 | 0.987 | 1.209 | 1.400 | 1.88 | 3.585 | 0.153 | 0.028 | 56.994 | 0.24 | 0.13 | 0.300 | 0.424 |
| 0.4000 | 0.896 | 0.969 | 7.073 | 1.224 | 0.440 | 0.966 | 1.199 | 1.400 | 1.90 | 0.581 | 0.149 | 0.031 | 51.156 | 0.26 | 0.14 | 0.312 | 0.417 |
| 0.4500 | 0.870 | 0.961 | 6.349 | 1.214 | 0.492 | 0.942 | 1.188 | 1.400 | 1.92 | 0.576 | 0.145 | 0.035 | 46.764 | 0.27 | 0.15 | 0.323 | 0.410 |
| 0.5000 | 0.843 | 0.952 | 5.775 | 1.206 | 0.543 | 0.914 | 1.176 | 1.400 | 1.94 | 0.571 | 0.141 | 0.038 | 43.398 | 0.29 | 0.16 | 0.333 | 0.404 |
| 0.5500 | 0.814 | 0.943 | 5.311 | 1.200 | 0.594 | 0.884 | 1.163 | 1.400 | 1.96 | 0.565 | 0.136 | 0.042 | 40.780 | 0.30 | 0.16 | 0.341 | 0.399 |
| 0.6000 | 0.784 | 0.933 | 4.928 | 1.194 | 0.645 | 0.852 | 1.150 | 1.400 | 1.99 | 0.559 | 0.131 | 0.045 | 38.731 | 0.31 | 0.17 | 0.348 | 0.395 |
| 0.6500 | 0.753 | 0.922 | 4.609 | 1.190 | 0.697 | 0.817 | 1.135 | 1.400 | 2.01 | 0.553 | 0.125 | 0.048 | 37.127 | 0.32 | 0.18 | 0.353 | 0.392 |
| 0.7000 | 0.721 | 0.911 | 4.339 | 1.188 | 0.750 | 0.781 | 1.120 | 1.400 | 2.04 | 0.546 | 0.120 | 0.051 | 35.881 | 0.33 | 0.18 | 0.357 | 0.389 |
| 0 7500 | 0.689 | 0.899 | 4.108 | 1.188 | 0.804 | 0.742 | 1.103 | 1.400 | 2.07 | 0.539 | 0.115 | 0.054 | 34.928 | 0.33 | 0.18 | 0.361 | 0.387 |
| 0.8000 | 0.656 | 0.887 | 3.909 | 1.194 | 0.864 | 0.699 | 1.084 | 1.400 | 2.10 | 0.531 | 0.109 | 0.057 | 34.222 | 0.33 | 0.18 | 0.363 | 0.386 |
| 0.8500 | 0.624 | 0.874 | 3.736 | 1.220 | 0.942 | 0.643 | 1.058 | 1.400 | 2.13 | 0.524 | 0.104 | 0.059 | 33.727 | 0.34 | 0.18 | 0.364 | 0.385 |
| 0.9000 | IMAGINARY SOLUTION | | | | | | | | | | | | | | | | |
| 0.9500 | IMAGINARY SOLUTION | | | | | | | | | | | | | | | | |
| 1.0000 | IMAGINARY SOLUTION | | | | | | | | | | | | | | | | |
| 1.0500 | IMAGINARY SOLUTION | | | | | | | | | | | | | | | | |
| 1.1000 | IMAGINARY SOLUTION | | | | | | | | | | | | | | | | |
| 1.1500 | 0.440 | 0 791 | 3.050 | 0.920 | 0.911 | 0.662 | 1.068 | 1.400 | 2.36 | 0.474 | 0.073 | 0.073 | 34.044 | 0.32 | 0.18 | 0.356 | 0.390 |
| 1.2000 | 0.412 | 0.776 | 2.974 | 0.853 | 0.866 | 0.691 | 1.083 | 1.400 | 2.40 | 0.465 | 0.069 | 0.075 | 34.538 | 0.31 | 0.17 | 0.347 | 0.396 |
| 1 2500 | 0.386 | 0.762 | 2.906 | 0.798 | 0.832 | 0.710 | 1.094 | 1.400 | 2.44 | 0.457 | 0.064 | 0.076 | 35.143 | 0.29 | 0.16 | 0.334 | 0.403 |
| 1.3000 | 0.361 | 0.747 | 2.844 | 0.750 | 0.803 | 0.724 | 1.103 | 1.400 | 2.48 | 0.448 | 0.060 | 0.078 | 35.855 | 0.27 | 0.15 | 0.319 | 0.413 |
| 1.3500 | 0.337 | 0.733 | 2.787 | 0.709 | 0.777 | 0.734 | 1.111 | 1.400 | 2.53 | 0.439 | 0.056 | 0.080 | 36.673 | 0.24 | 0.13 | 0.299 | 0.425 |
| 1.4000 | 0.314 | 0 718 | 2.735 | 0.673 | 0.755 | 0.740 | 1.118 | 1.400 | 2.57 | 0.431 | 0.052 | 0.081 | 37.597 | 0.20 | 0.11 | 0.276 | 0.438 |
| 1.4500 | 0.293 | 0.704 | 2.688 | 0.640 | 0.734 | 0.742 | 1.124 | 1.400 | 2.62 | 0.422 | 0.049 | 0.082 | 38.627 | 0.16 | 0.09 | 0.250 | 0.454 |
| 1.5000 | 0.272 | 0.690 | 2.645 | 0.611 | 0.716 | 0.742 | 1.130 | 1.400 | 2.66 | 0.413 | 0.045 | 0.084 | 39.764 | 0.11 | 0.06 | 0.220 | 0.472 |
| 1.5500 | 0.253 | 0.675 | 2.605 | 0.584 | 0.699 | 0.738 | 1.135 | 1.400 | 2.71 | 0.405 | 0.042 | 0.085 | 41.009 | 0.06 | 0.03 | 0.187 | 0.492 |
| 1.6000 | 0.235 | 0.661 | 2.568 | 0.560 | 0.683 | 0.733 | 1.139 | 1.400 | 2.76 | 0.396 | 0.039 | 0.086 | 42.365 | 0.00 | 0.00 | 0.151 | 0.514 |
| 1.6500 | 0.218 | 0.647 | 2.534 | 0.538 | 0.669 | 0.724 | 1.143 | 1.400 | 2.81 | 0.388 | 0.036 | 0.088 | 43.835 | -0.06 | -0.03 | 0.113 | 0.537 |
| 1.7000 | 0.203 | 0.634 | 2.503 | 0.519 | 0.655 | 0.715 | 1.147 | 1.400 | 2.86 | 0.380 | 0.034 | 0.089 | 45.420 | -0.13 | -0.07 | 0.071 | 0.563 |
| 1.7500 | 0.188 | 0.620 | 2.474 | 0.500 | 0.643 | 0.703 | 1.150 | 1.400 | 2.91 | 0.372 | 0.031 | 0.090 | 47.125 | -0.20 | -0.11 | 0.027 | 0.589 |
| 1 8000 | 0.174 | 0.607 | 2.447 | 0.484 | 0.631 | 0.690 | 1.153 | 1.400 | 2.96 | 0.364 | 0.029 | 0.091 | 48.953 | -0.28 | -0.15 | -0.020 | 0.618 |
| 1.8500 | 0.161 | 0.594 | 2.422 | 0.468 | 0.621 | 0.676 | 1.156 | 1.400 | 3.01 | 0.356 | 0.027 | 0.092 | 50.909 | -0.36 | -0.20 | -0.068 | 0.647 |
| 1.9000 | 0.149 | 0.581 | 2.399 | 0.454 | 0.611 | 0.660 | 1.159 | 1.400 | 3.06 | 0.348 | 0.025 | 0.092 | 52.997 | -0.44 | -0.24 | -0.119 | 0.678 |
| 1.9500 | 0.138 | 0.568 | 2.377 | 0.441 | 0.601 | 0.644 | 1.161 | 1.400 | 3.11 | 0.340 | 0.023 | 0.093 | 55.223 | -0.53 | -0.29 | -0.172 | 0.710 |
| 2.0000 | 0.126 | 0.556 | 2.356 | 0.429 | 0.593 | 0.627 | 1.164 | 1.400 | 3.16 | 0.333 | 0.021 | 0.094 | 57.591 | -0.62 | -0.34 | -0.227 | 0.743 |
| 2.0500 | 0.118 | 0.543 | 2.337 | 0.418 | 0.585 | 0.610 | 1.166 | 1.400 | 3.22 | 0.326 | 0.020 | 0.095 | 60.107 | -0.72 | -0.40 | -0.284 | 0.778 |

CONSTANT AREA CALCULATIONS
SUPERSONIC BRANCH
PRIMARY VAPOR: AIR   SECONDARY GAS:AIR
PR= 6.000 TR= 3.700 GP=1.400 GS=1.400 VR=  1.00 WP= 29.00 WS= 29.00
M.P/M.S=  0.100

| MS | P1S/ | T1S/ | VP/VS | VM/VS | MM | PM/ | TM/ | GM | MP | T1P/T0P | P1P/P0P | AP/AS | A/AP* | EFP0S | EFT0S | EFAVL | SR |
|---|---|---|---|---|---|---|---|---|---|---|---|---|---|---|---|---|---|
| 0.0500 | VIOLATION OF 2ND LAW: REQUIRES NEGATIVE TEMPERATURES | | | | | | | | | | | | | | | | |
| 0.1000 | VIOLATION OF 2ND LAW: REQUIRES NEGATIVE TEMPERATURES | | | | | | | | | | | | | | | | |
| 0.1500 | VIOLATION OF 2ND LAW: REQUIRES NEGATIVE TEMPERATURES | | | | | | | | | | | | | | | | |
| 0.2000 | VIOLATION OF 2ND LAW: REQUIRES NEGATIVE TEMPERATURES | | | | | | | | | | | | | | | | |
| 0.2500 | VIOLATION OF 2ND LAW: REQUIRES NEGATIVE TEMPERATURES | | | | | | | | | | | | | | | | |
| 0.3000 | VIOLATION OF 2ND LAW: REQUIRES NEGATIVE TEMPERATURES | | | | | | | | | | | | | | | | |
| 0.3500 | VIOLATION OF 2ND LAW FOR ADIABATIC SYSTEMS:REQUIRES WORK INPUT AND COOLING | | | | | | | | | | | | | | | | |
| 0.4000 | VIOLATION OF 2ND LAW FOR ADIABATIC SYSTEMS:REQUIRES WORK INPUT AND COOLING | | | | | | | | | | | | | | | | |
| 0.4500 | VIOLATION OF 2ND LAW FOR ADIABATIC SYSTEMS:REQUIRES WORK INPUT AND COOLING | | | | | | | | | | | | | | | | |
| 0.5000 | VIOLATION OF 2ND LAW FOR ADIABATIC SYSTEMS:REQUIRES WORK INPUT AND COOLING | | | | | | | | | | | | | | | | |
| 0.5500 | 0.814 | 0.943 | 5.311 | 3.033 | 1.908 | 0.217 | 0.721 | 1.400 | 1.96 | 0.563 | 0.136 | 0.042 | 40.780 | 0.96 | 0.53 | 0.786 | 0.129 |
| 0.6000 | 0.784 | 0.933 | 4.928 | 2.588 | 1.682 | 0.272 | 0.795 | 1.400 | 1.99 | 0.559 | 0.131 | 0.045 | 38.731 | 0.68 | 0.37 | 0.590 | 0.240 |
| 0.6500 | 0.753 | 0.922 | 4.609 | 2.239 | 1.511 | 0.327 | 0.855 | 1.400 | 2.01 | 0.553 | 0.125 | 0.048 | 37.127 | 0.51 | 0.28 | 0.480 | 0.313 |
| 0.7000 | 0.721 | 0.911 | 4.339 | 1.958 | 1.377 | 0.382 | 0.903 | 1.400 | 2.04 | 0.546 | 0.120 | 0.051 | 35.881 | 0.42 | 0.23 | 0.418 | 0.352 |
| 0.7500 | 0.689 | 0.899 | 4.108 | 1.728 | 1.265 | 0.437 | 0.944 | 1.400 | 2.07 | 0.539 | 0.115 | 0.054 | 34.928 | 0.37 | 0.20 | 0.386 | 0.372 |
| 0.8000 | 0.656 | 0.887 | 3.909 | 1.532 | 1.166 | 0.492 | 0.979 | 1.400 | 2.10 | 0.531 | 0.109 | 0.057 | 34.222 | 0.35 | 0.19 | 0.370 | 0.381 |
| 0.8500 | 0.624 | 0.874 | 3.736 | 1.348 | 1.063 | 0.558 | 1.016 | 1.400 | 2.13 | 0.524 | 0.104 | 0.059 | 33.727 | 0.34 | 0.19 | 0.365 | 0.385 |
| 0.9000 | IMAGINARY SOLUTION | | | | | | | | | | | | | | | | |
| 0.9500 | IMAGINARY SOLUTION | | | | | | | | | | | | | | | | |
| 1.0000 | IMAGINARY SOLUTION | | | | | | | | | | | | | | | | |
| 1.0500 | IMAGINARY SOLUTION | | | | | | | | | | | | | | | | |
| 1.1000 | IMAGINARY SOLUTION | | | | | | | | | | | | | | | | |
| 1.1500 | 0.440 | 0.791 | 3.050 | 1.078 | 1.162 | 0.530 | 1.002 | 1.400 | 2.36 | 0.474 | 0.073 | 0.073 | 34.044 | 0.33 | 0.18 | 0.358 | 0.389 |
| 1.2000 | 0.412 | 0.776 | 2.974 | 1.089 | 1.163 | 0.490 | 0.980 | 1.400 | 2.40 | 0.465 | 0.069 | 0.075 | 34.538 | 0.32 | 0.18 | 0.354 | 0.391 |
| 1.2500 | 0.386 | 0.762 | 2.906 | 1.093 | 1.217 | 0.455 | 0.961 | 1.400 | 2.44 | 0.457 | 0.064 | 0.076 | 35.143 | 0.31 | 0.17 | 0.349 | 0.394 |
| 1.3000 | 0.361 | 0.747 | 2.844 | 1.095 | 1.268 | 0.424 | 0.943 | 1.400 | 2.48 | 0.448 | 0.060 | 0.078 | 35.855 | 0.31 | 0.17 | 0.344 | 0.397 |
| 1.3500 | 0.337 | 0.733 | 2.787 | 1.096 | 1.317 | 0.395 | 0.925 | 1.400 | 2.53 | 0.439 | 0.056 | 0.080 | 36.673 | 0.30 | 0.16 | 0.339 | 0.401 |
| 1.4000 | 0.314 | 0.718 | 2.735 | 1.096 | 1.366 | 0.368 | 0.907 | 1.400 | 2.57 | 0.431 | 0.052 | 0.081 | 37.597 | 0.29 | 0.16 | 0.333 | 0.404 |
| 1.4500 | 0.293 | 0.704 | 2.688 | 1.096 | 1.413 | 0.343 | 0.890 | 1.400 | 2.62 | 0.422 | 0.049 | 0.082 | 38.627 | 0.28 | 0.15 | 0.326 | 0.408 |
| 1.5000 | 0.272 | 0.690 | 2.645 | 1.095 | 1.460 | 0.319 | 0.873 | 1.400 | 2.66 | 0.413 | 0.045 | 0.084 | 39.764 | 0.27 | 0.15 | 0.319 | 0.412 |
| 1.5500 | 0.253 | 0.675 | 2.605 | 1.095 | 1.507 | 0.297 | 0.856 | 1.400 | 2.71 | 0.405 | 0.042 | 0.085 | 41.009 | 0.25 | 0.14 | 0.312 | 0.417 |
| 1.6000 | 0.235 | 0.661 | 2.568 | 1.094 | 1.554 | 0.276 | 0.840 | 1.400 | 2.76 | 0.396 | 0.039 | 0.086 | 42.365 | 0.24 | 0.13 | 0.304 | 0.422 |
| 1.6500 | 0.218 | 0.647 | 2.534 | 1.094 | 1.600 | 0.257 | 0.824 | 1.400 | 2.81 | 0.388 | 0.036 | 0.088 | 43.835 | 0.23 | 0.13 | 0.295 | 0.427 |
| 1.7000 | 0.203 | 0.634 | 2.503 | 1.093 | 1.645 | 0.239 | 0.808 | 1.400 | 2.86 | 0.380 | 0.034 | 0.089 | 45.420 | 0.22 | 0.12 | 0.286 | 0.432 |
| 1.7500 | 0.188 | 0.620 | 2.474 | 1.092 | 1.691 | 0.222 | 0.792 | 1.400 | 2.91 | 0.372 | 0.031 | 0.090 | 47.125 | 0.20 | 0.11 | 0.277 | 0.438 |
| 1.8000 | 0.174 | 0.607 | 2.447 | 1.091 | 1.736 | 0.206 | 0.777 | 1.400 | 2.96 | 0.364 | 0.029 | 0.091 | 48.953 | 0.19 | 0.10 | 0.267 | 0.444 |
| 1.8500 | 0.161 | 0.594 | 2.422 | 1.091 | 1.781 | 0.191 | 0.762 | 1.400 | 3.01 | 0.356 | 0.027 | 0.092 | 50.909 | 0.17 | 0.09 | 0.257 | 0.450 |
| 1.9000 | 0.149 | 0.581 | 2.399 | 1.090 | 1.826 | 0.177 | 0.747 | 1.400 | 3.06 | 0.348 | 0.025 | 0.092 | 52.997 | 0.15 | 0.08 | 0.247 | 0.456 |
| 1.9500 | 0.138 | 0.568 | 2.377 | 1.089 | 1.870 | 0.165 | 0.733 | 1.400 | 3.11 | 0.340 | 0.023 | 0.093 | 55.223 | 0.14 | 0.07 | 0.236 | 0.463 |
| 2.0000 | 0.128 | 0.556 | 2.356 | 1.089 | 1.915 | 0.153 | 0.717 | 1.400 | 3.16 | 0.333 | 0.021 | 0.094 | 57.591 | 0.12 | 0.07 | 0.225 | 0.470 |
| 2.0500 | 0.118 | 0.543 | 2.337 | 1.088 | 1.959 | 0.142 | 0.705 | 1.400 | 3.22 | 0.326 | 0.020 | 0.095 | 60.107 | 0.10 | 0.06 | 0.213 | 0.477 |

## CONSTANT PRESSURE CALCULATIONS
### SINGLE SOLUTION
#### PRIMARY VAPOR: AIR   SECONDARY GAS:AIR

PR= 6.000 TR= 3.700 GP=1.400 GS=1.400 VR= 1.00 VP= 29.00 VS= 29.00

M.P/M.S= 0.100

| MS | PIS/ | TIS/ | VP/VS | VM/VS | MX | PM/ | TM/ | GM | MP | T1P/T0P | P1P/P0P | AP/AS | A/AP* | EFPOS | EFTOS | EFAVL | SR |
|---|---|---|---|---|---|---|---|---|---|---|---|---|---|---|---|---|---|
| 0.0500 | 0.998 | 1.000 | 54.485 | 5.862 | 0.264 | 0.998 | 1.228 | 1.400 | 1.83 | 0.599 | 0.166 | 0.004 | 363.038 | 0.12 | 0.07 | 0.227 | 0.468 |
| 0.1000 | 0.993 | 0.998 | 27.293 | 3.390 | 0.306 | 0.993 | 1.223 | 1.400 | 1.83 | 0.598 | 0.166 | 0.008 | 183.073 | 0.15 | 0.08 | 0.246 | 0.457 |
| 0.1500 | 0.984 | 0.996 | 18.252 | 2.568 | 0.349 | 0.984 | 1.216 | 1.400 | 1.84 | 0.597 | 0.164 | 0.012 | 123.455 | 0.18 | 0.10 | 0.263 | 0.447 |
| 0.2000 | 0.972 | 0.992 | 13.748 | 2.159 | 0.391 | 0.972 | 1.208 | 1.400 | 1.85 | 0.595 | 0.162 | 0.016 | 93.931 | 0.20 | 0.11 | 0.278 | 0.437 |
| 0.2500 | 0.957 | 0.988 | 11.059 | 1.914 | 0.434 | 0.957 | 1.200 | 1.400 | 1.86 | 0.592 | 0.160 | 0.020 | 76.449 | 0.22 | 0.12 | 0.292 | 0.429 |
| 0.3000 | 0.939 | 0.982 | 9.277 | 1.752 | 0.477 | 0.939 | 1.191 | 1.400 | 1.87 | 0.589 | 0.157 | 0.024 | 64.996 | 0.24 | 0.13 | 0.304 | 0.421 |
| 0.3500 | 0.919 | 0.976 | 8.013 | 1.638 | 0.521 | 0.919 | 1.181 | 1.400 | 1.88 | 0.585 | 0.153 | 0.028 | 56.994 | 0.26 | 0.14 | 0.316 | 0.415 |
| 0.4000 | 0.896 | 0.969 | 7.073 | 1.552 | 0.565 | 0.896 | 1.171 | 1.400 | 1.90 | 0.581 | 0.149 | 0.031 | 51.156 | 0.28 | 0.15 | 0.325 | 0.409 |
| 0.4500 | 0.870 | 0.961 | 6.349 | 1.486 | 0.609 | 0.870 | 1.159 | 1.400 | 1.92 | 0.576 | 0.145 | 0.035 | 46.766 | 0.29 | 0.16 | 0.334 | 0.403 |
| 0.5000 | 0.843 | 0.952 | 5.775 | 1.434 | 0.653 | 0.843 | 1.148 | 1.400 | 1.94 | 0.571 | 0.141 | 0.038 | 43.398 | 0.30 | 0.17 | 0.341 | 0.399 |
| 0.5500 | 0.814 | 0.943 | 5.311 | 1.392 | 0.698 | 0.814 | 1.135 | 1.400 | 1.96 | 0.565 | 0.136 | 0.042 | 40.700 | 0.31 | 0.17 | 0.348 | 0.395 |
| 0.6000 | 0.784 | 0.933 | 4.928 | 1.357 | 0.743 | 0.784 | 1.122 | 1.400 | 1.99 | 0.559 | 0.131 | 0.045 | 38.731 | 0.32 | 0.17 | 0.353 | 0.392 |
| 0.6500 | 0.753 | 0.922 | 4.609 | 1.328 | 0.788 | 0.753 | 1.108 | 1.400 | 2.01 | 0.553 | 0.125 | 0.048 | 37.127 | 0.33 | 0.18 | 0.357 | 0.390 |
| 0.7000 | 0.721 | 0.911 | 4.339 | 1.304 | 0.833 | 0.721 | 1.094 | 1.400 | 2.04 | 0.546 | 0.120 | 0.051 | 35.881 | 0.33 | 0.18 | 0.360 | 0.388 |
| 0.7500 | 0.689 | 0.899 | 4.108 | 1.283 | 0.878 | 0.689 | 1.079 | 1.400 | 2.07 | 0.539 | 0.115 | 0.054 | 34.928 | 0.33 | 0.18 | 0.362 | 0.386 |
| 0.8000 | 0.656 | 0.887 | 3.909 | 1.264 | 0.923 | 0.656 | 1.064 | 1.400 | 2.10 | 0.531 | 0.109 | 0.057 | 34.222 | 0.34 | 0.18 | 0.364 | 0.385 |
| 0.8500 | 0.624 | 0.874 | 3.736 | 1.247 | 0.969 | 0.624 | 1.049 | 1.400 | 2.13 | 0.524 | 0.104 | 0.059 | 33.737 | 0.34 | 0.18 | 0.364 | 0.385 |
| 0.9000 | 0.591 | 0.861 | 3.585 | 1.235 | 1.015 | 0.591 | 1.033 | 1.400 | 2.17 | 0.516 | 0.099 | 0.062 | 33.414 | 0.34 | 0.18 | 0.364 | 0.385 |
| 0.9500 | 0.559 | 0.847 | 3.452 | 1.223 | 1.060 | 0.559 | 1.017 | 1.400 | 2.20 | 0.508 | 0.093 | 0.064 | 33.268 | 0.33 | 0.18 | 0.363 | 0.386 |
| 1.0000 | 0.528 | 0.833 | 3.334 | 1.212 | 1.106 | 0.528 | 1.001 | 1.400 | 2.24 | 0.499 | 0.088 | 0.067 | 33.268 | 0.33 | 0.18 | 0.361 | 0.387 |
| 1.0500 | 0.498 | 0.819 | 3.228 | 1.203 | 1.152 | 0.498 | 0.984 | 1.400 | 2.28 | 0.491 | 0.083 | 0.069 | 33.403 | 0.33 | 0.18 | 0.359 | 0.388 |
| 1.1000 | 0.468 | 0.805 | 3.135 | 1.194 | 1.198 | 0.468 | 0.968 | 1.400 | 2.32 | 0.483 | 0.078 | 0.071 | 33.464 | 0.32 | 0.18 | 0.356 | 0.390 |
| 1.1500 | 0.440 | 0.791 | 3.050 | 1.186 | 1.244 | 0.440 | 0.951 | 1.400 | 2.36 | 0.474 | 0.073 | 0.073 | 34.044 | 0.32 | 0.17 | 0.352 | 0.392 |
| 1.2000 | 0.412 | 0.776 | 2.974 | 1.179 | 1.290 | 0.412 | 0.934 | 1.400 | 2.40 | 0.465 | 0.069 | 0.075 | 34.538 | 0.31 | 0.17 | 0.348 | 0.395 |
| 1.2500 | 0.386 | 0.762 | 2.906 | 1.173 | 1.334 | 0.386 | 0.918 | 1.400 | 2.44 | 0.457 | 0.064 | 0.076 | 35.143 | 0.30 | 0.17 | 0.343 | 0.398 |
| 1.3000 | 0.361 | 0.747 | 2.844 | 1.168 | 1.382 | 0.361 | 0.901 | 1.400 | 2.48 | 0.448 | 0.060 | 0.078 | 35.855 | 0.30 | 0.16 | 0.338 | 0.401 |
| 1.3500 | 0.337 | 0.733 | 2.787 | 1.162 | 1.428 | 0.337 | 0.884 | 1.400 | 2.53 | 0.439 | 0.056 | 0.080 | 36.673 | 0.29 | 0.16 | 0.332 | 0.405 |
| 1.4000 | 0.314 | 0.718 | 2.735 | 1.158 | 1.475 | 0.314 | 0.868 | 1.400 | 2.57 | 0.431 | 0.052 | 0.081 | 37.597 | 0.28 | 0.15 | 0.325 | 0.409 |
| 1.4500 | 0.293 | 0.704 | 2.688 | 1.153 | 1.521 | 0.293 | 0.852 | 1.400 | 2.62 | 0.422 | 0.049 | 0.082 | 38.627 | 0.27 | 0.15 | 0.318 | 0.413 |
| 1.5000 | 0.272 | 0.690 | 2.645 | 1.150 | 1.567 | 0.272 | 0.835 | 1.400 | 2.66 | 0.413 | 0.045 | 0.084 | 39.764 | 0.25 | 0.14 | 0.311 | 0.417 |
| 1.5500 | 0.253 | 0.675 | 2.605 | 1.146 | 1.613 | 0.253 | 0.819 | 1.400 | 2.71 | 0.405 | 0.042 | 0.085 | 41.007 | 0.24 | 0.13 | 0.303 | 0.422 |
| 1.6000 | 0.235 | 0.661 | 2.568 | 1.143 | 1.659 | 0.235 | 0.803 | 1.400 | 2.76 | 0.396 | 0.039 | 0.086 | 42.365 | 0.23 | 0.13 | 0.294 | 0.427 |
| 1.6500 | 0.218 | 0.647 | 2.534 | 1.139 | 1.705 | 0.218 | 0.788 | 1.400 | 2.81 | 0.388 | 0.036 | 0.088 | 43.835 | 0.21 | 0.12 | 0.285 | 0.433 |
| 1.7000 | 0.203 | 0.634 | 2.503 | 1.137 | 1.750 | 0.203 | 0.772 | 1.400 | 2.86 | 0.380 | 0.034 | 0.089 | 45.420 | 0.20 | 0.11 | 0.276 | 0.439 |
| 1.7500 | 0.188 | 0.620 | 2.474 | 1.134 | 1.796 | 0.188 | 0.757 | 1.400 | 2.91 | 0.372 | 0.031 | 0.090 | 47.125 | 0.18 | 0.10 | 0.266 | 0.444 |
| 1.8000 | 0.174 | 0.607 | 2.447 | 1.132 | 1.842 | 0.174 | 0.742 | 1.400 | 2.96 | 0.364 | 0.029 | 0.091 | 48.953 | 0.17 | 0.09 | 0.256 | 0.451 |
| 1.8500 | 0.161 | 0.594 | 2.422 | 1.129 | 1.888 | 0.161 | 0.727 | 1.400 | 3.01 | 0.356 | 0.027 | 0.092 | 50.909 | 0.15 | 0.08 | 0.245 | 0.457 |
| 1.9000 | 0.149 | 0.581 | 2.399 | 1.127 | 1.933 | 0.149 | 0.713 | 1.400 | 3.06 | 0.348 | 0.025 | 0.092 | 52.997 | 0.13 | 0.07 | 0.234 | 0.464 |
| 1.9500 | 0.138 | 0.568 | 2.377 | 1.125 | 1.978 | 0.138 | 0.699 | 1.400 | 3.11 | 0.340 | 0.023 | 0.093 | 55.223 | 0.12 | 0.06 | 0.223 | 0.471 |
| 2.0000 | 0.128 | 0.556 | 2.356 | 1.123 | 2.024 | 0.128 | 0.685 | 1.400 | 3.16 | 0.333 | 0.021 | 0.094 | 57.591 | 0.10 | 0.05 | 0.211 | 0.478 |
| 2.0500 | 0.118 | 0.543 | 2.337 | 1.122 | 2.069 | 0.118 | 0.671 | 1.400 | 3.22 | 0.326 | 0.020 | 0.095 | 60.107 | 0.08 | 0.04 | 0.199 | 0.485 |

CONSTANT AREA CALCULATIONS
SUBSONIC BRANCH
PRIMARY VAPOR: AIR   SECONDARY GAS:AIR
PR= 6.000 TR= 3.700 CP=1.400 GS=1.400 VR=  1.00 WP= 29.00 WS= 29.00
M.P/M.S=  0.500

| MS | PIS/ | TIS/ | VP/VS | VM/VS | MM | PM/ | TM/ | GM | MP | TIP/TOP | PIP/POP | AP/AS | A/AP* | EFPOS | EFTOS | EFAVE | SR |
|---|---|---|---|---|---|---|---|---|---|---|---|---|---|---|---|---|---|
| 0.0500 | 0.998 | 1.000 | 54.485 | 2.574 | 0.093 | 1.082 | 1.897 | 1.400 | 1.83 | 0.599 | 0.166 | 0.020 | 73.785 | 0.09 | 0.05 | 0.445 | 1.233 |
| 0.1000 | 0.993 | 0.998 | 27.293 | 2.374 | 0.173 | 1.141 | 1.889 | 1.400 | 1.83 | 0.598 | 0.166 | 0.041 | 37.795 | 0.16 | 0.09 | 0.476 | 1.165 |
| 0.1500 | 0.984 | 0.996 | 18.252 | 2.220 | 0.242 | 1.183 | 1.878 | 1.400 | 1.84 | 0.597 | 0.164 | 0.061 | 25.877 | 0.22 | 0.12 | 0.501 | 1.108 |
| 0.2000 | 0.972 | 0.992 | 13.748 | 2.096 | 0.306 | 1.211 | 1.865 | 1.400 | 1.85 | 0.595 | 0.162 | 0.081 | 19.979 | 0.27 | 0.15 | 0.522 | 1.061 |
| 0.2500 | 0.957 | 0.988 | 11.059 | 1.994 | 0.364 | 1.227 | 1.851 | 1.400 | 1.86 | 0.592 | 0.160 | 0.100 | 16.492 | 0.31 | 0.17 | 0.540 | 1.021 |
| 0.3000 | 0.939 | 0.982 | 9.277 | 1.908 | 0.419 | 1.233 | 1.836 | 1.400 | 1.87 | 0.589 | 0.157 | 0.120 | 14.213 | 0.35 | 0.19 | 0.555 | 0.987 |
| 0.3500 | 0.919 | 0.976 | 8.013 | 1.833 | 0.470 | 1.231 | 1.820 | 1.400 | 1.88 | 0.585 | 0.153 | 0.138 | 12.627 | 0.38 | 0.21 | 0.567 | 0.958 |
| 0.4000 | 0.896 | 0.969 | 7.073 | 1.768 | 0.518 | 1.223 | 1.803 | 1.400 | 1.90 | 0.581 | 0.149 | 0.157 | 11.475 | 0.40 | 0.22 | 0.580 | 0.933 |
| 0.4500 | 0.870 | 0.961 | 6.349 | 1.709 | 0.564 | 1.209 | 1.786 | 1.400 | 1.92 | 0.576 | 0.145 | 0.175 | 10.616 | 0.42 | 0.23 | 0.589 | 0.912 |
| 0.5000 | 0.843 | 0.952 | 5.775 | 1.655 | 0.607 | 1.191 | 1.769 | 1.400 | 1.94 | 0.571 | 0.141 | 0.192 | 9.963 | 0.44 | 0.24 | 0.598 | 0.894 |
| 0.5500 | 0.814 | 0.943 | 5.311 | 1.605 | 0.648 | 1.170 | 1.753 | 1.400 | 1.96 | 0.565 | 0.136 | 0.209 | 9.464 | 0.45 | 0.25 | 0.604 | 0.879 |
| 0.6000 | 0.784 | 0.933 | 4.928 | 1.557 | 0.685 | 1.148 | 1.737 | 1.400 | 1.99 | 0.559 | 0.131 | 0.225 | 9.088 | 0.47 | 0.26 | 0.610 | 0.866 |
| 0.6500 | 0.753 | 0.922 | 4.609 | 1.510 | 0.718 | 1.126 | 1.722 | 1.400 | 2.01 | 0.553 | 0.125 | 0.241 | 8.789 | 0.48 | 0.26 | 0.615 | 0.855 |
| 0.7000 | 0.721 | 0.911 | 4.339 | 1.462 | 0.747 | 1.105 | 1.709 | 1.400 | 2.04 | 0.546 | 0.120 | 0.256 | 8.572 | 0.48 | 0.27 | 0.619 | 0.847 |
| 0.7500 | 0.689 | 0.899 | 4.108 | 1.412 | 0.771 | 1.088 | 1.698 | 1.400 | 2.07 | 0.539 | 0.115 | 0.270 | 8.417 | 0.49 | 0.27 | 0.622 | 0.840 |
| 0.8000 | 0.656 | 0.887 | 3.909 | 1.359 | 0.788 | 1.075 | 1.690 | 1.400 | 2.10 | 0.531 | 0.109 | 0.284 | 8.314 | 0.49 | 0.27 | 0.624 | 0.835 |
| 0.8500 | 0.624 | 0.874 | 3.736 | 1.303 | 0.797 | 1.068 | 1.686 | 1.400 | 2.13 | 0.524 | 0.104 | 0.297 | 8.257 | 0.50 | 0.27 | 0.625 | 0.833 |
| 0.9000 | 0.591 | 0.861 | 3.585 | 1.244 | 0.800 | 1.066 | 1.684 | 1.400 | 2.17 | 0.516 | 0.099 | 0.309 | 8.240 | 0.50 | 0.27 | 0.625 | 0.832 |
| 0.9500 | 0.559 | 0.847 | 3.452 | 1.184 | 0.797 | 1.068 | 1.686 | 1.400 | 2.20 | 0.508 | 0.093 | 0.321 | 8.260 | 0.50 | 0.27 | 0.625 | 0.833 |
| 1.0000 | 0.528 | 0.833 | 3.334 | 1.124 | 0.789 | 1.073 | 1.690 | 1.400 | 2.24 | 0.499 | 0.088 | 0.333 | 8.314 | 0.49 | 0.27 | 0.623 | 0.836 |
| 1.0500 | 0.498 | 0.819 | 3.228 | 1.066 | 0.778 | 1.079 | 1.695 | 1.400 | 2.28 | 0.491 | 0.083 | 0.343 | 8.398 | 0.49 | 0.27 | 0.621 | 0.841 |
| 1.1000 | 0.468 | 0.805 | 3.135 | 1.011 | 0.765 | 1.084 | 1.701 | 1.400 | 2.32 | 0.483 | 0.078 | 0.354 | 8.512 | 0.48 | 0.26 | 0.618 | 0.847 |
| 1.1500 | 0.440 | 0.791 | 3.050 | 0.960 | 0.752 | 1.088 | 1.707 | 1.400 | 2.36 | 0.474 | 0.073 | 0.363 | 8.655 | 0.47 | 0.26 | 0.613 | 0.859 |
| 1.2000 | 0.412 | 0.776 | 2.974 | 0.913 | 0.737 | 1.089 | 1.714 | 1.400 | 2.40 | 0.465 | 0.069 | 0.373 | 8.825 | 0.46 | 0.25 | 0.608 | 0.870 |
| 1.2500 | 0.386 | 0.762 | 2.906 | 0.870 | 0.723 | 1.088 | 1.720 | 1.400 | 2.44 | 0.457 | 0.064 | 0.382 | 9.022 | 0.45 | 0.25 | 0.602 | 0.884 |
| 1.3000 | 0.361 | 0.747 | 2.844 | 0.830 | 0.710 | 1.084 | 1.726 | 1.400 | 2.48 | 0.448 | 0.060 | 0.390 | 9.246 | 0.43 | 0.24 | 0.594 | 0.901 |
| 1.3500 | 0.337 | 0.733 | 2.787 | 0.793 | 0.697 | 1.077 | 1.732 | 1.400 | 2.53 | 0.439 | 0.056 | 0.398 | 9.497 | 0.41 | 0.23 | 0.586 | 0.919 |
| 1.4000 | 0.314 | 0.718 | 2.735 | 0.760 | 0.684 | 1.068 | 1.737 | 1.400 | 2.57 | 0.431 | 0.052 | 0.405 | 9.775 | 0.39 | 0.22 | 0.577 | 0.939 |
| 1.4500 | 0.293 | 0.704 | 2.688 | 0.729 | 0.672 | 1.055 | 1.743 | 1.400 | 2.62 | 0.422 | 0.049 | 0.412 | 10.080 | 0.37 | 0.20 | 0.567 | 0.961 |
| 1.5000 | 0.272 | 0.690 | 2.645 | 0.701 | 0.660 | 1.041 | 1.748 | 1.400 | 2.66 | 0.413 | 0.045 | 0.419 | 10.414 | 0.35 | 0.19 | 0.557 | 0.985 |
| 1.5500 | 0.253 | 0.675 | 2.605 | 0.675 | 0.650 | 1.024 | 1.752 | 1.400 | 2.71 | 0.405 | 0.042 | 0.426 | 10.776 | 0.32 | 0.18 | 0.545 | 1.010 |
| 1.6000 | 0.235 | 0.661 | 2.568 | 0.651 | 0.639 | 1.005 | 1.756 | 1.400 | 2.76 | 0.396 | 0.039 | 0.432 | 11.167 | 0.30 | 0.16 | 0.533 | 1.037 |
| 1.6500 | 0.218 | 0.647 | 2.534 | 0.629 | 0.630 | 0.985 | 1.760 | 1.400 | 2.81 | 0.388 | 0.036 | 0.438 | 11.589 | 0.27 | 0.15 | 0.520 | 1.066 |
| 1.7000 | 0.203 | 0.634 | 2.503 | 0.609 | 0.621 | 0.963 | 1.764 | 1.400 | 2.86 | 0.380 | 0.034 | 0.443 | 12.041 | 0.24 | 0.13 | 0.507 | 1.096 |
| 1.7500 | 0.188 | 0.620 | 2.474 | 0.590 | 0.612 | 0.939 | 1.768 | 1.400 | 2.91 | 0.372 | 0.031 | 0.448 | 12.526 | 0.20 | 0.11 | 0.492 | 1.127 |
| 1.8000 | 0.174 | 0.607 | 2.447 | 0.573 | 0.604 | 0.915 | 1.771 | 1.400 | 2.96 | 0.364 | 0.029 | 0.453 | 13.045 | 0.17 | 0.09 | 0.478 | 1.160 |
| 1.8500 | 0.161 | 0.594 | 2.422 | 0.557 | 0.596 | 0.890 | 1.774 | 1.400 | 3.01 | 0.356 | 0.027 | 0.458 | 13.598 | 0.13 | 0.07 | 0.463 | 1.194 |
| 1.9000 | 0.149 | 0.581 | 2.399 | 0.542 | 0.589 | 0.864 | 1.777 | 1.400 | 3.06 | 0.348 | 0.025 | 0.462 | 14.188 | 0.10 | 0.05 | 0.447 | 1.229 |
| 1.9500 | 0.138 | 0.568 | 2.377 | 0.528 | 0.582 | 0.838 | 1.780 | 1.400 | 3.11 | 0.340 | 0.023 | 0.466 | 14.815 | 0.06 | 0.03 | 0.431 | 1.265 |
| 2.0000 | 0.128 | 0.556 | 2.356 | 0.515 | 0.575 | 0.812 | 1.782 | 1.400 | 3.16 | 0.333 | 0.021 | 0.471 | 15.481 | 0.02 | 0.01 | 0.414 | 1.301 |
| 2.0500 | 0.118 | 0.543 | 2.337 | 0.503 | 0.569 | 0.786 | 1.784 | 1.400 | 3.22 | 0.326 | 0.020 | 0.474 | 16.188 | -0.02 | -0.01 | 0.397 | 1.339 |

CONSTANT AREA CALCULATIONS
SUPERSONIC BRANCH
PRIMARY VAPOR: AIR   SECONDARY GAS:AIR
PR= 4.000 TR= 3.700 GP=1.400 GS=1.400 WR=   1.00 VP= 29.00 VS= 29.00
M.P/M.S=   0.500

| MS | PIS/ | TIS/ | VP/VS | VM/VS | MM | PM/ | TM/ | GM | MP | TIP/TOP | PIP/POP | AP/AS | A/AP* | EFPOS | EFTOS | EFAVL | SR |
|---|---|---|---|---|---|---|---|---|---|---|---|---|---|---|---|---|---|
| 0.0500 | VIOLATION OF 2ND LAW: REQUIRES NEGATIVE TEMPERATURES | | | | | | | | | | | | | | | | |
| 0.1000 | VIOLATION OF 2ND LAW: REQUIRES NEGATIVE TEMPERATURES | | | | | | | | | | | | | | | | |
| 0.1500 | VIOLATION OF 2ND LAW: REQUIRES NEGATIVE TEMPERATURES | | | | | | | | | | | | | | | | |
| 0.2000 | VIOLATION OF 2ND LAW: REQUIRES NEGATIVE TEMPERATURES | | | | | | | | | | | | | | | | |
| 0.2500 | VIOLATION OF 2ND LAW: REQUIRES NEGATIVE TEMPERATURES | | | | | | | | | | | | | | | | |
| 0.3000 | VIOLATION OF 2ND LAW FOR ADIABATIC SYSTEMS:REQUIRES WORK INPUT AND COOLING | | | | | | | | | | | | | | | | |
| 0.3500 | VIOLATION OF 2ND LAW FOR ADIABATIC SYSTEMS:REQUIRES WORK INPUT AND COOLING | | | | | | | | | | | | | | | | |
| 0.4000 | 0.896 | 0.969 | 7.073 | 5.777 | 2.446 | 0.179 | 0.865 | 1.400 | 1.90 | 0.581 | 0.149 | 0.157 | 11.475 | 0.99 | 0.54 | 0.873 | 0.281 |
| 0.4500 | 0.870 | 0.961 | 6.349 | 4.760 | 2.081 | 0.247 | 1.010 | 1.400 | 1.92 | 0.576 | 0.145 | 0.175 | 10.616 | 0.77 | 0.43 | 0.761 | 0.531 |
| 0.5000 | 0.843 | 0.952 | 5.775 | 4.017 | 1.843 | 0.314 | 1.132 | 1.400 | 1.94 | 0.571 | 0.141 | 0.193 | 9.963 | 0.66 | 0.36 | 0.702 | 0.663 |
| 0.5500 | 0.814 | 0.943 | 5.311 | 3.450 | 1.673 | 0.377 | 1.218 | 1.400 | 1.96 | 0.565 | 0.136 | 0.209 | 9.464 | 0.59 | 0.32 | 0.669 | 0.735 |
| 0.6000 | 0.784 | 0.933 | 4.928 | 3.027 | 1.548 | 0.437 | 1.284 | 1.400 | 1.99 | 0.559 | 0.131 | 0.225 | 9.080 | 0.55 | 0.30 | 0.651 | 0.774 |
| 0.6500 | 0.753 | 0.922 | 4.609 | 2.691 | 1.454 | 0.490 | 1.336 | 1.400 | 2.01 | 0.553 | 0.125 | 0.241 | 8.789 | 0.53 | 0.29 | 0.641 | 0.797 |
| 0.7000 | 0.721 | 0.911 | 4.339 | 2.427 | 1.383 | 0.536 | 1.374 | 1.400 | 2.04 | 0.546 | 0.120 | 0.256 | 8.572 | 0.52 | 0.29 | 0.636 | 0.808 |
| 0.7500 | 0.689 | 0.899 | 4.108 | 2.217 | 1.331 | 0.572 | 1.403 | 1.400 | 2.07 | 0.539 | 0.115 | 0.270 | 8.417 | 0.52 | 0.28 | 0.634 | 0.813 |
| 0.8000 | 0.656 | 0.887 | 3.909 | 2.053 | 1.297 | 0.599 | 1.422 | 1.400 | 2.10 | 0.531 | 0.109 | 0.284 | 8.314 | 0.51 | 0.28 | 0.633 | 0.815 |
| 0.8500 | 0.624 | 0.874 | 3.736 | 1.925 | 1.278 | 0.614 | 1.432 | 1.400 | 2.13 | 0.524 | 0.104 | 0.297 | 8.257 | 0.51 | 0.28 | 0.633 | 0.816 |
| 0.9000 | 0.591 | 0.861 | 3.585 | 1.826 | 1.272 | 0.619 | 1.435 | 1.400 | 2.17 | 0.516 | 0.099 | 0.309 | 8.240 | 0.51 | 0.28 | 0.633 | 0.816 |
| 0.9500 | 0.559 | 0.847 | 3.452 | 1.750 | 1.278 | 0.614 | 1.432 | 1.400 | 2.20 | 0.508 | 0.093 | 0.321 | 8.260 | 0.51 | 0.28 | 0.633 | 0.816 |
| 1.0000 | 0.528 | 0.833 | 3.334 | 1.691 | 1.294 | 0.601 | 1.424 | 1.400 | 2.24 | 0.499 | 0.088 | 0.333 | 8.314 | 0.51 | 0.28 | 0.632 | 0.816 |
| 1.0500 | 0.498 | 0.819 | 3.228 | 1.644 | 1.315 | 0.582 | 1.412 | 1.400 | 2.28 | 0.491 | 0.083 | 0.343 | 8.398 | 0.51 | 0.28 | 0.632 | 0.818 |
| 1.1000 | 0.468 | 0.805 | 3.135 | 1.607 | 1.342 | 0.560 | 1.397 | 1.400 | 2.32 | 0.483 | 0.078 | 0.354 | 8.512 | 0.51 | 0.28 | 0.631 | 0.820 |
| 1.1500 | 0.440 | 0.791 | 3.050 | 1.577 | 1.372 | 0.536 | 1.380 | 1.400 | 2.36 | 0.474 | 0.073 | 0.363 | 8.655 | 0.51 | 0.28 | 0.630 | 0.823 |
| 1.2000 | 0.412 | 0.776 | 2.974 | 1.551 | 1.405 | 0.510 | 1.362 | 1.400 | 2.40 | 0.465 | 0.069 | 0.373 | 8.825 | 0.50 | 0.28 | 0.628 | 0.826 |
| 1.2500 | 0.386 | 0.762 | 2.906 | 1.529 | 1.440 | 0.483 | 1.343 | 1.400 | 2.44 | 0.457 | 0.064 | 0.382 | 9.022 | 0.50 | 0.27 | 0.626 | 0.831 |
| 1.3000 | 0.361 | 0.747 | 2.844 | 1.511 | 1.476 | 0.457 | 1.323 | 1.400 | 2.48 | 0.448 | 0.060 | 0.390 | 9.246 | 0.49 | 0.27 | 0.624 | 0.836 |
| 1.3500 | 0.337 | 0.733 | 2.787 | 1.494 | 1.513 | 0.430 | 1.303 | 1.400 | 2.53 | 0.439 | 0.056 | 0.398 | 9.497 | 0.49 | 0.27 | 0.621 | 0.841 |
| 1.4000 | 0.314 | 0.718 | 2.735 | 1.480 | 1.551 | 0.405 | 1.283 | 1.400 | 2.57 | 0.431 | 0.053 | 0.405 | 9.775 | 0.48 | 0.27 | 0.618 | 0.848 |
| 1.4500 | 0.293 | 0.704 | 2.688 | 1.467 | 1.589 | 0.380 | 1.263 | 1.400 | 2.62 | 0.422 | 0.049 | 0.412 | 10.080 | 0.48 | 0.26 | 0.615 | 0.855 |
| 1.5000 | 0.272 | 0.690 | 2.645 | 1.456 | 1.627 | 0.356 | 1.243 | 1.400 | 2.66 | 0.413 | 0.045 | 0.419 | 10.414 | 0.47 | 0.26 | 0.612 | 0.862 |
| 1.5500 | 0.253 | 0.675 | 2.605 | 1.445 | 1.666 | 0.334 | 1.222 | 1.400 | 2.71 | 0.405 | 0.042 | 0.426 | 10.776 | 0.46 | 0.25 | 0.608 | 0.870 |
| 1.6000 | 0.235 | 0.661 | 2.568 | 1.436 | 1.704 | 0.312 | 1.202 | 1.400 | 2.76 | 0.396 | 0.039 | 0.432 | 11.167 | 0.45 | 0.25 | 0.604 | 0.879 |
| 1.6500 | 0.218 | 0.647 | 2.534 | 1.427 | 1.743 | 0.291 | 1.182 | 1.400 | 2.81 | 0.388 | 0.036 | 0.438 | 11.589 | 0.44 | 0.24 | 0.600 | 0.888 |
| 1.7000 | 0.203 | 0.634 | 2.503 | 1.420 | 1.782 | 0.272 | 1.162 | 1.400 | 2.86 | 0.380 | 0.034 | 0.443 | 12.041 | 0.43 | 0.24 | 0.596 | 0.898 |
| 1.7500 | 0.188 | 0.620 | 2.474 | 1.412 | 1.821 | 0.254 | 1.142 | 1.400 | 2.91 | 0.372 | 0.031 | 0.448 | 12.526 | 0.42 | 0.23 | 0.591 | 0.908 |
| 1.8000 | 0.174 | 0.607 | 2.447 | 1.406 | 1.860 | 0.237 | 1.123 | 1.400 | 2.96 | 0.364 | 0.029 | 0.453 | 13.045 | 0.41 | 0.23 | 0.586 | 0.919 |
| 1.8500 | 0.161 | 0.594 | 2.422 | 1.399 | 1.898 | 0.220 | 1.104 | 1.400 | 3.01 | 0.356 | 0.027 | 0.458 | 13.598 | 0.40 | 0.22 | 0.581 | 0.930 |
| 1.9000 | 0.149 | 0.581 | 2.399 | 1.394 | 1.937 | 0.205 | 1.086 | 1.400 | 3.06 | 0.348 | 0.025 | 0.462 | 14.188 | 0.39 | 0.21 | 0.576 | 0.941 |
| 1.9500 | 0.138 | 0.568 | 2.377 | 1.388 | 1.975 | 0.191 | 1.067 | 1.400 | 3.11 | 0.340 | 0.023 | 0.466 | 14.815 | 0.38 | 0.21 | 0.571 | 0.953 |
| 2.0000 | 0.128 | 0.556 | 2.356 | 1.383 | 2.013 | 0.178 | 1.049 | 1.400 | 3.16 | 0.333 | 0.021 | 0.471 | 15.481 | 0.37 | 0.20 | 0.565 | 0.966 |
| 2.0500 | 0.118 | 0.543 | 2.337 | 1.379 | 2.051 | 0.166 | 1.032 | 1.400 | 3.22 | 0.326 | 0.020 | 0.474 | 16.188 | 0.35 | 0.17 | 0.559 | 0.978 |

## CONSTANT PRESSURE CALCULATIONS
### SINGLE SOLUTION
### PRIMARY VAPOR: AIR    SECONDARY GAS:AIR

PR= 6.000 TR= 3.700 GP=1.400 GS=1.400 WR=  1.00 WP= 29.00 WS= 29.00

M.P/M.S=  0.500

| MS | P1S/ | T1S/ | VP/VS | VM/VS | MM | PM/ | TM/ | GM | MP | T1P/T0P | P1P/P0P | AP/AS | A/AP² | EFPOS | EFTOS | EFAVL | SR |
|---|---|---|---|---|---|---|---|---|---|---|---|---|---|---|---|---|---|
| 0.0500 | 0.998 | 1.000 | 54.485 | 18.828 | 0.717 | 0.998 | 1.723 | 1.400 | 1.83 | 0.599 | 0.166 | 0.020 | 73.785 | 0.36 | 0.20 | 0.560 | 0.977 |
| 0.1000 | 0.993 | 0.998 | 27.293 | 9.764 | 0.746 | 0.993 | 1.710 | 1.400 | 1.83 | 0.598 | 0.166 | 0.041 | 37.795 | 0.38 | 0.21 | 0.570 | 0.955 |
| 0.1500 | 0.984 | 0.996 | 18.252 | 6.751 | 0.776 | 0.984 | 1.696 | 1.400 | 1.84 | 0.597 | 0.164 | 0.061 | 25.877 | 0.40 | 0.22 | 0.579 | 0.935 |
| 0.2000 | 0.972 | 0.992 | 13.748 | 5.249 | 0.806 | 0.972 | 1.681 | 1.400 | 1.85 | 0.595 | 0.162 | 0.081 | 19.979 | 0.42 | 0.23 | 0.587 | 0.917 |
| 0.2500 | 0.957 | 0.988 | 11.059 | 4.353 | 0.838 | 0.957 | 1.666 | 1.400 | 1.86 | 0.592 | 0.160 | 0.100 | 16.492 | 0.43 | 0.24 | 0.594 | 0.901 |
| 0.3000 | 0.939 | 0.982 | 9.277 | 3.759 | 0.870 | 0.939 | 1.650 | 1.400 | 1.87 | 0.589 | 0.157 | 0.120 | 14.213 | 0.45 | 0.24 | 0.601 | 0.886 |
| 0.3500 | 0.919 | 0.976 | 8.013 | 3.338 | 0.903 | 0.919 | 1.634 | 1.400 | 1.88 | 0.585 | 0.153 | 0.138 | 12.627 | 0.46 | 0.25 | 0.607 | 0.873 |
| 0.4000 | 0.896 | 0.969 | 7.073 | 3.024 | 0.937 | 0.896 | 1.616 | 1.400 | 1.90 | 0.581 | 0.149 | 0.157 | 11.475 | 0.47 | 0.26 | 0.612 | 0.862 |
| 0.4500 | 0.870 | 0.961 | 6.349 | 2.783 | 0.971 | 0.870 | 1.599 | 1.400 | 1.92 | 0.576 | 0.145 | 0.175 | 10.616 | 0.48 | 0.26 | 0.617 | 0.852 |
| 0.5000 | 0.843 | 0.952 | 5.775 | 2.592 | 1.006 | 0.843 | 1.580 | 1.400 | 1.94 | 0.571 | 0.141 | 0.192 | 9.963 | 0.49 | 0.27 | 0.620 | 0.843 |
| 0.5500 | 0.814 | 0.943 | 5.311 | 2.437 | 1.042 | 0.814 | 1.561 | 1.400 | 1.96 | 0.565 | 0.136 | 0.209 | 9.464 | 0.49 | 0.27 | 0.624 | 0.836 |
| 0.6000 | 0.784 | 0.933 | 4.928 | 2.309 | 1.078 | 0.784 | 1.542 | 1.400 | 1.99 | 0.559 | 0.131 | 0.225 | 9.080 | 0.50 | 0.27 | 0.627 | 0.829 |
| 0.6500 | 0.753 | 0.922 | 4.609 | 2.203 | 1.115 | 0.753 | 1.522 | 1.400 | 2.01 | 0.553 | 0.125 | 0.241 | 8.789 | 0.51 | 0.28 | 0.629 | 0.825 |
| 0.7000 | 0.721 | 0.911 | 4.339 | 2.113 | 1.152 | 0.721 | 1.502 | 1.400 | 2.04 | 0.546 | 0.120 | 0.256 | 8.572 | 0.51 | 0.28 | 0.630 | 0.821 |
| 0.7500 | 0.689 | 0.899 | 4.108 | 2.036 | 1.190 | 0.689 | 1.481 | 1.400 | 2.07 | 0.539 | 0.115 | 0.270 | 8.417 | 0.51 | 0.28 | 0.632 | 0.818 |
| 0.8000 | 0.656 | 0.887 | 3.909 | 1.970 | 1.228 | 0.656 | 1.460 | 1.400 | 2.10 | 0.531 | 0.109 | 0.284 | 8.314 | 0.51 | 0.28 | 0.632 | 0.816 |
| 0.8500 | 0.624 | 0.874 | 3.736 | 1.912 | 1.267 | 0.624 | 1.438 | 1.400 | 2.13 | 0.524 | 0.104 | 0.297 | 8.257 | 0.51 | 0.28 | 0.633 | 0.816 |
| 0.9000 | 0.591 | 0.861 | 3.585 | 1.862 | 1.304 | 0.591 | 1.417 | 1.400 | 2.17 | 0.516 | 0.099 | 0.309 | 8.240 | 0.51 | 0.28 | 0.633 | 0.816 |
| 0.9500 | 0.559 | 0.847 | 3.452 | 1.817 | 1.345 | 0.559 | 1.395 | 1.400 | 2.20 | 0.508 | 0.093 | 0.321 | 8.260 | 0.51 | 0.28 | 0.632 | 0.817 |
| 1.0000 | 0.528 | 0.833 | 3.334 | 1.778 | 1.385 | 0.528 | 1.373 | 1.400 | 2.24 | 0.499 | 0.088 | 0.333 | 8.314 | 0.51 | 0.28 | 0.631 | 0.819 |
| 1.0500 | 0.498 | 0.819 | 3.228 | 1.743 | 1.425 | 0.498 | 1.351 | 1.400 | 2.28 | 0.491 | 0.083 | 0.343 | 8.398 | 0.51 | 0.28 | 0.630 | 0.822 |
| 1.1000 | 0.468 | 0.805 | 3.135 | 1.712 | 1.465 | 0.468 | 1.329 | 1.400 | 2.32 | 0.483 | 0.078 | 0.354 | 8.512 | 0.50 | 0.28 | 0.628 | 0.825 |
| 1.1500 | 0.440 | 0.791 | 3.050 | 1.683 | 1.506 | 0.440 | 1.307 | 1.400 | 2.36 | 0.474 | 0.073 | 0.363 | 8.655 | 0.50 | 0.27 | 0.626 | 0.830 |
| 1.2000 | 0.412 | 0.776 | 2.974 | 1.658 | 1.547 | 0.412 | 1.285 | 1.400 | 2.40 | 0.465 | 0.069 | 0.373 | 8.825 | 0.50 | 0.27 | 0.624 | 0.835 |
| 1.2500 | 0.386 | 0.762 | 2.906 | 1.635 | 1.587 | 0.386 | 1.263 | 1.400 | 2.44 | 0.457 | 0.064 | 0.382 | 9.022 | 0.49 | 0.27 | 0.621 | 0.841 |
| 1.3000 | 0.361 | 0.747 | 2.844 | 1.615 | 1.628 | 0.361 | 1.242 | 1.400 | 2.48 | 0.448 | 0.060 | 0.390 | 9.246 | 0.48 | 0.27 | 0.619 | 0.847 |
| 1.3500 | 0.337 | 0.733 | 2.787 | 1.596 | 1.670 | 0.337 | 1.220 | 1.400 | 2.53 | 0.439 | 0.056 | 0.398 | 9.497 | 0.48 | 0.26 | 0.615 | 0.854 |
| 1.4000 | 0.314 | 0.718 | 2.735 | 1.578 | 1.711 | 0.314 | 1.198 | 1.400 | 2.57 | 0.431 | 0.052 | 0.405 | 9.775 | 0.47 | 0.26 | 0.612 | 0.862 |
| 1.4500 | 0.293 | 0.704 | 2.688 | 1.563 | 1.752 | 0.293 | 1.177 | 1.400 | 2.62 | 0.422 | 0.049 | 0.412 | 10.080 | 0.46 | 0.25 | 0.608 | 0.870 |
| 1.5000 | 0.272 | 0.690 | 2.645 | 1.548 | 1.794 | 0.272 | 1.156 | 1.400 | 2.66 | 0.413 | 0.045 | 0.419 | 10.414 | 0.45 | 0.25 | 0.604 | 0.879 |
| 1.5500 | 0.253 | 0.675 | 2.605 | 1.535 | 1.835 | 0.253 | 1.135 | 1.400 | 2.71 | 0.405 | 0.042 | 0.426 | 10.776 | 0.44 | 0.24 | 0.600 | 0.888 |
| 1.6000 | 0.235 | 0.661 | 2.568 | 1.523 | 1.877 | 0.235 | 1.115 | 1.400 | 2.76 | 0.396 | 0.039 | 0.432 | 11.167 | 0.43 | 0.24 | 0.595 | 0.898 |
| 1.6500 | 0.218 | 0.647 | 2.534 | 1.511 | 1.918 | 0.218 | 1.095 | 1.400 | 2.81 | 0.388 | 0.036 | 0.438 | 11.589 | 0.42 | 0.23 | 0.591 | 0.909 |
| 1.7000 | 0.203 | 0.634 | 2.503 | 1.501 | 1.959 | 0.203 | 1.075 | 1.400 | 2.86 | 0.380 | 0.034 | 0.443 | 12.041 | 0.41 | 0.23 | 0.586 | 0.920 |
| 1.7500 | 0.188 | 0.620 | 2.474 | 1.491 | 2.001 | 0.188 | 1.055 | 1.400 | 2.91 | 0.372 | 0.031 | 0.448 | 12.526 | 0.40 | 0.22 | 0.581 | 0.931 |
| 1.8000 | 0.174 | 0.607 | 2.447 | 1.482 | 2.042 | 0.174 | 1.036 | 1.400 | 2.96 | 0.364 | 0.029 | 0.453 | 13.045 | 0.39 | 0.21 | 0.575 | 0.943 |
| 1.8500 | 0.161 | 0.594 | 2.422 | 1.474 | 2.083 | 0.161 | 1.017 | 1.400 | 3.01 | 0.356 | 0.027 | 0.458 | 13.598 | 0.38 | 0.21 | 0.570 | 0.956 |
| 1.9000 | 0.149 | 0.581 | 2.399 | 1.466 | 2.124 | 0.149 | 0.999 | 1.400 | 3.06 | 0.348 | 0.025 | 0.462 | 14.188 | 0.36 | 0.20 | 0.564 | 0.968 |
| 1.9500 | 0.138 | 0.568 | 2.377 | 1.459 | 2.165 | 0.138 | 0.981 | 1.400 | 3.11 | 0.340 | 0.023 | 0.466 | 14.815 | 0.35 | 0.19 | 0.558 | 0.982 |
| 2.0000 | 0.128 | 0.556 | 2.356 | 1.452 | 2.206 | 0.128 | 0.963 | 1.400 | 3.16 | 0.333 | 0.021 | 0.471 | 15.481 | 0.34 | 0.19 | 0.552 | 0.995 |
| 2.0500 | 0.118 | 0.543 | 2.337 | 1.446 | 2.247 | 0.118 | 0.945 | 1.400 | 3.22 | 0.326 | 0.020 | 0.474 | 16.188 | 0.32 | 0.18 | 0.545 | 1.009 |

APPENDIX B


DETAILED DESCRIPTION OF MACHINERY REQUIRED TO ACHIEVE ANY
DESIRED TOTAL PRESSURE FOR CONSTANT ENERGY STEADY FLOWS
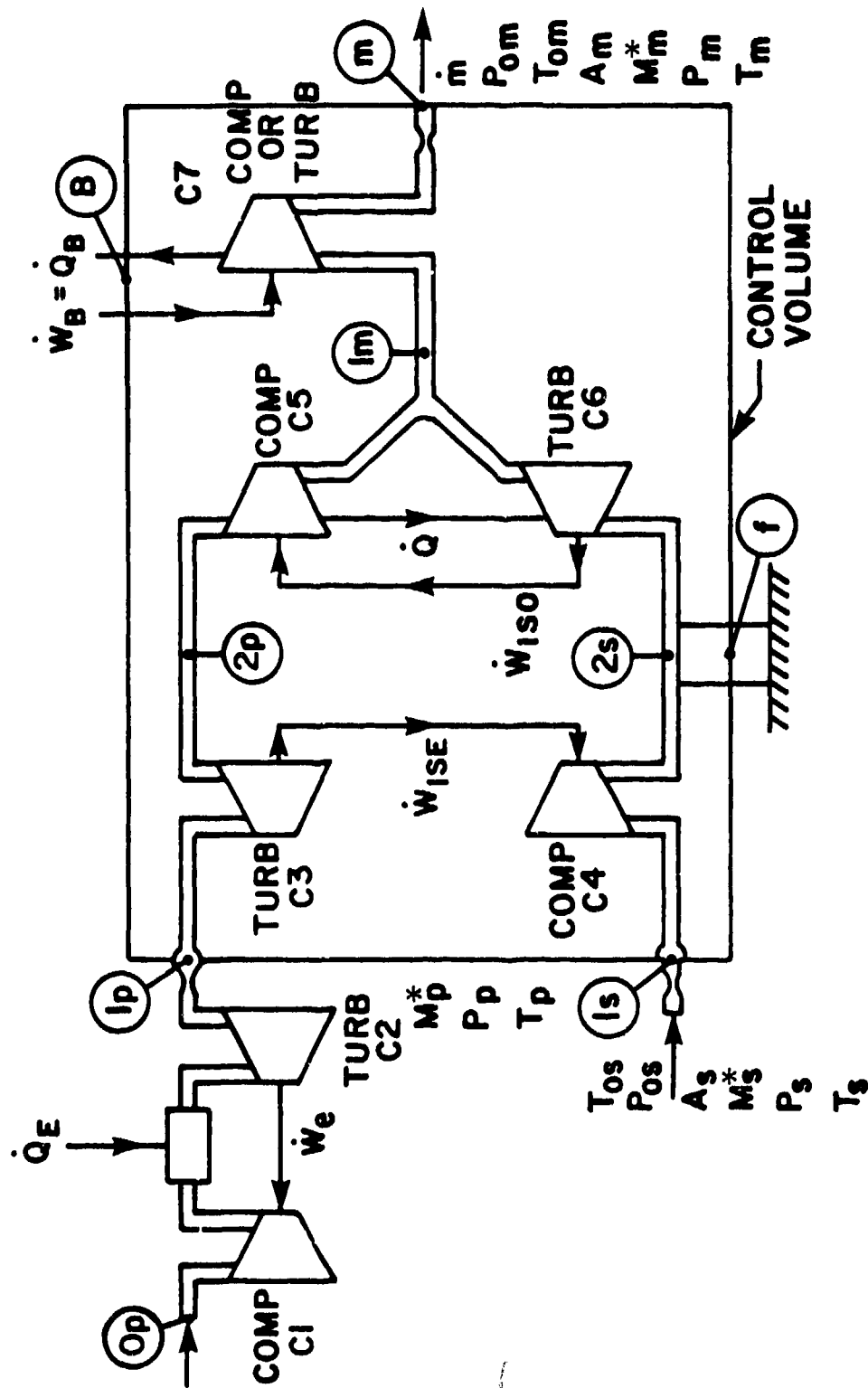
Figure B-1. Machinery for Producing Any Desired Total Pressure for Constant Enthalpy Steady Flows.

## Components of Figure B-1

1.  **Reversible adiabatic components:**

    C1: primary compressor

    C2: primary turbine that drives C1

    C3: primary turbine that drives C4

    C4: secondary compressor

2.  **Reversible isothermal components**

    C5: primary isothermal compressor

    C6: secondary isothermal turbine that drives C5 and exchanges heat with C5

    C7: Mixed flow isothermal compressor (or turbine) that adjusts final stagnation pressure to any desired value

## Stations

0p: We have shown a turbojet engine receiving mass flow $\dot{m}_p$ at $T_{os}$ and $P_{os}$ and supplying conditions of $P_{op}$ and $T_{op}$ at station 1p.

1p: Conditions $P_{op}$ and $T_{op}$ and $\dot{m}_p$. The nozzle produces any desired Mach number $M_p$ (or $M_p*$) at station 1p with static pressure $P_{1p}$ and static temperature $T_{1p}$. The flow can be diffused and fed to the reversible adiabatic turbine. Although we show that the stagnation conditions are supplied by a jet engine, they could also be provided by a boiler and the gas could be a primary vapor which may be a different gas than the secondary.

1s: A secondary gas flow is supplied at flow rate $\dot{m}_s$ and stagnation conditions $T_{os}$ and $P_{os}$. The nozzle supplies the flow at any desired Mach number, $M_s$ (or $M_s*$), at a static pressure of $P_{1s}$. The flow can be diffused to any desired value before entering the reversible adiabatic compressor C4.

2p: After passing through the reversible and adiabatic turbine the primary flow comes to the total temperature $T_{om}$ and a total pressure $P_{02p}$. Since the reversible adiabatic process is isentropic, the entropy is unchanged. Thus, $s_{2p} = s_{1p} = s_{op}$ (i.e., the stagnation value of the entropy at station 1p).

2s: The secondary flow is compressed in a reversible adiabatic process in compressor C4 to a stagnation temperature of $T_{om}$ at stagnation pressure $P_{02s}$. Since this is an isentropic process, we have: $s_{2s} = s_{1s} = s_{os}$ (i.e., the stagnation value of the entropy at station 1s).

Now the isentropic work, $W_{ISE}$, transfered from turbine C3 to compressor C4 is:

$$\dot{W}_{ISE} = \dot{m}_p \, C_p(T_{op} - T_{om}) = \dot{m}_s \, C_p(T_{om} - T_{os}) \quad .$$

277

Hence,

$$(\dot{m}_p + \dot{m}_s) T_{om} = \dot{m}_p T_{op} + \dot{m}_s T_{os} \quad . \tag{B-1}$$

Clearly, this is just the constant energy mixing condition.

lm: The conditions at lm result from mixing the secondary and primary gases that went through the reversible isothermal compressor C5 and the reversible isothermal turbine C6. We can relate the isothermal work to the heat transfer and to the entropy changes (since we have assumed reversible processes).

$$\dot{W}_{ISO} = \dot{Q} = \dot{m}_s T_{om}(s_m - s_{os}) = \dot{m}_p T_{om}(s_{op} - s_{om})$$

therefore

$$(\dot{m}_s + \dot{m}_p) s_{om} = \dot{m}_p s_{op} + \dot{m}_s s_{os} \quad . \tag{B-2}$$

Clearly, this is just the constant total entropy condition which is required for reversible mixing of the two incoming streams.

m: Finally, we take the mixed flow at conditions lm and compress the mixed flow with a reversible isothermal compressor C7. In this way, we can compress the mixed flow to any desired stagnation pressure while still keeping the total temperature the same: i.e., $T_{om}$. The work required for the compressor C7 is equal to the heat transfer. These quantities are shown crossing the control volume at the boundary station B. We amy expand the mixed flow through a nozzle to any Mach number and exit area that we wish.

If we write the momentum equation for the control volume shown in Figure B-1, we must in general include the force in the strut at the boundary station f. Since we are free to produce any stagnation pressure we want at station m, we can produce any force we desire at station f. (Note: the couplings at lp and ls have seals that do not contribute any force on the control volume).

278

Clearly, we can write the following equations for the control volume of Figure B-1 when we have steady flow conditions.

Continuity:

$$m = m_s + m_p \tag{B-3}$$

or

$$\rho_m \, A_m \, V_m = \rho_s \, A_s \, V_s + \rho_p \, A_p \, V_p \tag{B-3a}$$

Energy:

$$\dot{m} \, T_{om} = \dot{m}_s \, T_{os} + \dot{m}_p \, T_{op} \tag{B-4}$$

and momentum

$$P_m A_m - P_{1p} A_p = P_{1s} A_s + f = \dot{m}_p (V_p - V_m) + \dot{m}_s (V_s - V_m) \tag{B-5}$$

Now if we <u>arbitrarily</u> require that

$$A_m = A_p + A_s \tag{B-6}$$

and that the force in the strut is zero

$$f = 0 \tag{B-7}$$

We have a set of equations that are formally identical to those that we write for a constant area ejector.

The complete solution to these equations for a given set of inlet conditons can be used to produce efficiency maps as shown on Figures 4 and 5 of the main body of the report for subsonic and supersonic solution branches.

All of these solutions could be achieved with the machinery shown in Figure B-1 of this Appendix, but all of them could not be achieved with a constant area ejector.

It is also quite clear that the ideal machinery of Figure B-1 could be replaced with real, inefficient machines and ordinary heat exchangers such that Equations (B-3) thorugh (B-5) would still be valid. Thus, all of the solutions shown on Figures 4 and 5 of the main body of the report could be achieved with real machines. However, it is highly unlikely that such a device would have any practical significance.

279
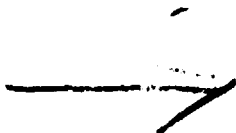
# THRUST AUGMENTING EJECTORS

by

Morton Alperin and Jiunn-Jenq Wu

July 1981

Table of Contents

## Abstract

A discussion of the development of the compact jet-diffuser ejectors utilized for hovering and low speed flight propulsion has been presented. This is followed by a description of ideal ejector performance as derived from a compressible flow theory, over the range of flight speeds from zero to supersonic speed. These analyses introduced the concepts of ejector configuration optimization and the validity of the so-called "second solution" to the mixing problem, wherein the flow after complete mixing is supersonic. The ideal performance of thrust augmenting ejectors designed under this "second solution" has been shown to be far superior to those designed by conventional methods. The ability of properly designed ejectors to utilize the thermal energy of injected gas for the production of useful energy has also been described. Finally, the influence of major losses has been discussed, including means for avoiding excessive performance degradation by proper optimization of the geometry of the ejector in view of these losses.

List of Figures

285

# List of Symbols

| | |
|---|---|
| A | duct area |
| a | primary jet area |
| C | coefficient |
| M | Mach number |
| NPR | nozzle pressure ratio ($= P_{or}/p_\infty$) |
| P | stagnation pressure |
| p | pressure |
| T | temperature |
| U | secondary or mixed flow velocity |
| V | jet velocity |
| X | duct width |
| $\alpha$ | inlet area ratio ($\alpha_\infty = A_2/a_\infty$; $\alpha_* = A_2/a_*$) |
| $\delta$ | geometric diffuser or outlet area ratio ($= X_3/X_2$) |
| $\eta$ | efficiency factor |
| $\Delta S$ | change of total entropy due to mixing |
| $\Delta P$ | primary jet pressure rise ($= P_{or} - P_{o\infty}$) |
| $\Delta T$ | primary jet temperature rise ($= T_{op} - T_{o\infty}$) |
| $\phi$ | thrust augmentation |

Subscripts

| | |
|---|---|
| di | inlet drag |
| dj | diffuser jet or jet diffuser |
| i | induced flow |
| N | primary nozzle thrust |
| p | primary jet |
| r | reservoir |
| o | stagnation |
| 1, 2, 3 | ejector stations |
| $\infty$ | undisturbed or ambient condition |
| * | sonic throat |

Thrust Augmenting Ejectors

Morton Alperin and Jiunn-Jenq Wu

Flight Dynamics Research Corporation

July 1981

## Introduction

Early theoretical and experimental work in ejector technology was related
primarily to the jet pump application. This work reported in References 1 and
2 for example, emphasized the inlet flow and assumed that a large subsonic
(diverging) diffuser was required at the outlet to return the flow to small
velocity at the ambient static pressure. The existence of two different resultant
flows after complete mixing of compressible fluids in a constant area duct was
observed in Reference 1, but the second solution, which represented supersonic
flow after complete mixing was not considered as being of practical importance.
These may have been proper conclusion for the jet pump application since the
objective was the achievement of large secondary flow compression and entrainment
ratios, rather than high momentum flux increment as is required in the case of
thrust augmenting ejectors.

The use of jet propulsion for aircraft created interest in the ejector
as a thrust augmenter. Unfortunately, the early work in thrust augmenting
ejectors borrowed the jet pump concept of large divergent diffusing outlets
as being desirable for high performance. This concept was reinforced by the
use of incompressible flow theory (References 3 and 4 for example), in the
analysis of the flow and performance of thrust augmenting ejectors, leading
to a limited understanding of the optimal capability of ejector thrusters.

Analyses using compressible flow theory also presented a bleak picture
of thrust augmenting ejector performance when the ejector was translating at
even small velocities in the thrust direction, and when the primary injected
gas was heated. Nagaraja, Hammond and Graetch (Reference 5) for example,
indicate a very rapid decrease of thrust augmentation with increasing velocity
and primary fluid stagnation temperature. It was noted in that document however,
that "as speed increased above about 400 ft/sec, the downward trend of thrust
augmentation begins to abate and indeed turns upward".

Very small performance improvement with increasing primary jet stagnation temperatures at speeds in excess of 400 ft/sec. is also illustrated in Reference 5, but the data terminated at speeds of about 600 ft/sec, and general conclusions appear to indicate a degradation of performance with increasing primary jet stagnation temperature.

As a result of the poor performance predicted by the incompressible flow analyses, and by compressible flow analyses as utilized in Reference 5 and others, very little effort was devoted to experimental work aimed at the application of ejectors as primary thrusters during high speed flight. Instead, the Air Force Aerospace Research Laboratory established a research program called Cold Thrust Augmentation (CTA), aimed at the development of ejectors using bleed or fan air for thrust vectoring and augmentation during hover and low speed flight. Under the assumption that ejectors should utilize cold gas injection, this program devoted itself to the investigation of methods for acceleration of the mixing process (References 4 and 6 for example). Other programs were sponsored by the Navy, Marine Corps, NASA, and the Air Force Flight Dynamics Laboratory in attempts to examine the fundamentals of ejector phenomena and to study the problems associated with integration of ejectors into realistic aircraft designs.

During that period of time other investigators have made valuable contributions to ejector technology and have in some measure overcome some of the objections to ejector utilization for V/STOL capability, however, the present remarks will be restricted primarily to work with which we are most familiar. This consists of efforts by Flight Dynamics Research Corporation to demonstrate the feasibility of designing very compact, high performance ejectors and to describe the realistic effects of injected gas characteristics and of translational velocities in the thrust direction, upon ejector performance.

Early investigations by FDRC resulted in demonstrating the feasibility of elimination of a discrete mixing section and of a very short wide-angle diffuser which diffused a fully attached flow to an area ratio of more than 3.0. This ejector developed under a Navy/Marine Corps program called STAMP (Small Tactical Aerial Mobility Platform), developed a thrust augmentation in excess of 2.0 with a configuration described in Reference 7 and shown on Figure 1a.

288

In this ejector, mixing was achieved by injection of the primary fluid upstream of the inlet of the ejector. The short 45 degree half-angle diffuser contained a diffuser jet which completely circumscribed the periphery of the diffuser, to prevent separation and to provide additional diffusion and mixing length beyond the exit of the solid surfaces of the diffuser. End plates extending beyond the diffuser exit were used to prevent collapse of the jet diffuser flow pattern thereby providing additional effective diffuser area ratio. This jet-diffuser ejector produced a thrust augmentation of 2.13 under stationary conditions and a net thrust augmentation of 2.68 at a tunnel speed of 66 ft/sec (perpendicular to the thrust), in the FDRC wind tunnel. This program is reported in detail in Reference 7.

The removal of the diffuser end plates from the STAMP ejector resulted in a decrease of thrust augmentation from 2.13 to 1.82. To avoid this deterioration of performance, a more sophisticated diffuser was designed by FDRC under the sponsorship of NADC. This diffuser, having a shape derived from the potential flow theory is shown on Figure 1b. It produced a thrust augmentation of 2.13 with a length (measured from the diffuser jet exit) of only 1.25 times the throat width of the ejector without the end plates required by the STAMP design. The curvature and divergence of the ends of the diffuser provided a means for avoiding the collapse of the jet diffuser flow downstream of the solid surfaces and provided a means for thrust vectoring in the longitudinal axis of the ejector as will be discussed later. Methods were developed for the design of this type of diffuser, which can conceptually be utilized for design of even shorter diffusers. Details of this effort are described in References 8 and 9.

Protruding primary nozzles were considered as undesirable by aircraft designers. Therefore a modification of the STAMP ejector injection system was carried out with joint NASA and NADC support. Many interesting observations were made during this effort, but briefly a set of nozzles was designed for attachment to the inlet of the ejector in a non-protruding manner, as illustrated on Figure 1b. Thrust augmentation of 2.02 was measured with the new nozzles and the diffuser described above. The entire ejector from inlet to end of the diffuser had a length equal to 2.4 times its throat width, and later modification reduced this to less than 2 times its throat width for aircraft integration. This work is reported in References 9 to 11.
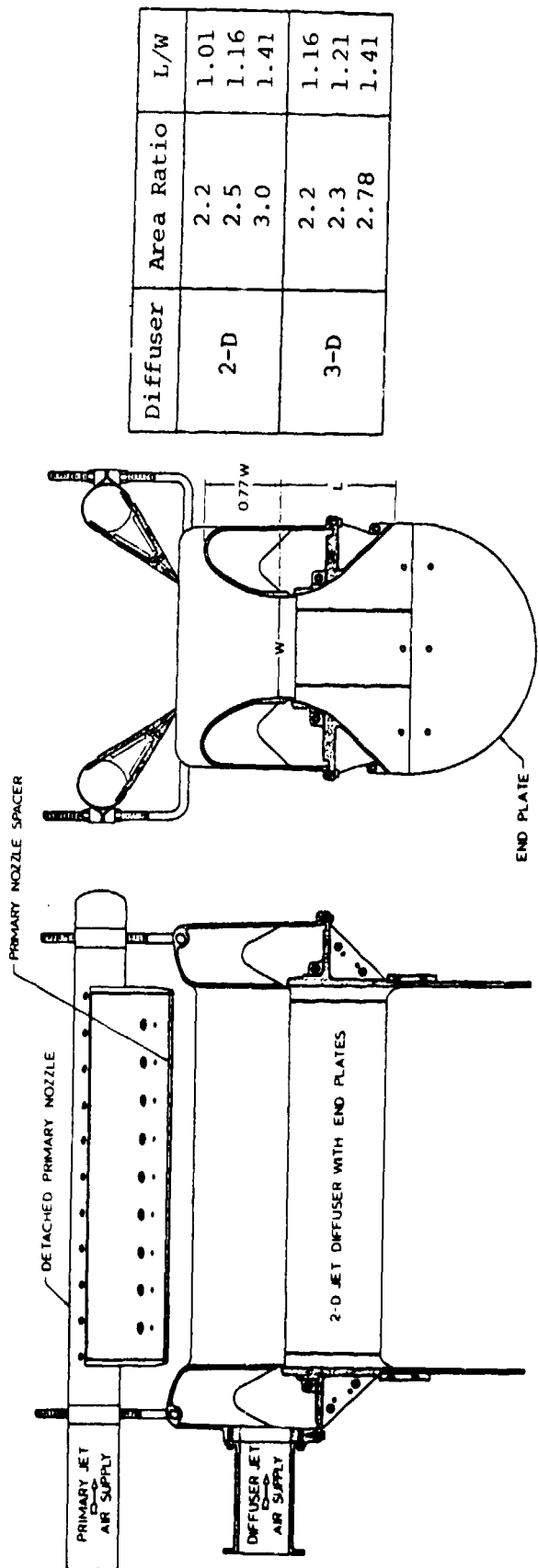
| Diffuser | Area Ratio | L/W |
|----------|-----------|------|
| 2-D | 2.2 | 1.01 |
|     | 2.5 | 1.16 |
|     | 3.0 | 1.41 |
| 3-D | 2.2 | 1.16 |
|     | 2.3 | 1.21 |
|     | 2.78 | 1.41 |



a) STAMP Jet-Diffuser Ejector
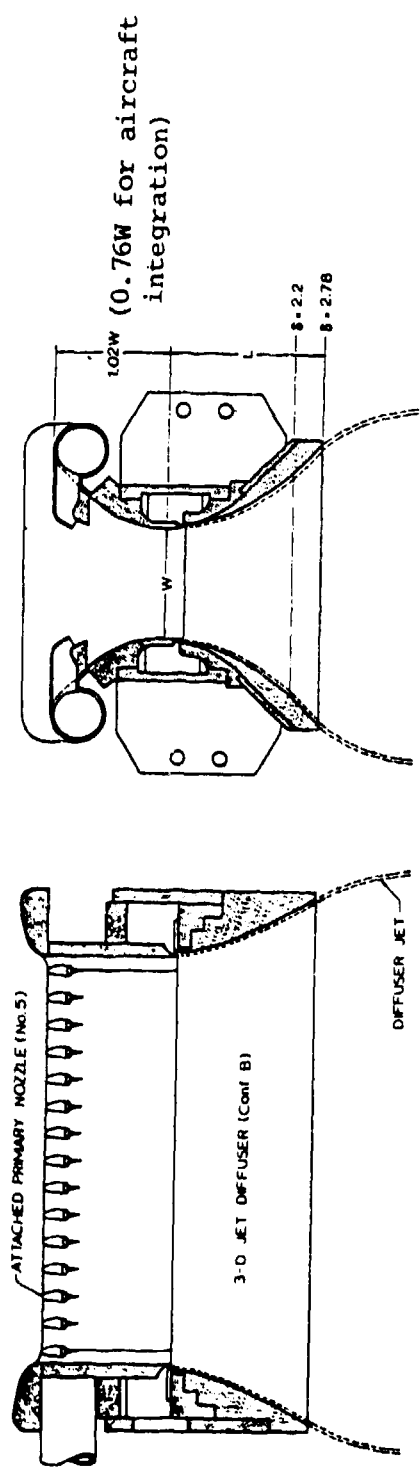


b) Ejector with Three-Dimensional Diffuser and Attached Nozzles

Figure 1. Jet-Diffuser Ejectors

Having developed this extremely small, high performance ejector, FDRC was given the opportunity to integrate the ejector into a supersonic fighter/ attack aircraft designed by General Dynamics and designated E205 (Figure 2). This effort was sponsored jointly by NADC and NASA. The achievement of the required ejector lift force corresponding to a wing loading of 118.3 psf at a nozzle pressure ratio of 3.0 while limiting the total size of the ejectors to fit within the structural limitations of the strake of the small supersonic fighter/attack aircraft necessitated a large injected momentum per unit throat area and a large thrust augmentation.

In this design, the ejectors are required to provide a thrust force to accelerate the aircraft to transition flight speeds, and the vertical force (lift) to achieve VTOL capability. This thrust vectoring is accomplished by an asymmetric extension of the rear ends of the diffusers and by use of specially designed thrust vector control jets within the ejector. The high value of thrust per unit area of ejector is achieved as a result of the effective use of injected gas at the diffuser jet in addition to the primary injection jets. This permits a high concentration of injected momentum while maintaining a high inlet area ratio and correspondingly high performance. Forces in the flight direction equivalent to 12% of the total thrust were measured with a single vector control jet in conjunction with an asymmetric extension of the rear end of the diffuser, in static tests at FDRC with a short ejector integrated into the forward end of the strake. The ejectors designed for the E205 are foldable and can be stowed completely within the strake during normal flight. Testing at high nozzle pressure ratios will be conducted at NASA Ames Research Center.

The design, based upon the use of unheated primary and diffuser gas appeared as illustrated on Figure 2. Further details are presented in Reference 11.

Ejector design considerations including performance predictions with high nozzle pressure ratio injected gas and estimated loss factors are discussed in a later section of this document.

Figure 2. V/STOL Fighter (one-fifth scale model)

| | | WING, Ref | CANARD | VERTICAL TAIL |
|---|---|---|---|---|
| AREA | ft² | 7.682 | 1.539 | 1.907 |
| | m² | 0.714 | 0.143 | 0.177 |
| SEMISPAN | | | | |
| ASPECT RATIO | | 3.62 | 2.16 | 1.28 |
| TAPER RATIO | | 0.19 | 0.37 | 0.43 |
| AIRFOIL | ROOT | NACA 64A204 | 64A005 | 5.3% Biconvex |
| | TIP | 64A204 | 64A003 | 4% Biconvex |

Unpowered Nacelle

SECTION BL 6.25 AND INBOARD

## Ideal Ejector Performance

These programs and others in a more advanced stage of development (Reference 12 for example) have given some indication that ejectors may be satisfactory for use in thrust vectoring and augmentation at zero translational velocity or at low speeds when oriented perpendicularly to the flight path. The adverse effect of high temperature injected gas has been considered as inevitable and some systems have been developed using bleed air or fan air exhaust to minimize this problem. The real advantage achievable by thrust augmenting ejectors has awaited a more thorough analytical treatment of the problem. Previous analyses which indicated very large performance degradations due to translational motion in the thrust direction and due to the injection of heated gas were lacking in several important aspects, which have become clear to us as a result of the effort sponsored by AFFDL and some considerable in-house efforts, some of which are reported in Reference 13, "High Speed Ejectors".

The analysis of the flow through an ejector under the assumption that the fluids are incompressible, yields results which are pertinent to those systems which operate underwater (References 14 and 15 for example). However, incompressible fluid analyses cannot provide information related to the effects of high pressure and temperature injected gas, nor those phenomena which are associated with heat transfer such as thermal choking. Therefore, realistic estimates of the performance and flow characteristics within a thrust augmenting ejector required to utilize the exhaust from conventional gas turbines, ramjets or rockets as the source of power, must utilize the theory of compressible flow.

In addition to the choice between compressible and incompressible theory, the analysis of ejector flow generally utilizes a choice between constant pressure and constant area mixing. The selection of one of these two cycles permits precise expression of the momentum theorem in the mixing section in a global analysis. Of these two choices, the use of constant pressure mixing results in the simpler mathematical formulation and better pumping characteristics (Reference 1) and has been utilized extensively in jet pump ejector literature.

293

Unfortunately the design of a constant pressure mixing duct becomes difficult since the exact shape of the duct cannot be determined by a global analysis and would require a complex, detailed analysis of the flow throughout the mixing process. A further disadvantage to the use of constant pressure mixing is related to the obvious restriction to the variation of the static pressure during mixing. The processes are restricted to those in which the pressure after mixing is identical to the pressure of the two individual flows at the start of mixing. The potential thermodynamic and aerodynamic advantages attributable to pressure changes during mixing are obviated by the assumption of constant pressure. This is immediately evident by observation of the character of the solution to the global treatment of the mixing problem under both assumptions. Clearly the constant area mixing problem has two solutions while constant pressure mixing has only one solution, and the freedom to permit pressure variations provides the opportunity to observe many types of flow patterns not possible within the constant pressure restriction.

The assumption of constant area mixing is also restrictive, but the feasibility of using a global analysis, of writing a precise momentum equation, and the geometric simplicity has prompted its use in analytical treatments of the mixing problem. It appears possible that some special mixing duct designs would result in better performance but no such analysis has been published to date to our knowledge. Therefore all further discussion of ejector flow and performance in this report will be based upon the assumption of constant area mixing of compressible flow, and will use the symbols and station designation presented on Figure 3.
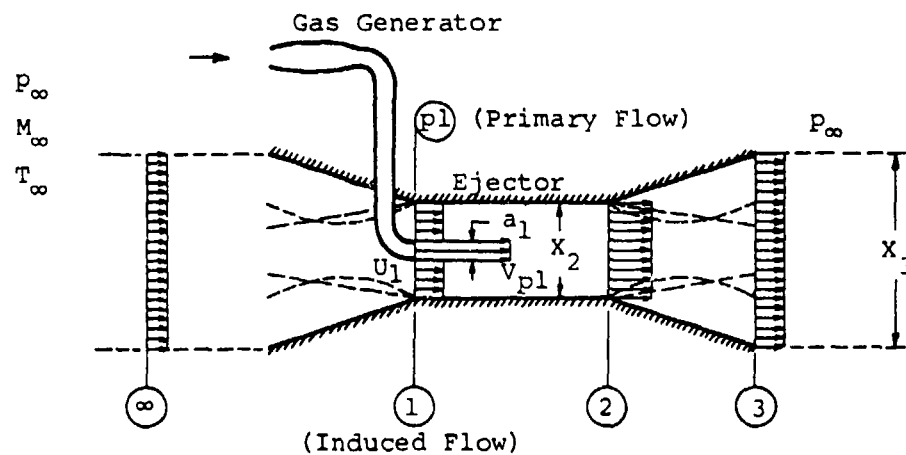


Figure 3. Ejector Configurations and Station Designation

294

As will be shown by means of the analyses described in the "High Speed Ejectors" report (Reference 13), high speed and hot gas injection need not have the adverse influence on ejector performance predicted by previous analyses. Although the reasons for these divergent views are complex in detail, there are several rather obvious differences in the treatment of ejector flow as presented in the "High Speed Ejector" report compared to the previous compressible flow analyses.

Most importantly, it has been observed that either of two distinct types of flow may exist after complete mixing of compressible fluid in a constant area duct. The so-called "first solution" always results in a subsonic (or sonic) flow after complete mixing, regardless of the conditions at the start of the mixing process. This solution dictates the geometric characteristics of the ejector required to return the mixed subsonic flow to ambient pressure at the outlet. The so-called "second solution" always results in a supersonic (or sonic) flow after complete mixing, regardless of the conditions at the start of the mixing process. Obviously the geometric characteristics of the ejector required to return this supersonic flow to ambient pres.ure will differ from those of the first solution. Since the mathematics allows only supersonic mixed flow under the second solution, it is obvious that certain conditions at the start of mixing may be inconsistent with physical reality. These conditions can be screened out by consideration of the Second Law of Thermodynamics. Although both solutions have been observed previously, to our knowledge, no use has been made of the second solution in the design of thrust augmenting ejectors to date.

Further, optimal geometries exist for all conditions examined by means of the compressible flow analysis. The optimal geometry is dependent upon the solution (first or second) utilized in the analysis, the operational and injected gas characteristics, and upon the losses within the ejector. As will be shown, the thrust augmentation achievable decreases rapidly on either side of the optimal inlet and outlet configurations. While some variations of outlet area have been examined, it is not apparent that those experiments were performed in the light of theoretical guidance nor that the geometries were even close to the optimal given by the theory.

In the following discussion, use is made of several unique parameters not generally used by theoreticians, but which we believe are important in relating theory to reality.

295

To evaluate the influence of any parameter on ejector performance, it is essential that the ejector size be fixed in relation to the size of its reference jet. To accomplish this it is necessary to define a reference jet as a free jet whose gas has the same stagnation properties and mass flow as those of the primary jet of the ejector. Then the relationship of the mixing section area of the ejector to that of its reference jet when expanded isentropically to ambient pressure $(\alpha_\infty)$, defines the ejector size. When the nozzle pressure ratio is supercritical, it is sometimes convenient to relate the size of the mixing section of the ejector to the throat area of the reference jet $(\alpha_*)$. In either case the comparison of ejector size to that of its reference jet remains constant as the pressure at the injection plane in the ejector varies as a result of changes in the ejector geometry.

When the ejector is in motion in its thrust direction, it is necessary to compare its performance with that of its reference jet while in motion under the same conditions. Thus the variation of nozzle pressure and temperature with changes in the translational velocity must be considered in a realistic manner. This can be accomplished with reasonable realism if the nozzle pressure and temperature ratios are expressed as increments in excess of the free stream ratios. Thus in the analyses presented, the nozzle pressure and temperature ratios are expressed in terms of $\Delta P/p_\infty$ and $\Delta T/T_\infty$. Obviously data presented for a fixed flight Mach Number can be related to fixed stagnation properties as is done on the maps to be described in the following discussion, but in presenting data on ejector performance as a function of its translational velocity, it is more realistic to utilize constant values of $\Delta P/p_\infty$ and $\Delta T/T_\infty$ and permit the nozzle pressure and temperature ratios to vary with the free-stream pressure and temperature ratios. Further, the net thrust of the ejector should be compared to the net thrust of its reference jet, to provide a meaningful indication of the ability of the ejector to augment the thrust of its reference jet.

These considerations have been utilized in the preparation of the data to be discussed in the following section.

296

Stationary Ejector

To illustrate the importance of a proper selection of the ejector configuration, we first examine the so-called stationary case in which the ejector is at rest with respect to the undisturbed medium or oriented so that its thrust vector is normal to the flight direction. Figure 4 illustrates the influence of ejector geometry upon the performance and thermodynamics of the flow in a stationary ejector. The chart was prepared with a fixed value of $\alpha_\infty$ (=20) to assure consideration of an ejector whose mixing duct area has a constant relationship to the area of the reference jet when fully expanded to ambient pressure. To simplify the presentation, the thrust augmentation, ratio of mechanical energies of ejector output to reference jet output, and the outlet area ratio required to return the mixed flow to ambient pressure are plotted versus the Mach Number ($M_1$) of the induced flow at the start of mixing. $M_1$ also determines the geometry at the inlet and outlet of the ejector for any given operational and injected gas characteristics. As indicated, there are three performance points where the thrust augmentation is optimal.

Under the first solution a maximum thrust augmentation always occurs with subsonic values of $M_1$. In this particular case it occurs very close to the lower limit of thermal choking. This optimal point varies with operational and injected gas characteristics.

The second solution usually displays a local maximum performance point with a supersonic value of $M_1$, which in this case occurs at the higher limit of choking, and a limiting performance at a subsonic value of $M_1$, limited by the Second Law of Thermodynamics.

It is interesting to note that in this ideal limiting situation, the total entropy of the mixed flow is equal to the sum of the entropies of the flows at the start of mixing and that the mechanical energy of the ejector discharge can be larger than that of the reference jet. Thus some of the thermal energy of the reference jet is converted to mechanical energy during the mixing process. Real gas effects and wave losses obviously preclude achieving the performance predicted by the $\Delta S = 0$ point, but achievement of this second solution flow pattern would obviously result in superior performance to that achieved by the conventional first solution.

297
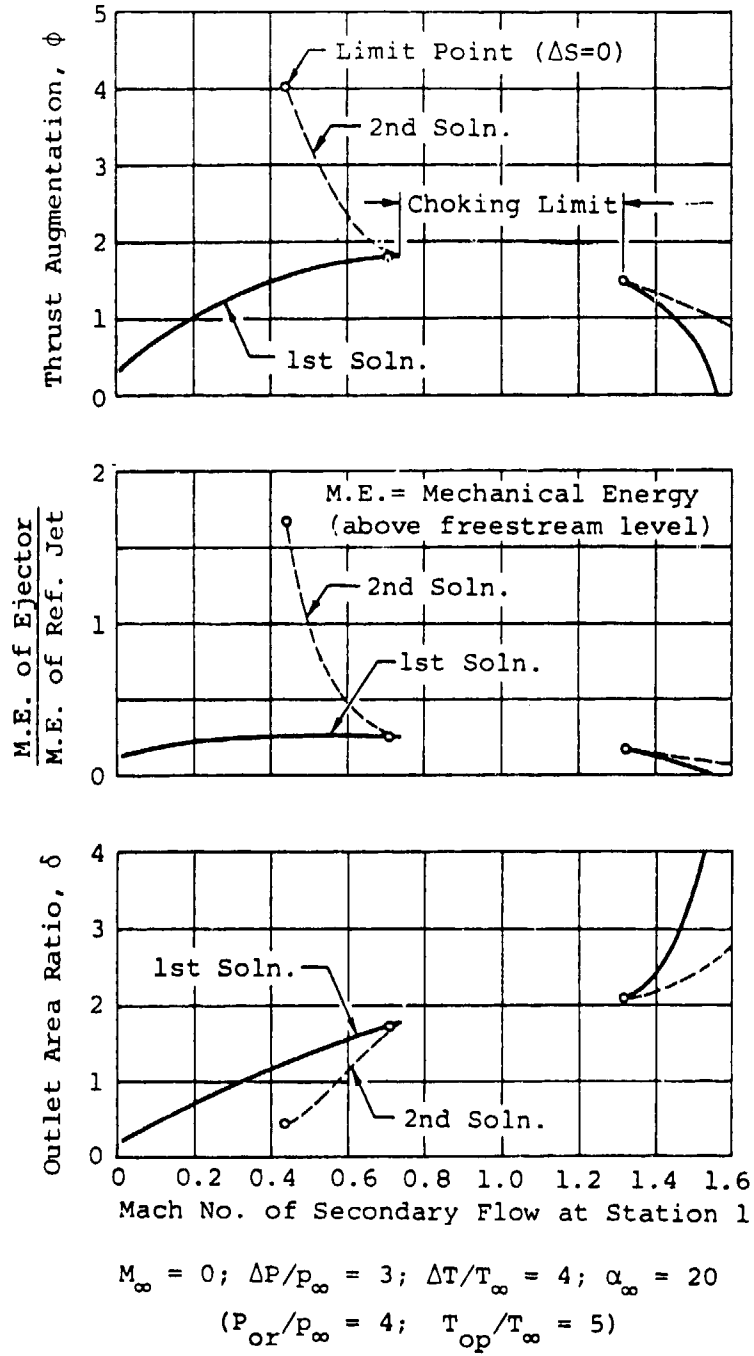
Figure 4. Example of Stationary Ejector

To illustrate the influence of primary fluid stagnation temperature and outlet geometry on stationary ejector performance, the variation of thrust augmentation is plotted versus outlet area ratio, for the first solution (Figure 5) and for the second solution (Figure 6), at an arbitrarily chosen primary nozzle pressure ratio and for several different primary nozzle stagnation temperatures. On these figures, the outlet area ratio is defined as the ratio of the area at the section where the pressure returns to ambient to the area of the mixing section of the ejector. On Figure 5, the outlet in the regions of practical interest (near maximum performance) is a diverging diffuser (area ratios greater than 1.0 and all discharged flow is subsonic). Both the thrust augmentation at a fixed outlet area ratio and the maximum achievable thrust augmentation decrease with increasing primary jet stagnation temperatures when the outlet area ratio is smaller than a certain critical value. At larger values of the outlet area ratio (supersonic mixing), the thrust augmentation increases with increasing primary jet stagnation temperatures when the outlet area ratio is fixed. Maximum thrust augmentation in this region however, decreases with increasing primary jet stagnation temperatures. The natural solution of this region, (where outlet area ratios correspond to supersonic values of $M_1$), is presumably the second solution.

Under the second solution (Figure 6), where the flow after complete mixing is supersonic, the ideal outlet (for the cases shown) is a converging or convergent-divergent diffuser. In order to distinguish between these two different types of outlets, dashed lines are used to represent the convergent diffuser while solid lines represent the convergent-divergent diffuser (which requires a sonic throat). As in the case of the first solution, increasing primary jet stagnation temperatures have an adverse influence on performance with a given outlet area ratio. Maximum limiting performance however, improves with increasing primary jet stagnation temperatures as a result of the ability to operate at smaller outlet area ratios without violation of the Second Law of Thermodynamics.

Comparison of Figures 5 and 6 disclose the considerable performance advantage in the use of second solution design criteria, even for the stationary ejector.
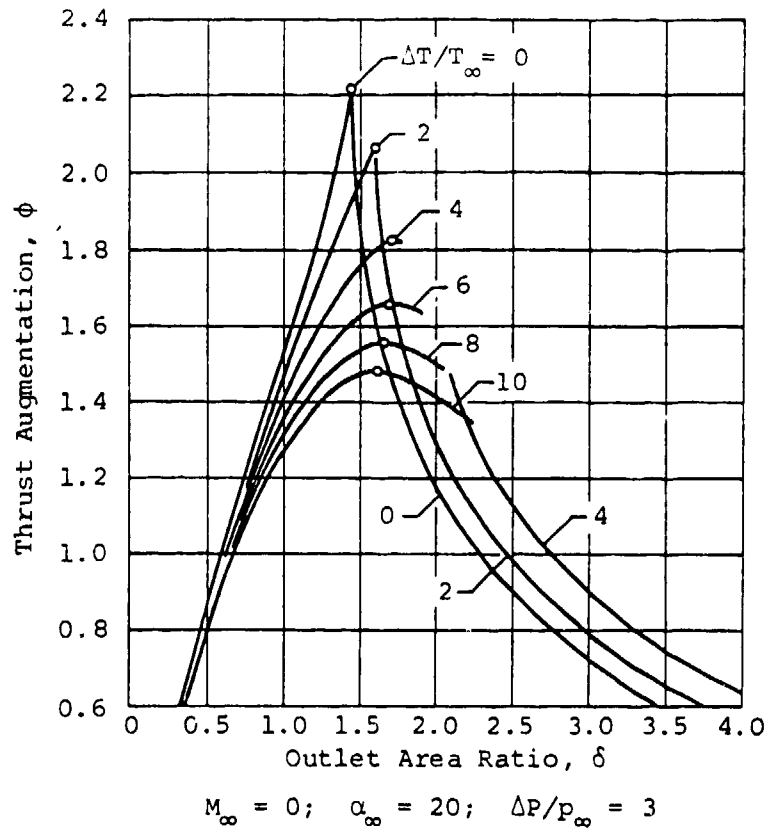
Figure 5. Stationary Ejector Performance - First Solution
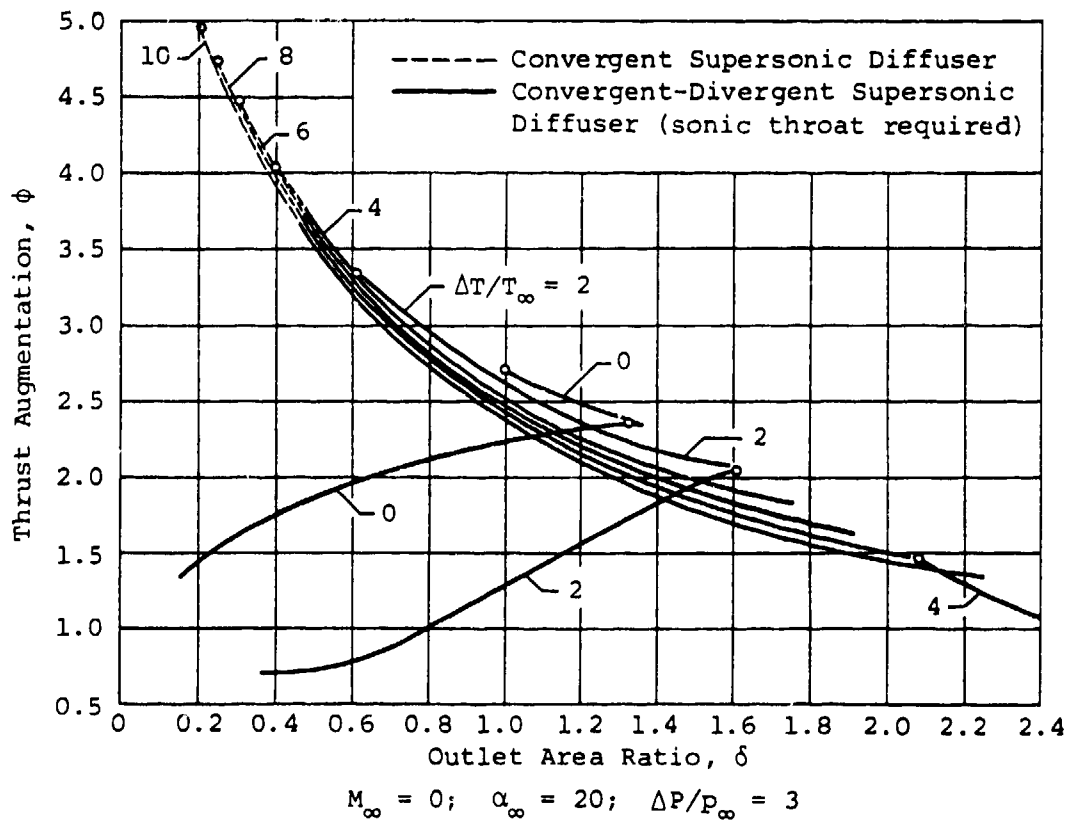


Figure 6. Stationary Ejector Performance - Second Solution

300

To provide a quick reference for determination of the influence of primary jet pressure and temperature ratios on ejector performance, maps showing ideal iso-augmentation lines with the appropriate configurations of inlet and outlet, on pressure-temperature surfaces are presented on Figures 7 to 9 for a stationary ejector with $\alpha_\infty = 20$ (a mixing duct having an area equal to 20 times that of the reference jet when fully expanded to ambient pressure).

Figure 7 represents the ideal performance of an ejector at rest or whose motion is normal to the thrust direction, designed with a geometry described by the optimal condition under the first solution. To our knowledge all thrust augmenting ejectors designed to date have utilized this design criterion but little effort has been devoted to optimization. As shown on Figure 7, ejectors designed under this criterion display a performance degradation with increasing primary jet pressure and temperature ratios. These ejectors require an accelerating inlet, and a subsonic diffuser or nozzle outlet for conditions within the boundary of Figure 7. The achievement of high performance ejector designs under this criterion lies in the effective design of diffusers, the minimization of component losses and the optimization of the geometry for any given set of injected gas characteristics, as will be illustrated on Figures 16 and 17.

Figure 8 represents the same operational conditions as those of Figure 7, but assumes that design criteria are established by use of the second solution with supersonic induced flow at the start of mixing, which requires a convergent-divergent accelerating inlet. As shown, increasing primary jet pressure and temperature ratios produce performance deterioration. Excessively high temperatures result in no analytical solution.

Use of the second solution with subsonic mixing is limited to the region where the total entropy change during mixing is greater than zero. At the limit ($\Delta S = 0$), ideal ejectors display a maximum performance limited by the Second Law of Thermodynamics and at this point the performance map is as presented on Figure 9. Under this design criterion the ideal performance is very high over the entire practical range of primary pressure and temperature ratios.

301

Using this design criterion, increasing primary jet stagnation temperature generally results in improved performance except at relatively low temperatures ($\Delta T/T_\infty < 1$) as illustrated.  As shown, within the boundary of Figure 9, the inlet is a subsonic accelerating duct, while the outlet is either a convergent-divergent supersonic diffuser, or a convergent supersonic diffuser.

Obviously losses due to wave drag, skin friction, blockage, etc., will result in some performance degradation.  These effects will be discussed in a later section of this document.
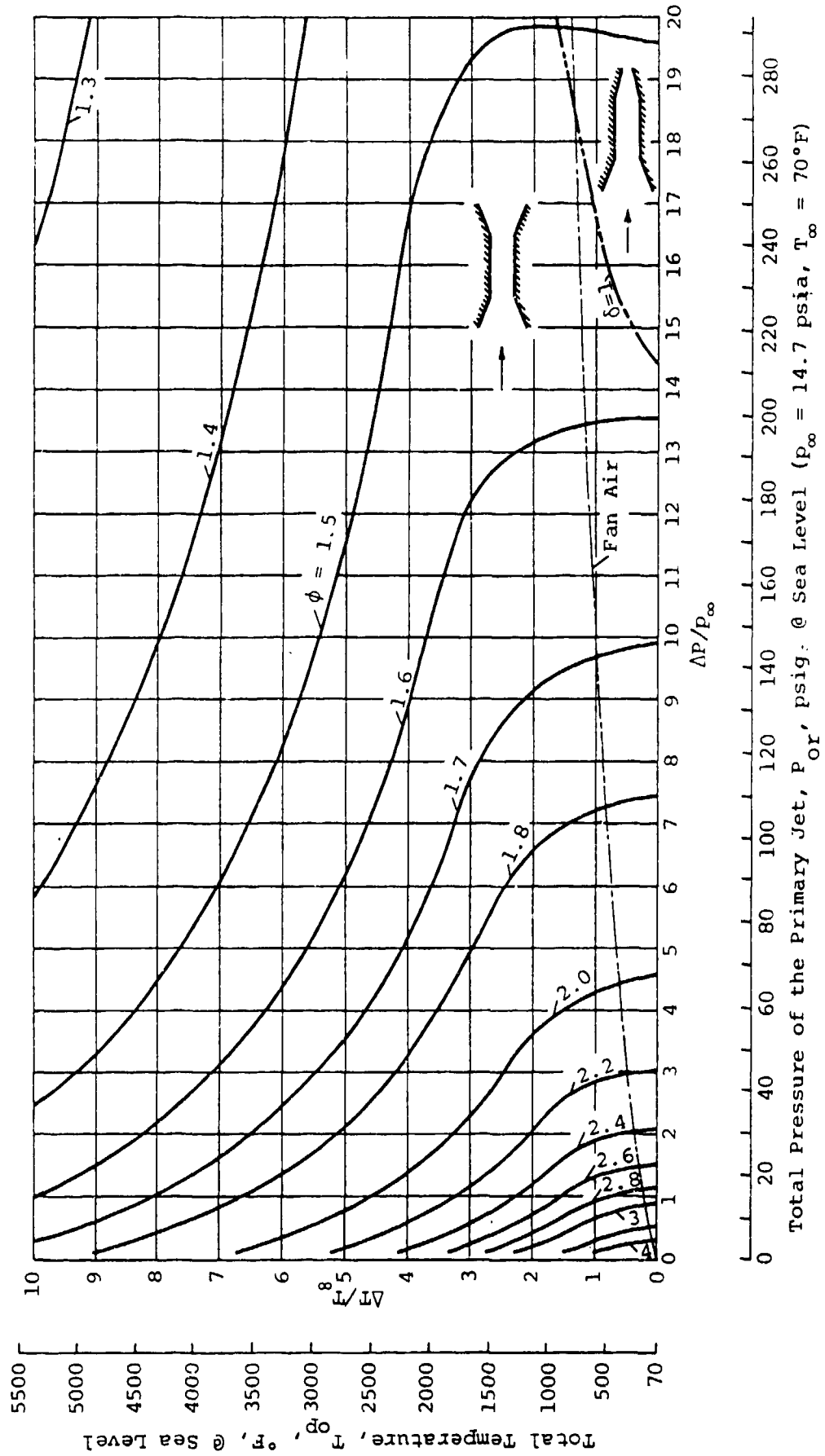
302

Figure 7. Ideal Ejector Performance Map
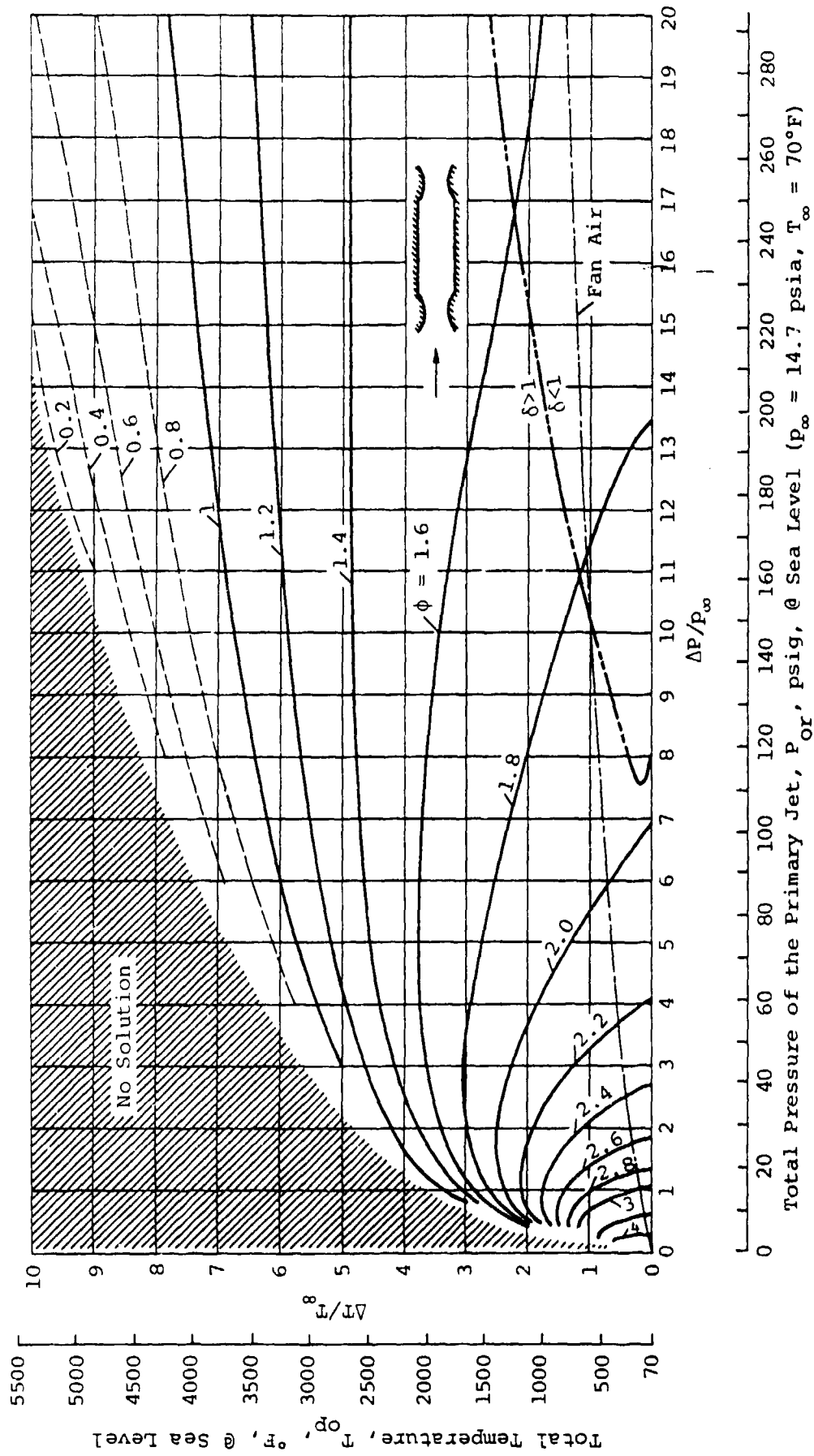
Freestream Mach Number: $M_\infty = 0$; Ejector: $\alpha_\infty = 20$, Maximum $\phi$ of First Solution (Subsonic Mixing)

303

Freestream Mach Number: $M_\infty = 0$; Ejector: $\alpha_\infty = 20$, Maximum $\phi$ of Second Solution (Supersonic Mixing)

Figure 8.  Ideal Ejector Performance Map

Figure 10. Ideal Ejector Performance Map

Freestream Mach Number: $M_\infty = 0.7$; Ejector: $\alpha_\infty = 20$, Maximum $\phi$ of First Solution (Subsonic Mixing)

Figure 9. Ideal Ejector Performance Map
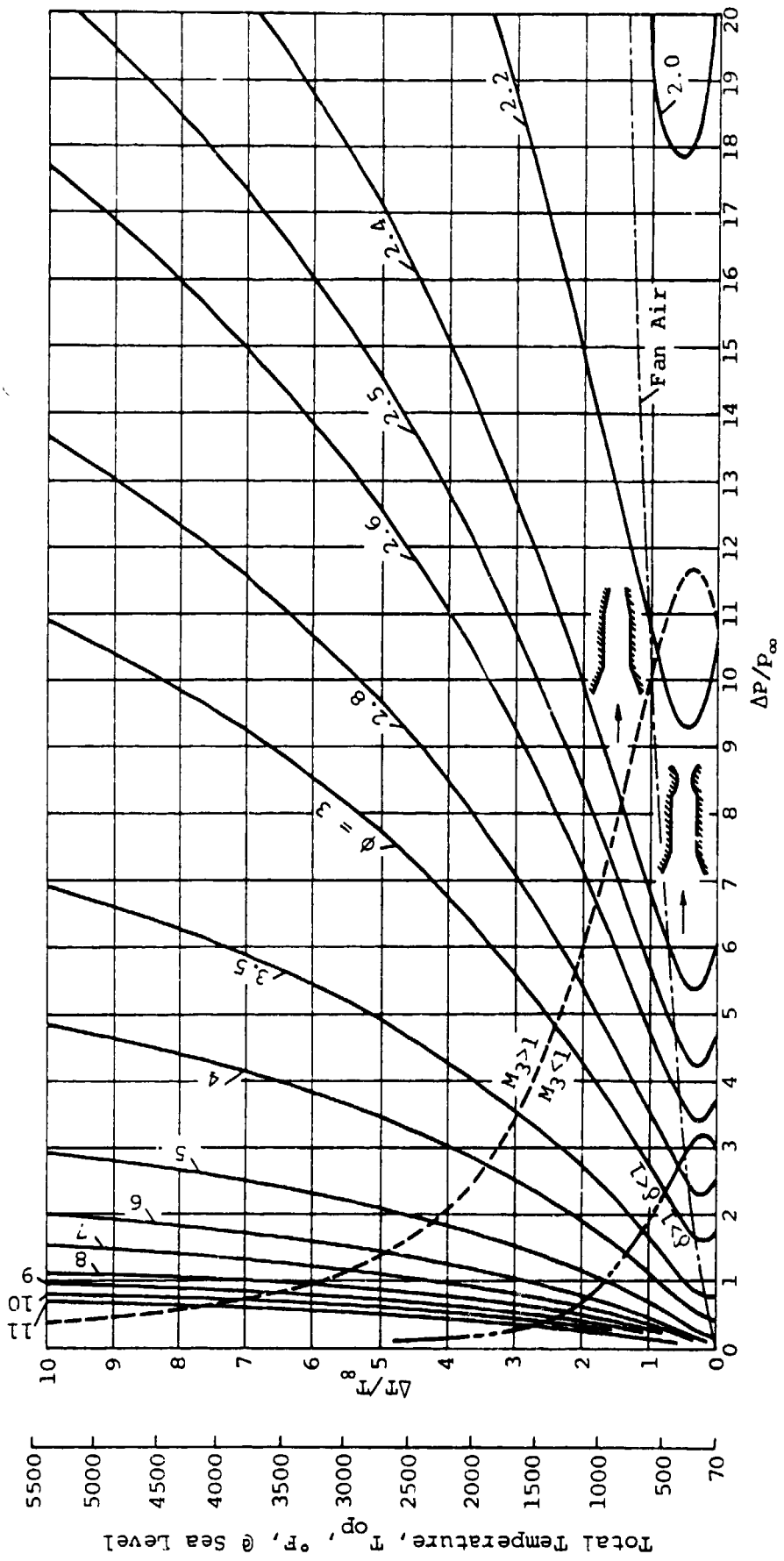
Freestream Mach Number: $M_\infty = 0$; Ejector: $\alpha_\infty = 20$, $\phi$ of Second Solution with Subsonic Mixing, $\Delta S = 0$

## Subsonic Flight Speeds

Thrust augmenting ejectors encounter their most difficult operational conditions in the mid-subsonic range of flight speeds. At these speeds, the beneficial effects of ram compression tend to be balanced by their adverse effects.

Optimal ejector designs based upon the first solution with subsonic mixing are distinctly divided into two types separated by the upper line of $\phi = 1$ on Figure 10. The first type is sketched below the $\phi = 1$ line and as shown has similar geometry to the conventional stationary ejector design which has an accelerating inlet and operates best with relatively low temperature injected gas (like fan air for example). The second type requires a compression inlet, and operates best at relatively low nozzle pressure ratios and high temperatures, or ramjet like injected gas. The first (conventional) type ejector can not achieve adequate performance at this flight speed, as shown. The performance of the second (ramjet) type ejector becomes significant and shows good performance at this flight Mach number (0.7) as illustrated on Figure 10. This is not evident in the stationary case (Figure 7). As will be shown later, the ramjet type ejector dominates the ejector design configuration under the first solution at higher speeds.

Ejectors operating at a flight Mach Number of 0.7 and designed under the second solution with supersonic mixing also display very poor optimal performance. The best performance, however, occurs at high primary nozzle pressure ratios and low primary temperature ratios as illustrated on Figure 11.

Figure 12 illustrates the tremendous advantage achievable through the use of the second solution with subsonic mixing. The ideal, limiting performance achievable by ejector designs prescribed by this type of flow can be very high over the entire practical range of primary pressure and temperature ratios. Further, the performance of these ejectors improves with increasing primary stagnation temperature (except for temperature below roughly the fan-air line), but falls off with increasing primary stagnation pressure. As indicated on Figure 12, the appropriate outlet design is a supersonic diffuser, either convergent or convergent-divergent. Therefore wave losses at the outlet become the major concern in designing this type of ejector for operation at this flight speed range.
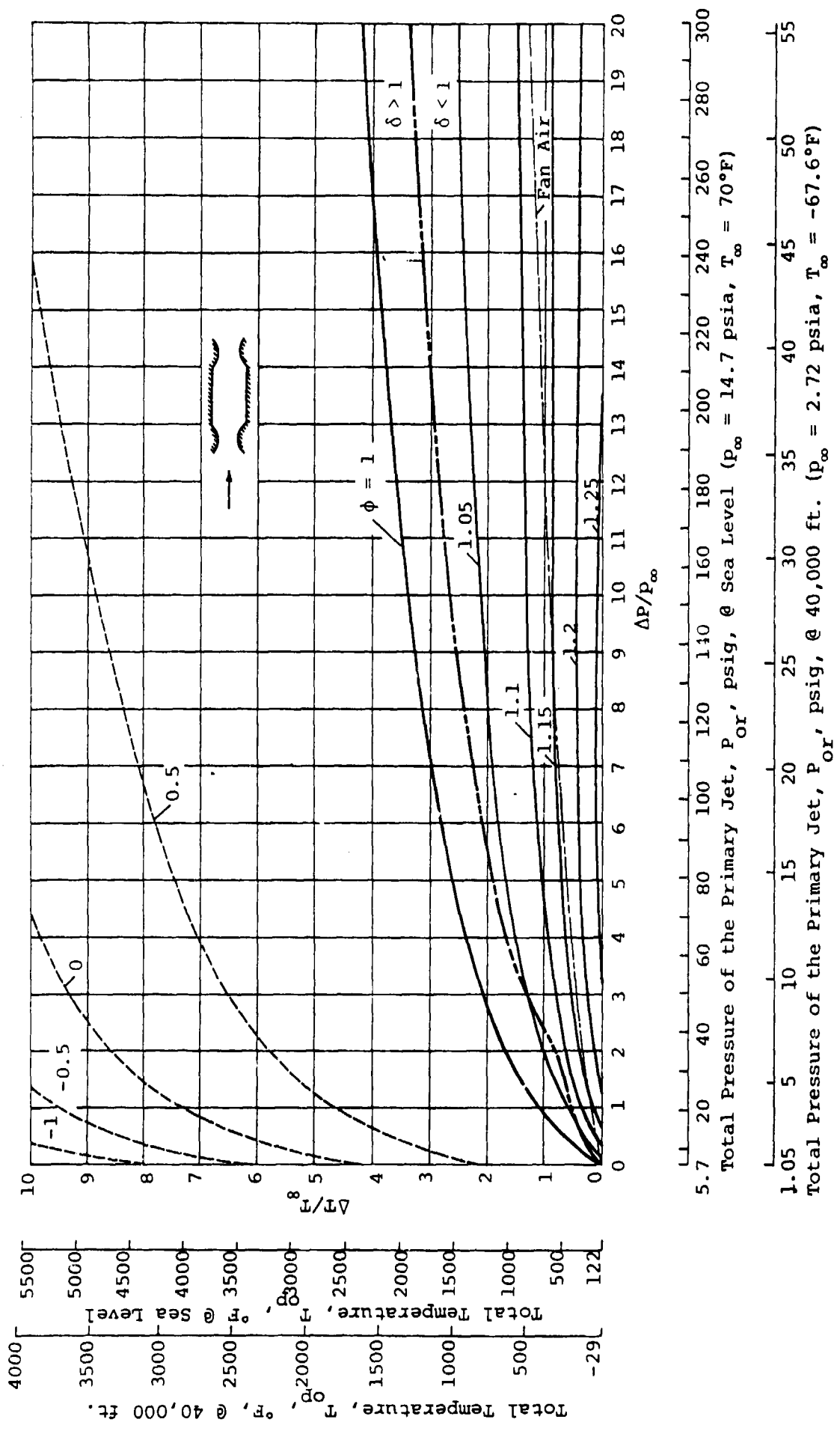
307

Figure 11. Ideal Ejector Performance Map
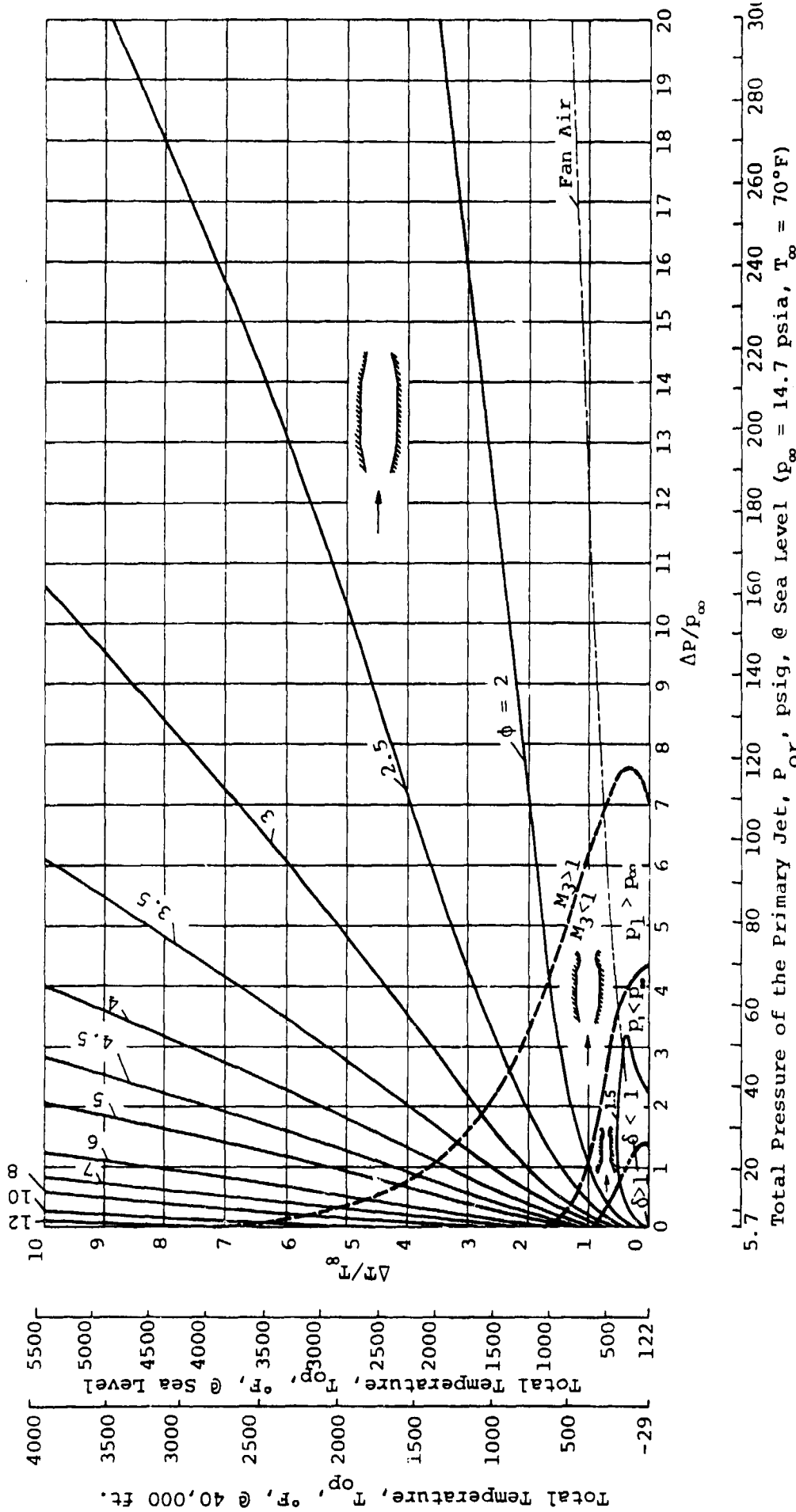
Freestream Mach Number: $M_\infty = 0.7$; Ejector: $\alpha_\infty = 20$, Maximum $\phi$ of Second Solution (Supersonic Mixing)

Figure 12. Ideal Ejector Performance Map

Freestream Mach Number: $M_\infty = 0.7$; Ejector: $\alpha_\infty = 20$, $\phi$ of Second Solution with Subsonic Mixing, $\Delta S = 0$

## Supersonic Flight Speeds

Ejectors translating at supersonic speeds can provide very large thrust augmentations provided the design criteria and injected gas characteristics are properly chosen and the configuration of the ejector is optimized.

Figure 13 illustrates the ideal performance of ejectors designed under the optimal conditions of the first solution, while translating at a Mach number of 2. As shown, better performance occurs at higher temperature and lower pressure ratio injected gas (ramjet type efflux), but the performance is a rather weak function of the nozzle pressure ratio, thus providing good performance even with turbojet or rocket type injected gas. As illustrated a supersonic convergent-divergent diffuser is required for ideal inlets and outlets over the range of specified conditions for flows resulting from this optimal design point.

Figure 14, illustrates the ideal, optimal thrust augmentation for ejectors translating at a Mach number of 2, when designed under the second solution with supersonic mixing. Better performance in this case also occurs when the injected gas has a higher stagnation temperature. The inlet is a supersonic converging diffuser, and the outlet is a diverging nozzle over most of the range of conditions illustrated.

Figure 15 illustrates the ideal, limiting thrust augmentation for ejectors translating at a Mach number of 2, and designed under the second solution with subsonic mixing. This limiting performance occurs at the condition where the total entropy after mixing is equal to the sum of the entropies of the primary and induced flows at the start of mixing. As shown, the limiting performance under this condition still achieves its maximum values (for a given temperature) with ramjet type injected gas, but the performance of ejectors designed under the second solution with subsonic mixing is considerably better than that achievable by ejectors designed under either of the other conditions. To achieve this type of flow at the prescribed flight Mach number it is essential that the ideal inlet be convergent-divergent, and the outlet be a divergent nozzle as illustrated. Therefore, inlet compression loss is likely to be a major factor controlling the ejector performance.

The influence of losses in the ejector flow upon optimal design criteria and performance are illustrated in the following discussion.
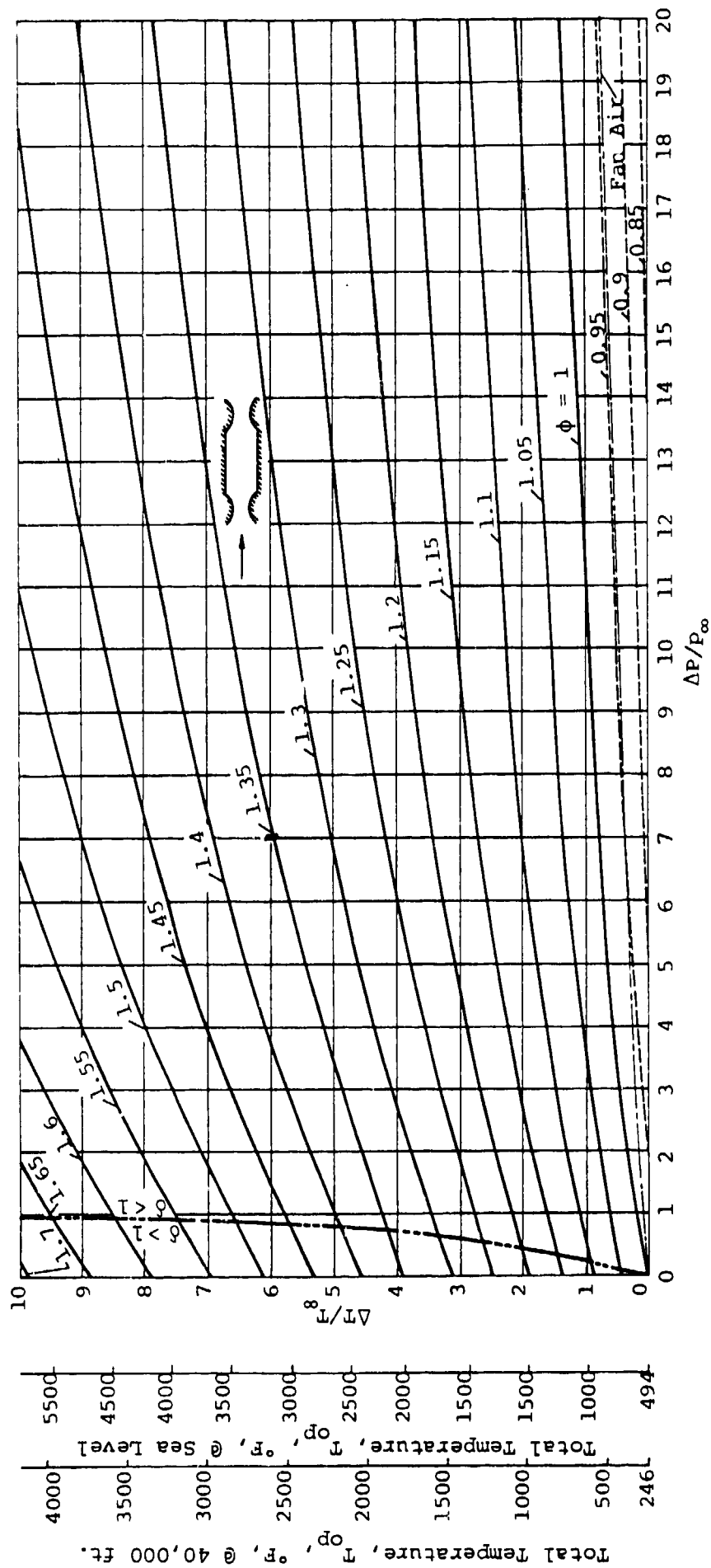
310

Figure 13. Ideal Ejector Performance Map
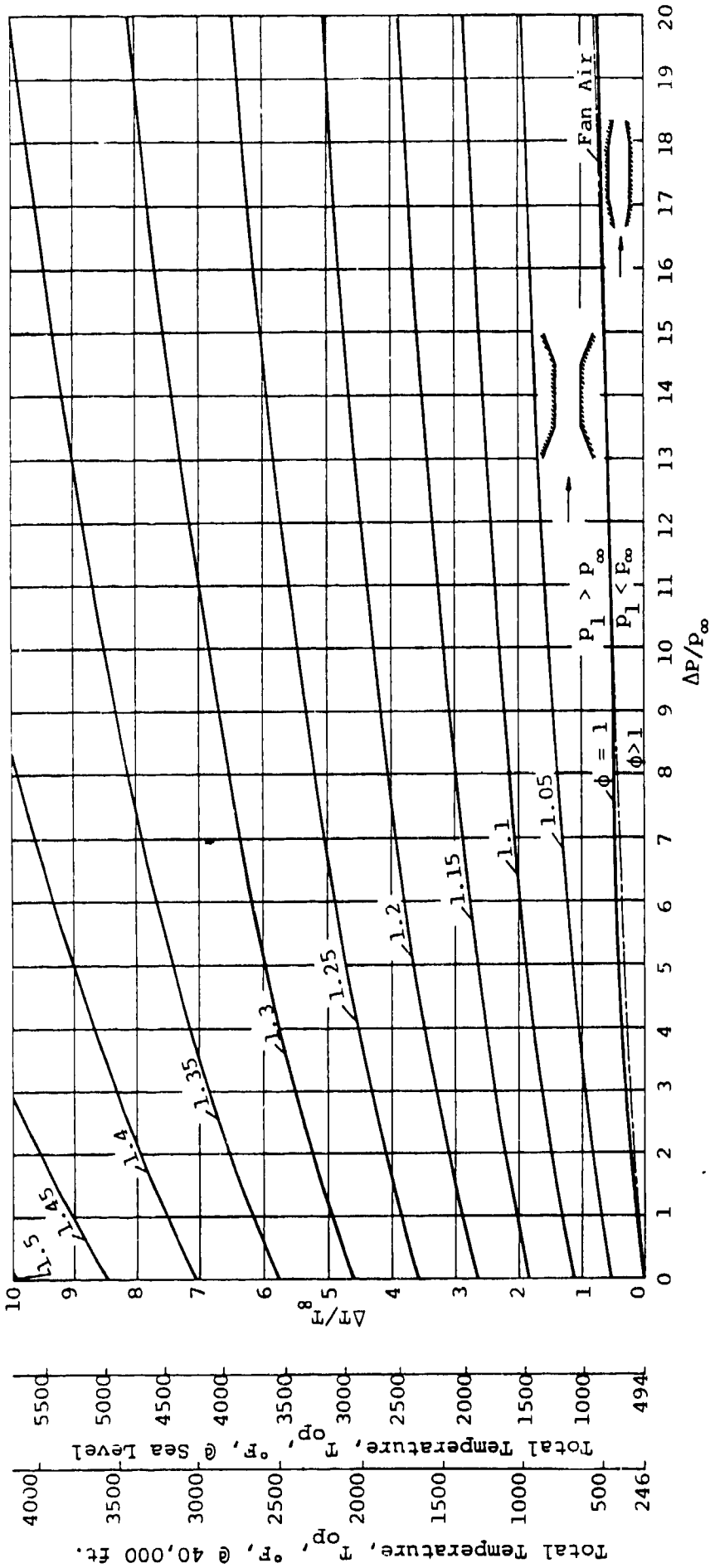
Freestream Mach Number: $M_\infty = 2$; Ejector $\alpha_\infty = 20$, Maximum $\phi$ of First Solution (Subsonic Mixing)

Figure 14. Ideal Ejector Performance Map
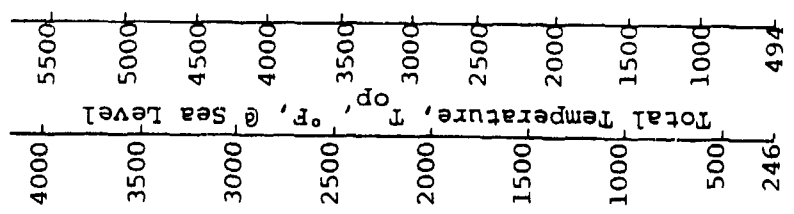
Figure 15. Ideal Ejector Performance Map
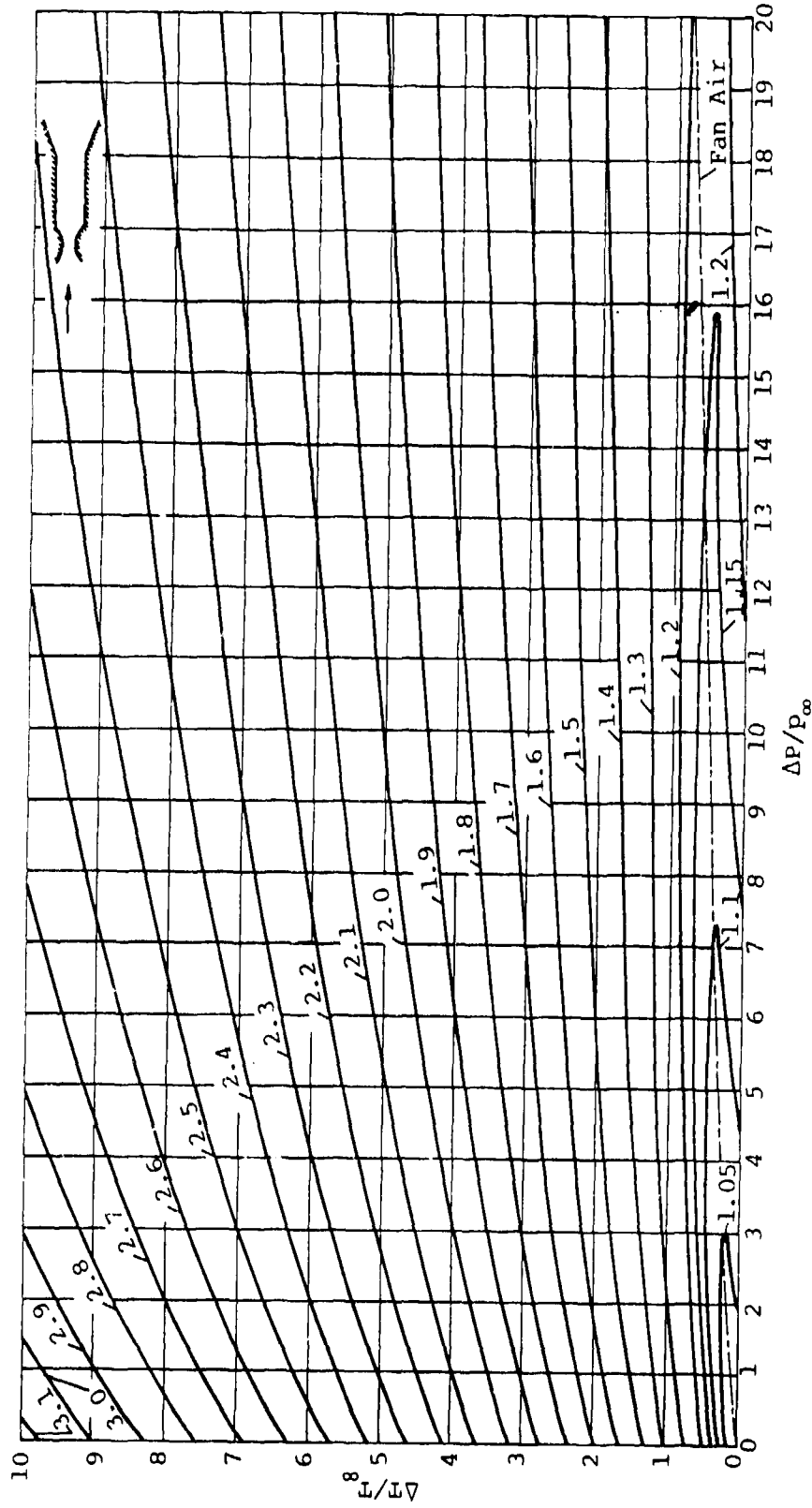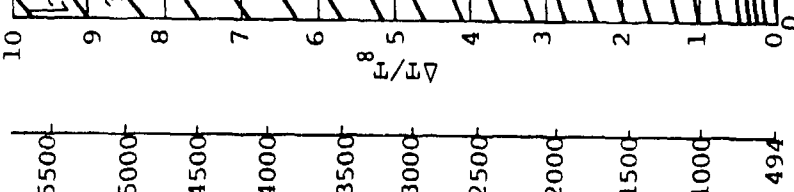
Freestream Mach Number: $M_\infty = 2$; Ejector: $\alpha_\infty = 20$, $\phi$ of Second Solution with Subsonic Mixing, $\Delta S = 0$.

313

## Influence of Losses on Ejector Performance

The actual performance of an ejector will obviously be degraded in comparison to that calculated under the assumption of ideal flow. This degradation of performance may be attributed to skin friction, blockage, incomplete mixing and where supersonic flow is involved, to wave losses. The actual realistic performance of ejectors can only be determined by precise evaluation of the various loss factors or by experiment. Exaggerated concepts of the amount of degradation due to the losses can result from overly pessimistic estimates of some loss factors or from a failure to properly optimize the ejector geometry in view of the losses.

Since thrust augmenting ejectors operate with an overall pressure ratio of 1 (ingestion and discharge are at ambient pressure), the processes occurring within the ejector generally require compression and expansion. Constant pressure throughout the cycle always results in very poor performance. Those operational and injected gas characteristics which can result in very high ideal performance virtually always require a high degree of compression (adverse pressure gradients or shock waves) at the inlet or outlet, or both.

Obviously, an ejector at rest with respect to the undisturbed medium must have an accelerating (expansion) inlet. Thus, as is well known, high performance requires high compression (diffusion) at the outlet.

Ejectors translating at high speed (subsonic or supersonic) may have either expansion or compression inlets at their optimal performance configuration, but high performance will generally require a compression process as a part of the cycle.

It is those compressive elements of the ejector which may significantly alter the ideal flow pattern (flow separation for example) and which must be carefully designed to avoid excessive losses if high performance is to be achieved. The following discussion is intended to illustrate the influence of those major losses on ejector design and performance.

### Subsonic Compression

In a conventional ejector configuration, the outlet generally consists of a subsonic diffuser. This is particularly true for ejectors designed under the first solution for operation at low subsonic speeds, with low stagnation pressure and temperature primary fluid (Figure 7 and the lower part of 10 for example).

314

At high subsonic speeds, subsonic compression inlets dominate the configurations which achieve optimal performance, as illustrated on Figures 10 and 12. This inlet configuration is somewhat similar to those utilized for subsonic jet engine inlets, but the details of these designs remain to be investigated.

The jet-diffuser ejector was created to overcome the subsonic compression problem involved in the conventional ejector outlet. However, other major obstacles to high performance include the primary nozzle attitude and mixing, which contribute to variations of the flow pattern. In addition, skin friction and inlet blockage can contribute to high losses. Methods utilized to evaluate and optimize these factors are described below.

### Jet-Diffuser Ejector - Designed Under the First Solution

To illustrate the advantage achievable by optimal ejector design, the analysis described in Reference 13 was used to evaluate the performance and to determine the optimal geometry of the stationary jet-diffuser ejector to be integrated into the E205 (as shown on Figure 2). The influence of geometric diffuser area ratio, nozzle pressure ratio and the loss factors upon the thrust augmentation of a jet-diffuser ejector with an appropriately designed inlet are described on References 9 - 11 and illustrated on Figures 16 and 17.

Nozzle thrust efficiency ($\eta_N$) had been evaluated experimentally at a low pressure ratio (NPR = 1.24) as reported in Reference 10. At this low pressure ratio, the nozzle thrust efficiency was determined to be 0.96, and it is estimated that at high pressure ratios, this factor will exceed 0.99 as a result of the Reynolds Number effect. The inlet drag coefficient ($C_{di}$) was determined by experiment and theoretical correlation to be 0.013 for a two-dimensional ejector. The increase of $C_{di}$ due to skin friction at the ends of the ejector is a function of the throat aspect ratio of the ejector and is taken into consideration in the performance calculations used to derive Figures 16 and 17. The effect of skin friction on the diffuser jet is evaluated with the aid of conventional boundary layer theory as described in Reference 13. To include viscous effects, the influence of manufacturing and flow non-uniformities, two and three-dimensional effects and finite longitudinal dimensions, a factor ($\eta_{dj}$) called jet-diffuser efficiency was used to represent the ratio of the effective to the geometric area ratio of the solid portion of the diffuser as described in Reference 13.

315

Figure 16 illustrates the existence of an optimal diffuser area ratio
for any given nozzle pressure ratio. The magnitude of this optimal diffuser
area ratio and the corresponding thrust augmentation achievable with this
optimal design depend upon the other geometric ejector factors and the loss
factors. Thus, as shown on Figure 16, an increase of the diffuser area ratio
can compensate somewhat for the performance degradation due to increased losses.
Conversely, diffuser area ratios in excess of the optimal values can result in
large performance losses.  The lowest dashed curve on Figure 16 is drawn to
indicate the correlation between analysis and experiment for the test conditions
utilized in the experiments.  The measured thrust augmentation of 1.95 achieved
during the testing is very close to the theoretical curve resulting from the
use of the factors derived for the ejector having a diffuser area ratio of 2.78.

As shown on Figure 16, testing of this same ejector at high pressure ratios
(greater than about 2.0 to 2.5) would result in operation beyond the optimal
point with drastic degradation of performance.  For example, at a nozzle
pressure ratio of 3.0, the thrust augmentation would be reduced from its
optimal value of 1.95 to about 1.32, if the diffuser area ratio remained
at 2.78.  To provide optimal performance at a nozzle pressure ratio of 3.0,
the solid diffuser area ratio must be reduced to about 2.3 if the losses at
this pressure ratio are as assumed. Experiments were conducted with the diffuser
cut down to an area ratio of 2.3 and, as illustrated, the measured thrust
augmentation was 1.93 at the nozzle pressure ratio of 1.24.  This experimental
point lies above the theoretical curve indicating an improvement of the
jet-diffuser efficiency $(\eta_{dj})$, due to the decreased diffuser area ratio.

Figure 17 illustrates the variation of the thrust augmentation of the
jet diffuser ejector as a function of nozzle pressure ratio for an ejector
with a fixed diffuser area ratio of 2.3.  As illustrated, a change of the
jet-diffuser efficiency from 0.7 to 0.8 results in a reduction of the cut-
off nozzle pressure ratio from 2.95 to 2.55.  Thus if the jet-diffuser
efficiency is increased as a result of the reduction of the area ratio,
testing at a nozzle pressure ratio of 3.0 would result in very poor performance,
since it would exceed the cut-off point shown on Figure 17.  In that case,
it would be desirable to reduce the nozzle pressure ratio to about 2.5 or to
further reduce the diffuser area ratio to about 2.0, or increase the stagnation
temperature of the primary jet.

A carefully planned experiment for correlation with this theory would be
of great value in the design of thrust augmenting ejectors.

316
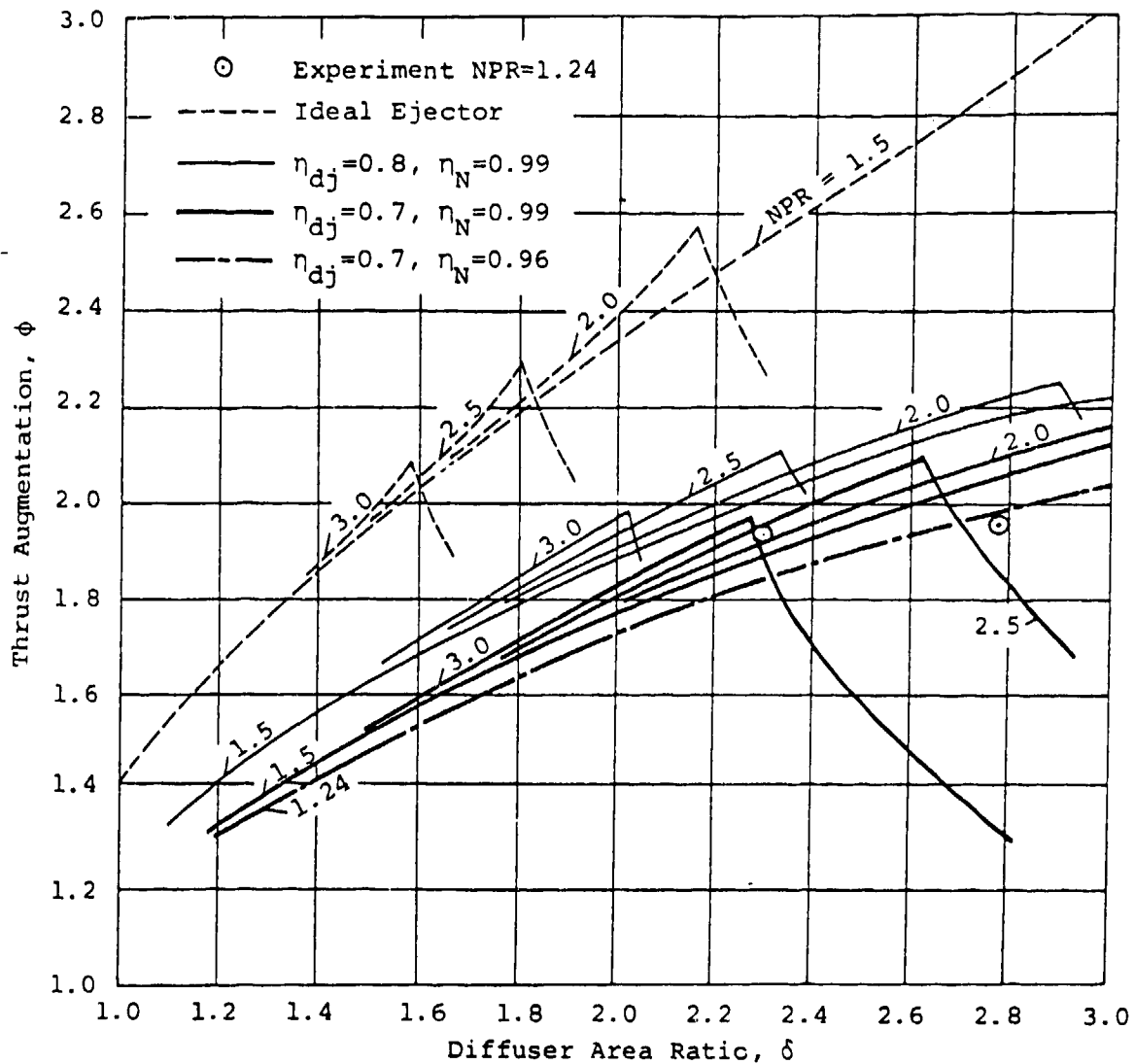
Air Source: Fan Air (isentropically compressed, @ sea level)
Ejector Throat: 10.16 cm wide, 38.1 cm long (4 in wide, 15 in. long)
Inlet Area Ratio: 32.14 (=throat area/primary nozzle area)
Diffuser Jet/Primary Jet Mass Flow Ratio: 0.7

Figure 16.   Stationary Jet-Diffuser Ejector Performance, as a
             Function of Diffuser Area Ratio

317

Figure 17. Stationary Jet-Diffuser Ejector Performance, as a Function of Nozzle Pressure Ratio

318

## Inlet Wave Losses

Ejectors translating at supersonic speeds generally have an expansion outlet (either subsonic to supersonic or supersonic to supersonic, as shown on Figures 13 to 15) or a very weak supersonic compression outlet at low supersonic flight speeds. Therefore compression losses at the outlet are not a concern to the ejector design. The ejector may have a subsonic or a supersonic Mach No. ($M_1$) at the start of mixing. With supersonic mixing ($M_1$ greater than 1.0), the inlet for optimal designs is usually decelerating, and requires some weak compression of the supersonic flow. Since high compression can be avoided in this case, the performance degradation compared to the ideal should be small and can be evaluated. With subsonic mixing ($M_1$ less than 1), ejectors generally perform better than with supersonic mixing, but the inlet wave loss is also significant.

Figure 18 illustrates the change in the optimal ejector configuration and the performance degradation of supersonic ejectors, resulting from inlet losses. The losses were evaluated with the use of the standard engine inlet compression loss specification as required by MIL-E-5007D, in an ejector translating at a Mach number of 2. As indicated, the inlet compression loss results in a performance reduction and a configuration change. The optimal geometry is modified by the losses for designs under the first solution. Consideration of performance in the light of known losses requires a smaller value of $M_1$ than in the ideal case, and if properly optimized, the performance degradation can be small. Under the second solution, with subsonic $M_1$, the design configuration change is small but the thrust augmentation is degraded from a value of 3.13 to 2.56 due to the inlet losses.

## Outlet Wave Losses

The performance achievable by ejectors designed under the second solution with subsonic mixing has been shown to be considerably better than that achieved by designs under the other optimal conditions over the entire range of flight conditions encountered by modern aircraft. This second solution with subsonic mixing design criterion is particularly important for flight from the mid-subsonic to transonic speed range, since other optimal conditions generally can not achieve the desired performance, with efficient gas generators. The actual achievement of the flows required to obtain this high performance involves the design of outlets capable of accepting supersonic flows at some arbitrary pressure and returning them to ambient pressure with minimal or acceptable wave losses.

319
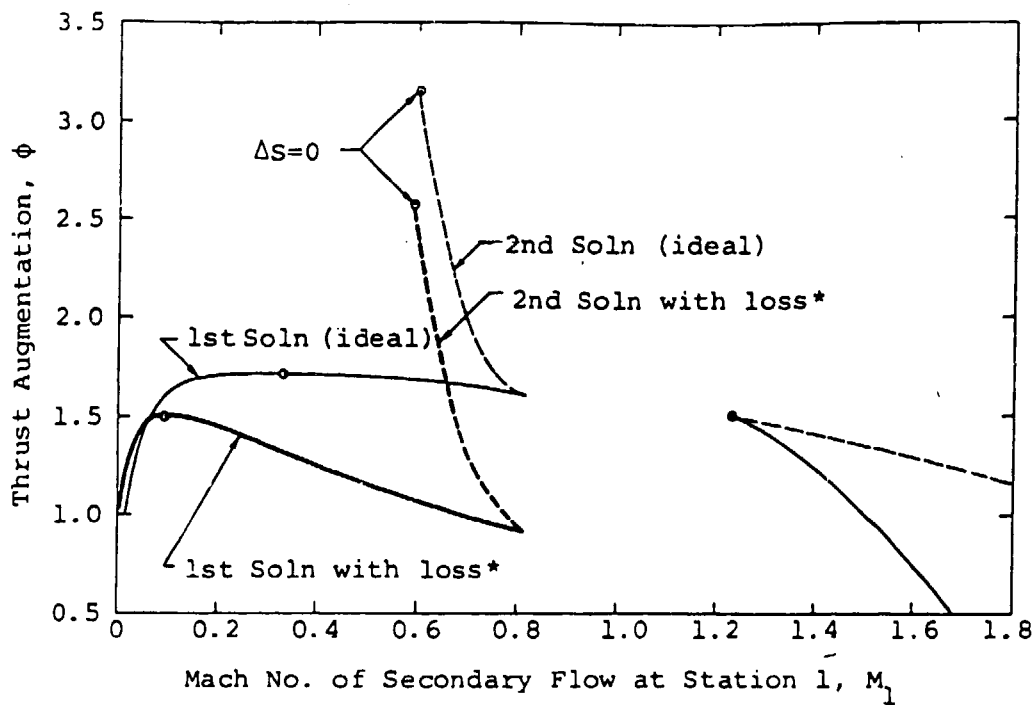
Condition: (Ram-jet) $M_\infty = 2$; $\Delta P/p_\infty = 0$; $\Delta T/T_\infty = 10$; $\alpha_\infty = 20$

*loss: MIL-E-5007D Inlet Recovery Factor

for $1 < M_\infty < 5$ is,

$$\eta_i = \frac{P_{o1}}{P_{o\infty}} = 1 - 0.075 \, (M_\infty - 1)^{1.35}$$

Figure 18. Supersonic Ejector with Inlet Compression Loss

In an attempt to demonstrate the feasibility of achieving the flow and performance attributable to second solution-subsonic mixing ejectors, FDRC with support from AFOSR and AFFDL, has initiated studies of the outlet design required by such ejectors. The study included an investigation of the starting problem for such supersonic flows and the losses and realistic performance of fixed geometry outlets capable of "swallowing" the starting shock wave and of avoiding excessive outlet losses. As a continuing part of this study, the use of simple, adjustable outlets have also been investigated.

Fixed Geometry Outlets

The starting problem can be avoided if the ideal isentropic outlet has a minimum area larger than that required for accomodating the mass flow when a normal shock wave is present in the mixing section, similar to the supersonic wind tunnel design discussed in Reference 16. In other words, the starting problem disappears if the mixed flow has a static pressure high enough to permit isentropic return to ambient pressure without excessive supersonic compression. Investigation to date showed that avoiding the starting problem is possible only at high flight speed (especially supersonic) and at high primary stagnation pressures and temperatures. These characteristics represent some realistic, in flight conditions and are encouraging from the point of view of the feasibility of designing operational systems which are quite simple. However, at supersonic speeds, the inlet compression loss becomes dominant, as discussed earlier. It has been observed that the utilization of an exit area large enough to accomodate the mass flow when a normal shock wave exists in the mixing section, can result in one of four possible outlet flows, described schematically on Figure 19.

When the steady state flow after mixing is supersonic and has a sufficiently high pressure to be returned isentropically to ambient pressure with very little or no supersonic compression, a shockless outlet can be utilized. In this case no starting problem exists. The outlet design for these conditions can appear as illustrated on Figures 19a and 19b.

In Figure 19a, the isentropic outlet design for starting as well as cruise operation is a divergent nozzle, which represents the case in which the supersonic flow at the end of mixing has a pressure in excess of ambient and must be expanded to return to ambient pressure.

321

Figure 19b illustrates the case in which the supersonic flow after mixing has a pressure less than ambient and isentropic compression to ambient pressure results in a smaller, but still supersonic Mach number, and with a minimum area larger than that required for accomodation of the subsonic mass flow behind a normal shock wave in the mixing section.

When the flow after mixing is supersonic and has properties such that its isentropic return to ambient pressure requires high compression, and results in low supersonic or subsonic exit velocities, it is impossible to avoid outlet shock waves if the starting problem is considered. The outlet flow pattern and schematic shapes for these situations are represented on Figures 19c and 19d.

Figure 19c illustrates the situation in which the ideal steady state operating outlet has a minimum area (either a "sonic throat" or the outlet opening) which is smaller than the minimum area required for starting (swallowing the starting shock wave). If the properties of the flow after mixing are such that a normal shock wave at the minimum starting area will result in exit pressure greater than ambient, and if the ejector outlet has an opening corresponding to the minimum starting area, the final compression of the flow to return to ambient pressure will be accomplished by a system of oblique waves. This situation appears to dominate ejectors which are translating at low subsonic to transonic speeds.

Figure 19d illustrates a situation in which the ideal steady state operating outlet has a minimum area which is smaller than that required for starting and in which a normal shock wave at the minimum starting area will result in an exit pressure which is smaller than ambient. This situation can result in either a stronger shock wave to satisfy the exit pressure requirement or, more desirably, a weak normal shock wave at the minimum area followed by a subsonic diffuser. The application for this type of outlet appears to be in the low subsonic flight speed regime, or low primary stagnation pressure and temperature gas at higher subsonic speeds.

The performance of ejectors suitable for laboratory study, using cold air supplies and translating at a Mach number of 0.65 and utilizing fixed geometry outlets is shown as a function of the nozzle pressure ratio on Figure 20. As indicated this type of outlet design for a second solution ejector with subsonic mixing is capable of performance which is considerably better than that obtained from ideal optimal first solution or second solution with supersonic mixing designs.

Note that $\alpha_*$ is 25 for the considerations presented on Figure 20. This means that the mixing duct area is fixed at 25 times the throat area (for supercritical pressure ratios) or 25 times the jet area when fully expanded to ambient pressure (for subcritical pressure ratios). Also, the entrainment ratio (induced mass flow rate/primary mass flow rate) for the conditions shown on Figure 20, decrease rapidly from about 21 at $\Delta P/p_\infty = 0.2$ to about 1 at $\Delta P/p_\infty = 20$ under the second solution at the limiting design point, $\Delta S = 0$.
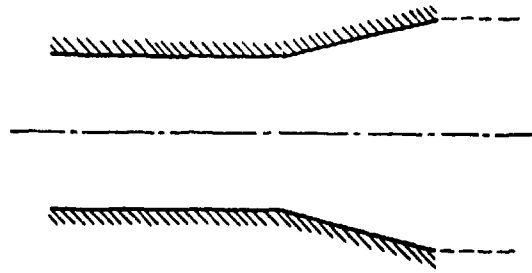
a) Shock-Free Supersonic Nozzle
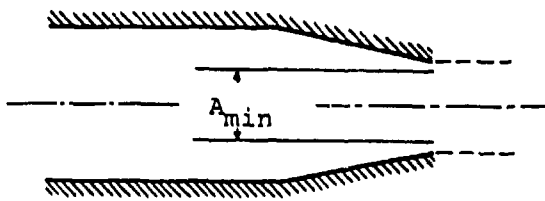
b) Shock-Free Supersonic Diffuser
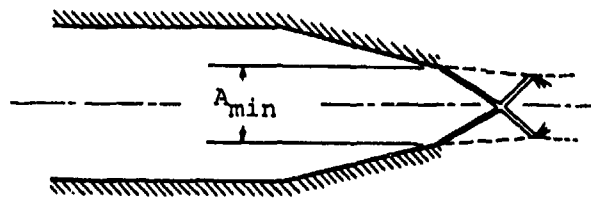
c) Supersonic Diffuser Followed by
Systems of Oblique Waves
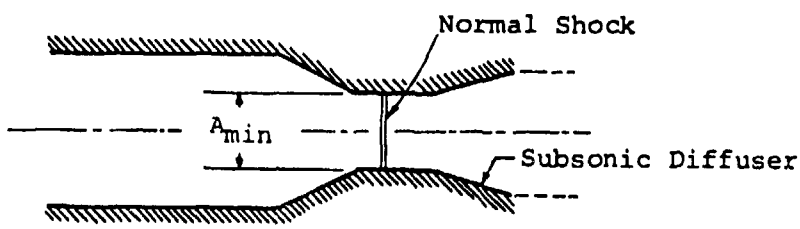
d) Supersonic Diffuser, Normal Shock Wave
Followed by a Subsonic Diffuser

Figure 19. Fixed Geometry Outlets For Thrusting Ejectors
Designed Under Second Solution

324
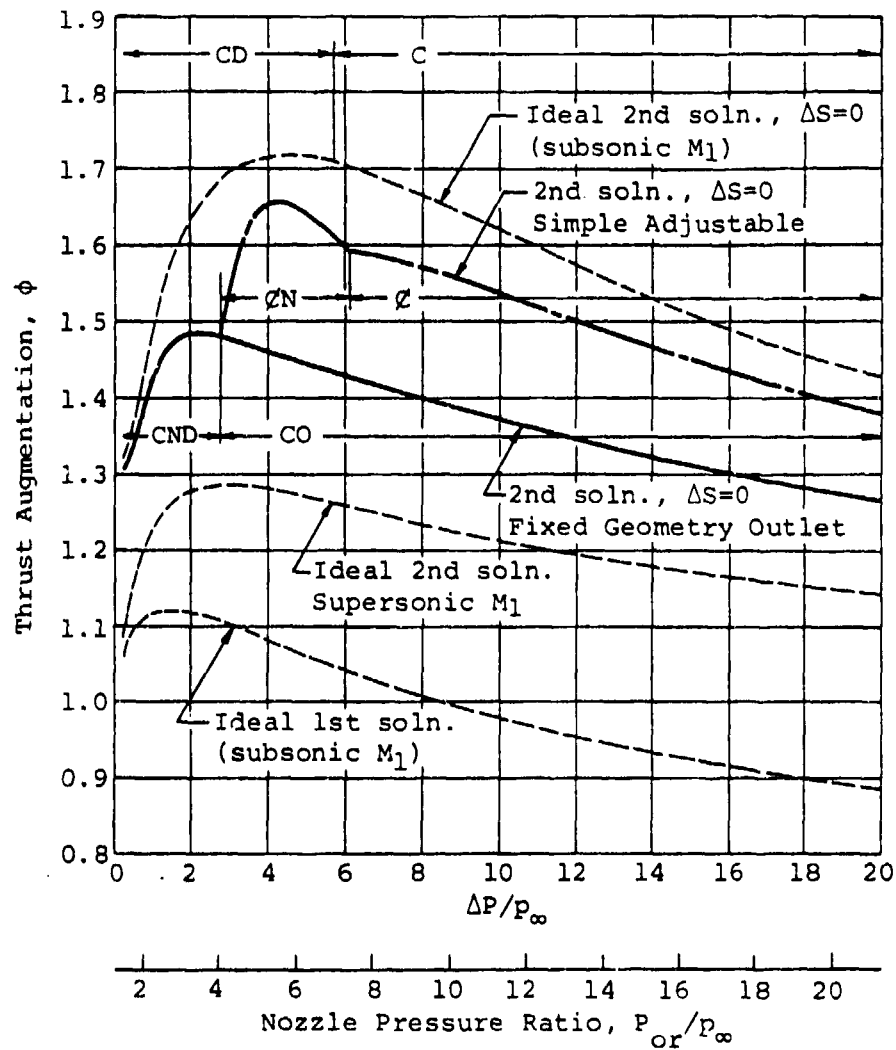
Configuration Notes:

C = Convergent supersonic diffuser (isentropic)

$\mathcal{C}$ = Convergent supersonic diffuser with flat wall and two oblique shock waves

D = Divergent subsonic diffuser (isentropic)

N = Normal shock wave, either at minimum starting section or at exit

O = Oblique wave systems required at the exit for final compression

Figure 20. Influence of Outlet Wave Losses on Ejector Performance
$M_\infty = 0.65$; $\alpha_* = 25$; $T_{op} = T_\infty$

325

## Simple Adjustable Outlet

Those conditions which require outlet designs in which the ideal minimum area cannot accomodate the mass flow under the starting condition are of two types illustrated on Figures 19c and 19d. Figure 19d, represents a configuration which requires a subsonic diffuser downstream of the minimum starting area. This would require a complex mechanism, similar to an adjustable second throat utilized in supersonic wind tunnels, for achieving an efficient outlet capable of swallowing the starting shock wave and providing an optimal outlet during cruise operation. Fixed geometry outlets corresponding to the starting condition are probably the most practical design for these conditions.

Figure 19c represents a more universal wave pattern which can provide acceptable but still quite degraded performance compared to the isentropic case as illustrated on Figure 20. By designing a simple adjustable outlet, the cruise performance of the ejector will be almost equivalent to that of the ejector with an isentropic outlet.

The simple adjustable outlet consists of a flat surface (in a two-dimensional ejector) on either side of the outlet, capable of very small rotation only, as illustrated on Figure 21. In the starting configuration these surfaces are adjusted to provide the required minimum starting area (Figure 19c or 21a). The surfaces can then be rotated to reduce the outlet area. The reduction of outlet area results in a reduction of the Mach number and an increase of the static pressure at the exit section. Obviously, the Mach number inside the exit section is still supersonic. When the increase of the static pressure is sufficient to compress the mixed flow to ambient pressure, the external starting oblique wave system (Figure 21a) will be eliminated during the outlet area adjustment, and the wave pattern associated with the cruise configuration will appear as shown on Figure 21c, which has a supersonic exit flow. When the increase of static pressure is not sufficient to return the mixed flow to ambient pressure, the external starting oblique shock wave system will require larger wave angles, due to the decreasing Mach number and finally form a normal shock wave at the exit section (Figure 21b), during the outlet area adjustment. Since the final compression of the mixed flow is accomplished by a normal shock wave, the discharged flow is subsonic.

The performance improvement resulting from the adjustment of the outlet is shown on Figure 20. This analysis for the simple adjustable outlet utilized the concept of two internal oblique shock waves as shown on Figure 21, for realistic evaluation of the wave loss. These wave losses have been shown to have very little effect upon the ejector performance both during starting or with fixed geometry configurations (Figure 19) and therefore the internal waves (if any) in the fixed geometry configurations have been neglected.
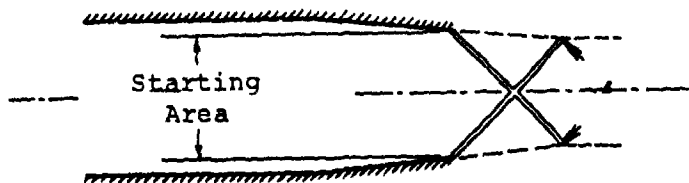
a) Starting Configuration
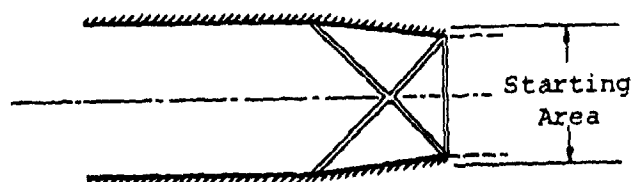


b) Cruise Configuration with a
Normal Shock at the Exit
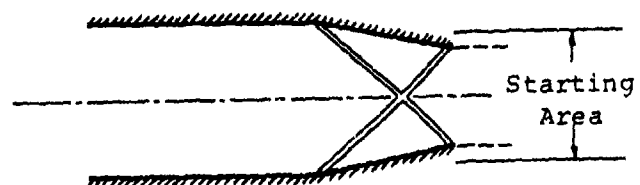


c) Cruise Configuration without a
Normal Shock at the Exit

Figure 21.  Simple Adjustable Outlets

328

## Conclusions

The process of mixing of compressible gases represents one of the most outstanding examples of the erroneous conclusions which can be drawn as a result of the use of incompressible flow theory where the fluids are actually compressible. Limitations implicit in the incompressible flow theory result in a failure to display the reality of a "second solution" which represents configurations having the best ideal performance over the entire ranges of operational and injected gas characteristics. Incompressible flow theory also fails to describe limitations due to thermal effects and choking.

The analysis of ejector flows based upon the use of compressible flow theory provides insights into the influence of motion in the thrust direction and thermal effects due to the injection of hot primary gas, which are of great value in the design of thrust augmenting ejectors operating in and with compressible fluids.

As shown by the compressible flow analysis, a properly designed ejector can derive beneficial performance from the utilization of the thermal energy content of its primary, injected fluid. Further, the performance of thrust augmenting ejectors need not deteriorate as rapidly due to motion in the thrust direction as is indicated by incompressible flow theory, provided the variation of stagnation characteristics of the injected and ingested gas are properly treated with changes of velocity.

The choice of ejector geometry required to achieve optimal performance is also essential to the design of high performance ejectors. The variation of optimal geometry with loss factors, in addition to the operational and injected gas characteristics must be considered in the final selection of ejector geometry.

Properly designed thrust augmenting ejectors can achieve high performance over the entire range of flight conditions, and can achieve large savings of energy (fuel consumption) in most aircraft applications.

# References

1.  Keenan, J. H., Neumann, E. P., and Lustwerk, F., "An Investigation of Ejector Design by Analysis and Experiment," ASME Trans. (J. of Applied Mechanics) Vol. 17, No. 3, September 1950, pp 299-309

2.  Fabri, J. and Siestrunck, R., "Supersonic Air Ejectors," Advances in Applied Mechanics, Volume No. 5, Academic Press, New York, 1958, pp 1-34

3.  Vaughan, J. C. III, "Performance of Jet Ejectors," ASD/XR 72-5 Aeronautical Systems Division, WPAFB, Ohio, February 1972

4.  Quinn, B., "Recent Developments in Large Area Ratio Thrust Augmentors," Aerospace Research Laboratories, WPAFB, Ohio, AIAA Paper No. 72-1174, AIAA/SAE 8th Joint Propulsion Specialist Conference, Nov 29 - Dec 1, 1972

5.  Nagaraja, K. S. Hammond, D. L. and Graetch, J.E., "One-dimensional Compressible Ejector Flows," AIAA Paper No. 73-1184, AIAA/SAE 9th Propulsion Conference, November 5-7, 1973

6.  Bevilaqua, P. M., "Evaluation of Hypermixing for Thrust Augmenting Ejectors," Journal of Aircraft, Vol. 11, No. 6, June 1974

7.  Alperin, M., Wu, J. J. and Smith, C. H., "The Alperin Jet-Diffuser Ejector (AJDE) Development, Testing and Performance Verification Report," Flight Dynamics Research Corporation, Naval Weapons Center NWC TP 5853, February 1976

8.  Alperin, M. and Wu, J. J., "End Wall and Corner Flow Improvements of the Rectangular Alperin Jet-Diffuser Ejector," Flight Dynamics Research Corp., Naval Air Development Center, NADC-77050-30, May 1978

9.  Alperin, M. and Wu, J. J., "Recent Development of a Jet-Diffuser Ejector," Flight Dynamics Research Corporation, AIAA-80-0231, AIAA 18th Aerospace Sciences Meeting, January 14-16, 1980

10. Alperin, M. and Wu, J. J., "Jet-Diffuser Ejector-Attached Nozzle Design," Flight Dynamics Research Corp., NASA, Ames Research Center and Naval Air Development Center, NASA CR 152361, May 1980

11. Alperin, M. and Wu, J. J., "A Jet-Diffuser Ejector for a V/STOL Fighter," Flight Dynamics Research Corp., NASA, Ames Research Center and Naval Air Development Center, NASA CR 166161, February 1981

12. Garland, D. B., "Phase I Wind Tunnel Tests of the J-97 Powered, External Augmentor V/STOL Model," The De Havilland Aircraft of Canada, Limited, NASA CR 152255, July 1980

13. Alperin, M. and Wu, J. J., "High Speed Ejectors," Flight Dynamics Research Corp., USAF Flight Dynamics Lab., AFFDL-TR-79-3048, May 1979

14. Alperin, M. and Wu, J. J., "Underwater Ejector Propulsion, Theory and Applications," Flight Dynamics Research Corp., Office of Naval Research, FDRC 0812-11-76, October 1976

15. Alperin, M. and Wu, J. J., "Underwater Jet-Diffuser Ejector Propulsion, Real Fluid Effects," Flight Dynamics Research Corp., Office of Naval Research, FDRC 0294-8-78, August 1978

16. Liepmann, H.W. and Roshko, A., "Elements of Gasdynamics," John Wiley and Sons, Inc., N.Y., 1957, pp 131-136
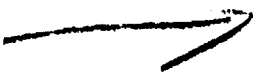
330

5

# AN OVERVIEW OF SUPERSONIC EJECTOR PERFORMANCE ANALYSES

A. L. (Tad) Addy
Professor and Associate Head
Department of Mechanical and Industrial Engineering
University of Illinois at Urbana-Champaign
1206 W. Green Street
Urbana, IL 61801

Telephone: (217) 333-1126

PRESENTATION SUMMARY

## AN OVERVIEW OF "SUPERSONIC" EJECTOR
## PERFORMANCE ANALYSES

Three general approaches are available for the analysis of "supersonic" ejector performance. In order of complexity, they are: (1) one-dimensional flow models, (2) combined one- and two-dimensional interactive flow models with a superimposed viscous mixing component, and (3) application of finite-difference approximations of the Navier-Stokes equations to the overall flowfield within the ejector. The constant-pressure and constant-area one-dimensional flow models are well developed and understood. The constant-area ejector model has the advantage in that this simplified model retains most of the essential features which are observed in ejector operation. The constant-pressure model is restricted in the features which can be included and in the range of ejector operating characteristics which can be predicted. The combined one- and two-dimensional interactive flow models have been developed during the past twenty years. These flow models provide a means for predicting overall supersonic ejector performance and details of the flowfield in the interaction region for non-constant area mixing ducts. Unfortunately, this approach is, in general, both tedious and computationally time consuming. The finite-difference approach to analyzing supersonic ejector performance is in the developmental stage. This general approach offers many positive incentives; however, there are still considerable difficulties to be overcome.

The objectives of this presentation will be to provide a brief overview of each of the methods for predicting "supersonic" ejector performance, to outline the significant features and advantages/disadvantages of each method, and to suggest possible future directions for consideration.

## NOMENCLATURE

### Symbols

| | |
|---|---|
| $C_p$ | Specific heat at constant pressure |
| $h$ | Specific enthalpy |
| $L$ | Length |
| $M$ | Mach number |
| $Mw$ | Molecular weight |
| $P$ | Pressure |
| $R$ | Gas constant |
| $r_d$ | Diffuser compression coefficient |
| $V$ | Magnitude of velocity |
| $w_a$ | Mass flowrate |
| $W$ | Work, shaft and shear |
| $\gamma$ | Ratio of specific heats |
| $\rho$ | Density |
| $\mu$ | Secondary-to-primary mass flowrate ratio, $w_s/w_p$ |

### Subscripts

| | |
|---|---|
| 0 | Stagnation state or location |
| 1, 2, 3, 4 | System locations |
| ATM | Atmosphere |
| B | Back |
| BO | Break-off conditions |
| M | Mixed |
| MAX | Maximum |
| P | Primary |
| S | Secondary |
| T | Total |
| $T_0$ | Refers to stagnation temperature function |
| X, Y | Upstream and downstream normal shock locations |

334

GENERAL EJECTOR CLASSIFICATIONS:

- "SUBSONIC" EJECTOR

  (1) SMALL COMPRESSION PRESSURE RATIO
  (2) LARGE SECONDARY (INDUCED) MASS FLOWRATE

- "SUPERSONIC" EJECTOR

  (1) LARGE COMPRESSION PRESSURE RATIO
  (2) SMALL SECONDARY (INDUCED) MASS FLOWRATE
  (3) EXHIBITS "CHOKING"/"LIMITING" FLOW
      PHENOMENA

POSSIBLE "SUPERSONIC" EJECTOR ENTRANCE FLOWS:

| PRIMARY (DRIVER) | SECONDARY (INDUCED) |
|---|---|
| SUPERSONIC | SUBSONIC |
| SUPERSONIC | SUPERSONIC |

"SUPERSONIC" EJECTOR FLOW REGIMES (AFTER FABRI) WITH
SUBSONIC/SUPERSONIC FLOWS:

- "MIXED" FLOW REGIME

- "SUPERSONIC" FLOW REGIME

- "SATURATED SUPERSONIC" FLOW REGIME

Mixing tube

$P_{M3}$

$P_B$

Static pressure wall taps

$P_{S0}$
$T_{S0}$

Secondary flow

Primary nozzle

$P_{P0}$
$T_{P0}$

Primary flow

Constant-area mixing section

Secondary
$M_{S1} < 1$

Primary
$M_{P1} > 1$

Uniform mixed flow
$M_{M3} < 1$

①        ②        ③
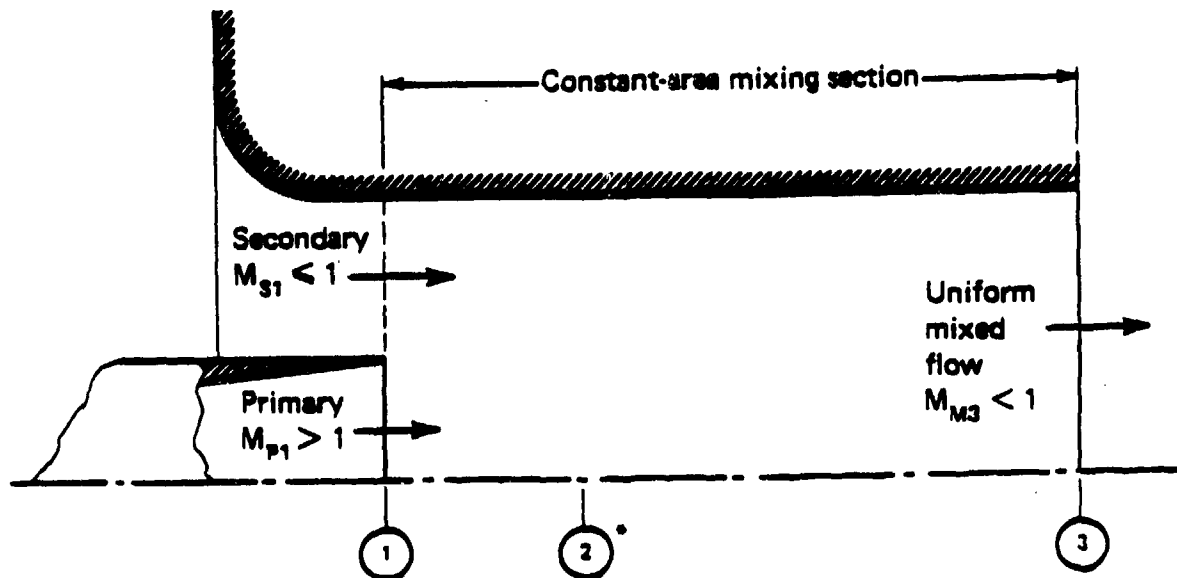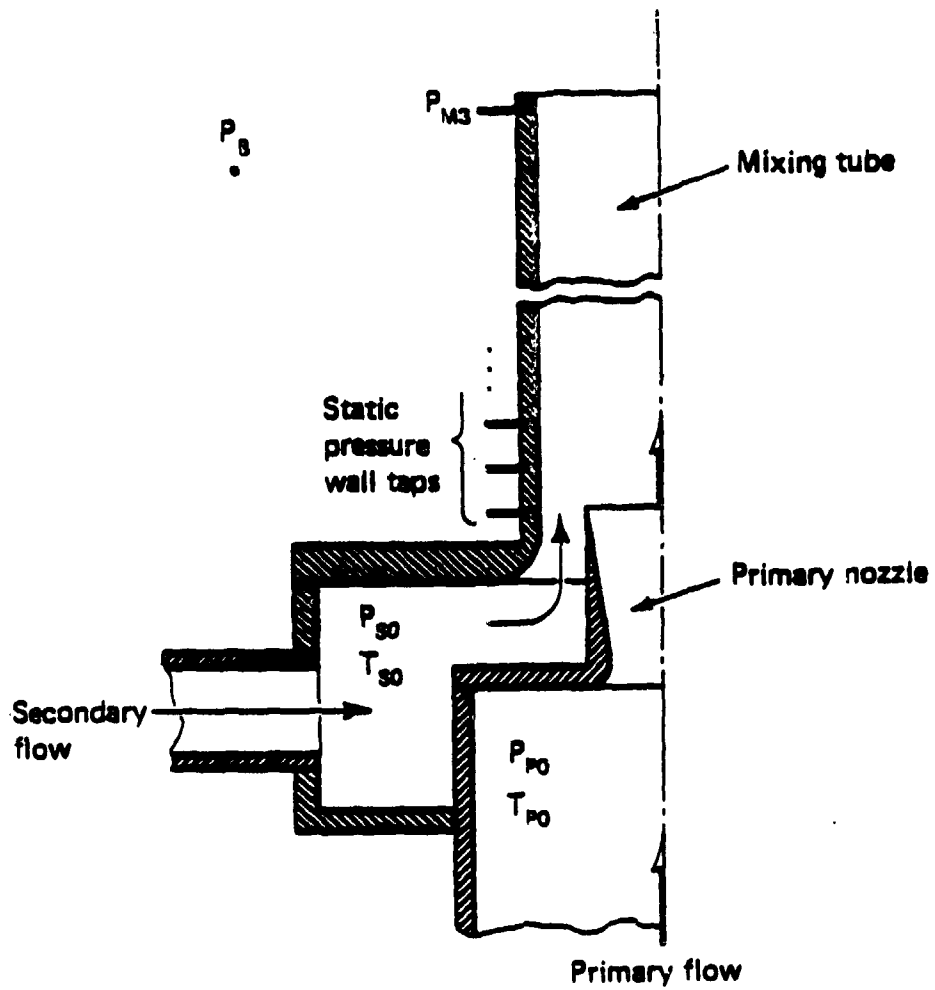
* Exists only for the "supersonic" regime

336

## EJECTOR FLOW REGIMES

"MIXED" FLOW REGIME CHARACTERISTICS:

- SECONDARY (INDUCED) FLOW IS UNCHOKED AND IS DEPENDENT ON THE DOWNSTREAM PRESSURE BOUNDARY CONDITION

- MIXING TUBE WALL PRESSURE DISTRIBUTION IS AFFECTED BY THE DOWNSTREAM PRESSURE BOUNDARY CONDITION

## EJECTOR FLOW REGIMES

"SUPERSONIC" FLOW REGIME CHARACTERISTICS:

- SECONDARY (INDUCED) MASS.FLOWRATE IS "CHOKED" AND IS INDEPENDENT OF THE DOWNSTREAM PRESSURE BOUNDARY CONDITION

- MIXING TUBE WALL PRESSURE DISTRIBUTION DOWN-STREAM OF THE AERODYNAMIC THROAT IS AFFECTED BY THE DOWNSTREAM PRESSURE BOUNDARY CONDITION

## EJECTOR FLOW REGIMES

"SATURATED-SUPERSONIC" FLOW REGIME CHARACTERISTICS:

- SECONDARY (INDUCED) FLOW IS "CHOKED" AT THE EJECTOR ENTRANCE AND IS INDEPENDENT OF THE DOWNSTREAM PRESSURE BOUNDARY CONDITION

- MIXING TUBE WALL PRESSURE DISTRIBUTION IS AFFECTED BY THE DOWNSTREAM PRESSURE BOUNDARY CONDITION

337

Planes of Constant $\bar{P}_{1S}$

Planes $\bar{P}_{OS}$ = constant

$\bar{P}_a$ - independent

Break-off Curve

$\bar{P}_a$ - dependent

338
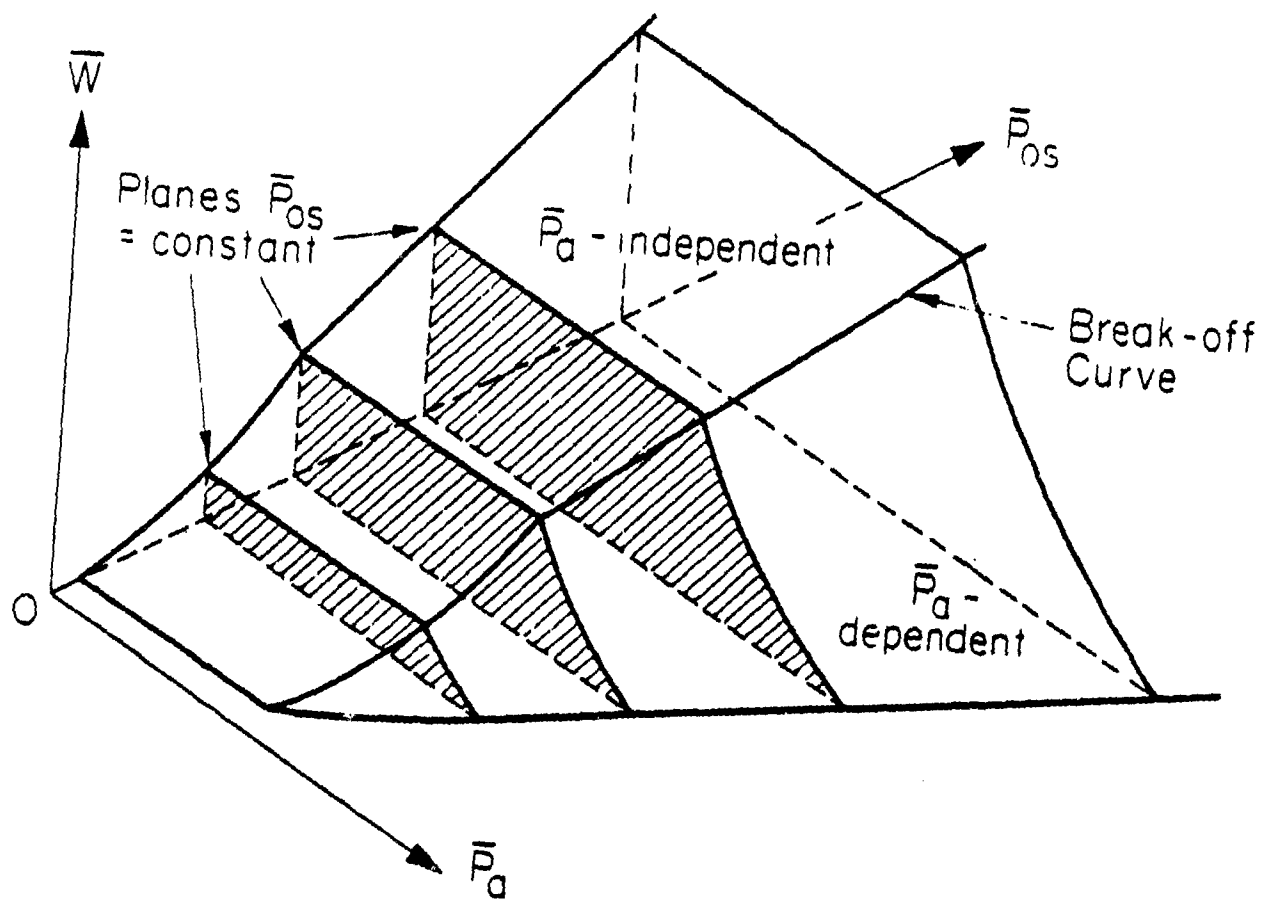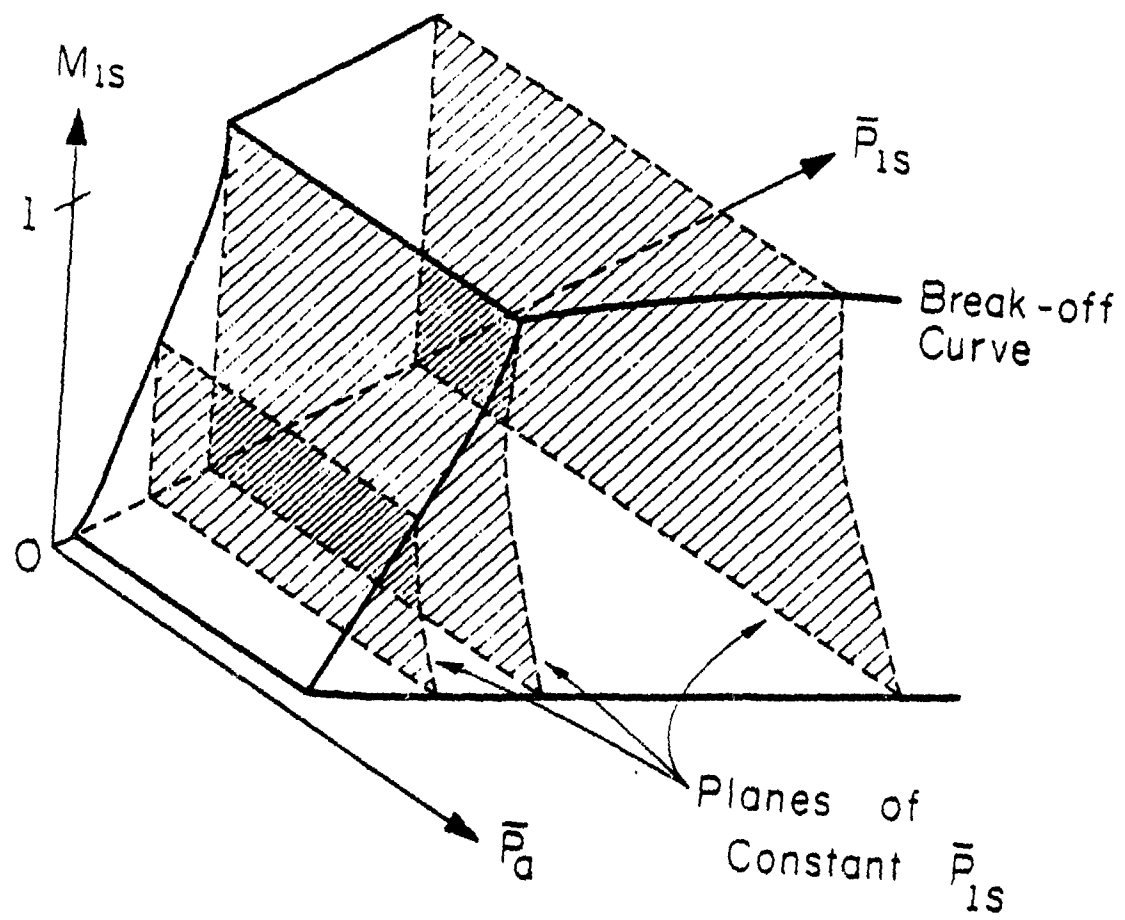
EJECTOR ANALYSES:

- QUASI-ONE-DIMENSIONAL EJECTOR FLOW MODELS

  - CONSTANT-PRESSURE EJECTOR FLOW MODEL
  - CONSTANT-AREA EJECTOR FLOW MODEL

- TWO-DIMENSIONAL EJECTOR FLOW MODELS

  - INVISCID INTERACTION COMPONENT
  - MIXING COMPONENT
  - RECOMPRESSION COMPONENT

- FINITE-DIFFERENCE EJECTOR FLOW MODELS


ONE-DIMENSIONAL ANALYSIS
OF
CONSTANT-PRESSURE EJECTOR SYSTEMS


CONSTANT-PRESSURE EJECTOR FLOW MODEL:

- SUPERSONIC PRIMARY NOZZLE

- VARIABLE-AREA, CONSTANT-PRESSURE MIXING SECTION

- DIFFUSER SECTION
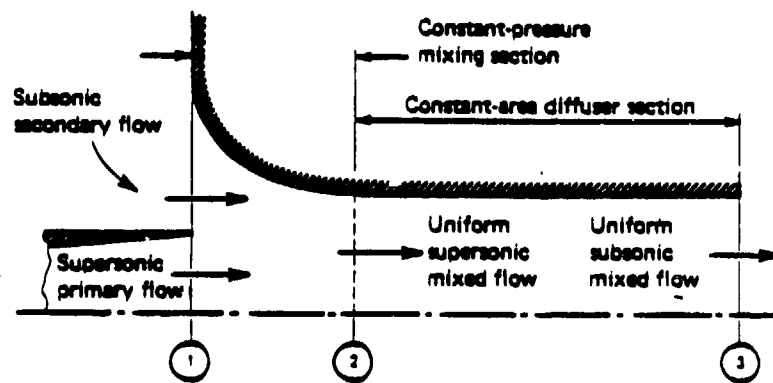
Axisymmetric constant-pressure ejector configuration
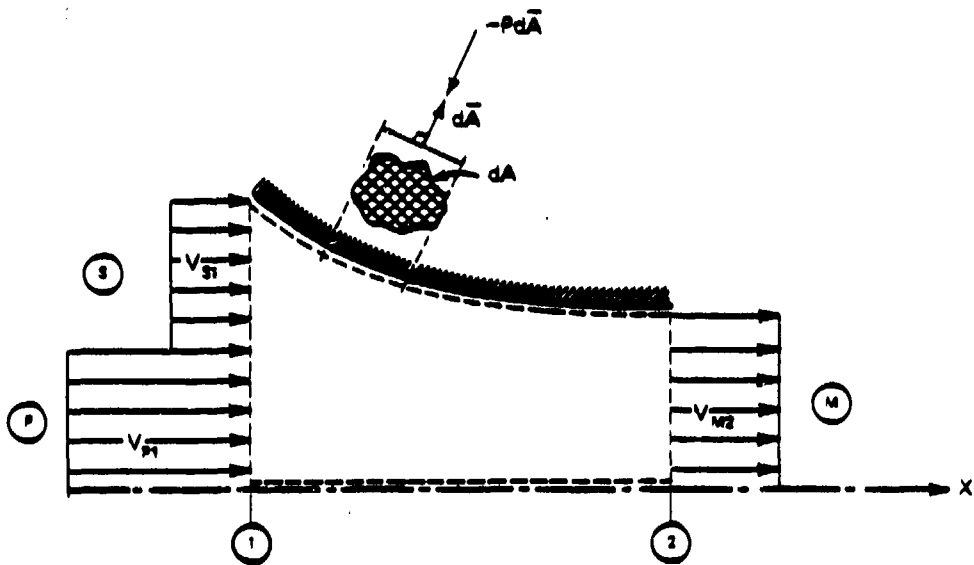
$P$, $\rho$, A, V, T, M, etc. are defined for each stream at sections 1 and 3.

Constant-pressure mixing section control volume

L/D > Minimum required value from Fig. 2.1-3.
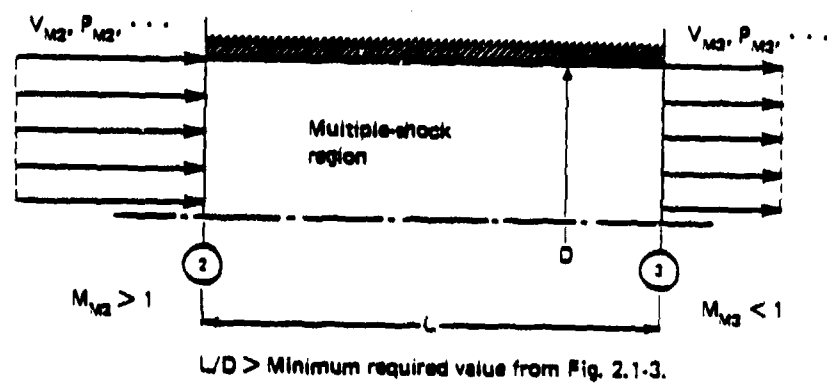
Constant-area supersonic diffuser notation

Empirical correlation for length-to-diameter ratio of constant-area supersonic diffusers

343
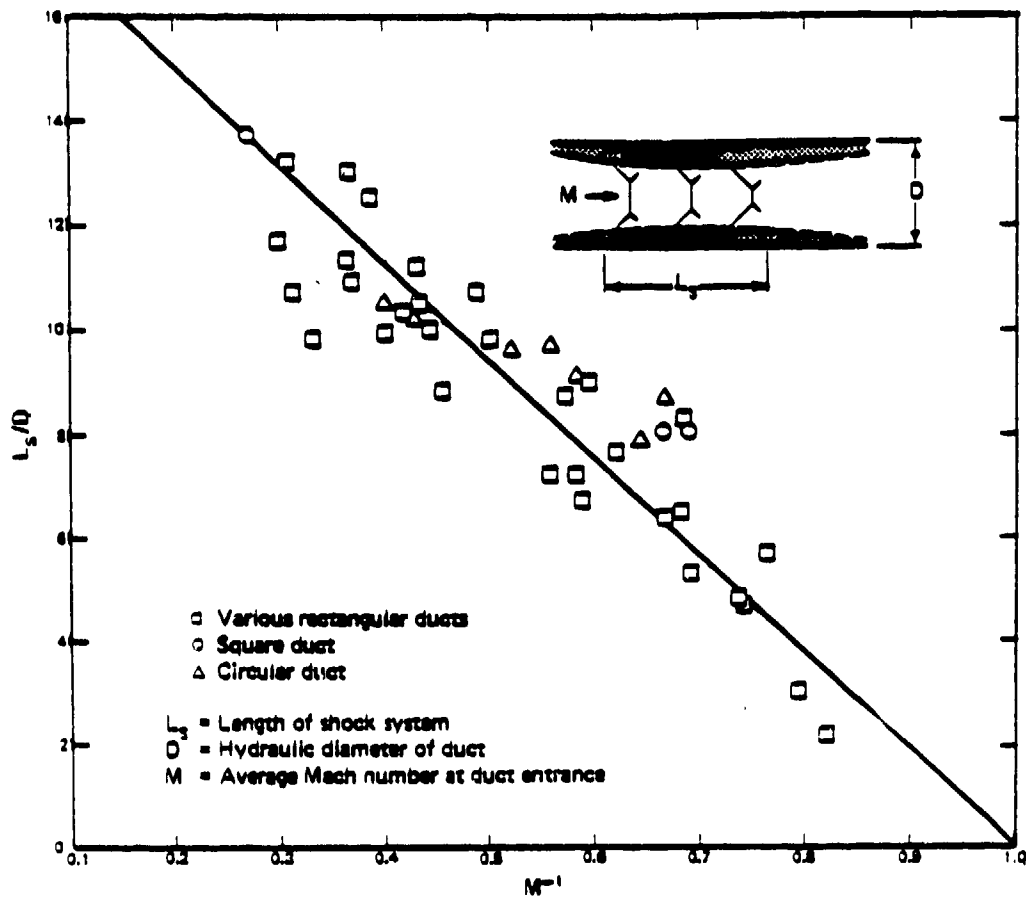
CONSTANT-PRESSURE EJECTOR ANALYSIS ASSUMPTIONS:

(1) STEADY FLOW

(2) PIECEWISE UNIFORM FLOWS AT SECTION 1 AND UNIFORM FLOW AT SECTIONS 2 AND 3

(3) PRIMARY AND SECONDARY GASES OBEY THE PERFECT GAS RELATIONSHIPS

(4) PRIMARY AND SECONDARY FLOWS ARE ISENTROPIC FROM THEIR RESPECTIVE STAGNATION STATES TO THE STATES AT SECTION 1

CONSTANT-PRESSURE EJECTOR ANALYSIS ASSUMPTIONS (Continued):

(5) PRIMARY AND SECONDARY STREAMS MIX IDEALLY TO FORM A MIXED, UNIFORM STREAM AT SECTION 2

(6) NEGLIGIBLE SHEAR STRESSES AT THE WALL

(7) ADIABATIC FLOW BETWEEN SECTIONS 1 AND 2

(8) NO SHAFT/SHEAR WORK BETWEEN SECTIONS 1 AND 2

CONSTANT-PRESSURE EJECTOR ANALYSIS ASSUMPTIONS (Concluded):

(9) THE INTEGRATED PRESSURE-AREA SURFACE FORCES ACTING IN THE FLOW DIRECTION ARE ZERO

THE CONSTANT-PRESSURE EJECTOR IS A SPECIAL CASE SATISFY-ING ASSUMPTION (9)

THE MIXING SECTION AREA VARIATION IS ASSUMED TO VARY SO THAT THE STATIC PRESSURE OF THE MIXING FLOW IS CONSTANT WITHIN THE MIXING SECTION

344

CONSERVATION OF MASS:

$$\oint_{CS} \rho\bar{V} \cdot d\bar{A} = 0$$

$$\rho_{P1}V_{P1}A_{P1} + \rho_{S1}V_{S1}A_{S1} = \rho_{M2}V_{M2}A_{M2}$$

$$w \equiv \rho AV, \quad w_P + w_S = w_M$$

$$\mu \equiv w_S/w_P$$

CONSERVATION OF MOMENTUM:

$$\rightarrow \sum F_X = \oint_{CS} V_X(\rho\bar{V} \cdot d\bar{A})$$

$$\rightarrow \sum F_X = P_{P1}A_{P1} + P_{S1}A_{S1} - P_{M2}A_{M2} - \hat{\imath}_X \cdot \int_{A_W} Pd\bar{A}$$

$$\gamma_P M_{P1}^2 + \frac{A_{S1}}{A_{P1}} \gamma_S M_{S1}^2 = \frac{A_{M2}}{A_{P1}} \gamma_M M_{M2}^2$$

CONSERVATION OF ENERGY:

$$\oint_{CS} (h_0)\rho\bar{V} \cdot d\bar{A} = 0$$

$$w_P h_{PO} + w_S h_{SO} = w_M h_{MO}$$

$$\frac{T_{MO}}{T_{PO}} = \frac{1}{(1+\mu)} \left[\frac{(C_P)_P}{(C_P)_M}\right] \left[1 + \mu \frac{(C_P)_S}{(C_P)_P} \cdot \frac{T_{SO}}{T_{PO}}\right]$$

345

Representative characteristics for a constant-
pressure ejector

346
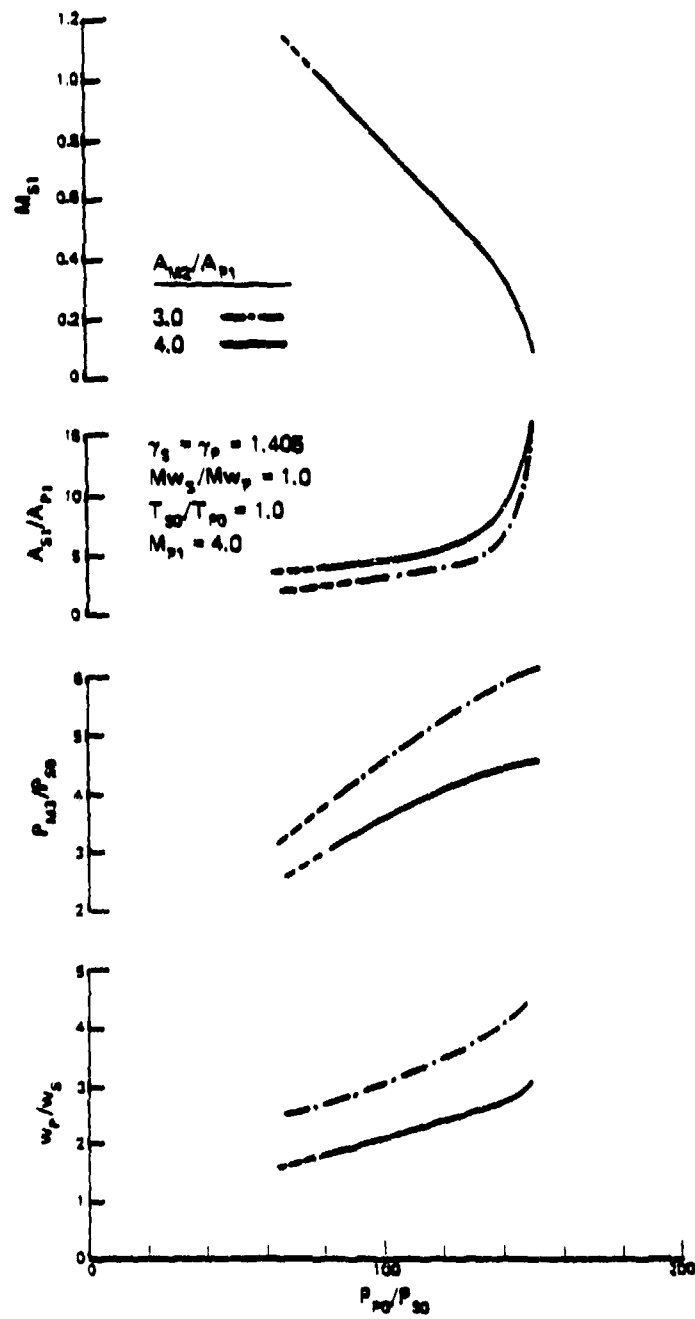
- **AREA DISTRIBUTION OF THE MIXING SECTION IS:**

  (1)  UNKNOWN,
  (2)  DEPENDENT ON THE EJECTOR OPERATING POINT, AND
  (3)  NOT DETERMINABLE FROM THE ANALYSIS.

- **FLOW MODEL DOES NOT INCLUDE KNOWN EJECTOR PHENOMENA AND REGIMES:**

  (1)  INTERACTION BETWEEN STREAMS AND
  (2)  "CHOKING".

ONE-DIMENSIONAL ANALYSIS
OF
CONSTANT-AREA EJECTOR SYSTEMS

CONSTANT-AREA EJECTOR FLOW MODEL:

- SUPERSONIC PRIMARY NOZZLE

- CONSTANT-AREA MIXING SECTION

347
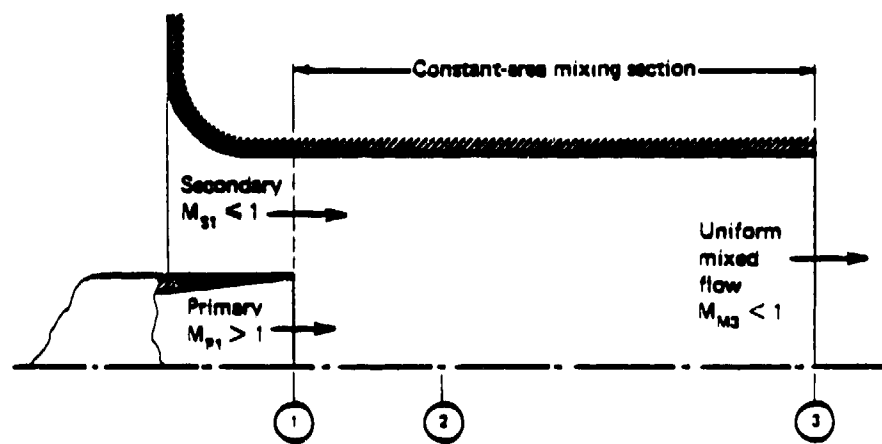
Axisymmetric constant-area ejector configuration
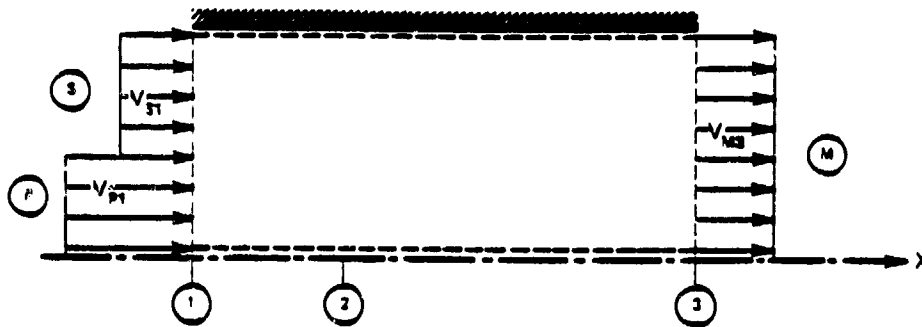
---- Control volume

P, $\rho$, A, V, T, M, etc. are defined for each stream
at sections 1 and 3.

*If "choking" exists

Constant-area mixing section control volume
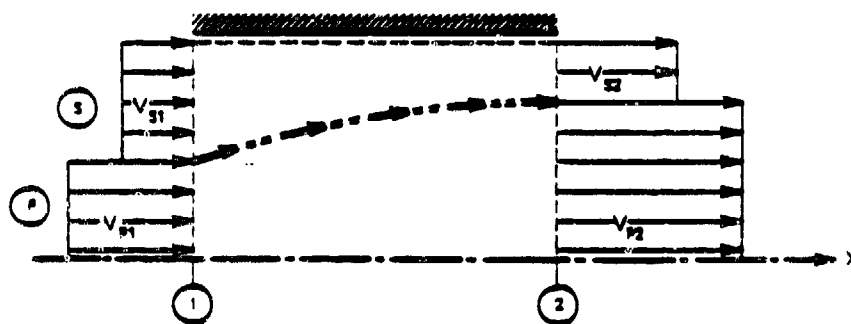


----Control volume

Control volume for Fabri "choking" analysis

CONSTANT-AREA EJECTOR ANALYSIS ASSUMPTIONS:

    (1)  STEADY FLOW

    (2)  PIECEWISE UNIFORM FLOWS AT SECTIONS 1 AND 2, AND
         UNIFORM FLOW AT SECTION 3

    (3)  PRIMARY AND SECONDARY GASES OBEY THE PERFECT GAS
         RELATIONSHIPS

    (4)  PRIMARY AND SECONDARY FLOWS ARE ISENTROPIC FROM
         THEIR RESPECTIVE STATES AT SECTION 1

CONSTANT-AREA EJECTOR ANALYSIS ASSUMPTIONS (Continued):

    (5)  PRIMARY AND SECONDARY STREAMS MIX TO FORM A UNI-
         FORM STREAM AT SECTION 3

    (6)  NEGLIGIBLE SHEAR STRESSES AT THE WALL

    (7)  ADIABATIC FLOW BETWEEN SECTIONS 1 AND 3

    (8)  NO SHAFT/SHEAR WORK BETWEEN SECTIONS 1 AND 3

FABRI'S "CHOKING" CRITERION --- ASSUMPTIONS:

    (1)  STREAMS REMAIN DISTINCT AND DO NOT MIX
         BETWEEN SECTIONS 1 AND 2.

    (2)  FLOW IS ISENTROPIC FOR EACH STREAM BETWEEN
         SECTIONS 1 AND 2.

    (3)  AVERAGE PRESSURE OF THE STREAMS CAN BE
         DIFFERENT AT EACH CROSS-SECTION.

    (4)  THE MACH NUMBER OF THE SECONDARY FLOW AT
         SECTION 2 IS $M_{S2} = 1$.

    (5)  THE STATIC PRESSURES ARE SUCH THAT
         $P_{P1} > P_{S1}$.

CONSERVATION OF MASS:

$$\oint_{CS} \rho \bar{V} \cdot d\bar{A} = 0$$

$$\rho_{P1} V_{P1} A_{P1} + \rho_{S1} V_{S1} A_{S1} = \rho_{M3} V_{M3} A_{M3}$$

$$w = \rho A V, \quad w_P + w_S = w_M$$

$$\mu = w_S / w_P$$

CONSERVATION OF MOMENTUM:

$$\rightarrow \sum F_X = \oint_{CS} V_X (\rho \bar{V} \cdot d\bar{A})$$

$$P_{P1} A_{P1} + P_{S1} A_{S1} - P_{M3} A_{M3} =$$

$$\rho_{M3} A_{M3} V_{M3}^2 - (\rho_{P1} A_{P1} V_{P1}^2 + \rho_{S1} A_{S1} V_{S1}^2)$$

CONSERVATION OF ENERGY:

$$\oint_{CS} h_0 (\rho \bar{V} \cdot d\bar{A}) = 0$$

$$w_P h_{P0} + w_S h_{S0} = w_M h_{M0}$$

$$\frac{T_{M0}}{T_{P0}} = \frac{1}{(1+\mu)} \left[ \frac{(C_P)_P}{(C_P)_M} \right] \left[ 1 + \mu \frac{(C_P)_S}{(C_P)_P} \cdot \frac{T_{S0}}{T_{P0}} \right]$$

351

CONSTANT-AREA EJECTOR OPERATING REGIMES:

- "MIXED" REGIME ... BACK-PRESSURE DEPENDENT

- "SUPERSONIC" AND "SATURATED SUPERSONIC" REGIME ...
  BACK-PRESSURE INDEPENDENT

- TRANSITION BETWEEN REGIMES OCCURS ALONG THE
  "BREAK-OFF" CURVE

"MIXED" FLOW REGIME:

- $M_{S1} < 1$
- $P_{S1}/P_{P1} \lessgtr 1$
- $M_{S2} < 1$
- $W_S/W_P = f(P_{S0}/P_{P0}, P_{M3}/P_{P0}, \ldots)$

"SUPERSONIC" FLOW REGIME:

- $M_{S1} < 1$
- $P_{S1}/P_{P1} < 1$
- $M_{S2} = 1$
- $W_S/W_P = f(P_{S0}/P_{P0}, \ldots)$

"SATURATED-SUPERSONIC" FLOW REGIME:

- $M_{S1} = 1$
- $P_{S1}/P_{P1} \geq 1$
- $W_S/W_P = f(P_{S0}/P_{P0}, \ldots)$

INVISCID INTERACTION CHARACTERISTICS AND CRITERIA:

- SUBSONIC/SUPERSONIC ENTRANCE FLOWS

    - SECONDARY FLOW ACCELERATES TO FORM AN AERODYNAMIC THROAT

    - "CHOKING" AT AERODYNAMIC THROAT

    - UNEQUAL AVERAGE STATIC PRESSURES AT AERODYNAMIC THROAT

INVISCID INTERACTION CHARACTERISTICS AND CRITERIA (CONT'D)

- SUPERSONIC/SUPERSONIC ENTRANCE FLOWS

    - SECONDARY FLOW DECELERATES TO FORM AN AERODYNAMIC THROAT

    - "LIMITING" MACH NUMBER OF ONE AT AERO-DYNAMIC THROAT

    - UNEQUAL AVERAGE STATIC PRESSURES AT AERODYNAMIC THROAT

    - INDUCED FLOW SEPARATION MAY LIMIT PERFORMANCE
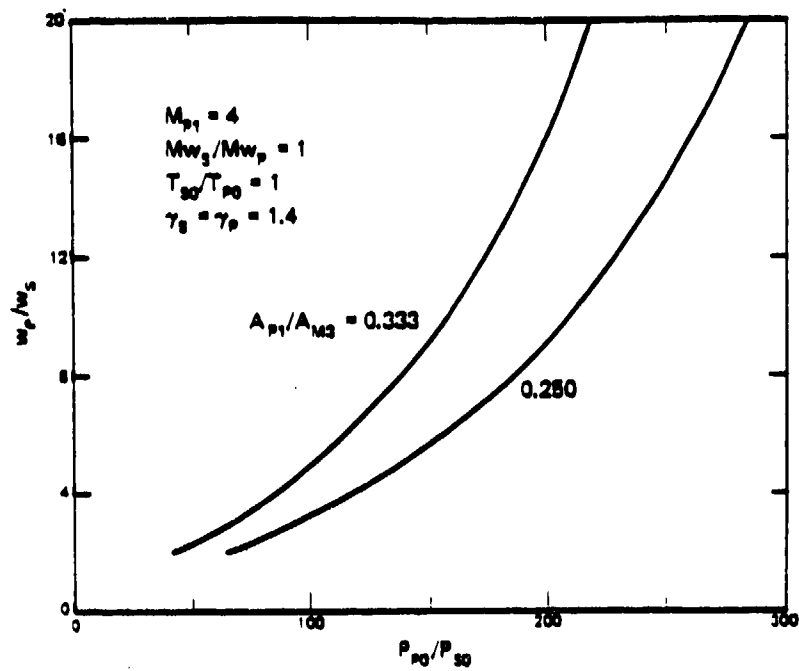
353

(a) Mass flowrate characteristics

Constant-area ejector characteristics

354
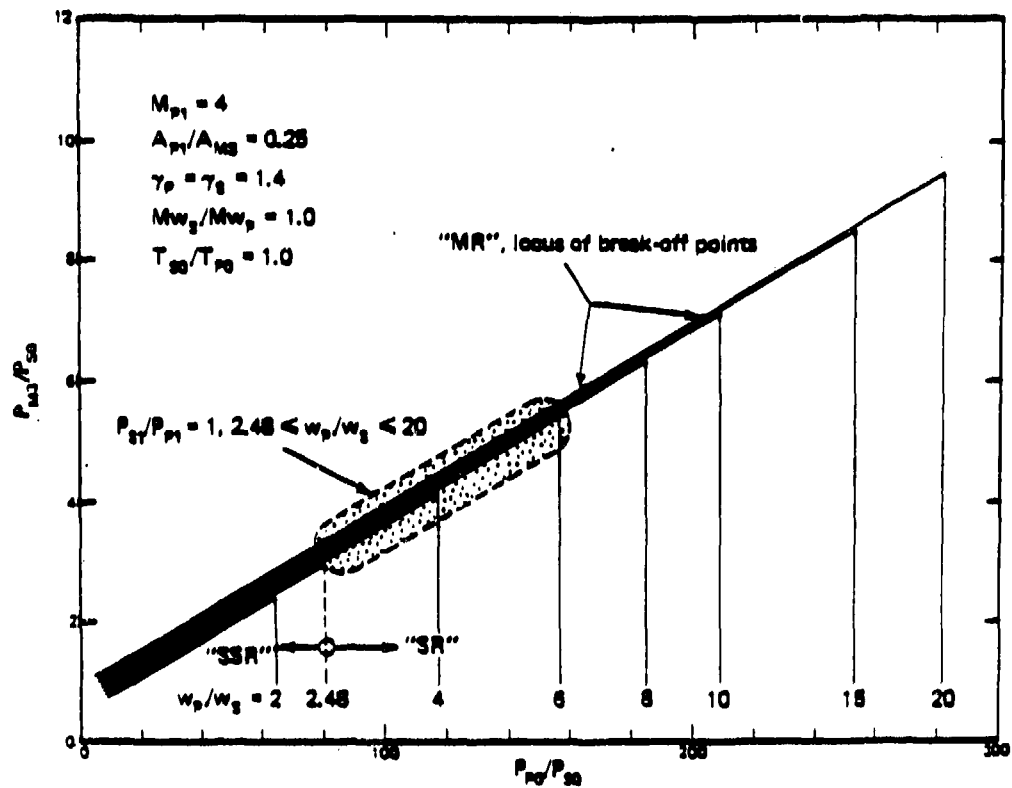
(b)  Compression characteristics

CONSTANT-AREA EJECTOR FLOW MODEL

- ● POSITIVE FEATURES:

    - ● INCLUDES EXPERIMENTALLY OBSERVED FLOW REGIMES
    - ● INCLUDES "CHOKING" PHENOMENA
    - ● CONVENIENT AND RAPID ANALYSIS

- ● NEGATIVE FEATURES:

    - ● CONSTANT-AREA RESTRICTION
    - ● "LONG" MIXING SECTIONS
    - ● POOR AGREEMENT WITH EXPERIMENT FOR CERTAIN
      SMALL SECONDARY FLOWRATE CONDITIONS
    - ● LACK OF FLOWFIELD DETAILS


▷ TWO-DIMENSIONAL EJECTOR ANALYSES


TWO-DIMENSIONAL EJECTOR FLOW MODELS:

- ● "ZERO" AND "SMALL" SECONDARY FLOWRATES

    - ● TURBULENT MIXING
    - ● FLOW-WALL INTERACTION
    - ● FLOW RECOMPRESSION

- ● "HIGHER" SECONDARY FLOWRATES

    - ● INVISCID PRIMARY-SECONDARY INTERACTION
    - ● TURBULENT MIXING
    - ● SOLUTION CRITERIA AND BOUNDARY CONDITIONS
    - ● FLOW DIFFUSION

TWO-DIMENSIONAL INVISCID INTERACTION:

- MUTUAL INTERACTION BETWEEN FLOWS WITHIN AVAILABLE FLOW AREA

- MATCHED STATIC PRESSURE AT MUTUAL FLUID BOUNDARY

- FORMATION OF AERODYNAMIC THROAT

- "CHOKING" CRITERIA AT AERODYNAMIC THROAT

TWO-DIMENSIONAL MIXING COMPONENT:

- INVISCID VELOCITIES AT FLUID SLIPLINE BOUNDARY

- SUPERIMPOSE FULLY DEVELOPED MIXING PROFILE

- ESTIMATE ENTRAINMENT AND DISPLACEMENT EFFECTS

EJECTOR OPERATING REGIMES:

- "MIXED" REGIME...BACK-PRESSURE DEPENDENT

- "SUPERSONIC" AND "SATURATED-SUPERSONIC" REGIME...BACK-PRESSURE INDEPENDENT

- TRANSITION BETWEEN REGIMES OCCURS ALONG THE "BREAK-OFF" CURVE

357

Ejector mass flow characteristic surface. $\bar{W} = f(\bar{P}_{os}, \bar{P}_a)$
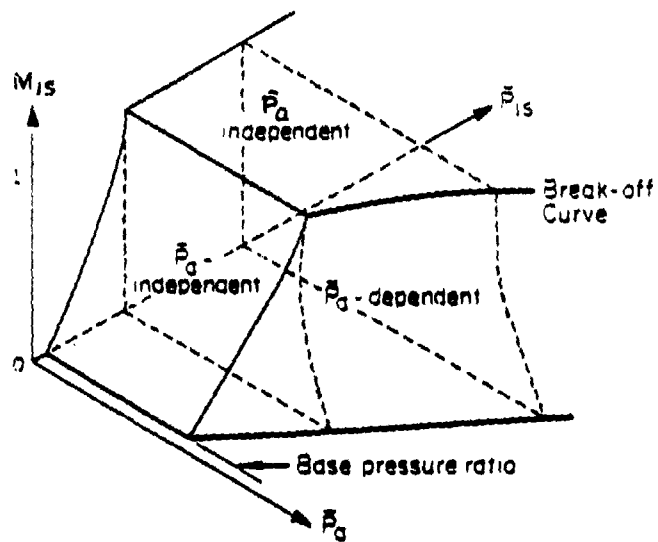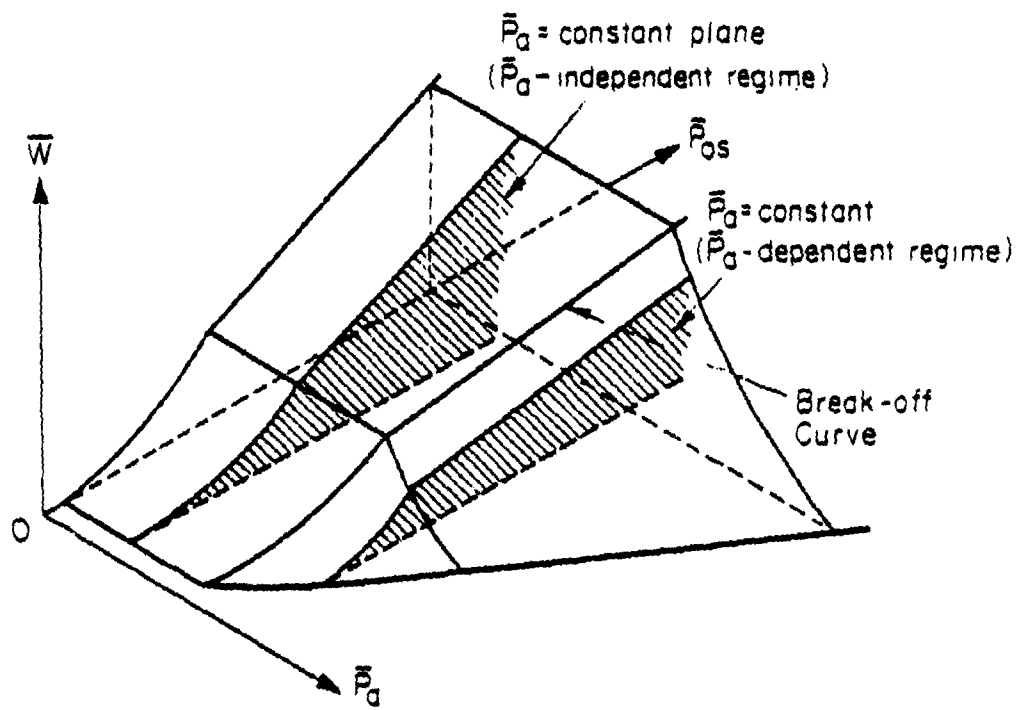


Ejector characteristic surface $M_{is} = f(\bar{P}_{is}, \bar{P}_a)$

$\bar{P}_a$ = constant plane
($\bar{P}_a$ – independent regime)

$\bar{P}_{os}$

$\bar{P}_a$ = constant
($\bar{P}_a$ – dependent regime)

Break-off
Curve

$\bar{W}$

O

$\bar{P}_a$

Intersection of the $\bar{W}$-surface with planes of constant $P_a$



$\bar{W}$

$\bar{P}_{os}$

Planes $\bar{P}_{os}$
= constant

$\bar{P}_a$ – independent

Break-off
Curve

$\bar{P}_a$ –
dependent

O

$\bar{P}_a$
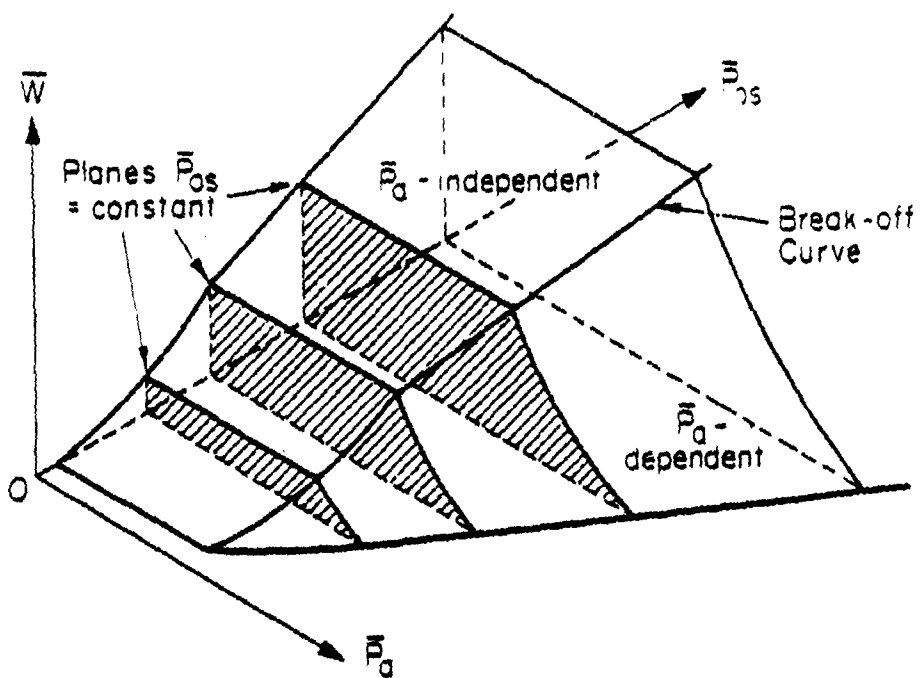
Intersection of the $\bar{W}$-surface with planes of constant $P_{os}$

359

Intersection of the $M_{ts}$-surface with planes of constant $\bar{P}_a$



Intersection of the $M_{ts}$-surface with planes of constant $\bar{P}_{1s}$

360
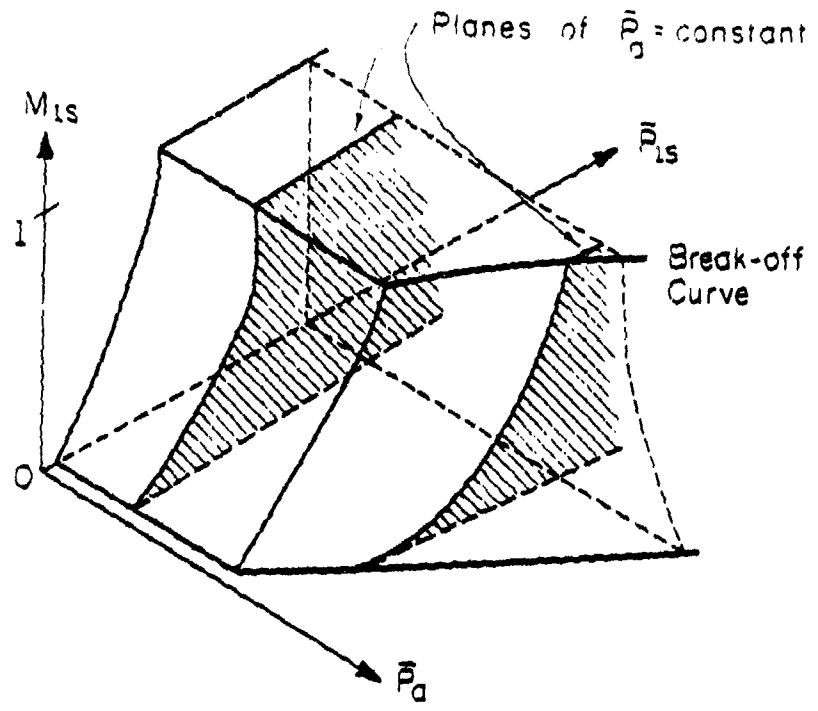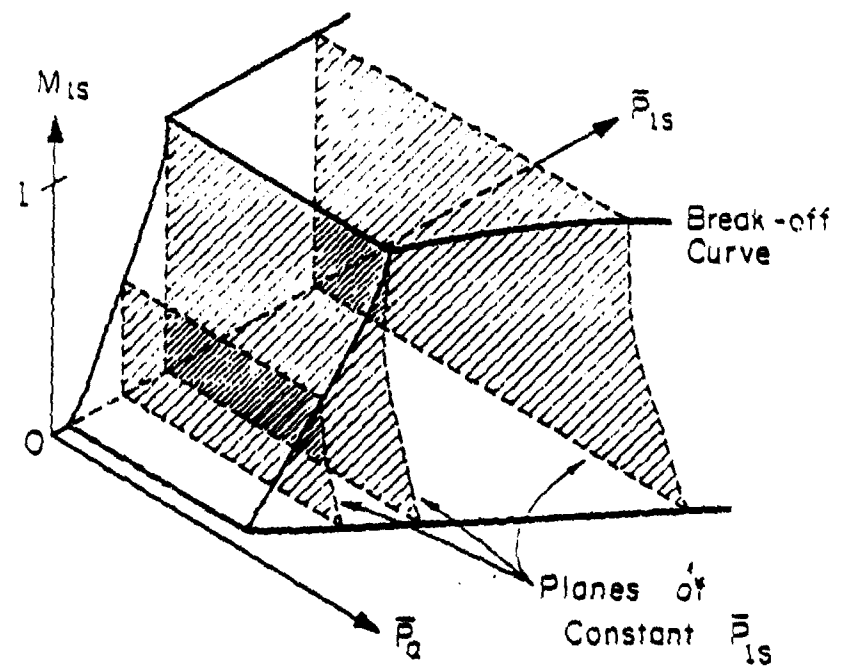
Flow field for "zero" flow regime
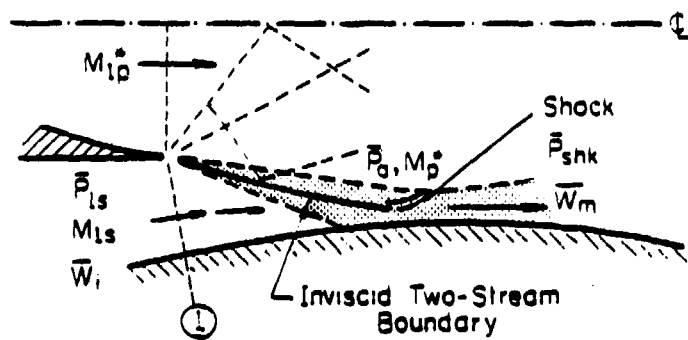


Flow model for "small" flow regime
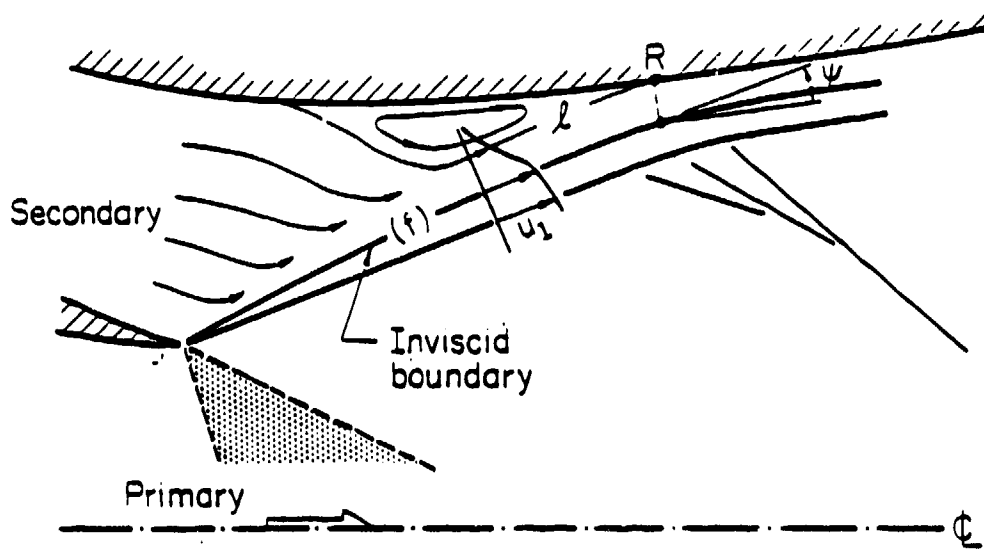
Schematic of theoretical reattachment ONERA
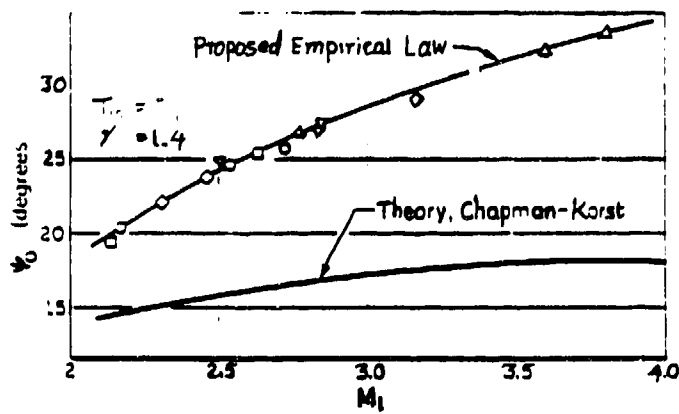


Empirical law of angular reattachment ONERA
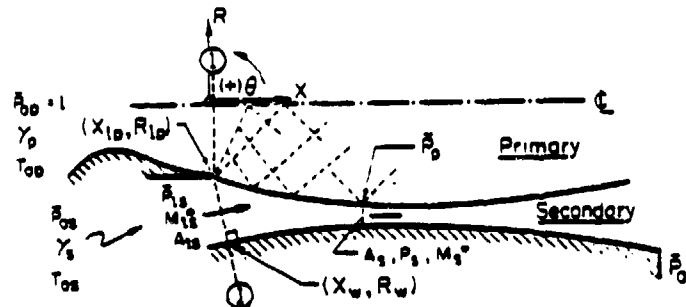
Two-stream inviscid flow model



$$X_{min} \begin{cases} \dfrac{dA_s}{dX} = 0 \\[2mm] (M_s^*)_{min} \leq 1 \\[2mm] (A/A^*)_s = \text{minimum} \end{cases}$$

where
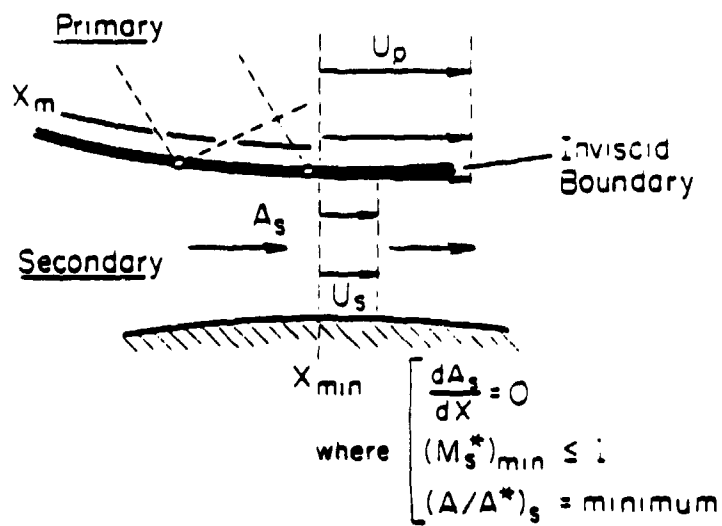
Inviscid velocity profile at the "choking" point
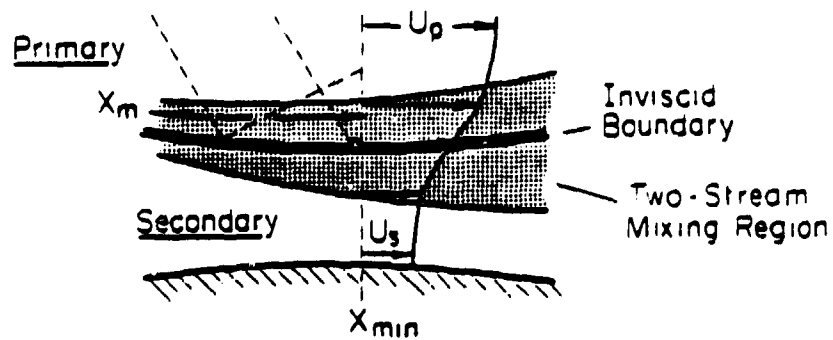


Viscid approximation at the "choking" point

363
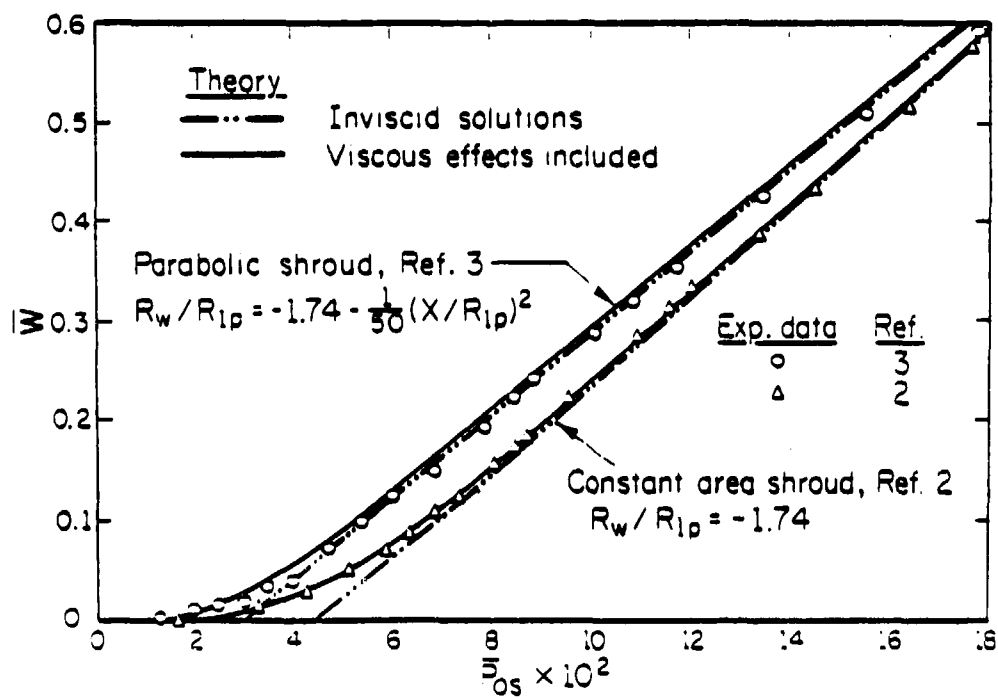
Comparison of theory and experiment for the pumping characteristics of two ejector systems (After References 2 and 3)
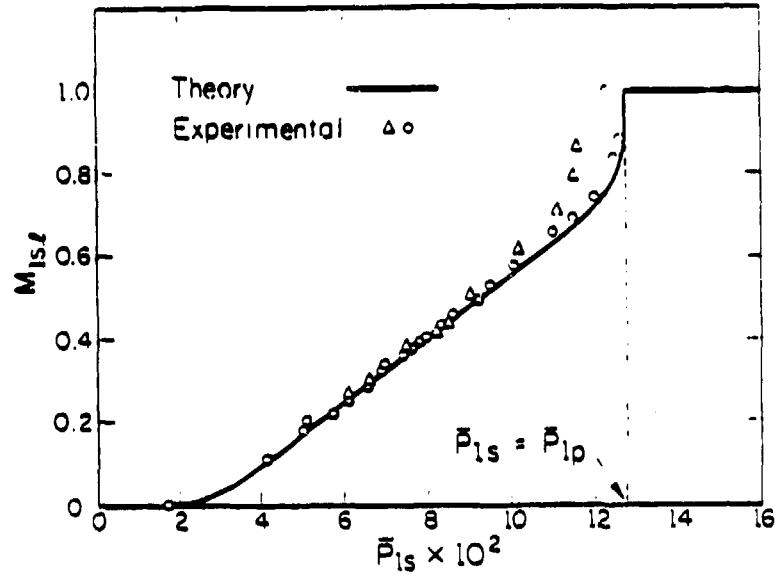
Comparison of theory and experiment for the "limiting initial secondary Mach number" for a constant shroud area ejector system. ($M_{1p} = 2$, $A_w/A_{1p} = 3.06$) (Ref. 2)

$\bar{P}_{1s}$ Table

| Inviscid Theory | | Experimental | |
|---|---|---|---|
| Line | Value | Symbol | Value |
| ——— | 0.06574 | o | 0.0658 |
| —·—· | 0.090 | △ | 0.092 |
| — — — | 0.110 | □ | 0.111 |
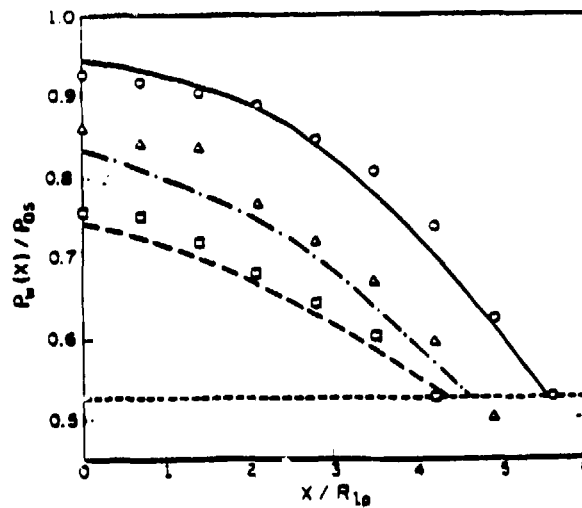


Comparison of theory and experiment for the pressure distribution up to the "choking" point ($M_{1p} = 2$, $A_w/A_{1p} = 3.06$) (Ref. 2)

365

TWO-DIMENSIONAL INTERACTION MODEL

● POSITIVE FEATURES:

   ● INCLUDES EXPERIMENTALLY OBSERVED FLOW
     REGIMES
   ● INCLUDES "CHOKING" PHENOMENA
   ● ANALYZE NON-CONSTANT AREA MIXING DUCTS
   ● AGREES WELL WITH EXPERIMENTS THROUGHOUT
     OPERATIONAL REGIME

● NEGATIVE FEATURES:

   ● TEDIOUS SOLUTION PROCEDURE
   ● TIME-CONSUMING COMPUTATIONS
   ● NOT APPLICABLE TO "LONG" NON-CONSTANT
     AREA MIXING DUCTS

# EXPERIMENTAL EJECTOR RESULTS
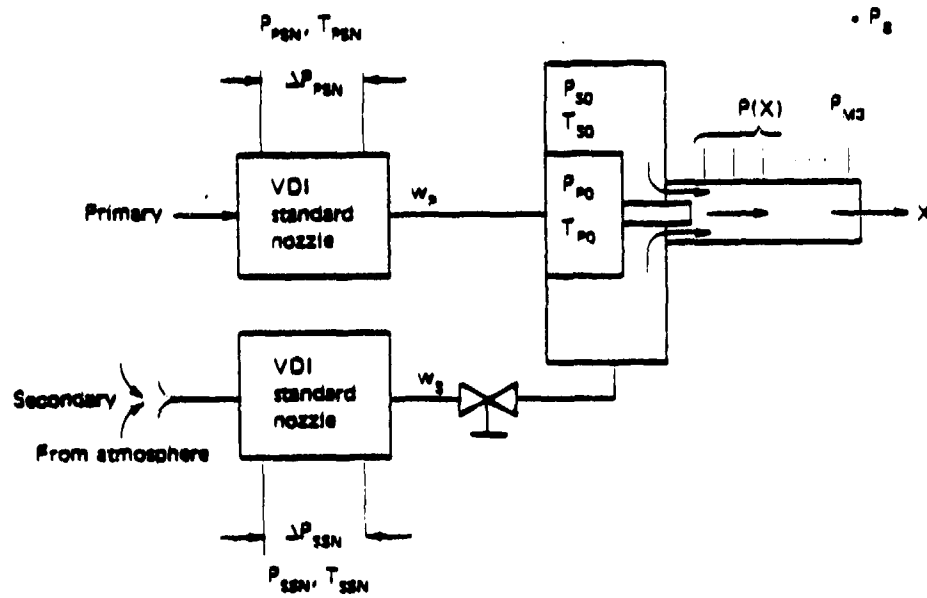


Experimental ejector set-up and notation
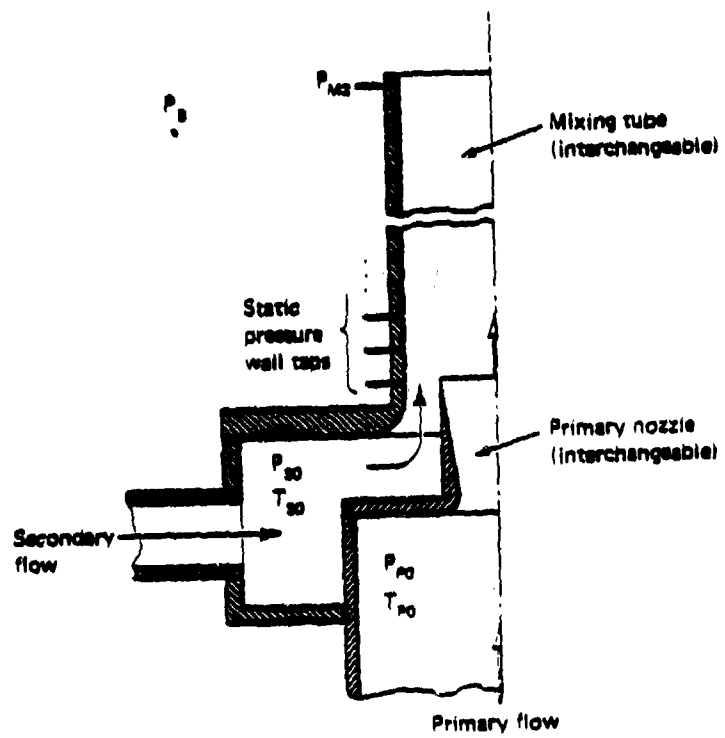
Schematic of axisymmetric ejector configuration

Labels in figure:
$P_{B}$
$P_{M3}$
Mixing tube (interchangeable)
Static pressure wall taps
Primary nozzle (interchangeable)
$P_{S0}$
$T_{S0}$
Secondary flow
$P_{P0}$
$T_{P0}$
Primary flow

(a) Basic conical nozzle.

(b) Slotted extension for nozzle.
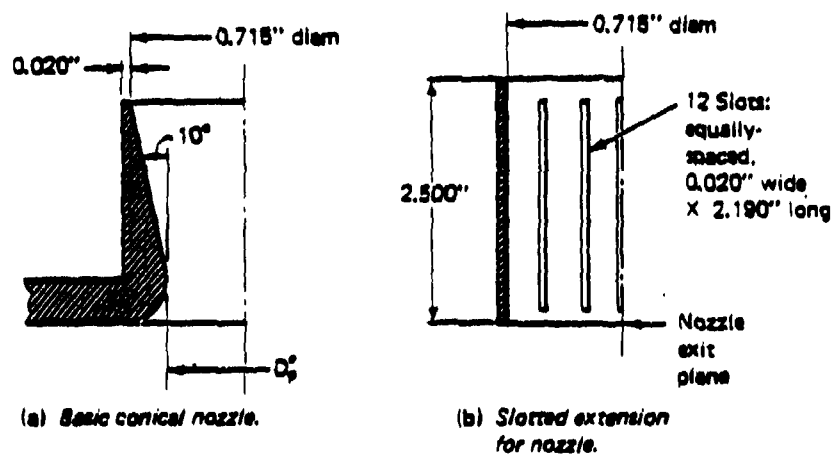
| Nozzle | $M_{p_1}$ | $D_p^c$ in. |
|--------|-----------|-------------|
| 1 | 2.0 | 0.550 |
| 2 | 2.5 | 0.440 |
| 3* | 2.5 | 0.440 |
| *Slotted nozzle | | |

(c) Nozzle specifications.

Schematics and specifications of ejector primary nozzles

369
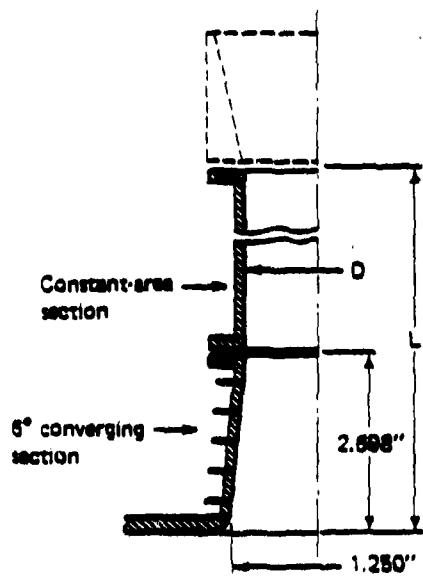
(a) *Variable-area mixing section.*
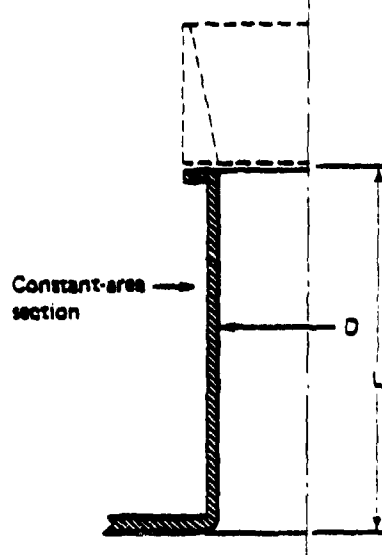
(b) *Constant-area mixing section.*

| Mixing tube | D in. | L in. |
|---|---|---|
| 1 | 0.995 | 12.500 |
| 2 | 1.245 | 13.000 |
| 3* | 0.995 | 12.882 |
| *With 6° converging section | | |

(c) *Mixing section specifications.*
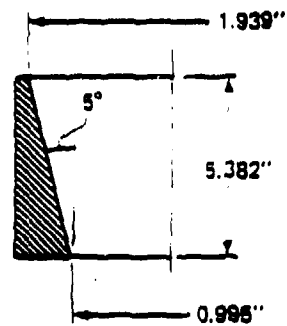
(d) *Subsonic diffuser section.*

Schematics and specifications of ejector mixing sections
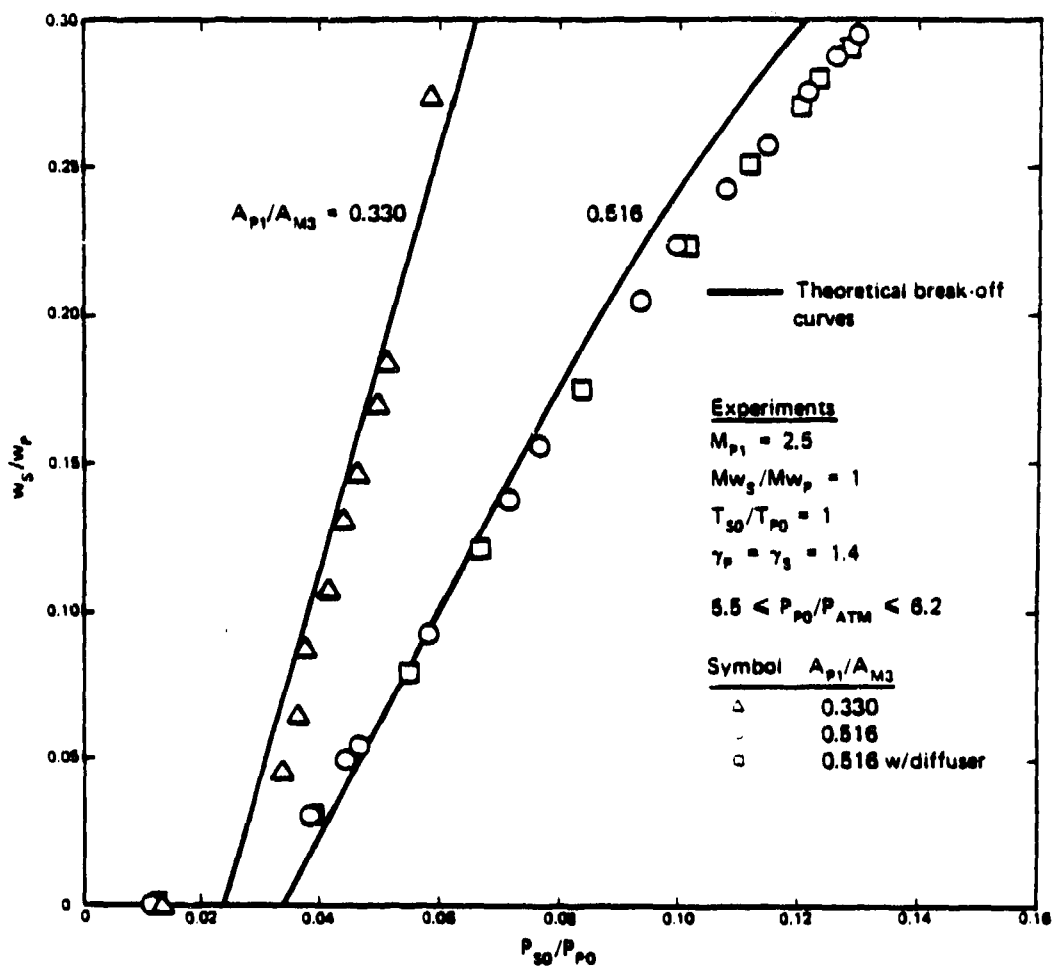
Constant-area ejector mass flow characteristics
$(A_{P_1}/A_{M3} = 0.330, 0.516$ and $M_{P_1} = 2.5)$
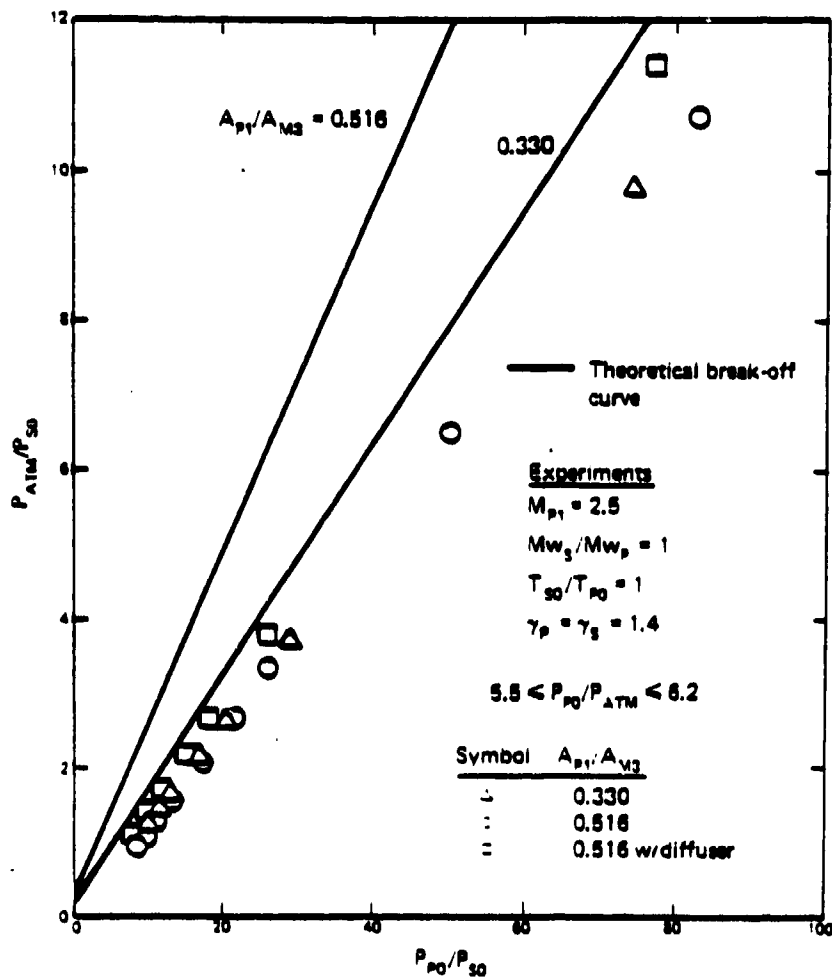
Constant-area ejector compression characteristics
($A_{P_1}/A_{M_3}$ = 0.330, 0.516 and $M_{P_1}$ = 2.5)
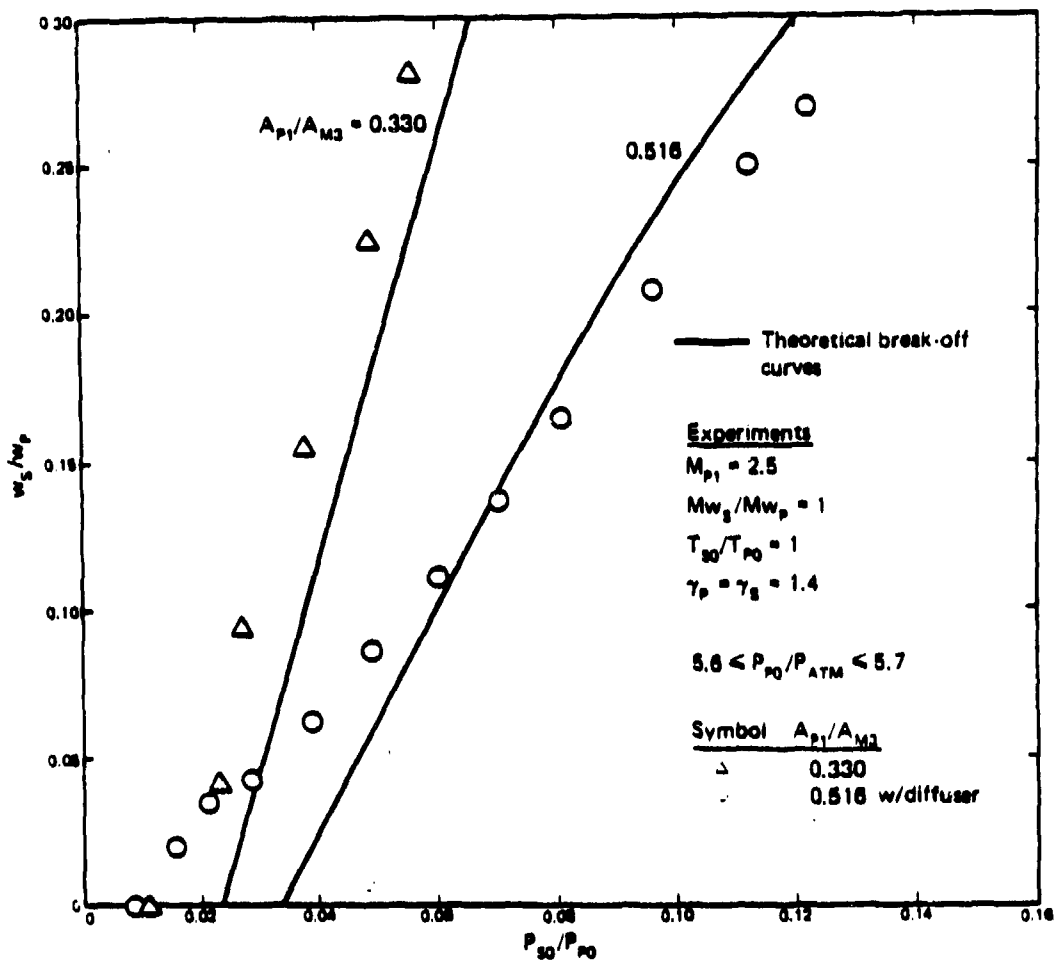
Constant-area, slotted-nozzle ejector mass flow characteristics
($A_{P_1}/A_{M3}$ = 0.330, 0.516 and $M_{P_1}$ = 2.5)
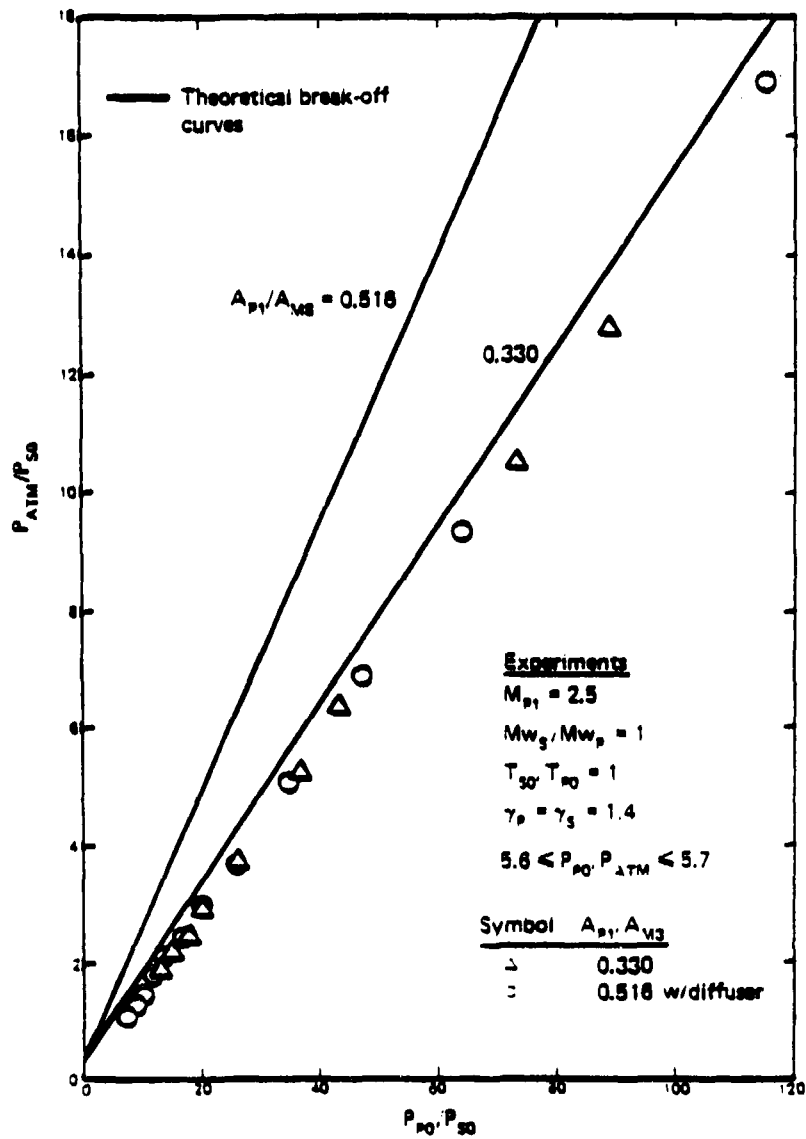
Constant-area, slotted-nozzle ejector compression
characteristics $(A_{p_1}/A_{M3} = 0.330, 0.516$ and
$M_{p_1} = 2.5)$
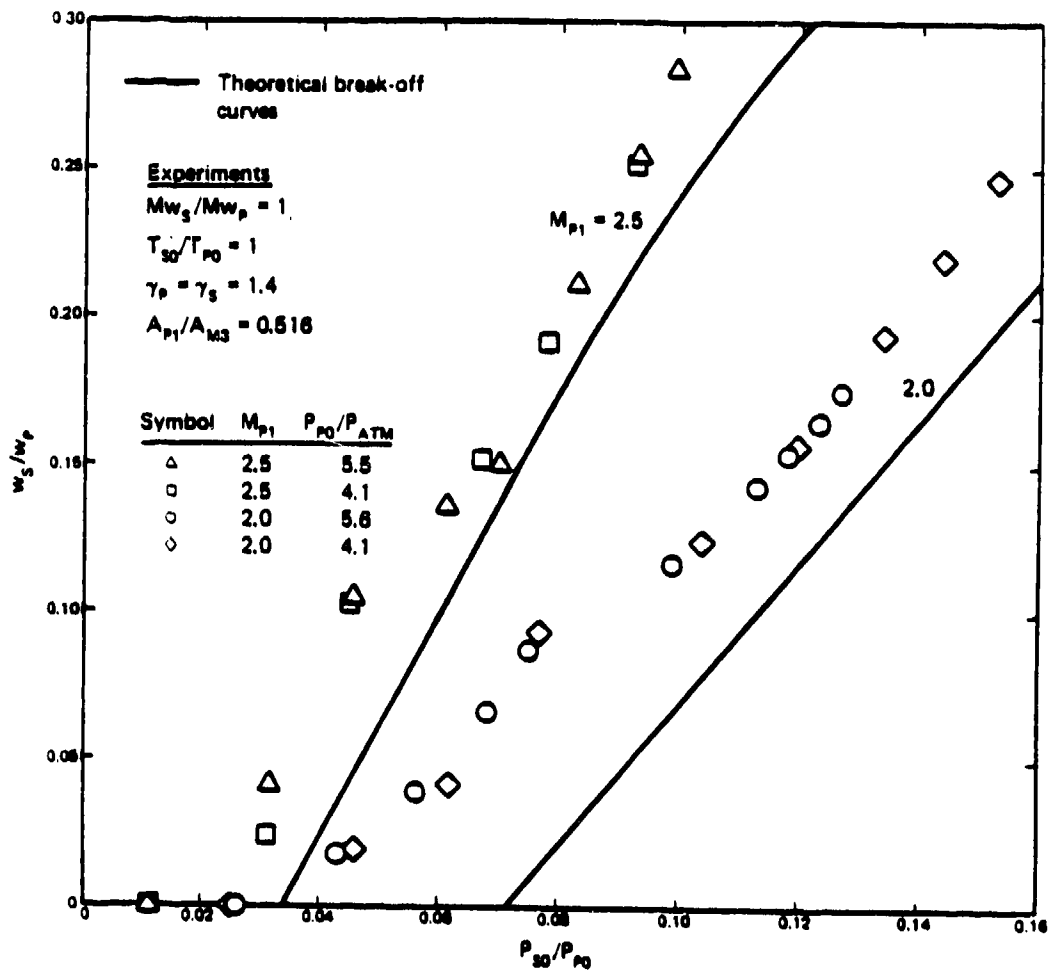
Variable-area ejector mass flow characteristics
$(A_{P_1}/A_{M5} = 0.516$ and $M_{P_1} = 2.0, 2.5)$
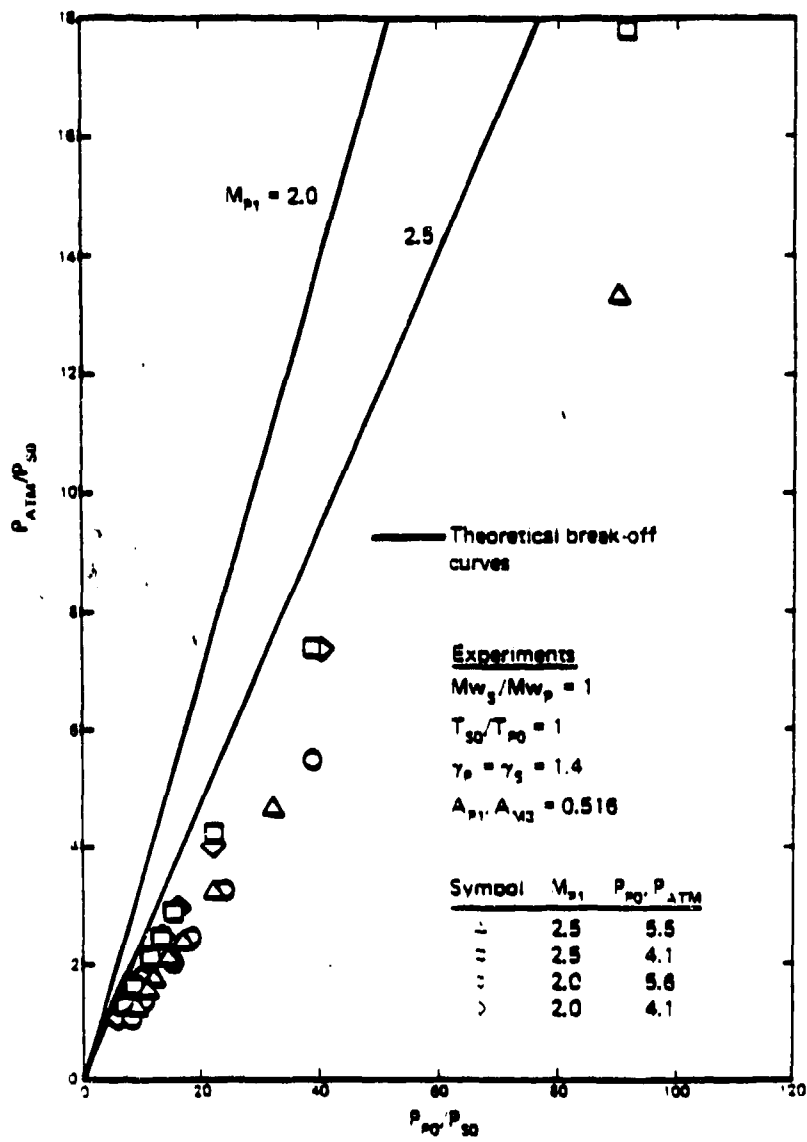
Variable-area ejector compression characteristics
$(A_{P_1}/A_{M3} = 0.516$ and $M_{P_1} = 2.0, 2.5)$
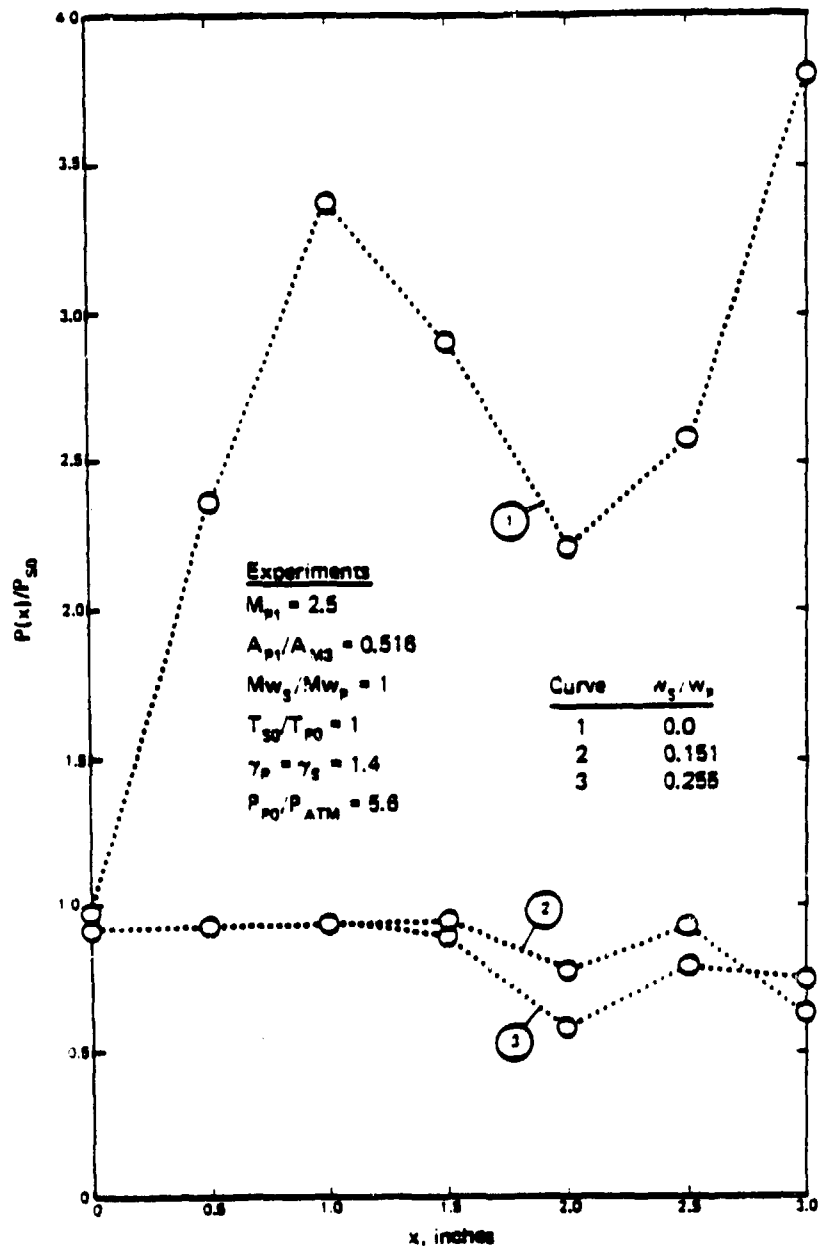
Variable-area ejector wall pressure distributions
$(A_{P_1}/A_{M_3} = 0.516, M_{P_1} = 2.5, P_{P_0}/P_{ATM} = 5.6)$
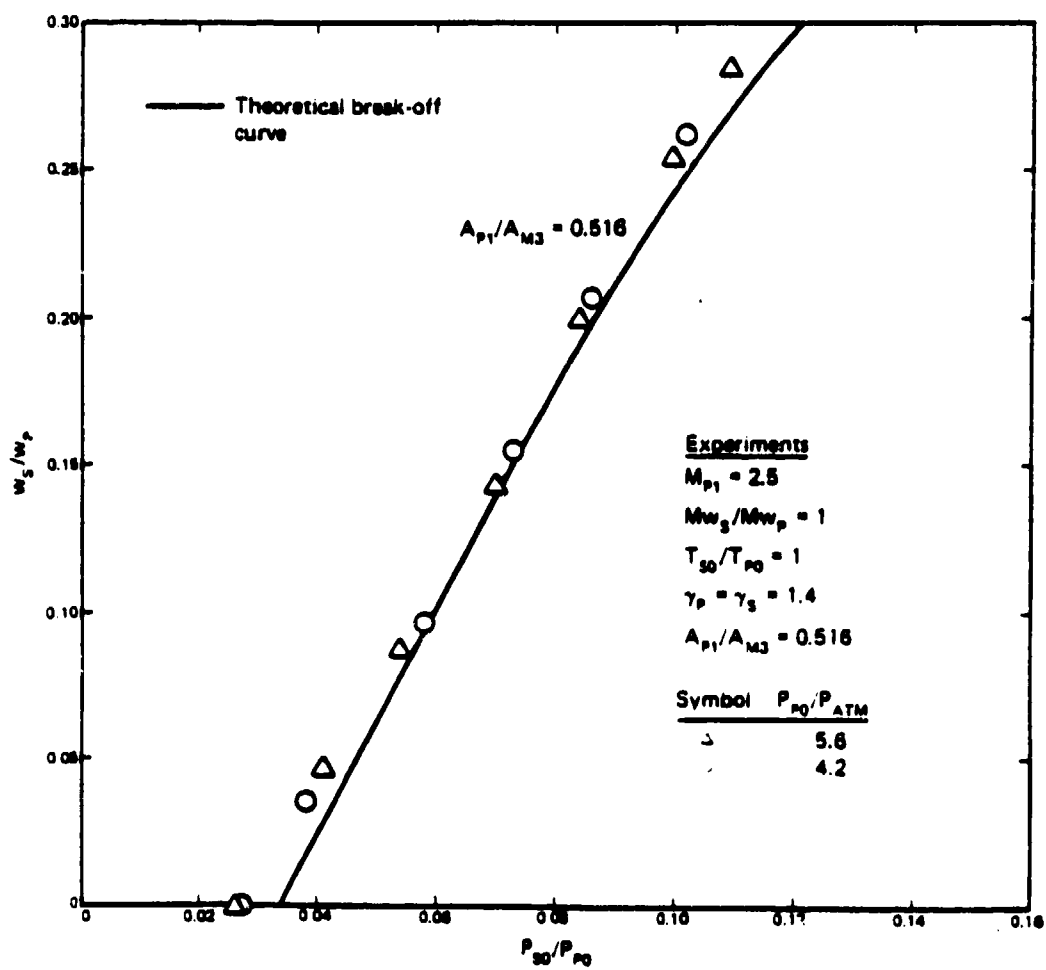
Variable-area, slotted-nozzle ejector mass flow characteristics
$(A_{P_1}/A_{M_3} = 0.516$ and $M_{P_1} = 2.5)$
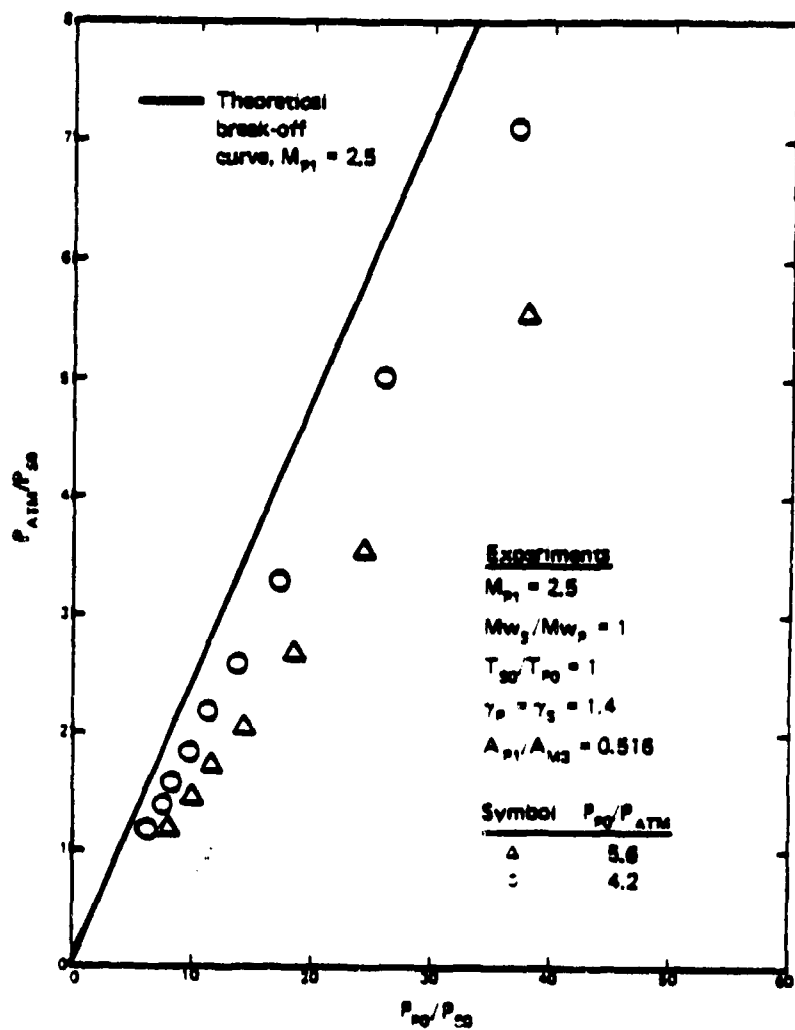
Variable-area, slotted-nozzle ejector compression characteristics ($A_{p_1}/A_{M3} = 0.516$ and $M_{p_1} = 2.5$)
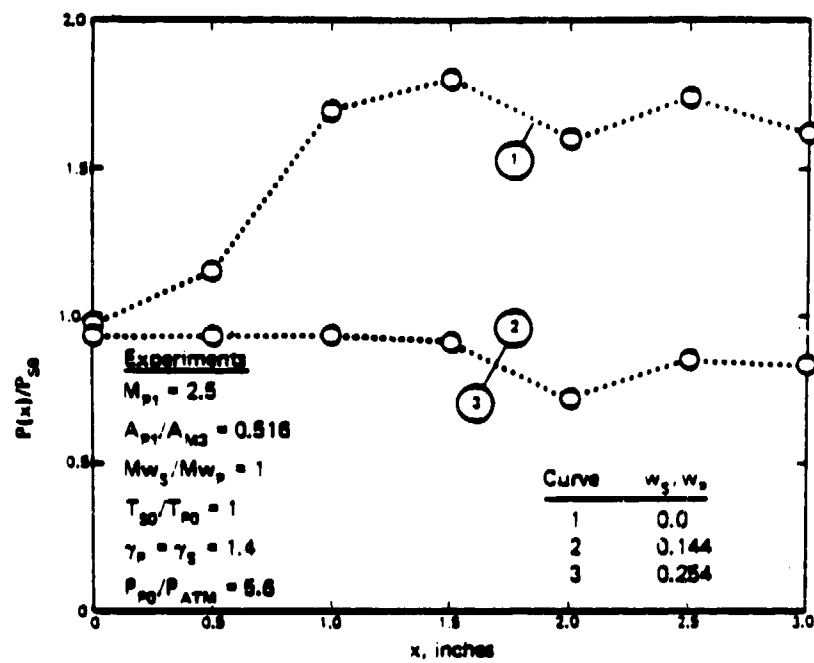
Variable-area, slotted-nozzle ejector wall pressure distributions ($A_{p_1}/A_{m3}$ = 0.516, $M_{p_1}$ = 2.5, and $P_{p0}/P_{ATM}$ = 5.6)

NEW DIRECTIONS IN EJECTOR FLOW MODELS

- COMBINED INVISCID-VISCID MODEL

- IMPROVED MODEL(S) FOR MIXING PHENOMENA

- IMPROVED "CHOKING" CRITERION

- IMPROVED "DOWNSTREAM" DIFFUSER MODELS

- INTEGRATED BOUNDARY-LAYER ANALYSIS

NEW DIRECTIONS IN EJECTOR SYSTEM DESIGN

- MULTIPLE-STREAM PRIMARY FLOW

- LONGITUDINALLY DISTRIBUTED PRIMARY FLOW

- UNSTEADY PRIMARY FLOW

- SEGMENTED DIFFUSER (MIXING SECTION)

- SUPERSONIC-SUPERSONIC SYSTEMS

NEW DIRECTIONS IN EJECTOR DESIGN -- PRIMARY
FLOW

- STEADY-STATE NOZZLE SYSTEM
    (1) NOZZLE DISTRIBUTION
    (2) LONGITUDINAL NOZZLE DISTRIBUTION

- UNSTEADY OR PERIODIC NOZZLE SYSTEM
    (1) PULSATING FLOW
    (2) OSCILLATING FLOW
    (3) STRONG ACOUSTIC EXCITATION OF
        MIXING REGIONS

# SELECTED LITERATURE

Fabri, J., and Paulon, J., "Theory and Experiments on Supersonic Air-to-Air Ejectors," NACA TM 1410 (1958).

Fabri, J., and Siestrunck, R., "Supersonic Air Ejectors," _Advances in Applied Mechanics_, New York, N.Y., Academic Press, Vol. V, pp. 1-34 (1958).

Chow, W. L., and Addy, A. L., "Interaction between Primary and Secondary Streams of Supersonic Ejector Systems and their Performance Characteristics," AIAA Journal, 2(4):686-695 (1964).

Chow, W. L., and Yeh, P. S., "Characteristics of Supersonic Ejector Systems with Non-Constant Area Shroud," AIAA Journal, 3(3):525-527 (1965).

Korst, H. H., Addy, A. L., and Chow, W. L., "Installed Performance of Air-Augmented Nozzles Based on Analytical Determination of Internal Ejector Characteristics," Journal of Aircraft, 3(6): 498-506 (1966).

Addy, A. L., "The Analysis of Supersonic Ejector Systems," _Supersonic Ejectors_, AGARDograph No. 163, pp. 31-101 (1972).

Ginoux, J. J., Editor, _Supersonic Ejectors_, AGARDograph No. 163, 1972, 5 Papers.

Addy, A. L., and Mikkelsen, C. D., "An Investigation of Gas-Dynamic Flow Problems in Chemical Laser Systems," Department of Mechanical and Industrial Engineering, University of Illinois at Urbana-Champaign, Report No. UILU-ENG-74-4009 (1974).

Addy, A. L., "The Analysis of Supersonic Ejector Systems," _Ejectors_, von Karman Institute, Lecture Series 79 (1975).

Delery, J., "Methods d'étude des éjecteurs supersonique Application aus tuyéres double-flux," _Ejectors_, von Karman Institute, Lecture Series 79 (1975).

# An Experimental Study on the Mixing of

## Two-Dimensional Jets.

By

M.A. BADRI NARAYANAN.
&
S. RAGHU
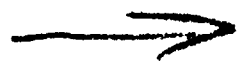
SUMMARY:

This paper deals with the experiments carried out on the mixing of a pair of two dimensional subsonic jets with different exit velocities placed adjacent to each other. The flow field downstream of the jets was investigated for its growth, for turbulent fluctuations and for the entrainment of mass. Some preliminary studies were also made on the spread of the jets due to artificial disturbances.

INTRODUCTION:

The performance of an ejector heavily depends on the mixing of primary and secondary flows. High rate of mixing enhances the efficiency of the ejector system which is required for achieving larger augmentation in thrust (Ref. 1,2,3). Mixing process in fluid dynamics is basically a turbulence phenomenon. The mechanism of turbulent mixing involves different scales of motion ranging from large scales comparable to the width of the mixing zone to micro

* Professor
- Experimental Fluid Dynamics

+ Graduate Student
  Both Department of Aeronautical Engineering
  Indian Institute of Science,
  Bangalore - 560 012.
  INDIA.

scales responsible for dissipation. In the case of an ejector the large scale motions play the significant role since they are primarily responsible for the transport of mass and momentum across the flow. Small scale mixing is a localised phenomenon and its involvement has different importance.

Brown et al (Ref.4) have observed that in free shear layers the large scale motions are orderly and coherent in nature and recent investigation by Wygnanski (Ref.5) further supports this view. Based on the above observation one is tempted to energise these large scale fluctuations in a selective manner to achieve greater momentum transfer across the flow. Platzer et al (Ref.6) and Hermann Viets (Ref.7) have recently shown that by the introduction of sinusoidal fluctuations at selected frequencies it is possible to enhance mixing appreciably in jets. In this tuned system the input energy is efficiently utilized. This selective pulsation may have applications in ejector technology as well.

The present investigation was aimed towards the study of the effect of velocity gradient on mixing process. A pair of two dimensional jets having different exit velocities was chosen for this purpose. The measurements consisted of mean as well as turbulent quantities in the mixing region for different jet exit velocity ratios ( $\frac{U_1}{U_2}$ ). Attention was focussed towards entrainment, growth of the mixing zone and the large scale structures. Attempts were made to enhance mixing by artificial means.

## Experimental Set-up:

The experimental set-up consisted of a pair of two dimensional

jets placed adjacent to each other as shown in figure.1. At the exit, the width of the jets was 2.5 cms and length 30 cms (aspect ratio 12). The flow in the mixing region was enclosed between two side plates kept parallel to each other to prevent expansion in the lateral direction. Both the jets were operated by a single blower powered by a 3 H.P. motor. In between the blower and the jets a large silencing chamber with a set of screens and two honey combs was incorporated to damp out the fluctuations produced by the blower and other flow disturbances. The velocity in one of the jets was controlled by introducing a suitable screen in its flow path. Four screens were employed which produced velocity ratios ( $\frac{U_1}{U_2}$ ) of 0.37, 0.53, 0.65, 0.87. The turbulence level at the exit was about 0.1%. The turbulent as well as mean velocities were measured using hot-wires All the electronic circuits for the above purpose were locally fabricated. For studying the instantaneous fluctuations the hot-wire traces were recorded using a continuous feed camera.

## Experimental Results:

The mean velocity profiles were measured at a number of stations downstream of the exit ($x/D = 1$ to 11) for the different values of $U_1/U_2$(1.0, 0.87, 0.65, 0.53, 0.37). Except for the case $U_1/U_2 = 1.0$ all the profiles were initially unsymmetric, however they became symmetric around $x/D = 8.0$ even for the smallest velocity ratio of 0.37 (Fig. 2,3.). In addition, the mean velocity profiles exhibited similarity at and beyond $x/D$ of 9.0 when plotted in the form $\frac{U}{U_m}$ versus $\frac{2y}{\delta.5}$ (Fig.4) and coincided with that of a two dimensional single turbulent jet under equilibrium conditions (Ref.8). The value of $\delta$.5 was chosen as the thickness of the jet corresponding to a velocity

equal to half that of the local maximum ($U_m$).

The growth of the jet (based on $\delta.5$) was slow to begin with but increased rapidly beyond $x/D \simeq 4$, linearly with x. Based on this linear behaviour, neglecting the initial region, the virtual origin ($x_0$) of the combined jets was estimated. $x_0$ varied from negative to positive values ranging from - 25 cms for $\frac{U_1}{U_2}$ = 1.0 to +7.6 cms for $\frac{U_1}{U_2}$ = 0.37, (Fig.5). The thickness of the boundary layer, at the exit, was about one millimeter on all the four walls.

The maximum velocity ($U_m$) of the jet varied linearly with $\sqrt{(x-x_0)}$ except in the vicinity of the exit and this trend was conspicious for the case $\frac{U_1}{U_2}$ = 0.37 (Fig.6), an altogether different behaviour from that of a two dimensional jet where $U_m$ is supposed to vary with $1/\sqrt{(x-x_0)}$. A plot of $U_m$ versus $1/\sqrt{(x-x_0)}$ is also shown in figure.6 for comparison.

Based on the mean velocity profiles the entrainment of mass was estimated (within permissible errors). For the case $\frac{U_1}{U_2}$ = 1.0 the entrainment ratio ( $\frac{m}{m_0}$ ) is around 2.0 (Fig.7) at $x/D$ of 12 and 2.8 for $\frac{U_1}{U_2}$ = 0.37 at the same location, $m_0$ and m being the mass flow rates at x=0 and x respectively. This result clearly indicates that the initial shear has significant effect on mixing.

The longitudinal velocity fluctuations ( $\tilde{u} = \sqrt{\overline{u'^2}}$ ) were measured at many x locations for all the cases and the results showed (Figs.8&9) that $\tilde{u}'$ profiles do not reach similarity conditions even at large values of $x/D$. The $\tilde{u}'$ distribution exhibited two distinct peaks with the turbulence intensities higher for $\frac{U_1}{U_2}$ = 0.37 than for $\frac{U_1}{U_2}$ = 1.0. Similar trend was observed with $\overline{u'v'}$ (Fig.11) but the $\tilde{v}'$ profile did

not exhibit the two peaks (Fig.10).

The correlations $R_{uu}$ (Z) in the lateral direction (Z) was measured at $x/D = 9$ for the case $\dfrac{U_1}{U_2} = 0.37$. $R_{uu}$ rapidly decreased to zero within a distance ($\triangle Z$) of 40 mm, however this trend was reversed when the high frequency part of the hot wire signals was filtered. At low frequencies the correlation was 0.2 even beyond $\triangle Z=180$ mm (Fig. 12&13). This result if of great significance (Ref.4) since it suggests that the large scale fluctuations maintain their two dimensinnality, as well as orderly motion for considerable distances, downstream of their origin.

Some preliminary attempts were made to identify the large scale structures from the hot-wire signals. A single inclined hot-wire ($45^{\circ}$) was employed for this purpose, since it is sensitive to both u' as well as v' fluctuations. The hot-wire signals were recorded on a 35 mm film using a continuous feed oscilloscope camera. A low pass filter was employed to remove the unwanted high frequency noise like signals. Only signals between 4 to 600 cycles/sec were recorded. From the oscilloscope traces the large scale structures were counted. These experiments were carried out along the center line for $\dfrac{U_1}{U_2} = 0.37$ at few x stations. The frequency of occurance of the large scale structures f, was found to be nearly constant all along x and the value was around 170 per second in this experiment,(Fig.14) the nondimensional strouhal number ( $\dfrac{fD}{U_m}$ ) being equal to 0.16 approximately

Attempts were made to increase the spread of the jet as well as the entrainment of mass using artifical disturbances. The disturbances were produced by the vortex shed by two circular rods 2 mm

in diameter placed in the flow near the end of the dividing plate as
shown in figure 15. In this experiment only the mean velocities were
measured. Analysis of the results indicated the following trends:
(a) The width of the jet increased appreciably. However the virtual
origin ($x_0$) did not change from that of the undisturbed flow the
values of $x_0$ being 25 cms and 24.9 cms for the undisturbed and
disturbed cases respectively. The growth of the jet was linear
(Fig.5) except near the exit and the increase in the spread was
larger by a factor of about 1.5.
(b) The enhancement in entrainment rate was about 20% greater than
the undisturbed case (Fig.7).

When the above experiment was conducted for the case $\dfrac{U_1}{U_2} = 0.37$
the increase in entrainment was negligible when compared to the
corresponding undisturbed flow.

CONCLUSIONS:

(1) The spread as well as the entrainment ratio of a two-dimensional
subsonic jet can be increased appreciably by introducing shear in the
flow. Similar results could also be obtained with artificial disturbances.

References:

1. McCormick B.W.                   Aerodynamics of V/STOL Flight
                                    Academic Press, New York, London
                                    (1967).

2.  Qwinn.B.                    Compact ejector Thrust Augmentation.
                               J. of Aircraft Vol. 10, No.8.
                               August (1973).

3.  Bevilaque P.M.             Analytical Description of Hypermixing
                               and Test of an Improved Nozzle. J. of
                               Aircraft Vol. 13, No.1, Jan. (1976).

4.  Brown,G.L.Roshko.A.        On Density Effects and Large Struc-
                               ture in Turbulent Mixing Layers J.
                               Fluid Mech, 64. 175 (1974).

5.  Wygnanski et al            On the Preservance of a Quasi-Two-
                               Dimensional Eddy-Structure In a
                               Turbulent Mixing Layer J.Fluid Mech.
                               Vol. 93. Part.2.(1979).

6.  M.F.Platzer               Entrainment characteristics of
    J.M. Simmons               Unsteady subsonic Jets AIAA Journal
    & K. Bremhort              (Technical note) vol.16 No.3 March
                               1978.

7.  Viets.H.                  Flip-Flop Jet Nozzle AIAA Journal,
                               Vol.13, October 1975 PP 1375-1379.

8.  Schlichting.H.            Boundary Layer Theory, Pergamon
                               Press. 1955. New York. London Paris.
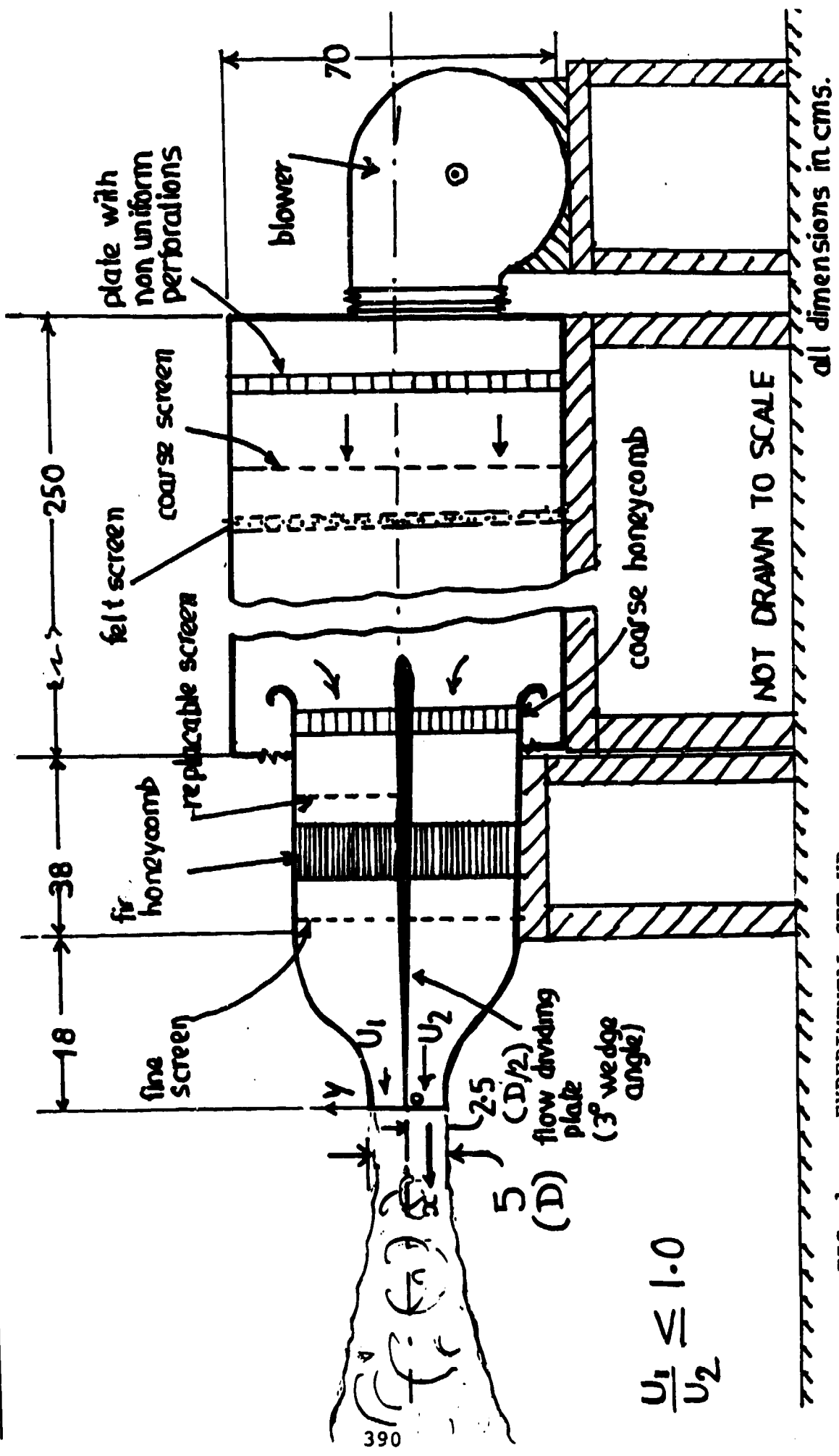
FIG. 1. EXPERIMENTAL SET-UP
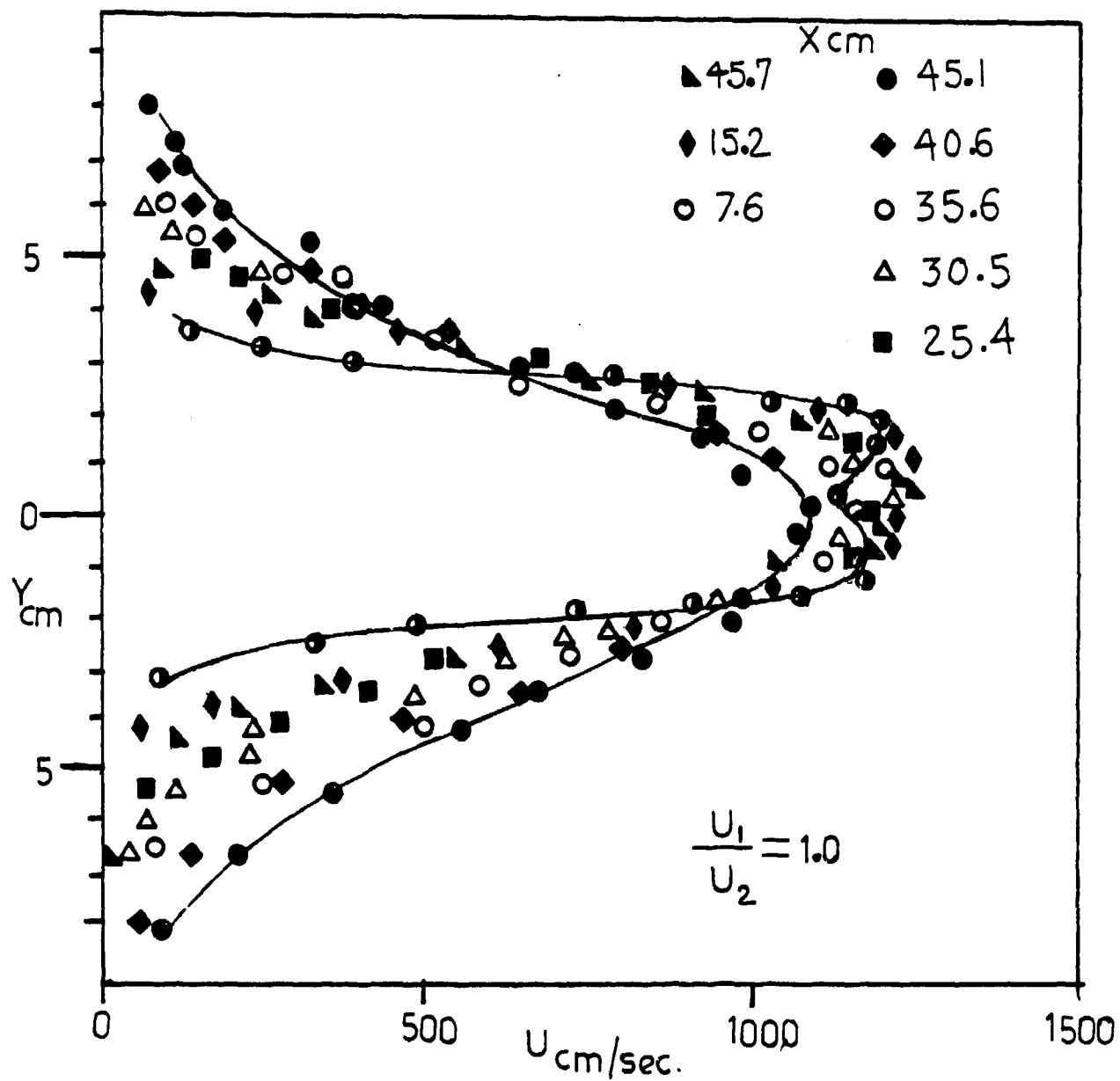
FIG. 2.    MEAN VELOCITY PROFILE $\frac{U_1}{U_2} = 1.0$
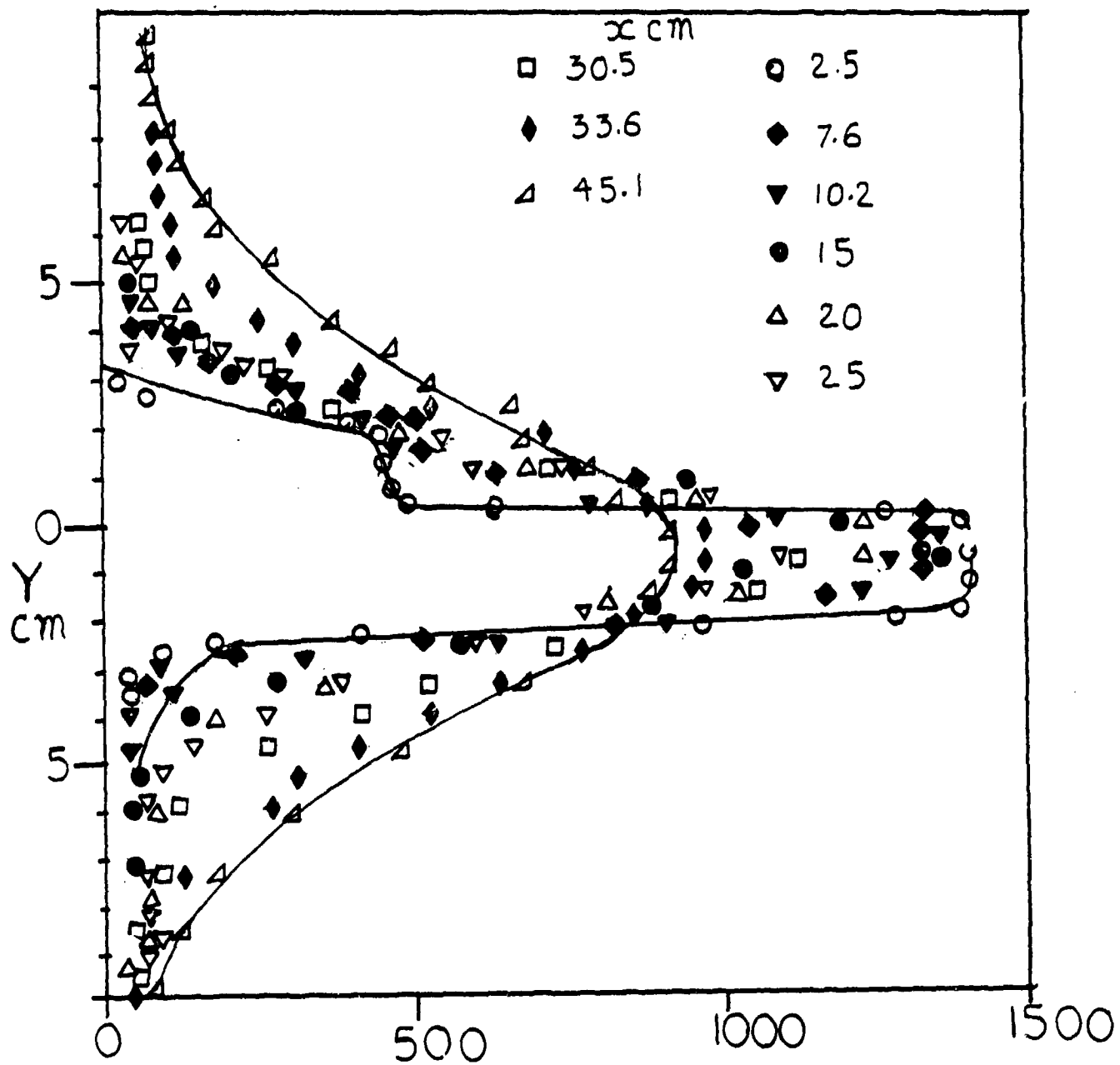
FIG. 3.    MEAN VELOCITY PROFILE $\dfrac{U_1}{U_2} = 0.37$
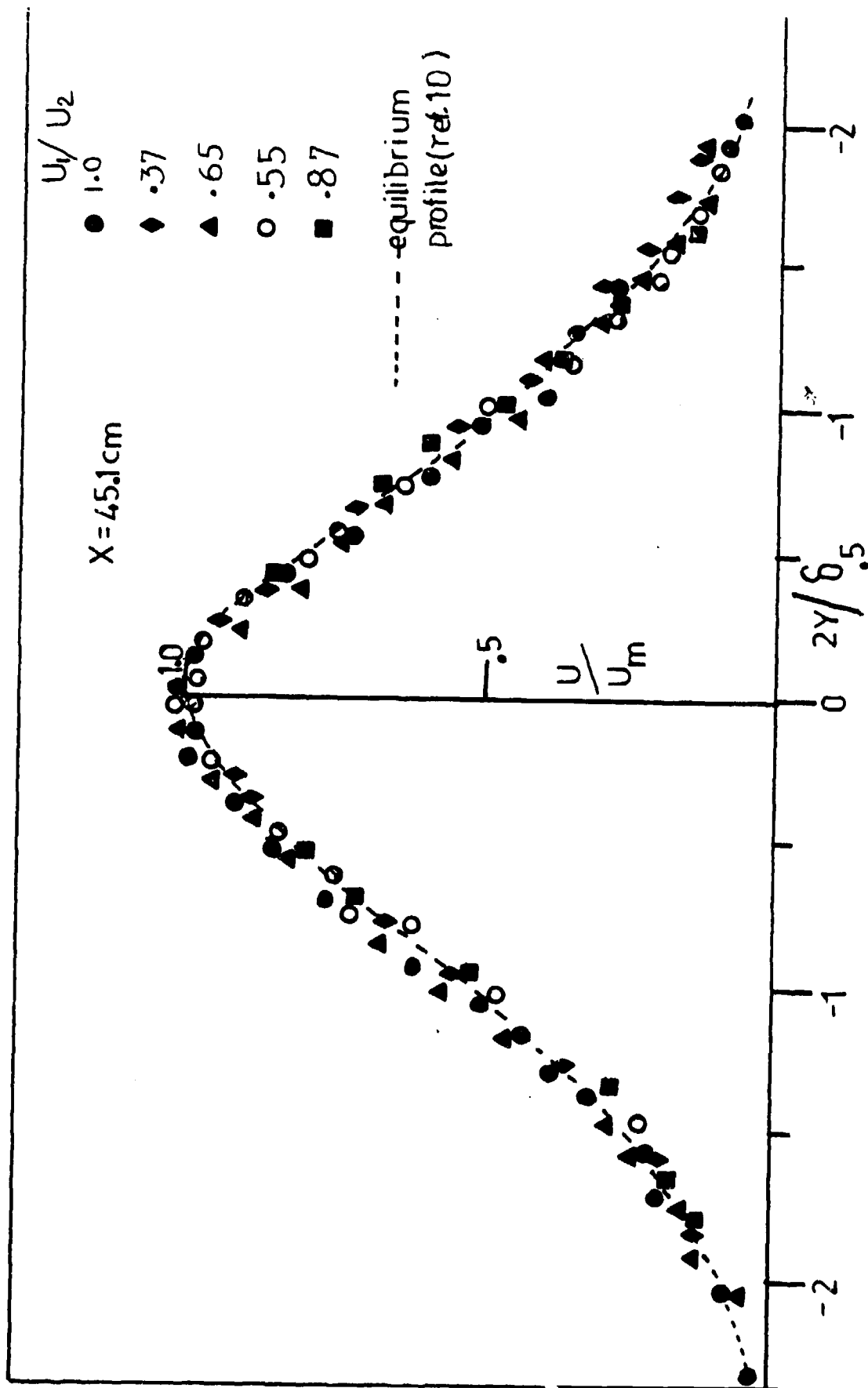
FIG. 4. SIMILARITY OF THE MEAN VELOCITY PROFILES
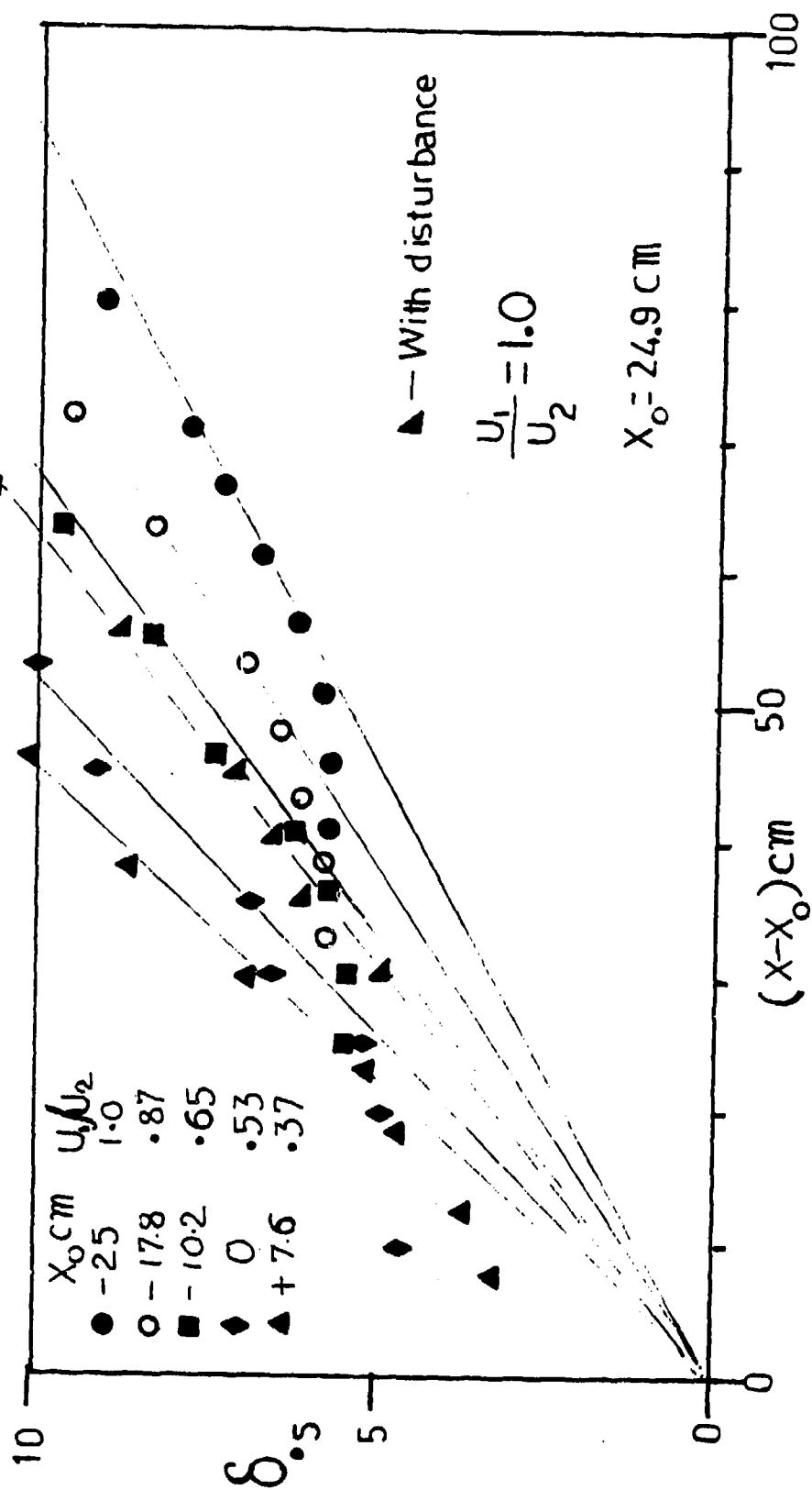
FIG. 5.    GROWTH OF THE JET WIDTH
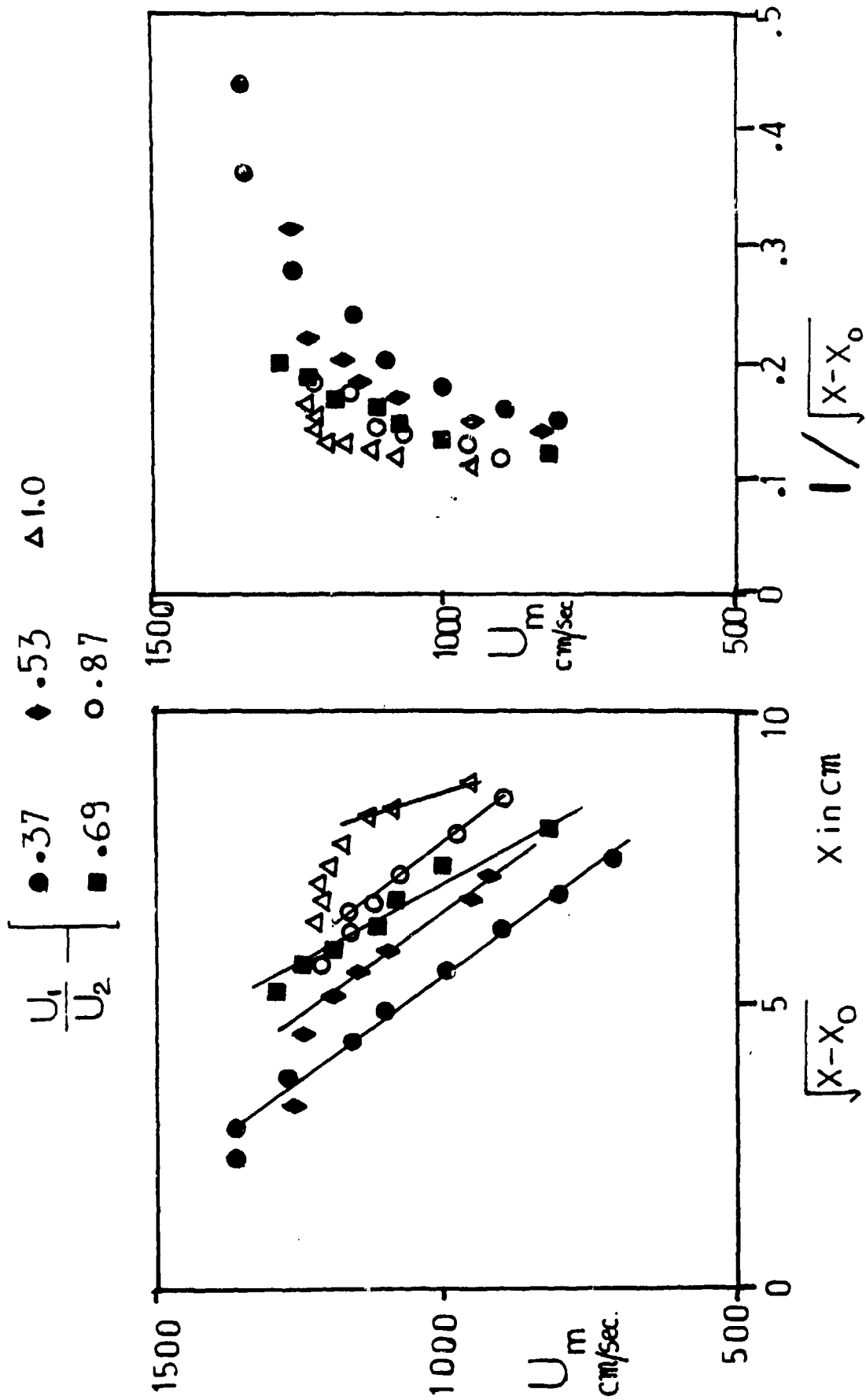
FIG. 6. VARIATION OF THE MAXIMUM VELOCITY ALONG THE JET
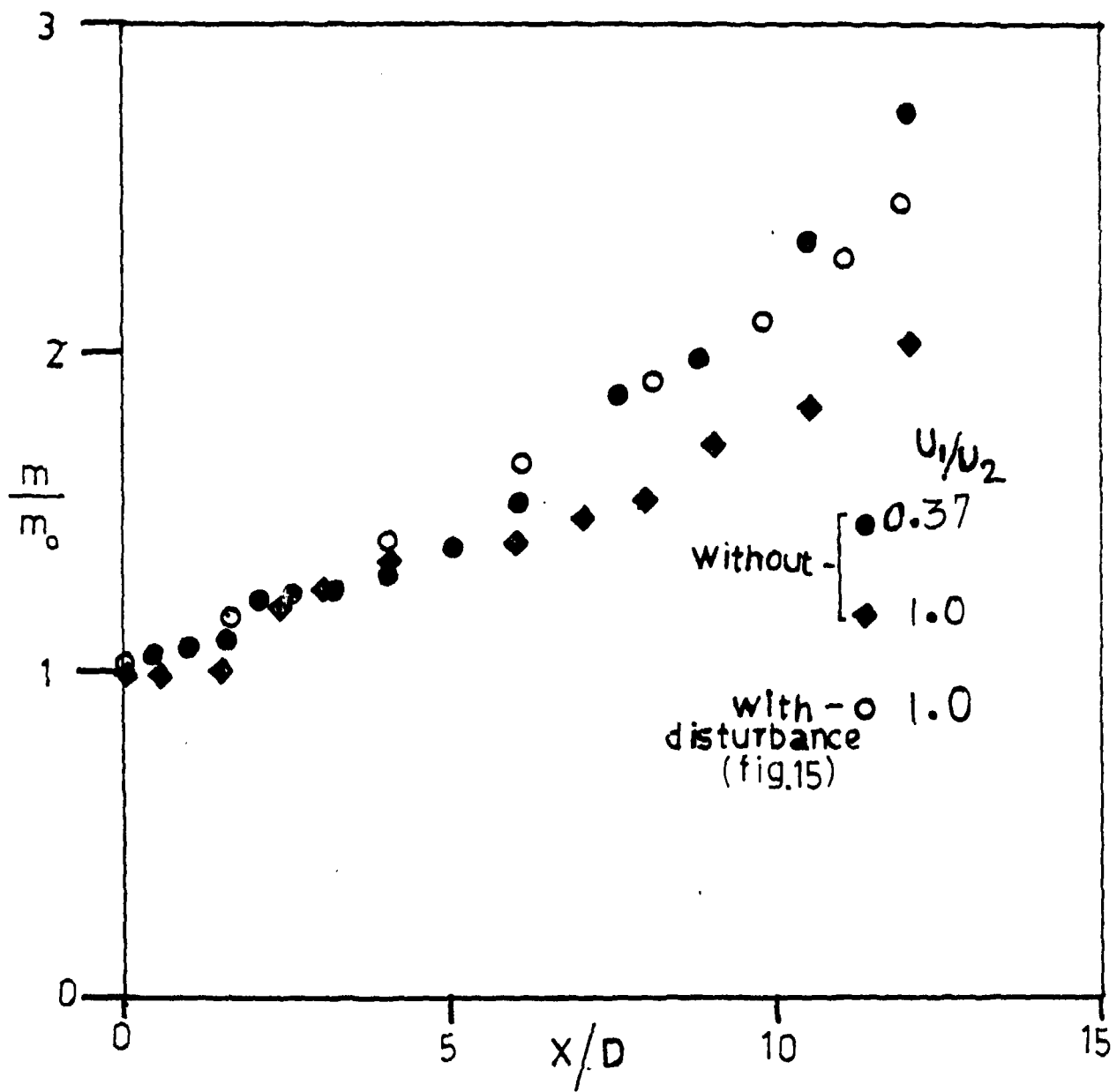
FIG. 7.    ENTRAINMENT RATIO
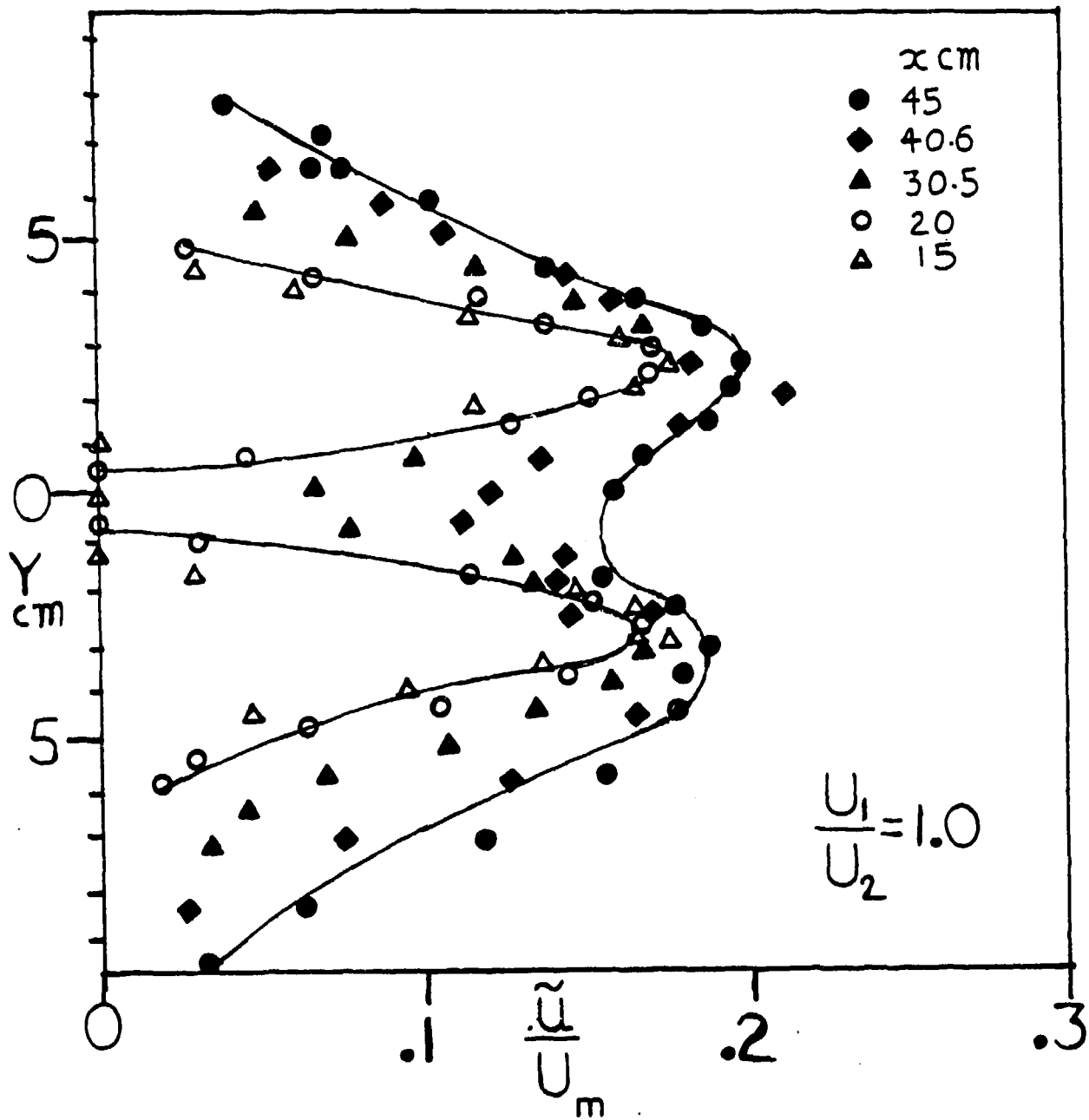
FIG. 8.    LONGITUDINAL VELOCITY FLUCTUATIONS ( $\frac{U_1}{U_2} = 1.0$ )
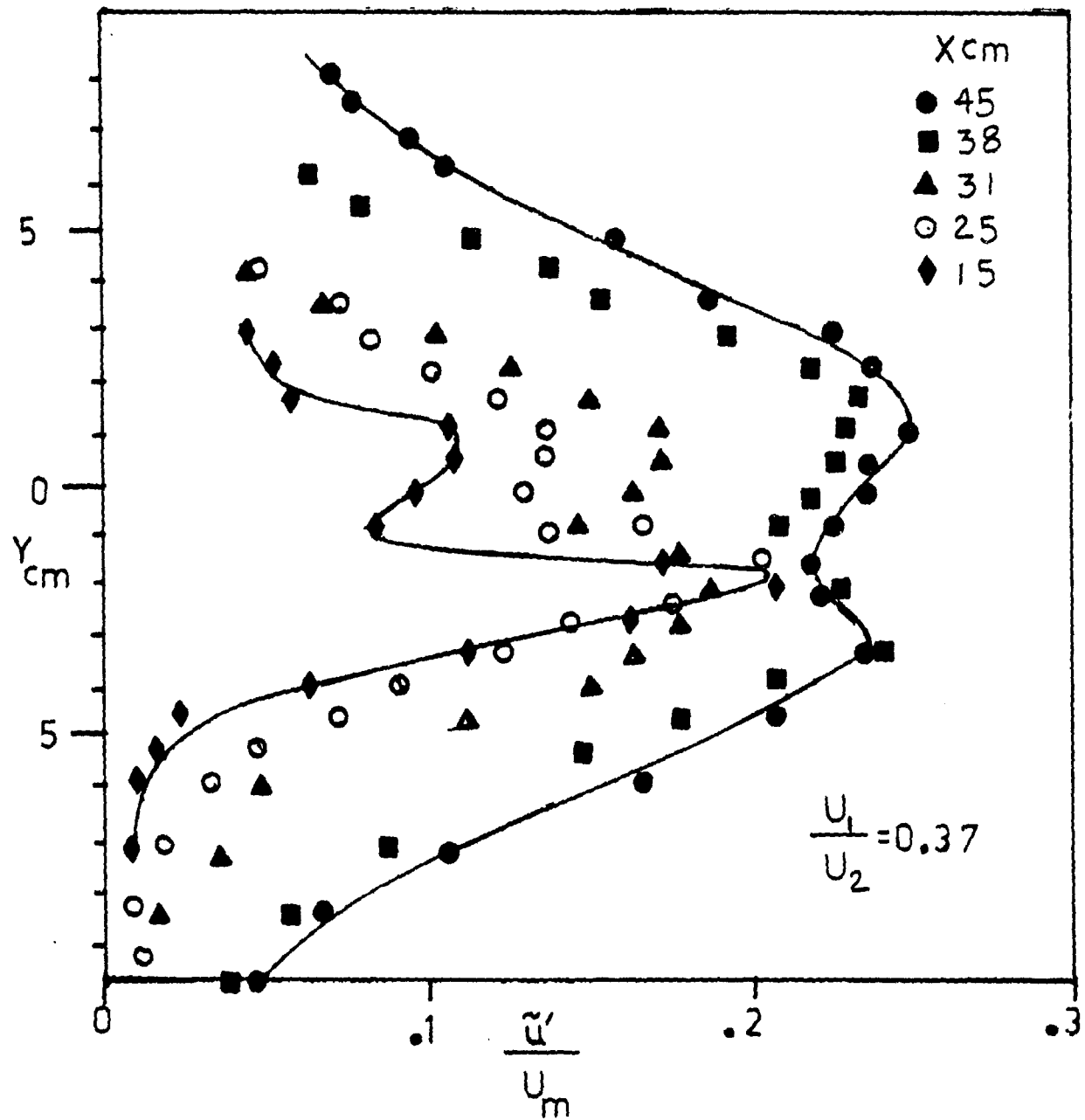
FIG. 9.    LONGITUDINAL VELOCITY FLUCTUATIONS ( $\frac{U_1}{U_2}$ = 0.37 )
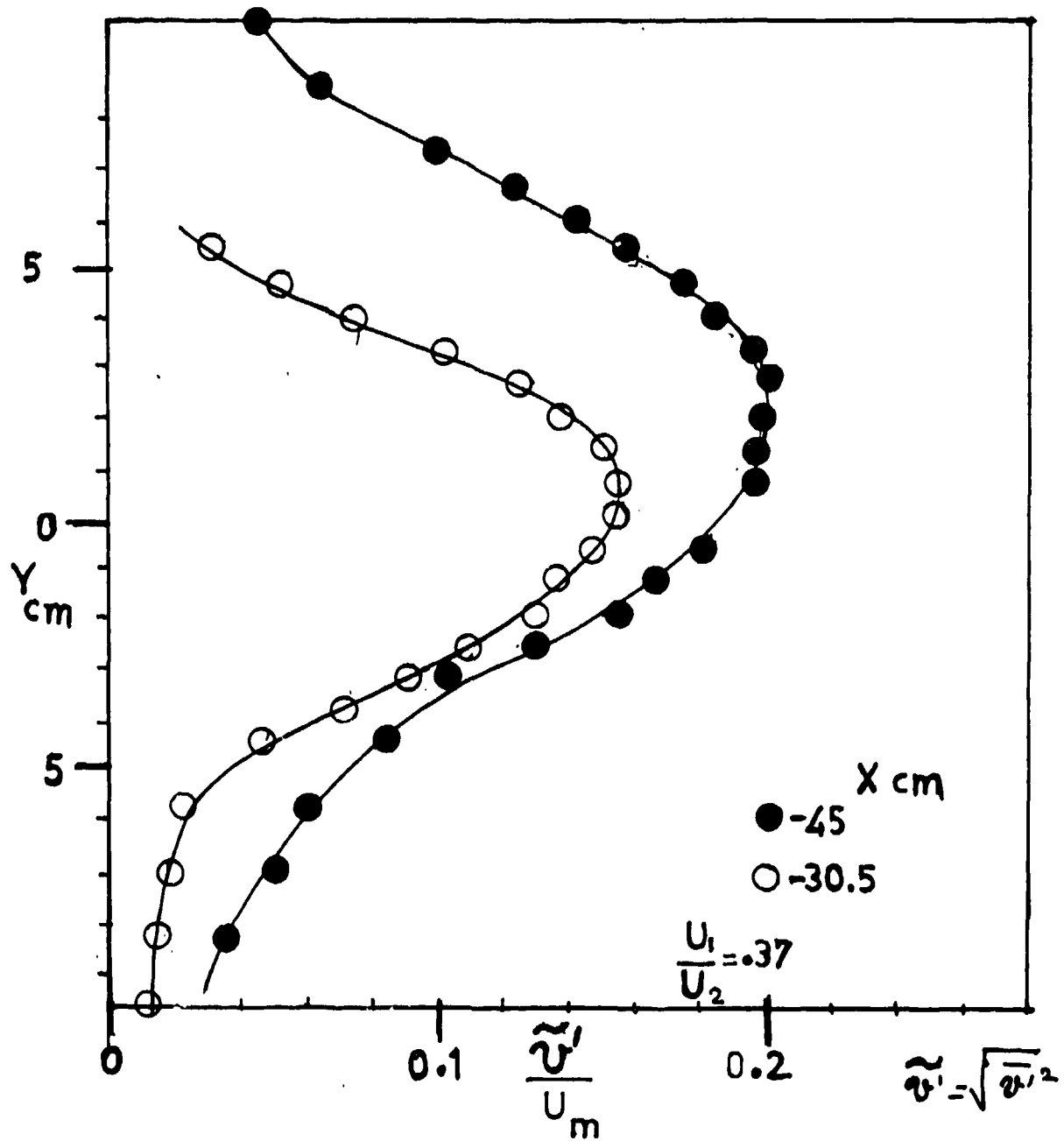
FIG.10. DISTRIBUTION OF THE VERTICAL VELOCITY FLUCTUATIONS ACROSS THE JET

400
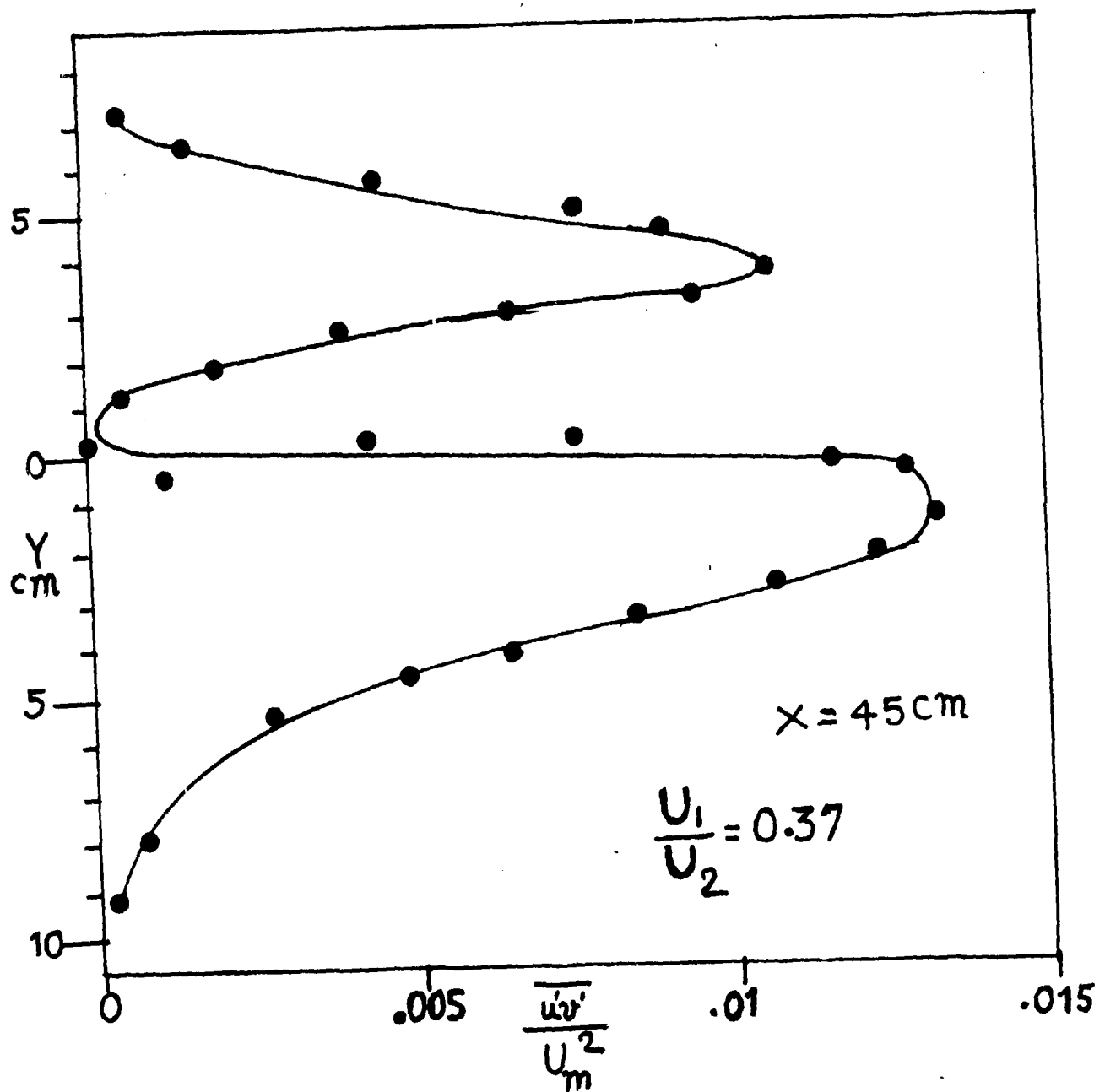
FIG.11. DISTRIBUTION OF REYNOLDS STRESS ACROSS THE JET

401
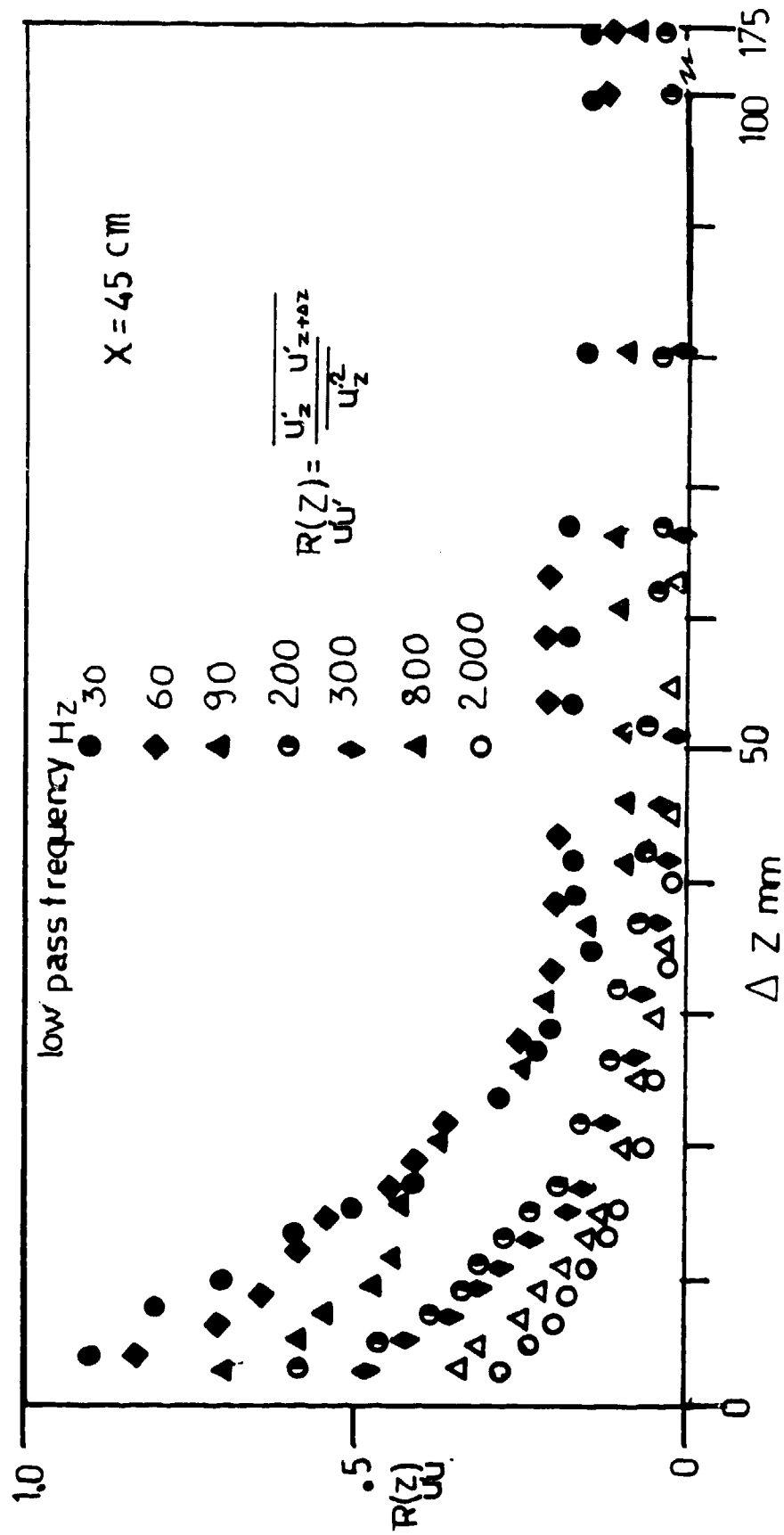
FIG. 12. CORRELATION AT DIFFERENT FREQUENCIES

402
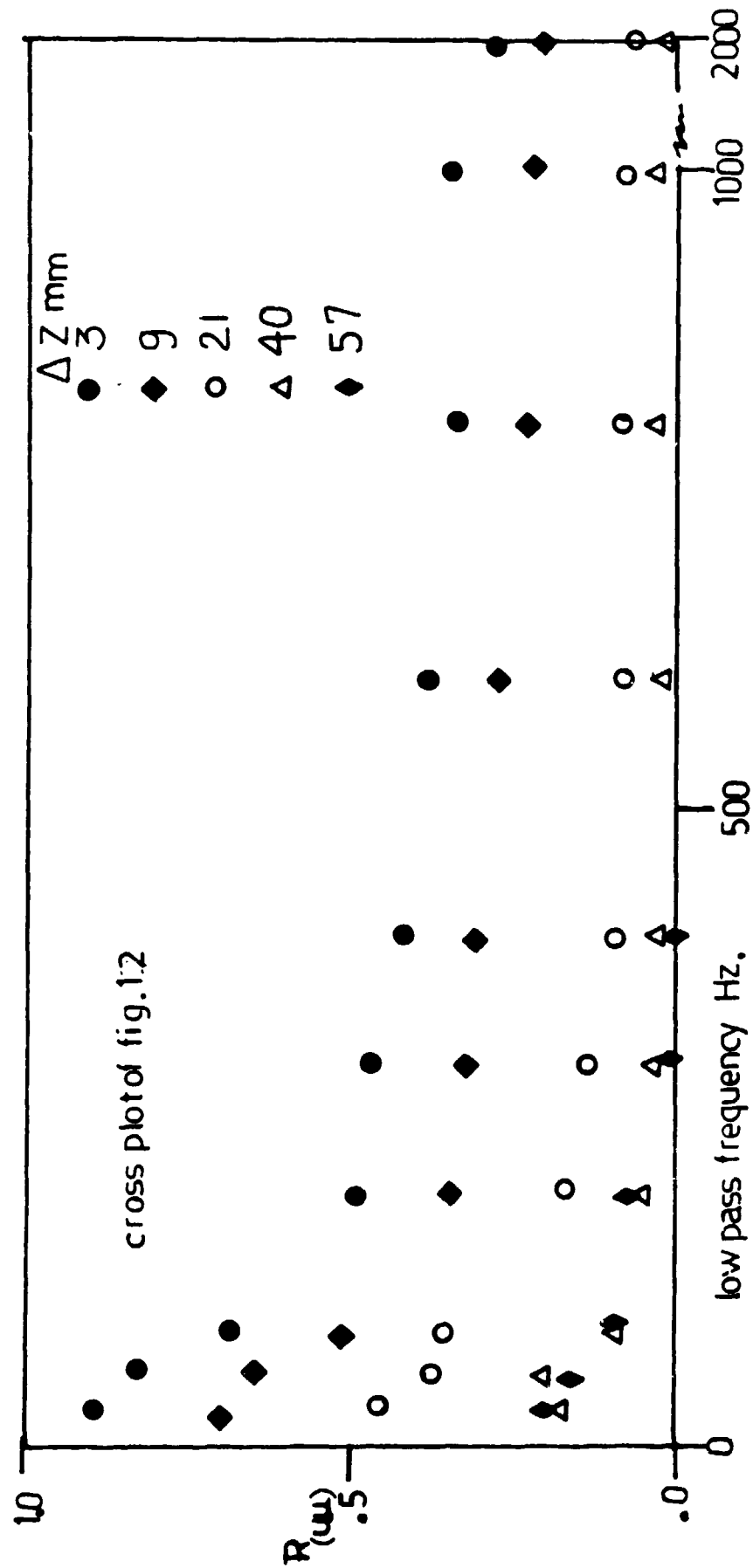
FIG. 13. VARIATION OF CORRELATION FOR A GIVEN Δz, WITH FREQUENCY

FIG. 14  HOT WIRE SIGNALS AT VARIOUS DISTANCES (X) ALONG THE CENTER LINE

NUMBER OF FLUCTUATIONS IN THIS TRACE.

X cm

1.5 → 67

15 → 65

25 → 72

38 → 70

45 → 75

Y=0

$U_2 \simeq 1200 \ Cm/sec$    $\dfrac{U_L}{U_2} \approx 37$    $f = 170/sec$

500 Hz
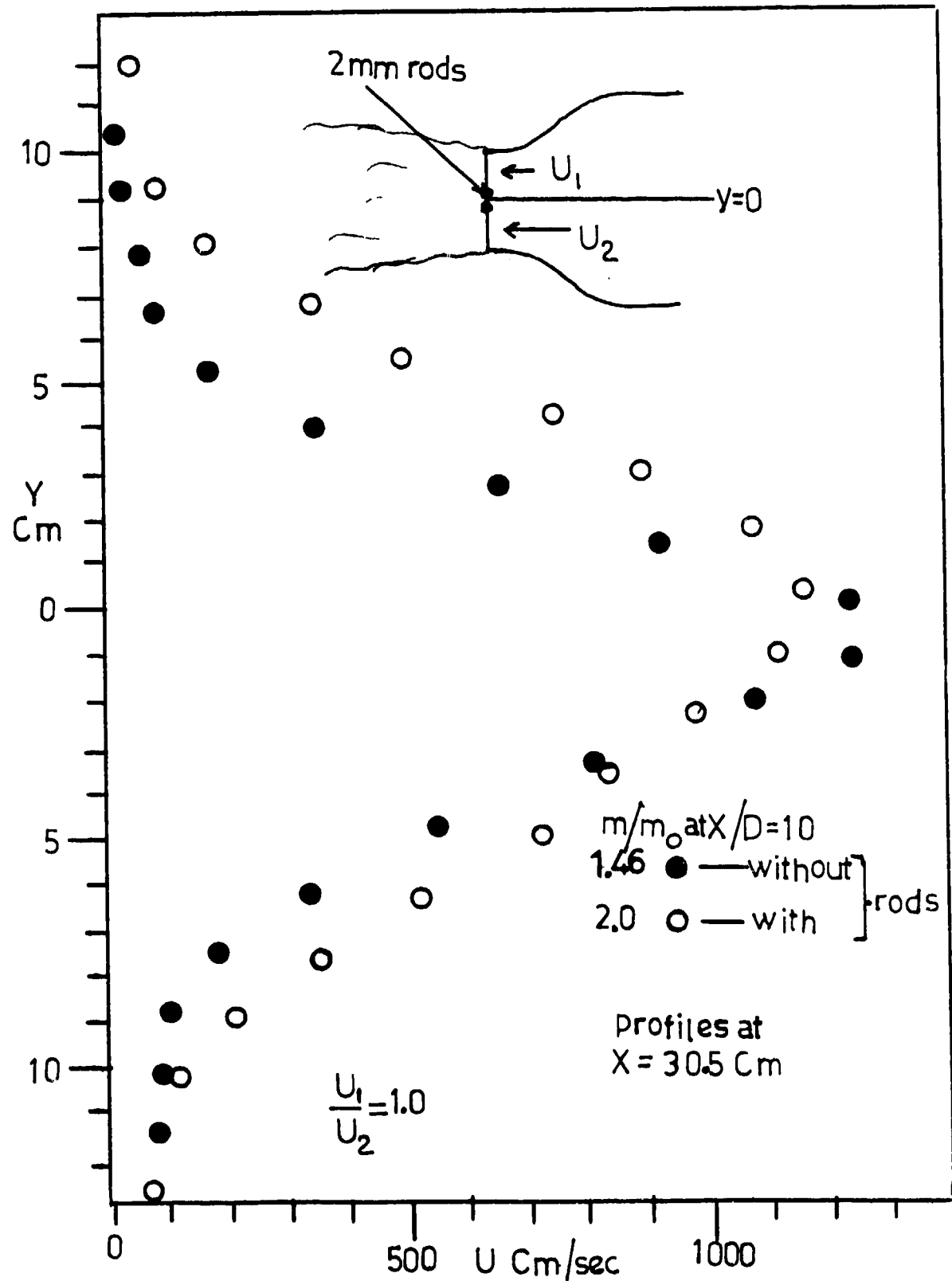
FIG. 15. MEAN VELOCITY PROFILES WITH AND WITHOUT RODS

405

# THEORETICAL PERFORMANCE LIMITS FOR NON-STATIC
# EJECTOR THRUST AUGMENTORS

James S. Petty
Air Force Aero Propulsion Laboratory
Air Force Wright Aeronautical Laboratories
Wright-Patterson Air Force Base, OH 45433

# FOREWORD

The study reported herein was undertaken as the result of several conversations with Dr. Hans J. P. von Ohain, then Chief Scientist of the Air Force Aero Propulsion Laboratory.

The effort was conducted in-house in the Air Force Aero Propulsion Laboratory, Air Force Systems Command, Wright-Patterson Air Force Base, Ohio, under Project 3066, Task 06, Work Unit 02 by Dr. James S. Petty (AFWAL/POTC) during the period February 1979 through September 1979. The author submitted the report in November 1979.

The author wishes to express his gratitude to Dr. von Ohain and to Drs. Kervyn D. Mach (AFWAL/POTC) and K. S. Nagaraja (AFWAL/FIMM) for their comments and suggestions. Special appreciation is due to Mrs. Carla Morter for typing this report.

The paper is included in the workshop proceedings because the results of the effort reflect new ideas on ejector performance domains in a range of flight Mach numbers of interest. Although the author did not present the paper in the workshop, the paper is included here as it strikes new ground, thereby extending the state-of-the-art of ejector technology. The paper is also published as an AFWAL technical report bearing the number AFWAL-TR-79-2120.

PRECEDING PAGE BLANK-NOT FILMED

# ABSTRACT

An analytical study was performed to determine the theoretical limits on the performance of non-static ejector thrust augmentors. Idealizing assumptions were made, such as inviscid compressible working fluids, isentropic flows in inlets, diffusers, nozzles and ducts, constant pressure mixing, and thermally and calorically perfect fluids. By ignoring details of the primary flow "pump", the performance of ejector augmentors was found in terms of three parameters (the secondary/primary mass flow ratio, a pressure parameter and a temperature parameter) in a form which was not an explicit function of the flight Mach number. It was also shown that multi-stage ejectors offered no performance improvement over ideal single-stage ejectors. Two primary "pump" devices, a turbine engine gas generator and an isentropic compressor, were considered. With them, the Mach number dependent behavior of ideal ejectors was determined. As a result of this study, the following conclusions were drawn: 1) The performance of ideal ejector is severely degraded by increasing the primary fluid temperature; 2) The performance of ideal ejectors is degraded faster than that of ideal turbofans as the flight Mach number is increased; 3) Neither the turbine engine nor the isentropic compressor is a suitable "pump" for ideal ejectors, except at very low Mach numbers, 4) Ejector augmentors should be most useful for low flight speed applications, e.g., V/STOL.

TABLE OF CONTENTS

412

# LIST OF ILLUSTRATIONS

413

LIST OF SYMBOLS

| SYMBOL | QUANTITY |
|--------|----------|
| $C_p$ | specific heat at constant pressure |
| $f$ | specific thrust, $F/\dot{m}_p u_\infty$ |
| $F$ | thrust |
| $h$ | enthalpy, $C_p T$ |
| $\tilde{h}$ | nondimensional temperature or enthalpy, $T/T_\infty$ |
| $M$ | Mach number |
| $\dot{m}_p$ | primary or core mass flow rate |
| $p$ | pressure |
| $s$ | entropy |
| $T$ | absolute temperature |
| $u$ | velocity |
| $\tilde{u}$ | nondimensional velocity, $u/h_\infty^{1/2}$ |
| $\alpha$ | turbine engine compressor parameter (Page 15) |
| $\beta$ | secondary/primary mass flow ratio (bypass ratio) |
| $\gamma$ | ratio of specific heats |
| $\Delta\tilde{h}_c$ | nondimensional combustor temperature rise |
| $\Delta T_c$ | combustor temperature rise |
| $\Delta s$ | difference of entropy variables |
| $\zeta$ | mixing pressure parameter, $(1-\frac{1}{\pi_m})/(1-\frac{1}{\pi_{ts}})$ |
| $\mu$ | temperature parameter, $(T_{ts}/T_{tp})^{1/2}$ |
| $\nu$ | pressure parameter, $(1-\frac{1}{\pi_{ts}})^{1/2}/(1-\frac{1}{\pi_{tp}})^{1/2}$ |
| $\xi$ | mass flow fraction (Page 9) |
| $\pi$ | nondimensional pressure variable, $(p/p_\infty)^{\frac{\gamma-1}{\gamma}}$ |
| $\phi$ | augmentation ratio, $f/f_{\beta=0}$ |

SUBSCRIPTS

| | |
|--|--|
| a | at ambient pressure |
| c | compressor exit condition (except in $\Delta\tilde{h}_c$ and $\Delta T_c$) |
| e | in the exhaust |
| ej | ejector |

414

| SYMBOL | QUANTITY |
|---|---|

SUBSCRIPTS

| | |
|---|---|
| isen | isentropic compressor |
| m | at or in the mixer |
| p | primary (core) flow (except in $C_p$) |
| s | secondary (bypass) flow |
| t | first subscript - stagnation (total) condition |
| | second subscript - at the turbine inlet |
| tf | turbofan |
| $\infty$ | ambient static (freestream) condition |

SUPERSCRIPTS

| | |
|---|---|
| * | optimum |
| (i),(n),(N) | stage number (multi-stage ejector) |

# SECTION I

## INTRODUCTION

### 1. BACKGROUND

The idea of using ejector devices to obtain thrust augmentation for gas turbine engines is not new. However, it has received increased attention during the past decade or so, due in part to the significant advances which have been realized in the design and performance of static (stationary) ejector augmentors.

In his 1966 paper[1], Heiser reported on an analytic study of thrust augmentation, in which he used a few basic assumptions and the conservation laws. His analysis of ejector augmentors was limited to static devices with constant area mixers and incompressible flows. He showed that, except for small bypass ratios (secondary/primary mass flow ratio), the thrust augmentation ratios attainable by ejectors were considerably less that those of ideal thrust augmentors, and were limited to values of less than two.

In an earlier note[2], Knox briefly discussed the optimum performance of the nonstationary, constant pressure mixing ejector augmentor. His results indicate that potential performance is possible which is considerably better than Heiser's predictions. The only flaw we find with Knox's results is that he did not consider the primary (high pressure) fluid to have been collected from the atmosphere, and hence, did not include its contribution to the ram drag.

In this study, we have sought to ascertain the theoretical limits of performance for nonstationary ejector augmentors, compared with those of turbofan engines. To do this, we have essentially re-derived and extended Knox's results by also examining turbofans, multistage ejectors and various "pump" devices.

Using an aerothermodynamic cycle analysis, the performance of the ideal ejector augmentor is examined without making any assumptions about the primary "pump" device which supplies the high pressure working fluid. Both single and multiple stage ejectors are considered. The ideal mixed-flow turbofan is also analyzed for comparison. Finally, the influences of two "pump" devices - an isentropic compressor and a turbine engine gas generator are addressed.

## 2. ASSUMPTIONS

In order to make our analysis ideal (and tractable), we have made a number of assumptions about the working fluids and the thrust augmenting devices:

- Perfect gases - Both the primary and secondary gasses are calorically and thermally perfect, and both have the same value for $\gamma$, the ratio of the specific heats.

- Inviscid, compressible flow - Both the primary and secondary flows are inviscid and compressible.

- Uniform flows - All flow fields are uniform in the direction normal to the flow direction, e.g., no transverse pressure gradients.

- Isentropic or adiabatic processes - All flows in inlets, diffusers, nozzles, ducts, compressors and turbines are isentropic; i.e., no shock losses, or skin friction or heat transfer losses. All mixing processes are adiabatic; i.e., no skin friction or heat transfer losses.

- Constant pressure mixing - All mixing processes occur at constant pressure.

These assumptions generally produce performance estimates for thrust augmentation devices which are greater than those

418

physically attainable, and thus, can serve as optimistic
upper bounds for performance. The possible exception is the
assumption of perfect gases. We will not, however, address
the effects of thermal and caloric imperfections on ejector
performance.

## 3. DESCRIPTION OF AN IDEAL EJECTOR AUGMENTOR

Figure 1* is a schematic sketch of an ideal ejector
augmentor with a temperature-entropy (T-S) diagram for the
ejector cycle assuming complete mixing of the primary and
secondary flows. The operation of the ejector augmentor may
be described as follows:

Ambient air is captured by the inlet and isentropically
diffused to stagnation conditions. On the T-S diagram,
this is represented by the vertical line from $(p_\infty, T_\infty, s_\infty)$
to $(p_{ts}, T_{ts}, s_\infty)$.

A portion of this diffused flow is then pumped by some means
to the primary reservoir conditions $(p_{tp}, T_{tp}, S_p)$. The
remainder of the captured flow forms the secondary, or bypass,
flow. The mass fractions of the captured air in the primary
and secondary flows are $\frac{1}{1+\beta}$ and $\frac{\beta}{1+\beta}$, where $\beta$ is the secondary/
primary mass flow ratio (bypass ratio).

The primary and secondary flows are expanded through nozzles
to some mixing pressure $p_m$. This is represented on the T-S
diagram by the vertical lines from the primary and secondary
reservoir conditions down to the mixing pressure isobar.

The two flows are completely mixed adiabatically at constant
pressure, as represented by the lines along the $p_m$ isobar to
the mixed flow isentrope.

---

*All illustrations appear at the end of this report.

The mixed flow is then expanded or diffused, as required, through the exhaust nozzle to ambient pressure. We consider this to be a two-step process; the first step being the isentropic recovery of the flow to stagnation conditions $(p_{tm}, T_{tm}, s_m)$, and the second step being the isentropic expansion of the stagnant flow to ambient pressure. This is represented on the diagram by moving vertically along the mixed flow isentrope upward to the mixed flow total temperature isotherm and then downward to the ambient pressure isobar.

## SECTION II

## IDEAL CYCLE ANALSES

1. EQUATION OF STATE

For convenience in the following analyses, we will use a modified form of the equation of state with nondimensional enthalpy, entropy and pressure variables. Since the gas is assumed to be thermally and calorically perfect, the temperature, pressure and entropy are related by the equation.[3]

$$T/T_\infty = (p/p_\infty)^{\frac{\gamma-1}{\gamma}} e^{(s-s_\infty)/C_p}$$

where $(\ )_\infty$ refers to ambient conditions. Defining the nondimensional variables

$$\hbar = T/T_\alpha$$
$$\pi = (p/p_\alpha)^{\frac{\gamma-1}{\gamma}}$$
$$\sigma = e^{(s-s_\infty)/C_p}$$

the equation of state which we use is obtained:

$$\hbar = \pi\sigma$$

Since $h/h_\infty = T/T_\infty$ for a calorically perfect gas, $\hbar$, is also the nondimensional specific enthalpy. These variables have the minor advantage that constant pressure, temperature and entropy curves in a T-S diagram are all straight lines on the equivalent $\hbar$-s diagram.

In the remainder of this Section, when we refer to temperature (or enthalpy), entropy or pressure, we mean the equivalent non-dimensional variable, $\hbar$, $\sigma$ or $\pi$, unless otherwise specified.

## 2. EJECTOR AUGMENTOR (SINGLE STAGE)

The analysis of the single stage ejector augmentor cycle shown in Figure 1 is relatively straightforward. Given the total conditions ($\hbar_{tp}$, $\pi_{tp}$, $\hbar_{ts}$, $\pi_{ts}$) of the primary and secondary flows and the mixing pressure $\pi_m$, the primary and secondary static enthalpies ($\hbar_{mp}$, $\hbar_{ms}$) at the entrance to the mixer are determined, and hence, the primary and secondary mixing velocities:

$$\hbar_{mp} = \hbar_{tp}\pi_m/\pi_{tp} \tag{1}$$

$$\tilde{u}_p^2 = 2(\hbar_{tp} - \hbar_{mp}) \tag{2}$$

etc., where $\tilde{u} = u/h_\infty^{\frac{1}{2}}$ is a nondimensional velocity. The mixing process itself is described globally by the conservation of energy and momentum. Since the mixing is assumed to be adiabatic and inviscid, the conservation of energy gives

$$(1 + \beta)\ \hbar_{tm} = \hbar_{tp} + \beta\hbar_{ts} \tag{3}$$

where $\beta$ is the secondary/primary mass flow ratio. Under the assumption of constant pressure mixing and inviscid flow, the pressure and viscous terms drop out of the momentum equation, and the conservation of momentum gives simply

$$(1 + \beta)\ \tilde{u} = \tilde{u}_p + \beta\tilde{u}_s \tag{4}$$

At the end of the mixing zone, the static enthalpy and entropy are given by

$$\hbar_m = \hbar_{tm} - \tfrac{1}{2}\ \tilde{u}_m^2 \tag{5}$$

$$\sigma_m = \hbar_m/\pi_m \tag{6}$$

Finally, the expansion of the mixed flow through the exhaust nozzle to ambient conditions gives the exhaust velocity

$$\tilde{u}_e = \sqrt{2} \ (\hbar_{tm} - \hbar_{am})^{\frac{1}{2}}$$

$$= \sqrt{2} \ (\hbar_{tm} - \pi_\infty \sigma_m)^{\frac{1}{2}}$$

$$= \sqrt{2} \ (\hbar_{tm} - \sigma_m)^{\frac{1}{2}} \qquad (7)$$

(the latter because $\pi_\infty = 1$), and the specific thrust ($f = F/\dot{m}_p u_\infty$)

$$f = (1 + \beta)(\tilde{u}_e/\tilde{u}_\infty - 1) \qquad (8)$$

In this equation for the specific thrust, we assume that both the primary and secondary fluids consist of captured ambient air, and hence, contribute to the ram drag.

The solution of these equations is relatively straight-forward. However, we are not particularly interested in the solution for arbitrary mixing pressures, but only in the solution at the mixing pressures which maximize the specific thrust.

As can be seen from examination of Equations (7) and (8), the specific thrust is maximized by minimizing the entropy $\sigma_m$ of the mixed flow. With a little algebraic manipulation of Equations (1) through (6), the entropy of the mixed flow can be expressed as

$$\sigma_m = \frac{\hbar_{tm}}{\pi_m} - \frac{1}{(1 + \beta)^2} \left[ (\frac{\hbar_{tp}}{\pi_m} - \sigma_p)^{\frac{1}{2}} + \beta(\frac{\hbar_{ts}}{\pi_m} - \sigma_s)^{\frac{1}{2}} \right]^2 \qquad (9)$$

Taking the derivative of this equation with respect to $\pi_m$, setting it equal to zero and solving for $\pi_m$, we obtain the following solutions for the optimum mixing pressure:

$$\pi_m^* = (\hbar_{tp} - \hbar_{ts})/(\frac{\hbar_{tp}}{\pi_{ts}} - \frac{\hbar_{ts}}{\pi_{tp}}), \ \frac{\hbar_{tp} - \hbar_{ts}}{\sigma_p - \sigma_s} \qquad (10)$$

Examination shows that the first solution has the minimum entropy if $\hbar_{tp} \geqslant \hbar_{ts}$ and $\pi_{tp} \geqslant \pi_{ts}$, and the second solution has the minimum entropy if $\hbar_{tp} \leqslant \hbar_{ts}$ and $\pi_{tp} \geqslant \pi_{ts}$. We will not

consider the second solution further, because $\hbar_{tp} > \hbar_{ts}$ for ejector thrust augmentors for gas turbine engines. Note that the optimum mixing pressure $\pi_m^*$ is independent of the mass flow ratio $\beta$. By substituting the first solution of Equation (10) into Equation (9), the minimum mixed flow entropy is found to be

$$\sigma_m^* = \frac{1}{(1 + \beta)^2} (\hbar_{tp} + \beta\hbar_{ts}) (\frac{1}{\pi_{tp}} + \beta\frac{1}{\pi_{ts}}) \qquad (11)$$

and the maximum exhaust velocity

$$\tilde{u}_e^* = \frac{\sqrt{2}}{1 + \beta} (\hbar_{tp} + \beta\hbar_{ts})^{\frac{1}{2}} ([1 - \frac{1}{\pi_{tp}}] + \beta[1 - \frac{1}{\pi_{ts}}])^{\frac{1}{2}} \qquad (12)$$

We now define two parameters; a "temperature" parameter

$$\mu = (\hbar_{ts}/\hbar_{tp})^{\frac{1}{2}} \qquad (13)$$

and a "pressure" parameter

$$\nu = \left(\frac{1 - \frac{1}{\pi_{ts}}}{1 - \frac{1}{\pi_{tp}}}\right)^{\frac{1}{2}} \qquad (14)$$

Using these parameters we may rewrite Equation (12) as

$$\tilde{u}_e^* = [2\hbar_{ts} (1 - \frac{1}{\pi_{ts}})]^{\frac{1}{2}} \frac{1}{1 + \beta} (\frac{1}{\mu^2} + \beta)^{\frac{1}{2}} (\frac{1}{\nu^2} + \beta)^{\frac{1}{2}} \qquad (15)$$

We have assumed that the secondary flow air is obtained by isentropic recovery from ambient conditions, so

$$\hbar_{ts} = \pi_{ts} = 1 + \frac{\gamma - 1}{2} M_\infty^2, \quad \sigma_s = 1$$

$$\tilde{u}_\infty^2 = (\gamma - 1)M_\infty^2 = 2(\hbar_{ts} - 1) \qquad (16)$$

Substituting from Equations (15) and (16) into Equation (8), the specific thrust is found to be

$$f = (\frac{1}{\mu^2} + \beta)^{\frac{1}{2}} (\frac{1}{\nu^2} + \beta)^{\frac{1}{2}} - (1 + \beta) \qquad (17)$$

and the augmentation ratio $\phi$ (defined to be $f/f_{\beta=0}$)

$$\phi = \frac{1}{1 - \mu\nu} [(1 + \beta\mu^2)^{\frac{1}{2}}(1 + \beta\nu^2)^{\frac{1}{2}} - (1 + \beta)\mu\nu] \qquad (18)$$

These two equations give the maximum values for the specific thrust and augmentation ratio which can be obtained from an ejector augmentor with complete mixing, given the parameters $(\beta, \mu, \nu)$.

As an aside, if the mixing pressure is not optimum ($\pi_m \neq \pi_m^*$), then the specific thrust is

$$f = [\frac{1}{\mu^2\nu^2} + \beta(\frac{1}{\mu^2} + 1)\zeta + \beta^2 +$$

$$2\frac{\beta}{\mu}(\frac{1}{\nu^2} - \zeta)^{\frac{1}{2}}(1 - \zeta)^{\frac{1}{2}}]^{\frac{1}{2}} - (1 + \beta)$$

where we have introduced the parameter

$$\zeta = \frac{1 - \frac{1}{\pi_m}}{1 - \frac{1}{\pi_{ts}}}$$

For optimum mixing pressure, $\zeta^* = (1 - \mu^2/\nu^2)/(1 - \mu^2)$. This can be used to evaluate off-optimum ejector augmentor performance.

3. EJECTOR AUGMENTOR (MULTI-STAGE)

The question naturally occurs as to whether or not the performance of the ideal ejector augmentor with a single constant pressure mixing stage can be improved by using an ideal multi-stage mixer in which the secondary flow is introduced incrementally, and in which each stage is optimized.

Consider the incremental mixer stage displayed schematically in Figure 2. As shown, the output of the $(n-1)^{st}$ stage forms the primary flow for the $n^{th}$ stage, and an increment $\xi_s^{(n)}$ of secondary mass flow is added at the $n^{th}$ stage.

Conservation of mass gives, for the $n^{th}$ stage,

$$\xi_p^{(n)} = \xi_m^{(n-1)} \tag{19}$$

$$\xi_m^{(n)} = \xi_p^{(n)} + \xi_s^{(n)} \tag{20}$$

conservation of energy gives

$$\hbar_{tp}^{(n)} = \hbar_{tm}^{(n-1)} \tag{21}$$

$$\hbar_{tm}^{(n)} = (\xi_p^{(n)} \hbar_{tp}^{(n)} + \xi_s^{(n)} \hbar_{ts}) / \xi_m^{(n)} \tag{22}$$

and conservation of momentum, for constant pressure mixing, gives

$$\tilde{u}_m^{(n)} = (\xi_p^{(n)} \tilde{u}_p^{(n)} + \xi_s^{(n)} \tilde{u}_s^{(n)}) / \xi_m^{(n)} \tag{23}$$

The assumption of isentropy between stages gives

$$\sigma_p^{(n)} = \sigma_m^{(n-1)} \tag{24}$$

For a specified mixing pressure $\pi_m^{(n)}$, the mixing velocities of the primary and secondary flows are, respectively,

$$\tilde{u}_p^{(n)} = \sqrt{2} \ (\hbar_p^{(n)} - \pi_m^{(n)} \sigma_p^{(n)})^{\frac{1}{2}} \tag{25}$$

$$\tilde{u}_s^{(n)} = \sqrt{2} \ (\hbar_{ts} - \pi_m^{(n)} \sigma_s)^{\frac{1}{2}}$$

and the entropy of the mixed flow is

$$\sigma_m^{(n)} = [\hbar_{tm}^{(n)} - \frac{1}{2} \ (\tilde{u}_m^{(n)})^2] / \pi_m^{(n)} \tag{26}$$

Given that $\xi_p^{(1)} = 1$, Equations (19) and (20) may be immediately solved to give

$$\xi_m^{(n)} = 1 + \sum_{i=1}^{n} \xi_s^{(i)} \tag{27}$$

426

and, given that $\hbar_{tp}^{(1)} = \hbar_{tp}$, Equations (21) and (22) have the solution

$$\hbar_{tm}^{(n)} = (\hbar_{tp} + \hbar_{ts}\sum_{i=1}^{n} \xi_s^{(i)})/\xi_m^{(n)} \tag{28}$$

Our analysis of the single stage mixer shows (Equation (10)) that the optimum mixing pressure for the $n^{th}$ stage should be

$$\pi_m^{*(n)} = (\hbar_{tp}^{(n)} - \hbar_{ts})/(\frac{\hbar_{tp}^{(n)}}{\pi_{ts}} - \frac{\hbar_{ts}}{\pi_{tp}^{(n)}})$$

$$= (\hbar_{tm}^{(n-1)} - \hbar_{ts})/(\frac{\hbar_{tm}^{(n-1)}}{\pi_{ts}} - \frac{\hbar_{ts}}{\hbar_{tm}^{(n-1)}} \sigma_m^{(n-1)})$$

This choice minimizes the entropy increase in each stage. (Which implies that the overall entropy increase of the multi-stage mixer will also be minimized.) With this, Equations (19) through (26) and some algebraic manipulation, the following relation for the entropy of the mixed flow is found:

$$\sigma_m^{(n)} = \frac{\hbar_{tm}^{(n)}}{\hbar_{tm}^{(n-1)} - \hbar_{ts}} \left[ (\hbar_{tm}^{(n-1)} - \hbar_{tm}^{(n)})\frac{\sigma_s}{\hbar_{ts}} + (\hbar_{tm}^{(n)} - \hbar_{ts})\frac{\sigma_m^{(n-1)}}{\hbar_{tm}^{(n-1)}} \right]$$

With the initial condition $\sigma_m^{(o)} = \hbar_{tp}/\pi_{tp}$, the solution of this recursion relation may be shown to be

$$\sigma_m^{(n)} = \hbar_{tm}^{(n)} [\frac{1}{\pi_{tp}} + \frac{1}{\pi_{ts}} \sum_{i=1}^{n} \xi_s^{(i)}]/\xi_m^{(n)} \tag{29}$$

and the optimum mixing pressure $\pi_m^{*(n)}$ for the $n^{th}$ stage is then found to be

$$\pi_m^{*(n)} = (\hbar_{tp} - \hbar_{ts})/(\frac{\hbar_{tp}}{\pi_{ts}} - \frac{\hbar_{ts}}{\pi_{tp}}) \tag{30}$$

which is a constant, independent of either stage number or mass flow ratio.

If we choose $\xi_s^{(i)}$ such that, for N stages,

$$\beta = \sum_{i=1}^{N} \xi_s^{(i)}$$

then Equations (27), (28) and (29) give

$$\xi_m^{(N)} = 1 + \beta$$

$$\hbar_{tm}^{(N)} = (\hbar_{tp} + \beta\hbar_{ts})/(1 + \beta)$$

$$\sigma_m^{(N)} = \frac{1}{(1 + \beta)^2} (\hbar_{tp} + \beta\hbar_{ts})(\frac{1}{\pi_{tp}} + \beta\frac{1}{\pi_{ts}})$$

which results, including Equation (30), are identical to those for a single stage mixer for the same mass flow ratio $\beta$. Therefore, ideal incremental staging offers no performance advantage over an ideal single stage.*

## 4. MIXED-FLOW TURBOFAN

Figure 3 shows a schematic drawing and a T-S diagram for an ideal mixed-flow turbofan. The primary (or core) fluid is isentropically expanded through the turbine to extract power to drive the fan which isentropically compresses the secondary (or bypass) flow. The fan and turbine are matched so that the total pressures of the core and bypass flows are the same at the entry to the mixer. The flows are mixed adiabatically at zero velocity in the mixer and expanded to ambient pressure in the exhaust nozzle.

---

*This result appears to constitute one step in a proof that the constant pressure mixer is the optimum mixer, i.e., the mixer with the least entropy increase.

The turbofan cycle may be analyzed by using the T-S diagram of Figure 3(b). The work performed by the turbine must equal the work required by the fan, so

$$(\hbar_{tp} - \hbar_{tpm}) = \beta(\hbar_{tsm} - \hbar_{ts})$$

The total pressures at the turbine and fan exits must be equal, so

$$\hbar_{tsm}/\sigma_s = \hbar_{tpm}/\sigma_p = \pi_{tm}$$

Since the flow mixing is adiabatic and at zero velocity, conservation of energy gives

$$\hbar_{tpm} + \beta\hbar_{tsm} = (1 + \beta)\hbar_{tm}$$

The entropy of the mixed flow is given by

$$\sigma_m = \hbar_{tm}/\pi_{tm}$$

and the exhaust velocity is

$$\tilde{u}_e = \sqrt{2}\ (\hbar_{tm} - \hbar_{am})^{\frac{1}{2}}$$
$$= \sqrt{2}\ (\hbar_{tm} - \sigma_m)^{\frac{1}{2}}$$

The solution of these equations is straightforward and will not be detailed here. The results are

$$\hbar_{tm} = (\hbar_{tp} + \beta\hbar_{ts})/(1 + \beta)$$

$$\sigma_m = (\sigma_p + \beta\sigma_s)/(1 + \beta)$$
$$= (\hbar_{tp}/\pi_{tp} + \beta\hbar_{ts}/\pi_{ts})/(1 + \beta) \tag{31}$$
$$\pi_{tm} = \hbar_{tm}/\sigma_m$$
$$\tilde{u}_e = (\frac{2}{1 + \beta})^{\frac{1}{2}}\ [\hbar_{tp}(1 - \frac{1}{\pi_{tp}}) + \beta\hbar_{ts}(1 - \frac{1}{\pi_{ts}})]$$

In the manner used above for the ejector augmentor, we find the specific thrust and augmentation ratio to be, respectively,

$$f = (1 + \beta)^{\frac{1}{2}}(\frac{1}{\mu^2\nu^2} + \beta)^{\frac{1}{2}} - (1 + \beta) \qquad (32)$$

$$\phi = \frac{1}{1 - \mu\nu} [(1 + \beta)^{\frac{1}{2}}(1 + \beta\mu^2\nu^2)^{\frac{1}{2}} - (1 + \beta)\mu\nu] \qquad (33)$$

where we have introduced the parameters $\mu$ and $\nu$ defined in Equations (13) and (14).

It can be shown, although we will not do it here, that the best performance which can be achieved by a nonmixed-flow turbofan is the same as that given above for the mixed-flow turbofan, and is achieved when the primary and secondary flows have the same exhaust velocities.

## 5. THE ISENTROPIC COMPRESSOR

Up to this point, we have not made any stipulations concerning the nature of the "pump" which is used to compress captured ambient air from its stagnation conditions to the primary flow reservoir conditions for either the ejector augmentor or the turbofan. The most efficient device for the primary flow pump is an isentropic compressor. (We assume that a suitable power source is available to drive it.) For such a compressor, the parameters $\mu$ and $\nu$ are related, since

$$\pi_{tp} = \pi_{ts}\, \hbar_{tp}/\hbar_{ts}$$

for isentropic compression. One then finds the relationship

$$\nu_{isen} = [\frac{\pi_{ts} - 1}{\pi_{ts} - \mu^2}]^{\frac{1}{2}}$$

from Equations (13) and (14). This may be expressed, using Equation (16), as

$$\nu_{isen} = [\frac{\gamma-1}{2}M_\infty^2/(1 - \mu^2 + \frac{\gamma-1}{2}M_\infty^2)]^{\frac{1}{2}} \qquad (34)$$

which shows explicitly the Mach number dependence of the relationship.

## 6. CORE TURBINE ENGINE GAS GENERATOR

We now assume the "pump" to be a simple turbine engine gas generator, since this is what is most commonly used in practice. With this assumption, we can derive the primary reservoir conditions ($\hslash_{tp}$, $\pi_{tp}$, $\sigma_p$) in terms of the turbine engine compressor pressure ratio ($p_{tc}/p_{ts}$) and the combustor temperature rise ($\Delta T_c$).

The T-S diagram for an ideal turbine engine gas generator is shown in Figure 4. We define nondimensional compressor pressure ratio and combustor temperature rise parameters

$$\alpha = (p_{tc}/p_{ts})^{\frac{\gamma-1}{\gamma}}$$

$$\Delta\hslash_c = \Delta T_c/T_\infty$$

Then by definition

$$\pi_{tc} = \alpha\pi_{ts}$$

$$\hslash_{tt} = \hslash_{tc} + \Delta\hslash_c$$

and, since the turbine and compressor works must match,

$$(\hslash_{tc} - \hslash_{ts}) = (\hslash_{tt} - \hslash_{tp})$$

The compression is assumed to be isentropic, so

$$\hslash_{tc} = \hslash_{ts}\,\pi_{ts}/\pi_{ts} = \alpha\hslash_{ts}$$

Assuming isentropic expansion in the turbine and solving the above equations, we find

431

$$\sigma_p = 1 + \frac{1}{\alpha} \frac{\Delta \hbar_c}{\hbar_{ts}}$$

$$\hbar_{tp} = \hbar_{ts}(1 + \frac{\Delta \hbar_c}{\hbar_{ts}}) \tag{35}$$

$$\pi_{tp} = \pi_{ts}(1 + \frac{\Delta \hbar_c}{\hbar_{ts}}) / (1 + \frac{1}{\alpha} \frac{\Delta \hbar_c}{\hbar_{ts}})$$

for the primary reservoir conditions. The "temperature" and "pressure" parameters, $\mu$ and $\nu$, can be expressed in terms of the turbine engine parameters, $\alpha$ and $\Delta \hbar_c$:

$$\mu = [1 + \frac{\Delta \hbar_c}{\hbar_{ts}}]^{-\frac{1}{2}}$$

$$\nu = [1 + (1 - \mu^2)(1 - \frac{1}{\alpha}) / (\pi_{ts} - 1)]^{-\frac{1}{2}} \tag{36}$$

Since

$$\hbar_{ts} = \pi_{ts} = 1 + \frac{\gamma - 1}{2} M_\infty^2$$

the relationship between $(\mu, \nu)$ and $(\alpha, \Delta \hbar_c)$, and hence between $(f, \phi)$ and $(\alpha, \Delta \hbar_c)$, are Mach number dependent.

Finally, if the compressor pressure ratio is made infinitely large then the turbine engine gas generator becomes, in essence, an isentropic compressor. This can be seen by examining Equations (35) and (36) in the limit $(\alpha \to \infty)$.

432

# SECTION III

## DISCUSSION

### 1. MAXIMUM THRUST AUGMENTATION AND THE TURBOFAN

In his analysis, Heiser obtained results for the maximum performance of a passive augmentor which are essentially the same as those we have derived in Section II.4 for the ideal turbofan. However, it is theoretically possible to exceed the maximum performance found by Heiser by using energy transfer processes which are thermodynamically reversible.[4] Examples of thermo-dynamically reversible devices are ideal turbocompressors and ideal counterflow heat exchangers (under some conditions). In the Appendix, it is shown that the maximum augmentation ratio achievable by a passive augmentor using reversible thermodynamic processes is

$$\phi_{max} = \frac{[1 + \beta]^{\frac{1}{2}} [(\hbar_{tp} + \beta\hbar_{ts}) - (1 + \beta)\sigma_p \frac{1}{1+\beta}]^{\frac{1}{2}} - [1 + \beta][\hbar_s - 1]^{\frac{1}{2}}}{[\hbar_{tp} - \sigma_p]^{\frac{1}{2}} - [\hbar_{ts} - 1]^{\frac{1}{2}}}$$

for given initial flow conditions $(\beta, \hbar_{tp}, \hbar_{ts}, \sigma_p, \sigma_s = 1)$. This equation unfortunately, unlike those for the ejector augmentor and turbofan, cannot be cast into a Mach number-independent form in terms of the temperature and pressure parameters $\mu$ and $\nu$. Because of this, because the ideal mixed-flow turbofan performance is only slightly worse (~5%) than the theoretical maximum for practical flow conditions and because the turbofan is the most common form of passive thrust augmentor, we will use the ideal mixed-flow turbofan as the standard for comparison in the following discussion.

### 2. COMPARISON OF ENTROPIES

The first comparison we make is between the nondimensional entropies of the mixed flows for the ejector augmentor and the turbofan. From Equations (11) and (31):

$$\Delta\sigma_m = \sigma_{mej} - \sigma_{mtf} = \frac{\beta}{(1+\beta)^2} (\hbar_{tp} - \hbar_{ts})(\frac{1}{\pi_{ts}} - \frac{1}{\pi_{tp}})$$

433

This is always positive if $T_{tp} \geqslant T_{ts}$ and $P_{tp} \geqslant P_{ts}$. (If $T_{tp} < T_{ts}$ and $P_{tp} \geqslant P_{ts}$, then the second solution given in Equation (10) for the optimum mixing pressure must be used, which gives the result $\Delta\sigma_m = 0$.) Therefore, an ideal ejector augmentor with complete mixing can never be more efficient than an ideal turbofan for the same ($\beta$, $T_{tp}$, $P_{tp}$, $T_{ts}$, $P_{ts}$). This is not unexpected since the mixing in the ideal turbofan occurs at negligible velocity, while the mixing in the ejector generally occurs at high relative velocities.

## 3. IDEAL PERFORMANCE CONTOUR MAPS

In Figure 5*, we present constant specific thrust and constant augmentation ratio contours for ideal ejector augmentors, plotted as functions of $\mu$ and $\nu$ for various mass flow ratios using Equations (17) and (18). The most obvious feature of the figure is that, when $\mu = \nu$, the augmentation ratio is unity; that is, no thrust augmentation is realized. The reason for this is as follows:

> When $\mu = \nu$, the optimum mixing pressure, given by
> Equation (10), is equal to the ambient static pressure
> ($\pi_m^* = 1$). Now, in an ejector with constant pressure
> mixing, no net thrust is developed in the mixer
> (conservation of momentum); the thrust augmenting
> forces are developed in the inlet, the secondary
> flow nozzle and the exhaust nozzle. If the mixing
> occurs at ambient static pressure, then, from
> conservation of momentum, the secondary flow cannot
> develop any net thrust in either the inlet and
> secondary flow nozzle, or the exhaust nozzle; hence,
> there can be no thrust augmentation of the primary
> flow.

A second feature of the contour maps in Figure 5 and of Equations (17) and (18), is the symmetry in $\mu$ and $\nu$ of both the specific thrust and augmentation ratio contours (diagonal symmetry).

---

*The reader should bear in mind that this figure and those to follow, do not show the performance of a single augmentor. Rather, each point in the figures represents the performance of a different optimized ideal augmentor.

As can be seen in the figure, for ideal ejector augmentors the maximum value of the augmentation ratio for a particular mass flow ratio $\beta$ is obtained when $(\mu, \nu)$ is $(0,1)$ or $(1,0)$. From Equation (18), this value is

$$\phi_{max} = (1 + \beta)^{\frac{1}{2}}$$

Thus, the augmentation ratio theoretically attainable by an ideal ejector augmentor, which uses compressible gasses and a constant pressure mixer, can exceed the limiting value of two which Heiser found assuming incompressible flow and constant area mixing.

For an ideal ejector, the case $\mu = 1$ (i.e., $T_{tp} = T_{ts}$) is that of a "pure ejector," that is, an ejector in which the energy added to the bypass flow comes entirely from the pressure of the primary flow. The case $\nu = 1$ (i.e., $p_{tp} = p_{ts}$) is that of a "pure ramjet"; the only energy added to the bypass flow is thermal energy from the primary flow. For this reason, we refer to the region of the $\mu$-$\nu$ map which lies above the diagonal $(\mu > \nu)$ in Figure 5 as the "ejector side" of the map and the region below the diagonal $(\mu < \nu)$ as the "ramjet side." The optimum mixing pressure, as given by Equation (10), is below the ambient static pressure on the ejector side and above ambient on the ramjet side. In the limits, the optimum mixing pressure for the pure ejector is zero, and for the pure ramjet, the freestream total pressure.

Since the energy (fuel) consumption is more or less proportional to the stagnation temperature difference between the primary and secondary flows, one would prefer an ejector device which operates on the ejector, rather than ramjet, side of the map, where the total temperature difference is low ($\mu$ near unity).

In Figure 6, we show constant specific thrust and augmentation ratio contours for several mass flow ratios for the ideal mixed-flow turbofan, as given by Equations (32) and (33).

Comparison of this figure with Figure 5 shows a striking difference in the augmentation ratio contours. In particular, for the turbofan, useful augmentation can be obtained anywhere in the region of the maps, whereas, for the ejector augmentor, useful augmentation can be obtained only away from the diagonal ($\mu = \nu$).

## 4. MACH NUMBER DEPENDENCE OF LIMITS ON PERFORMANCE

Although the specific thrust and augmentation ratio contours of Figures 5 and 6 are not Mach number dependent, the values of $\mu$ and $\nu$ are (for specified $p_{tp}$ and $T_{tp}$). In particular, the theoretically accessible region of the figures is Mach number dependent, since $\nu$ has a limiting non-zero value as the primary total pressure becomes infinitely large. From Equations (14) and (16),

$$\nu_{min}(M_\infty) = \frac{\frac{\gamma-1}{2}M_\infty^2}{(1 + \frac{\gamma-1}{2}M_\infty^2)^{\frac{1}{2}}}$$

This is a mathematical limit and contains no assumptions concerning the thrust augmentation device (other than that $\nu$ is a valid parameter for describing its performance). Thus, it is equally applicable to the ideal turbofan and to the ideal ejector augmentor. The consequence of this minimum attainable $\nu$ is that the regions of high augmentation ratio along the left border of the $\mu-\nu$ maps are beyond reach unless the flight Mach number is low. The regions of high augmentation ratio along the lower boundary are practically unattainable because the required primary flow total temperature is too high:

$$T_{tp} = T_\infty (1 + \frac{\gamma-1}{2}M_\infty^2)\frac{1}{\mu^2}$$

(from Equations (13) and (16)). If, for the sake of illustration, we choose a maximum practical value of nine for $T_{tp}/T_\infty$, then

$$\mu_{min} = \frac{1}{3} (1 + \frac{\gamma-1}{2}M_\infty^2)^{\frac{1}{2}}$$

This and $\nu_{min}$, which is defined above, define accessible regions
of the $\mu-\nu$ maps as functions of the freestream Mach number.
These regions are shown in Figure 7 for selected Mach numbers.
This figure may be overlaid on the $\mu-\nu$ maps of Figures 5      to
see, graphically, the effect of the Mach number on the at.. .al.e
performance for ideal ejector augmentors and turbofans.

5.  EJECTOR AUGMENTOR WITH AN ISENTROPIC COMPRESSOR

We now examine the case in which the primary "pump" of our
ideal thrust augmentors is an isentropic compressor.  In Figure 8,
are shown the $\mu-\nu$ curves for isentropic compressors for various
Mach numbers, as given by Equation (34).  The horizontal tick
mark on each curve is at the value of $\mu$ for which $T_{tp}/T_{\infty} = 9$, the
temperature used previously in Figure 7.  As with Figure 7, this
figure may be overlaid on any of the maps of Figures 5 and 6.  As
one would expect, the use of an isentropic compressor further
restricts the accessible regions of the $\mu-\nu$ maps.  This restric-
tion is particularly bad for low primary stagnation temperatures
($\mu \approx 1$) where the ejector augmentor performance is best.  The
effect on turbofan performance is not as severe because the
turbofan has good performance near the $\mu-\nu$ diagonal, whereas the
ejector augmentor does not.

Since an ideal turbine engine gas generator with infinite
compressor pressure ratio is an isentropic compressor, and since
an ideal turbofan is at best an isentropic compressor, Figure 8
also represents the outer limits for the accessible regions of
the $\mu-\nu$ maps for turbine engines and turbofans used as primary
"pumps."  (We project this statement, without proof, to include
all heat engines.)  As a result, Figure 8 overlaid on any of the
maps of Figures 5 and 6 will show the theoretical limits of
ejector augmentor and turbofan performance for the given Mach
numbers and mass flow ratio. :

437

## 6.  EJECTOR AUGMENTOR WITH TURBINE ENGINE GAS GENERATOR

Finally, we consider the case in which the primary "pump" is a simple turbine engine gas generator, as described in Section II.6.  In Figure 9, constant specific thrust and augmentation ratio contours are shown for a mass flow ratio of five at Mach numbers of 0.2, 0.7 and 1.4, plotted as functions of the gas turbine compressor pressure ratio and the combustor temperature rise.  The contours were obtained from Equations (17), (18) and (36).  In these maps, the area to the right of the $\phi = 1$ contour is on the ejector side and the area to the left is on the ramjet side, as defined above.  As can be seen, for the low Mach number case, useful thrust augmentation can be obtained.  However, the maximum augmentation requires an unrealistically low combustor temperature rise in the turbine engine.  (Such a low temperature rise would make the gas generator too large and heavy.)  As the temperature is raised to more reasonable levels, the thrust augmentation is reduced, but remains useful.  For higher Mach numbers, the attainable augmentation drops to practically useless levels.  At supersonic Mach numbers, some thrust augmentation is realized on the ramjet side, but this is a relatively useless benefit, because higher thrust can be achieved for the same fuel consumption (which is proportional to combustor temperature rise) simply by raising the compressor pressure ratio and forgetting about the augmentor device.

To further clarify the relationship between the Mach number-independent maps of Figure 5 and the Mach number-dependent maps of Figure 9, we have plotted in Figure 10 the boundaries of the temperature rise - pressure ratio region of the maps of Figure 9 as functions of $\mu$ and $\nu$ for selected Mach numbers.  This figure is similar in concept to Figures 7 and 8.  For each Mach number, the region of interest is to the right of the curved line, which is itself the contour for compressor pressure ratio equal to 32.  These curves are independent of mass flow ratio and may be overlaid on both the ejector augmentor and turbofan maps of Figures 5 and 6.  Comparing Figures 8 and 10, we see that the use of a gas turbine as a core device further restricts the accessible regions of the $\mu$-$\nu$ performance maps for both ejector augmentors and turbofans.

# SECTION IV

## CONCLUSIONS

The preceding analyses and discussion have all focused on the maximum performance which is theoretically attainable by ejector thrust augmentors. All flow processes were assumed to be isentropic, except for the flow mixing, which cannot be isentropic due to the second law of thermodynamics. The performance of real ejector augmentors will not be as good because of viscous and heat transfer losses, shock losses, incomplete mixing, non-optimum mixing conditions, etc. For this reason and considering the results of the present analytic study, we cannot be very optimistic about the efficacy of ejector devices for thrust augmentation for other than relatively low subsonic flight Mach numbers. We have found that the turbofan offers better performance than does the ejector augmentor for all forward flight conditions (for the same mass flow ratios).

As a result of this study, we have drawn the following conclusions:

- The ejector augmentor is theoretically capable of respectable performance. However, this performance is severely degraded if the primary flow is hot.

- The turbine engine is not a particularly suitable "pump" for an ejector augmentor because the turbine engine exhaust gases are too hot, and as a result, degrade the potential ejector performance to nearly useless levels, except at low Mach numbers. We may also turn this statement around: Ejector devices are not very suitable for thrust augmentation of turbine engines, except at low subsonic Mach numbers. (This conclusion also applies to isentropic compressors and turbofans used as pumps for ejector devices.)

- As the flight Mach number increases, the performance of an ejector augmentor is degraded faster than that of a turbofan.

439

The ejector augmentor should be most beneficial for lift and thrust enhancement at low speeds (e.g., V/STOL operations). It may also be useful for some special applications where geometric considerations mitigate against the use of a turbofan. However, the turbofan will probably remain the better device in terms of performance, because of its advanced state of development and high component efficiencies.

Lest these conclusions be assumed to apply to all ejector-like devices, we close with the following caveat:

> We have assumed throughout this study of ejector
> thrust augmentors that the primary and secondary
> flows are completely mixed and that all momentum
> and energy transfer processes occur in the mixer.
> For ejector-like devices for which these assumptions
> do not apply (e.g., the so-called "jet compressor"),
> our conclusions do not necessarily apply either.

# APPENDIX

## MAXIMUM THRUST AUGMENTATION

Assume that we have two fluid flows - a primary flow with initial stagnation conditions $(h_{tp}, s_p)$ and a secondary flow with initial stagnation conditions $(h_{ts}, s_s)$ - with a secondary/primary mass flow ratio $\beta$. Further assume that the two flows interact and proceed through some thermodynamic processes to final stagnation conditions $(h'_{tp}, s'_p)$ and $(h'_{ts}, s'_s)$. The two flows are then expanded isentropically through nozzles to ambient static pressure to provide thrust.

The exhaust velocities of the two flows are given by

$$
u_{ep} = \sqrt{2}\,[h'_{tp} - h'_{ap}]^{\frac{1}{2}}
$$
$$
u_{es} = \sqrt{2}\,[h'_{ts} - h'_{as}]^{\frac{1}{2}}
\qquad (A.1)
$$

where $h'_{ap}$ and $h'_{as}$ are static enthalpies at ambient static pressure:

$$
h'_{ap} = h_{\infty} e^{(s'_p - s_{\infty})/C_p}
$$
$$
h'_{as} = h_{\infty} e^{(s'_s - s_{\infty})C_p}
\qquad (A.2)
$$

The resultant specific thrust is

$$
f = (u_{ep} + \beta u_{es})/u_{\infty} - (1 + \beta)
\qquad (A.3)
$$

The initial and final stagnation conditions are related by the laws of thermodynamics,

$$
h'_{tp} + \beta h'_{ts} = h_{tp} + \beta h_{ts}
\qquad (A.4)
$$
$$
s'_p + \beta s'_s \geqslant s_p + \beta s_s
$$

The latter inequality can be written as

$$s_p' + \beta s_s' = s_p + \beta s_s + (1 + \beta)C_p \varepsilon \qquad (A.5)$$

where $\varepsilon \geqslant 0$.

We now seek the maximum specific thrust for fixed initial flow conditions by varying first $h_{tp}'$, then $s_p'$ and finally $\varepsilon$. Using Equations (A.1) through (A.4), the first variation

$$\frac{\partial f}{\partial h_{tp}'} = 0$$

has the solution

$$h_{tp}' = h_{tp} - \frac{\beta}{1+\beta} [h_{tp} - h_{ap}' - h_{ts} + h_{as}']$$

which gives upon substitution into Equations (A.1) and (A.3):

$$u_{ep} = u_{es} = (\frac{2}{1+\beta})^{\frac{1}{2}}[h_{tp} + \beta h_{ts} - (h_{ap}' + \beta h_{as}')]^{\frac{1}{2}}$$

Using this result and Equation (A.5) in Equation (A.3), the second variation

$$\frac{\partial f}{\partial s_p'} = 0$$

is performed, which gives

$$s_p' = s_s' = \frac{s_p + \beta s_s}{1+\beta} + C_p \varepsilon$$

and thence,

$$h_{tp}' = h_{ts}' = \frac{h_{tp} + \beta h_{ts}}{1+\beta}$$

The specific thrust is

$$f = \sqrt{2(1+\beta)} \ [h_{tp} + \beta h_{ts} - (1+\beta)h_\infty e^{(\frac{s_p + \beta s_s}{1+\beta} - s_\infty)/C_p} \ e^\varepsilon]^{\frac{1}{2}}/u_\infty$$
$$- (1+\beta)$$

Cursory examination of this expression shows that the specific thrust is maximized when $\varepsilon = 0$, that is, when the flow processes are reversible.

Finally, assuming isentropic diffusion in the inlet ($s_s = s_\infty$), we obtain for the maximum attainable specific thrust:

$$f_{max} = [\frac{1+\beta}{\hbar_{ts}-1}]^{\frac{1}{2}}[\hbar_{tp} + \beta\hbar_{ts} - (1+\beta)\sigma_p^{1/1+\beta}]^{\frac{1}{2}} - (1+\beta)$$

where we have introduced the nondimensional parameters used in Section II. The process which gives this maximum performance is one in which the two initial flows interact through a reversible thermodynamic process to move to the same final thermodynamic state, i.e.,

$$h'_{tp} = h'_{ts}$$

$$s'_p = s'_s$$

$$\varepsilon = 0$$

The augmentation ratio is

$$\phi_{max} = \frac{[1+\beta]^{\frac{1}{2}}[(\hbar_{tp} + \beta\hbar_s) - (1+\beta)\sigma_p^{1/1+\beta}]^{\frac{1}{2}} - [1+\beta][\hbar_{ts} - 1]^{\frac{1}{2}}}{[\hbar_{tp} - \sigma_p]^{\frac{1}{2}} - [\hbar_{ts} - 1]^{\frac{1}{2}}}$$

443
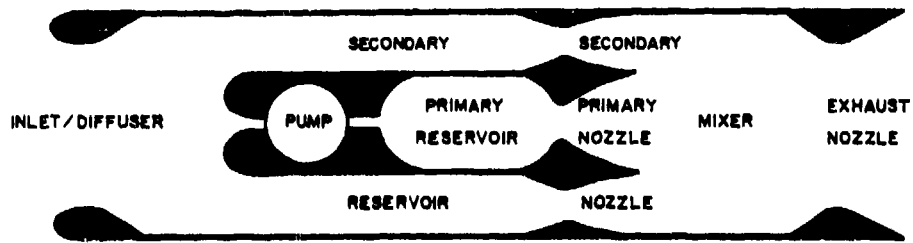
a) SCHEMATIC DRAWING
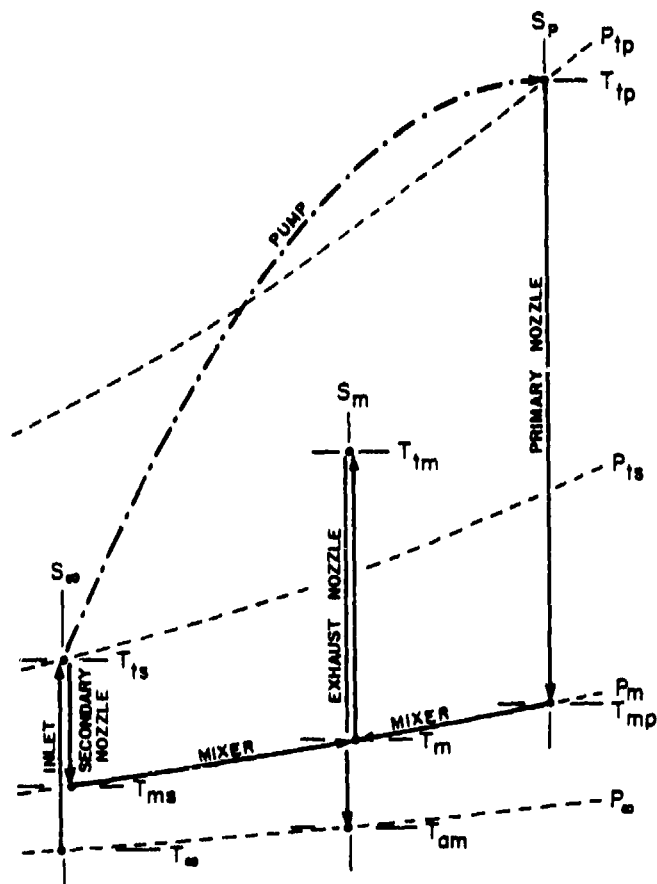
b) T-S DIAGRAM

FIGURE 1   Ejector Thrust Augmentor
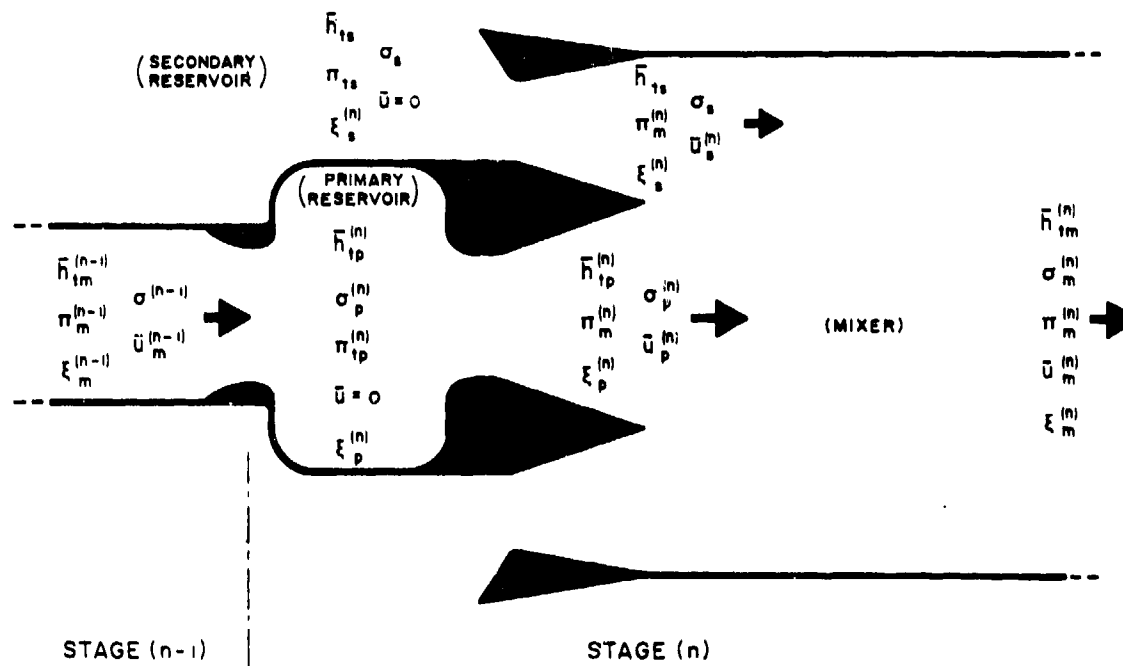
FIGURE 2   Schematic of One Stage of a Multi-Stage Ejector Augmentor
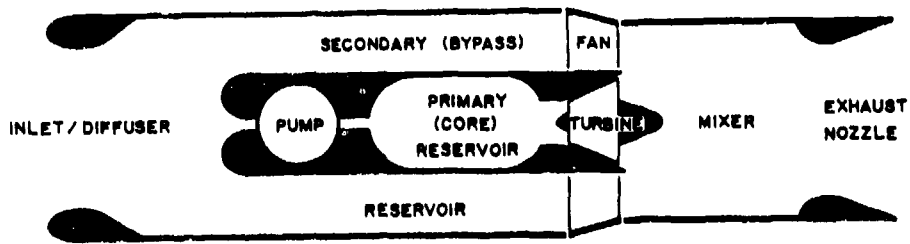
a) SCHEMATIC DRAWING
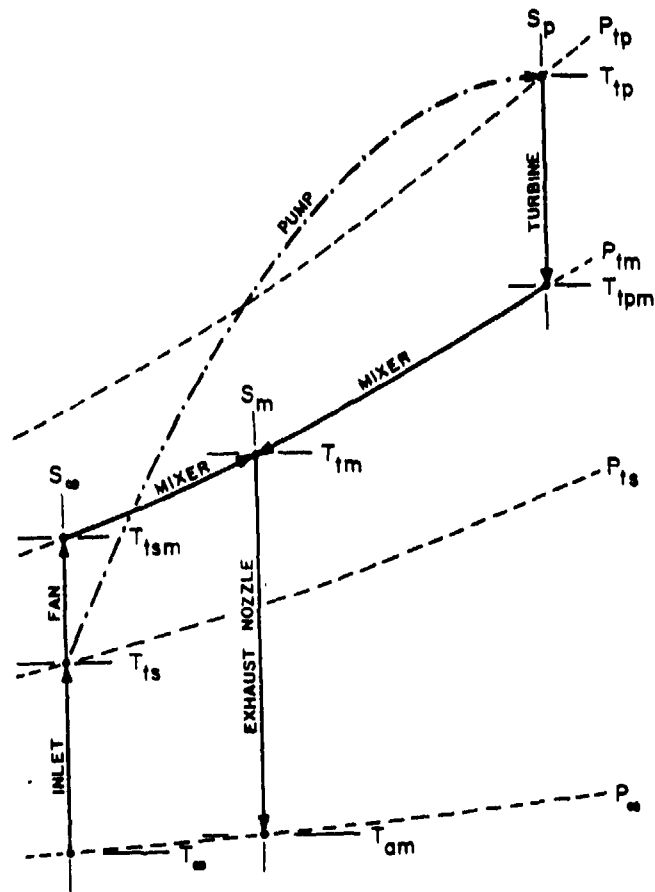


b) T-S DIAGRAM

FIGURE 3   Turbofan Engine
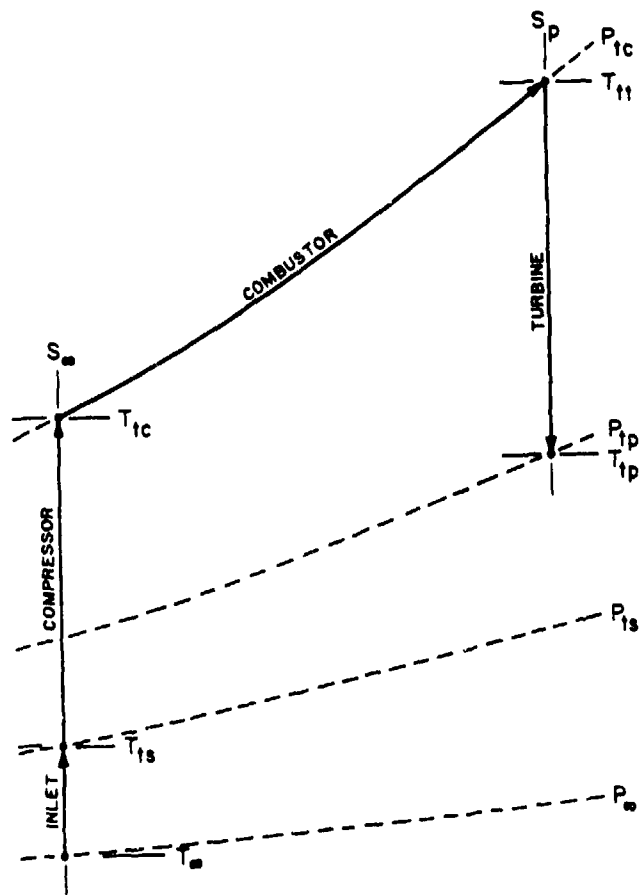
FIGURE 4   T-S Diagram for an Ideal Turbine Engine Gas Generator
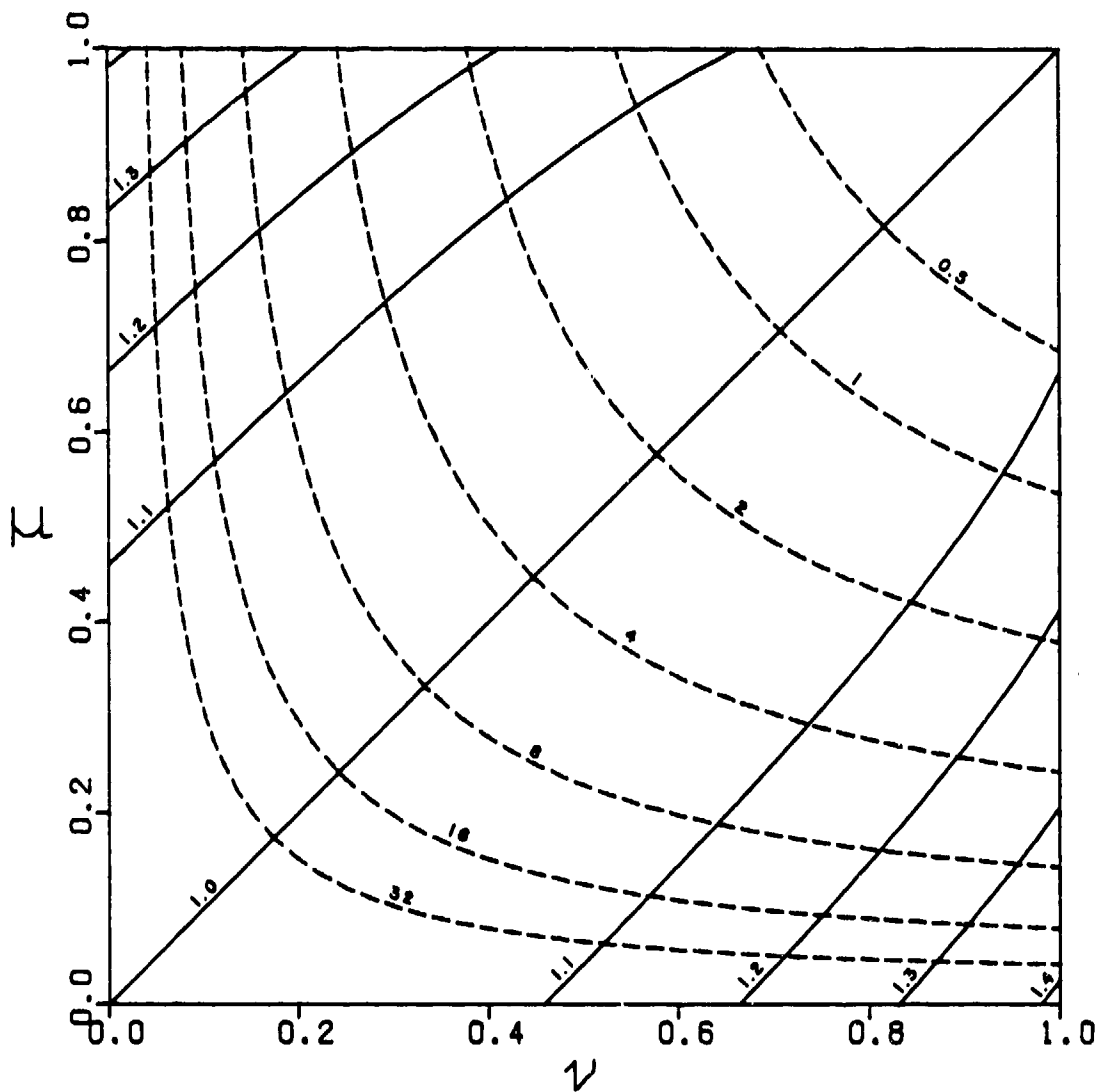
FIGURE 5   Performance Maps for Ideal Ejectors

a)   Secondary/Primary Mass Flow Ratio β = 1
     (—Augmentation Ratio φ, ---Specific Thrust f)

FIGURE 5   Performance Maps for Ideal Ejectors

b)   Secondary/Primary Mass Flow Ratio β = 2
     (—Augmentation Ratio φ, ---Specific Thrust f)
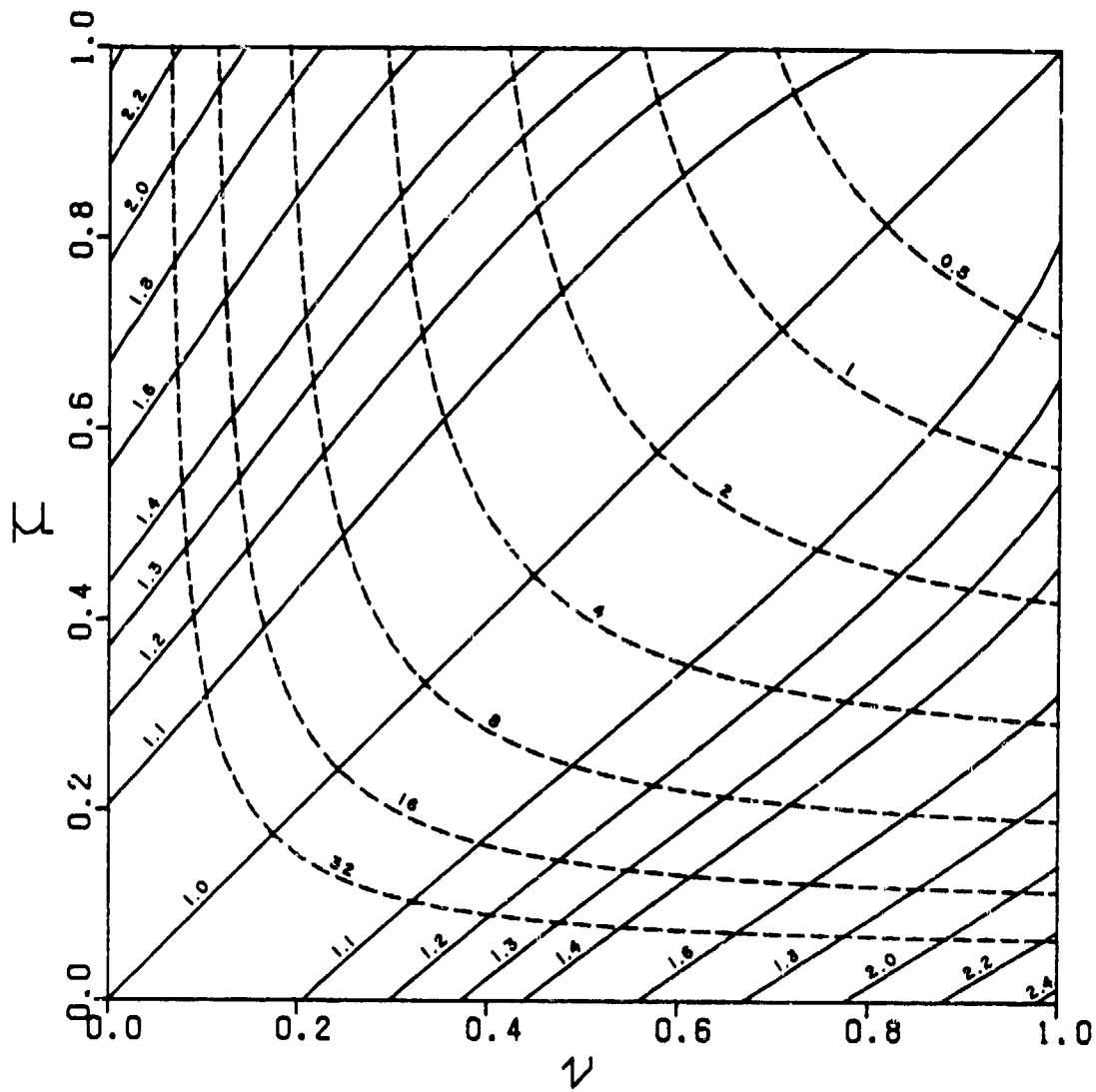
FIGURE 5    Performance Maps for Ideal Ejectors

c)    Secondary/Primary Mass Flow Ratio β = 5
(——Augmentation Ratio φ, ---Specific Thrust f)

450
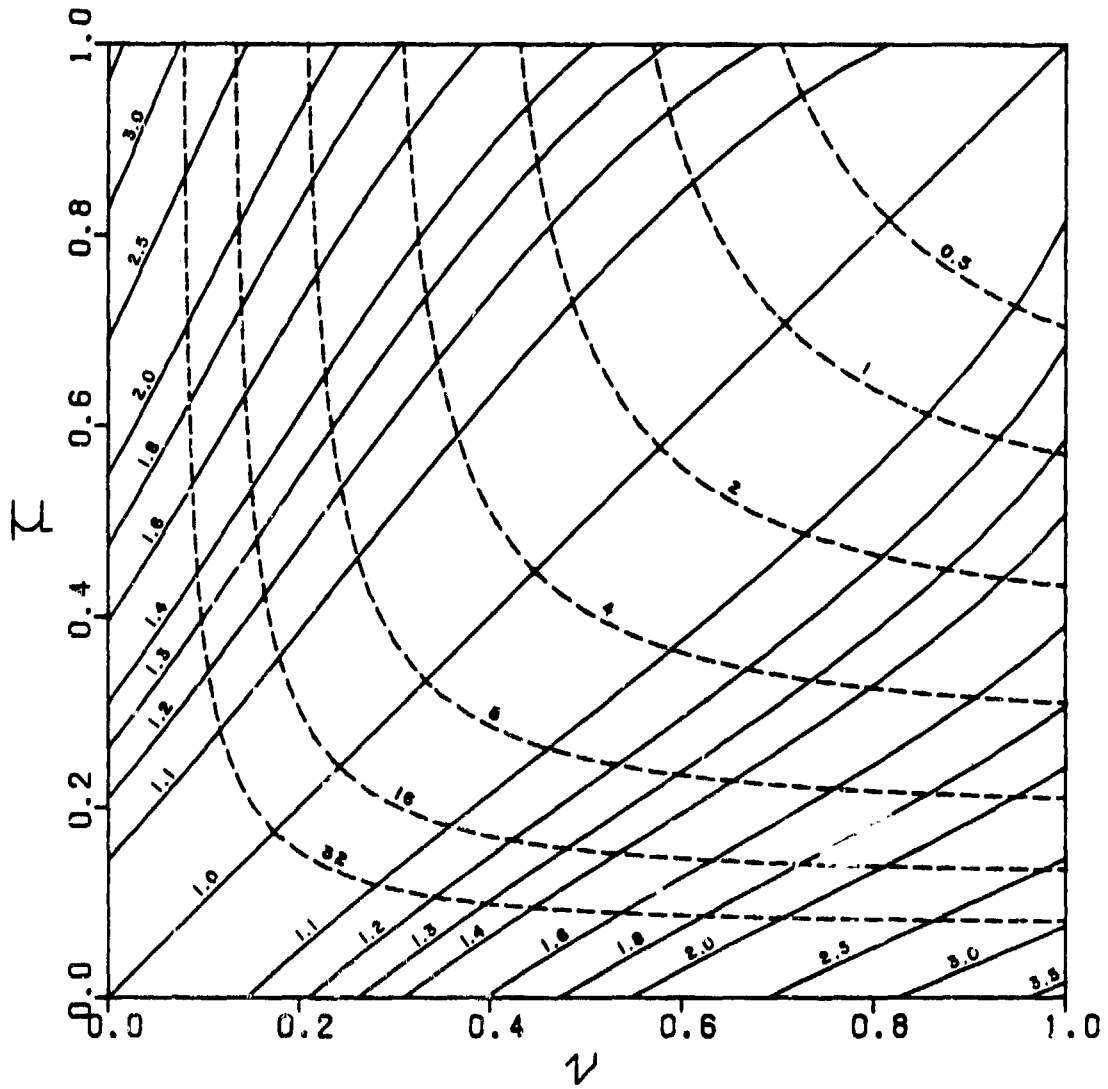
FIGURE 5  Performance Maps for Ideal Ejectors

d) Secondary/Primary Mass Flow Ratio β = 10
   (——Augmentation Ratio φ, ---Specific Thrust f)

451
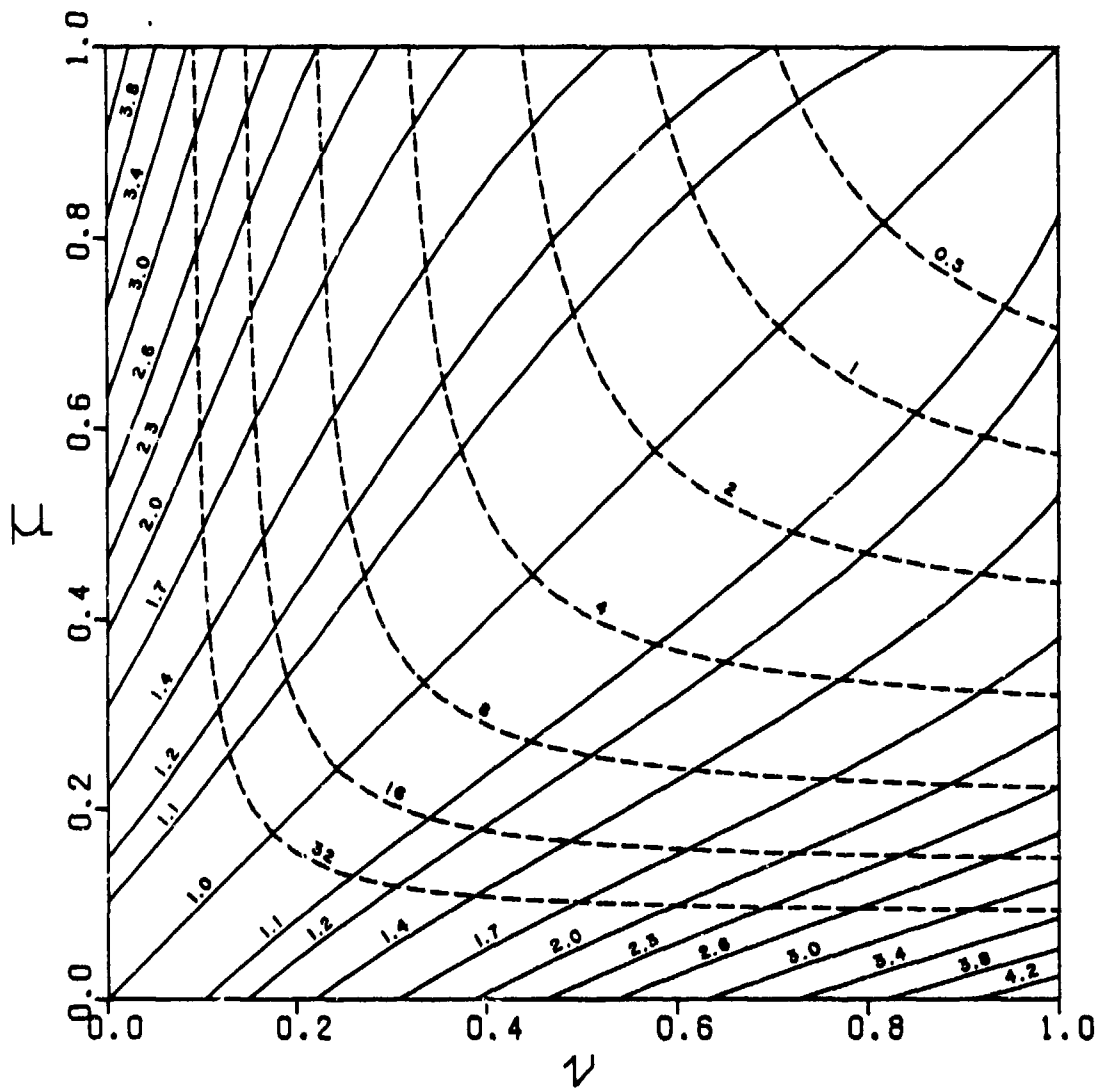
FIGURE 5   Performance Maps for Ideal Ejectors

e)   Secondary/Primary Mass Flow Ratio β = 20
    (—Augmentation Ratio φ, ---Specific Thrust f)

452
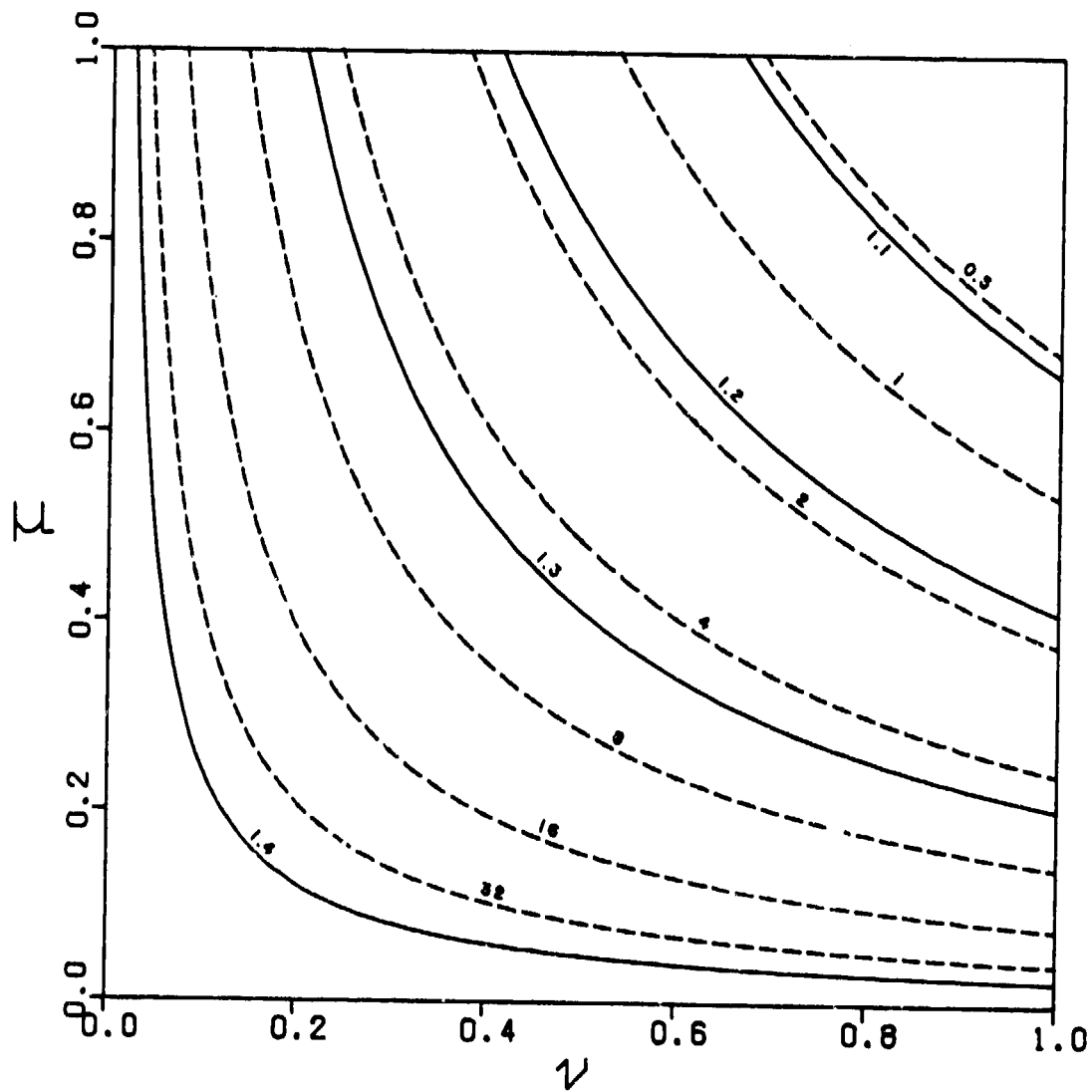
FIGURE 6   Performance Maps for Ideal Turbofans

    a)  Secondary/Primary Mass Flow Ratio $\beta = 1$
        (—Augmentation Ratio $\phi$, ---Specific Thrust f)
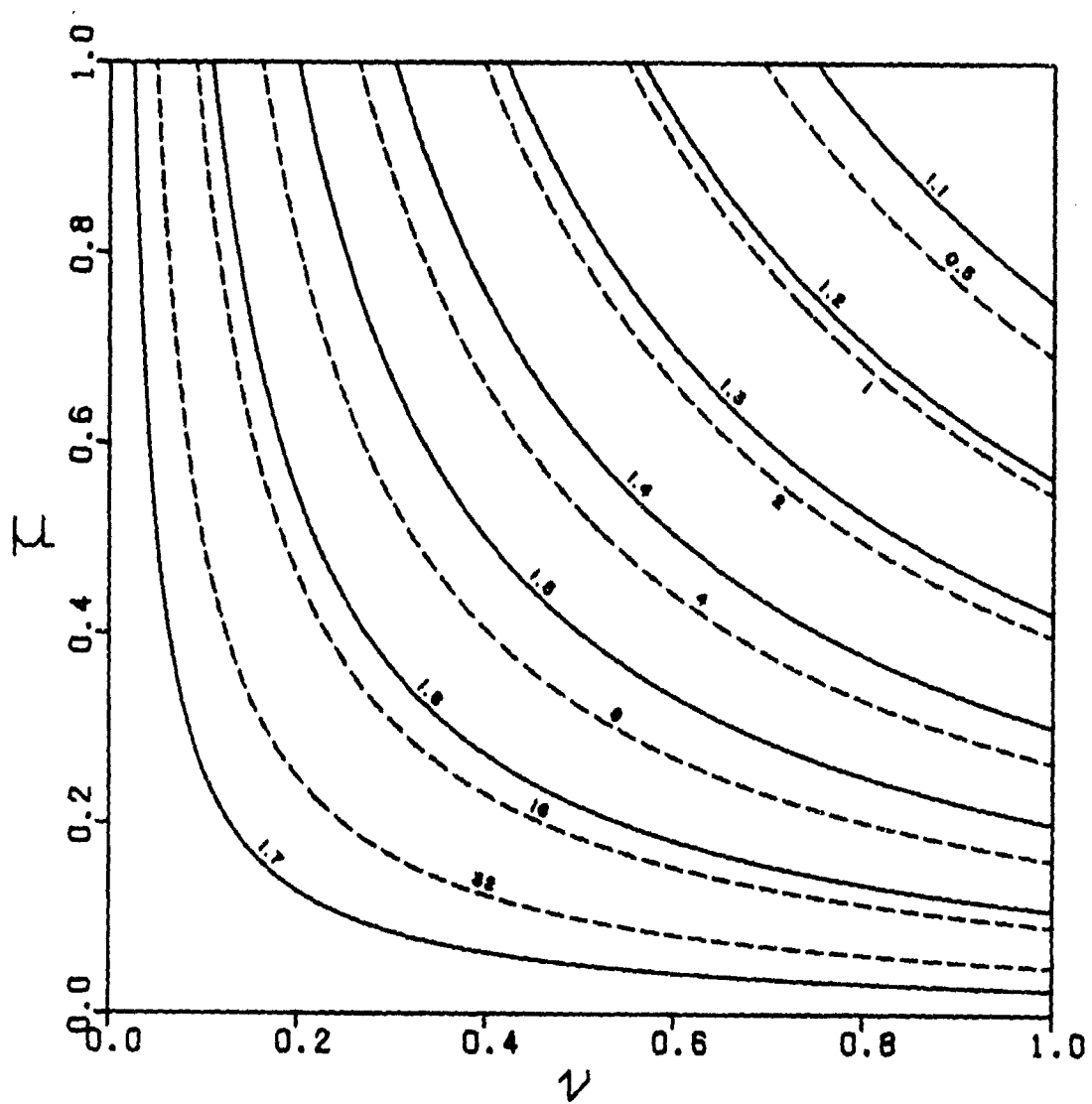
FIGURE 6   Performance Maps for Ideal Turbofans

b)   Secondary/Primary Mass Flow Ratio β = 2
(——Augmentation φ,   ———Specific Thrust f)
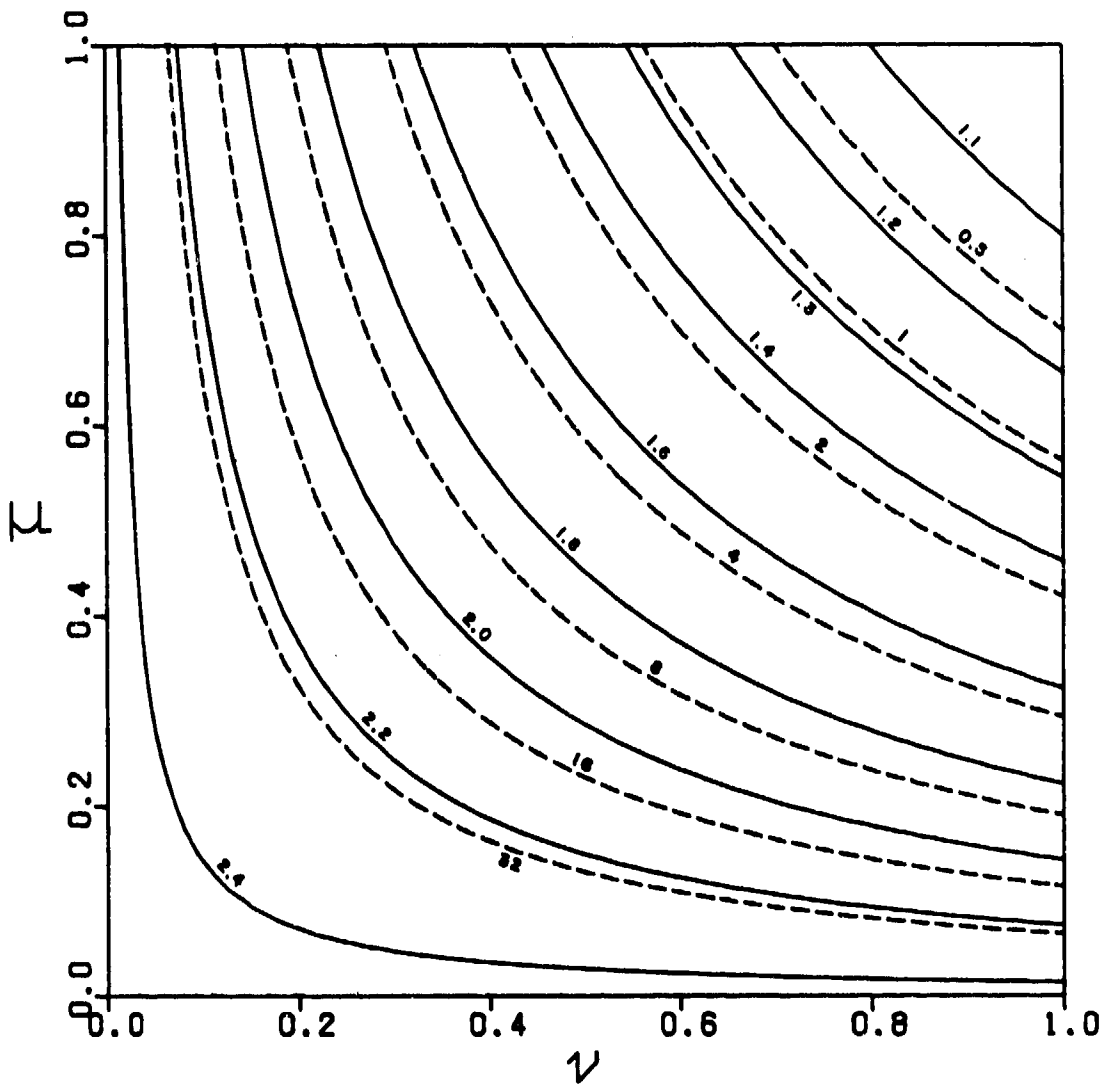
FIGURE 6   Performance Maps for Ideal Turbofans

c)   Secondary/Primary Mass Flow Ratio β = 5
     (——Augmentation φ, ———Specific Thrust f)

455
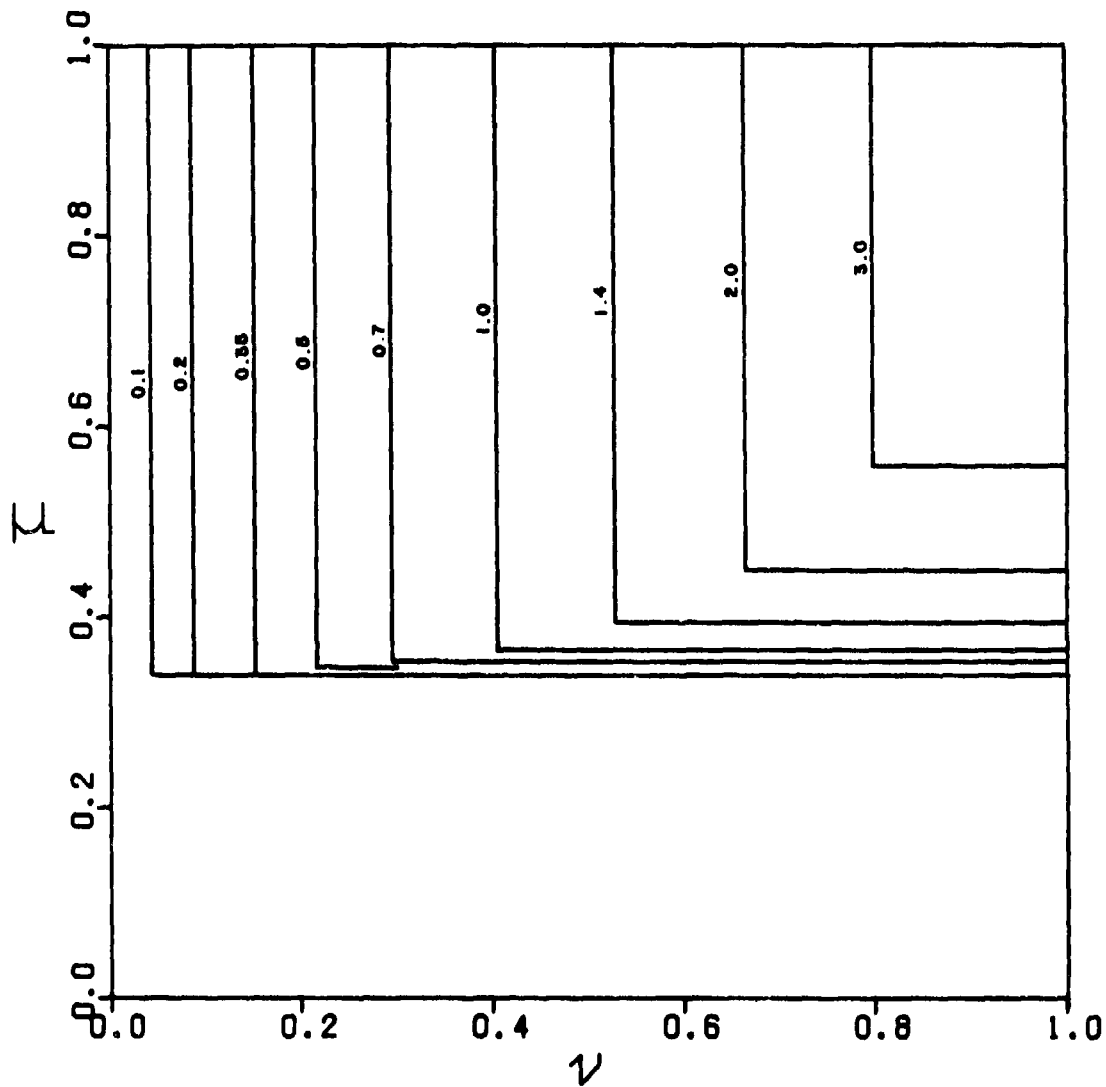
FIGURE 7  Attainable Regions of Performance Maps for
Various Mach Numbers

(The regions are to the right of the curves.)
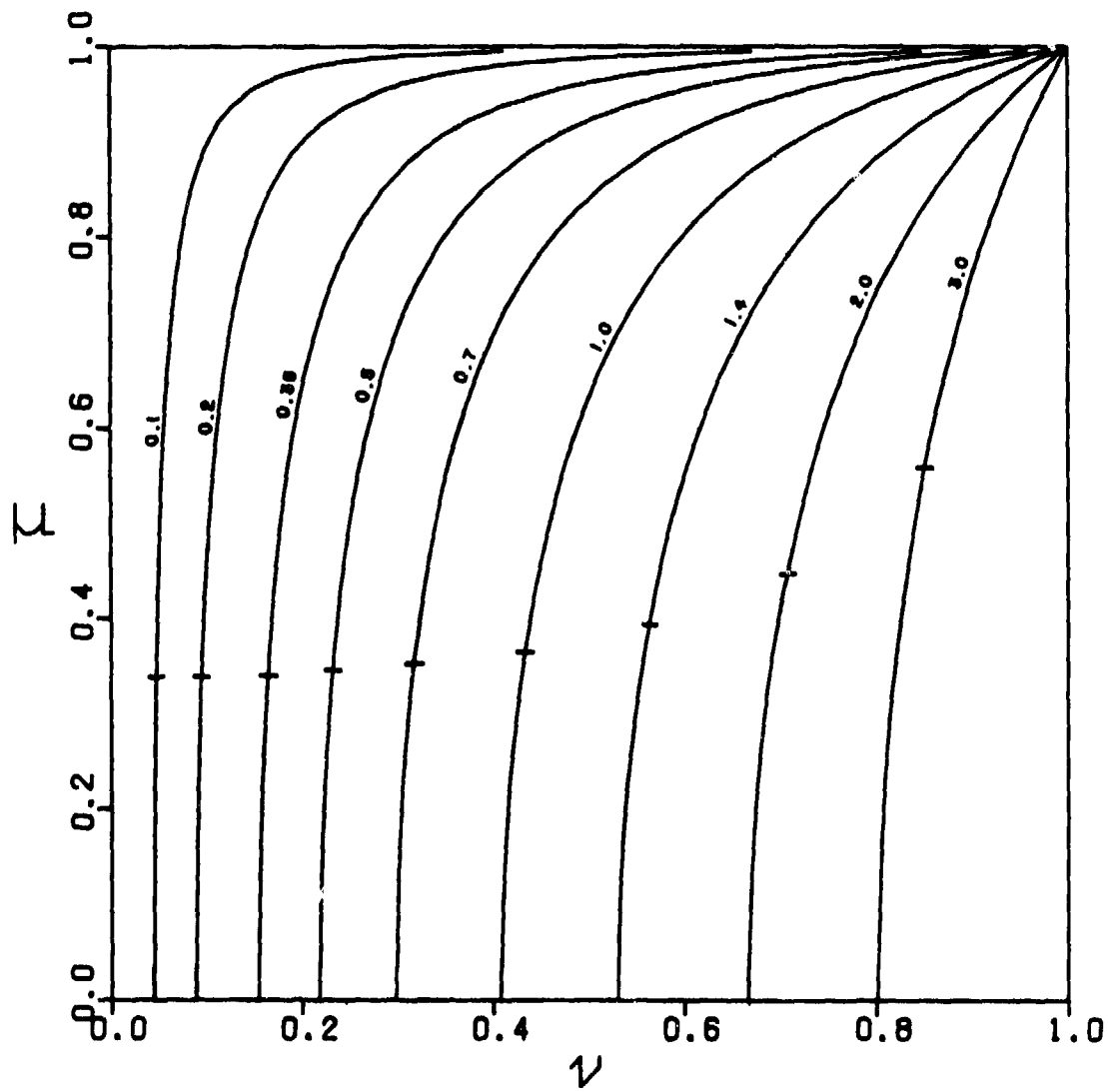
FIGURE 8   Isentropic Compressor Curves for Various
Mach Numbers
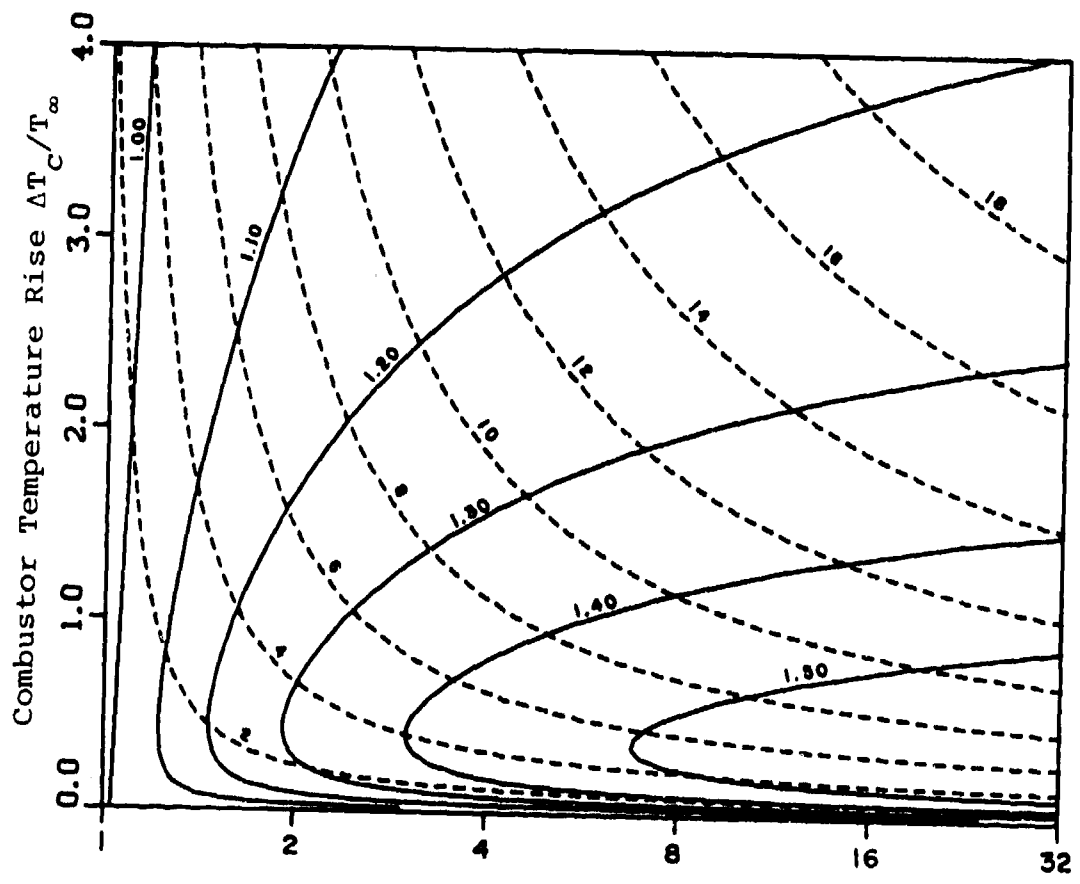
Core Turbojet Compressor Pressure Ratio - $P_{tc}/P_{ts}$

FIGURE 9   Performance Map for Ideal Ejectors with Turbine Engine Cores (Secondary/Primary Mass Flow Ratio $\beta = 5$)

a)   Mach Number $M_\infty = 0.2$
     (——Augmentation Ratio $\phi$, ---Specific Thrust f)
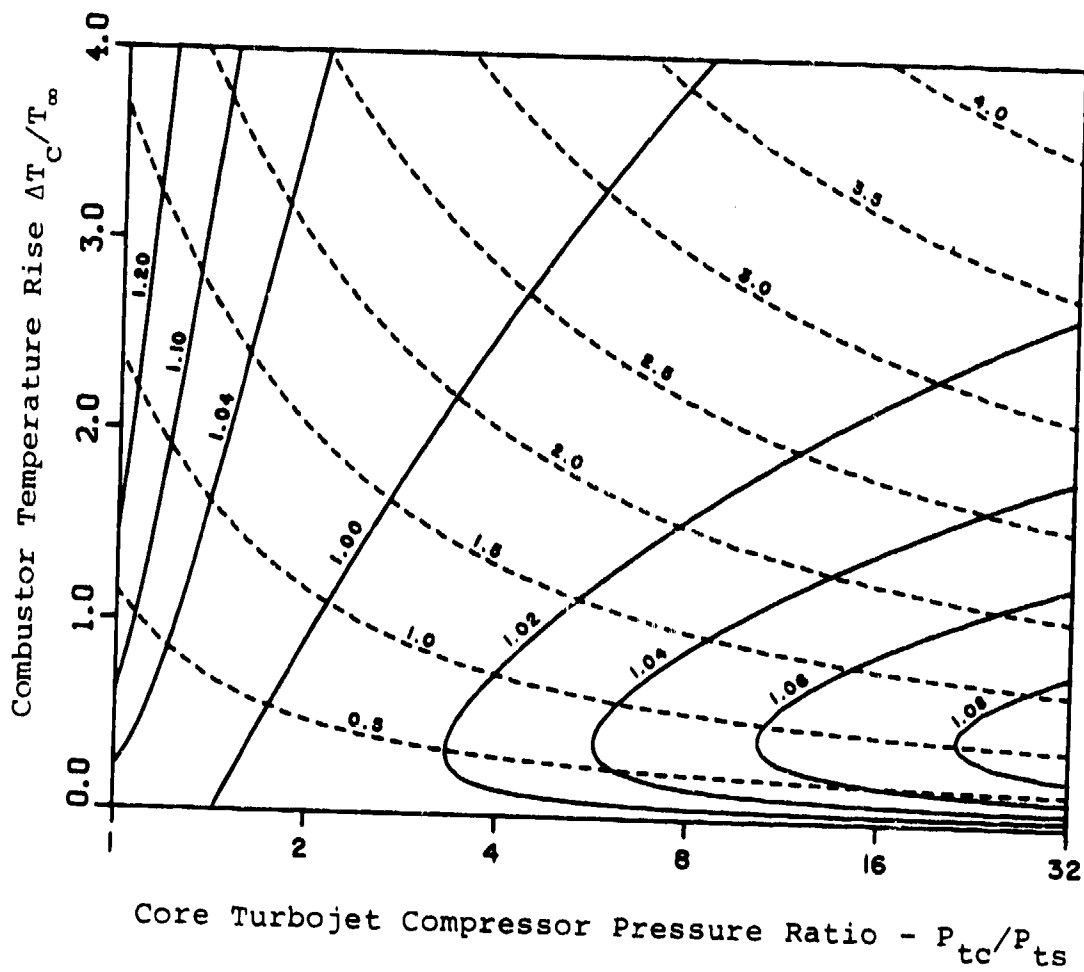
458

FIGURE 9   Performance Map for Ideal Ejectors with
Turbine Engine Cores (Secondary/Primary
Mass Flow Ratio β = 5)

b)   Mach Number $M_\infty$ = 0.7
(——Augmentation Ratio φ, ———Specific Thrust f)
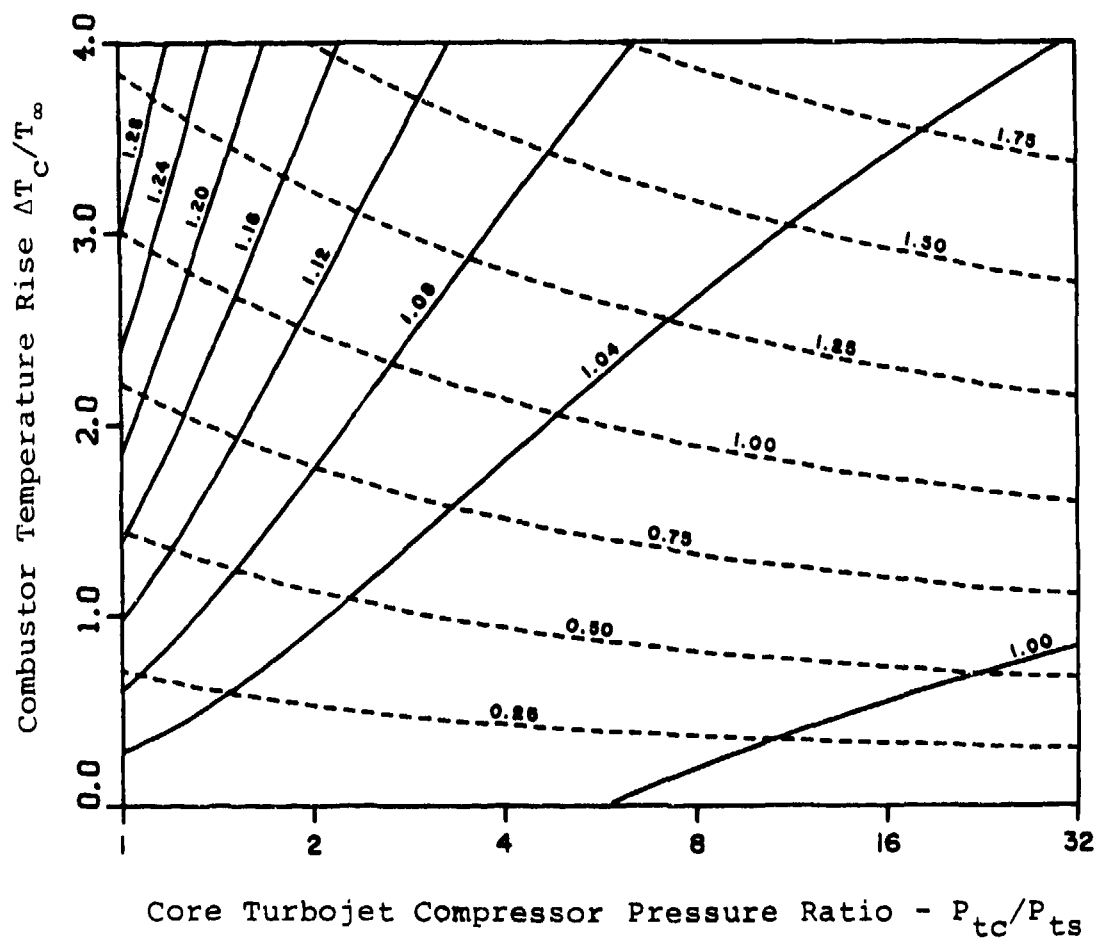
459

FIGURE 9  Performance Map for Ideal Ejectors with
Turbine Engine Cores (Secondary/Primary
Mass Flow Ratio β = 5)

c)  Mach Number $M_\infty$ = 1.4
(——Augmentation Ratio ϕ, ---Specific Thrust f)
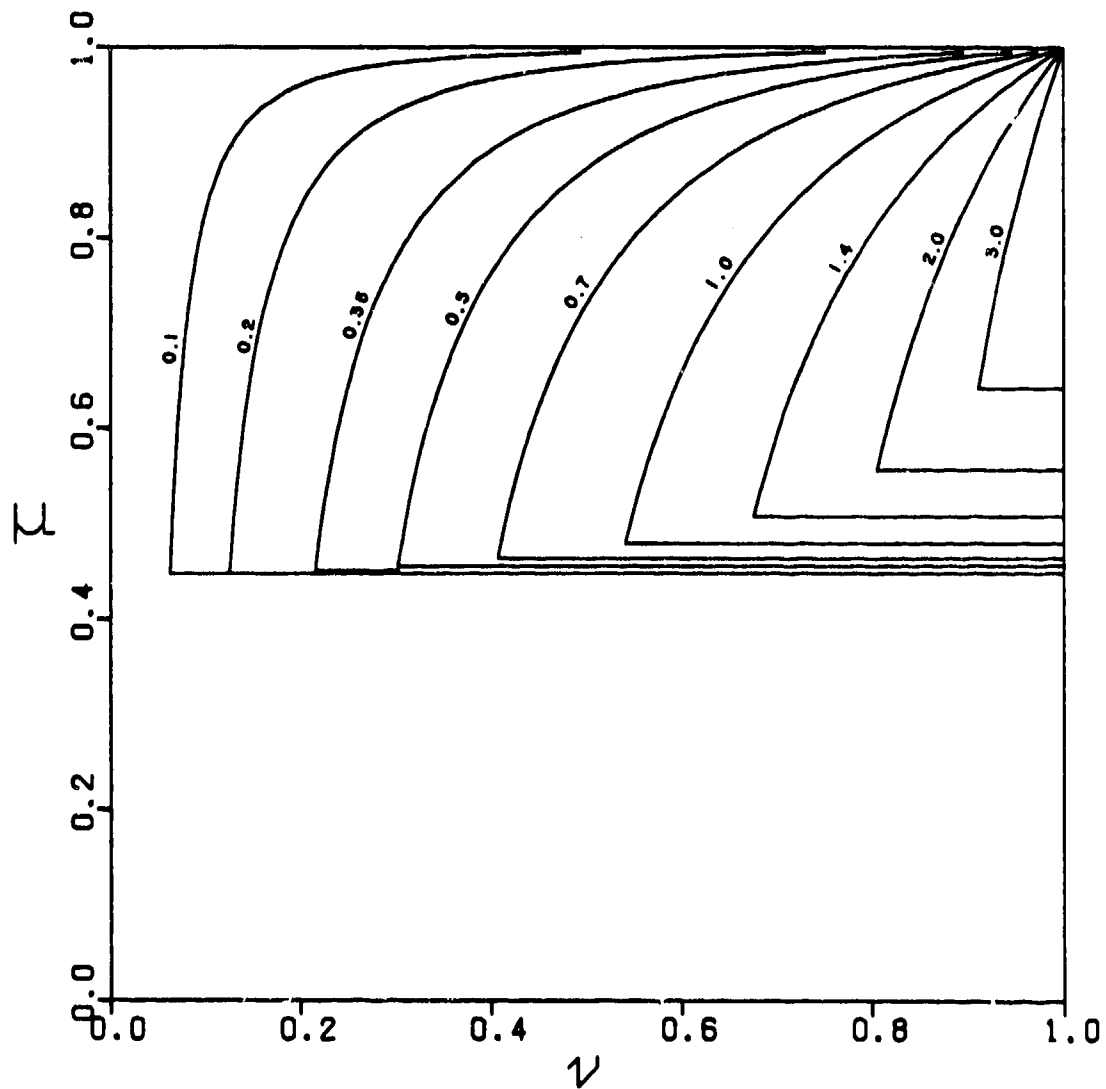
FIGURE 10    Mapping of the Core Turbine Engine of
            Figure 8 for Various Mach Numbers ($P_{tc}/P_{ts}$
            = 1-32, $\Delta T_C/T_\infty$ = 0-4)

(The regions are to the right of the curves.)

461

# REFERENCES

1. W. H. Heiser, "Thrust Augmentation," Journal of Engineering for Power (ASME Transactions), Vol 89, No 1, January 1967, pp 75-82.

2. R. M. Knox, "The Optimized Ejector-Nozzle Thrust Augmentor," Journal of the Aerospace Sciences, Vol 29, No 4, April 1962, pp. 470-471.

3. Equations, Tables and Charts for Compressible Flow, NACA Report 1135, 1953.

4. J. L. Porter, (Private Communication), August 1979.
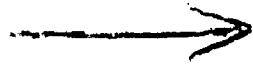
# Experimental Investigation

## of

## Oscillating Subsonic Jets

D. J. Collins and M. F. Platzer
Department of Aeronautics
Naval Postgraduate School


J. C. Lai and J. M. Simmons
Department of Mechanical Engineering
University of Queensland, Australia

# Experimental Investigation

## of

## Oscillating Subsonic Jets

D. J. Collins and M. F. Platzer
Naval Postgraduate School

and

J. C. S. Lai and J. M. Simmons
University of Queensland
Brisbane, Australia

The enclosed paper was first presented at the symposium on "Numerical and Physical Aspects of Aerodynamic Flows," California State University, Long Beach, California, 19–21 January 1981. A revised version will appear in the symposium proceedings to be published by the Springer Publishing House.

Work completed since January 1981 includes the set-up of a two-component laser system for the simultaneous measurement of the streamwise and normal velocity components. A first series of measurements has been completed indicating substantial agreement with the earlier measurements. The new measurements permit a more precise determination of the jet momentum.

EXPERIMENTAL INVESTIGATION
OF
OSCILLATING SUBSONIC JETS

D. J. Collins and M. F. Platzer
Naval Postgraduate School
Monterey, CA

and

J. C. S. Lai and J. M. Simmons
University of Queensland
Brisbane, Australia

## Abstract

The entrainment mechanisms in turbulent jets
and methods to increase the entrainment have been
a subject of considerable basic and applied inter-
est for many years. Recently, this problem has
attracted increased attention because of the need
to develop compact, yet highly efficient thrust
augmenting ejectors for VSTOL applications. Sev-
eral new techniques have been introduced or pro-
posed to increase the jet entrainment, e.g. hyper-
mixing, swirling, acoustic interactions, and un-
steady jet flows. Measurements are described for
two-dimensional turbulent free jets which are ex-
cited by forced vibration of a small vane located
in the jet potential core. Mean velocity measure-
ments using pitot tubes and hot wire or laser-
doppler anemometry show significantly increased
entrainment rates over the steady turbulent jet.
Measurement details and the effect of various pa-
rameters, such as nozzle pressure ratio, amplitude
and frequency of vane oscillation, are summarized.

## Introduction

Steady two-dimensional jet flows have at-
tracted the interest of many investigators due to
the fundamental and practical importance of such
flows. Much of the currently available informa-
tion has been summarized by Harsha (1971),
Rajaratnam (1976) and Everitt & Robins (1978).
Significant interest in unsteady jet flow effects
first was sparked by the development of the pulse
jet engine, especially when Bertin (1955) and
Lockwood (1963) noted the favorable effect of pul-
sating jet flow on secondary flow entrainment.
Lockwood (1963) also identified the generation of
ring vortices in pulsing flow, a phenomenon later
verified more clearly by Curtet & Girard (1973).
Further investigations of pulsating jet flows were
performed by Johnson & Yang (1968), Didelle, et al
(1972), Binder & Favre-Marinet (1973), Crow &
Champagne (1971) and, most recently, Bremhorst &
Harch (1977) and Bremhorst & Watson (1980). A
different type of unsteady jet flow is produced
by time-varying jet deflection, either by mechan-
ical oscillation of the jet nozzle or by fluidic
jet actuation. The flow patterns produced by a
mechanically oscillated jet exhausting into a
secondary flow recently were measured in some
detail by Simmons, et al (1978), whereas fluidic
jet nozzles were developed and investigated by
Viets (1975, 1979). A comparison of the entrain-
ment rates produced by pulsating or oscillating
jets, presented by Platzer, et al (1978), shows
remarkably different rates depending on the type of
jet unsteadiness.

The present investigation was motivated by the
quest for a simple, yet efficient method to in-
crease the jet entrainment for potential use in
thrust augmenting ejectors. As pointed out by
Schum (1975), the augmenter performance is criti-
cally dependent on achieving high entrainment rates
while maintaining high nozzle efficiencies if
volume is to be minimized for a desired augmenta-
tion ratio. Pulsating or fluidic jet nozzles have
the disadvantage of a more complicated nozzle
design and of decreased efficiency, hence a new
jet excitation scheme was adopted in the hope to
achieve a good compromise between enhanced jet
entrainment and decreased nozzle efficiency. For
this purpose a small vane situated in the poten-
tial core was excited into small pitch oscilla-
tions such that both frequency and amplitude of
oscillation could be varied over a significant
range. The investigation of this type of jet ex-
citation was stimulated by the encouraging results
reported by Fiedler & Korschelt (1979) who used a
freely vibrating vane for jet excitation.

In the following sections the experimental
set-up, the measuring techniques and results ob-
tained to date are presented. This paper consti-
tutes the second phase of an investigation begun
at the University of Queensland and reported
earlier by Simmons, et al (1979).

## Experiments

Mean velocity measurements were made in a vane
excited turbulent jet of air which issued into
stationary air from a plenum chamber through a
rectangular nozzle of length L = 300mm and width
h = 6mm (Fig. 1). Wire gauges and honeycombs were
installed upstream of the nozzle to reduce the tur-
bulence at the jet exit. No side plates were used
to contain the jet. The chamber pressure and tem-
perature were continuously monitored          σ t.
experiment through a manometer and a          coup_e
respectively.

A vane which had a symmetric air. l section
with a thickness of 1.3mm, a span of 360mm and a
chord of 10mm was located symmetrically in the
potential core at 1.42h from the nozzle. The vane
was oscillated by a reciprocating rod with an ec-
centricity e driven through a motor. Various
frequencies and amplitudes of oscillation of the
vane about a mean position set at zero angle of
attack could be attained by varying respectively
the power input to the motor and the eccentricity
e . Since the vane fluttered at high nozzle pres-
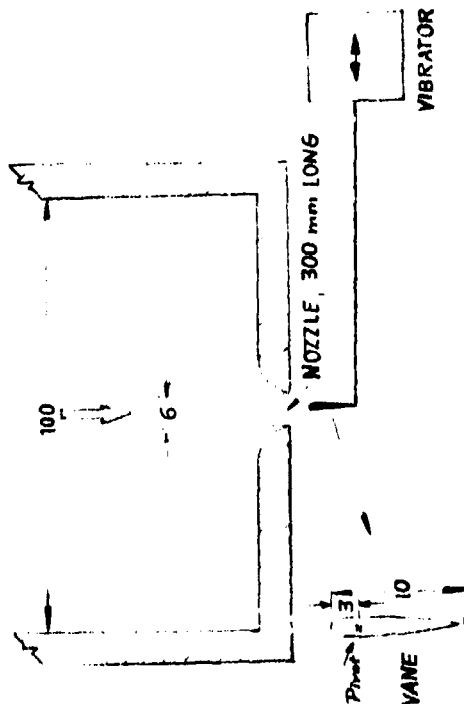
Fig. 1  Configuration of Nozzle and

Oscillating Vane (All dimensions in millimeters).

sure ratio of operation, it was supported with two
bearings 4.5mm thick each and 123mm apart, hence
reducing the nozzle's aspect ratio to an effective
value of 1:20. This aspect ratio is still con-
sidered acceptable for two-dimensional jets, e.g.
Forthmann (1946), Zijnen (1958) and Goldschmidt
and Eskinazi (1965).

Typical jet temperatures on the center line
at the exit, 20, 40 and 60 nozzle widths down-
stream, were $7^oC$, $3^oC$, $1^oC$ and $0.5^oC$ respectively
above ambient. However, these will not have any
significant effect on the jet measurements.

For the convenient operation of the Laser
Doppler Velocimeter, the facility was designed such
that a velocity traverse across the jet was ob-
tained by fixing the probe (pitot-tube or LDV) in
space and moving the jet with a hydraulic lifting
device.

The mean velocity measurements were made
across the width of the jet at its midspan and at
distances of 20, 40 and 60 nozzle widths downstream
of the nozzle for the following range of parameters:

## Instrumentation

### Pitot-Static Tube

A pitot-static tube of hole internal diameter
0.74mm was used by aligning it with the mean flow
direction. The tube had four static holes located
symmetrically around the periphery at 17 tube dia-
meters. The mean pressure obtained with a pitot-
static tube in a fluctuating flow is generally
given by

$$P_t - P_s = \frac{1}{2} \rho \cdot [U^2 + K_1 \overline{u^2} + K_2 (\overline{v^2} + \overline{w^2})]$$

where $P_t$ and $P_s$ are the total and static pres-
sures, $U$ the mean velocity, $u$, $v$ and $w$ the
velocity fluctuations in the streamwise and the
two transverse directions. $K_1$ and $K_2$ are of
order unity. Bradshaw and Goodman (1968) con-
cluded that in highly turbulent jets, for dis-
tances less than 150 nozzle widths, the measured
static pressure is higher than the actual value.
Harsha (1971, page 69) noted that the deviation of
the total head tube reading caused by changes in
turbulence intensities is commonly ignored.
Alexander, et al (1953) observed that the total
pressure decreased markedly with increasing rela-
tive turbulence level. On the other hand, Krause,
Dudzinski and Johnson (1974) observed that in pul-
sating flows total pressure tubes indicate values
higher than the true average pressure. In the
present measurements no attempt was made to correct
for errors due to fluctuating flow effects. How-
ever, it was noted that for both the steady and
vane excited jet it was necessary to measure the
static pressure simultaneously with the total head
pressure because of a significant static pressure
variation throughout the jet. Such variations were
reported earlier by Miller and Comings (1957).

### Hot Wire Anemometer[*]

A constant temperature hot-wire anemometer was
used, the wire being a platinum alloy 10 μm dia-
meter with its 4mm length aligned parallel to the
length of the nozzle. The anemometer was operated
at a constant resistance ratio of 1.3 which gives a

---

x)The hot wire measurements were performed by the
last three authors on a set-up at the University of
Queensland quite similar to the one shown in Fig. 1.
The pitot-tube and LDV measurements were performed
by the first three authors at the Naval Postgrad-
uate School.

mean wire temperature of the order of $700^\circ K$. Typical jet temperatures on the centre line at 20, 40 and 60 nozzle widths downstream were $4^\circ C$, $3^\circ C$ and $2^\circ C$ respectively above ambient so that the cold resistance of the wire varied by at most 1%. An analysis showed that a temperature change of $8^\circ C$ gives a change of only 2% in the temperature sensitivity of the wire. Hence a first order temperature correction to the anemometer calibration was adequately achieved by operating the wire at a constant resistance ratio with its cold resistance determined by local jet conditions.

## Laser Doppler Anemometer

A single component, dual beam laser-doppler velocimeter was used in the forward scatter mode with an on-axis photomultiplier for detecting the signals. The laser was a Spectra-Physics Model 164 Argon-Ion laser operated at a wavelength of 514.5nm with 200 to 500 mw of power. The optics system was that of a DISA two color system with a beam separation of 27.6mm and 9.2mm. The two beams of the laser were focused on the measurement point by means of a 600mm lens. Frequency shifting was used to separate the pedestal from the doppler signal. Particles, generated from olive oil by a TSI Model 3075 constant output atomizer, were seeded at a rate of 0.3cc/mm in the plenum chamber upstream of the nozzle. Also, before actual measurements were taken, the surrounding environment of the jet was heavily seeded to ensure a uniform distribution of particles both in the fluid originating from the nozzle and the surrounding so that bias due to non-uniform seeding could be managed. Particle sizes, though variable, never exceeded 1 μm. The particles therefore had a size of the order of the fringe spacing in the operating mode of beam separation used and thus yielded signals with full modulation. Dynamic calculations indicate that the seed particles will track the flow with a relaxation time of the order of $10^{-6}$ sec. The Doppler signals received by the photomultiplier were transmitted to a DISA 55L90 LDA counter for further processing. Counters, alternatively known as burst-signal processors which measure the velocity of individual particles, are, by far, the most versatile LDV signal processors as compared with trackers, frequency analyzers and photocorrelators and are especially suitable for low particle concentration provided that the signal to noise ratio is adequate. The signals were first band-pass filtered to remove the high frequency noise and the low frequency pedestal. The filters were used in conjunction with threshold window adjustments which set the upper amplitude limit to reject signals from large particles and amplifier gain control which attenuated the input signal to reduce the noise signal to below the circuit trigger level. The signals were then validated based on a 5/8 comparison mode with a tolerance accuracy of ±1.5% or ±3%. Details of the validation circuit and operation of the counter are available in the DISA instruction manual (1976). The validated signals were further reduced on-line by an HP9825A microcomputer to extract the mean axial velocity component $U$ and the aggregate axial turbulence $\bar{u}^2$. Histograms, were taken of selected points during the experiment. The histograms were used to determined the filter bandpass setting and on-line graphs of the experimental results were also obtained.

Using computer simulation Hoesel and Rodi (1975) showed that the error in LDV mean velocity is inversely proportional to the bandwidth of the bandpass filter. Throughout the experiments, the signal-to-noise ratio was continuously monitored to give a value of 20 which is adequate for LDV data processed by counters. On-line histogram plots of particle velocity distribution were used to help select the most appropriate band pass filter values and the value of the shift frequency. Validated signals were received at a rate of about 200-600/ sec. Assuming that the particle velocity distribution is Gaussian, 95% of the data should fall within $\pm 2\sigma$ limits, where $\sigma$ is the standard deviation. These limits were used to ensure that the band-pass filters were wide enough to accept at least 95% of the data.

## Results

Figure 2 shows the mean velocity profiles obtained by hot wire anemometry at 60 nozzle widths from the jet exit. The vane amplitude was 5.2 degrees zero-to-peak, the vane chord was 10mm and the vane leading edge was located at 3.3mm from the jet exit. The jet exit velocity was 36.4m/sec. The vane oscillation produces a substantial spreading of the jet which is accompanied by a much faster center velocity decay than is obtained for the steady jet. However, it should be noted that the hot wire measures the velocity magnitude rather than the u-velocity component. Hence, the hot wire measurements overestimate the entrainment, as is indeed confirmed by the pitot tube and LDV measurements.

Figures 3 and 4 depict typical center-line velocity decays and jet spreading trends as a function of downstream distance, measured by the pitot tube. These results were obtained for a pressure ratio of 1.137 and a vane amplitude of 2.6 degrees zero-to-peak. Jet spreading is seen to increase with increasing frequency, which is accompanied by a decrease in centerline velocity with increasing frequency. Figures 5 show a comparison of the velocity profiles measured by the pitot-static tube and by the laser-doppler velocimeter for several parameter combinations.

It can be seen that the LDV consistently measures low compared to the pitot tube, even in steady jet flow and especially in the high turbulence regions of the jet. Further measurements are clearly needed to evaluate the accuracy of both measuring techniques in these regions.

Table 1 lists the entrainment results obtained to date for three pressure ratios, three vane amplitudes, three frequencies (20, 30, 40Hz) at three downstream stations (20, 40, 60x/h). Both the LDV and pitot tube measurements are shown. The following trends can be recognized:

a) Increasing vane amplitude and frequency substantially increase the entrainment.

b) Entrainment decreases with increasing pressure ratio.

Typical entrainment increases range from 10% to 175% depending on frequency, amplitude and pressure ratio. For example, at the highest pressure ratio
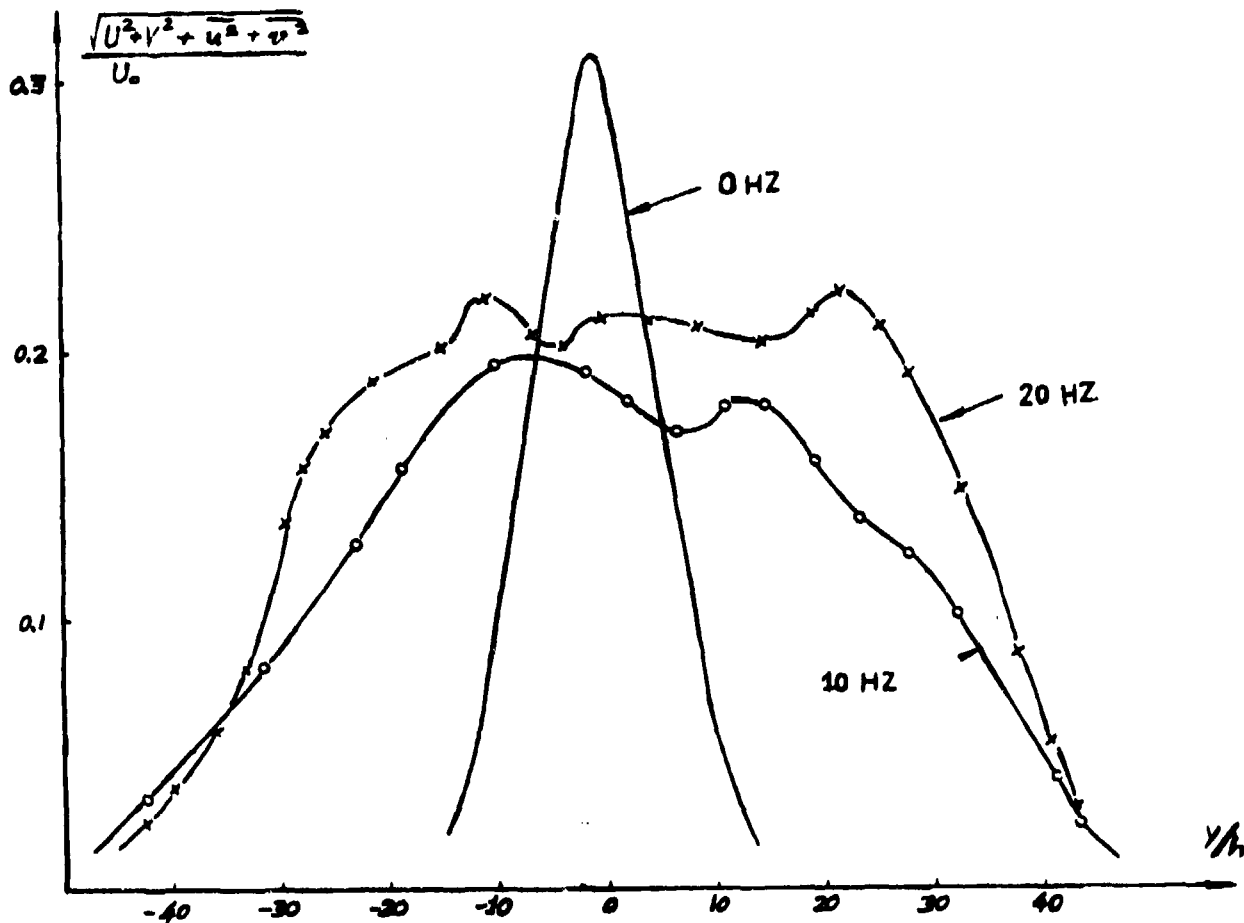
Fig. 2 Profiles of Mean Jet Velocity Magnitude Measured with Hot Wire at 60 Nozzle Widths downstream of Nozzle. Vane is Located 3.3mm from Nozzle and Amplitude of Oscillation is 5.2 degrees aero-peak. Jet Exit Velocity $u_0 = 36.4$ m/sec.
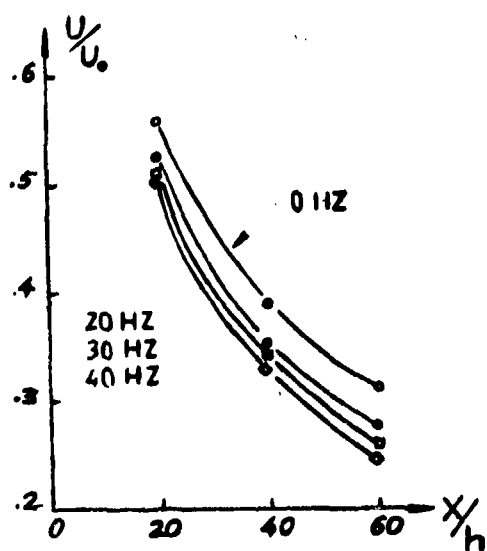


Fig. 3 Mean Center-Line Velocity Decay as a Function of Downstream Distance, Measured with Pitot Tube at a Vane Frequency of 0,20 30,40 Hz, Amplitude of 2.6 Degrees, Pressure Ratio 1.137
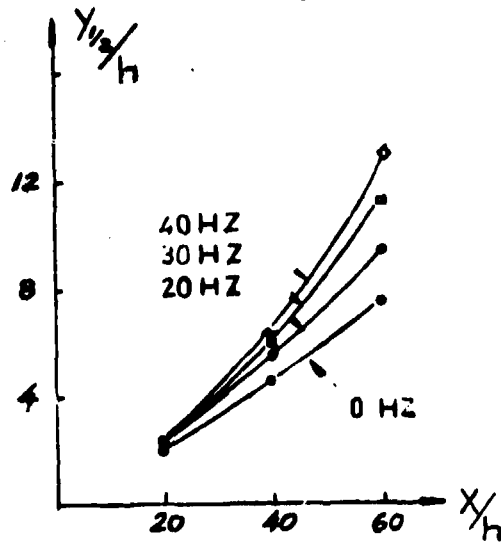


Fig. 4 Mean Jet-Spreading (Jet Half-Width) as a Function of Downstream Distance, Measured with Pitot Tube at a Vane Frequency of 0,20,30,40 Hz, Amplitude of 2.6 Degrees, Pressure Ratio 1.137

468
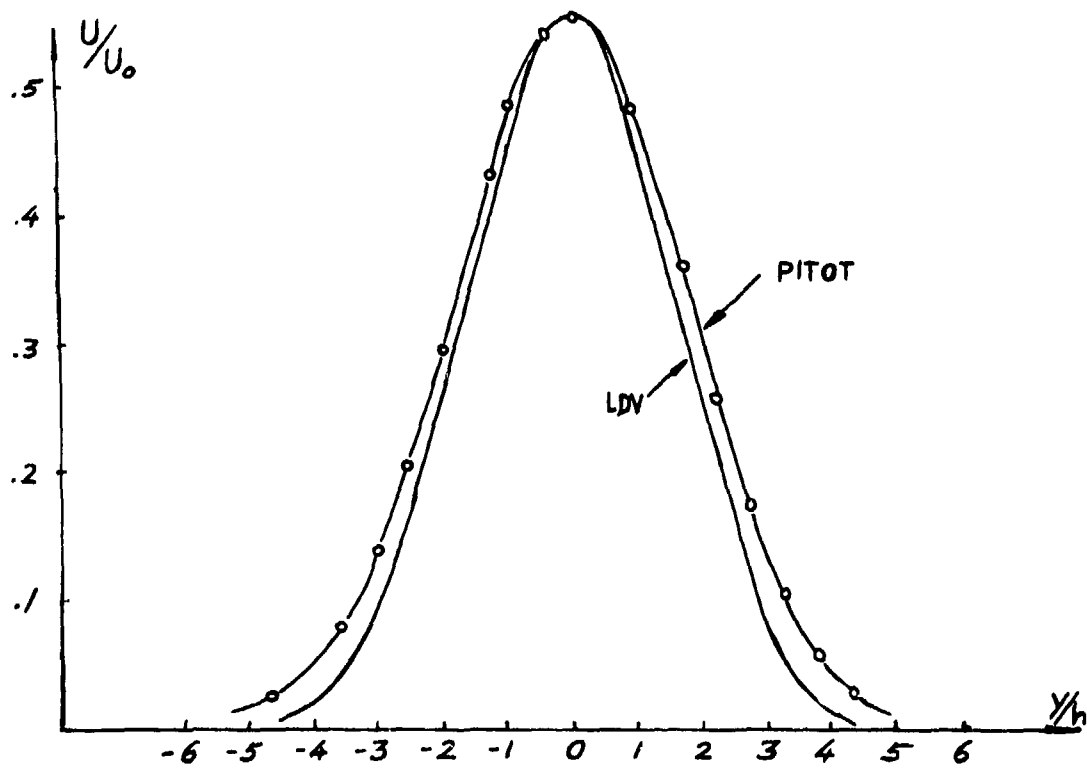
Fig. 5A  Comparison between Measured Velocity Profiles at 20 Nozzle Widths, Pressure
Ratio 1.137, Zero Frequency and Amplitude.
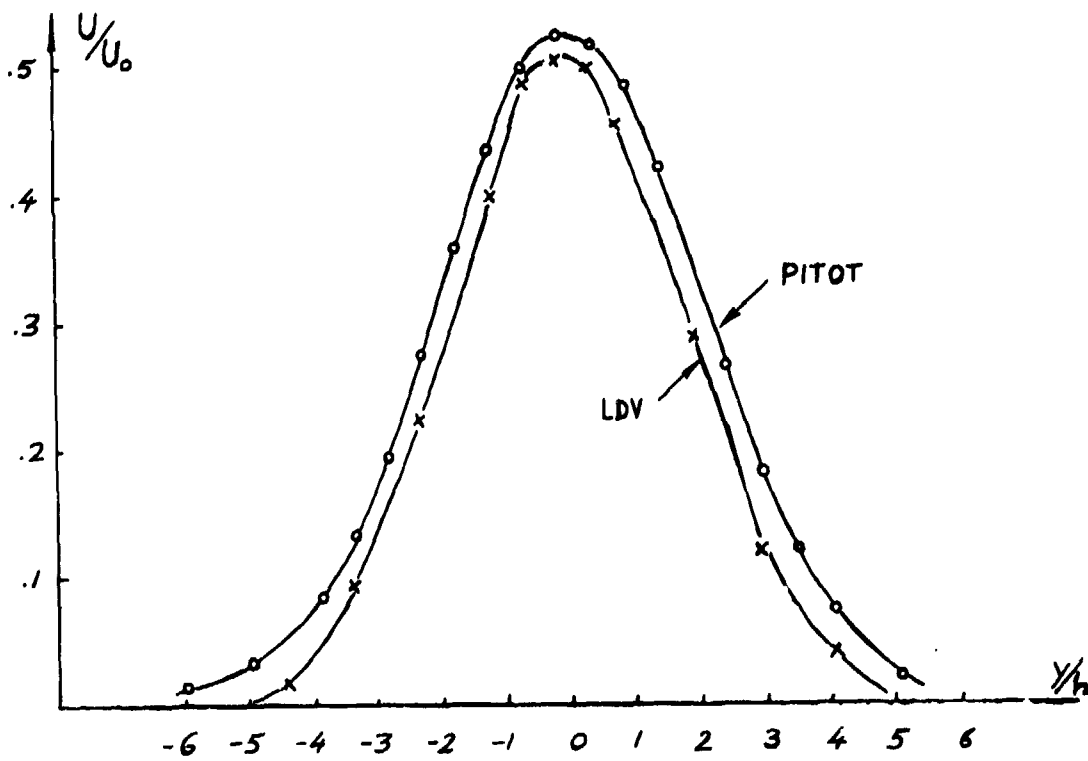


Fig. 5B  Comparison between Measured Velocity Profiles at 20 Nozzle Widths, Pressure
Ratio 1.137, Vane Amplitude 2.6 degrees zero-to-peak, Frequency 30Hz.
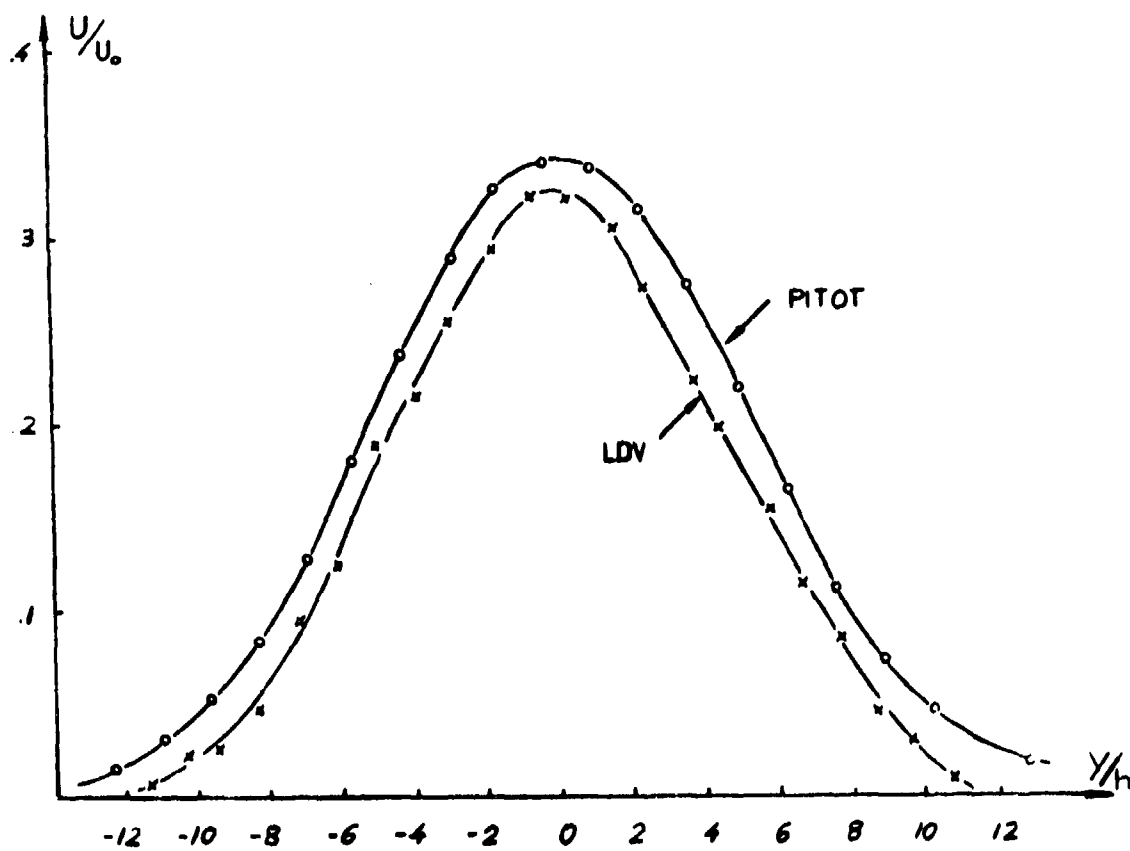
Fig. 5C Comparison between Measured Velocity Profiles at 40 Nozzle Widths, Pressure
Ratio 1.137, Vane Amplitude 2.6 degrees zero-to-peak, Frequency 30Hz.
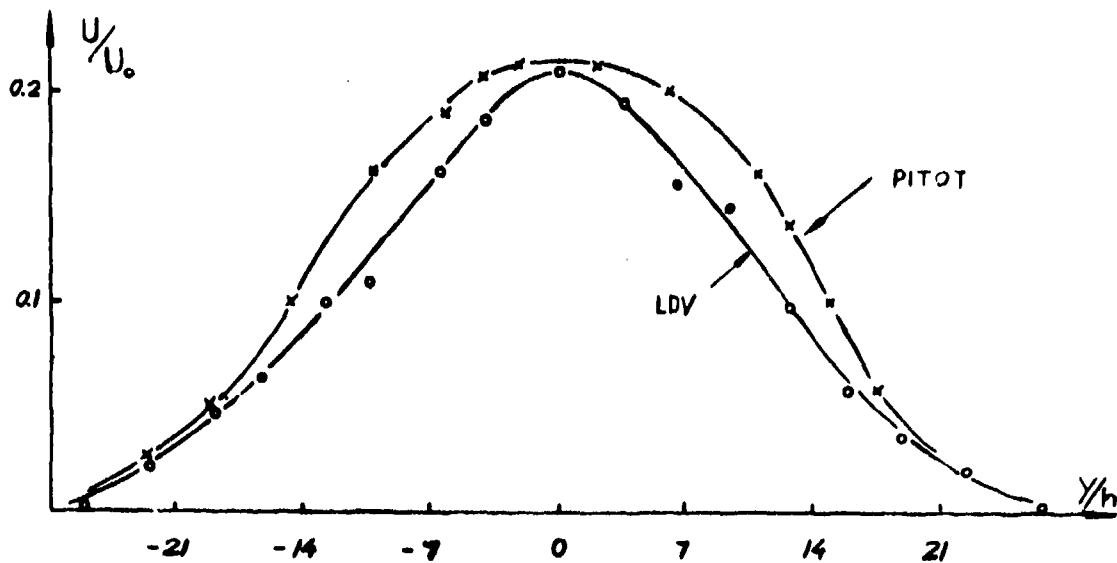


Fig. 5D Comparison between Measured Velocity Profiles at 60 Nozzle Widths, Pressure
Ratio 1.268, Vane Amplitude 4.6 degrees, zero-to-peak, Frequency 30Hz.

470

| | Vane | Station 20x/h | | Station 40x/h | | Station 60x/h | |
|---|---|---|---|---|---|---|---|
| Frequency | Amplitude | LDV | Pitot | LDV | Pitot | LDV | Pitot |
| 0 | 0 | 1.45 | 1.45 | 2.52 | 2.7 | | 3.8 |
| 20 | 2.6 | 1.79 | 1.6 | 4.11 | 3.75 | | 5.9 |
| 30 | 2.6 | 1.89 | 1.8 | 4.2 | 4.1 | | 7.25 |
| 40 | 2.6 | 2.09 | 2 | 4.31 | 4.4 | | 7.75 |
| 20 | 4.6 | 2.57 | 2.1 | 5.18 | 4.6 | | |
| 30 | 4.6 | 2.92 | 2.4 | 5.53 | 5.1 | | |
| 40 | 4.6 | 3.24 | 2.7 | 6.02 | 5.7 | | |
| 20 | 6.9 | 3.16 | 2.5 | 5.7 | 4.9 | | |
| 30 | 6.9 | 3.19 | 2.9 | 6.19 | 5.4 | | |
| 40 | 6.9 | 3.26 | 3.1 | 6.98 | 5.9 | | |

Table 1A   Entrainment $\dfrac{Q(x)}{Q_E} - 1$   at Pressure Ratio 1.008

| | Vane | Station 20x/h | | Station 40x/h | | Station 60x/h | |
|---|---|---|---|---|---|---|---|
| Frequency | Amplitude | LDV | Pitot | LDV | Pitot | LDV | Pitot |
| 0 | 0 | 1.18 | 1.5 | 2.2 | 2.8 | 3.6 | 4 |
| 20 | 2.6 | 1.39 | 1.6 | 2.4 | 3.1 | 3.83 | 4.7 |
| 30 | 2.6 | 1.29 | 1.7 | 2.56 | 3.3 | 4.3 | 5.2 |
| 40 | 2.6 | 1.28 | 1.7 | 2.58 | 3.5 | 4.42 | 5.6 |
| 20 | 4.6 | 1.41 | 1.9 | 2.18 | 3.6 | 4.55 | 5.2 |
| 30 | 4.6 | 1.44 | 2 | 2.47 | 3.9 | 4.96 | 6.2 |
| 40 | 4.6 | 1.39 | 2 | 2.8 | 4.2 | 5.34 | 6.7 |
| 20 | 6.9 | 1.48 | 3.1 | 2.32 | 3.9 | 5.49 | 5.8 |
| 30 | 6.9 | 1.65 | 3.1 | 2.72 | 4.3 | 6.4 | 6.9 |
| 40 | 6.9 | 1.71 | 3.3 | 3.31 | 4.9 | 6.69 | 7.8 |

Table 1B   Entrainment $\dfrac{Q(x)}{Q_E} - 1$   at Pressure Ratio 1.137

| | Vane | Station 20x/h | | Station 40x/h | | Station 60x/h | |
|---|---|---|---|---|---|---|---|
| Frequency | Amplitude | LDV | Pitot | LDV | Pitot | LDV | Pitot |
| 0 | 0 | 1.08 | 1.5 | 2.2 | 2.7 | 3.16 | 3.8 |
| 20 | 2.6 | 1.11 | 1.6 | 2.2 | 2.9 | 3.17 | 4.2 |
| 30 | 2.6 | 1.15 | 1.6 | 2.3 | 3.1 | 3.6 | 4.5 |
| 40 | 2.6 | 1.00 | 1.7 | 2.43 | 3.2 | 4 | 4.8 |
| 20 | 4.6 | 1.01 | 1.8 | 2.24 | 3.3 | 3.67 | 4.8 |
| 30 | 4.6 | 1.30 | 1.9 | 2.24 | 3.6 | 4.22 | 5.5 |
| 40 | 4.6 | 1.33 | 2 | 2.36 | 3.9 | 5.87 | 6 |
| 20 | 6.9 | 1.20 | 2 | 2.30 | 3.7 | 4.14 | 5.5 |
| 30 | 6.9 | 1.21 | 2.1 | 2.63 | 4 | 5.7 | 6.1 |
| 40 | 6.9 | 1.17 | 2.3 | 2.79 | 4.5 | 6.4 | 7.1 |

Table 1C   Entrainment $\dfrac{Q(x)}{Q_E} - 1$ at Pressure Ratio 1.268

measured (1.268), the entrainment increase at station 60 is still between 30% to 100% for an amplitude of 6.9 degrees at frequencies ranging from 20 to 40 Hz.

Considerable differences can be noted in some cases between the pitot tube and LDV results, especially for large frequencies and amplitudes. This is to be expected due to the measuring uncertainties of pitot tubes in oscillatory flow. However, significant differences also are obtained in steady jet flows which occur mainly in the high turbulence regions of the velocity profiles, Figures 5.

Salter, ARL-Report 75-0132, gives the following formula for the entrainment of steady rectangular jets

$$\frac{Q(x)}{Q_E} = (0.6 - 0.04 \frac{P_c}{P_A}) (\frac{x}{h})^{1/2}$$

which produces the following values for the three pressure ratios and stations measured:

471

$$\frac{Q(x)}{Q_E} - 1 = 1.5, \quad 2.54, \quad 3.33 \quad \text{at } P_c/P_A = 1.008$$

20x/h  40x/h  60x/h

$$= 1.48, \quad 2.51, \quad 3.3 \quad \text{at } P_c/P_A = 1.137$$

$$= 1.46, \quad 2.47, \quad 3.26 \quad \text{at } P_c/P_A = 1.268$$

## Analysis

Tennekes and Lumley (1972) show that for plane turbulent jets the cross-stream momentum equation

$$U\frac{\partial V}{\partial x} + V\frac{\partial V}{\partial y} + \frac{\partial}{\partial x}(\overline{uv}) + \frac{\partial}{\partial y}(\overline{v^2}) = -\frac{1}{\rho}\frac{\partial P}{\partial y} + \nu(\frac{\partial^2 V}{\partial x^2} + \frac{\partial^2 V}{\partial y^2})$$

can be approximated by retaining only the two terms

$$\frac{\partial}{\partial y}(\overline{v^2}) = -\frac{1}{\rho}\frac{\partial P}{\partial y} \tag{1}$$

Here $U$, $V$ are the mean velocities in the $x$ and $y$ directions, $u$, $v$ the velocity fluctuations, $P$ the static pressure and $\nu$ the kinematic viscosity. This approximation assumes that the turbulence intensities are about half an order of magnitude smaller than the jet velocity, i.e.,

$$\frac{u}{U_s} = 0(\frac{\ell}{L})^{1/2}$$

where $U_s$ is the maximum jet velocity, $\ell$ is the cross-stream length scale and $L$ the streamwise length scale. The velocity scale for the turbulence is indicated by $u$, so that

$$-\overline{uv} = 0(u^2) \; ; \quad \overline{u^2} = 0(u^2) \; ; \quad \overline{v^2} = 0(u^2)$$

Integrating Eg. (1) and assuming no imposed external pressure gradient leads to

$$\frac{1}{\rho}\frac{\partial P}{\partial x} + \frac{\partial}{\partial x}(\overline{v^2}) = 0 \tag{2}$$

Hence, the streamwise momentum equation

$$U\frac{\partial U}{\partial x} + V\frac{\partial U}{\partial y} + \frac{\partial}{\partial x}(\overline{u^2} - \overline{v^2}) + \frac{\partial}{\partial y}(\overline{uv}) = \nu(\frac{\partial^2 U}{\partial x^2} + \frac{\partial^2 U}{\partial y^2})$$

becomes

$$U\frac{\partial U}{\partial x} + V\frac{\partial U}{\partial y} + \frac{\partial}{\partial y}(\overline{uv}) = 0 \tag{3}$$

where only the first, second and fourth term have been retained and where it has been assumed that

$$\frac{U_s}{u} \cdot \frac{1}{\text{Re}}(\frac{\ell}{L}) \to 0$$

which is always satisfied for sufficiently large Reynolds number Re .

Integration of Eq. (3) with respect to $y$ gives the well known condition of momentum conservation

$$\rho \int_{-\infty}^{+\infty} U^2 \, dy = M_o \tag{4}$$

where $M_o$ is the total amount of momentum put into the jet at the origin per unit time.

The third and fourth terms in the streamwise momentum equation differ by a factor of order $0(\frac{\ell}{L})$. For the vane excited jet the cross-stream length scale $\ell$ will be significantly larger than for the non-excited jet. This suggests to retain these terms thus leading to the following more accurate condition for momentum conservation

$$\int_{-\infty}^{+\infty} (U^2 + \overline{u^2} - \overline{v^2}) \, dy = \text{Const} \tag{5}$$

In Table 2

$$M_1 = \int_{-\infty}^{+\infty} U^2 \, dy \quad \text{and} \quad M_2 = \int_{-\infty}^{+\infty} (U^2 + \overline{u^2}) dy \quad \text{are}$$

plotted from the available LDV data. For the lowest pressure ratio, 1.008, a significant increase in both jet momentum values is observed in the excited jet. The additional momentum imparted to the flow by the oscillating vane in this case is likely to be a substantial percentage of the initial jet momentum. Since this imparted momentum remains essentially constant at the higher pressure ratios, its contribution becomes less significant in comparison to the available initial jet momentum. Indeed, the momentum values at the two higher pressure ratios exhibit no significant differences between the steady and the excited jet momentum values. However, it can be noted that the $M_2$-values increase with increasing downstream distance and with increasing vane amplitude, in apparent violation of momentum conservancy. Here, it must be remembered that the condition for momentum conservation Eq. (5) contains at least another additional term, i.e., the fluctuating cross-flow momentum. Therefore, any definite statements about momentum conservation must await the measurement of the cross-flow fluctuations. Such measure- are planned in the next phase of this investigation. Also, a more detailed analysis will be attempted based on the unsteady shear layer equations for turbulent flow. Prescribing sinusoidal jet deflection these equations will be solved using the Cebeci-Keller box method similar to the analysis of pulsating jets by Lai & Simmons (1980) and by Carrion (1980). Finally, it is interesting to note that the $M_1$ and $M_2$ values differ only by about 10% for the steady jet, thus indicating the small contribution of the turbulent fluctuations. In contrast, the excited jet exhibits quite substantial variations between these two momentum integrals again indicating the need for more detailed measurements and analyses of this type of jet flow.

## Momentum $M_2$ at Pressure Ratio 1.008

| Frequency | Amplitude | Station 20 x/h | Station 40 x/h | Station 60 x/h |
|---|---|---|---|---|
| 0 | 0 | 1.13 | 1.1 | |
| 20 | 2.6 | 1.34 | 1.58 | |
| 30 | 2.6 | 1.33 | 1.56 | |
| 40 | 2.6 | 1.45 | 1.52 | |
| 20 | 4.6 | 1.66 | 1.85 | |
| 30 | 4.6 | 1.81 | 1.74 | |
| 40 | 4.6 | 1.94 | 1.82 | |
| 20 | 6.9 | 1.96 | 1.83 | |
| 30 | 6.9 | 1.91 | 1.8 | |
| 40 | 6.9 | 1.79 | 1.96 | |

## Momentum $M_1$ at Pressure Ratio 1.008

| Frequency | Amplitude | Station 20 x/h | Station 40 x/h | Station 60 x/h |
|---|---|---|---|---|
| 0 | 0 | 1.03 | 0.99 | |
| 20 | 2.6 | 1.15 | 1.36 | |
| 30 | 2.6 | 1.11 | 1.36 | |
| 40 | 2.6 | 1.17 | 1.32 | |
| 20 | 4.6 | 1.38 | 1.58 | |
| 30 | 4.6 | 1.5 | 1.5 | |
| 40 | 4.6 | 1.64 | 1.57 | |
| 20 | 6.9 | 1.59 | 1.54 | |
| 30 | 6.9 | 1.49 | 1.53 | |
| 40 | 6.9 | 1.43 | 1.68 | |

## Momentum $M_2$ at Pressure Ratio 1.137

| Frequency | Amplitude | Station 20 x/h | Station 40 x/h | Station 60 x/h |
|---|---|---|---|---|
| 0 | 0 | .97 | .97 | 1.03 |
| 20 | 2.6 | 1.09 | 1.02 | 1.09 |
| 30 | 2.6 | 1.05 | 1.05 | 1.12 |
| 40 | 2.6 | 1.04 | 1.01 | 1.06 |
| 20 | 4.6 | 1.13 | .97 | 1.18 |
| 30 | 4.6 | 1.13 | 1 | 1.12 |
| 40 | 4.6 | 1.08 | .99 | 1.14 |
| 20 | 6.9 | 1.07 | 1 | 1.2 |
| 30 | 6.9 | 1.13 | 1.02 | 1.2 |
| 40 | 6.9 | 1.13 | 1.08 | 1.15 |

## Momentum $M_1$ at Pressure Ratio 1.137

| Frequency | Amplitude | Station 20 x/h | Station 40 x/h | Station 60 x/h |
|---|---|---|---|---|
| 0 | 0 | .85 | .85 | .92 |
| 20 | 2.6 | .90 | .84 | .84 |
| 30 | 2.6 | .84 | .83 | .86 |
| 40 | 2.6 | .83 | .77 | .85 |
| 20 | 4.6 | .83 | .83 | .85 |
| 30 | 4.6 | .79 | .62 | .82 |
| 40 | 4.6 | .76 | .62 | .9 |
| 20 | 6.9 | | .54 | .84 |
| 30 | 6.9 | | .53 | .92 |
| 40 | 6.9 | | .63 | .94 |

Table 2 Momentum Values $M_1$ and $M_2$

## Momentum $M_2$ at Pressure Ratio 1.268

| Frequency | Amplitude | Station 20 x/h | Station 40 x/h | Station 60 x/h |
|---|---|---|---|---|
| 0 | 0 | 0.94 | .98 | 1 |
| 20 | 2.6 | 0.97 | .98 | 1.01 |
| 30 | 2.6 | 0.99 | .98 | 1.13 |
| 40 | 2.6 | 0.90 | 1 | 1.17 |
| 20 | 4.6 | 0.97 | .94 | 1.1 |
| 30 | 4.6 | 1.08 | .89 | 1.13 |
| 40 | 4.6 | 1.12 | .89 | 1.17 |
| 20 | 6.9 | 0.97 | .95 | 1.19 |
| 30 | 6.9 | 0.94 | .92 | 1.37 |
| 40 | 6.9 | 0.88 | .89 | 1.4 |

## Momentum $M_1$ at Pressure Ratio 1.268

| Frequency | Amplitude | Station 20 x/h | Station 40 x/h | Station 60 x/h |
|---|---|---|---|---|
| 0 | 0 | 0.85 | 0.86 | 0.88 |
| 20 | 2.6 | 0.79 | 0.81 | 0.79 |
| 30 | 2.6 | 0.80 | 0.72 | 0.82 |
| 40 | 2.6 | 0.70 | 0.79 | 0.85 |
| 20 | 4.6 | 0.74 | 0.66 | 0.77 |
| 30 | 4.6 | 0.62 | 0.59 | 0.74 |
| 40 | 4.6 | 0.77 | 0.57 | 0.79 |
| 20 | 6.9 | 0.60 | 0.54 | 0.7 |
| 30 | 6.9 | 0.58 | 0.54 | 0.9 |
| 40 | 6.9 | 0.51 | 0.53 | 0.97 |

Table 2 Momentum Values $M_1$ and $M_2$

## Summary

Velocity measurements using pitot tube, hot wire and laser-doppler anemometry have been performed in jets which exhausted into still air and which were excited by a small oscillating vane located in the jet's potential core. Entrainment results obtained to date for three pressure ratios (1.008, 1.137, 1.268), three vane amplitudes (2.6, 4.6, 6.9 degrees zero-to-peak), three frequencies (20, 30 40Hz) at three downstream stations (20, 40, 60 nozzle widths) show significant entrainment increases over the steady jet. In particular, the following trends were identified: entrainment increases with increasing vane amplitude and frequency, but decreases with increasing pressure ratio.

## References

Alexander, L.G., Baron, T., Comings, E.W., 1953, "Transport of Momentum, Mass and Heat in Turbulent Jets", Bulletin 413, May, University of Illinois Engineering Department Station.

Bertin, J., "Dilution Pulsatoire sur Reacteur, Comptes Rendus, Academie des Sciences (Paris), Vol. 240, May 1955, pp. 1855-1857.

Binder, G. and Favre-Marinet, M., "Mixing Improvement in Pulsating Turbulent Jets", Proceedings of ASME Symposium on Fluid Mechanics of Mixing, Atlanta, GA., June 1973, pp. 167-172.

Bradshaw, P., and Goodman, D.C., 1968, "The Effect of Turbulence on Static-Pressure Tubes", Aero. Research Council, R & M 3527.

Bremhorst, K. and Harch, W.H., "Near Field Velocity Measurements in a Fully Pulsed Subsonic Air Jet", In Turbulent Shear Flows ed. by Durst, F., Launder, B.E., Schmidt, F.W. and Whitelaw, J.H., Springer-Verlag, Berlin, Heidelberg, 1979, pp. 37-54.

Bremhorst, K. and Watson, R.D., "Velocity Field and Entrainment of a Pulsed Core Jet", to be published in ASME Journal of Fluids Engineering.

Carrion, S.C., "Calculation of Pulsating Turbulent Jets", M.S. Thesis, California State University at Long Beach, to be published.

Crow, S.C. and Champagne, F.H., "Orderly Structure in Jet Turbulence", Journal of Fluids Mechanics, Vol. 48, Aug. 1971, pp. 547-591.

Curtet, R.M. and Girard, J.P., "Visualization of a Pulsating Jet", Proceedings of ASME Symposium on Fluid Mechanics of Mixing, Atlanta, GA, June 1973, pp. 173-180.

Didelle, H., Binder, G., Craya, A., and Laty, R., "L'Augmentation de la Poussee d'une trompe a Jet Inducteur Pulsant: Resultats des Essais", Laboratoires de Mecanique des Fluides, Univ. Grenoble, June 1972.

Everitt, K.W. and Robbins, A.G., "The Development and Structure of Turbulent Plane Jets", J. Fluid Mechanics, Vol. 88, Part 3, pp. 563-583, 1978.

Fiedler, H. and Korschelt, D., "The Two-dimensional Jet with Periodic Initial Condition", 2nd Symposium on Turbulent Shear Flows, Imperial College, July 1979.

Forthmann, E., 1934, "Uber Turbulente Strahlausbreitung", Ing. Archiv, 5., pp. 4254 (see also NACA TM No. 789, 1936).

Goldschmidt, V.W. and Eskinazi, S., 1965, "Two-Phase Turbulent Flow in a Plane Jet", J. Appl. Mech., ASME, pp. 735-747, December.

Harsha, P.T., 1971, "Free Turbulent Mixing: A Critical Evaluation of Theory and Experiment", Arnold Engineering Development Center, Report No. AEDC-TR-71-36.

Hoesel, W. and Rodi, W., 1975, "Errors Occuring in LDA-Measurements with Counter Signal Processing", Proceedings of the LDA-Symposium Copenhagen, 1975, pp. 251-257.

Johnson, W.S. and Yang, T., "A Mathematical Model for the Prediction of the Induced Flow in a Pulse-jet Ejector with Experimental Verification", ASME Winter Annual Meeting and Energy Systems Exposition, Paper 68-WA/FE-33, New York, Dec. 1968.

Krause, L.N., Dudzinski, T.J. and Johnson, R.C., "Total Pressure Averaging in Pulsating Flows", Instrumentation for Airbreathing Propulsion, Progress in Astronautics & Aeronautics, Vol. 34, pp. 193-203, 1974.

Lai, J.C.S. and Simmons, J.M., "Numerical Solution of Steady and Periodically Pulsed Two-Dimensional Turbulent Free Jets", Naval Postgraduate School Technical Report, to be published, 1980.

Lockwood, R.M., "Pulse Reactor Lift-Propulsion System Development Program", Hiller Aircraft Company, Rpt. No. ARD-308, March 1963.

Miller, D.R. and Comings, E.W., 1957, "Static Pressure Distribution in the Free Turbulent Jet", J. Fluid Mec., Vol. 3, Part 1, pp. 1-16.

Platzer, M.F., Simmons, J.M., and Bremhorst, K., 1978, "Entrainment Characteristics of Unsteady Subsonic Jets", AIAA Journal, Vol. 16, March, pp. 282-284.

Rajaratnam, N., "Turbulent Jets", Elsevier Scientific Publishing Company, New York, 1976.

Schum, E.F., "Techniques for Increasing Jet Entrainment Rates in Ejector Augmenters", Proceedings of the Workshop on Prediction Methods for Jet V/STOL Propulsion Aerodynamics, Naval Air Systems Command, July 1975, pp. 639-652, (available from DDC as AD-A024023).

Simmons, J.M., Platzer, M.F., and Smith, T.C., 1978, "Velocity Measurements in an Oscillating Plane Jet Issuing into a Moving Airstream", J. Fluid Mech., Vol. 84, pp. 33-53.

Simmons, J.M., Lai, J.C.S. and Platzer, M.F., 1979, "Jet Excitation by an Oscillating Vane", University of Queensland, Brisbane, Australia, Department of Mechanical Engineering Research Report No. 10/79.

Tennekes, H. and Lumley, J.L., 1972, "A First Course in Turbulence", MIT Press, Cambridge, MA.

Viets, H., "Flip-Flop Jet Nozzle", AIAA Journal, Vol. 13, Oct. 1975, pp. 1375-1379.

Viets, H., "Coherent Structures in Time Dependent Shear Flows", AGARD Conference Proceedings on Turbulent Boundary Layers", The Hague, Netherlands, September 1979.

Zijnen, B.G., Van der Hegge, 1958, "Measurements of the Velocity Distribution in a Plane Turbulent Jet of Air", App. Sci. Res., Sec. A, Vol. 7, pp.256-276.

# AN INVESTIGATION OF PLANAR, TWO-DIMENSIONAL
# EJECTORS WITH PERIODIC OR STEADY SUPERSONIC DRIVER FLOW

H. L. Petrie
Graduate Research Assistant

and

A. L. (Tad) Addy
Professor and Associate Head
Department of Mechanical and Industrial Engineering
University of Illinois at Urbana-Champaign
1206 W. Green Street
Urbana, IL   61801

Telephone:   (217) 333-1126

PRESENTATION SUMMARY


AN INVESTIGATION OF PLANAR, TWO-DIMENSIONAL EJECTORS
WITH PERIODIC OR STEADY SUPERSONIC DRIVER FLOW*


The results of an experimental and theoretical investigation of a
planar, two-dimensional constant area ejector with a periodically pulsed
or a steady, supersonic driver flow will be presented.  The purpose of
this investigation was to determine the potential of using unsteady flow
techniques to enhance the mixing between high-speed streams interacting
within a duct and to improve the overall pressure recovery obtained
within an ejector system.  This research was motivated by mixing problems
which were encountered in high-energy chemical laser systems at the laser
fuel-oxidizer nozzle array and within the ejector-diffuser system required
to pump the laser effluent for atmospheric discharge.

A large scale fluidic oscillator was developed to pulse the ejector
driver flow stagnation pressure about a constant valve at frequencies up
to 250 Hz.  Driver flow frequencies of 142 Hz and 250 Hz were used in a
series of ejector experiments; for comparison, a series of steady driver
flow experiments were also conducted.  A wide range of ejector flow condi-
tions were experimentally investigated for three values of ejector mixing
duct length-to-height ratios.  All of the ejector experiments were con-
ducted in the "supersonic" or "mixed" regimes of operation.  In the
"supersonic" regime, the ejector driver flow expands against the induced

flow as both flows enter the mixing duct and chokes the induced flow at an aerodynamic throat formed within the mixing duct; in the "mixed" regime, the induced ejector flow is not choked and the driver flow may or may not expand against the induced flow at the mixing duct inlet.

A one-dimensional, quasi-steady control volume analysis was successfully employed to model these ejector flows. Periodic ejector flows were found to be well modeled by the quasi-steady analysis. The driver-to-induced flow inlet static pressure ratios and mass flowrate ratios of the steady driver flow ejector were accurately predicted by the one-dimensional analysis. The mean values of these inlet flow parameters obtained with the periodic driver flow ejector were not significantly different from the steady driver flow results. The experimentally determined steady driver flow ejector compression ratios were approximately 25% lower than predicted by the analysis. The pressure recovery obtained with the ejector operating at given inlet flow conditions for both periodic and steady driver flows increased slightly with driver flow frequency. At the frequencies investigated, the pulsation of the driver flow was found to have a small effect on ejector operation and the mixing and entrainment characteristics did not appear to be altered significantly by the pulsed driver flow. However, the mixing duct wall static pressures in the steady driver flow ejector experiments were found, unexpectedly, to be unsteady under most flow conditions. The unsteady and highly disturbed character of the flow within the mixing duct of the steady driver flow ejector may be an inherent ejector characteristic which could have masked some of the potential differences in performance between the periodic and steady driver flow ejectors. In the periodic driver flow experiments, the

478

results indicate that the Strouhal number of the periodic driver flows was not sufficiently high to alter significantly the dynamics of mixing between the high-speed, ducted streams.

The steady driver flow ejector experiments raise two questions: (i) Are the unsteady flow phenomena observed in these experiments a characteristic of plane, two-dimensional ejectors? and (ii) Do similar unsteady flows occur in an axisymmetric ejector?

## NOMENCLATURE

### Symbols

| | |
|---|---|
| A | Area |
| $C_p$ | Specific heat at constant pressure |
| $C_v$ | Specific heat at constant volume |
| h | Specific enthalpy |
| L | Mixing duct length |
| M | Mach number |
| Mw | Molecular weight |
| P | Pressure |
| R | Universal gas constant |
| St | Strouhal number |
| t | Time |
| T | Absolute temperature |
| V | Magnitude of velocity |
| w | Mass flowrate |
| $w_{sp}$ | Secondary to primary mass flowrate ratio |
| W | Mixing duct width |
| X | Longitudinal or flow-direction coordinate |

480

OBJECTIVES:

- TO DEVELOP AN EFFICIENT LARGE-SCALE FLUID OSCILLATOR TO PULSE THE EJECTOR DRIVER FLOW ABOUT A MEAN VALUE.

- TO INVESTIGATE THE EFFECTS OF A PERIODIC DRIVER FLOW ON EJECTOR PERFORMANCE.

- TO INVESTIGATE THE SAME EJECTOR CONFIGURATIONS WITH A STEADY DRIVER FLOW.

- TO MODEL THE EJECTOR OPERATION WITH PERIODIC DRIVER FLOW.
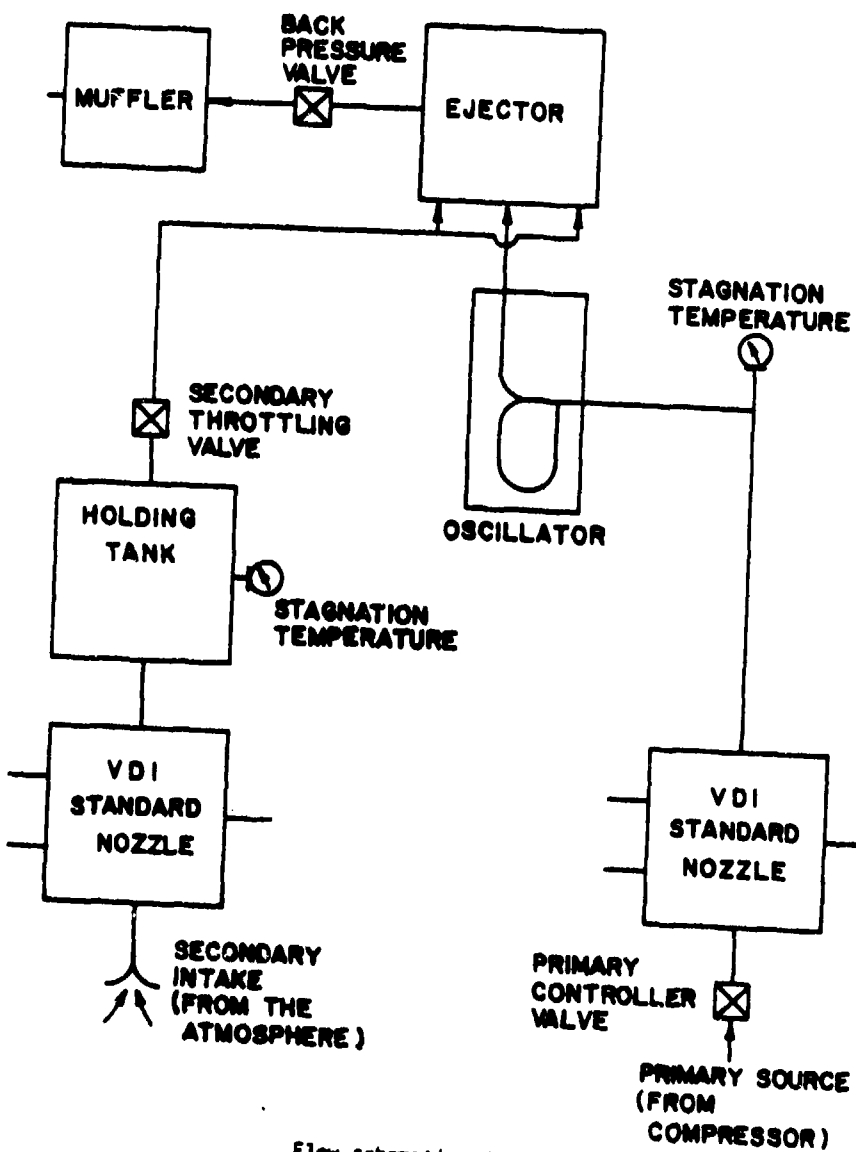
Flow schematic of the test rig
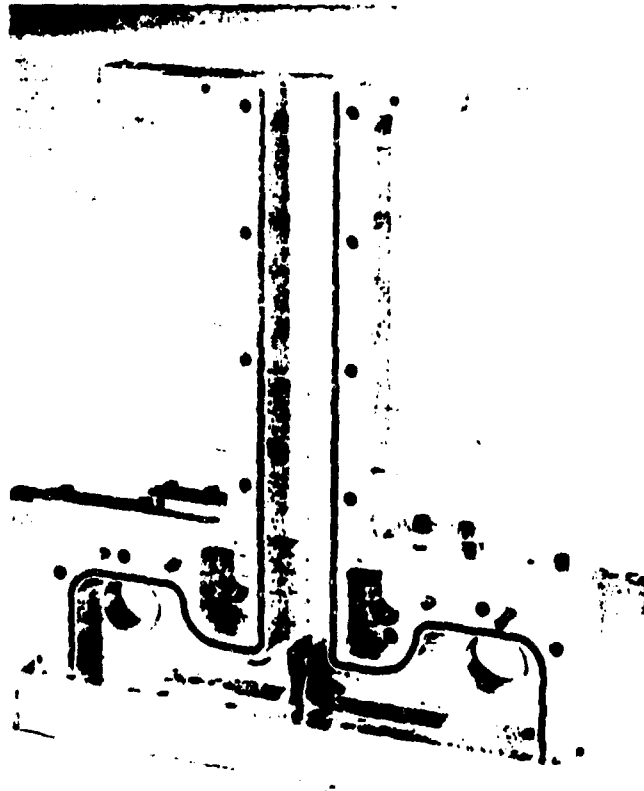
The partially assembled ejector unit (L/W = 9.0)
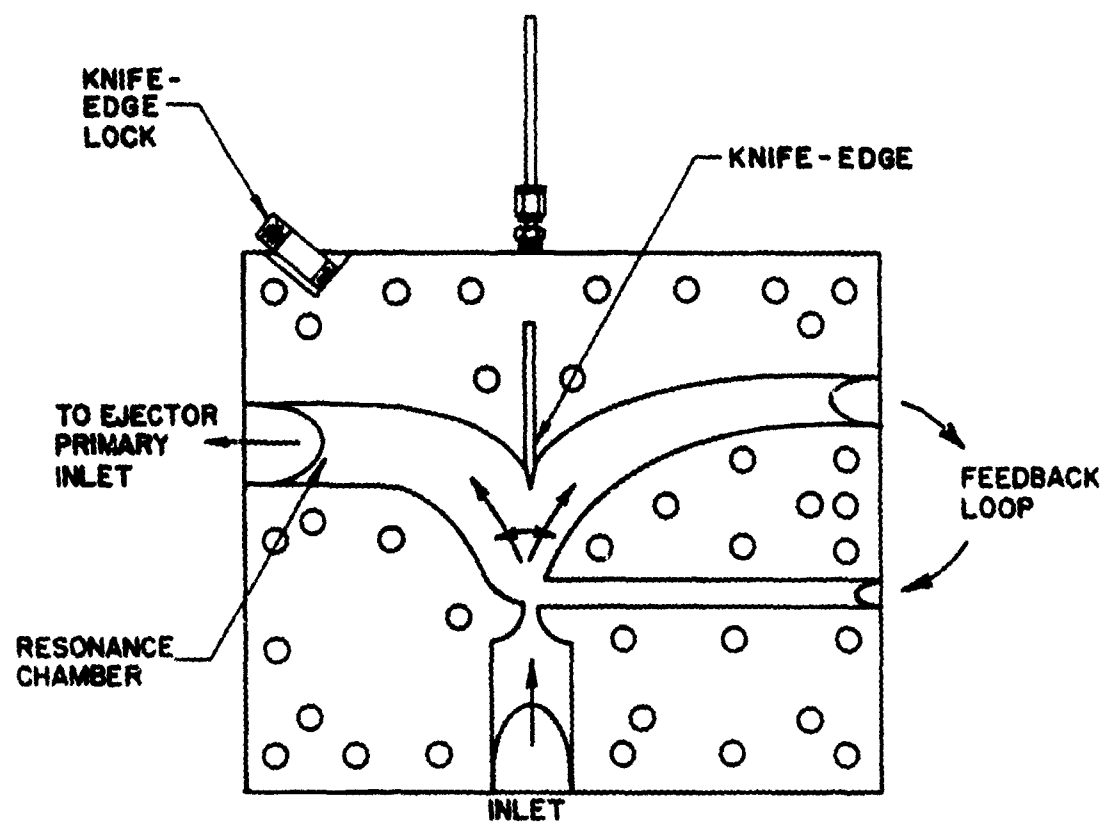
View of the partially assembled oscillator body

CEC TYPE 4–312
PRESSURE
TRANSDUCERS

CEC TYPE 1–183
SIGNAL CONDITIONER

BIOMATION 1015
WAVEFORM RECORDER

DATOS 305
DATA
INTERFACE

OSCILLOSCOPE

MEMODYNE
RECORDER

T.I.
SILENT 700
TERMINAL

CDC
CYBER 175
COMPUTER
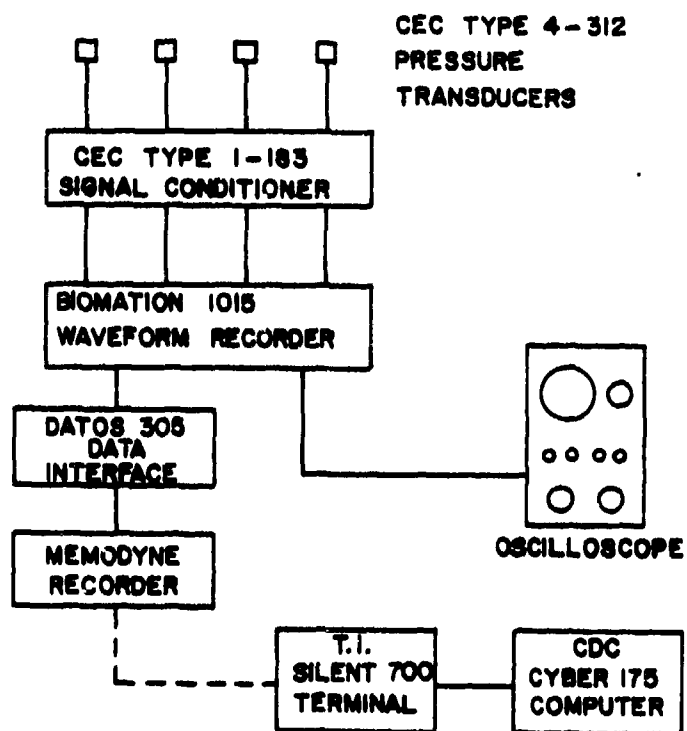
Schematic detailing the data acquisition system

485
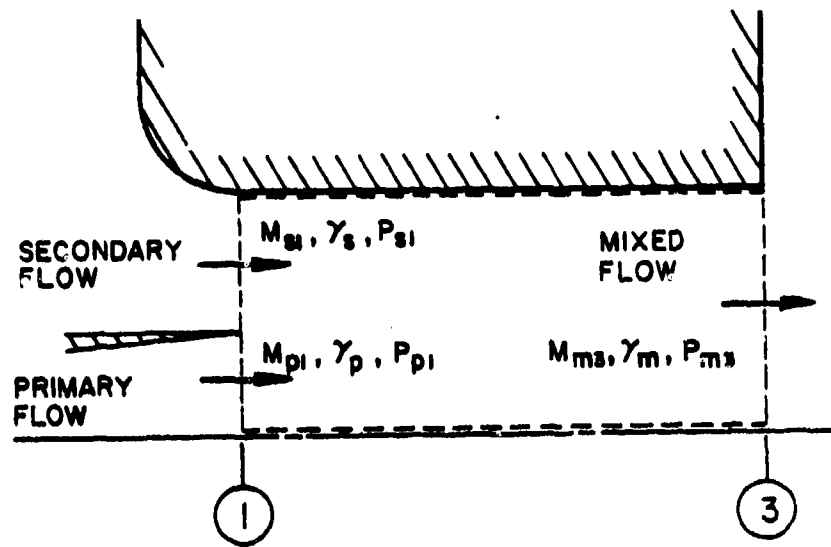
Control volume used in the overall analysis
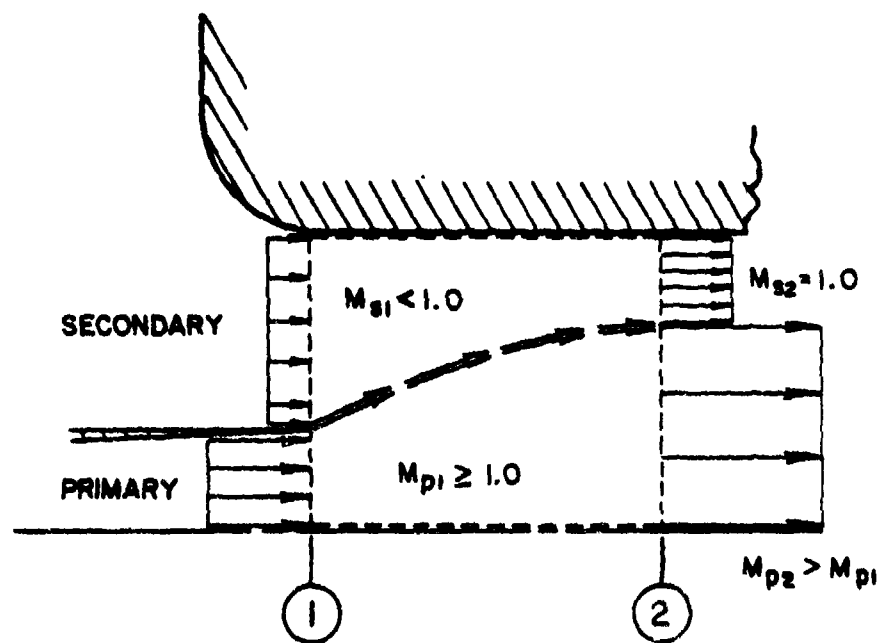
Control volume used in the supersonic regime analysis
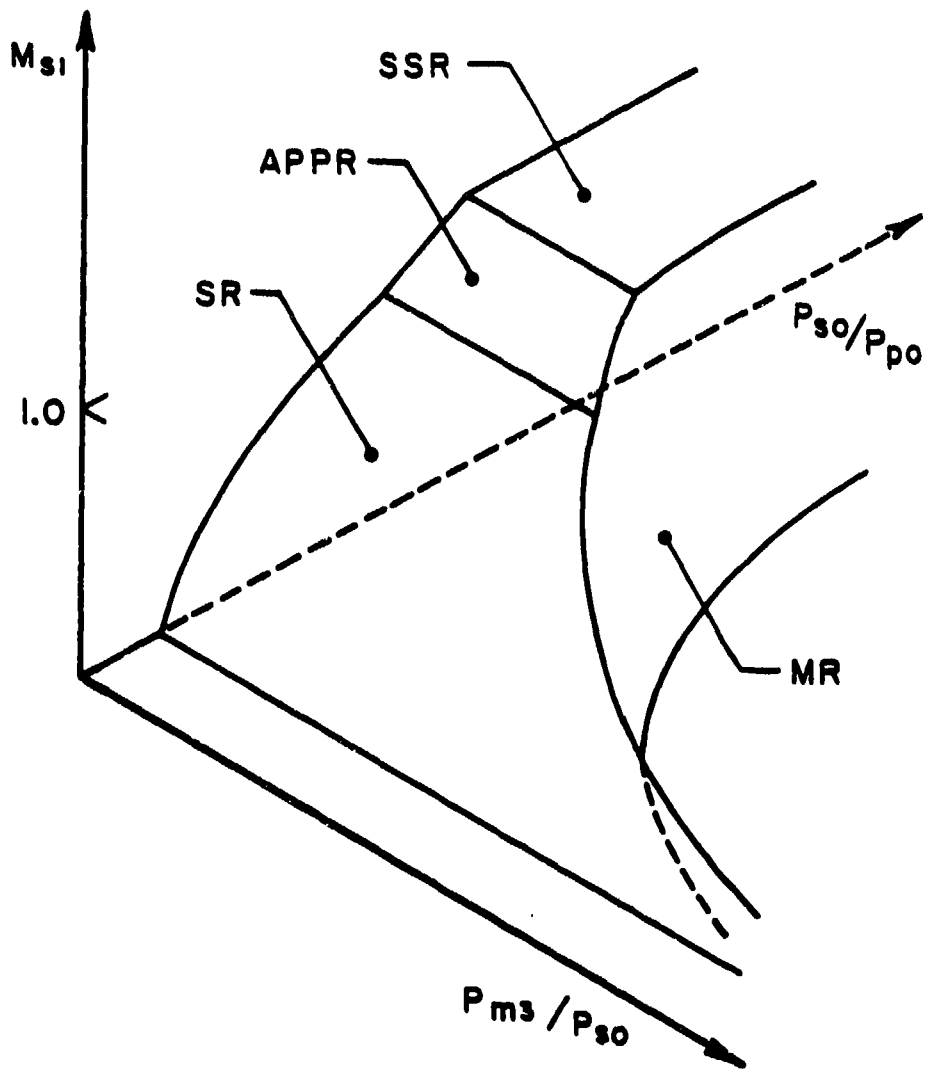
The one-dimensional inviscid analysis solution surfaces

Back pressure independent steady flow values of $P_{s1}/P_{p1}$ versus $P_{s0}/P_{p0}$

489

Back pressure independent steady flow values of $w_s/w_p$ versus $P_{so}/P_{po}$
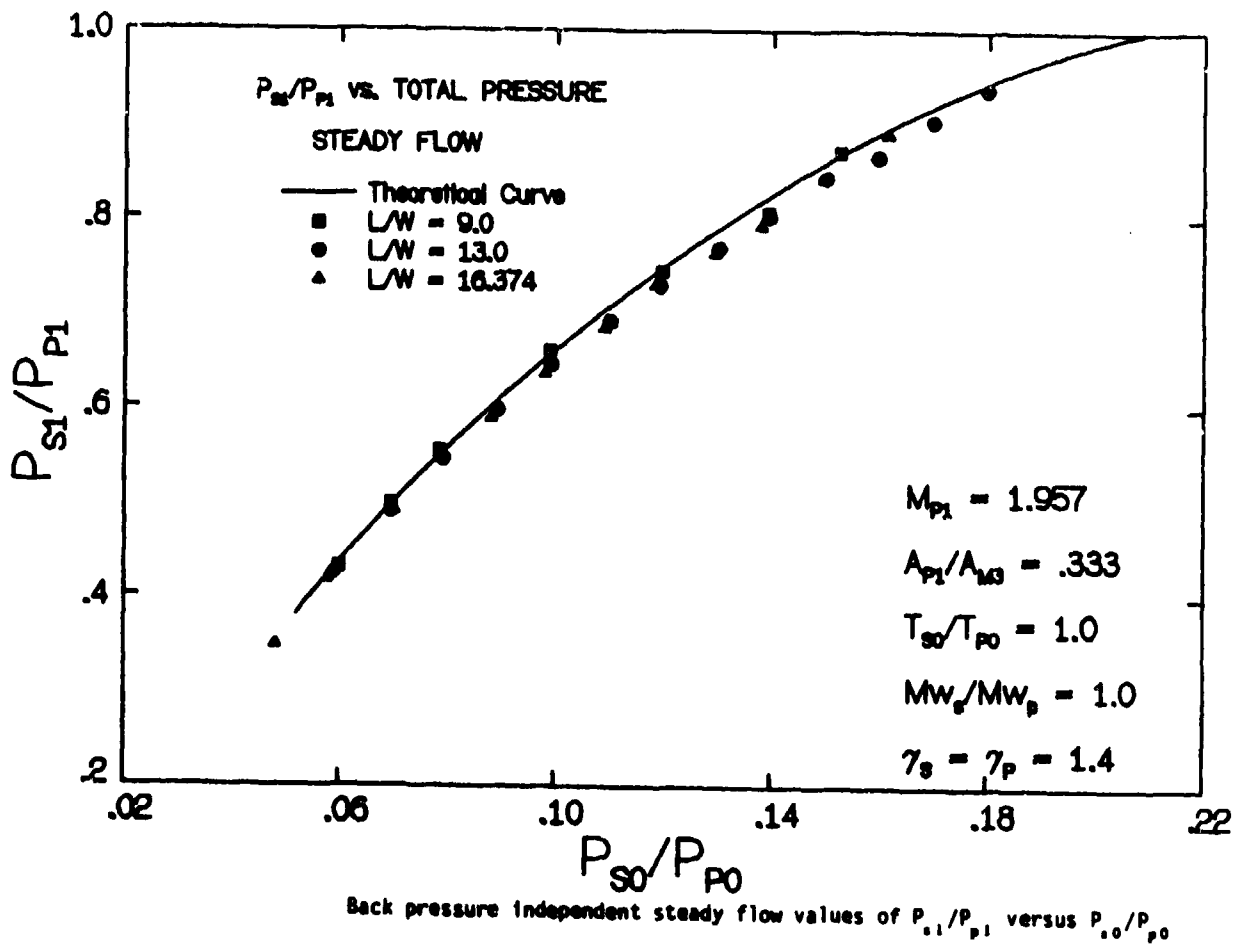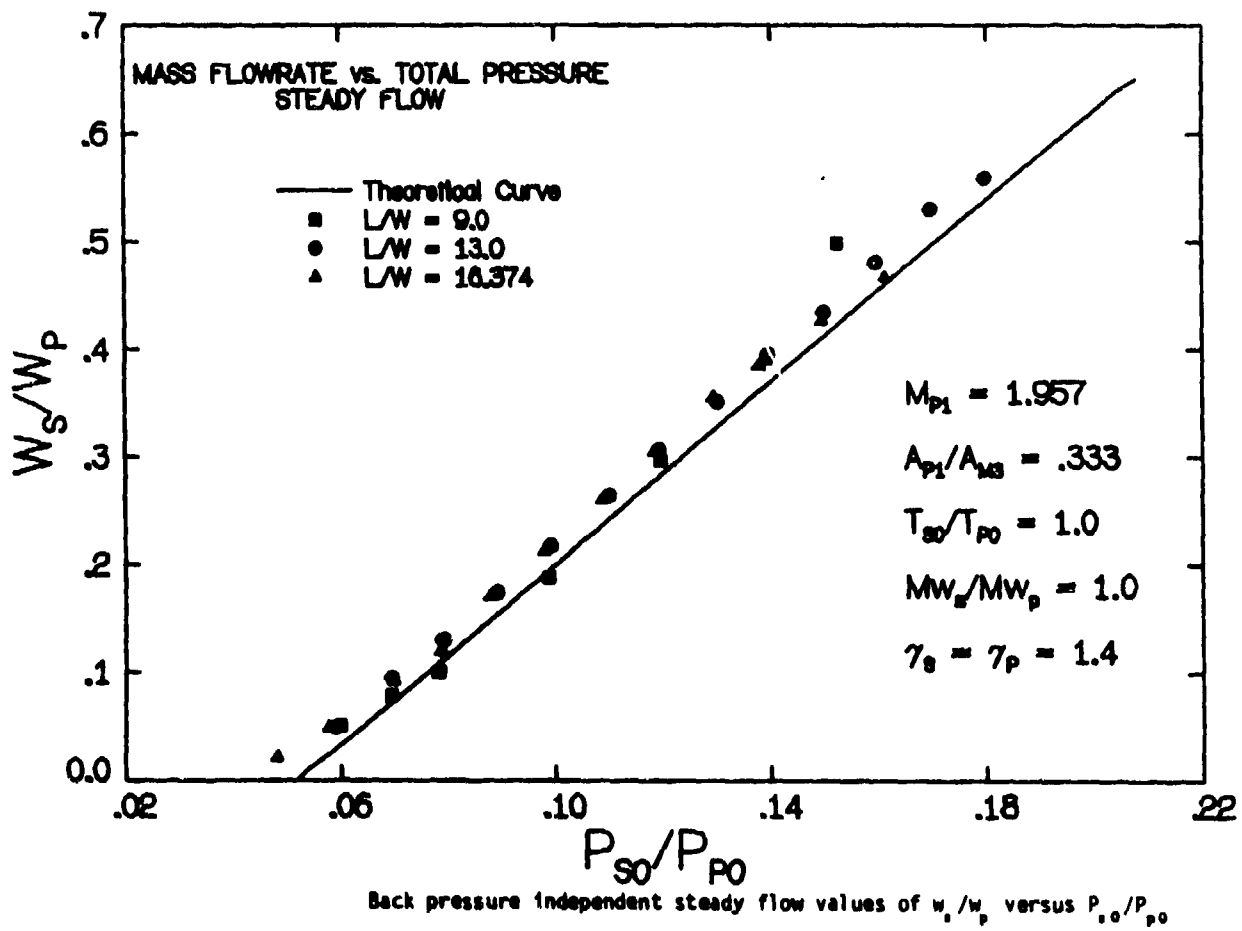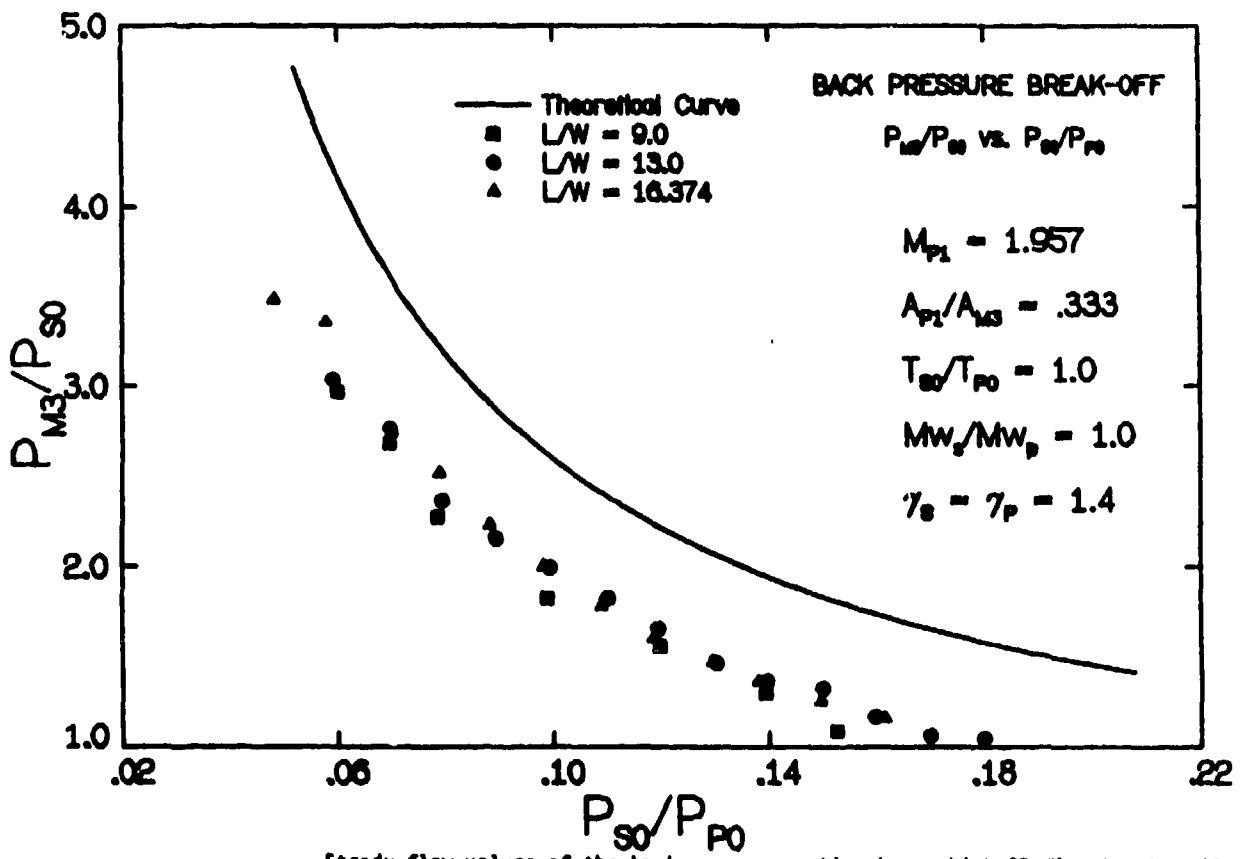
Steady flow values of the back pressure ratio above which SR flow breaks-off
to MR flow versus $P_{s.o}/P_{p.o}$

491
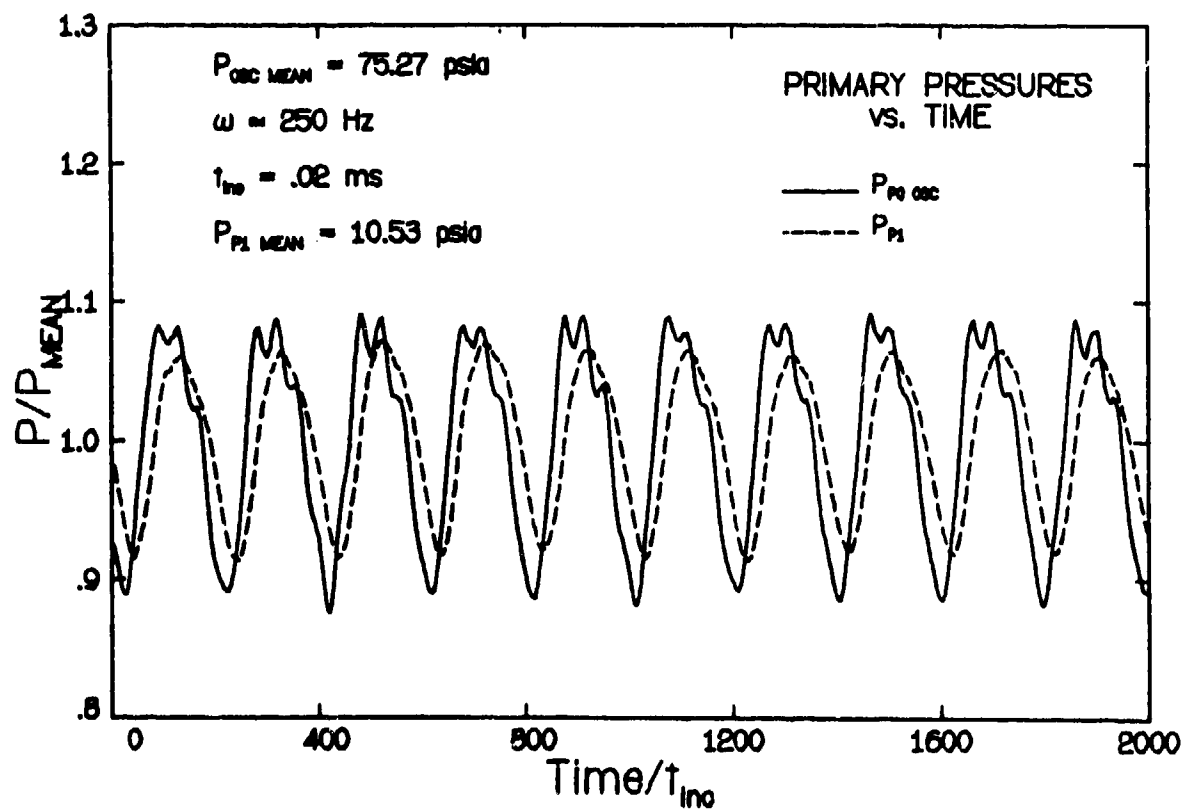
Simultaneously recorded values of $P_{p1}$ and $P_{po}$ versus time at the 250 Hz driver frequency

492
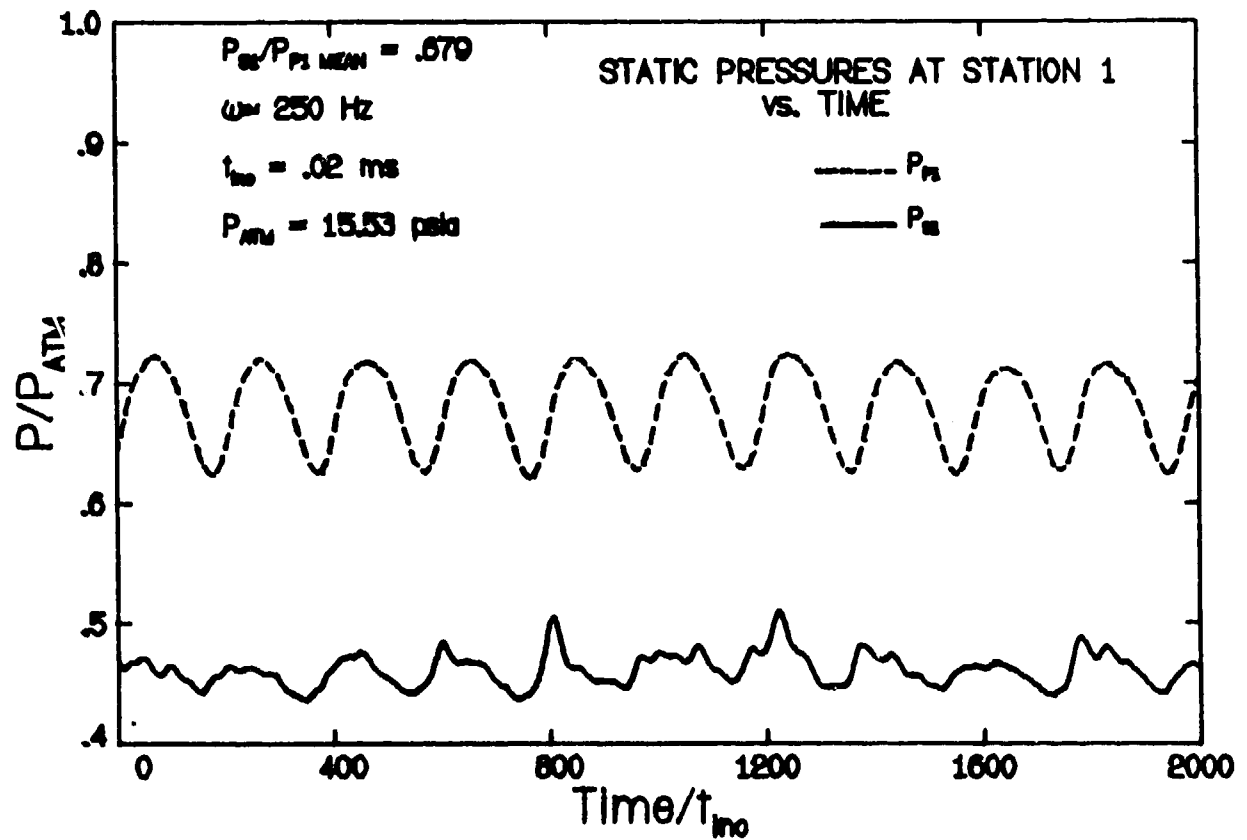
Primary and secondary static pressures at Station 1 for the 250 Hz driver ejector flow versus time (L/W = 9.0, $P_{so}/P_{po} = .100$)
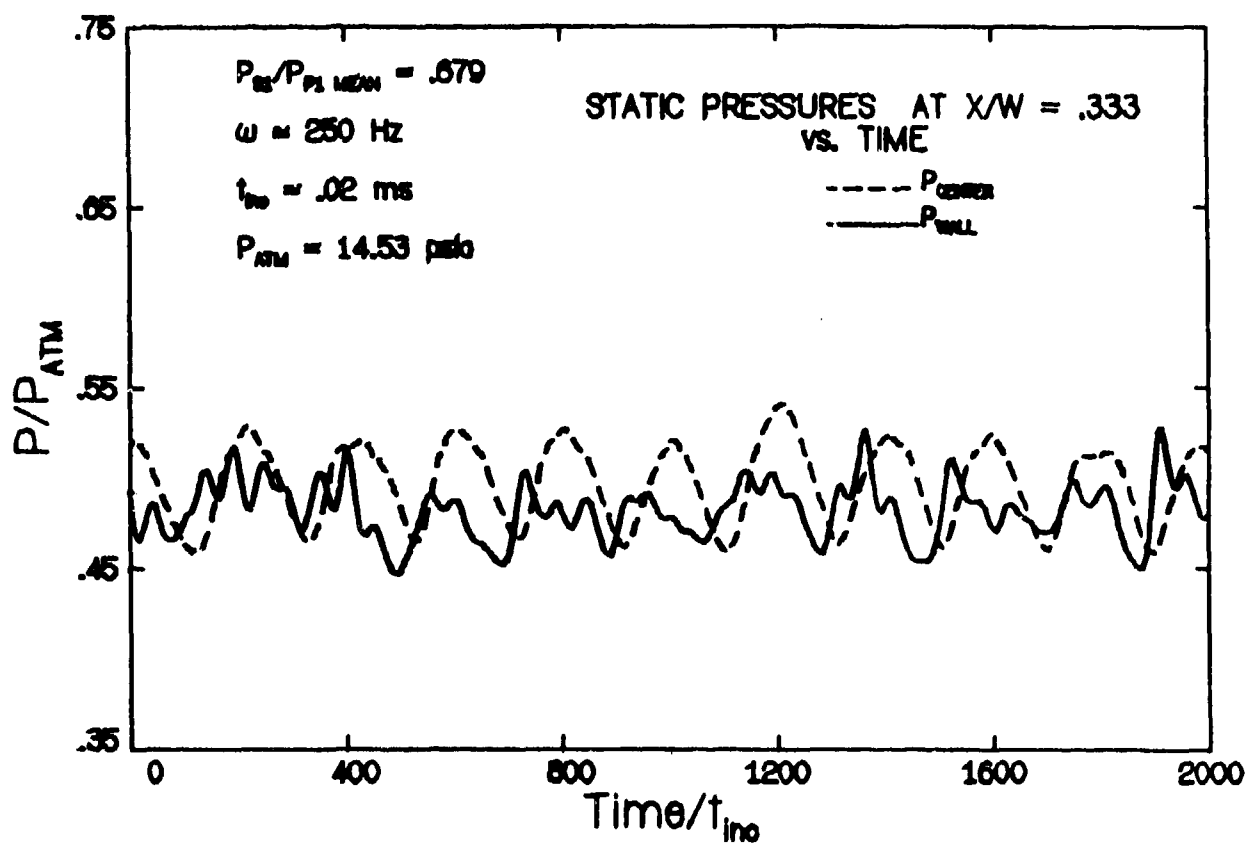
Static pressures versus time in the 250 Hz driver ejector flow at X/W = .333 (L/W = 9.0, $P_{so}/P_{po}$ = .100)
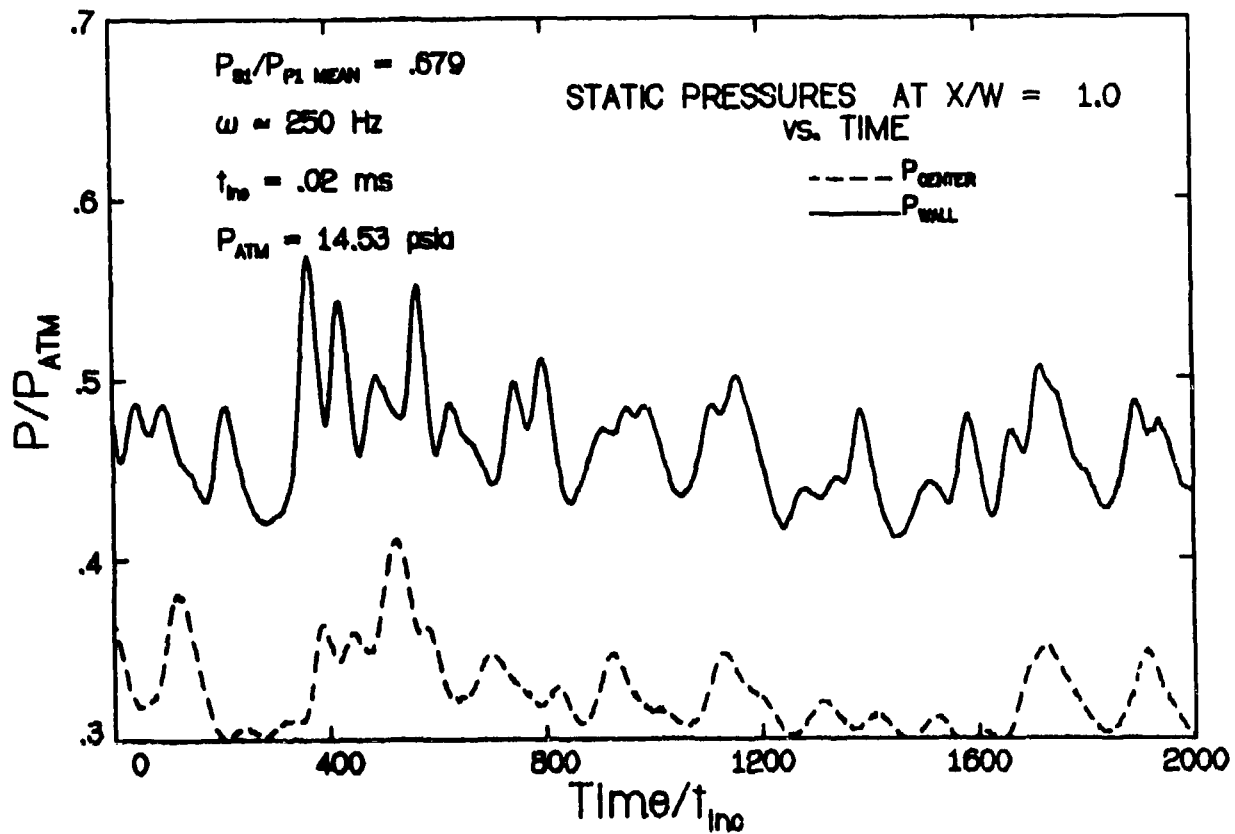
Static pressures versus time in the 250 Hz driver ejector flow
at X/W = 1.00 (L/W = 9.0, $P_{so}/P_{po}$ = .100)

Static pressures versus time in the 250 Hz driver ejector flow at X/W = 1.333 (L/W = 9.0, $P_{so}/P_{po}$ ≈ .100)

Static pressures versus time in the 250 Hz driver ejector flow at X/W = 4.0 (L/W = 9.0, $P_{s,0}/P_{p,0}$ = .100)
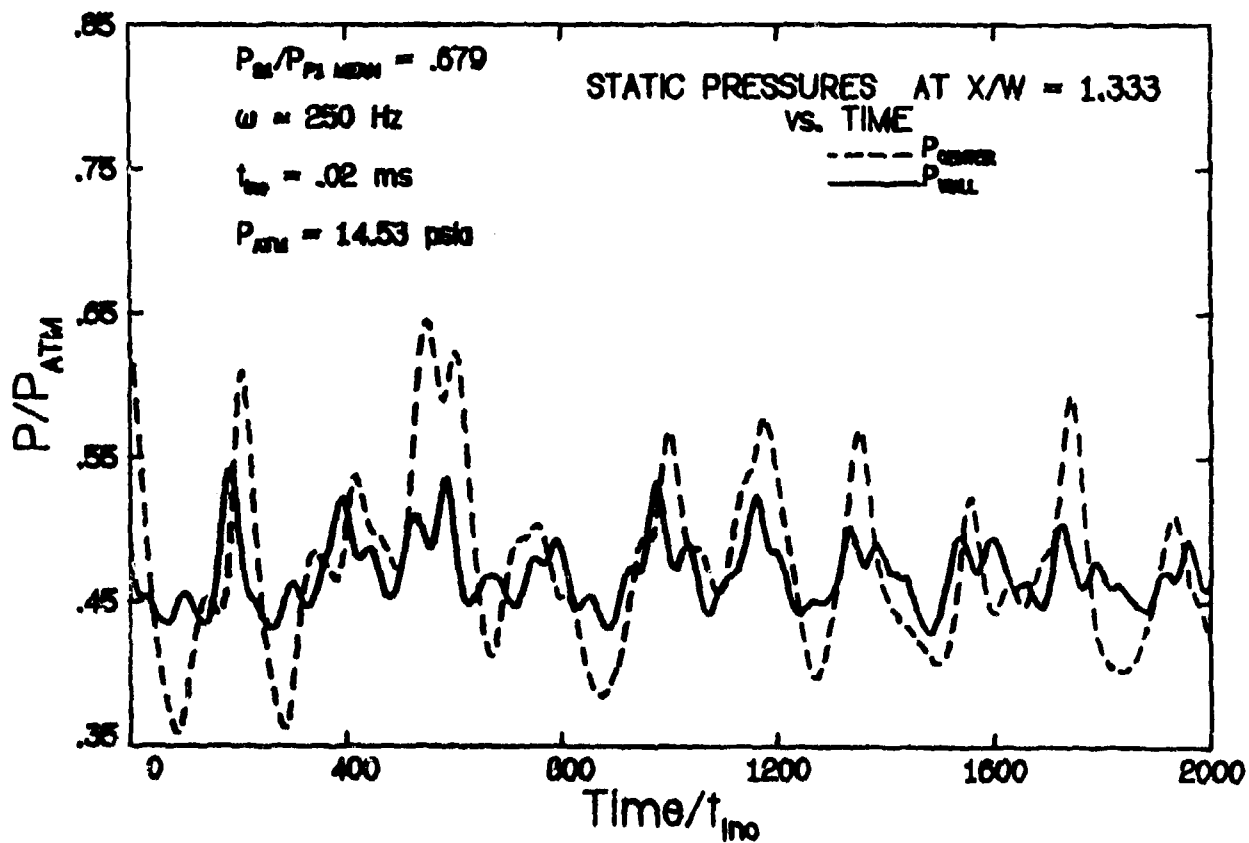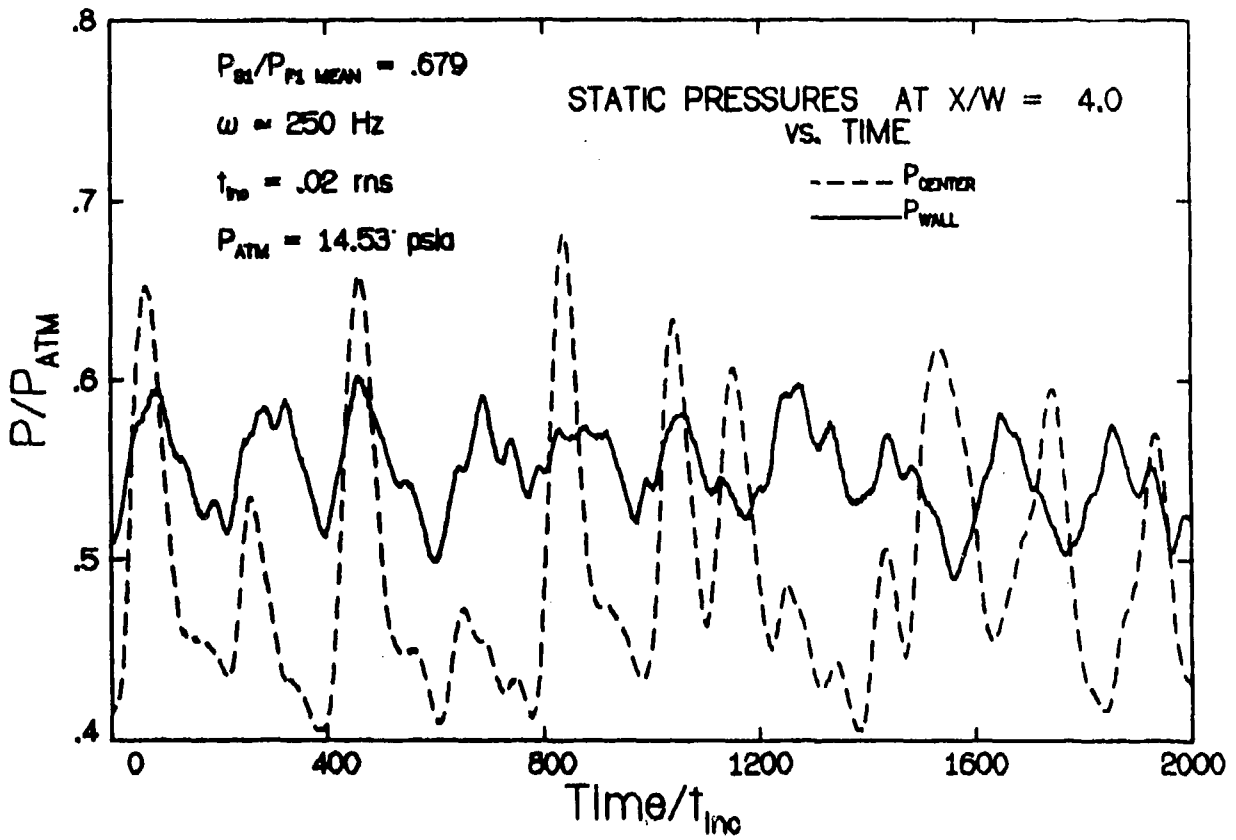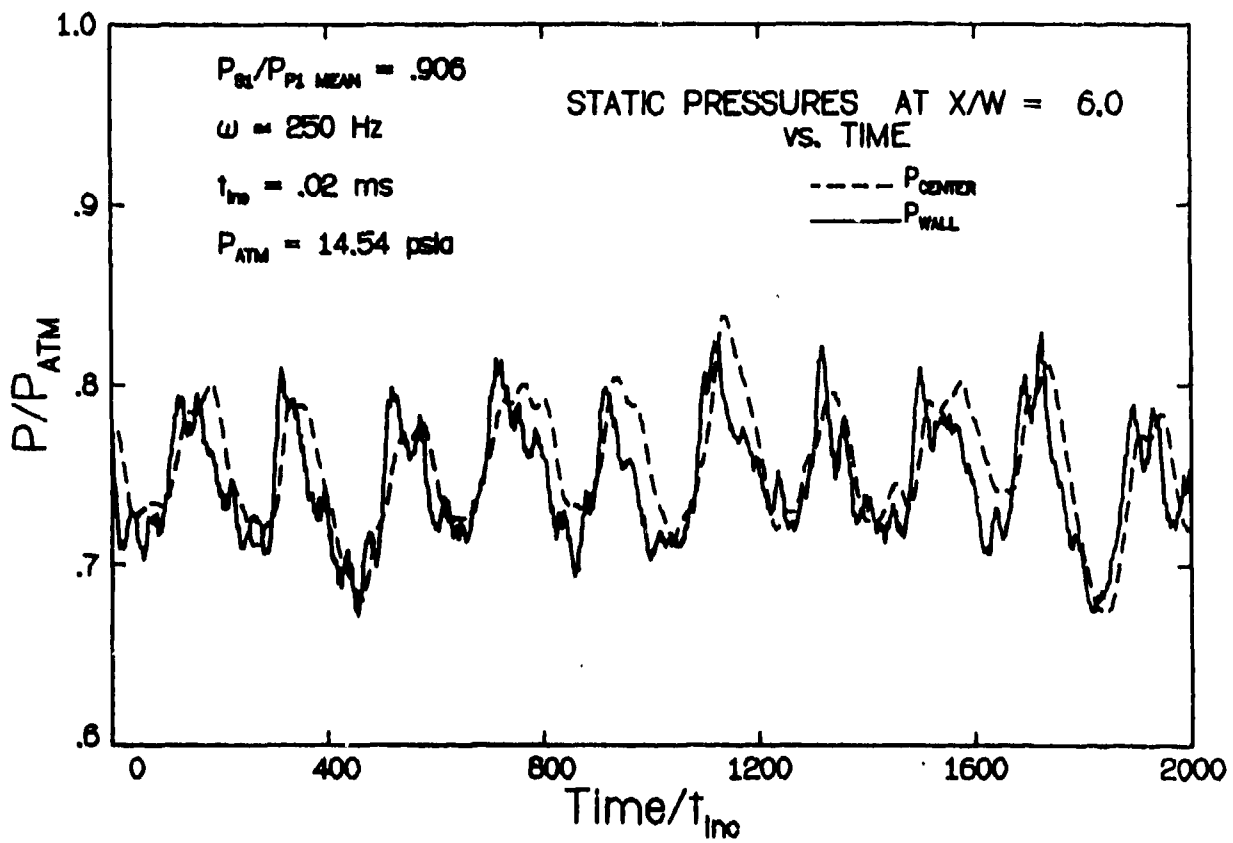
Static pressures versus time in the 250 Hz driver ejector flow at X/W = 6.0 (L/W = 9.0, $P_{so}/P_{po}$ = .160)
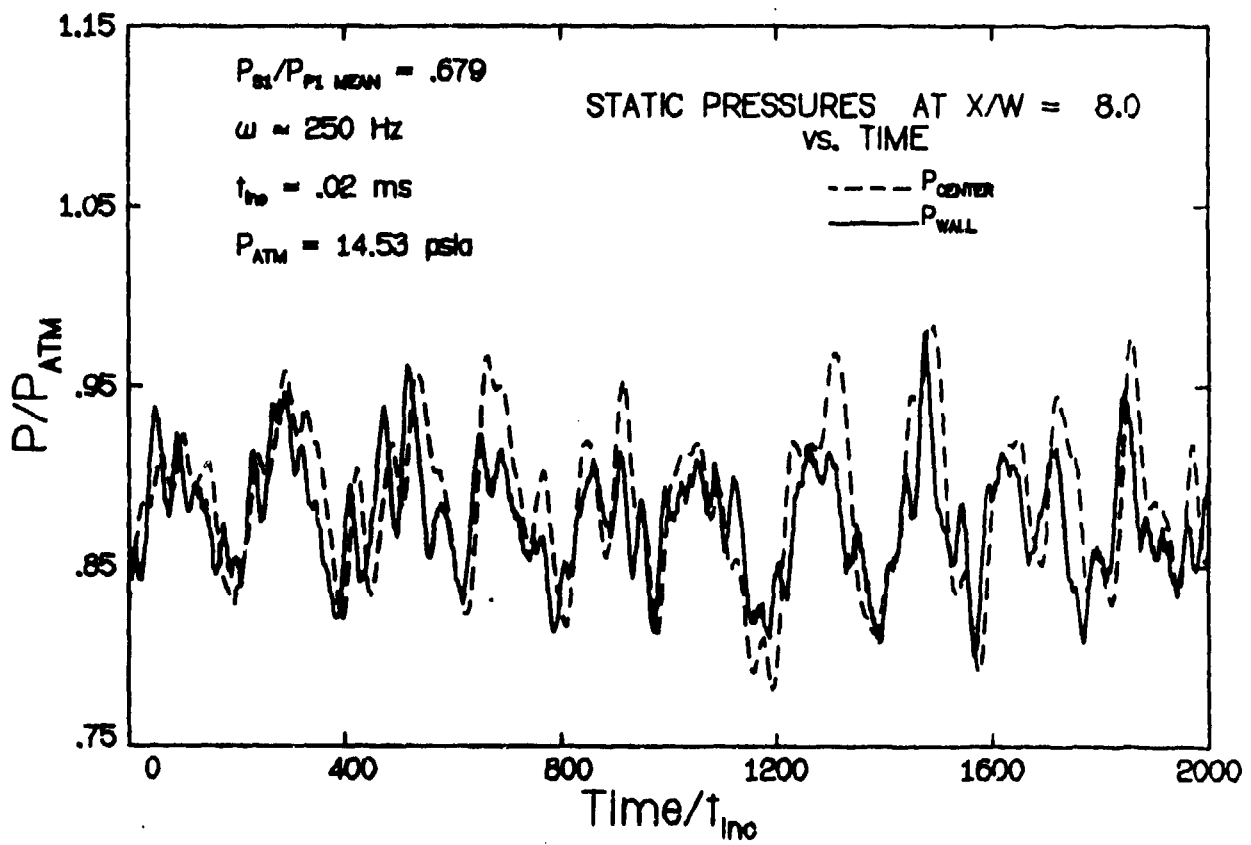
Static pressures versus time in the 250 Hz driver ejector flow at X/W = 8.0 (L/W = 9.0, $P_{so}/P_{po}$ = .100)
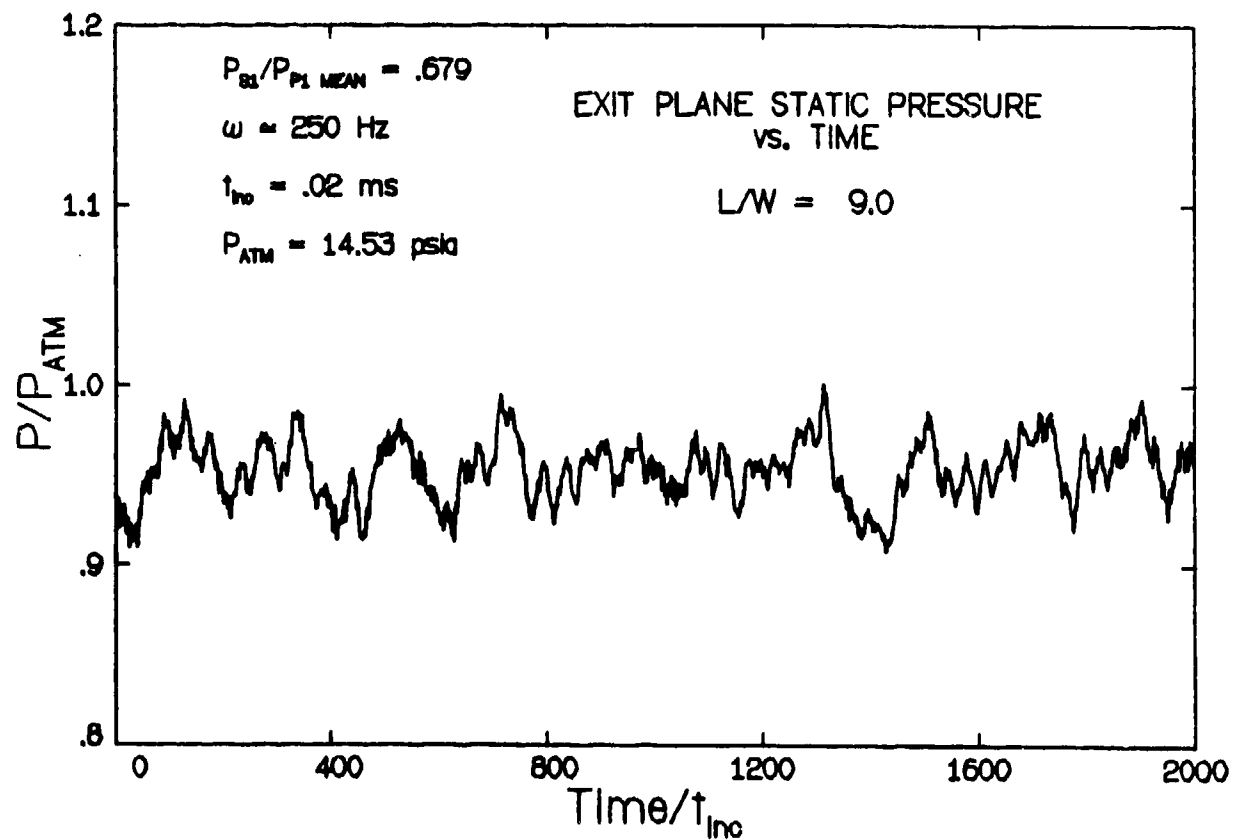
The exit plane static pressure versus time on the primary flow centerline (L/W = 9.0, $P_{so}/P_{po}$ = .100)
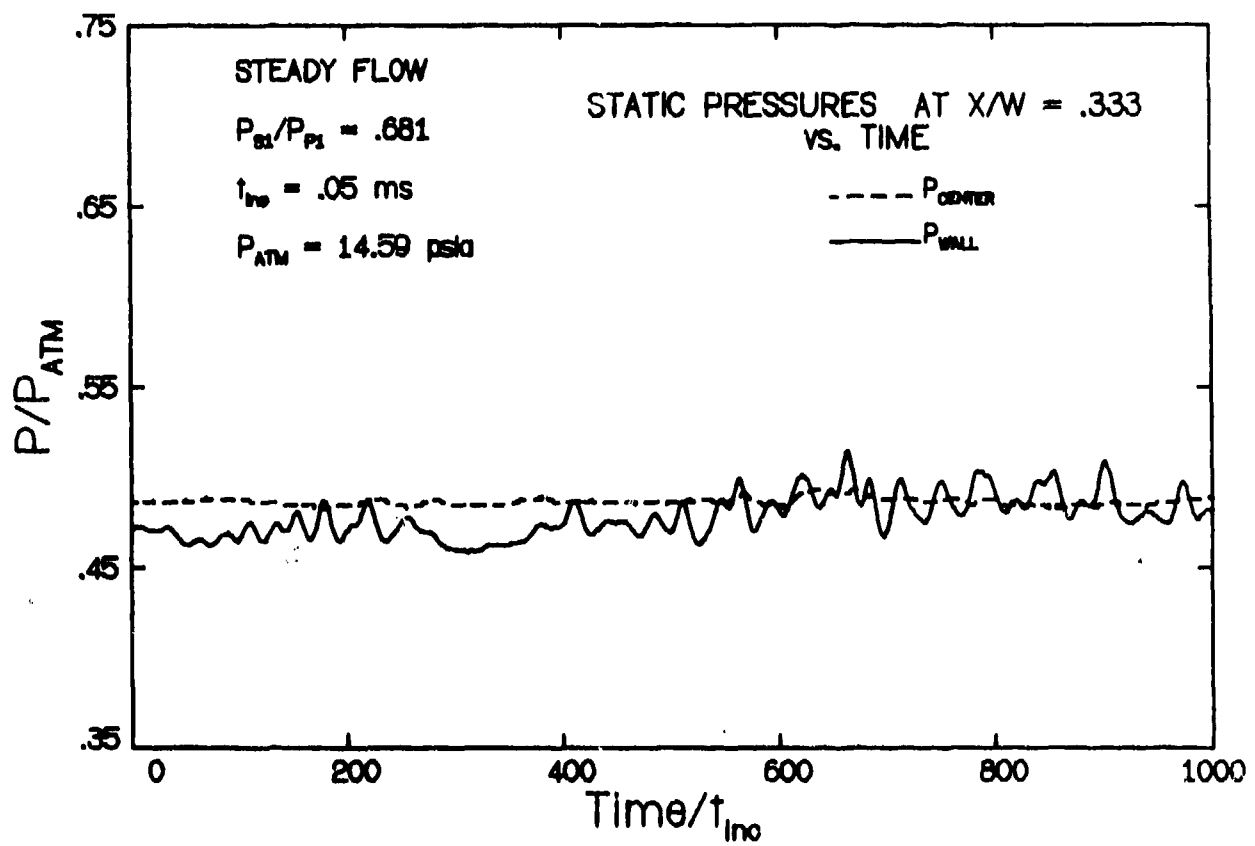
Small disturbances in the subsonic wall flow of the steady driver
ejector flow (L/W = 9.0, $P_{ao}/P_{po}$ = .100)
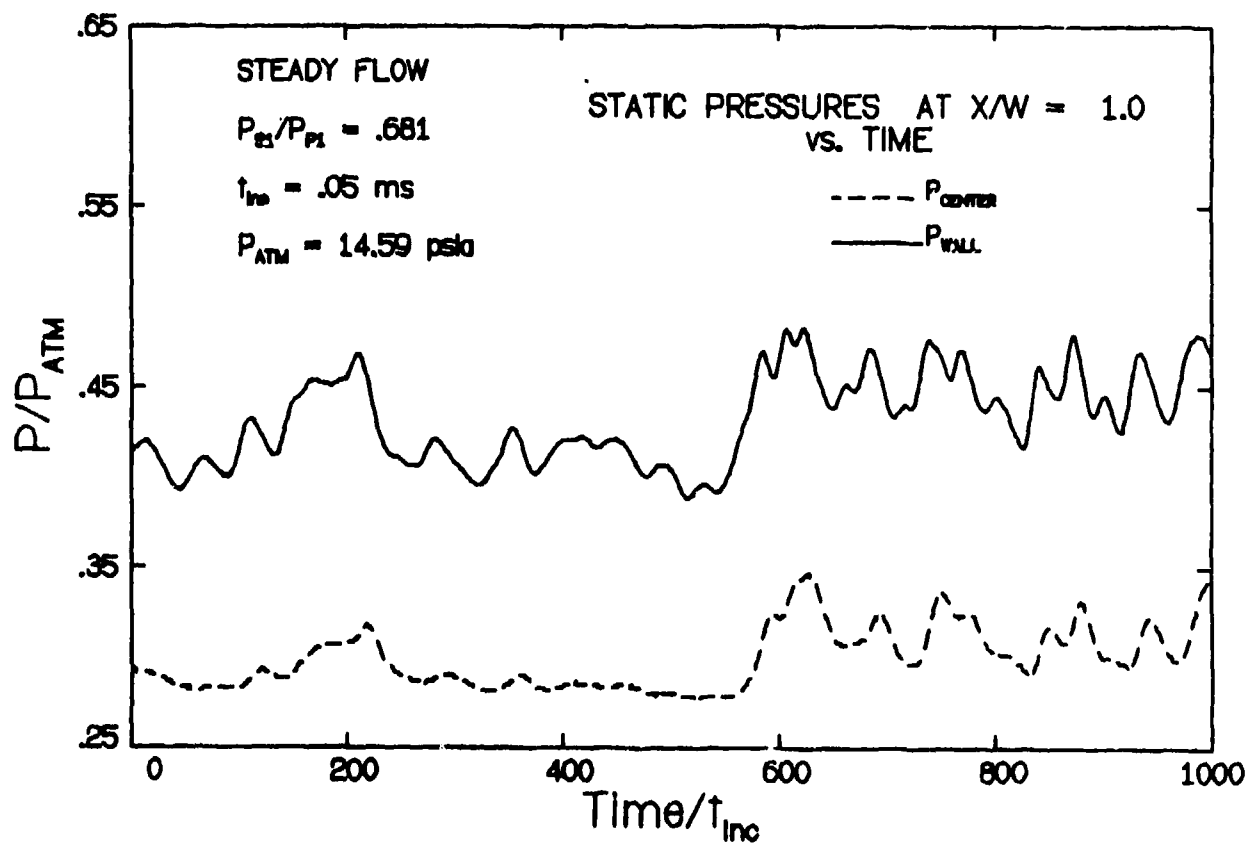
501

Static pressures versus time in the steady driver ejector flow at X/W = 1.00 (L/W = 9.0, $P_{s0}/P_{p0}$ = .100)

502

Static pressures versus time in the steady driver ejector flow at $X/W = 1.333$ ($L/W = 9.0$, $P_{s0}/P_{p0} = .100$)

503

Static pressures versus time in the steady driver ejector flow
at X/W = 4.0 (L/W = 9.0, $P_{so}/P_{po}$ ≈ .100)

Static pressures versus time in the steady driver ejector flow
at X/W = 8.0 (L/W = 9.0, $P_{so}/P_{po}$ = .100)

MASS FLOWRATE RATIO vs. BACK PRESSURE
$P_{so}/P_{po}$ = .070    L/W = 9.0

+ 250 Hz
★ 142 Hz
⊕ STEADY FLOW

$W_S/W_P$ vs. $P_{M3}/P_{SO}$

$w_s/w_p$ versus $P_{m3}/P_{so}$ for flows that have passed the break-off
point and are in the mixed regime (L/W = 9.0, $P_{so}/P_{po}$ = .070)

506

$w_s/w_p$ versus $P_{m3}/P_{so}$ for flows that have passed the break-off point and are in the mixed regime (L/W = 9.0, $P_{so}/P_{po}$ = .100)

MASS FLOWRATE RATIO vs. BACK PRESSURE
$P_{S0}/P_{P0}$ = .130    L/W = 9.0

+ 250 Hz
★ 142 Hz
● STEADY FLOW
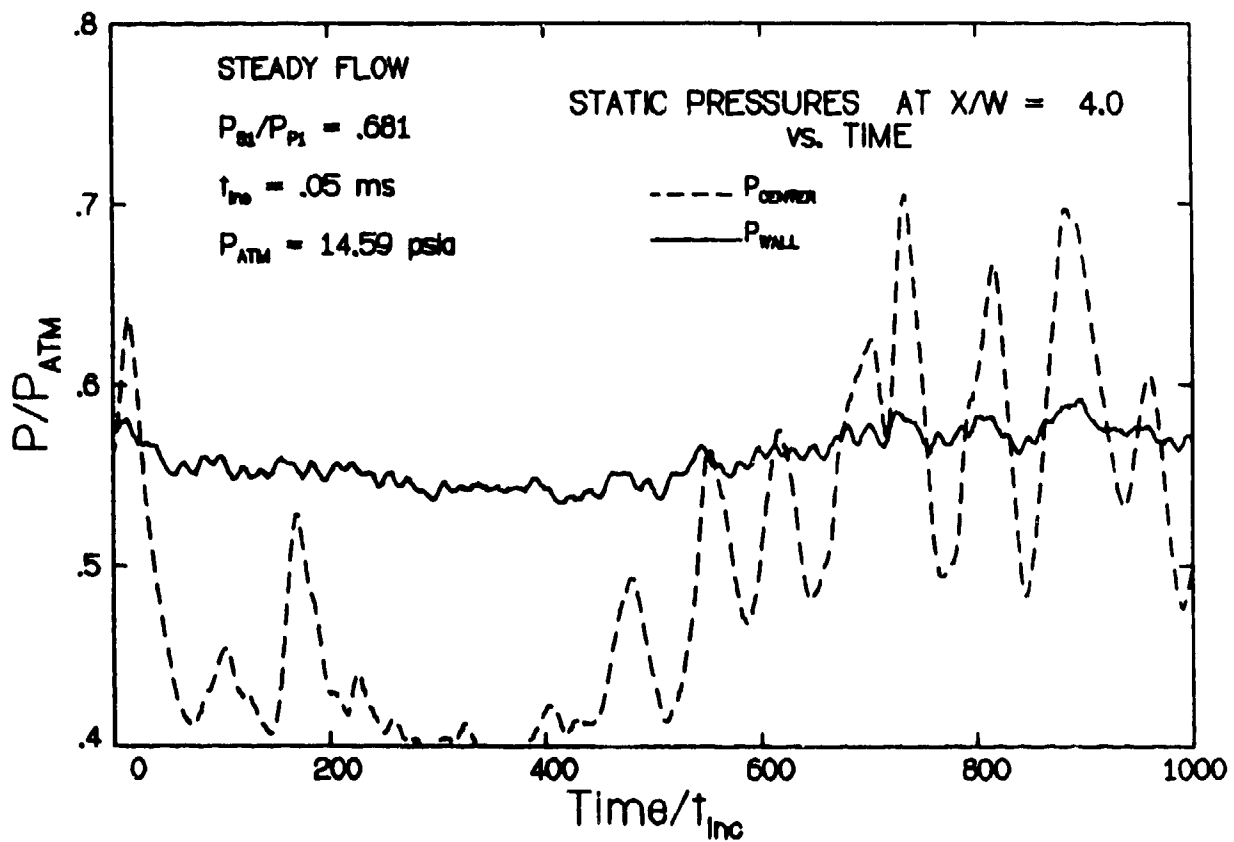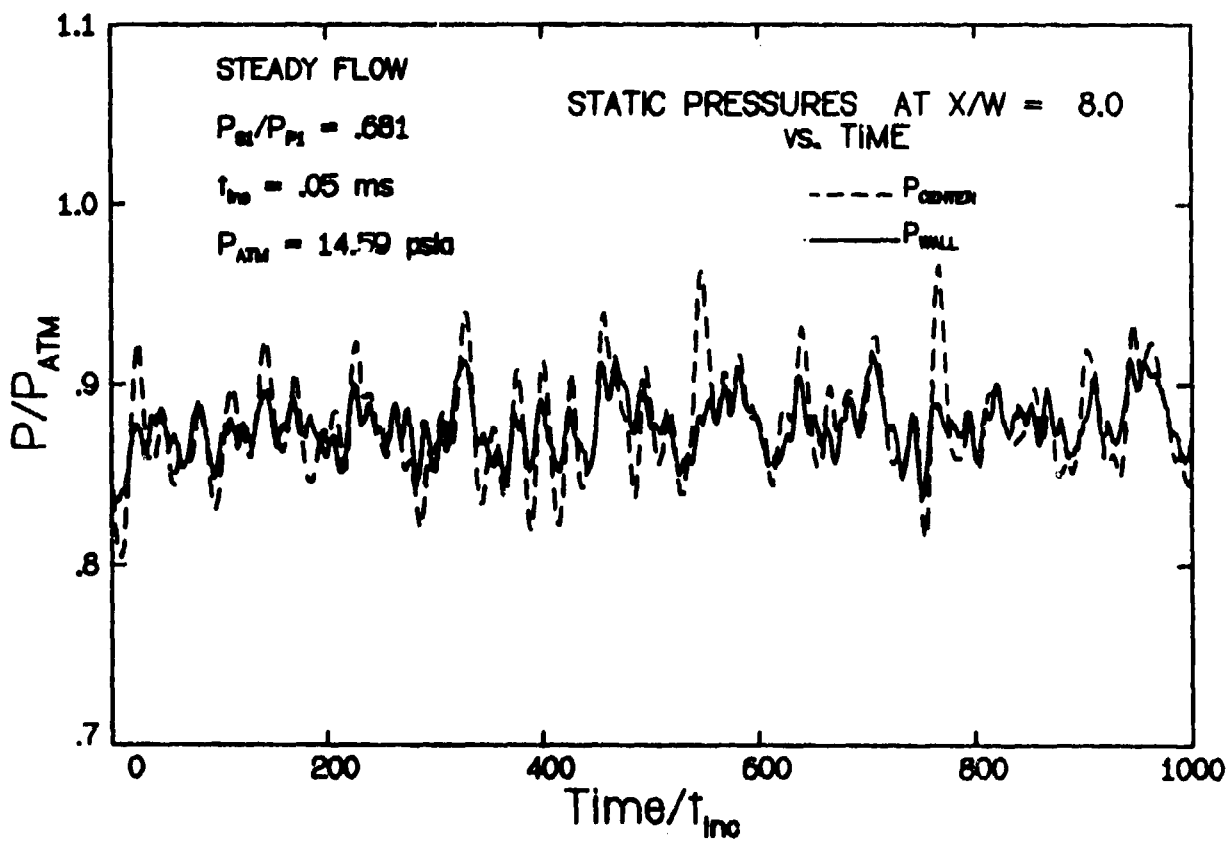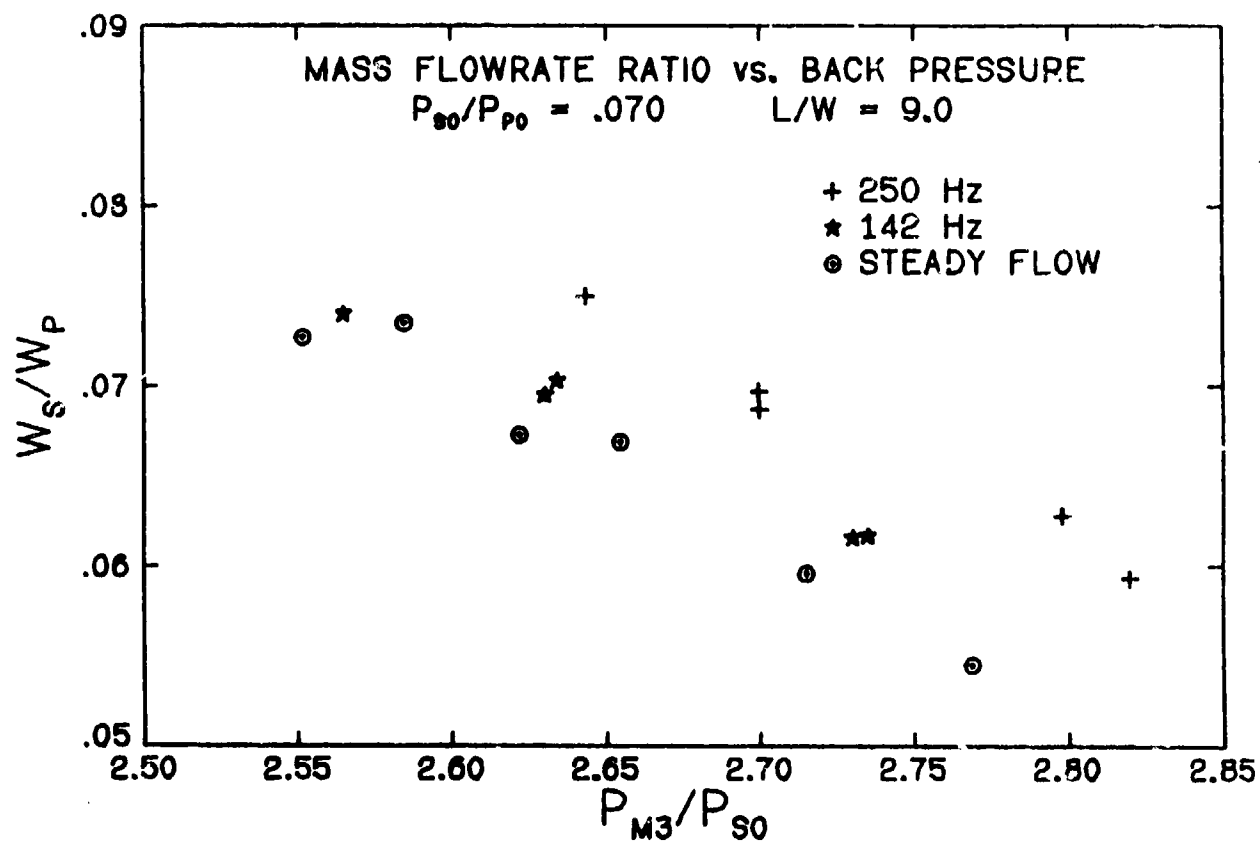
$W_S/W_P$

$P_{M3}/P_{S0}$

$w_s/w_p$ versus $P_{M3}/P_{S0}$ for flows that have passed the break-off point and are in the mixed regime (L/W = 9.0, $P_{S0}/P_{P0}$ = .130)

508

FINDINGS:

- EJECTORS WITH PERIODIC DRIVER FLOWS WERE WELL
  MODELED BY A QUASI-STEADY, ONE-DIMENSIONAL
  ANALYSIS.

- EJECTORS WITH STEADY DRIVER FLOWS WERE WELL
  MODELED BY ONE-DIMENSIONAL ANALYSIS.

FINDINGS (CONT'D):

- THE MEAN FLOW EJECTOR RESULTS WITH A PERIODIC
  DRIVER WERE NOT SIGNIFICANTLY DIFFERENT FROM
  THE STEADY DRIVER RESULTS.

- THE FLOW WITHIN THE MIXING DUCT WAS FOUND TO
  BE UNSTEADY FOR BOTH STEADY AND PERIODIC DRIVER
  FLOWS.

FINDINGS (CONT'D):

- UNSTEADY AND HIGHLY DISTURBED CHARACTER OF
  THE FLOW WITHIN MIXING DUCT COULD HAVE MASKED
  PERIODIC DRIVER EFFECTS.

- PERIODIC DRIVER FLOW EXPERIMENTS PROBABLY
  REQUIRED HIGHER STROUHAL NUMBERS TO ALTER
  MIXING DYNAMICS.


FINDINGS (CONT'D):

- IS OBSERVED UNSTEADY AND DISTURBED FLOW IN
  MIXING DUCT CHARACTERISTIC OF PLANAR, TWO-
  DIMENSIONAL EJECTORS?

- DO SIMILAR UNSTEADY FLOWS OCCUR IN AN
  AXISYMMETRIC EJECTOR?

## LITERATURE

Shapiro, A. H., <u>The Dynamics and Thermodynamics of Compressible Fluid Flow</u>, Vol. 1, Ronald Press Co., New York, 1953.

Fabri, J. and Paulon, J., "Theory and Experiments on Supersonic Air-to-Air Ejectors," NACA TM 1410, September 1958.

Chow, W. L. and Addy, A. L., "Interaction Between Primary and Secondary Streams of Supersonic Ejector Systems and their Performance Characteristics," AIAA Journal, Vol. 2, April 1964, pp. 686-695.

Chow, W. L. and Yeh, P. S., "Characteristics of Supersonic Ejector Systems with Non-Constant Area Shroud," AIAA Journal, Vol. 3, March 1965, pp. 525-527.

Nelson, J. R., "Investigation of the Mixing Region Between the Primary and Secondary Streams of a Two-Dimensional Supersonic Air-Air Ejector System," Masters Thesis, Air Force Institute of Technology, Air University, June 1966.

Johnson, J. K., Jr., "An Analytical and Experimental Investigation of Ejector Performance for Nonsteady Flow Conditions," Clemson University, College of Engineering, Engineering Experiment Station Bulletin 107, July 1966.

McCormack, P. D., Cochran, D., and Crane, L., "Periodic Vorticity and Its Effect on Mixing," The Physics of Fluids, Vol. 9, August 1966, pp. 1555-1560.

Sparks, C. R., "A Study of Pulsating Effects on Orifice Metering of Compressible Flow," ASME, Flow Measurement Symposium, K. C. Cotton (editor), Pittsburg, Pennsylvania, September 26-28, 1966.

Zarek, J. M., "The Neglected Parameters in Pulsating Flow Measurement," ASME, <u>Flow Measurement Symposium</u>, K. C. Cotton (editor), Pittsburg, Pennsylvania, September 26-28, 1966.

Townsend, A. A., "The Mechanisms of Entrainment in Free Turbulent Flows," Journal of Fluid Mechanics, Vol. 26, Part 4, 1966, pp. 689-716.

Halbach, C. R., Otsap, B. A., and Thomas, R. A., "A Pressure Insensitive Fluidic Temperature Sensor," Advances in Fluidics, ASME, Brown, F. T. (editor), 1967, pp. 298-312.

Johnson, W. S., "A Performance Comparison of the Wave Energy Exchanger and the Steady Flow Ejector," Ph.D. Thesis, University of Tennessee, Mechanical and Aerospace Engineering Department, 1967.

Glass, D. R., "Effects of Acoustic Feedback on the Spread and Decay of Supersonic Jets," AIAA Journal, Vol. 6, October 1968, pp. 1890-1897.

Becker, H. A. and Massoro, T. A., "Vortex Evolution in a Round Jet," Journal of Fluid Mechanics, Vol. 31, Part 3, 1968, pp. 435-448.

Johnson, W. S. and Yang, T., "A Mathematical Model for the Prediction of the Induced Flow in a Pulsejet Ejector with Experimental Verification," ASME Paper No. 68-WA/FE-33, 1968.

Rudinger, G., Nonsteady Duct Flow: Wave Diagram Analysis, Dover Publications Inc., New York, 1969, pp. 94-106.

Bevilaqua, P. M. and Lykoudis, P. S., "Mechanisms of Entrainment in Turbulent Wakes," AIAA Journal, Vol. 9, 1971, pp. 1657-1659.

Crow, S. C. and Champaign, F. H., "Orderly Structure in Jet Turbulence," Journal of Fluid Mechanics, Vol. 48, Part 3, 1971, pp. 547-591.

Kovaszney, L. S. G., "The Structure of Turbulence in Shear Flows," AGARD-CP-93, 1971.

Addy, A. L., "The Analysis of Supersonic Ejector Systems," Supersonic Ejectors, AGARD-CP-163, 1972, pp. 31-101.

Binder, G. and Favre-Marinet, M., "Mixing Improvement in Pulsating Turbulent Jets," Fluid Mechanics of Mixing, ASME, Symposium Proceedings of the Joint Meeting, Georgia Institute of Technology, June 20-22, 1973, pp. 167-172.

Baker, L. R., Jr. and McDermit, J. H., "Survey of Pressure Recovery Methods for Chemical Laser Applications," Chemical Laser Analysis and Development, Vol. VI, Lockheed Missile and Space Co., Technical Report RK-CR-73-2, October 1973.

Khare, J. M., "An Analytical and Experimental Investigation of an Unsteady Flow Ejector," University of Calgary, Mechanical Engineering Department, Report No. 53, 1973.

Olivari, D., "Analysis of an Axisymmetrical Turbulent Pulsating Jet," von Karman Institute Technical Note No. 104, November 1974.

Addy, A. L. and Mikkelsen, C. D., "An Investigation of Gas Dynamic Flow Problems in Chemical Laser Systems," Department of Mechanical and Industrial Engineering, University of Illinois at Urbana, Report No. UILU-ENG-74-4009, 1974.

Brown G. and Roshko, A., "The Effect of Density Differences on the Turbulent Mixing Layer," Journal of Fluid Mechanics, Vol. 64, Part 4, 1974, pp. 775-816.

Brown, S. L. and Murphy, R. D., "Design and Testing of Thrust Augmenting Ejectors," V/STOL Aerodynamics, AGARD-CP-143, 1974.

Papailiou, D. D. and Lykoudis, P. S., "Turbulent Vortex Streets and Entrainment," Journal of Fluid Mechanics, Vol. 62, Part 1, 1974, pp. 11-31.

Gilbert, G. B. and Hill, P. G., "Analysis and Testing of Two-Dimensional Slot Nozzle Ejectors with Variable Area Mixing Sections," NASA CR-2251, May 1975.

Hasinger, S. H., "Performance Characteristics of Ejector Devices," former Aerospace Research Laboratories, Wright-Patterson Air Force Base, Technical Report ARL TR 75-205, June 1975.

Tai, T. C., "Analysis and Design of Thrust Augmenting Ejectors," Prediction Methods for Jet V/STOL Propulsion Aerodynamics, Vol. 2, M. F. Platzer (editor), Proceedings of a Naval Air Systems Command Research and Technology Group Workshop, Institute for Defense Analysis, Arlington, Virginia, July 28-31, 1975, pp. 702-721.

Viets, H., "Flip-Flop Jet Nozzle," AIAA Journal, Vol. 13, October 1975, pp. 1375-1379.

Ejectors, von Karman Institute, Lecture Series 79, two volumes, 1975, Addy, A. L., "The Analysis of Supersonic Ejector Systems"; Delery, J., "Methods d'étude des éjecteurs Supersonic Application aus tuyéres double-flux;" Olivari, D., "Jets and Mixing Phenomena"; Viets, H., "Thrust Augmenting Ejectors"; Walker, B. J., "Chemical Laser Pumping Systems"; Schmitt, H., "Summary of Possible Applications and Present Status of Various Ejector Techniques."

Bradshaw, P., "Interacting Shear Layers in Turbomachines," Turbulence in Internal Flows, Murthy, S. N. B. (editor), A Project SQUID Workshop, Warrenton, Virginia, June 14-15, 1976, pp. 35-65.

Roshko, A., "Structure of Turbulent Shear Flows: A New Look," AIAA Journal, Vol. 14, October 1976, pp. 1349-1357.

Dimotakis, P. E. and Brown, G. L., "The Mixing Layer at High Reynolds Numbers: Large Structure Dynamics and Entrainment," Journal of Fluid Mechanics, Vol. 76, Part 3, 1976, pp. 535-560.

Mikkelsen, C. D., Sandberg, M. R., and Addy, A. L., "Theoretical and Experimental Analysis of the Constant Area Supersonic-Supersonic Ejector," Department of Mechanical and Industrial Engineering, University of Illinois at Urbana, Report No. UILU-ENG-76-4003, 1976.

Bremhorst, K. and Harch, W. H., "Near Field Velocity Measurements in a Fully Pulsed Subsonic Air Jet," Turbulent Shear Flows, Symposium Proceedings, Pennsylvania State University, April 18-20, 1977, pp. 2.41-2.50.

Viets, H., "Thrust Augmenting Ejector Analogy," Journal of Aircraft, Vol. 14, April 1977, pp. 409-411.

Quinn, B., "Interactions Between Screech Tones and Ejector Performance," Journal of Aircraft, Vol. 14, May 1977, p. 467.

Simpson, R. L., "Features of Unsteady Turbulent Boundary Layers as Revealed from Experiments," Unsteady Aerodynamics, AGARD-CP-227, September 1977.

Telionis, D. P., "Unsteady Boundary Layers, Separated and Attached," Unsteady Aerodynamics, AGARD-CP-227, September 1977.

DeJoode, A. D. and Pantankar, S. V., "Prediction of Three-Dimensional Turbulent Mixing in an Ejector," AIAA Journal, Vol. 16, February 1978, pp. 145-150.

Platzer, M. F., Simmons, J. M., and Bremhorst, K., "Entrainment Characteristics of Unsteady Subsonic Jets," AIAA Journal, Vol. 16, No. 3, March 1978, p. 282.

Stover, T. R., "Development of a Large-Scale Fluidic Oscillator for Application to an Unsteady Aerodynamic Ejector System Using the Hydraulic Analogy," Masters Thesis, Department of Mechanical and Industrial Engineering, University of Illinois at Urbana, 1978.

SOME OBSERVATIONS ON MIXING OF FREE AND
CONFINED UNDEREXPANDED RECTANGULAR JETS

By

A. Krothapalli, Y. Hsia,
D. Baganoff, and K. Karamcheti

Joint Institute for Aeronautics and Acoustics
Stanford University

Paper Presented at the
Ejector Workshop for Aerospace Applications
August 3 - 5, 1981
Dayton, Ohio

# ABSTRACT

A continuing series of experimental investigations is being carried
out on an underexpanded jet of air issuing from a convergent rectangular
nozzle in both free and confined configurations. Schlieren pictures of
the flow field along with hot wire and microphone data were obtained for
different operating conditions and configurations of the jet.

In our study of factors influencing jet mixing and concomitant sound
production the following observations were made for a free jet. At a
pressure ratio for maximum screech sound radiation, which occurs at a
pressure ratio of 3.7, Schlieren photographs show a very strong organized
cylindrical wave pattern on either side of the jet with their respective
sources located at the end of the third shock cell. Associated with
this wave pattern is a large angular spread of the jet of about 36 degrees,
compared with a normal spread of about 20 degrees. When small rigid sur-
faces were introduced near the nozzle exit, we found that the flow can be
either destabilized, characterized by a large spreading of the jet or
stabilized, depending on the position of the surfaces. These effects
show that solid surfaces and their placement have a profound effect on
mixing characteristics of jets.

Some experiments on partially confined jet (plates placed parallel
to the long dimension of the nozzle) indicate that the jet spreads very
rapidly and fills the channel within about one channel width downstream
of the nozzle exit. The organized wave pattern present in a free jet is
replaced by a very complicated wave system. In a fully confined (ejector)
configuration with its greater secondary flow velocity these sound waves
are not present, and less rapid mixing between the primary and secondary
streams is observed.

## NOMENCLATURE

| | |
|---|---|
| a | Speed of sound |
| AR | Aspect ratio |
| D | Width of the nozzle |
| L | Length of the nozzle |
| $L_1$ | Distance between the plates in x,z, plane |
| $L_2$ | Distance between the plates in x,y plane |
| $\ell, L_3$ | Length of the confining surfaces |
| M | Mach number |
| $P_a$ | Ambient pressure |
| $P_o$ | Stagnation pressure |
| $P_{o2}$ | Pitot tube pressure |
| $P_s$ | Surface pressure on the confining surfaces |
| R | Pressure ratio |
| U | Mean velocity |
| $U_{CL}$ | Mean velocity along the centerline of the jet |
| $\sqrt{\overline{u^2}}$ | rms velocity fluctuation |
| x | Coordinate along the jet axis |
| y | Coordinate along the small dimension of the nozzle |
| $y_{\frac{1}{2}}$ | Local half width of the U profile along the y axis |
| z | Coordinate along the long dimension of the nozzle |

# INTRODUCTION

A continuing series of experiments is being carried out to study the basic fluid mechanical properties of single and multiple rectangular jets in a free and confined environment. This work was motivated by the use of these jets in a augmentor wing considered by NASA Ames Research Center. The configuration which is of interest here is shown in Figure 1. Also shown in the figure is a slot nozzle augmentor wing. The gross characteristics of a multi lobe augmentor wing was reported by Aiken (1). These results show that the lobe augmentor gives higher static thrust augmentation than slot nozzle augmentor at a given value of mixing length ($\ell/L$ or $\ell/D$). Combining the lobed nozzle with a lined augmentor reduces the noise of the augmentor wing as compared to a slot nozzle augmentor (2). With these advantages in mind, and to further improve the performance of multi-element nozzle ejector, a long range program was initiated at Stanford. This program has the following main objectives to the general problem of mixing processes in a multiple three dimensional confined jet (ejector).

- Investigate the characteristics of a single rectangular free jet
- Study the characteristice of a free jet in a multilobe configuration
- Include the confining surfaces, and determine the nature of changes in the flow as a result of confining walls
- Develop a semi-analytical method for predicting the performance of multilobe nozzle ejector

519

Most of the results dealing with incompressible single and multiple
jets in free and partially confined configurations were reported by
Krothapalli et al. (3,4,5). Experiments on a subsonic compressible
rectangular free jet were recently completed, and the results are
reported by Hsia et al. (6). The purpose of the present paper is to
present and discuss the results of experiments with an underexpanded
rectangular jet in free and confined configurations.

The flow under consideration will depend mainly on the following
parameters: the aspect ratio of the nozzle (lobe), the pressure ratio
R, the Mach number M, and Reynolds number Re of the jet near the exit,
the state of the flow at the exit of the nozzle, configuration of the
confining surfaces, in particular the inlet geometry, and conditions
of the ambient medium into which the jet is issuing. The range of
parameters considered in this experiment is compared with the augmentor
wing and are shown in Figure 2. In the present investigation, two
nozzle aspect ratios of 16.7 and 10 were considered. The pressure
ratio R, was varied from 2.0 to 5.4. This corresponds to a Mach
number range based on isentropic flow of 1.05 to 1.8. The Reynolds
number employed was based on the width D (small dimension) of the
nozzle and given by $Re = M \frac{aD}{\nu}$ , where a and $\nu$ are the speed of sound
and kinematic viscosity of the ambient medium. This Reynolds number
was varied from $7.2 \times 10^4$ to $1.8 \times 10^5$.


APPARATUS, INSTRUMENTATION AND PROCEDURES


A blow down air supply system was used, the details of which
can be found in Reference 3. Two nozzle sizes were used in the present

study. The dimensions of the rectangular exit of the small nozzle used was 50mm long (L) by 3mm wide (D)  The exit dimensions of the large nozzle were 50mm long and 5mm wide.  The nozzle exit in each case was preceeded by a 40mm long smooth rectangular channel (50mm x 3mm, and 50mm x 5mm).  The 3mm nozzle used in this investigation was one central lobe of a multilobed nozzle employed in previous investigation (see Figure 3). All other lobes were blocked while measurements were made on the central lobe.  The 5mm nozzle employed was single lobed nozzle, but otherwise all other dimensions were the same. This nozzle was used in all the experiments concerning the confining jet.  For the partially confined jet configuration two plates were symmetrically placed parallel to the long dimension of the nozzle.  The separation distance between the plates can be adjusted from 0 to 80mm.  For the ejector configuration, two additional parallel plates are symmetrically placed normal to the long dimension of the nozzle.  The separation distance between them can also be adjusted, however kept at 50mm for the present experiment.  A schematic arrangement of the confining surfaces is shown in Figure 4.  Also shown in the figure is a cartesian coordinate system (x,y,z) with its origin located at the center of the nozzle exit, with x axis oriented along the centerline of the jet.

A conventional Schlieren system was used for flow visualization. Measurements were made using a pitot-tube and hot wire anemometry. A standard DISA normal wire in conjunction with a DISA 55 M01 constant temperature anemometer was used.  Surface pressure measurements were made using a 96 port scanning valve which is interfaced with a PDP 11/23 minicomputer.  For the most part the hot wire was used in regions

where the flow is known to be subsonic, thus minimizing errors present due to compressibility.

The controlling parameter in this investigation was the stagnation pressure $p_o$, which was varied from 30psia to 85psia. This corresponds to a range of nozzle pressure ratios from 2 to 5.8. This pressure was maintained to an accuracy better than one percent. Most of the Schlieren pictures were taken to display the flow field in the plane containing the small dimension of the nozzle. For a free jet, experiments were conducted for a number of pressure ratios using both nozzles, however only a limited selection is presented here. In the case of a confined jet only the 5mm nozzle was used.

## RESULTS AND DISCUSSION

### Free Jet

Typical Schlieren pictures of the jet issuing from the 3mm nozzle, at three different pressure ratios are shown in Figure 5. For a pressure ratio R>1.9, the flow at the nozzle exit is chocked and results in the formation of a series of shock cells downstream of the nozzle exit as shown in the figure. The most striking observation for the three cases shown in the figure are large change in the angle of spread of the jet, the appearance of a very strong organized wave pattern, and the development of a Mach wave radiation pattern at the highest pressure ratio. For example, the total angle of spread of the jet is about 20° for both the lowest (R=2.2) and the highest (R=5.4) pressure ratios, while the total angle of spread is about 35° at the pressure ratio for maximum screech sound radiation (R=3.7). As will be shown later, that the jet spreads

522

linearly in all these cases; i.e. $\frac{d\delta}{dx} = \delta' = \delta/(x-x_o) = C$, where, $\delta$, is some measure of the local scale of the flow; a thickness defined in some particular way. If an asymptotic value of $\delta' = C$ can be determined from the picture then $x_o$ is determined from the tangent, $\delta = C(x - x_o)$. Using this procedure the spreading rate is obtained for various pressure ratios of the jet and it is plotted in Figure 6. At a pressure ratio for maximum screech sound radiation, which occurs at a pressure ratio of 3.7, the spreading rate is higher by almost 50 percent as compared to the same at other pressure ratios. Associated with this large spreading rate is an organized cylindrical double wave pattern which originates alternatively from each side of the jet. The source for the wave system is approximately located at the end of the third shockcell. Detailed structure of the near sound field of this flow was described by Krothapalli et al. (7). Figure 7 gives an example of the flow from the 5mm nozzle for the same conditions as in Figure 5b. In this case the aspect ratio of the nozzle is lower (10) than for the 3mm nozzle (16.7). On comparing the two flows, one finds a single-wave pattern is present in Figure 7, while a double-wave pattern is present in Figure 5b.

To study the degree of two dimensionality present in the experiments, photographs were taken at right angles to the view in Figure 5. The results are presented in Figures 8a and 8b. Three shock cells can be identified in the figures by three bright lines in the jet, and very little spreading of the jet occurs in this plane indicating the flow is fairly two dimensional.

It has been shown by Poldervaart et al. (8) that the placement of a reflective surface near the exit of rectangular jet has an important effect on the flow. To further investigate this effect several reflector geo-

metries were used; and a typical geometry of 90° is shown in Figure 9. The most striking conclusion drawn from the experiments was that the flow can be either destabilized characterized by a large spreading of the jet or stabilized by a small plate, and the effect is present with the plate located on only one side and in almost all positions. Figure 9 gives such a comparison where the plate position was adjusted holding the plate parallel to the jet axis to cause this effect.

To obtain the detailed structure of the jet, measurements were made using pitot tube and hot wire at selected operating conditions. Some of the typical results are presented in the next few figures. The variation of the pitot pressure along the centerline of the jet for a pressure ratio of 3.7 is shown in Figure 10. The absolute values are divided by the ambient pressure and plotted agianst the nondimensionalized downstream distance. These measurements cannot be transferred directly into velocity or Mach number, neither are they the true pitot pressure. In supersonic flow, maxima in pitot pressure corresponds to minima in Mach number and vice versa. Also shown in the figure is the location of the source for the sound waves observed in Schlieren photographs (Figure 5b). It is observed that the downstream decay of the pitot pressure is considerably accelerated after about 10D, and subsonic flow is realized beyond x/D of about 15.

The variation of the centerline mean velocity $U_{CL}$ with downstream distance x, for x/D greater than 30, and for three different pressure ratios, is shown in Figure 11. The mean velocity $U_{CL}$, is normalized with respect to the corresponding exit velocity of the jet, which is computed from the isentropic flow tables (with the assumption that the flow is fully expanded near the nozzle exit). Also included in the figure are the

typical variations of two dimensional and axisymmetric jets. For x/D

greater than 60, and for both lowest (R=2.7) and highest (R=5.4) pressure

ratios, the velocities decay at a rate roughly the same as that of a two

dimensional jet, while for the pressure ratio of 3.7 (screeching condition)

the velocity decays faster than the two dimensional jet. Figure 12 shows

the distribution of the mean velocity U across the jet in the x,y plane

at different downstream stations ranging from 40 to 100 widths at a pressure

ratio of 3.7. The velocity U is normalized with respect to $U_{CL}$ at each

station, while the distance y is normalized by the distance x to the station

in question. The profiles do not display any geometrical similarity, which

is in contrast to geometrically similar profiles for a high speed subsonic

rectangular jet (6).

The growth of the jet in x,y plane with downstream distance for three

different pressure ratios is shown in Figure 13. The ordinate $y_{\frac{1}{2}}$ is the

distance from the centerline of the jet to the point where the mean velocity

is equal to one-half of its centerline value. The jet in the x,y plane

spreads linearly with x and the locus of half velocity points is given by

$$y_{\frac{1}{2}} = k(x - x_o).$$

For planar jets, the value of k varies between 0.09 and 0.12. For the

lowest and highest pressure ratios the variation is linear and identical

to each other with values for k=0.095 and $x_o$=-7D. For the screeching

condition the variation is also linear with k=0.138 and $x_o$=20D. Also included

in the figure are the data for a subsonic rectangular jet and an under-

expanded axisymmetric jet (exiting from a 2mm diameter nozzle).

Profiles in the x,y plane of the rms values of the velocity at

different downstream locations x, for a pressure ratio of 3.7, are shown

525

in Figure 14. These values are normalized with respect to the local mean velocity on the centerline. The profiles do not indicate any geometrical similarity and show a distinct saddle shape for $\frac{x}{p}$ less than 70. After examination of this data along with the data at other pressure ratios, it appears that the overall structure of an underexpanded screeching jet may be quite different from that of nonscreeching and subsonic jets.

## Confined Jet

Typical Schlieren pictures of a partially confined jet issuing from the 5mm nozzle, at a pressure ratio of 3.4 (35psig), and at three different spacings ($L_2$) are shown in Figure 15. The striking observation is that the jet spreads very rapidly and fills the channel within about one channel width ($L_2$) downstream of the nozzle exit. The organized sound wave pattern present in a free jet is replaced by a very complicated wave system. Considerable enhancement of large vortical motions were observed. The static pressure distribution along the plates were measured at a spacing $L_2$ equal to 10D, for four different stagnation pressures. The results are shown in Figure 16. The pressure distribution on the plate placed on either side of the jet was found to be identical, thus measurements on only one of the plates are presented here. For x less than about 8cm, the pressure is almost equal to the ambient pressure; thus suggesting very little secondary flow is induced into the channel.

Figure 17 gives an example of the flow in an ejector ($L_1/L = 1.0$) for the same conditions as in Figure 15. On comparing the two flows one finds that the jet spreads very slowly and less rapid mixing between

526

the primary and secondary flows is observed. With the confining plates

normal to the long dimension of the nozzle, the jet seems to be less

sensitive to the variation of the spacing between the plates (placed

parallel to the long dimension of the nozzle). With its greater secondary

flow velocity sound waves are not present. For larger spacings ($L_2 \geq$ 70mm)

weak sound waves are found in the ejector. Figure 18 gives the surface

pressure distribution for the same conditions as in Figure 16. For the

entire length of the wall the pressure was negative and in each case a

minimum value was found at about 3cm from the nozzle exit. The lowest

magnitude noted in this data was about -2.5psig at 3cm downstream of the

nozzle exit for a stagnation pressure of 40psig. This corresponds to a

secondary flow Mach number of about 0.48.

To compare the flow for the two cases in the entire length of the

duct at the same operating conditions picutres were taken for a pressure

ratio of 3.5 as shown in Figure 19. In the ejector configuration the

significant mixing between the primary and secondary flows takes place

for a downstream distance of about 2.5 channel widths.

## CONCLUDING REMARKS

The following conclusions can be drawn from the measurements of a free jet. From the Schlieren pictures it was observed, in the range of pressure ratios from 3 to 4 that an organized cylindrical wave pattern emerges alternately from each side of the jet. Associated with this wave pattern is a large angular spread of the jet of about 36° compared with a normal spread of about 20°. The mean velocities and rms velocity profiles in the x,y plane do not show any similarity. The structure of such a jet may be quite different from that of a compressible subsonic and nonscreeching underexpanded jet. There is some evidence that the structure of a nonscreeching underexpanded jet may be quite similar to that of a subsonic jet. The present studies are still not complete enough to enable a detailed understanding of the complex flow development of the jet issuing from an underexpanded rectangular nozzle. All the implications of the results obtained are not yet understood. Further experiments are underway to obtain the information to properly character-ize and elucidate the flow structure.

Experiments on a partially confined jet indicate that the jet spreads very rapidly and fills the channel within about one channel width down-stream of the nozzle exit. The static pressure distribution on the sur-face depicts that very little secondary flow is induced into the channel. The organized wave pattern present in a free jet is replaced by a very complicated wave system. In a fully confined configuration with its greater secondary flow velocity these sound waves are not present; and less rapid mixing between the primary and secondary streams is observed. Further detailed investigations are planned to obtain the flow details within these confining geometries.

# REFERENCES

1.  Aiken, N. T., "Advanced Augmentor Wing Research", STOL Technology, NASA SP-320, October 1972.

2.  Falarski, D. M., Aoyagi, K., and Koenig , G. D., "Acoustic Charac-teristics of Large Scale STOL Models", STOL Technology, NASA SP-320, October 1972.

3.  Krothapalli, K., Baganoff, D., and Karamcheti, D., "Development and Structure of a Rectangular Jet in a Multiple Jet Configuration", AIAA Journal, August 1980, pp 945-950.

4.  Krothapalli, K., Baganoff, D., and Karamcheti, K., "Partially Confined Multiple Jet Mixing", AIAA Journal, March 1981, pp 324-328.

5.  Krothapalli, K., Baganoff, D., and Karamcheti, K., "On the Mixing of a Rectangular Jet", Journal of Fluid Mechanics, Vol. 107, 1981, pp 201-220.

6.  Hsia, Y., Krothapalli, K., Baganoff, D., and Karamcheti, K., "Effects of Mach Number on the Development of a Rectangular Jet", JIAA TR (to be published) September 1981.

7.  Krothapalli, K., Baganoff, D., Hsia, Y., and Karamcheti, K., "Some Features of Tones Generated by an Underexpanded Rectangular Jet" AIAA paper no. 81-0060, January 1981.

8.  Poldervaart, J. L., Wijnauds, J. P. A., and Brankhurst, L., "Aerosonic Games with the Aid of Control Elements and Externally Generated Pulses", Noise Mechanisms AGARD CP-131, 1973.

**SLOT** **D**

**LOWER GAP**

**FLAP**

**SHROUD**

$\ell$

SECTION

PERSPECTIVE

**LOBE**

**SHROUD**

**L**

**FLAP**

**L₁**

**S**

SECTION

PERSPECTIVE
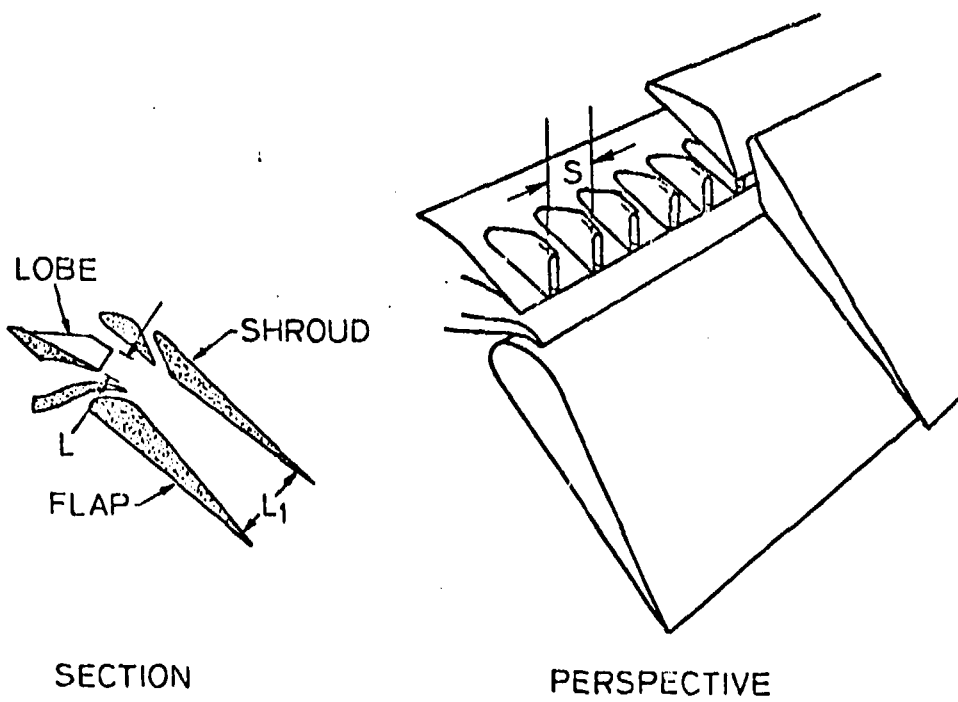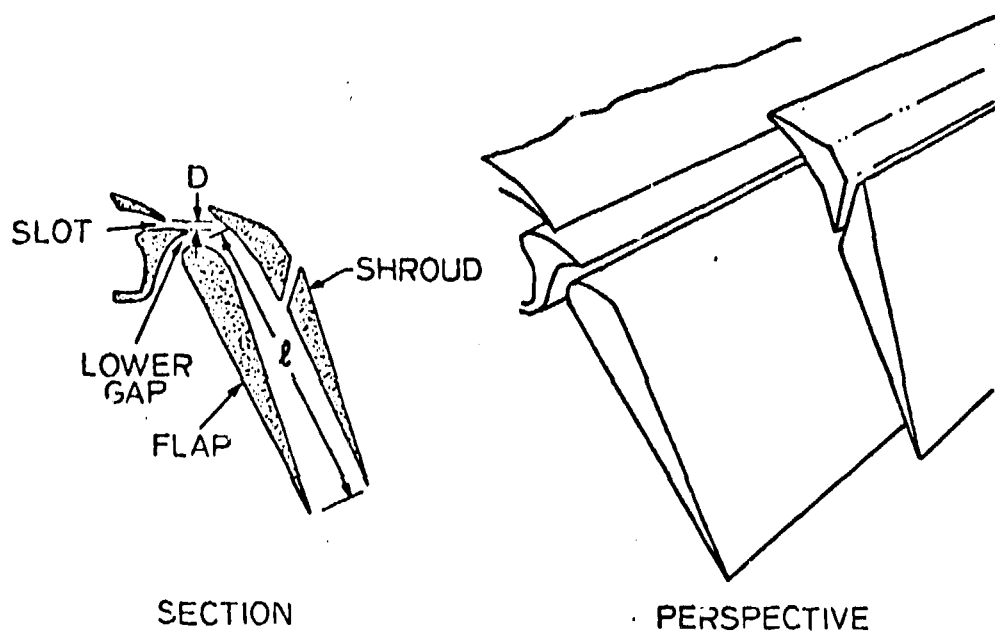
FIGURE 1. SECTIONAL VIEWS OF AN AUGMENTOR

## RANGE OF PARAMETERS

| | AUGMENTOR WING | EXPERIMENT |
|---|---|---|
| AIRCRAFT SPEED | $\leq 200$ KNOTS | 0 KNOTS |
| PLENUM PRESSURE RATIO | 2 - 3 | 1.3 - 5.5 |
| NOZZLE ASPECT RATIO | 0 - 15 | 5 - 16.7 |
| VENTILATION RATIO | $\leq 10$ | 4 - 10 |
| FLAP EXIT VELOCITY | 60 - 200 M/S | 60 - 300 M/S |
| REYNOLDS NUMBER (BASED ON NOZZLE WIDTH) | 40,000 - 130,000 | 12,000 - 180,000 |

FIGURE 2.
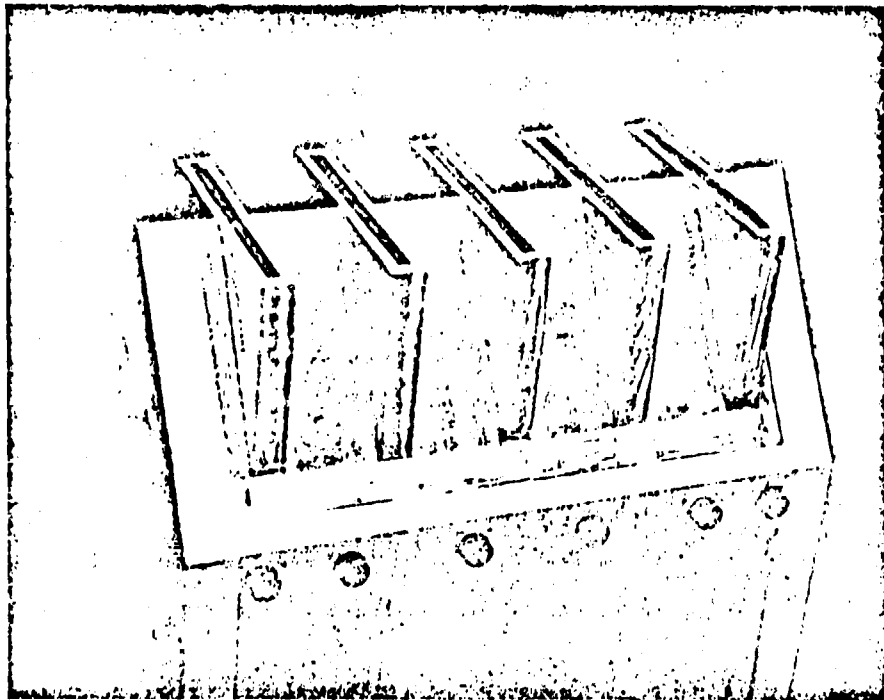
FIGURE 3. THE MULTILOBE NOZZLE
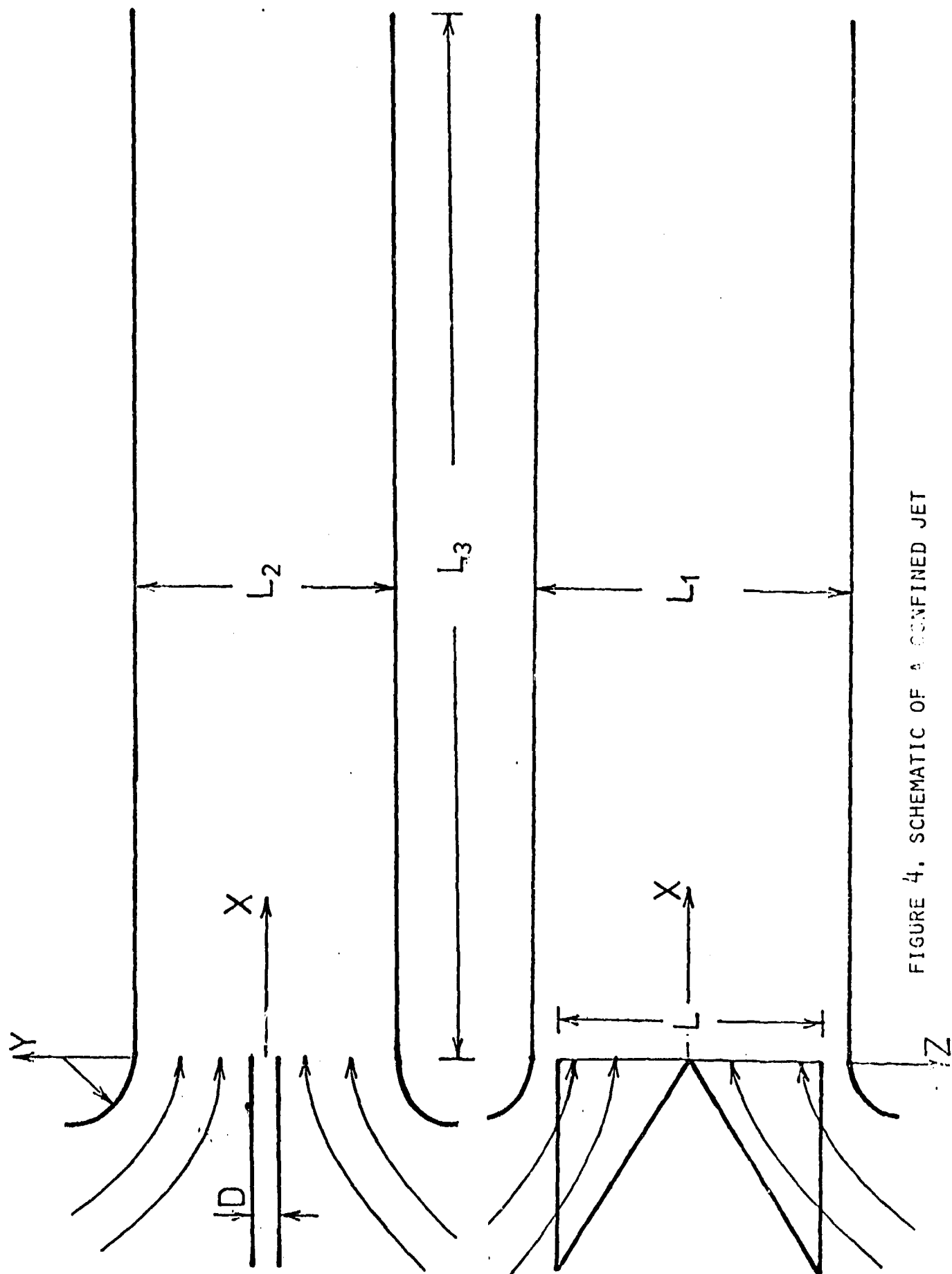
FIGURE 4. SCHEMATIC OF A CONFINED JET

533

R=3.7
5b

R=22
5a

534
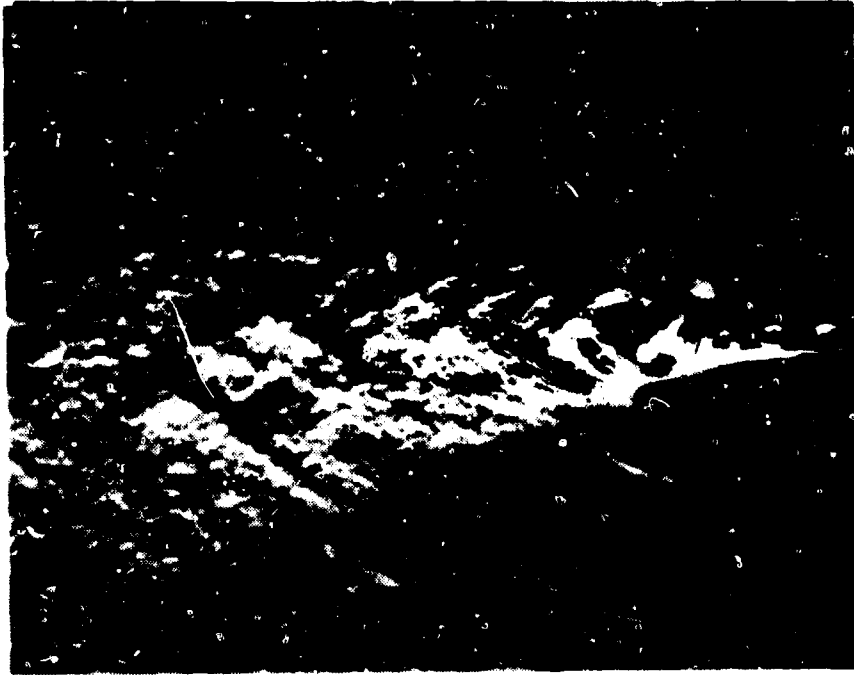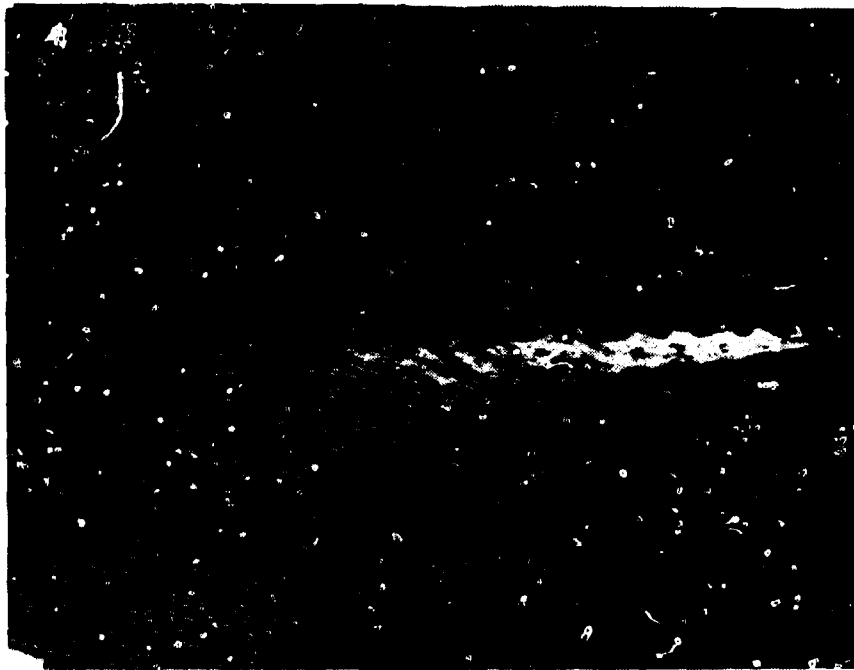
R=5.4
5c

FIGURE 5. SCHLIEREN PICTURES OF THE JET FROM 3MM NOZZLE.
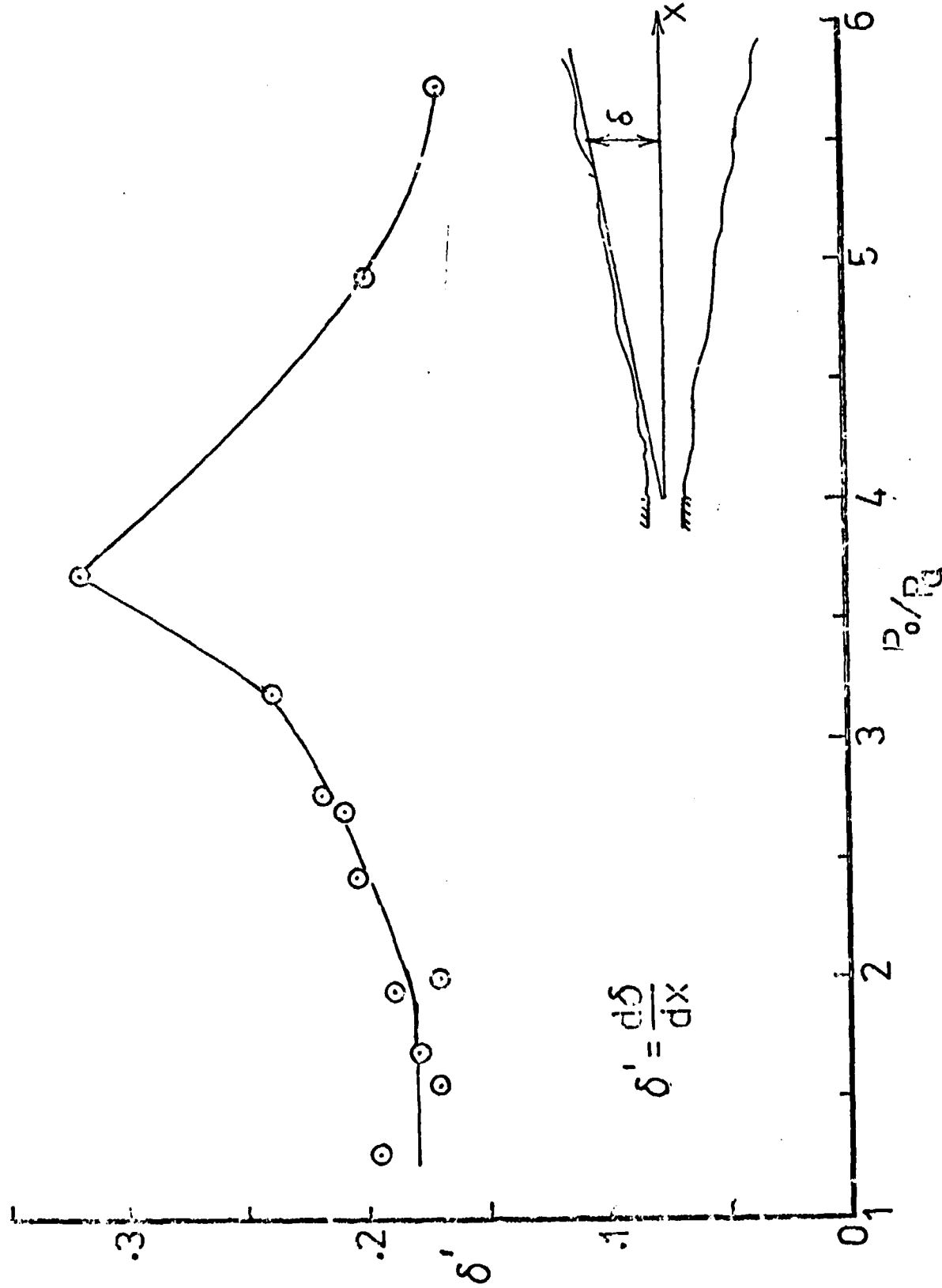
FIGURE 6. VARIATION OF THE SPREADING RATE WITH PRESSURE RATIO.

R=3·7

FIGURE 7. SCHLIEREN PICTURE OF THE JET FROM 5MM NOZZLE.
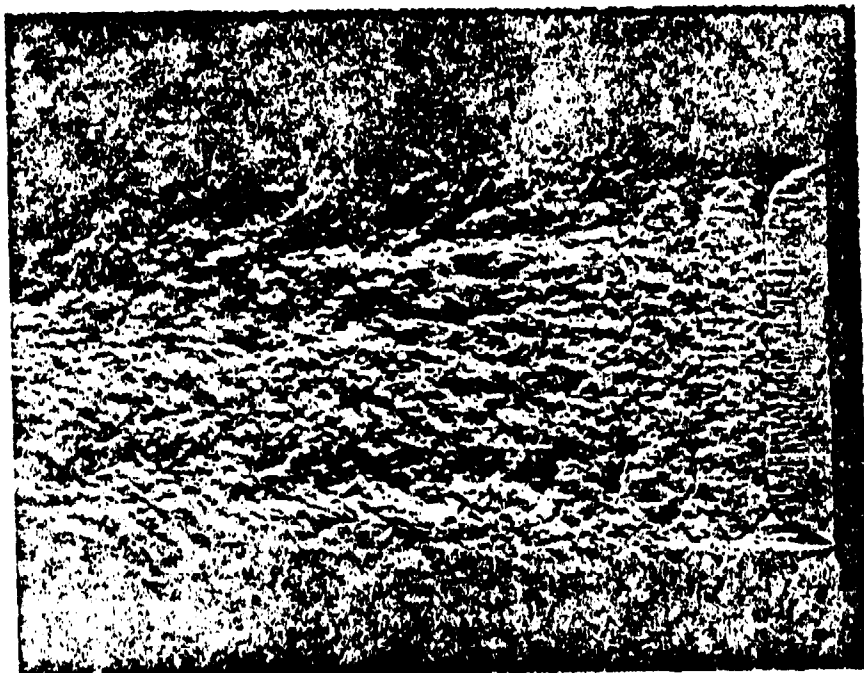
R=5.4
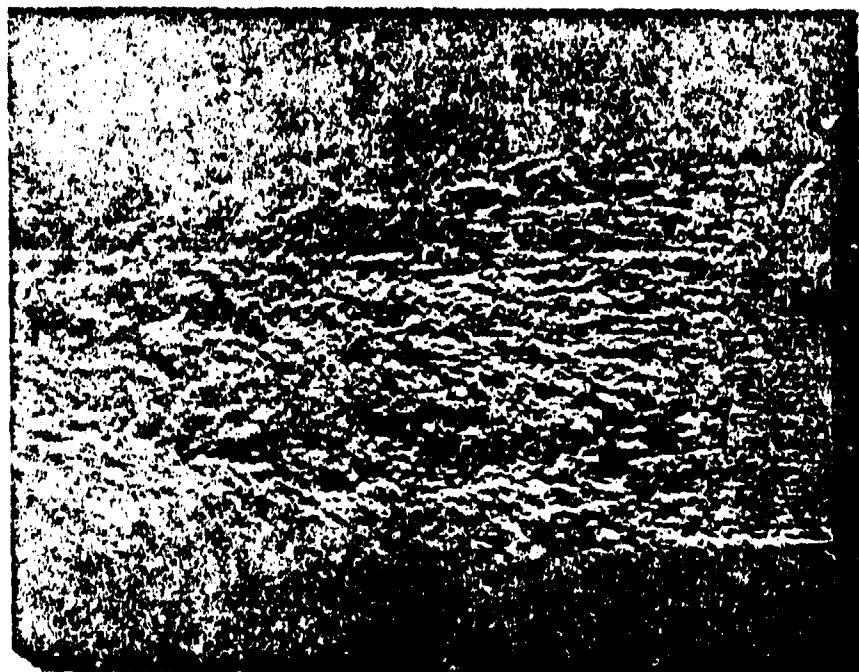
R=3.7

FIGURE 8. SCHLIEREN PICTURES OF THE JET FROM 3MM NOZZLE
(LOOKING AT THE LONG DIMENSION OF THE NOZZLE)
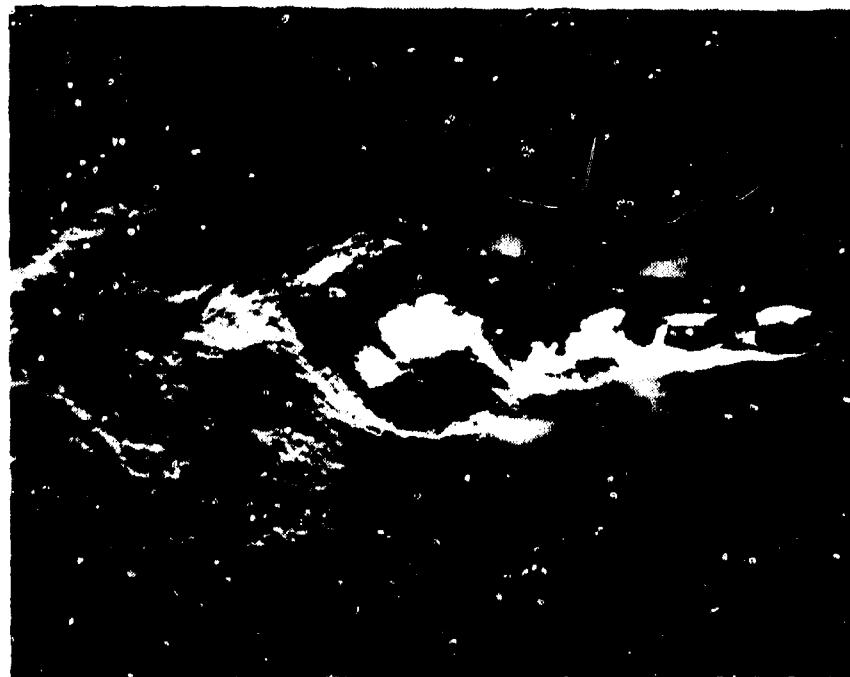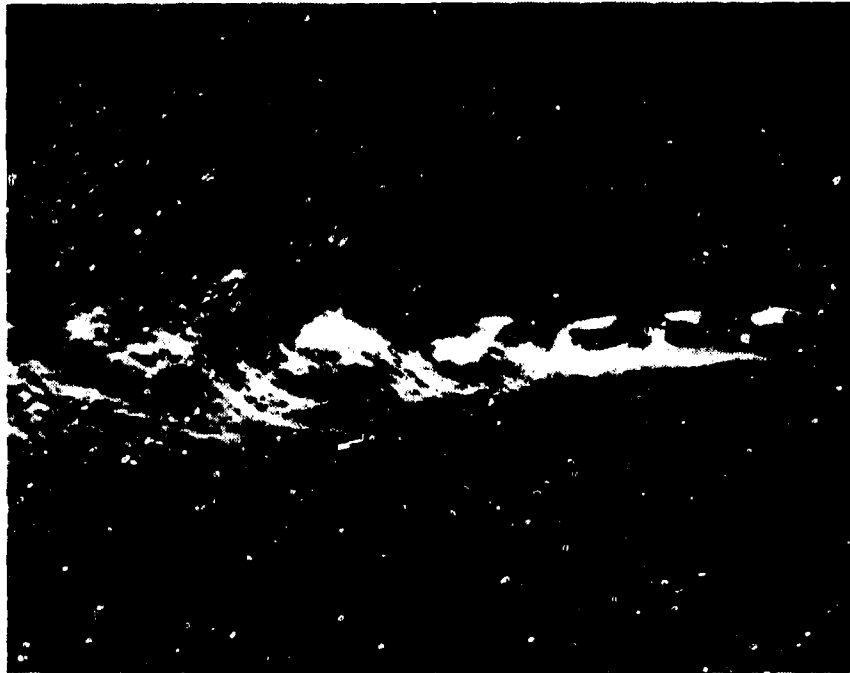
R=3.7

FIGURE 9. SCHLIEREN PICTURES OF THE JET WITH A REFLECTIVE SURFACE.
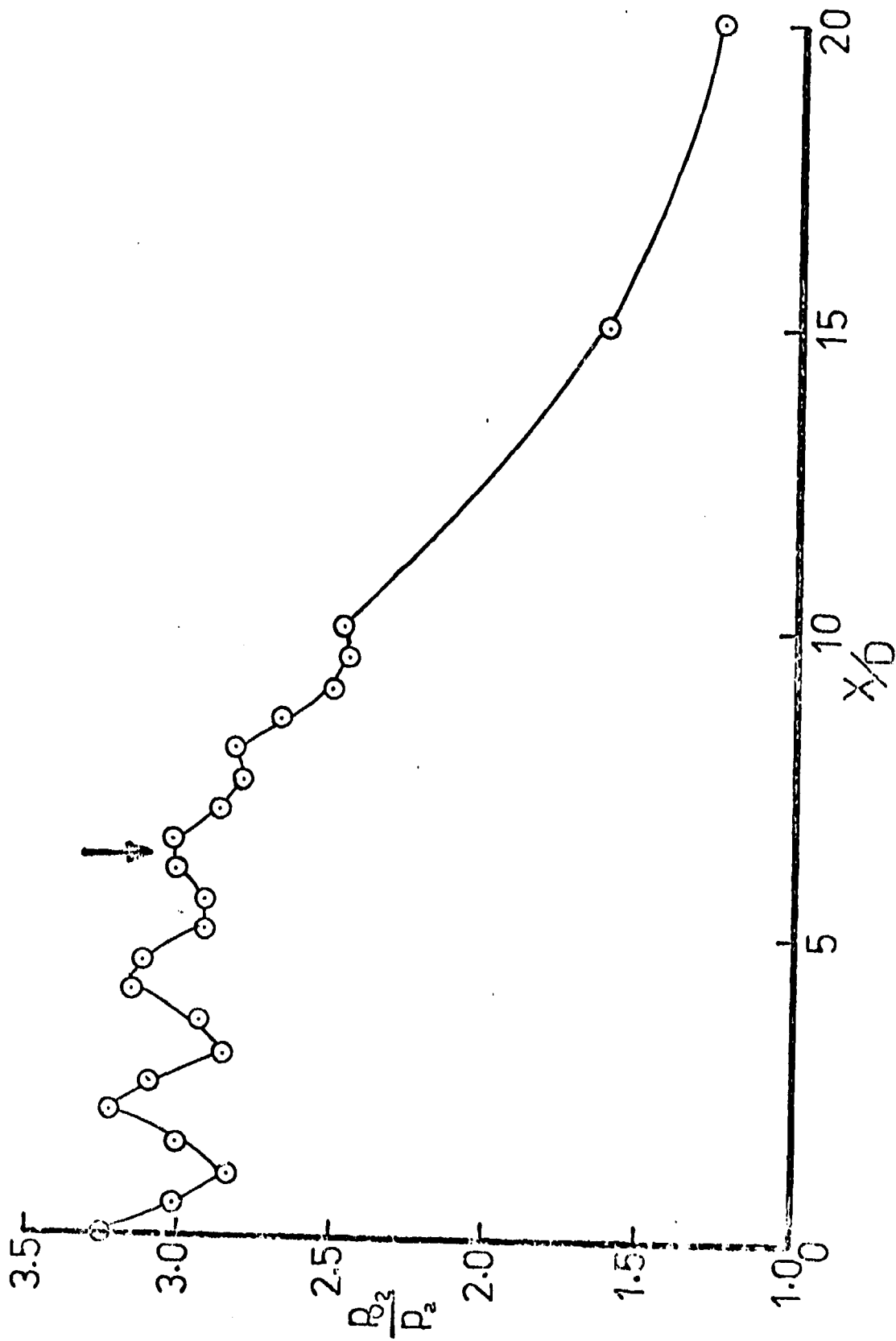
FIGURE 10. VARIATION OF THE PITOT PRESSURE ALONG THE CENTER LINE OF THE JET.

540
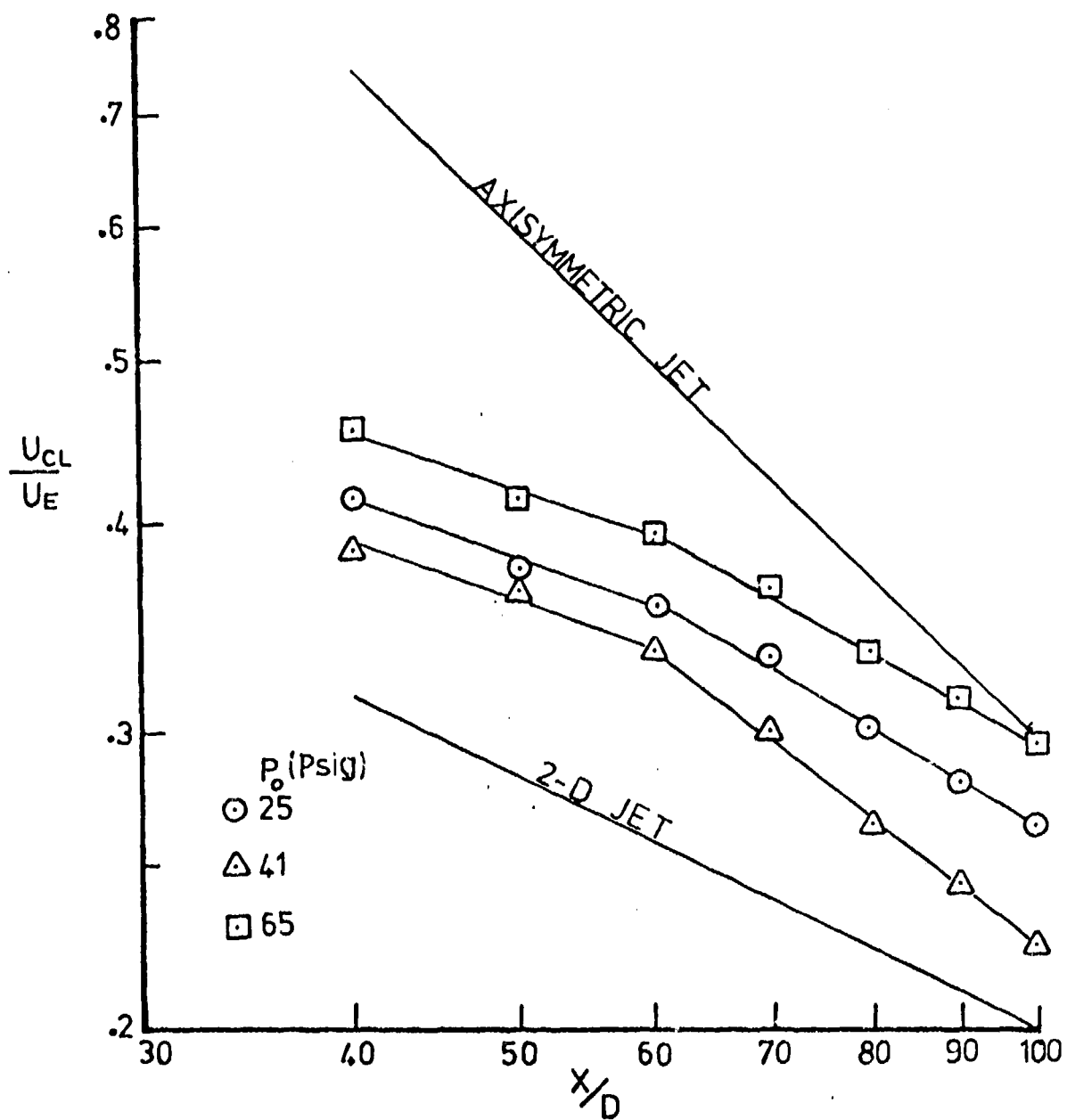
FIGURE 11. THE DECAY OF THE MEAN VELOCITY ALONG
THE CENTERLINE OF THE JET.

541
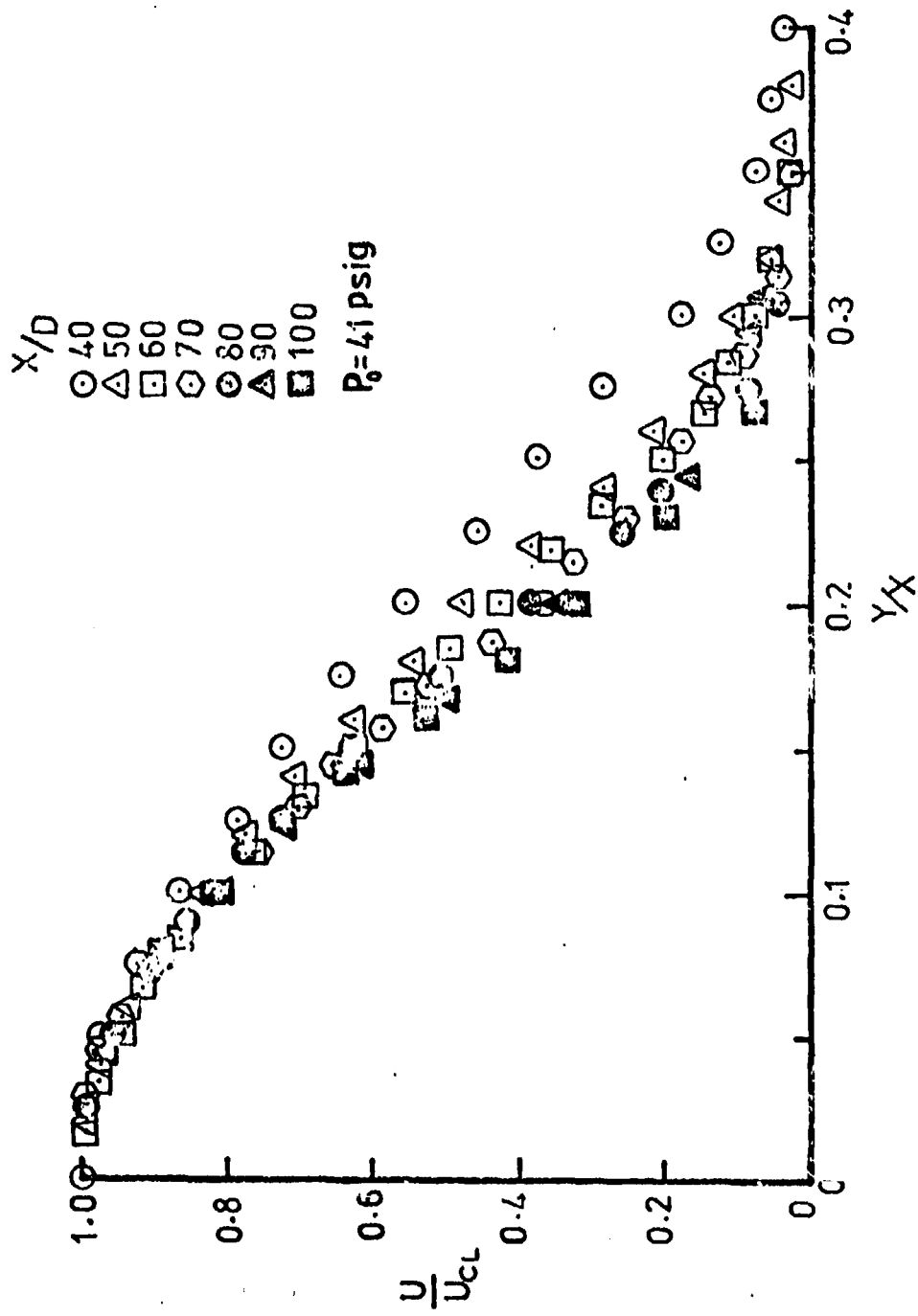
FIGURE 12. MEAN VELOCITY PROFILES IN THE CENTRAL X,Y PLANE.
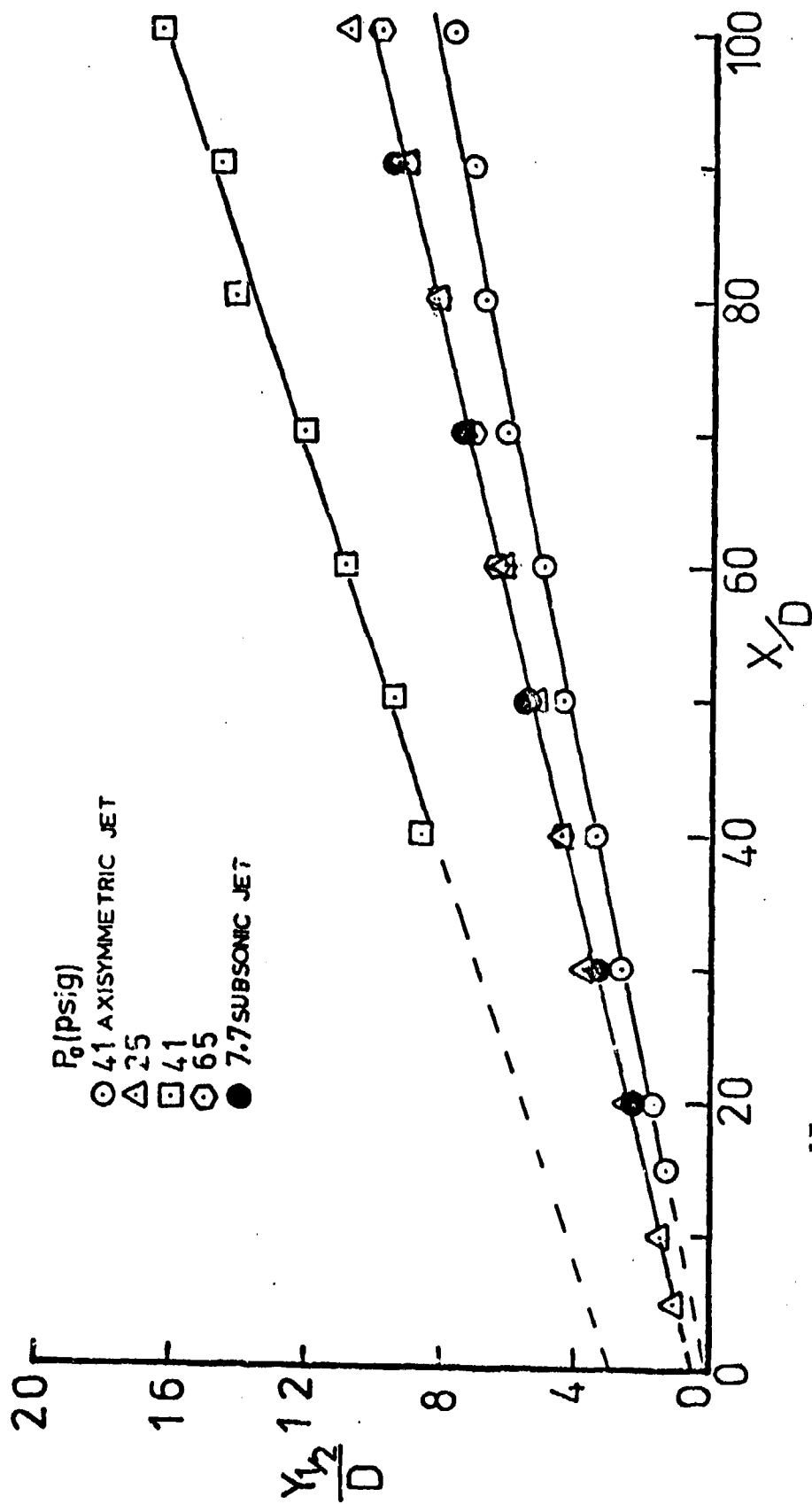
FIGURE 13. GROWTH OF THE JET IN THE X,Y PLANE WITH DOWNSTREAM DISTANCE.

543
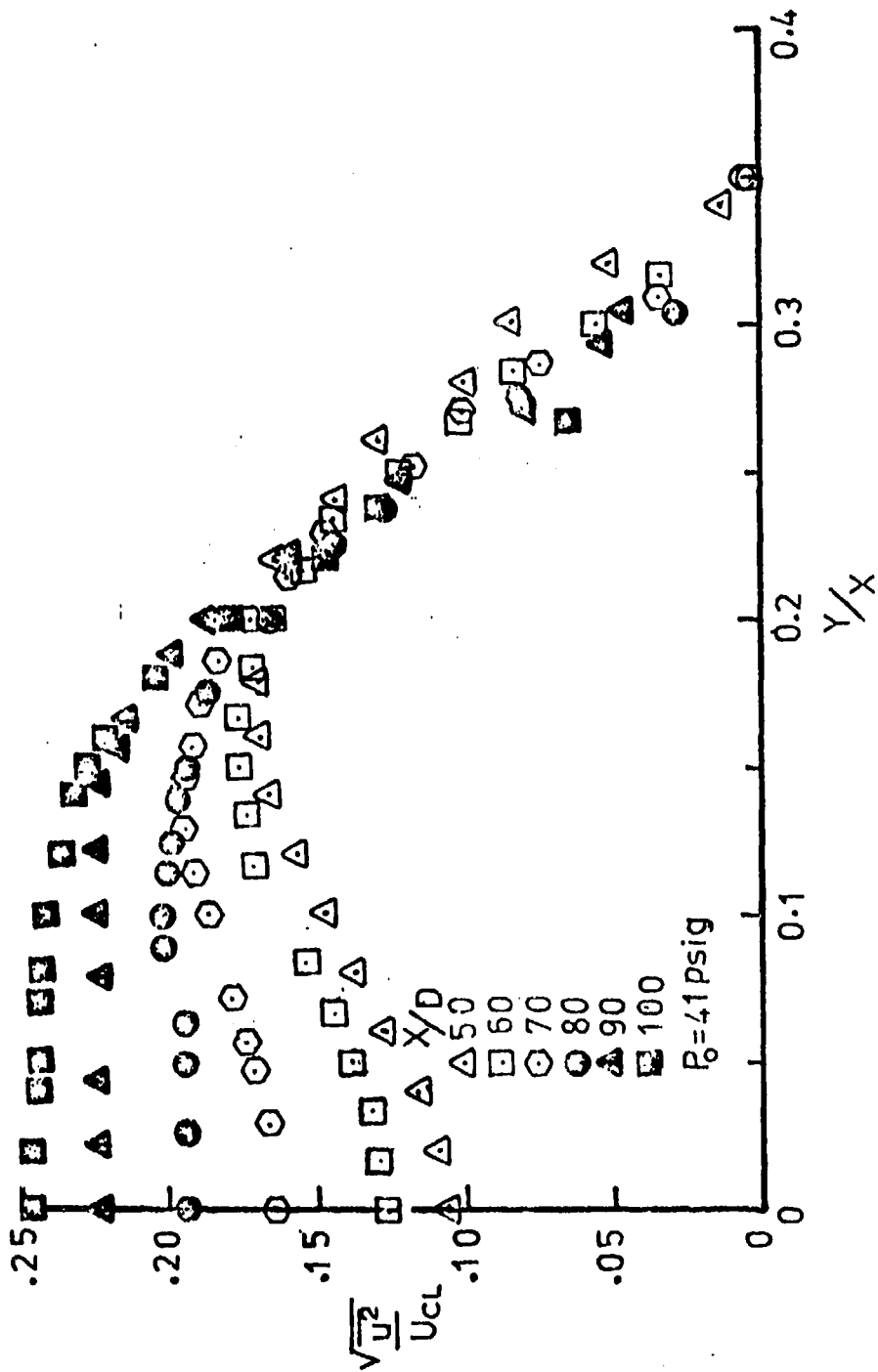
FIGURE 14. DISTRIBUTION OF THE VELOCITY FLUCTUATIONS IN THE CENTRAL X,Y PLANE.

544
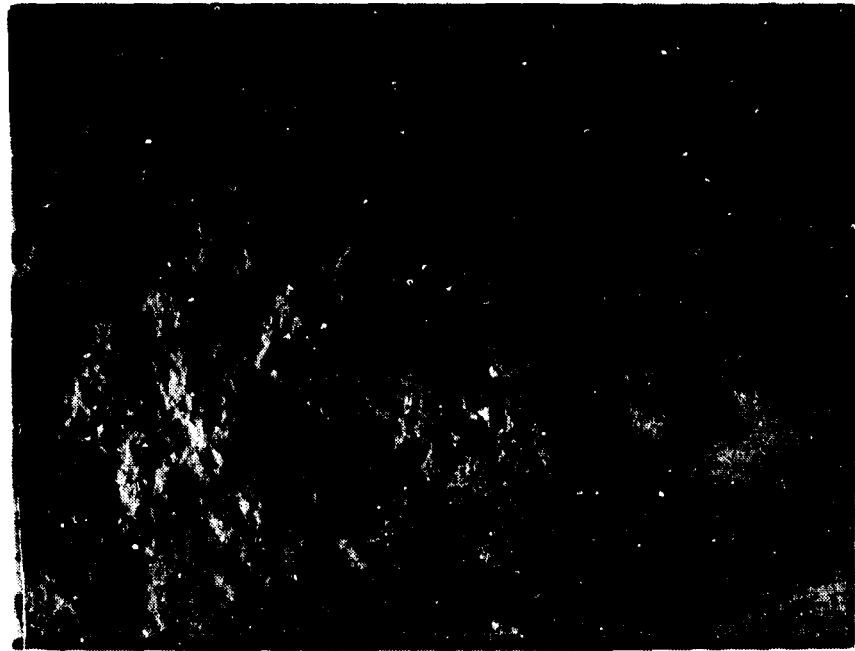
FIGURE 15. SCHLIEREN PICTURES OF A PARTIALLY CONFINED JET FOR R=3.4.
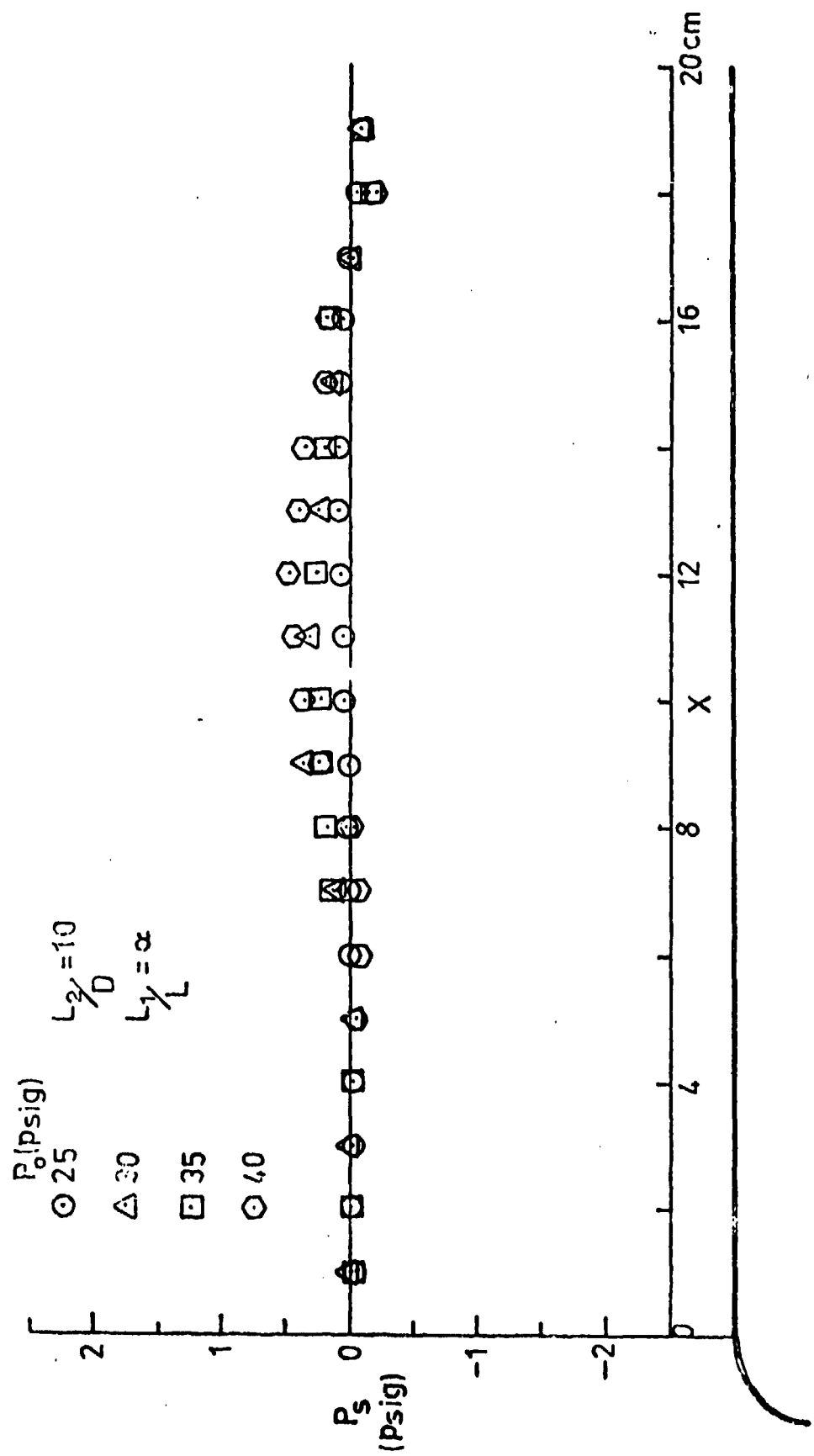
FIGURE 16. STATIC PRESSURE VARIATION ON THE WALL OF A CHANNEL.
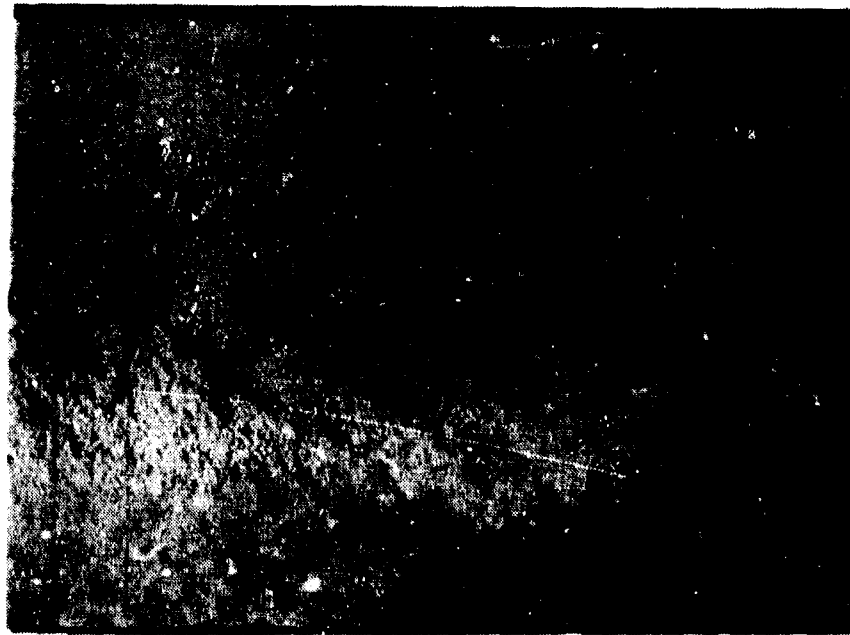
FIGURE 17. SCHLIEREN PICTURES OF A FULLY CONFINED JET FOR R=3.4.

$\frac{L_2}{D}$

8

12

16
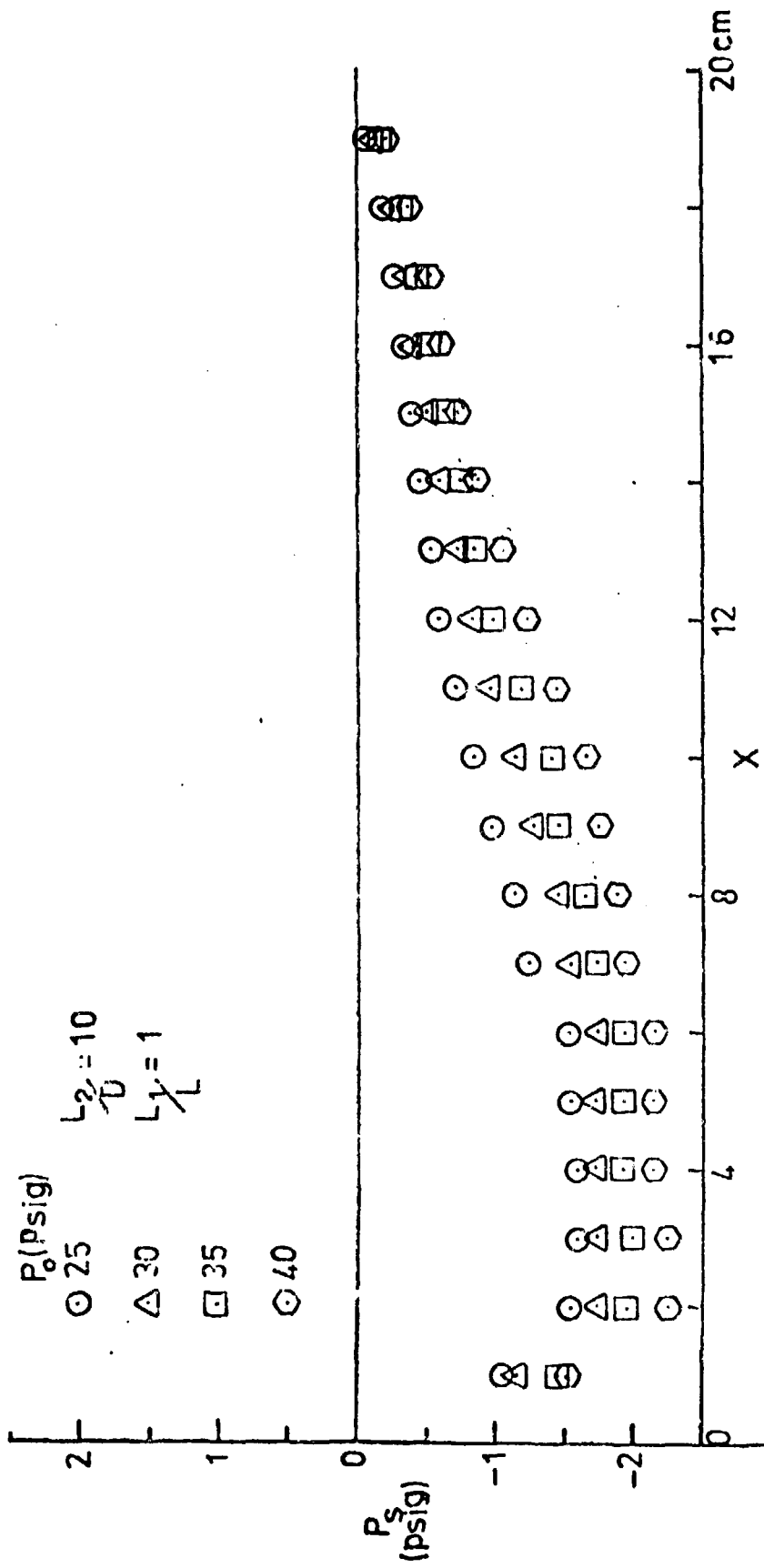
FIGURE 18. STATIC PRESSURE VARIATION ON THE WALL OF AN EJECTOR.

PARTIALLY CONFINED JET

EJECTOR

FIGURE 19. SCHLIEREN PICTURES OF THE JET IN PARTIALLY
CONFINED AND EJECTOR CONFIGURATIONS FOR R=3,4.
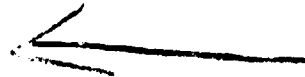
# Experimental Investigation of Thrust

## Augmenting Ejector Flows

L. Bernal and V. Sarohia
Fluid Dynamics and Thermal Sciences Group

Jet Propulsion Laboratory
California Institute of Technology
Pasadena, California 91109

## Introduction

The results of two investigations, one recently completed on pulsatile ejector flows[1] and the second currently in progress on a two-dimensional ejector configuration are presented. The objective of these investigations is to determine the role of entrained fluid and its mixing with the primary jet on ejector performance. Results will also be presented on the effects of entrance geometry on ejector entrainment and thrust augmentation.

Recent realization of the presence of large-scale structures[2,3,4,5] in turbulent shear flows has generated an interest in advancing the understanding of their role in entrainment and mixing. To determine the influence of the organization of the primary flow on ejector performance, direct thrust measurements were made to characterize the ejector performance as a function of frequency and amplitude of primary jet pulsations. The effect of the primary jet pulsations on the shroud surface pressure distribution was also documented. Flow visualization, direct thrust measurements, ejector shroud surface pressure measurements and velocity measurements are being utilized to determine the evolution of the mean velocity profiles in the ejector shroud and its relationship to entrainment and mixing.

## Results of Pulsatile Axisymmetric Ejector Flow

The facility used in these experiments is shown in Figure 1. The primary flow nozzle, at the center of the figure, and the ejector shroud, to its right, are mounted on a thrust balance. The flow enters the primary nozzle stagnation region perpendicular to the axis to the ejector to minimize any possible contribution of its momentum to the system thrust. The flow in the plenum chamber could be modulated between 100 and 2000 Hz by first passing the flow through a pneumatic transducer, shown at the left of Fig. 1. The primary jet nozzle exit diameter was 2.5 cm. The exit Mach number, $M_e$, could be varied between 0.1 to 0.7. The rms longitudinal velocity fluctuations at the center of the nozzle exit plane ranged from 1% (no excitation) to as high as 17% of the mean jet velocity. The mean mass flow through the system was maintained constant at different excitation amplitudes by means of a shocked orifice upstream of the pneumatic transducer. Flow visualization shadowgraph pictures of the free jet were obtained by injecting a small amount of $CO_2$ into the primary flow, upstream of the plenum chamber. Typical pictures are shown in Figures 2 and 3 for the steady jet and the excited jet, respectively. These pictures reveal the organization of the large scale structure by the imposed excitation and the resulting increase of the jet growth rate.

The ejector shroud used in these experiments had an area ratio of 12.3. A constant area mixing chamber was used, with a length to diameter ratio of 3.4. The entrance was of the bell-mouth type, its radius normalized with that of the mixing chamber was 0.36. The location of the shroud relative to the primary jet was optimized for maximum thrust augmentation, a distance of 2.5 cm was used. The effect of frequency of pulsations on thrust augmentation ratio is presented in Table 1, where $T_0$ is the measured thrust of the primary jet at the same exit Mach number, $M_e = 0.5$, without pulsations. At low

frequencies the thrust augmentation ratio is 1.2, the value obtained for the steady flow ejector. At frequencies above 200 Hz, the thrust augmentation ratio is 1.3, an increase of 8% over the value for the steady flow ejector. 200 Hz gives a normalized value $fd/U_e = 0.03$ where f is frequency of pulsation, d is primary jet diameter and $U_e$ is flow velocity at nozzle exit.

The effect of amplitude of the velocity fluctuations at the primary exit on system thrust are given in Figure 4 at an exit Mach number of 0.4 and frequency of 500 Hz, $fd/U_e = 0.01$. Since the imposed pulsations result in an increase thrust of the primary jet different normalizations were used, as shown in Figure 4. The ejector thrust with pulsations normalized with the primary jet thrust without pulsations showed an increase in thrust up to 1.27 at largest amplitude. The increase in thrust of the primary jet alone due to the pulsations is shown in Figure 4. The thrust of the ejector with pulsations normalized with the thrust of the primary jet with pulsations is also shown. The improvement in thrust associated with the pulsations only is given by the dashed area. An increase with pulsations amplitude up to a value of 8% of the value for steady ejector flow was observed at an amplitude of 17% of the exit velocity.

The effects of primary jet pulsation on ejector shroud surface pressure are presented in Figure 5, where the pressure coefficient is defined as the local pressure minus the ambient pressure normalized with the steady jet dynamic pressure. These results show a large suction at the entrance followed by a rapid pressure recovery, a region of approximately constant pressure and an additional pressure recovery near the exit. The effect of pulsations is to increase the suction within the ejector. The shape of the profiles is not modified, as shown in Figure 5.

The surface pressure measurements suggest that the flow around the

553

entrance of the ejector plays an important role in the performance of the
ejector. These effects were investigated further using two bell-mouth-type
entrances of different radii, a flat plate located perpendicular to the
ejector axis at the entrance and a mixing chamber without entrances fairing.
In all cases the mixing chamber diameter, length and location relative to the
primary jet were the same as in the experiments previously described. The
thrust efficiency for these four configurations as a function of primary
nozzle exit Mach number is shown in Figure 6. Both bell-mouth entrance, the
wooden and lucite nose which have a radii of 0.61 and 0.25 times the mixing
chamber diameter respectively, have similar thrust augmentation ratio, on the
order of 1.2. The results for the other two configurations which are
characterized by a sharp edge at the entrance of the mixing chamber show
thrust augmentation on the order of 1.05. How these changes influence
entrainment of the primary jet is shown in Figure 7. These results indicate
that the loss of thrust augmentation is accompanied by a loss of entrainment
by the primary jet.

## Two-Dimensional Ejector Flow Results

The two-dimensional ejector facility is shown in Figure 8. The primary
nozzle and ejector shroud were mounted on a balance for direct thrust
measurements. Also shown in this picture is the Laser Doppler Velocimeter
used for the velocity measurements. The ejector has a constant area mixing
chamber with a bell-mouth entrance. The area ratio is 13.3. The mixing chamber
length is 3 times its width and the bell-mouth radius normalized with the
mixing chamber width is 0.25. The primary jet width is 0.8 cm and the span of
the facility is 50.8 cm. The ejector is located one mixing chamber width from
the primary nozzle.

The tnrust of the ejector system normalized with the measured thrust of the primary nozzle as a function of primary nozzle pressure ratio is presented in Figure 9. A maximum value of 1.23 is found at a primary flow pressure ratio of 1.94. The efficiency of the ejector decreases at higher pressure ratios. Surface pressure measurements cn the ejector shroud are shown in Figure 10. The general features of the pressure distribution are similar to those for the axisymmetric ejector (Figure 5). However, the values of the pressure coefficient are significantly lower in 2-dimensional as compared with axisymmetric configuration . The sharp pressure rise at the entrance of the mixing chamber increases with primary jet exit Mach number. The pressure recovery at the back of the ejector, however, does not significantly change for the range of primary jet pressure ratios investigated. Laser Doppler velocity measurements inside the ejector are presented in Figure 11. These velocity profiles show a continuous decrease of velocity at the centerline with downstream distance. While close to the ejector shroud ($Y = \mp 4.0$ cm), the velocity first decreases in the entrance region and increases further downstream.

## Conclusions

The effect of primary jet pulsations is to increase the thrust augmentation ratio,provided that their frequency is within the range of receptivity of the jet, i.e. $fd/U_e > 0.03$, where f is the frequency of pulsations, d the primary jet diameter, and $U_e$ is the exit velocity. The gain in ejector thrust increases with the amplitude of the pulsations. Entrance geometry has a relatively small effect on thrust augmentation provided the flow separation does not occur. If flow separation does occur, relatively little thrust augmentation is observed. Flow separation of ejector walls also

results in a reduction of ejector entrainment. The surface pressure distribution on a two-dimensional configuration shows the development of a sharp pressure increase at the entrance of the mixing chamber, suggesting the possibility of flow separation in this area. Laser Doppler measurements show a decrease of the velocity near the wall, thus further suggesting the possibility of flow separation.

## Acknowledgements

# References

1. V. Sarohia, L. Bernal and T. Bui, "Entrainment and Thrust Augmentation in Pulsatile Ejector Flows", JPL Publication 81-36.

2. Crow, S.E. and Champagne, F.H., "Orderly Structure in Jet Turbulence", Journal of Fluid Mechanics, Vol. 48, 1971, pp. 547-591.

3. Brown, G.L. and Roshko, A., "On Density Effects and Large Scale Structure in Turbulent Mixing Layers", Journal of Fluid Mechanics, Vol. 64, 1974, pp. 775-816.

4. Browand, F.K. and Weidman, P.D., "Large Scales in the Developing Mixing Layers", Journal of Fluid Mechanics, Vol. 76, pp. 127-144.

5. Winant, C.D. and Browand, F.K., "Vortex Pairing: The Mechanism of Turbulence Mixing-Layer Growth at Moderate Reynolds Numbers", Journal of Fluid Mechanics, Vol. 63, 1974, pp. 237-255.

Table 1 - Influence of the Frequency of Pulsations on Ejector Performance

$M_e = 0.50$

| Frequency of Pulsations | $\dfrac{fd}{U_e}$ | $\sqrt{\overline{u'2}}/U_e$ | $T_{ejector}/T_o$ |
|---|---|---|---|
| 0 | 0 | 0.01 (Random) | 1.2 |
| 50 | .007 | 0.08 | 1.22 |
| 100 | 0.015 | 0.08 | 1.21 |
| 200 | 0.03 | 0.08 | 1.22 |
| 300 | 0.046 | 0.06 | 1.28 |
| 400 | 0.062 | 0.08 | 1.30 |
| 500 | 0.08 | 0.08 | 1.24 |
| 600 | 0.09 | 0.08 | 1.27 |
| 700 | 0.10 | 0.08 | 1 |
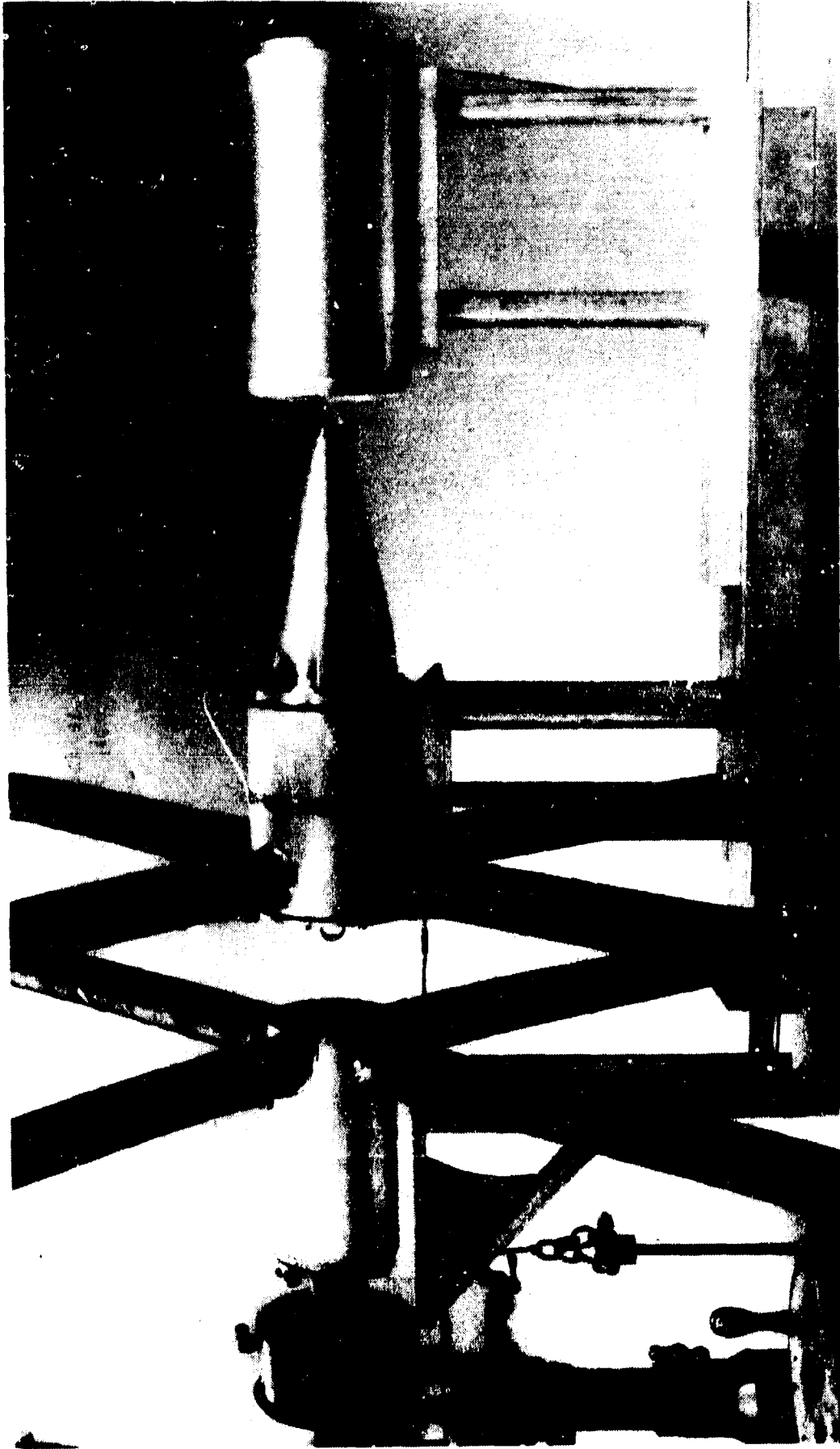
Figure 1. Primary Jet and Constant-Area Ejector
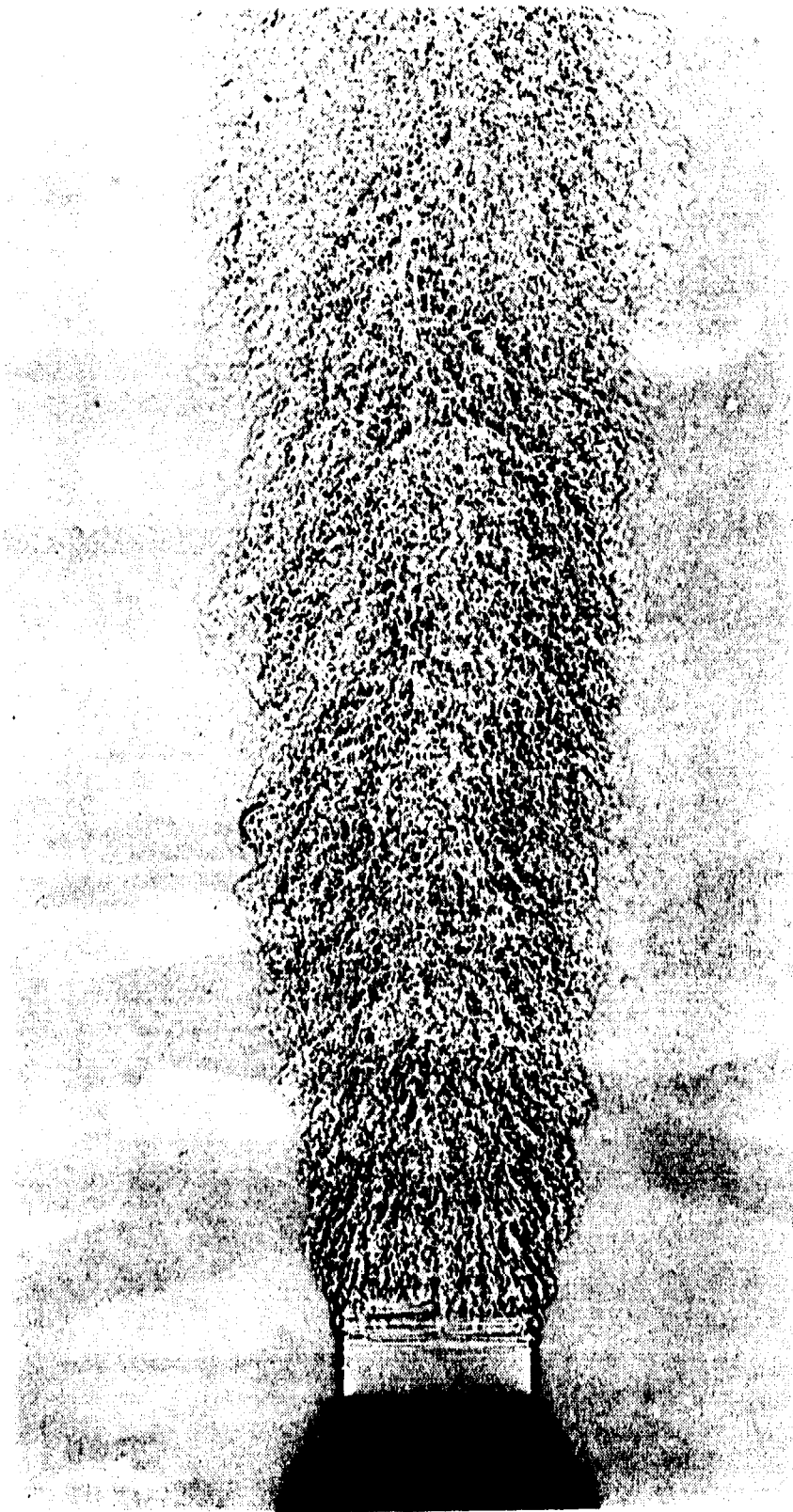
Figure 2. Subsonic Exhausting Into Ambient Air Without Upstream Pulsations. Velocity at Nozzle Exit = 52 m/s.
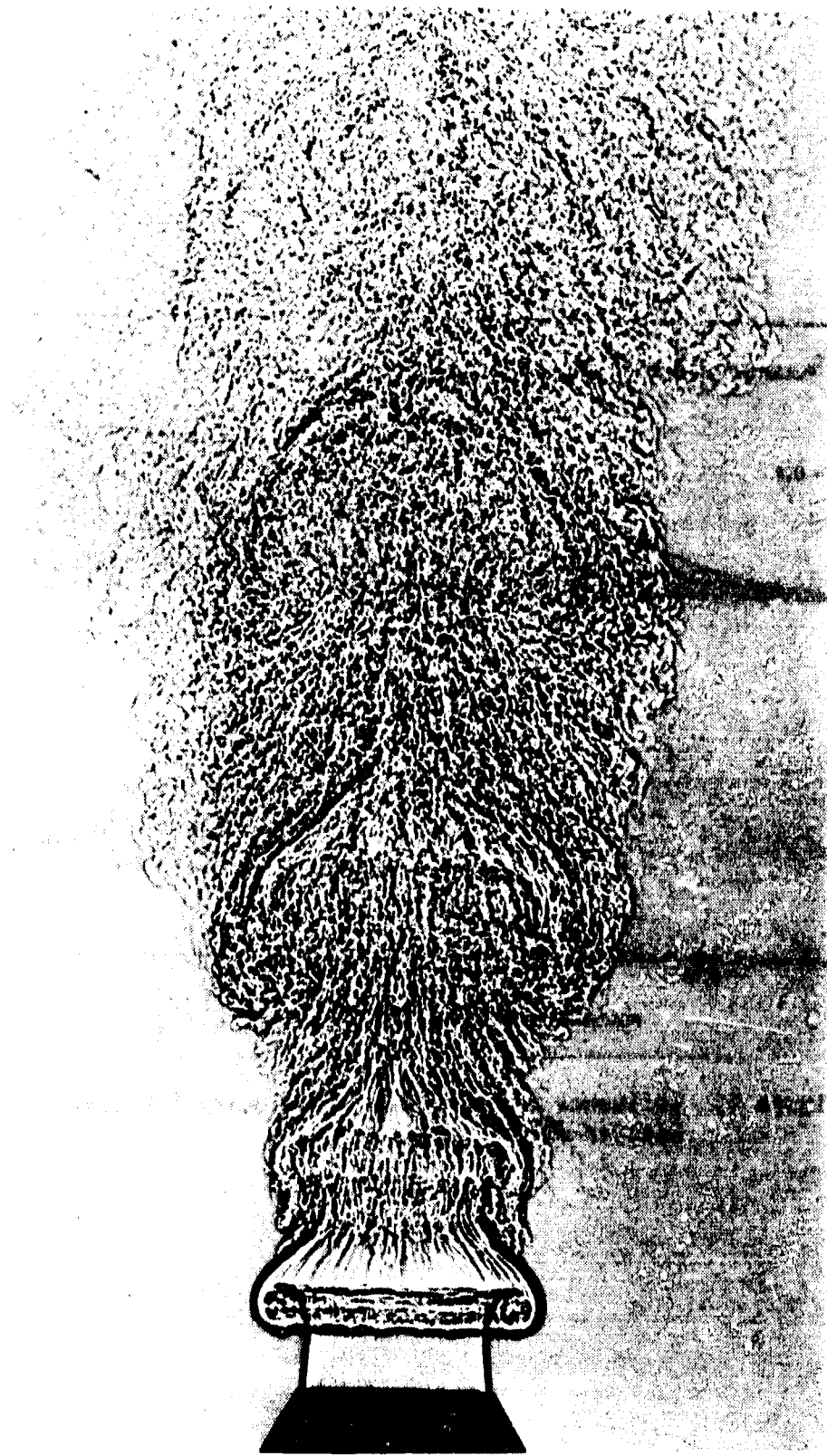
Figure 3. Subsonic Jet Exhausting Into Ambient Air With Upstream Pulsations. Velocity at Nozzle Exit = 52 m/s. Frequency $fd/U_e = 0.3$.
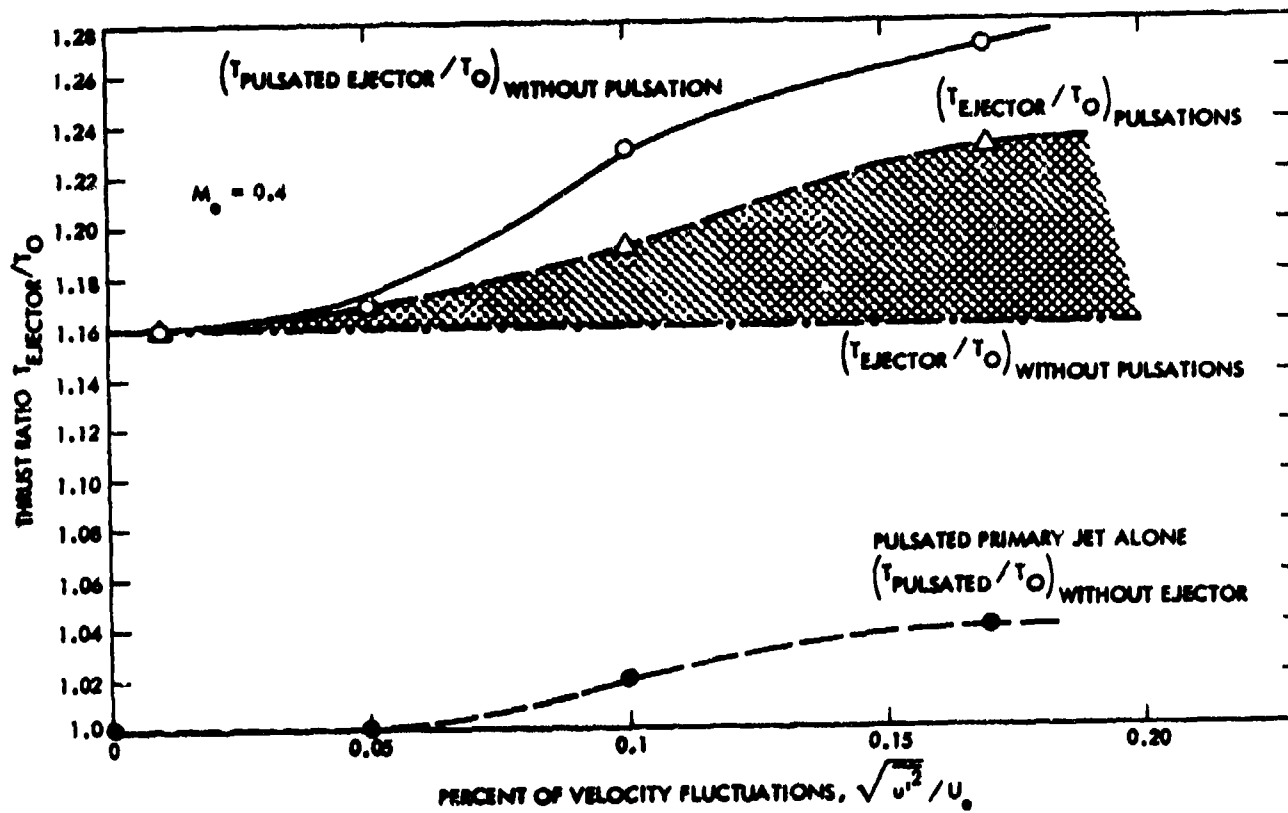
Figure 4. Influence of Amplitude of Velocity Fluctuations on Ejector Performance.
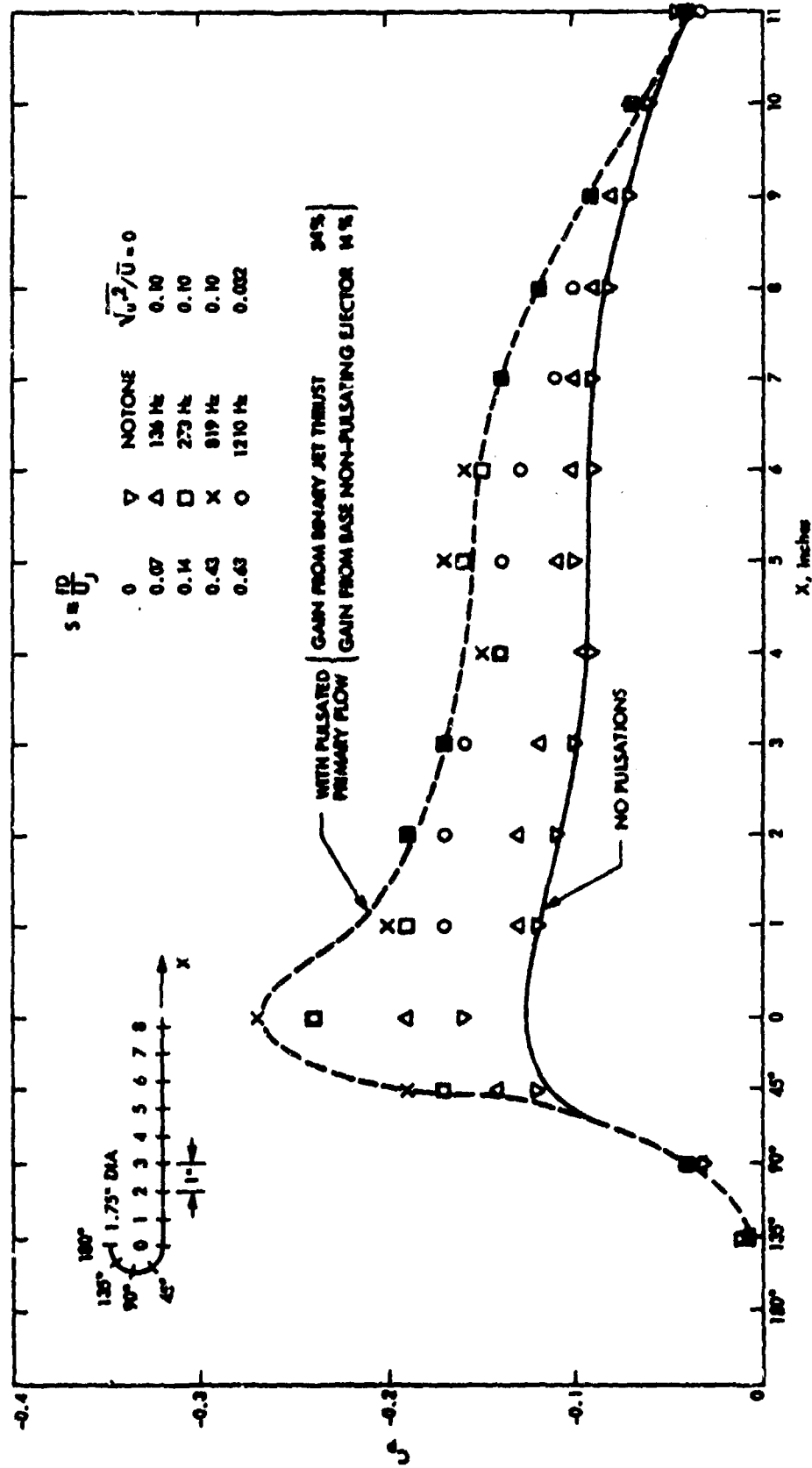
Figure 5. Pressure Distribution Along Ejector Wall With and Without
Pulsating Primary Jet.
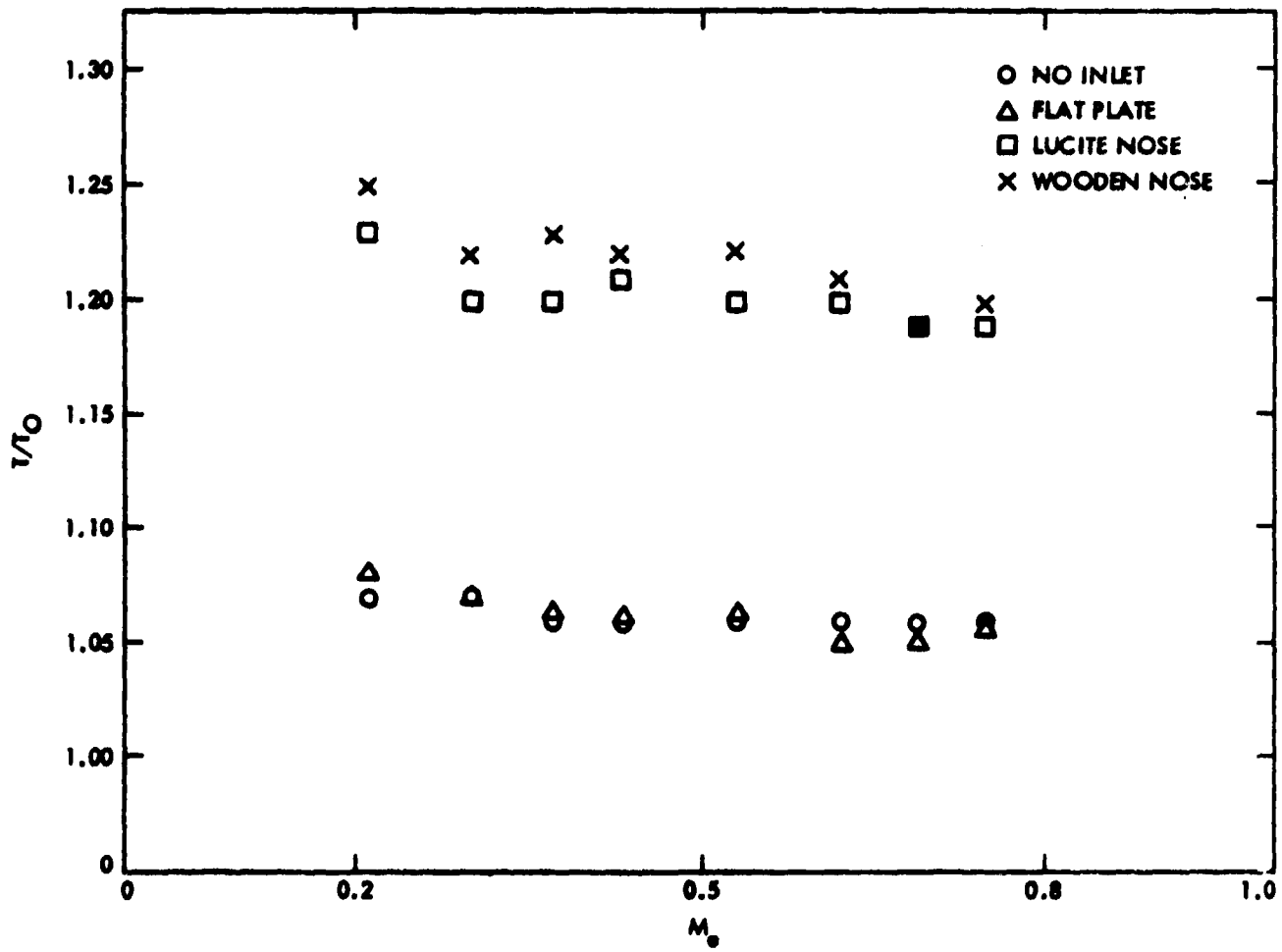
Figure 6.  Ejector Inlet Effects.

564
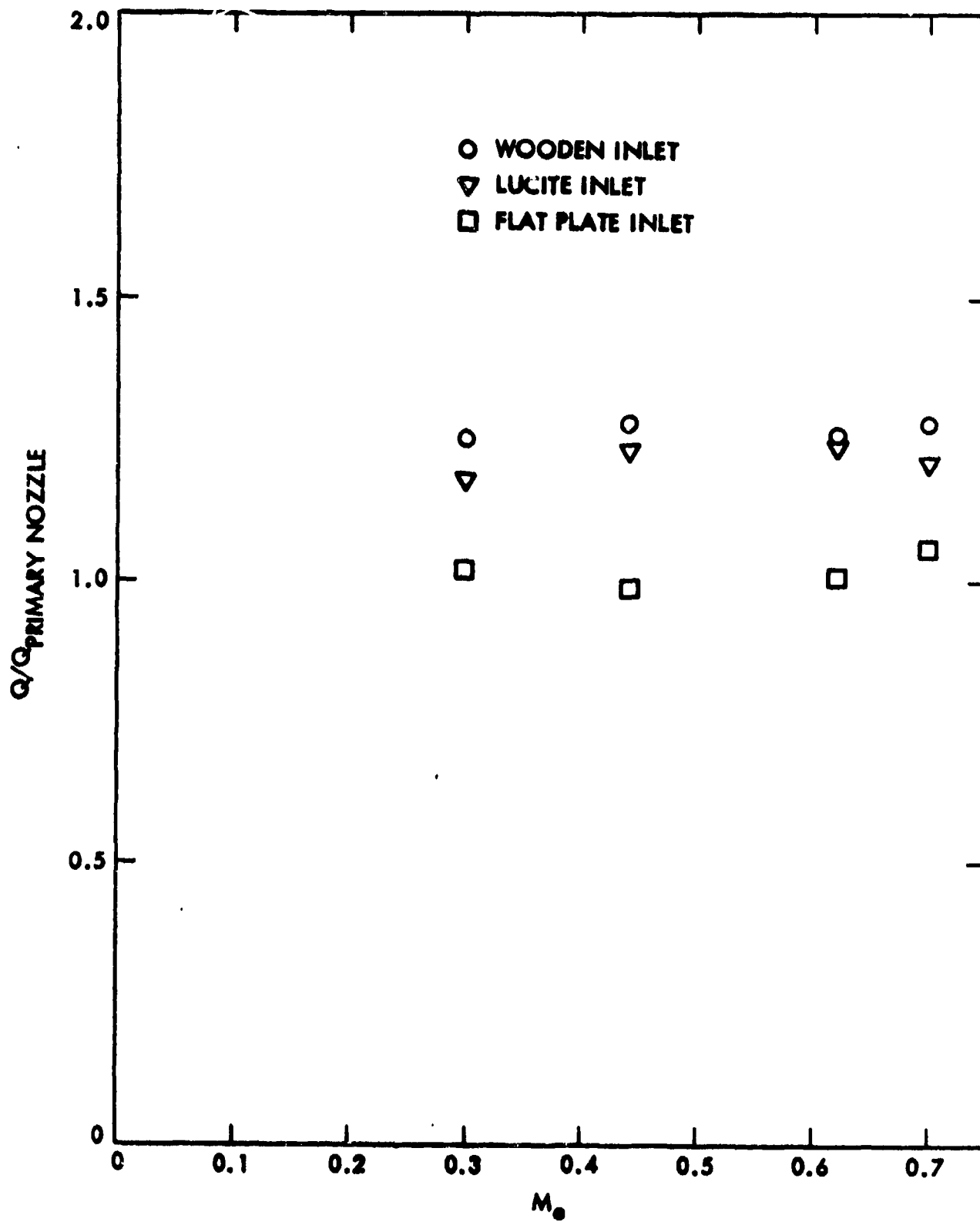
Figure 7. Influence of Ejector Inlet Flow on Entrainment.
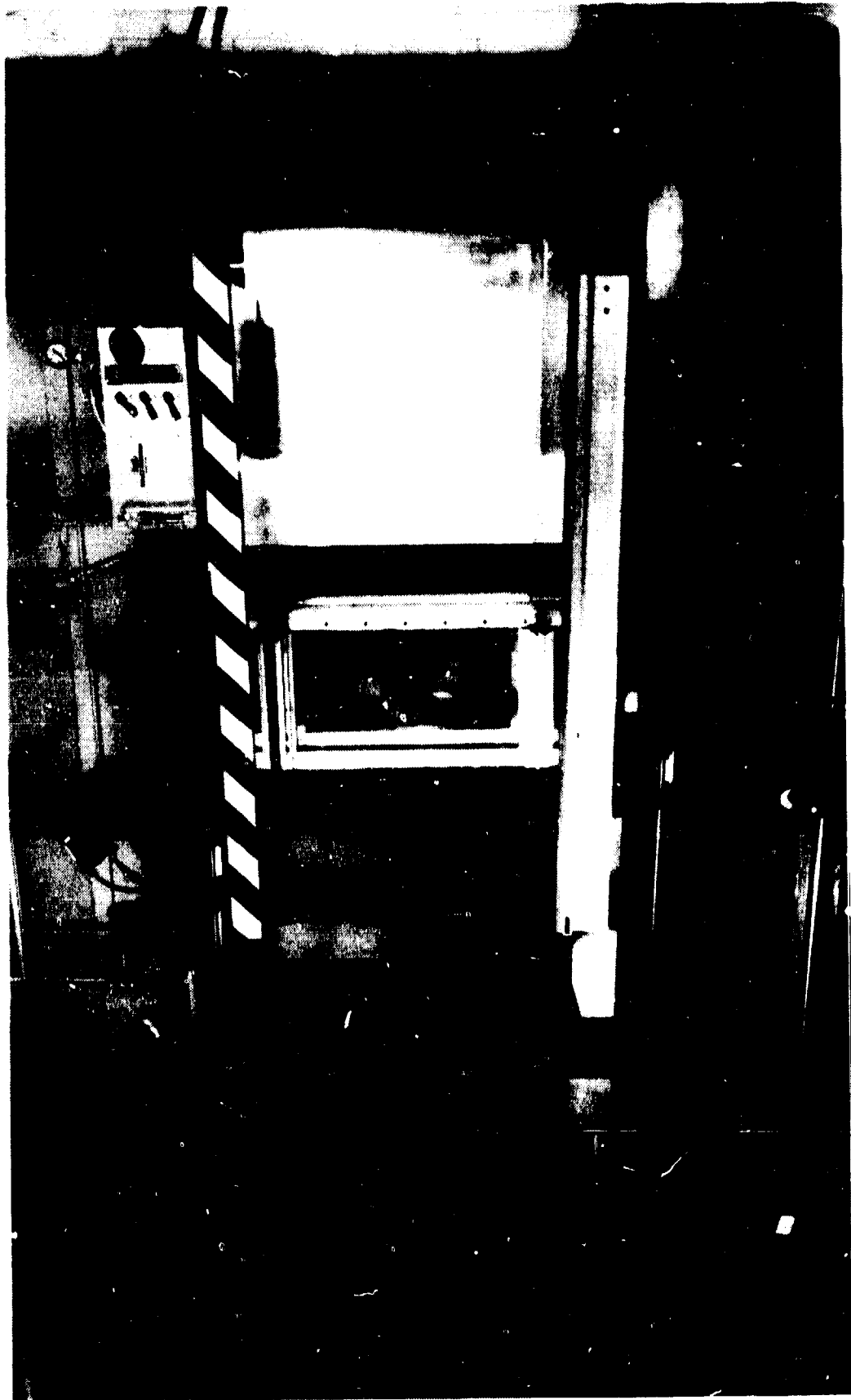
Figure 8. Two-Dimensional Ejector Facility.
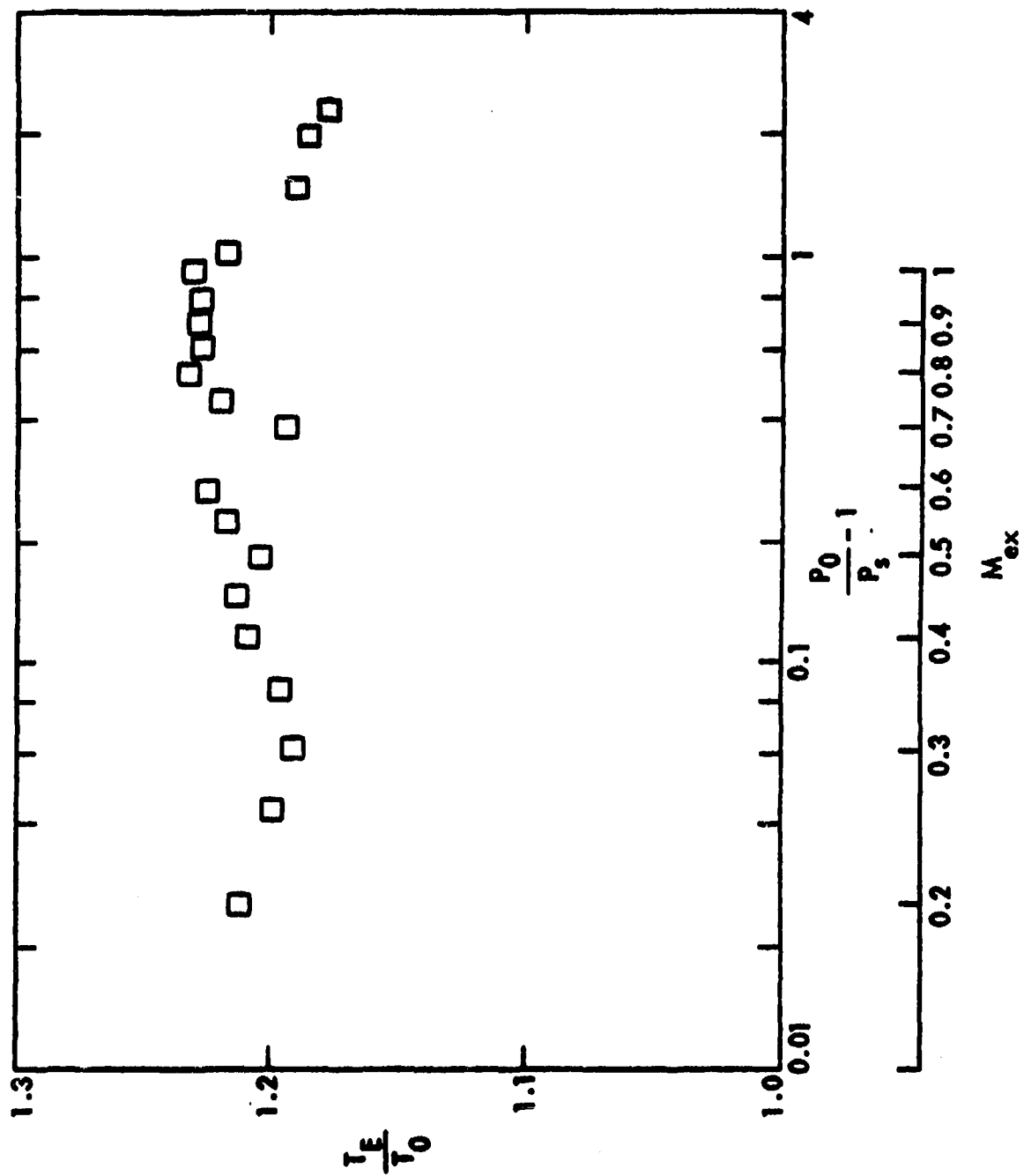
Figure 9.  Thrust Augmentation Ratio of Two-Dimensional Ejector.
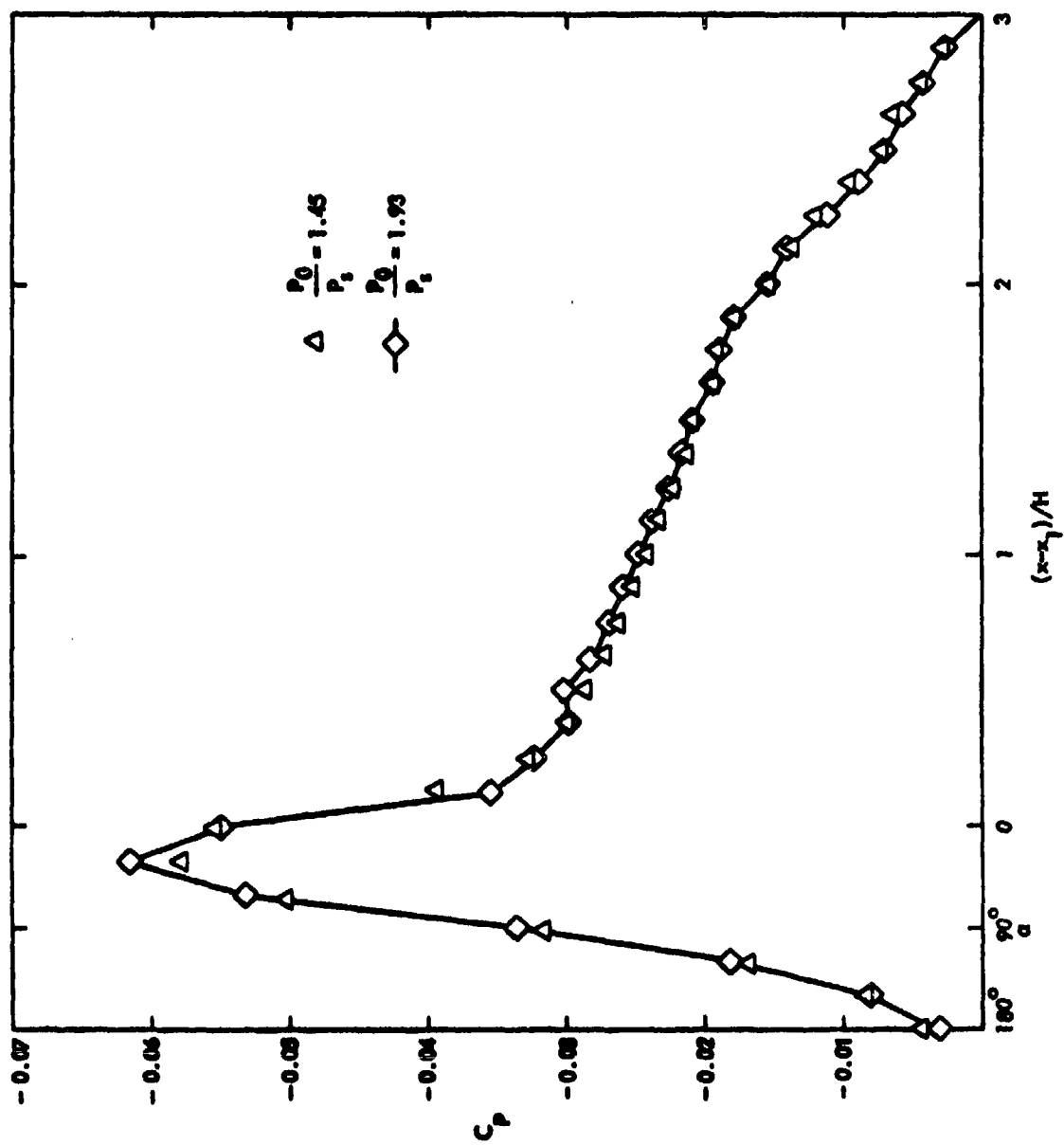
Figure 10. Surface Pressure Coefficient on Two-Dimensional Ejector Shroud.
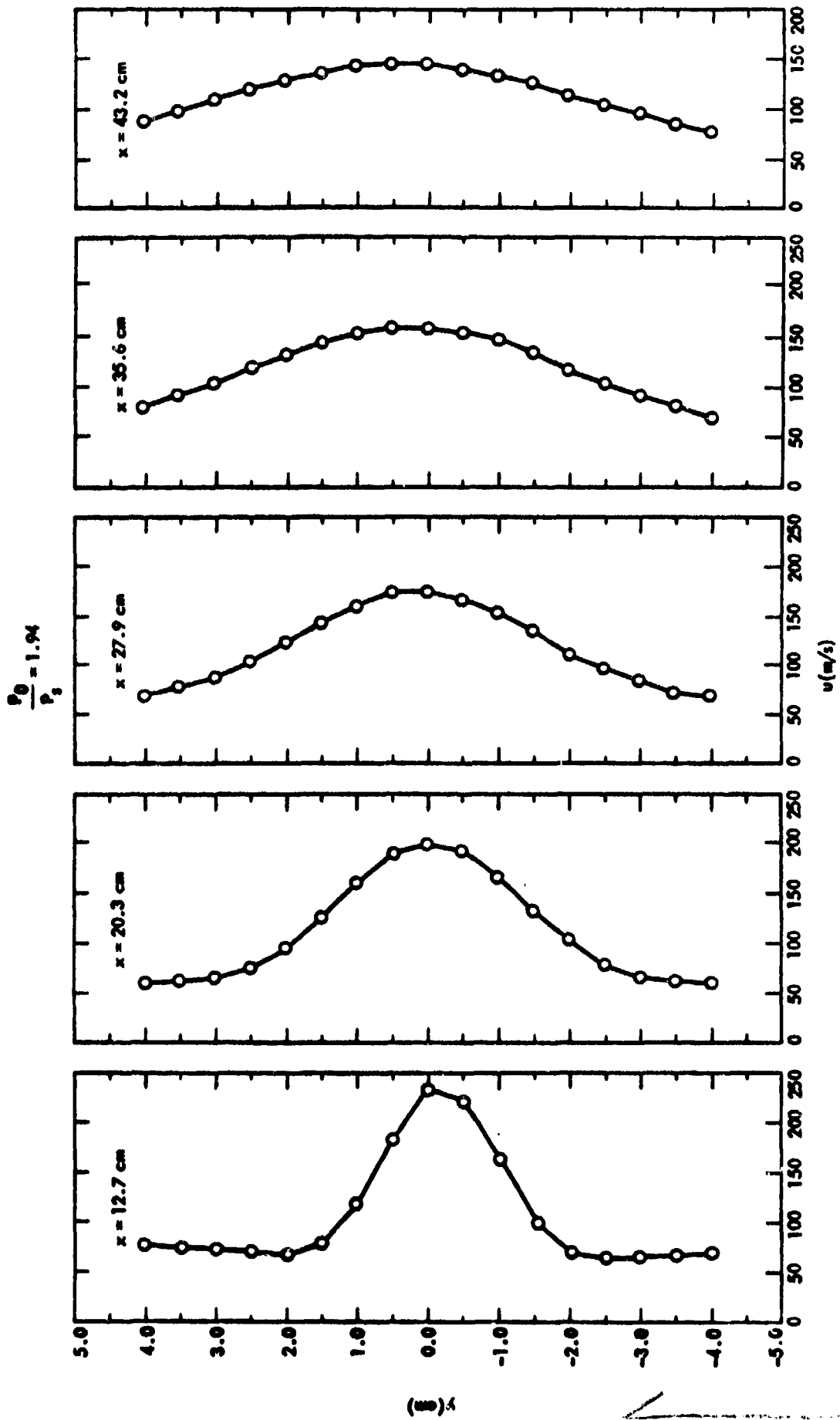
Figure 11. Downstream Velocity Profiles Inside Ejector Shroud.

# THE MIXING OF SWIRLING FLOWS

Gordon C. Oates
University of Washington
Seattle, WA.

The results of an investigation of the effects of swirling the inner stream upon the mixing rate of co-annular flows will be presented. The presentation will consist of three major sections:

## MODEL OF AN IDEAL MIXER WITH SWIRL

The overall investigation was motivated by the desire to lead to understanding of some of the mechanisms existing in real aircraft mixers. To this end, the effects of swirl upon the performance of ideal mixers was determined so that the unavoidable losses due to the presence of non-axial momentum etc. could be determined (in comparison to conventional ideal mixers).

In the example to be described here, a mixer consisting of constant radius inner and outer ducts is considered. When swirling is considered, the swirl is introduced far upstream in the inner stream. Mixing of the two streams is assumed to occur with no sidewall friction, with the (far) downstream condition being that of solid body rotation. The swirl is then removed from the flow by an actuator disc, following which the flow is expanded through a nozzle.

Comparisons are made of the performance of such a mixer with a conventional constant area mixer with the same stagnation properties at inlet. Some detailed calculational examples will be shown, and the various assumptions of the analysis emphasized.

## EXPERIMENTAL PROGRAM

A large high pressure air storage system has been adapted to provide flow rates of up to a total of ten pounds per second. The flows can be throttled to a variety of stagnation pressures, and in the present investigation two streams are provided. A large co-annular settling chamber provided with honey-comb and screens is utilized to reduce the turbulence levels prior to entry into the test section.

The accompanying figure shows the contraction section and swirl generator used to provide the test flows. The following test section consists of inter-

changeable segments of tube (of length 2,4,8,16 and 32 inches) that allow flow
traverses to be made at a succession of axial locations.

Mean flow properties were measured throughout the flow field. Detailed
static pressure measurements were taken along the inner and outer annuli
as well as on the upstream inner surface of the intermediate annulus. Two five
hole probes were used for measurement of the flow conditions within the stream
(one probe for use in cases when no outer annulus was present, the other for use
when the flow was enclosed). Use of the five hole probes allowed determination
of the fluid velocity magnitude and direction as well as determination of the
static and stagnation pressures.

Calibration of the five hole probes required extensive measurements and
data reduction, and the method utilized will be described.

PRELIMINARY RESULTS

An extensive series of tests has been run, and the data is in the process
of being reduced and interpreted. Some of the extensive results will be shown
in the presentation. The attached graphs show the behavior of the wall static
pressure and tangential velocity for the case where the ratio of the mass flow
in the outer stream to that in the inner (swirling) stream is 0.77. These results
and others will be considered in detail in the presentation.
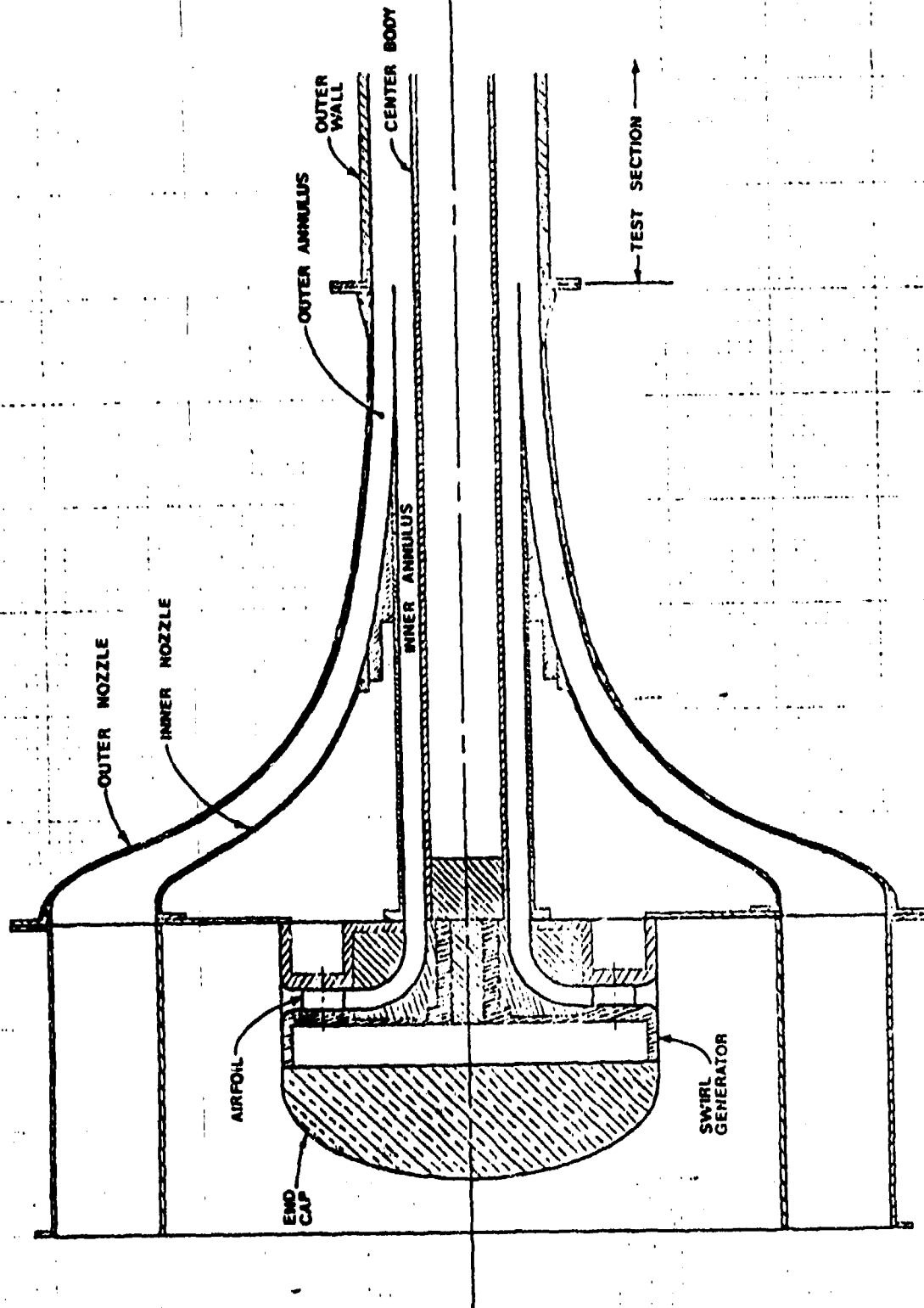
SWIRL GENERATOR & NOZZLES

STATIC PRESSURE ON 4 INCH TUBE

574
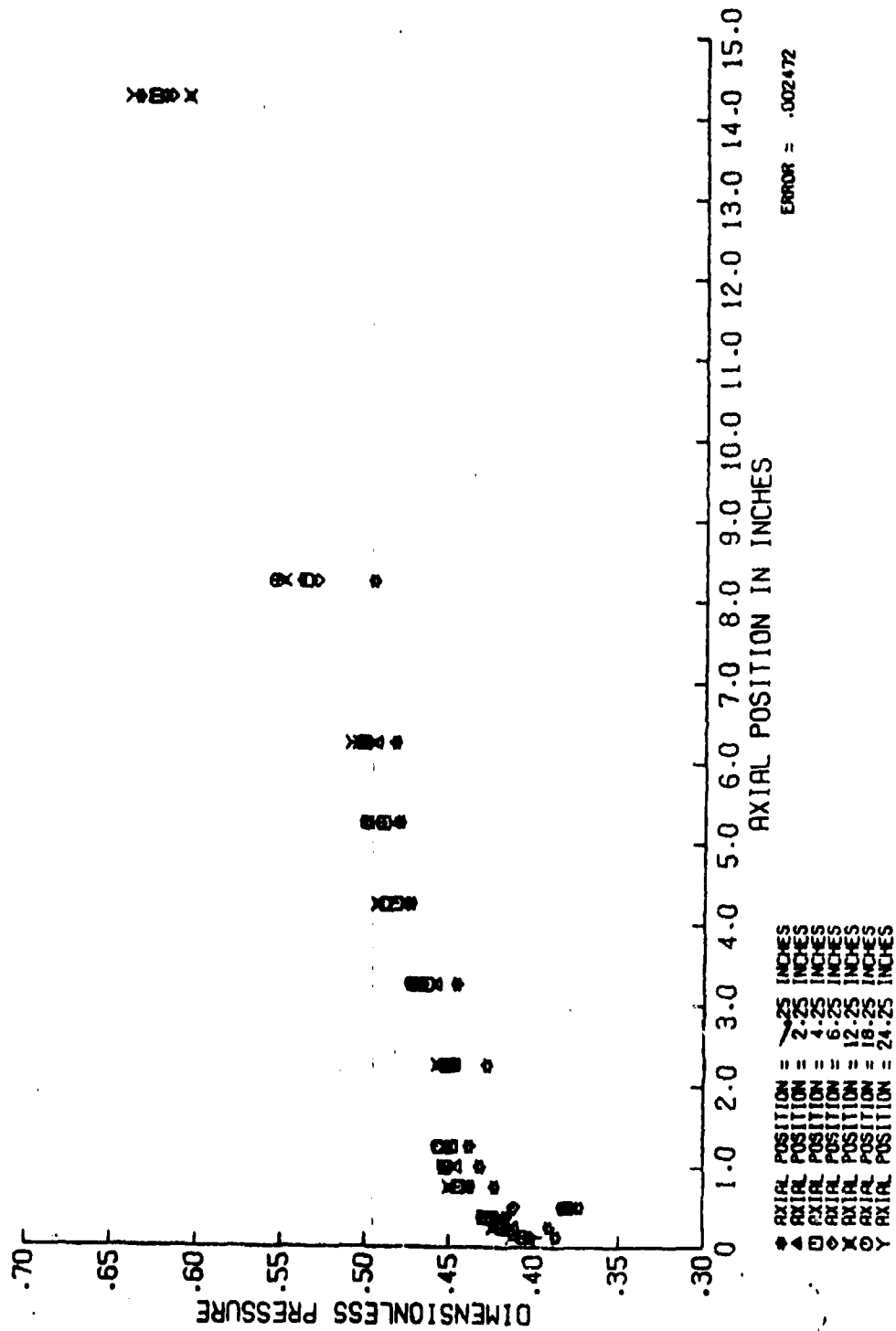
STATIC PRESSURE ON 6 INCH TUBE

ERROR = .002472

AXIAL POSITION IN INCHES

DIMENSIONLESS PRESSURE

* AXIAL POSITION = .25 INCHES
▲ AXIAL POSITION = 2.25 INCHES
□ AXIAL POSITION = 4.25 INCHES
◇ AXIAL POSITION = 6.25 INCHES
× AXIAL POSITION = 12.25 INCHES
⊙ AXIAL POSITION = 18.25 INCHES
Y AXIAL POSITION = 24.25 INCHES
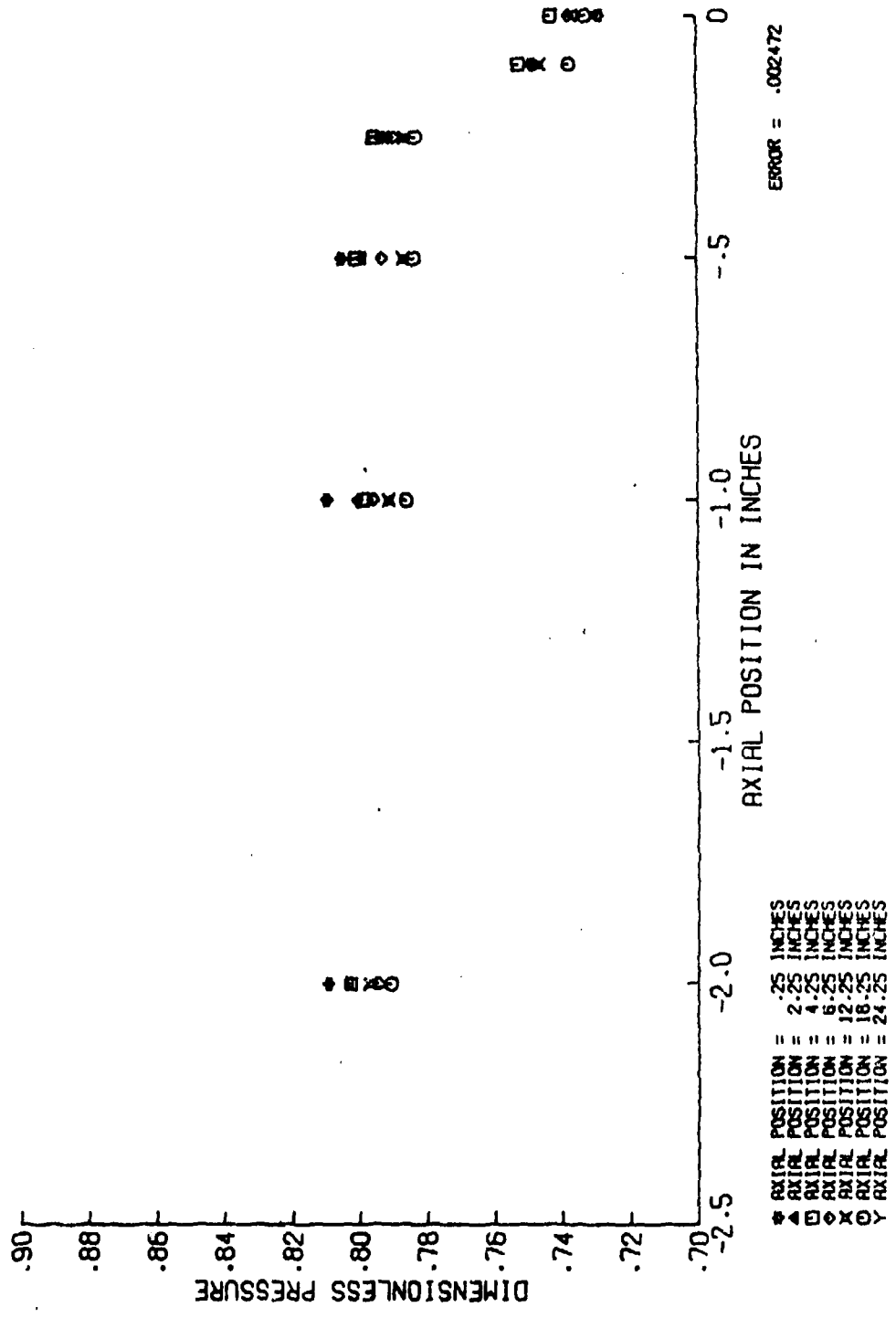
STATIC PRESSURE ON 8 INCH TUBE

DIMENSIONLESS PRESSURE

AXIAL POSITION IN INCHES

◇ AXIAL POSITION = .25 INCHES
▲ AXIAL POSITION = 2.25 INCHES
⊟ AXIAL POSITION = 4.25 INCHES
◇ AXIAL POSITION = 6.25 INCHES
✕ AXIAL POSITION = 12.25 INCHES
⊙ AXIAL POSITION = 18.25 INCHES
Y AXIAL POSITION = 24.25 INCHES

ERROR = -.002472

AXIAL POSITION IN INCHES

RADIAL POSITION IN INCHES

DIMENSIONLESS TANGENTIAL VELOCITY

AXIAL POSITION = .25 INCHES
AXIAL POSITION = 2.25 INCHES
AXIAL POSITION = 4.25 INCHES
AXIAL POSITION = 6.25 INCHES
AXIAL POSITION = 12.25 INCHES
AXIAL POSITION = 18.25 INCHES
AXIAL POSITION = 24.25 INCHES

# UNSTEADY FLOWS APPLICABLE TO EJECTOR MECHANICS[*]

Hermann Viets,[**] Michael Piatt,[***] Mont Ball,[†]
Richard Bethke[††] and David Bougine[†††]

Wright State University
Dayton, Ohio 45435

## I. ABSTRACT

As a result of the size and weight constraints on the application of ejectors to aerospace vehicles, there is a continuing search for improvements to meet those constraints within performance limits.  The objective of the present research program is to examine the effect of forced unsteady motions on the mean flow.  The specific geometries include fluidically and mechanically driven unsteady jets, airfoils, rearward facing ramps and steps, driven diffusers and the detailed identification of large scale structures in unsteady flows.

[**]Professor; Presently Associate Dean and Professor, College of Engineering West Virginia University, Morgantown, W.Va.

[***]Research Assistant; Presently with the Mead Corp., Dayton, Ohio

[†]Senior Technician

[††]Associate Professor

[†††]Research Assistant; Presently with the Aeronautical Systems Div., Wright Patterson AFB.

## II.  INTRODUCTION

The application of ejectors to aerospace vehicles, especially Vertical
and Short Takeoff and Landing (V/STOL) aircraft, places severe constraints on
the allowable size and weight of such structures.  To meet these constraints
and yet achieve acceptable performance requires systems where the mixing
process between the primary and secondary flows is very rapid and relatively
complete in a short distance.  In addition, component devices such as inlets
and diffusers must also meet the length (and weight) constraint.

Many techniques have been proposed to deal with these constraints, two
of the more successful being the hypermixing primary nozzle[1,2] (which introduces
streamwise vorticity to enhance the mixing process) and the jet flap diffuser[3]
(which allows a portion of the diffusion process to take place outside the
physical diffuser).  A different approach was taken by other investigators who
attempted to intoduce unsteadiness into the ejector flow in order to enhance
the rate of mixing and diffusion.

The purpose of the present paper is to examine the uses of unsteady flows
which find application to ejectors.  The emphasis is on those areas investigated
by our own research group at Wright State University under U.S. Air Force
sponsorship.  The unsteady work is an outgrowth of previous efforts at the
U.S. Air Force Aerospace Research Laboratories in the early 1970's.  Much of
that work is described briefly in Reference 4.  A more detailed presentation of
the recent efforts described here is found in Reference 5.  The details of the
latest efforts concerning acoustically driven ejectors appear in Reference 6.

The following material is presented as it relates to ejector components,
in particular jets, wings and ramps (or surfaces in general), diffusers and
boundary layers.

## III.  FLOWFIELD OF AN UNSTEADY JET

Various methods have been proposed to induce unsteady flow in jets.[7-18] In general, the objective is to affect the rate at which the jet mixes with its surroundings.  The particular jet nozzle design employed in the present study is described in Reference 9 and consists of a modified fluidic element with a feedback mechanism.

The nozzle design and the jet it produces are shown in Figure 1.  In this case the feedback loop is built around the nozzle body in order to minimize its influence on any external flow.  The jet oscillates from side to side in a quasi-sinusoidal fashion and rapidly mixes with the coflowing stream or the ambient fluid.  The oscillation is produced without the need for moving parts.

a.  Flow visualization

The fluidic nozzle shown in Figure 1 is mounted in a smoke tunnel to illustrate the dynamic interaction between the jet and the surrounding fluid. The smoke is produced by allowing kerosene to drip on an inclined resistance heater.  The kerosene vapor is forced out through tubes and then entrained into the open circuit smoke tunnel inlet.  The instantaneous streakline pattern is shown in Figure 2 for a coflowing stream to jet velocity ratio of 28% and a frequency of 30.5 Hz.  A sinusoidal-like structure may be seen, with a strong interaction between the jet and coflowing stream.  The shear forces between the two flows produce an apparent vortex structure which is swept downstream.  The presence of the large scale structures enhances the mixing process.

b.  Quantitative results

Mounting the nozzle between two Plexiglas sheets to minimize three dimensional effects, as shown in Figure 3, the field is traversed with a hot wire anemometer.

A composite picture of the streamwise time averaged velocity profiles at their relative downstream positions for a frequency of 12 Hz is shown in Figure 4. The behavior of the time averaged velocity distribution can be described in a three step process. Near the nozzle exit the double peak profiles are formed and diverge from each other, entraining fluid from outside the jet and from the center valley. Farther downstream, the velocity in the valley reaches a minimum. The transverse flow begins to move toward the jet centerline, filling the valley while entraining fluid from outside the jet. The final process is the development of a typical two dimensional jet velocity profile with a single peak on the centerline.

The centerline velocity decay and halfwidth growths corresponding to this jet are shown in Figure 5. Since the maximum velocity is not always on the jet centerline, the velocity decay may be based on the centerline velocity or the maximum velocity. Likewise, the halfwidth growth may be based on either velocity and thus both rates are shown in the decay and growth curves of Figure 5. Of course, the two sets of curves coalesce when the double peak disappears.

The time averaged velocity decays and halfwidth growths (Figure 5) are rather weak functions of frequency, if they are based on the peak velocity at each streamwise position. However, based on the centerline velocity, both the velocity decay and the jet growth are strong functions of oscillation frequency. At low frequencies, the centerline velocity decays very rapidly and then rises somewhat under the influence of the double jet peaks. At higher frequencies, the decay is much weaker and leads to the conclusion that at very high frequencies, it is possible that only a single velocity peak appears. This is indeed the case for the acoustic interaction experiment described in Section XII

582

c. Instantaneous velocities

In order to determine the flow structure at a particular instant, the hot wire must sample at precise times and these samples must be taken when the jet itself is in a known orientation. Thus the sampling of the hot wire circuit must be conditioned by the knowledge of the overall jet orientation. The jet orientation is determined by an additional hot wire probe referred to as a trigger.

Three composite Figures showing the instantaneous jet structure at three instants of time are shown in Figures 6-8. The situation where the jet is instantaneously pointing downstream and moving from an upward to a downward orientation is illustrated in Figure 6. The shaded area approximates the jet itself. Figure 7 shows the jet in an extreme downward orientation while in Figure 8 the jet is again oriented directly downstream and moving from a downward to an upward orientation. It is clear from Figures 6-8 that the acoustic stimulation has caused a strong time dependency in the jet structure.

## IV. LARGE SCALE STRUCTURE IN AN UNSTEADY JET

The existence of coherent structures in turbulent shear flows[19] has greatly complicated the task of modeling these flows. Since the use of local transport properties does not appear to be adequate, future descriptions of turbulent flows will probably rely more heavily on phenomenalogical models. The flow may then be based on some observations of its structure. A very simple example would be to model the coherent large scale structure of a free jet by a number of vortices being convected downstream in a jet without a large scale structure. Of course, other difficulties arise; in particular, the questions of how this strucutre is initially formed[20] and the geometrical relationships involved.[21]

The motivation, then, for studying unsteady flows is due to their own usefulness and also as a guide to the modeling of "steady" flows.

The large scale coherent struct re in free shear layers, as demonstrated by Roshko and Brown[22] (see also Ref. 19), is difficult to model due to the lack of detailed understanding of its origin. Although it is clear that the large scale structure is born in the turbulent shear layer, its growth and geometrical spacing have not been predicted analytically. However, it has been shown that the scale must increase with streamwise distance[20] and that the spacing also increases by amalgamation of adjoining structures.[21] A simpler problem, from the modeling point of view, is the unsteady flow in which the origin of the largest scale structure is more evident.

In Figure 2, the large scale unsteady structure is evident in the jet at position A. Even more interesting is the structure at position B where the turbulent flow is clearly rotating in a clockwise sense. Since the flow is unsteady, the smokelines are not streamlines but streaklines so the interpretation is less straight forward. However, it appears that of the two streaklines at position B, the lower one is deflected around the large scale structure while the upper streakline is being entrained into the turbulent large scale structure which is the jet. This interpretation is verified by observing the oscillation with a strobe light which is tuned so that there is a small frequency difference between the strobe frequency and the jet oscillation frequency. Then the jet appears to flap in slow motion and the rotational motion may be clearly seen. Thus, the large scale unsteady structure behaves in the same way as the large scale undriven flow structure described by Roshko[19] and entrains fluid on the upstream side. A similar entrainment pattern for the turbulent wake has been found by Bevilaqua and Lykoudis.[23] The effect may be seen for the

larger structure at position C in Figure 2 where the turbulent flow is entraining the coflowing stream on the upstream side of the large scale structure.

a.  Modeling the usteady jet

To understand the production of the large scale unsteady structure in the unsteady jet, it is useful to construct a very simple phenomonalogical model of the process.  It appears that the growth of the unsteady structure greatly resembles the growth and subsequent breaking of a water wave.  This may be seen by examining three positions of the developing large scale structure shown schematically in Figure 9, where $u_j(s)$ and $u_c$ are the jet and coflowing stream velocities, respectively.  The original deformation of the jet surface is a relatively small amplitude wave.  This wave travels downstream (left to right) at a velocity $u_{wave}$ such that $u_c < u_{wave} < u_j$.  Therefore, the wave is in a shear flow which causes it to curl in a counter-clockwise direction and entrain fluid into itself.  Even without shear, it can be shown that the top of the wave outruns the bottom and curling results.[24]  After the curling up is completed, the vortex-like structure continues to entrain fluid.  The photographs of Figure 9 are taken from positions A, B & C of Figure 2, where position B has been printed as it would appear on the upper surface of the jet.  They clearly verify the schematics of the upper part of the Figure.

If one considers a breaking water wave, the schematic of Figure 9 corresponds to the wave shape at three instants of time, however with the wave traveling from right to left.  Position A is the earliest swelling of wave.  As the wave travels to the left, its forward face steepens and finally breaks as shown at position B.  By position C the wave has broken and resembles a vortex like structure.  The energy of the breaking wave is transformed partially into

585

turbulence, which is eventually dissipated as heat, and partially serves to energize the undertow[24] which is the jet velocity itself in the present analogy. The analogy is incomplete, however, because the water wave is driven by gravity and somewhat by viscous effects while the jet structure is entirely a viscous phenomenon. In spite of this, once the viscosity has created a vortex sheet at the interface, the deformation of this sheet may be modeled inviscidly[20,21] with considerable success.

The main point then is not that the steady and unsteady flow structures are the same but rather that they may have similar origins. As the unsteady structure grows from a large amplitude surface wave, so that steady structure may grow from a small amplitude surface wave.

b.   Quantitative confirmation

Looking back at the schematic of the unsteady jet field in Figure 1, a growing sinusoidal wave traveling downstream, where should one look for the existance of the vortex strucutre observed in the smoke photographs?  The question is answered by another look at the model of Figure 9.  As the bulge of the jet flow curls up to create a vortex structure, it necessarily does so by breaking toward the upstream direction (as driven by the slower coflowing stream or ambient fluid).  Thus the vortex produced would be expected to exist at a position somewhat upstream of the initial jet bulge, which in this case is the extreme off axis position of the instantaneous jet centerline.

A portion of the jet flowfield, for the case of a frequency of 18 Hz and an extreme downward orientation of the jet at the nozzle exit, is shown in Figure 10a taken from Ref. 25.  The lengths of the arrows are proportional to the local velocity and the angles are determined from the measured axial and transverse velocities.  The instantaneous jet centerline is also shown, from which it may be

estimated that if a vortex is present, it should be centered roughly between 16 and 22 jet diameters downstream. No vortex-like structure is evident in this region.

Several investigators have shown, however, that in order to see the coherent motion of a group of particles, the observer must be traveling with the velocity of the center of mass of those particles. Probably the first examination of this effect was made by Prandtl[26] who photographed a boundary layer by traveling at various speeds relative to the flow. Each photograph then revealed a different coherent structure.

In order to see the structure in the flowfield of Figure 10a, a nominal velocity of the vortex center is assumed and that streamwise velocity subtracted from each of the data points in the field. The result is shown in Figure 10b and clearly shows a vortex located in the very region where one would expect it based on the flow visualization results presented above.

Based on the phenominological model of Figure 9 and the quantitative results of Figure 10, one can then make more predictions of the location of large coherent vortices in a family of instantaneous jets as shown in Figure 11 corresponding to the composites of Figs. 6-8. The vortices are drawn in the positions where they might be expected to be found based on the previous results.

Searching at the three positions closest to the nozzle exit, A, C and E leads to the conclusion that coherent vortices do not exist at those positions. This is, however, entirely consistent with the model proposed in Figure 9. It is clear from the flow visualization experiments that it takes some time (or equivalently, distance) for the bulge on the jet to curl up into a coherent structure. The positions near the jet exit simply have not allowed enough time (or distance) for this process to take place. The other vortices identified have been shown to exist in Ref. 27.

587

c.   Instantaneous velocity decay.

Further evidence of the existance of a large scale vortex structure in the unsteady jet may be found in the instantaneous decay of the jet centerline velocity. In the case of steady jets, the centerline velocity decay is a monotonically decreasing function of streamwise distance. In the unsteady jet case, the centerline velocity decay (where the centerline is a quasi-sinusoidal shape) has a typical behavior[25] shown in Figure 12. The velocity decays with streamwise distance, reaches a local minimum and starts to increase again. A peak is reached, where upon the decay begins anew. The location of the peak corresponds to the existence of a vortex at that position.

Considering the induced velocity distribution due to the vortex and superimposing that velocity on a monotonically decaying centerline velocity results in the typical distribution of Figure 12. Thus the visual observation of a vortex structure in the unsteady jet is consistent with the quantitative measurements, specifically the instantaneous velocity structure and its centerline decay.

## V.   MULTIPLE UNSTEADY JET FLOWFIELD

The unsteady jets described to this point do not have any fixed phase relationship if they exit in a multijet configuration. In order to have a phase control on the jet, a mechanical control was proposed[28] consisting of rotating valves on each side of the nozzle. Then instead of a feedback loop, the control parts on either side of the nozzle are alternately opened and closed relative to the ambient pressure as shown in Figure 13. Thus a pressure difference is created across the jet by rotating the valves out of phase with each other, so that one side is open while the other is closed. The resulting flow always attaches to the closed side and thus produces a jet which oscillates from one side to the other.

The multiple jet geometry has been proposed as a gust tunnel[28,29] because of the control available over the amplitudes and frequencies of the unsteady components as well as the possibility for a traveling transverse disturbance which can be controlled. The system can be used as well in an ejector where the magnitudes and frequencies can be tuned for maximum performance.

a. Instantaneous velocity profiles

If the nozzle flows are all oscillated in phase, they produce a rather large oscillation in transverse velocity (orthogonal to the mean tunnel direction). The instantaneous velocity distribution produced by the nozzles at the instant the nozzle flow is in the extreme upward position is shown in Figure 14. Since the distance from the nozzle exits is not large (20 nozzle exit sizes), there is still the evidence of the jet nozzles in the streamwise velocity profiles. However, even this close to the exits, the velocity ratio between the peaks and valleys has been reduced from more than four at the nozzle exit to less than two, indicating a strong mixing rate.

To oscillate the jets out of phase, the relative phases of the four jets are set such that the two upper jets are 180° out of phase with the two lower jets. The two sets of jets are then alternately aimed toward and away from each other. The flowfield corresponding to these two situations measured at a position twenty jet thicknesses downstream, are shown in Figures 15 and 16 respectively. It may be seen that in each case the transverse velocity is roughly zero at the channel centerline (after being corrected for the tunnel bias) and consistant with the jet orientations for positions off the channel axis.

The effect of the entrainment of the channel flow by the unsteady jets themselves is evident, especially in the upper portion of Figure 16. There the v velocity component is expected to be positive (upward) but in fact is somewhat downward (negative) reflecting the presence of the entrainment velocity. The

589

possibility of tuning such a multijet device to an ejector geometry has not yet been investigated.

## VI.   FORCED UNSTEADY FLOW OVER A WING

The unsteady jet methods discussed in the previous sections offer potential performance improvements which are due to the increased mixing rate between the jet and the coflowing stream.  The present section and the following one concern themselves with a mechanical device which causes the flow near a wall to be unsteady.  Such a concept could thus be applied at various points in an ejector where separation could be a problem.  The origin of the present mechanical system lies in experiments on oscillating airfoils.

As reported by McCroskey,[30] Kramer[31] was the first investigator to discover that an oscillation about a mean angle of attack delayed the onset of stall.  That is, the flow remained attached to the upper surface at higher angles of attack in the dynamic case than in the static condition.  Several investigators have performed flow visualization studies and found that the oscillating airfoil produces a vortex structure on the upper surface as shown in Figure 17.  Apparently the vortices act to energize the boundary layer on the airfoil and thereby delay separation.

A similar vortex structure may be generated by a number of simple techniques, one of which is illustrated in Figure 18.  The vortices are created by a cam shaped rotor moving in the counter-clockwise direction as shown.  Each time the rotor surface discontinuity sweeps by, a vortex is generated in much the same manner as the recirculation region behind a rearward facing step but with increased strength.  The vortex spacing depends upon the local velocity and the frequency of generation.

In order to illustrate the ability of the rotor vortex generator to energize the boundary layer, the flow over an airfoil with the rotor mounted near the leading edge is visualized with kerosine vapor. The Reynolds number, based on the airfoil chord, is approximately 100,000.

On the airfoil, separation first occurs in a limited fashion at an angle of attack of 14° and the flow is fully separated at 20°. This is determined by observation of the smoke flow structure as well as pressure measurement at the single static pressure port in the separated region.

The structure of the flow about the airfoil at an angle of attack of 20° and the rotor withdrawn into the body is shown in Figure 19a. In order to avoid acoustic interaction between the flow and the rotor cavity, the cavity has been covered by tape. Without any other changes (except removing the tape) the rotor described above is activated at a rotational frequency of 2400 rpm and the resulting flow visualization shown in Fgiure 19b.

The effect of the active rotor is to draw the streamlines down closer to the surface of the airfoil and thereby reduce the size of the separated region. In addition, a streamline which passes below the airfoil in the case of no rotor activity ($\omega = 0$), appears above the airfoil for $\omega = 2400$ rpm. This indicates an increase in the airfoil lift and a reduction in the upper surface pressure.

A limited amount of quantitative data is also available (Reference 32) to substantiate the ability of the rotor to energize the boundary layer. The purpose of the present section is not simply to propose the vortex rotor as a method to delay separation, but rather to point out the utility of a time dependent method of boundary layer control. In this regard, there is no assurance that the rotor method is superior to, say, an oscillating plate[33,34] which

591

alternately protrudes from and withdraws into the surface of the airfoil. The choice of the rotor was due to the obvious vibration advantages of a rotor motion over the reciprocating motion. This is especially true if the rotor is designed so that it is dynamically balanced. There are certainly other time dependent devices which are capable of producing the same vortex structures, such as an oscillating air brake configuration.

## VII. UNSTEADY FLOW OVER A REARWARD FACING RAMP

The previous section discussed the ability of the unsteady rotor to energize a boundary layer thinner than its own protrusion into the flow. In this section the boundary layer thickness at the rotor position is greater than the height of the fully extended rotor.and the boundary layer is fully turbulent.

The time dependent vortex structure considered in this section is produced by the cam shaped rotor discussed in the last section. The discontinuity in the rotor surface generates one lateral vortex for each turn of the rotor. The effect of the vortices is to energize the lower portion of the boundary layer and enable the flow to withstand stronger pressure gradients. The mechanism by which this is accomplished is probably the actual exchange of low energy fluid in the boundary layer for higher energy fluid from the mainstream. It should be emphasized that the direction of rotation of the cam is such that it does not push the flow. Thus the energy put into the rotor is only the small amount required for the mass exchange, not the energy put into the boundary layer (which comes from the freestream).

Figure 20 shows the particular geometry of interest here, a half boat tail geometry (which could also be considered a half diffuser from the point of view of internal flows). Such a method is a possible way of filling the wake of a bluff body to reduce its drag. More generally, the technique is representative

of a positive view of unsteady flow which searches for beneficial aspects of unsteady flows as opposed to those leading to performance degradation.

The experiments are performed in a low speed smoke tunnel. The remainder of the tunnel is constricted so that all the flow is forced through the duct and over the rearward facing ramp. The velocity produced upstream of the ramp is nominally 32 m/sec resulting in a Reynolds number of $1.97 \times 10^6$ per meter. Further details are found in Reference 35.

For a ramp angle of 28°, as shown in Figure 21, the pressure distribution varies only slightly from the freestream value if the rotor is unused (ie $\omega = 0$). This indicates the flow is separated at the ramp and therefore the effective area that the flow experiences is nearly a constant area duct. The use of the rotor at 1000 rpm reduces the pressure distribution at the beginning of the ramp, indicating that the flow more easily negotiates the turn.

As the rotor speed increases above 1000 rpm, the static pressure on the ramp decreases, indicating improved flow performance. The performance at rotor speed of 4000 and 5000 rpm is virtually indistinguishable, suggesting that this speed range may contain the maximum performance in terms of $\omega$ for this particular case.

As the ramp angle is increased to 30°, the separated flow (for $\omega = 0$) reacts even less to the presence of the ramp; the pressure distribution deviates even less from the freestream value. The general behavior of the flowfield with increasing $\omega$ is similar to that at 28°. As the rotor speed is increased, the pressure distribution on the ramp decreases. Again, the difference between the 4000 and 5000 rpm values is very small.

a. Flow visualization

Kerosine vapor is entrained into the tunnel flow and some longer time exposures of the field are shown in Figure 22. The wall angle is 28° and the rotor speed varies between $\omega = 0$ in Figure 6a to $\omega = 4000$ in Figure 22 d. As the

rotor speed increases, the positions of the mean streamlines move closer and closer to the ramp, indicating better flow attachment and verifying the pressure measurements of Figure 21.

Perhaps of even more interest are the high speed photographs of Figure 23 a-f for various rotor speeds at a ramp angle of 28°. For a zero rotor speed and the cavity taped, the flow clearly separates as shown in Figure 23a. There is some large scale structure in the separated shear layer but not enought momentum transfer to lead to reattachment. If the rotor is activated with $\omega$ = 1000 rpm (Figure 23b), the separated flow curves down toward the ramp surface, very much in the same manner as the time averaged picture at the same rotor speed, Figure 22b.

With a rotor speed of 2500 rpm (Figure 23c), the curvature of the flow toward the ramp becomes more pronounced. In addition, the time dependent structure becomes significantly larger. A vortex may be seen in Figure 23c, with a region farther downstream which appears to be separated. The sequence of events appears to be as follows: Suppose the flow is initially separated. The rotor generates a vortex which causes the flow to attach for a moment before it is forced to detach again by the adverse pressure gradient. At this time the flow needs a new vortex to force it to attach again. If the speed (or effectively, the generation frequency) is sufficiently high, the necessary vortex is available.

The flow situation described above may be seen in Figures 23d and 23e for both of which $\omega$ = 4000 rpm. The two photographs indicate considerably different flow patterns. Actually they are examples of the same time dependent flow at two different times. These are the extreme positions of the oscillatory flow pattern at 4000 rpm. The mean pressure distribution on the ramp reflects the time average of the oscillatory flow. The instantaneous flow patterns, Figures 23d and e are fully consistent with the time average flow pattern of Figure 22d, where the

594

apparent lack of smoke near the wall is due to the fact that the streakline is there only intermittently. It should be noted that the position of the incoming smoke is unchanged in the sets of photographs resulting in Figures 22 and 23.

The transition between the flow patterns of Figures 23d and e is shown in Figure 23f (for a speed of 5000 rpm). The flow far down the ramp is clearly separated while that nearer to the corner is relatively attached. The attached flow is produced by the vortex sweeping downstream, momentarily overcoming the adverse pressure gradient, as discussed above.

A three dimensional rotor (i.e. tapered in the transverse direction) has also been tested and is reported in Reference 27. Its general behavior is similar to that described above.

The unsteady structure can also be accomplished by various other devices such as oscillating spoilers, plates or even membranes. The advantage of the rotor system is primarily that the reciprocating motion has been avoided. In addition, with the use of modern composities, the rotor could be built as designed and yet be well balanced, again avoiding troublesome vibration.

## VIII.  SUDDEN EXPANSION GEOMETRY

A sudden expansion (i.e. rearward facing step) geometry is sometimes used in combustors and is referred to as a dump combustor. The recirculation region thus produced acts as a flameholder and keeps the flame from being blown downstream by the high speed flow. Therefore, the recirculation region is designed to act as an ignition for the main flow passing through the duct. In order for ignition to be accomplished, there must be an interaction between the two flow regions. It is the purpose of this section to illustrate a simple mechanical rotor (Figure 24) which indicates a potential performance improvement

since it increases the fluid dynamic interaction between the recirculation region and the main flow. The experimental details may be found in Ref. 36.

The method proposed here is demonstrated in a two-dimensional arrangement although most dump combustor applications for ramjets are axisymmetric. This is due to the relative simplicity of the 2-D device but the same principle can be applied to the axisymmetric case, probably in the form of segmented rotors or several rotors around the periphery of the duct.

a.  Flow visualization

The flow is rendered visible by the entrainment of smoke into the inlet of the open circuit wind tunnel. The resulting time averaged streamlines are shown in Figure 25 for the case of no rotor motion (i.e., the rotor withdrawn into the surface and the cavity covered). The length of the recirculation region is approximately eight or nine step heights as compared to a length of eight step heights in a comparable high speed axisymmetric experiment.[37] That the activation of the rotor decreases the average length of the recirculation region may be seen in Figure 25b where the rotor speed is 1000 rpm. The reduced length is approximately 7-8 step heights. Increasing the rotational speed produces yet a further reduction in the average recirculation zone length, as seen in Figure 25 c-e. The time dependent motion as may be seen in Figure 26, showing the streaklines for the case of no rotor activity ($\omega = 0$). The breakdown of the shear layer into a larger scale structure may be seen near the end of the separated region. The length of this recirculation region is approximately 8-9 step heights as was estimated from the time averaged photograph, Figure 25a.

The introduction of unsteady flow by means of the rotor results in very significant time dependent changes in the flow structure. Some indication of

596

this effect is seen in Figure 25 b-e where the spreading of the streamlines indicate their extreme positions. More dramatic evidence is presented in the following set of figures for the case of $\omega$ = 2500 rpm. Figure 27a shows the structure of the flow as not much different from that of zero rotor speed, Figure 26. However, at another instant of time, Figure 27b, the tail of the recirculation region has been swept away while the upstream portion is relatively unchanged. At yet another instant, Figure 27c, the recirculation region has again attained the expected elliptical shape but with a much decreased length. The interaction of the two flow regions is very strong with the length of the recirculation region effectively pulsing back and forth.

b.  Quantitative results

The flow visualization results are verified by the static pressure distributions presented in Figure 28. The basic effect of unsteadiness on the time average flow is seen to be the shortening of the recirculation region length. That is, the pressure reaches its maximum at a streamwise distance which is inversely proportioned to rotor speed. The maximum pressure position is not the re-attachment point since it has been shown,[37] based on flow visualization, that reattachment occurs upstream of where the maximum pressure is attained. Thus the reattachment, in the case of the withdrawn rotor ($\omega$ = 0) should occur before ten step heights (where the maximum pressure is attained).

From the point of view of ejectors, if the length constraint is especially severe, such an active "dump" device may merit more attention as a diffuser.

## IX.  UNSTEADY DIFFUSERS

Artificially induced large scale flow structures have been employed success-fully in the past to improve performance. Two examples are the common stream-wise vortex generators sometimes used to control the flow over an aircraft

597

wing and to maintain attached flow in large angle diffusers. In each case, streamwise vortices are created which cause a transfer of energy from the other flow to the boundary layer. The large scale streamwise structures are created by the passive vortex generators simply mounted in the surfaces.

The objective of this section is to examine the potential performance advantages of a diffuser in which the flow is forced to be unsteady by the use of the rotor described above.

The device employed in this experiment is simply a spiral shaped rotor mounted in the wall on each side of the channel just upstream of the diffuser section. The rotor surface has a discontinuity which ends in a cusp. The rotor turns in such a direction that the motion of the portion exposed to the flow is always against the flow, i.e. the upper rotor turns in a clockwise direction while the lower rotor turns in the counter-clockwise sense.

Each time the surface discontinuity of the rotor is swept through the fluid, a vortex is formed which then is convected downstream. The rotors (and hence the vortices) can have an arbitrary phase relationship. In Figure 29a the rotors appear simultaneously and thus the vortices are formed in phase with each other and are symmetrically positioned. Figure 29b illustrates the out of phase condition where the discontinuities appear alternately and thus the vortices formed are staggered as they sweep downstream. The use of the rotors is designed to allow the diffuser to operate at a larger area ratio without separation. The unsteady vortex structure energizes the boundary layer and allows it to overcome a larger pressure gradient.

a. Flow visualization

As the rotor speed increases with a fixed tunnel speed, the spacing of the consecutive vortices decreases, as well as the size of the vortices themselves.

598

This effect may be seen in Figure 30 where the streamwise velocity through the diffuser has been held artificially low in order to more clearly illustrate the structure. The lowest photograph is at a rotor speed of $\omega$ = 1000 rpm with an increase of 1000 rpm to each photograph above. Thus the number of vortices seen in the photographs is proportional to the rotor speed.

A comparison of the flow patterns with and without the use of a rotor is shown in the photographs of Figure 31. In this case the exposure time of the film is much longer and the result is an effective time average resulting in a streamline pattern. In each case the diffuser angle is $2\theta$ = 30°. The upper case employs no rotor and strong separation is apparent from the lower wall of the diffuser. The lower photograph employs a rotor at a nondimensional speed of $\bar{\omega}$ = 11.84 with the rotors in phase with each other. The separated region has moved to the upper wall and has been significantly reduced in size.

b. Performance

The performance of the various diffuser combinations are compared by means of the nondimensional pressure rise (or pressure recovery) through the device. The nondimensional pressure, $\bar{P}$ is defined as the difference between the wall pressure within the diffuser and the inlet pressure, divided by the inlet dynamic pressure,

$$\bar{P} = \frac{P_{wall} - P_{inlet}}{\frac{1}{2}\rho V^2}$$

The pressure rise with nondimensional streamwise distance is shown in Figures 32-34 for the case of an out of phase orientation of the two rotors. The pressure rise is plotted for various rotor speeds including the case of $\bar{\omega}$ = 0 which corresponds to no rotor and having the rotor cavities covered to avoid acoustic interactions. The lowest angle case is shown in Figure 32,

Since no separation exists, the use of rotors cannot improve the performance and, in fact, results in a performance reduction.

Increasing the diffuser angle to $2\theta = 24°$ results in a separated flow as verified by the pressure distributions of Figure 33 for $\bar{\omega} = 0$. In this case, the use of the rotors results in roughly the same performance although there is a positive trend with rotor speed. In addition, with the use of the rotor, the pressure distribution on both walls assumes the shape corresponding to attached flow. At the highest angular setting, $2\theta = 30°$, the overall performance decreases. However, the use of the in-phase rotors results in a significant performance improvement compared to the no rotor condition.

The corresponding results for the out of phase rotor orientation show a small performance improvement. Perhaps even more important is the positive trend with rotor speed (vortex frequency) which is evident.

c.   Flow structure

Instantaneous velocity profiles are taken within the diffuser by employing a hot wire anemometer along with a conditioned sampling device. The input required to define the rotor position comes from a magnetic pickup on the rotor drive shaft. A more detailed description of the data aquisition system is given in Reference 38.

The instantaneous streakline patterns can be an aid to the identification of the large scale flow structures. The in-phase configuration for an angle of $2\theta = 24°$ is shown in Figure 35. It is evident that the basic flow is attached to the upper wall and that the forced unsteadiness modifies that condition. The flow visualization reveals a strong vortex near the lower wall at a phase angle of $\phi = 180°$. Since the rotors are in-phase there is a corresponding mirror image vortex near the upper wall which does not appear to be as

600

large and also is located further downstream. Both of these effects are consistent with the flowfield since the growth of the vortex is inhibited by the proximity of the wall and the vortex is convected more rapidly due to the higher velocity near the fully attached wall. The presence of the vortex at the 180° phase angle is verified by the superimposed instantaneous streamwise velocity profile which is enhanced near the center of the channel and reduced in the region between the vortex and the wall. Both effects are caused by the induced velocity due to the presence of the vortex pair.

With the rotors in the in-phase orientation, the flowfield is expected to have a pulsating character due to the time dependent change of the blockage at the diffuser inlet. This effect is evident in the flow visualization result at $\phi = 90°$ where the pulsing appears to be almost symmetrical. The effect may also be seen by comparing the instantaneous velocity profile at $\phi = 90°$ to that at $\phi = 180°$. The former profile is wide and relatively uniform while the latter is constricted at the edges and accelerated near the center.

Streaklines with superimposed velocity profiles are shown in Figure 36 for an out of phase rotor orientation and a larger diffuser angle $2\theta = 30°$. In this case the basic flow is attached to the lower wall of the diffuser. The instantaneous phase angles of the individual rotors are indicated on each side of the diffuser. Due to the out of phase orientation of the rotors, the flowfield has essentially a flapping character. This is most evident in Figure 36d. The vortices appear to be located in the vicinity of the measuring station in (b) and (d). In each case, the upper vortex in (b) and the lower vortex in (d), the presence of the vortex results in a decreased velocity near the wall and an increased value near the centerline. These velocity changes may again be attributed to the induced velocity of the vortex structure.

601

In order to more clearly specify the effect of a vortex on the flowfield (and thus be more capable of identifying the vortex location) consider the schematics of Figure 37. The objective is to demonstrate the local change in velocity, both streamwise (u') and transverse (v'), produced by the presence of the vortices which are shown schematically as swirling fluid near each wall. The vortex near the upper wall is rotating in the counter clockwise direction while the vortex near the lower wall rotates in the clockwise direction. The qualitative transverse velocity changes, u', (equivalent to the induced velocity) may be seen not to depend upon whether the profile is taken in front or in back of the vortex location but does depend upon the sense of rotation of the vortex. Thus the streamwise velocity profiles can be used to determine the sign of the vorticity.

The qualitative effect on the transverse velocity change (v') indicates that there is a sign change from the upstream to the downstream side of the vortex and also a sign change with the sign of the rotation itself. However, it is not possible to distinguish between, for example, the upstream side of a counter clockwise vortex from the downstream side of a clockwise vortex. Thus both velocity profiles are required, but knowing both can result in the identification of the vortex.

In order to verify the schematics of Figure 37, consider some data taken from the in-phase results of Figure 35. In particular, compare the velocity profiles for the case where a vortex pair is present ($\phi = 180°$) near the measuring plane to a case where no vortices are present ($\phi = 90°$). This comparison is presented in Figure 38. The difference in the streamwise velocity corresponds, for both the upper and lower vortex, to the situation of the profile being taken on the downstream side of the vortex as in Figure 37. This is certainly consistent with

602

the flow visualization results at $\phi$ = 180° of Figure 35.  Comparison of the

transverse velocity profiles verifies this conclusion since the difference

qualitatively agrees with the schematic profiles downstream of the vortices

in Figure 37.

Consider now the case of the out of phase results of Figure 36.  A vortex is

evident near the upper wall of Figure 36b while none appears near that wall

in Figure 36d.  A comparison of the streamwise and transverse velocity profiles

of these cases is presented in Reference 38.  From the streamwise comparison,

it is clear that the vortex is turning in the counter clockwise direction.

The difference between transverse velocity profiles indicates that the profile

containing the vortex (Figure 36b, $\phi$ = 90°) was taken upstream of the vortex.

This result may be seen to be consistent with the streakline photograph of Figure

36b.

Thus the forced time dependent diffuser flows appear to have potential to

improve the performance of the device.  In the present case, the time dependency

has been mechanically created.  Of course, other possibilities exist which may

have advantages in terms of construction, reliability or cost.

## X.   DETAILS OF THE ROTOR FLOWFIELD

The preceding section on unsteady diffuser flows has described some of the

vortex structure in the diffuser.  Some of the earlier sections also revealed

the vortex structure for various geometries.  In this section the simplest rotor

configuration is considered, the rotor on a flat plate as shown in Figure 39.

a.   Flow visualization

Typical of the desired vortex generation is the result shown in Figure 40

for a rotor speed of 3000 rpm.  The strobe lighted photographs have been arranged

603

in the order of their occurrence, from top to bottom. As the rotor tip sweeps from right to left, the first hint of the vortex produced is seen in the lowest smokeline which begins to curl up in Figure 40a. By Figure 40b the rotor tip has disappeared and the vortex is evident, slightly farther downstream. The streaklines still appear to be relatively laminar but in Figure 40c the vortex flow appears to be turbulent with a smaller scale structure visibly. By Figure 40d the size of the vortex structure has grown considerably and it has translated downstream as well as rising higher above the surface of the plate. Its position yet farther downstream is shown in Figures 40 a, b and c where its continued growth and interaction with the outer streaklines is evident. In summary, the vortex is produced by the rotor shape, grows and transitions to a turbulent state and is convected downstream.

The tip of the rotor is moving in the upstream direction in the previous case and a strong vortex is apparent. Turning the rotor in the opposite direction at the same speed (i.e. ~ 3000 rpm) generates vortices at the same frequency and rotating in the same sense. This indicates that the relative velocity between the rotor and freestream is still in the same sense. In general, for rotation in the clockwise direction the strength of the vortex is greatly reduced by the lowered relative velocity. Such cases are presented in Ref. 39.

Thus the flow visualization results clearly show the existence of a vortex structure downstream of the spinning rotor. The frequency of generation depends upon the rotational frequency since each rotation produces one vortex. The strength of the vortex depends upon the relative velocity between the motion of the cusp tip and the freestream velocity.

b.   Quantitative results

The flowfield downstream of the rotor is examined by a conditionally sampled

604

sampled hot wire. The entire flowfield can be depicted by plotting the magnitude of the total velocity and its orientation as the length and angle of vector arrows in a field. Such a field is shown in Figure 41a, where the rotor is in the $\theta = 0°$ (i.e. the maximum extension) position. The velocity vectors shown are the instantaneous values at that particular phase position of the rotor.

Examining Figure 41a, there is no evidence of the existence of a vortex in the flowfield. However, in order to see the coherent motion of a portion of matter, the observer should be in a frame of reference moving with its center of mass (as discussed in relation to unsteady jets). In the field of Figure 41a, this can be accomplished by simply subtracting the velocity of the center of the particular vortex Of course, the location of the vortex center is unknown, so the process involves some trial and error. However, the flow structure which leads to a vortex can be isolated. It consists of a curved instantaneous streamline in the vicinity of which the magnitudes of the velocity vectors simultaneously increase with distance from the center of curvature of the streamline.

Employing this method to identify the location of the vortex and subtracting the streamwise velocity at that point from all the velocities in the field reveals the vortex structure in Figure 41b. The vortex center is located at approximately $X = 7.5$, $Y = 3.5$. No other vortex is apparent.

The same method can be applied to the flowfields produced at various phase positions (see Ref. 39). When the vortex locations are known, the vortex trajectories may be determined as shown in Figure 42 and the trajectory of the vortex is found to be an almost linear rise after its structure is established. Based on the trajectory, the translational velocity of the vortex is approximately constant and equal to the undistrubed freestream velocity.

The trajectory of the vortex, as shown in Figure 42, also explains why the vortex generator is so effective even if it is submerged within a boundary layer.

605

The vortex is created with a very small core which grows rapidly and it rises out of the boundary layer. Thus the scale of its influence becomes larger as it moves downstream and it moves into a better position from which to energize the boundary layer.

## XI.  DATA ANALYSIS TO IDENTIFY LARGE SCALE VORTEX STRUCTURES

As described in the preceding section, the large scale vortex structures of the various unsteady flowfields are of both fundamental and applied interest. The present method applies a discrete Fourier transformation to a general velocity field on a point by point basis. The resulting transformed field yields a distinctive signature of the passing large scale structure. Then knowing the locations of the large scale structure, the convection of these points can be determined. The details of the present analysis are given in Ref. 40.

a.  The transformation technique

The discrete Fourier transformation maps a complex matrix of size $N_1$ by $N_2$ into another complex matrix of the same size by the equation:

$$F(m,n) = \sum_{k=0}^{N_1-1} \sum_{\ell=0}^{N_2-1} f(k,\ell) e^{-j\left(\frac{2\pi}{N_1} km + \frac{2\pi}{N_2} \ell n\right)} \tag{1}$$

where $f(k,\ell)$ is the discrete function in the original plane at points $K, \ell$ and $F(m,n)$ is the corresponding spectrum. The basis of the transformation technique is that any shift of the vortex location from the centerline of the physical plane results in a change in the phase angle of every point in the transformed plane. The new phase angle is proportional to the product of the vortex shift distance and the particular matrix location. This technique was tested on several artificial

606

vortex fields,[40] on real flowfields produced by jets and rotors and even on fields with multiple vortices.

b.    Vortex identification in a real flow.

The instantaneous flowfield structure of an oscillating jet has been determined[25,27] and found to contain large scale unsteady vortices which are convected downstream.  A time slice of this flowfield is shown in Figure 6 and corresponds to the instant that the jet is in the horizontal position and sweeping from top to bottom.  No vortex is apparent in Figure 6 because the convected velocity is superimposed on the vortex.  Transforming the velocities of Figure 6 by Equation (1) and applying the techniques of Ref. 40 results in identifying the vortex center shifted $X = 8.34$, $Y = 2.15$ from the upper left corner point.  The total velocity at that point is found and subtracted from every point in the physical plane, Figure 6, and results in the structure shown in Figure 43.  Here the coordinate frame is moving with the velocity of the point identified as the vortex center and indeed a vortex is apparent, centered at the identified point.

The technique developed for the locating of a single vortex convected with the flow has been extended in Reference 40 to include an arbitrary number of vortices.  Additional techniques are currently being examined to make the identification of multiple coherent structure more precise and rapid.

## XII.  CURRENT EFFORTS IN UNSTEADY FLOWS

The continuing research program in unsteady flows is presently directed into two major areas.  The structure of the coherent vortex near a flat plate has been examined from the point of view of two-dimensionality.[39]  However, the vortex is not really uniform in the transverse direction.  The structure actually assumes a three dimensional shape, having some resemblence to the vortex loop found by

607

some investigators in a transitioning boundary layer. Further understanding of this flow could lead to a better ability to control the vortex and hence the energization of boundary layers by its use.

Another area of interest to ejector mechanics is the question of acoustic interaction. Quinn[41,42] found that an underexpanded choked jet in ejector shroud can lead to acoustic interaction between the screech tones generated by the jet and the ejector shroud. This can lead to a resonance in the ejector with standing transverse waves in the duct. This, in turn, drives the jet unsteady and can improve the ejector performance. The rectangular analog of Quinn's axisymmetric experiments was reported by Viets, Campbell and Korken.[43]

The current unsteady flow program is examining the flowfield of flapping jets of rather high frequency[6] (1000 Hz and above) in an attempt to produce standing transverse waves in an ejector shroud. The high frequency nozzles were originally developed for two phase flow of liquid into air.[11] The performance of one of these nozzles in terms of mass flow ratio (total mass flow/primary mass flow) is shown in Figure 44. For very short ejectors, the unsteady performance is superior to that of the steady ejector with a simple slot nozzle. It should also be noted that no attempt was made to optimize the performance of the unsteady nozzles.

The transverse dimension of the ejector shroud was chosen to allow resonance at approximately 1000 Hz. When the primary jet is oscillating at roughly that frequency, standing waves exit which are related to that frequency and other wave shapes exist at high harmonics of that frequency. These wave shapes are shown in Figure 45 and demonstrate the possibility of improving the flow in the ejector by taking into account the acoustical properties of the flow in addition to the larger scale unsteady pheonomena.[6]

608

## XIII.  CONCLUSION

The foregoing is an attempt to examine the possibilities of including unsteady flows to improve the performance of ejectors.  As with nominally steady flows, the unsteady ejector is a complex device from the point of view of optimization.  However, it is apparent that the inclusion of the unsteadiness, sufficiently understood, could lead to significant performance improvements in ejectors.

# XIV. REFERENCES

1. Quinn, B., "Compact Ejector Thrust Augmentation," J. Aircraft, Vol. 10, No. 8, Aug. 1973, pp. 481-486.

2. Bevilaqua, P.M., "Evaluation of Hypermixing for Thrust Augmenting Ejectors," J. Aircraft, Vol. 11, No. 6, June 1974, pp. 348-354.

3. Alperin, M., "A Coanda Inlet/Jet Flap Diffuser Ejector," AF Flight Dynamics Lab Report TR-72-106, Aug. 1972.

4. Viets, H., "Thrust Augmenting Ejectors," U.S. Air Force Aerospace Research Laboratories Report ARL 75-0224, June 1975.

5. Viets, H.; Piatt, M.; Ball, M.; Bethke, R.J. and Bougine, D., "Problems in Forced Unsteady Fluid Mechanics," To be issued as a Flight Dynamic Laboratory Report, 1981.

6. Viets, H., "Unsteady Ejectors," NATO/AGARD Symposium on Fluid Dynamics of Jets with Applications to V/STOL, Lisbon, Portugal, Nov. 1981.

7. Crow, S.C. and Champagne, F.H., "Orderly Structure in Jet Turbulence," J. Fluid Mech., Vol. 48, Part 3, 1971, pp. 547-591.

8. Binder, G. and Favre - Marinet, M., "Mixing Improvement in Pulsating Turbulent Jets," ASME Symposium on Fluid Mechanics of Mixing, June 1973.

9. Viets, H., "Flip-Flop Jet Nozzle," AIAA Journal, Vol. 13, No. 10, October 1975, pp. 1375-1379. (See also U.S. Patent No. 3,926,373.)

10. Williams, J.R., Ambrosiani, J.P. and Palmer, W.E., "Analysis of a Pulsating Wall Jet," Columbus Aircraft Division/North American Rockwell Report NR 72H-325, October 1972.

11. Viets, H., Balster, D. and Toms, H.L., "Time Dependent Fuel Injectors," AIAA Paper No. 75-1305, AIAA/SAE 11th Propulsion Conference, Anaheim, California, 1975 (See also U.S. Patent No. 3,998,386).

12. Simmons, J.M., Platzer, M.F. and Smith, T.C., "Velocity Measurements in an Oscillating Plane Jet Issuing Into a Moving Air Stream," J.F.M., Vol. 84, Part 1, 1978, pp. 33-53.

13. Hill, W.G. and Green, P.R., "Self Excited Superturbulence: The Whistler Nozzle," Grumman Research Dept. Rept. RE-488, Oct. 1974.

14. Collins, D.J.; Platzer, M.F.; Lai, J.C.S. and Simmons, J.M., "Experimental Investigation of Oscillating Subsonic Jets," Symposium on Numerical and Physical Aspects of Aerodynamic Flows, Calif. State Univ., Long Beach, Ca., Jan. 1981.

15. Rockwell, D.O., "External Excitation of Planar Jets," J. Applied Mech., Dec. 1972, pp. 883-890.

16. Foa, J.V., "A Vaneless Turbopump," AIAA Journal, Vol. 1, No. 2, Feb. 1963, pp. 466-7.

17. McCormack, P.D.; Cochran, D. and Crane, L., "Periodic Vorticity and its Effect on Jet Mixing," Phys. Fluids, Vol. 9, No. 8, Aug. 1966, pp. 1555-60.

18. Brown, G.B., "On Vortex Motion in Gaseous Jets and the Origin of their Sensitivity to Sound," Proc. Phys. Soc. Vol. 47, 1935, pp. 703-732.

19. Roshko, A., "Structure of Turbulent Shear Flows: A New Look," AIAA Journal, Vol. 14, No. 10, 1976, pp. 1349-1357.

20. Michalke, A., "On Spatially Growing Disturbances in an Inviscid Shear Layer," J. Fluid Mech., Vol. 23, Part 3, 1965, pp. 521-544.

21. Moore, D.W. and Saffman, P.G., "The Density of Organized Vortices In A Turbulent Mixing Layer, J. Fluid Mech., Vol. 69, 1975, pp. 465-473.

22. Brown, G.L. and Roshko, A., "The Effect of Density Difference on the Turbulent Mixing Layer, Turbulent Shear Flows," AGARD-CP-93, 1971, pp. 23 (1-12).

23. Bevilaqua, P.M. and Lykoudis, P.S., "Mechanism of Entrainment in Turbulent Wakes," AIAA Journal, Vol. 9, No. 8, Aug. 1971, pp. 1657-59.

24. Stoker, J.J., Water Waves, Interscience Publishers, New York, 1957.

25. Piatt, M. and Viets, H., "Conditioned Sampling in an Unsteady Jet," AIAA Paper No. 79-1857, AIAA Aircraft Systems and Technology Meeting, New York City, August 1979.

26. Schlichting, H., Boundary Layer Theory, McGraw-Hill Book Co., Inc., New York, 1960, pg. 400.

27. Viets, H., "Coherent Structures in Time Dependent Flow," Proceedings of the NATO/AGARD Specialists Meeting on Turbulent Boundary Layers, The Hague, Netherlands, September 1979, AGARD CP-271.

28. Viets, H., "High Frequency Gust Tunnel," AGARD Conference Proceedings No. 174 on Windtunnel Design and Testing Techniques, London, England, Oct. 1975. (See also U.S. Patent No. 4,074,568.

29. Viets, H., Ball, M. and Piatt, M., "Experiments in a Subscale Pilot Gust Tunnel," AIAA Paper No. 80-0453, Aerodynamic Testing Conference, Colorado Springs, Colo., March 1980. Also AIAA Journal, Vol. 19, No. 6, June 1981, pp. 820-822.

30. McCroskey, W.J., "Recent Developments in Dynamic Stall," Unsteady Aerodynamics, R.B. Kinney, Ed., University of Arizona, 1975.

31. Kramer, M., "Die Zunahme des Maximalauftriebes von Tragflugeln bei plotzlicher Anstellwinkelvergrosserung (Böeneffeckt), Z. Flugtech. u. Motorluftshif, Vol. 23, 1932, pp. 185-189, (Also NACA T.M. 678. 1932.)

32. Viets, H., Piatt, M., and Ball, M., "Unsteady Wing Boundary Layer Energization," Proceeding of the U.S.A.-Germany Data Exchange Meeting, Meersburg, West Germany, April 1979 (also AIAA Atmospheric Flight Mechanics Meeting, Paper No. 79-1631, Boulder, Colo., August 1979).

33. Keesee, J.E., Francis, M.S. and Lang, J.D., "Technique for Vorticity Measurement in Unsteady Flow," AIAA Journal, Vol. 17, No. 4, April 1979.

34. Keesee, J.E., Francis, M.S., Sparks, G.W., Jr., and Sisson, G.E., "Aerodynamic Characteristics of an Unsteady Separated Flow," AIAA Journal, Vol. 17, No. 12, Dec. 1979, pp. 1332-1339.

35. Viets, H., Piatt, M. and Ball, M., "Boundary Layer Control by Unsteady Vortex Generation," Proceedings of the Symposium on the Aerodynamics of Transportation, June 1979, Published by the ASME. Also J. of Wind Eng. and Indust. Aero., Vol. 7, 1981 pp. 135-144.

36. Viets, H. and Piatt, M., "Induced Unsteady Flow in A Dump Combustor," (with M. Piatt), Proceedings of the 7th International Colloquium on Gasdynamics of Explosions and Reactive Systems, Gottingen, Germany, August 1979. Also AIAA Progress in Aeronautics and Astronautics Series. In Press.

37. Drewry, J.E., "Fluid Dynamic Characteristization of Sudden-Expansion Ramjet Combustor Flowfields," AIAA Journal, Vol. 16, April 1978, pp. 313-319.

38a. Viets, H., Ball, M. and Bougine, D., "Large Scale Structures in Driven Unsteady Diffuser Flows," Proceedings of the International Flow Visualization Symposium, Ruhr University, Bochum, Germany, Sept. 1980.

38b. Viets, H., Ball, M., and Bougine, D., "Performance of Forced Unsteady Diffusers," AIAA Paper No. 0154, Aerospace Sciences Meeting, St. Louis, Mo., Jan. 1981.

39. Viets, H., Piatt, M. and Ball, M., "Forced Vortices Near A Wall," Proceedings of the U.S.-Germany Data Exchange Meeting, U.S. Naval Academy, Annapolis, Md., April 1980. Also AIAA Paper No. 81-0256, Aerospace Sciences Meeting, St. Louis, Mo., Jan. 1981.

40. Bethke, R.J. and Viets, H., "Data Analysis to Identify Coherent Flow Structures," AIAA Paper No. 80-1561, AIAA Atmospheric Flight Mechanics Conference, Danvers, Mass., Aug. 1980.

41. Quinn, B., "Effect of Acoustic Interactions on Ejector Performance," J. Aircraft, Vol. 12, No. 11, Nov. 1975, pp. 914-916.

42. Quinn, B., "Interactions Between Screech Tones and Ejector Performance," J. Aircraft, Vol. 14, No. 5, May 1977, pp. 467-473.

43. Viets, H., Campbell, J. and Korkan, K., "Acoustic Interactions in Ejectors," AIAA Paper No. 81-2045, AIAA 7th Aeroacoustic Conf., Palo Alto, Calif., Oct. 1981.
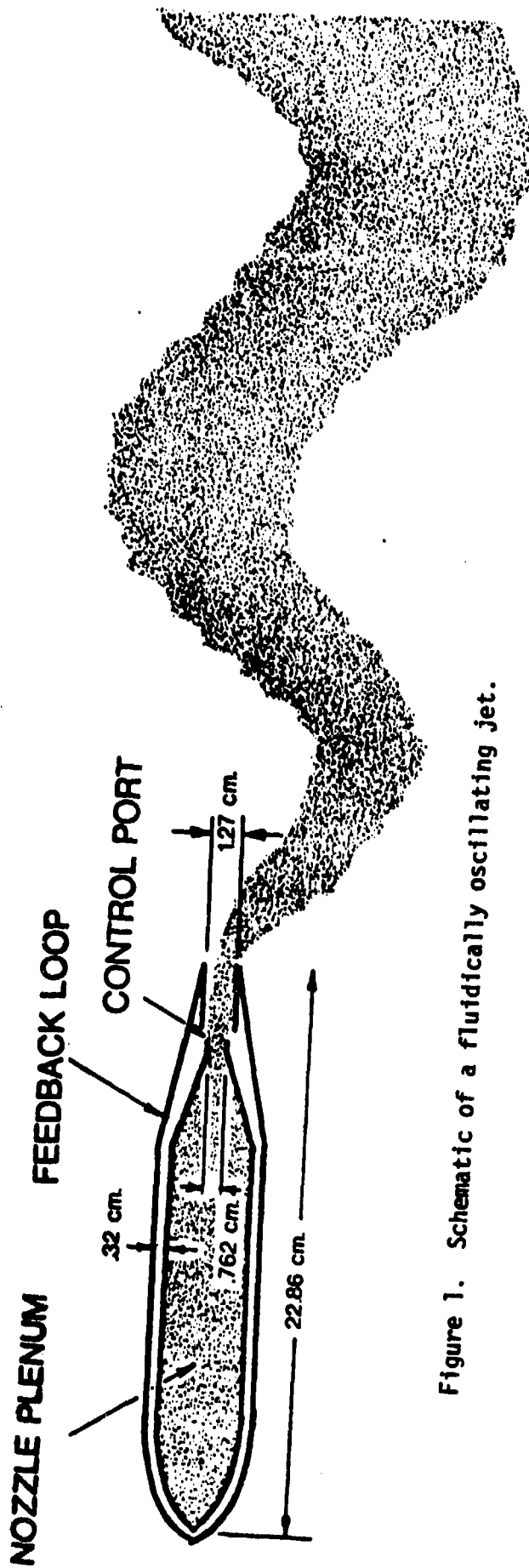
Figure 1. Schematic of a fluidically oscillating jet.

NOZZLE PLENUM

FEEDBACK LOOP

CONTROL PORT

.32 cm.

.762 cm.

22.86 cm.

.127 cm.
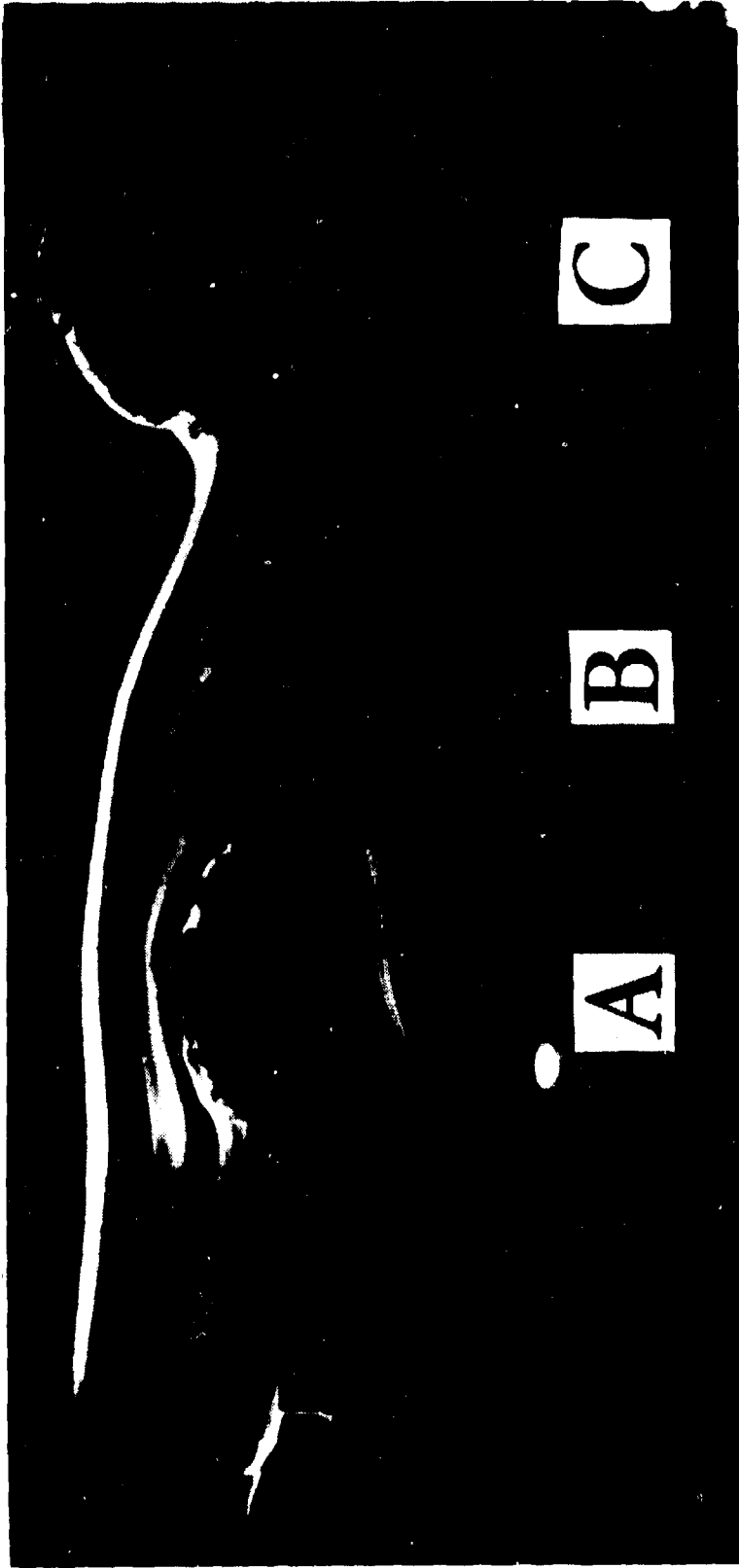
Figure 2. Smoke flow visualization of the oscillating jet in a coflowing stream of 28% of the jet velocity.
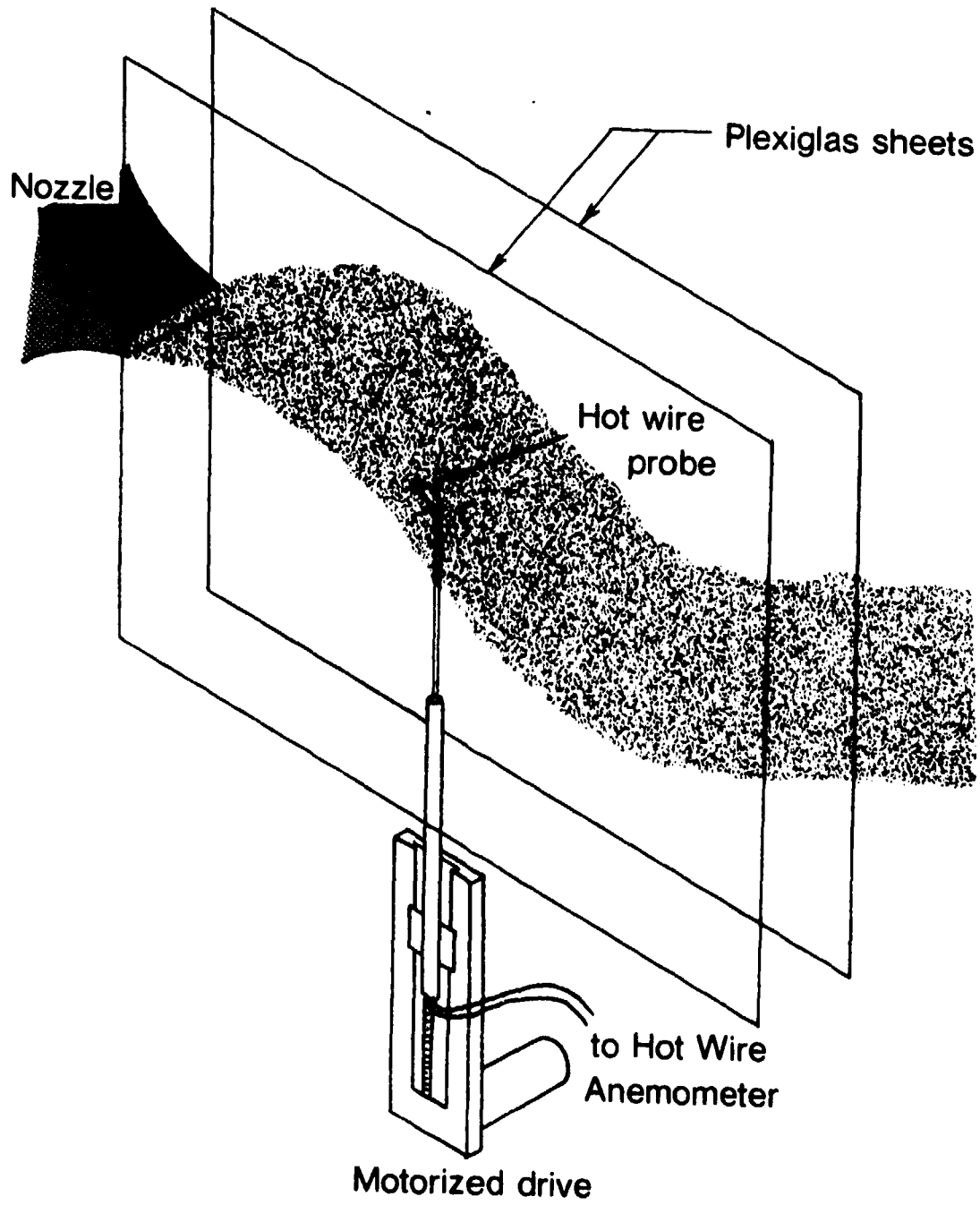
Figure 3. Experimental setup.
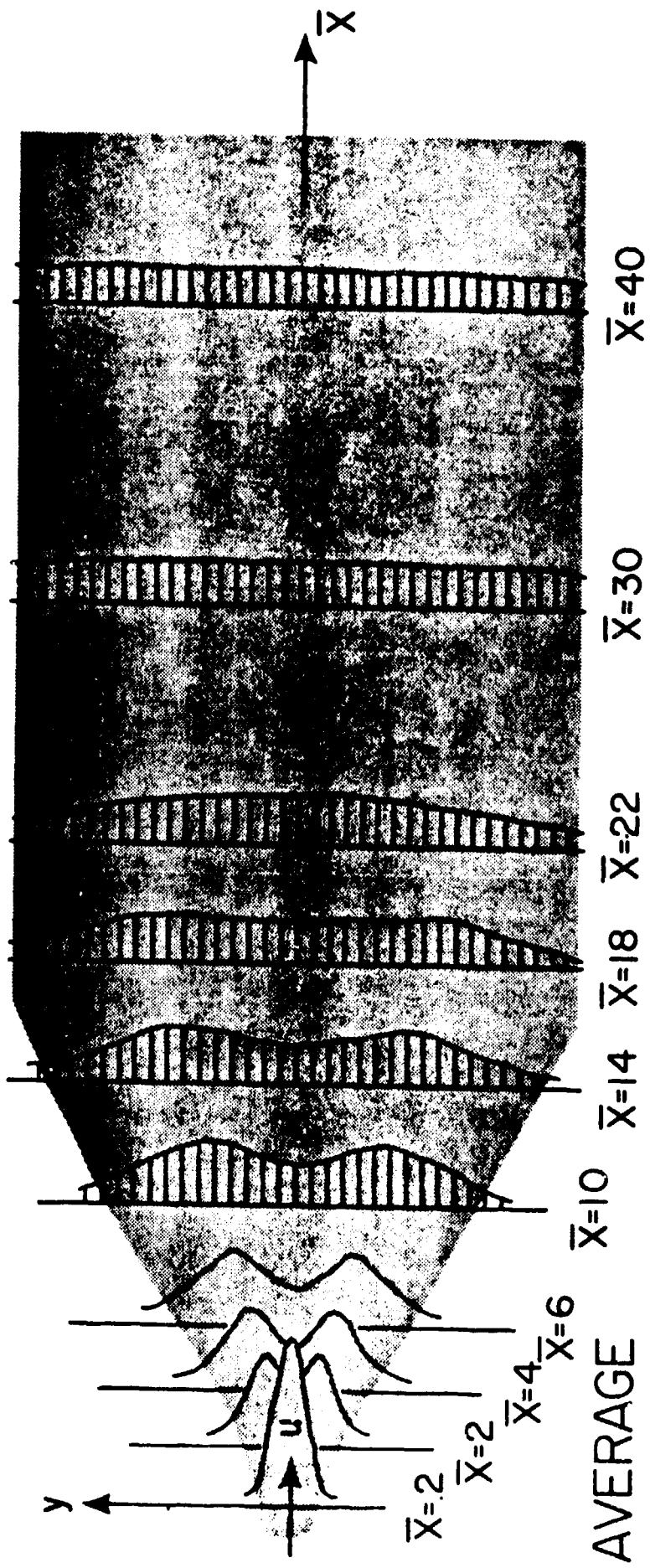
Figure 4. Composite view of the time average oscillating jet.

AVERAGE

$\bar{X}=2$ $\bar{X}=4$ $\bar{X}=6$ $\bar{X}=10$ $\bar{X}=14$ $\bar{X}=18$ $\bar{X}=22$ $\bar{X}=30$ $\bar{X}=40$
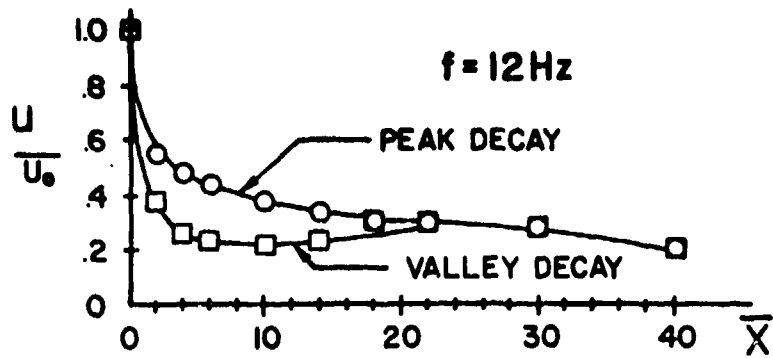
Centerline and peak velocity decay
in the time averaged oscillating jet.
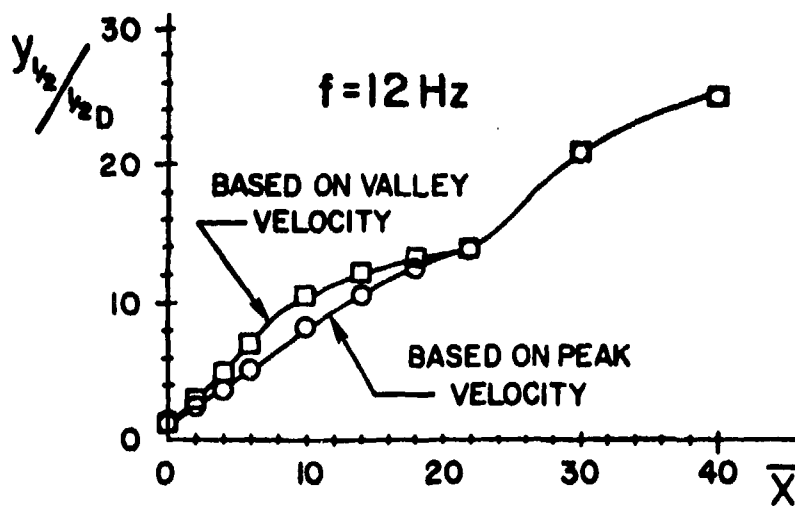


Figure 5. Half width growth in the time averaged oscillating jet

617
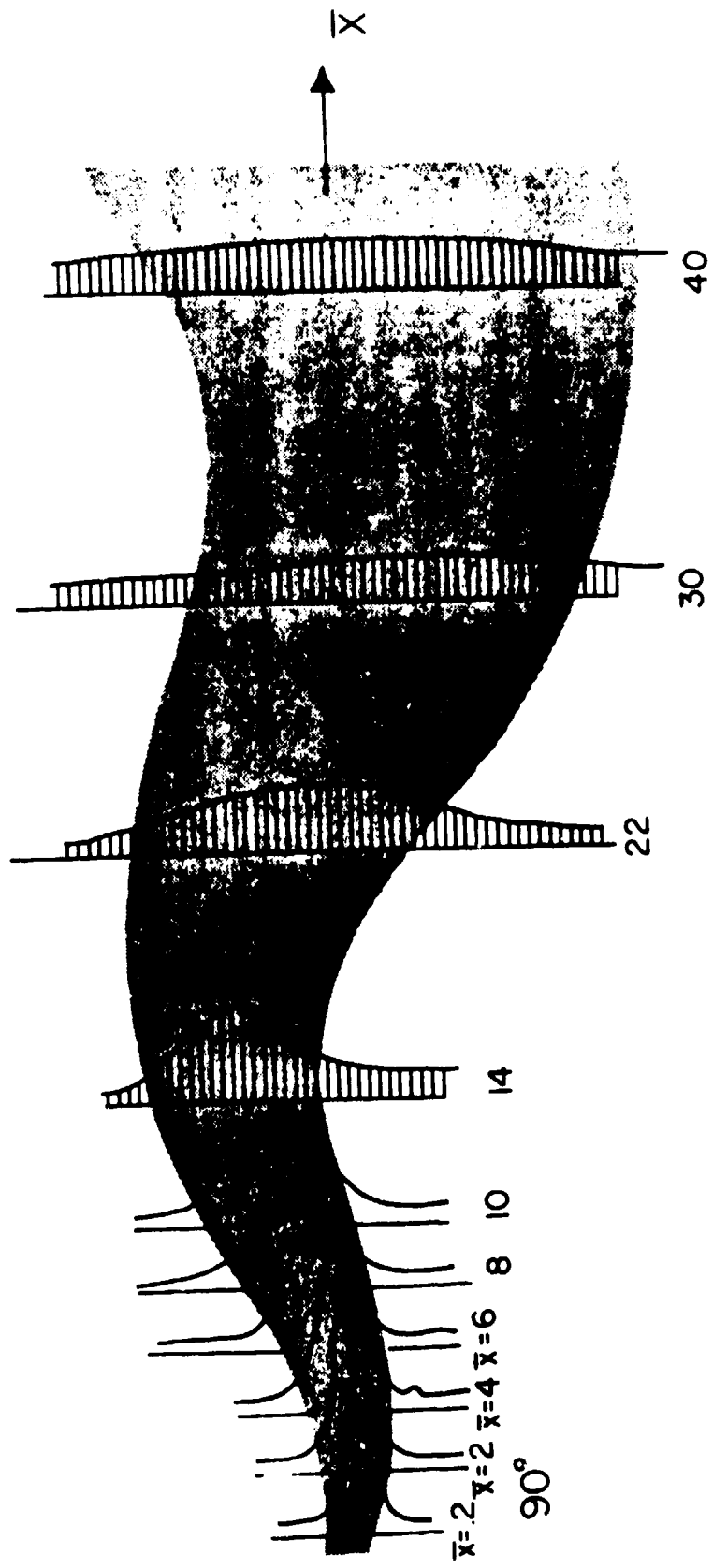
Figure 6. Composite of the instantaneous streamwise velocity profiles for f=12 Hz, θ=90°.
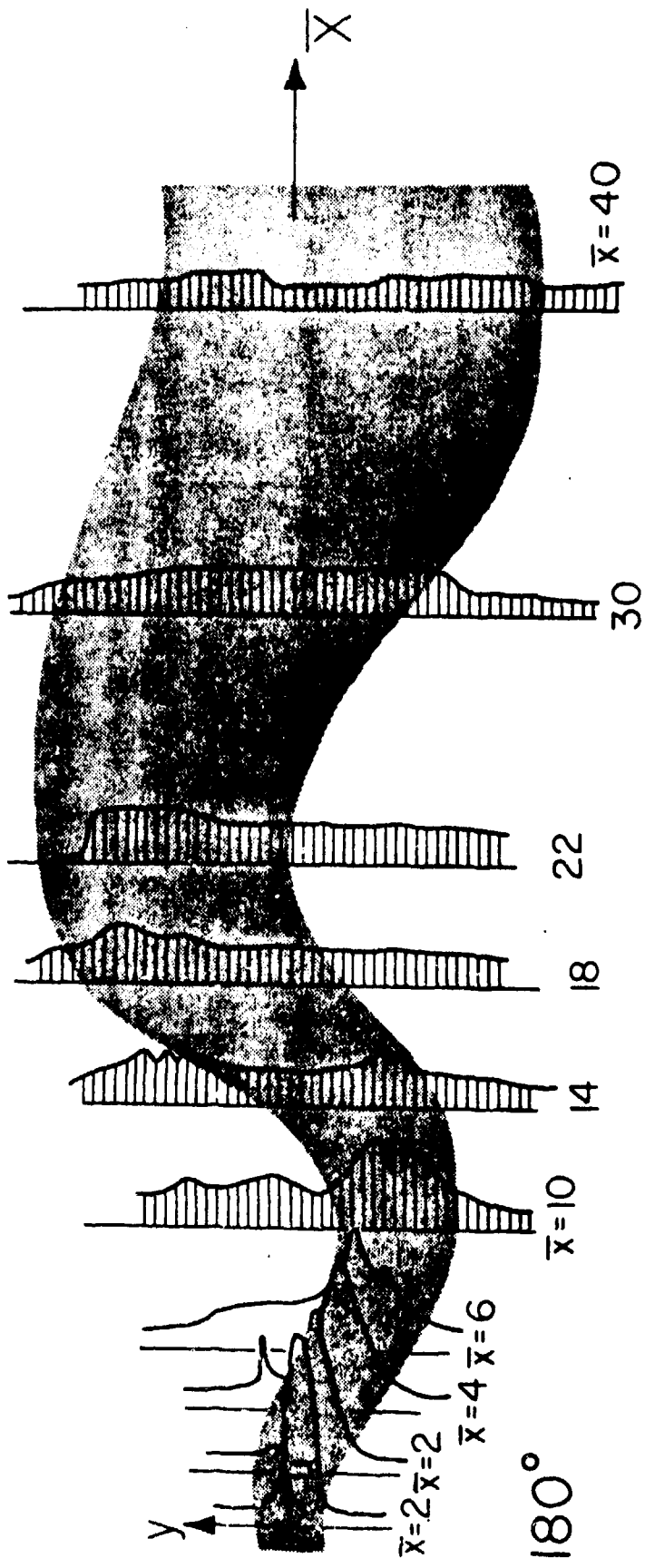
Figure 7. Composite of the instantaneous velocity profiles for f=12 Hz, θ=180°.
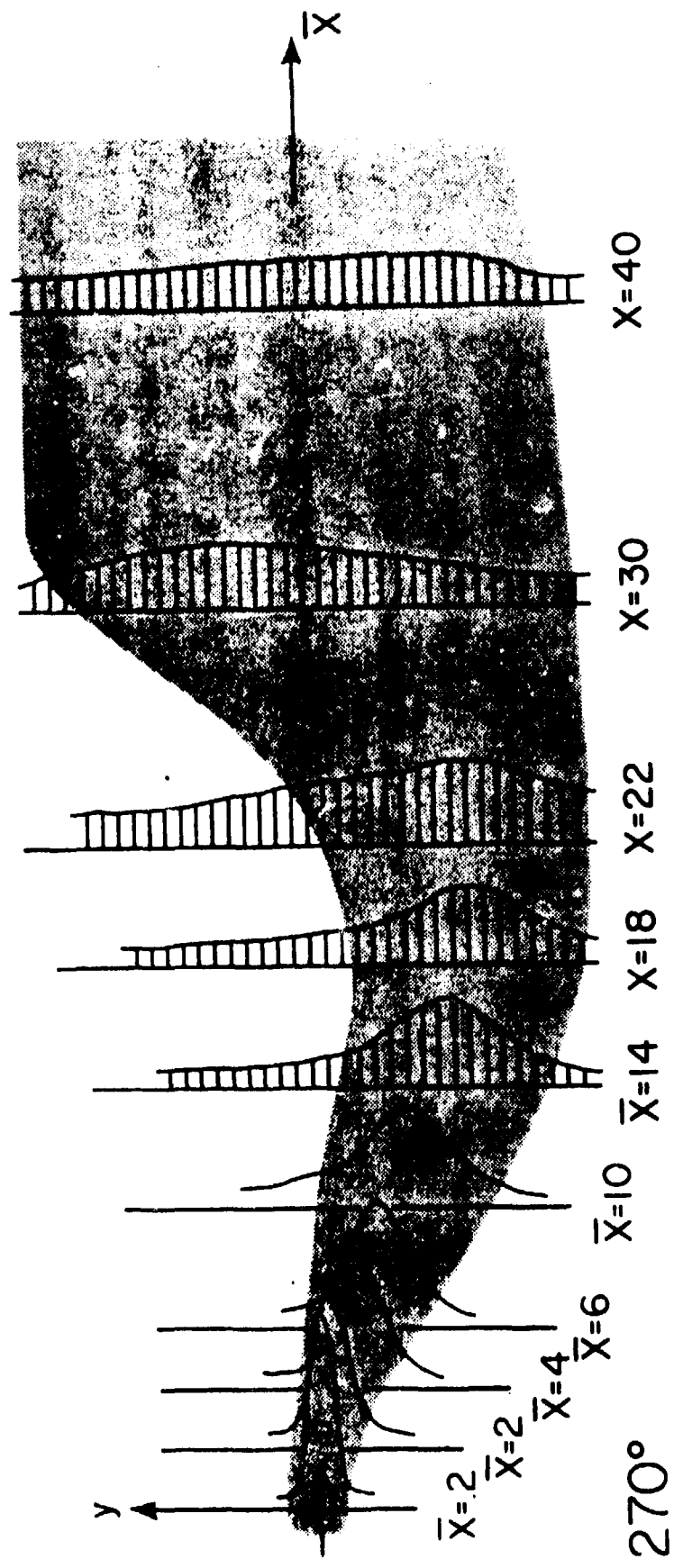
Figure 8. Composite of the instantaneous velocity profiles for f=12 Hz, θ=270°.
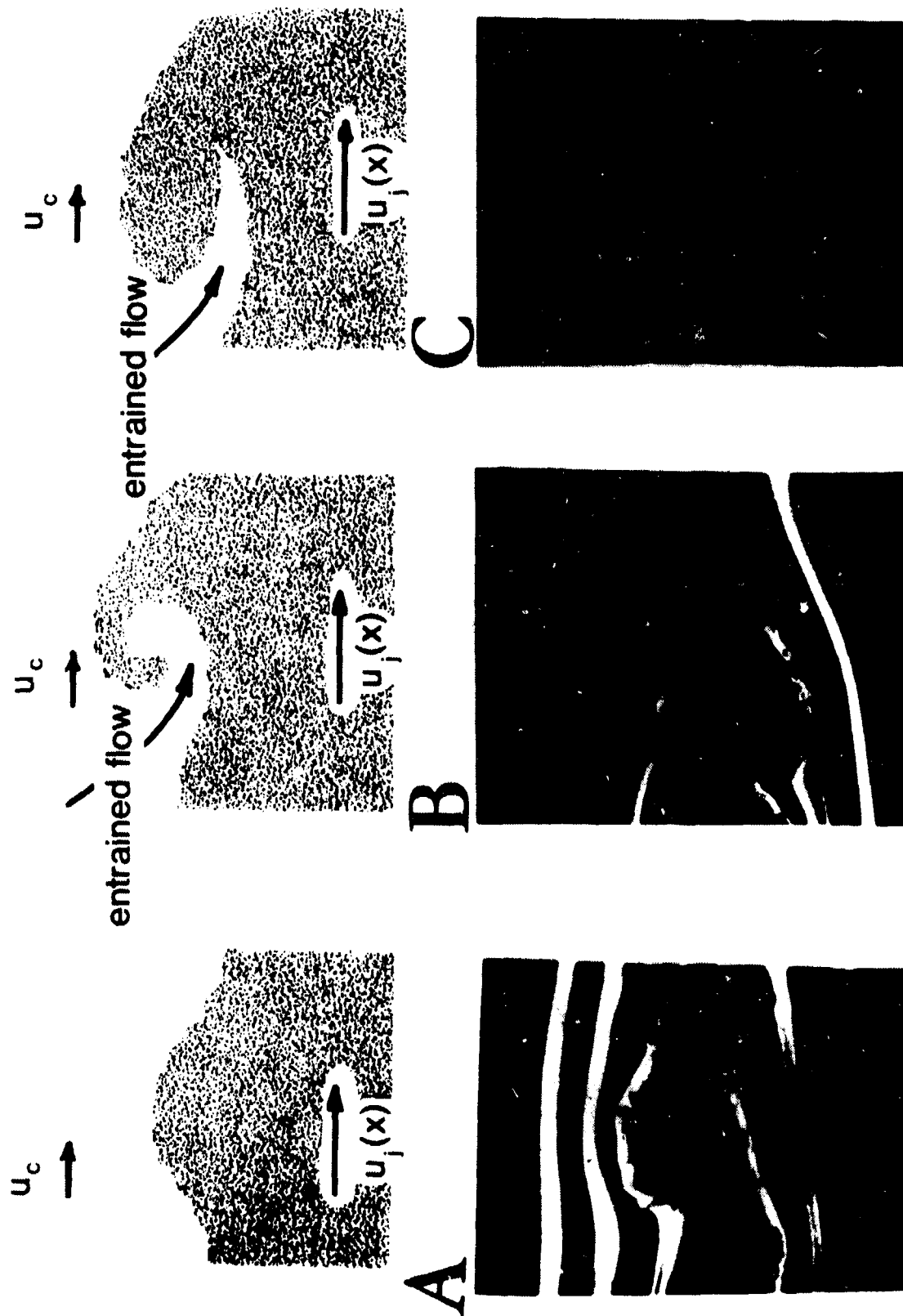
Figure 9. Evolution of the jet surface waves.
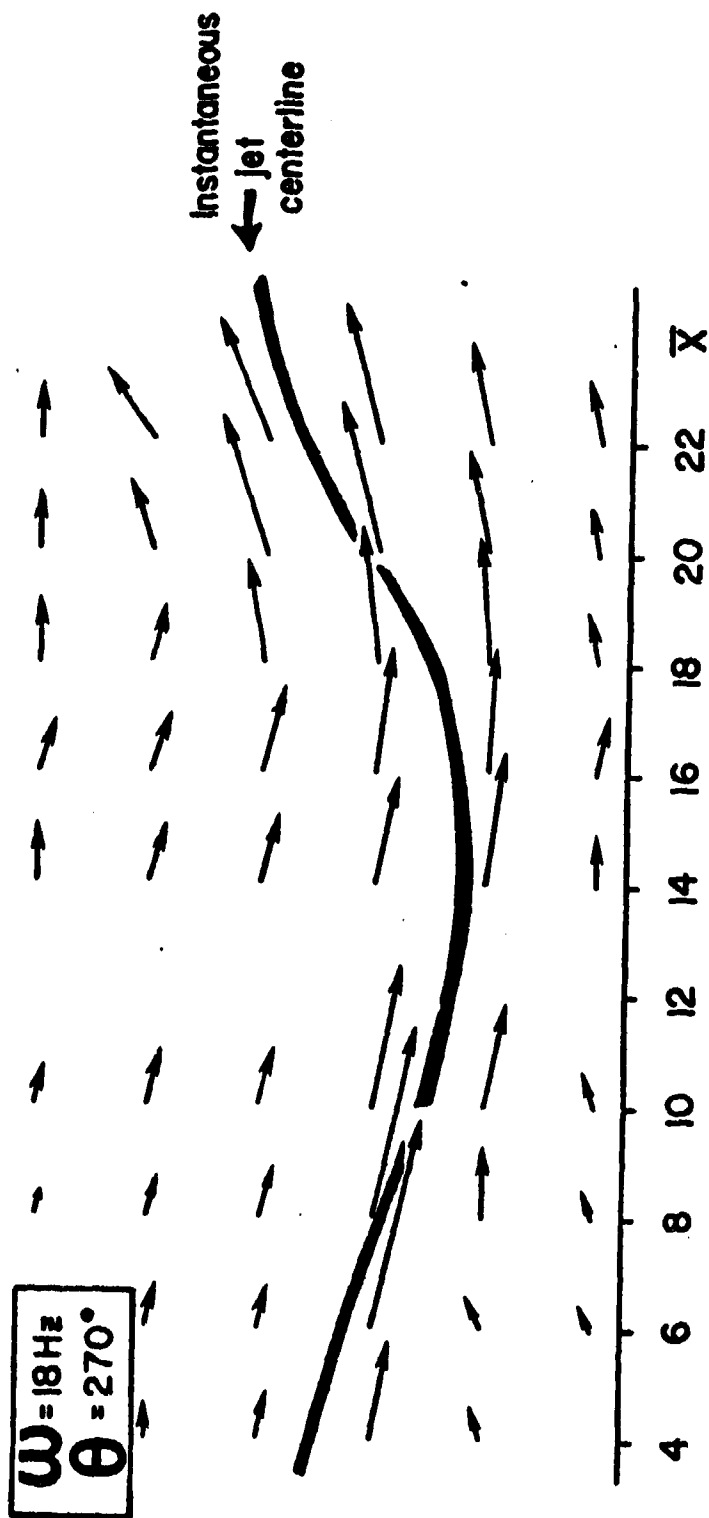
Figure 10α. Jet velocity field at a frequency ω=18 Hz and phase angle θ=270°.
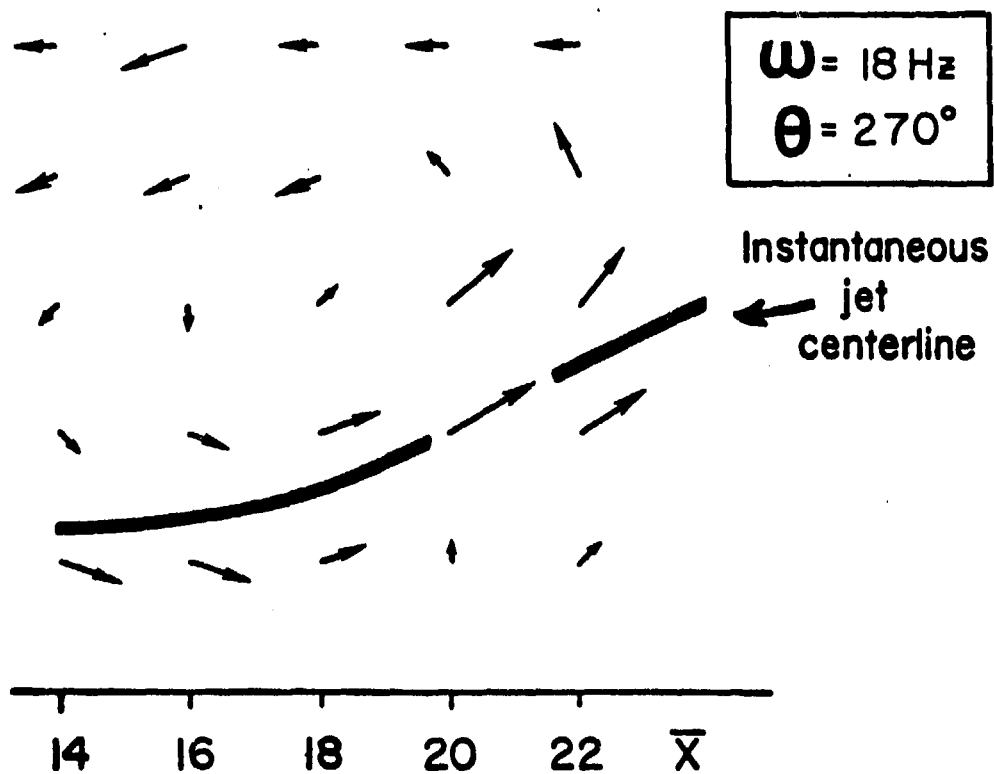
Figure 10b. Coherent structure of the jet seen in a moving coordinate system.
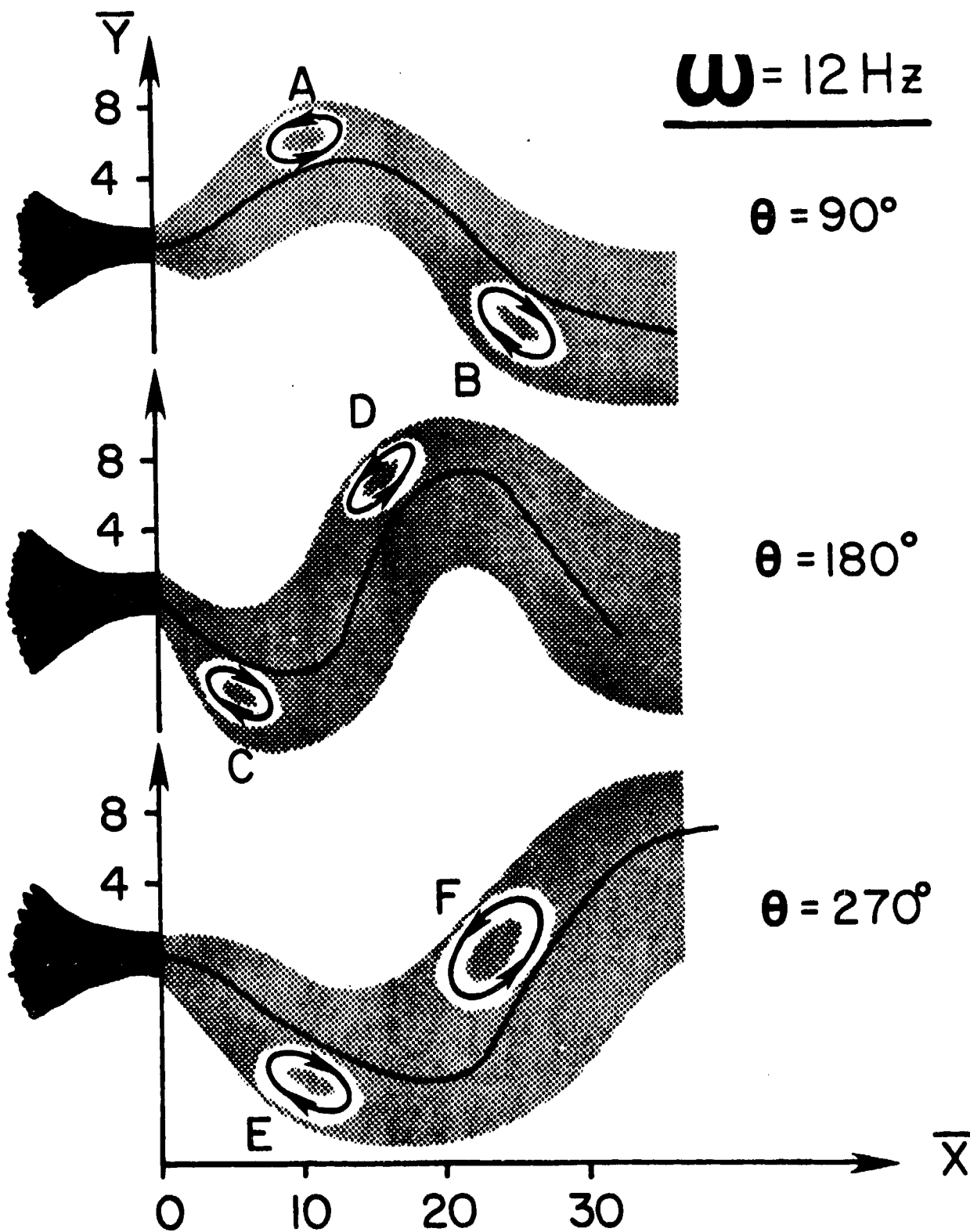
Figure 11. Anticipated vortex locations based on flow visualization results.
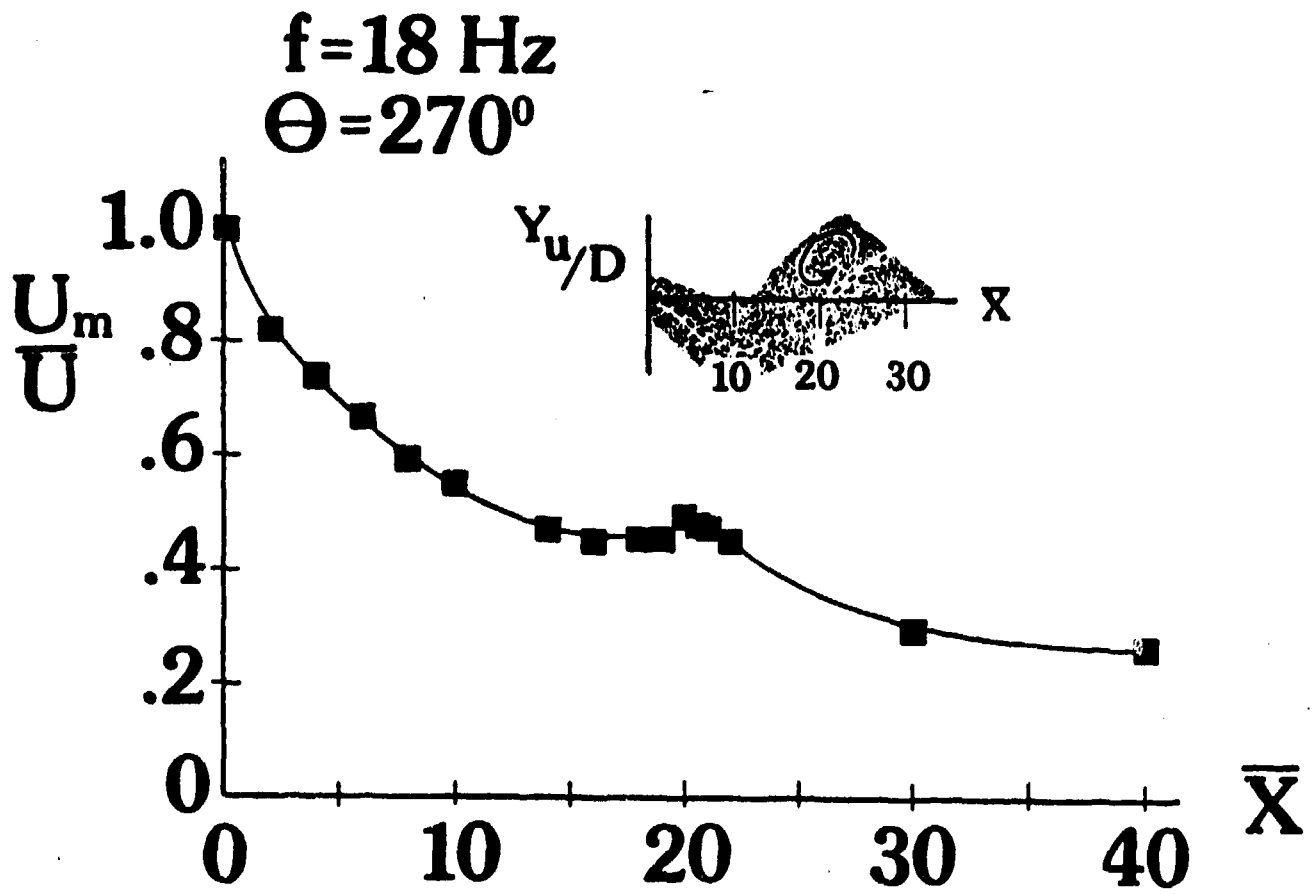
Figure 12. Effect of the vortex structure on the instantaneous jet velocity decay.
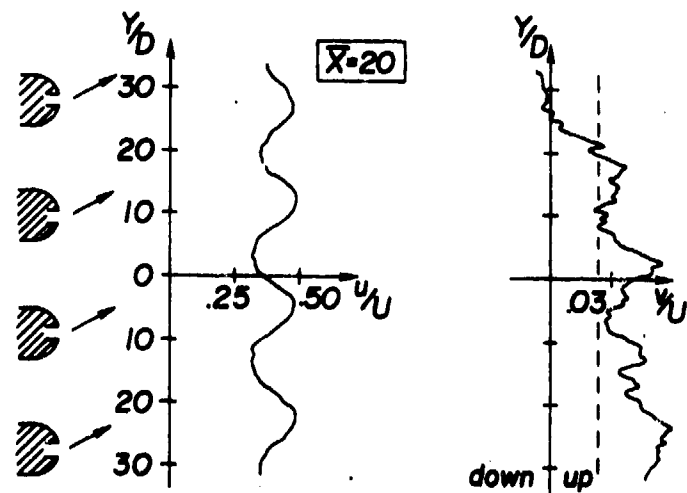
Figure 13. Flowfield at $\bar{X}$ = 20 for the in-phase configuration in the upward orientation.
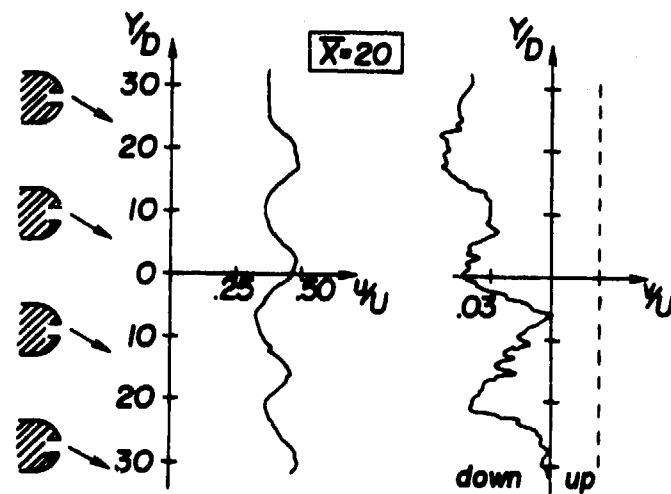


Figure 14. Flowfield at $\bar{X}$ = 20 for the in phase configuration in the downward orientation.

626
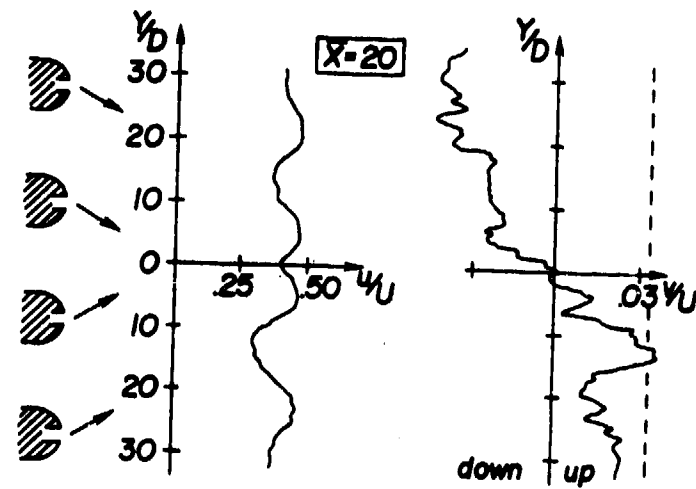
Figure 15. Flowfield at $\bar{X}$ = 20 for the out of phase configuration and an inward orientation.
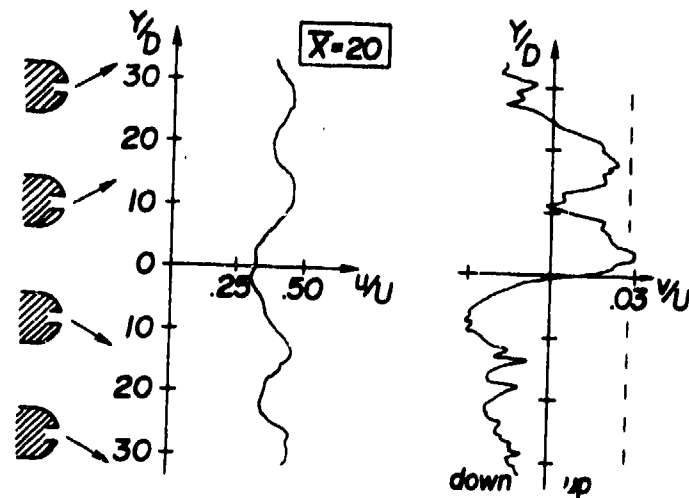


Figure 16. Flowfield at $\bar{X}$ = 20 for the out of phase configuration and an outward orientation.

$$\alpha = \alpha_0 + \alpha' \sin \omega t$$

a.

b.
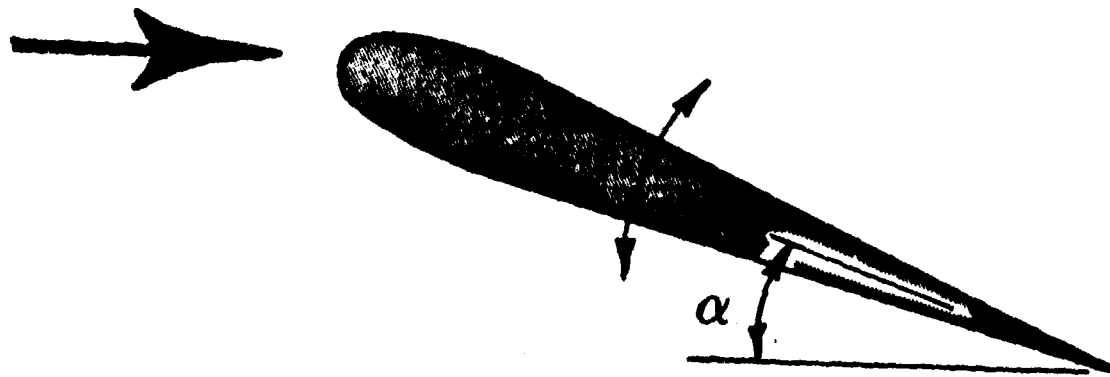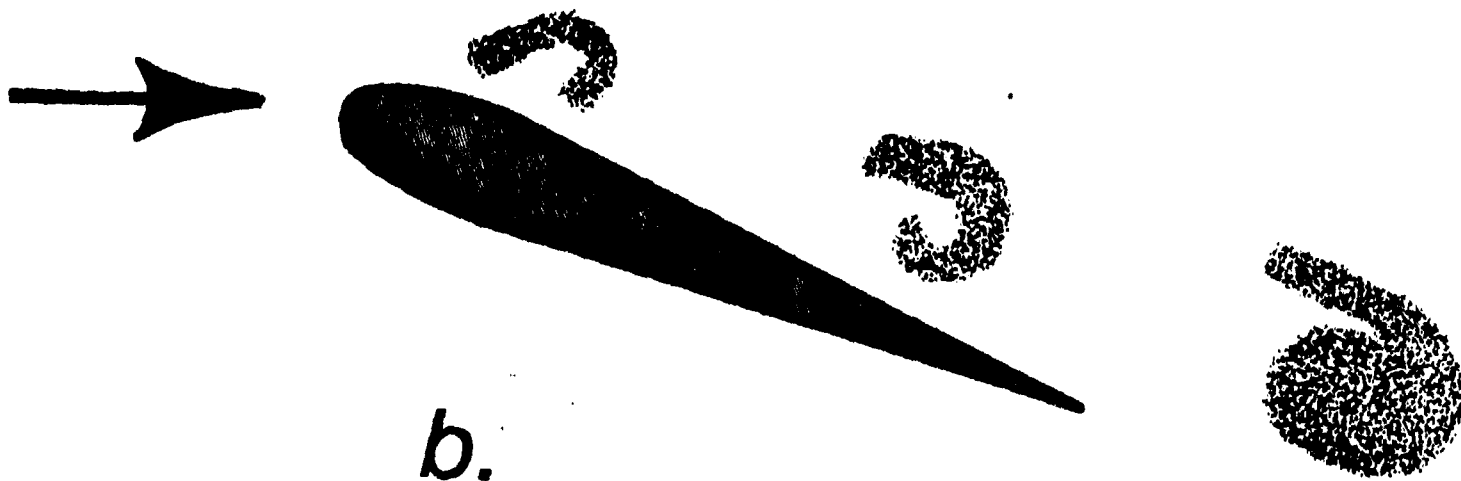
Figure 17. Geometry and Flowfield of an Oscillating Airfoil.
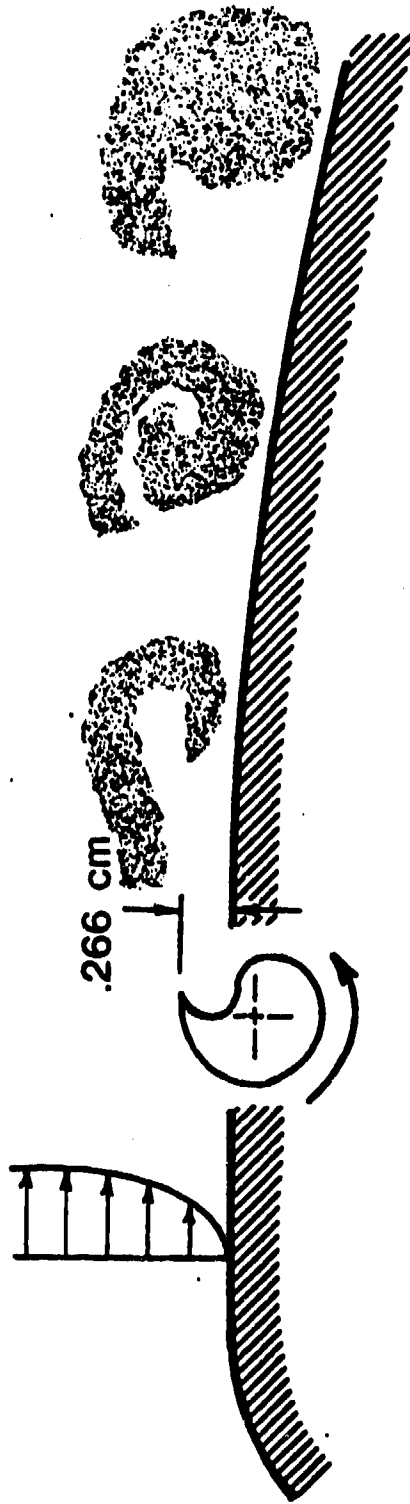
Figure 18. Vortex Generation by an Embedded Rotor.

.266 cm

**a.** $\omega=0$
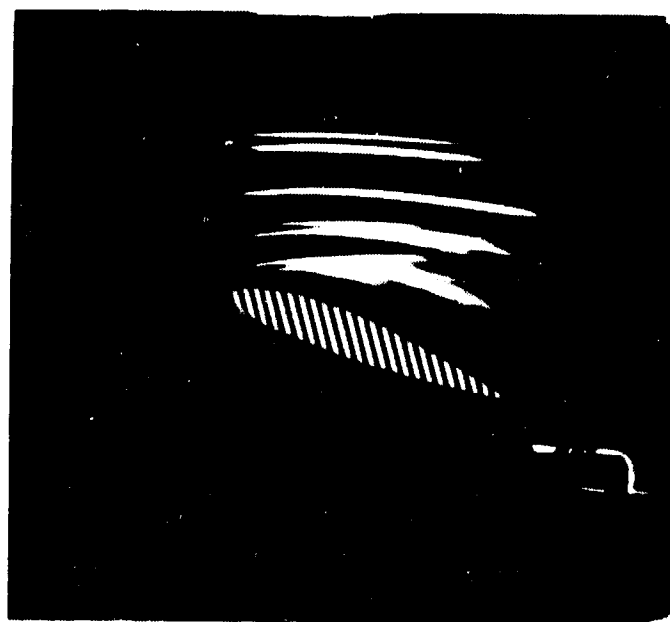


**b.** $\omega=2400$

Figure 19. Flow Visualization of the Flow Structure at $\alpha = 20°$.
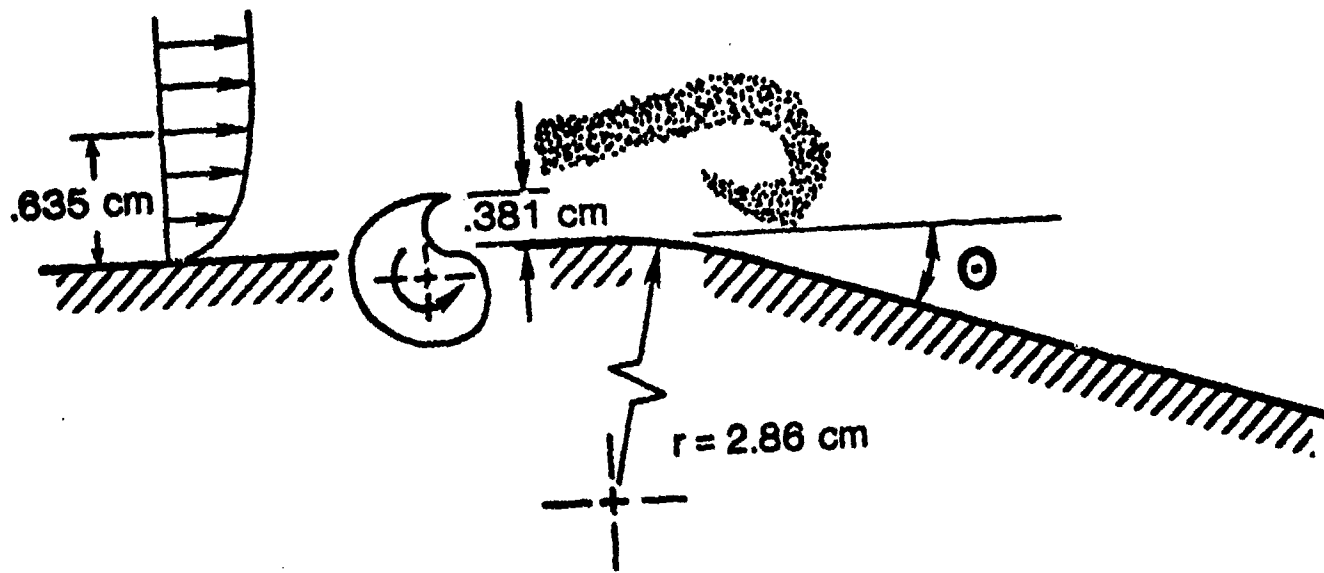
Figure 20a.  Unsteady Ramp Flow Configuration
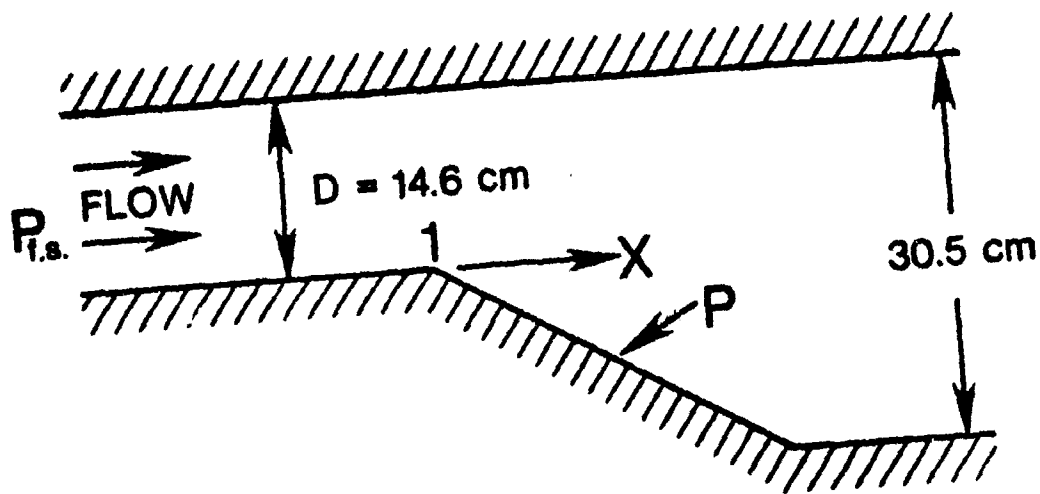


Figure 20b.  Tunnel Geometry

631
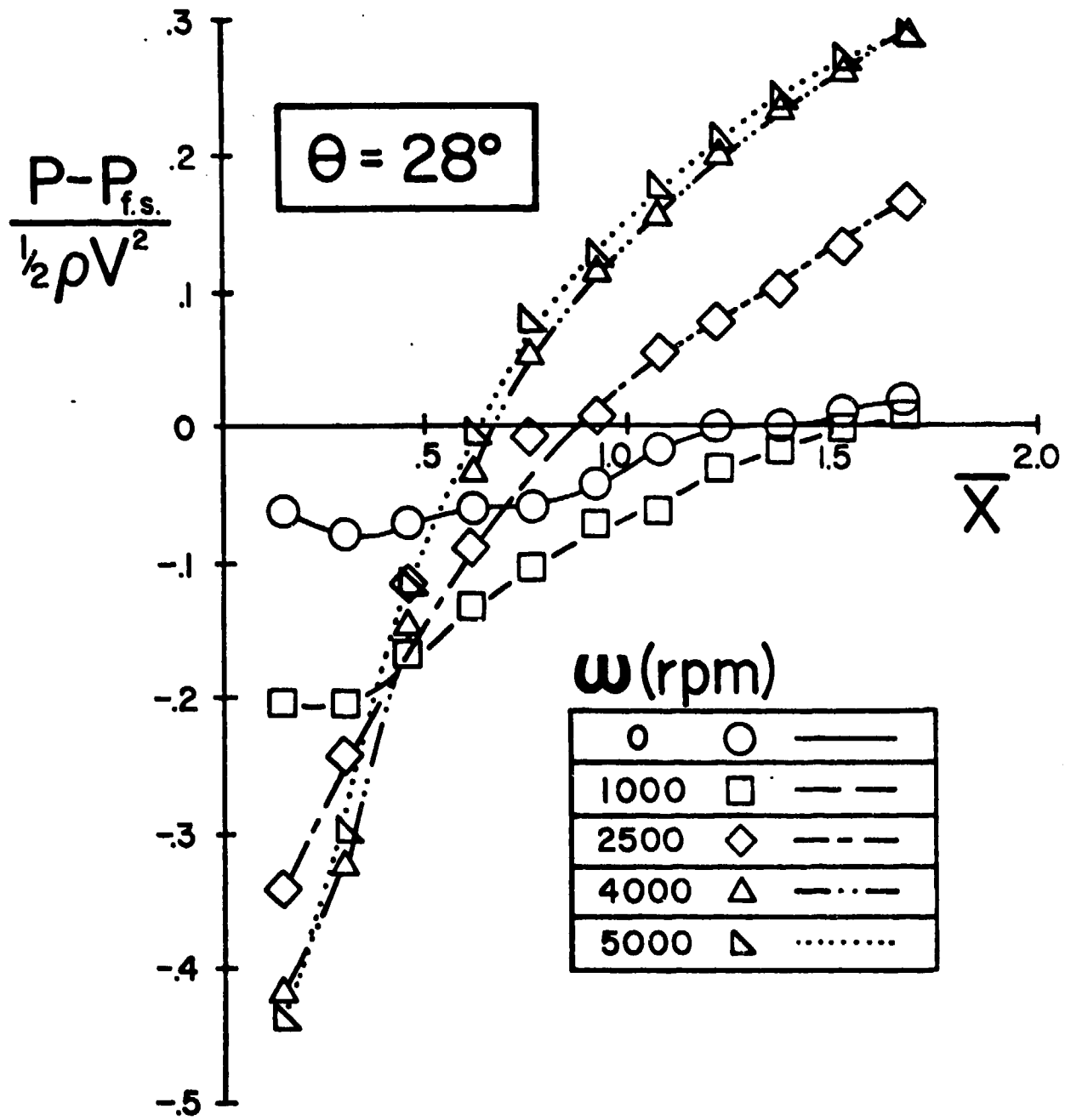
Figure 21. Pressure Distribution on the Ramp for
θ = 28°.

Figure 22. Time averaged Flow for $\theta = 28°$.

633
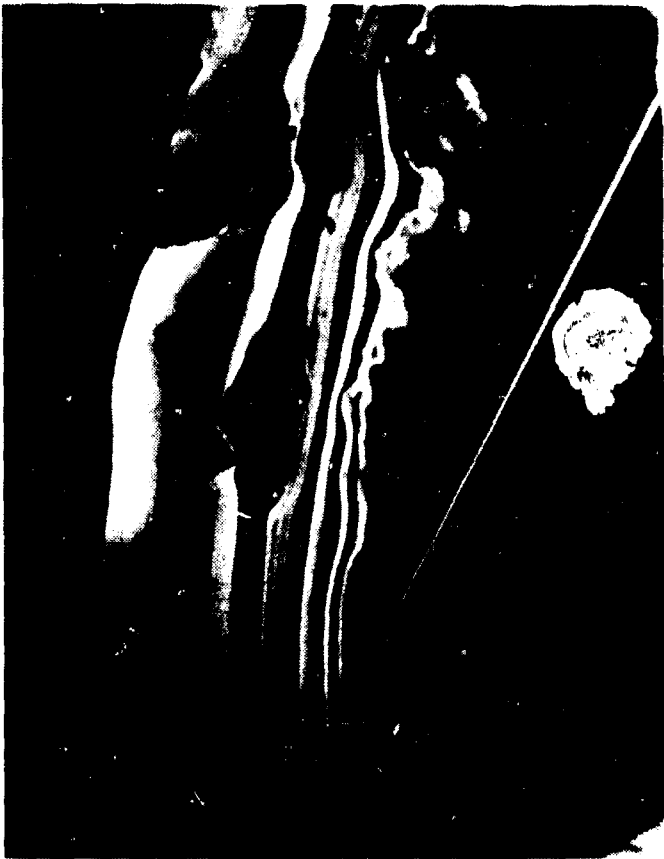
Figure 23 Instantaneous Streakline Photographs for Various Ro' ⌐ Speeds at θ = 28°.

e.

f.

d.

Figure 23. Continued

635

$$\bar{x} = x/h$$

$$\bar{h} = h/d$$

d

h

x

a.

.381cm

.953cm

.478cm

b.
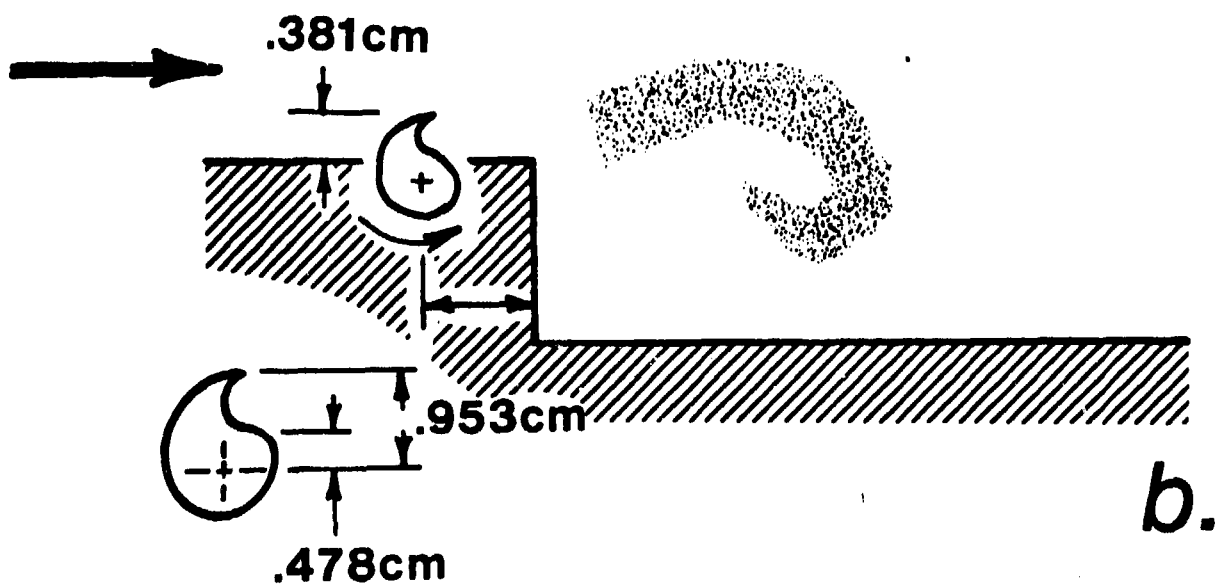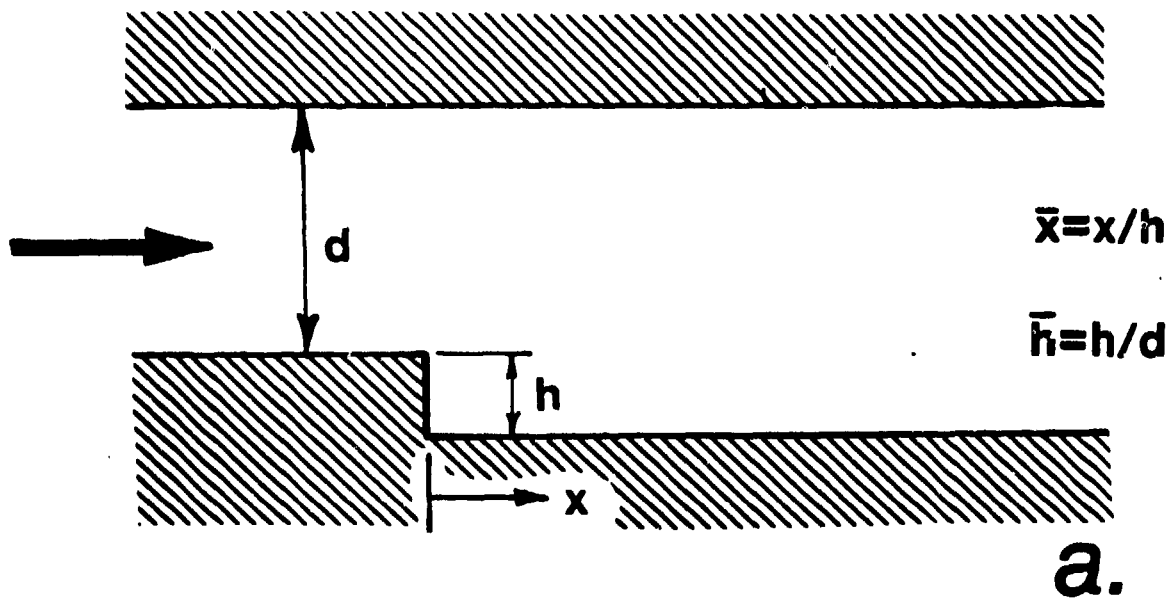
Figure 24. Experimental Geometry and Rotor Flowfield.

636
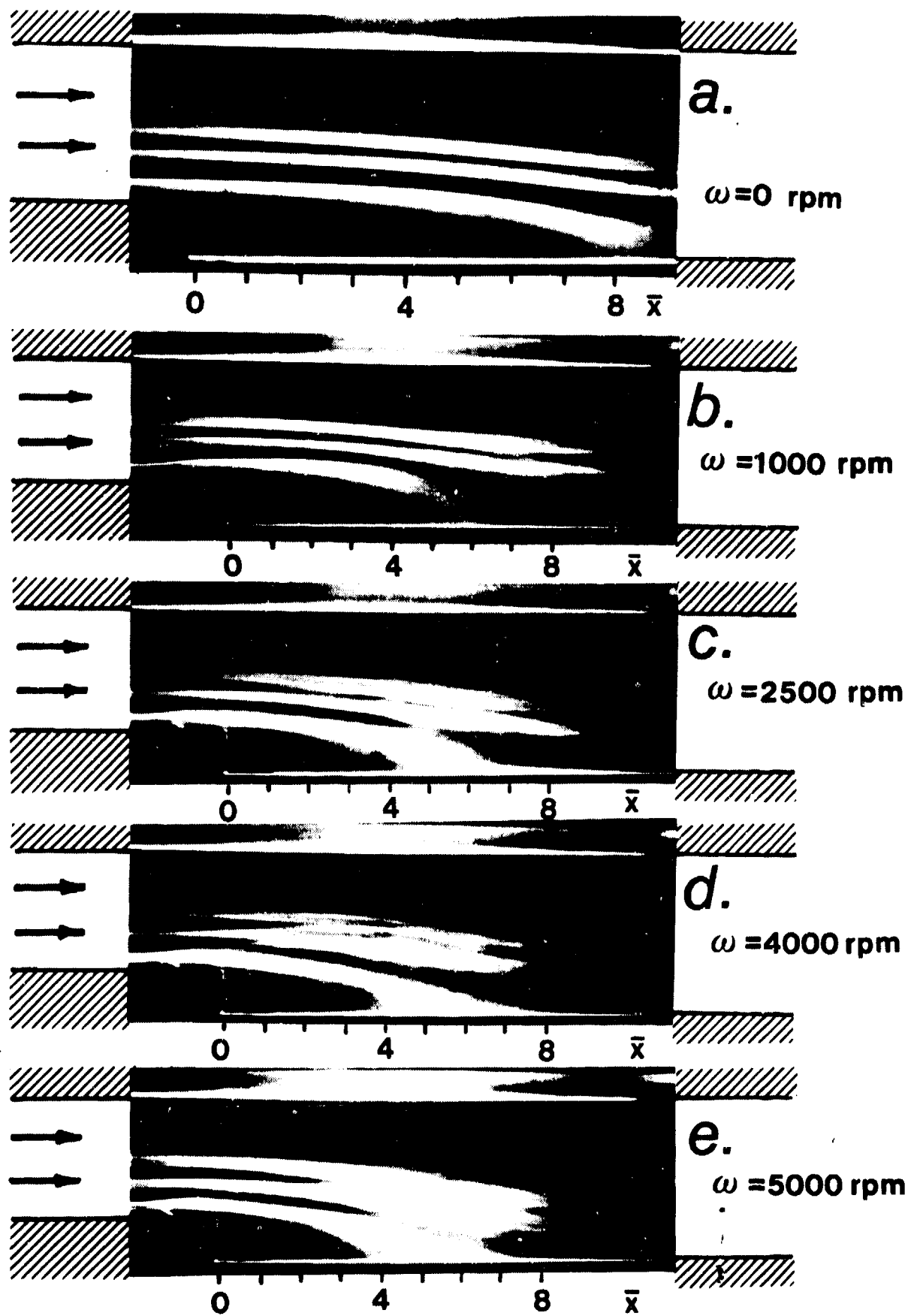
Figure 25. Streamline Shapes for Various Rotor Speeds, $\bar{h} = 1/3$.
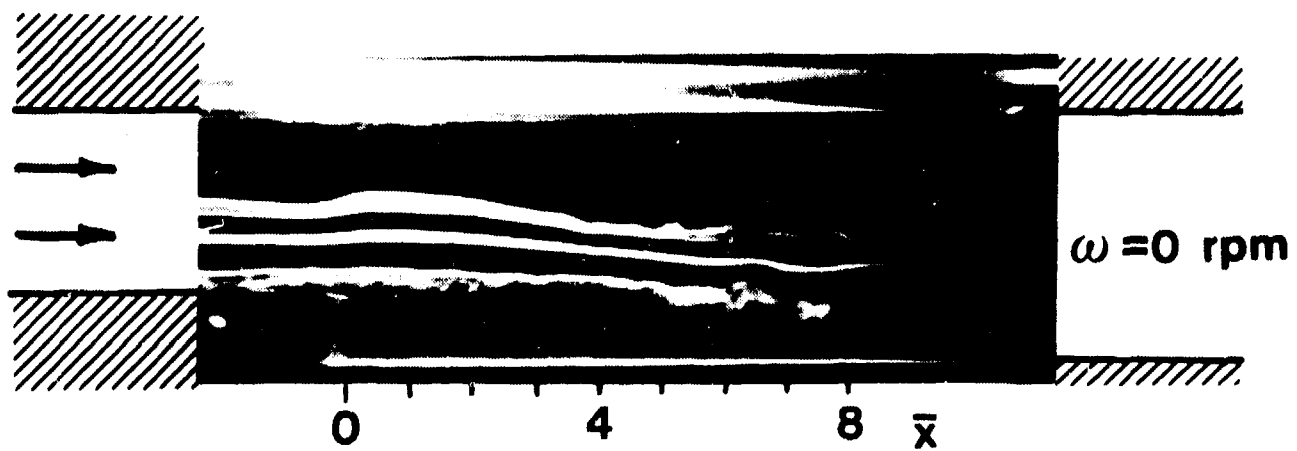
Figure 26. Instantaneous Streaklines for
$\omega = 0$, $\bar{h} = 1/3$.

a. ω =2500rpm

b. ω =2500rpm
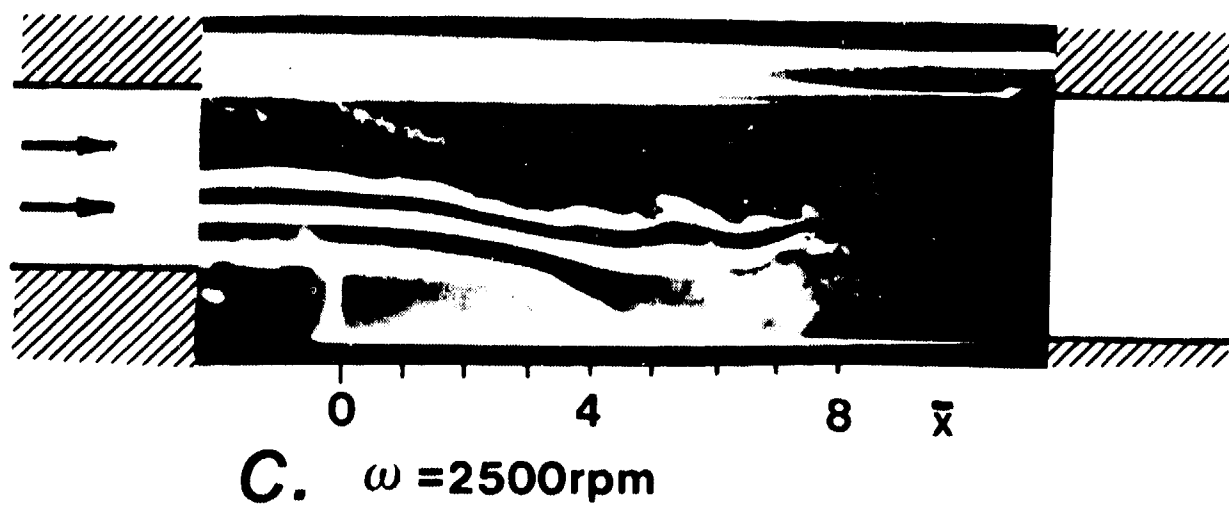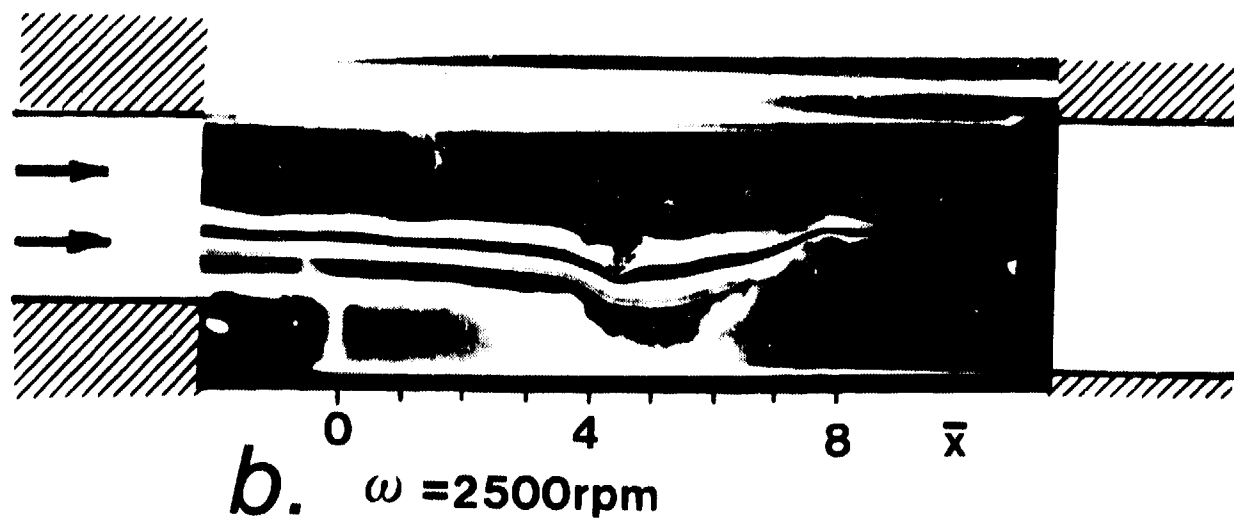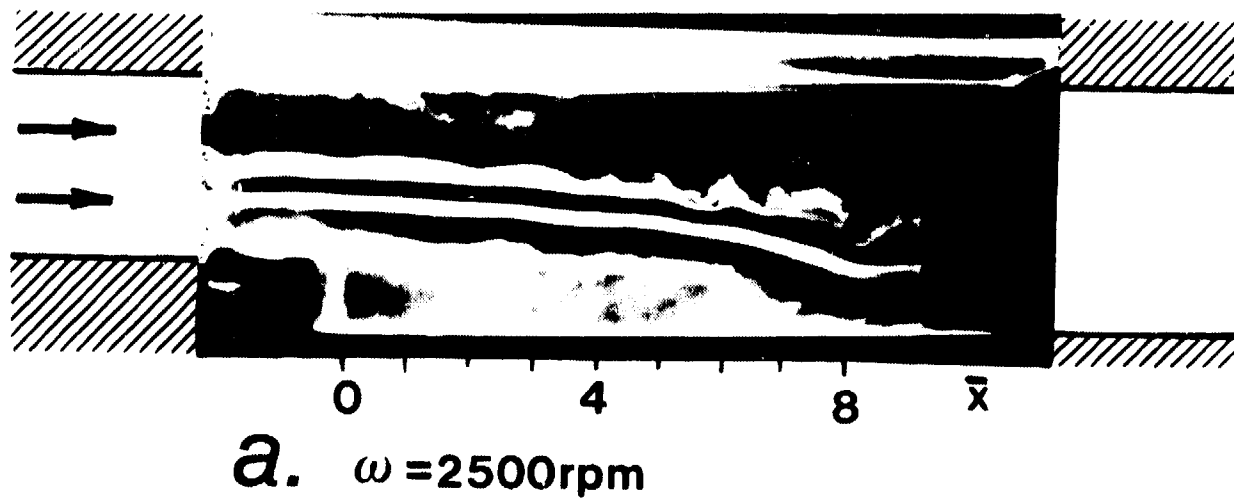
c. ω =2500rpm

Figure 27. Streaklines at Three Different Instants,
ω = 2500 rpm, h̄ = 1/3.

639
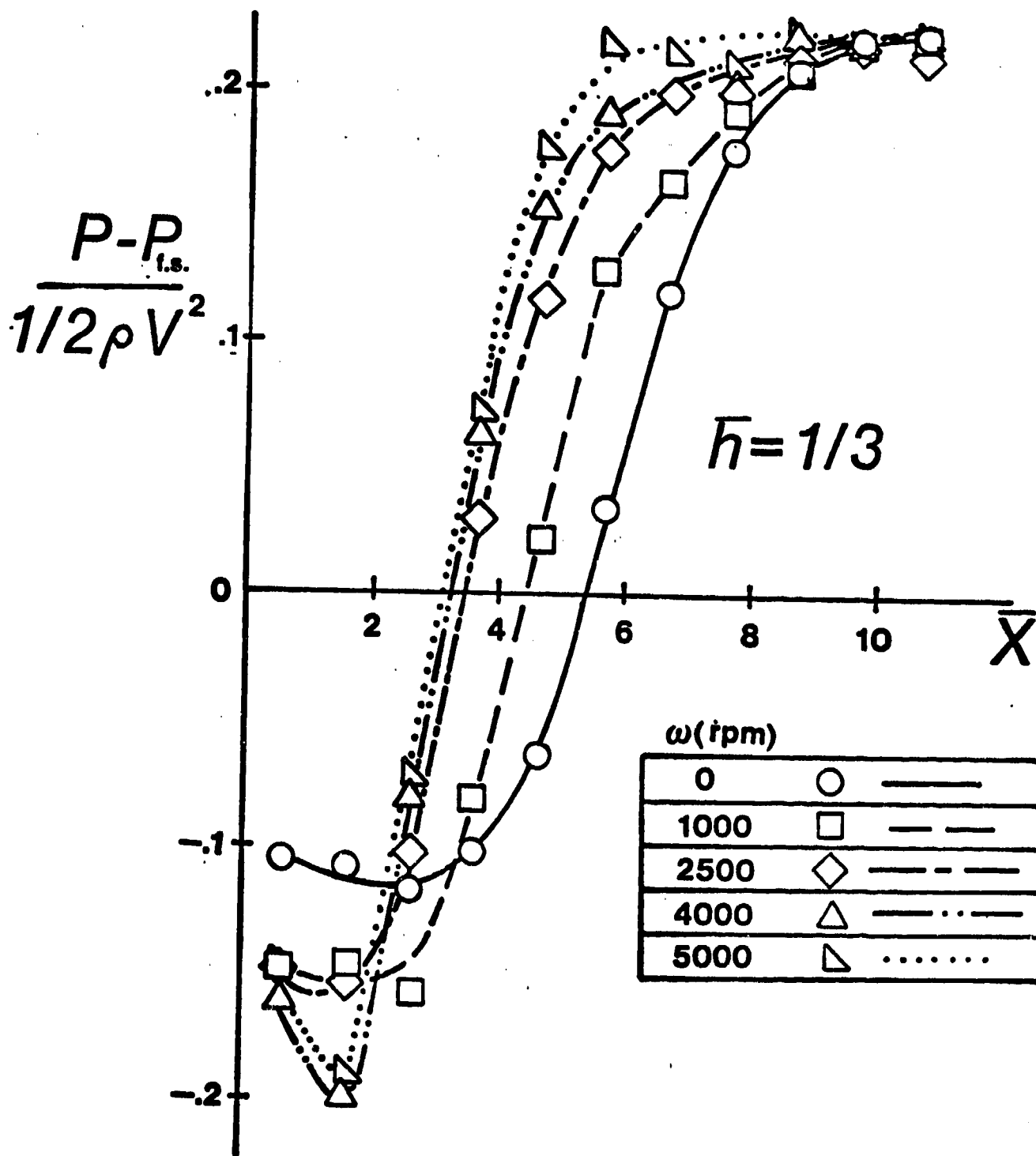
Figure 28. Pressure Distribution Downstream of the Dump Station; $\bar{h} = 1/3$, Various Rotor Speeds.

(a) In Phase
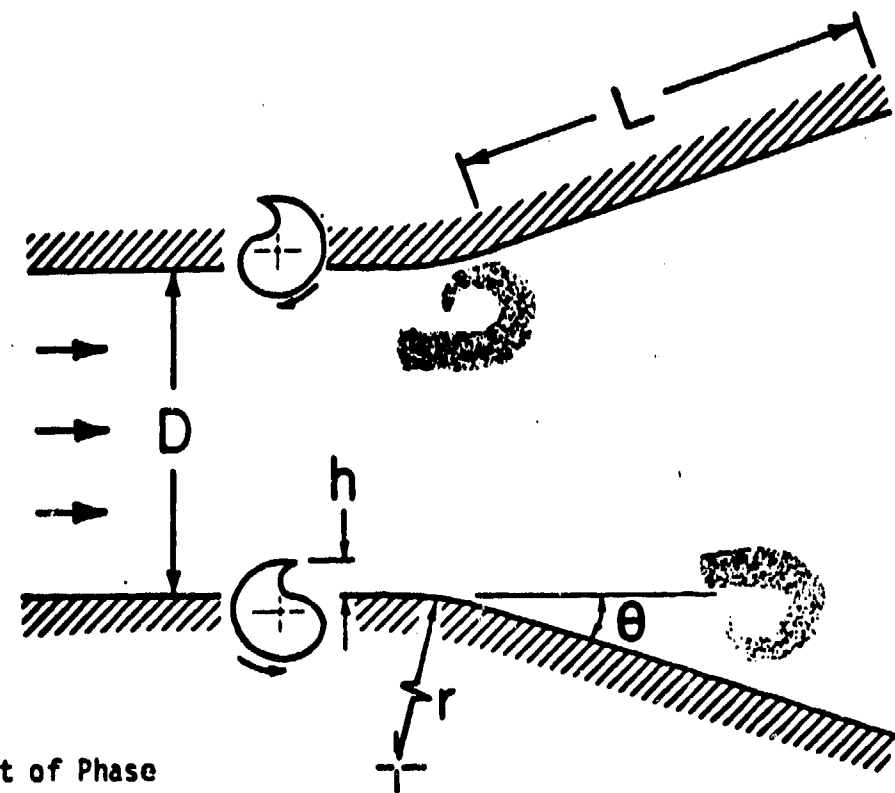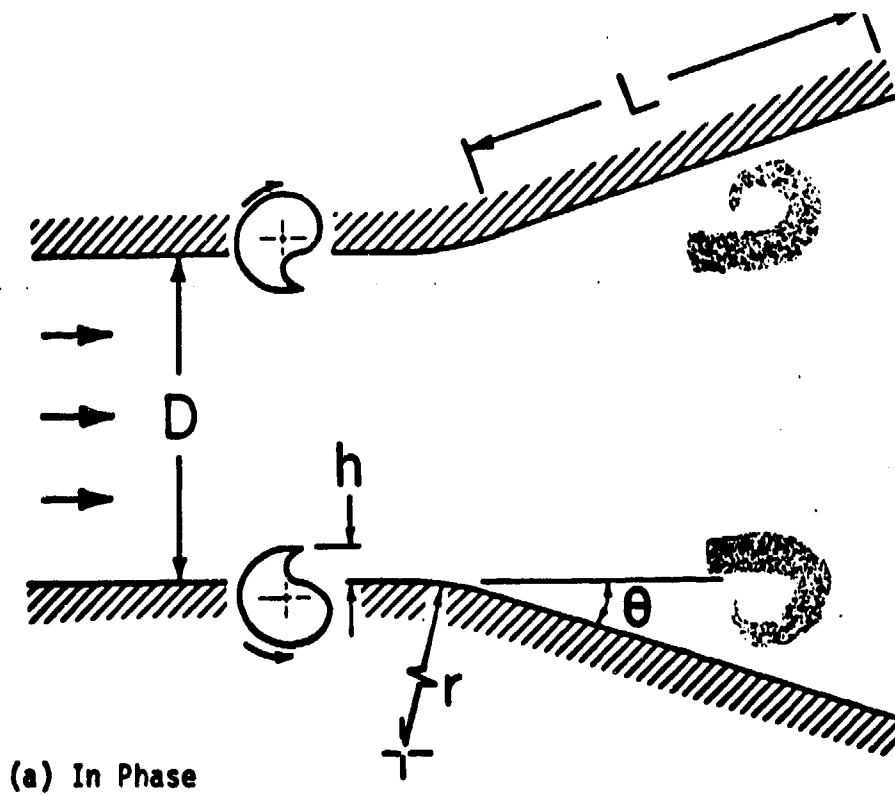
(b) Out of Phase

Figure 29.   In phase and out of phase rotor orientations.
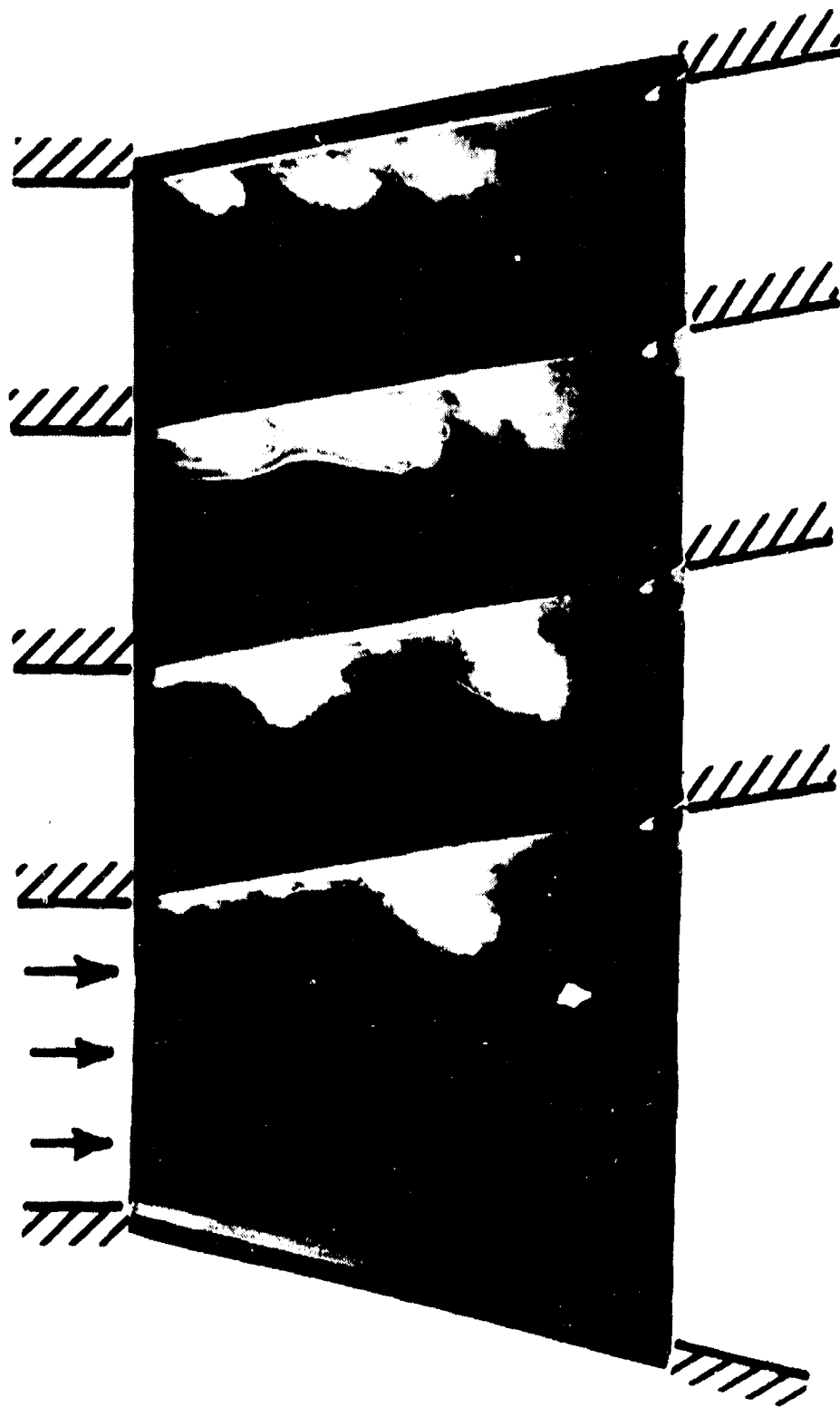
Figure 30. Multiple vortices produced in the diffuser by increasing the speed of the rotor.
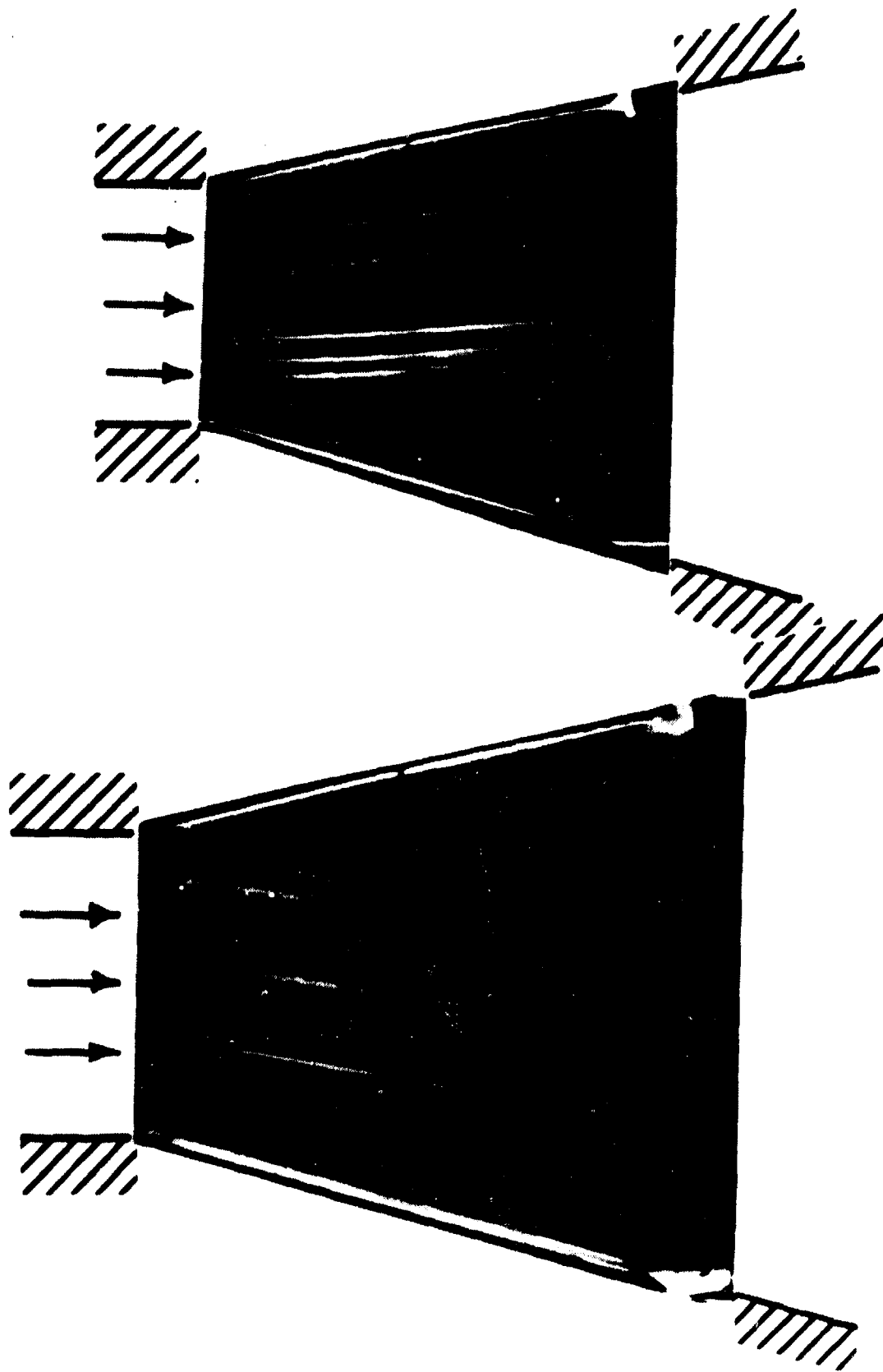
Figure 31. Longer exposure streamline photographs for
$2\Theta = 30°$. (a). Separation at the bottom
for $\bar{\omega} = 0$ (b). Weaker separation at the top
for $\bar{\omega} = 11.84$ (both in phase)
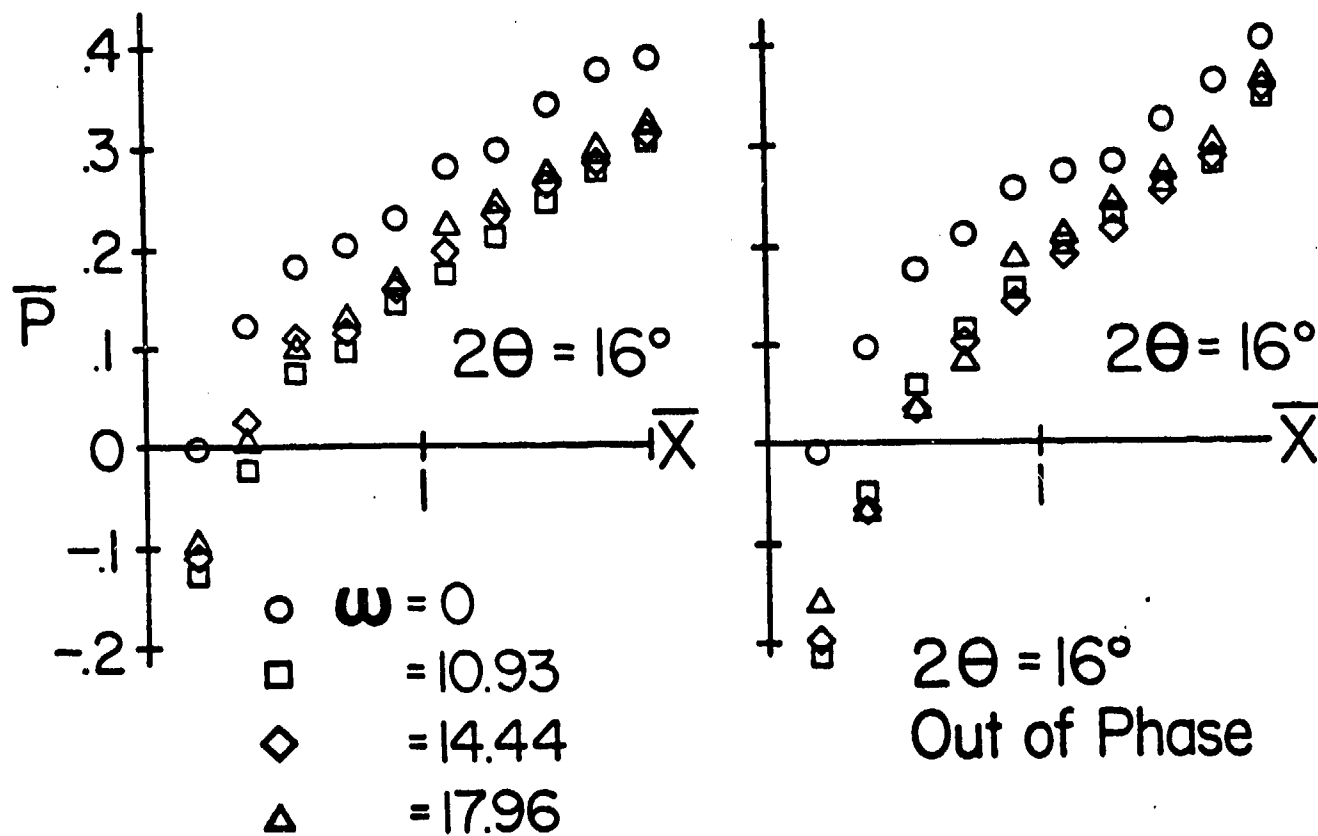
Figure 32. Pressure rise through the diffuser for 2θ=16 and various rotor speeds, out of phase.
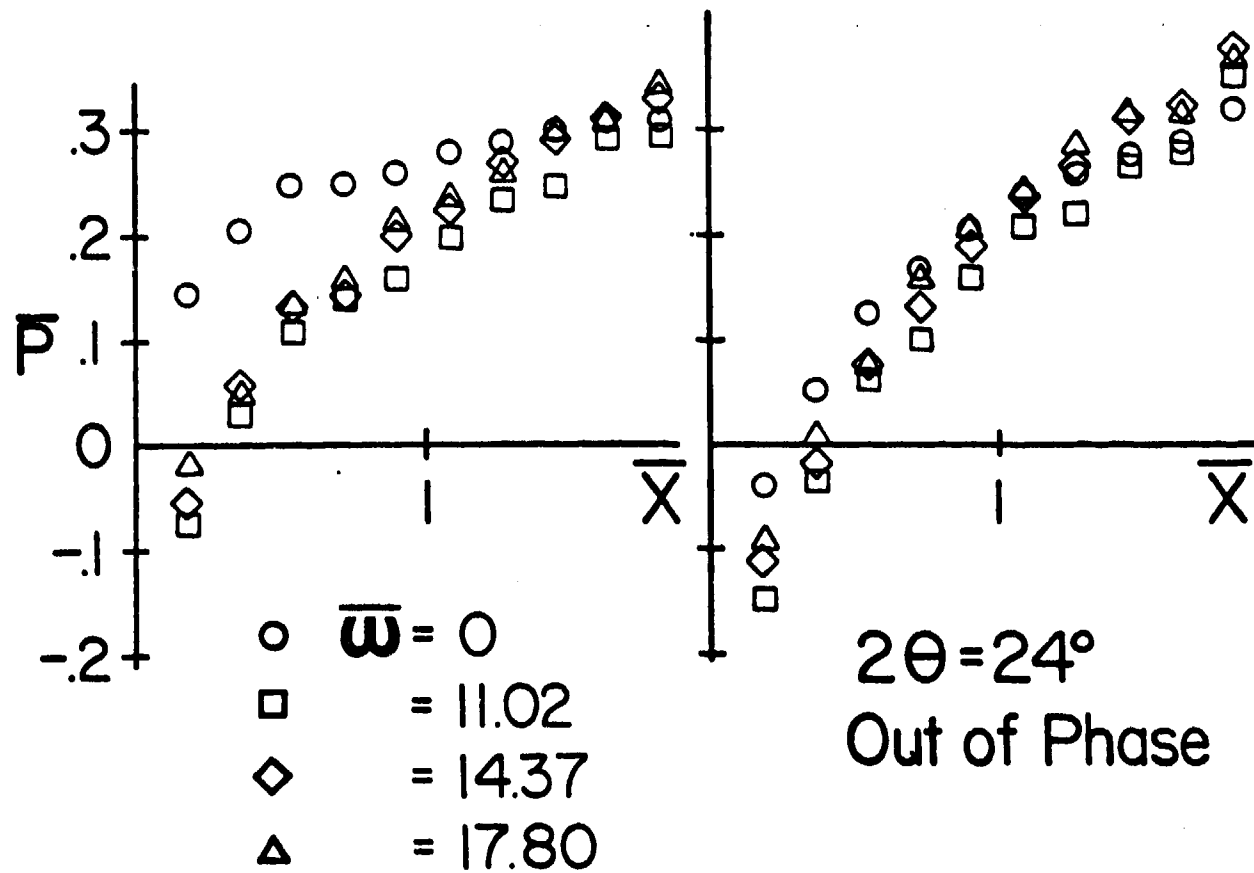
Figure 33. Pressure rise for larger angle diffuser, 2θ = 24°, out of phase.
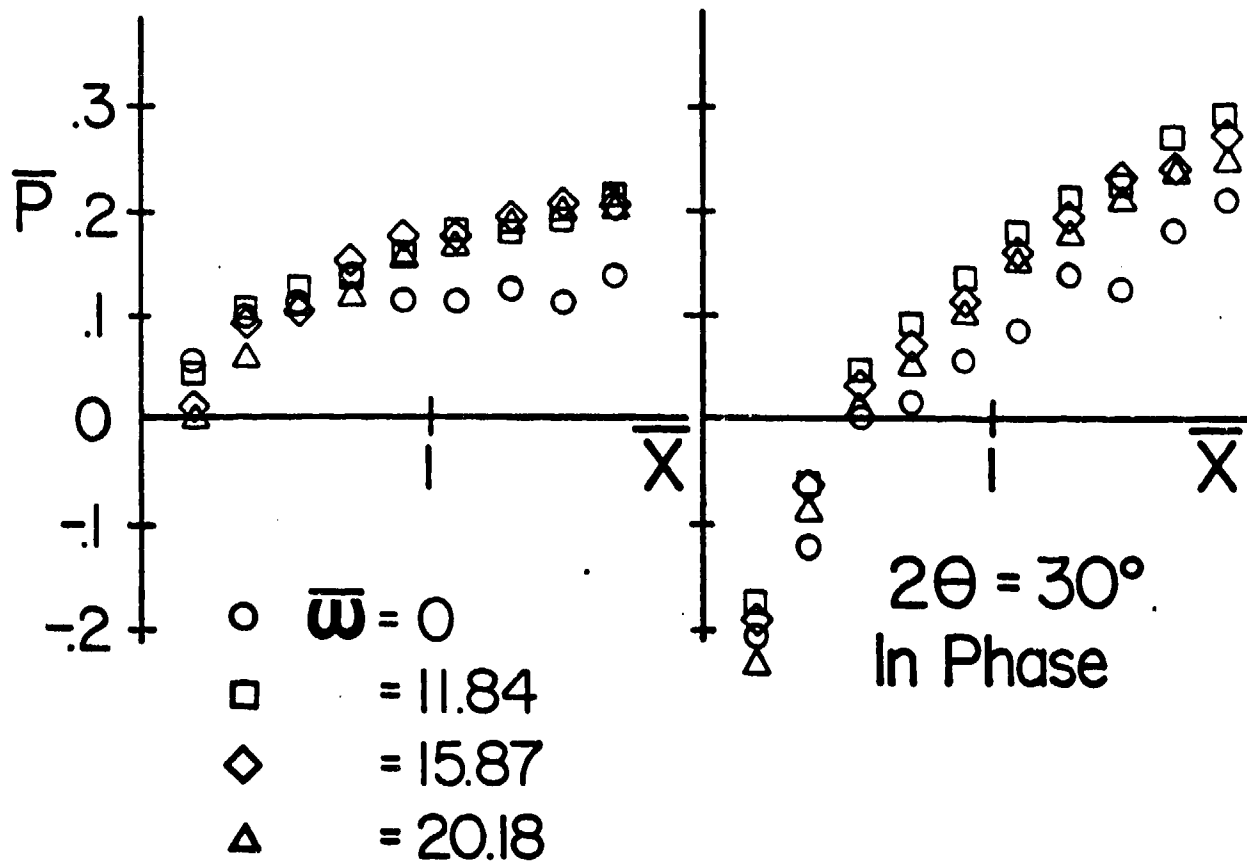
Figure 34. In phase pressure rise for $2\theta = 30°$, and rotors in phase.
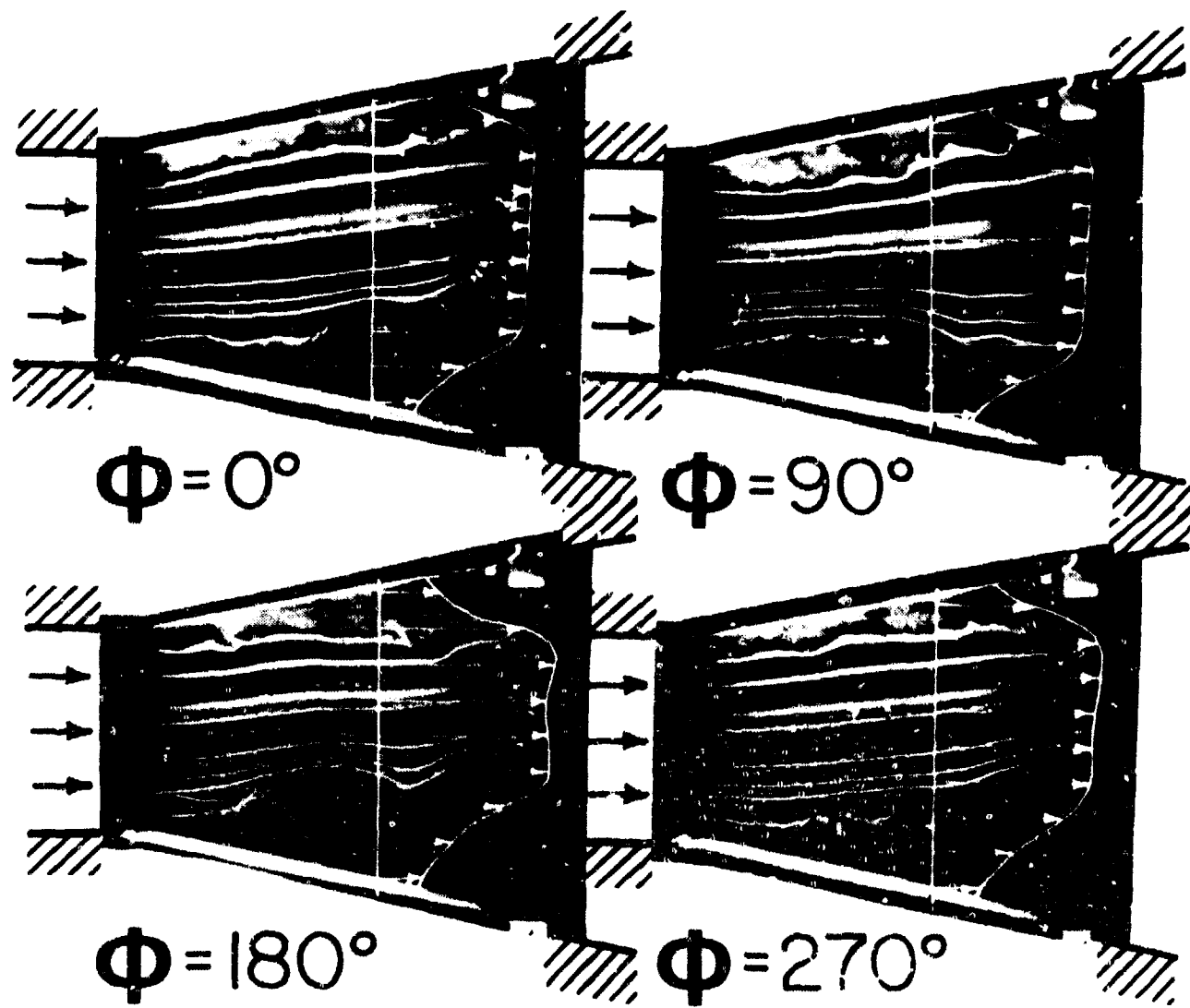
$$2\theta = 24° \; ; \; \overline{\omega} = 11.23$$

In Phase

Figure 35. Streakline photographs of the diffuser flow at different phase positions with superimposed instantaneous velocity profiles.
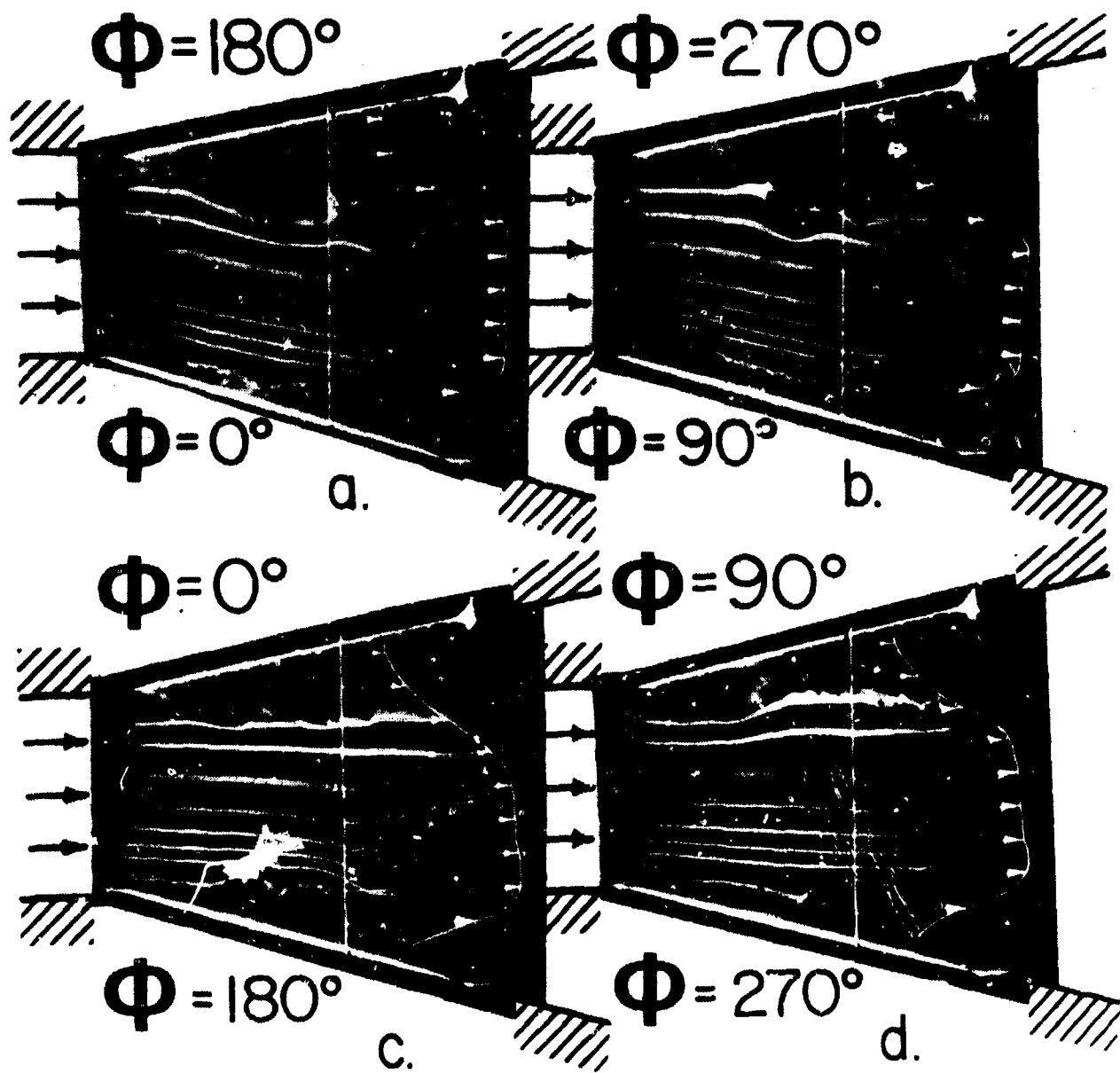
$$2\boldsymbol{\theta} = 30°\;;\;\overline{\boldsymbol{\omega}} = 13.14$$

Out of Phase

Figure 36. Streakline photographs for a larger diffuser angle and for the out of phase rotor orientation.
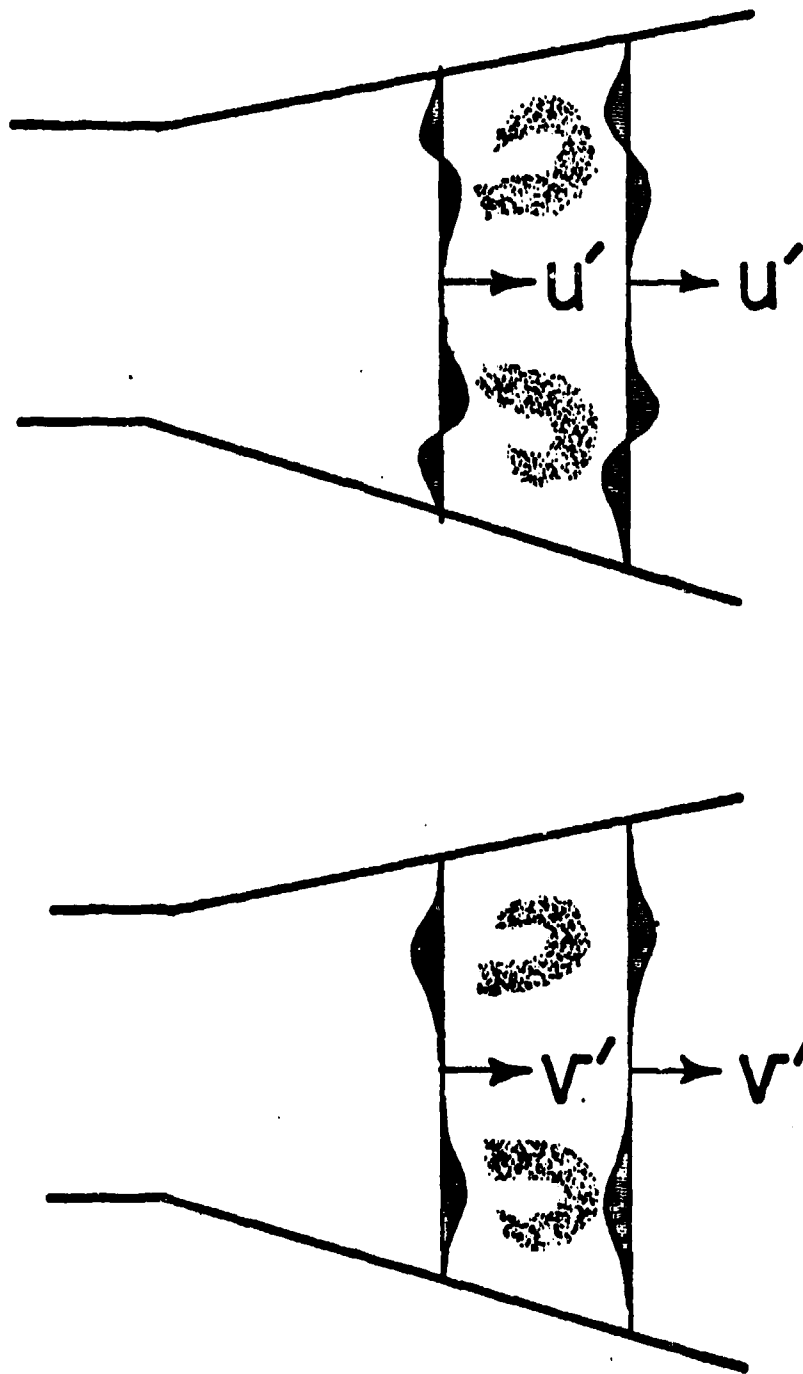
Figure 37. The presence of a counter-clockwise vortex near the upper wall or a clockwise vortex near the lower wall leads to instantaneous velocity changes in the streamwise (u') and transverse (v') directions.

649
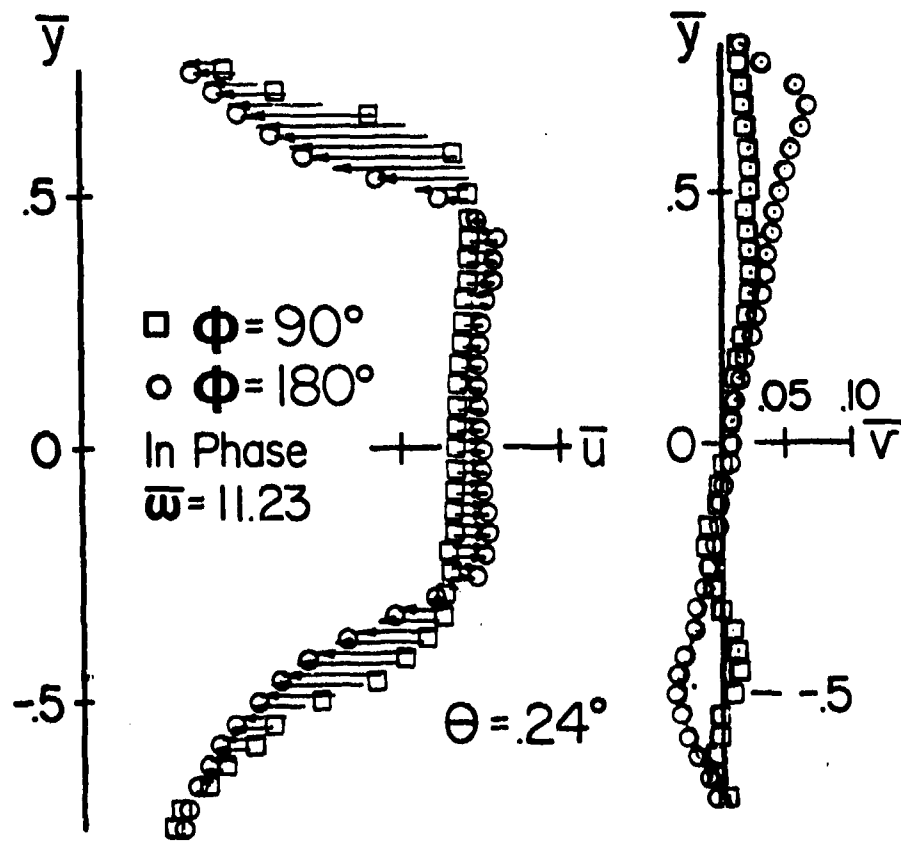
Figure 38. Velocity difference between the presence of
a vortex pair ($\phi$ = 180°) and no vortex
($\phi$ = 90°).

650
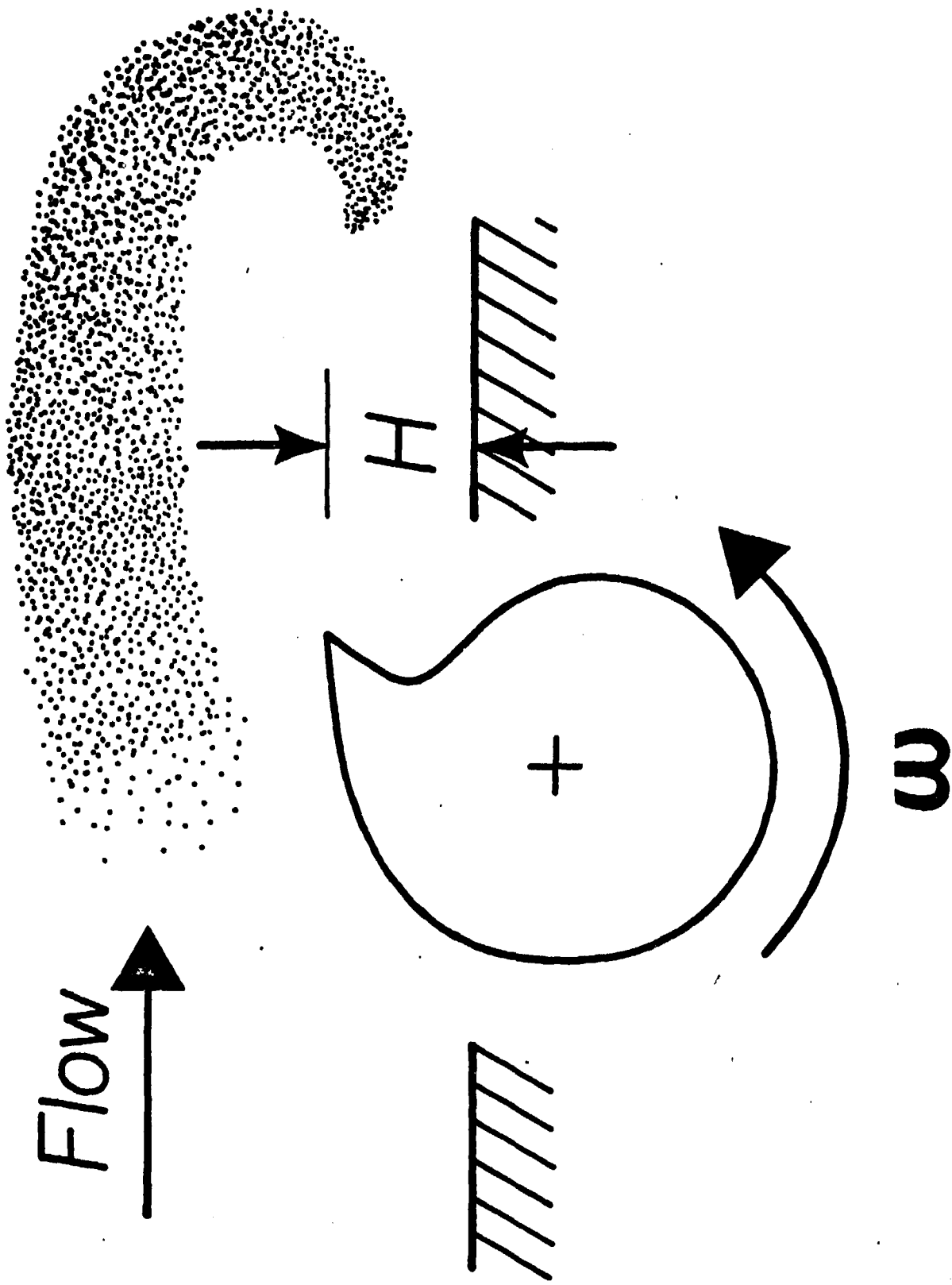
Figure 39. Schematic of the vortex flow generated by a cam shaped rotor.
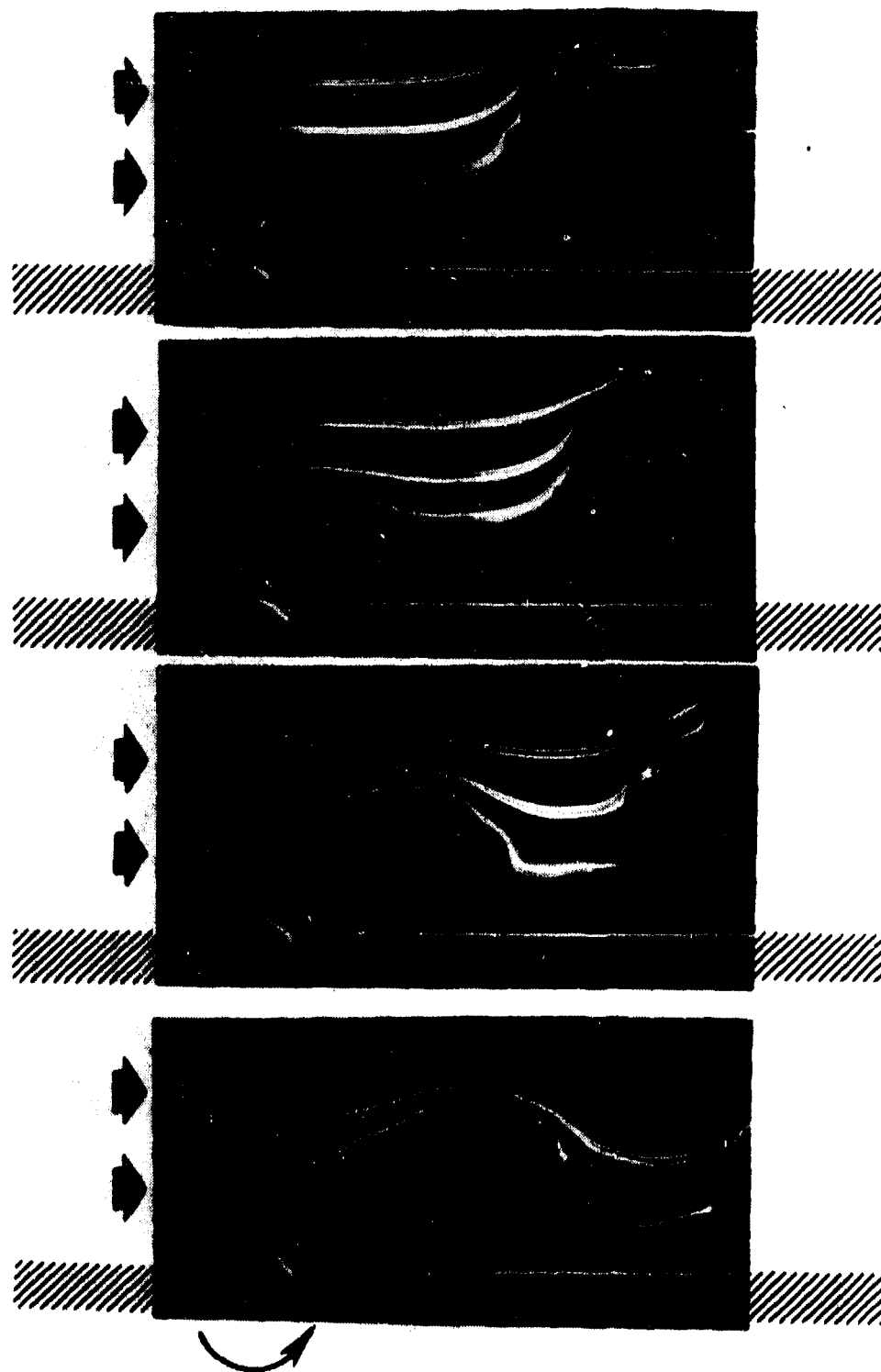
$$\omega = + 3000 \text{ rpm}$$

Figure 40. Flow visualization of vortex structure produced by the vortex generator with $\omega$ = 3000 rpm.

652
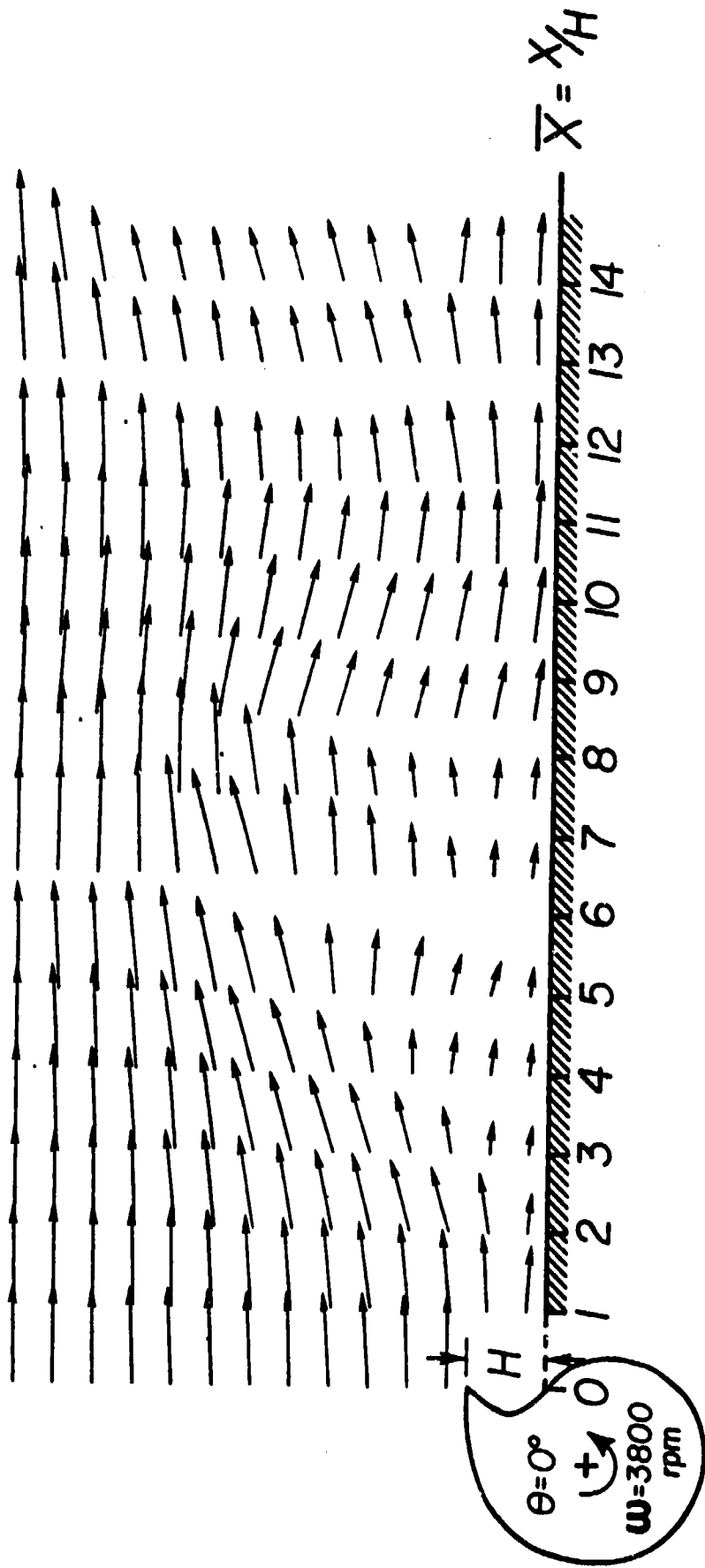
Figure 41a. Instantaneous velocity field with the rotor fully extended in the θ = 0° position.

653
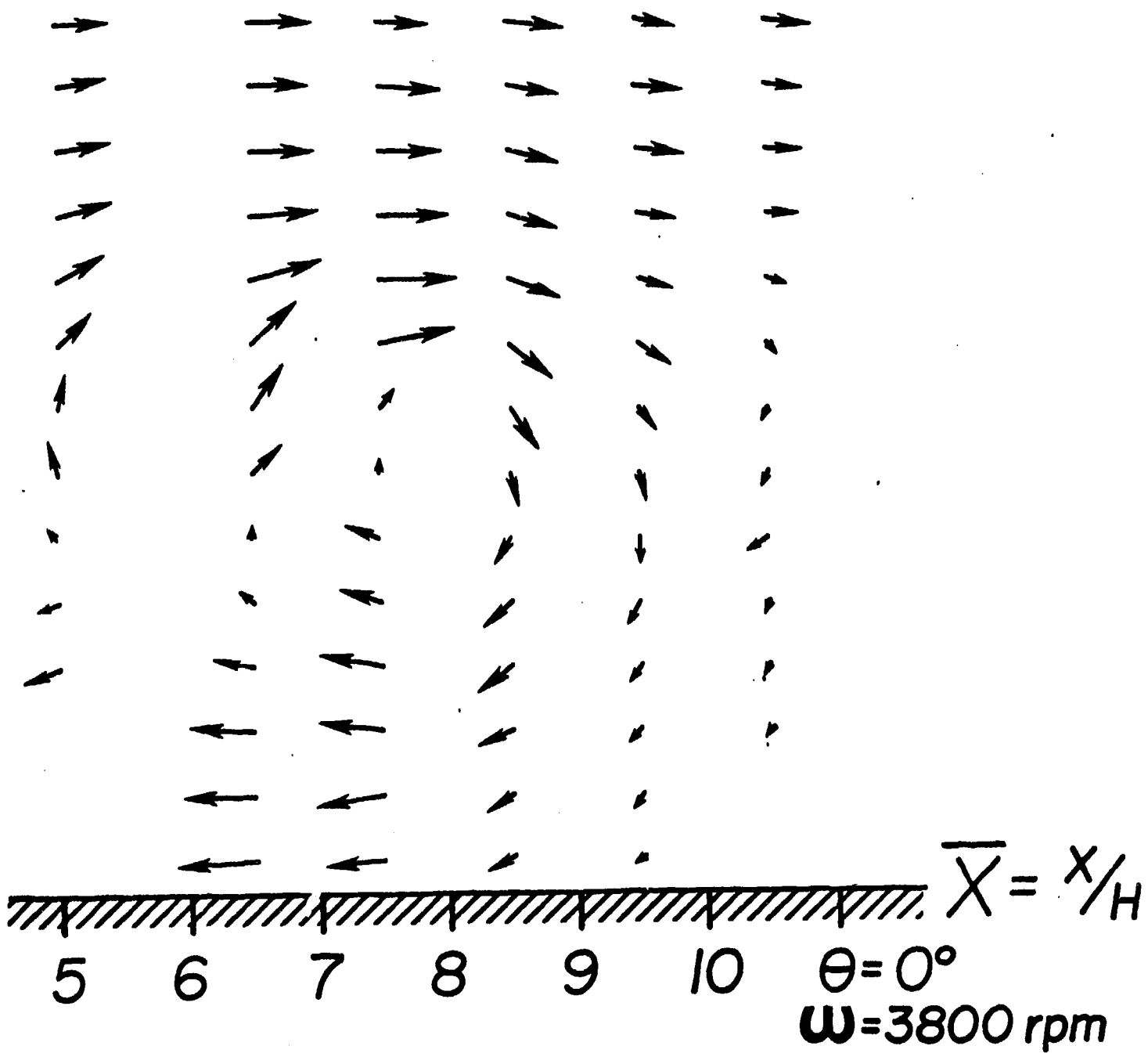
Figure 41b. Identification of a vortex structure in a reference frame moving at 11.5 m/sec.
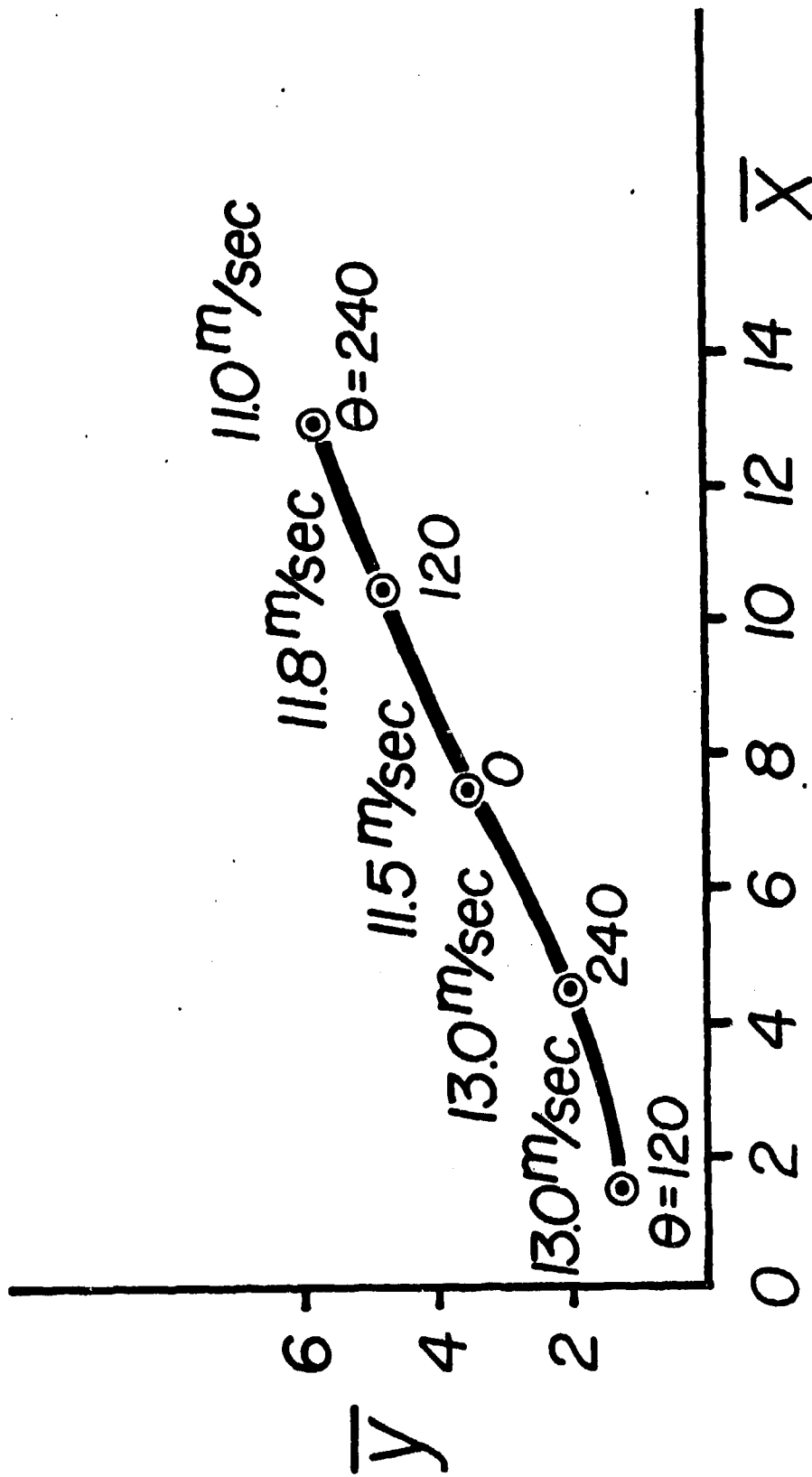
Figure 42. Trajectory of the vortex center as it moves downstream.
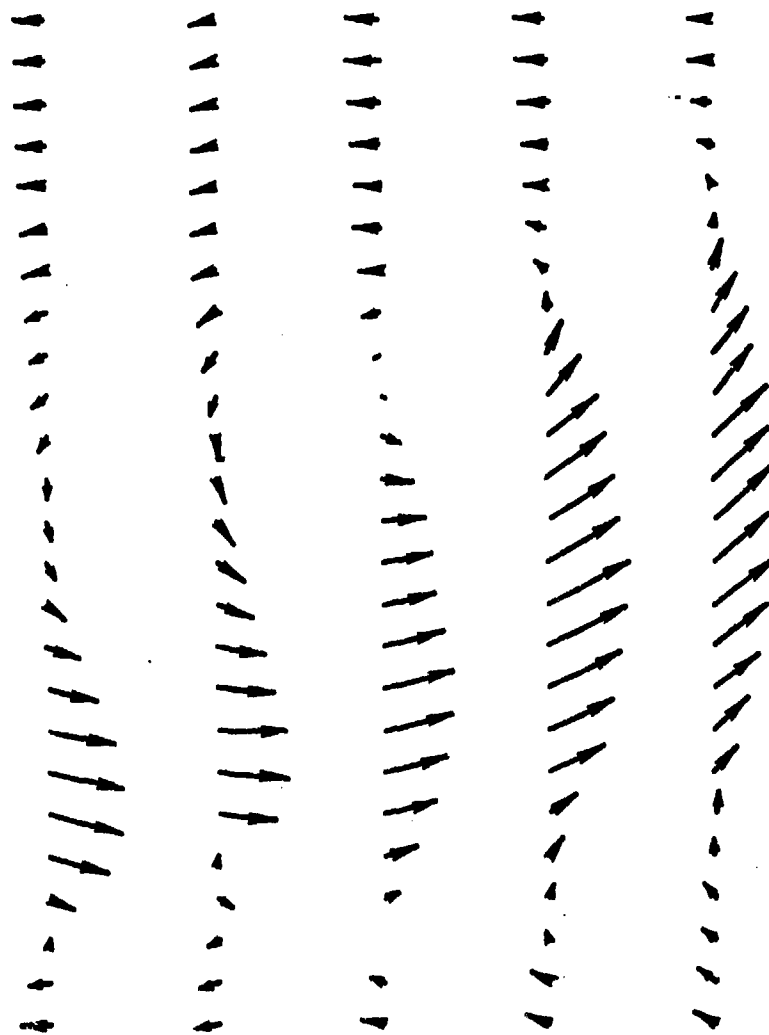
Figure 43. Flow structure in a reference frame moving with the velocity at the point identified as the vortex center.
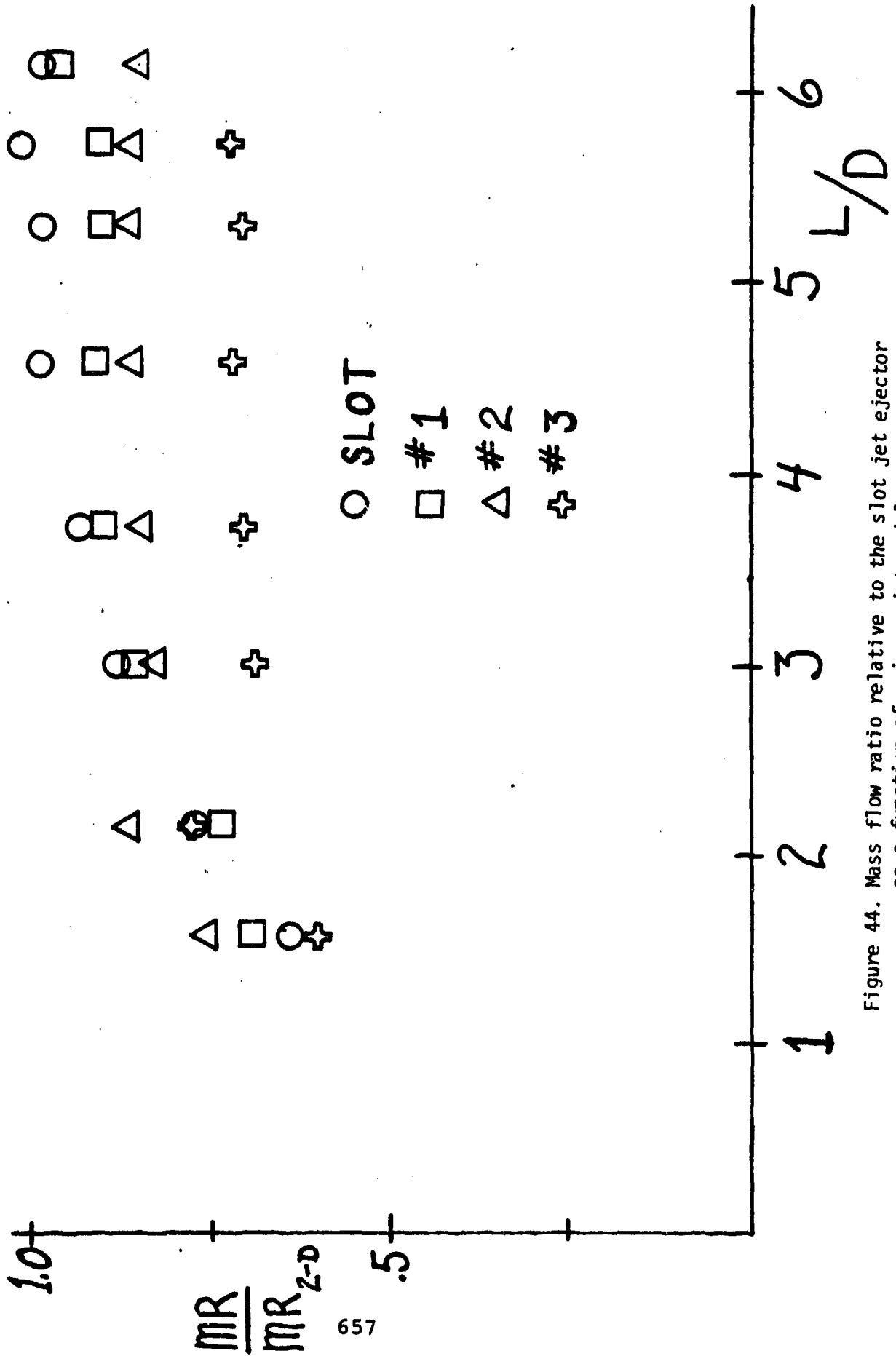
Figure 44. Mass flow ratio relative to the slot jet ejector as a function of primary jet and length
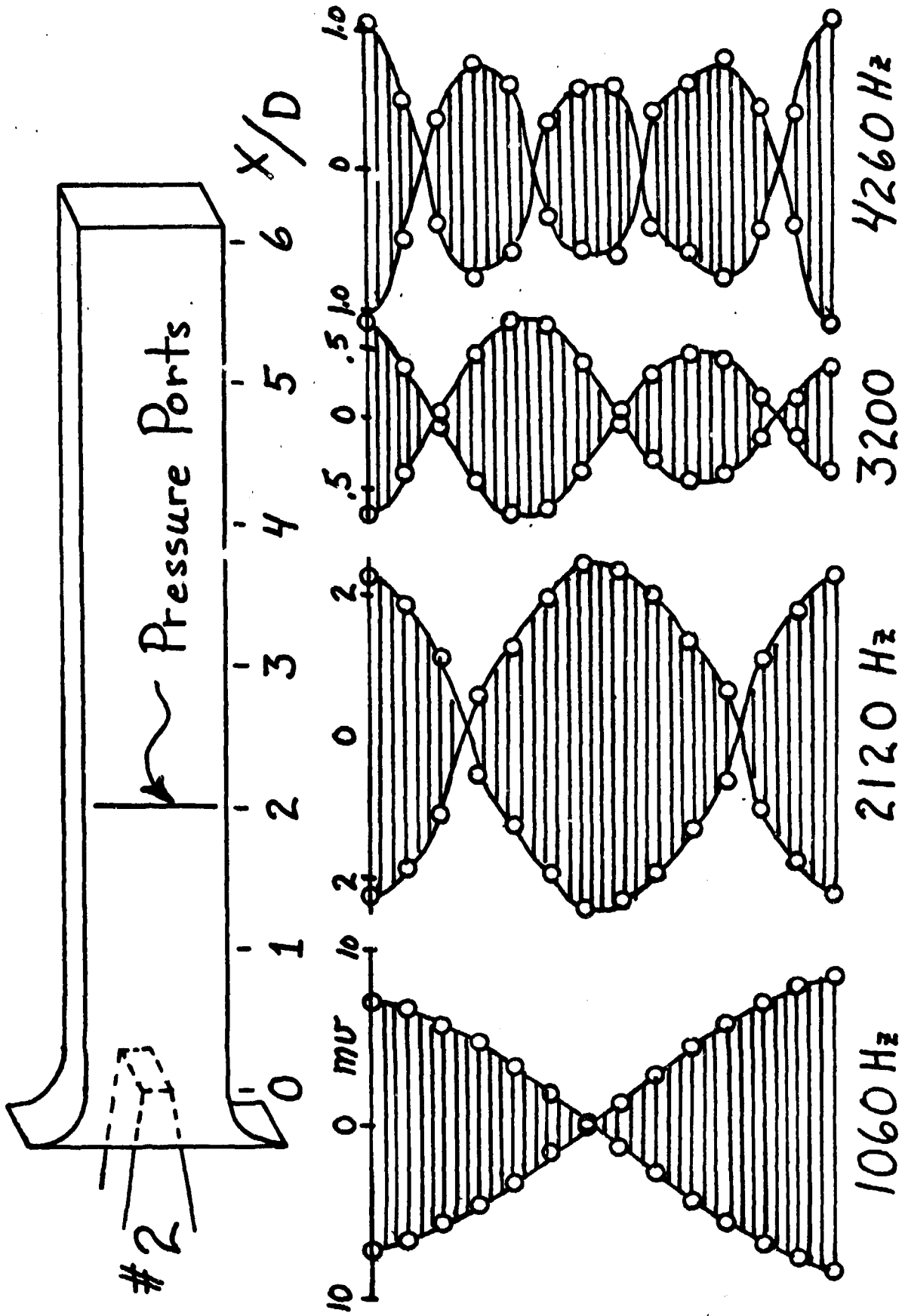
Figure 45. Wave structure in a rectangular ejector with an oscillating jet

CONSIDERATIONS

ON
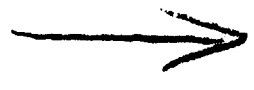
STEADY- AND NONSTEADY-FLOW EJECTORS

by Joseph V. Foa
The George Washington University
Washington, D.C.   20052

## ABSTRACT

A broad examination is made of the flow induction spectrum, from the steady-flow to the pulsating-flow ejector, with special attention to the relationships of dissipation and performance to nonsteadiness, size of migrating eddies, and diffusion. A boundary-value approach is recommended for the comparative evaluation of induction modes. The limits of attainable thrust or lift augmentation are shown to be in some cases a good deal higher than those predicted by initial-value analyses.

## I.   INTRODUCTION

A review of the state of the art, accompanied by an extensive bibliography, has recently been presented by Porter and Squyres [1][1].

The object of this paper is to provide a basis for comparison of the potential merits of the various ejector mechanisms that have so far been considered, as well as of such others as may be proposed in the future. Much of the discussion is based on simple analytical models of a kind that has often proven useful in the prediction of ejector performance [2,3,4,]. Illustrations will focus on thrust augmenters in static operation.

## II.   NATURE OF THE PROBLEM

Consider a thrust augmenter in which the exit flow is steady and uniform, although the interaction may involve nonsteady processes. Given the area ratio $A_e/A_p$, and the boundary conditions, the conservation equations

---

[1]Numbers in brackets designate References at end of paper.

uniquely determine the thrust augmentation ratio $\Phi$ as a function of the dissipation $\delta$, which in turn depends on the chosen mode of flow induction (cf, e.g., Ref. 5).

We are dealing here with a boundary-value problem. Treating it as an initial-value problem -- say, using the mass flow ratio $\mu$ as an independent variable -- may still produce useful relationships, but may also lead to erroneous interpretations or predictions if account is not taken of the fact that the control variables do not include the flow conditions at the merger station.

Figures 1 and 2 show, as an example, the relationships of $\mu$ and $\Phi$ to $\delta$ for a thrust augmenter operating statically on incompressible fluids of equal densities. The beneficial effect of a reduction of $\delta$ on the thrust augmentation ratio is seen to be due in large part to the attendant increase of mass flow ratio.

Figure 3 illustrates, for a specific case, the error that may result from the use of an initial-value (i.v.) approach instead of the boundary-value (b.v.) approach in the prediction of the effect that a change of $\delta$, reflecting a change in the mode of flow induction, may have on performance. The specific case is that of a thrust augmenter of area ratio $A_e/A_{p'} = 25$, which in its original mode produces a static thrust augmentation of 1.4. The dissipation, energy transfer efficiency, and mass flow ratio in this original mode turn out to be 0.67, 0.29, and 4.9, respectively. The error is seen to be significant. For the ideal limit of performance -- the augmentation that would be produced with $\delta=0$ ($\eta_\tau=1.0$) -- the i.v. treatment gives $\Phi_{o_{max}} = (1+\mu)^{\frac{1}{2}} = 2.43$, whereas the b.v. treatment gives $\Phi_{o_{max}} = (A_e/A_{p'})^{1/3}$

= 2.92 (a performance level, that, according to the former treatment, would require an energy transfer efficiency of about 160%!). The condition $\delta \to 0$ is, of course, unrealistic. It is, however, equally unrealistic in both contexts.

As already mentioned, using $\mu$ as an independent variable may also lead to misinterpretation of important relationships and effects. For example, in comparative assessments of different ejector mechanisms, if $A_e/A_p$, and the boundary conditions are stipulated to be the same for all (as they normally are), fixing $\mu$ uniquely determines $\delta$, regardless of the mode of flow induction. This strange result has, mistakenly but understandably, been taken by some to mean, among other things, that the only beneficial effect that can be derived from the introduction of non-steadiness in the ejector mechanism is the promotion of mixing.

In the following, a variety of flow induction modes will be examined from a consistent, boundary-value viewpoint, with the ratio $A_e/A_p$, as a control variable. Special attention will given to the effect of nonsteadiness.

### III. STEADY-FLOW EJECTOR

The incompressible-flow, uniform-density, constant-area ejector in static operation may be taken as a baseline. The dash line in Fig. 2 shows the performance for this case.[1] Secondary-fluid entrainment takes place here because, in constant-area mixing, $p_i$ is always lower than $p_\infty$. Of course, for any given area ratio and boundary conditions, the lower $p_i$, the larger the entrainment, and the obvious way to lower $p_i$ is to

---

[1]The performance plotted here differs from that calculated for the same case by Von Kármán [4] only in that it is not based on the assumption $u_{pi} = u_p$.

exhaust the flow through a diffuser. In the baseline device, as just noted, the pressure rises from $\underline{i}$ to $\underline{e}$, so that mixing and diffusion may be said to take place concurrently. The diffuser function is carried out rather inefficiently in this case, because of the entropy that is produced in mixing, and the question arises under what conditions better results could be obtained through a separation of the two functions, i.e., by having the mixing phase as nearly completed as possible prior to diffusion.

The answer to this question depends, of course, on the constraints that are placed on the comparison.

In Fig. 4 the performance of the baseline ejector is compared with that of an ejector of equal maximum lateral dimensions, in which, however, mixing takes place at constant pressure and is followed by reversible diffusion. The latter configuration always produces a higher augmentation than the baseline one. As one might expect, this result is at variance from those of analyses based on other constraints.

More generally, if mixing takes place at constant pressure, the dissipation is proportional to the square of the difference between the velocities of the two flows at the merger station. This velocity difference normally decreases as $p_1$ is decreased (hence, as the diffuser area ratio $A_e/A_f$ is increased), but the effect is not always monotonic. There are, in fact, situations in which a merger p     e can be identified that will optimize performance. It can readily be erified, from Euler's equation and the condition $d(u_{p1} - u_{s1}) = 0$, that the optimum mixing pressure is the one that causes the product $\rho_1 u_1$ to be the same for the two flows, regardless of

662

whether the two fluids are compressible or not. In short, for best performance, the mixing pressure should be either equal to the optimum (where an optimum exists) or as low as possible. Ideal upper bounds of performance, as determined in this manner for incompressible-flow inter-actions, are plotted in Figs. 5(a), (b), and (c). The charts give $\delta$ and $\mu$ for any set of values of $A_e/A_p$, and $p_{\tau p}/p_{\tau s}$. The exit velocity and the thrust augmentation are then readily calculated for each point from these quantities. The charts also confirm that the performance of the steady-flow ejector improves when the secondary-to-primary density ratio is increased, in constrast to what most often happens in nonsteady-flow devices [6,7].

The only advantage of assessing performance in terms of $\delta$ is that it brings to light the value of certain trade-offs. For example, in the use of longitudinal swirls [8,9] or of wall jets [10,11] to stabilize the flow in wide-angle diffusers, a sacrifice of primary available mechanical energy is accepted for the purpose of avoiding the larger loss that would result from flow separation [10]. Similarly, in the generation of the longitudinal vortices of "hypermixing" arrangements [10,12], for use where compactness is at a premium, the kinetic energy of rotation within the vortices represents a deliberate sacrifice of mechanical energy, but this sacrifice is small compared to the loss that would result from incomplete mixing [12].

Among the steady-flow improvements on the baseline mechanism, mention should be made of the effect of cross-sectional nonuniformities in the secondary-flow velocity distribution at the merger station [4]. Fig. 6 shows the performance improvement that could result from the introduction

663

of such a nonuniformity in the baseline device, calculated both with the assumption $u_{pi} = u_p$, [4] and without it. The nonuniformity is seen to have a beneficial effect. It is not clear, however, how a nonuniform velocity distribution could be maintained across straight parallel streamlines in a potential flow, except at a stationary pressure discontinuity.

## IV.  NONSTEADY-FLOW EJECTOR

The only nondissipative component of energy transfer in flow induction is the work of interi͟ace forces (now commonly designated "pressure exchange"). This component is obviously absent in steady-flow interactions, because pressure forces acting on a stationary interface do no work. It follows that higher energy transfer efficiencies, hence better performance, should be achievable in nonsteady flow induction than in the steady modes.

The distinction between steady and nonsteady modes is somewhat blurred by the fact that the transition from one to the other is actually continuous. Even in the conventional ejector, which is normally thought of and analyzed as a steady-flow device, the migration of finite-size lumps or eddies from each flow into the other generates a measure of nonsteadiness. Attendant -- predicted or observed -- improvements of performance have, as already mentioned, been attributed to the higher mixing rates resulting from the increased interface area [13 through 18]. It seem unlikely, however, that this effect could be significant. Far more importantly, such migrations give rise to interface pressure forces which do work, thereby contributing a nondissipative component to the transfer of mechanical energy. Changes of scale of the migrating masses may, as a consequence, have a more significant effect on the dissipation (hence, on the efficiency of energy transfer) than

they have on the mixing rate. When the scale is very large, the contribution of mixing to flow induction may be expected to become less important than that of pressure exchange.

Consider first a baseline model as shown in Fig. 7, in which the two flows exchange finite-size irrotational lumps of mass. The penetration of such lumps from one flow into the other generates flow fluctuations in both flows at the merger station, but, if the static pressure $p_i$ is assumed to be uniform at each instant, the amplitude of the fluctuations is greater in the secondary, because of its lower stagnation pressure, than in the primary flow. Then, neglecting the primary-flow fluctuations, the extent to which the velocity $u_{si}$ departs from steadiness may be measured, in analogy to von Kármán's approach, by a coefficient of timewise nonuniformity $\Lambda = \overline{u_{si}^2}/(\overline{u_{si}})^2$, the value of which is always greater than 1.0, except when the flow is steady. The analysis then proceeds in the same manner as for the effect of spacewise nonuniformities. A typical result is presented in Fig. 8.

This procedure is probably valid only for low values of $\Lambda$. However, the calculated improvement of augmenter performance that results from an increase of $\Lambda$ confirms, if only qualitatively, that, in the mixing of two flows, the migration of finite-size lumps of mass from each flow into the other has the effect of reducing the dissipation in the overall process.

The situation is more complicated when, as is mostly the case, the migrating masses are vortical eddies, because the attendant dissipation may be large enough to offset much of the benefit of pressure exchange.

665

An extreme situation of this kind is that illustrated in Fig. 9, which is taken from a paper by Lockwood [19] relating to a series of tests aimed at a comparative performance evaluation of steady- and pulsating-flow thrust augmenting ejectors. In the latter, induction takes place through the work of pressure forces acting on the surface of a succession of primary-fluid "pistons", within a considerably shorter interaction length than in the steady-flow ejector. Ideally, mixing plays no role in this mode of flow induction, and the transfer of momentum and energy from the primary to the secondary fluid takes place without dissipation. Indeed, the test results reported by Lockwood [19] confirm the superiority of the nonsteady-flow process (Fig. 10). It must be noted, however, that the plotted thrust augmentation ratio of the pulsating-flow ejector is the measured ratio between the thrust of the entire device and the thrust produced by the pulsating primary alone, in the absence of a shroud. The primary is, however, originally available, in most cases, as a steady flow. The performance that matters is, therefore, the augmentation relative to the thrust that would be produced by the unshrouded original flow. This is, of course, true not only in the extreme case of the pulsating-flow ejector, but whenever finite-size eddies, generated out of steady flows, are participating in the induction process.

My colleague Professor Charles A. Garris is presently directing, at The George Washington University, an experimental study of the energetics of eddy formation under conditions similar to those of ejector flows. While waiting for the results of this study, an approximate evaluation of the effect of eddy scale can be made on the basis of available information and simple physical reasoning. Consider again, for simplicity, a constant-area,

666

incompressible-flow, uniform-density ejector in static operation. At one

end of the spectrum of its possible mechanisms of flow induction is the

steady-flow mode, in which pressure exchange is absent and the dissipation

associated with the transfer of momentum and energy from the primary to the

secondary is that of the baseline mode (Section III). At the other end is

the pulsating-flow ejector, where the transfer efficiency can be taken to

be 1.0 but the cost of generating the primary "pistons" may be considerable.

In evaluating this cost, the primary pistons may be assumed to be

generated by a "chopping up" of the originally steady flow, and their

initial structure may be assumed to be that of tight vortex rings. The

chopping up produces throttling and wave losses. Throttling losses can,

in principle, be made as small as desired by making the opening and closing

times of the chopper as short as possible. The losses associated with

wave processes in the primary supply duct have been found to be suprisingly

large in some cases. They are, however, absent when the flow is incompressible,

as it has been stipulated to be in the analytical model considered here.

The chopping-up costs will, accordingly, be neglected. There remains, how-

ever, an important item of cost to be considered: the dissipation of that

portion of the initially available mechanical energy that becomes trapped

in the vortex ring as kinetic energy of rotation.

The trapped energy can be calculated as the difference between the

kinetic energies of bulk motion of the pulsed discharge and of the fully

formed vortex ring prior to energy exchanges with the surroundings. Photo-

graphic records of vortex ring formation [21] show that the primary, as it

rolls up into a toroidal vortex, captures within its folds a nonnegligible

mass of ambient fluid. The attendant decrease of kinetic energy of bulk

motion of the ring is not a loss; it is, rather, a component of pressure

667

exchange, since momentum is imparted in the process to the captured mass.
The mass is, of course, also induced to rotate within the ring, but in
the absence of any kind of information on this motion, the attendant dis-
sipation of kinetic energy will be assumed to be negligible.

Some guidance as to what the initial kinetic energy of translation
of the fully formed ring would be in the absence of entrainment may be
obtained from existing theories, which do not account for entrainment.
The Kármán-Burgers solution [22] gives the circulation $\Gamma$ around the core
of the vortex as a function of the duration of the discharge and of the
impulsive pressure causing it, and the Kelvin-Lamb formula [23] then gives
the translational velocity of the ring as a function of $\Gamma$ and of the ring-
to-core diameter ratio $\psi$.

Application of this procedure has revealed that, while the flow-
induction process of the pulsating-flow ejector is one that involves
pressure exchange alone, and is therefore essentially nondissipative,
the loss associated with the formation of the driving primary pistons
can be large enough to reduce the performance very significantly. For
values of $\psi$ representative of reported observations [24], the dissipation
$\delta_1$ associated with the formation of the ring (ratio between the trapped
energy, as calculated by this procedure, and the initial available mechanical
energy of the primary) turns out to be about 0.5.

Intermediate modes between the steady-flow and the pulsating-flow
ejector involve some measure of pressure exchange, arising from the inter-
penetration of migrating eddies, and some measure of mixing. In general,
therefore, the "cost" of the overall process is made up of the formation
loss $\delta_1$ and of an interaction loss $\delta_2$ (ratio between the loss of available

668

mechanical energy in the subsequent interaction and the initial kinetic energy of translation of the fully formed ring ). The total dissipation is then $\delta = \delta_1 + (1-\delta_1)\delta_2$.

Nothing is known about the effect of eddy scale on $\delta_1$ and $\delta_2$, except that, as the average size of the eddies increases, $\delta_1$ increases and $\delta_2$ decreases. Some information on the overall effect may be obtained on the basis of the educated guess: $\delta_1 = a_1 + b_1\xi^2$, $\delta_2 = a_2 - b_2\xi^2$, where the _a_'s and the _b_'s are constants and $\xi$ is the ratio between the diameter of the eddy and the radius of the interaction duct. The constants are determined by the values of $\delta_1$ and $\delta_2$ for $\xi = 0$ and $\xi = 1.0$, which are known.

The thrust augmentation ratio, as calculated in this manner for $A_e/A_{p'} = 10$, is plotted as a function of average eddy size in Fig. 11. The optimum eddy diameter turns out to be very large -- about one third of the duct diameter -- but the optimum is a weak one. Even if it were feasible to hold the eddies, on the average, to the desired size, the performance advantage that could be derived from such a control would hardly be worth the trouble. This is all the more evident when it is considered that the optimum mode turns out to be pretty nearly that of the pulsating-flow ejector, in the analysis of which, as will be recalled, some of the costs of eddy generation have been neglected.

With larger area ratios, the optimum eddy size, as determined by this procedure, would be even closer to the extreme one of eddies spanning the entire interaction space. Since this is an improbable situation when the area ratio is large, the information developed here, concerning the effect of eddy size, is applicable only to ejectors of small or moderate area ratios.

669

## V.  CRYPTOSTEADY-FLOW EJECTOR

The preceding section has dealt with the conversion penalties that are associated with the introduction of a pressure exchange component -- necessarily nonsteady -- in the extraction of energy from an initially steady flow.  These penalties are avoided in cryptosteady flow induction, where the primary is allowed to remain steady but its discharge nozzle is imparted a transverse motion, thereby causing the interfaces to move.  When, as in the rotary jet [25], the motion of the primary nozzle is such that the resultant of the interface pressure forces is always in a direction to promote flow induction, the overall dissipation is always less, all else being equal, then if pressure exchange were absent.

No attempt will be made here to review the work that has been done on this subject (e.g., Refs. 6,7, 25-27), except to note that practically all of it so far has focused, both theoretically and experimentally, on models with little or no  diffusion.  Since this mode of flow induction stands to benefit as much as all others from a lowering of the merger pressure, a meaningful assessment of its potential merit will have to include consideration of its predicted and  measured performance when coupled with diffusers of various area ratios.

## VI.  CONCLUSIONS

1.  The limits of attainable thrust or lift augmentation are significantly
    higher than those predicted by analyses based on an initial-value approach.

2.  The performance of constant-pressure-mixing ejectors is always better
    than that of the constant-area-mixing ejectors of the same maximum
    lateral dimensions, under the same operating conditions.

3. The performance of constant-pressure-mixing ejectors does not always improve monotonically when the mixing pressure is reduced.

4. In the mixing of parallel flows, the generation of finite-size eddies results in a loss of available mechanical energy. On the other hand, the migration of such eddies from one flow into the other gives rise to eddy-surface pressure forces which do work, thereby introducing a pressure exchange (nondissipative) component in the energy transfer process. The net effect on efficiency may be a gain or a loss, depending on the size of the eddies, but the performance improvements that can be achieved through eddy-scale control do not appear to be important enough to warrant the added complication of a controlling device.

5. Mixing in the diffuser may have a stabilizing effect on the flow, but has, apart from that, an adverse effect on diffuser efficiency. Where mixing is the main component of the flow induction process and compactness is sought, the mixing chamber and the diffuser should independently be made as short as possible, and other methods should be used to delay or prevent flow separation in the diffuser.

6. Where pressure exchange is part of the induction process, it may take place partly or entirely in the diffuser. It should, however, be completed before any significant mixing has taken place.

<div align="center">ACKNOWLEDGMENT</div>

# REFERENCES

1. Porter, J. L., and Squyres, R. A., "A Summary/Overview of Ejector Augmentor Theory and Performance," Vought Corporation ATC Report No. R-91100-9CR-47, April 1980.

2. Keenan, J. H., Neumann, E. P., and Lustwerk, F., "An Investigation of Ejector Design by Analysis and Experiment," Journal of Applied Mechanics, Vol. 17, No. 3, September 1950, pp. 299-309.

3. Shapiro, A. H., in discussion of preceding reference, Journal of Applied Mechanics, Vol. 18, No. 1, March 1951, p. 117.

4. von Kármán, Th., "Theoretical Remarks on Thrust Augmentation," H. Reissner Anniversary Volume, J. W. Edwards, Ann Arbor, 1949.

5. Foa. J. V., "Ejectors and Rotary Jets as Thrust Augmenters," in Marine Propulsion, J. Sladky editor, ASME, New York, 1976.

6. Hohenemser, K. H., and Porter, J. L., "Contribution to the Theory of Rotary Jet Flow Induction," Journal of Aircraft, Vol. 3, No. 4, July-August 1966, pp. 339-346.

7. Costopoulos, Th., "Constant-Area Flow Interaction in Cryptosteady-Flow Thrust Augmenters," The George Washington University, Tech. Rept. No. TR-UTA-773, April 1977.

8. Peters, H., "Conversion of Energy in Cross-Sectional Divergencies Under Different Conditions of Inflow," NACA Tech. Memo 734, 1934.

9. Van Dewoestine, R. V., "An Experimental Investigation of Boundary Layer Development and Swirling Flow in Conical Diffusers," Ph.D. Thesis, Purdue University, 1969.

10. Quinn, B., "Recent Developments in Large Area Ratio Thrust Augmenters," AIAA/SAE 8th Joint Propulsion Specialists Conference, New Orleans, Louisiana, 1976.

11. Alperin, M., Wu, J. J., and Smith, C. A., "The Alperin Jet-Diffuser Ejector (AJDE)," Rept. No. NWC TP5853, Naval Weapons Center, China Lake, Cal., Feb. 1976.

12. Bevilaqua, P. M., "Evaluation of Hypermixing for Thrust Augmenting Ejectors," Journal of Aircraft, Vol. 11, No. 6, June 1974, pp. 348-354.

13. Heiser, W. H., "Thrust Augmentation," Journal of Engineering for Power (Transactions of the ASME), January 1967, pp. 75-82.

14. Bremhorst, K., and Harch, W. H., " The Mechanism of Jet Entrainment," AIAA Journal, Vol. 16, No. 10, October 1978, pp. 1104-1105.

15. Binder, G., and Favre-Martinet, M., "Mixing Improvement in Pulsating Turbulent Jets," ASME Symposium on Fluid Mechanics of Mixing, Atlanta, Ga. June 20-22, 1973.

16. Viets, H., "Oscillating Jet Nozzles for V/STOL Application," AIAA/SAE 10th Propulsion Conference, San Diego, Cal., October 21-23, 1974.

17. Viets, H., and Piatt, M., "Linearized Unsteady Jet Analysis," Workshop on Thrust Augmenting Ejectors, Ames Research Center, Moffett Field, Cal., June 28-29, 1978.

18. Binder, G., and Didelle, H., "Improvement of Ejector Thrust Augmentation by Pulsating or Flapping Jets," 2nd Symposium on Jet Pumps and Ejectors and Gas Lift Techniques, Cambridge, U.K., organized by BHRA (British Hydromechanics Research Association), Cranfield, Bedford, March 24-26, 1975.

19. Lockwood, R. M., and Patterson, W. G., "Energy Transfer From an Intermittent Jet to a Secondary Fluid in an Ejector-Type Thrust Augmenter," Hiller Aircraft Company, Interim Rept. ARD-305, 30 June 1962.

20. Morrisson, R., "Jet Ejectors and Augmentation," NACA ACR 37, September 1942.

21. Magarvey, R. H., and MacLatchy, C. J., "The Formation and Structure of Vortex Rings," Canadian Journal of Physics, Vol. 42, 1964, pp. 678-683.

22. von Kármán, Th., and Burgers, J. M., "General Aerodynamic Theory - Perfect Fluids," Division E. Chapter III. Section 3, in Aerodynamic Theory, W. F. Durand editor, 1934.

23. Lamb, H., Hydrodynamics, Dover (6th Ed.), pp. 236-241.

24. Sullivan, J. F., Widnall, S. E., and Ezekiel, S., "Study of Vortex Rings Using A Laser Doppler Velocimeter," AIAA Journal, Vol. 11, October 1973, pp. 1384-1389.

25. Hohenemser, K. H., "Preliminary Analysis of a New Type of Thrust Augmenter," Proceedings of the 4th U.S. National Congress of Applied Mechanics, ASME, New York, 1962, pp. 1291-1299.

26. Hohenemser, K. H., " Flow Induction by Rotary Jets," Journal of Aircraft, Vol. 3, January-February, 1966, pp. 18-24.

27. Costopoulos, Th., "A Wide-Jet Strip Analysis of Cryptosteady-Flow Thrust Augmenters," The George Washington University, Tech. Repts. TR-UTA-771 and 772, March 1977.

## NOMENCLATURE

### Symbols

| | |
|---|---|
| A | cross-sectional area |
| $\dot{m}$ | mass flow rate |
| p | static pressure |
| $p_T$ | total (or stagnation) pressure |
| t | time |
| u | axial component of flow velocity |

$$\bar{u} = \frac{1}{A} \int_A u\, dA$$

$$\overline{u^2} = \frac{1}{A} \int_A u^2\, dA$$

$$\bar{\bar{u}} = \frac{1}{t} \int_t u\, dt$$

$$\overline{\overline{u^2}} = \frac{1}{t} \int_t u^2\, dt$$

$$\delta = \Delta / \tfrac{1}{2}\, \dot{m}p\, u_p^2,$$

$\Delta$    dissipation

$\eta_\tau$    efficiency of energy transfer

$\lambda = \overline{u^2}/(\bar{u})^2$

$\Lambda = \overline{\overline{u^2}}/(\bar{\bar{u}})^2$

$\mu = \dot{m}_s/\dot{m}_p$

$\rho$    density

$\Phi$    thrust or lift augmentation ratio

$\Phi_o$    static thrust or lift augmentation ratio

### Subscripts

| | |
|---|---|
| e | discharge station |
| f | station at which mixing is practically completed |
| i | merger station (upstream end of interaction space) |
| p | primary |
| p' | primary conditions on isentropic and isoenergetic expansion to ambient pressure |
| s | secondary |
| ∞ | ambient |

674

# DEFINITIONS

Available mechanical energy of a body of fluid in a flow. The kinetic
energy of bulk motion that the body of fluid would possess on isoen-
ergetic and isentropic expansion or compression to a preselected
reference pressure.

Dissipation. Difference between the fluxes of available mechanical
energy at the entrance into and at the exit from the interaction space.

Efficiency of energy transfer. Ratio between the available mechanical
energy gained by the secondary and that lost by the primary in the
interaction.

Interaction space. The space in which momentum and energy are transferred
from one flow to the other.

Pressure exchange. The work of interface pressure forces.

Thrust augmentation. The ratio between the thrust produced by a flow
induction device and the thrust that would be produced by its primary
alone on isoenergetic and isentropic expansion to ambient pressure.

675
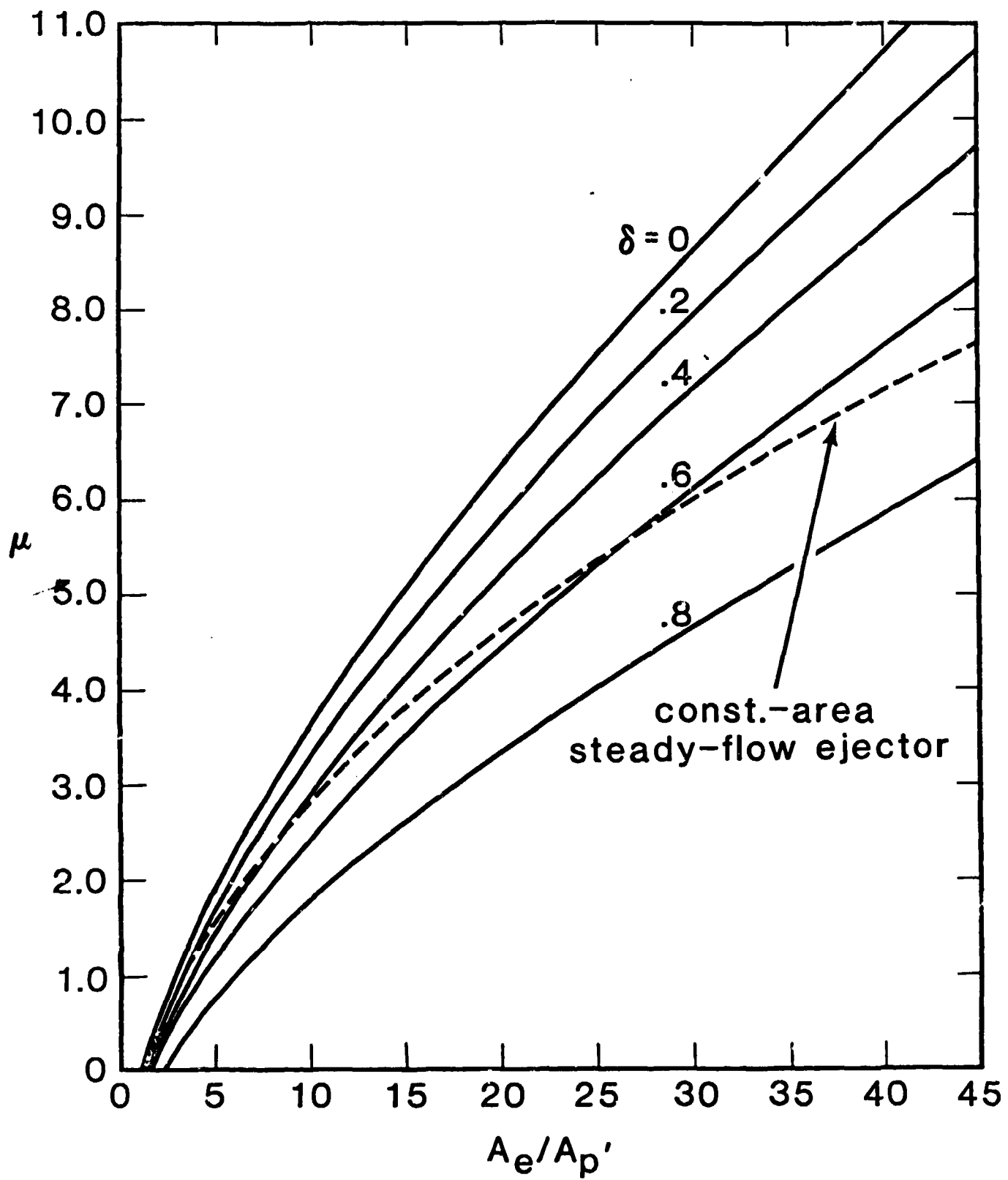
Fig. 1. – Effect of dissipation on mass flow ratio
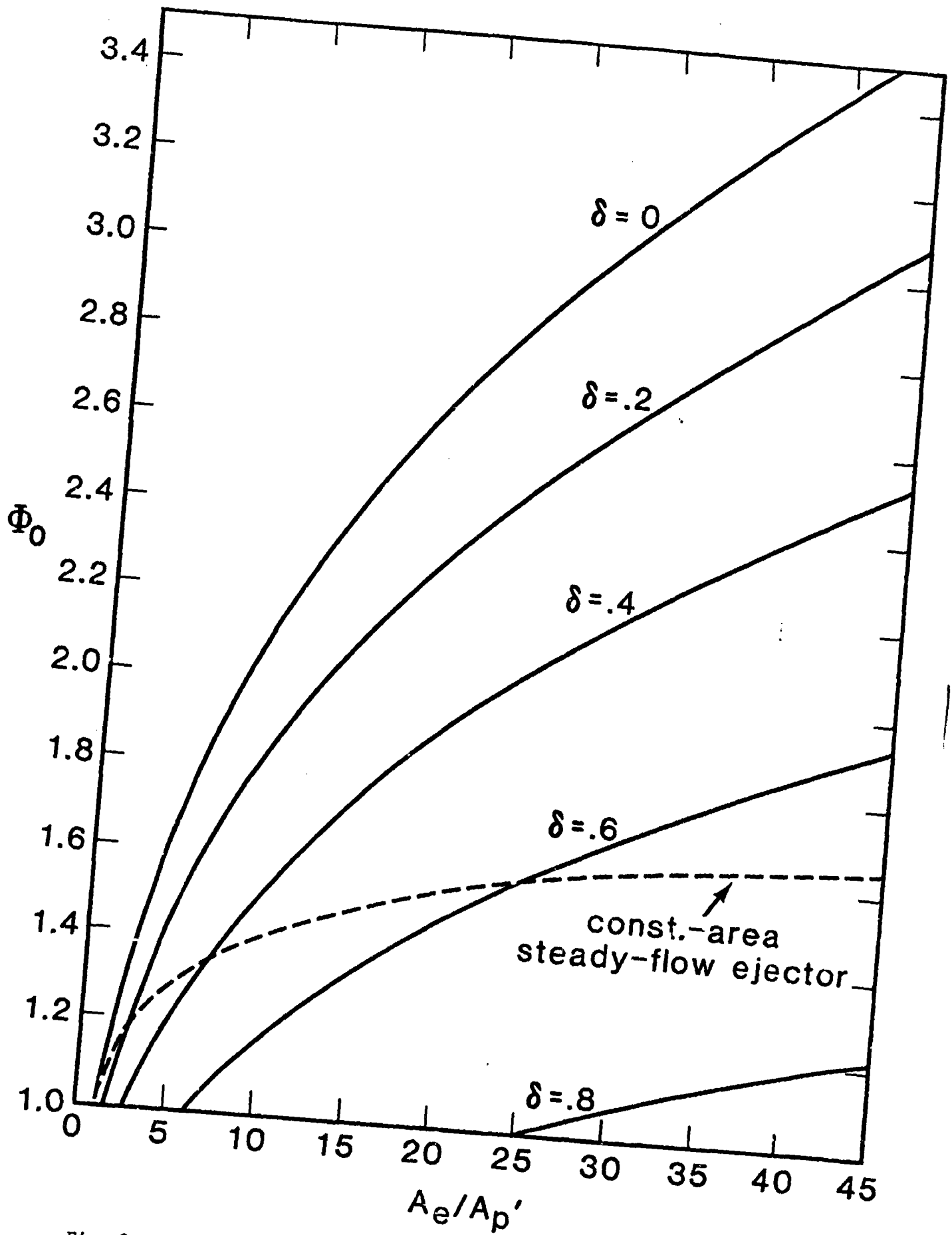
Fig. 2. — Effect of dissipation on static thrust augmentation
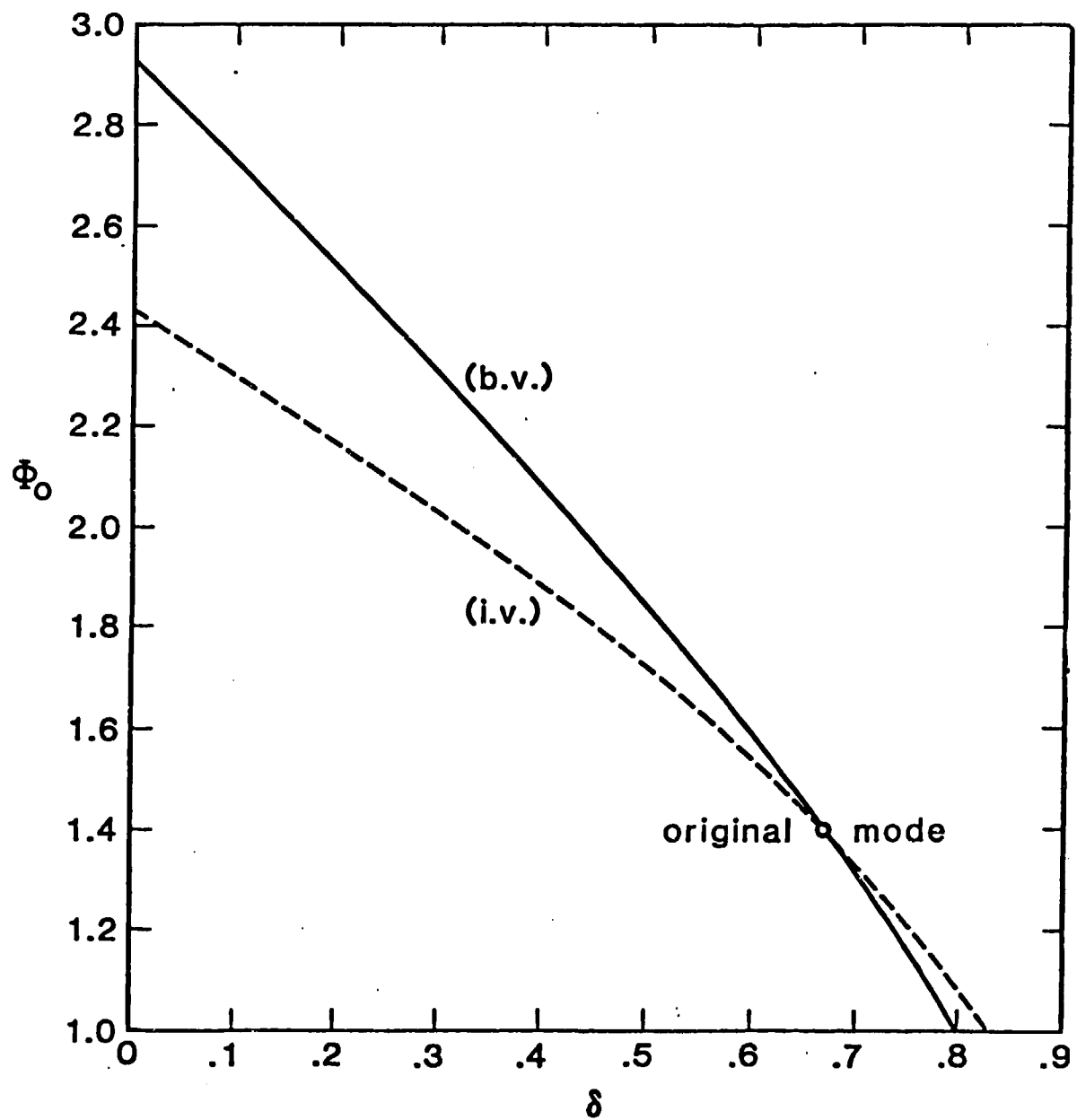
Fig. 3 – Predicted effect of mode changes, based on
boundary-value (b.v.) and initial-value (i.v.)
analyses
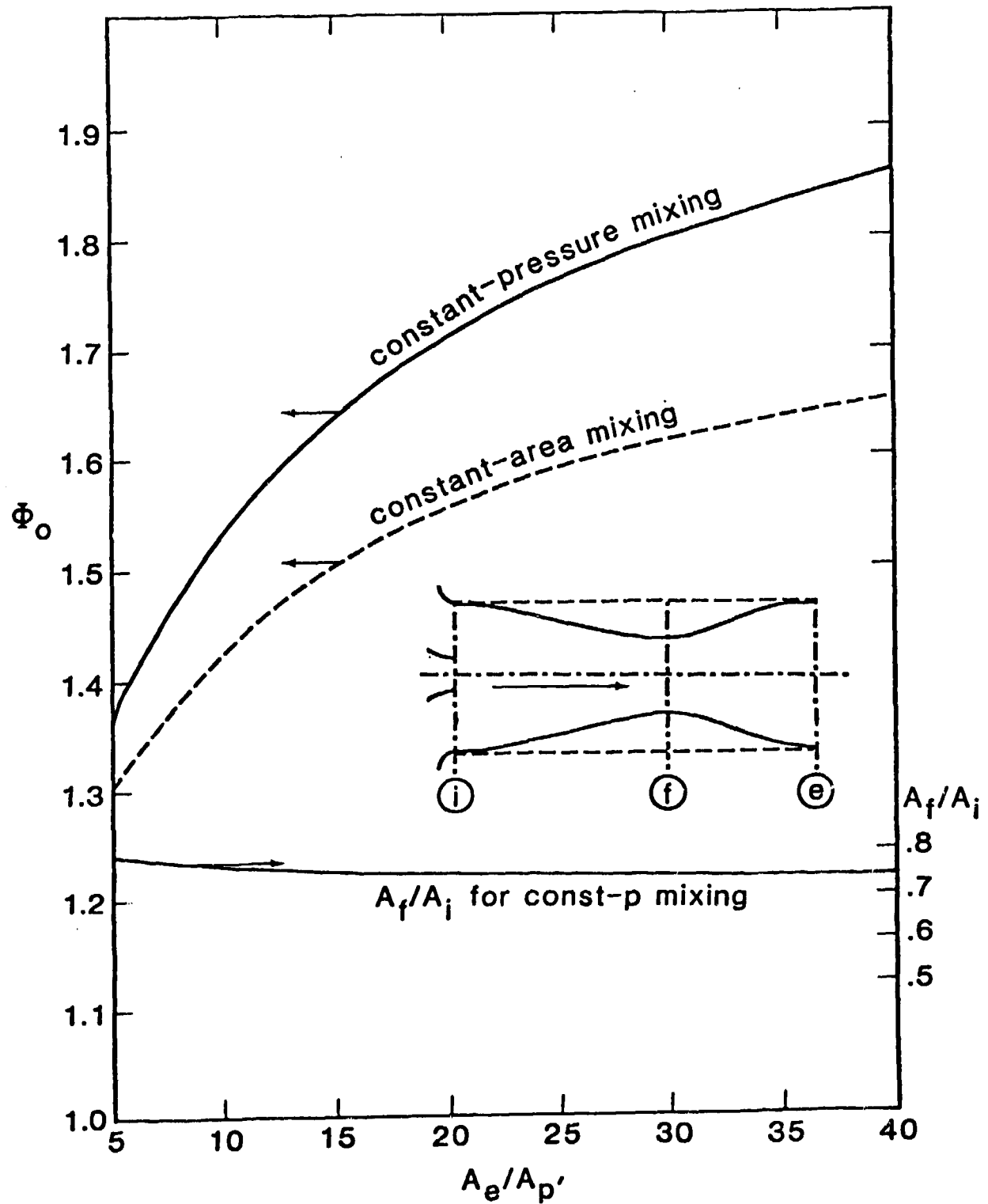
Fig. 4 — Comparison of constant-pressure- and constant-area-mixing
ejectors of equal maximum transversal dimensions.
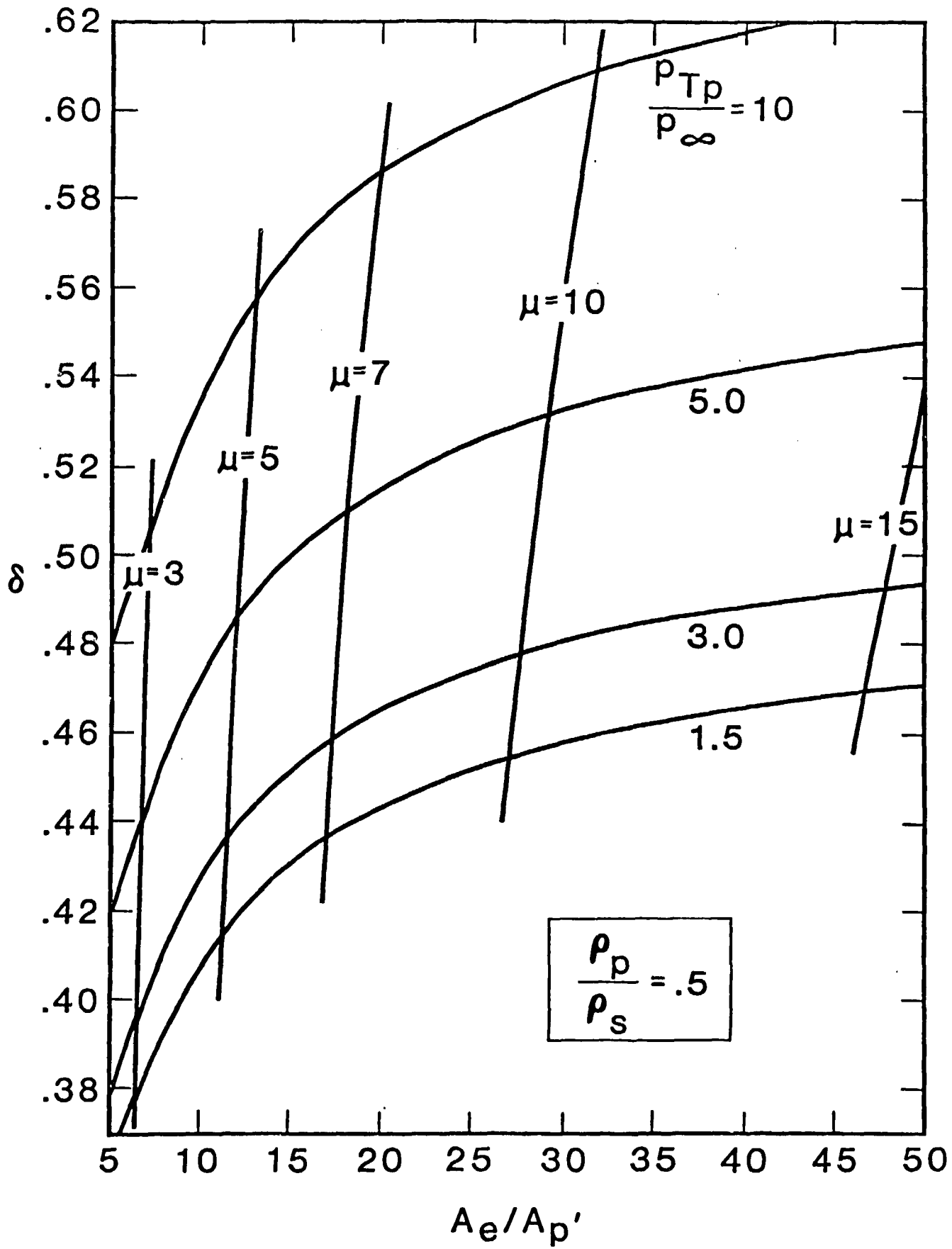
Fig. 5. – Ideal performance of incompressible steady-flow, constant-pressure
(a) – $\rho_p/\rho_s = 0.5$

680
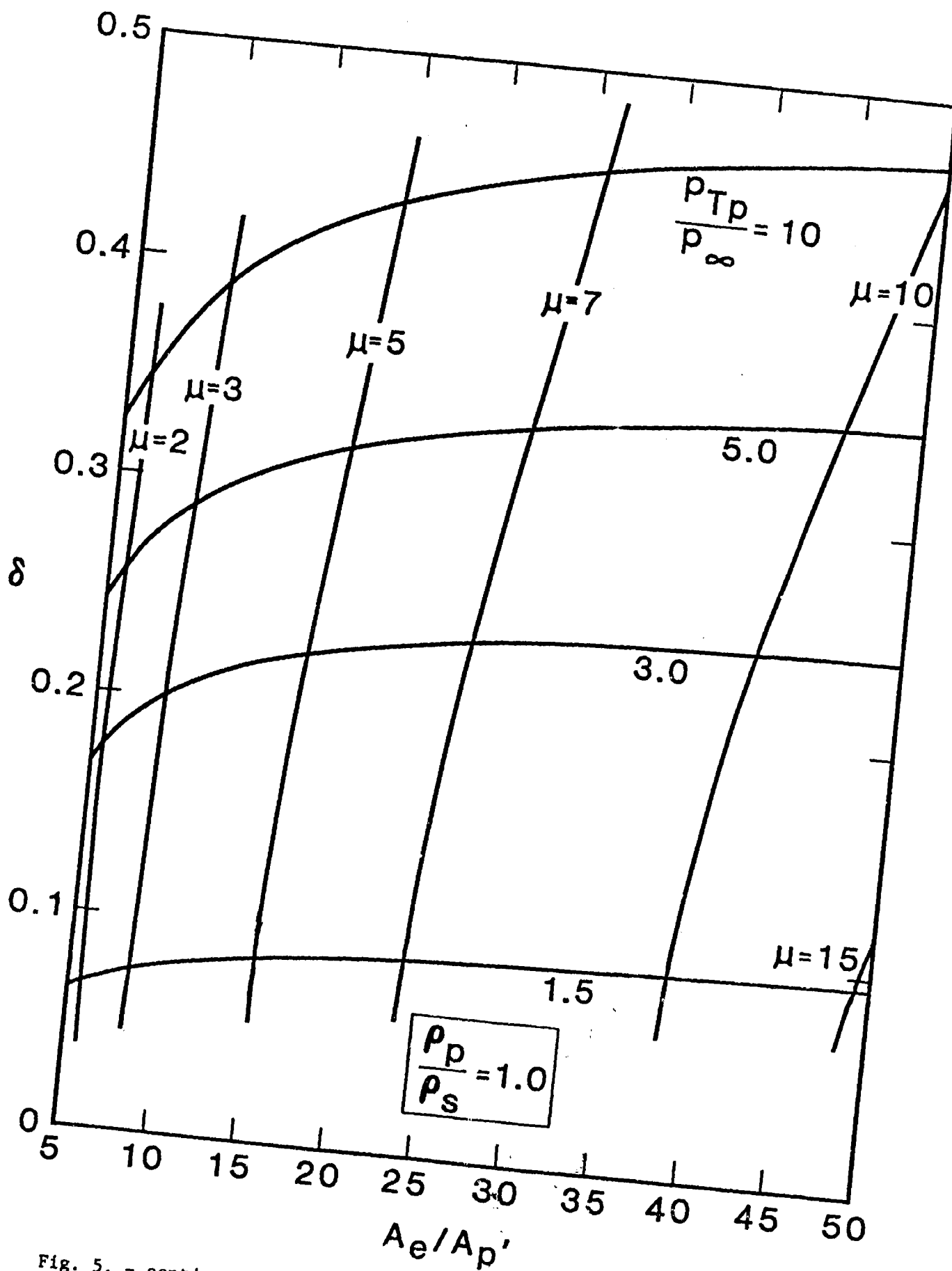
Fig. 5. - continued: (b) $\rho_p/\rho_s = 1.0$

681
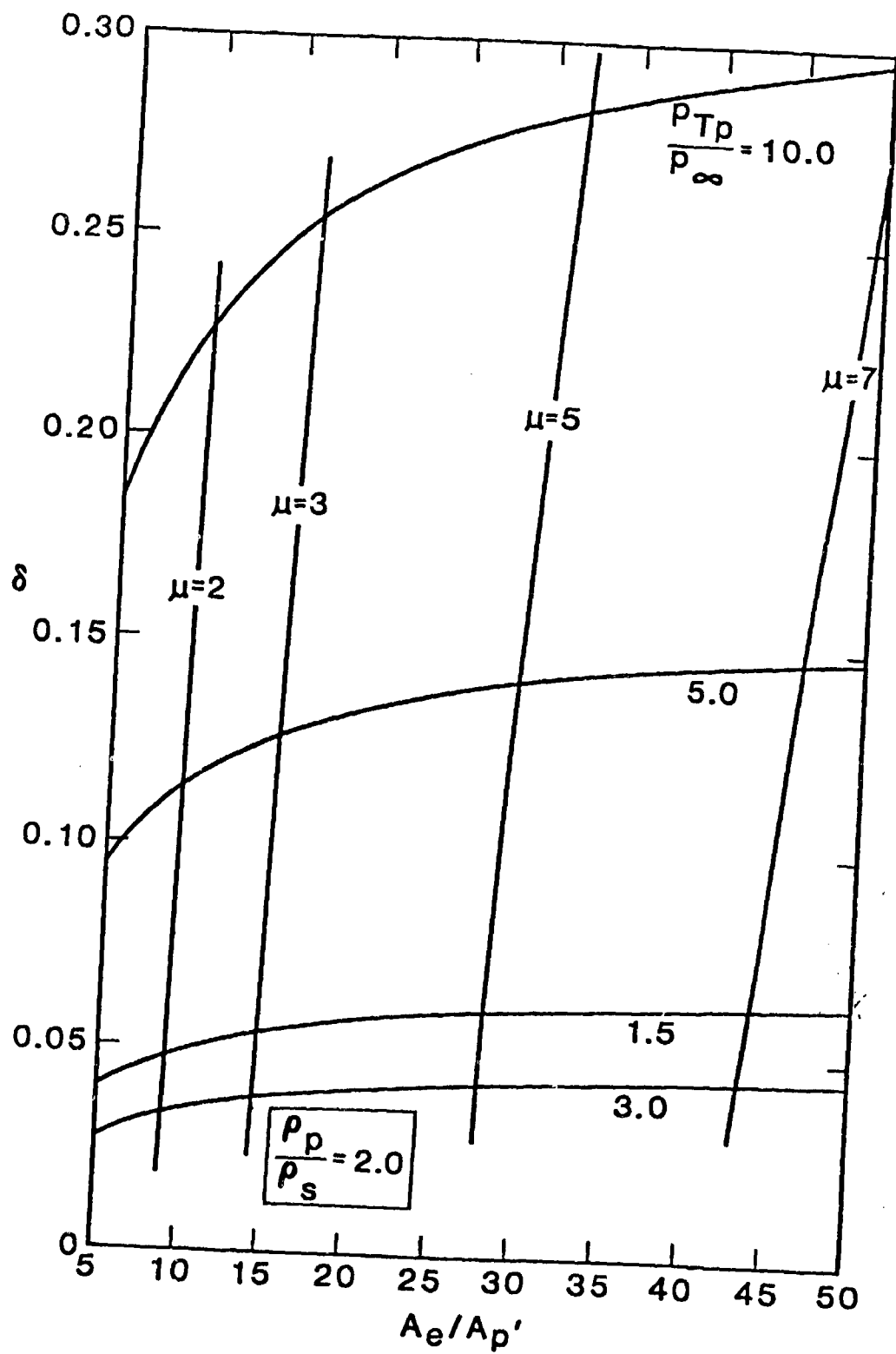
Fig. 5, cont'd. - (c) $\rho_p/\rho_s$ = 2.0
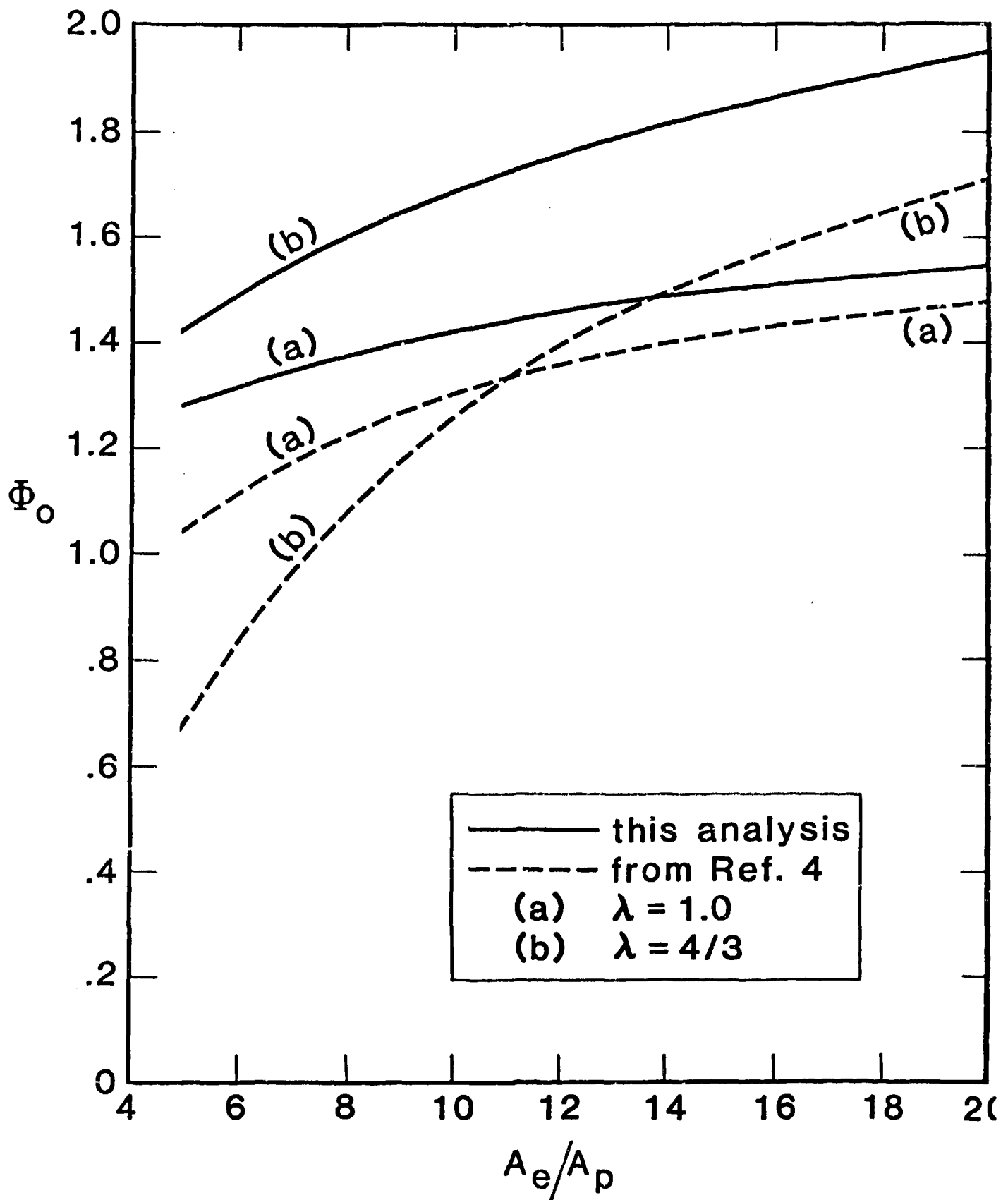
Fig. 6 – Steady-flow ejector.  Effect of secondary-flow nonuniformity at merger station
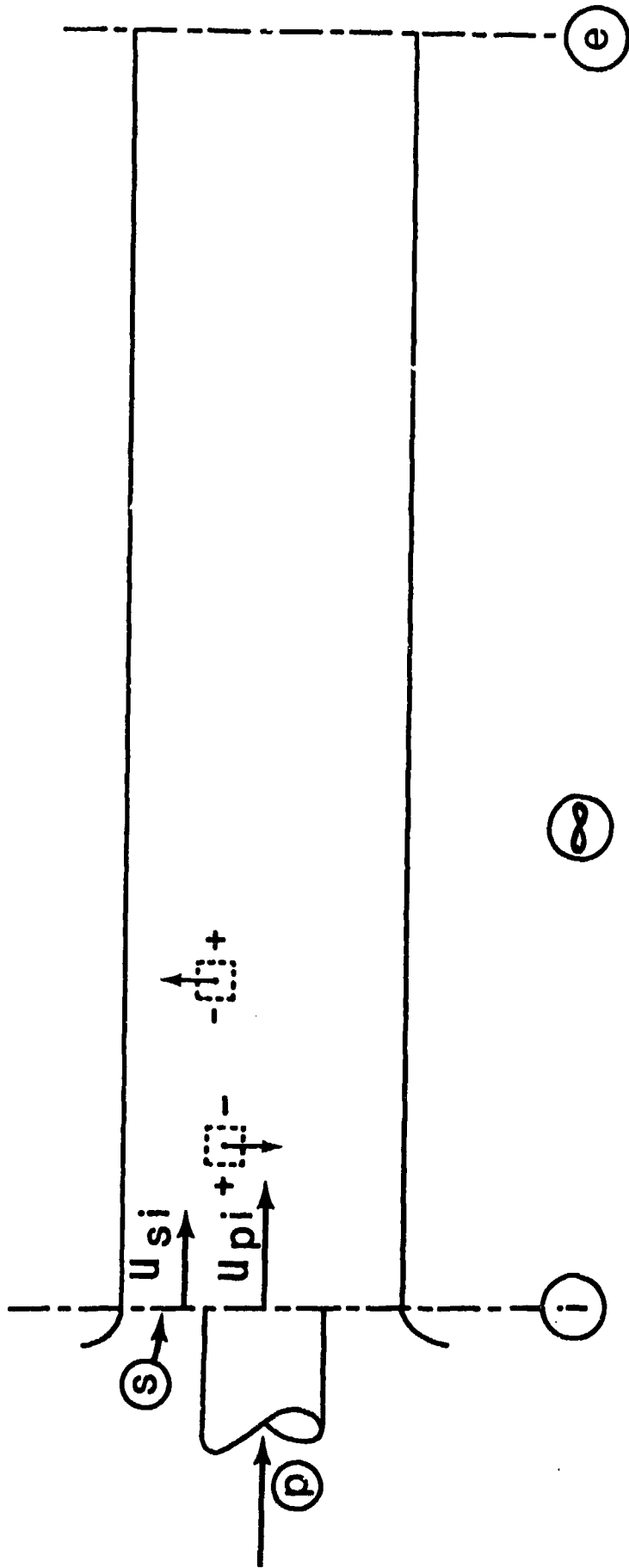
Figure 7. Schematic of Exchange of Mass in Lumps Which are Irrotational.
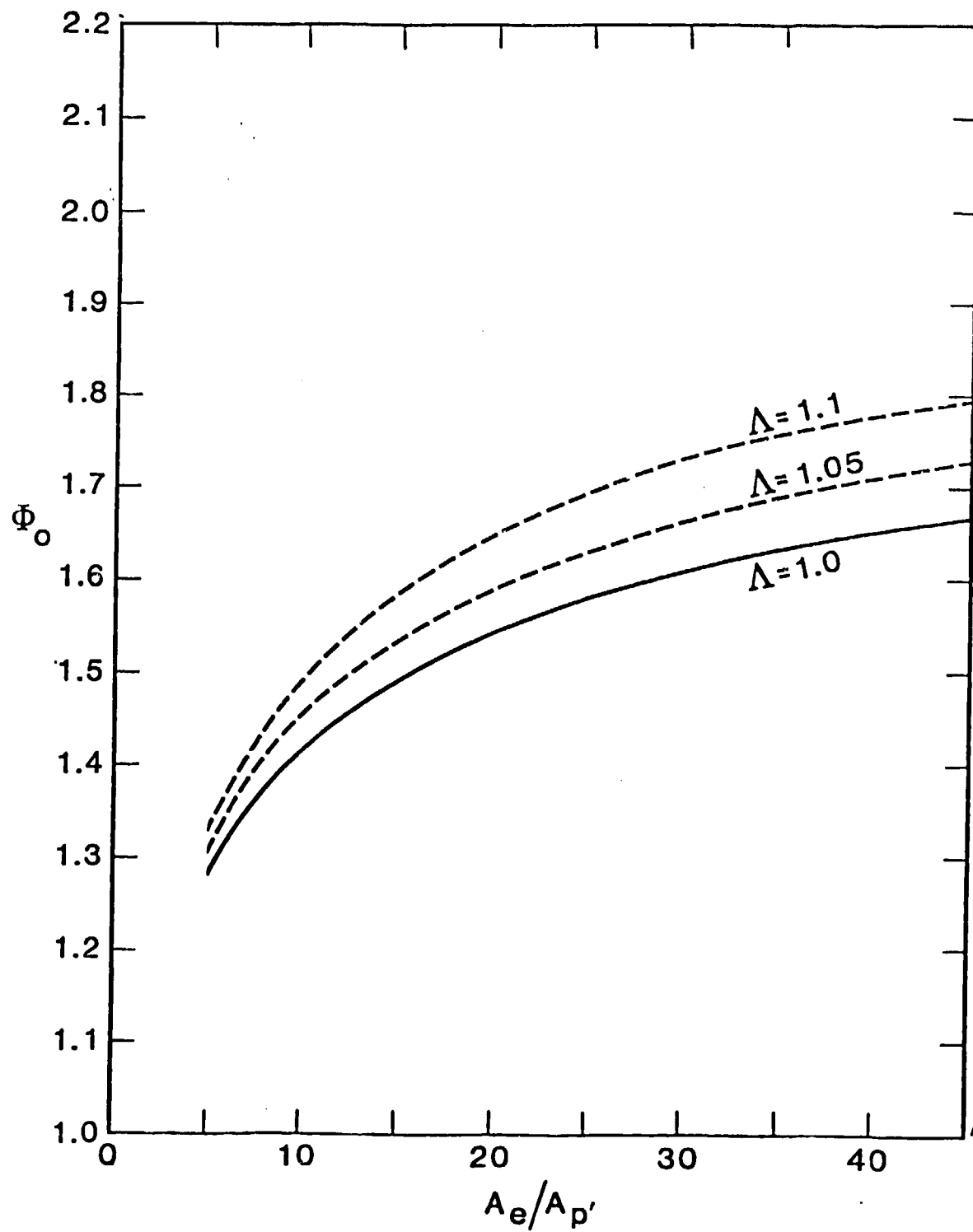
Fig. 8 – Effect of inlet nonsteadiness resulting from
lump migration in mixing
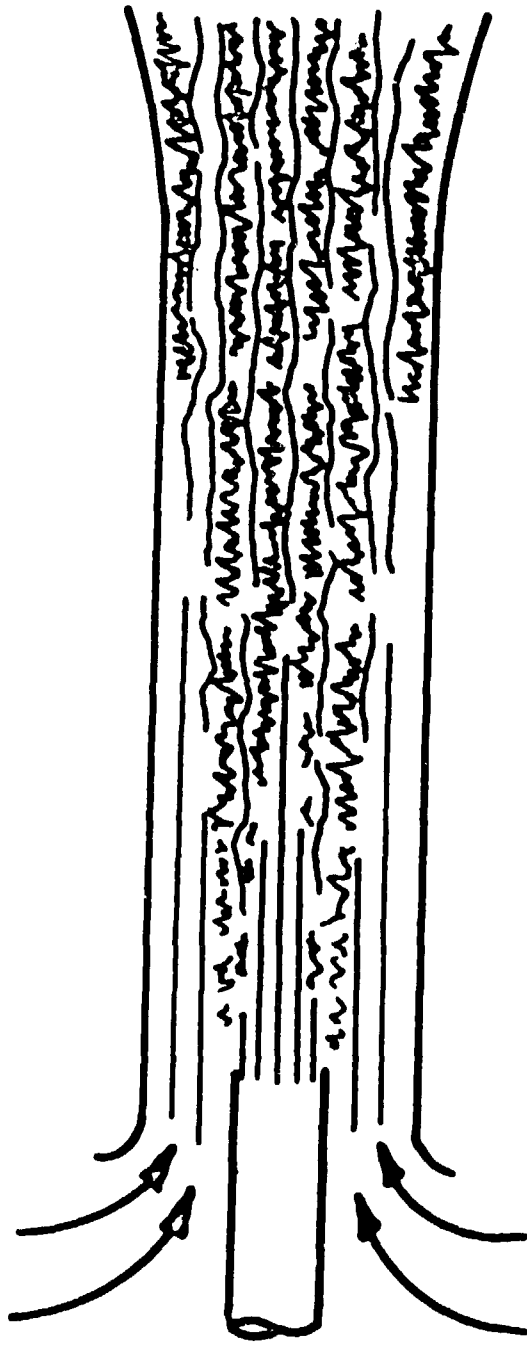
**STEADY-FLOW EJECTOR**
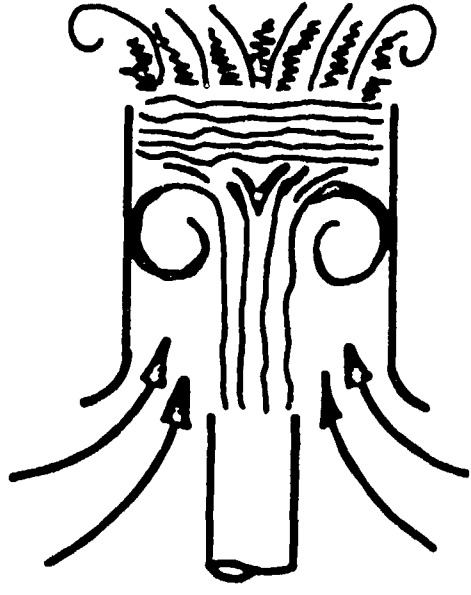
**PULSATING-FLOW EJECTOR**

Fig. 9 - Models compared by Lockwood [19]

686
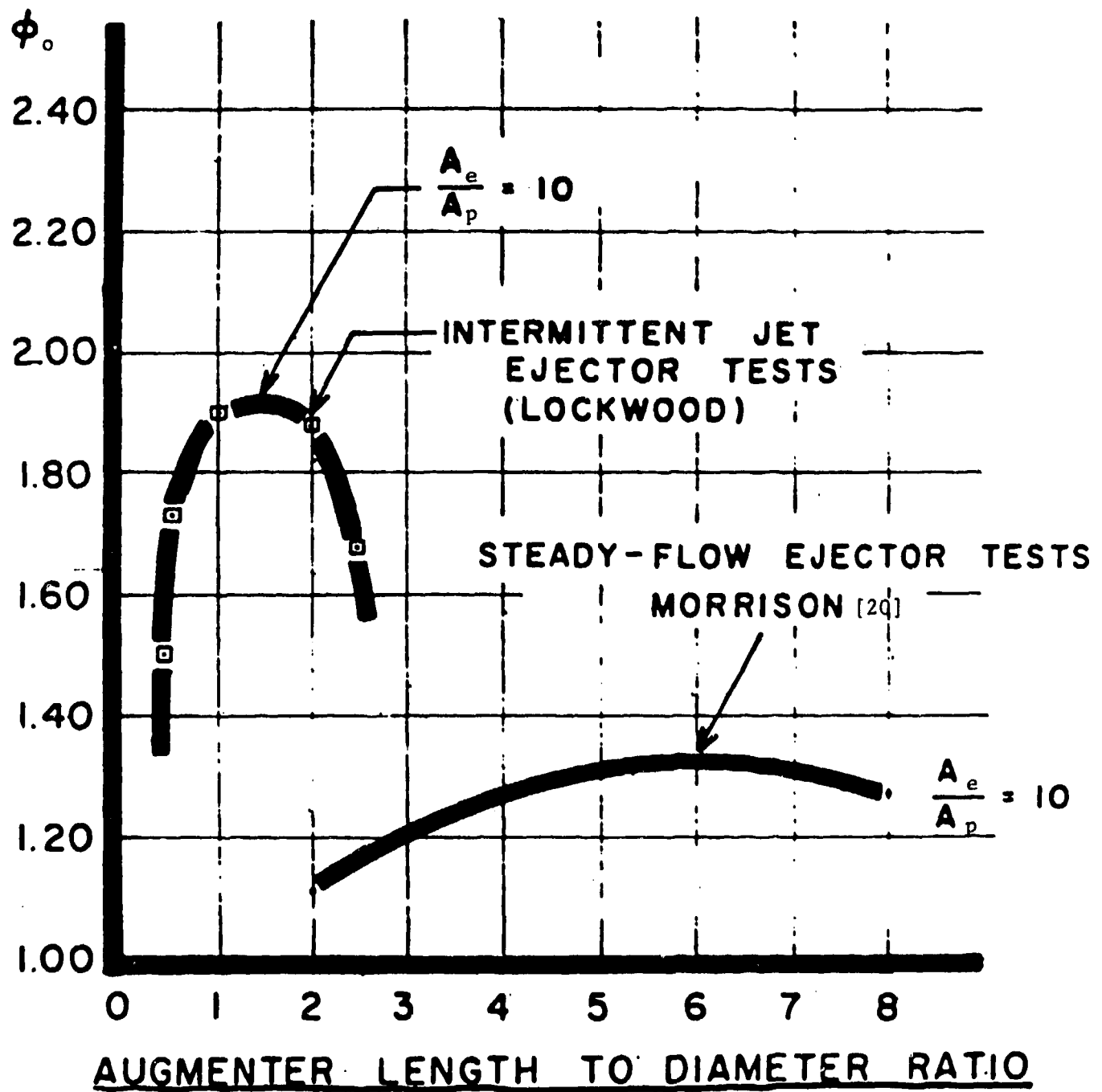
Fig. 10 – Performance comparison of models shown in Fig. 9 [19]
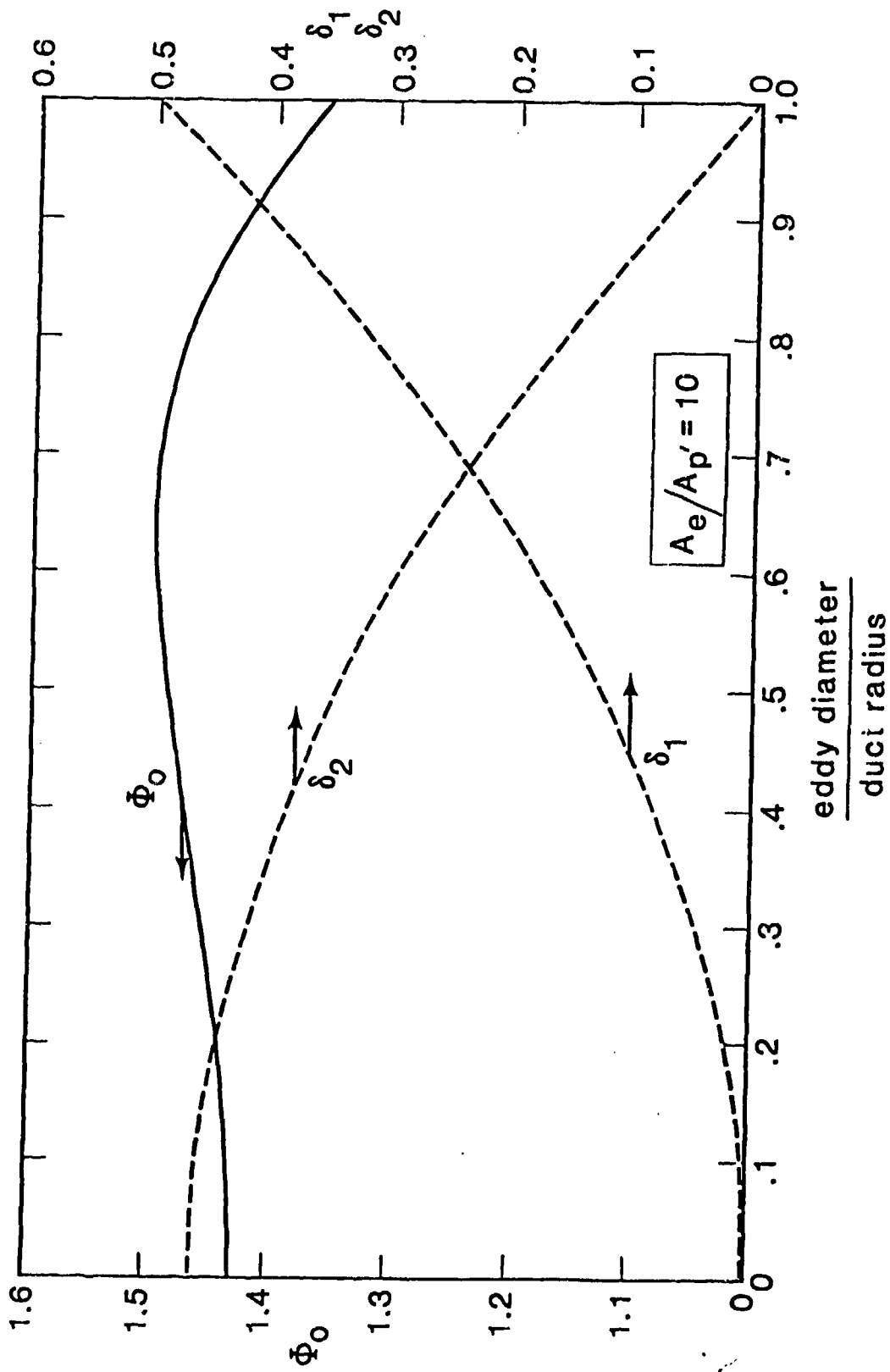
Fig. 11 - Effect of eddy size on ejector performance

# A PRELIMINARY STUDY OF VORTEX
# FORMATION FROM PULSED JETS

By

J. Z. Irdmusa* and C. A. Garris**

Department of Civil, Environmental,
and Mechanical Engineering
The George Washington University
Washington, D.C.   20052

## Introduction

It is known that superior thrust augmentation may be obtained in
ejectors by the use of pulsed jets as opposed to steady flow jets.  Pulsed
jets and other unsteady flow devices offer the advantage that they can
capitalize on the reversible work of interface pressure forces as well as
the usual irreversible turbulent mixing.  The latter alone is employed in
steady flow ejectors.

When a pulsed jet discharges into a duct or an open environment, the
jet forms a toroidal vortex ring which acts as a piston pushing the ambient
fluid in its path.  The configuration of this vortex ring can be extensively
controlled by proper control of the boundary conditions at the exit of the
jet.

The present work is a preliminary study of the configurations of the
vortex rings produced by different boundary conditions and of their sub-
sequent behavior.  It is hoped that such a study will illuminate some
avenues of improvement for pulsed-jet ejector technology.

---

*Research Assistant
**Associate Professor of Engineering

This work is distinct from most of the available literature on vortex rings (Refs. 1-6) in that it focuses on the highly viscous formation stage of vortex development rather than on the fully developed vortex commonly studied.

## Experimental Investigation

The principal vortex parameters considered in this study were:

1. Vortex size and shape

2. Vortex translational motion

3. Vortex entrainment of ambient fluid

Particular attention was devoted to the dev lopmental period of the vortex from emergence of the jet, through formation, to the fully formed vortex ring.

The control parameters were:

1. Exit configuration (sharp edged orifice, chimney, duct, etc.)

2. Intensity of jet (outlet velocity)

The methods employed were principally photographic. Both multi-flash-strobe-open-shutter photos with a 35mm still camera and high speed motion pictures with a HYCAM 16mm Cine camera were used. In order to get a better picture of the entrainment processes, some runs were taken with laser sheet illumination.

The vortices were produced in still air by means of a large loud-speaker. Pulse intensity as well as pulse duration and wave-form could be controlled. The exit jet was monitored after setting up the instrumentation with a hot-wire anemometer, but the anemometer was then removed immediately

690

prior to testing to avoid probe interference.  Flow visualization was achieved by injecting cigarette smoke into an enclosure surrounding the loudspeaker.  When the speaker was energized, the emerging jet and its transformation to a vortex ring could then be observed photographically.

## Results and Discussion

Figure 1 is a two-flash open-shutter photograph of a single vortex ring generated from a sharp-edged orifice.  Figure 2 is a similar photograph of a vortex produced from a sharp-edged chimney of the same diameter. The exit velocities were adjusted to be the same in both runs.  To facilitate comparison, the time between exposures is the same and the scales are approximately the same in both figures, as noted in the subtitles of the respective figures.

Comparison of the two figures reveals several features:

1. Size:  The vortices produced with the chimney are appreciably larger than those produced with the simple orifice.  The difference is on the order of 25%.

2. Translational Speed of Ring:  Note the larger distance travelled between exposures by the orifice-produced vortex of Fig. 1 than by the chimney-produced vortex of Fig. 2. This indicates that the vortices produced by the orifices propagate considerably faster than those produced by the chimneys for a given jet pulse strength and jet diameter. The difference is on the order of 30-35%.

3. Entrainment:  Note the very clear spiral entrainment patterns of Fig. 2 as well as the large number of rings as compared with those of Fig. 1.  This shows that the slower moving,

691

larger vortices tend to entrain more ambient fluid. This increased entrainment accounts for its larger size and, in part, for its slower speed. This will be discussed further later.

4. Formation Characteristics: Comparison of Figs. 1 and 2 shows that the orifice-generated vortices tend to form very rapidly whereas the chimney-generated vortices travel farther downstream before they are fully developed.

In Figs. 3 and 4, data taken from high-speed movies of several vortices are summarized, again highlighting the comparison between orifice-generated and chimney-generated vortices.

Fig. 3 further shows that, upon emerging, the vortex experiences a brief period of deceleration and then propagates at nearly constant speed. Fig. 4 shows that after formation, the vortices change little in size.

Further comparisons were made between vortices formed from chimneys of equal diameter but varying height, while maintaining equal exit jet speeds. The resulting effect on the vortex configuration was observed to be small.

To understand the physics of these observations, one must consider the energetics of the phenomenon. In all cases, a pulse of a given amount of kinetic energy is injected into still ambient fluid. However, if appreciable entrainment occurs, this kinetic energy must be shared by a greater amount of fluid mass, hence, one would expect a slower vortex translation. To further complicate matters, the vortex possesses both translational and

rotational kinetic energies. Hence if the vortex circulation is very high, one might expect a slower vortex as well since more of the initial kinetic energy is absorbed in the rotational mode, and less in the translational mode.

The clear, delicate spiral structure of the chimney-generated vortices of Fig. 2 demonstrates considerable entrainment. Since the spiral structure persists many diameters downstream, it appears that mixing within the vortex is very slow. The structure of the orifice-generated vortex of Fig. 1, however, demonstrates much less entrainment as indicated by its more homo- geneous appearance. This relatively homogeneous appearance may also be partly due to greater internal mixing resulting from greater circulation, however, this cannot be substantiated due to lack of quantitative information on the circulation.

We believe that although there are several differences in the fluid mechanics of the orifice-generated vortex and the chimney-generated vortex, the most significant one is that ambient air enters the vortex more freely in the latter than in the former, as the ring forms. The boundary layer over the outer surface of the orifice plate in Fig. 1 impedes the influx of ambient air. This impediment is not present around the chimney, and, as a consequence, the entrained mass is larger and the translational velocity is lower, as has been observed.

## Concluding Remarks

The present work demonstrates that considerable control over vortex characteristics may be obtained by the proper choice of exit boundary con- ditions. Further control may be obtained by choice of the history and duration of the pulsed jet. This aspect is still under study.

The preliminary work discussed here has shown the need for better quantification of vortex flow fields and entrainment characteristics. It is hoped to study the flow fields in the future using Laser Velocimetry and thereby obtain quantitative information about the vortex circulation under various conditions. Efforts are now under way to better understand the entrainment characteristics by direct time-resolved concentration mapping by means of Laser-Tomography.

After learning the degree of control one may exercise over vortex characteristics, those characteristics which are ideal for pulsed jet ejectors must be determined. It is now believed that the reversible work of interface pressure forces must be capitalized upon. Hence, it may be that the energy of rotation in the vortex may be lost and not imparted to the to the secondary flow in the ejector. In such case, one may wish to minimize the circulation. However, high circulation may promote vortex stability and, hence, vortex persistence, which perhaps is a favorable characteristic. Thus, an optimum amount of circulation for pulsed jet ejectors may exist.

## Acknowledgements

## References

1. Sullivan, J., Widnall, S.: "Study of Vortex Rings Using a Laser Doppler Velocimeter", AIAA Journal, October 1973, Vol. II, p. 1384.

2. Okabe, J., Inoue, S.: "The Generation of Vortex Rings", Report, Research Institute for Applied Mechanics, Vol. VIII, 32, 1961, 91.

3. Okabe, J., Inoue, S.: "The Generation of Vortex Rings II", Report, Research Institute for Applied Mechanics, Vol. IX, 36, 1961, 147.

4. Maxworthy, T.: "Some Experimental Studies of Vortex Rings", Journal of Fluid Mechanics, Vol. 81, No. 3, pp. 465-495, 1977.

5. Magarvey, R. H., MacLatchy, C. S.: "The Formation and Structure of Vortex Rings", Canadian Journal of Physics, Vol. 42, p. 678, 1964.

6. Maxworthy T.: "The Structure and Stability of Vortex Rings", Journal of Fluid Mechanics, Vol. 51, No. 1, pp. 15-32, 1972.

Fig. 2 - Vortex from Chimney. Chimney diameter 1", height
1", Jet pulse velocity 33 Inches/Sec. Vortex velocity
16.5 Inches/Sec, time between exposures 1/10 Sec.scale 1/2.5
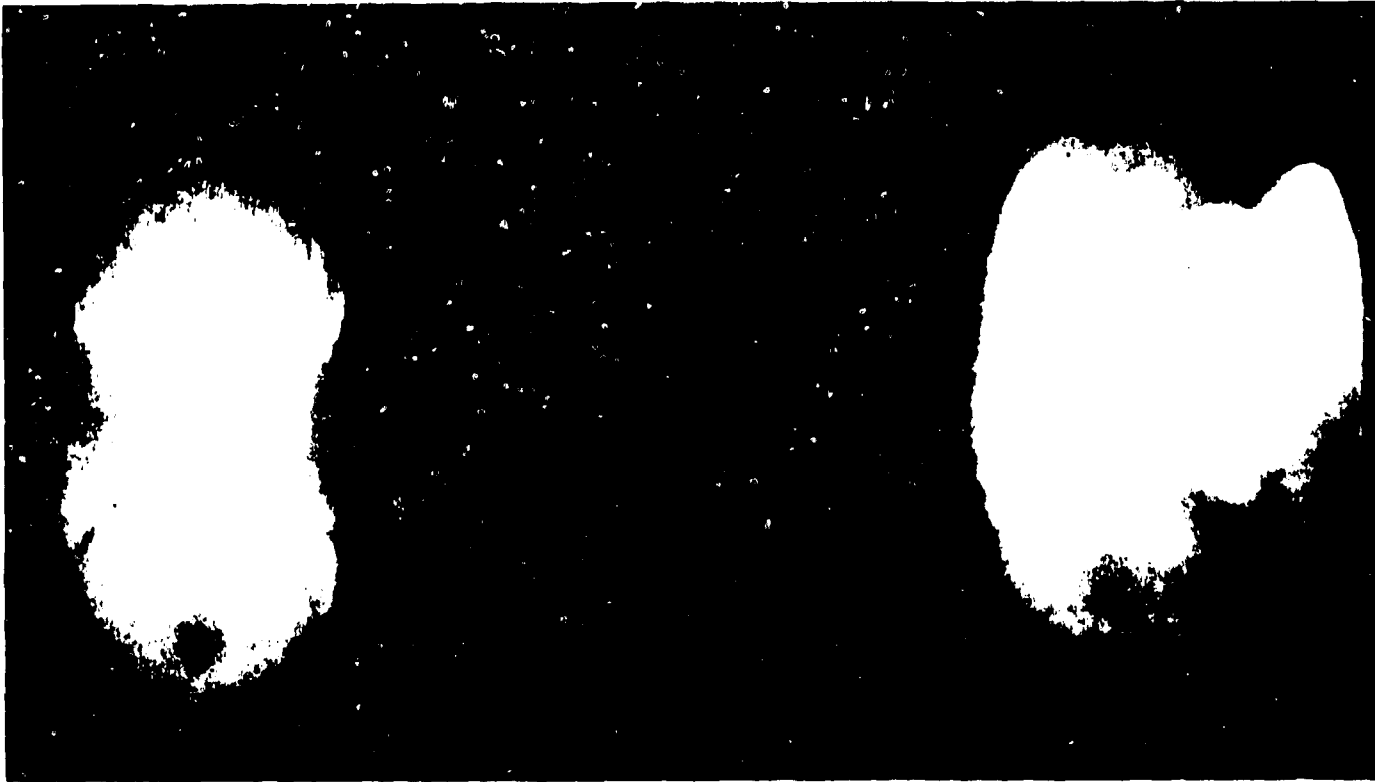


Fig. 1 - Vortex from simple orifice. Orifice diameter 1",
Jet pulse velocity 33 Inches/Sec. Vortex velocity 21.6
Inches/Sec, time between exposures 1/10 Sec,scale 1/2.3
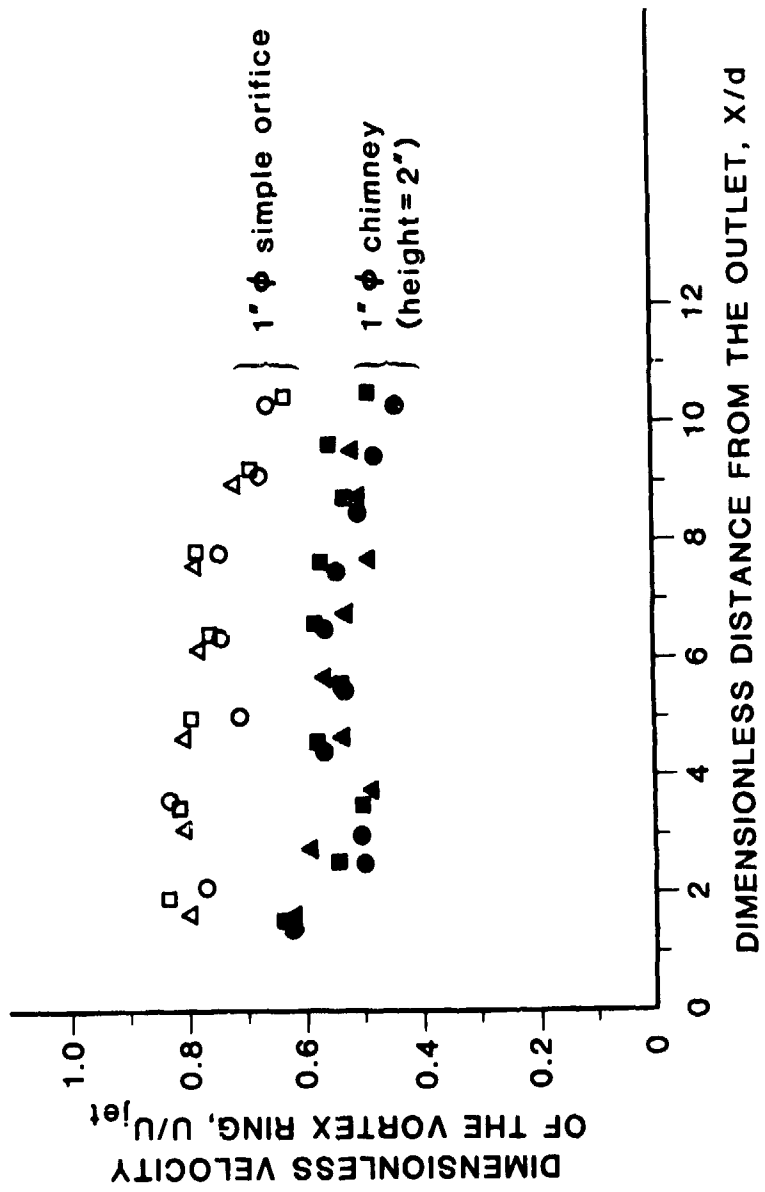
Fig. 3 – Comparison of Vortex Translational Velocities vs. Distances from Outlet for Simple Orifice (unfilled symbols) and for Chimney (filled symbols). Data are obtained from High-Speed movies and different shapes of symbols denote different vortices. For all data, initial jet pulse velocity = 33 inches/sec.
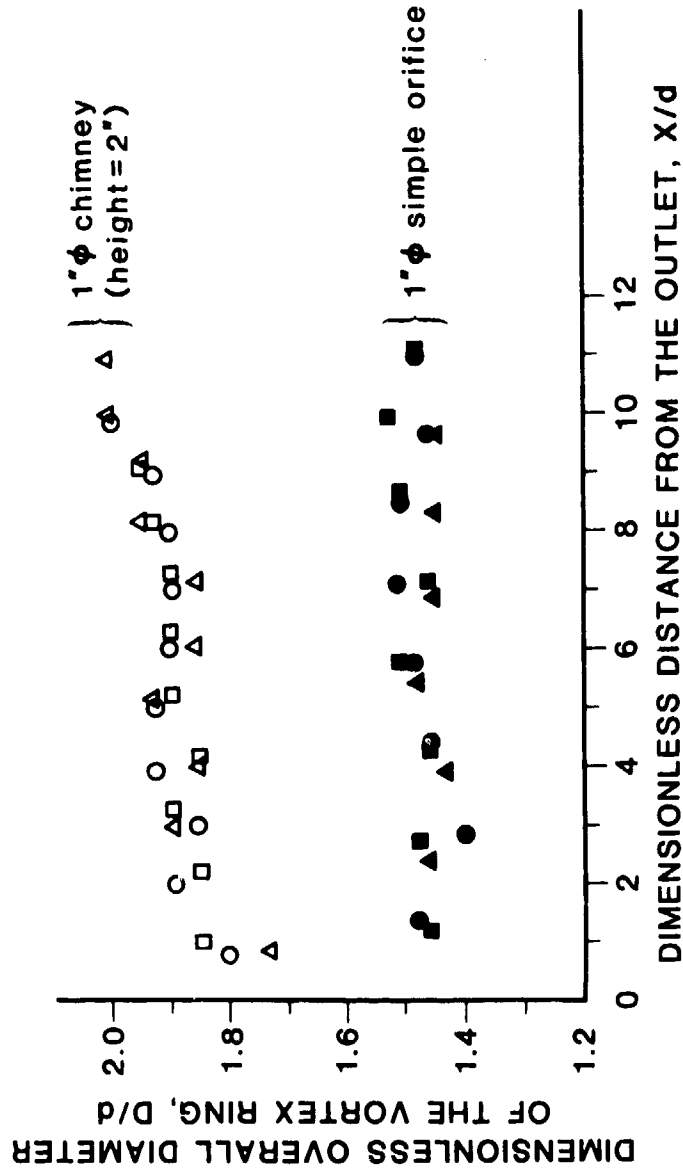
Fig. 4 - Comparison of Vortex Diameters vs. Distances from Outlet for Simple Orifice (filled symbols) and chimney (unfilled symbols). Data are obtained from High-Speed movies and different shapes of symbols denote different vortices. For all data, initial jet pulse velocity = 33 inches/sec.

698

# STUDY OF THREE-DIMENSIONAL THRUST-AUGMENTING EJECTORS

Ramesh K. Agarwal*
McDonnell Douglas Corporation
St. Louis, Missouri 63166

## ABSTRACT

A theory is presented for the prediction of thrust augmentation characteristics of a three-dimensional ejector configuration in which a series of rectangular-hypermixing nozzles pumps the secondary air in a constant-area or slowly diverging channel. Based on the theory, a computer program is developed which requires the ejector design parameters, the empirical constants in the eddy viscosity model, and the nozzle pressure ratio as input and calculates the entrained secondary mass flow, the secondary and exit velocities, the net thrust and the thrust augmentation ratio. Good agreement is found between the theoretical prediction and the experimental data.

## NOMENCLATURE

| | |
|---|---|
| $A$ | area |
| $A_t$ | throat area |
| $U$ | velocity |
| $\bar{V}_e$ | average exit velocity |
| $p$ | static pressure |
| $p_t$ | total pressure |
| $\rho$ | density |
| $T$ | temperature |
| $L$ | ejector length |
| $H_t$ | throat height |
| $b_o$ | nozzle half width |
| $t_o$ | nozzle half height |
| $h$ | spacing between the nozzles |
| $R$ | gas constant |
| Re | Reynolds number |
| $g_{\bar{c}}$ | gravitational constant |
| $E$ | entrainment ratio |
| $C_D$ | discharge coefficient |
| $\Phi$ | augmentation ratio |
| $\theta$ | diffuser half angle |
| $\eta_D$ | diffuser efficiency |
| $\eta_N$ | nozzle efficiency |
| $\eta_T$ | thrust efficiency |

### Subscripts

| | |
|---|---|
| S | secondary condition |
| e | exit condition |
| N | nozzle condition |
| a | ambient |

---

*Scientist, McDonnell Douglas Research Laboratories

AD P000524

## INTRODUCTION

In V/STOL aircraft, lift and thrust augmentation is needed to achieve vertical or short take-offs and landings. A number of devices have been suggested to achieve high lift and thrust. Excellent reviews of such devices have been given recently by Korbacher[1] and Smith.[2] One such device is an ejector in which entrainment by a jet of primary fluid is used to pump secondary flow through a duct. The thrust of the mixed flow generally exceeds that of the primary jet alone and thus can serve to augment and deflect the thrust of a cruise engine to achieve vertical or short take-offs and landings.

A large number of theoretical and experimental investigations have been conducted to understand the mechanics of ejector performance and thus evaluate its suitability for V/STOL aircraft application. Most of the theoretical investigations[3-5] base their analyses on a simplified model of the ejector in which the turbulent mixing of parallel primary and secondary uniform streams in a constant-area channel or a constant-pressure channel is considered with or without a diffuser at the end of the mixing duct. Experiments have been conducted by simulating this simplified model in the laboratory.[5-7] These investigations show that ejectors of long length are needed to achieve significant levels of augmentation. However, the increase in the rate of mixing and the diffusion of the mixed flow can result in significant increase in the augmentation ratio. In order to promote mixing, hypermixing nozzles have been suggested which seem to show promise.[7] While the simplified model helps in understanding why an ejector works, it is not capable of predicting the performance of a real ejector behind a wing. Two major configuration effects which must be taken into account to reasonably predict the performance of a real ejector behind a wing under static conditions are (a) the effect of multiple jets shooting into the ejector channel and (b) the effect of inclination of the ejector axis to the wing chord. The evaluation of the overall performance of an augmentor wing, however, also must take into account the effect of flow over the wing and that of the jet emerging from the ejector channel.

In the present investigation, we consider an ejector configuration in which a series of equally spaced, rectangular-hypermixing nozzles pumps the secondary air in a constant-area or slowly diverging channel, as shown in Fig. 1. In the most general case, the height of the nozzle may be smaller than the channel width at the throat, although in many of the ejectors designed (including the experimental model at NASA Ames Research Center), the height of the nozzle is equal to the width of the ejector channel inlet. As a first step towards this study, we determined the flowfield of an array of turbulent three-dimensional jets issuing from rectangular-hypermixing nozzles immersed in a secondary stream in an unbounded space or in a constant-area channel. For computing the thrust augmentation attributable to an ejector configuration shown in Fig. 1, we used these flowfield descriptions in the yz plane at the exit and employed one-dimensional control-volume-type analysis in the xz plane. For a constant-area channel, such an approach is quite accurate. For a slowly diverging channel, the approach is adequate if an appropriate area correction factor is introduced. A computer program was written to solve the coupled one-dimensional compressible flow continuity and momentum equations. The program requires the ejector design parameters, the empirical description of the hypermixing-eddy viscosity model, and the nozzle pressure ratio as input and calculates the entrained secondary mass flow, the secondary and exit velocities, the net thrust, and the thrust augmentation ratio. Results are presented and a comparison is made with the experimental data of Aiken.[8]
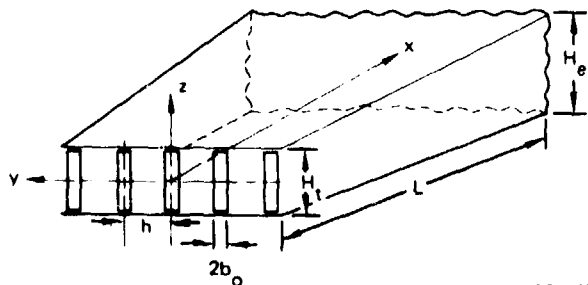


Fig. 1 Ejector configuration.

GP11 0850-1

700

# FLOWFIELD OF A 3-D RECTANGULAR-HYPERMIXING JET
## IMMERSED IN AN EXTERNAL STREAM IN UNBOUNDED SPACE

Consider a three-dimensional turbulent jet of an incompressible viscous fluid of uniform velocity $U_N$ issuing from a rectangular nozzle of width $2b_o$ and height $2t_o$ into a secondary stream of velocity $U_S$. We employ the cartesian coordinate system with x-coordinate along the axis of the jet as shown in Fig. 2. Assuming that the velocity components can be expressed as $v_i = u_i + u_i'$ (i = 1,2,3), where $u_i$ represents the mean value and $u_i'$ the fluctuating part, the governing equations are the continuity and the time-averaged Navier-Stokes equations:

$$\frac{\partial u_j}{\partial x_j} = 0 , \tag{1}$$

$$u_j \frac{\partial u_i}{\partial x_j} = - \frac{1}{\rho} \frac{\partial p}{\partial x_i} + v \frac{\partial^2 u_i}{\partial x_i \partial x_j} + \frac{\partial \tau_{ij}}{\partial x_j} , \tag{2}$$

and

$$x_i = (x, y, z), \ u_i = (u, v, w), \ \tau_{ij} = - \overline{u_i' u_j'} .$$

In Eq. (2), $v$ denotes the laminar viscosity and $\tau_{ij}$ are the turbulent stresses. Nondimensionalizing the equations, velocity components with $U_N$, the coordinates with $2t_o$, and the pressure with $\rho U_N^2$,

$$\frac{\partial \bar{u}_j}{\partial \bar{x}_j} = 0 \tag{3}$$



Rectangular nozzle

GP11 0650 2
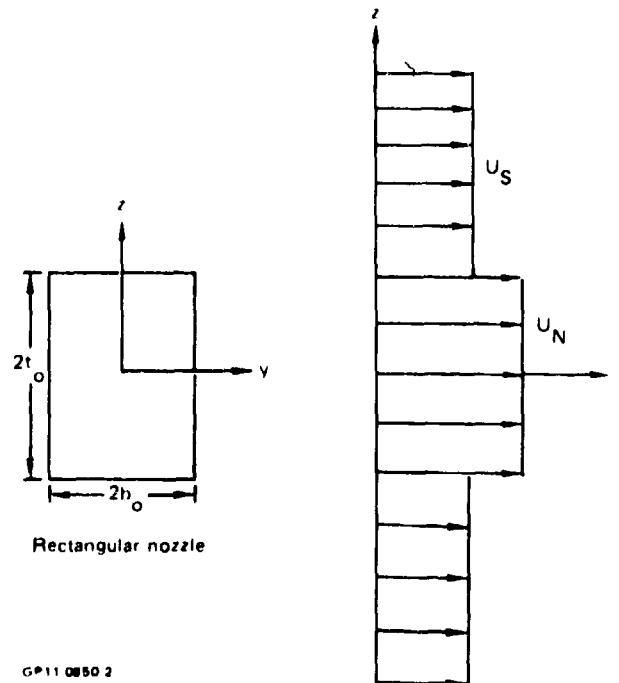
Fig. 2  Velocity profile in the xz plane at the exit of
the nozzle.

701

and

$$\bar{u}_j \frac{\partial \bar{u}_i}{\partial \bar{x}_j} = - \frac{\partial \bar{p}}{\partial \bar{x}_i} + \frac{1}{Re} \frac{\partial^2 \bar{u}_i}{\partial \bar{x}_i \partial \bar{x}_j} + \frac{\partial \bar{\tau}_{ij}}{\partial \bar{x}_j},$$ (4)

where Re is the Reynolds number.

Now we introduce the usual boundary-layer variables:

$$Y = \sqrt{Re}\ \bar{y}; \qquad Z = \sqrt{Re}\ \bar{z}, \qquad X = \bar{x}$$

and assume the following expansions for the velocity components, pressure, and turbulent shear stresses:

$$\bar{u} = \bar{u}_o + \frac{1}{\sqrt{Re}}\ \bar{u}_1 + \ldots$$

$$\bar{v} = \frac{1}{\sqrt{Re}}\ \bar{v}_1 + \ldots$$

$$\bar{w} = \frac{1}{\sqrt{Re}}\ \bar{w}_1 + \ldots$$

$$\bar{p} = \bar{p}_o + \frac{1}{\sqrt{Re}}\ \bar{p}_1 + \frac{1}{Re}\ \bar{p}_2 + \ldots$$

$$\bar{\tau}_{xx} = \frac{1}{\sqrt{Re}}\ \bar{\tau}_{1xx} + \ldots$$ (5)

Taking the limit Re $\to \infty$, we arrive at the boundary-layer equations for the three-dimensional turbulent jet flow:

$$\frac{\partial \bar{u}_o}{\partial X} + \frac{\partial \bar{v}_1}{\partial Y} + \frac{\partial \bar{w}_1}{\partial Z} = 0$$ (6a)

$$\bar{u}_o \frac{\partial \bar{u}_o}{\partial X} + \bar{v}_1 \frac{\partial \bar{u}_o}{\partial Y} + \bar{w}_1 \frac{\partial \bar{u}_o}{\partial Z} = - \frac{\partial \bar{p}_o}{\partial X} + \frac{\partial^2 \bar{u}_o}{\partial Y^2} + \frac{\partial^2 \bar{u}_o}{\partial Z^2} + \frac{\partial \bar{\tau}_{1xy}}{\partial Y} + \frac{\partial \bar{\tau}_{1xz}}{\partial Z}$$ (6b)

$$\bar{u}_o \frac{\partial \bar{v}_1}{\partial X} + \bar{v}_1 \frac{\partial \bar{v}_1}{\partial Y} + \bar{w}_1 \frac{\partial \bar{v}_1}{\partial Z} = - \frac{\partial \bar{p}_2}{\partial Y} + \frac{\partial^2 \bar{v}_1}{\partial Y^2} + \frac{\partial^2 \bar{v}_1}{\partial Z^2} + \frac{\partial \bar{\tau}_{1xy}}{\partial X} + \frac{\partial \bar{\tau}_{2yy}}{\partial Y} + \frac{\partial \bar{\tau}_{2yz}}{\partial Z}$$ (6c)

$$\bar{u}_o \frac{\partial \bar{w}_1}{\partial X} + \bar{v}_1 \frac{\partial \bar{w}_1}{\partial Y} + \bar{w}_1 \frac{\partial \bar{w}_1}{\partial Z} = - \frac{\partial \bar{p}_2}{\partial Z} + \frac{\partial^2 \bar{w}_1}{\partial Y^2} + \frac{\partial^2 \bar{w}_1}{\partial Z^2} + \frac{\partial \bar{\tau}_{1xz}}{\partial X} + \frac{\partial \bar{\tau}_{2yz}}{\partial Y} + \frac{\partial \bar{\tau}_{2zz}}{\partial Z}$$ (6d)

$$- \frac{\partial \bar{p}_o}{\partial Y} = - \frac{\partial \bar{p}_o}{\partial Z} = 0$$ (6e)

702

$$\frac{\partial \bar{p}_1}{\partial Y} = \frac{\partial \bar{\tau}_{1yy}}{\partial Y} + \frac{\partial \bar{\tau}_{1yz}}{\partial Z} , \qquad \frac{\partial \bar{p}_1}{\partial Z} = \frac{\partial \bar{\tau}_{1yz}}{\partial Y} + \frac{\partial \bar{\tau}_{1zz}}{\partial Z} \tag{6f}$$

Eqs. (6a–6f) represent the complete set of boundary-layer equations governing the flowfield of a three-dimensional rectangular jet. An eddy viscosity model or a closure hypothesis is needed to represent the turbulent shear stresses in terms of the mean-flow velocity gradients. Further simplification is obtained by recognizing that the turbulent stress terms are an order of magnitude larger than the laminar viscous terms:

$$\frac{\partial \bar{u}_o}{\partial X} + \frac{\partial \bar{v}_1}{\partial Y} + \frac{\partial \bar{w}_1}{\partial Z} = 0 \tag{7a}$$

$$\bar{u}_o \frac{\partial \bar{u}_o}{\partial X} + v_1 \frac{\partial \bar{u}_o}{\partial Y} + w_1 \frac{\partial \bar{u}_o}{\partial Z} = -\frac{\partial \bar{p}_o}{\partial X} + \frac{\partial \bar{\tau}_{1xy}}{\partial Y} + \frac{\partial \bar{\tau}_{1xz}}{\partial Z} \tag{7b}$$

$$\bar{u}_o \frac{\partial \bar{v}_1}{\partial X} + \bar{v}_1 \frac{\partial \bar{v}_1}{\partial Y} + \bar{w}_1 \frac{\partial \bar{v}_1}{\partial Z} = -\frac{\partial \bar{p}_2}{\partial Y} + \frac{\partial \bar{\tau}_{1xy}}{\partial X} + \frac{\partial \bar{\tau}_{2yy}}{\partial Y} + \frac{\partial \bar{\tau}_{2yz}}{\partial Z} \tag{7c}$$

$$\bar{u}_o \frac{\partial \bar{w}_1}{\partial X} + \bar{v}_1 \frac{\partial \bar{w}_1}{\partial Y} + \bar{w}_1 \frac{\partial \bar{w}_1}{\partial Z} = -\frac{\partial \bar{p}_2}{\partial Z} + \frac{\partial \bar{\tau}_{1xz}}{\partial X} + \frac{\partial \bar{\tau}_{2yz}}{\partial Y} + \frac{\partial \bar{\tau}_{2zz}}{\partial Z} \tag{7d}$$

$$-\frac{\partial \bar{p}_o}{\partial Y} = -\frac{\partial \bar{p}_o}{\partial Z} = 0 \tag{7e}$$

$$\frac{\partial \bar{p}_1}{\partial Y} = \frac{\partial \bar{\tau}_{1yy}}{\partial Y} + \frac{\partial \bar{\tau}_{1yz}}{\partial Z} , \qquad \frac{\partial \bar{p}_1}{\partial Z} = \frac{\partial \bar{\tau}_{1yz}}{\partial Y} + \frac{\partial \bar{\tau}_{1zz}}{\partial Z} \tag{7f}$$

Now we assume that the static pressure remains constant in the entire flowfield (an appropriate assumption) so that $\partial \bar{p}_o / \partial X = 0$. Also the velocity difference ($U_N - U_S$) is considered small (essentially valid far downstream from the nozzle) so that we can write $\bar{u}_o = U_S/U_N + \hat{u}$. Linearizing Eqs. (7a–7f) such that the terms second-order in $\hat{u}$, $\bar{v}_1$, $\bar{w}_1$ and their gradients are neglected, we find that the flow field due to the fluid mechanical mixing of the jet with the external stream can be described by the equation

$$\frac{U_S}{U_N} \cdot \frac{\partial \hat{u}}{\partial X} = \frac{\partial \bar{\tau}_{1xy}}{\partial Y} + \frac{\partial \bar{\tau}_{1xz}}{\partial Z} . \tag{8}$$

Defining $\bar{\tau}_{1xy}$ and $\bar{\tau}_{1xz}$ in terms of an eddy viscosity and assuming that the eddy viscosity is a function of X only, Eq. (8) can be written as

$$\frac{U_S}{U_N} \cdot \frac{\partial \hat{u}}{\partial \bar{X}} = \bar{\epsilon}(X) \left( \frac{\partial^2 \hat{u}}{\partial Y^2} + \frac{\partial^2 \hat{u}}{\partial Z^2} \right) . \tag{9}$$

Writing Eq. (9) in terms of dimensional variables,

$$U_S \frac{\partial u}{\partial x} = \epsilon(x) \left( \frac{\partial^2 u}{\partial y^2} + \frac{\partial^2 u}{\partial z^2} \right) . \tag{10}$$

The description for $\epsilon$ is provided by formulating a suitable model which gives best agreement of the theory with experiment. Bevilaqua[7] has shown that the effect of hypermixing can be incorporated by defining an eddy viscosity whose length and velocity scales are proportional to the vortex size and rotational spread of the hypermixing vortices. In case of hypermixing, he shows that

$$\epsilon = \epsilon_0 + \epsilon_H = \epsilon_0 + C \left( u/U_S \right) \Big/ \int_{-x_0}^{x} dx/u , \tag{11}$$

where $\epsilon_0$ is the conventional eddy viscosity related to Reynolds stresses and $\epsilon_H$ is the eddy viscosity related to vortex-induced stresses, $x_0$ is the distance from apparent origin of the vortices to the actual origin of the jet, and C is an empirical constant. Combining Eqs. (10) and (11), the governing equation for the flowfield becomes

$$U_S \frac{\partial u}{\partial x} = \left\{ \epsilon_0 + U_S C \left( x + x_0 \right)^{-1} \right\} \left[ \frac{\partial^2 u}{\partial y^2} + \frac{\partial^2 u}{\partial z^2} \right] . \tag{12}$$

Introducing a stretching transformation

$$\frac{\partial \xi}{\partial x} = \alpha + C \left( x + x_0 \right)^{-1}, \qquad \alpha = \frac{\epsilon_0}{U_S} ,$$

Eq. (12) becomes

$$\frac{\partial u}{\partial \xi} = \frac{\partial^2 u}{\partial y^2} + \frac{\partial^2 u}{\partial z^2} . \tag{13}$$

We are interested in the solution of Eq. (13) subject to the following boundary conditions:

$$\text{At } x = 0, u = U_N - U_S \quad \text{for} \quad |y| \le b_0, |z| \le t_0$$

$$= 0 \quad \text{for} \quad |y| > b_0, |z| > t_0$$

$$\text{At } x > 0, u \to 0 \quad \text{for} \quad y \to \infty, z \to \infty .$$

Employing the method of separation of variables, the solution can be written as

$$u = u_0 - U_S = \frac{U_N - U_S}{4}\left[ \text{Erf } \frac{b_0 - y}{2\sqrt{\xi}} + \text{Erf } \frac{b_0 + y}{2\sqrt{\xi}} \right]\left[ \text{Erf } \frac{t_0 - z}{2\sqrt{\xi}} + \text{Erf } \frac{t_0 + z}{2\sqrt{\xi}} \right], \quad (14)$$

where

$$\text{Erf } \zeta = \frac{2}{\sqrt{\pi}} \int_0^\zeta e^{-t^2} dt .$$

An analogous solution for a laminar jet has been obtained by Pai and Hsieh.[9]

In case of a 2-D jet of width $2b_0$, $t_0 \to \infty$ and the solution becomes

$$u = u_0 - U_S = \frac{U_N - U_S}{2}\left[ \text{Erf } \frac{b_0 - y}{2\sqrt{\xi}} + \text{Erf } \frac{b_0 + y}{2\sqrt{\xi}} \right] . \quad (15)$$

From Eq. (14), we can draw conclusions regarding the decay of jet-centerline velocity and the spread of the jet in various directions.

**Decay of Centerline Velocity of the Jet**

The maximum velocity $u_m$ of the jet at a given station x occurs on the jet axis, i.e., at $y = 0$, $z = 0$. Eq. (14) gives

$$\frac{u_m}{U_N - U_S} = \frac{u_{om} - U_S}{U_N - U_S} = \text{Erf}\left( \frac{b_0}{2\sqrt{\xi}} \right) \text{Erf}\left( \frac{t_0}{2\sqrt{\xi}} \right) . \quad (16)$$

In Fig. 3, we plot $u_m/(U_N - U_S)$ as a function of $\sqrt{\xi}$ for $b_0 = 1$ and various values of $t_0$. The decay rate of $u_m/(U_N - U_S)$ with $\xi$ decreases as $t_0$ increases (large aspect ratio). In jet mixing problems the decay rate of maximum velocity decreases as the total momentum of the jet increases. In Fig. 3, the total momentum of the jet increases with $t_0$ so that the rate of decay of maximum velocity decreases as the aspect ratio of the nozzle increases.
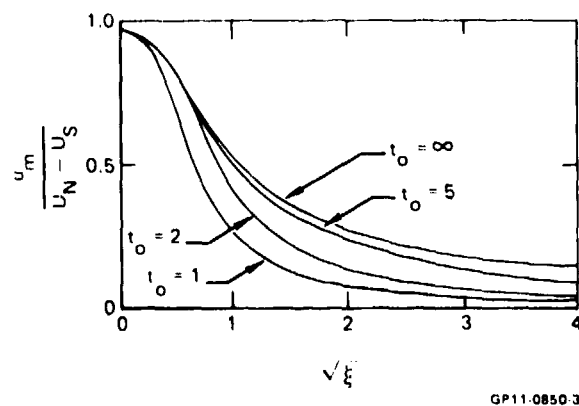
Fig. 3 Centerline velocity of the jet as a function of
distance downstream from the nozzle exit for
various aspect ratios ($b_0 = 1$).

## Spread of the Jet in Various Directions

The main feature of the three-dimensional jet mixing is that the spread of the jet is different in different directions. A contour of constant u at a given x can be used to describe the spread of the jet.

Let $r_k = \sqrt{y_k^2 + z_k^2}$ be the radial distance from the x-axis at a given $\xi$, where the subscript k refers to the point where $u(\xi, k) = k \cdot u_m (\xi)$ and $0 < k < 1$. It is evident that $r_k$ is different in different directions. In Fig. 4, $r_k$ is plotted in both the y-direction, $r_k = s_{ky}$ (z = 0), and the z-direction, $r_k = s_{kz}$ (y = 0), for k = 0.5 and 0.75. The spread $s_{kz}$ along the direction of the side $t_o > 1$ is slower than that along the shorter side. The points '0' give the locations where $s_{0.5y} = s_{0.5z}$ in Fig. 4a. In Fig. 4b, we find that the width of the jet will first decrease with increasing of $\xi$ until a minimum point is reached, after which the width increases with $\xi$; such behavior exists for all values of k between 0.5 and 1.

In order to examine closely what happens downstream of point '0' in Fig. 4a, whose location is a function of $t_o$, we calculate the width of the jet for large values of $\xi$. The asymptotic expressions of $s_{ky}$ and $s_{kz}$ for large values of $\xi$ can be obtained as

$$s_{ky}^2 = 4(1 - k)\left[ \xi - \frac{b_o^2}{12} \right] \tag{17a}$$

$$s_{kz}^2 = 4(1 - k)\left[ \xi - \frac{t_o^2}{12} \right]. \tag{17b}$$

At large values of $\xi$, $s_{ky} > s_{kz}$ for $t_o > b_o$. Equations (17) also show that at large values of $\xi$, $s_{ky} \simeq s_{kz}$. Therefore, the widths of the jet in the major (z-axis) and the minor (y-axis) axes of the nozzle will cross over (only one crossover) and tend to become equal. Far downstream, therefore, the rectangular jet tends to become axisymmetric.

706
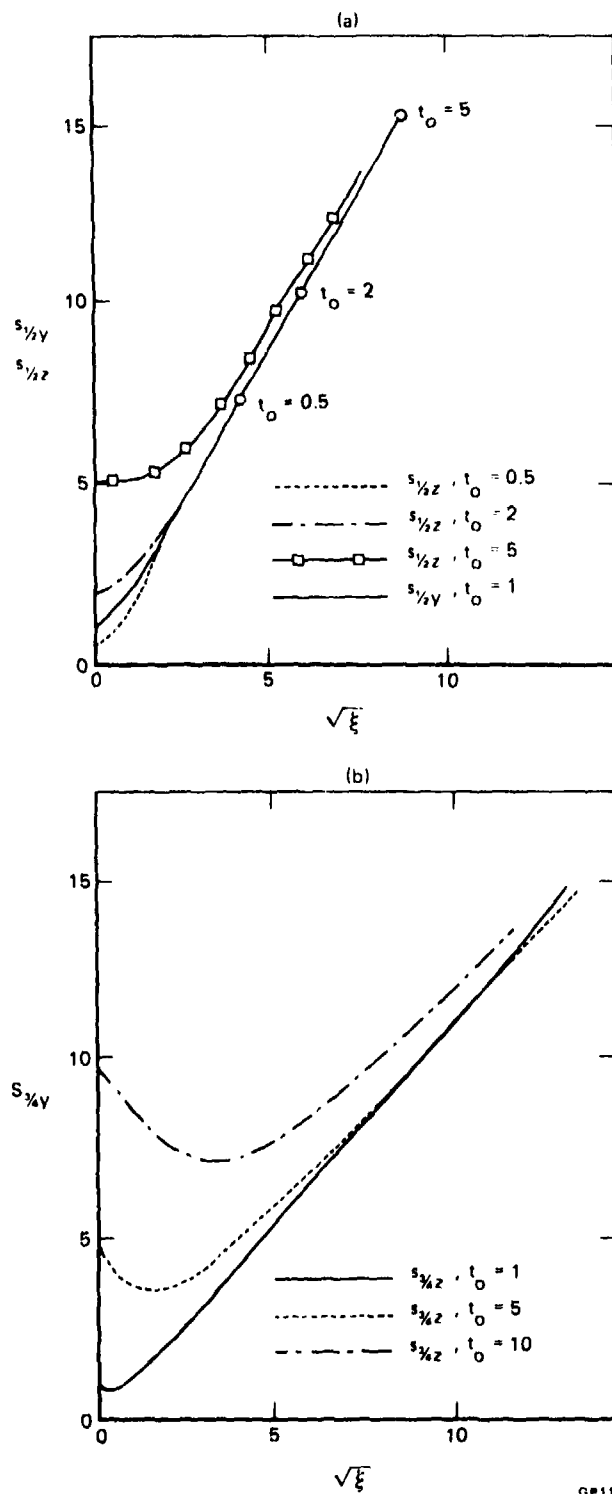
Fig. 4 Jet width, $s_{ky}(z = 0$ plane) and $s_{kz}$ ($y = 0$
plane), at $u = k\,u_m$ as a function of distance
downstream from exit; (a) $k = 0.5$ and
(b) $k = 0.75$. (o) denotes the point where
$s_{1/2y} = s_{1/2z}$ for various $t_o$.

## FLOWFIELD OF AN ARRAY OF 3-D RECTANGULAR-HYPERMIXING JETS IMMERSED IN AN EXTERNAL STREAM IN UNBOUNDED SPACE OR IN A CONSTANT-AREA CHANNEL

Since Eq. (13) is linear, the flowfield resulting from an array of equally spaced nozzles, with their centerlines at a distance h apart, issuing jets of uniform velocity $U_N$ into an external stream of velocity $U_S$ ($U_S < U_N$) is given by the superposition of individual jet flowfields. Therefore, for the configuration shown in Fig. 5, the streamwise velocity is given by

$$\frac{u_o - U_S}{U_N - U_S} = \frac{1}{4}\left[\text{Erf}\,\frac{t_o - z}{2\sqrt{\xi}} + \text{Erf}\,\frac{t_o + z}{2\sqrt{\xi}}\right] \cdot \sum_{n=-N}^{M}\left[\text{Erf}\,\frac{b_o - y - nh}{2\sqrt{\xi}} + \text{Erf}\,\frac{b_o + y - nh}{2\sqrt{\xi}}\right],$$

(18)



yz-plane



Apparent origin

xz-plane
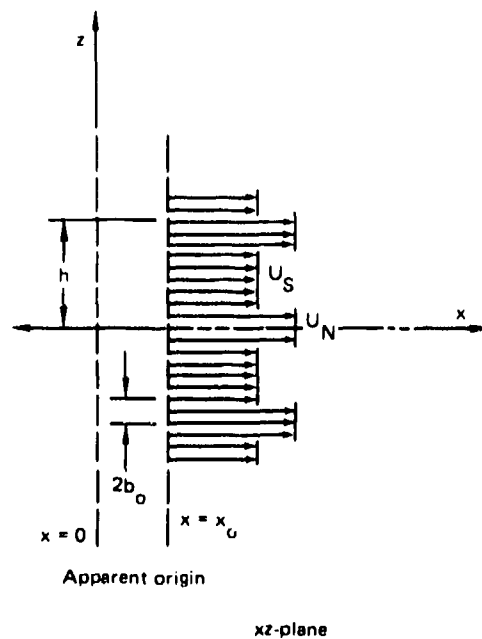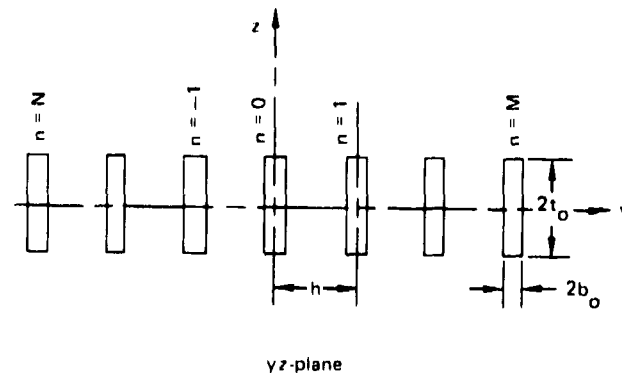
GP11-0850-5

Fig. 5 Velocity profile in the throat region of the ejector due to an array of rectangular nozzles.

708

where the total number of nozzles is $(M + N + 1)$.

If the array of Fig. 5 is symmetrically confined between two parallel plates at a distance $H_t$ apart, the solution for the streamwise velocity $u_o(\xi, y, z)$ is given by

$$\frac{u_o - U_S}{U_N - U_S} = \frac{1}{2} \sum_{n=-N}^{M} \left[ \text{Erf} \frac{b_o + y - nh}{2\sqrt{\xi}} + \text{Erf} \frac{b_o - y + nh}{2\sqrt{\xi}} \right]$$

$$\cdot \left[ \frac{2t_o}{H_t} + \frac{2}{\pi} \sum_{m=1}^{\infty} \frac{1}{m} \sin \frac{2m\pi t_o}{H_t} \cos \frac{2m\pi z}{H_t} \cdot \exp\left\{ -\left(\frac{2m\pi}{H_t}\right)^2 \xi \right\} \right]. \quad (19)$$

When $2t_o = H_t$, i.e., the nozzle height is equal to the width of the channel, Eq. (19) reduces to the solution for an array of 2-D jets. In the subsequent discussion, we denote $4\xi = 4[\alpha x + C \ln (1 + x/x_o)]$ as $b^2(x)$, where $b$ is a standard notation to describe the width of the mixing zone, $\alpha$ and $C$ are constants determined experimentally, and $x_o$ is determined by the condition that at $x = x_o$, $b = b_o$ (half width of the nozzle):

$$x_o = \frac{1}{\alpha} \left( \frac{b_o^2}{4} - C \ln 2 \right). \quad (20)$$

## THEORY FOR THE PREDICTION OF EJECTOR PERFORMANCE

For computing the thrust augmentation and entrained secondary flow resulting from the ejector configuration shown in Fig. 1, we use the flowfield Eq. (19) in the yz plane at the exit and employ one-dimensional control volume type analysis in the xz plane.

From Eq. (19), for a constant-area ejector, at the exit section 'e',

$$\frac{u_e - U_S}{U_N - U_S} = \frac{1}{2} \sum_{n=-N}^{M} \left[ \text{Erf} \frac{b_o + y - nh}{b_L} + \text{Erf} \frac{b_o - y + nh}{b_L} \right]$$

$$\cdot \left[ \frac{2t_o}{H_t} + \frac{2}{\pi} \sum_{m=1}^{\infty} \frac{1}{m} \sin \frac{2\pi m t_o}{H_t} \cdot \cos \frac{2m\pi z}{H_t} \cdot \exp\left\{ -\left(\frac{m\pi b_L}{H_t}\right)^2 \right\} \right]. \quad (21)$$

where

$$b_L^2 = b^2(x) \Big|_{x = x_o + L} = 4 \left[ \alpha(x_o + L) + C \ln \left( 2 + \frac{L}{x_o} \right) \right]$$

and $x_o$ is given by Eq. (20).

The momentum at the exit is given by

$$J_e = \rho_e \int_{-H_t/2}^{H_t/2} \int_{-(N+1/2)h}^{(M+1/2)h} u_e^2 \, dy \, dz \, . \tag{22}$$

For a diverging channel of exit area $A_e$ and throat area $A_t$, we introduce an area correction factor in Eq. (22) so that the exit momentum is given by

$$J_e = \rho_e \frac{A_t}{A_e} \int_{-H_t/2}^{H_t/2} \int_{-(N+1/2)h}^{(M+1/2)h} u_e^2 \, dy \, dz \, . \tag{23}$$

Let $\bar{V}_e$ be the average velocity at the exit of the diverging channel. The average momentum at the exit is then

$$J_{av} = \rho_e (M + N + 1) h H_e \bar{V}_e^2 \, . \tag{24}$$

A momentum correction factor $\kappa_{me}$ is defined as

$$\kappa_{me} = J_e / J_{av} \, . \tag{25}$$

One-dimensional control volume analysis is applied between the throat and exit sections in x-z plane. The continuity and momentum equations, respectively, are

$$\rho_S A_S U_S + \rho_N A_N U_N = \rho_e A_e \bar{V}_e \tag{26}$$

$$A_N p_N + A_S p_S + \frac{\rho_N A_N U_N^2}{g_c} + \frac{\rho_S A_S U_S^2}{g_c} + \frac{p_N A_N + p_S A_S + p_a A_e}{A_e + A_t} \left( A_e - A_t \right)$$

$$= A_e p_a + \kappa_{me} \cdot \frac{\rho_e A_e \bar{V}_e^2}{g_c} + \Delta p_f \cdot \frac{A_e + A_t}{2} + \Delta p_D \cdot \left( A_e - A_t \right) \tag{27}$$

where

$$\Delta p_f = \text{pressure loss term attributable to wall friction} = \frac{1}{2} c_f L \rho_e \bar{V}_e^2 D_h$$

$$c_f = 0.0095$$

$$D_h = \frac{A_e + A_t}{[(M + N + 1)h + H_e]}$$

$$\Delta p_D = \text{pressure loss term due to imperfect diffusion} = \frac{1 - \eta_D}{\eta_D} (p_a - p_S)$$

$$\eta_D = \text{diffuser efficiency} = 0.95 - 0.6 \sin^2 2\theta$$

$$\theta = \text{diffuser half angle} = \tan^{-1} \frac{H_e - H_t}{2L}$$

$$U_N = \left[ 2 g_c \eta_N \frac{\gamma}{\gamma - 1} R T_a \left\{ 1 - \left[ \left( \frac{p_S}{p_a} \right) \middle/ \left( \frac{p_t}{p_a} \right) \right]^{\frac{\gamma - 1}{\gamma}} \right\} \right]^{1/2}, \quad \text{if } \frac{p_t}{p_a} < 1.89$$

$$= (\gamma R g_c \eta_N T_a)^{1/2}, \quad \text{if } \frac{p_t}{p_a} > 1.89 \text{ (choked flow)}$$

$$U_S = \left[ 2 g_c \frac{\gamma}{\gamma - 1} R T_a \left\{ 1 - \left( \frac{p_S}{p_a} \right)^{\frac{\gamma - 1}{\gamma}} \right\} \right]^{1/2}$$

$$\eta_N = \left\{ 1 - 0.16 \left( \frac{p_t}{p_a} \right) \right\}^2$$

$$\begin{pmatrix} \rho_N \\ \rho_S \\ \rho_e \end{pmatrix} = \begin{pmatrix} p_N \\ p_S \\ p_a \end{pmatrix} \middle/ R \begin{pmatrix} T_N \\ T_S \\ T_e \end{pmatrix}$$

$$T_N = T_a - \left( \frac{\gamma - 1}{\gamma} \right) \frac{U_N^2}{2 R g_c}, \quad \text{if } \frac{p_t}{p_a} < 1.89$$

$$= \frac{2}{\gamma + 1} T_a, \quad \text{if } \frac{p_t}{p_a} > 1.89 \text{ (choked flow)}$$

$$\begin{pmatrix} T_S \\ T_e \end{pmatrix} = T_a - \frac{\gamma - 1}{2\gamma R g_c} \begin{pmatrix} U_S^2 \\ \bar{V}_e^2 \end{pmatrix}$$

$A_N$ = total area covered by the nozzles $= 4 (M + N + 1) b_o t_o$

$A_t$ = throat area $= (M + N + 1) h H_t$

$A_e$ = exit area $= (M + N + 1) h H_e$

$A_S = A_t - A_N$ .

Substituting for $\Delta p_f$, $\Delta p_D$, $U_N$, $U_S$, $\rho_N$, $\rho_S$, and $\rho_e$ in Eqs. (26) and (27), we obtain a set of coupled equations for the unknowns $\bar{V}_e$ and $p_S$ which can be determined in terms of the geometric parameters of the ejector and the nozzle pressure ratio $p_t/p_a$.

From the nature of the Eqs. (26) and (27), it is obvious that an explicit solution cannot be obtained. Therefore a computer program is written based on an iterative scheme. The program requires the ejector design parameters, the empirical constants in the eddy viscosity model, and the nozzle pressure ratio as input and calculates the entrained secondary mass flow, the secondary and exit velocities, the net thrust, and the thrust augmentation ratio.

The net thrust is given by

$$\Pi = \kappa_{me} \rho_e A_e \bar{V}_e^2$$

and the isentropic augmentation ratio is defined as

$$\Phi = \frac{\kappa_{me} \rho_e A_e \bar{V}_e^2}{(\rho_N A_N U_N) U^*} , \tag{28}$$

where

$$U^* = \left[ 2 g_c \frac{\gamma}{\gamma - 1} R T_a \left\{ 1 - \left( \frac{p_a}{p_t} \right)^{\frac{\gamma - 1}{\gamma}} \right\} \right]^{1/2} , \quad \text{if } \frac{p_t}{p_a} < 1.89$$

$$= (\gamma R g_c T_a)^{1/2} , \quad \text{if } \frac{p_t}{p_a} > 1.89 \text{ (choked flow).} \tag{29}$$

The entrainment ratio is defined as

$$E = \frac{\text{Secondary mass flow}}{\text{nozzle mass flow}} = \frac{\rho_S A_S U_S}{\rho_N A_N U_N} . \tag{30}$$

712

## RESULTS AND DISCUSSION

The results of the computations are presented in three parts.

Case (A): The theory is applied for predicting the performance of the model ejector at NASA Ames Research Center. The geometric characteristics of the experimental model at NASA-Ames are as follows:

**Nozzle specifications:**

8:1 hypermixing nozzle, normal to the exit plane makes a 45° angle with the jet centerline, nozzle width $(2 b_o) = 0.5055$ cm (0.2 in.), nozzle height $(2 t_o) = 10.16$ cms (4 in.), number of nozzles $= M + N + 1 = 16$ ($M = 8$, and $N = 7$), and spacing between the nozzles (h) = 5.08 cms (2 in.)

**Ejector Specifications**

Length L = 36.576 cms. (14.4 in.), area ratio $A_t/A_N = 15$, and $H_t = 2t_o$. From Bevilaqua's paper[7], we find the constants for the eddy viscosity model:

$$\alpha = 0.02, \quad C = 0.0006.$$

Using the above specifications, we calculate the nozzle mass flow $M_N = (\rho_N A_N U_N)$ and the net thrust $\Pi \ (= \kappa_{me} \rho_e A_e \tilde{V}_e^2)$ for various pressure ratio $p_t/p_a$ and area ratio $A_e/A_t$. We also calculate the ideal nozzle mass flow $\overset{\bullet}{M}_N$ and ideal thrust of the ejector $\Pi^{\bullet}$, given by the expressions:

$$M_N^{\bullet} = \rho_N A_N U^{\bullet}, \tag{31}$$

$$\Pi^{\bullet} = \rho_e A_e \tilde{V}_e^{\bullet 2} \tag{32}$$

where $U^{\bullet}$ is given by Eq. (29) and $\tilde{V}_e^{\bullet}$ is computed from Eqs. (26) and (27) with $\kappa_{me} = 1$, $\eta_D = 1$, and $\Delta p_f = 0$. We define discharge coefficient $C_D = M_N/M_N^{\bullet}$ and thrust efficiency $\eta_T = \Pi/\Pi^{\bullet}$; the variation of $C_D$ and $\eta_T$ with $p_t/p_a$ and $A_e/A_t$ is plotted in Figs. 6 and 7. The agreement between the theoretical predictions and the experimental data of Aiken[8] is excellent; experimentally measured mass flow and thrust are also normalized using Eqs. (31) and (32) respectively. The main empiricism involved in the theory is in the relations for $\eta_N$ and $\eta_D$. A careful choice of $\eta_N$ and $\eta_D$ and is essential for obtaining such an excellent agreement between the theory and experiment. The influence of the choice of $\eta_N$ and $\eta_D$ on theoretical predictions is illustrated in the following test computations:

Case (B): The thrust augmentation ratio and entrainment ratio E are calculated for various $A_e/A_t$ and $p_t/p_a$ by varying different design parameters, viz. the length L of the ejector, the ratio of the channel height to the nozzle height $H_t/2t_o$, and the nozzle spacing to width ratio $h/2b_o$. In these computations we assume $\eta_N = \eta_D = 1$. These results (Figs. 8–13) serve to illustrate the influence of various geometric parameters and can be used to determine an optimum design.

Case (C): We assume $\eta_N = 0.95$ and

$$\eta_D = 0.95 - 0.6 \sin^2 2\theta, \tag{33}$$

where $\theta = \tan^{-1} \dfrac{H_e - H_t}{2L}$. The results (Figs. 14 and 15) show a large drop in thrust augmentation for large

values of $A_e/A_t$ and at smaller lengths L. Although $\eta_D$ may not be defined by Eq. (33) for all ejectors, this example does illustrate its importance in correctly predicting the ejector performance. Fancher[10] finds that the Eq. (33) is quite adequate for wide range of $A_e/A_t$.
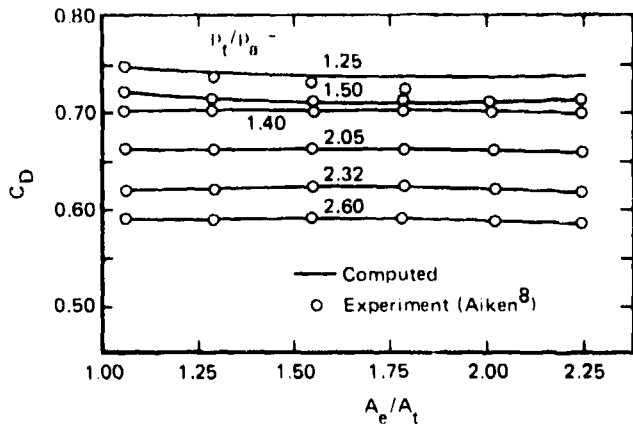
Fig. 6  Case (A) - comparison between the
experimental and theoretical values of
discharge coefficients, $C_D$, for various area
ratio ($A_e/A_t$) and pressure ratio ($p_t/p_a$).
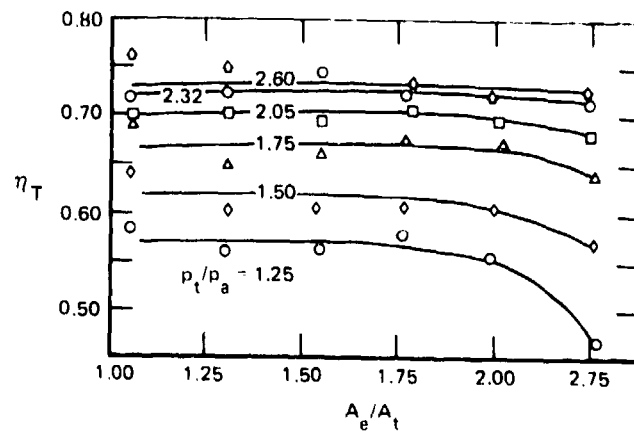


Fig. 7  Case (A) - comparison between the
experimental and theoretical values of ejector
thrust efficiency, $\eta_T$, for various values of
area ratio ($A_e/A_t$) and pressure ratio ($p_t/p_a$).
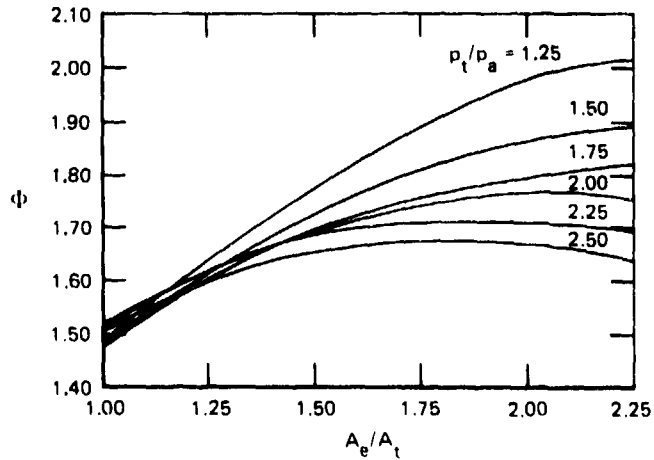


Fig. 8  Case (B) - theoretical variation of the
thrust-augmentation-ratio, $\Phi$, with area ratio
($A_e/A_t$) for various pressure ratios ($p_t/p_a$);
$\eta_N = \eta_D = 1$.
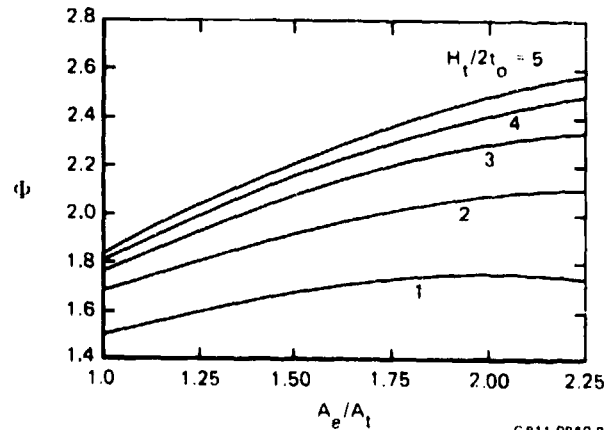


Fig. 9  Case (B) - theoretical variation of the
thrust-augmentation-ratio, $\Phi$, with area ratio
($A_e/A_t$) for various $H_t/2t_0$ (throat
height/nozzle height) at $p_t/p_a = 2.05$;
$\eta_N = \eta_D = 1$.

714
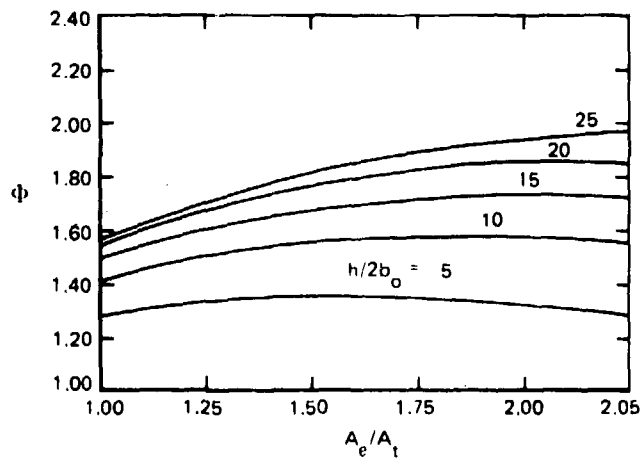
Fig. 10 Case (B) - theoretical variation of the thrust-augmentation-ratio, $\Phi$, with area ratio $(A_e/A_t)$ for various $h/2b_0$ (spacing between the nozzles/nozzle width) at $p_t/p_a = 2.05$; $\eta_N = \eta_D = 1$.
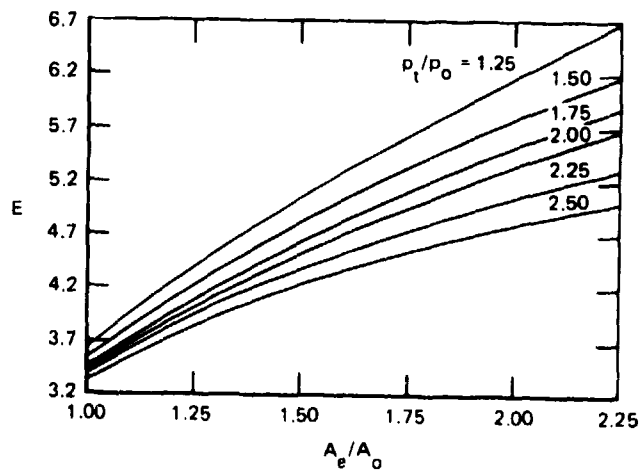
Fig. 11 Case (B) - theoretical variation of the entrainment ratio, E, with area ratio $(A_e/A_t)$ for various pressure ratios $(p_t/p_a)$; $\eta_N = \eta_D = 1$.
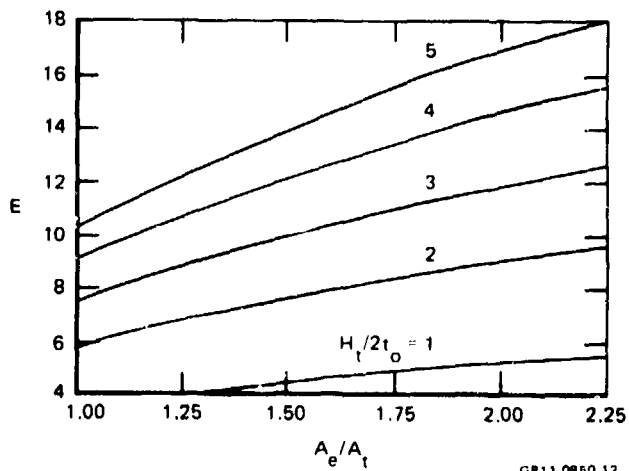
Fig. 12 Case (B) - theoretical variation of the entrainment ratio, E, with area ratio $(A_e/A_t)$ for various $H_t/2t_0$ (throat height/nozzle height) at $p_t/p_a = 2.05$; $\eta_N = \eta_D = 1$.
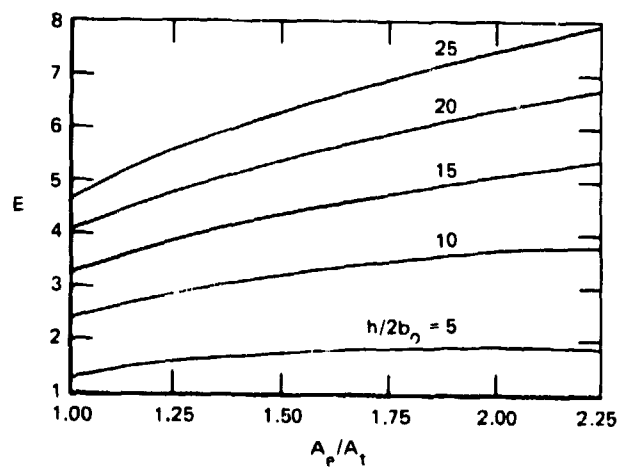
Fig. 13 Case (B) - theoretical variation of the entrainment ratio, E, with area ratio $(A_e/A_t)$ for various $h/2b_0$ (spacing between the nozzles/nozzle width) at $p_t/p_a = 2.05$; $\eta_N = \eta_D = 1$.

715
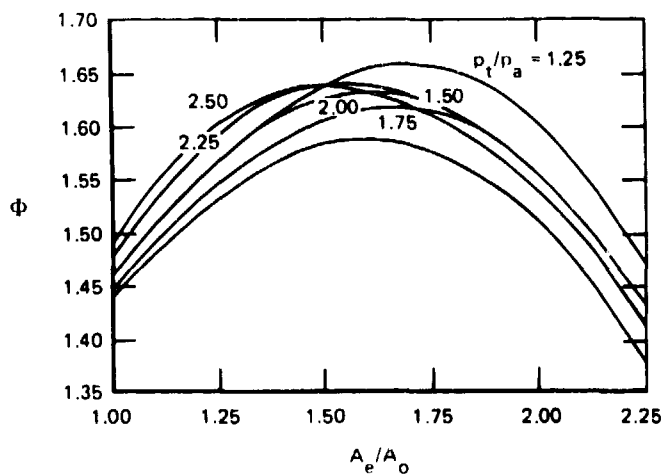
Fig. 14: Case (C) - theoretical variation of thrust-augmentation-ratio, $\Phi$, with area-ratio $(A_e/A_t)$ for various pressure ratio $(p_t/p_a)$;
$\eta_N = 0.95$, $\eta_D = 0.95 - 0.6$
$\sin^2\left\{2\left(\tan^{-1}\dfrac{H_e - H_t}{L}\right)\right\}$.
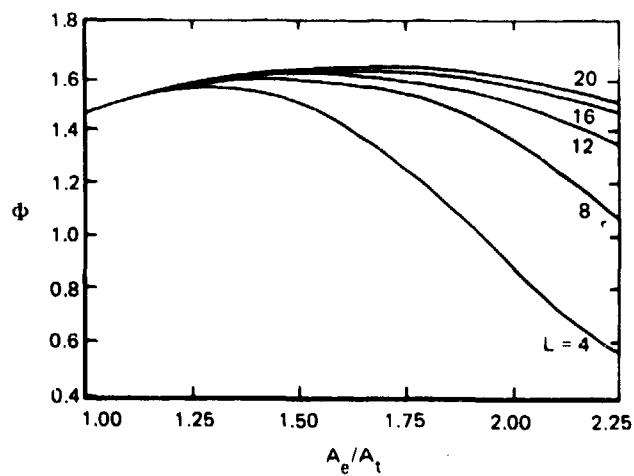
Fig. 15 Case (C) - theoretical variation of thrust-augmentation-ratio, $\Phi$, with area-ratio $(A_e/A_t)$ for various ejector lengths;
$\eta_N = 0.95$, $\eta_D = 0.95 - 0.6$
$\sin^2\left\{2\left(\tan^{-1}\dfrac{H_e - H_t}{L}\right)\right\}$.

## ACKNOWLEDGMENT

## REFERENCES

1. Korbacher, G. K., "Aerodynamics of Powered High Lift Systems," Annual Rev. Fluid Mech., Vol. 6, 1974, pp. 319-358.

2. Smith, A. M. O., "High Lift Aerodynamics," J. Aircraft, Vol. 12, 1975, pp. 501-530.

3. Von Karman, T., "Theoretical Remarks on Thrust Augmentation," Reissner Anniversary Volume, Edward Bros., Ann Arbor, Mich., 1949, pp. 461-468.

4. Hill, P. G., "Turbulent Jets in Ducted Streams," J. Fluid Mech., Vol. 22, 1965, pp. 161-186.

5. Bevilaqua, P. M., "Evaluation of Hypermixing for Thrust Augmenting Ejectors," J. Aircraft, Vol. II, 1974, pp. 348-354.

6. Gilbert, G. B., and Hill, P. G., "Analysis and Testing of Two-Dimensional Slot Nozzle Ejectors with Variable Area Mixing Section," NASA CR-2251, May 1973.

7. Bevilaqua, P. M., "Analytical Description of Hypermixing and Test of an Improved Nozzle," J. Aircraft, Vol. 13, 1976, pp. 43-48.

8. Aiken, T. N., Unpublished data, NASA Ames Research Center, July 1976.

9. Pai, S. I. and Hsieh, T. Y., "Linearized Theory of Three-Dimensional Jet Mixing With and Without Walls," J. Basic Engineering, 1970, pp. 93-100.

10. Fancher, R. B., "Low-Area Ratio, Thrust Augmenting Ejectors," J. Aircraft, Vol. 9, 1972, pp. 243-248.

# INVESTIGATION OF THE SUPERSONIC-SUPERSONIC EJECTOR*

J. C. Dutton
Department of Mechanical Engineering
Texas A&M University
College Station, Texas

## ABSTRACT

An investigation of the constant area, supersonic-supersonic ejector has been conducted wherein one supersonic stream is pumped directly by another inside a confining duct. The theoretical analysis is based on simplified, one-dimensional models of the constant area mixing section and inviscid interaction region. The parametric dependence of the ejector pressure recovery performance on each of seven dimensionless variables is presented. A series of small scale, axisymmetric ejector experiments indicates that the theory predicts maximum ejector compression ratios which are 15 to 22 percent higher than the measured values and that the ejector is susceptible to separation of the secondary stream at the confluence point of the primary and secondary streams.

## NOMENCLATURE

| | |
|---|---|
| A | area |
| B | quantity defined in Eq. (8) |
| D | diameter |
| $f_1, f_2, f_3, f_4$ | functions of $\gamma$ and M defined by Eqs. (2), (4), (9), and (14), respectively |
| M | Mach number |
| MW | molecular weight |
| P | pressure |
| Re | Reynolds number |
| T | temperature |
| V | velocity |
| W | mass flow rate |
| $\gamma$ | specific heat ratio |
| $\mu$ | absolute viscosity |
| $\rho$ | density |

## Subscripts and Superscripts

| | |
|---|---|
| lim | limiting condition |
| M | mixed |
| P | primary |
| s | secondary |
| T | throat |
| o | stagnation |
| 1,2,3 | stations 1, 2, or 3 in Fig. 2 |
| * | sonic condition |

## INTRODUCTION

Supersonic ejector-diffuser systems have many applications both as pressure recovery and thrust augmentation devices. However, the application which provides the primary motivation for this work is the high-energy chemical laser. In the continuous wave chemical laser, alternate, interleaved streams of fuel ($H_2$ or $D_2$) and oxidant (F) enter the laser cavity at high Mach numbers and a low static pressure. These streams then mix and react to establish the lasing zones between the streams. Accompanying the chemical reactions, a significant quantity of heat is released to the laser flow which tends qualitatively to increase the static pressure, to decrease the stagnation pressure, and to decrease the Mach number of the "mixed" supersonic laser flow. At the laser cavity exit the flow is hot (T=1500K), highly corrosive, supersonic (1.5<M<3.5), and at low static pressure (1<P<10 kPa). This stream must then be pumped to ambient conditions so that the lasing process can be started and sustained.

The conventional approach to the pressure recovery problem, Fig. 1(a), has been to first diffuse the laser flow using a constant area supersonic diffuser followed by a subsonic diffuser and then to pump the resulting subsonic flow with a supersonic ejector. The mixing tube of this subsonic-supersonic ejector is then generally followed by a second subsonic diffuser. An alternate approach to the problem is the supersonic-supersonic ejector, Fig. 1(b). In this system the diffusers located between the cavity exit and the ejector are eliminated and the supersonic laser cavity flow is pumped directly with a supersonic ejector. This concept offers the advantage of reducing the overall device length with a possible increase in performance. Since the physical size of the combined laser/pumping system is dominated by the pressure recovery equipment, it may also result in a substantial weight and volume reduction for the system. The objective of the present paper is to present the results of an integrated theoretical and experimental investigation of the supersonic-supersonic ejector.

## PREVIOUS WORK

The topic of ejectors has been extensively studied over the years as evidenced by Mikkelsen's[1] compilation of over 350 references concerning ejector systems and related topics. However, the overwhelming majority of these publications is concerned with pumping a subsonic, or even stagnant, secondary stream; this is not surprising when one considers the wide variety of industrial applications for such devices.

The earliest work concerned with the ejector pumping of supersonic streams appears to be that of

717

Spiegel, et al.[2] which was reported in 1953. This report was the first of four NACA reports[2-5] concerned with the possibility of using supersonic air injection to reduce the required starting and running pressure ratios of supersonic and hypersonic wind tunnels. Both Spiegel, et al.[2] and Hunczak and Rousso[3] performed one-dimensional analyses of the tunnel circuit including auxiliary supersonic air injection just downstream of the test section. Experiments were also performed which demonstrated that reduced pressure ratios were obtained with the supersonic injection, although the pressure recovery was not as favorable as that obtained from variable-geometry, second-throat-diffuser tunnels. Hasel and Sinclair[4] experimentally investigated the possibility of using supersonic injection in conjunction with a variable geometry diffuser for increasing the pressure recovery of supersonic wind tunnels. They found that the injection enhanced the tunnel pressure recovery, particularly for the higher test section Mach numbers which were considered, $3 \leq M \leq 5$. Stokes[5] also reported use of supersonic air injection together with a variable geometry diffuser in a hypersonic tunnel. Unfortunately, no pressure recovery data was reported.

As mentioned in the introduction, the recent development of the chemical laser has spawned renewed interest in the supersonic-supersonic ejector as a means of pumping the supersonic laser cavity flow directly. Zimet[6] performed an experimental study of the steady state and transient operation of a supersonic ejector with both a subsonic and supersonic secondary flow. It was concluded that the supersonic-supersonic mode showed good potential for weight-volume reductions at increased performance but that starting problems were more critical than for the conventional subsonic-supersonic configuration.

## THEORY

There are several methods available to analyze the pumping performance of the supersonic-supersonic ejector; these include one-dimensional analysis, the method of integral relations, the method of characteristics, and finite difference techniques. For the latter methods the flowfield may be described in increasing detail but the computer time necessary both to develop the appropriate programs and to calculate individual cases increases proportionately. Since the purpose of the present study was to develop a simplified, general theory for the pressure recovery performance of the supersonic-supersonic ejector and to investigate parametrically the feasibility of utilizing this device to pump laser cavity flow, a one-dimensional approach was adopted. As such, the method is computationally simple and is well-suited to parametric studies and optimization procedures although it provides little insight into the details of the actual flowfield.

The analysis is similar to that performed by Fabri, et al.[7,8] for the subsonic-supersonic ejector. The conservation equations are applied to an overall control volume contained within the constant area ejector mixing tube assuming uniform velocity and pressure distributions for the primary and secondary streams at the tube entrance and a fully mixed, uniform stream at the exit. These relations allow determination of the exit conditions, but it is well-known[1,7,8,9,10] that all arbitrary

combinations of inlet conditions are not possible. In particular, as the static pressure of the primary stream at the mixing tube inlet is increased above that of the secondary, a condition is eventually reached for which the secondary stream is compressed to sonic conditions at the "aerodynamic throat" formed just downstream of the tube inlet, much like an ideal, variable area supersonic diffuser. A second set of control volume relations is used to predict the operation of the ejector at this "upper limit point."

## Overall Control Volume Analysis

The continuity, momentum, and energy conservation equations are applied[1,7,8] to a control volume spanning the mixing tube from the inlet to exit, stations 1 to 3 in Fig. 2. Assuming the steady, frictionless, adiabatic flow of an ideal gas with constant specific heats, the conditions at the tube exit can be determined upon specification of the following eight parameters: the inlet Mach numbers of the primary and secondary streams, $M_{p1}$ and $M_{s1}$; the specific heat ratios, $\gamma_p$ and $\gamma_s$; the stagnation temperature and molecular weight ratios, $T_{op}/T_{os}$ and $MW_p/MW_s$; and the inlet stagnation pressure and area ratios of the primary-to-secondary streams, $P_{op1}/P_{os1}$ and $A_{p1}/A_{s1}$.

The stagnation pressure ratio at the inlet is first transformed to the equivalent static pressure ratio by using the isentropic flow function,

$$\frac{P_{p1}}{P_{s1}} = \frac{P_{op1}}{P_{os1}} \frac{f_1(\gamma_s, M_{s1})}{f_1(\gamma_p, M_{p1})} \tag{1}$$

where $\quad f_1(\gamma, M) \equiv \left(1 + \frac{\gamma-1}{2} M^2\right)^{\gamma/(\gamma-1)} \tag{2}$

The primary to secondary mass flow ratio can then be determined from the mass flow function as

$$\frac{W_p}{W_s} = \frac{P_{p1}}{P_{s1}} \frac{A_{p1}}{A_{s1}} \left[\frac{MW_p}{MW_s} \frac{T_{os}}{T_{op}}\right]^{1/2} \frac{f_2(\gamma_p, M_{p1})}{f_2(\gamma_s, M_{s1})} \tag{3}$$

where $\quad f_2(\gamma, M) \equiv M\left[\gamma\left(1 + \frac{\gamma-1}{2} M^2\right)\right]^{1/2} \tag{4}$

With this information, the specific heat ratio and molecular weight ratio of the fully mixed exit flow are found from

$$\gamma_M = \gamma_s \cdot \frac{1 + \frac{W_p}{W_s} \frac{\gamma_p}{\gamma_s} \frac{(\gamma_s-1)}{(\gamma_p-1)} \frac{MW_s}{MW_p}}{1 + \frac{W_p}{W_s} \frac{(\gamma_s-1)}{(\gamma_p-1)} \frac{MW_s}{MW_p}} \tag{5}$$

$$\frac{MW_M}{MW_s} = \frac{1 + \frac{W_p}{W_s}}{1 + \frac{W_p}{W_s} \frac{MW_s}{MW_p}} \tag{6}$$

Likewise, the stagnation temperature ratio of the mixed flow can be determined from the energy and continuity equations as

$$\frac{T_{OM}}{T_{os}} = \frac{1 + \frac{W_P}{W_s}\frac{\gamma_P}{\gamma_s}\frac{(\gamma_s-1)}{(\gamma_P-1)}\frac{MW_s}{MW_P}\frac{T_{OP}}{T_{os}}}{1 + \frac{W_P}{W_s}\frac{\gamma_P}{\gamma_s}\frac{(\gamma_s-1)}{(\gamma_P-1)}\frac{MW_s}{MW_P}} \qquad (7)$$

By combining the continuity and momentum equations written for the overall control volume, the exit Mach number and pressure ratios can be calculated using

$$B \equiv \frac{\left(1 + \frac{W_P}{W_s}\right)f_2(\gamma_s,M_{s1})\left[\frac{T_{OM}}{T_{os}}\cdot\frac{MW_s}{MW_M}\right]^{1/2}}{f_3(\gamma_s,M_{s1}) + \frac{P_{P1}}{P_{s1}}\frac{A_{P1}}{A_{s1}}f_3(\gamma_P,M_{P1})} \qquad (8)$$

where $\quad f_3(\gamma,M) \equiv 1 + \gamma M^2 \qquad (9)$

and $\quad M_{MS}^2 = \frac{\gamma_M(1-2B^2) \pm \left[\gamma_M^2-2B^2\gamma_M^2-2B^2\gamma_M\right]^{1/2}}{2B^2\gamma_M^2 - \gamma_M^2 + \gamma_M} \qquad (10)$

$$\frac{P_{MS}}{P_{s1}} = \frac{f_3(\gamma_s,M_{s1}) + \frac{P_{P1}}{P_{s1}}\frac{A_{P1}}{A_{s1}}f_3(\gamma_P,M_{P1})}{f_3(\gamma_M,M_{MS})\left(1 + \frac{A_{P1}}{A_{s1}}\right)} \qquad (11)$$

$$\frac{P_{OMS}}{P_{OS1}} = \frac{P_{MS}}{P_{s1}}\frac{f_1(\gamma_M,M_{MS})}{f_1(\gamma_s,M_{s1})} \qquad (12)$$

Note that two roots are indicated for the square of the exit Mach number, $M_{MS}^2$, since it is obtained from the solution of a quadratic equation. The root obtained using the positive sign is a supersonic solution and may be thought of as the uniform supersonic Mach number "equivalent" to the piecewise uniform primary and secondary Mach numbers at the mixing tube entrance. The root obtained with the negative sign is a subsonic solution and is the one utilized here since it is assumed that the mixing tube is sufficiently long so that the exit flow is fully mixed and diffused to subsonic conditions. It is interesting to note that if the supersonic solution is allowed to diffuse through a normal shock wave the subsonic solution is obtained. This result should not be surprising since the relations developed here are a multistream equivalent of the one-dimensional Fanno-Rayleigh relations for a normal shock wave.

## Control Volume Analysis of the Inviscid Interaction Region

If the primary-to-secondary inlet static pressure ratio is greater than one $(P_{P1}/P_{s1}>1)$, the secondary flow is compressed by the mutual interaction of the primary and secondary streams within the mixing tube, Fig. 2. As previously mentioned, this process is limited, in a one-dimensional sense,

to a compression of the secondary to sonic flow conditions at the aerodynamic throat formed just downstream from the mixing tube inlet. This limiting condition is analyzed by writing integral conservation relations for control volumes which extend from the tube entrance to the aerodynamic throat location, stations 1 to 2 in Fig. 2. It is assumed that the streams remain distinct and do not mix in this initial interaction region and that the flow for each stream is isentropic between stations 1 and 2. These assumptions, together with the facts that the mixing tube area is constant and that the secondary Mach number at the aerodynamic throat is unity, $M_{s2}=1$, allow determination of this limiting operating condition. One consequence of this model is that the average, one-dimensional static pressures of the streams can be different at a given axial location. Of course, the true, two-dimensional boundary conditions across the slipline between the streams are equality of static pressure and flow direction.

By writing continuity equations for each individual stream and a momentum equation for the combination of the two, the limiting point of operation can be determined from the following computations. First the primary Mach number at the choking location, $M_{P2}$, is found as the supersonic solution of the following implicit relation,

$$f_4(\gamma_P,M_{P2}) = f_4(\gamma_P,M_{P1})\left[1 + \frac{f_4(\gamma_s,M_{s1})-1}{\frac{A_{P1}}{A_{s1}}f_4(\gamma_s,M_{s1})}\right] \qquad (13)$$

where the function $f_4$ is the isentropic area ratio function, $A/A^*$,

$$f_4(\gamma,M) = \frac{A}{A^*}(\gamma,M) \equiv$$

$$\frac{1}{M}\left[\left(\frac{2}{\gamma+1}\right)\left(1 + \frac{\gamma-1}{2}M^2\right)\right]^{(\gamma+1)/2(\gamma-1)} \qquad (14)$$

With $M_{P2}$ determined, the primary-to-secondary inlet static pressure ratio at the limit condition can be calculated from

$$\left(\frac{P_{P1}}{P_{s1}}\right)_{lim} = [f_5(\gamma_s,M_{s1})-f_2(\gamma_s,M_{s1})f_3(\gamma_s,1)/f_2(\gamma_s,1)]/$$

$$\frac{A_{P1}}{A_{s1}}[f_2(\gamma_P,M_{P1})f_3(\gamma_P,M_{P2})/f_2(\gamma_P,M_{P2})-f_3(\gamma_P,M_{P1})] \qquad (15)$$

A given operating point satisfies the aerodynamic compression criterion for started supersonic secondary flow if $(P_{P1}/P_{s1})<(P_{P1}/P_{s1})_{lim}$.

If the primary static pressure at the inlet is less than that of the secondary, $P_{P1}/P_{s1}<1$, this limit condition analysis can be repeated where compression of the primary stream to sonic conditions is now of concern. However, for operating points near the point of maximum ejector pressure recovery, the condition $P_{P1}/P_{s1}>1$ prevails. Further details concerning the theoretical analysis may be found in Refs. 1 and 11.

719

## Parametric Study

Utilizing the simplified, one-dimensional analysis described in the preceding sections, it is a straightforward task to perform a parametric study to determine the dependence of the ejector's pressure recovery performance on the dimensionless variables of importance. As previously mentioned, the analysis identifies eight such parameters: $M_{P1}$, $M_{s1}$, $\gamma_P$, $\gamma_s$, $T_{OP}/T_{OS}$, $MW_P/MW_s$, $A_{P1}/A_{s1}$, and $P_{OP1}/P_{OS1}$. Because of this large number of variables, a rational scheme for conducting the study is needed. The method used is to define a baseline case and then to vary a single parameter at a time about this case. The baseline configuration is defined by: $M_{P1}=4.0$, $M_{s1}=2.0$, $\gamma_P=\gamma_s=1.4$, $T_{OP}/T_{OS}=MW_P/MW_s=1.0$, and $A_{P1}/A_{s1}=0.5$. In this study, the primary-to-secondary stagnation pressure ratio at the tube inlet, $P_{OP1}/P_{OS1}$, is used as the independent variable in obtaining primary-to-secondary mass flow variations so that curves of pressure recovery versus mass flow ratio can be developed.

The ejector operating plane for the baseline case is presented in Fig. 3 where the exit-to-secondary inlet stagnation pressure ratio is plotted as a function of the primary-to-secondary mass flow ratio. The stagnation pressure ratio has been utilized as the pressure recovery variable in the parametric study since the stagnation pressure of the mixed flow is a measure of the pressure against which the ejector can pump if the exit flow is further diffused through an ideal subsonic diffuser. The upper line is the series of maximum compression ratio operating points defined by the overall control volume analysis assuming a uniform, fully mixed, subsonic flow at the exit of the constant area mixing tube. The vertical line at the right is the limiting condition defined in the preceding section by compression of the secondary to sonic conditions at the aerodynamic throat. For larger mass flow ratios, the one-dimensional model of tne inviscid interaction region predicts that started supersonic flow of the secondary is not possible. The vertical line at the left is the lower limit of useful ejector operation where the mixed-to-secondary stagnation pressure ratio is unity. Also marked is the operating point at which the static pressures of the primary and secondary streams at the mixing tube inlet are equal. As can be seen in the figure the maximum ejector compression ratio increases with increasing primary-to-secondary inlet static pressure ratio. It is interesting to note that the relation between the maximum ejector pressure ratio and the mass flow ratio is very nearly linear although the set of equations, (1)-(12), used to determine it are decidedly nonlinear.

Figures 4-9 present the parametric dependence of the ejector pressure recovery performance on the variables $M_{P1}$, $M_{s1}$, $\gamma_P$, $\gamma_s$, $MW_P/MW_s$, $T_{OP}/T_{OS}$, and $A_{P1}/A_{s1}$. Although the molecular weight and stagnation temperature ratios are, in general, independent parameters their effect on the ejector operating plane is identical in this study since only one of these parameters at a time is varied while the other remains at unity. The influence of the $MW_P/MW_s$ and $T_{OP}/T_{OS}$ variations has been combined in Fig. 8.

By inspecting these figures, it is seen that in terms of increased compression ratios for a given primary-to-secondary mass flow ratio, the ejector pumping performance is only weakly dependent on the inlet primary Mach number, moderately dependent on the specific heat and entrance area ratios, and strongly dependent on the secondary inlet Mach number and stagnation temperature and molecular weight ratios. The matched inlet static pressure points, $P_{P1}/P_{s1}=1.0$, have been marked on each operating curve by vertical bars when they occur within the bounds of the figures: $P_{OMS}/P_{OS1}\geq1$, $0<W_P/W_s<5$. Note that the compression ratio at which the matched static pressure point occurs increases strongly as $M_{P1}$ is increased and $M_{s1}$ is decreased and is relatively independent of the other five parameters. This observation is important since the experiments indicate that as the inlet primary static pressure is increased above that of the secondary, separation of the secondary stream at the confluence point occurs with an accompanying degradation in the ejector performance. Therefore, the most effective means for improving ejector pressure recovery are to compress the secondary stream toward sonic conditions, either upstream of the ejector or in the mixing tube, and to employ a high Mach number, low molecular weight, high stagnation temperature primary gas.

## EXPERIMENTS

A series of small scale, cold flow, air-to-air ejector experiments has been conducted both to compare with the previously described theoretical analysis and to obtain a more detailed flowfield description than is provided by the one-dimensional, control volume approach.

### Experimental Equipment and Apparatus

A half-section schematic of the axisymmetric, supersonic-supersonic ejector is shown in Fig. 10. The primary flow enters the ejector from a large stagnation chamber at the bottom of the apparatus and is accelerated through the centrally located supersonic primary nozzle. The secondary flow enters the secondary stagnation chamber from two sides and is accelerated through the annular passage formed by the outer wall of the primary nozzle and the mixing tube base. Both the primary and secondary nozzles have elliptical entrance sections and were designed by the method-of-characteristics to produce uniform distributions of velocity and pressure at their confluence point. The Mach numbers and primary-to-secondary area ratios at the mixing tube entrance for the five ejector configurations tested are given in Table 1.

Static pressure taps were installed along the mixing tube wall from the nozzle exit plane to the mixing tube exit at increments of one tube radius. A series of six static wall taps, not shown in Fig. 10, was equally spaced about the mixing tube axis at the nozzle exit plane to check the concentricity of the nozzle and mixing tube. An additional five wall pressure taps, also not shown, were located upstream of the nozzle exit plane at increments of 2.54 mm to ensure that the entering secondary flow was supersonic. It should be noted that in all but one series of experiments the constant area mixing tubes were 10 tube diameters in length.

Table 1 Inlet Mach numbers and area ratios for the supersonic-supersonic ejector experiments

| | $M_{P1}$ | $M_{S1}$ | $A_{P1}/A_{S1}$ |
|---|---|---|---|
| 1 | 2.50 | 1.50 | 0.51 |
| 2 | 2.50 | 1.75 | 0.51 |
| 3 | 2.50 | 2.00 | 1.13 |
| 4 | 2.50 | 2.50 | 1.13 |
| 5 | 4.00 | 2.00 | 1.13 |

A final stagnation chamber and back pressure control valve were located downstream from the mixing tube exit. The purpose of the stagnation chamber was to prevent local disturbances at the control valve from influencing the velocity and pressure distributions of the mixed, subsonic flow at the tube exit. For one experiment, a traversing pitot probe was added between the mixing tube and final stagnation chamber for measurement of the exit Mach number distribution.

The experiments were conducted in the Mechanical Engineering Laboratory utilizing both the continuous air flow facility and a specially designed and constructed high-pressure supply system. Mass flow rates for the primary and secondary streams were measured with standard VDI nozzles. Depending on its level, pressure data was recorded with precision Bourdon-tube gauges, manometers, or with a strain gauge transducer-digital counter system. The accuracy of the pressure measurements was approximately within $\pm$ 1.5 kPa and the data was repeatable to within approximately $\pm$ 1%.

## Experimental Procedure

Maximum compression ratio data for each experimental ejector configuration was obtained in the following manner. With the back pressure control valve fully open, the secondary stagnation pressure, $P_{os1}$, was set at a fixed value to be maintained by the secondary automatic controller. The automatic controller for the primary stagnation pressure, $P_{oP1}$, was then set such that the mass flow ratio, $W_P/W_s$, would lie within the operating plane for the ejector configuration being considered. The back pressure valve was then closed until the secondary inlet static pressure, $P_{s1}$, began to rise indicating maximum compression conditions. At this point the mixing tube axial wall pressure distribution and exit pressure were recorded. This process was repeated for various combinations of $P_{os1}$ and $P_{oP1}$ until the entire mass flow ratio range was covered unless otherwise restricted by the facility supply pressure. Reference 1 can be consulted for additional information regarding the experimental equipment and procedure.

## Results and Discussion

The maximum compression characteristics for the experimental, constant area, supersonic-supersonic

ejector configurations listed in Table 1 are presented in Figs. 11-15. In contrast to the parametric results given in the previous section, the pressure recovery variable for the experiments is taken as the exit-to-secondary inlet static pressure ratio since these static pressure data are of principal interest for laser system applications. In addition, the results are presented over the range of mass flow ratios from the point of matched static pressure between the primary and secondary streams to the previously defined upper limit point.

For each ejector configuration investigated, the compression ratio data was recorded at one or two secondary nozzle throat Reynolds numbers,

$$Re_{ST} = \frac{\rho V}{\mu} (D_{MS} - D_s^*) \qquad (16)$$

where $\rho$, $V$, and $\mu$ are the density, velocity, and absolute viscosity, respectively, of the secondary stream evaluated at the throat and $(D_{MS} - D_s^*)$ is the difference between the outer and inner diameters at the throat. In addition, at each operating point the pressure ratio was determined and plotted against two independent variables: (1) the mass flow ratio, $W_P/W_s$, as determined from the VDI nozzle measurements, and (2) the primary stagnation-to-secondary static pressure ratio at the inlet, $P_{oP1}/P_{s1}$. These two points should exactly coincide since $W_P/W_s$ is theoretically proportional to $P_{oP1}/P_{s1}$. However, by examining the figures it can be seen that the VDI measurements yield $W_P/W_s$ values which are 0 to 44 percent greater than the $P_{oP1}/P_{s1}$ values. In addition, it was found that the magnitude of the disagreement increases as the secondary Reynolds number decreases and as $W_P/W_s$ (and, therefore, $P_{P1}/P_{s1}$) increases. These observations are strong evidence that the boundary layer of the secondary stream may separate at the primary/secondary confluence point. Referring to Fig. 2, it is seen that for $P_{P1}/P_{s1} > 1$ the secondary boundary layer approaching the confluence point must negotiate a compression (adverse pressure gradient) with the associated change in direction. For strong adverse pressure gradients the boundary layer will separate somewhere upstream, so that the secondary stream will not be "flowing full" at the mixing tube inlet. For this condition, values of $W_P/W_s$ based on the geometrical area, $A_{s1}$, and the pressure measurement, $P_{s1}$, will therefore be too low. This confluence point separation problem is similar in nature to the plume-induced separation occurring in the base region of power-on missile flows.

It can also be seen in Figs. 11-15 that the experimentally measured maximum compression ratios are less than the values predicted by the simplified, one-dimensional theory. Based on $P_{oP1}/P_{s1}$ values, the experimental ejector pressure recovery is 15 to 22 percent less than the theoretical values over the range of parameters investigated. Considering the simplicity of the one-dimensional model, an error of this magnitude is not surprising. Complex phenomena occurring in the mixing tube such as primary/secondary mixing, boundary layer growth and separation, shock wave-boundary layer-mixing layer interactions, etc.,

have been ignored. These results do indicate, however, that if an empirical pressure recovery factor of roughly 0.8 is applied to the one-dimensional model, compression ratios within a few percent of the experimental values can be expected.

Axial wall pressure distributions were also obtained for each configuration investigated. Distributions for the $M_{p_1}/M_{s_1} = 2.5/2.0$ ejector, corresponding to maximum compression conditions near the matched pressure point, upper limit point, and an intermediate operating point, are presented in Fig. 16. At the matched pressure point, the wall pressure is initially constant followed by a monotonic increase which then levels off to the exit value. At the upper limit point, the wall pressure exhibits an initial rise followed by a nearly linear increase to the exit. The initial pressure rise can be attributed to the diffusion of the secondary stream as it is compressed by the primary in the initial interaction region.

At the upper limit point and the intermediate operating point in Fig. 16 it appears that the static pressure is still rising at the tube exit. Thus it appears that the mixing tube was not of a sufficient length for the diffusion process to be completed. This, in turn, may explain some of the discrepancies between the theoretical predictions and experimental measurements of the compression ratio presented in Figs. 11-15. However, a further series of experiments was conducted for the $M_{p_1}/M_{s_1} = 2.5/2.0$ ejector with five mixing tube lengths: L/D=5, 7.5, 10, 12.5, and 15. These experiments demonstrated that the overall ejector performance was essentially identical for all configurations with L/D≥7.5. Only for the L/D=5 mixing tube was the ejector performance significantly degraded due to the inadequate mixing and recompression length available.

For the same ejector and similar operating conditions as presented in Fig. 16, the exit Mach number distributions were also measured. The results are presented in Fig. 17. These measurements demonstrate that the exit flow is reasonably well mixed and uniform since distinct primary and secondary streams cannot be identified at the tube exit.

## CONCLUSIONS

A theoretical and experimental investigation of the constant area, supersonic-supersonic ejector has been conducted. A simplified theory which is based on one-dimensional models of the constant area mixing section and inviscid interaction region has been developed to predict the pressure recovery performance of the device. The analysis identifies seven variables of importance, and the parametric dependence of the compression ratio on each of these variables is presented. It was found that the dependence on the primary and secondary inlet Mach numbers and the primary-to-secondary molecular weight and stagnation temperature ratios is strong. Therefore, the ejector performance can be maximized by compression of the secondary stream and by use of a low molecular weight, high stagnation temperature, high Mach number primary gas.

A series of small scale, axisymmetric experiments has also been conducted for five ejector

configurations. These experiments indicate that as the primary-to-secondary static pressure ratio at the mixing tube inlet is increased, separation of the secondary stream occurs, thus degrading ejector performance. Comparison of the measured and predicted compression ratios for the configurations studied suggests that application of an empirical factor of 0.8 to the one-dimensional theory will provide pressure recovery information of acceptable accuracy for engineering purposes.

## REFERENCES

1. Mikkelsen, C. D., Sandberg, M. R., and Addy, A. L., "Theoretical and Experimental Analysis of the Constant-Area, Supersonic-Supersonic Ejector," Department of Mechanical and Industrial Engineering, University of Illinois at Urbana-Champaign, Report No. UILU-ENG-76-4003, Oct. 1976.

2. Spiegel, J. M., Hofstetter, R. V., and Kuehn, D. M., "Applications of Auxiliary Air Injectors to Supersonic Wind Tunnels," NACA RM A53I01, 1953.

3. Hunczak, H. R. and Rousso, M. D., "Starting and Operating Limits of Two Supersonic Wind Tunnels Utilizing Auxiliary Air Injection," NACA TN 3262, 1954.

4. Hasel, L. E. and Sinclair, A. R., "A Preliminary Investigation of Methods for Improving the Pressure-Recovery Characteristics of Variable-Geometry Supersonic-Subsonic Diffuser Systems," NACA RM L57H02, 1957.

5. Stokes, G. M., "Description of a 2-Foot Hypersonic Facility at the Langley Research Center," NASA TN D-939, 1961.

6. Zimet, E., "Steady State and Transient Operation of an Ejector for a Chemical Laser Cold Flow Mixing Experiment," NSWC/WOL/TR 76-142, Oct. 1976.

7. Fabri, J. and Paulon, J., "Theory and Experiments on Supersonic Air-to-Air Ejectors," NACA TM 1410, 1958.

8. Fabri, J. and Siestrunck, R., "Supersonic Air Ejectors," Advances in Applied Mechanics, Vol. V, Academic Press, New York, 1958, pp. 1-34.

9. Addy, A. L., "The Analysis of Supersonic Ejector Systems," Supersonic Ejectors, AGARDograph No. 163, 1972, pp. 31-101.

10. Addy, A. L., "The Analysis of Supersonic Ejector Systems," Ejectors, von Karman Institute, Lecture Series No. 79, 1975.

722

11. Dutton, J. C. and Addy, A. L., "One-Dimensional Analyses of Supersonic-Supersonic Ejector-Diffuser Systems for Chemical Laser Applications," Department of Mechanical and Industrial Engineering, University of Illinois at Urbana-Champaign, Report No. UILU-ENG-78-4015, Sept. 1978.

FIGURES
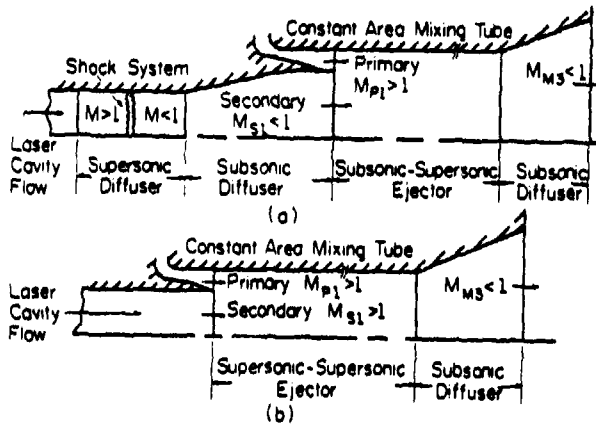


Figure 1  Alternate approaches to pumping laser cavity flow (a) subsonic-supersonic ejector (b) supersonic-supersonic ejector
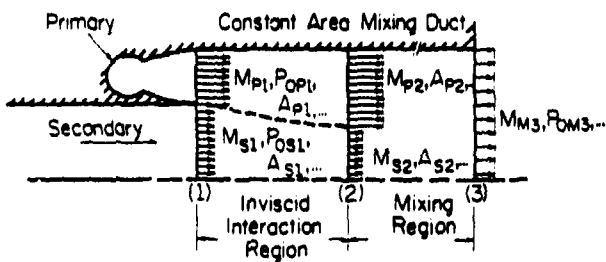


Figure 2  Schematic of the models and nomenclature used in the analysis of the constant area, supersonic-supersonic ejector
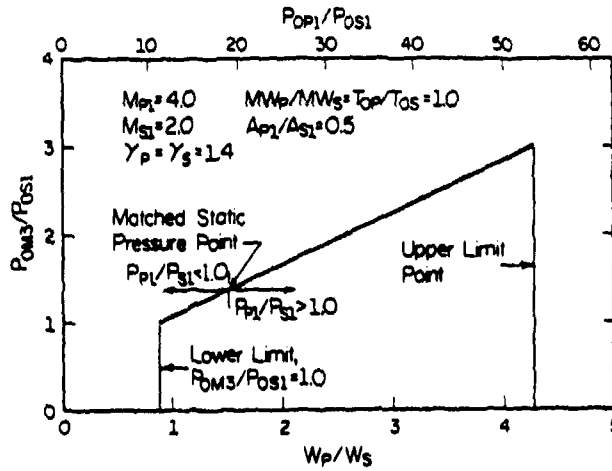


Figure 3  Operating plane for the baseline case of the constant area, supersonic-supersonic ejector
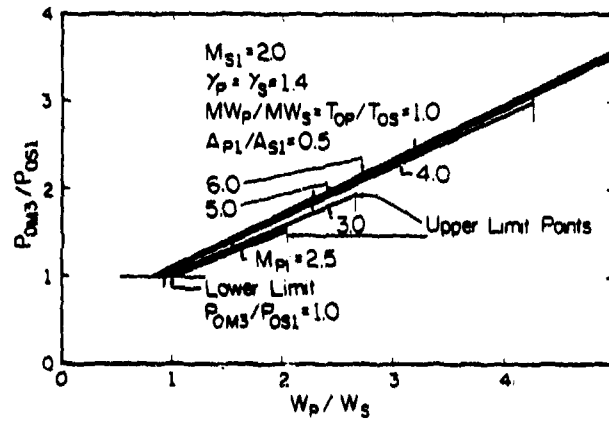


Figure 4  Parametric effect of $M_{P_1}$ on ejector pressure recovery
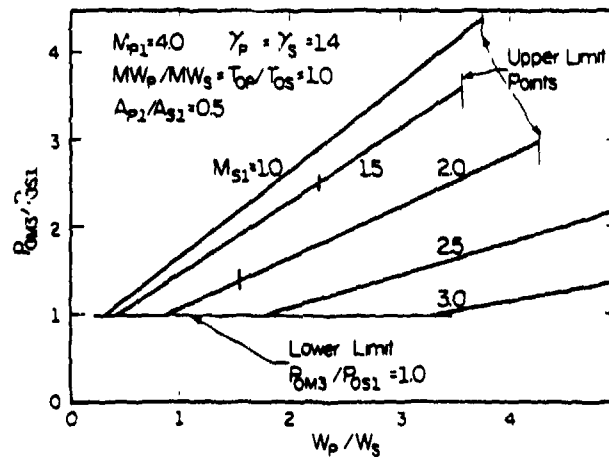


Figure 5  Parametric effect of $M_{S_1}$ on ejector pressure recovery

723
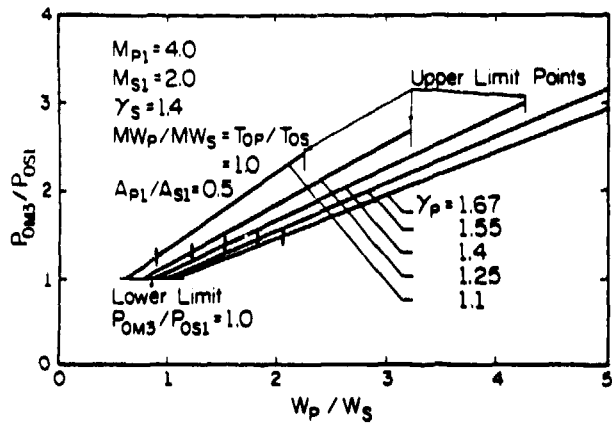
Figure 6   Parametric effect of $\gamma_P$ on ejector pressure recovery
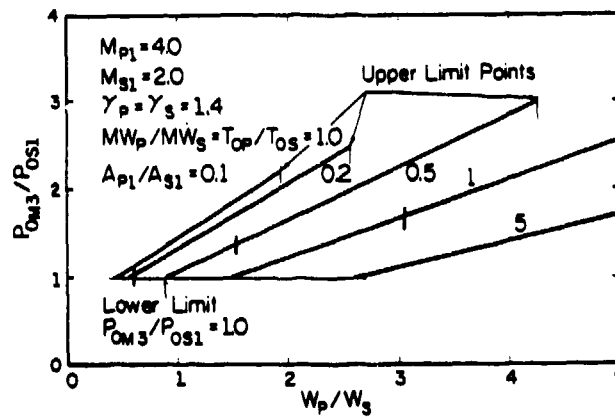


Figure 9   Parametric effect of $A_{P1}/A_{S1}$ on ejector pressure recovery
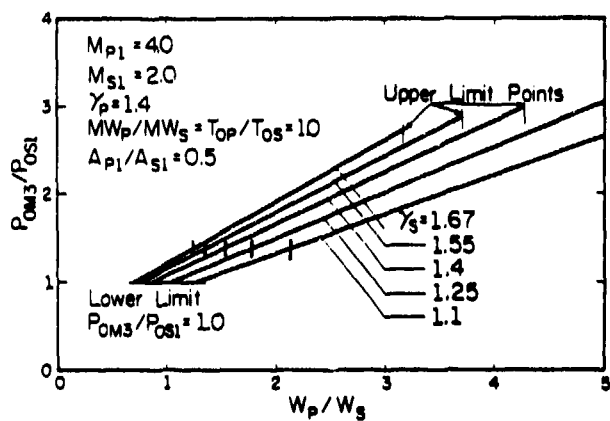


Figure 7   Parametric effect of $\gamma_S$ on ejector pressure recovery
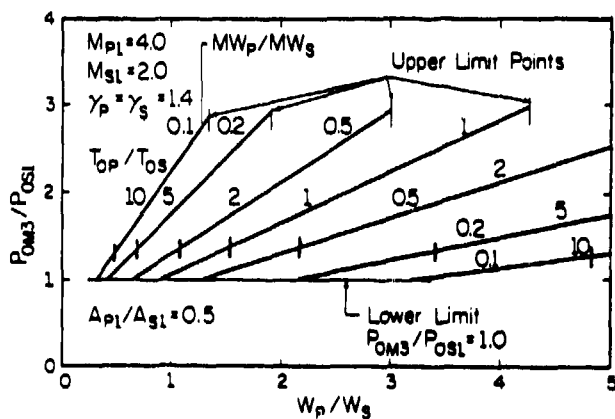


Figure 8   Parametric effects of $MW_P/MW_S$ and $T_{OP}/T_{OS}$ on ejector pressure recovery
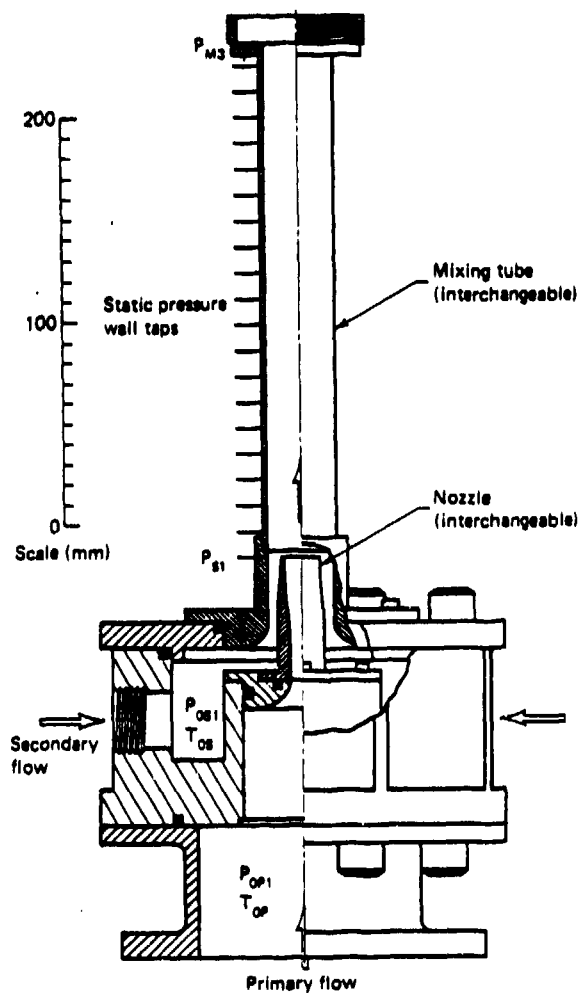


Figure 10   Half-section schematic of the axisymmetric, supersonic-supersonic ejector apparatus

724
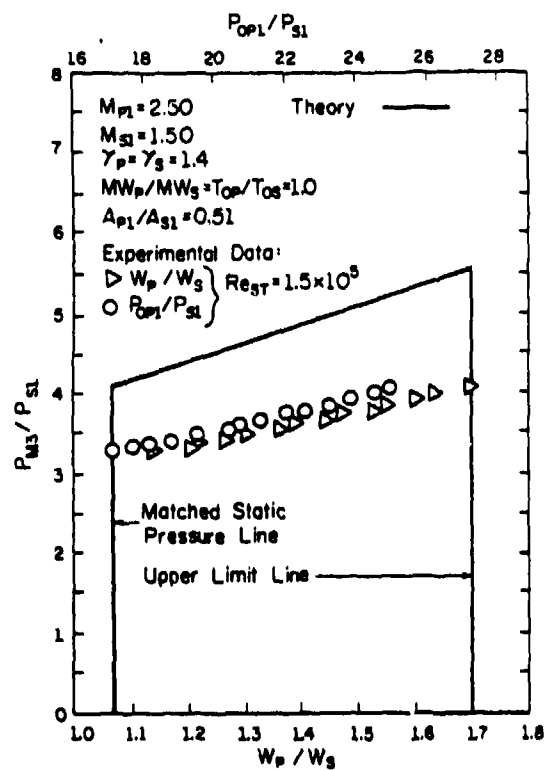
Figure 11 Comparison of experimental and theoretical ejector compression characteristics, $M_{P_1}/M_{S_1}$ = 2.5/1.5

Figure 12 Comparison of experimental and theoretical ejector compression characteristics, $M_{P_1}/M_{S_1}$ = 2.5/1.75
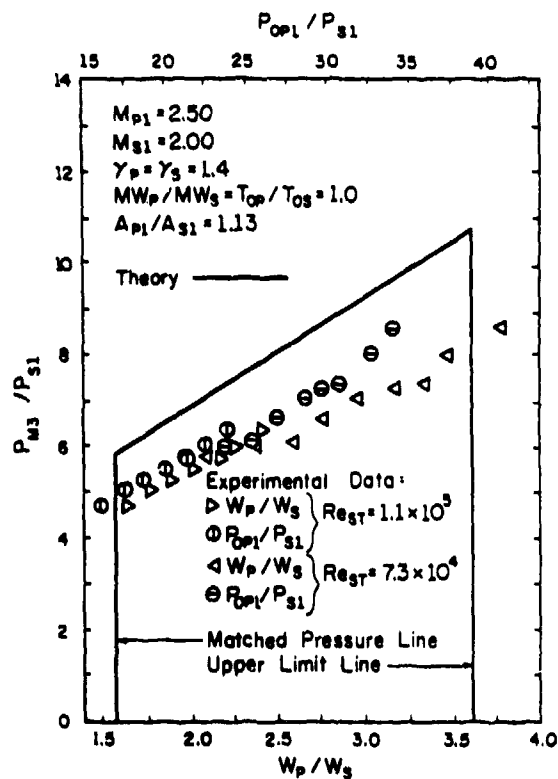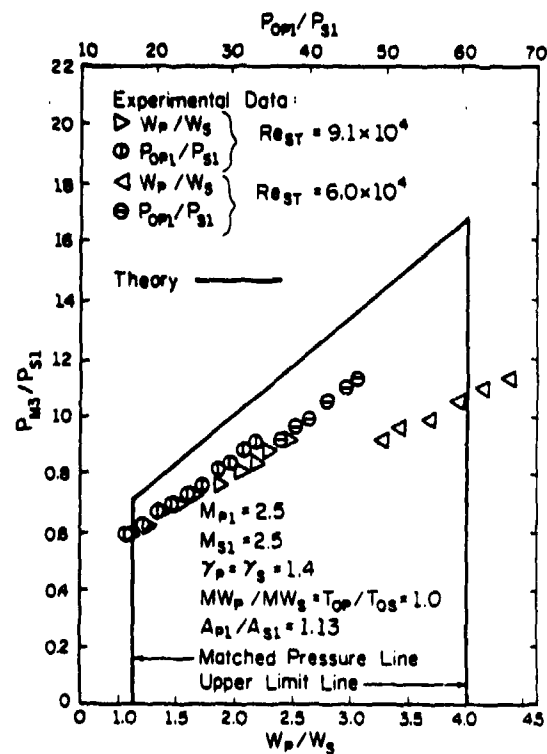
Figure 13 Comparison of experimental and theoretical ejector compression characteristics, $M_{P_1}/M_{S_1}$ = 2.5/2.0

Figure 14 Comparison of experimental and theoretical ejector compression characteristics, $M_{P_1}/M_{S_1}$ = 2.5/2.5
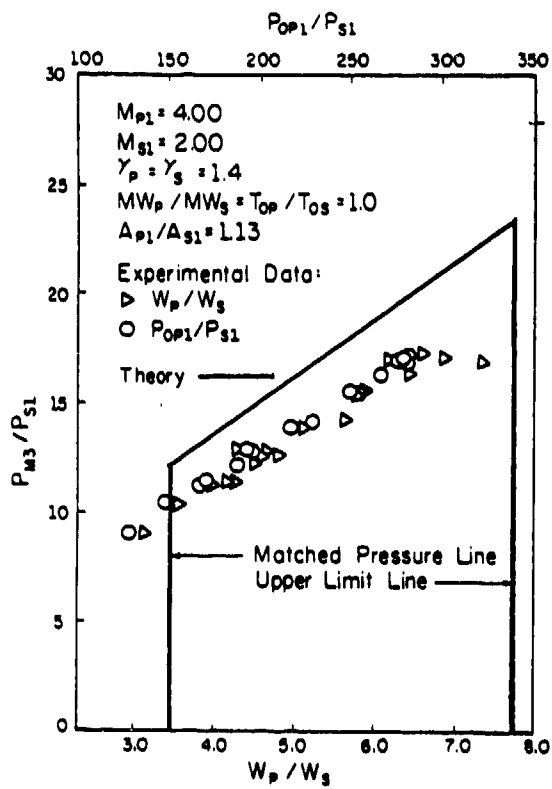
725

$P_{OP1}/P_{S1}$

100  150  200  250  300  350

$M_{P1} = 4.00$
$M_{S1} = 2.00$
$\gamma_P = \gamma_S = 1.4$
$MW_P / MW_S = T_{OP}/T_{OS} = 1.0$
$A_{P1}/A_{S1} = 1.13$

Experimental Data:
▷  $W_P / W_S$
○  $P_{OP1}/P_{S1}$

Theory ———

$P_{M3}/P_{S1}$

Matched Pressure Line
Upper Limit Line

3.0  4.0  5.0  6.0  7.0  8.0
$W_P / W_S$

Figure 15  Comparison of experimental and theoretical ejector compression characteristics, $M_{P1}/M_{S1} = 4.0/2.0$

Theory ———

$M_{P1} = 2.50$
$M_{S1} = 2.00$
$\gamma_P = \gamma_S = 1.4$
$MW_P / MW_S = 1.0$
$T_{OP}/T_{OS} = 1.0$
$A_{P1}/A_{S1} = 1.13$

$r/R_{M3}$

Experimental Data:

| $P_{OP1}/P_{S1}$ | $P_{M3}/P_{S1}$ | $Re_{ST}$ |
|---|---|---|
| ○ 32.3 | 7.87 | $7.07 \times 10^4$ |
| (Upper Limit) | | |
| △ 24.4 | 6.51 | $1.06 \times 10^5$ |
| □ 16.5 | 5.00 | $1.05 \times 10^5$ |
| (Matched Pressure) | | |

0  0.2  0.4  0.6  0.8  1.0
$M_{M3}$
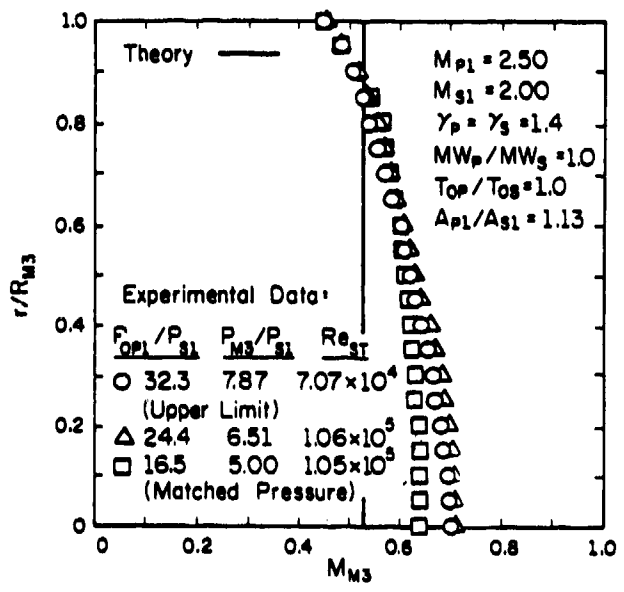
Figure 17  Exit Mach number distributions for the ejector at maximum compression conditions, $M_{P1}/M_{S1} = 2.5/2.0$

| $P_{OP1}/P_{S1}$ | $Re_{ST}$ | |
|---|---|---|
| ○ 34.0 | $7.34 \times 10^4$ | (Upper Limit) |
| △ 23.9 | $1.08 \times 10^5$ | |
| □ 16.1 | $1.09 \times 10^5$ | |
| (Matched Pressure) | | |

$M_{P1} = 2.50$  $MW_P/MW_S = 1.0$
$M_{S1} = 2.00$  $T_{OP}/T_{OS} = 1.0$
$\gamma_P = \gamma_S = 1.4$  $A_{P1}/A_{S1} = 1.13$

$P(x)/P_{S1}$

0  2  4  6  8  10
$x/D_{M3}$
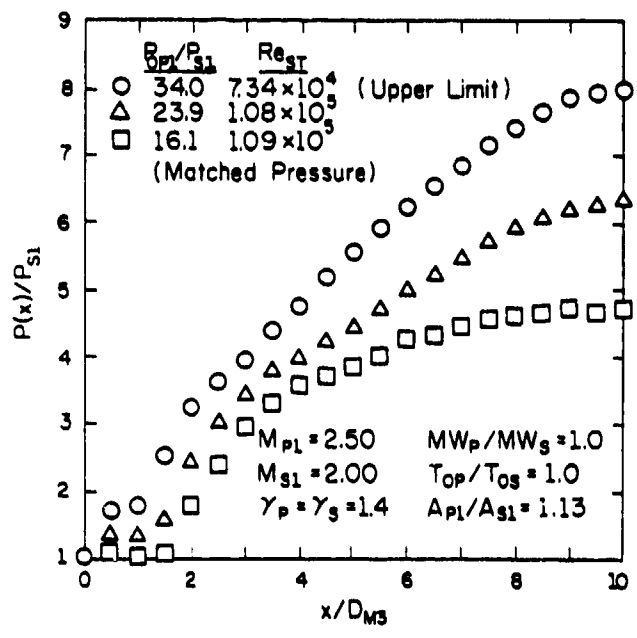
Figure 16  Mixing tube wall pressure distributions for the ejector at maximum compression conditions, $M_{P1}/M_{S1} = 2.5/2.0$

726

# ROTATIONAL FLOW IN A CURVED-WALL DIFFUSER DESIGNED BY USING THE INVERSE METHOD OF SOLUTION OF POTENTIAL FLOW THEORY*

Tah-teh Yang and Francois Ntone
Mechanical Engineering Department, Clemson University
Clemson, South Carolina

## ABSTRACT

Curved wall diffusers designed by using an inverse method of solution of potential flow theory have been shown to be both short and highly efficient. These features make this type of diffuser attractive in thrust ejector applications. In ejectors, however, the flow at the diffuser inlet is nearly a uniform shear flow. This paper presents a method used in examining the flow velocity along the diffuser wall and some of the analytical results for diffusers designed with potential flow theory and receiving a rotational flow. The inlet flow vorticity and the diffuser area ratios prescribed in the inverse solution of the irrotational flow are the parameters of the study. The geometry of a sample ejector using such a diffuser and its estimated thrust augmentation ratio are also presented.

## INTRODUCTION

The existing "Clemson Inverse Design Program for Short Curved Wall Diffusers"[1] is based on irrotational flow theory. Much experimental data have been examined for inlet flows having thin boundary layers with core flows well represented by potential flow theory. In such cases, experimentally obtained wall pressure distributions agree with the theoretically prescribed distributions very well. In ejectors, however, the diffuser inlet flow is significantly different from irrotational flow.

Based on the inlet velocity measurements reported by Hill and Gilbert[2] it appears that diffuser inlet flow should be represented by a shear flow of uniform vorticity. Under this condition (admitting a shear flow) the wall pressure distribution could be significantly different from that which was prescribed for the particular diffuser inlet design. Specifically, this raises a concern about the presence of an adverse pressure gradient or a deceleration in diffuser wall velocity which may result from the inlet shear flow. A moderate deceleration upstream of the suction slot may be overcome by increasing the suction flow rate. A strong deceleration will result in flow separation. A combination of large design area ratio and inlet vorticity could also result in a flow reversal at the diffuser exit because of the shear flow requirement, even in an inviscid flow. It becomes apparent, therefore, that a method of calculating the wall velocity of a shear flow in this type curved diffuser is necessary to assure no adverse pressure gradient along the diffuser wall. And this will allow us to obtain the high thrust augmentation benefit afforded by using a short, curved wall diffuser section in the ejector design.

# METHOD OF SOLUTION

## 1. Equations of Motion

The coordinate system is defined by Figure 1. For axisymmetric flow, the continuity equation is:

$$\frac{\partial u}{\partial r} + \frac{\partial w}{\partial x} + \frac{u}{r} = 0 \tag{1}$$

Define the stream function $\Psi(r,x)$ such that:

$$w = \frac{1}{r}\frac{\partial \Psi}{\partial r} \quad \text{and} \quad u = -\frac{1}{r}\frac{\partial \Psi}{\partial x} \tag{2a,b}$$

Then equation (1) becomes:

$$\frac{1}{r^2}\frac{\partial \Psi}{\partial x} - \frac{1}{r}\frac{\partial^2 \Psi}{\partial r \partial x} + \frac{1}{r}\frac{\partial^2 \Psi}{\partial x \partial r} - \frac{1}{r}\left(\frac{1}{r}\frac{\partial \Psi}{\partial x}\right) = 0$$

In addition, $\Psi$ satisfies the vorticity equation which in cylindrical coordinates for an axisymmetric shear flow is:

$$\frac{\partial u}{\partial x} - \frac{\partial w}{\partial r} = B \tag{3}$$

Substituting equations (2a,b) into equation (3) yields the following

$$\frac{\partial^2 \Psi}{\partial x^2} + \frac{\partial^2 \Psi}{\partial r^2} = \frac{1}{r}\frac{\partial \Psi}{\partial r} - Br \tag{4}$$

which is an elliptic partial differential equation.

## 2. Boundary Conditions

In the numerical solution of equation (4) for shear flow, we used the same grid network as for irrotational flow. The boundary conditions used are as follows.

(1) Inlet

At the diffuser inlet, there is a parallel flow in the x-direction, and consequently $u = 0$. The $\Psi$'s are obtained from equations (2a,b) as follows

$$\frac{1}{r}\frac{\partial \Psi}{\partial r} = w \quad \text{and} \quad -\frac{1}{r}\frac{\partial \Psi}{\partial x} = 0$$

Therefore $\psi$ only changes with r, hence

$$\frac{d\Psi}{dr} = wr$$

For shear flow,

$$w = w_{o,in} - Br$$

therefore

$$\Psi = \int_0^r r(w_{o,in} - Br)dr$$

Which yields

$$\Psi = \frac{1}{2} r^2 w_{o,in} - \frac{1}{3} Br^3 \qquad (5)$$

From equation (5), we have:

$$\Psi_{wall} = \frac{1}{2} R_{in}^2 w_{o,in} - \frac{1}{3} BR_{in}^3 \qquad (6)$$

where $R = r(\Psi_{wall})$

For irrotational flow and uniform parallel inlet velocity $q_{irr}$, we have:

$$\Psi_{irr} = \int_0^{R_{in}} r q_{irr} \, dr$$

At the wall:

$$(\Psi_{irr})_{wall} = \frac{1}{2} q_{irr} R_{in}^2 \qquad (7)$$

However, $\Psi_{wall}$ may not necessarily be equal to $(\Psi_{irr})_{wall}$, which means that for the same diffuser geometry, flow rates for the irrotational and rotational (shear) cases may not be the same.

Define $\gamma$ such that

$$(\Psi_{irr})_{wall} = \gamma \Psi_{wall}$$

and then

$$q_{irr} = \gamma (w_{o,in} - \frac{2}{3} BR_{in}) \qquad (8)$$

For the shear flow solution, we will need to (i) specify, for the inlet boundary condition, the values of $w_{o,in}$ and $\gamma$; (ii) obtain B from equation (8); and (iii) specify the streamline according to equation (5).

Another possibility is that both B and $w_{o,in}$ are specified, and $\gamma$ is to be calculated from equation (8).

In the inverse design program if we have prescribed parallel but non-uniform irrotational flows at the inlet and the exit, then the boundary condition at the inlet would be as follows:

$$(\Psi_{irr})_{wall} = \gamma \left[ \frac{1}{2} R_{in}^2 w_{o,in} - \frac{1}{3} BR_{in}^3 \right]$$

729

For known $B$ and $w_{o,in}$, $\gamma$ can be calculated from the following

$$\gamma = \frac{(\Psi_{irr})_{wall}}{\frac{1}{2} R_{in}^2 w_{o,in} - \frac{1}{3} BR_{in}^3} \tag{9}$$

and the streamlines can be calculated from equation ($\smile$).

(2) Centerline

Along the centerline, we have $\Psi = 0$.

(3) Wall, upstream of slot

Along the wall, upstream of the slot, we have $\Psi = \Psi_{wall}$, where $\Psi_{wall}$ is the same as the one calculated at the inlet.

(4) Wall, downstream of slot and inside of slot

Let $\beta$ and $\beta_{irr}$ be the fractions of the flow into the slot for the rotational and irrotational cases respectively. These $\beta$'s are related to the stream functions as shown in the following expressions.

$$\beta_{irr} = 1 - \frac{\Psi_{irr,st}}{\Psi_{irr,wall}} \tag{10}$$

and

$$\beta = \frac{\Psi_{wall} - \Psi_{st}}{\Psi_{wall}}$$

or

$$\Psi_{st} = \Psi_{wall}(1 - \beta) \tag{11}$$

$\beta$ is specified as an input to the analysis. The $\Psi$ values for lines AB and AC in Figure 2 are determined from equation (10).

(5) Diffuser Exit

Letting $Q_{irr}$ = Volumetric flow rate at the diffuser exit for irrotational flow and

$Q$ = Volumetric flow rate at diffuser exit for shear flow

results in:

$$Q_{irr}/(1 - \beta_{irr}) = \gamma Q/(1 - \beta) \tag{12}$$

It can be shown that for parallel flow

$$\dot{w}_{o,e} = \frac{2}{3} BR_{NSTAGU} + \frac{2(\Psi_{irr})_{wall}(1 - \beta)}{\gamma R_{NSTAGU}^2} \tag{13}$$

730

Here B is specified, $\Psi_{irr}$ and $R_{NSTAGU}$ are obtained from the Clemson Inverse Solution Computer Program, and $w_{o,e}$ is the center line velocity at the diffuser exit. ($R_{NSTAGU}$ is the radius at the stagnation point A of Figure 2.)

(6) Exit of Slot

At the slot exit, a shear flow having vorticity B is assumed.

Referring to Figure 4:

$$R - R_o = y \sin(90^\circ - \alpha) = y \cos \alpha$$

or

$$R = R_o + y \cos \alpha \tag{14}$$

The following development is to determine the stream function in the slot.

$$\Psi_y - \Psi_{st} = \int_0^y qR\,dy \tag{15}$$

But from Figure 3 we see that, $q = q_{o,sl} - By$

and therefore

$$\Psi_y = \Psi_{st} + R_o q_{o,sl}\, y + \frac{1}{2}(q_{o,sl} \cos \alpha - R_o B)y^2 - \frac{1}{3} By^3 \cos \alpha \tag{16}$$

The $\Psi$'s at the exit of the slot can be prescribed using equation (15) where $y$ is replaced by $\dfrac{(R-R_o)}{\cos \alpha}$, viz.

$$q_{o,sl} = \frac{\beta \Psi_{wall} + \frac{1}{2} R_o B \dfrac{R_{w,sl}-R_o}{\cos \alpha}^2 + \frac{1}{3} B \dfrac{R_{w,sl}-R_o}{\cos \alpha}^3 \cos \alpha}{R_o \dfrac{R_{w,sl}-R_o}{\cos \alpha} + \frac{1}{2} \dfrac{R_{w,sl}-R_o}{\cos \alpha}^2 \cos \alpha} \tag{17}$$

3. Computational Procedures

(1) For irrotational flow, prescribe $q_{irr}$ parallel at inlet and exit of diffuser. Prescribe a slightly increasing velocity distribution at wall, upstream and downstream of the slot, with desired deceleration across the slot region.

(2) Solve the inverse problem for irrotational flow. The grid work in terms of x's and r's and the velocity distributions at inlet and exit of the diffuser and at the slot exit are then obtained.

(3) Solve the rotational flow equation for $\Psi$ using the previously discussed boundary conditions.

(4) Solve for the velocity distribution at the wall. If the velocity distribution at the wall is slightly increasing with an abrupt deceleration across the slot, the diffuser geometry is satisfactory. If there is a deceleration along the wall, change the irrotational wall velocity distribution and go back to (2).

731

Using equations (2a,b) we may compute the velocity distribution along the wall from the Ψ distribution, i.e., with

$$q = \sqrt{(\frac{1}{r} \frac{\partial \Psi}{\partial r})^2 + (\frac{1}{r} \frac{\partial \Psi}{\partial x})^2} \qquad (18)$$

In the wall velocity computation, the vorticity is to be specified as one of the parameters at the diffuser inlet, and in ejector application this parameter is determined from the mass ratio of the primary and the secondary flow rates and the geometry of the mixing chamber. Using this method, computations were carried out on the University's IBM 370/3033 digital computer. Before a more generalized inverse design program is formulated, the method outlined above will be used to examine the wall velocity distribution to assure the absence of any adverse pressure gradient in ejector design. A more detailed version of the analysis will be published as Mr. Francois Ntone's thesis for a Master of Science Degree in Mechanical Engineering at Clemson University, which is expected to be completed by May 1981. Results of the sample computations using the above outlined analysis are presented in the next section.

## ANALYTICAL RESULTS

Figure 5 represents an axisymmetric diffuser having an area ratio of 2.5 to 1. Figure 6 shows the velocity distributions along the diffuser walls. The circles denote the velocity distribution prescribed to the "Inverse Design Program" for irrotational flow, and the triangles represent the velocity distribution along the diffusers depicted in Figure 5. The second velocity distributions were computed for inlet shear flow having a nondimensional vorticity value of 0.33 where velocity and length are normalized by inlet center line velocity and inlet width respectively. It is apparent that even though the prescribed diffuser wall velocity distribution upstream of the slot has a strong acceleration, the wall velocity distributions may experience deceleration in the diffuser when a shear flow is admitted. In actual operation a flow separation would most likely take place.

Figure 7 shows three velocity distributions for the diffuser depicted in Figure 5; these are specifically for inlet vorticity values of 0.33, 0.5, and 0.65. There is a significant change in the magnitude of the velocities, but their gradients vary only slightly. As expected, larger vorticity results in more deceleration. The larger change of wall velocity magnitude results from the assumption in our analysis that the diffuser center line velocity is kept constant, therefore the wall velocity decreases more when the inlet shear flow vorticity increases more. Judging from the distributions of this figure, a flow separation would likely take place in all three cases. Figure 8 shows the wall velocity distributions for the diffuser depicted in Figure 5, under the conditions of (i) admitting an inlet shear flow with a vorticity of 0.5 and (ii) three different slot suction rates. A suction rate Of 5.6% was the design value. At a suction rate of 8.5%, the velocity gradient upstream of the slot has not improved significantly in comparison to the distribution resulting from the 5.6% suction flow. Perhaps none of these distributions will yield a fully attached flow throughout the diffuser.

Figure 9 shows a diffuser designed for irrotational flow and having an area ratio of 2.5 to 1 with its suction slot slightly modified. Figure 10 shows the rotational velocity distribution along the walls of diffusers depicted in Figures 1 and 5 with inlet vorticity of 0.5. Apparently, there is no significant difference in wall velocity distribution for these two shear flow inlet cases. Figure 11 shows a diffuser designed for irrotational flow and having an area ratio of 2 to 1. Figure 12 shows wall velocity distributions for the diffuser depicted in Figure 11. The velocity distribution represented by circles is for irrotational flow, and that represented by triangles is for shear flow with velocity of 0.5. In this case hardly any deceleration is detected for the rotational flow, therefore, one should expect a highly effective diffuser even when a shear flow inlet condition is imposed at the curved wall diffuser inlet. Figures 13 and 14 are similar to Figure 12 and are for an area ratio of 1.5 to 1.

## SAMPLE EJECTOR

Now the variation of wall velocity distribution due to vorticity is understood, and one may select ejector design parameters in such a way that no deceleration takes place along the diffuser wall and the diffuser flow can be maintained attached without excessive boundary layer suction.

Figure 15 shows an example of an air-to-air ejector for thrust augmentation with the area ratio of the secondary flow to the primary flow at the mixing chamber inlet of 40 to 1, and the mass ratio of the secondary flow to primary flow of 12 to 1. This ejector has a static pressure of -1.25/psig at the exit of a mixing chamber. From this pressure level one may use a highly effective short diffuser with an area ratio of 2.2 to achieve an exit pressure of the ambient level.

Based on the conventional definition of thrust augmentation ratio $\phi$, namely; the momentum of the mixture of the primary and secondary flows at the ejector exit to the momentum of the primary flow at the mixing chamber inlet, this sample ejector has a vlaue of $\phi$ of 2.182. Since the short diffuser of the sample ejector uses boundary layer control, an auxilliary ejector will be used to achieve the necessary boundary layer suction. The removed air will be discharged in the same direction as the thrust ejector and thus contributes to the overall thrust. Therefore a modified thrust augmentation ratio $\phi_2$, defined as the total momentum at the ejector exit to the sum of the momentum of the primary flows at the mixing chamber inlet and the suction chamber, must be used for this type of ejector. We found that for the sample ejector, $\phi_2$ has a value of 1.830 provided that a suction fraction of 10% is adequate for the boundary layer control, and the mass ratio of the auxilliary ejector of 4 to 1 can be accomplished. These assumptions are considered to be reasonable. It is noteworthy that the overall length of the ejector is much reduced relative to the ones having diffusers designed by using the concept of incipient separation. The performance level in thrust augmentation ratio compared favorably to those reported in reference 3.

REFERENCES

1.  Nelson, C.D. and T. Yang, "Design of Bounded and Unbounded Axially Symmetrical Ducts with Specified Distributions", AIAA Journal, Vol. 15, No. 9, Sept. 1977.

2.  Gilbert, G.B. and P.G. Hill, "Analysis and Testing of Two-Dimensional Slot Nozzle Ejectors with Variable Area Mixing Sections", NASA CR 2251, Nov. 1972.

3.  Tai, T.C., "Optimization of Axisymmetric Thrust Augmenting Ejectors", Proceedings of AIAA 10th Fluid and Plasmadynamics Conference, Alberquerque, New Mexico, June 27-29 1977, paper 77-707.
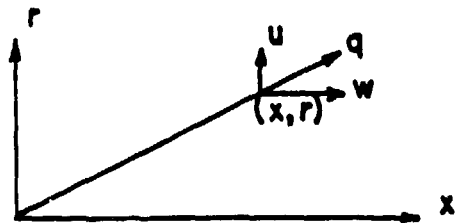
Figure 1.  Coordinate System and        Figure 2.  Wall Streamlines and
           Velocity Components.                    the Branching Point.
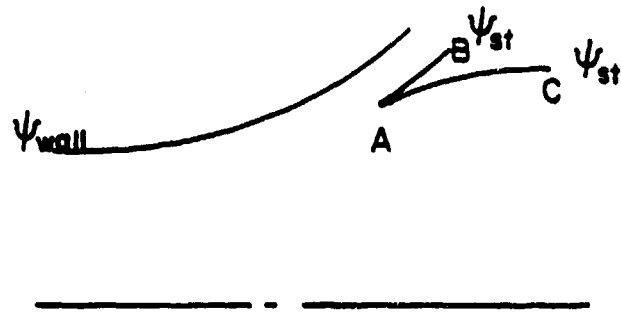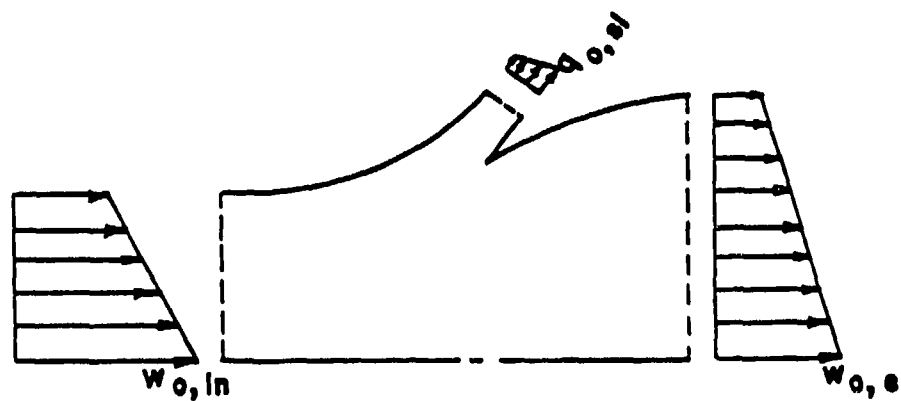


Figure 3.  Velocity Distributions for Shear Flow.
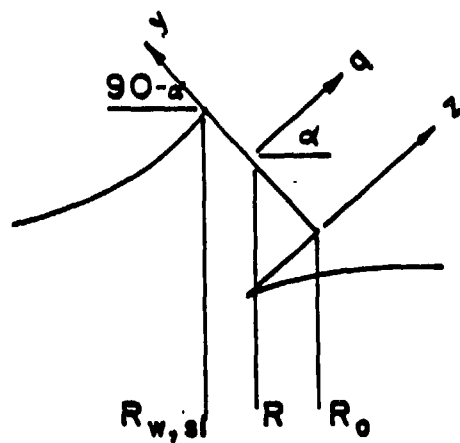


Figure 4.  Coordinate System at Slot Exit.
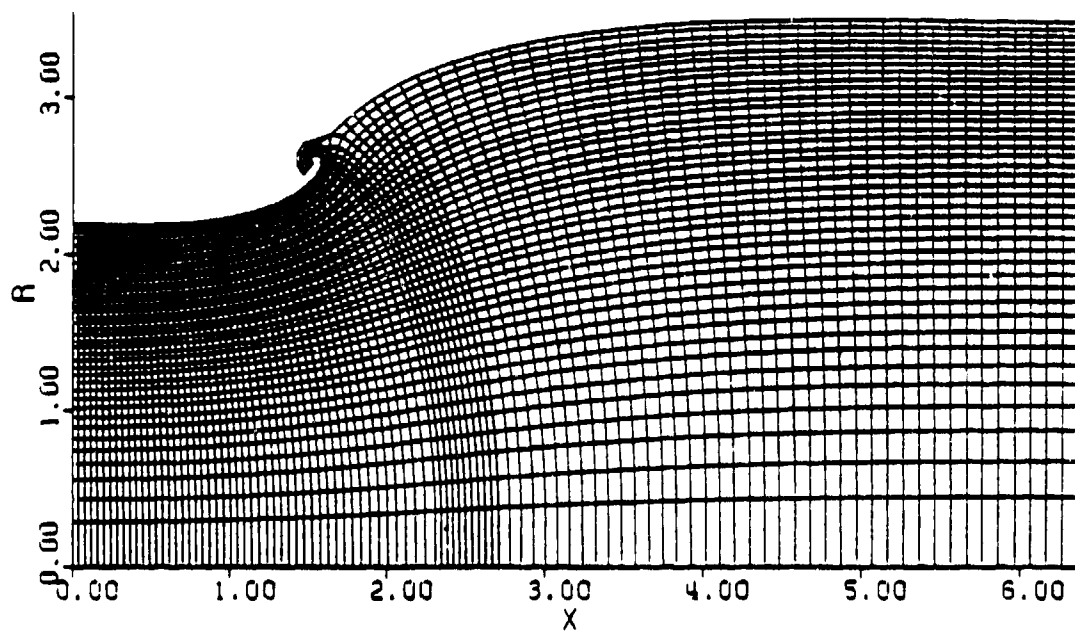
Figure 5.  Computer Plot of $\phi - \Psi$ Grid for an Axisymmetric Diffuser, AR = 2.5, Suction Rate = 5.6%.
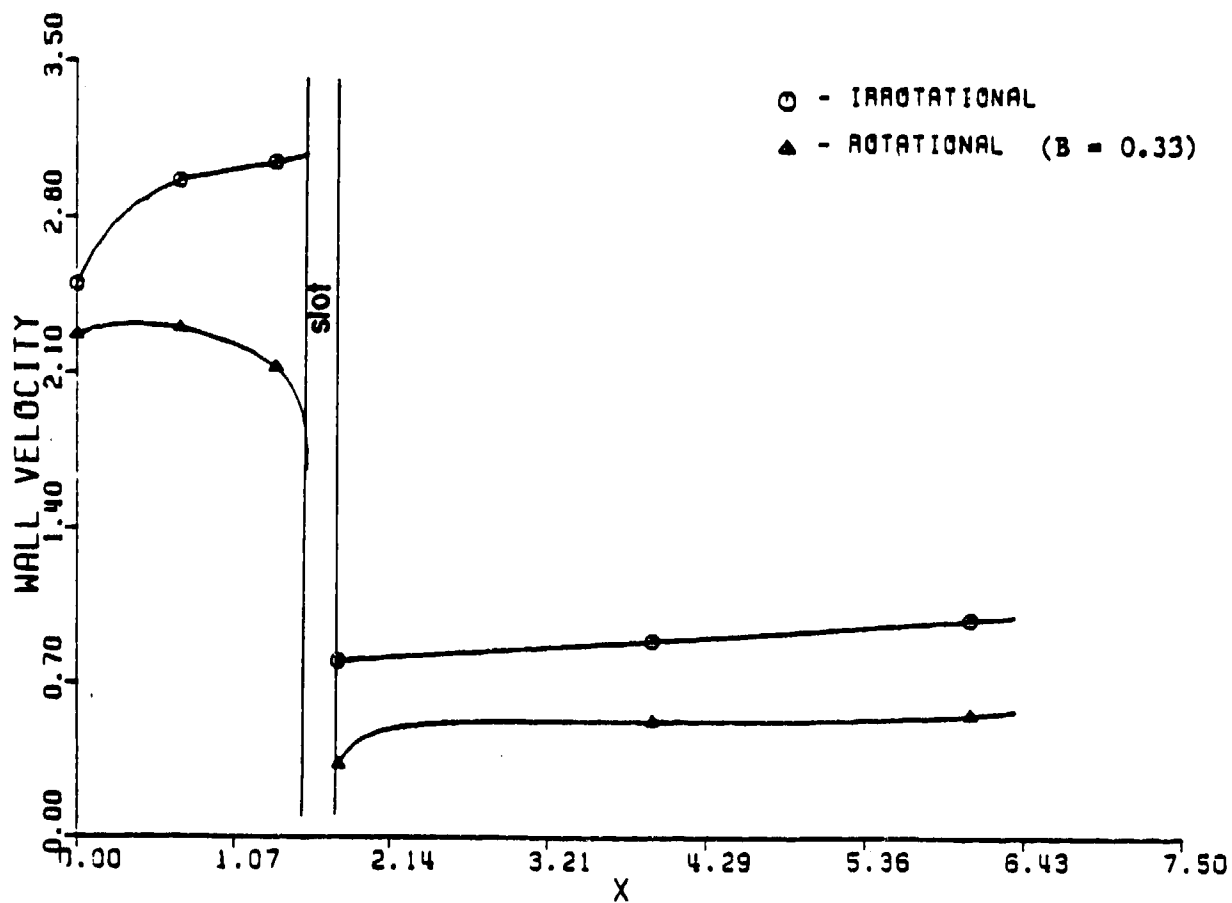


Figure 6.  Velocity Distributions for Rotational and Irrotational Flow.

736
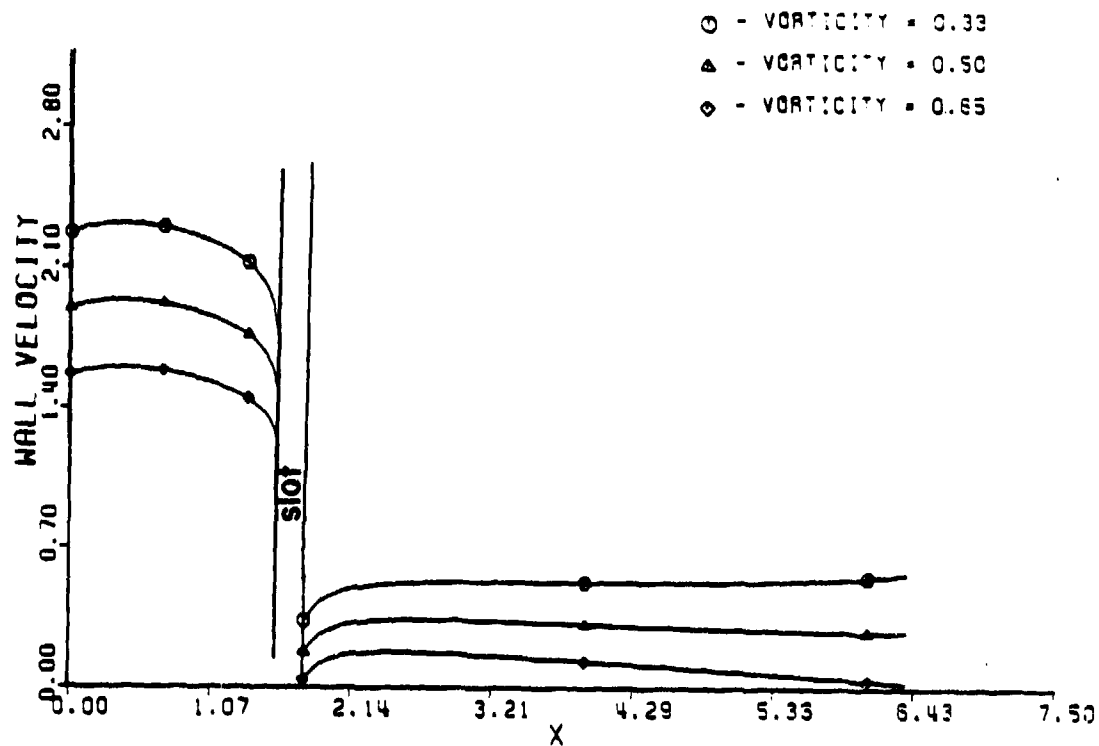
**Figure 7.** Velocity Distributions for Three Rotational Flows with Suction Rate of 5.6%
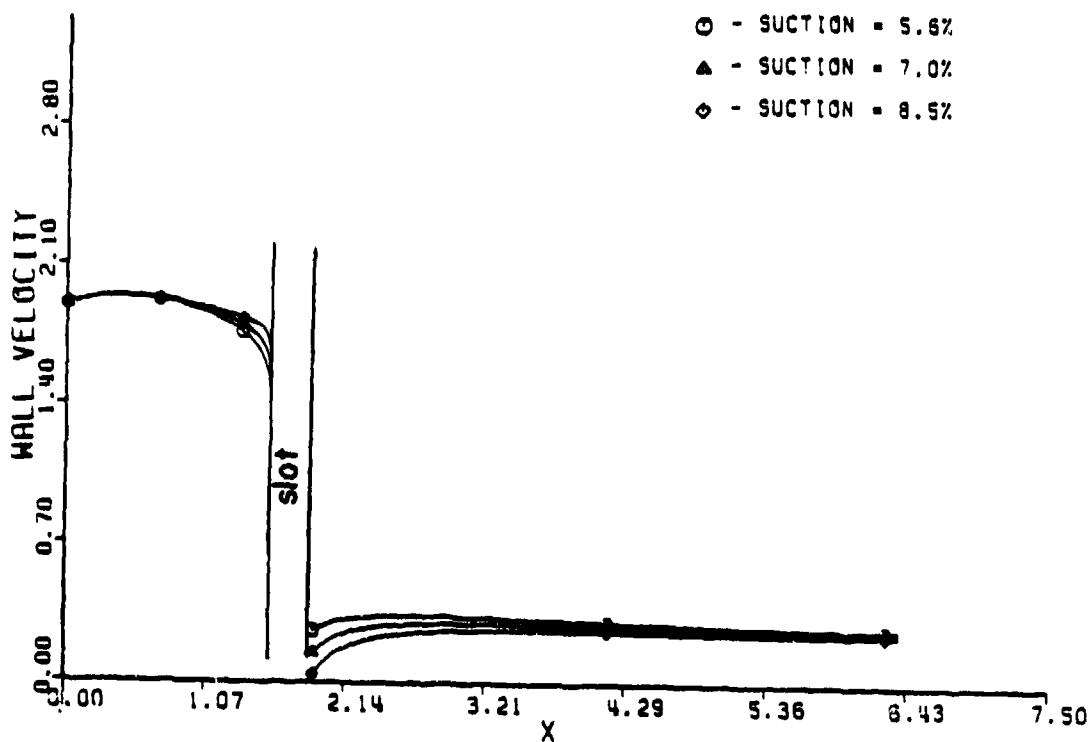


**Figure 8.** Velocity Distributions for Rotational Flow with B = 0.5 and Three Suction Rates.
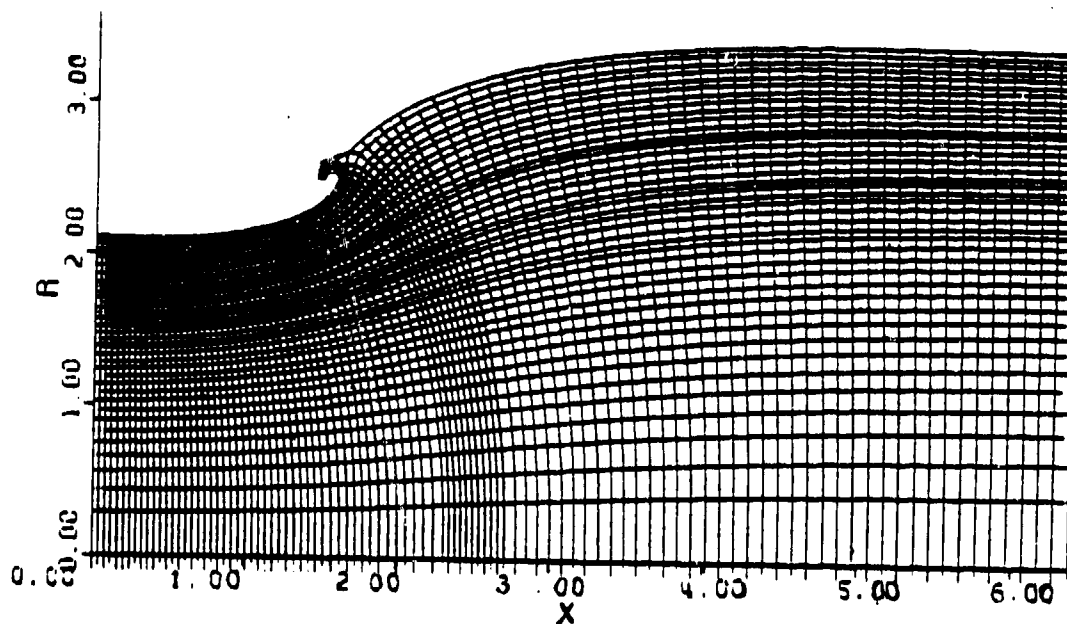
Figure 9. Computer Plot of φ-Ψ Grid for an Axisymmetric Diffuser, AR = 2.5, Suction Rate = 5.6% (Change in Suction Slot).
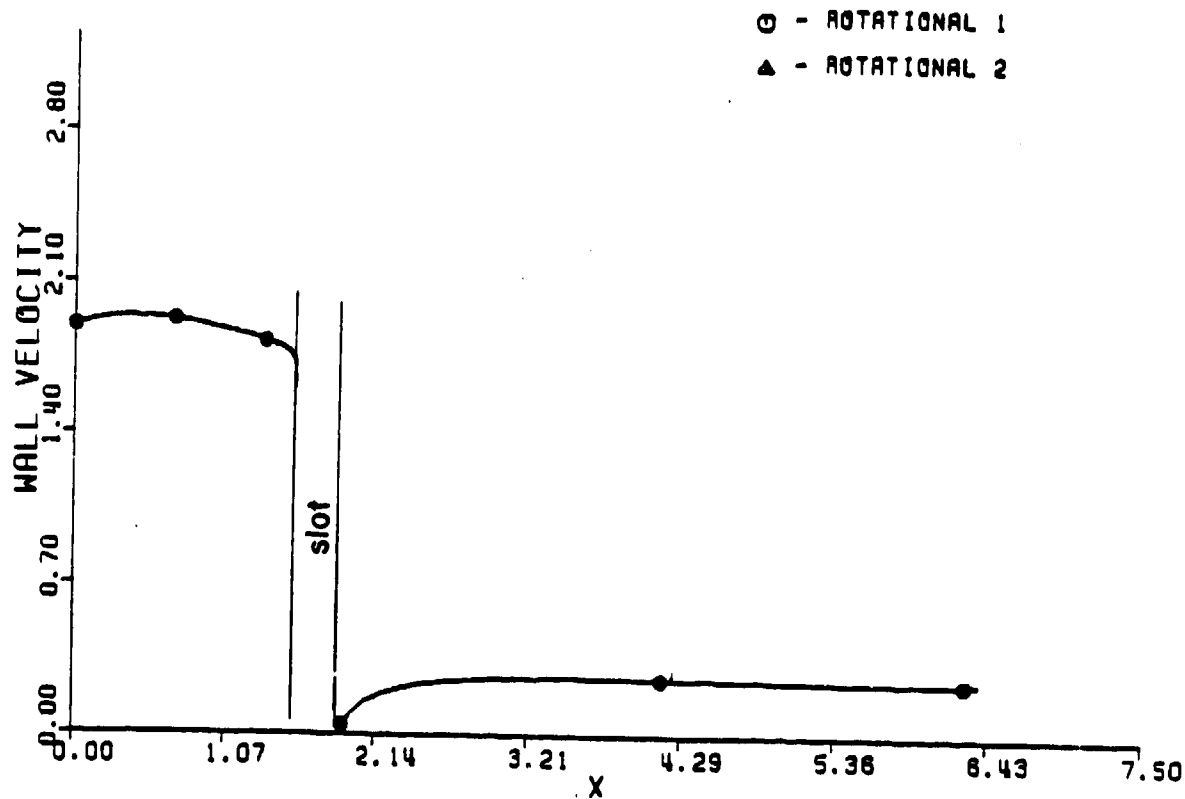


Figure 10. Velocity Distributions for Diffusers Represented in Figures 5 and 9 (B = 0.5, Suction Rate = 8.5%).

738
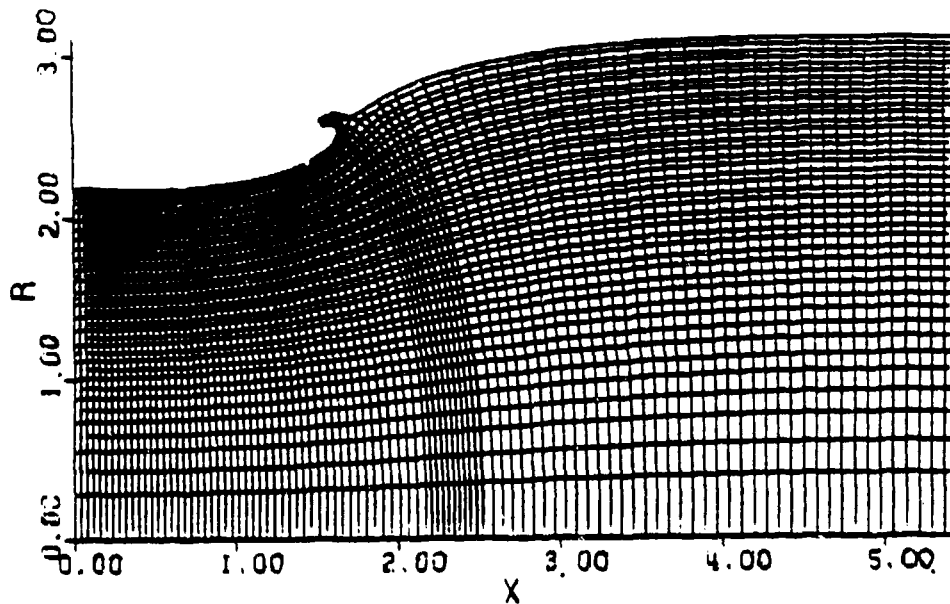
Figure 11.    Computer Plot of φ–ψ Grid for an Axisymmetric Diffuser, AR = 2.0, Suction Rate = 5.6%.
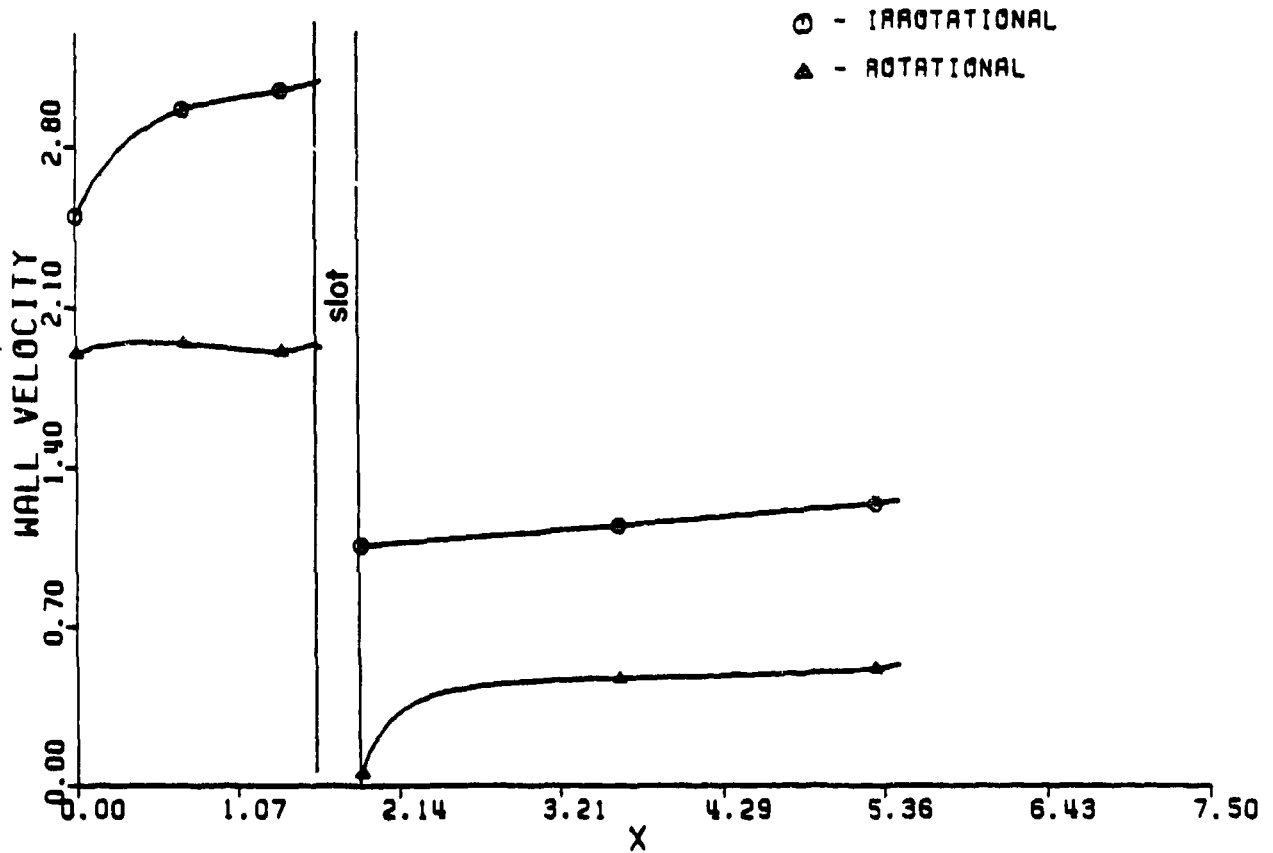


Figure 12.    Velocity Distributions for Rotational and Irrotational Flows, B = 0.5, Suction Rate = 8.5%

739
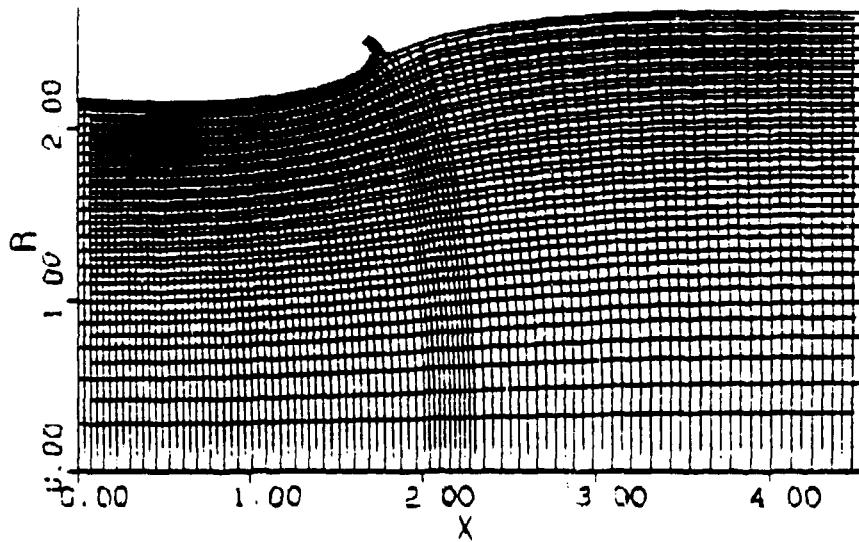
Figure 13. Computer Plot of φ-ψ Grid for an Axisymmetric Diffuser, AR = 1.5, Suction Rate = 8.5%
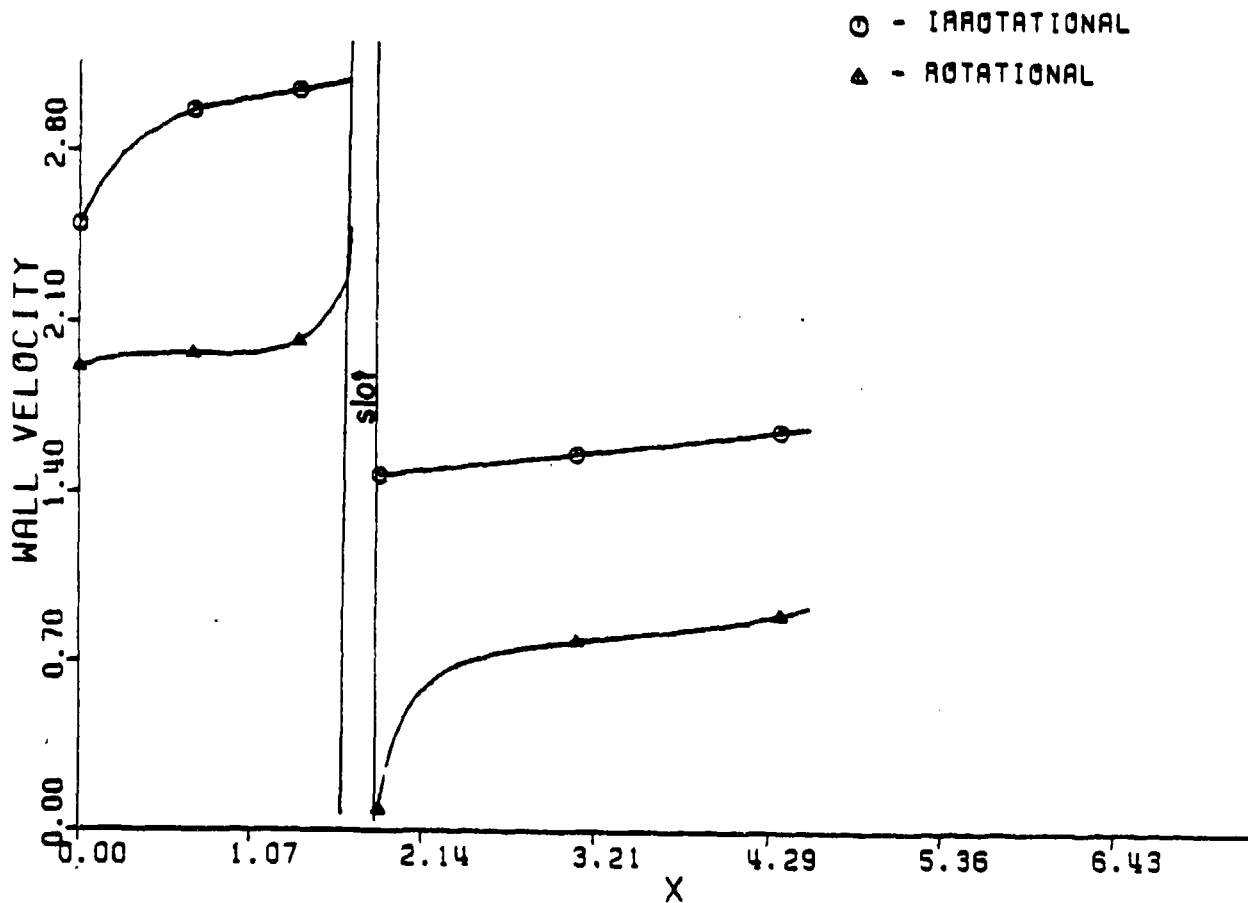


Figure 14. Velocity Distributions for Rotational and Irrotational Flows, B = 0.5, Suction Rate = 8.5%.

740
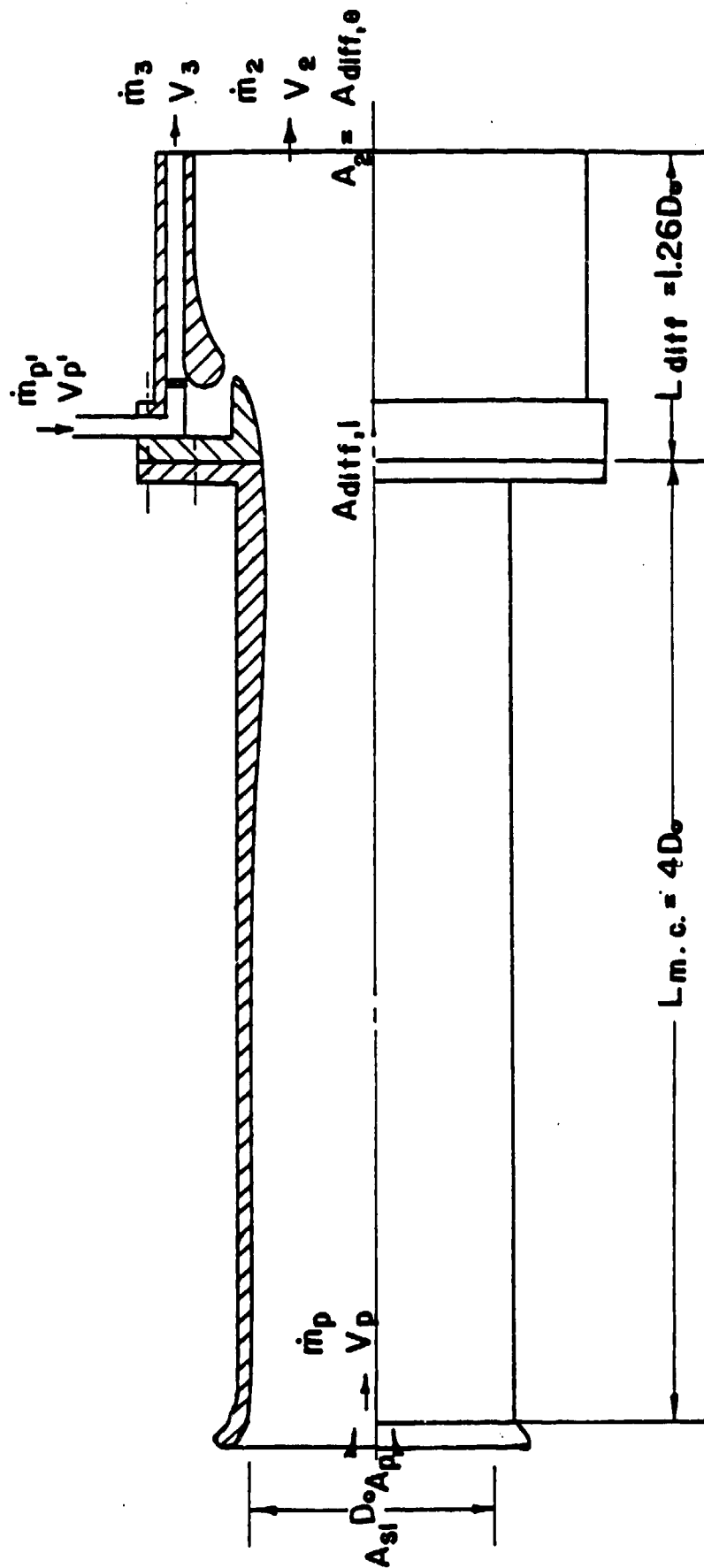
$$\frac{A_2}{A_{si}} = AR = 2 \qquad \frac{A_{diff,e}}{A_{diff,i}} = AR_2 = 2.2 \qquad \phi_2 = \frac{\dot{m}_2 V_2 + \dot{m}_3 V_3}{\dot{m}_p V_p + \dot{m}_{p'} V_{p'}} = 1.83$$

Figure 15. A Sample Air-to-Air Ejector with 10% Contraction for Mixing Chamber. No Deceleration Along Diffuser Wall.

# INLET AND DIFFUSER EFFECTS ON
# THRUST AUGMENTING EJECTORS[1]

S. G. Reznick[2]
Air Force Wright Aeronautical Laboratories
Wright-Patterson AFB OH 45433

M. E. Franke[3]
Air Force Institute of Technology
Wright-Patterson AFB OH 45433

## ABSTRACT

Effects of primary jet inlet nozzle configuration and diffuser geometry on the thrust augmentation of circular and rectangular ejectors are investigated in an experimental study. The rectangular ejector inlet nozzle configurations consist of either one, two, or three slot nozzles. The circular ejector inlet nozzles consist of slot nozzles placed either across the inlet or around the inlet periphery. Diffuser geometry is varied primarily by changing the diffuser area ratio. Effect on thrust performance of the primary flow injection angle relative to the inlet walls is investigated. Effects of side-wall, end-wall, and diffuser blowing on thrust performance and diffuser stall also are considered.

AD P000526

## INTRODUCTION

The development of thrust augmenting ejectors has been aggressively pursued since their potential was suggested by von Kármán in his classic paper on the subject in 1949 [1]. Ejectors have been developed and tested in several experimental aircraft, including an augmentor-wing STOL aircraft [2, 3] and the XFV-12A [4]. Although primary air for an ejector in a jet aircraft application is readily available from engine bleed air or engine exhaust, the designs have met with limited success [2, 5]. The performance of ejector-equipped aircraft indicates that either the existing ejectors must be more effectively integrated into aircraft designs or new ejector devices possessing superior performance must be developed to make ejector thrust augmentation a more useful technology. The weight penalty and the ducting pressure losses must be overcome. It is possible that a mix of different ejector approaches, such as high-performing, fixed geometry ejectors mounted in the fuselage and lower performing but collapsible ejectors integrated into the wing, will give a combined performance which is adequate for thrust requirements. Further development work is therefore needed to make ejectors a more viable option. Ejector developments can be stimulated also as more new theories and analogies [6-8] are developed for the analysis and design of these thrust augmenting devices.

The purpose of this investigation is to examine the effects of primary jet nozzle configuration and diffuser geometry on the thrust of both rectangular and axisymmetric, circular ejectors.

## EXPERIMENTAL APPARATUS

### Rectangular Ejector

The rectangular ejector was configured with one, two, or three primary slot injection nozzles at the inlet. A photograph of the rectangular ejector with two inlet nozzles is shown in Fig. 1. Blowing capability existed at the two inlet cylinders, at the four small end-wall slot nozzles, and at the two diffuser cylinders. A schematic of the ejector geometry is shown in Fig. 2. A small diameter pressure tap was located in each nozzle plenum to measure static pressure. This pressure was very close to the stagnation pressure due to the low flow velocity in the plenum. The nozzles contained internal baffle chambers and flow straighteners to provide a more uniform spanwise velocity profile at the nozzle exit. The primary nozzles were designed to pivot as well as to translate vertically and horizontally. Thus, the injection angle and the position of the primary nozzles relative to each other and to the inlet walls could be varied. The exit dimensions of the primary nozzles were 0.08 in by 5.7 in.

Two primary nozzles were mounted symmetrically on either side of the inlet and could be adjusted to direct the primary flow at different angles relative to the inlet side walls. This dual-nozzle configuration is similar to that of Alperin et al [8-10]. A primary center nozzle could be inserted by itself in the inlet or between the other two nozzles to form a triple-nozzle configuration. The three nozzles in the triple configuration either had the same exit plane or the center nozzle was positioned in front to provide a staged effect.

744

The rectangular ejector was constructed with a 3-in-long section that served either as a constant area mixing chamber or as a variable angle diffuser. This section was followed by a second variable angle diffuser stage. The throat height of the mixing chamber as well as the wall angle could be varied. The parameters that define the positioning of the inlet nozzles, the diffuser lengths and wall angles, and the inlet cylinder blowing angle are shown in Fig. 2. Extensions, which reduced inlet losses, could be attached to the metal side walls and plexiglass end walls of the diffuser. The extensions increased the diffuser length by 1.5, 2.5, and 3.5 in.

Circular Ejectors

The two circular ejectors consisted of wooden inlets, fiberglass mixing chambers and fiberglass or metal diffuser sections. Both ejectors had 2-in radius-of-curvature inlets followed by a constant area mixing chamber 3 in long. The ejectors had mixing chamber diameters of 4.4 in and 6 in respectively. The smaller ejector had detachable conic diffuser sections which permitted two or three stage diffusion as follows: $\psi_1$ = 3 deg, $\psi_2$ = 3, 4, or 5 deg, and $\psi_3$ = -3, 0, or 2 deg. The diffuser sections of the large circular ejector were similar.

Three types of primary injection nozzles were designed for the inlet. These slot nozzles are referred to as the spoke, circumferential, and annular nozzles. The spoke and circumferential nozzles were used in various combinations on the large circular ejector, and the circumferential nozzles and the annular nozzle were used separately on the small ejector.

The spoke nozzle configuration consisted of eight symmetrically-positioned, slot nozzles that extended from the perimeter to the center of the ejector. This configura _n is shown in Fig. 3. The slots were 2.75 in long with a gap of 0.0 in.

The 8-nozzle circumferential configuration is shown in Fig. 4. The 8 nozzles were spaced symmetrically around the inlet perimeter and designed to provide flow tangent to the curved inlet surface, but not on the surface. The nozzles had a slot length of 0.94 in and a slot gap of 0.06 in and could be used in combination with the spoke nozzles or by themselves. A 16-nozzle circumferential configuration was obtained by adding 8 more nozzles around the perimeter to the 8-nozzle configuration.

The annular nozzle, Fig. 5, was designed to provide a continuous annular slot flow of air approximately tangent to the walls at the inlet The slot gap was 0.065 in.

Test Stand

A test stand was designed to supply compressed air to the ejector apparatus and measure the ejector thrust with a strain gage load cell. The test stand consisted of a pipe arrangement which pivoted as a pendulum about two low-friction annular bearings in a "tee" bearing support at the pivot point. The ejector was bolted to the swinging end of the pipe. Compressed air flowed through the open center of the "tee" bearing, through the length of pipe (pendulum), and then through tygon tubing to the ejector manifolds and jet nozzles. A standard orifice, located mid-

745

way along the length of the pendulum, was used to measure the mass flow rate in accordance with ASME specifications [11].

## EXPERIMENTAL PROCEDURES

Thrust was measured by a floor-mounted strain gage load cell that was connected to the ejector by cables. A position-adjustable pulley arrangement allowed the cables to turn 90 deg corners. Thrust readings were obtained using a strain gage indicator or a digital multivoltmeter and a set of standard calibrated weights.

Pressure readings were obtained with water and mercury manometers. A pressure tap was located in each nozzle plenum. A pitot tube rake with tines spaced $\frac{1}{4}$ in apart was used to scan the ejector exit flow for the total pressure, Fig. 6. The Bernoulli equation was used to determine velocity profiles. Fine cotton threads taped to the diffuser walls and a hand-held slender rod tipped with cotton thread were used to provide flow visualization.

Steady-state tests were run to determine the thrust augmentation ratio $\phi$ and to approximate the mass augmentation ration $\dot{m}_0/\dot{m}_1$. The thrust augmentation ratio is defined as

$$\phi = \frac{F_m}{F_i}$$

where $F_m$ is the force developed by the ejector and measured by the strain gage apparatus and $F_i$ represents the force the primary nozzle flow would have generated upon discharge isentropically to the ambient atmosphere in the absence of the rest of the ejector apparatus. $F_i$ is given by

$$F_i = 7A_1P_a \left[ (p_t/p_a)^{0.286} - 1 \right]$$

The mass augmentation ratio, which represents the mass flow rate of secondary air $\dot{m}_0$ to the mass of primary air $\dot{m}_1$, was calculated for some of the configurations. The mass flow rate from the primary nozzles was calculated from the nozzle pressure ratio or by use of the test stand orifice meter. The exit mass flow rate was obtained from the exit velocity profile. The secondary mass flow rate $m_0$ was determined from the difference between the exit mass flow rate $\dot{m}_s$ and the primary mass flow rate $\dot{m}_1$.

### Room Effects

Since the tests were conducted indoors, a room effects study was accomplished to determine whether the walls of the room or objects within the room would affect thrust augmentation performance. A flat wooden barrier (7 ft by 7 ft) was positioned at specific distances normal to the ejector flow both in front of and behind the ejector with circumferential nozzles. The thrust augmentation ratio remained constant until the barrier was within 17 in of the ejector inlet or within 30 in of the ejector exit. Since the test room walls, floor and ceiling were all greater than 5 ft from the mounted ejector, it is assumed that the room did not affect ejector performance and measurements.

# RESULTS

The tests were run at primary to ambient pressure ratios $p_t/p_a$ of 1.1 to 1.5. At these pressure ratios, the primary jet nozzle velocities ranged from approximately 300 to 900 fps. The average diffuser exit velocities were approximately 100 fps. The primary nozzle exit Reynolds numbers Re were based on exit velocity and on the nozzle gap as the characteristic length and ranged from 14,000 to 24,000. At the diffuser exit, Re varied from 200,000 to 300,000 based on exit velocity and exit diameter or width as the characteristic length.

## Rectangular Configurations

The importance of using inlet end-wall extensions and a curved entry to each side wall, Fig. 2, was noted by Kedem [12]. The use of end-wall extensions and a curved entry was found to increase the thrust augmentation ratio by approximately 10 percent over a wide range of exit area ratios. For this reason the curved entry and exit end-wall extensions were used in all the tests.

Tests were run with the dual inlet nozzles to determine the effects of diffuser area ratio $A_3/A_2$ on thrust performance. Various area ratios were obtained by varying the diffuser wall angle. The results are shown in Fig. 7. The trend of $\phi$ with $A_3/A_2$ is similar to results reported by others, such as Quinn [13] and Bevilaqua [14], in that $\phi$ increases, reaches a maximum and then decreases with increasing $A_3/A_2$. Figure 7 shows $\phi$ was maximum for an $A_3/A_2$ in the range of 1.8 to 1.9. The diffuser influences the pressure in the ejector, and at low values of diffuser area ratio the pressure in the ejector is not low enough to aid the flow of secondary fluid. On the other hand, large diffuser area ratios that would lead to favorable pressure distributions in the ejector do not necessarily achieve this due to flow separation in the diffuser. In some cases, blowing along the diffuser side walls eliminates stall or permits wider diffuser angles without stall; however, the shear losses due to the blowing may decrease performance. Figure 8 shows that for an unstalled case, $\phi$ decreased slightly as the percent of primary flow through the diffuser nozzles was increased.

End-wall and inlet side-wall blowing were also employed. Except in the cases where this blowing prevented large scale separation, the blowing was generally detrimental to the thrust augmentation ratio $\phi$. This was especially the case with the dual primary nozzles. The dual nozzles provide primary flow near the side-walls and do not require as much additional blowing to prevent stall and separation.

The dual-nozzle configuration also was tested at different injection angles $\alpha$ while holding h, $\ell$, and the diffuser configuration constant. The results of these runs, shown in Fig. 9, indicate that the angle the jet makes with the inlet wall affects the thrust augmentation ratio significantly. The best performance was obtained when the primary jet was directed approximately tangent to the curved inlet side walls. For injection angles less than this optimum angle, the flow strikes the side wall and causes a force that acts opposite to the desired thrust vector.

For larger injection angles, the flow does not appear to attach to the curved inlet, but instead separates from the wall in the ejector throat. The dual nozzle positions were changed by varying h, and ℓ. Yet, maximum performance still was obtained when the injection angle was approximately tangent to the inlet side wall, Fig. 10. These results show that thrust augmentation was very sensitive to this tangency condition and relatively insensitive to nozzle position.

Tests with a triple-nozzle configuration showed a decrease in performance compared with the dual-nozzle configuration. This is shown in Fig. 11 where the results indicate that $\phi$ decreased as the amount of air issuing from the center nozzle exceeded approximately 15 percent of the total primary flow. Between 0 and 15 percent, there was little change in thrust augmentation. Also, it should be noted that by just inserting the center nozzle in the inlet, $\phi$ decreased from 1.48 to 1.4. The results (not shown) for the single nozzle indicated that $\phi$ was less than 1.3 even with side-wall blowing and even though the single nozzle inlet area ratio was twice that of the dual nozzles. For the limited tests conducted, the dual-nozzle configuration appears to be superior to the other configurations. An exit velocity profile obtained with the dual-nozzle configuration is shown in Fig. 12. The profile shows that the velocity is higher near the walls than at the center of the ejector exit plane. This type of distribution apparently leads to better flow attachment at the walls and less chance for flow separation than with a profile where the velocity is highest at the center.

Circular Configurations

The circumferential nozzle performance results with the smaller ejector are shown in Fig. 13. The effect of diffuser area ratio on $\phi$ shows trends typical to those described previously for the rectangular ejector, Fig. 7; however, the values of $\phi$ for the circular ejector exceeded those of the dual-nozzle rectangular ejector. It should be noted, however, that although the cross sectional throat areas of the rectangular ejector and circular ejector were approximately the same, the inlet area ratios differ by about two. This occurs since the total area of the 8 circumferential nozzles was about half the total area of the dual-nozzle configuration. The maximum $\phi$ of approximately 1.9 is somewhat less than the augmentation ratio reported by Alperin and Wu [15] but considerably less than that reported by Campbell and von Ohain, although they used a different performance index. The exit velocity profile is shown in Fig. 14. As expected the exit velocity is much higher near the walls than at the center. This is similar to that found with the dual-nozzle rectangular ejector. It appears that it might be desirable to increase the mixing, since this should increase performance further as pointed out by Bevilaqua [14]. Alperin and Wu [8] suggest, however, that an increase in effective diffuser area ratio can compensate for incomplete mixing.

The thrust augmentation obtained with the annular nozzle was significantly less than that with the 8 circumferential nozzles ($\phi$ = 1.3 vs 1.75). Possible causes for this lower performance include the difference in inlet area ratio, that the discrete circumferential nozzles may achieve a hypermixing effect, and that the 8 circumferential

748

nozzles did not block the inlet as much as the annular nozzle. The $\phi$ obtained for the 16-circumferential nozzle configuration was approximately 1.55. This was somewhat better than that obtained with the annular nozzle, but less than that with the 8-nozzle configuration.

The results with the larger ejector showed that the spoke nozzle arrangement alone did not develop any thrust augmentation. A possible explanation for this is that the velocity profile (not shown) indicated that the highest velocity occurred near the center of the exit or just the opposite of that found with the 4.4 in circular ejector with the circumferential nozzles. As a result, the flow with spoke nozzles was more prone to stall. When circumferential nozzles were positioned between the spoke nozzles, significant thrust augmentation was obtained. The results are shown in Fig. 15. The thrust augmentation decreased as more flow was injected through the spoke nozzles. The thrust augmentation ratio obtained in this ejector with only the 8-circumferential nozzles was approximately 1.7 while the augmentation ratio with flow only through the 8-circumferential nozzles in the combined arrangement was 1.55, as shown in Fig. 15.

## CONCLUSIONS

1. The inlet primary nozzle configuration has a large effect on the thrust augmentation of both rectangular and circular ejectors.

2. Inlet primary nozzles placed near but not on the side walls with the flow directed parallel to each side wall provided good thrust augmentation in both the rectangular and circular ejectors.

3. Diffuser stall and separation for a given diffuser area ratio occurred more readily with primary nozzles placed across the inlet in a spoke or single nozzle configuration than with those placed around the inlet periphery or near the side walls.

4. Discrete nozzles placed around the inlet periphery of a circular ejector provided somewhat better thrust augmentation than an annular nozzle at approximately the same location.

5. Side-wall, end-wall, and diffuser blowing tended to reduce thrust augmentation, when not required to prevent separation.

6. The circular ejector had a thrust augmentation ratio greater than that of the rectangular ejector.

## REFERENCES

1. Von Kármán, T., "Theoretical Remarks on Thrust Augmentation," Contributions to Applied Mechanics", Reissner Anniversary Volume, Ann Arbor MI, 1949, pp. 461-468.

2. Aiken, T. N., "Thrust Augmentor Application for STOL and V/STOL," NASA Technical Memorandum, NASA TM X-73241, June 1977.

3. Korbacher, G. K., "Aerodynamics of Powered High-Lift Systems," Annual Review of Fluid Mechanics, Vol. 6, 1974, pp. 319-358.

4. Mark, L. and Dehart, J. H., "High Speed Aerodynamic Design of an Innovative V/STOL Canard-Wing Configuration," AIAA Paper 76-910, AIAA Aircraft Systems and Technology Meeting, Dallas TX, September 1976.

5. Murphy, R. and Lewis, E. L., "XFV-12A Thrust Augmented Wing (TAW) Prototype Aircraft," Proceedings of the Workshop on Thrust Augmenting Ejectors, NASA Ames Research Center CA, June 1978, NASA Conference Publication 2093, September 1979, pp. 473-480.

6. Bevilaqua, P. M., "A Lifting Surface Theory for Thrust Augmenting Ejectors." AIAA Journal, Vol. 16, No. 5, May 1978, pp. 475-481.

7. Viets, H., "Thrust Augmenting Ejector Analogy," Journal of Aircraft, Vol. 14, No. 4, April 1977, pp. 409-411.

8. Alperin, M. and Wu, J. "Consideration of Some Critical Ejector Problems," Proceedings of the Workshop on Thrust Augmenting Ejectors, NASA Ames Research Center CA, June 1978, NASA Conference Publication 2093, September 1979, pp. 363-384.

9. Alperin, M. and Wu, J., "The Alperin Jet Diffuser Ejector (ASDE) Development, Testing, and Performance Verification Report." Naval Weapons Center CA, NWC TP 5853, 1976.

10. Alperin, M. and Wu, J., "Recent Development of a Jet-Diffuser Ejector." AIAA Paper 80-0231, January 1980.

11. Flowmeter Computation Handbook, The American Society of Mechanical Engineers, New York, 1971.

12. Kedem, E., An Experimental Study of Static Thrust Augmentation Using a 2-D Variable Ejector, MS Thesis, Air Force Institute of Technology, Wright-Patterson AFB OH, 1979.

13. Quinn, B., "Compact Ejector Thrust Augmentation," Journal of Aircraft, Vol. 10, No. 8, August 1973, pp. 481-486.

14. Bevilaqua, P. M., "Evaluation of Hypermixing for Thrust Augmenting Ejectors," Journal of Aircraft, Vol. 11, No. 6, June 1974, pp. 348-354.

15. Alperin, M. and Wu, J., "End Wall and Corner Flow Improvements of the Rectangular Alperin Jet-Diffuser Ejector," NADC-77050-30, May 1978.

16. Campbell, W. C. and von Ohain, H., "Thrust Augmentation for V/STOL: ARL's Research and Concepts." Aerospace Research Laboratories, ARL 67-0065, April 1967.

| | |
|---|---|
| A | cross sectional area |
| $A_0/A_1$ | inlet area ratio |
| $A_3/A_2$ | diffuser exit area ratio |
| F | thrust |
| h | distance between pivot points of dual nozzles |
| $\ell$ | distance from primary nozzle exit to ejector throat |
| L | diffuser length |
| $\dot{m}$ | mass flow rate |
| $P_a$ | ambient pressure |
| $P_s$ | static pressure |
| $P_t$ | total pressure |
| $\alpha$ | primary injection angle |
| $\theta$ | inlet cylinder blowing angle |
| $\phi$ | thrust augmentation ratio |
| $\psi$ | diffuser wall angle |

## Subscripts

| | |
|---|---|
| 0 | inlet secondary flow |
| 1 | primary nozzle exit or first stage diffuser |
| 2 | ejector throat or second stage diffuser |
| 3 | ejector exit or third stage diffuser |
| i | isentropic |
| m | measured |

Fig. 1    Photograph of Rectangular Ejector with
Dual Nozzles
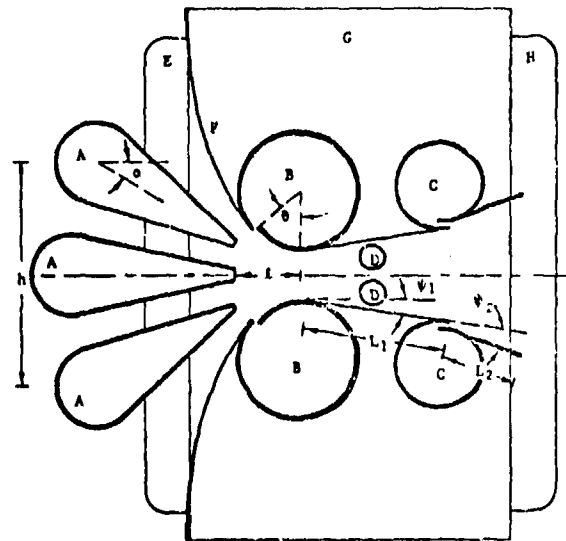


| | |
|---|---|
| A    Primary nozzles | E    Inlet end-wall extension |
| B    Inlet cylinders | F    Inlet side wall |
| C    Diffuser cylinders | G    End wall |
| D    End-wall nozzles | H    Exit end-wall extension |

Fig. 2    Schematic of Rectangular Ejector with
Three Nozzles



Fig. 3    Photograph of Circular Ejector with
Spoke Nozzles



Fig. 4    Photograph of Circular Ejector with
8 Circumferential Nozzles

752

Fig. 5    Photograph of Annular Nozzle
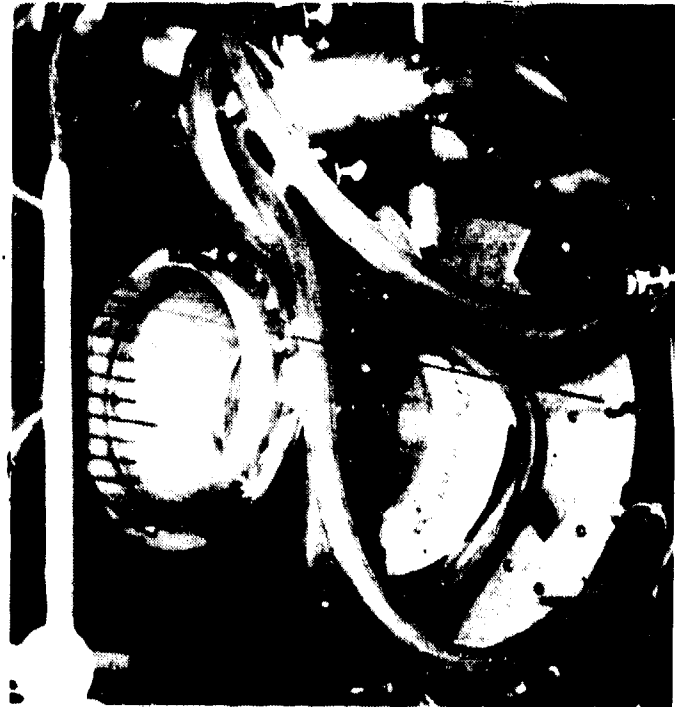


Fig. 6    Photograph of Pitot Tube Rake with
Circular Ejector
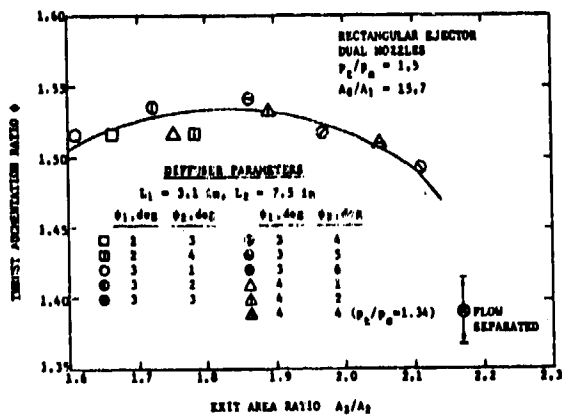


Fig. 7    Effect of Diffuser Geometry on Thrust
Augmentation Ratio
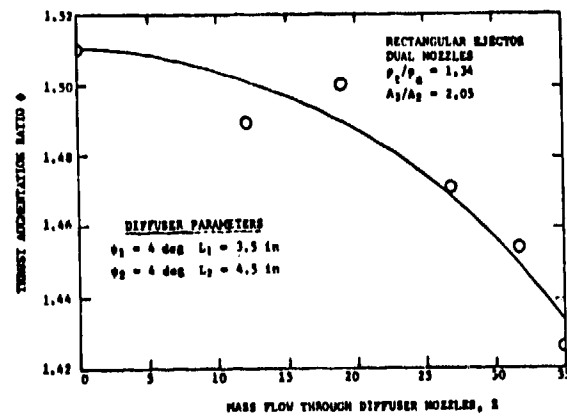


Fig. 8    Effect of Diffuser Side-Wall Blowing
on Thrust Augmentation Ratio
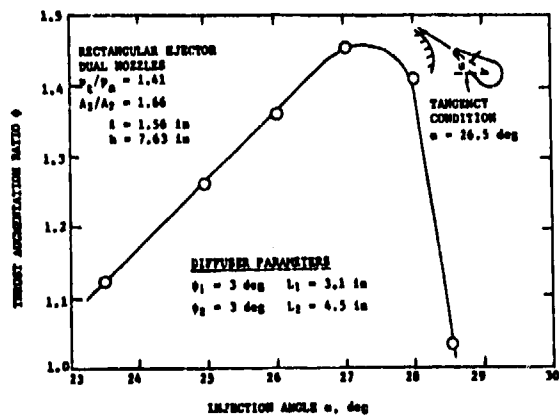


Fig. 9    Effect of Primary Jet Injection Angle
on Thrust Augmentation Ratio
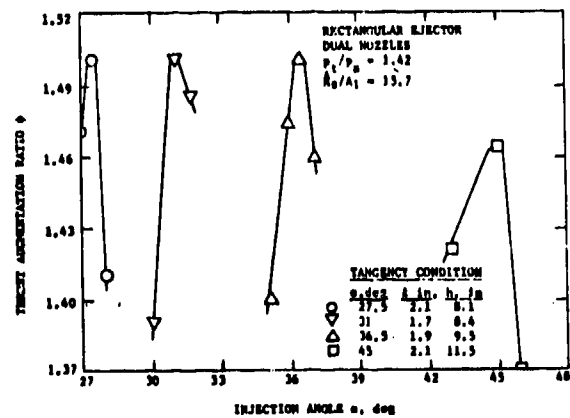


Fig. 10    Effect of Primary Jet Injection Angle
and Position on Thrust Augmentation
Ratio

753
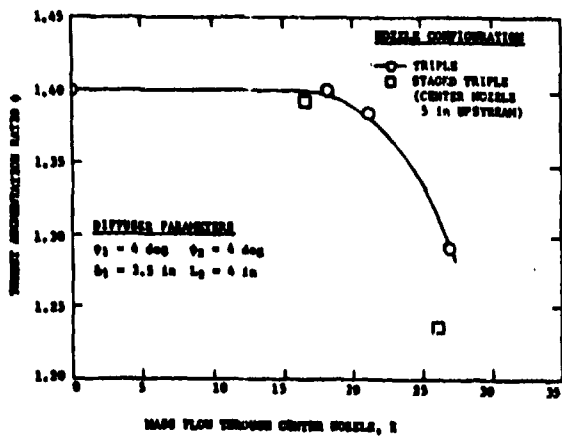
**Fig. 11** Performance of Rectangular Ejector with Triple-Nozzle Configurations
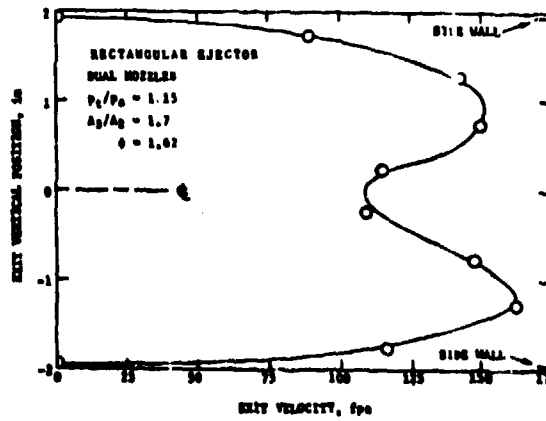


**Fig. 12** Exit Velocity Profile
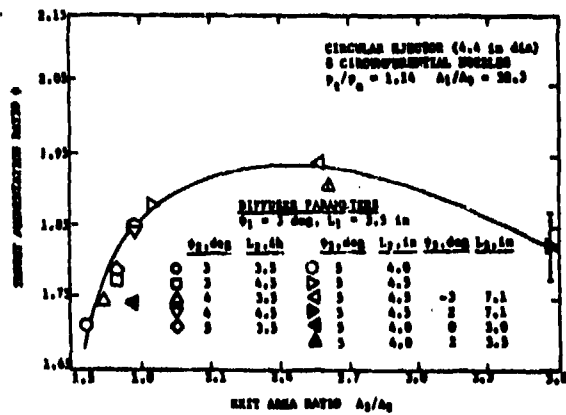


**Fig. 13** Performance of Circular Ejector with Circumferential Nozzles
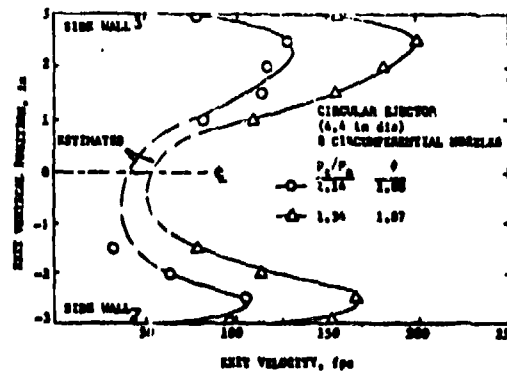


**Fig. 14** Exit Velocity Profiles
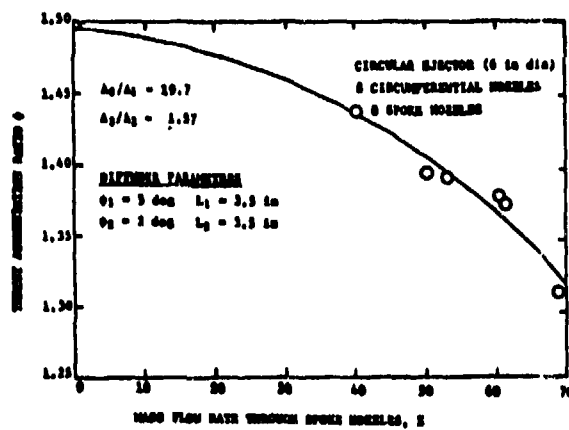


**Fig. 15** Combined Performance of Spoke and Circumferential Nozzles

754

33

# FLOW STRUCTURES ASSOCIATED WITH UPPER SURFACE BLOWN AIRFOILS

N.D. Malmuth*, W.D. Murphy**, and V. Shankar**
Rockwell International Science Center
Thousand Oaks, California 91360
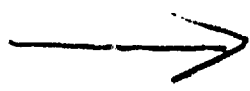
J.D. Cole[†]
University of California at Los Angeles
Los Angeles, California 90024

E. Cumberbatch[††]
Purdue University
West Lafayette, Indiana 47906

## ABSTRACT

Asymptotic and computational methods have been utilized to study the incompressible and transonic flow over upper surface blown airfoils. To provide a framework for other approximate simulations which are subsequently discussed, a full potential formulation is indicated. In this and other models, the problem has been decomposed into the treatment of the fine structure of the jet and the analysis of the flow outside it. Asymptotic expansions of limit process type have been used to treat the jet in a thin layer approximation using suitable strained variables. Although vorticity must be accounted for in matching with the external flow, its effect on the Spence

*Manager, Fluid Dynamics
**Mathematical Sciences Group
†Professor, Structures and Mechanics Department
††Professor, Department of Mathematics

boundary conditions derived under irrotational assumptions is nil in regions away from the trailing edge and jet exit. Computational results for a USB airfoil indicate significant enhancements in lift with blowing. Comparisons with experiments indicate that viscous wall jet effects, wave interaction phenomena with the mixing zones near the jet exit and trailing edge layers must be incorporated into the model for improved simulation of the flow physics. A viscous module treating the interaction of the jet with the airfoil boundary layers is used to quantify shock induced separation delay for various blowing rates.

## 1.0 INTRODUCTION

Upper surface blowing (USB) has been proposed as a means of increasing usable lift and thereby enhancing V/STOL capability at low speeds in landing configurations. At transonic Mach numbers, it has the further application of achieving low turn radii in dogfight scenarios. The attendant high accelerations are accomplished through elimination of separation by suppression of adverse pressure gradients in the viscous boundary layer, and also movement of shocks downstream of the trailing edge, thereby discouraging shock induced separation and buffet at high manuever incidences. Further applications of laminar flow control through stabilization using tangential blowing to achieve favorable pressure gradients is of strong interest currently. In the application of this concept, the engine bleedoff, thrust, and structural penalties required to achieve the foregoing aerodynamic advantages is of importance to the designer. To obtain this relationship, a knowledge of the associated flow fields is required. Although attention has been given to the jet flap in theoretical investigations, relatively little analysis has been performed on upper surface blown configurations. For incompressible speeds, the work of Spence[1] represents the classical thin airfoil treatment of the jet flap problem. At transonic Mach numbers, a computational jet flap solution based on small disturbance theory was developed for airfoils, and generalized for three-dimensional wings by Malmuth and Murphy.[2,3] In these analyses, the classical Karman-Guderley model was applied with a generalized version of the Murman-Cole successive line overrelaxation scheme[4] to treat the free-jet

757

boundaries. The jet was assumed to be thin, and it was assumed on a heuristic basis that the Spence boundary conditions were applicable across it. These conditions involve equilibration between the normal pressure gradient and the centrifugal force associated with the momentum in the jet.

In this paper, the applicability of the conditions will be analyzed for a compressible rotational jet in the context of blowing upstream of the trailing edge on the upper surface, i.e., upper surface blowing in contrast to the jet flap configuration in which the jet emanates from the trailing edge. The aspect of the paper involving fine-structure of the jet layer represents an extension of the earlier work of Malmuth and Murphy[5] on transonic wall jets. From these analyses, the paper will describe the numerical approach to treat the USB problem, and various results showing possibilities for lift augmentation will be presented.

Pressure distributions arising from these solutions will be presented and compared with experimental data. Sources of error will be identified, particularly those associated with wave interaction phenomena at the jet exit. Others involving viscous modifications of the wall jet will be considered. In particular, the impact of the tangential blowing on the boundary layers will be analyzed as the first step of a viscous interaction procedure to be presented elsewhere for such flows. Results from the computational methods will be presented that provide inexpensive quantifications for the first time of shock induced separation delay due to tangential blowing.

758

## 2.0 FORMULATION AND ANALYSES

### 2.1 Full Potential Theory

In Fig. 1, a USB configuration is shown. For purposes of providing a general framework for the subsequent sections which deal with a small disturbance mode, a subsumptive full potential formulation is indicated. Two separate potentials are introduced, $\phi_I$ and $\phi_E$ for the jet and external flow respectively. Appropriate to the solution of the full potential equation indicated, boundary conditions on the airfoil surface and slip lines such as AB are shown. Additional conditions of pressure continuity across the latter jet boundaries also hold. These are discussed in addition to far field and trailing edge aspects in Ref. 6.

### 2.2 Thin Jet Theory

As an essential ingredient of a small disturbance formulation, the jet structure is developed in this section for purposes of specification of the boundary conditions. In particular, it will be shown how the Spence theory of Ref. 1 and the heuristic framework of Ref. 2 which is crudely speaking a small deflection approximation of t' mulation of the preceding section can be derived from a systematic approximation procedure. For this purpose, we relax the irrotational assumptions implicitly embodied in the previous section.

Referring to Fig. 2, a section of the jet of Fig. 1 is detailed. A curvilinear coordinate system is embedded in the jet as indicated. The lines $\eta$ = constant are parallel to a reference line (the $\xi$ axis) which only under special circumstances coincides with the centerline of the jet. Otherwise, the $\xi$ axis is a reference line which is the centerline of an approximate parallel flow to be discussed subsequently. In this coordinate system, the lines $\xi$ = constant are normals to $\xi$ axis. In what follows, the incompressible case will be discussed. The generalizations to compressible flow are straightforward.

To obtain an approximate incompressible set of equations prototypic of the compressible case, the thin jet limit is considered. The character-istic jet thickness is shown in Fig. 2, where the jet boundary is denoted as $\eta = \tau b(\xi) = \tau b_0 + \tau^2 b_1 + \ldots$ .

We now define a thin jet limit

$$\tau \to 0, \quad \xi, n^* = n/\tau \text{ fixed} \tag{1}$$

where the boundary layer coordinate $n^*$ is introduced to keep the jet slip lines in view in the limit process. In (7), the appropriate representation of the velocity components $q_\xi$, $q_\eta$ shown in Fig. 2 and the pressure p to yield a non-trivial structure are

$$\frac{q_\xi(\xi,\eta;\tau)}{U} = \frac{1}{\sqrt{\tau}} u_0(\xi.n^*) + \sqrt{\tau} \, u_1(\xi,n^*) + \ldots \tag{2a}$$

760

$$\frac{q_\eta}{U} = \sqrt{\tau}\, v_0 + \tau^{3/2}\, v_1 + \ldots \tag{2b}$$

$$\frac{p}{\rho U^2} = p_0 + \tau p_1 + \ldots \tag{2c}$$

where U is some typical freestream velocity and all coefficients of the gauge functions involving $\tau$ are $O(1)$ as $\tau \to 0$. These orders are consistent with the massless momentum source model of Spence.[1]

Substitutions of these expansions into the exact equations and boundary conditions gives a hierachy of problems for the various terms in these developments. Details of the solutions for the first and second order quantities are given in Ref. 6. For a constant velocity jet exit, i.e., $q_\xi\,(0,n^\ast) = C$, $q_\eta\,(0,n^\ast) = 0$, leads to the following solution

$$u_0 = u_0(\psi) = C \tag{3a}$$

$$v_0 = 0 \tag{3b}$$

$$p_0(\xi,n^\ast) = (1-\eta^\ast)\frac{C^2}{R} + q_u(\xi) \tag{3c}$$

$$b_0 = 1 \tag{3d}$$

$$\psi = Cn^\ast \tag{3c}$$

where $\psi$ is the zeroth order stream function, and $q_u$ is the pressure on the upper slip line in units of twice the freestream dynamic pressure.

761

## Discussion

Equations (3) describe a parallel flow jet. The total jump in pressure across the jet from (3c) is

$$[p_0] = p(\xi,1) - p(\xi,-1) = 2c^2/R \tag{4}$$

where R is the radius of curvature of the jet centerline. Equations (3) are consistent with the Spence model. It should be noted that in contrast to the latter, no assumption regarding irrotationality is required to obtain (4), in contrast to the results of previous workers. The radius of curvature of the jet is approximately R upstream of the trailing edge which in turn is approximately given by that of the blown upper surface. Downstream of the trailing edge, R is determined from applying (4) to the treatment of the flow outside of the jet. Upstream of the trailing edge, the wall pressure is evaluated by (4) since R is known and is given by

$$p(\xi,-1) = \frac{2c^2}{R} + q_u(\xi) \quad . \tag{5}$$

## External Flow

At distances large compared to the jet width, the fine structure of the jet is important only insofar as it provides matching conditions to the irrotational flow field outside itself. In incompressible flow, this external "outer" flow can be determined by thin airfoil theory. At transonic speeds,

762

small disturbance theory is appropriate for this region. Details of the asymptotic matching procedure have been discussed in Ref. 6. Based on these developments and the earlier ones for arbitrary deflection thin jets in Section 2.2, the boundary conditions for the outer flow in the incompressible and transonic cases for the jet flap and upper surface blowing are now indicated.

### Jet Flap

Representing the equation of the jet as

$$y = \delta g(x)$$

where $\delta$ is the thickness ratio of the airfoil and in a small disturbance approximation considering the "outer" expansion pressure coefficient to be given as

$$\frac{p - p_\infty}{\rho U^2} = \delta P(x,y) + \ldots$$

then by virtue of a generalization of (4) we obtain

$$[P(x,0)] = - C_j g''(x) = - 2[\phi_x] \quad , \qquad (6)$$

where

$$C_j \equiv \rho \int_{-\tau}^{\tau} q_\xi^2 d\eta \left/ \rho U^2 = O(1) \right. \tag{7a}$$

and $\phi$ is a perturbation potential.

Equation (6) is used in conjunction with the jet tangency relation

$$\phi_y(x,0) = g'(x) \tag{7b}$$

and the airfoil boundary conditions to determine the external flow field. These relations coincide with those derived by Spence. They can be generalized for transonic flow by placing the $\rho$ inside the integrand in (7a).

### Upper Surface Blowing

To treat conditions on the blown part of the airfoil, Eq. (6) can be applied by approximating the radius R by $(f")^{-1}$ to obtain the wall pressures, and using the airfoil and jet boundary conditions to determine the upper slip line jet pressures.

From the arbitrary deflection thin jet theory derived in Section 2.2, it can be seen that rotational flow produces the same pressure jumps across the jet in the dominant approximation as the irrotational Spence models. Correspondingly, it can be shown that to within factors involving the density, qualitatively similar results are obtained for transonic flow. Another

764

important aspect of the asymptotic representations derived here is that they lead to higher approximations for the structure of the jet and external flow which can be systematically obtained. Finally, the analytical solutions described above and in Ref. 6 allow the systematic assessment of the effects of initial vorticity and skewness which are inaccessible to other theories.

## 3.0 RESULTS AND DISCUSSION FOR TRANSONIC UPPER SURFACE BLOWING

A successive line overrelaxation (SLOR) scheme within a Karman-
Guderley framework[2] has been used to compute the flow field over an upper
surface blown airfoil. On the blown portion, the jump conditions across the
jet are determined by the asymptotic results given in previous sections,
i.e., Eqs. (6) and (7b). Providing that the region is not too close to the
jet exit or trailing edge, the streamwise gradients can be neglected in the
entropy and velocity component parallel to the wall. Away from these regions,
the pressure gradient perpendicular to the streamlines is balanced by
centrifugal force. For the region near the jet exit, these assumptions become
invalid. Here, the scale of the gradients in the streamwise direction become
important, principally due to the influence of wave interactions with the slip
line. Similar fine structures occur near the trailing edge where the flow can
stagnate on the unblown side, depending on the ratio of the stagnation
pressure of the jet to the ambient stagnation value. For incompressible flow,
Ref. 6 discusses the tri-stable equilibrium at the trailing edge corresponding
to the value of the stagnation pressure ratio, which leads to the dividing
streamline leaving tangent to the upper surface if this is greater than
unity. Consistent with the previous discussion, the appropriate generaliza-
tion to transonic flow was assumed also to be this arrangement for a single
valued pressure without a shock in that location. This assumption has been
altered to assess the sensitivity of the flow to the dividing streamline
angle. In this connection, surface pressures for the dividing streamline

766

bisecting the trailing edge angle (as it would be incompressible flow) were compared with those for the upper surface tangent configuration. Based on these studies, significant differences are anticipated only for large incidences and trailing edge angles.

Typical results obtained from the computational model are shown in Fig. 3 in which the flow over a thick airfoil designed at Rockwell's Columbus Aircraft Division (CAD) was analyzed with the SLOR code. Here, the pressures for various values of the blowing coefficient $C_j$ are compared against those for the unblown case at a freestream Mach number $M_\infty = 0.703$, and angle of attack $\alpha = 0°$. Substantial lift augmentation is evident for blowing. Also evident is the associated rearward motion of the shock with increased blowing and sectional loading as if the incidence is increased.

In Fig. 4 the corresponding increase in lift coefficient $C_L$ with slot downstream movement is also shown as well as the increase in the size of the supersonic region.

Similar increases of lift with blowing coefficient as well as the size of the supersonic region has been illustrated in Ref. 6.

Tests of the adequacy of the foregoing model to simulate realistic transonic USB airfoil flows have been inhibited by the lack of suitable experimental data. Information exists only for highly three-dimensional configurations, large thickness, or incidence in ranges beyond the validity of the assumptions of small disturbance theory. Another restriction is the unavailability of the associated geometric data and flow diagnostics

767

accompanying the tests. The results of Yoshihara[7] and his coworkers were useful in this connection and allowed us to compare the jet flap specialized version of the USB theory in Reg. 2. For the simulations described in this paper, tests performed by N.C. Freeman at NPL on a USB modified 6% thick RAE 102 airfoil and described in Ref. 8, appear to be the most suitable results for comparison at present. Unfortunately, the angle of attack associated with the NPL data is 6$^\circ$ which is marginal for the application of a small disturbance model.

Figure 5 indicates comparisons of chordwise pressures for various values of $C_j$. Also shown are schlierens indicating the associated flow field structure. Turning to the $C_j = 0$ results (Part (a)), massive shock induced separation is indicated and is apparently initiated at the downstream limb of the lambda shock on the upper surface. This is reflected in the classical erosion of the suction plateau and is responsible for the indicated disagreement between the inviscid computational results and the data. For these tests, nominal tangential blowing with a slot height of 0.07% of the chord was used. The slot location is 15% downstream of the nose. The Mach number $M_\infty$ immediately above the slip line at the slot (point A in Fig. 1) is approximately 1.29 for both $C_j$'s indicated. For $C_j = 0.017$, the slot Mach number $M_e$ has been estimated as 1.79 for $C_j = 0.048$, $M_e \approx 2.36$.

Comparison between theory and experiment in Part (b) of Fig. 5 indicates reduced discrepancies on the upper surface associated with the limited separation. In Part (c), the agreement is correspondingly further improved.

To achieve adequate realism, it is important to discuss factors responsible for the disagreements. One feature not captured by the USB simulation is the pressure spike at the slot location. Based on the slot size, the streamwise scale for this phenomenon is at least an order of magnitude greater than the characteristic wavelength of a Mach diamond pattern in the wall jet. These fluctuations may not be resolvable with conventional pressure tap arrangements for the thin slot employed in the tests. If a rough model of a coflowing inviscid supersonic wall jet over a flat plate is used to describe the flow near the slot, the approach to a final steady state may be damped oscillatory or monotone depending on whether the reflection coefficient R which is given by

$$R = \frac{\lambda - 1}{\lambda + 1}$$

where

$$\lambda = M_e^2 \beta / M^2 \beta_e \quad , \quad \beta = \sqrt{M^2 - 1} \quad , \quad \beta_e = \sqrt{M_e^2 - 1}$$

is respectively positive or negative.

The relaxation length L to achieve the downstream pressure in units of the exit height is of the order of $\ln R$ which can be approximately 5 to 50 in the present case depending on the accuracy of the estimate for $M_e$. Note in this connection that

769

$$R < 0 \text{ for } 1 < M < \frac{M_e^2}{\beta_e} \quad , \text{ and } M_e < M < \infty$$

$$R > 0 \text{ for } \frac{M_e^2}{\beta_e} < M < M_e \quad .$$

For the submerged case, $R \to 1$, ($M_e >> M$), and the Prandtl periodic pattern is obtained, with no radiation of energy to the external flow.

These facts suggest that one factor that may be responsible for the observed spike is the internal decay process in the jet. If transonic effects and wall curvature are accounted for, the presence of "ballooning" and throats in the jet may also be contributory. These aspects are further discussed in Ref. 6.

Turning now to the discrepancy of the values shown on the rear surface (downstream of 0.5c) in Fig. 5c, we note that in spite of the obvious elimination of separation, a thick viscous wall jet is present. Downstream diffusion will affect the application of the Spence relation on the blown portion as well as the shock jump. In view of the wall jet thickness shown on the schlierens, this factor appears to be more significant than obliqueness at its foot. A near term refinement is being implemented employing a coupled inviscid-viscous model using second order boundary layer corrections to the Spence boundary conditions accounting for axial gradients of the displacement and momentum thickness. The first phase of this model involves a blown boundary layer module. Preliminary results from this component illustrating the effectiveness of blowing in delaying separation is provided in the next section.

770

# 4.0  VISCOUS EFFECTS

A laminar boundary layer module has been constructed based on a generalization of the box method of Ref. 11 to tangential blowing. Results have been computed by coupling this element to the inviscid framework previously discussed to provide a blown boundary layer algorithm, formulational details of which will be reported elsewhere. Using a NACA 0012 airfoil shown in Fig. 6 with a smoothed small disturbance SLOR chordwise pressure distribution on its upper surface for $M_\infty = 0.7$ and $\alpha = 3°$ as a basis of illustration, typical results are shown in Fig. 7 which indicates the streamwise evolution of velocity profiles upstream of the slot and uncorrected for viscous interaction effects on the external flow field. The normal coordinate $\zeta$ is a Blasius reduced version of the normal curvilinear physical coordinate n. Despite the rather severe adverse pressure gradients, particularly those associated with the nose singularity, and their significant influence on the source term in the momentum equations as the coefficients of the reduced form in the Blasius variables, the box scheme is robust enough to treat such variations. For the case at hand, the loss in fullness in the profile resulting from the adverse pressure gradient is evident. Associated decreasing wall shear stress is also apparent.

Regarding the influence of slot blowing, Fig. 8 shows evolution for the same airfoil of the profiles downstream of a slot located at $x^* = 0.2$ in which $(x^*, y^*)$ refer hereinafter to Cartesian coordinates erected at the mean camber line in the usual way. For the examples selected, an initial parabolic

slot profile was utilized in which the velocity function at the slot station $x^* = x_s^*$ is given by

$$\frac{u}{u_e} = f'(x_s^*,\zeta^*) = - A(\zeta^*-\zeta_d)\zeta^* \quad , \quad 0 < \zeta^* < \zeta_d \tag{8a}$$

$$A = \frac{4\left(\dfrac{u}{u_e}\right)_{max}}{\zeta_d^2} \quad , \quad \zeta^* = \zeta + \zeta_d$$

and for the range of $\zeta^*$ above the slot lip,

$$f'(x_s^*+,\zeta^*) = f'(x_s^*-,\zeta^*) \quad , \quad \zeta_d < \zeta^* < \infty \tag{8b}$$

where the solution which had been marched from upstream to the slot location is assumed to have a continuous velocity component at the slot (excluding the pathological case of shocks at the slot location.

From (8a),

$$f = - \frac{A\zeta^{*3}}{3} + A\zeta_d \frac{\zeta^{*2}}{2} \quad 0 < \zeta^* < \zeta_d \tag{9a}$$

$$f(\zeta_d) = \frac{A\zeta_d^3}{6} \quad . \tag{9b}$$

For more general slot profiles in which

772

$$f'(x_s^*, \zeta^*) = F'(\zeta^*) \quad , \quad 0 < \zeta^* < \zeta_d \quad ,$$

the blowing coefficient $= C_\mu = \dfrac{J\delta^{1/3}M_\infty^{3/4}}{\rho_\infty U^2 c}$ , where $J$ = momentum flux/unit

span, $c$ = chord is given by

$$C_\mu = \frac{M^{3/4}\delta^{1/3}\sqrt{x_s^*}}{\sqrt{Re_\infty}} \int_0^{\zeta_d} F'^2(\zeta^*)d\zeta^* \quad , \tag{10}$$

where $Re_\infty$ is the freestream Reynolds number based on the chord, and $x_s^*$ is the streamwise position of the slot in units of the chord. Actually, (10) is an approximation to within terms of $O(\varepsilon^{2/3})$. In (10), the quantity $\zeta_d$ is given by:

$$\zeta_d = \left(\frac{d}{c}\right)\sqrt{\frac{\bar{\rho}}{\rho_e}\frac{Re_\infty}{x_s^*}} \tag{11}$$

where $d$ is the dimensional slot height and $\bar{\rho}$ is the mean density across the slot.

For the example indicated in Fig. 8, the slot was located at 20% chord, very close to the onset of separation, which occurred at 27.6% chord

for this case. It should also be noted that the location of the shock which had been slightly smoothed for purposes of initial checkout of the algorithm (which can handle non-smooth cases) is at about 23% chord. The characteristic diffusion of the profile associated with mixing of the jet is evident in the figure. More significant and not clearly indicated (but shown later), is the fact that the separation point has now been moved downstream to 79% chord. Other calculations show that with modest further increases in $\zeta_d$, separation can be completely eliminated. (Note in this context that the peak velocity for (8a) is $A\zeta_d^2/4$.)

In Ref. 6 the corresponding profile development for an "underblown" case where the peak is less than the freestream value is discussed. Relaxation to a conventional profile occurs as previously. However, this blowing configuration actually results in premature separation as compared to the case of no blowing. This is indicated in Fig. 9 where the effect of blowing on the separation point location is shown. Despite the initially higher shear stress at the slot in the underblown case $\zeta_d = 1$, $A = 2$, the higher vorticity diffusion and lower overall momentum in the layer leads to earlier separation which can be seen as the leftmost solid circle in Fig. 9. This level should be related to the unblown result shown in dashed lines in the same plot. Moreover, the case $\zeta_d = 2.65$, $A = 1$, moves the separation point substantially downstream to almost 80% chord. Other cases are shown in Fig. 9, such as the one corresponding to the slot position at approximately 11% chord. This demonstrates the dramatic role of the slot location and upstream boundary layer thickness in delaying separation; where for the same slot height, the

upstream slot location gives an almost trivial downstream movement of the separation location, in contrast to the potent effect of the downstream slot position.

The results of Fig. 9 can be replotted as in Fig. 10 to show the trends as a function of a momentum flux parameter which is proportional to $C_\mu$. By Eq. (10), $C_\mu \sim A^2 \zeta_d^5$ for a parabolic profile. For the limited number of cases run, there is a suggestion in Fig. 10 that the curves of Fig. 9 collapse to a single universal band of results. In view of the roles of the pressure gradient, and the multiple extrema in the velocity profile, this assertion must be regarded as tentative at best. <u>What is significant however, is that for the first time, the delay effect of tangential blowing on natural and shock induced separation over transonic airfoils has been inexpensively quantified</u>.

## 5.0 CONCLUSIONS

Asymptotic and computational models have been used to obtain the flow over upper surface blown (USB) airfoils at incompressible and transonic speeds. The treatment involves a detailed analysis of the flow in the jet. The analytical and computational results indicate that

- In the thin jet small deflection approximation, the pressure jumps associated with the Spence theory prevail even if the flow is rotational and compressible.

- The asymptotic developments provided allow further systematic refinements.

- Effects associated with initial skewness and vorticity inaccessible to other theories can be assessed.

- Computational results obtained for transonic USB configurations indicate significant enhancement of lifting pressures associated with blowing.

- Comparisons with experiment indicate the need for refinements incorporating wave interaction phenomena near the jet exit as

well as viscous interaction processes in the downstream portion of the wall jet.

- Substantial downstream movements in the shock-induced separation point are achievable with application of tangential blowing. By computational schemes, these delays can be inexpensively quantified as compared to experimental methods.

With the viscous module and the appropriate iterative coupling algorithm to the external flow to be implemented in the near future, optimization between separation suppression, wave drag minimization, and supercirculation control will be possible. It is envisioned that the design techniques contained in Refs. 12-14 will augment this capability by providing methods to modulate shock formation in concert with the blowing effects.

### Acknowledgement

777

REFERENCES

1.  Spence, D.A., "The Lift Coefficient of a Thin Jet Flapped Wing," Proc. Roy. Soc., Ser. A, 238, December 1956, pp. 46-48.

2.  Malmuth, N.D. and Murphy, W.D. "A Relaxation Solution for Transonic Flow Over Jet Flapped Airfoils," AIAA J. 14, September, 1976, pp. 1250-1257.

3.  Murphy, W.D. and Malmuth, N.D., "A Relaxation Solution for Transonic Flow over Three-Dimensional Jet-Flapped Wings," AIAA J., 15, January 1977, pp. 46-53.

4.  Murman, E.M. and Cole, J.D., "Calculation of Plane Steady Transonic Flows," AIAA J., 9, January 1971, pp. 114-121.

5.  Malmuth, N.D. and Murphy, W.D., "An Inviscid Model for Submerged Transonic Wall Jets," AIAA Paper 77-174 (1977).

6.  Malmuth, N.D., Murphy, W., Shankar, V., Cole, J. and Cumberbatch, E., "Studies of Upper Surface Blown Airfoils in Incompressible Flow," AIAA Paper 80-0270, presented at the AIAA Aerospece Sciences Meeting, January 14-16, 1980, Pasadena, California.

7.  Yoshihara, H., Carter, W.V., Fatta, J.G. and Magnus, R.G., "Aeronautical Exploratory Research on Jet Flapped Airfoils," Convair Report L-112173, February 1972.

8.  Pearcy, H.H., "Shock Induced Separation and Its Prevention by Design and Boundary Layer Control," Boundary Layer and Flow Control, Lachmann, G.V., ed., Pergamon, Oxford, London 1961, pp. 1166-1344.

9.  Malmuth, N.D. and Murphy, W.D., Quarterly Letter Progress Report No. 14 on ONR Contract N00014-76-C-0350, SC5055.14QR, Auguest 20, 1979.

10. Malmuth, N. and Murphy, W.D., Quarterly Letter Progress Report No. 13 on ONR Contract N00014-76-C-0350, SC5055.13QR, May 14, 1979.

11. Keller, H.B. and Cebeci, T., "Accurate Numerical Methods for Boundary Layers, II, Two-Dimensional Turbulent Flows," AIAA J., 10, September 1972, pp. 1197-1200.

12. Shankar, V., Malmuth. N.D. and Cole, J.D., "Computational Transonic Airfoil Design in Free Air and A Wind Tunnel," AIAA Paper 78-103, AIAA 16th Aerospace Sciences Meeting.

13. Shankar, V., Malmuth, N.D. and Cole, J.D., "A Consistent Design Procedure for Supercritical Airfoils in Free Air and A Wind Tunnel," invited paper

presented at NASA-Langley Conference on Advanced Technology Research, also in Proceedings, March 1978.

14. Shankar, V., Malmuth, N.D. and Cole, J.D., "A Computational Inverse Procedure for Three-Dimensional Wings and Wing-Body Combinations," AIAA Paper 79-0344, presented at the 17th Aerospace Sciences Meeting, New Orleans, Louisiana, January 15-17, 1979.

FIGURE CAPTIONS

Fig. 1    Transonic upper surface blowing - full potential equation
          formulation.

Fig. 2    Section of jet and curvilinear coordination system.

Fig. 3    Effect of blowing coefficient, $(C_j)$, variations on chordwise
          pressures for CAD USB supercritical airfoil, $M_\infty = 0.703$, $\alpha = 0^\circ$,
          (slot location at 65% chord).

Fig. 4    Behavior of $C_L$ and criticality as a function of extent of blowing,
          CAD USB airfoil, $C_j = 0.1$, $M_\infty = 0.703$, $\alpha = 0^\circ$.

Fig. 5    Comparison of USB theory of this paper with NPL tests of Freeman
          (Ref. 8), $M_\infty = 0.75$, $\alpha = 6^\circ$, c = chord, t = maximum thickness.

Fig. 6    Upper surface pressure distribution on NACA 0012 airfoil $M_\infty = 0.7$, $\alpha$
          $= 3^\circ$.

Fig. 7    Unblown streamwise profile development for case of Fig. 6.

Fig. 8    Blown profiles, A = 1, $\zeta_d = 2.65$.

Fig. 9    Position of separation point, $x_s^*$, with blowing - NACA 0012, $M_\infty = 0.7$,
          $\alpha = 3^\circ$.

Fig. 10   Reduced plot of separation location $x_s^*$ as a function of momentum flux
          parameter $A^2\zeta_d^5$.

$$L[\phi] = (a^2 - \phi_x^2) \, \phi_{xx} - 2 \, \phi_x \phi_y \phi_{xy} + (a^2 - \phi_y^2) \, \phi_{yy} = 0$$

JET
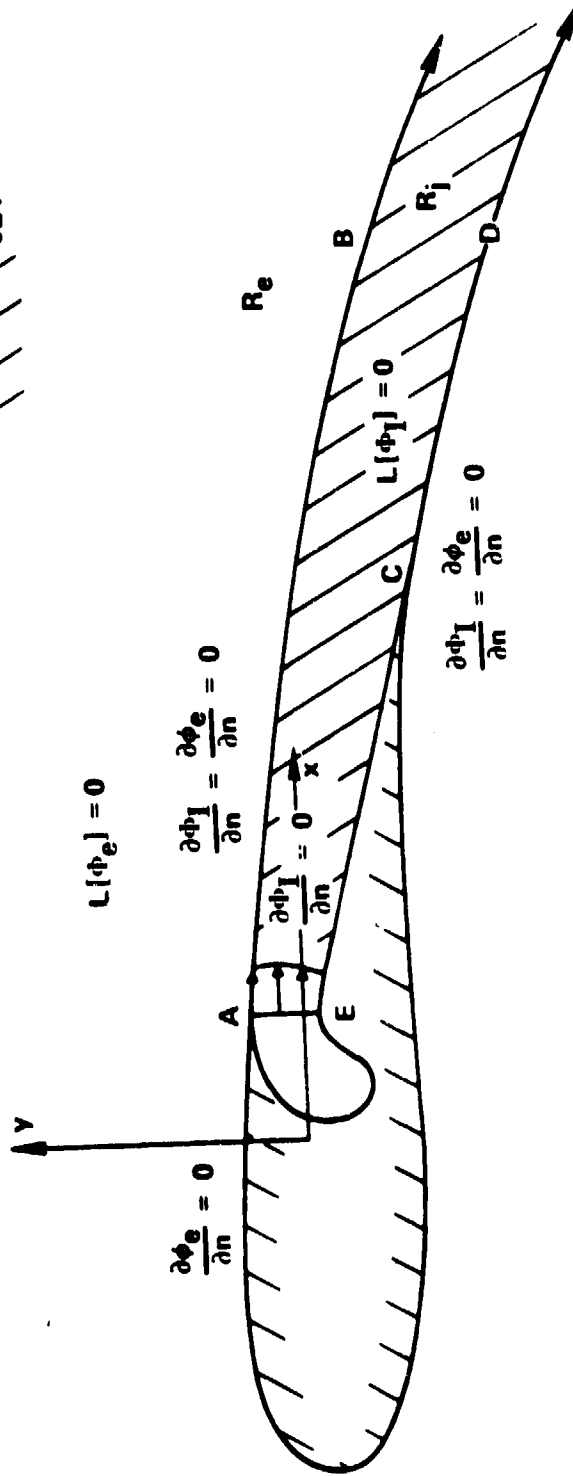
$R_e$

B

$R_j$

$L[\phi_e] = 0$

$L[\phi_j] = 0$

D

$\dfrac{\partial \phi_I}{\partial n} = \dfrac{\partial \phi_e}{\partial n} = 0$

$\dfrac{\partial \phi_I}{\partial n} = \dfrac{\partial \phi_e}{\partial n} = 0$

C

A

$\dfrac{\partial \phi_I}{\partial n} = 0$

x

E

$L[\phi_e] = 0$

y

$\dfrac{\partial \phi_e}{\partial n} = 0$

Fig. 1. Transonic Upper Surface Blowing — Full Potential Equation Formulation
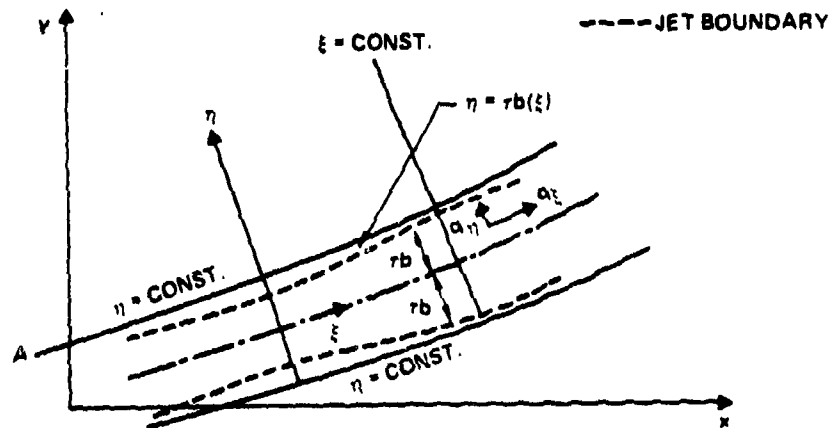
Fig. 2. Section of Jet and Curvilinear
Coordinate System



Fig. 3. Effect of Blowing Coefficient, ($C_j$), Var-
iations on Chordwise Pressures for CAD
USB Supercritical Airfoil, $M_\infty = 0.703$,
$\alpha = 0°$, (Slot Location at 65% Chord)

782
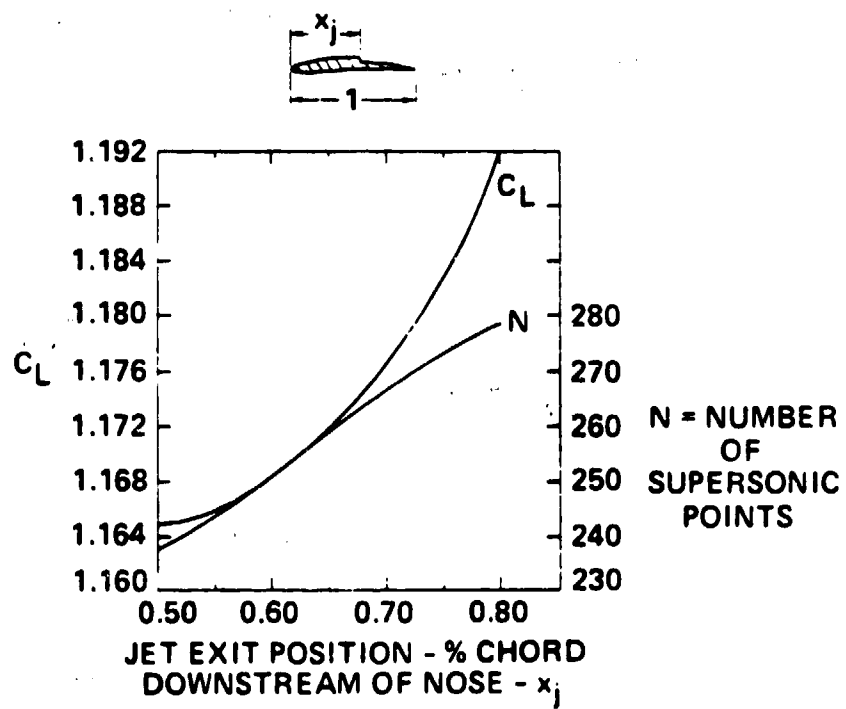
Fig. 4. Behavior of $C_L$ and Criticality as a Function of Extent of Blowing, CAD USB Airfoil, $C_j=0.1$, $M_\infty=0.703$, $\alpha=0°$

Fig. 5.  Comparison of USB Theory of This Paper
with NPL Tests of Freeman (Ref. 8),
$M_\infty = 0.75$, $\alpha = 6°$, c = Chord,
t = Maximum Thickness

Fig. 6. Upper Surface Pressure Distribution on Upper Surface of NACA 0012 Airfoil, $M_\infty = 0.7$, $\alpha = 3°$



Fig. 7. Unblown Streamwise Profile Development for Case of Fig. 6.

Fig. 8    Blown Profiles, $A = 1$, $\zeta_d = 2.65$



Fig. 9.    Position of Separation Point, $x_s^*$, with
Blowing — NACA 0012, $M_\infty = 0.7$, $\alpha = 3°$

786
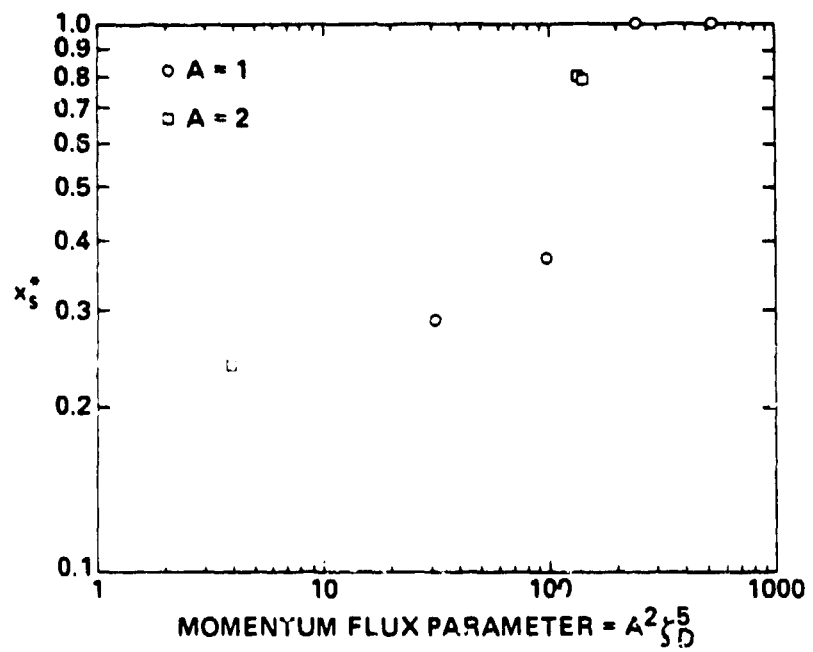
Fig. 10. Reduced Plot of Separation Location $x_s^*$ as a Function of Momentum Flux Parameter $A^2 \zeta_d^5$

# PROGRESS TOWARDS A THEORY OF JET FLAP THRUST RECOVERY

by

P. M. Bevilaqua, E. F. Schum, and C. J. Woan

Rockwell International, North American Aircraft Division

## ABSTRACT

A combination of analysis and testing has been utilized to develop a
theory of jet flap thrust recovery at the low speeds and large
deflection angles characteristic of ejector wing lift systems.  The
contribution of jet drag to the reduction in recovery has been
computed with a viscid/inviscid interaction analysis. Computational
results are  compared to wake survey and airfoil surface pressure
measurements made with a two-dimensional jet flapped airfoil model.
The thrust recovery is nearly complete for small values of the jet
deflection angle, but for larger angles, the recovery decreases as
the thrust coefficient increases.  It is concluded that the loss of
recovery is due to the jet drag for values of the thrust coefficient
less than unity; for larger values, the loss is increased by flow
separation from the airfoil.

## INTRODUCTION

Incorporating the ejector into the trailing edge of a wing, as shown in Figure 1, produces an especially effective lift/propulsion system. An ejector wing aircraft converts smoothly from hover to wing-borne flight, since the loss of reaction lift as the jets are deflected for conversion is balanced by an increase of wing lift induced by the jet flap effect (Davidson, 1956). The lift of the jet flap is greater than the vertical component of the jet thrust because interaction of the jet with the free stream changes the wing surface pressure distribution. Similarly, the jet flap induces a net thrust on the wing greater than the horizontal component of jet thrust.

Various analytical methods have been developed to predict the lift increment induced by the jet flap. These are based on Spence's (1956) now classical jet flap theory in which the inertia of the jet sheet is related to the strength of an equivalent vortex sheet. On the other hand, there are no methods for predicting the thrust recovery. Stratford (1956) pointed out that in ideal fluids, the total jet thrust would be recovered as a horizontal force, but that in real fluids, the recovery is reduced by the drag due to jet entrainment. Williams, et. al. (1961) noted that leading edge separation would also cause a loss of thrust, while Tsongas (1962) argued that the recovery is reduced by separation from the jet flap itself. Since the mechanism of thrust recovery is not well understood, empirical data is used to specify the thrust loss, although complete recovery is assumed for calculating lift (McCormick, 1967).
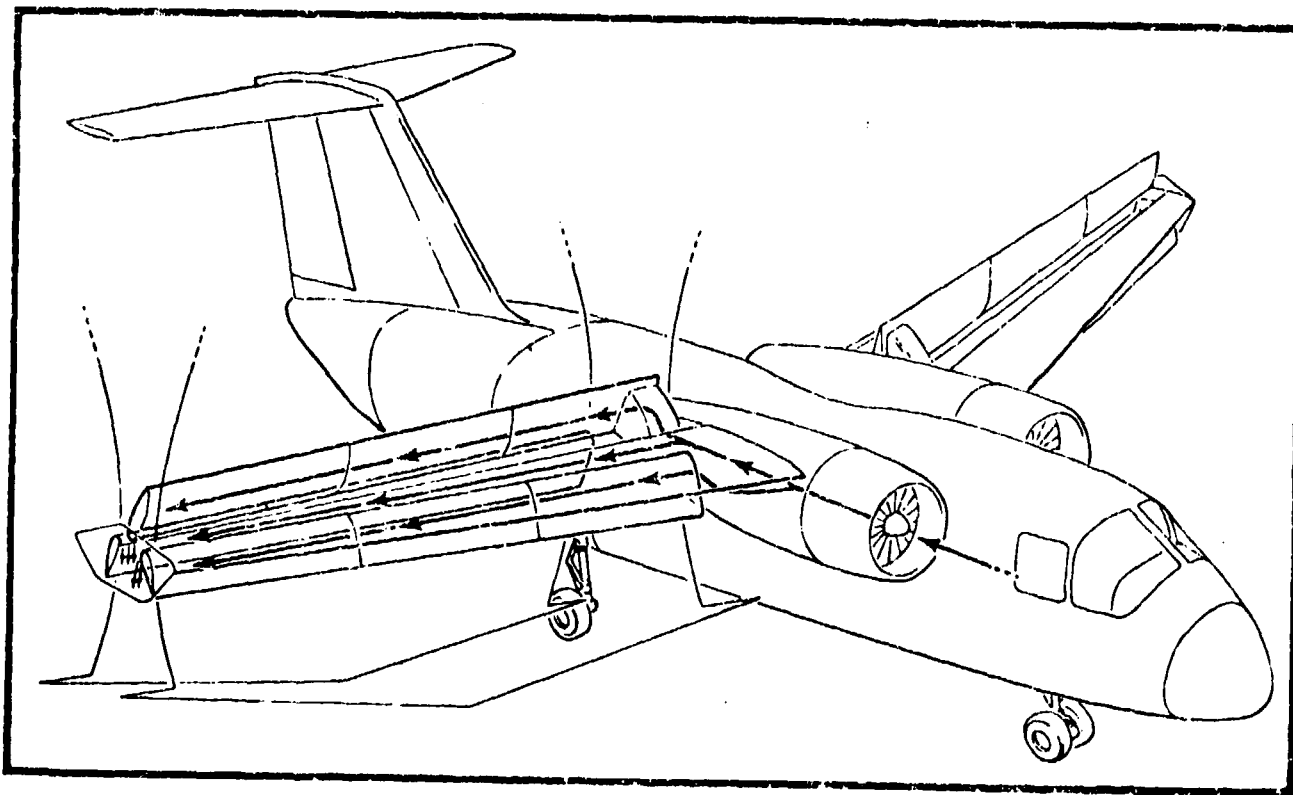


Figure 1. Ejector Wing V/STOL Aircraft

The purpose of this paper is to summarize progress in developing a quantitative theory for predicting thrust recovery. A combination of analysis and testing has been used to distinguish between the effects of jet drag and flow separation. It is concluded that the jet drag covers a significant loss of recovery, but that bursting of the leading edge separation bubble covers an additional loss of recovery at large values of the jet thrust coefficient and deflection angle. A more complete description of these results is given by Bevilaqua, et. al. (1980).

JET DRAG ANALYSIS

The thrust recovery is generated by equal but opposite pressure forces induced on the airfoil and jet sheet. According to Spence's (1956) theory, the inertial forces which resist deflection of the jet sheet are balanced by a pressure difference in the external flow along the upper and lower boundaries of the jet. This pressure difference can be related to the strength of an equivalent vortex sheet located along the jet axis. Then, in mathematical terms, the vorticity in the jet sheet induces an upwash on the vorticity bound in the airfoil; the airfoil therefore experiences a thrust. Similarly, the airfoil vorticity induces a downwash on the jet, which experiences a reaction force that increases the jet thrust. Simultaneously, the interaction of the main stream with the jet transfers the vertical component of the jet thrust to the main stream. The forces on the airfoil, jet, and a surrounding control volume are shown in Figure 2. In an ideal fluid, the net thrust on the airfoil is equal to the total
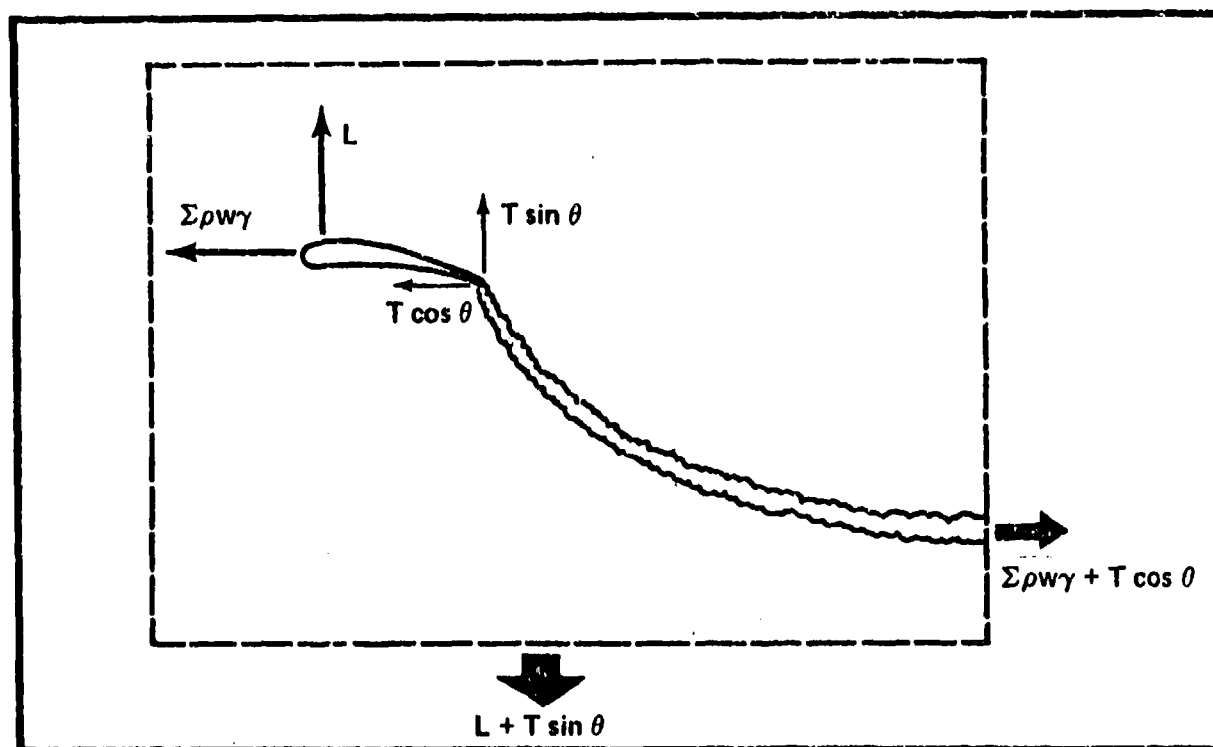


Figure 2. Forces on the Airfoil and Jet

791

jet thrust, because the jet is ultimately turned in the direction of the free stream.

Real fluid effects reduce the thrust recovery through two separate mechanisms: jet entrainment induces a form drag on the airfoil, and boundary layer separation covers a loss of suction which reduces the thrust on the airfoil. The entrainment drag and corresponding loss of jet thrust can be represented by the mutually induced forces on the vortex sheet bound in the wing and sink distribution which represents the entrainment of the jet. In order to compute the contribution of the jet drag to the reduction in thrust recovery, the equal but opposite forces on the airfoil and jet have been computed by matching a potential flow solution for the path of the jet to a viscous flow solution for the entrainment and thrust of the jet.

In order to determine the jet path, the mathematical problem is to find a velocity potential which is harmonic, and satisfies the boundary conditions of uniform flow at infinity and flow tangent to the surface of the airfoil and centerline of the jet. The balance between the inertia force due to jet curvature and the pressure difference across the jet becomes an additional, dynamic boundary condition. In the present analysis, the jet thrust is not assumed to be constant, but has a distribution prescribed from the viscous analysis.

Vortex panel methods are used to solve the mathematical problem. The airfoil and jet are presented by linear vorticity distributions as shown in Figure 3. Since the position of the jet is initially unknown, the
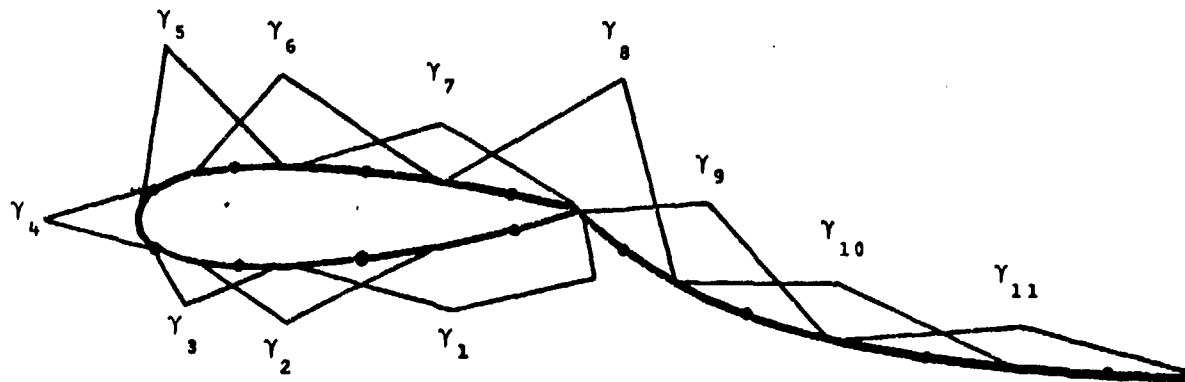


Figure 3. Linear Vorticity Distributions on the Airfoil and Jet

solution is obtained by iterating between the dynamic and kinematic boundary conditions. For each iteration, the problem reduces to solving a set of linear equations with unknown vortex strengths. A Gaussian elimination procedure is used.

For the viscous solution, a finite difference analysis was developed. The basic scheme is that derived by Patankar and Spalding (1970) for thin shear layers: the full Navier Stokes equations are reduced to a simpler set by the assumption that there is a primary direction of flow (along the jet) and that diffusion is negligible in that direction. Launder and Spalding's (1972) two-equation turbulent kinetic energy model, modified for the effects of curvature by Schum, et. al. (1980) was used to compute the mixing.

Because the influence of the jet flap is determined by the jet momentum, the streamwise variation of the excess momentum

$$T_{XS} = \rho \int_{-\infty}^{\infty} (U_T^2 - U_S^2) \, dy$$

is used in the inviscid solution. Here, $U_T$ is the total velocity and $U_S$ is the secondary velocity. This integral vanishes outside the jet, where $U = U_S$. Similarly, the sink strengths are determined from the variation of the excess mass, because only the change in the excess mass has an effect on the flow outside the jet. It is important to note that these sinks do not represent the quantity of mass entrained by the jet, but only the effect of the entrainment on the external flow.

The viscid and inviscid analyses are matched by iterating until the computed reduction of jet thrust and the jet drag induced on the airfoil are the same. Generally, three to four iterations are required for convergence.

EXPERIMENTAL PROGRAM

In order to minimize the induced drag, the jet flap airfoil model was tested in a high aspect ratio, two dimensional wind tunnel designed especially for powered lift testing. This tunnel is an open circuit type, powered by a multi nozzle ejector downstream of the test section. The test section is nominally 50 cm wide, 365 cm high, and 370 cm long. Smooth flow into the tunnel is achieved with an elliptical bellmouth section. The sidewalls diverge at approximately 0.2° on each side to allow for boundary layer growth in the test section. The maximum velocity of the main stream is approximately 30 meters/sec. A sketch of the tunnel is shown in Figure 4.

The model is mounted 150 cm from the inlet section and 210 cm above the tunnel floor. It is mounted in aluminum plates installed flush with the tunnel sidewalls. A pair of plexiglass windows are installed in each plate to permit flow visualization. A set of boundary layer control nozzles are also provided, one located just upstream of the model, and the other over the model at the midchord. The speed of the main flow is measured with calibrated static pressure taps in the tunnel walls just downstream of the bellmouth.
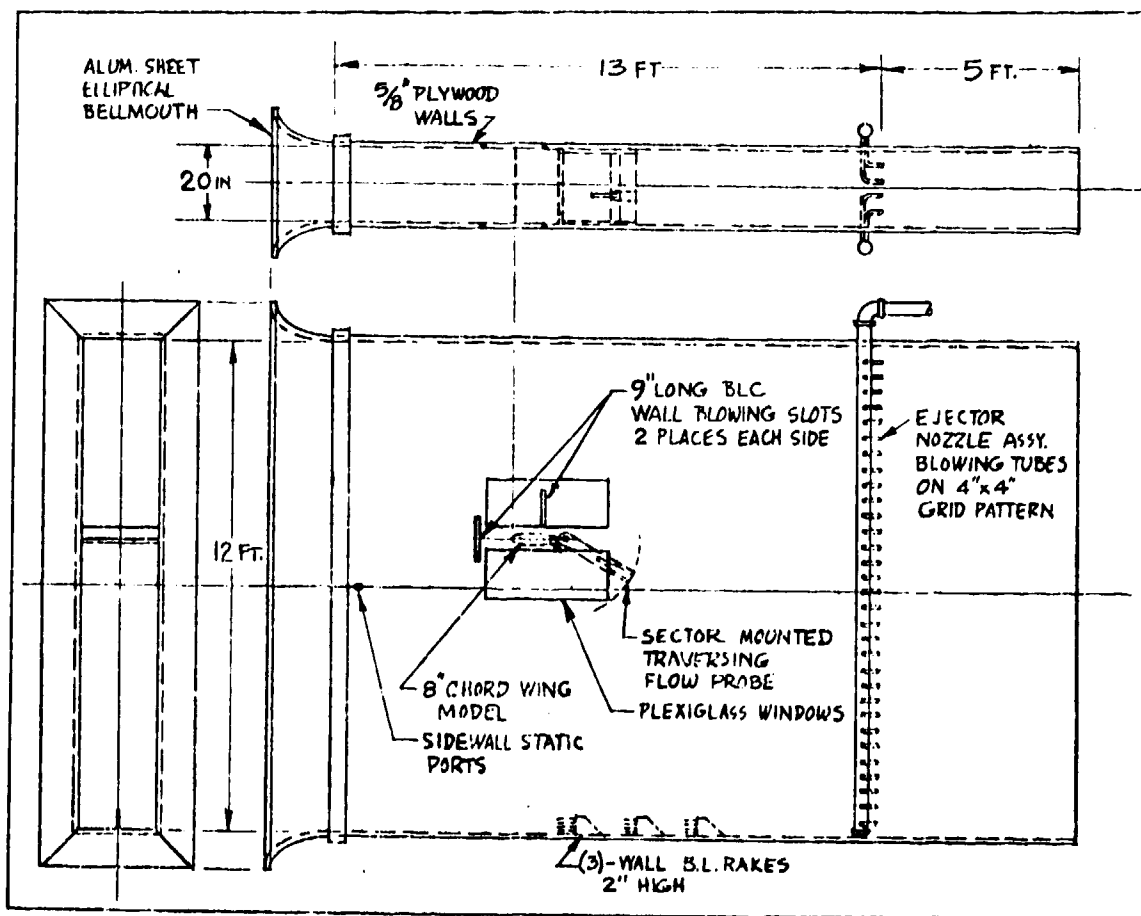
Figure 4.   Ejector Powered Wind Tunnel

The jet flap airfoil model has a 20% thick uncambered elliptical section, modified near the trailing edge to include a short 10% chord flap.  The thick elliptical section has an equivalent leading edge radius of approximately 5.5% which was designed to alleviate leading edge separation.  The jet nozzle is located on the upper surface and blows parallel to the model chord.  The jet is turned to the proper deflection by the Coanda effect on the short flap.  Seventy-four pressure taps are located at the midspan of the model.  An additional eight taps are located in two spanwise rows on the upper surface to monitor two-dimensionality.  The model is constructed of aluminum with steel end fittings, which also serve as the air supply inlets.

The practical difficulties in measuring two-dimensional force data on a blown model were avoided by integrating the midspan surface pressure distribution to obtain lift, and integrating the jet wake to determine thrust.  A five-port pressure probe was used for the wake survey, in order to determine the magnitude and direction of the jet thrust vector.  The method of Betz (Schlichting, 1960) modified to include flow angularity, was used to integrate the wake survey data.

794

## RESULTS AND DISCUSSION

The effect of the initial deflection angle on the measured jet trajectory for a thrust coefficient of unity ($C_\mu = 1$) is shown in Figure 5. As expected, the penetration of the jet increases with the deflection angle. The variation in the measured trajectory with thrust coefficient for a constant deflection ($\theta = 30°$) is shown in Figure 6. The jet tends to straighten out as the thrust is increased.
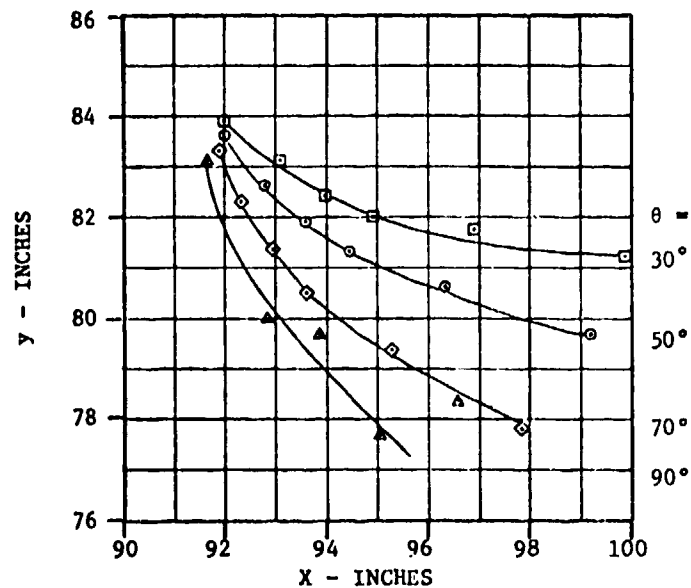


Figure 5. Variation of Jet Shape with Deflection Angle, $C_\mu = 1.0$
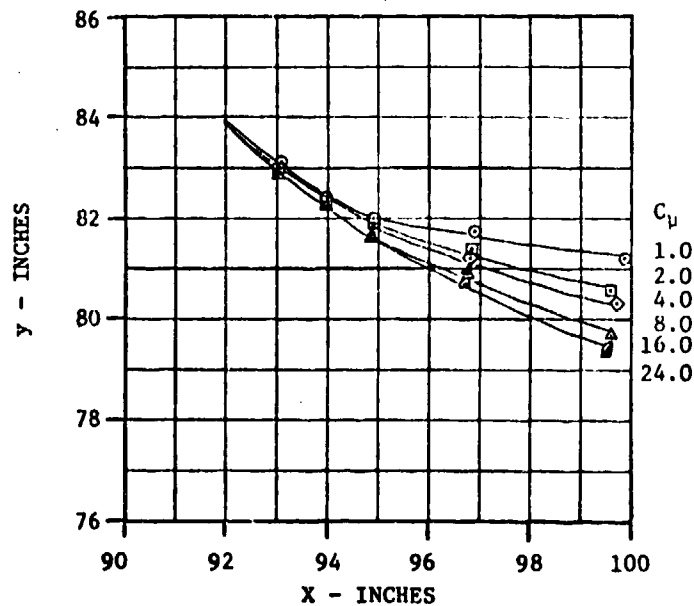


Figure 6. Variation of Jet Shape with Deflection Angle, $\phi = 30°$

795

The measured variation of the thrust recovery with the jet blowing coefficient and deflection angle is shown in Figure 7. There is a discontinuous change in the recovery for values of $C_\mu \sim 2$. Comparison of the measured and computed airfoil surface pressure distributions, at the change point shown in Figures 8 and 9 reveals that this change is due to the "bursting" of the leading edge separation bubble.

The bursting of this bubble depends on the Reynolds number and Mach number of the flow, and the leading edge radius of the airfoil, so that these curves cannot be generally applied. However, it can be concluded that the loss in recovery due to jet drag is discontinuously increased when the leading edge bubble does burst.
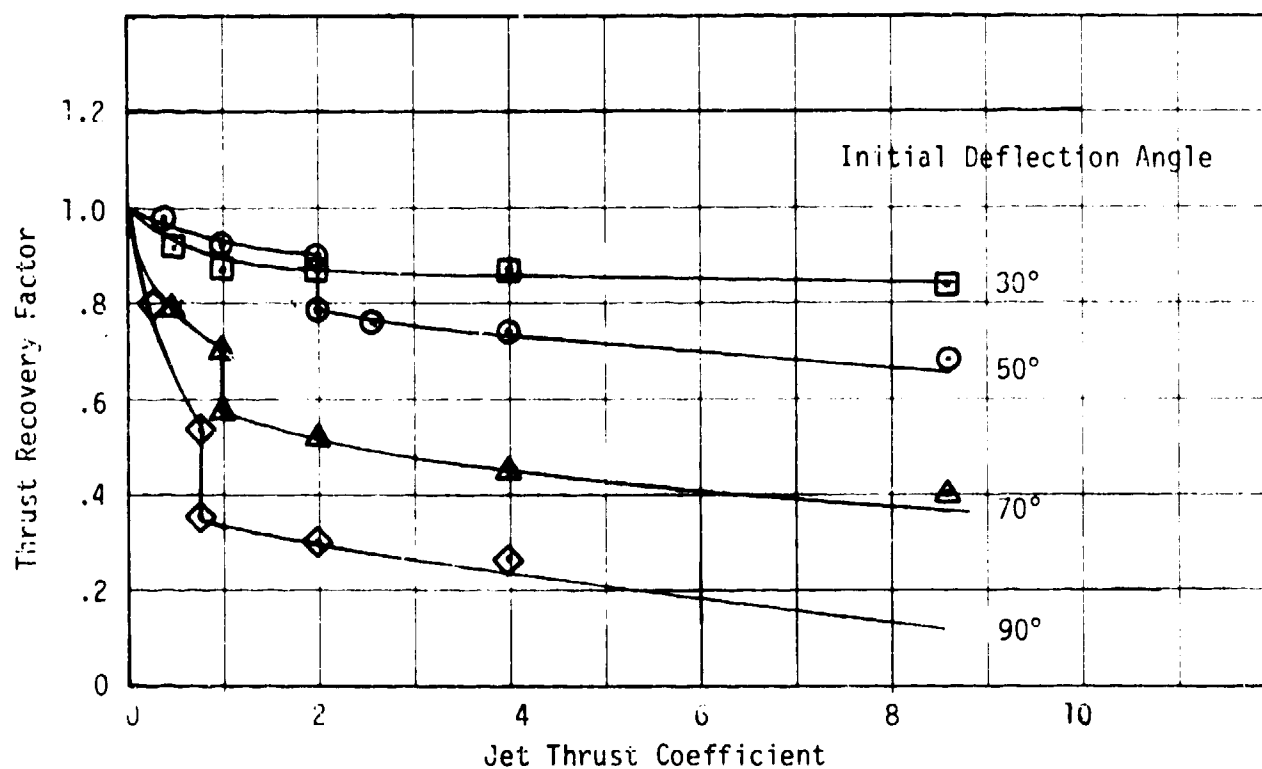


Figure 7. Variation of the Thrust Recovery Factor
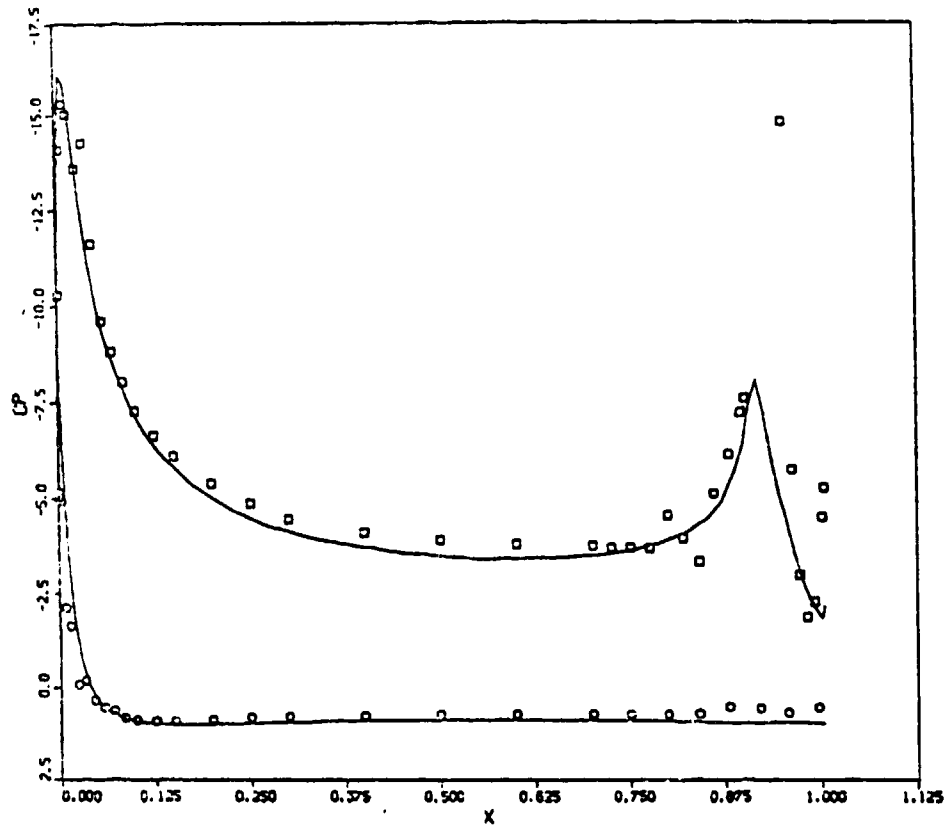
Figure 8.  Comparison of Measured and Ideal Airfoil Pressure Distributions, $C_\mu = 2$, $\theta \doteq 50°$ Unseparated Flow
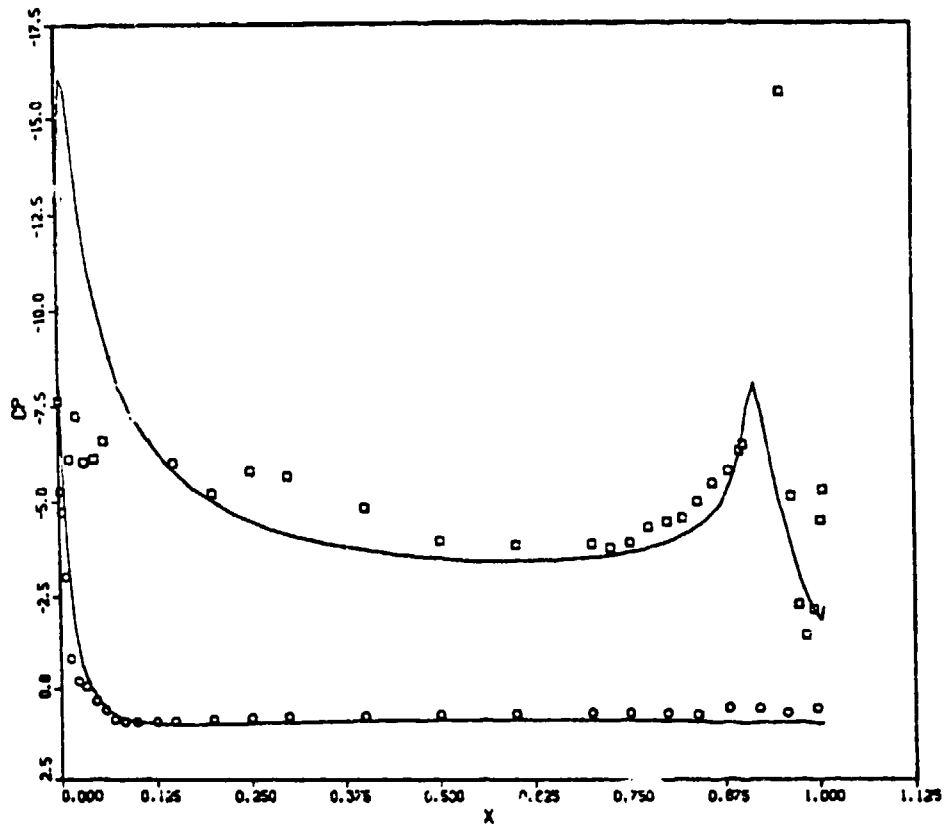


Figure 9.  Comparisons of Measured and Ideal Airfoil Pressure Distributions, $C_\mu = 2$, $\theta = 50°$ Separated Flow

797

CONCLUSIONS

The thrust recovery is a function of both the thrust coefficient and jet deflection angle. In general, the recovery is nearly complete for small values of the thrust coefficient ($C_\mu < 1$), but decreases to the horizontal component of the jet reaction force at large values of thrust ($C_\mu \approx 15$). The effect of jet mixing is to reduce the thrust recovery about 10% at small values of the thrust coefficient and deflection angle. As these parameters are increased, flow separation causes a further loss in recovery. For a fixed deflection angle, there is a discontinuous change in the recovery factor at $C_\mu \sim 2$, as the character of the separation changes from a "short" bubble which re-attaches to the airfoil near the leading edge, to a "long" bubble which re-attaches near the trailing edge. The flow is bistable in the transition region. At higher values of $C_\mu$, the bubble does not re-attach to the airfoil at all, but is entrained into the wake.

REFERENCES

Bevilaqua, P. M.; Woan, C. J.; and Schum, E. F.; "Viscid/Inviscid Inter- action Analysis of Ejector Wings," NASA CR 166172, in review, 1981.

Davidson, I. M., "The Jet Flap," Journal of the Royal Aeronautical Society, Jan 1956, pp. 25-50.

McCormick, B. W., "Aerodynamics of V/STOL Flight," Academic Press, New York, 1967.

Launder, B. E. and Spalding, D. B., "Mathematical Models of Turbulence, Academic Press, 1972.

Patankar, S. V. and Spalding, D. B., "Heat and Mass Transfer in Boundary Layers, " International Textbook Co., Ltd., London, 1970.

Schlichting, H., "Boundary Layer Theory," McGraw-Hill Book Co., New York, 1960

Schum, E. F.; Bevilaqua, P. M.; and Patankar, S. V.; "Computation of the Turbulent Mixing in Curved Ejectors, ONR-CR212-249-2F, April 1980.

Spence, D. A., "Lift Coefficient of a Thin, Jet-Flapped Wing," Proceedings of the Royal Society of London, Vol. A238, 1956, pp. 46-68.

Stratford, B. S., "Mixing and the Jet Flap," Aeronautical Quarterly, May 1956.

Tsongas, G. A., "Verification and Explanation of the Controllability of Jet Flap Thrust," SUDAER No. 138, October 1962.

Williams, J.: Butler, S. F.: and Wood, M. N.; "The Aerodynamics of Jet Flaps," ARC R&M 3304, January 1961.
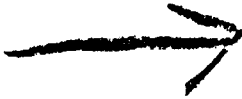
# EJECTOR SHROUD AERODYNAMICS

by

J. H. DeHart and S. J. Smrdel

Rockwell International, North American Aircraft Division

## ABSTRACT

An experimental and analytical study has been conducted to determined the effect of shroud parameters on ejector thrust augmentation. The ejector shroud is analogous to a wing operating in a non-linear stream and potential flow methods were utilized to predict ideal pressure distributions on the shroud. Scale model tests were conducted to determine actual forces and pressure distributions on shroud components. Experimental data were obtained for symmetrically increased flap lengths (L/W) and asymmetric flap lengths. It is shown that flap length increases produce higher thrust augmentation ratios by delaying stall to higher diffuser area ratios.

## INTRODUCTION

An ejector may be described as an air pump which uses a primary jet to entrain secondary air through the shroud. The additional mass and its velocity will produce more thrust than the individual primary jets acting alone.

The ejector wing configuration being developed at Rockwell International/ Columbus for the XFV-12A aircraft is shown in Figure 1. It consist of two blown flaps and a centerbody nozzle. The streamlines of the entrained flow indicate the direction of the secondary flow as it is drawn into the ejector "shroud". The two flaps may be considered as wings "flying" in the entrained velocity field and they will experience induced lift and drag forces similar to a conventional wing airfoil. The augmentation ratio may then be defined as the ratio of the primary jet thrust (T) plus the sum of axial forces on the flaps (F), to the isentropic thrust of the primary mass (ṁv).

$$\phi = \frac{T + F}{\dot{m}v}$$

Augmentation may therefore be increased by providing a shroud with a geometry which maximizes the "lift" for a particular center-body nozzle. The forces generated on the shroud are carried as a pressure loading around the shroud surface, and any separation or downward rotation of the resultant force vector will affect the performance of the augmenter. It is important therefore to understand the shroud as an ejector component. This paper presents some significant aspects of the shroud aerodynamics of the XFV-12A ejector wing.

### EFFECT OF FLAP LENGTH

One variable of ejector geometry which is known to increase augmentation ratio is flap length. The effect of increased flap length on thrust augmentation ratio ($\phi$) is shown on Figure 2 for length/width (L/W) ratios of 1.5, 2.0, and 2.5. It is seen that for diffuser area ratios (DAR) below about 1.6, little difference in $\phi$ or throat velocity is noted. However, increases in $\phi$ are obtained for diffuser area ratios greater than 1.6. Similar results have been previously obtained for a comparable ejector. These results may be shown to be due to several causes (both favorable and adverse) in and around the shroud which vary with diffuser area ratio. The net effect determines whether a gain in $\phi$ will be realized.

Figure 3 compares the aft flap surface pressures for two diffuser area ratios and two shroud lengths (L/W). It is seen that L/W has little effect on the distribution of pressure around the Coanda surfaces. A similar trend was noted on the forward flap. However, flow measurements at the exit of the augmenter indicate an increase in mass flow through the ejector in both cases. This data for a 3.5 inch section of the span is shown in Figure 4.

To understand this anomaly, the surface pressure data is plotted in Figures 5 and 6 to show the distribution of up and down loads. At the higher DAR (2.25), there is no appreciable difference in upload. However, the longer flap has less download, the net result being increased $\phi$. At the lower diffuser area ratio (DAR = 1.5), increased flap length produces a decrease in both the up and down loads.

The independence of $\phi$ with flap length for area ratios less than 1.6 is thought to be due to at least two cancelling effects. First, for a given diffuser area ratio, an increased flap length results in a reduced flap angle, i.e., the flaps are "flying" at a lower angle of attack, which would tend to lower the throat velocities. However, the throat velocity surveys, shown in Figure 7, indicate no effect due to flap length. There-fore, it is likely that increased mixing cancels the effect of angle.

In order for a gain in $\phi$ to be realized (due to increased mixing) at higher area ratios but not at lower area ratios, the mixing process at higher area ratios must be more effective than at lower area ratios. This is verified by comparing the reduction in velocity profile shape factor for the two cases. Figure 8 shows the improvement for a low and high diffuser area ratio case. The improvement obtained with increased L/W was much greater at $A_3/A_2 = 1.97$ versus $A_3/A_2 = 1.18$.

FLAP LENGTH ASYMMETRIES

It should be noted that ejectors currently under study are generally not free to take any size, shape, or geometry, but are constrained by packaging limitations to be able to fold up within the contour of a supersonic wing airfoil of a specific aircraft. Design studies of a possible wing ejector alternative for the XFV-12A resulted in an ejector configuration with unequal flap lengths. A test program was initiated to determine the effects of asymmetric flap lengths on augmenter performance.

The results of a test in which the aft flap was 25% longer than the forward flap is shown in Figure 9. Because of the unequal flap lengths, the diffuser area ratio was defined in two ways as indicated on Figure 9, and the data presented accordingly. It can be seen that the increase in aft flap length did not change the peak $\phi$, although the curve of $\phi$ versus diffuser area ratio is changed somewhat. An examination of the data from the lift and drag measuring load cells revealed no skewness in the thrust vector.

LOCAL SEPARATION EFFECTS (BUBBLES)

Careful study of the thrust augmentation ($\phi$) variation with diffuser area ratio (DAR) shown in Figure 10 shows a characteristic that was typical for some of the high performing nozzles under development, i.e., a break in $\phi$ between DAR's of 1.6 and 1.8. This characteristic is thought to be due to a local separation that first occurs on the forward flap Coanda surface and then, at a slightly higher DAR, on the aft flap. Figure 11 presents a comparison of the pressure distribution on the forward flap surface for

802

for both narrow and wide cross slot nozzles. Figures 11a and 11b show that both nozzles produce the same pressure distributions, however, the wide nozzle produces a more negative value of pressure. The irregularities in pressure occurring at about 20 nozzle thicknesses (s/t) around the surfaces are thought to be due to local separation. The possibility of expansion and compression waves has been ruled out because of the relatively large distance from the nozzle.

This Coanda surface pressure data has been replotted in Figure 12 to show the variation of surface pressure with diffuser area ratio for a given pressure tap location. Figure 12a (forward flap) shows that at the first three tap locations, similar pressure variations for both nozzles are obtained. However, at the fourth tap (s/t ≅ 20) the previously discussed irregularities can be clearly seen.

Additional data which show the possibility of local separation on the Coanda surfaces is shown in Figure 13. These data show the effect of artificial surface roughness (grit) on surface pressure. The pressures are plotted versus arc length (measured from nozzle exit). The grit was placed between pressure taps three and four. The pressure distributions on the forward flap are very similar with and without grit, i.e., local separation is indicated. The aft flap is seen to have a relatively smooth pressure distribution without grit. However, the addition of grit creates an apparent local separation with a pressure loss downstream of the separation point. The character of the aft flap pressure distribution with grit and the forward flap pressure distribution without grit are similar. The effect of grit on ejector performance was found to be a loss in $\phi$ of at least .04.

It is concluded, based on these data, that both the forward and aft flaps experience local separation at s/t ≈ 20. The indicated separation location is near the point at which the pressure gradient becomes adverse.

INVISCID ANALYSIS OF SHROUD

The increase in thrust that results from the turbulent mixing of the primary jet and secondary streams appears as a reaction force on the ejector shroud. The reaction force is the integral of the surface pressure distribution on the shroud. In order to evaluate the measured pressure distribution, it is desirable to compute the ideal pressure distributions. A method for calculating these distributions will be described in this section and results of its application presented.

A potential flow solution for the ejector wing was obtained by Bevilaqua and DeJoode (1978) by replacing the shroud elements and jets with equivalent flow singularities. The flow is assumed to be irrotational, incompressible and attached. Since the flow satisfies Laplace's equation, the flow velocities at any field point may be obtained by superimposing the induced velocity due to all the flow singularities. The tangential and normal components of the resultant velocity at the $i^{th}$ panel control point may be expressed as follows:

803

$$V_{t_i} = \Sigma\, A_{s_{ij}}\, \sigma_j + \Sigma\, A_{v_{ij}}\, \gamma_j$$

$$V_{N_i} = \Sigma\, B_{s_{ij}}\, \sigma_j + \Sigma\, B_{v_{ij}}\, \gamma_j$$

where $\sigma$ and $\gamma$ are the source and vortex strengths, respectively, and $A_s$, $A_v$, $B_s$, $B_v$ are the influence coefficients which depend only upon panel geometry.

The shroud surfaces are represented by a series of curved parabolic panels. The continuous distribution of flow singularity densities corresponding to an exact distribution is approximated by piecewise linear distributions of both source and vortex densities on each curved panel. The sink strengths and distributions are used to simulate jet entrainment. Vortex densities are the only unknowns in this potential flow formulation and these can be determined by appropriate boundary conditions on the ejector wing elements.

Application of the Newmann boundary condition, that is, specifying the normal velocity at each control point of the panel elements, results in a system of linear equations in the unknown vortex strengths, $\gamma$. Having determined the singularity strengths by solving these equations, the panel velocities, pressures and off body velocities can then be obtained. Details of this inviscid solution for an ejector wing were presented by Bevilaqua and DeJoode (1978) for the static case, and by Bevilaqua, Woan, and Schum (1981) for the case of an ejector in forward flight.

An analysis of the shroud has been made using this method. The procedure employed was to set the secondary flow rate through the shroud by adjusting the strengths of an assumed center jet sink distribution. The strengths were adjusted so that the throat velocity obtained from the inviscid computer code was equal to a desired value (obtained from experiment or the jet mixing analysis).

Figure 1 shows the model used to represent the .2 scale rectangular wing at a diffuser area ratio of 2.0. The computer streamlines are also shown. Figure 14 presents a comparison of experimental and computed velocities at the ejector throat. Figure 15 shows a comparison of chordwise flow angles at the inlet plane and Figure 16 shows the corresponding velocities. Each figure presents experimental data at a span station under a cross slot nozzle and one under the span slot. The secondary flow is seen to be almost two dimensional. The agreement between test and theory is excellent and shows that the inviscid code is quite useful in determining inlet flow characteristics.

A comparison of computer and experimental surface pressures are shown in Figure 17. The pressure due to Coanda jet turning, i.e., $\Delta P = \dfrac{\text{Thrust}}{\text{Radius}}$, has been removed from the experimental data. The computed pressure distributions are in good agreement with the data.

Interestingly, the lowest pressures do not occur at the throat. It is concluded that the shroud surface pressures are composed of a part due to channel-type flow and a part due to airfoil-type flow. The superposition of the two types moves the minimum pressure away from the throat and towards the shroud leading edge.

804

Figure 18 presents a comparison of the computed shroud pressure distribution with experimental data. The comparisons shown have the largest discrepancy at the "leading edge." The potential flow solution indicates a large adverse pressure gradient just upstream of the nozzle. It is possible that the flow could be separated in this region and be re-entrained further downstream. An analogy can be drawn between this "postulated separation" and typical airfoil leading edge separation. In the latter, leading edge separation results in a rapid increase in drag with no appreciable change in lift. Separation of this type for the ejector would be quite detrimental to performance and difficult to detect without further detailed instrumentation. Further study of ejector leading edge separation was planned. Thus, there are two possible separation bubbles, one under the primary jet on the Coanda surface, and one possibly upstream of the nozzle exit.

CONCLUSIONS

1. Improvements in augmentation ratio, with longer shrouds, are the result of more effective diffuser mixing.

2. Modest asymmetries in ejector flap lengths do not necessarily degrade augmentation ratio.

3. For XFV-12A-type ejector wing configurations, local areas of separation and reattachment have been identified.

4. A potential flow solution for an XFV-12A ejector has been obtained and compares favorably with experimental results.

REFERENCES

1. Bevilaqua, P. M., and DeJoode, A. D., "Viscid/Inviscid Interaction Analysis of Thrust Augmenting Ejectors," Feb. 1978.

2. Bevilaqua, P. M.; Woan, C. J.; Schum, E. F.; "Viscid/Inviscid Interaction Analysis of Ejector Wings," April 1981.
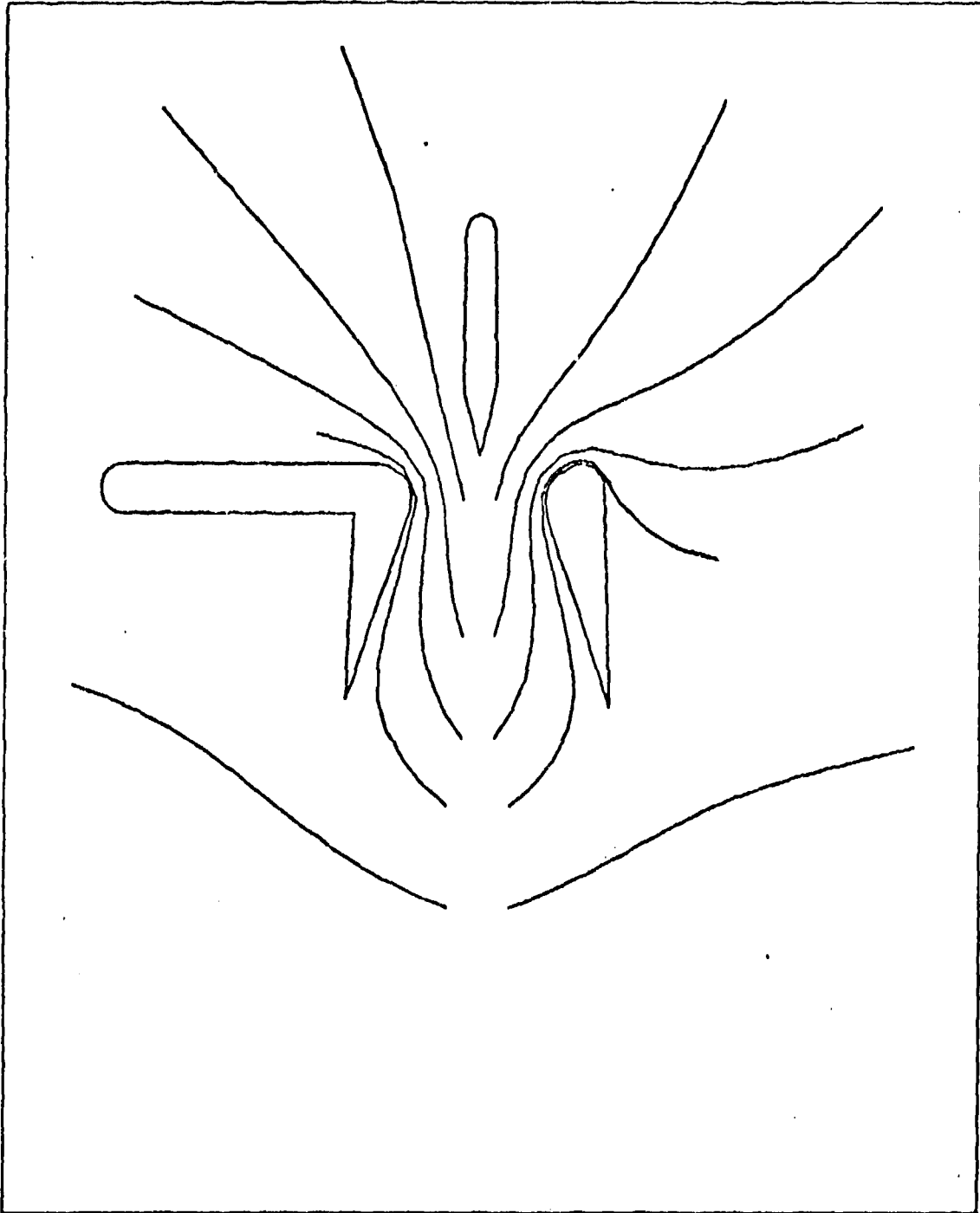
Figure 1.   Entrainment by the Primary Jet Induces a Secondary Flow
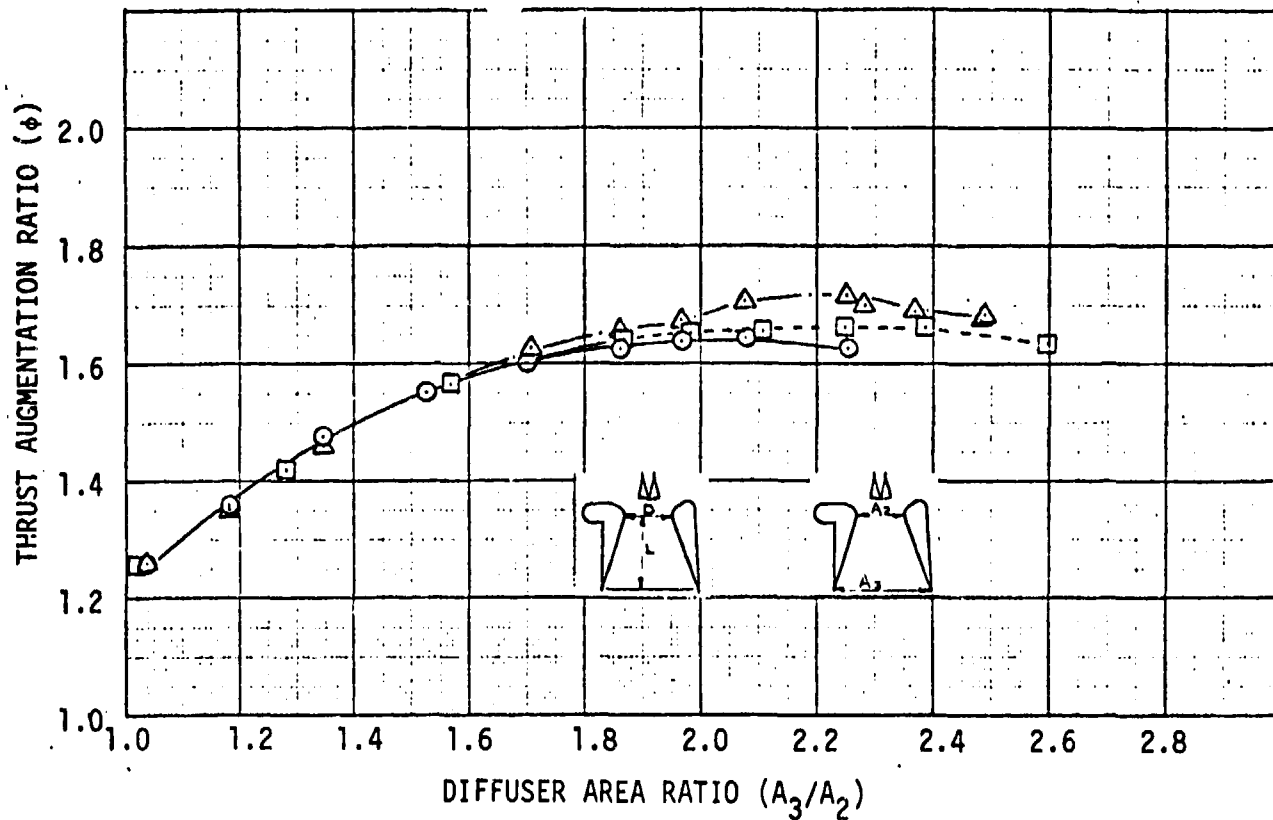
Figure 2. Effect of Flap Length on Thrust Augmentation Ratio
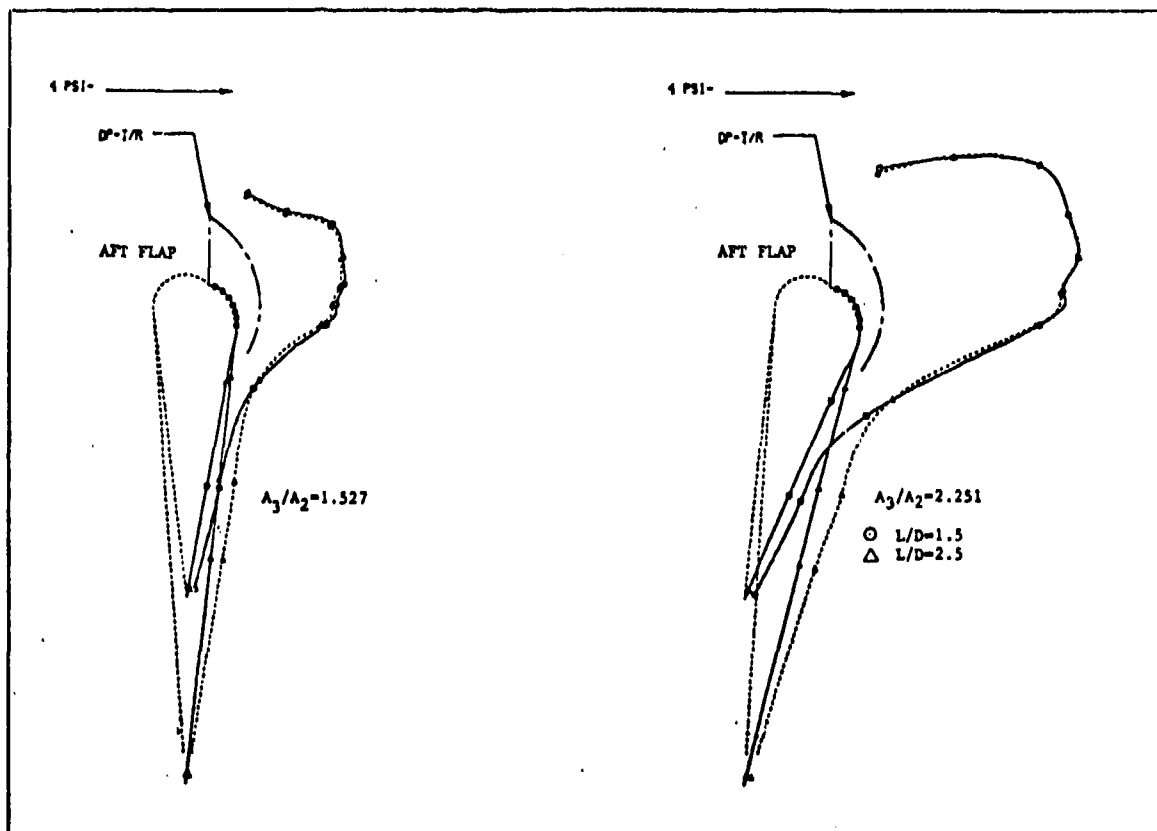


Figure 3. Effect of Flap Length on Surface Pressure Distribution

EFFECT OF FLAP LENGTH ON SECTION MASSFLOW
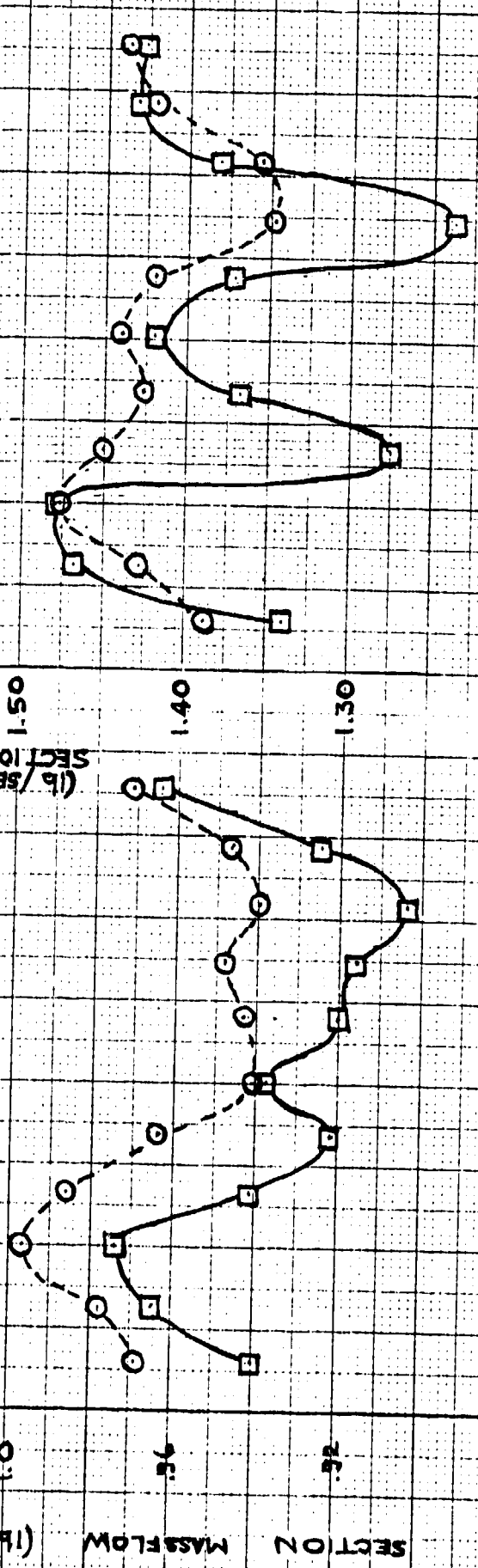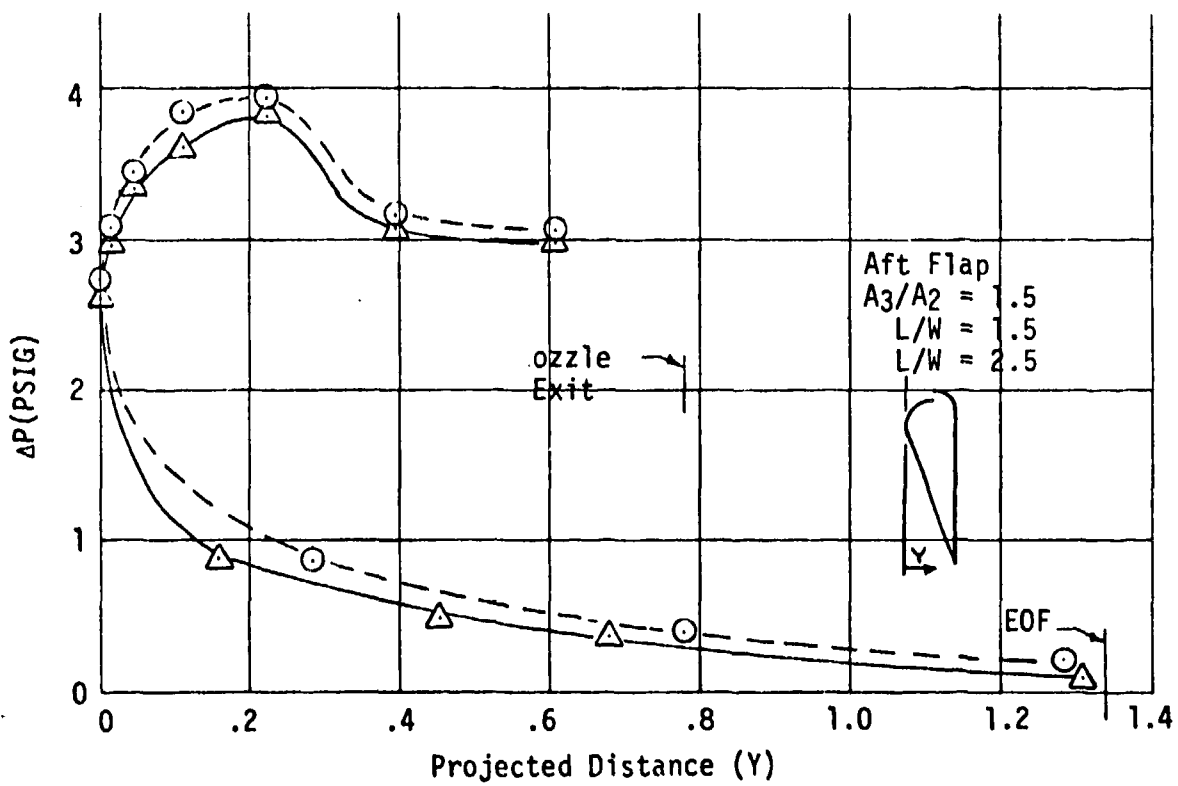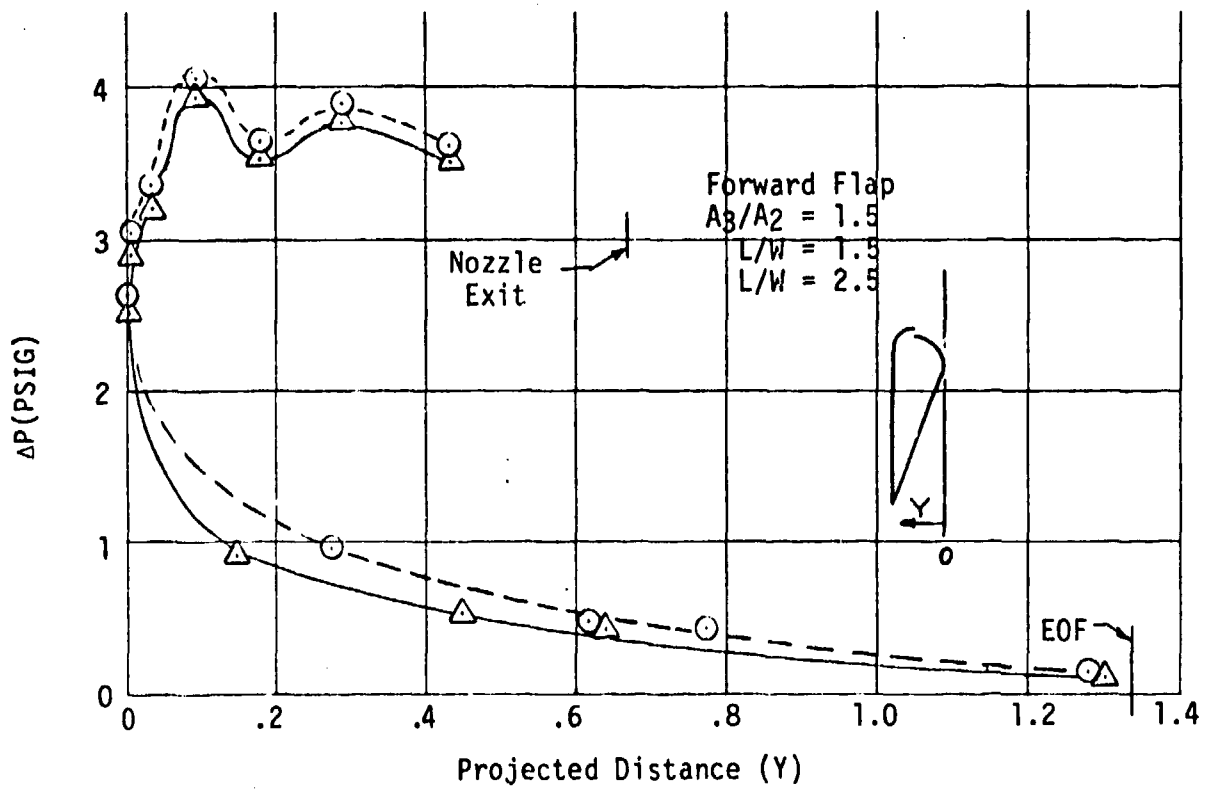
FIGURE 4

Figure 5. Effect of Flap Length on Shroud Surface Pressures
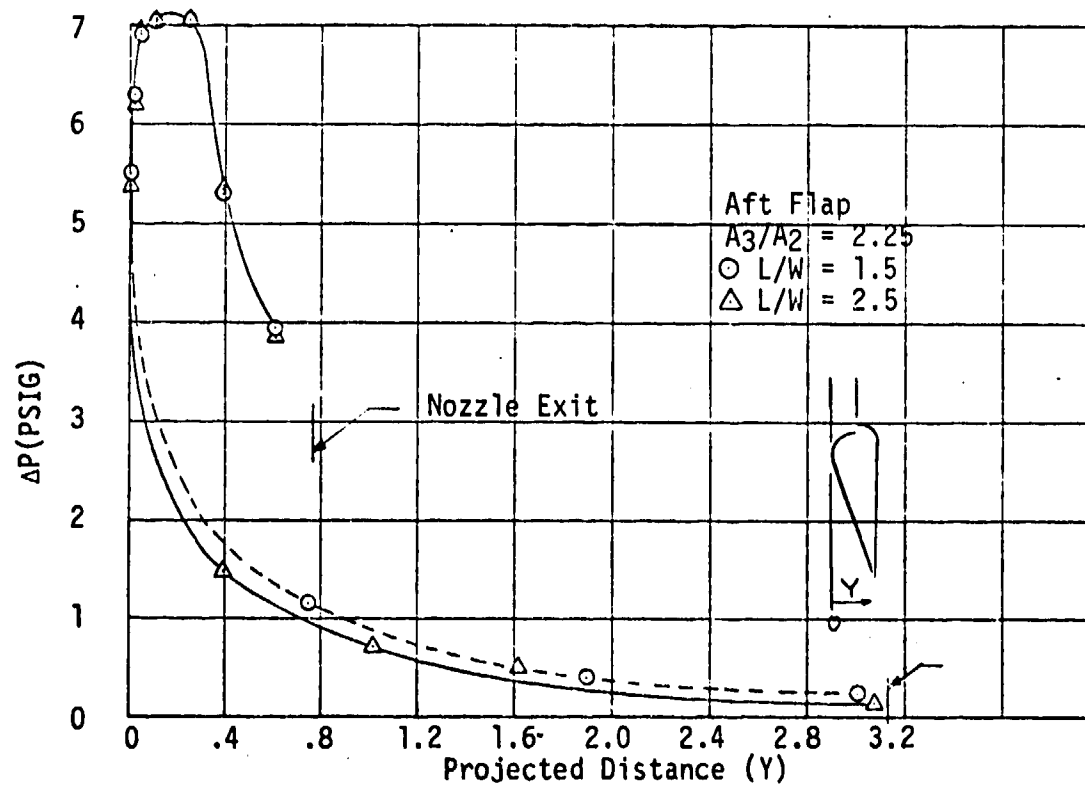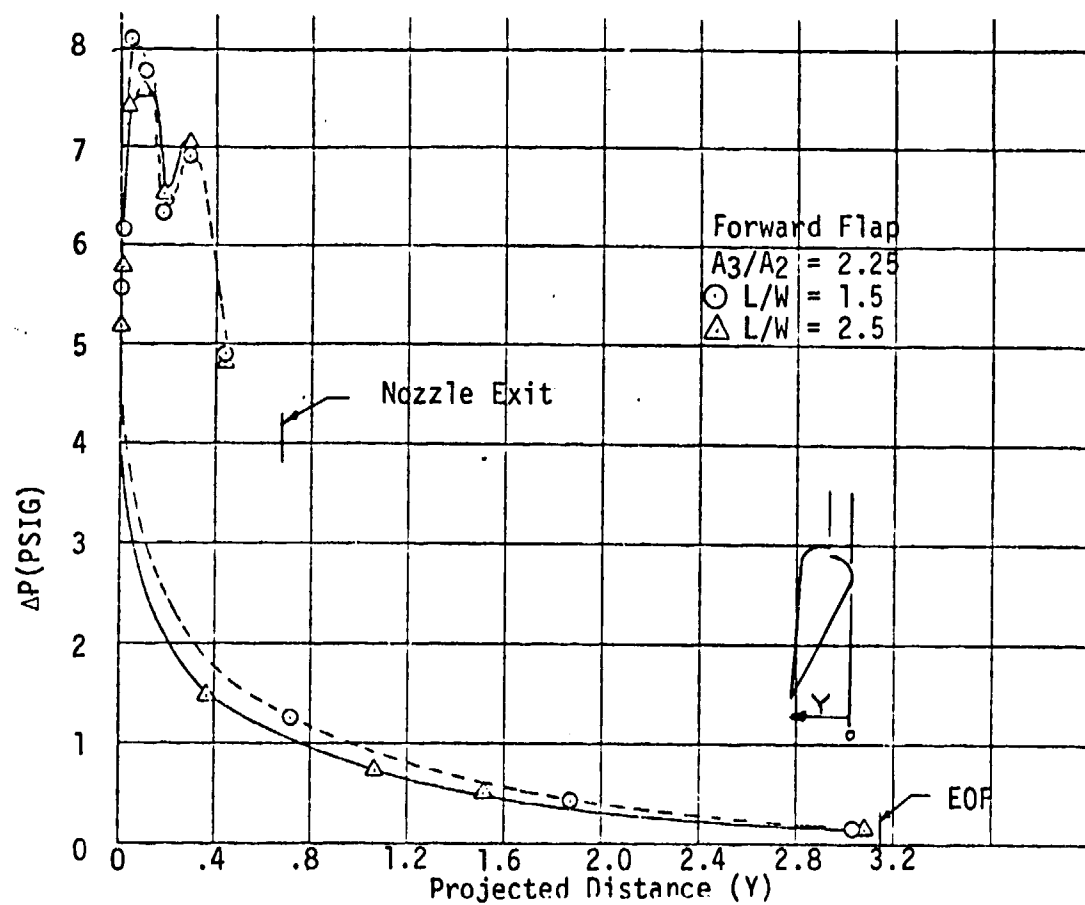
Figure 6.  Effect of Flap Length on Shroud Surface Pressures

810
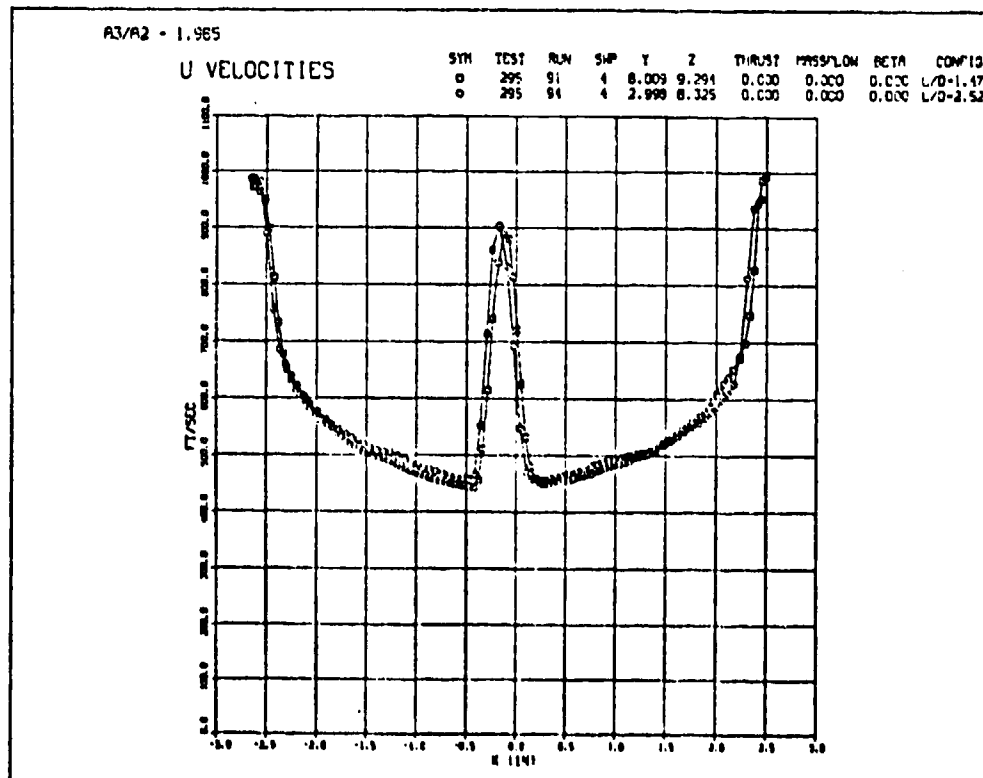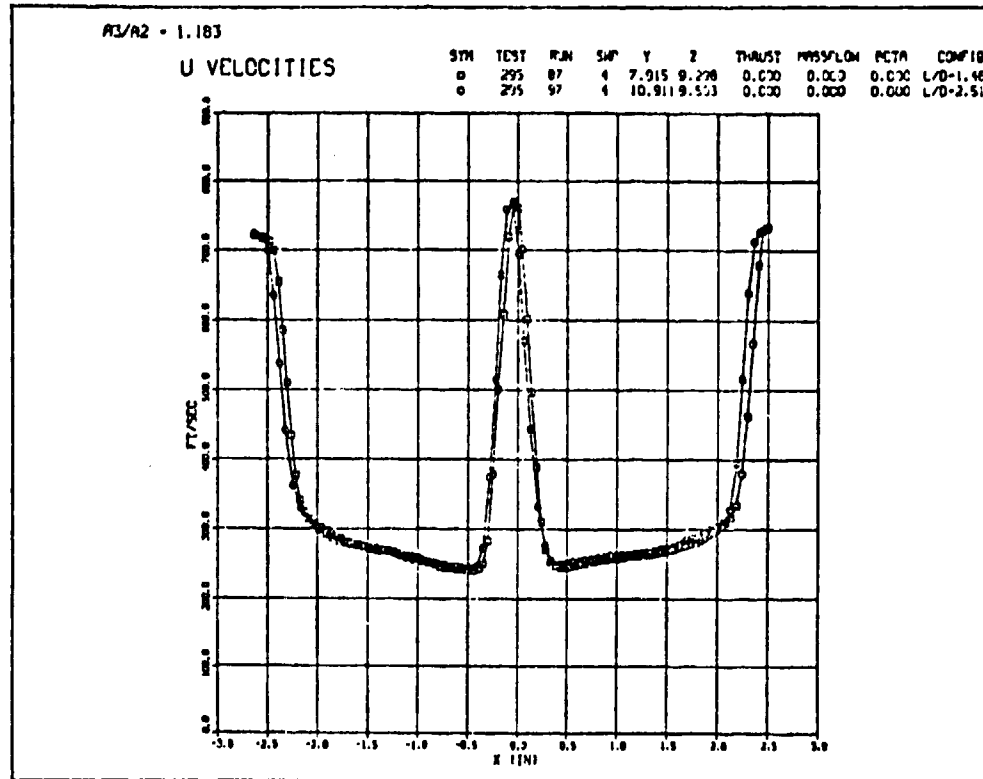
Figure 7.   Effect of Flap Length on Throat Velocity

811

EFFECT OF FLAP LENGTH ON VELOCITY PROFILE SHAPE FACTOR
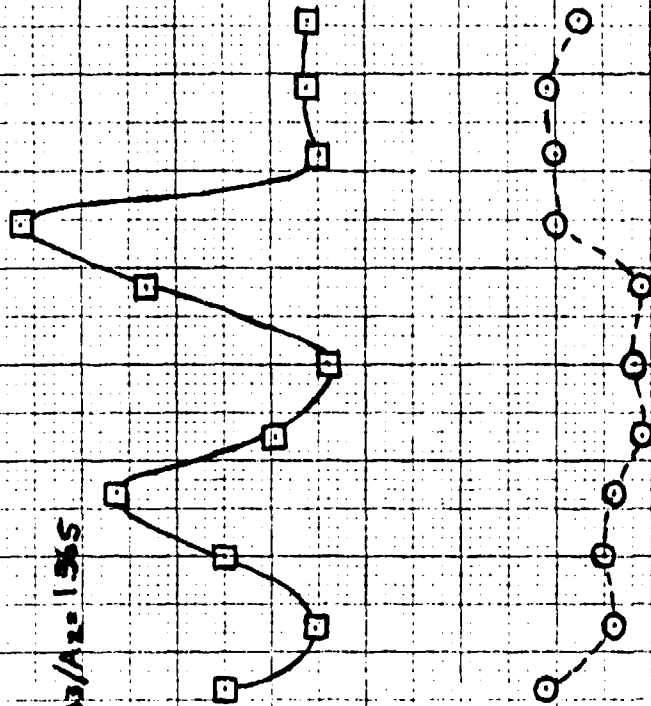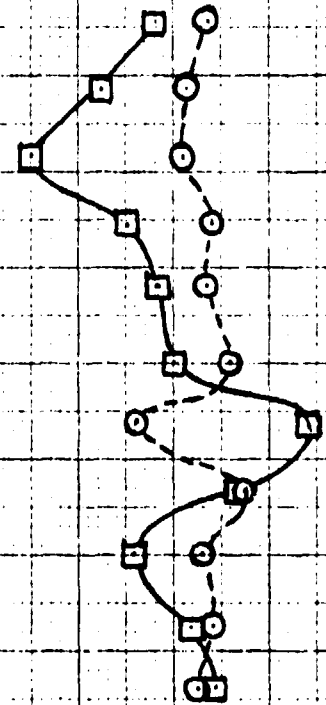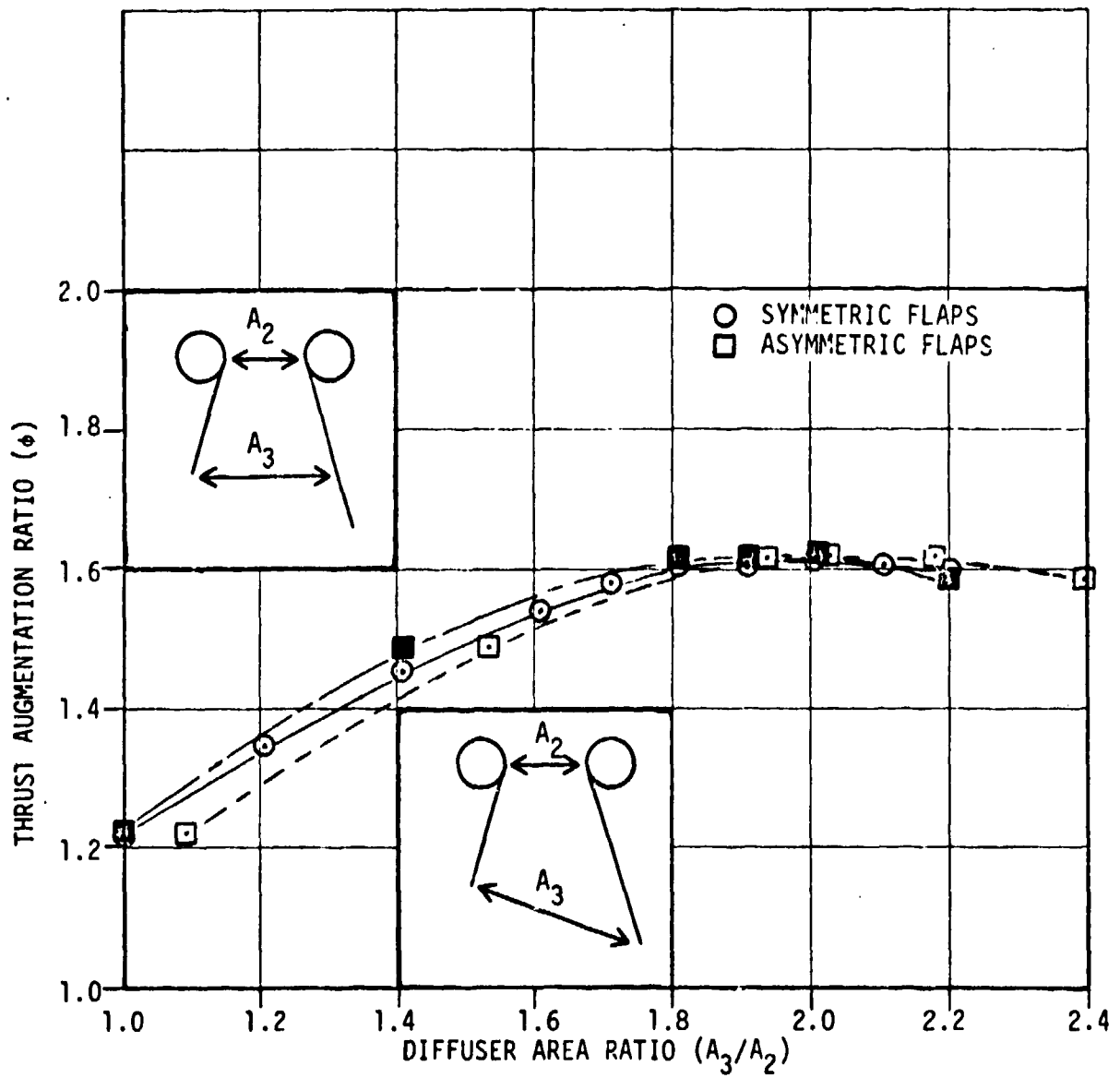
FIGURE 8

Figure 9. Effect of Asymmetric Flap Length on $\phi$

813
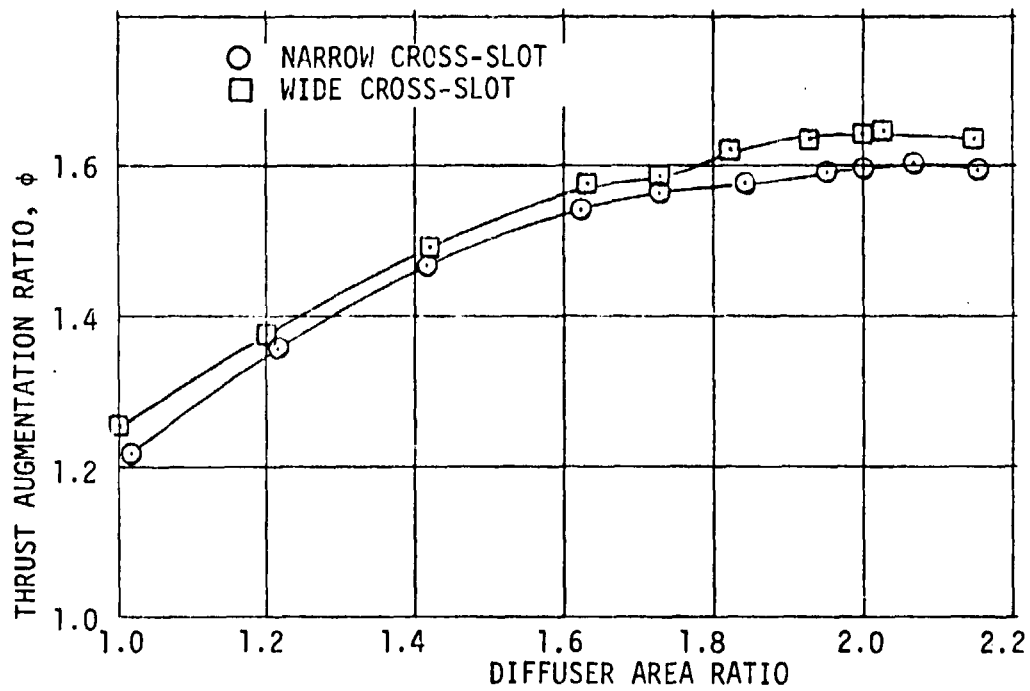
Figure 10.   Effect of Cross-Slot Width on Thrust Augmentation Ratio

FORWARD FLAP SURFACE PRESSURES FOR SCS-1 AND SCS-2 NOZZLES

Figure 11.

815
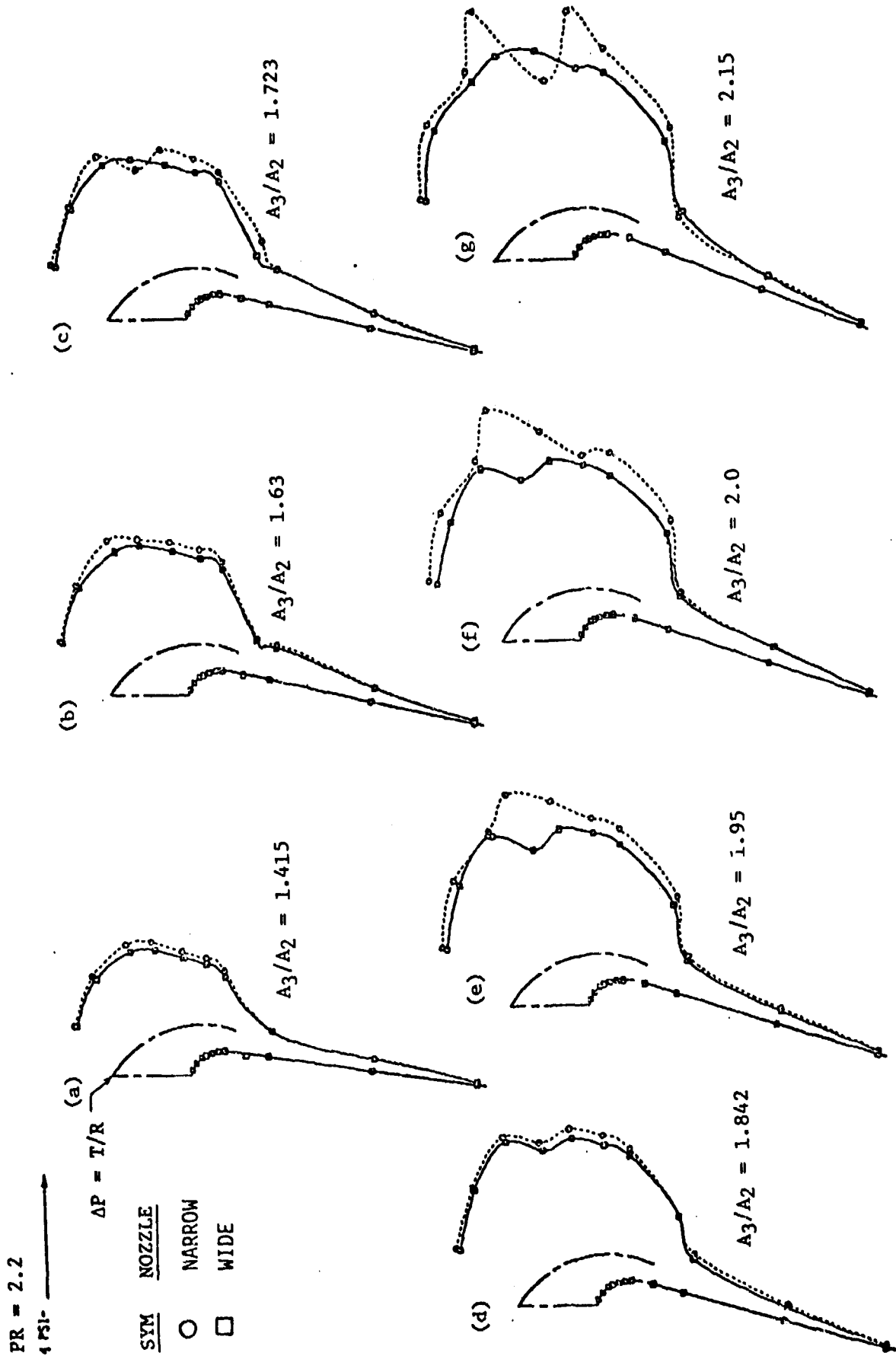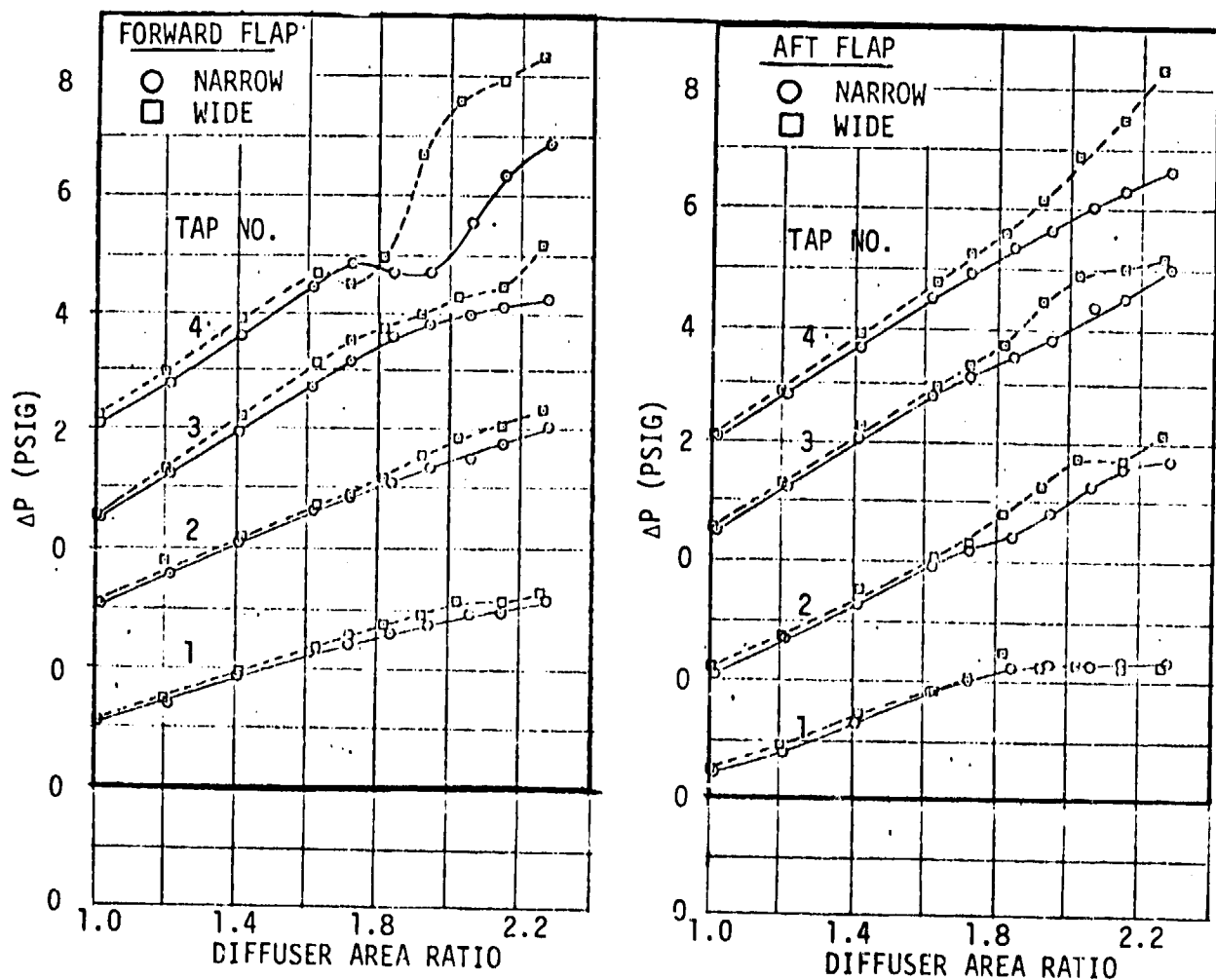
Figure 12. Variation of Surface Pressure With Diffuser Area Ratio
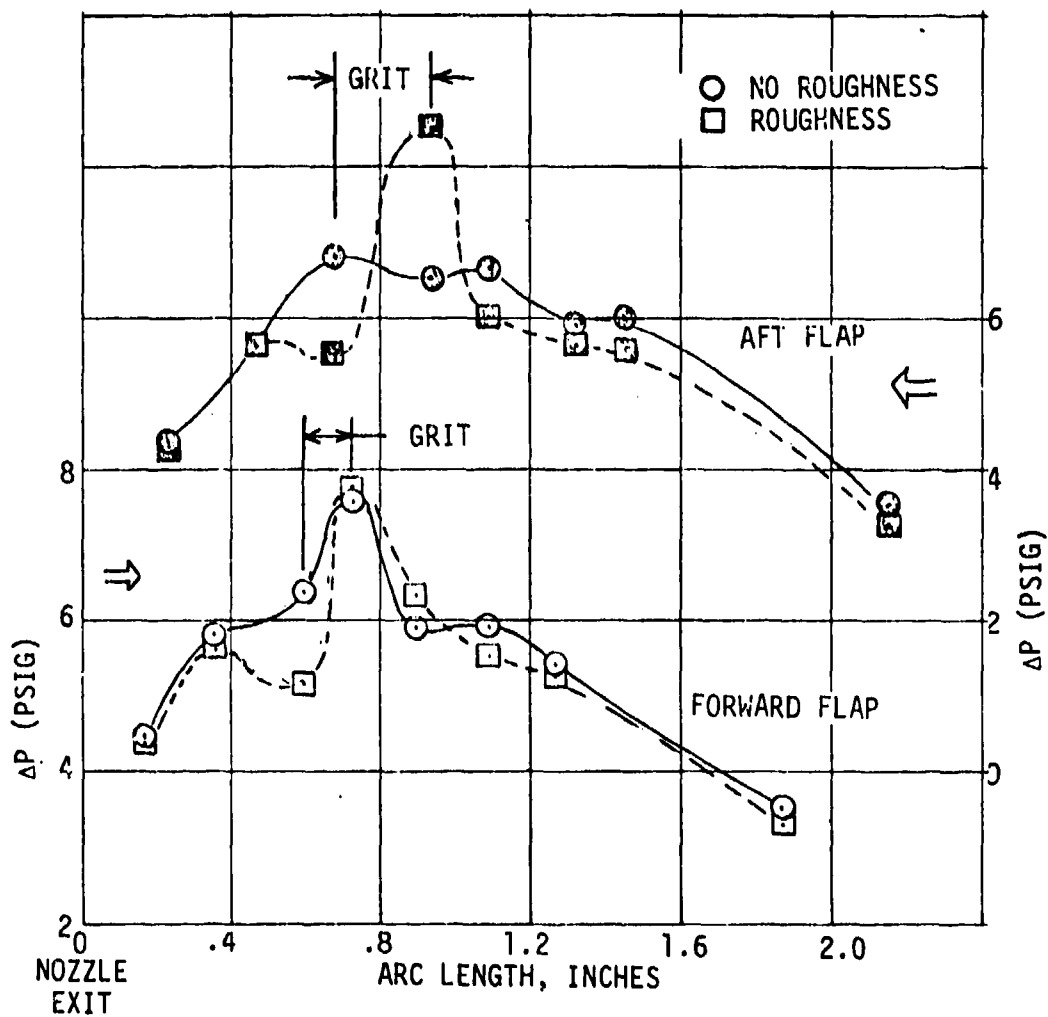
Figure 13. Effect of Roughness on Coanda Surface Pressures

817
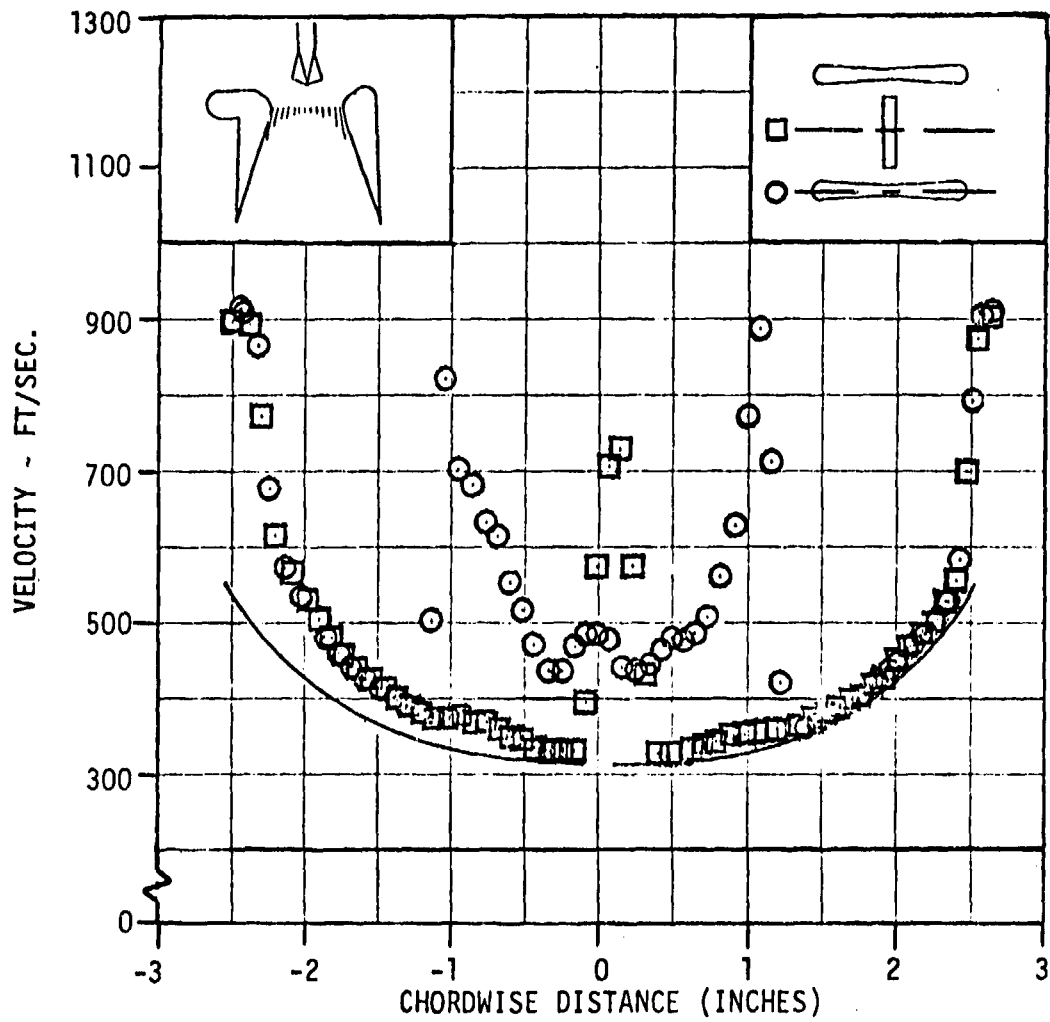
Figure 14.  Comparison of Experimental and Theoretical Velocities
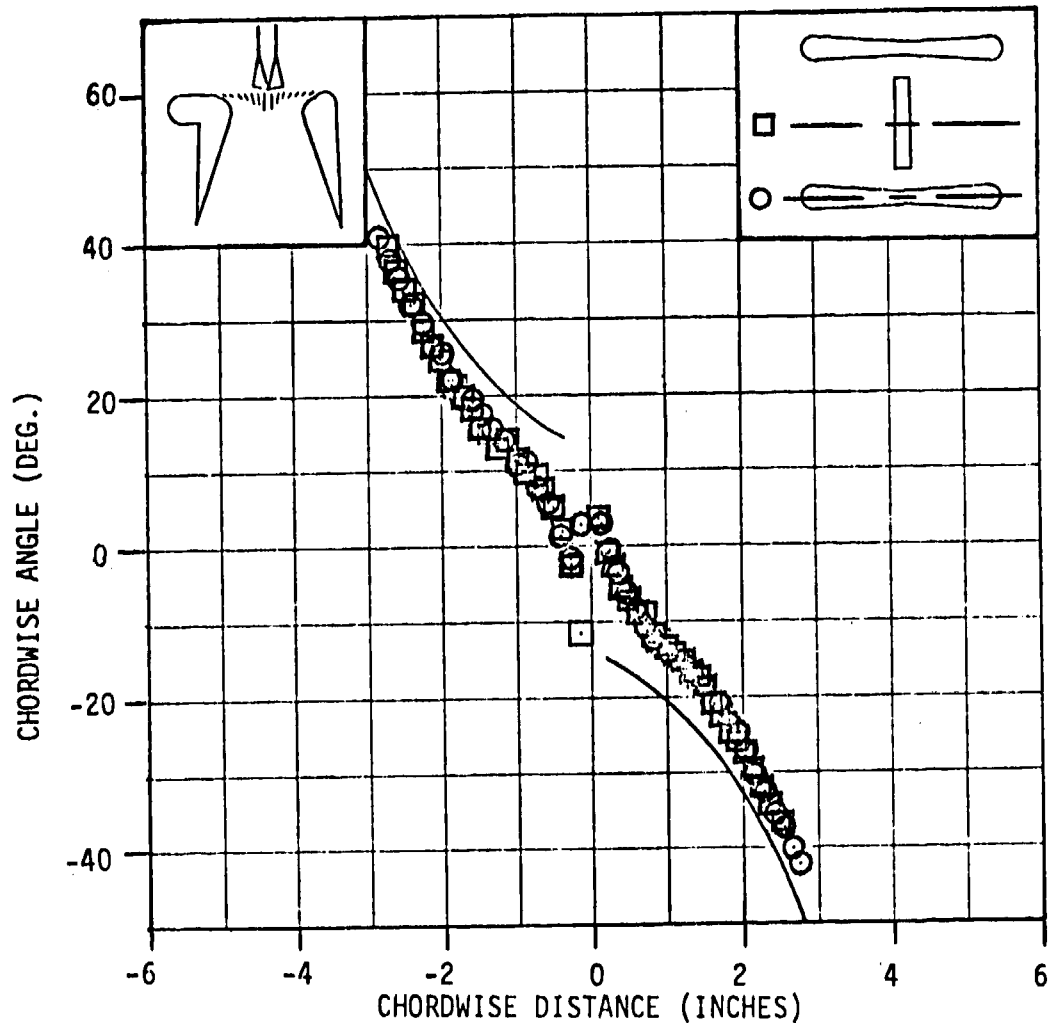
Figure 15. Comparison of Experimental and Theoretical Flow Angles
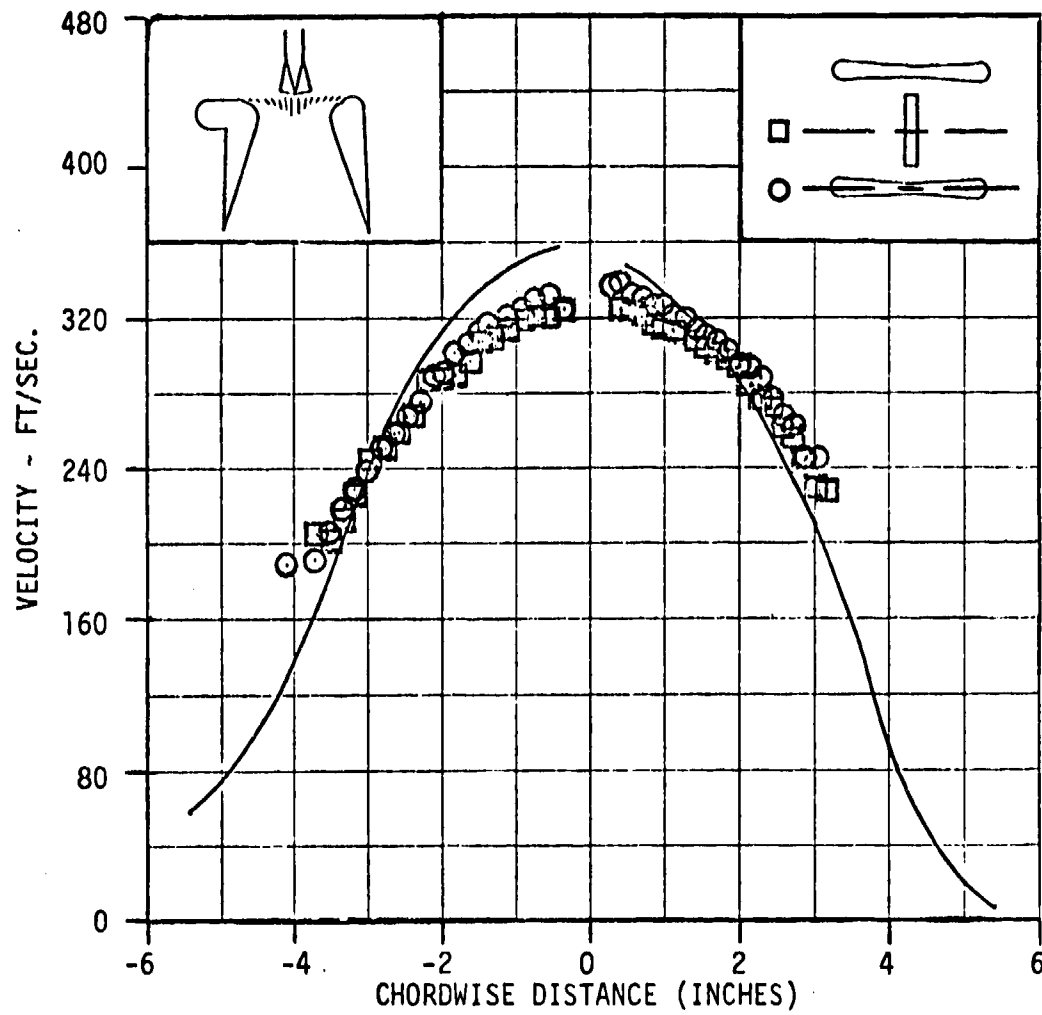
Figure 16.   Comparison of Experimental and Theoretical Velocities
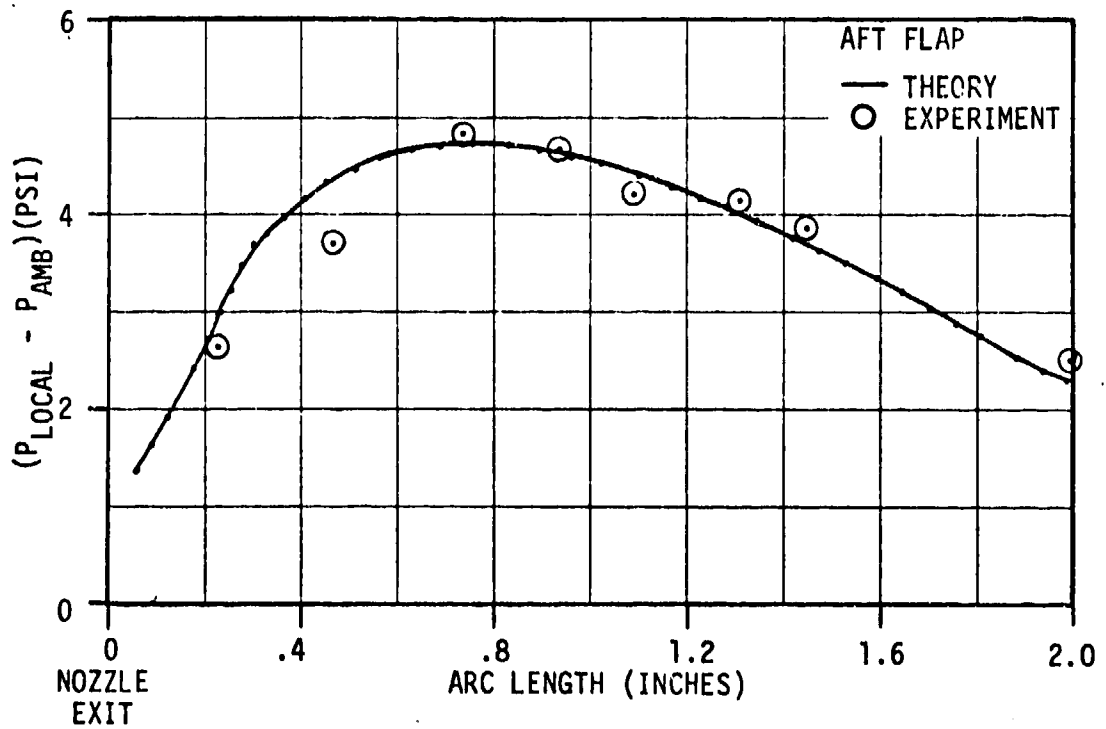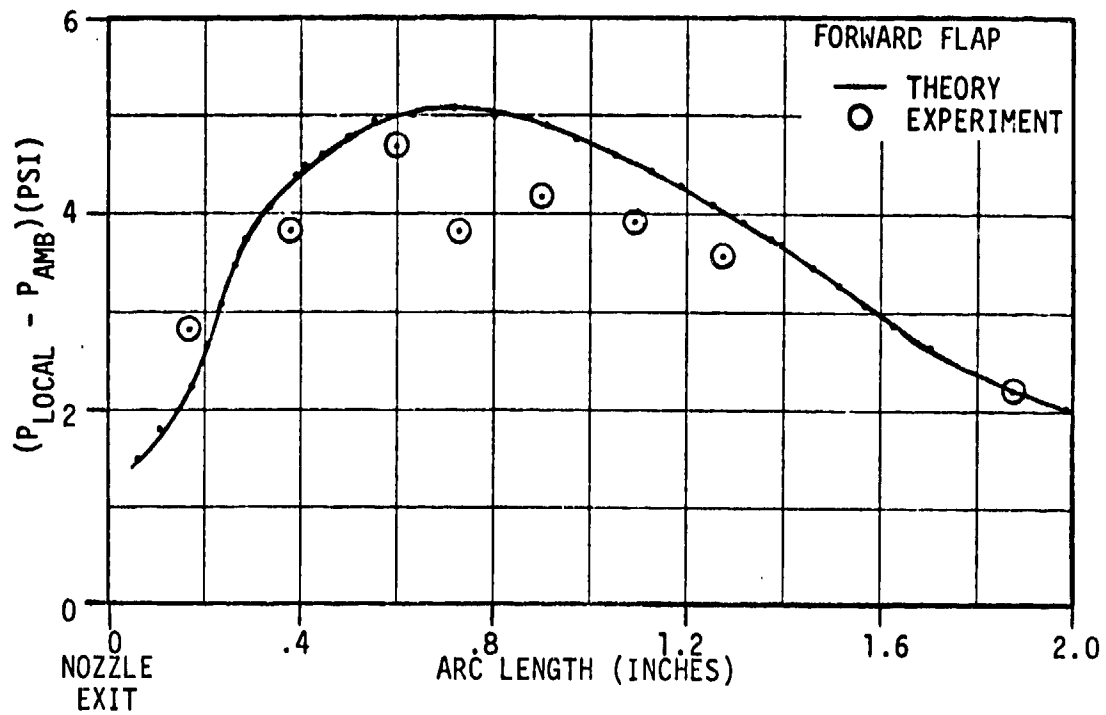
Figure 17. Comparison Experimental and Theoretical Surface Pressures
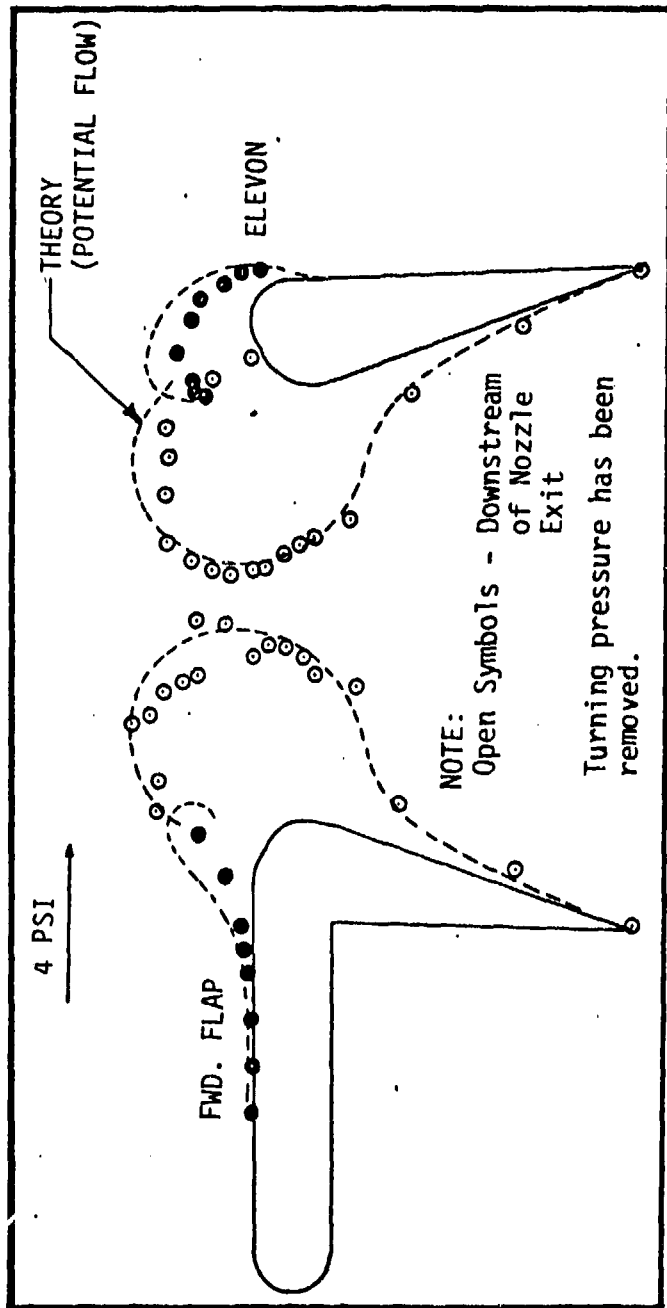
Figure 18. Comparison of Predicted and Experimental Shroud Pressure Distributions

822

# EJECTOR NOZZLE DEVELOPMENT
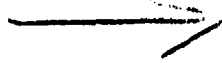
by

E. J. Schum and J. H. DeHart

Rockwell International, North American Aircraft Division

## ABSTRACT

A combination of computer analysis and scale model testing was utilized to develop a nozzle which would increase the performance of thrust augmenting ejectors. Scale model tests were conducted on various multi-lobed and vortex generating nozzles. Predicted jet characteristics were obtained by calculating a finite difference solution of Reynolds equations for the three dimensional flow field. A two-equation turbulence kinetic energy model was used for closure. It is demonstrated that the thrust augmentation of the XFV-12A ejector can be increased from 1.45 to 1.64 by the addition of lobes to the baseline nozzle, and a corresponding increase of throat width.

# INTRODUCTION

The static thrust of turbojet engines can be significantly increased by diverting the exhaust flow through an ejector pump. According to the laws of momentum and energy conservation, greatest thrust is obtained from a given energy input by accelerating a large mass of air to a low exhaust velocity. Within an ejector, thrust is increased by transferring the kinetic energy of the engine exhaust stream to a larger mass of air drawn from the atmosphere. The ejector duct experiences a reaction force which is equal but opposite to the momentum change of the accelerated stream. Details of this process have been discussed by Bevilaqua.[1]

The mechanism of this energy transfer is the turbulent mixing of the two streams. Thus, increases in ejector thrust augmentation can be obtained by increasing the turbulent mixing rate. Appreciable increases in mixing and augmentation have been achieved with the so-called hyper-mixing[2,3]. The alternating exit of the hypermixing nozzle serves to introduce a row of streamwise vortices into a plane jet (Figure 1).
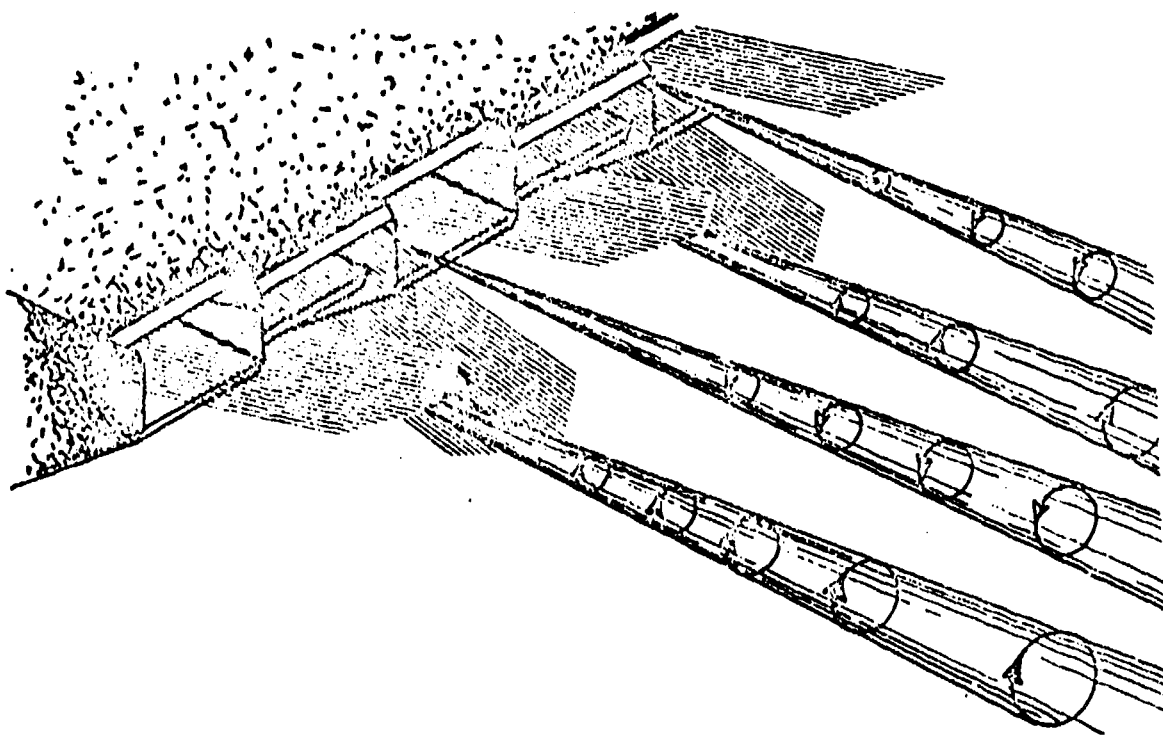


Figure 1. Hypermixing Nozzle Exit

825

These vortices serve to accelerate the turbulent mixing and thus to entrain additional fluid into the ejector. Because of their favorable entrainment characteristics, hypermixing nozzles in the centerbody were used in the XFV-12A airplane. Figure 2 illustrates how the ejector components fold into the shape of a wing for forward flight. This study is concerned with the development of the centerbody nozzle.
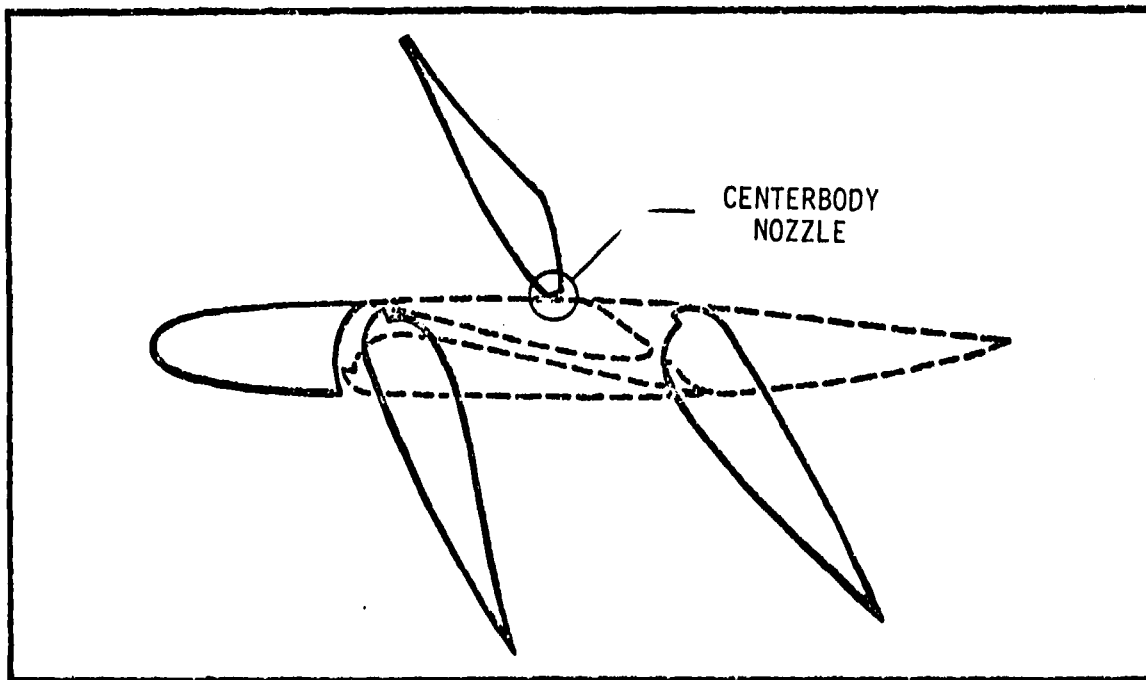


Figure 2. Deflected Ejector wing

The specific objective of this investigation was to develop and demonstrate centerbody nozzles that would provide increased augmentation, exceeding the peak value of 1.45 obtained for the hypermix configuration.

In the following sections, a "master plan" is presented including a brief description of the 3-dimensional, turbulent kinetic energy program (3D-TKE) used to calculate the viscous mixing. Analytical and experimental results for both symmetric and asymmetric, centerbody nozzle configurations are discussed.

## NOZZLE DEVELOPMENT PLAN

The overall program consisted of three phases.

**Phase I**  To Improve Analytical Capability for Calculating 3-Dimensional, Turbulent Flow by:

- Identifying inlet turbulent kinetic properties for augmenters ($k$, $\mu_t$, $\varepsilon$)

- Inlet grid generation program

- Simplification for incompressible flow

**Phase II**  To Compare Analyses with Experiment for Hypermixing Nozzles to Update Analytical Technique

**Phase III**  To Develop and Demonstrate Centerbody Nozzles that Increase Augmentation

ANALYTICAL MODEL AND NUMERICAL APPROACH

## Governing Equations

The program equations, in cartesian coordinates, include:

Equation of State

$$\rho = \frac{P}{RT}$$

Continuity

$$\frac{\partial}{\partial X}(\rho U) + \frac{\partial}{\partial Y}(\rho V) + \frac{\partial}{\partial Z}(\rho W) = 0$$

Momentum

(1)

$$\frac{\partial}{\partial X}(\rho U^2) + \frac{\partial}{\partial Y}(\rho UV) + \frac{\partial}{\partial Z}(\rho UW) = \frac{\partial \tau_{YX}}{\partial Y} + \frac{\partial \tau_{ZX}}{\partial Z} - \frac{\partial P}{\partial X}$$

$$\frac{\partial}{\partial X}(\rho UV) + \frac{\partial}{\partial Y}(\rho V^2) + \frac{\partial}{\partial Z}(\rho VW) = \frac{\partial \tau_{YY}}{\partial Y} + \frac{\partial \tau_{ZY}}{\partial Z} - \frac{\partial P'}{\partial Y}$$

$$\frac{\partial}{\partial X}(\rho UW) + \frac{\partial}{\partial Y}(\rho VW) + \frac{\partial}{\partial Z}(\rho W^2) = \frac{\partial \tau_{YZ}}{\partial Y} + \frac{\partial \tau_{ZZ}}{\partial Z} - \frac{\partial P'}{\partial Z}$$

827

Energy

$$\frac{\partial}{\partial X}(\rho U H) + \frac{\partial}{\partial Y}(\rho V H) + \frac{\partial}{\partial Z}(\rho W H) = \frac{\partial}{\partial Y}\left(\frac{\mu_t}{Pr}\frac{\partial H}{\partial Y}\right) + \frac{\partial}{\partial Z}\left(\frac{\mu_t}{Pr}\frac{\partial H}{\partial Z}\right)$$

where U, V, and W are the time averaged components. These equations are regarded as parabolic in the longitudinal coordinate, X, and elliptic in the transverse coordinates; Y and Z. A more complete description of the program is given by DeJoode and Patankar[4].

The turbulent shear stresses, $\Gamma_{ij}$, are expressed in terms of a turbulent viscosity, $\mu_t$, and velocity gradients. The two-equation turbulence model of Launder and Spalding[5] expresses the turbulent viscosity in terms of two parameters, K and $\epsilon$, for which two differential equations are solved. The expression for $\mu_t$ is:

$$\mu_t = c_\mu \, \rho \, K^2 / \epsilon \tag{2}$$

where $c_\mu$ is an empirical constant and K and $\epsilon$ are obtained from the solution of:

$$\frac{\partial(\rho U K)}{\partial X} + \frac{\partial(\rho V K)}{\partial Y} + \frac{\partial(\rho W K)}{\partial Z} = \frac{\partial}{\partial Y}\left(\frac{\mu_t}{\sigma_K}\frac{\partial K}{\partial Y}\right) + \frac{\partial}{\partial Z}\left(\frac{\mu_t}{\sigma_K}\frac{\partial K}{\partial Z}\right) + G - \rho\epsilon$$

$$\frac{\partial(\rho U \epsilon)}{\partial X} + \frac{\partial(\rho V \epsilon)}{\partial Y} + \frac{\partial(\rho W \epsilon)}{\partial Z} = \frac{\partial}{\partial Y}\left(\frac{\mu_t}{\sigma_\epsilon}\frac{\partial \epsilon}{\partial Y}\right) \tag{3}$$

$$+ \frac{\partial}{\partial Z}\left(\frac{\mu_t}{\sigma_\epsilon}\frac{\partial \epsilon}{\partial Z}\right) + (c_1 G - c_2 \rho\epsilon)\left(\frac{\epsilon}{K}\right)$$

G is the rate of generation of K by the action of velocity gradients. Since the only significant gradients are $\partial U/\partial Y$ and $\partial U/\partial Z$, the expression for G becomes

$$G = \mu_t \left[\left(\frac{\partial U}{\partial Y}\right)^2 + \left(\frac{\partial U}{\partial Z}\right)^2\right] \tag{4}$$

828

Values of the constants (Reference 5) include:

| $c_\mu$ | $c_1$ | $c_2$ | $\sigma_K$ | $\sigma_\epsilon$ |
|---------|-------|-------|------------|-------------------|
| 0.09    | 1.44  | 1.92  | 1.0        | 1.3               |

The above equations were put in finite difference form. From known conditions at an upstream cross section, X, the flow field at the downstream cross section, $X + \Delta X$ is computed. This streamwise marching process is continued until the domain of interest has been covered.

### Boundary Conditions

Figure 3 presents a typical ejector configuration, containing a hypermix centerbody nozzle. Other types of centerbody nozzle designs can also be analyzed. Needed geometric parameters include the throat to inlet primary flow area, $A_2/A_0$, the ejector exit to throat area, $A_3/A_2$, the diffuser length, L, the Coanda surface shape, and the flow split or division of the primary flow between the centerbody nozzle and Coanda jets.
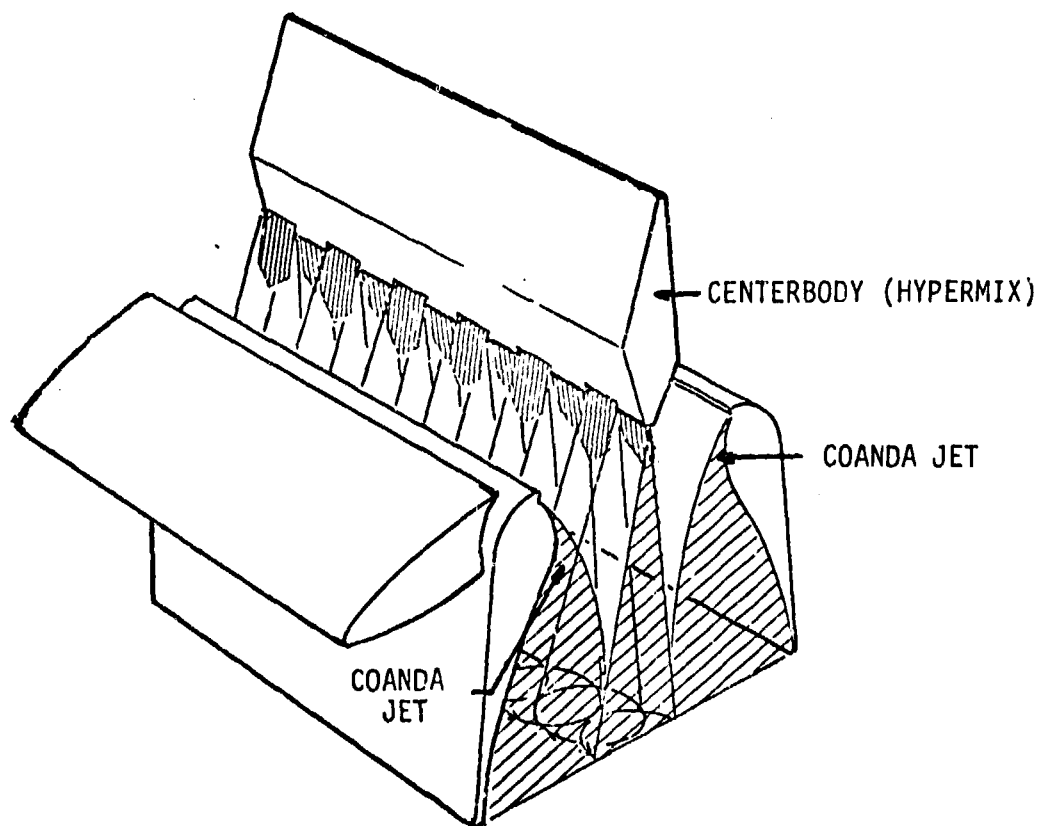


Figure 3. Typical Ejector Wing Configuration

The computational boundaries are outlined in Figure 4 for the hypermix type configuration. Symmetry planes are used as computational boundaries in the spanwise direction because most nozzle designs are "periodic" along the span.
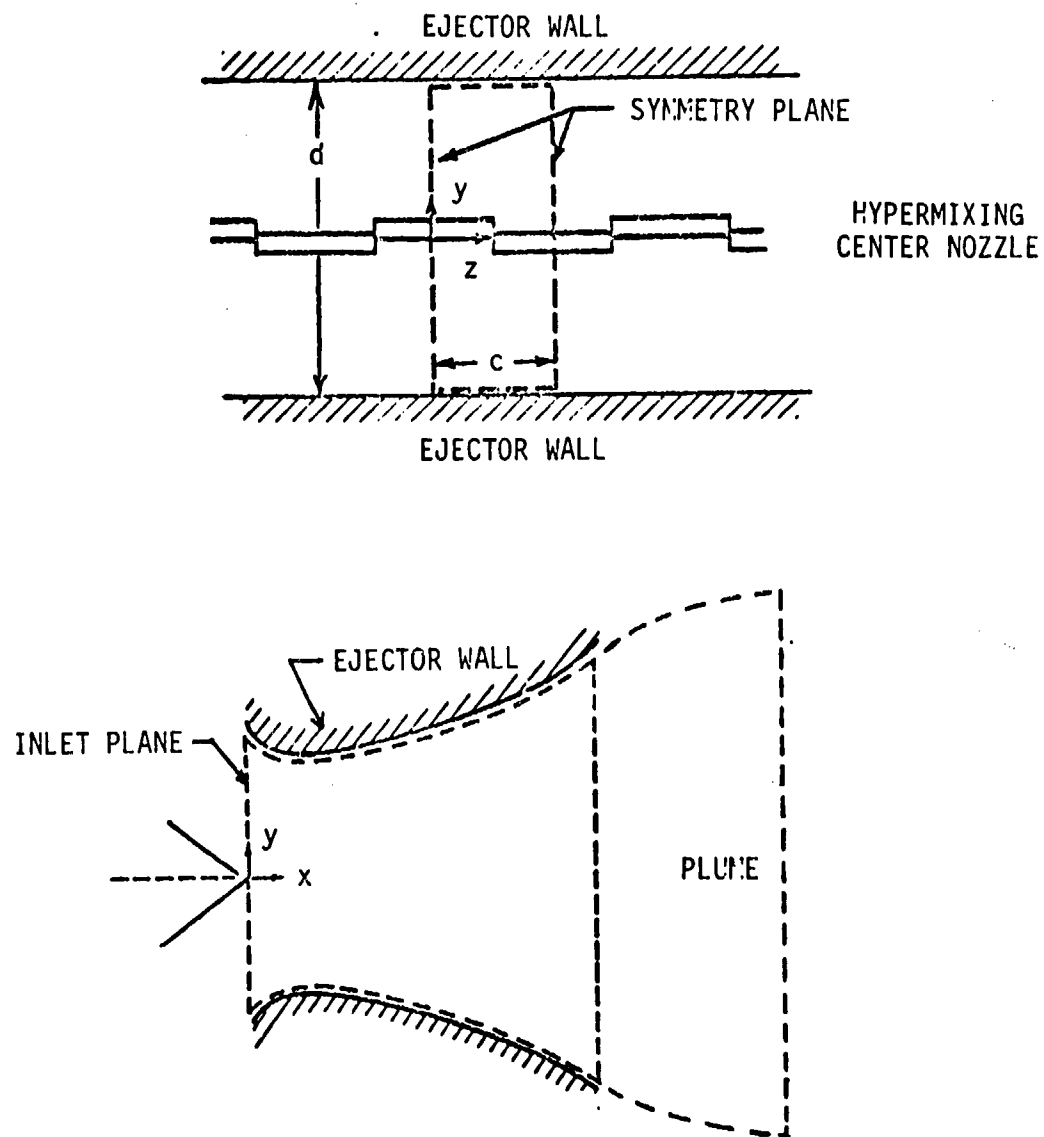


Figure 4. Computational Boundaries

830

## Initial Conditions

Primary jet velocities were calculated from the conventional isentropic relation using a velocity coefficient of 0.925 (reference 6). The mean static pressure along with the ambient pressures are used in Bernoulli's equation to calculate the inlet secondary stream velocities. The inlet static pressure is obtained in the iterative solution of the viscous flow field and is discussed in the "Closure Scheme". Values of the initial turbulence conditions ($K$, $\mu_t$, $\varepsilon$) are discussed in a later section.

## Inlet Grid Generator

At the inlet computational plane of the ejector, it is necessary that the flow area be subdivided into a grid of approximately 1500 to 3000 control areas (volumes) with corresponding velocities (primary or secondary). To reduce the usual 20 hour setup time to an hour or less and also eliminate the arbitrariness of the subdivision, a computer program was written to generate the grid where only the ejector and nozzle dimensions are the primary input. A grid for the hypermix configuration is shown in Figure 5 and contains approximately 3000 control volumes. At the upper and lower surfaces, the grid appears to be shaded because in the Coanda jet region, a much finer grid is used.

## Closure Scheme

Closure is obtained by iterating on the inlet pressure until the calculated pressure at the end of the exhaust plume is ambient. The plume exit pressure is dependent upon the curvature of the jet sheet leaving the trailing edge of the ejector shroud as well as the plume length, both determined by the difference between the ambient pressure and the ejector exit pressure. This "jet flap" effect is discussed in more detail in reference 4.

The thrust augmentation ratio, $\phi$, is defined to be the ratio of the ejector stream thrust to the isentropic thrust obtained by expanding the same mass of primary fluid to atmospheric pressure. The thrust of the ejector is evaluated by integrating the exit momentum flux and pressure force,

$$T = \int_{A_3} \rho U^2 \, dY \, dZ - (P_\infty - P_3)A_3$$

in which $P_3$ and $A_3$ are the static pressure and area at the exit. $\phi$ is defined as:

$$\phi = \frac{T}{\dot{m}_{pri} U_{isent}}$$

COANDA
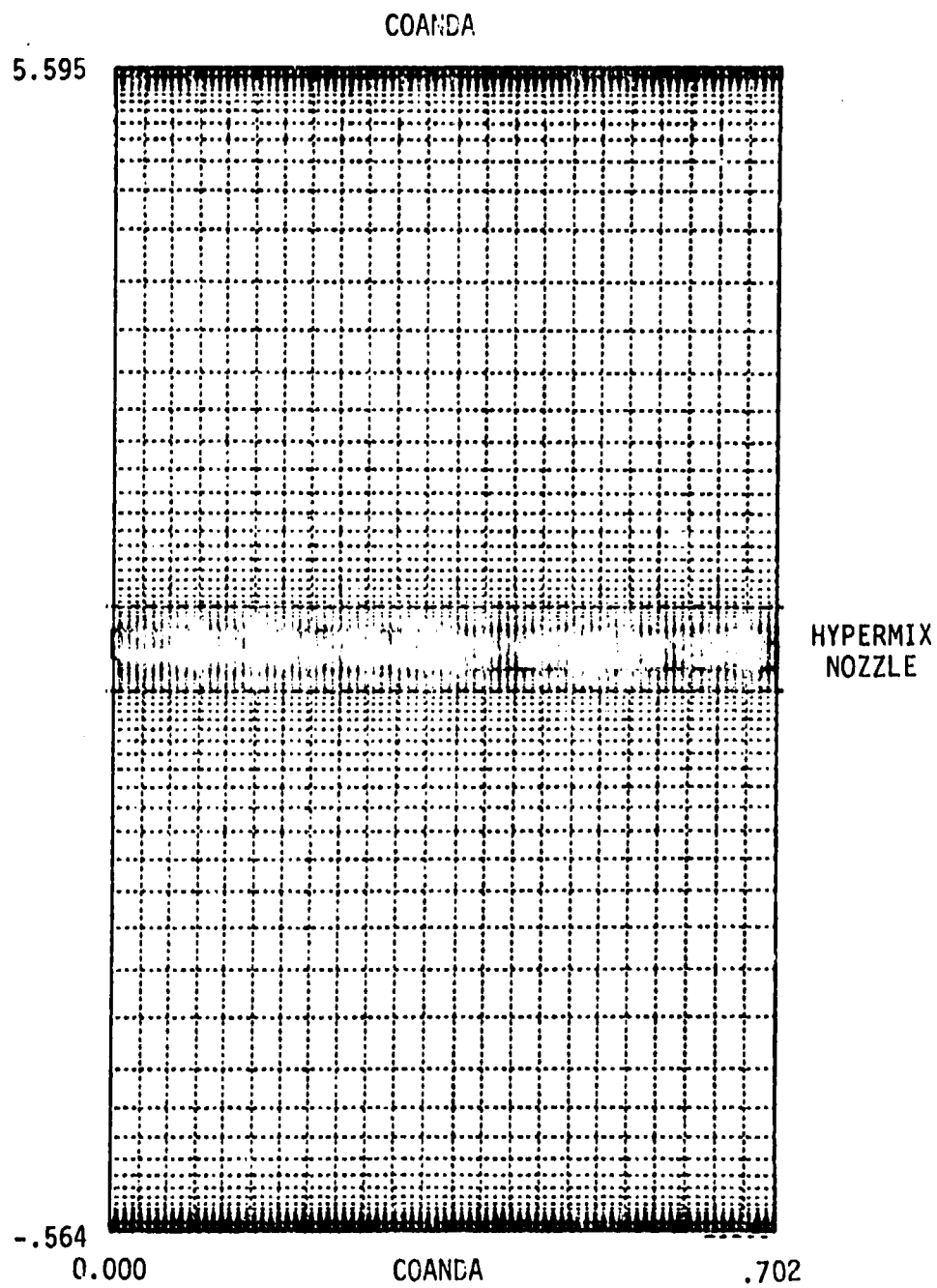


Figure 5. Computational Grid for Hypermixing
Centerbody Configuration.

## Simplification for Incompressible Flow

To reduce computer time the analysis was conducted using the incompressible option in the program. With this, density is assumed constant and the state and energy equations are bypassed. To verify that this was a valid approach, both compressible and incompressible computer runs were made for a hypermix configuration at a pressure ratio of 2.2 and primary gas temperatures of 80°F (usual test conditions). There was little difference in the ejector calculated exit velocity profiles. This afforded a saving of about 30.percent or 10 minutes of CPU time on the CDC-176 computer.

## RESULTS AND DISCUSSION

The following sections describe how the hypermix test results interacted with the computer program development (Phase II) so that it could be used to identify higher performance symmetric and/or asymmetric nozzle configurations (Phase III).

## Hypermixing Nozzles

To improve the analytical design methods, angularity measurements were made of the secondary flow at the ejector inlet. These data were generalized and incorporated into the program. Initial values of the kinetic energy for use at the inlet computational plane were obtained from hot film measurements.

Figure 6 presents the calculated, 2-dimensional mainstream velocity distribution along with the calculated and measured profiles for two lateral positions, corresponding to the middle of the hypermix element and between adjacent elements. It should be noted that the Coanda velocities are not in good agreement since Coanda curvature effects have not been included in the computer program. In the 2-dimensional velocity distribution, the nearby Coanda velocities were purposely omitted from the plot in order that the intermediate velocity distribution could be shown.

Calculated $\phi$'s are compared with measured values in Figure 7. Analytical results were normalized at a $\phi$ of 1.45 at 7° since the computer program predicts a $\Delta\phi$. The 7° reference point corresponds to the $\phi$ measured for the 7° hypermixing nozzle configuration, used in the XFV-12A airplane. Results are for an $A_3/A_2 = 1.9$, $A_2/A_0 = 16.2$, and an $L/D = 1.8$, where D is the throat width. Up to about 20°, the predicted trend agrees with measured values. Beyond 20°, calculated $\phi$'s decreased while the measured values remained essentially constant.
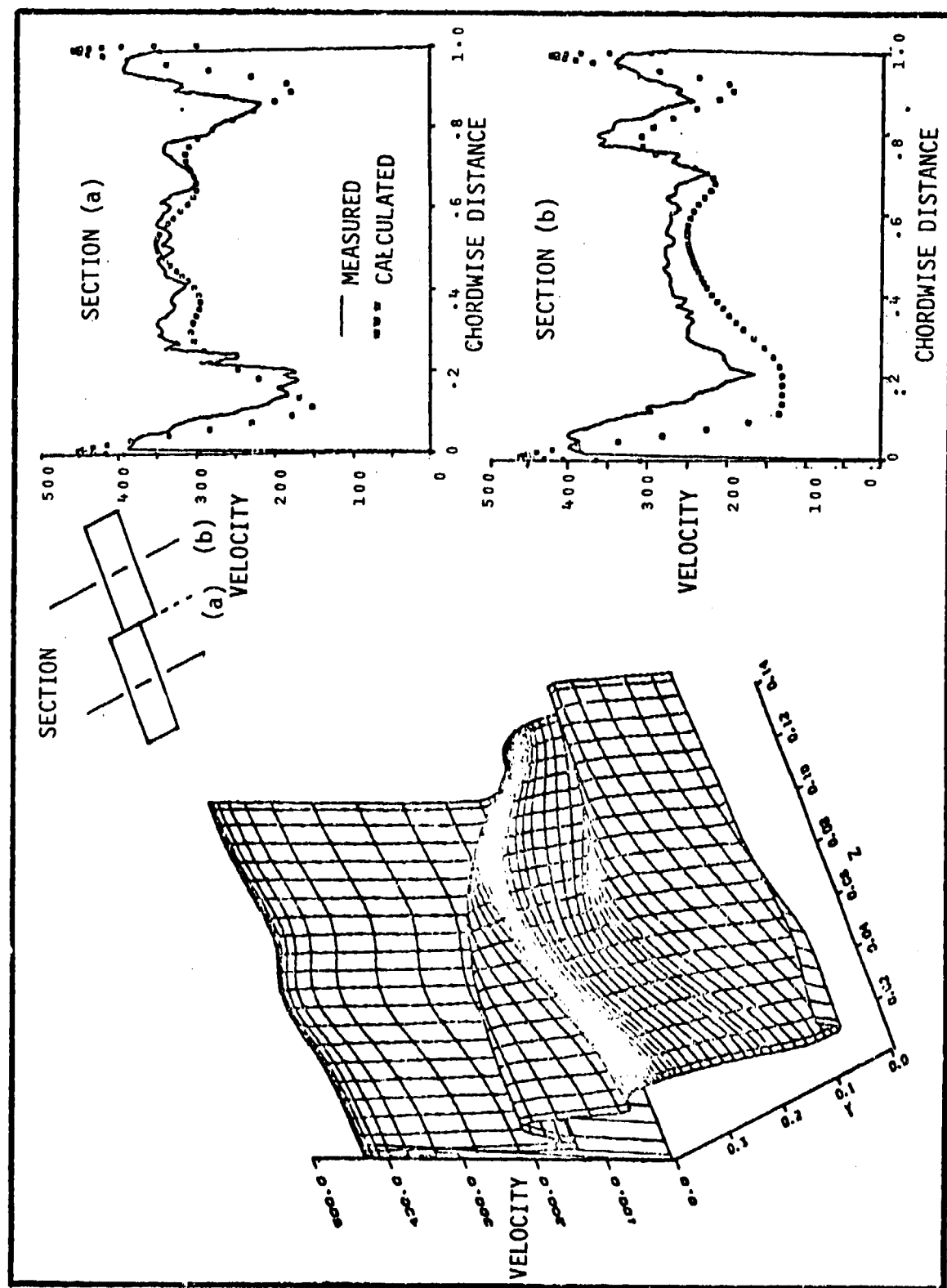
Figure 6. Comparison of Calculated and Measured Velocity Profiles at Ejector Exit for 22.5° Hypermix Nozzles
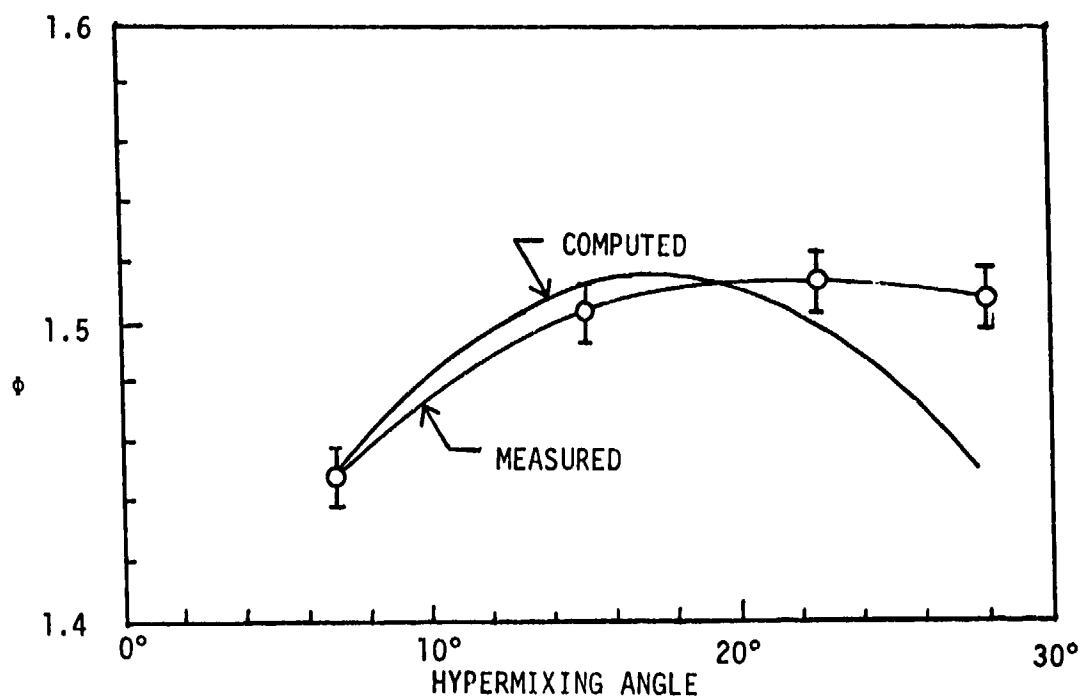
Figure 7. Comparison of Measured and Computed Augmentation

With the increasing hypermixing angle, the swirling or vortex action should increase and therefore additional swirl terms (originally deleted to reduce computer time) should be included in the turbulence generation term, G (Equation 4). With the addition of all swirl terms in G for the 28° case, the calculated $\phi$ increased by only 0.01. The lack of agreement beyond about 20° is attributed to a limitation in the manner used to solve the flow equations, in that the V and W velocity components should be much smaller than the mainstream velocity, U. At high swirl angles this may not be true.

Since good agreement of calculated and measured velocities were obtained along with the general $\phi$ trends, the computer program was used in the design and analyses of other nozzle configurations, discussed in the following sections.

Asymmetric Nozzles

This type nozzle was developed in an effort to capitalize on the generally superior entrainment characteristics of the symmetric cross-slot nozzle configuration while maintaining packaging limits imposed by supersonic airfoil contours. The design combines a series of aft facing, spanwise slot nozzles with an alternating series of cross-slots on the

forward side. An upstream view of the 14 element, asymmetric centerbody nozzle along with a side view is shown in Figure 8. The aspect ratio of the span slot is 5.5.
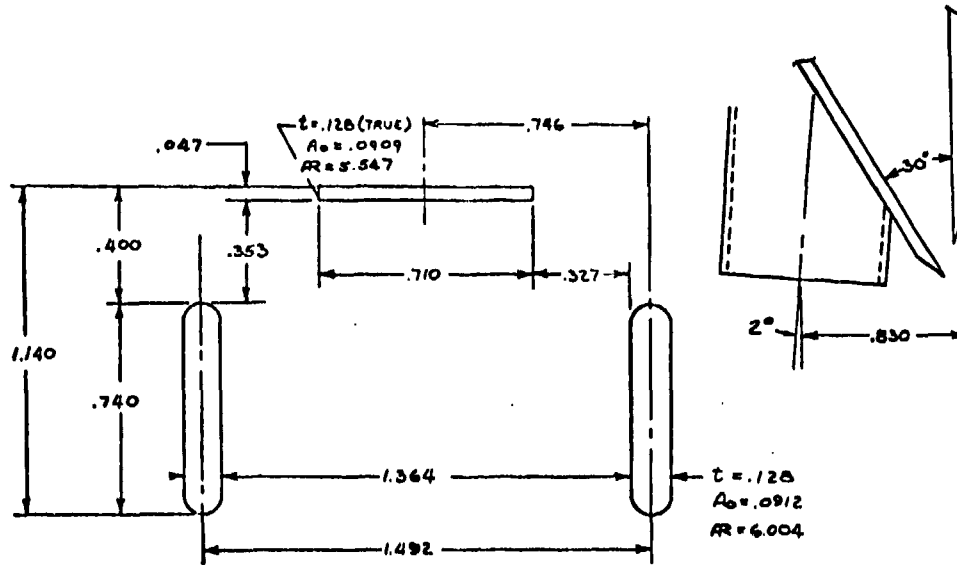


Figure 8. 14 Element Asymmetric Nozzle

The computer program was used to indicate expected $\Delta\phi$ trends. Tests were then used to confirm the predicted trends. For example, to increase $\phi$ it was analytically shown that for this type nozzle, it is necessary to increase the throat width, $A_2$, to prevent the merging of the cross-slot and Coanda jets. In Figure 9 the measured maximum $\phi$ for the 5.4 aspect ratio configuration, wide throat was 1.53, an increase of 0.02 over the hypermixing peak value (Figure 7).

836
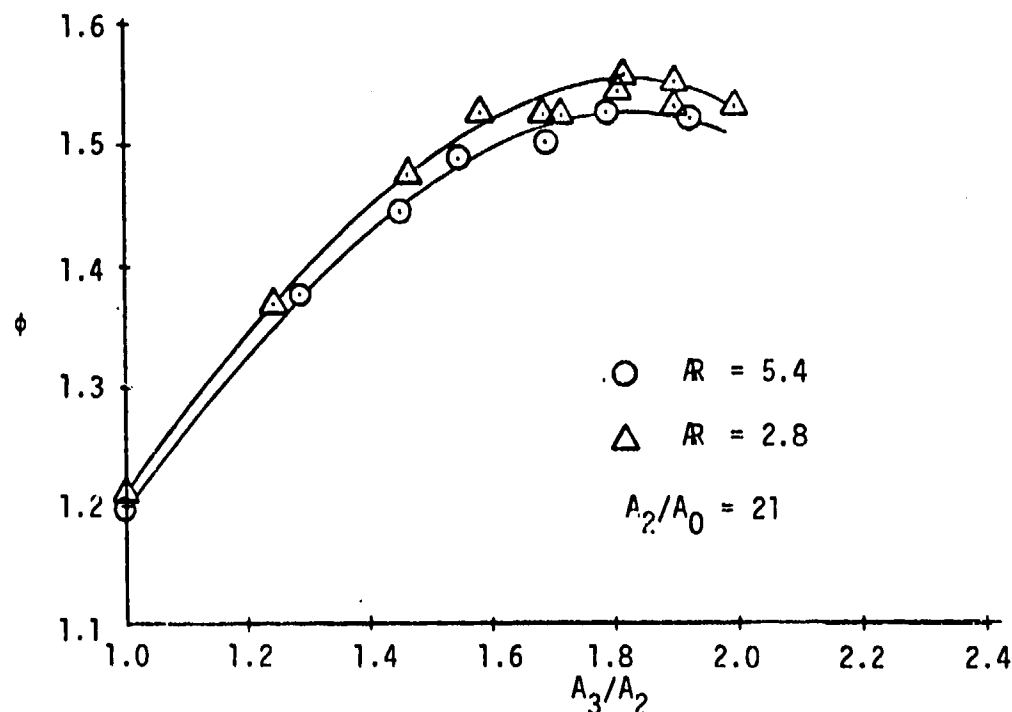
Figure 9. Effect of Span Slot Aspect Ratio, Asymmetric Nozzles

Further analyses showed that when the aspect ratio of the span slot is reduced from 5.5 to 2.8, the $\phi$ should increase by 0.03. Measurements (Figure 9) showed a gain of 0.02. The peak $\phi$ for the asymmetric con-figuration was 1.55, a $\Delta\phi$ of 0.04 above the peak for the hypermixing nozzles.

Calculated and measured velocities for the smaller aspect ratio con-figuration are shown in Figure 10. Velocity profiles are similar.

## Symmetric Nozzles

Based on the previous analytical and experimental results neither the hypermixing or asymmetric nozzles provided a $\phi$ of the order of 1.65, the target value. The computer program, however, has been proven useful in their design and evaluation. To obtain reliable results, the program does require an accurate description of the flow conditions at the inlet computational plane, particularly that of the primary flow. Secondary flow angularity was discussed earlier. Therefore, the study of the symmetric nozzles was concerned with primary flow angularity measurements, the design and testing of a nozzle to capitalize on these measurements, and finally the effect of geometric variations on $\phi$.
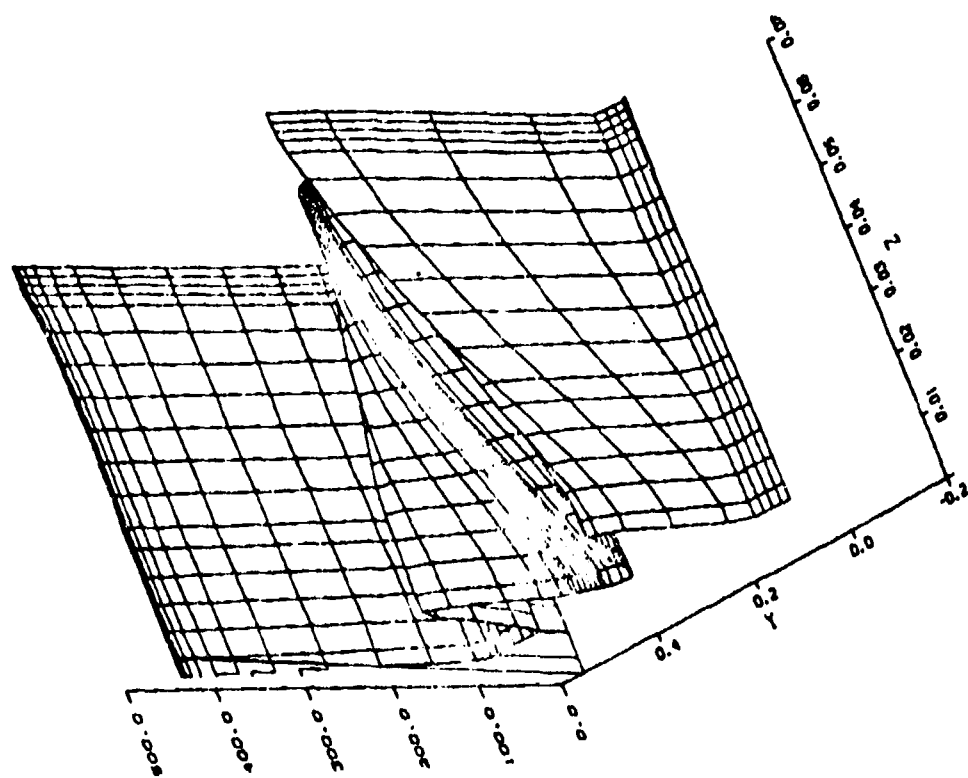
COMPUTED
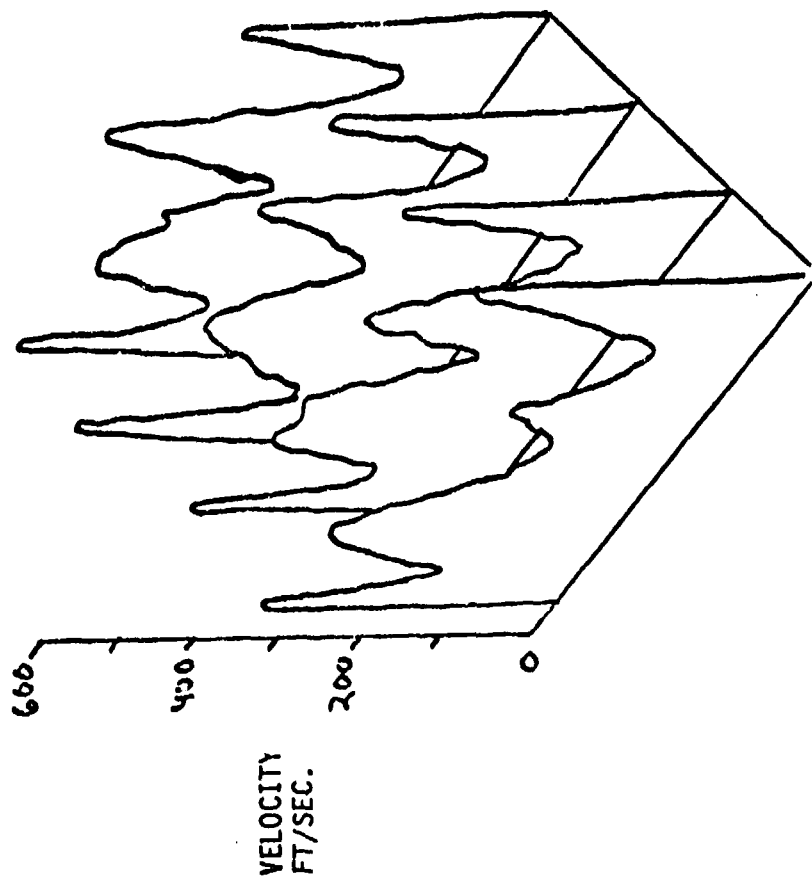
MEASURED

Figure 10. Comparison of Velocity Profiles at Ejector Exit for Asymmetric Nozzles

The symmetric nozzle configurations consist of either a series of symmetric cross slots or a series of cross slots with intermediate span slots. Figure 11 shows schematically the downstream vortex action for symmetric cross slots, in the absence of span slots.



Figure 11. Symmetric Cross Slot Flow Pattern

Figure 12 presents a typical cross slot-span slot configuration. In this configuration the thickness of the cross slot gap is shown to vary linearly from the centerline. In other configurations this thickness is held constant. Geometric design parameters are shown in Figure 13.



Figure 12. Typical Cross Slot-Span Slot Configuration

1　　BOAT-TAIL ½ ANGLE
2　　LAUNCH ANGLE
3　　WEDGE ANGLE
4　　½ WIDTH
5　　INNER GAP
6　　OUTER GAP

BOWTIE RATIO = OUTER GAP/INNER GAP

CROSS SLOT ASPECT RATIO = $(\text{WIDTH} - \text{SPLITTER})^2/\text{AREA}$

Figure 13.　Cross Slot Geometric Parameters

840

Cross Slot Primary Flow Discharge Angle: Angularity measurements were made. Figure 14 presents the data for four nozzle configurations having the following wedge and launch angles: (a) 0°, 21°; (b) 21°, 21°; (c) 11°, 17.2°; and (d) 21°, 9°. Schematics of the corresponding nozzles are also shown. The abscissa is the nondimensional distance from the center-line to the edge of the nozzle. Measurements were made under four nozzles in each configuration. There is some scatter due to slight manufacturing differences for the small scale model augmenters, evident in Figure 14(c). For analytical purposes, the profile shapes were approximated by straight lines. Calculated $\Delta\phi$'s are shown in Figure 15 for a linearly varying and for a constant angular distribution. The abscissa is the average of the angle at $S = 0$ and $S = 1$. Analytically, a nozzle having the linearly varying flow angle provides a greater $\Delta\phi$. To verify the trend, a cross slot nozzle was designed to provide this type profile (Figure 16). Figure 17 presents a comparison of the measured flow angularity with the desired linear distribution. The results demonstrate that a nozzle can be designed to provide a desired distribution. For this configuration the predicted $\Delta\phi$ was 0.30. The measured value was 0.24 (Figure 15).

Bowtie Ratio: A "bowtie nozzle" shape (cross slot nozzle gap varying, as shown in Figure 12) should increase entrainment and, hence, $\phi$ by placing more primary flow into the "dog bone" vortices at the cross slot tips (Figure 11). Analytical results are compared with experimental results in Figure 18. Up to a bowtie ratio of about 2, $\phi$ does increase as predicted.

Span Slot-Cross Slot Flow Split: Both analytical and experimental tests were conducted with the cross slot-span slot configurations to determine the effect of flow split. Flow split is defined as the ratio of the flow through the span slots to the total primary flow. Results are compared with data in Figure 19. Best performance is obtained when the flow to the span slot is about 40 percent or less. These results are understandable since the downstream jet expansion from the span slot can generate destructive interference with the flow from the cross slot.
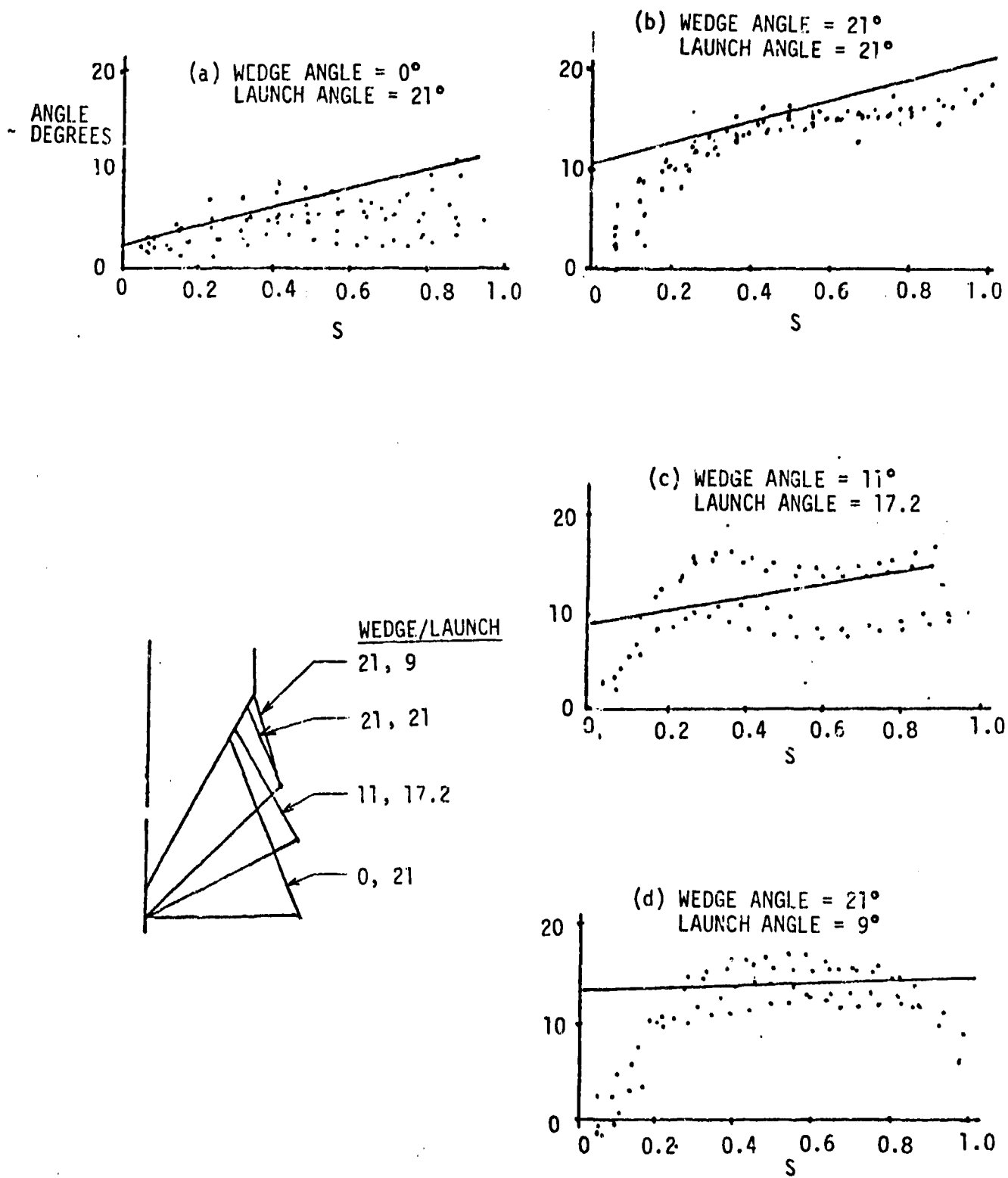
Figure 14. Cross Slot Nozzle Exit Flow Angles
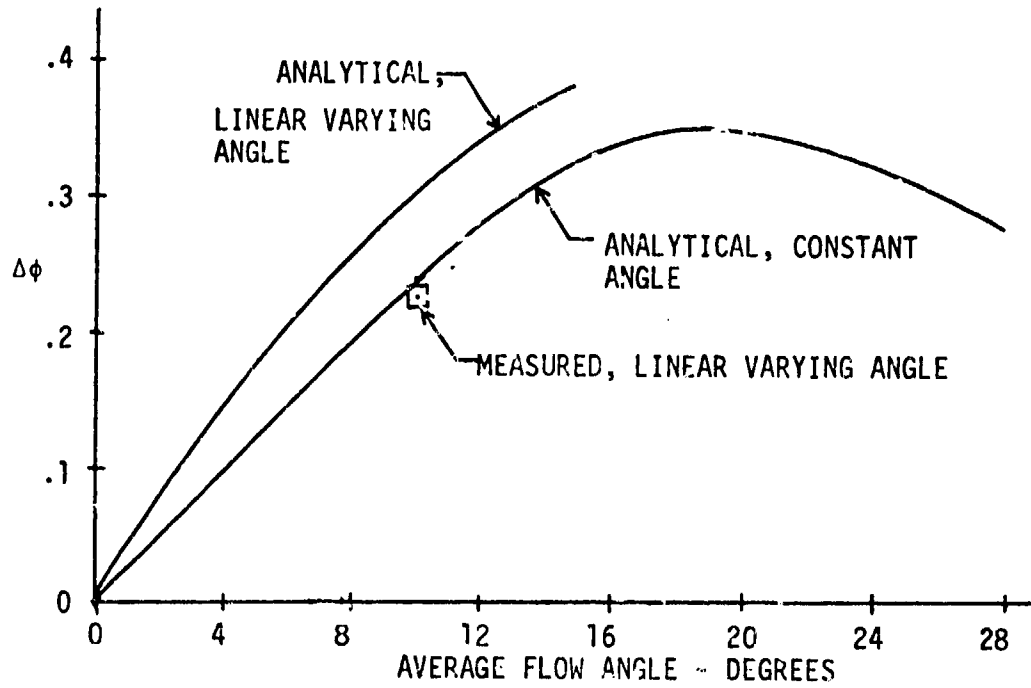
Figure 15. Effect of Constant and Linearly Varying Cross Slot Exit Angularity on Δφ.
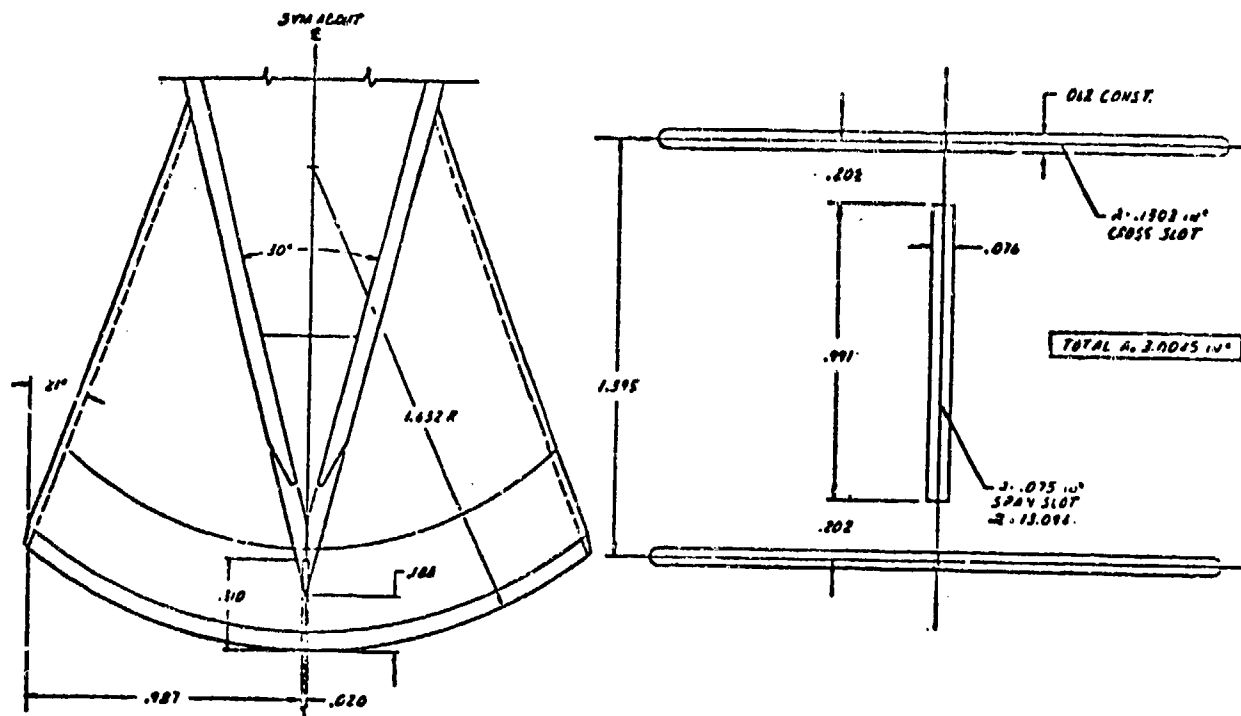


Figure 16. Cross Slot-Span Slot Nozzle with a Linearly Varying Exit Profile.

843
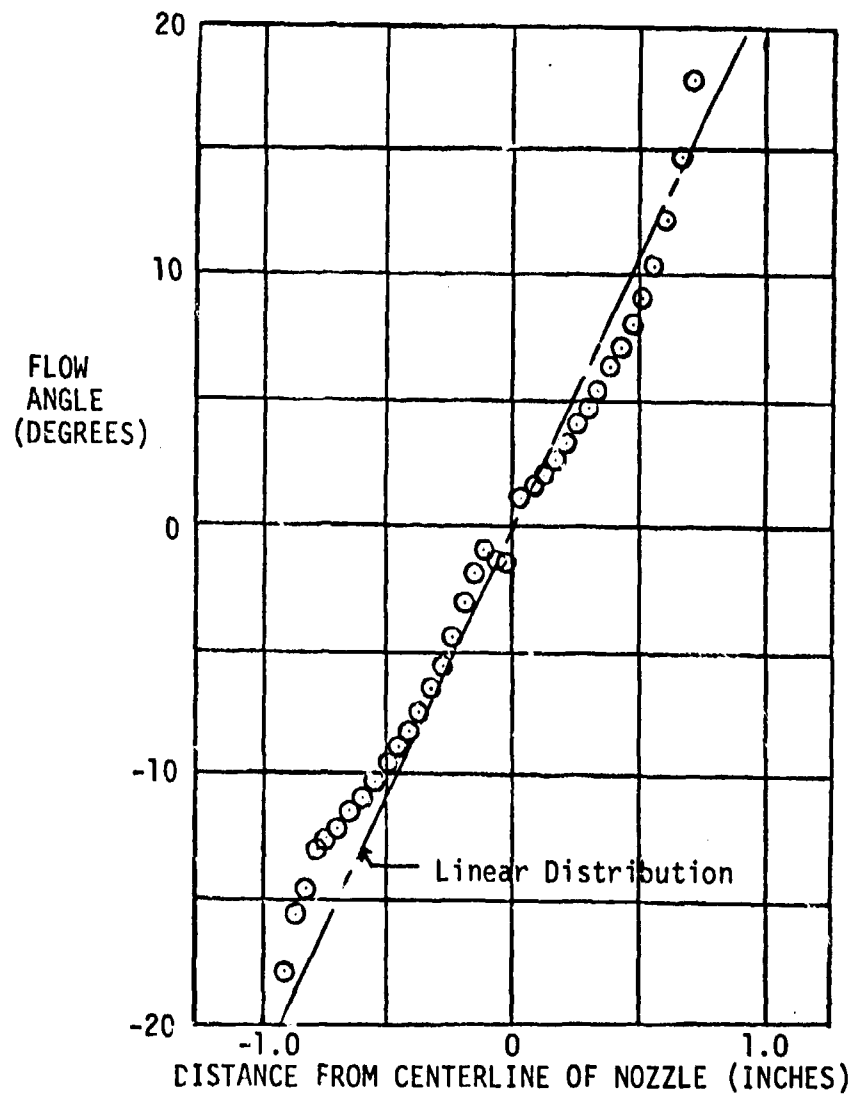
Figure 17. Measured Flow Angles for Linearly Varying Slot Nozzle Configuration.
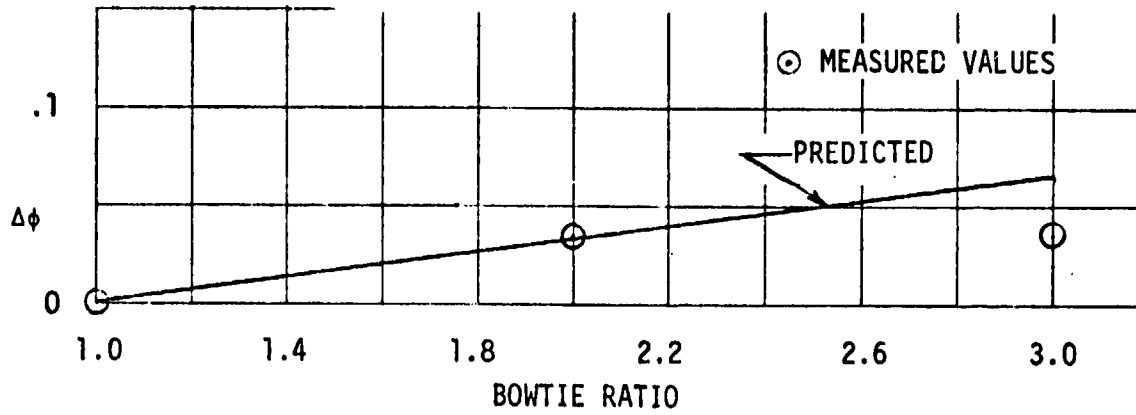
Figure 18. Effect of Bowtie Ratio
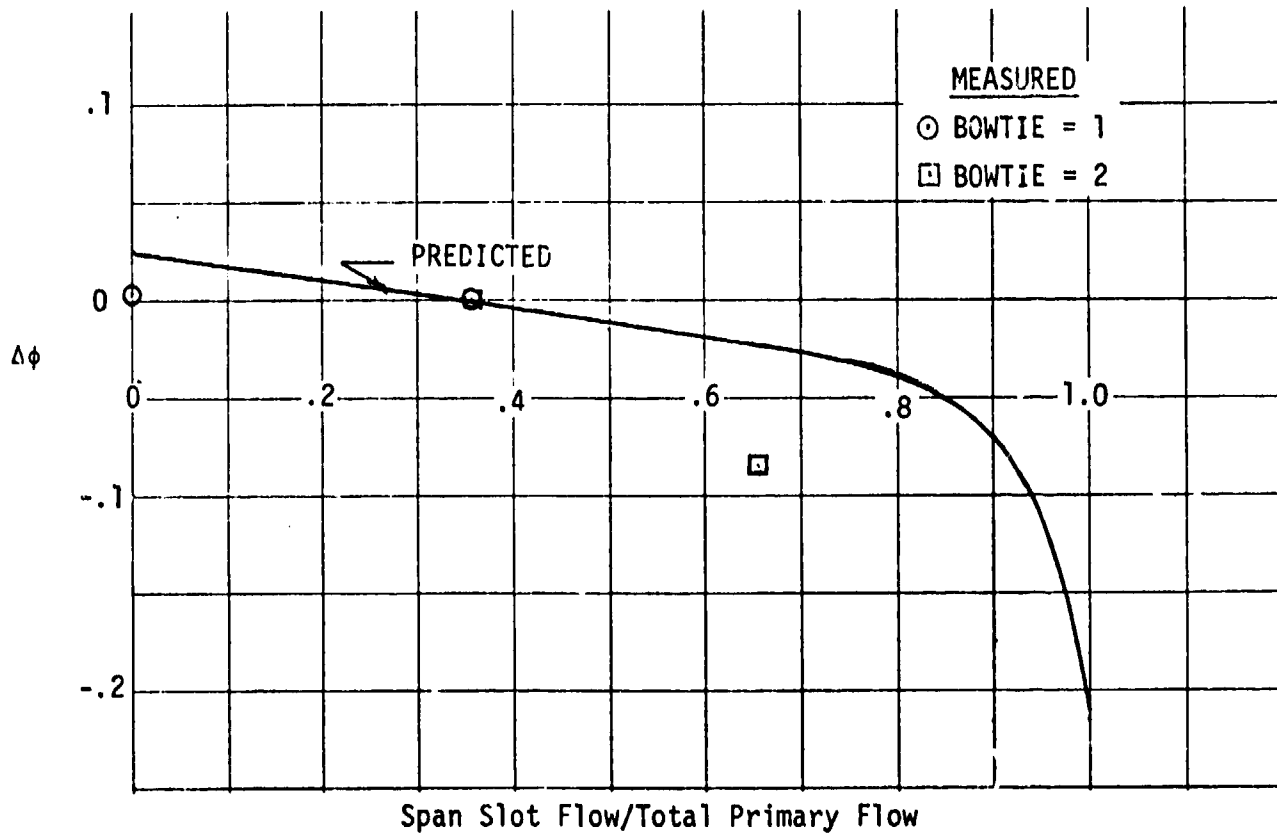


Figure 19. Effect of Flow Split

845

Cross Slot Aspect Ratio: Since the results in the previous section showed that the percent primary flow to the cross slot nozzle should be increased, the next logical step was to investigate the effect of cross slot aspect ratio. Earlier work by Peschke[7] showed that the entrainment for 2-dimensional free jets is increased with aspect ratio. Predicted results for augmenters (Figure 20) show that $\Delta\phi$ is increased with cross slot aspect ratio; however, physical width constraints must be considered.
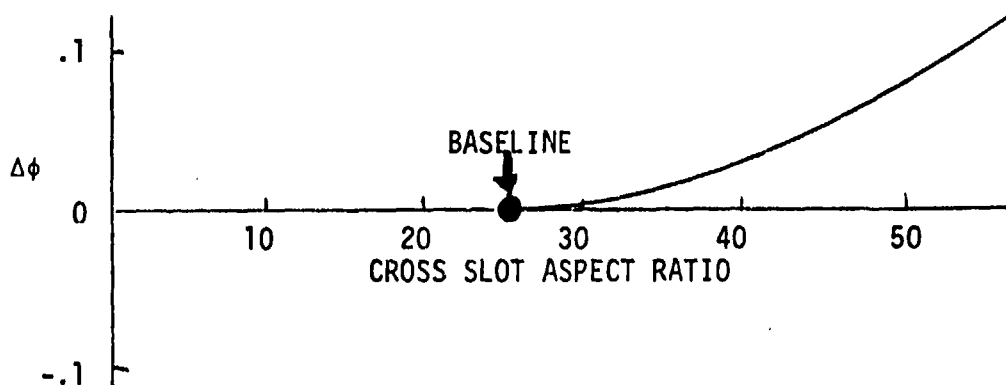


Figure 20. Effect of Cross Slot Aspect Ratio

Symmetric Nozzle Overall Performance: By combining the computer program with tests of the inlet flow angularity, geometric variations, etc., a measured peak $\phi$ of 1.64 was demonstrated for a cross slot-span slot configuration (Figure 16).


CONCLUSIONS


The following results were obtained from a combined analytical and experimental investigation of centerbody nozzle configurations.

.  By combining the data of hypermixing nozzle configurations with a 3-dimensional, turbulent kinetic energy computer program, an analytical procedure was developed for predicting the flow field in ejectors and their augmentation, $\phi$.

.  The measured $\phi$ for the 7° hypermixing nozzle, used in the XFV-12A airplane, was 1.45. It was analytically and experimentally shown that a peak $\phi$ of 1.51 could be obtained by increasing the hypermixing angle to 22°.

- Data for the asymmetric nozzle showed a peak $\phi$ of 1.55.

- Although larger $\phi$'s were obtained by extending the width of the cross slot, optimization studies and tests showed that to increase $\phi$ it was necessary to increase the bowtie ratio, relative flow to the cross slot, cross slot aspect ratio, and to provide a cross slot, exit velocity angularity which varied linearly with distance.

- By combining the computer program with test data of inlet flow angularity, geometric variations, etc., a measured peak $\phi$ of 1.64 was demonstrated for the cross slot-span slot configuration in which the exit angularity of the cross slot varied linearly with distance.

## REFERENCES

1. Bevilaqua, P. M., Lifting Surface Theory for Thrust-Augmenting Ejectors, AIAA Journal, Vol. 16, No. 5, May 1978, pp. 475-581.
2. Quinn, B. P., Compact Ejector Thrust Augmentation, Journal of Aircraft, Vol. 10, No. 8, August 1973, pp. 481-486.
3. Bevilaqua, P. M., Evaluation of Hypermixing for Thrust Augmenting Ejectors, Journal of Aircraft, Vol. 11, No. 6, June 1974, pp. 348-354.
4. DeJoode, A. D. and Patankar, S. V., Prediction of Three Dimensional Turbulent Mixing in an Ejector, AIAA Journal, Vol. 16, No. 2, February 1978, pp. 145-150.
5. Launder, B. E. and Spalding, D. B., The Numerical Computation of Turbulent Flows, Computer Methods in Applied Mechanics and Engineering, Vol. 3, No. 2, March 1974, pp. 269-289.
6. Mefferd, L. A. and Bevilaqua, P. M., Computer-Aided Design Study of Hypermixing Nozzles, NR78H-91, NASC Contract N00019-77-C-0527, July 1978.
7. Peschke, W., Advanced Ejector Thrust Augmentation Study - Mass Entrainment of Axisymmetric and Rectangular Free Jets, AFFDL-TR-73-55, April 1973.

# THEORY AND PRACTICE OF EJECTOR SCALING

by

P. M. Bevilaqua and C. P. Combs

Rockwell International, North American Aircraft Division

Columbus, Ohio

Paper Presented at

Ejector Workshop for Aerospace Applications

August 3-5, 1981/Dayton, Ohio

Rockwell International

849

# THEORY AND PRACTICE OF EJECTOR SCALING

by

P. M. Bevilaqua and C. P. Combs

Rockwell International, North American Aircraft Division

## ABSTRACT

Procedures are described for utilizing scale models for the development of thrust augmenting ejectors. Physical reasoning and the methods of dimensional analysis are used to argue that the Mach numbers must be matched, but that the Reynolds number is not a relevant parameter if its value is large. Numerical analysis is used to show that almost no change in performance may be expected from the use of cold air jets. Experimental data is presented to support these results. Thus, it is concluded that scale model ejectors powered by cold jets provide a close approximation to the performance of full size ejectors powered by hot jet exhaust flows.

# INTRODUCTION

Scale model testing of thrust ejector systems and their associated components provides a convenient low cost alternative to full size test and development programs. The applicability of model scale test data in the prediction of conventional aircraft performance through the use of certain scaling laws has long been accepted practice. Unfortunately, the development of full size thrust ejector systems utilizing model scale testing is not as universally accepted.

Inconsistencies in the results of available ejector scaling studies imply that we cannot simply scale an ejector model geometrically and assume that its performance will be representative of its full size counterpart. However, by the use of physical reasoning and mathematical analysis, a scaling rationale for the design of useful model tests has been developed. Applying physical reasoning and the laws of dimensional analysis, it will be shown that the performance of model scale ejectors driven by cold air jets should approximate the performance of their full size counterparts driven by aircraft gas turbine propulsion systems.

Utilization of this rationale in conjunction with highly controlled specific test procedures and methods has resulted in providing substantiation for utilizing model scale ejectors in the development for full size ejector systems.

## Ejector Scaling Rationale

In order to set up a meaningful test, the fundamental parameters on which the thrust augmenting force depends must be identified. If it is assumed that this force is a function of the jet thrust, the ejector shroud geometry, and the physical properties of the fluid, dimensional analysis yields for the scaling law

$$F/T = f(Re, M, L/W, \delta)$$

in which the force coefficient, $F/T$, is the ratio of the augmenting force to the jet thrust, Re and M are the jet Reynolds number and Mach number, and $L/W$ and $\delta$ give the length to width ratio and divergence angle of the ejector shroud. The force coefficient also depends on the surface roughness and ambient turbulence level, but these parameters should be controlled to insure that their effect is small. Temperature effects are usually assumed to be implicit in the variation of the Mach and Reynolds numbers; however, an additional effect of temperature on the turbulent mixing will be discussed separately.

The geometry of a scale model can easily be made to duplicate the full size prototype, but it is not possible to simultaneously match the Mach and Reynolds numbers of the prototype; for example, if the Mach numbers are matched, then the change in scale means the model Reynolds number will be smaller. Similarly, if the Reynolds numbers are matched

852

by increasing the model velocity, then the model Mach number will be larger. However, because the velocity of the prototype jet is large (M > 1), the Reynolds number is also large (Re ≈ $10^6$), so that the flow is turbulent and the effects of viscosity are small. In this case, changes in the Reynolds number only affect the very smallest scales of the turbulence, which do not interact directly with the main flow. According to this principle of asymptotic invariance, the Reynolds number is not a relevant parameter if its value is large.

Therefore, if the Mach numbers are matched and the Reynolds numbers are large, scale model tests can be used to determine the variation of ejector thrust with nozzle geometry and diffuser angle for a given ejector configuration. On the other hand, the angle at which the flow separates, and other phenomena which relate to the exact details of the viscous stresses, are dependent on the Reynolds number. Thus, unless the Reynolds number is matched, model values of the separation angle cannot always be used to predict full size separation angles. Typically, separation will occur at a smaller angle on the scale model due to the predominance of the viscous stresses resulting from the lower value of Reynolds number. Therefore, the assumption that the full size ejector separates at the same angle as the scale model should be a conservative estimate.

As previously noted, the first order effects of temperature on the physical properties of the jet (density, viscosity, and compressibility) are implicit in scaling the Mach and Reynolds numbers. In particular, the Mach number (M ≈ V/a) is independent of temperature, since both the jet velocity, V, and the speed of sound, a, have the same dependence on temperature:

$$\text{jet velocity} \qquad V = \left[ \frac{2\gamma}{\gamma - 1} RT_0 \left( 1 - \left( \frac{P}{P_0} \right)^{\frac{\gamma - 1}{\gamma}} \right) \right]^{\frac{1}{2}}$$

$$\text{speed of sound} \qquad a = \left( \gamma \, RT_0 \right)^{\frac{1}{2}}$$

The jet thrust is also independent of temperature, since the velocity increase is balanced by a decrease in density. The variation of Reynolds number with temperature is shown in Figure 1. The effect of reducing the jet temperature by 1000°F, as in the present case, does not change the order of magnitude of the Reynolds number.

The effect of temperature on the rate of turbulent mixing is not as straightforward. For small density differences, the mixing rate is proportional to the velocity difference between the two streams. If the density difference is large, the mixing rate is proportional to the momentum difference. Thus, a small temperature difference will probably increase the mixing rate ($\Delta V \sim T_0^{\frac{1}{2}}$) while a large temperature change will probably decrease mixing ($\Delta \rho V \sim T_0^{-\frac{1}{2}}$), although this has not been proven.

The net effect of the 1000° temperature decrease used for these scale model tests was calculated with the TKE program to be a .03 increase in augmentation. This is almost within the accuracy of the calculation procedure; however, the available data seem to support this result.[1-4] This is shown in Figure 2. Although all the data except that of Lockheed also included a scale or configuration change, the trend is consistent. Thus, a small increase in performance may be expected as a result of using cold jets in the scale model testing. However, for the temperature range of interest, the temperature effect is almost within the range of computational and experimental error.

Therefore, based on theoretical arguments, if primary flow Mach numbers are matched while Reynolds numbers are held large enough to assure turbulent flow, it may be concluded that model scale ejectors powered by cold jets should approximate the performance of large scale ejectors powered by hot flow jets.

A study of ejector scale effects performed at Pennsylvania State University indicated that the thrust augmentation increases with ejector scale. However, aircraft scale ejectors built by both Boeing and DeHavilland produced less augmentation than the laboratory models from which they were developed. While initially these results appear inconclusive, it is believed that the inconsistencies may relate to differences between the model scale and full size tests. Model construction techniques, primary jet temperature, and test procedures all must be accounted for during investigations of ejector scale.

## Ejector Test Techniques

In order to minimize the influence of experimental error which may in some part explain the observed inconsistencies in previous ejector scale investigations, attention must be given to developing well controlled test procedures and methods.

At Rockwell, scale model ejector tests are normally performed at the Columbus plant's thermodynamics laboratory utilizing test stands specially designed and fabricated for ejector test applications. Each test stand is basically a floating frame attached to an outer fixed frame through a set of load cells to measure the ejector's forces. Figure 6. Tension is maintained on the load cells with dead weight cable suspended preloads. Air flow is supplied from the laboratory's compressor via four individually controlled supply lines. The air supply system is equipped with particle filters and dryers in order to remove contaminants from the primary air supply. Excessive variations in air flow temperature are eliminated through the use of a compressor system cooling tower.

Each air supply line has a venturi meter with the necessary instrumentation attached to calculate mass flows using standard venturi meter equations. The four lines are fed to the diffuser, centerbody, elevon, and endwall blowers (BLCS) through four flexible 2-inch hoses. These flexible lines prevent excessive tare when bringing the lines across the metric part of the load stand.

Load cells, pressure transducers, and thermocouples are connected at appropriate test points on the load stand, model, and air supply system to monitor forces, pressures, and temperatures. These transducers are periodically calibrated using standard laboratory practice with calibration equipment traceable to the National Bureau of Standards.

The Thermo Lab's data system is capable of monitoring 48 channels of transducer analog output data and incorporates all signal conditioning and amplification prior to signal processing by an IBM 1800 computer. The data system also has the capability of performing an electrical test of the transducer's bridge integrity by use of a resistance calibration test (R-CAL). This is routinely done by the computer prior to each test run, and any drift in transducer excitation or signal amplification is automatically compensated for by the computer. Prior to each test run, the load cells are checked by preloading with calibrated lead weights, thus assuring their accuracy before collecting test data.

Data acquisition and reduction is handled by an IBM 1800 computer that contains a 48 channel multiplexer and a 14 bit plus sign analog to digital converter.

Data reduction is accomplished by appropriate user-written computer programs. Conversion constants for all transducers are contained in the software and utilized to convert transducer electrical outputs to equivalent engineering units. Appropriate equations are programmed to calculate augmenter air flow parameters such as isentropic thrust, flow coefficients, velocity Reynolds number, etc. A typical printout of relative ejector performance parameters is shown in Figure 3. Selected parameters are calculated and punched into cards for additional data analysis utilizing a timeshared IBM 370 computing system.

Data Error and Repeatability

Prior to applying model scale test results to the development of full size ejector systems, it is useful to develop an understanding of the test data accuracy and repeatability. The definition of augmentation ratio ($\phi$), utilized in Rockwell's ejector development program is

$$\phi = \frac{\text{Ejector Lift (Thrust)}}{\text{Nozzle Isentropic Thrust}} = \frac{\text{Load Cell Measured Lift}}{\underset{\text{Measured}}{(\text{Mass Flow})} \quad \underset{\text{Isentropic}}{(\text{Velocity})}}$$

Therefore, the fractional error in $\phi$ may be computed by:

$$\frac{\Delta\phi}{\phi} = \sqrt{\frac{\Delta\text{Lift}}{\text{Lift}}^2 + \frac{\Delta\text{Mass Flow}}{\text{Mass Flow}}^2 + \frac{\Delta\text{Velocity}}{\text{Velocity}}^2}$$

where the ($\Delta$) symbol signifies the probable error in the parameter of interest.

855

A close examination of the calibration accuracies of the instrumentation utilized to isolate the major parameters in the augmentation ratio ($\phi$) definition resulting in

Lift (load cell accuracy and hose tare corrections)   =   .25%

Mass Flow (calibration accuracy venturi and associated pressure transducers) = 1.29%

Velocity (calibration or pressure transducers)   =   .117%

Therefore:

$$\Delta\phi = \sqrt{(.0025)^2 + (.0129)^2 + (.00117)^2} = .0132$$

Therefore, an expected error in measured performance of 1.32% can be related to the accuracy of the instrumentation utilized during the scale model test program.

To determine the possible variation in augmenter performance over a short period of time and the possible error encountered by taking lift and pressure data at an instantaneous time slice, a series of runs were made comparing results where ten data samples were taken, averaged, and compared to results of a single sample data point. Figure 4 presents a comparison plot of single sample/data point vs. ten samples/per data point (@ one sec. time interval between samples). Results show that $\phi$ at any given time is comparable to $\phi$ over a period of ten seconds.

This sampling/averaging technique was further tested by increasing the time between samples from one sec. to ten secs. The lower plot on Figure 5 shows the results of one sample/sec. vs. one sample/ten sec. for a ten sample data point.

Based on these investigations the 10 sample-1 sample/sec. technique was incorporated as the standard sampling method in the data reduction routines.

Long term data repeatability was established by periodically restoring the model to a baseline configuration and examining its performance. Figure 10 presents a $\phi$ vs $A_3/A_2$ comparison of a four run series over a two week time period. The maximum scatter in $\phi$ was on the order of $\pm.013 \Delta\phi$.

By collectively evaluating the experimental error due to instrumentation accuracy and the data repeatability, it is possible to establish a band of experimental data scatter. For the example discussed this band was about $\pm.02 \Delta\phi$. Isolating and controlling the experimental data quality is an integral part of effective ejector scaling.

## Experimental Data

A survey of large scale ejectors previously developed by Rockwell International provides substantiating evidence that model scale ejectors can be utilized in the design of prototype scale ejector systems. In general large scale ejector systems have performed as well as or slightly better than their model scale counterparts. Figures 7 and 8. In one case shown in Figure 9 where a great deal of attention was given to exact geometric scaling, the same level of augmentation ratio ($\phi$) was achieved.

## CONCLUSION

Through the use of physical reasoning, mathematical analysis, and carefully controlled test techniques, scale model testing can be utilized in the development of large scale ejector systems. Experimental data have been obtained which provide substantiating evidence that model scale ejectors powered by cold air jets provide a close approximation to the performance of full size ejectors powered by hot jet exhaust flows. Further study of ejector scale and temperature effects is recommended to establish scaling relationships for ejector systems.

## REFERENCES

1) Phillips, J. D., Temperature and Pressure Effects on Thrust Augmentation, M.S. Thesis, The Ohio State University, 1975.
2) Dejneka, R., Influence of Driving Air Temperature on Thrust Augmenting Ejector Performance, NADC-PE-41, August 1930.
3) Gates, M. F., Cochran, C. L., Evaluation of Annular Nozzle Ejector, ARD-280, November 1980.
4) Rabeneck, G. L.; Shumpert, P. K.; and Sutton, J. F., Steady Flow Ejector Research Program, Lockheed Aircraft Corporation, Georgia Division, Final Contract Report NONC-3067(00), December 1980.
5) Fought, D. E., Test and Analysis of a Coanda Thrust Augmentation Nozzle, (A Thesis in Aeronautical Engineering), The Pennsylvania State University, January 1960.
6) Wang, T.; Wright, R.; and Mahal, Design Integration and Noise Studies for Jet STOL Aircraft, The Boeing Company, NASA CR114286, May 1972.
7) Whittley, D. C., Augmenter-Wing Technology for STOL Transport Aircraft, DeHavilland Aircraft of Canada, Ltd., High Lift Technology Course, Univ. of Tenn., 27 October 1975.
8) Mefferd, L. A.; Alden, R. E.; and Bevilaqua, P. M., Design and Test of Prototype Scale Ejector Wing, Paper at Workshop of Thrust Augmenting Ejectors, NASA Ames Research Center, June 1978.

REYNOLDS NUMBER

$$R_N = \frac{\rho V}{\mu} \qquad \rho \quad \text{DECREASES AS } T^{-1}$$
$$V \quad \text{INCREASES AS } T^{\frac{1}{2}}$$
$$\mu \quad \text{INCREASES AS } T^{\frac{1}{2}}$$

$$R_N \sim T^{-1}$$

REYNOLDS NUMBER DECREASES WITH
INCREASING TEMPERATURE
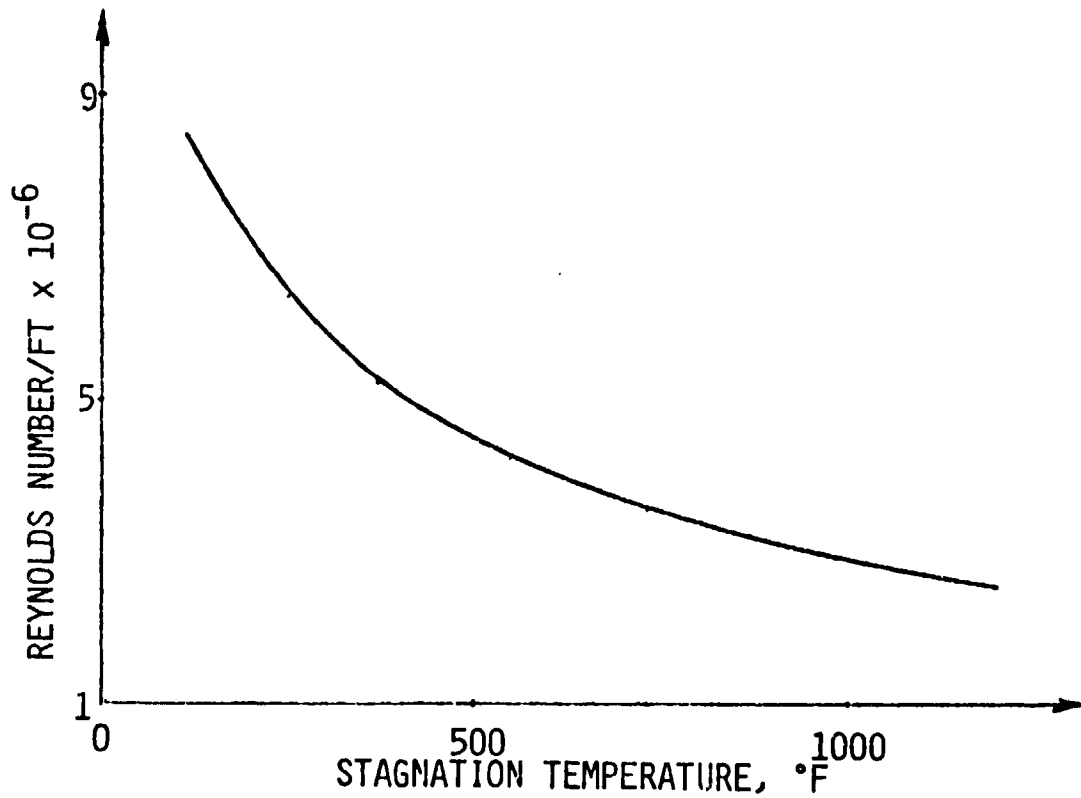


Figure 1.

# TEMPERATURE EFFECT
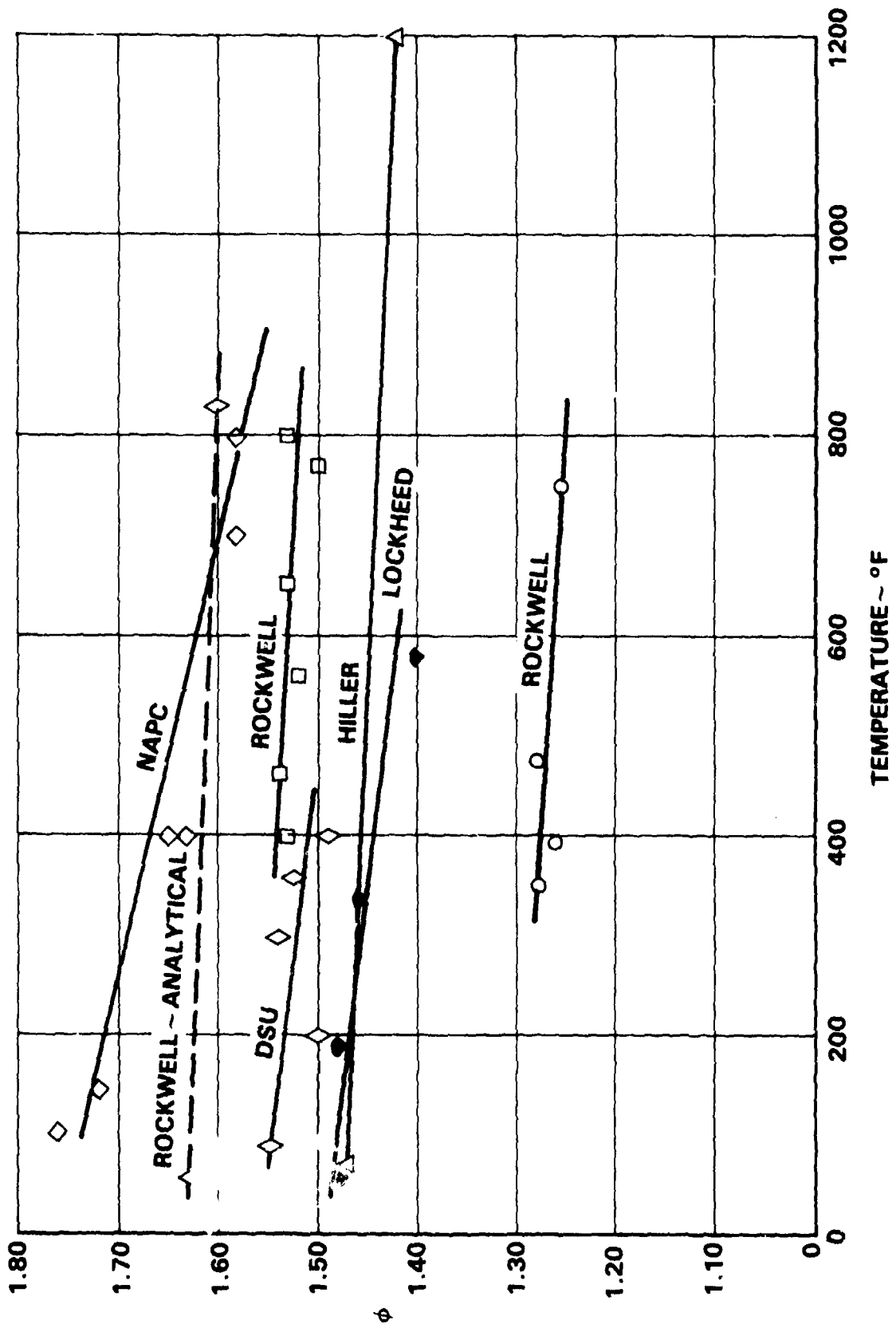


Figure 2.

FOD 924 0.2 RECT WG,15EL CRUC BT HT=1.60,CBA=0,F=24,(ORIG),EX=11.37, TH=5.019,A3/2=2.265,CB TAPS OFF,FRNGS

PT 3

|  |  |  | FWD COANDA | CENTERBODY | AFT COANDA | BLC |
|---|---|---|---|---|---|---|
| PHI 1.6543 | TFGI 126.0674 |  | FGI1 22.6879 | FGI2 75.0328 | FGI3 22.9383 | FGI4 5.4084 |
|  |  |  | FGI5 ********** |  |  |  |
| 1FEJC 208.5585 | AVCDN 0.9879 |  | CDN1 1.0113 | CDN2 0.9777 | CDN3 1.0224 | CDN4 0.8841 |
|  |  |  | CDN5 ********** |  |  |  |
| TWFN 3.6179 |  |  | WFN1 0.6359 | WFN2 2.1728 | WFN3 0.6354 | WFN4 0.1736 |
|  |  |  | WFN5 ********** |  |  |  |
| TWFV 3.5710 | PHIL 1.6543 |  | WFV1 0.6431 | WFV2 2.1246 | WFV3 0.6496 | WFV4 0.1535 |
|  |  |  | WFV5 ********** |  |  |  |
|  |  |  | PWFV1 | PWFV2 | PWFV3 | PWFV4 |
|  |  |  | PWFV5 ********** |  |  |  |
|  |  |  | PRN1 18.0107 | PRN2 59.4955 | PRN3 18.1931 | PRN4 4.3004 |
| DELTF 24.0000 | AVPRN 2.1988 |  | PRN1 2.1942 | PRN2 2.2006 | PRN3 2.1982 | PRN4 2.1958 |
|  |  |  | PRN5 ********** |  |  |  |
| DELTD 90.0000 | TAREA 5.0005 |  | AREA1 0.8812 | AREA2 3.0006 | AREA3 0.8788 | AREA4 0.2400 |
|  |  |  | AREA5 0.0000 |  |  |  |
| PBAR 14.2802 |  |  | VELN1 1135.8420 | VELN2 1137.1628 | VELN3 1136.8634 | VELN4 1133.9904 |
|  |  |  | VELN5 ********** |  |  |  |
| CLIFT 208.5585 | ULIFT 207.5764 |  | MNN1 1.0000 | MNN2 1.0000 | MNN3 1.0000 | MNN4 1.0000 |
|  |  |  | MNN5 ********** |  |  |  |
| CSIDE 0.0000 | USIDE 0.0000 |  | PTN1 31.3344 | PTN2 31.4263 | PTN3 31.3912 | PTN4 31.3577 |
|  |  |  | PTN5 ********** |  |  |  |
| CDRAG 0.0000 | UDRAG 0.0000 |  | PS1 89.8149 | PS2 42.3319 | PS3 91.8718 | PS4 33.1919 |
|  |  |  | PS5 ********** |  |  |  |
|  |  |  | RNV1 0.776E 06 | RNV2 0.194E 07 | RNV3 0.788E 06 | RNV4 0.185E 06 |
|  |  |  | RNV5 0.000E 00 |  |  |  |
|  |  |  | PV1 113.3789 | PV2 110.1443 | PV3 113.2390 | PV4 113.6570 |
|  |  |  | PV5 ********** |  |  |  |
|  |  |  | DPV1 2.2578 | DPV2 7.4836 | DPV3 2.3645 | DPV4 0.1291 |
|  |  |  | DPV5 ********** |  |  |  |
|  |  |  | TV1 534.0676 | TV2 533.5381 | TV3 533.9327 | TV4 531.8807 |
|  |  |  | TV5 ********** |  |  |  |

LFT LD CELL-NTH    LFT LD CELL-STH
109.4089           98.1674

DRG LD CELL-EST    DRG LD CELL-WST
0.0000             0.0000

SDE LD CEL-N.E.    SDE LD CEL-S.E.
0.0000             0.0000

SDE LD CEL-N.W.    SDE LD CEL-S.W.
0.0000             0.0000

CH-SAT1    CH-SAT2    CH-SAT3    CH-SAT4
0          0          0          0
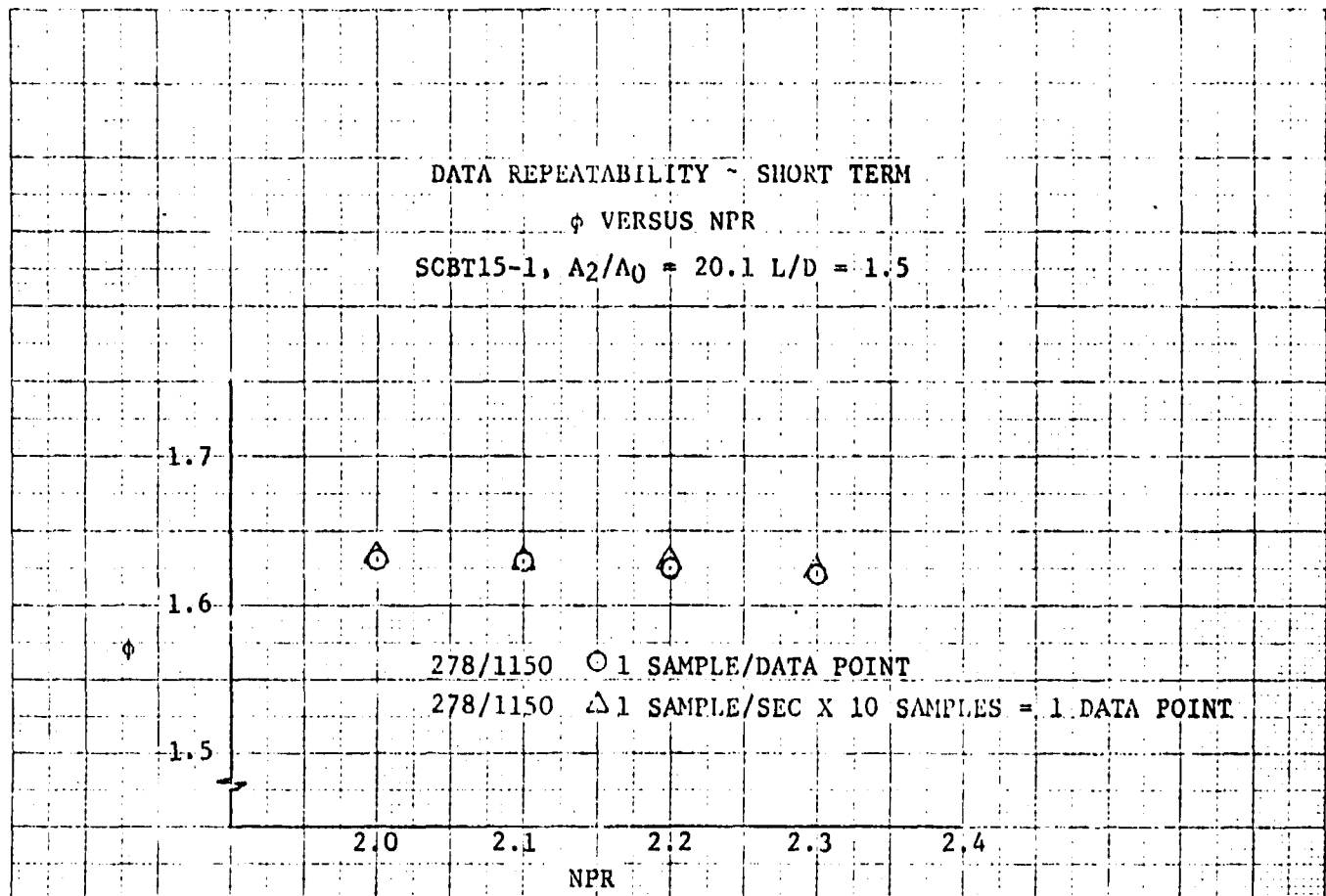
Figure 3.

Figure 4.



Figure 5.

Figure 6.

862
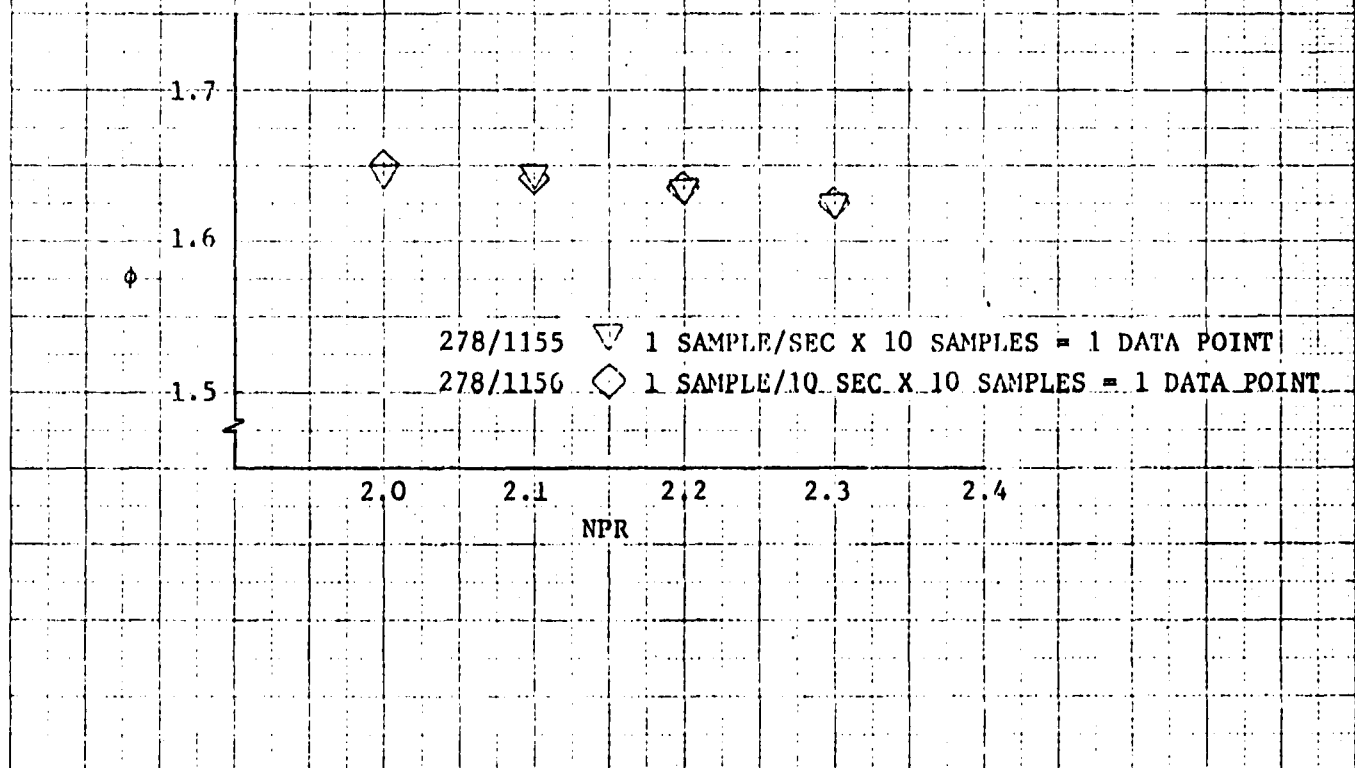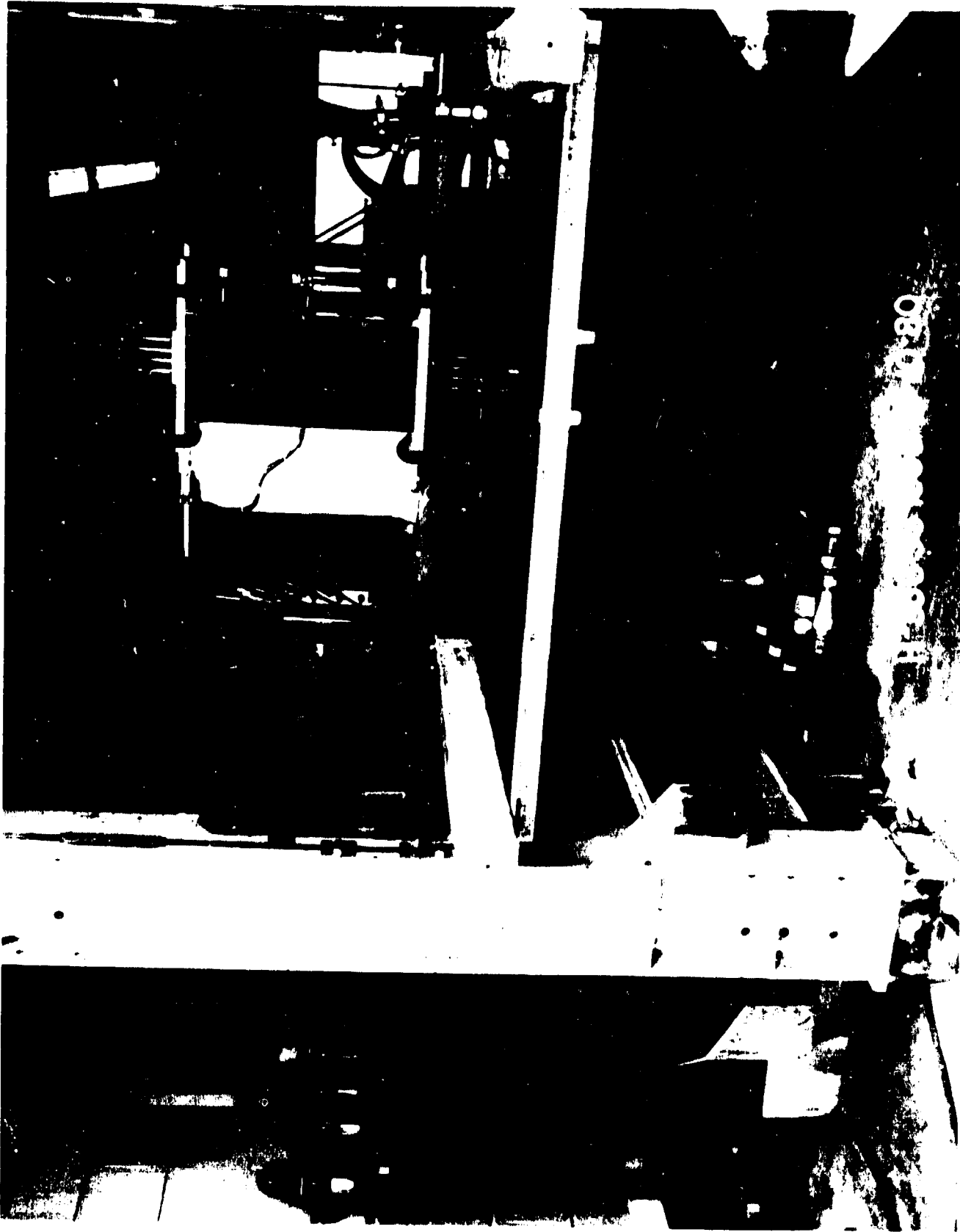
SUMMARY WING $\phi$ VS. $\delta_F$

Figure 7.

CAD 16000
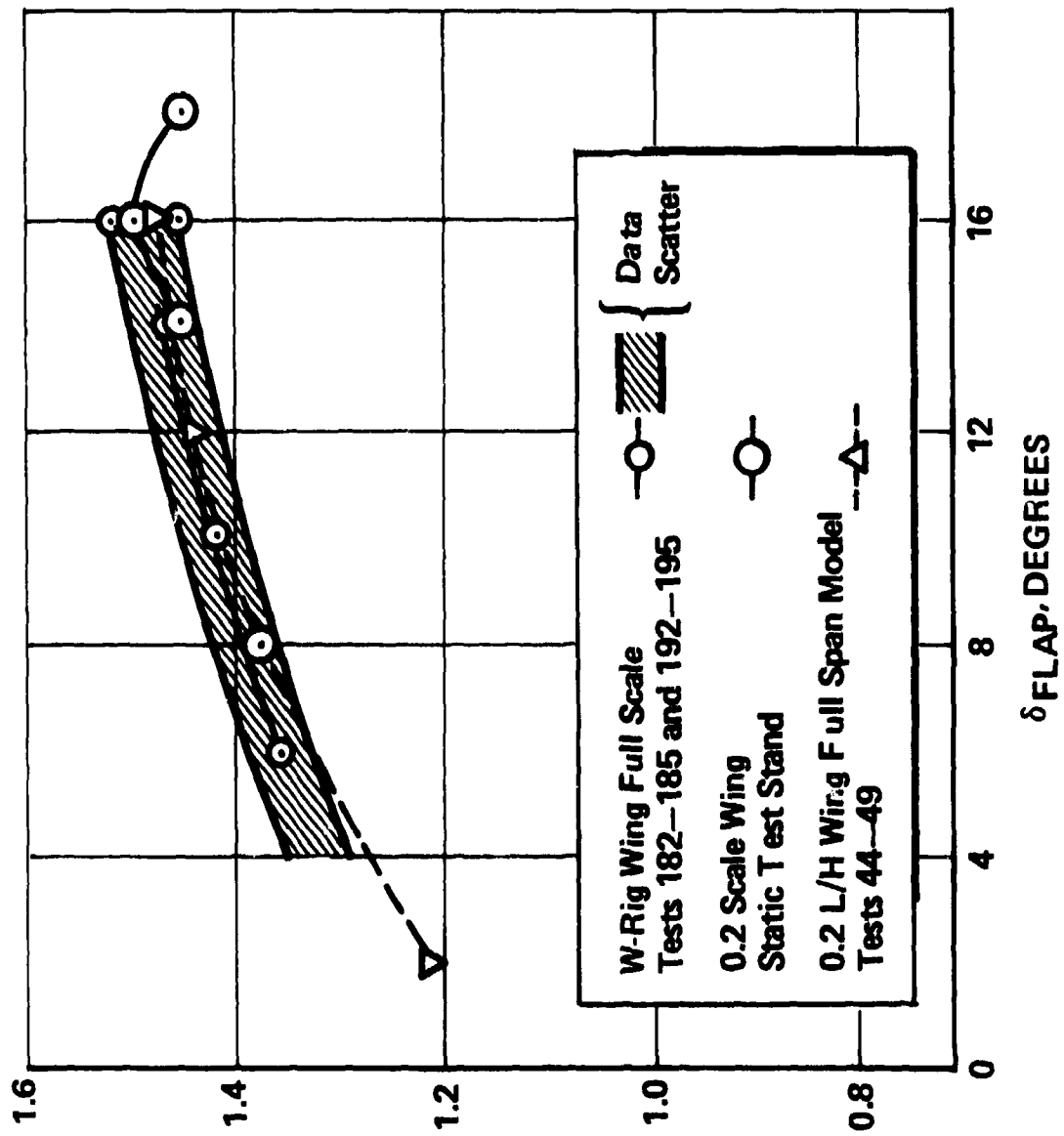
# SUMMARY CANARD $\phi$ VS. $\delta_F$



Figure 8.
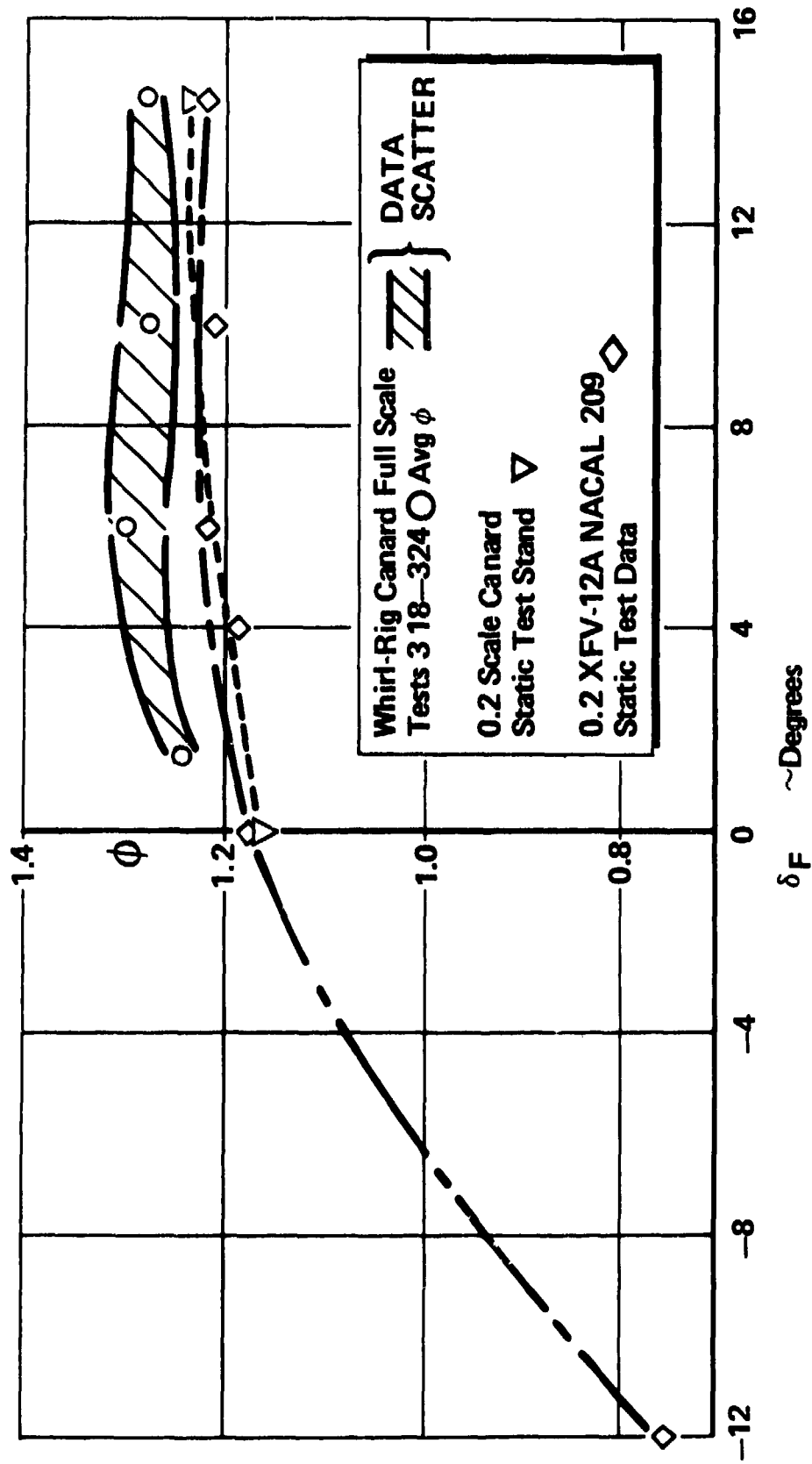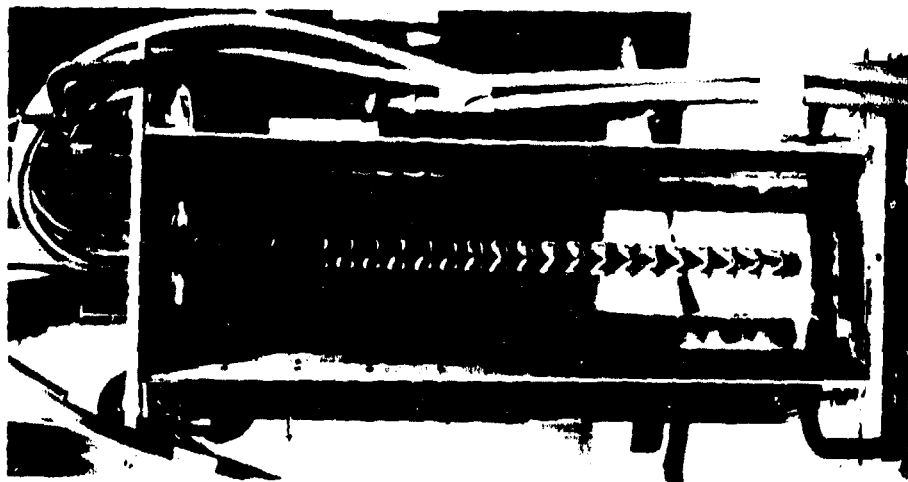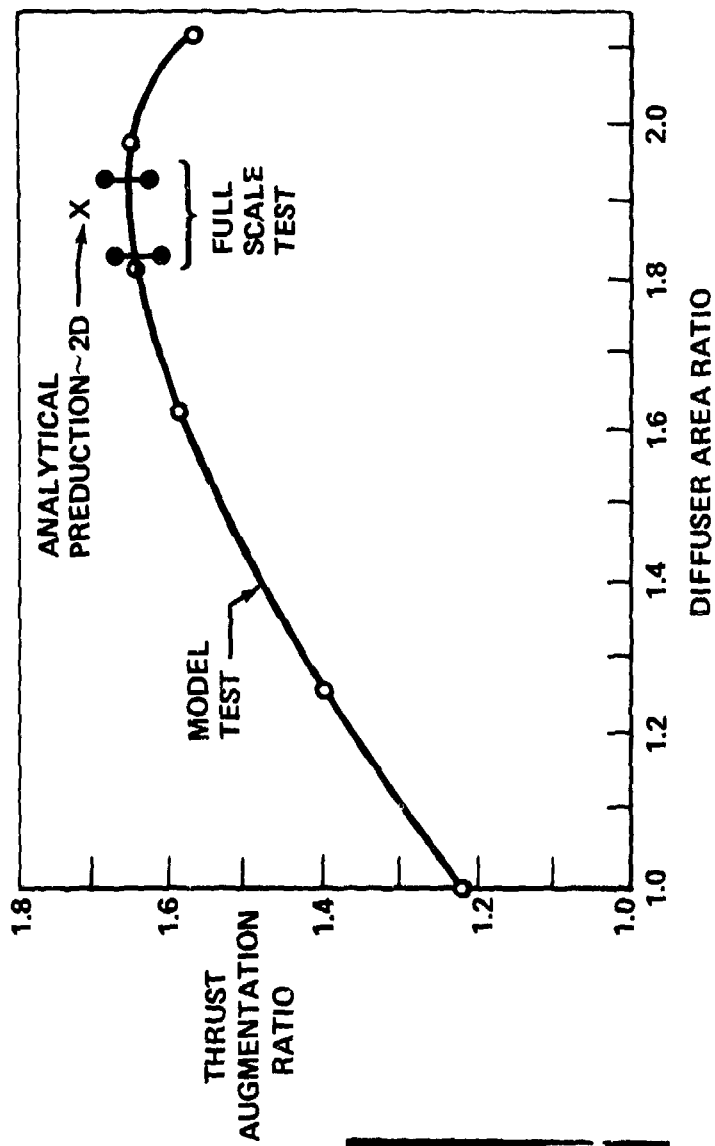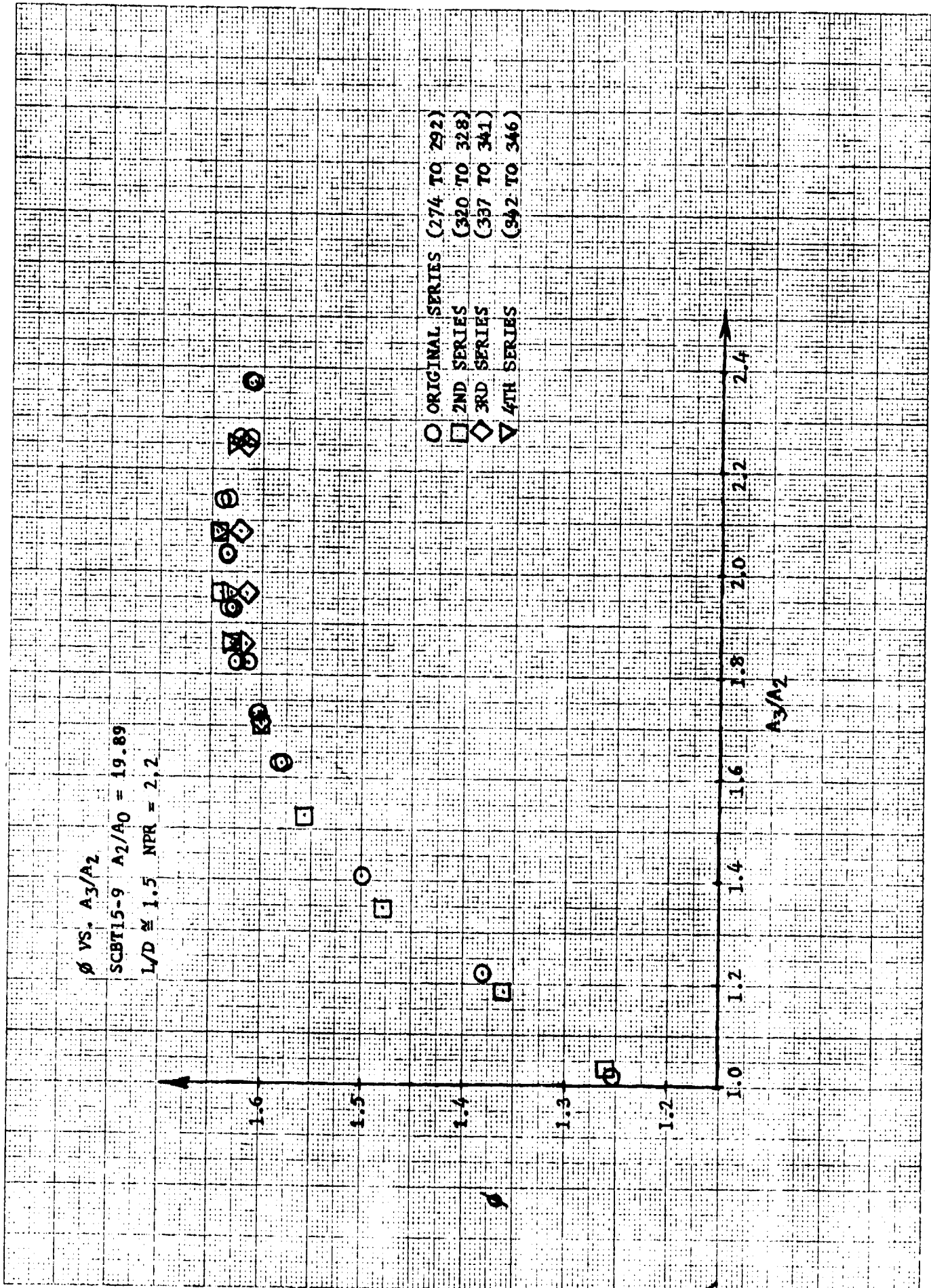
864

CAD 16031

Figure 9.

Figure 10.

866

VISCID/INVISCID INTERACTION ANALYSIS OF EJECTOR WINGS

by

P. M. Bevilaqua, C. J. Woan, and E. F. Schum

Rockwell International, North American Aircraft Division

Columbus, Ohio

Paper Presented at

Ejector Workshop for Aerospace Applications

August 3-5, 1981/Dayton, Ohio

Rockwell International

# VISCID/INVISCID INTERACTION ANALYSIS OF EJECTOR WINGS*

by

P. M. Bevilaqua, C. J. Woan, and E. F. Schum

Rockwell International, North American Aircraft Division

## ABSTRACT

A method has been developed to predict the lift and thrust of an ejector wing by iterating between a viscous solution for the turbulent entrainment of the primary jets, and an inviscid solution for the ejector wing flow field. A two-dimensional analysis, which utilizes a turbulent kinetic energy model for the jet mixing calculation and a higher order panel method for the inviscid flow calculation, is described. The complete ejector wing geometry is analyzed. Detailed surface pressures both inside and outside the ejector can be calculated. A sample calculation for a typical ejector wing configuration is compared to experimental data.

# INTRODUCTION ·

Although analytic methods are necessary for conceptual studies and to reduce test requirements, there is no satisfactory theory for predicting ejector wing performance. Methods have been developed to calculate the surface pressure distributions induced by an ejector of given thrust. These calculations are based on the now classical vortex sheet model of the pure jet flap devised by Spence (ref. 1). Linearized, thin airfoil models of the ejector wing were developed by Chan (ref. 2) and Woolard (ref. 3), who added a sink on the upper surface of a jet-flapped wing to represent the entrainment into the ejector. Wilson (ref. 4) extended this approach by including the effects of thickness and camber, as well as deflection of the jet wake. More recently, Dillenius and Mendenhall (ref. 5) studied three-dimensional effects. In all these methods, experimental data are used to specify the variation in ejector thrust during conversion from hover to conventional flight.

Such an empirical approach is useful for estimating pressure distributions or for performing parametric analysis. However, a theory for predicting both the thrust augmentation ratio and the initial thrust angle is necessary to evaluate significant design changes, or new configurations for which there is no data base. Bevilaqua and DeJoode (ref. 6) developed a method for predicting the thrust augmentation of stationary ejectors by iterating between a viscous solution for the entrainment of the primary jets and an inviscid solution for the pressures induced on the ejector duct by the entrained flow. The purpose of this paper is to describe an extension of this analysis developed to predict the lift and thrust of the more complex ejector wing in transition flight.

Calculation of the flow field is more difficult in this case because deflection of the exhaust jet by the free stream influences both the thrust of the ejector and the lift of the wing. A two-dimensional analysis, which utilizes a turbulence kinetic energy model for the jet mixing calculation and a higher order panel method for calculating the surface pressures, has been developed.

A description of this analysis, together with a computed result is given in the following sections.

## MATHEMATICAL MODEL

The interactions between the ejector and wing flow fields are computed without solving the full Navier-Stokes equations by iterating between a viscous solution for the flow through the ejector and an inviscid solution for the flow around the wing. Because the primary direction of flow is through the ejector, the governing elliptic equations can be reduced to a parabolic set which can be solved by marching through the ejector in the streamwise direction. The mixing

of the turbulent jets can then be used to define an equivalent sink distribution. The requirement that the ejector wing and jet boundaries must be streamlines of the flow together with appropriate jet dynamic boundary conditions determines the strength of the wing circulation. The circulation and jet shapes, in turn, control the entrainment calculated in the next iteration for the viscous solution.

## Potential-Flow Calculation

The geometry of the two-dimensional ejector wing considered in this study is shown in Figure 1. It has three main components: a plain flapped wing, a central nozzle, and an aft flap. Primary jets are injected at the knee of the forward flap, the trailing edge of the central nozzle, and near the leading edge of the aft flap. The three jets grow and merge to define the jet wake, which has higher total pressure than the free stream does. Consequently, the flow consists of two regions with different total pressure, thus it is inhomogeneous

According to Küchemann and Weber (ref. 7), the inhomogeneous flow may be made homogeneous without changing the flow velocity field by subtracting the total pressure difference between the jet wake and the main stream from the static pressure inside the jet wake. In the resulting homogeneous flow, the jet boundaries are unknown and to be determined as part of solution subjected to the usual tangential flow (kinematic) condition and an additional dynamic boundary condition

$$\Delta H = \rho U \gamma \tag{1}$$

where $\rho$ is the fluid density (both jet and main stream), U is the mean velocity of the jet boundary, $\gamma$ is the velocity difference across the jet boundary, and $\Delta H$ is the total pressure difference between the main stream and jet wake.

However, if the jets are not completely mixed by the ejector exit, each jet before complete mixing is treated as a thin jet using the classical thin jet theory. According to Spence (ref. 1), the static pressure jump, $\Delta p$, across a thin jet is balanced by the rate of change of jet momentum, J, due to jet curvature, 1/R, and is related to the vortex strength, $\gamma$, (equivalent to the velocity difference across the jet) of the jet sheet as follows:

$$\Delta p = \rho U \gamma = \frac{J}{R} \tag{2}$$

The solution of a thin jet is obtained by satisfying this dynamic boundary condition together with its kinematic boundary condition. All the flow singularities which determine the potential-flow solution are shown in Figure 1. The cross line source is added to combine with the line sink to simulate the doublet effects on the flow field for modeling

870

the effect of the jet, which acts like an elongated actuator disk to draw air through the ejector.

The potential flow just described is calculated by using the Hess (ref. 8) higher-order panel method. Both airfoil and jet boundaries are defined by a series of discrete points, so-called corner points, as shown in Figure 2. Between two successive corner points, the true geometry is approximated by a curved parabolic panel. A linear vortex distribution and a linear source distribution are placed on each of these panels. Source singularity strengths are chosen a priori and set equal to twice the local jet entrainment velocity. Vortex singularity strengths and the jet shapes are determined by satisfying the airfoil and jet kinematic boundary conditions and the jet dynamic boundary conditions, equations (1) and (2).

Since the jet dynamic boundary conditions, equations (1) and (2), are nonlinear and the jet shapes are not known, a priori, an iterative procedure shown in Figure 3 is adopted to obtain the potential-flow solution. Details of the computational procedure are given in ref. 9.

## Jet-Mixing Calculation

The jet-mixing calculation is a partially parabolic method described in detail in ref. 10. The flow governing equations are derived from Reynolds' equations for turbulent flows, by neglecting streamwise diffusion and including curvature effects. A TKE turbulent model (ref. 11) modified to include the curvature effect is used to determine the turbulent viscosity. A set of finite-difference equations are formed by integrating the governing differential equations over a small control volume. The resulting finite difference equations are solved iteratively for velocity and pressure fields. Briefly, the iterative procedure begins with an initial guess of the pressure field, solves the momentum equations for the velocity components using a triadiagonal matrix algorithm, corrects the pressure and velocity fields to satisfy the continuity equation, and repeats the process until convergence is obtained.

## SOLUTION MATCHING PROCEDURE

The solution is iterative, since the two individual flow problems and their coupling are nonlinear. The iterative procedure used is summarized schematically by the flow chart of Figure 4. Details of the computational procedure are described in ref. 9. Presently, the potential-flow program and the jet-mixing program are separated and communicate through external data transformation.

## EXAMPLE SOLUTION

To test the present matching solution procedure for ejector wings, the model wing "Configuration Augmenter 1" (Figure 7) of ref. 12 was analyzed at a transition operating condition. The tunnel velocity was 34.4 m/sec (113 ft/sec) for a tunnel static pressure of 1.024 atmospheres. The effective angle of attack was 2 degrees and the momentum coefficient was 2. Figures 8 through 12 show the calculated results and Stewart's (ref. 12) experimental data.·

Comparison of the distributions reveals that the differences between the experimental and theoretical pressure are dramatically reduced when ·jet entrainment effects are included in the calculations. Examination of the experimental data shows large discrepancies near the leading edge and on the upper surface of the centerbody. These are most likely due to flow separation in these regions. The flow separation may be due to the high local angle of attack as indicated by the calculated flow streamline pattern about the ejector wing shown in Figure 12. The present computer program cannot calculate a separated flow.

## CONCLUSIONS

1. A viscid/inviscid interaction analysis has been developed to predict the thrust augmentation ratio and initial thrust angle of ejector wing configurations. This provides an advance over classical methods of analysis, which require these parameters to be specified as an input.

2. Comparison of the predicted surface pressure distributions with experimental data establishes confidence in the model of the flow field. But in addition, a greater understanding of the performance of ejector wings has been obtained from the analysis.

3. Examination of the computed streamlines and surface pressures reveals the somewhat surprising result that the forward stagnation point is located near the trailing edge of the forward flap. This is a result of the large circulation induced by the jet flap effect and suggests that a leading edge device may be required to achieve maximum lift and thrust. Further, the surface pressure distributions on the other two elements suggest that the flow is more likely to separate from the central nozzle than the aft flap. Since the flow into the ejector is being accelerated past the nozzle, this was also an unexpected result.

4. The present analysis can be improved by including boundary-layer and three-dimensional effects.

5. It would be useful to have test data for a two-dimensional configuration, since no comparison with available three-dimensional data can be exact.

## REFERENCES

1. Spence, D. A.:  The Lift Coefficient of a Thin, Jet-Flapped Wing, Royal Society of London, Proceedings, vol. 238, January 1957, pp. 46-68.

2. Chan, Y. Y.:  Lift Induced by Suction Flaps on Augmenter Wings, Canadian Aeronautics and Space Institute Transactions, vol. 3, no. 2, Sept. 1970, p. 107.

3. Woolard, H. W.:  Thin-Airfoil Theory of an Ejector-Flapped Wing Section, AIAA Journal of Aircraft, vol. 12, no. 1, January 1975, p. 26.

4. Wilson, J.:  Thrust Augmented Wing Section in Potential Flow, PhD Dissertation, West Virginia University, 1973.

5. Dillenius, M. F. and Mendenhall, M. R.:  Theoretical Analysis of an Augmenter Wing for a VTOL Fighter, NASA CR-152254.

6. Bevilaqua, P. M. and DeJoode, A. D.:  Viscid/Inviscid Interaction Analysis of Thrust Augmenting Ejectors, Report ONR-CR212-249-1, February 1978.

7. Kuchemann, D. and Weber J.:  Aerodynamics of Propulsion, McGraw-Hill, Chapter 3, New York, 1953.

8. Hess, J. L.:  Higher-Order Numerical Solution of the Integral Equations for the Two-Dimensional Neumann Problem, Computational Methods in Applied Mechanics and Engineering, vol. 2, no. 1, February 1973.

9. Bevilaqua, P. M.; Woan, C. J.; and Schum, E. F.:  Viscid/Inviscid Interaction Analysis of Ejector Wings, NASA CR 166172, in review, 1981.

10. Schum, E. F.; Bevilaqua, P. M.,; and Patankar, S. V.:  Computation of the Turbulent Mixing in Curved Ejectors, ONR-CR212-249-2F, April 1980.

11. Launder, B. E. and Spalding, D. B.:  Mathematical Models of Turbulence, Academic Press, 1972.

12. Stewart, V. R.:  A Study of a VTOL Thrusting Ejector in  Low Speed Flight, vol. 1 and 2, NASA CR-166137, March 1981.

Figure 3. Inviscid Numerical Procedure
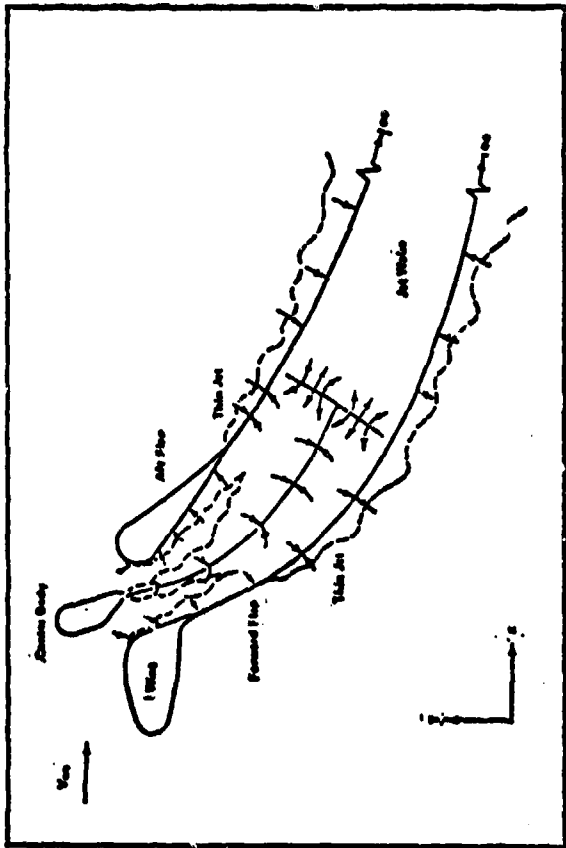


Figure 1 Mathematical Model of the Generalized Ejector Wing
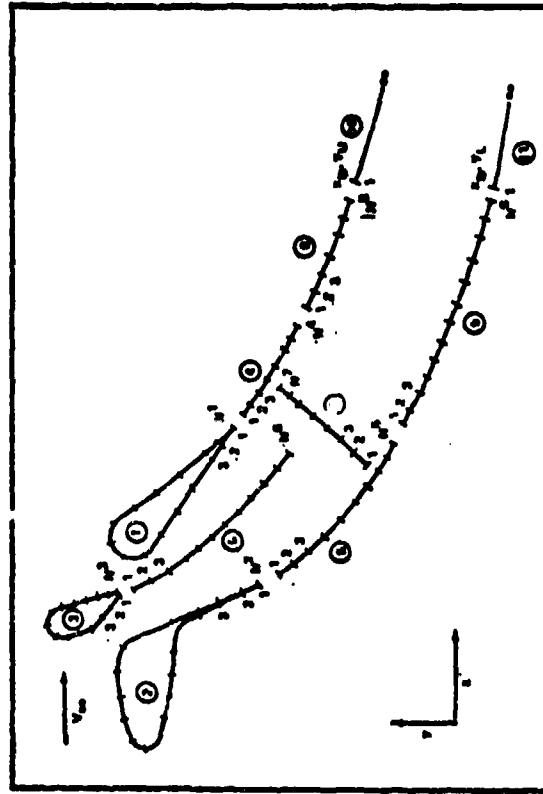


Figure 2. Isolated Elements and Direction of Indexing the Corner Points
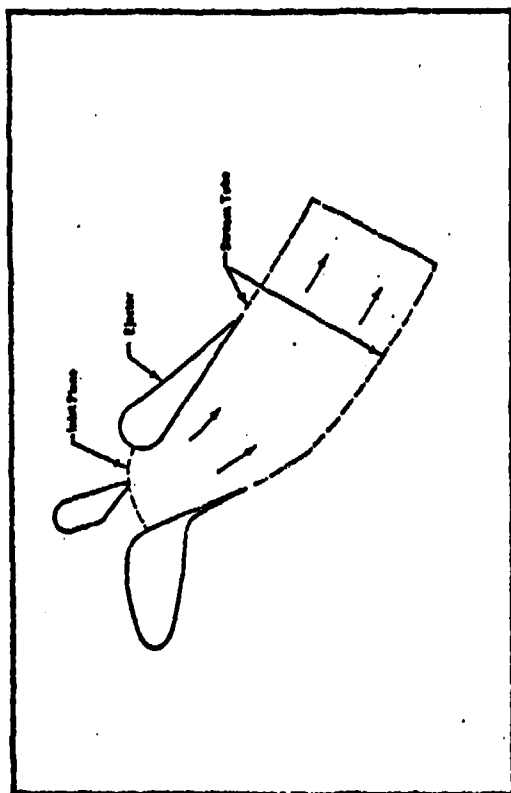
Figure 5. Flow Field Boundaries



(a) Non-orthogonal Grid

(b) Orthogonal Grid
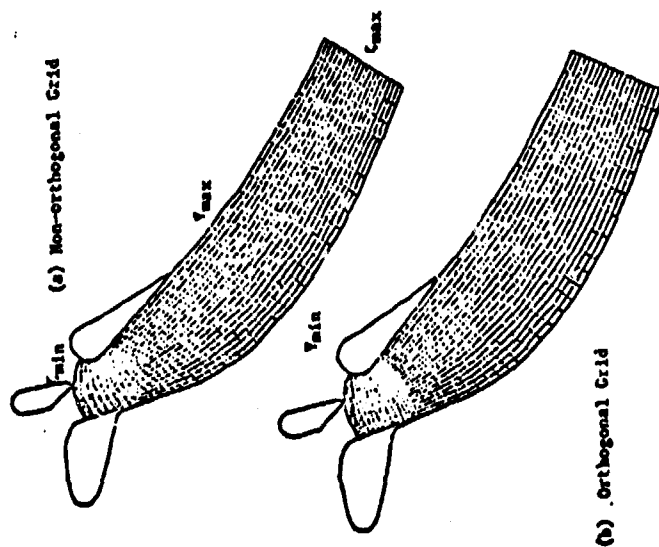
Figure 6. Boundary-Oriented Grids
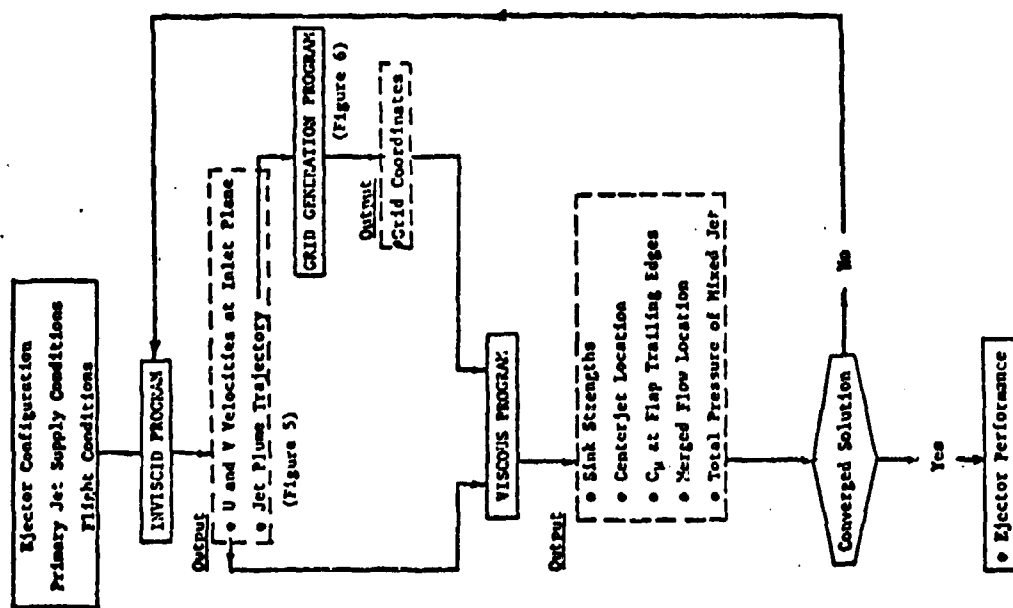


Figure 4. Inviscid/Viscid Matching Procedure

875

Figure 9. Comparison of the Calculated Pressure Coefficients with the Experimental Data for the Kestrel Flap.



Figure 10. Comparison of the Calculated Pressure Coefficients with Experimental Data for the Aft Flap of the Kestrel Wing



Figure 7. Experimental Model Configuration



Figure 8. Slot Strengths
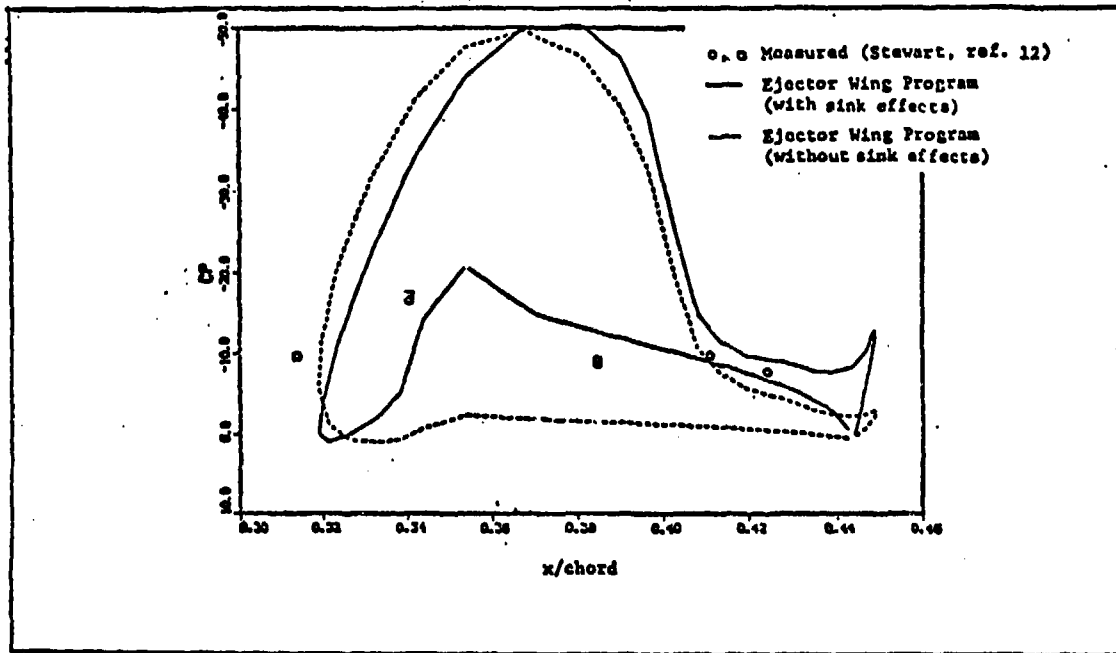
**Figure 11.** Comparison of the Calculated Pressure Coefficients with the Experimental Data for the Centerbody
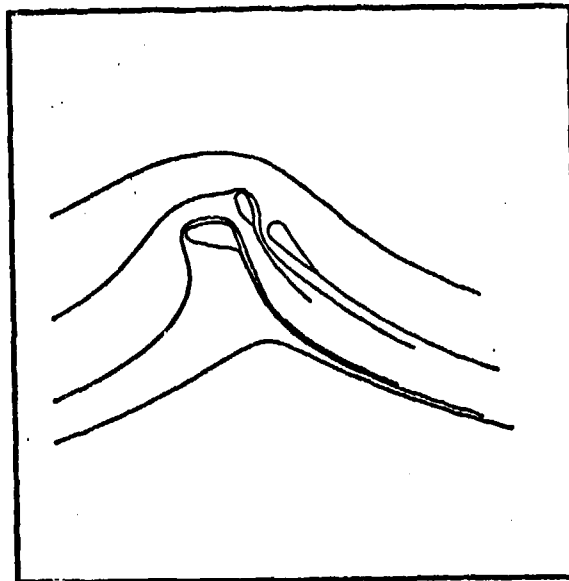


**Figure 12.** Calculated Flow Streamline Pattern about the Ejector Wing
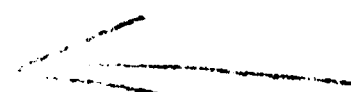
Turbulence Measurements in
an Ejector Wing Flow Field

by

G. D. Catalano
Louisiana State University
Baton Rouge, Louisiana


H. E. Wright and D. Stevens
Air Force Institute of Technology
Wright Patterson AFB, Ohio


K. S. Nagaraja
AF Wright Aeronáutical Labs
Wright Patterson AFB, Ohio

# I. Introduction

Consider the principle of an ejector[1]. In the simplest cast,
coaxial jets are confined to a duct rather than a constant pressure atmos-
phere. For this flow field, the mass flow rate averaged mean axial momen-
tum is not conserved and the static pressure may vary with downstream
location. There will be an increase of pressure with increasing down-
stream position as the jet cores are being consumed by rapid shear layer
mixing. In fact, the pressure may also continue to rise in the developing
flow zone downstream of the disappearance of the cores. This pressure
rise can be considered the source of the pumping effect of the ejector.

Significant and fundamental developments in thrust augmenting ejec-
tors have been accomplished in the last several years. Hypermixing
nozzles have been developed with a resultant increase in ejector compact-
ness realized[2]. Mixing and diffusion of flows have been achieved
simultaneously with performance advantage. Thrust augmentation ratios on
the order of two in an ejector of inlet area ratio 23 have been achieved
experimentally[3]. A theoretical methodology which can evaluate the
performance of the ejectors subject to a wide range of variation in the
thermodynamic parameters of the injected and the entrained fluids has been
developed for incompressible and compressible flows for a constant area
duct[4]. High lift characteristics of an ejector-flapped wing have
been evaluated[5]. A numerical prediction of three dimensional
ejector flows has been proposed[6].

Although the literature on ejectors in general and, particularly,
thrust augmenting ejectors, is quite extensive, the turbulence field has
been essentially ignored. The information that is available is predomin-
antly concerned with flows in constant area pipes with Razinley and

881

Brighton[7] presenting an extensive set of one point statistical measurements for varying mean velocity ratios and jet/pipe diameter ratios.

The purpose of this investigation is to conduct an extensive survey of the resultant velocity flow field of a given ejector wing design. The effectiveness of the ejector will be assessed by comparing the flow field with the ejector powered and with the ejector unpowered. The data in this experiment is obtained by use of a laser velocimeter in conjunction with a photon correlation processing technique. Photon counting offers improved system sensitivity by permitting velocity measurements to be made even when insufficient signal photons are available to define a classical scattering signal. When required for an improved signal to noise ratio, the naturally occuring contaminant particles are augmented by kerosene vapor. The use of the kerosene vapor allows a flow visualization technique to be employed as well.

The relevance of this investigation is reinforced by one of the major conclusions of the Workshop in 1979 which is that a significant amount of basic research using smaller models (cold or hot air supply) and analytical development should be continued vigorously for both static and at airpeed conditions[8].

## II. Experimental Equipment and Technique

The facility used for this investigation is a two dimensional smoke tunnel. This facility employs an open return system of flow, capable of subsonic incompressible velocities up to 23 meters/second, using two diffuser isolated 1.5 horsepower motor driven fans. All measurements are taken at a nominal freestream velocity of 8 m/sec. The velocity was monitored at first by a Prandtl type pitot probe and a microamanometer.

These were later discarded in favor of the laser velocimeter as a means of setting and checking the freestream velocity.

The removable front test section measures 1.5 m in length, 1.0 m in height and 0.07 m in width. The back wall of the test section is of laminated plate glass, whereas the front wall is of 0.0097 m thick plexiglass. This window arrangement is acceptable in light of the fact that the laser velocimeter is operated in the backscatter mode. The test section is noted as having a downhill gradient of 0.05 m in 1.5 m.

The flow marker particles are introduced into the flow system in thin streamtubes by a stack and injector apparatus, positioned in the tunnel contraction region. The stack is of airfoil shape with sixty five 0.60 cm inside diameter injector tubes issuing from it. The marker particles are generated in a process where, two 900 watt inconel heaters boil kerosene fuel at 605 degrees Kelvin, creating vapor particles that are then mixed under turbulent conditions with cool air to produce a dense white nontoxic and noncorrosive smoke. Water vapor is condensed out of the smoke in a condensing chamber prior to entrance into the stack/injector apparatus, thereby eliminating water condensation in the injector tubes and the test section.

A great deal of effort was spent in reducing turbulence levels in this flow system. These efforts included installation of a 0.2 m radius bell mouth to the tunnel inlet, in an attempt to correct for a low concentration ratio of 11.5 to 1.0. Immediately downstream of this location a 0.076 m thick section of honeycomb, with a cell length to diameter ratio of 8.0, was installed to reduce large scale turbulent structures. In addition a series of screens (progressively finer downstream) were mounted prior to the stack/injector location. From measurements taken in the freestream, it would appear that turbulent intensities approach a value

883

of 0.01 in the smoke streamtubes. These values must be attributed to the shape of the stack/injector system, its location and the process of issuing a secondary flow into the mainstream through the injectors.

The specific flow field investigated is an ejector wing design conceived by Vought under contract with the Flight Dynamics Laboratory at Wright Patterson AFB (Figure 1)[9]. A two dimensional model is constructed and placed in the test section of the wind tunnel. The ejector plenum is supplied from the laboratory compressed air reservoir. The design of the ejector is presented in Figure 2. Considerable effort was expended in attempting to achieve a uniform exit velocity profile with relatively low values of the turbulent intensities. The aspect ratio of the rectangular nozzle is 4.1:1 and the solidity ratio is 0.327:1. The mean velocity at the nozzle exit plane, $U_2$, is kept at a constant 16 m/sec.

The laser used for all measurements is a Helium-Neon Laser of 15 milliwatts intensity at $6328.0 \times 10^{-10}$ m, plus associated power unit. The laser beam diameter is 1.1 m at the $1/e^2$ points. The transmitting optics consisted of a transmitter beamsplitter and polarization unit mounted to the laser head, a frequency shifting electro-optic phase modulating crystal, two front surface silvered plane mirrors mounted at 45 degrees to the horizontal and a convex focussing lens of 100 cm focal length. The beamsplitter takes the incident beam from the laser and divides it into two equal intensity, 1.1 mm diameter beams.

The frequency shifting phase modulator is required in the optical train to eliminate any flow direction sense ambiguities and provide measurements in regions of high turbulent intensity. In principle a uniform shifting of the fringes in the control volume (point of laser beam intersection) is possible with an application of a sawtooth voltage to

884

the phase modulator's two electro-optical crystals. A resulting increase

or decrease in the doppler frequency of the flow enables the flow direc-

tion to be determined. A drive unit is required for the phase modulator

unit as well as a frequency counter for accurate determination of the

doppler frequency shift applied.

The electronic processing scheme is composed of a digital photon

correlator and data storage unit, associated power supply and oscilliscope

for visual observation of the autocorrelation function growth with time.

The correlator possesses a resolution time of from 50 nanoseconds to 1

second. Measurements were taken in the single clipped autocorrelation

mode and at an infinite sample rate.

Special note should be made of the turbulent intensities measurement

technique. Care is taken in order to minimize the problems of background

flare light and photon pileup. The effects of these two phenomena can

result in a skewness or a distortion of the photon correlation function

from which the mean velocity and local turbulent intensity are calculated.

Therefore a numerical technique[10] is employed which results in the

alleviation of the skewness problem.

## III.  Experimental Results and Discussion

### A.  Flow Visualization

A series of photographs depicting qualitatively the resultant flow

field about the ejector wing model as shown in Figure 3 through 9. For

all photographs the ratio between the ejector exit plane mean velocity,

$U_2$, and the tunnel speed, V, is equal to 2:1. The angle of attack, $\alpha$,

between the wing model chord line and the incoming tunnel flow is varied

from $-5^{\circ}$ to $+25^{\circ}$. For each value of $\alpha$, the case with the ejector powered

885

and the unpowered case are examined.

By examining each set of figures, three general observations are made concerning the effects of the ejector. First, significantly more smoke (hence, tunnel airflow) is entrained into the constant area duct between the lower and upper airfoils in the powered case. In fact, it appears that near stagnation conditions are reached downstream of the nozzle with jet flow off. Secondly, with the ejector powered, there is an increase in curvature of the streamlines in the vicinity of the leading edge stagnation point. As will be discussed later in this report, this is evidence of the shift of the wing model's stagnation point further downstream on the lower surface of the front airfoil. Thirdly, the smoke streamlines above the wing are shifted downward towards the airfoil surface in the powered case. Thus, qualitative evidence exists that one of the effects of the ejector is to decrease the resultant wake flow behind the wings.

B. Mean Velocities and Turbulent Intensities

In Figure 10, the location of the mean velocity and turbulent intensity data obtained are shown. Note that in all cases, x is measured, longitudinally, from the leading edge and z is measured vertically from the airfoil surfaces.

Turbulent intensity is defined here as the ratio between the root mean square of the velocity fluctuations, $u_{rms}$, non-dimensionalized by the local mean velocity, U.

Figure 11 shows mean velocity profiles upstream of the ejector wing while the turbulent intensity profiles are presented in Figure 12. The effect of the ejector shown in the mean velocity profiles is to accelerate the mean flow above the upper surface and to decelerate the mean flow beneath the ejector wing. This effect is quite pronounced immediately

886

upstream of the leading edge. The turbulent intensities are not as well behaved but the value of $u_{rms}/U$ does seem to increase above the upper surface with the ejector powered.

Mean velocity and turbulent intensity profiles are shown for the downstream locations $x/c = 0.2$, (F), and $x/c = 0.5$, (I), in Figures 13 and 14. Both these locations are above the upper surface and the mean flow is consistently faster in the ejector powered case. The turbulent intensity data reinforces an observation made with reference to flow visualization evidence. The value of the turbulent intensities reduce to the free stream value closer to the wing surface with the ejector working. This would again indicate a shift of the potential flow down toward the upper surface.

Consider the data presented for the lower surface locations for $x/c = .02$, $x/c = .04$, and $x/c = 0.2$. In figures 15 through 17, at each flow location, the mean longitudinal velocity, U, is less in the powered case. This suggests the movement of the stagnation further along the lower surface as can be argued from Figure 18. As the stagnation point moves downstream, the apparent angle of attack of the airfoil will increase. With the increase of $\alpha$, the mean velocity measured in the longitudinal direction will necessarily decrease close to the stagnation point.

The mean and turbulent velocity field downstream of the ejector nozzle is examined in Figures 19 through 21 for $x/c = 0.44$, 0.58, and 0.72. Note that the flow for both cases actually accelerates after it enters the constant area mixing duct. Also consider the relatively high turbulent intensities in the confining duct for the ejector powered case. Values of $u_{rms}/U$ equal to 0.25 are measured which is indicative of jet mixing rather than characteristic of duct type flow. Once again for the field above the wing, the velocity returns to the free stream turbulence

887

condition faster with the jet working. For example, for $z = 10$ cm in Figure 21, $u_{rms}/U$ is equal to .05 for the nonpowered case but possesses a value of .01 for the ejector working case.

## IV. Summary

An experimental investigation of the resultant turbulent flow field about an ejector wing design incorporating a constant area mixing duct is made. Mean velocities and turbulent intensities are calculated from the photon correlation functions. Comparison between the ejector powered and non-powered cases are made. Qualitative information as well is obtained from a flow visualization technique. The following results are obtained.

1) The ejector consistently accelerated the flow field above the wings' upper surface. The influence is felt upstream of the model's leading edge.

2) The stagnation point moved further downstream along the lower surface for the ejector powered case, indicating an apparent increase in the effective angle of attack.

3) The turbulent intensities in the confining duct are more indicative of free or coaxial jet turbulence levels.

4) The streamlines above the wing's upper surface are compressed downwards toward the airfoil indicating a reduction in the turbulence and, hence, the wake region.

# References

1. Johnston, J. P., "Internal Flows", Turbulence ed. P. Bradshaw, Topics in Applied Physics, Vol. 12, Springer-Verlag, New York, 1978, pp. 154-157.

2. Quinn, B., "Compact Ejector Thrust Augmentation", J. Aircraft, Vol. 10, No. 8, August 1973.

3. Quinn, B., "Experiments with Hypermixing Nozzles in an Area Ratio 23 Ejector, ARL 72-0084, June 1972.

4. Nagaraja, K. S., Hammond, D. L., and Graetch, J. E., "One Dimensional Compressible Ejector Flows", AIAA Paper 73-1184, Nov. 1973.

5. Woolard, H. W., "Thin Airfoil Theory of an Ejector-Flapped Wing Section", J. Aircraft, Vol. 12, Jan. 1975.

6. Roberts, D. W. and Paynter, G. C., "Numerical Prediction of 3-D Ejector Flows", Workshop on Thrust Augmenting Ejectors, Ames Research Center, Moffett Field, California, June 28-29, 1978, pp. 55-70.

7. Razinsky, E., and Brighton, J. A., "Confined Jet Mixing for Nonseparating Conditions", Trans ASME, D, Vol. 93, September, 1971, pp. 333-349.

8. Koenig, D. G., "NASA Overview", Workshop on Thrust Augmenting Ejectors, Ames Research Center, Moffett Field, California, June 28-29, 1978, pp. 23-40.

9. Ejector Wing Design, Vought Corporation Advanced Technology Center, ATC Report No. R-91100/9CR-44, September 1979.

10. Catalano, G. D., Walterick, R. E., and Wright, H. E., "Improved Measurement of Turbulent Intensities by Use of Photon Correlation", AIAA Journal.
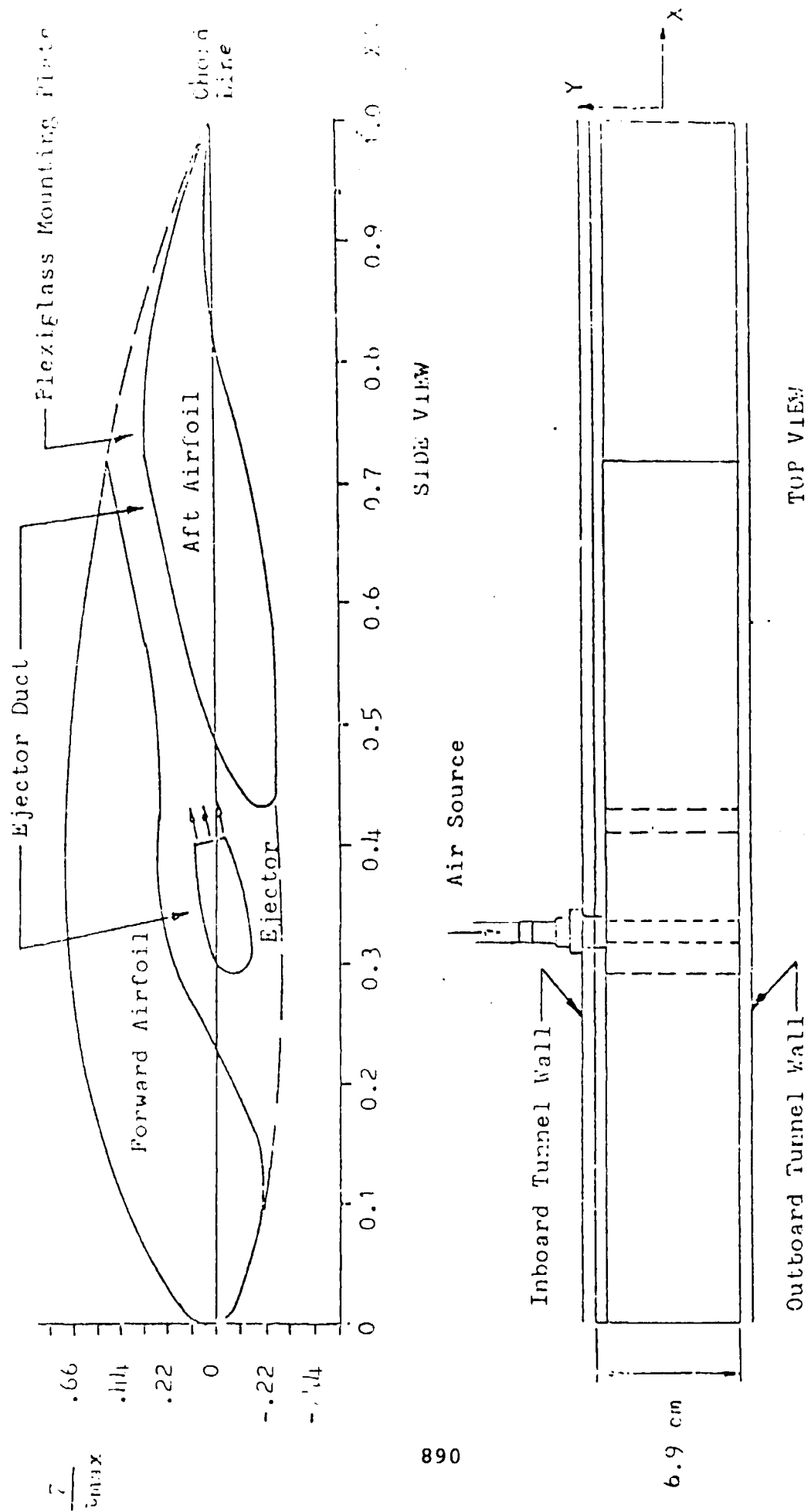
Figure 1. Ejector Wing Design
Chord Length, $C$, = 58.1 cm
Maximum thickness, $t_m$, = 11.1 cm

Air

1.27 cm ID

.793 cm ID    1.1 cm

.554 cm

.516 cm

.390 cm

Screen

Flow Straighteners

6.66 cm

Y

X

Ejector Face

Blowing Tube

2.87 cm

TOP VIEW

2.2 cm

1.6 cm

Air

Z

Y
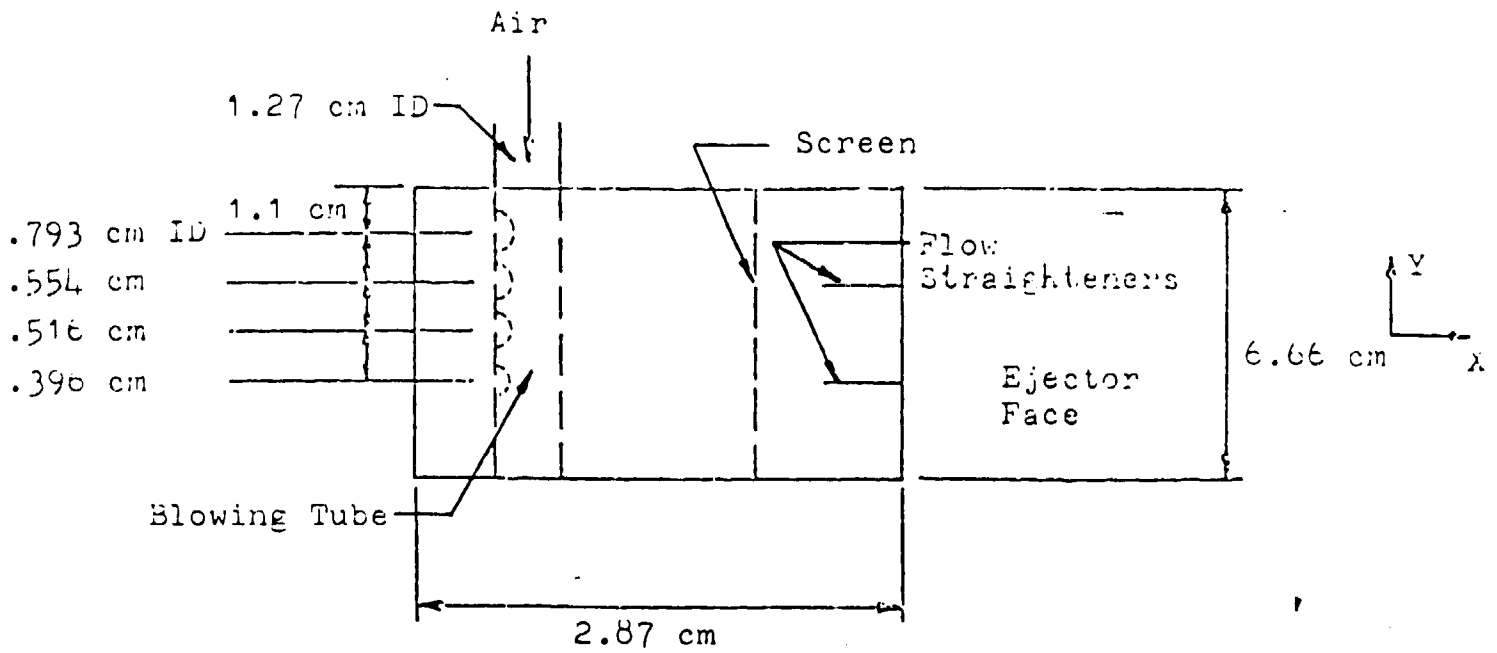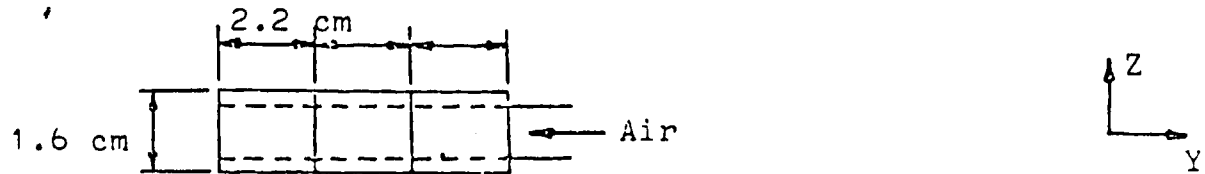
Ejector Face Area = 10.66 cm$^2$

FRONT VIEW
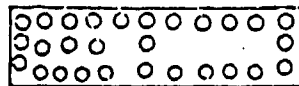
225 holes
.132 cm ID each
Screen Hole Area = 3.49 cm$^2$

SCREEN

Figure 2.      EJECTOR      891
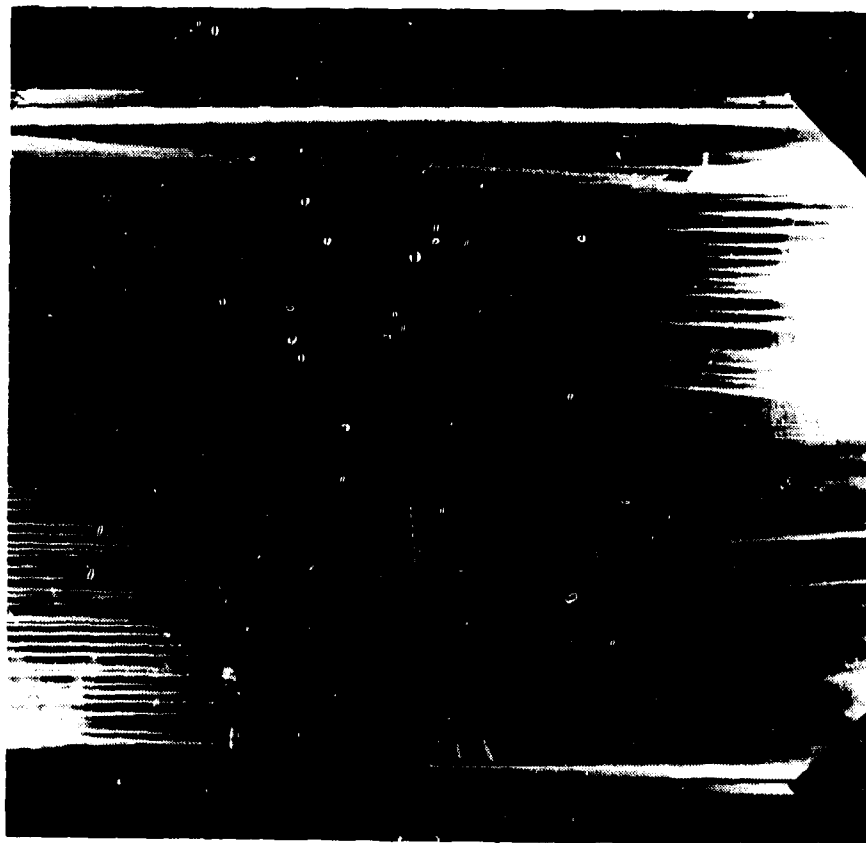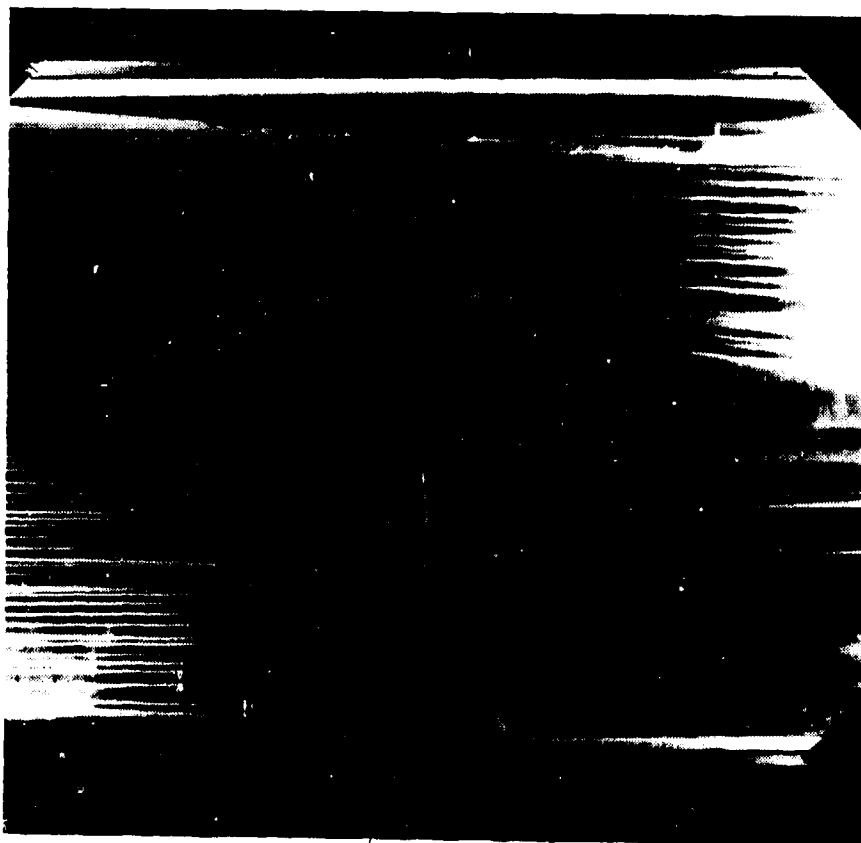
Unpowered

Powered

Figure 3.  Flow Visualization for  $\alpha = -5^{\circ}$.
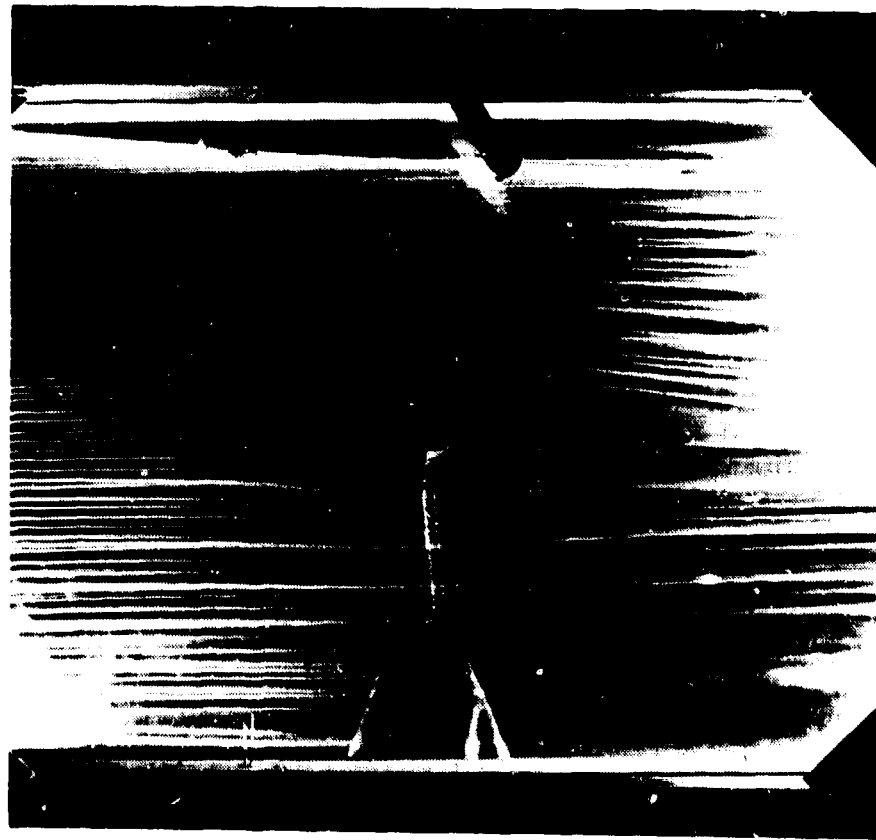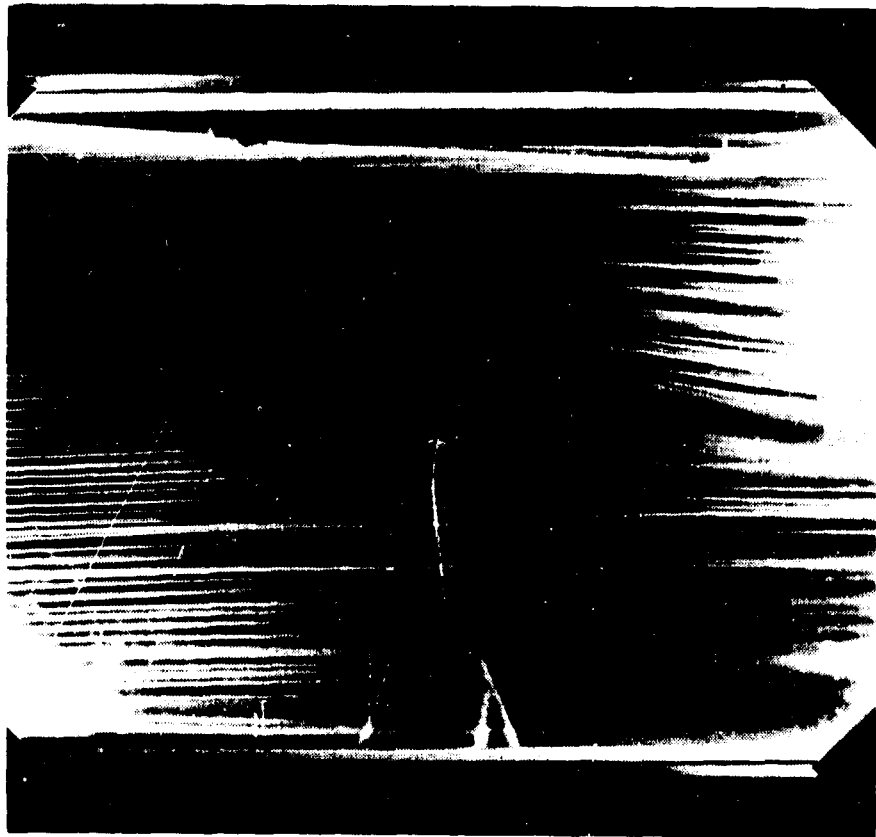
Unpowered

Powered

Figure 4.    Flow Visualization for $\alpha = 0^{o}$.

893
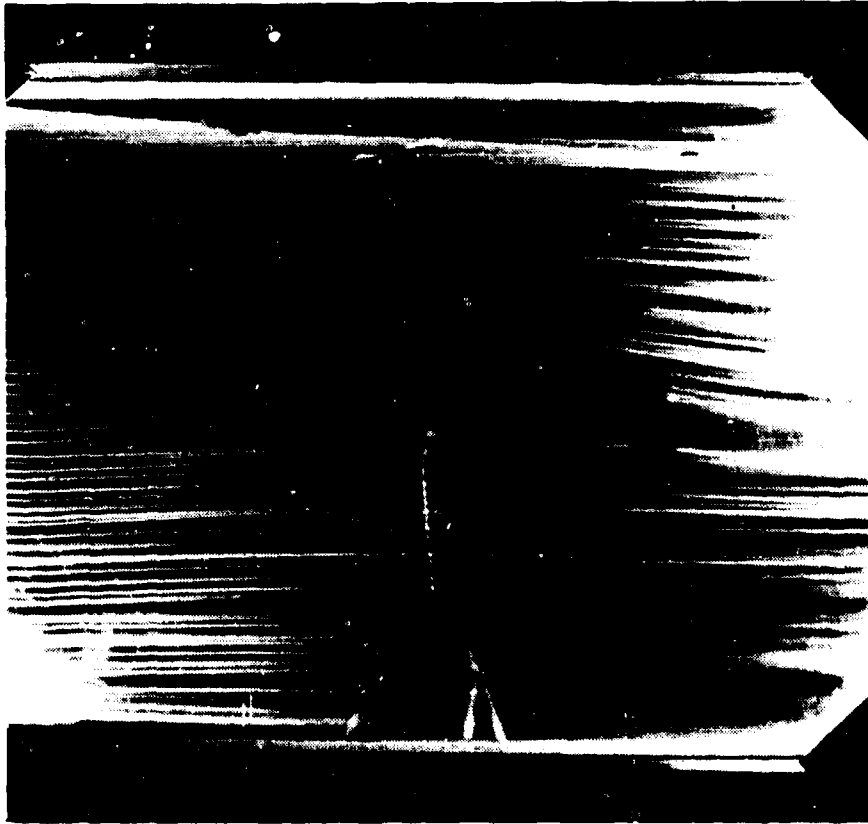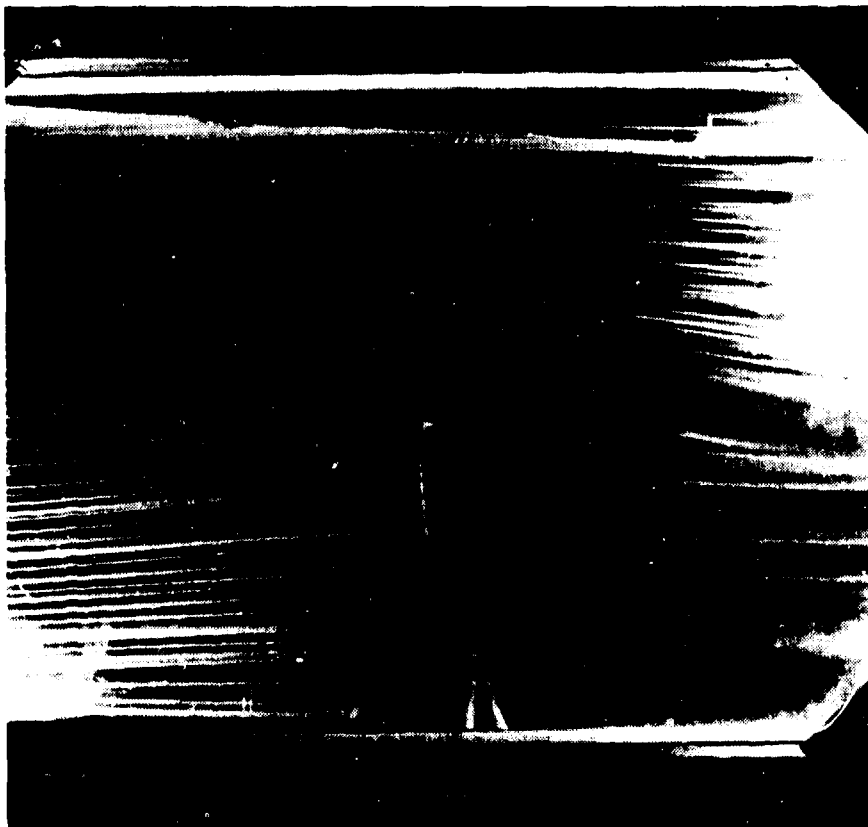
Unpowered

Powered

Figure 5.    Flow Visualization for $\alpha = 5^{\circ}$.
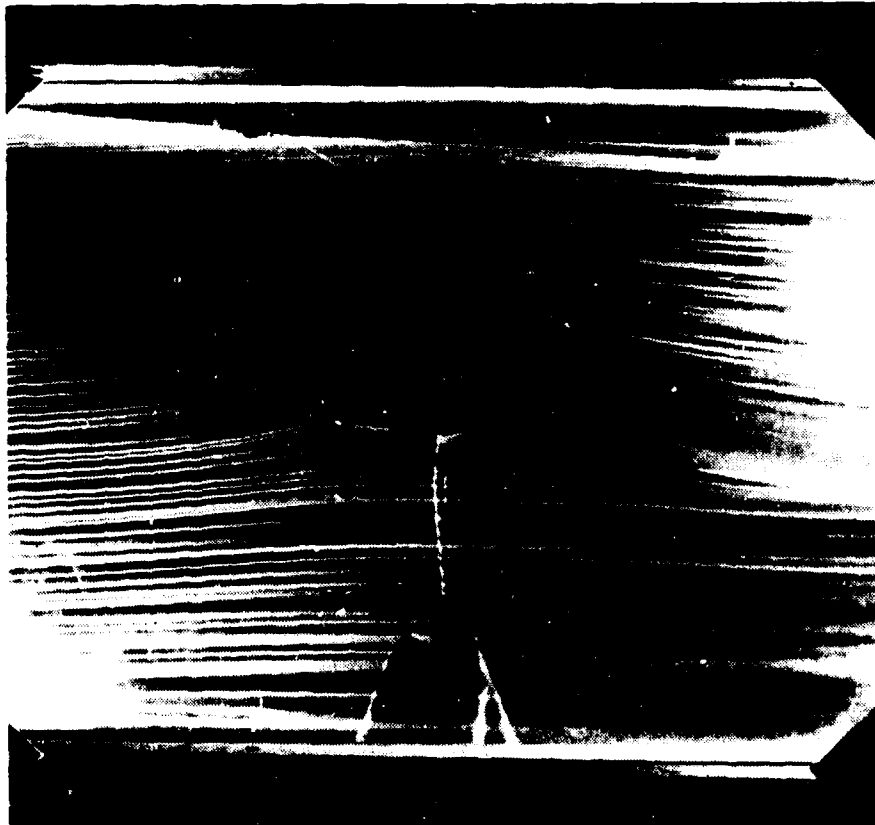
Unpowered

Powered

Figure 6. Flow Visualization for $\alpha = 10^\circ$.

895
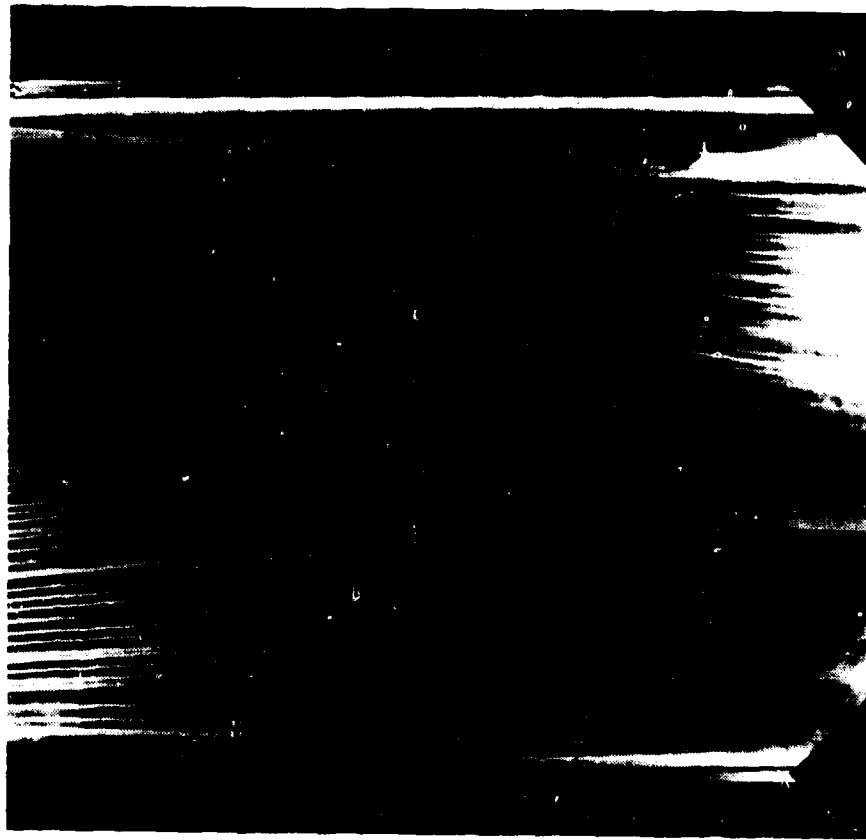
Unpowered

Powered

Figure 7.  Flow Visualization for  $\alpha = 15^{\circ}$

896

Unpowered

Powered

Figure 8.   Flow Visualization for $\alpha = 20^{\circ}$.

897
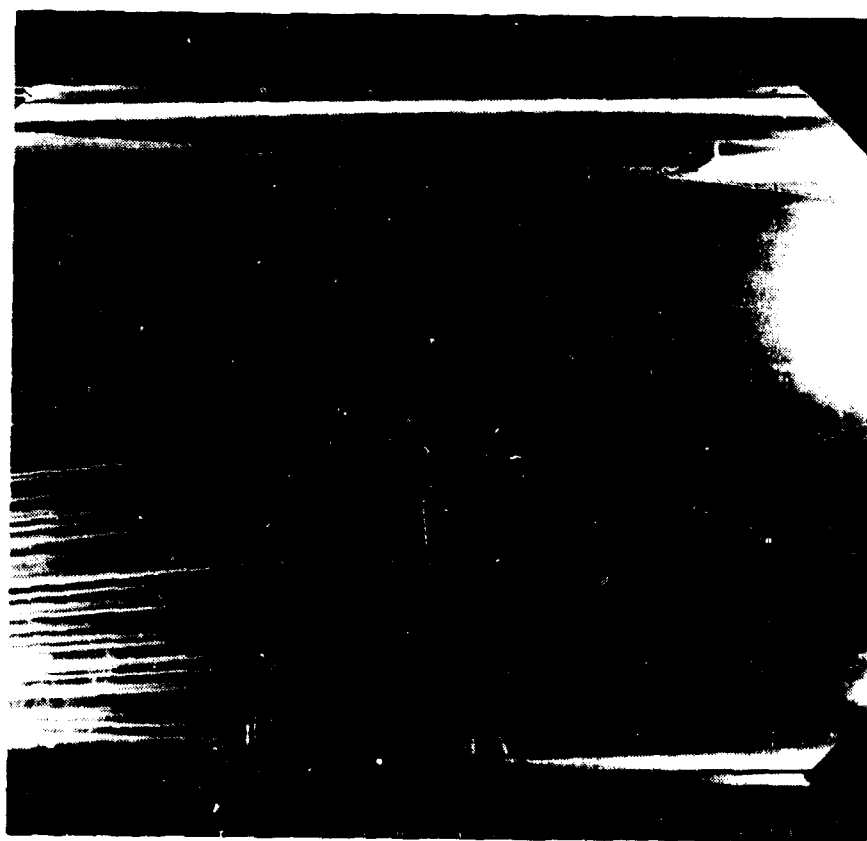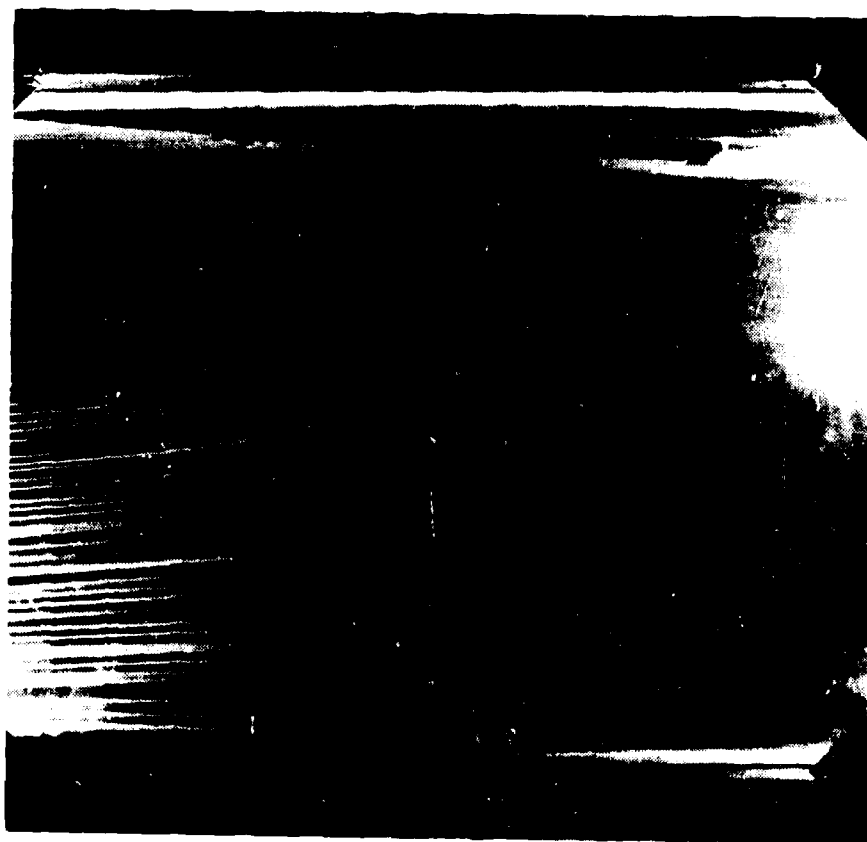
Unpowered

Powered

Figure 9. Flow Visualization for $\alpha = 25^{\circ}$.
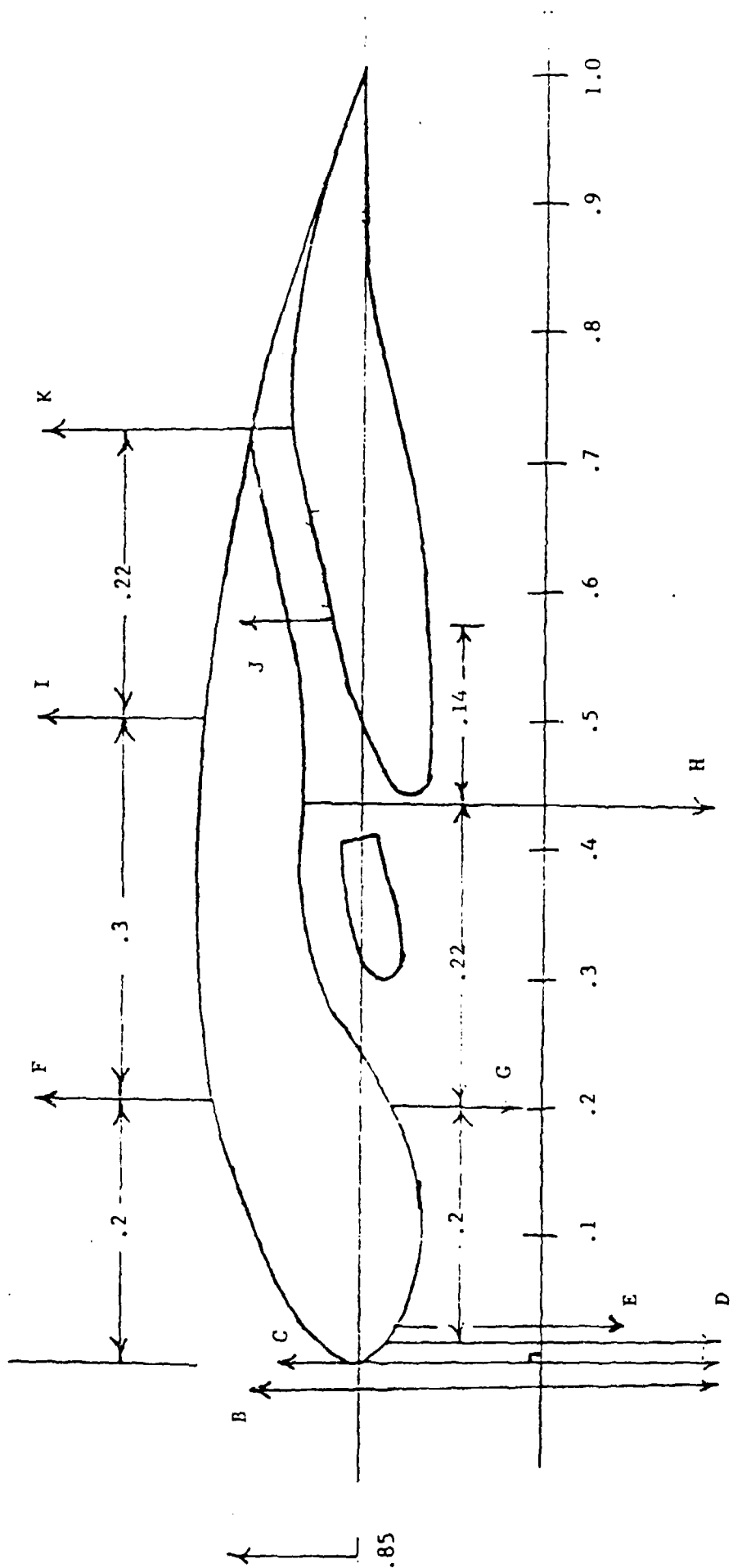
Figure 10. Measurement Locations for Ejector Wing Flow Field

899
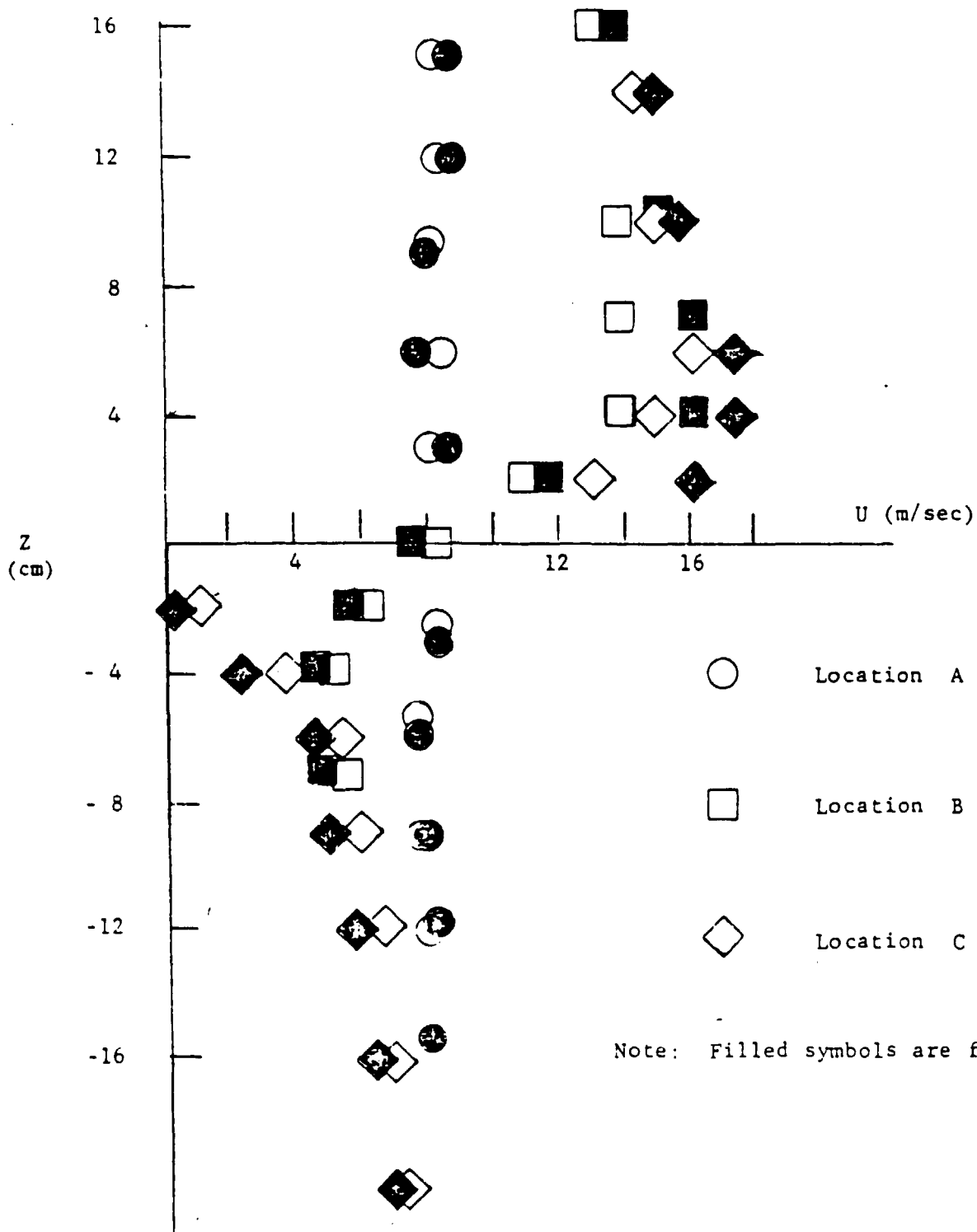
Figure 11.   Mean Velocity Profiles for Ejector Wing.

Figure 12.   Turbulent Intensity Profiles for Ejector Wing.

901
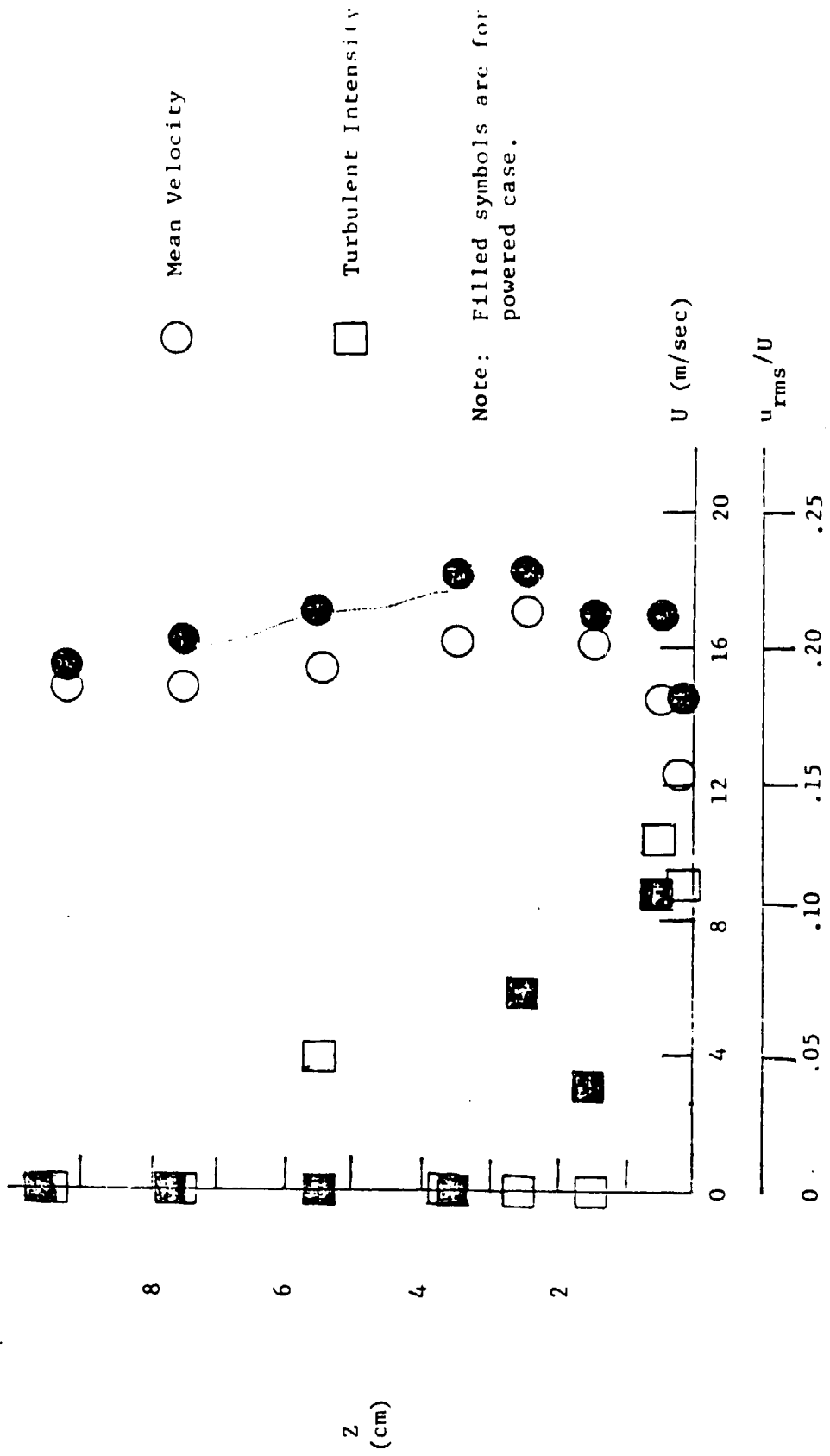
Figure 13. Mean Velocities and Turbulent Intensities at Location x/c = 0.2 (F).
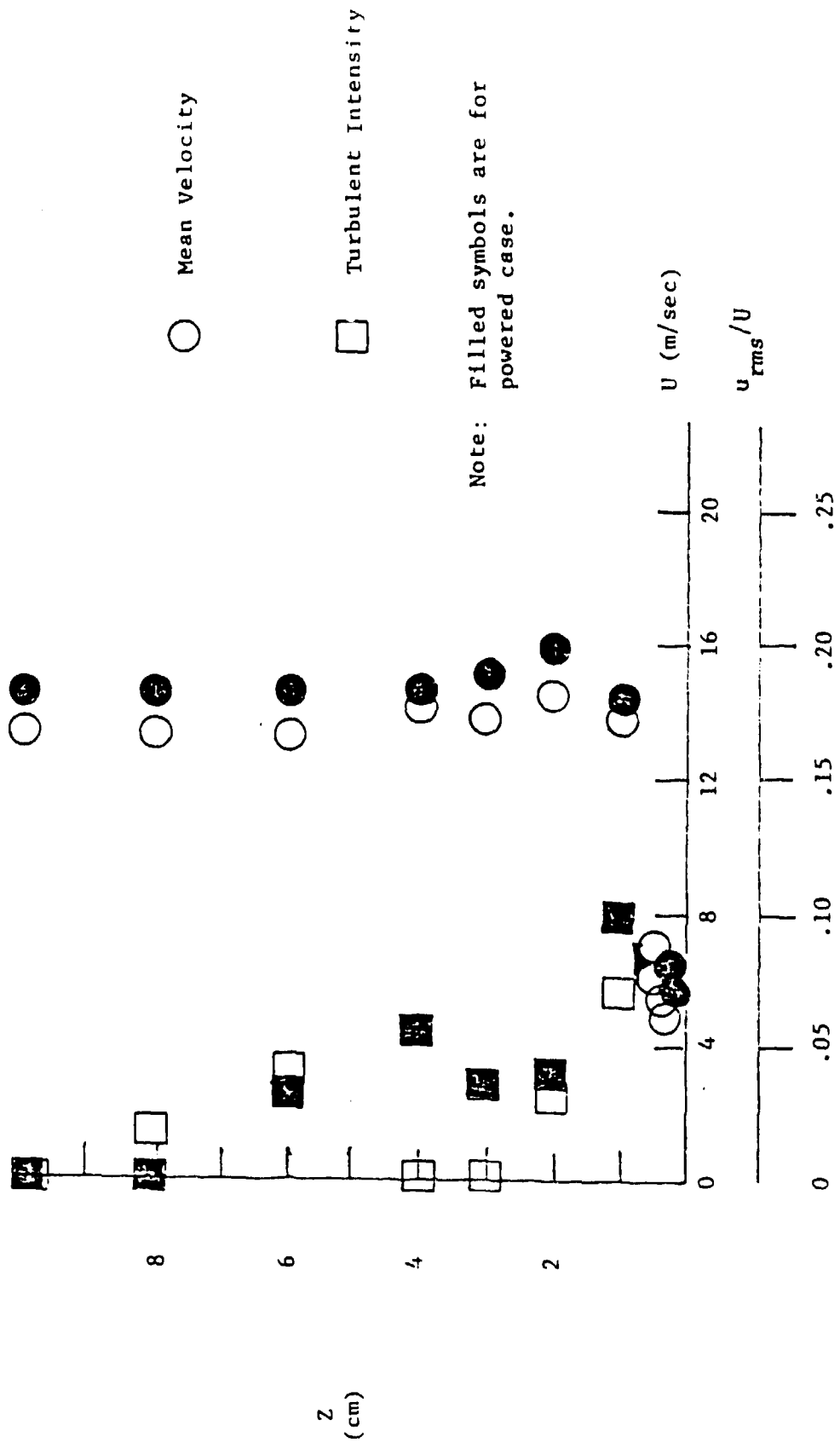
Figure 14. Mean Velocities and Turbulent Intensities at Location x/c = 0.5 (I).
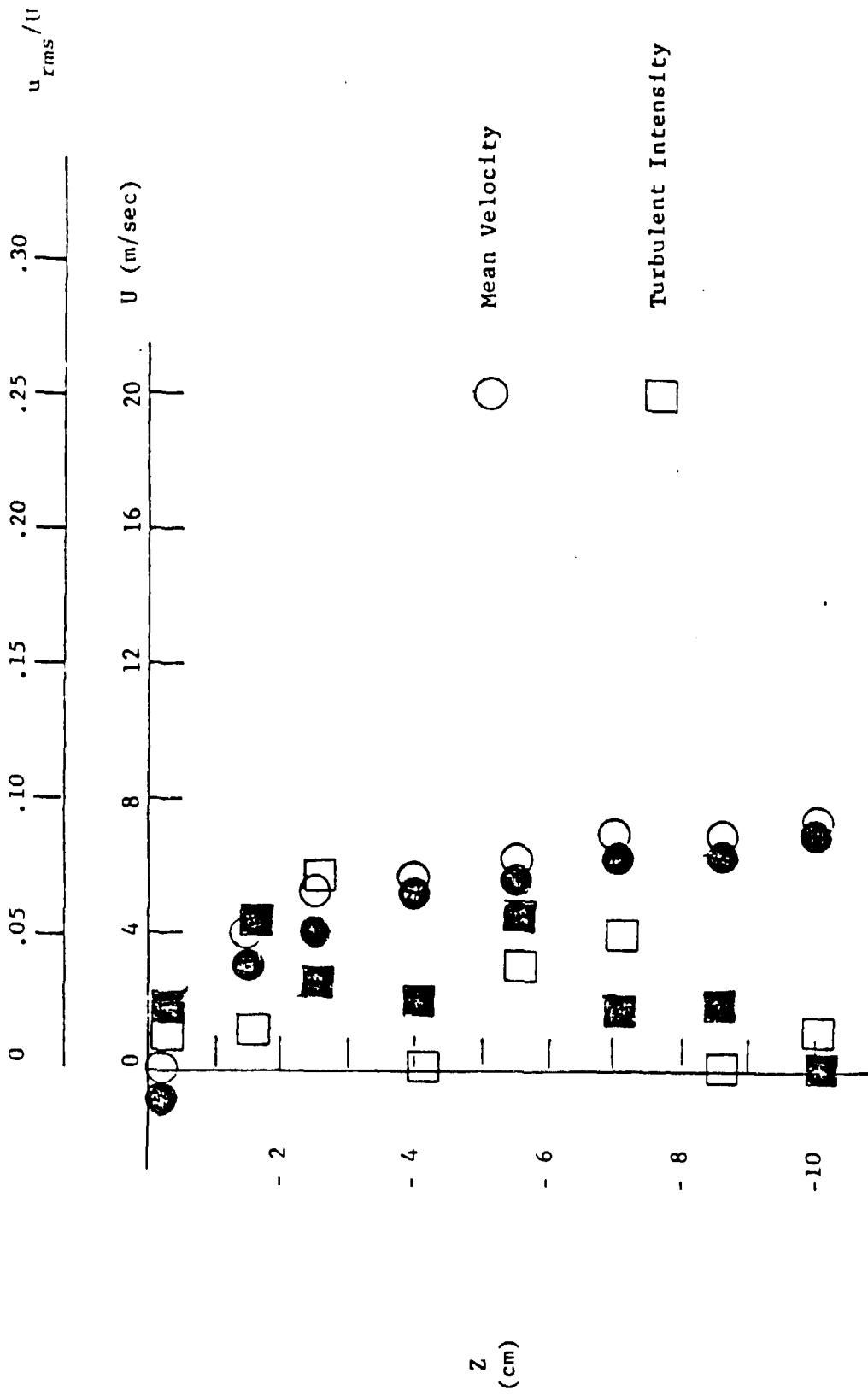
Figure 15. Mean Velocities and Turbulent Intensities at Location x/c = .02 (D).

Figure 16.  Mean Velocities and Turbulent Intensities
at Location  x/c = .04 (E).
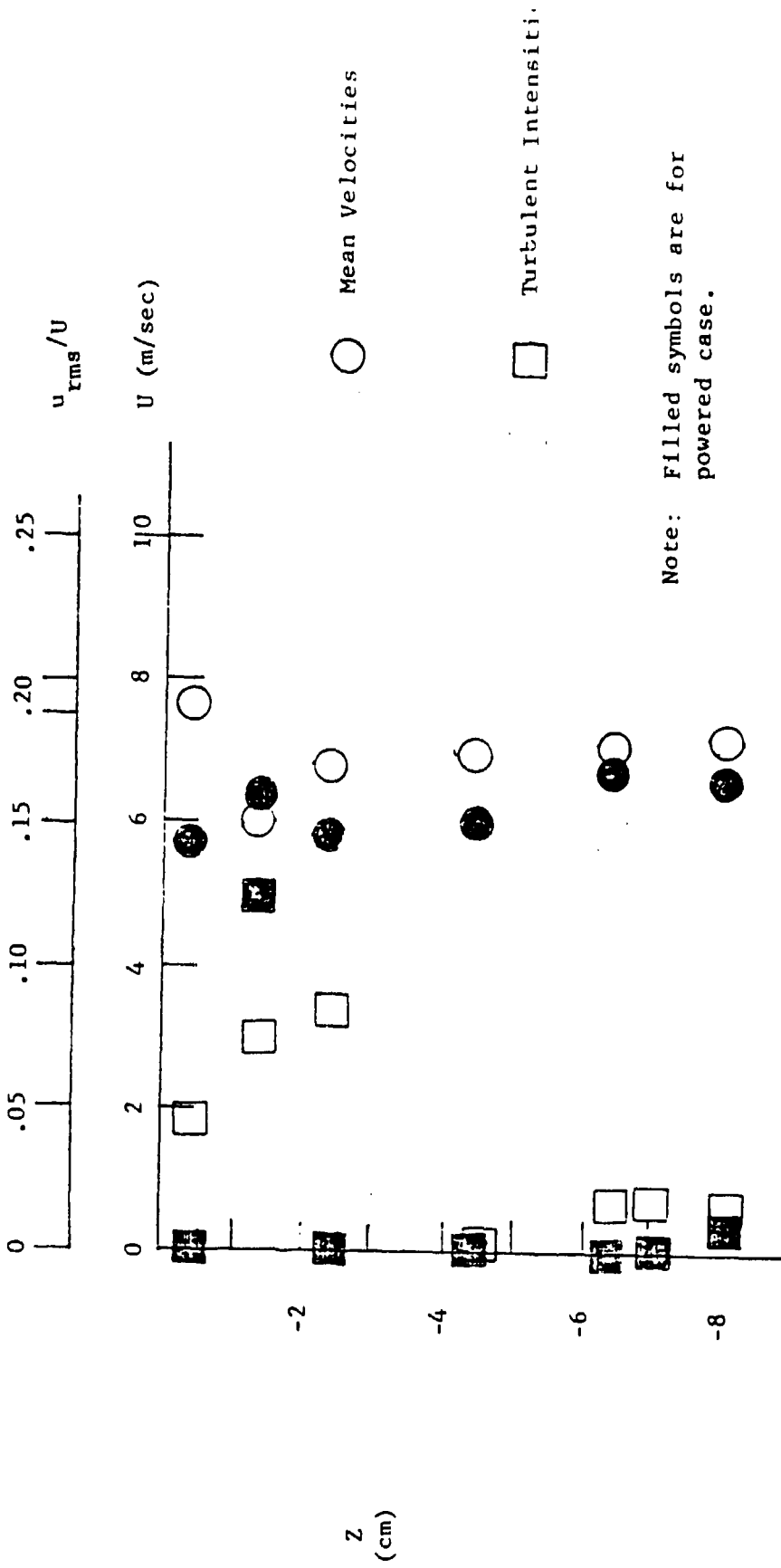
Figure 17. Mean Velocities and Turbulent Intensities at Location x/c = 0.2 (G).
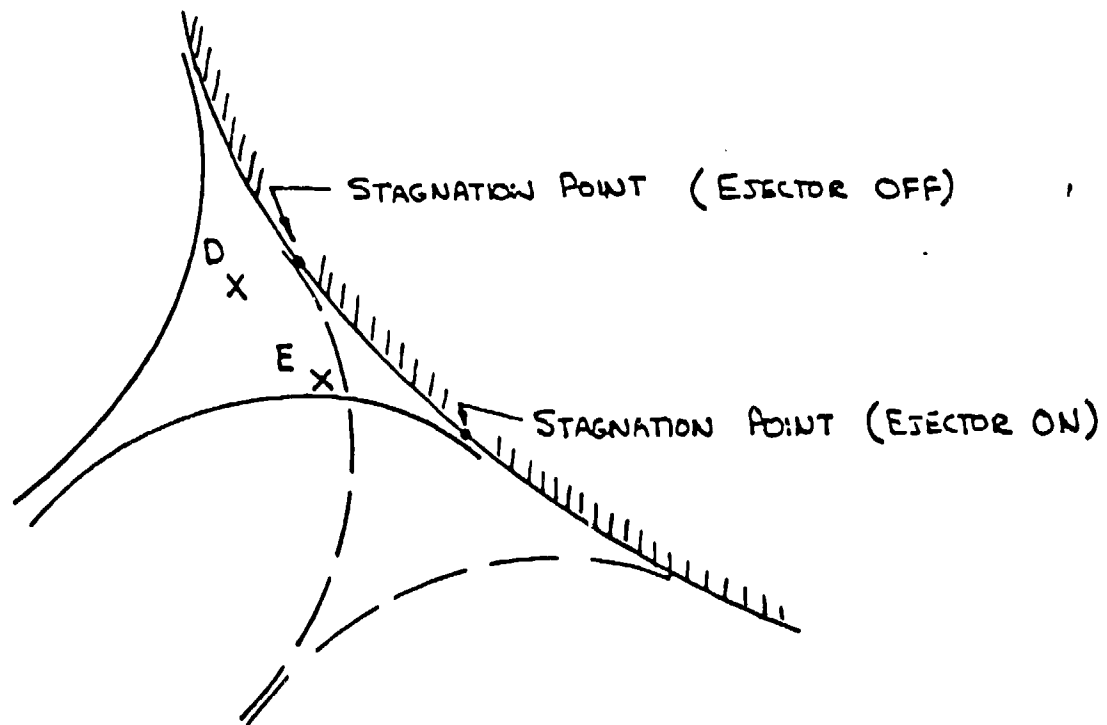
Figure 18.    Shift of Stagnation Point Location
              Caused by Powered Ejector.

907

Figure 19. Mean Velocities and Turbulent Intensities at
Location x/c = 44 (II).
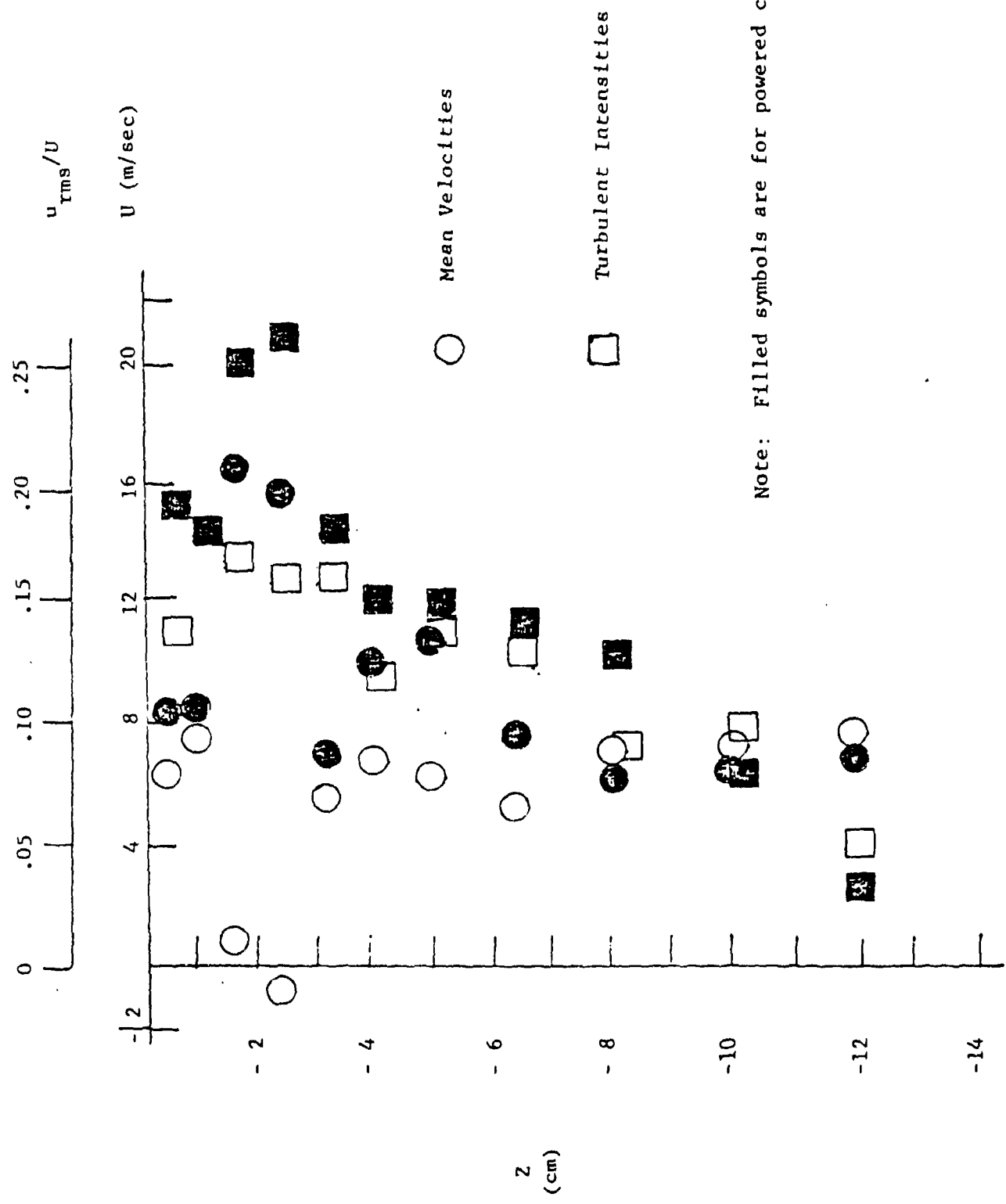
Note: Filled symbols are for powered case.

○ Mean Velocities

□ Turbulent Intensities
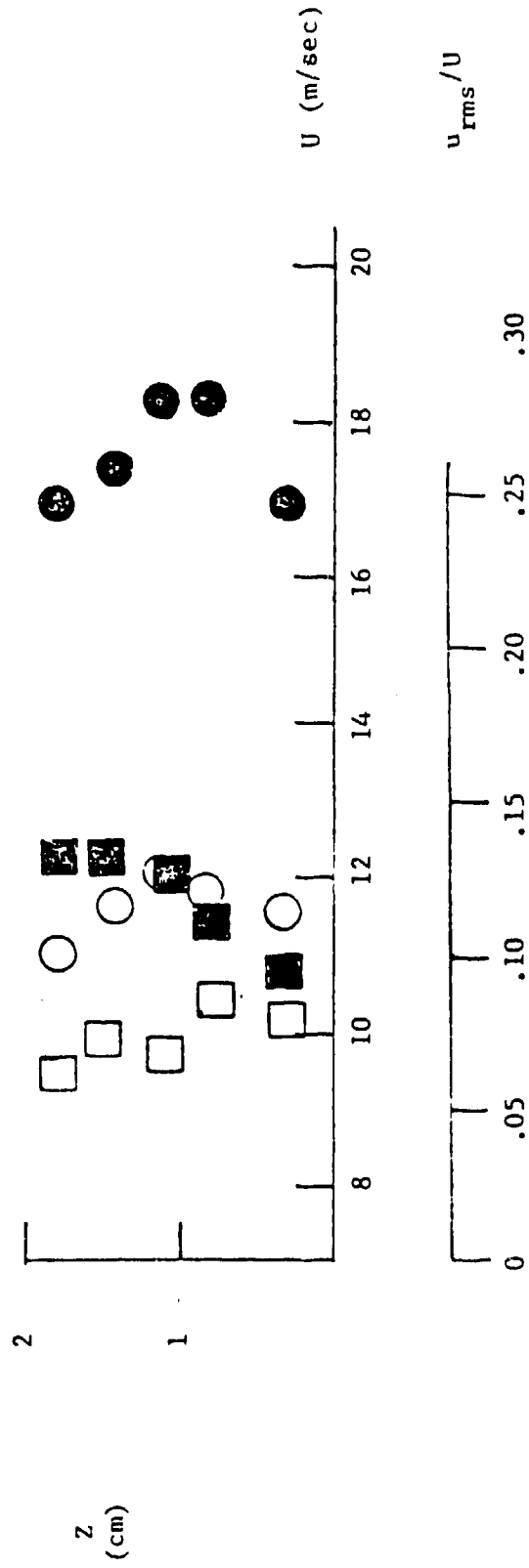
Figure 20. Mean Velocities and Turbulent Intensities
at Location x/c = .58 (J).

909
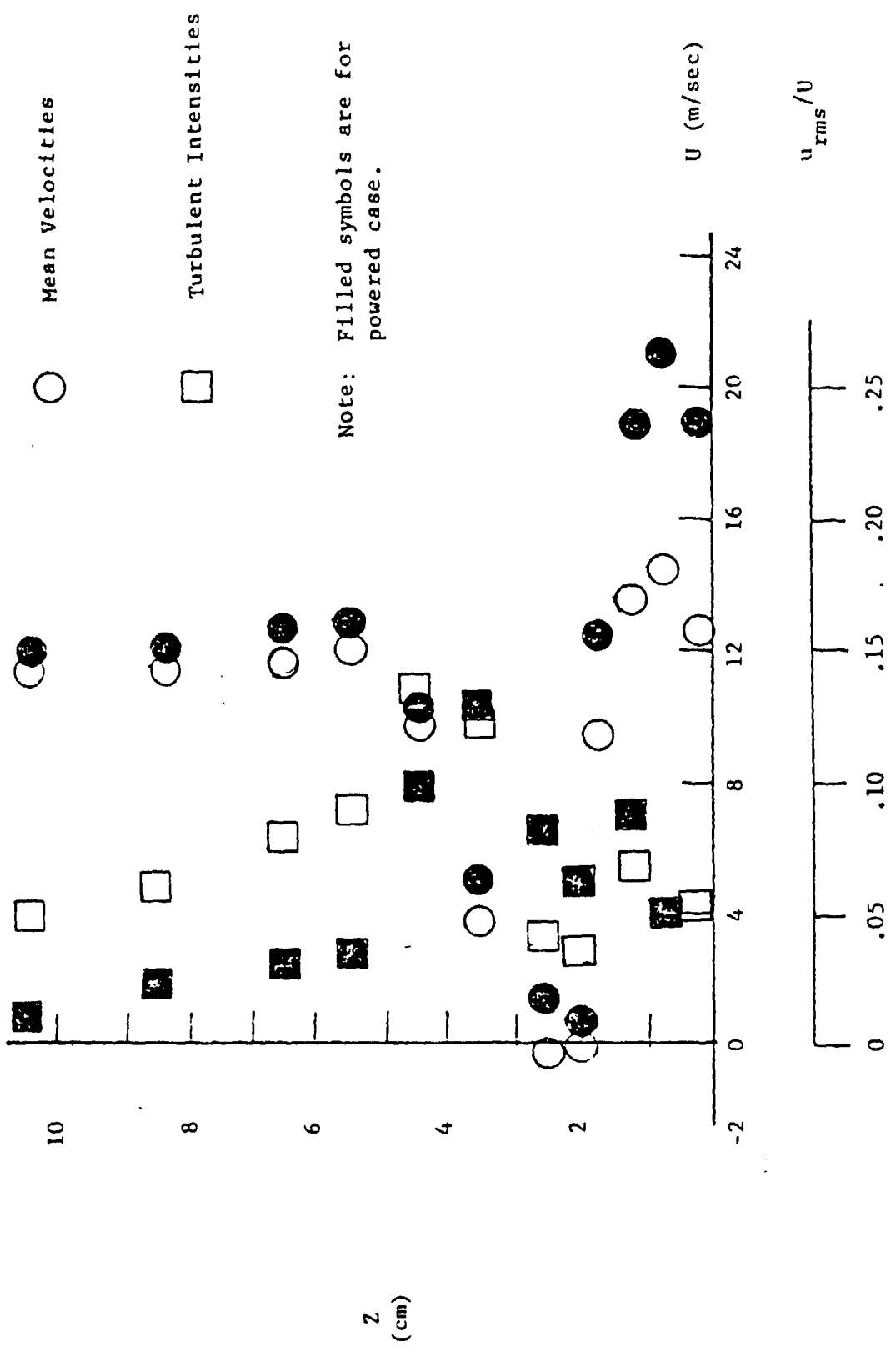
Figure 21. Mean Velocities and Turbulent Intensities at Location $x/c = .72$ (K).

# EJECTOR THRUST AUGMENTATION LIFT SYSTEMS FOR SUPERSONIC V/STOL AIRCRAFT

BY

LCDR JAMES M. FARLEY
RONALD D. MURPHY
NAVAL AIR SYSTEMS COMMAND
WASHINGTON, D.C.

EJECTOR WORKSHOP
W-P AFB
AUG, 1981

911

# THRUST AUGMENTED WING (XFV-12A)
## TECHNOLOGY DEMONSTRATION PROGRAM
## (HISTORICAL REVIEW)

- NOV 1971 – "LETTER TYPE" RFP FOR V/STOL TECHNOLOGY DEMONSTRATOR
  LONG ENDURANCE (SUBSONIC)/FIGHTER-ATTACK (SUPERSONIC)
  COMPATIBLE WITH SEA CONTROL SHIP
  IMAGINATIVE IDEAS WHICH EXPLORE TECHNOLOGY OPPORTUNITIES.

- OCT 1972 – ROCKWELL SELECTED TO DEVELOP XFV-12A

- THRUST AUGMENTATION BENEFITS:
  HIGHLY RESPONSIVE LIFT CONTROL SYSTEM
  BENIGN ENVIRONMENT
  OVERALL MISSION PERFORMANCE
  REDUCED POWER PLANT COSTS

- PROGRAM OBJECTIVES:
  COMPATIBILITY OF ENGINE AND DIVERTER
  EFFICIENT DUCTING TO AUGMENTERS
  AUGMENTATION RATIO FOR VTOL
  VTOL AND TRANSITION HANDLING QUALITIES
  FLYING QUALITIES WITH LOW CANARD (CTOL)

# XFV-12A CONFIGURATION



ENHANCED MIXING
CENTERBODY NOZZLE

AFT DIFFUSER FLAP
(ELEVON)

FORWARD
DIFFUSER FLAP

$\delta_0$

VTOL MODE

CTOL MODE
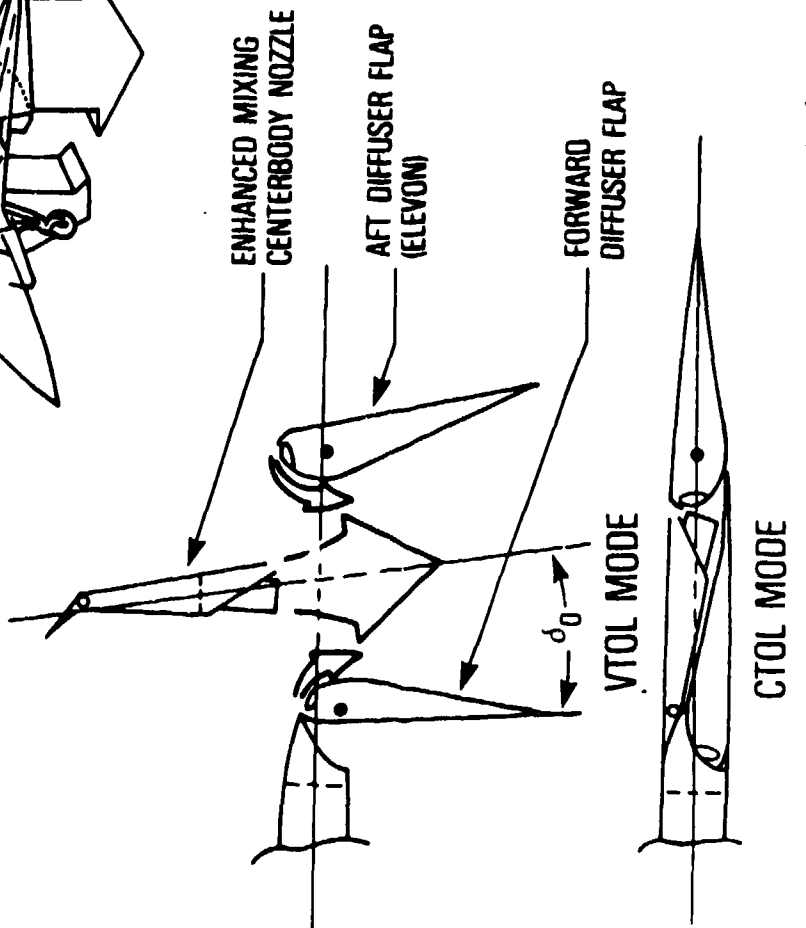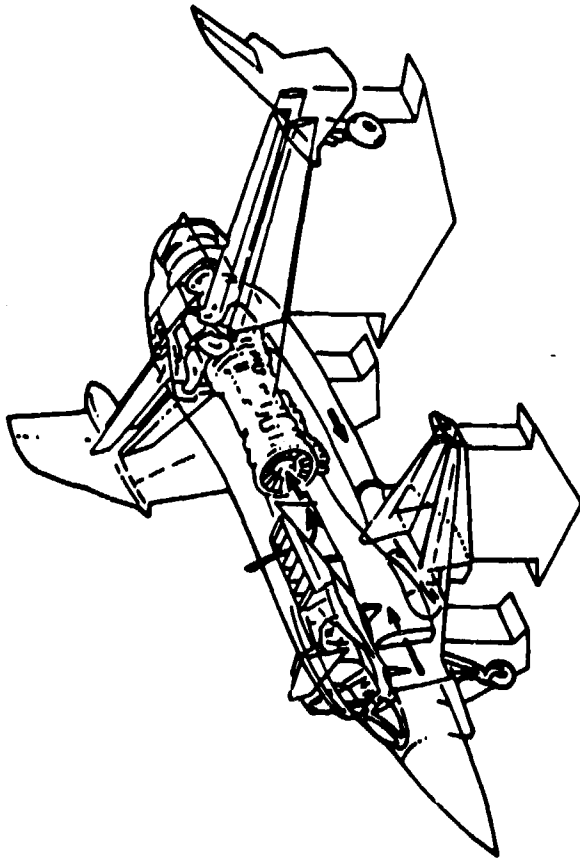
AUGMENTATION
RATIO – $\phi$

$\dfrac{LIFT}{F_{N_{ISEN}}}$

DIFFUSER HALF ANGLE – $\delta_D$
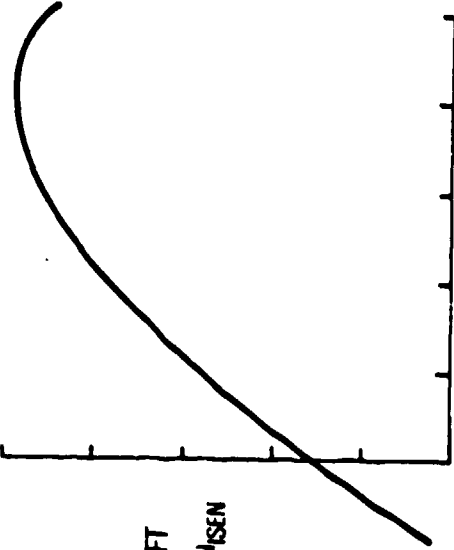
# RESULTS OF TETHERED HOVER TESTING AT NASA – LANGLEY

**GOOD NEWS** FUNCTIONAL COMPATIBILITY: ENGINE/DIVERTER
CONTROL MECHANIZATION
COCKPIT CONTROLS

EFFICIENT DIVERTER/DUCTING SYSTEM: 3% $F_N$ LOSS DUE TO LEAKAGE
10% $F_N U$ LOSS DUE TO $P_T$ LOSS

BENIGN ENVIRONMENT

EFFICIENT TRIFRICATED INLET ~ 97-98%

NO POWER PLANT PROBLEMS: 28.8 HRS RUN TIME AT LRC
5.4 HRS INTERMEDIATE AT LRC

STRUCTURAL INTEGRETY – HOT GAS FLOW: SUPER PLASTIC FORMING
(ONLY TWO DUCTING FAILURES)             HONEYCOMB PANELS
                                        BELLOWS AND SEALS

VTOL CONTROLS: NO HYSTERESIS PROBLEMS
EXCELLENT CONTROL/FORCE RESPONSE

CONFIRMED POSITIVE G/E CHARACTERISTICS

VERIFICATION OF UNIQUE VTOL TEST FACILITY

**BAD NEWS**    WING:      $\Phi_{GOAL} = 1.50$    $\Phi_{ACHIEVED} = 1.26$

CANARD:    $\Phi_{GOAL} = 1.30$    $\Phi_{ACHIEVED} = 1.11$

914

# WING AUGMENTER DIAGNOSTIC TESTING

**WHIRL RIG**   RECONFIGURE THE MODEL: SIMULATE DIVERTER
                                        SIMULATE FUSELAGE

UTILIZE AIRCRAFT DUCTING AND AUGMENTER
VALIDATION OF $\Phi_W = 1.26$

**COMPONENT TEST**   COLD FLOW:   FORWARD DIFFUSER
                                  AFT DIFFUSER
                                  I/B AND O/B END WALL NOZZLES
                                  CENTERBODY SEGMENT

HOT FLOW:    FORWARD DIFFUSER
             AFT DIFFUSER
             CENTERBODY

RESULTS:     POOR MIXING OF CENTERBODY NOZZLE
             LOW COMPONENT $C_T$'s
             FLOW ANGULARITY PROBLEMS
             POOR $P_T$ DISTRIBUTIONS

CONCLUSIONS: GEOMETRIC VARIATIONS OF
             (1) AUGMENTER GEOMETRY
             (2) FEED SYSTEM

**RECOMMENDATIONS**   INITIATE A REMEDIAL DEVELOPMENT PROGRAM
                      WING, CANARD, LRC

915

# WING AUGMENTER REMEDIAL DEVELOPMENT PROGRAM

- 0.20 SCALE MODEL SYSTEMATIC TESTING
  COANDA GEOMETRY
  RECTANGULAR AUGMENTER (MIDSPAN GEOMETRY)
  TAPERED AUGMENTER

- MORE EMPHASIS ON ANALYTICAL CAPABILITY

- FULL SCALE COMPONENT DEVELOPMENT
  AFT DIFFUSER SEGMENT MODEL
  CENTERBODY FEED MODEL
  CENTERBODY SEGMENT MODEL
  ENDWALL NOZZLES
  COLD FLOW TESTING OF FINAL COMPONENT

- FULL SCALE TESTING ON WHIRL RIG
  COMPONENT TESTING
  AUGMENTER SHROUD
  FULL AUGMENTER

- REQUIREMENTS:  φ (RECTANGULAR) = 1.65
                  φ (TAPER)       = 1.60

- RECOMMENDATIONS: UPON OBTAINING THE REQUIRED WING PERFORMANCE A
  CANARD REMEDIAL DEVELOPMENT PROGRAM SHOULD BE
  INITIATED

916

# WING AFT DIFFUSER (ELEVON) DEVELOPMENT
## (FULL SCALE)



917
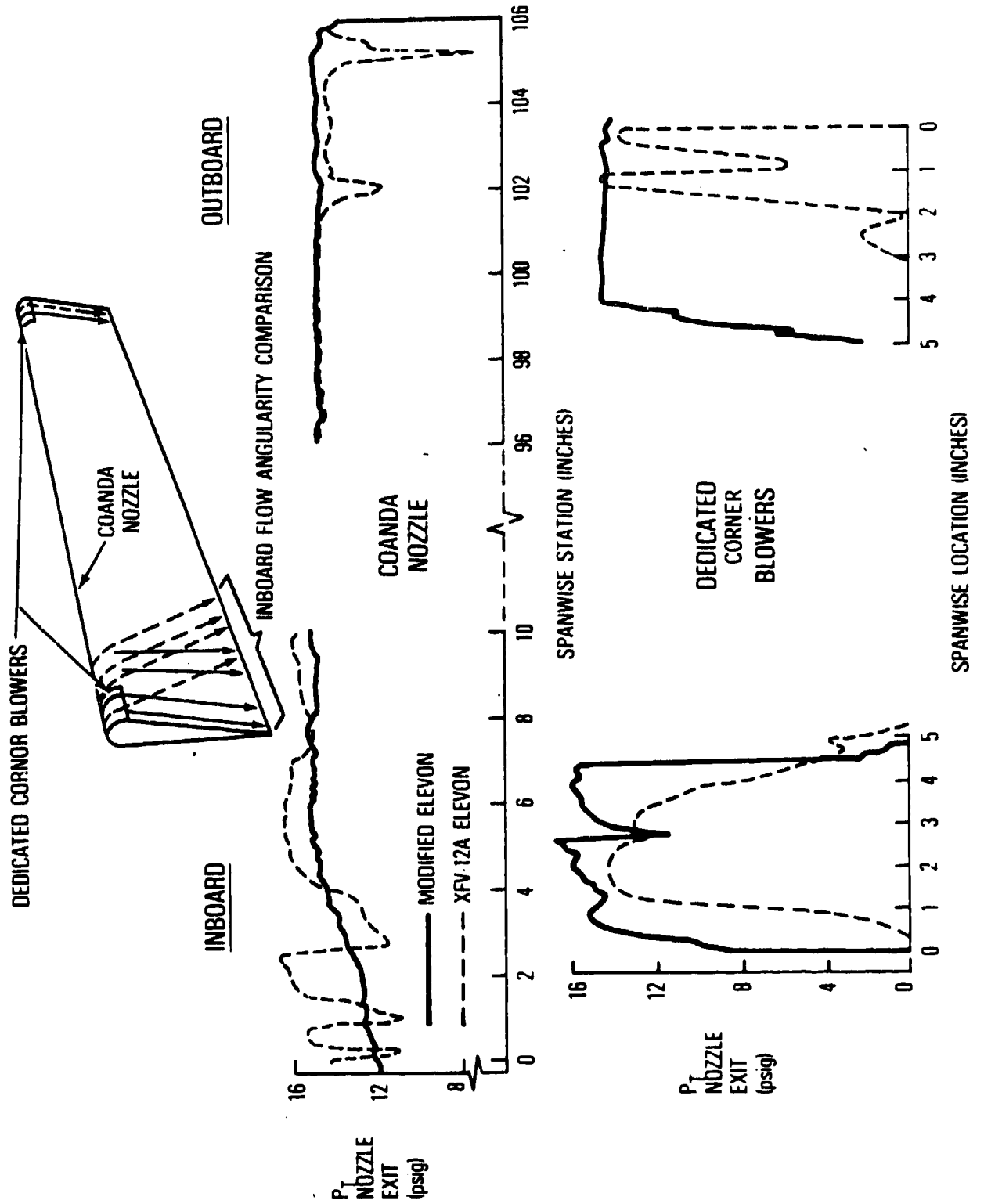
WING AUGMENTER CENTERBODY NOZZLE
DEVELOPMENT
(0.20 SCALE)
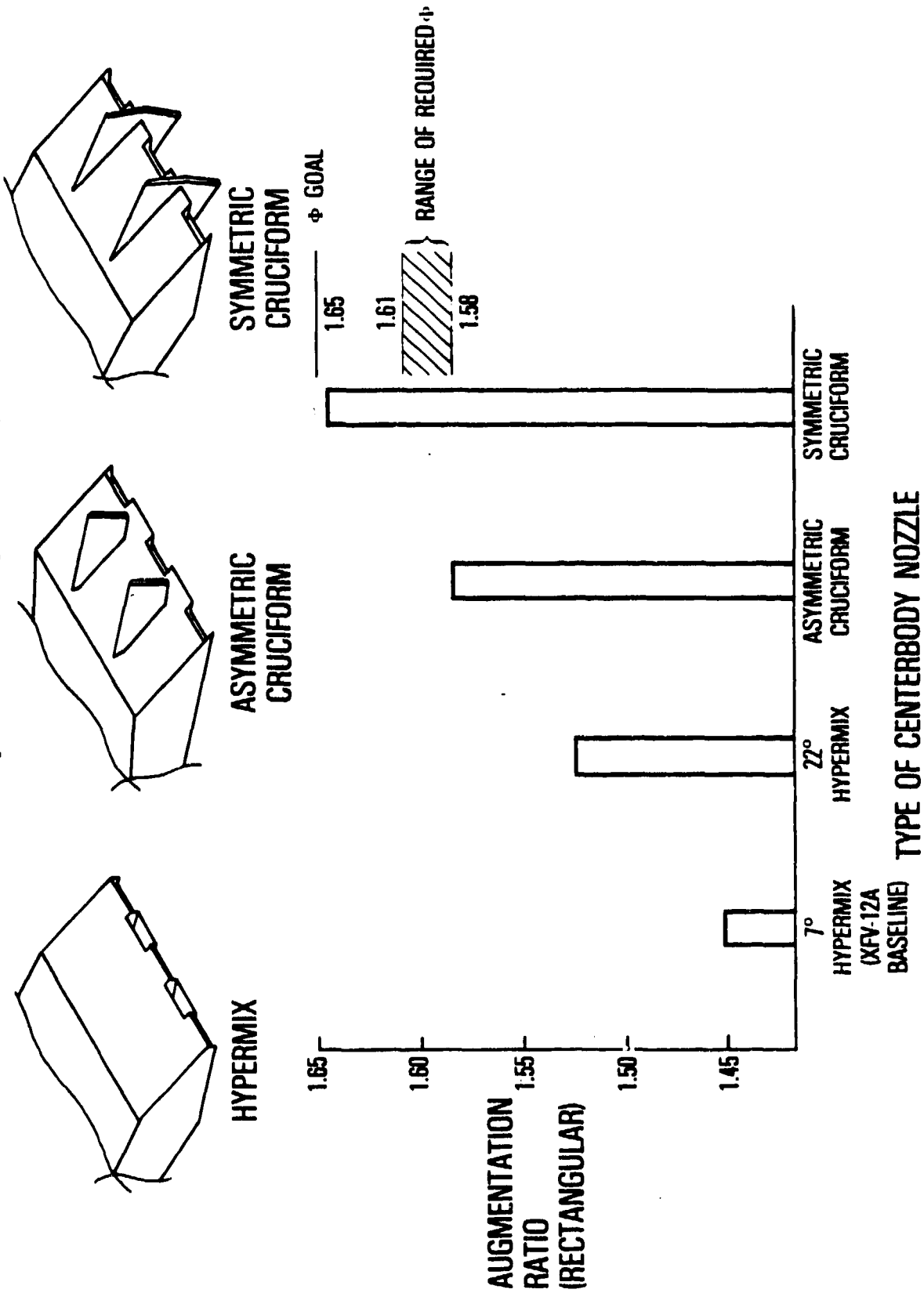
# AUGMENTER INTEGRATION COMPARISON
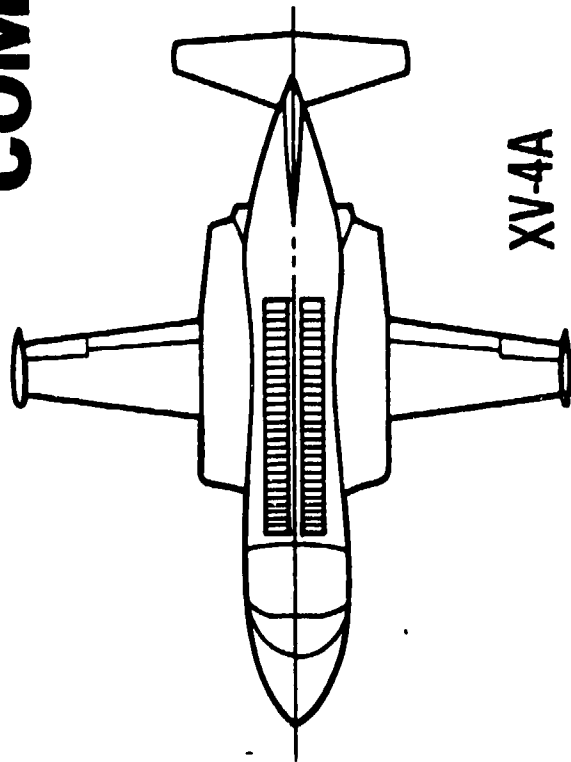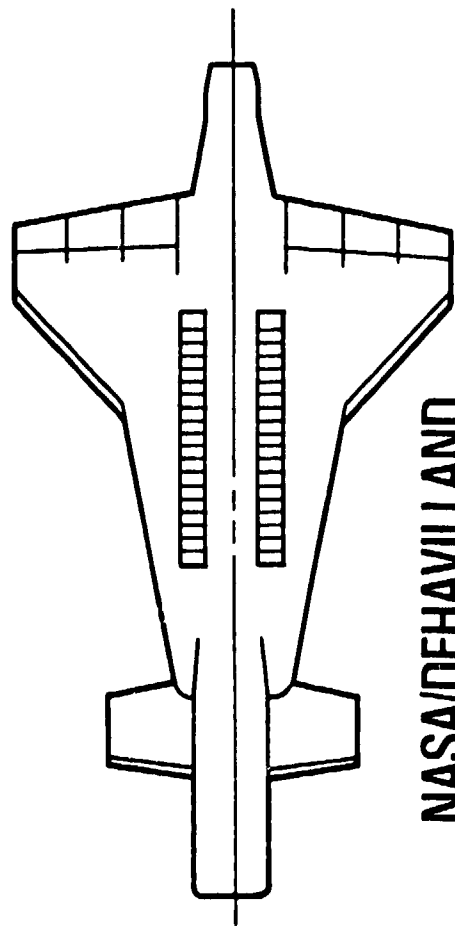
NASA/DEHAVILLAND AUGMENTER
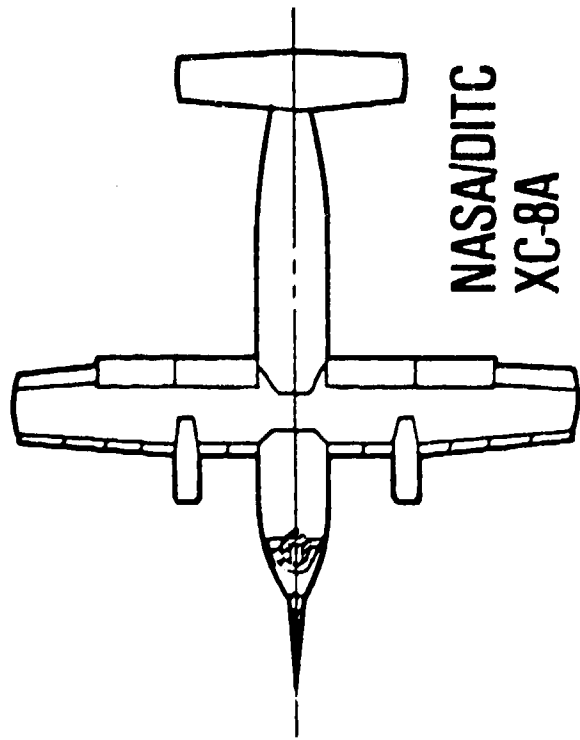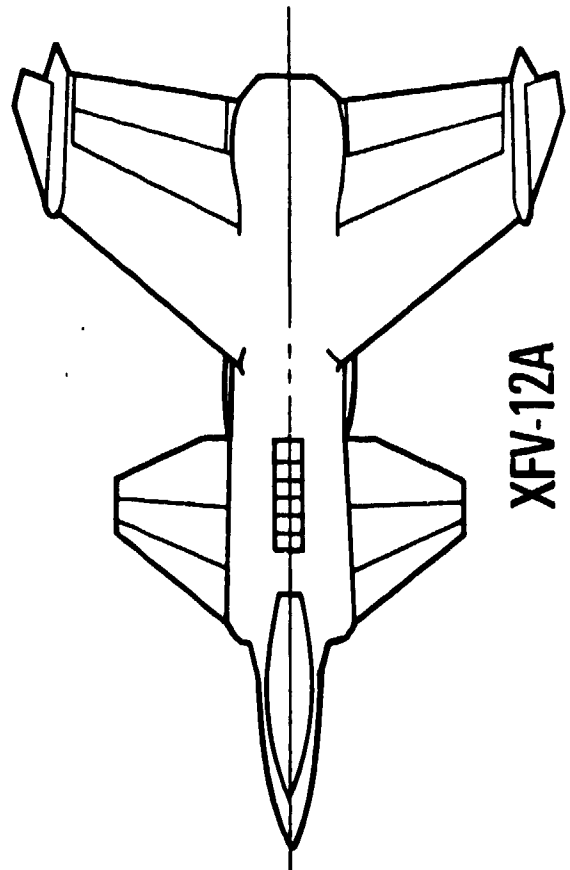
XFV-12A

XV-4A

NASA/DITC XC-8A

# AUGMENTER GEOMETRY COMPARISON
## (NORMALIZED TO THROAT WIDTH)



XFV-12A

XV-4A

NASA/DITC XC-8A

NASA/DEHAVILLAND AUGMENTER
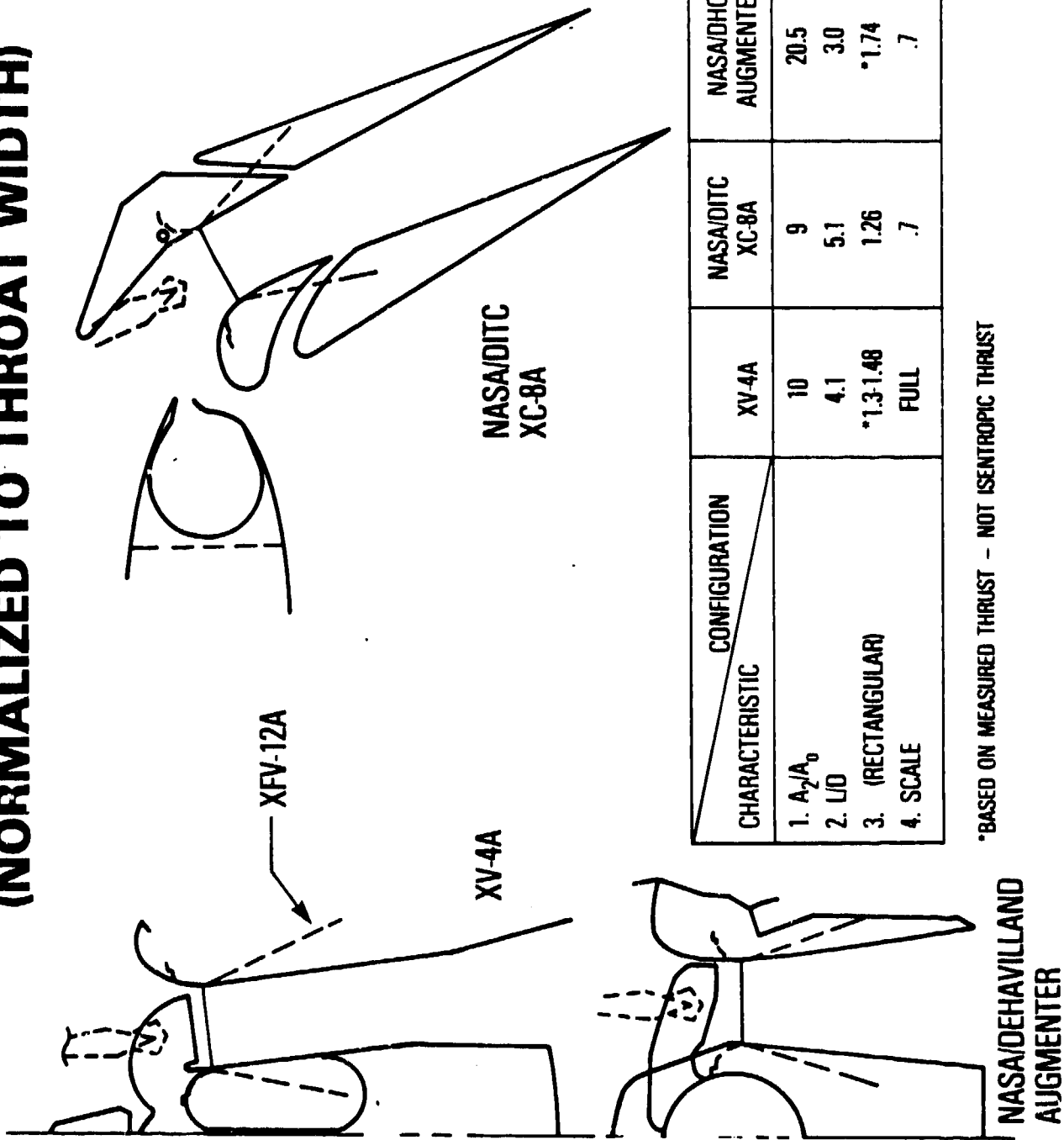
| CHARACTERISTIC / CONFIGURATION | XV-4A | NASA/DITC XC-8A | NASA/DHC AUGMENTER | XFV-12A |
|---|---|---|---|---|
| 1. $A_2/A_0$ | 10 | 9 | 20.5 | 20.1 |
| 2. L/D | 4.1 | 5.1 | 3.0 | 1.5 |
| 3. (RECTANGULAR) | *1.3-1.48 | 1.26 | *1.74 | 1.62-1.64 |
| 4. SCALE | FULL | .7 | .7 | .2 |

*BASED ON MEASURED THRUST – NOT ISENTROPIC THRUST

920

# AIRCRAFT MODIFICATION FOR RECTANGULAR AUGMENTERS
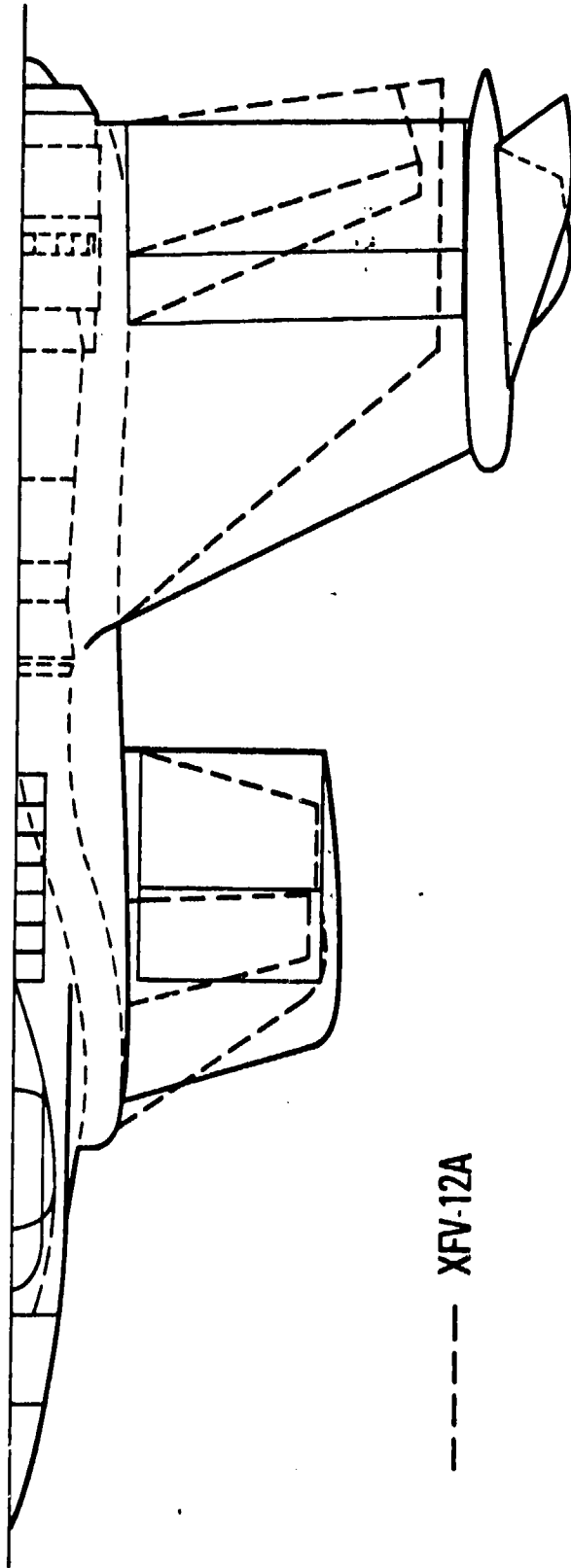


--- XFV-12A

| AUGMENTER CHARACTERISTICS | $A_0$ | $A_2$ | $A_2/A_0$ | L/D | SPAN | THROAT WIDTH | THROAT AR | 0 |
|---|---|---|---|---|---|---|---|---|
| WING MODEL (SCBT15-12) | 5.0 | 100.0 | 20.1 | 1.44 | 20.0 | 5.0 | 4.0 | 1.62 |
| *AIRCRAFT (WING) | 4.8 | 97.5 | 20.5 | 1.60 | 23.7 | 4.1 | 5.7 | 1.60 |
| (CANARD) | 6.1 | 84.8 | 13.8 | 1.24 | 12.9 | 6.6 | 1.96 | 1.45 |

*0.20 SCALE

# NAVY ASSESSMENT OF AIRCRAFT
# DEMONSTRATOR DEVELOPMENT PROGRAM

TECHNICAL ISSUES:  Φ PREDICTION

- SMALL SCALE ⟶ LARGE SCALE
- COLD TO HOT
- MECHANIZATION

f (Φ PERFORMANCE)

- GROUND EFFECT
- REINGESTION
- CONTROL POWER

PROGRAM ISSUES:  COST/RISK TRADEOFF

NAVY V/STOL OBJECTIVES GUIDANCE

# NAVY PROGRAM DECISION

- DELAY DEMO AIRCRAFT DEVELOPMENT PROGRAM

- CONSIDERATION OF ADDITIONAL AUGMENTER INTEGRATION CONCEPTS

- REASSESS ETA PROGRAM

  - NAVY V/STOL PROGRAM GUIDANCE
  - NAVY V/STOL PRIORITIES
  - HIGH SPEED CONCEPT VERIFICATION

# AUGMENTER INTEGRATION PHILOSOPHY (SUPERSONIC)

CHORDWISE AUGMENTER

CHARACTERISTICS

SPANWISE AUGMENTER

| CHARACTERISTICS | CHORDWISE AUGMENTER | SPANWISE AUGMENTER |
|---|---|---|
| VOLUME AVAILABILITY | HIGH | LOW |
| ENHANCED MIXING | NO | YES |
| COANDA BLOWING | NO | YES |
| END WALL BLOWING | NO | YES |
| MECHANIZATION | SIMPLIFIED | DIFFICULT |
| CLOSEOUT-CTOL | SIMPLIFIED | DIFFICULT |
| TRANSITION | UNKNOWN | GOOD |

POTENTIAL OPTIMUM CONFIGURATION

924

# EJECTOR THRUST AUGMENTATION DEVELOPMENT PLAN

FUNDAMENTALS

SCALE EFFECTS

SMALL SCALE TESTS

PRELIMINARY DESIGN

FULL SCALE ETA VALIDATION TESTS

INTEGRATION

AIRCRAFT TECHNOLOGY DATA BASE

DESIGN SYNTHESIS

OPERATIONAL CONCEPT

FLIGHT TEST DEMO

CONCEPT VALIDATION

TECHNOLOGY DEMONSTRATOR CONCEPT

REFINED ETA REQUIREMENTS

REQUIRED ADVANCED TECHNOLOGY DEVELOPMENT

# NAVAIR RECOMMENDATIONS

- PURSUE JOINT INVOLVEMENT IN ETA DEVELOPMENT

- DEVELOPMENT PLAN (NEAR TERM)

  ETA VALIDATION: SMALL SCALE COLD
  
                                SMALL SCALE HOT
  
                                FULL SCALE MECHANIZED
  
                                (ALL WITH GEOMETRIC SIMILARITY WITH
  
                                CLOSE OUT CAPABILITY)

  ANALYSIS:      FUNDAMENTAL MODELING
  
                        AUGMENTER PERFORMANCE

- DESIGN STUDIES

- GROUND BASED TESTING FOR CONFIGURATION CONCEPT VALIDATION

- TECHNOLOGY DEMONSTRATION OF ETA V/STOL AIRCRAFT
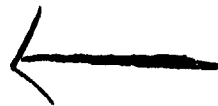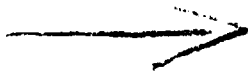
926

SOME APPLICATIONS OF EJECTOR TECHNOLOGY
TO STOL AND V/STOL AIRCRAFT PROJECTS

BY D.B. GARLAND

THE DE HAVILLAND AIRCRAFT OF CANADA, LIMITED
DOWNSVIEW, ONTARIO, CANADA


EJECTOR WORKSHOP FOR AEROSPACE APPLICATIONS
AUGUST 3-5, 1981, DAYTON, OHIO.

927

SOME APPLICATIONS OF EJECTOR TECHNOLOGY
TO STOL AND V/STOL AIRCRAFT PROJECTS

BY D.B. GARLAND

THE DE HAVILLAND AIRCRAFT OF CANADA LIMITED

ABSTRACT

A discussion of some elements of ejector technology,
as developed at DHC, is presented.  Three operational
areas are considered, i.e.

(a)  Static or hovering condition

(b)  Low forward speed (STOL regime)

(c)  High subsonic cruise

Subsequently, three project study aircraft are introduced
to illustrate the application of ejectors in their
respective operational areas.  These aircraft are:

(a)  An advanced turbo fan powered STOL transport

(b)  A STOVL supersonic combat aircraft

(c)  A STOVL subsonic support aircraft.

## INTRODUCTION

This presentation describes some tec... al aspects of ejector technology as developed at DHC and ways in which such technology may be incorporated in high performance aircraft to overcome some of the penalties normally associated with powered lift.

Three operational areas for ejectors are discussed, viz.

      (a)   Static thrust augmentation

      (b)   Augmentation in the STOL regime

      (c)   High subsonic cruise operation.

Subsequently, three project study aircraft are introduced to illustrate the application of ejectors in their various operational areas.  These aircraft are:

      (a)   An advanced turbo fan powered STOL transport

      (b)   A STOVL supersonic combat aircraft

      (c)   A STOVL subsonic support aircraft.

EJECTOR TECHNOLOGY AT DHC

Some of the aspects of augmentor technology which have been considered
at DHC in recent years are discussed below.  They are grouped for convenience
under headings relating to three operating speed regimes, i.e. static (zero
forward speed), low forward speed typical of STOL take-off and climb-out, and
high subsonic cruise speed.

(a) Static Thrust Augmentation

The well established requirements for maximizing thrust augmentation
ratio can be expressed as:

(i)     Large secondary/primary area ratio

(ii)    Large diffuser area ratio (DAR)

(iii)   Uniform velocity distribution at diffuser exit

(iv)    Low inlet and friction losses.

Each of these requirements is compromised to some extent when an ejector
is integrated with an airframe, the so-called 'packaging restraints'.  Diffuser
area ratio may be limited by flow separation or unsteady flow, by choking of
the augmentor throat or by the dominant effect of inlet or friction losses.
The last two requirements given above are functions also of the design approach,
especially of the primary nozzle array.

The approach taken at DHC has been towards a simple arrangement, as
shown in Figure 1, which eliminates the need for separate devices for control
of flow separation in the diffuser.  The high aspect ratio lobe nozzles essen-
tially span the throat and the flow from the nozzles is arranged to 'blow' the
diffuser walls - the gap between the nozzle extremities and walls is optimized
experimentally to suit the DAR for maximum thrust augmentation.  Additionally,
the gap between the end nozzles and the end-walls is also optimized to control
flow separation there.  The net result is that diffuser flow breakdown is
postponed to values of DAR beyond that for maximum thrust augmentation ratio.
This is seen in Figure 2 where some typical experimental data are displayed.
Here it should be noted that the gross thrust augmentation ratio, $\phi_G$ , is
defined as the measured thrust divided by the actual (not ideal) nozzle thrust
which would be generated by expanding the same nozzle flow from the same nozzle
total pressure to ambient pressure.  The peak wall Mach number, $M_w$, is calculated
from the wall static pressure assuming that the local total pressure is ambient,
i.e. no inlet losses or jet mixing increments are considered significant at the
throat between nozzles where $M_w$ static taps are located.

930

Uniformity of diffuser exit velocity distribution is a function of nozzle pitch, nozzle width and augmentor length. Nozzle designs other than plain convergent slots can sometimes be used to improve jet mixing rate and uniformity of exit flow. The choice of nozzle pitch depends on trade-offs of inlet losses and weight of nozzles against exit uniformity. DHC laboratory models have air supplied axially to the nozzles whereas some large-scale models powered by jet engine exhaust have hot gas supplied transversely to the nozzles (see Figure 3). In this case the entry duct is approximately airfoil shaped and the entry Mach number is about 0.3 to minimize the nozzle cross-section and hence inlet losses. The transverse velocity component at the nozzle exit plane, due to the duct entry velocity, is counteracted by the swept nozzle exit plane.

The effects of operating ejectors at high nozzle pressure ratio (NPR) have been studied extensively in our work. The importance of high pressure, of course, is that duct sizes and/or pressure losses can be minimized. Nozzle exit area is also reduced for the same thrust and ejector secondary/primary area ratio is thereby increased. The ejector length/nozzle width ratio is also improved and a greater thrust augmentation ratio generally occurs. This is in spite of degradations in $\phi_G$ which occur as a result of high NPR per se and as a result of lower optimum DAR at higher pressure ratio.

Experimentally, it is found that the diffuser area ratio for maximum $\phi_G$ is reduced as NPR is increased. This effect can be duplicated theoretically by inclusion of a simple frictional loss term in the compressible ejector equations. It then appears that the frictional losses due to the high secondary flow velocities at high NPR preclude the use of higher diffuser area ratios. Another limit to useable DAR occurs for some ejector geometries with low secondary/primary area ratios where the throat velocity becomes sonic. Increasing DAR then merely generates a supersonic region, especially near the curved diffuser walls, which is terminated by a shock which separates the diffuser flow. A completely supersonic secondary/mixed flow is presumably achievable under some very high NPR conditions.

Operations of ejectors with hot gas primary flow (temperatures up to 700°C) showed no significant performance difference as compared with room temperature air operation, based on our limited experience.

931

(b)  Augmentation at Low Flight Speeds

At forward speed the performance of an ejector is commonly expressed as $X_{NET}/X_N$ versus $V_\infty/V_J$, where

$X_{NET}$ = Augmentor exit gross thrust - inlet momentum drag

$X_N$ = Primary nozzle thrust

$V_\infty$ = Flight velocity

$V_J$ = Primary jet velocity, expanded to ambient pressure

Both theory and experiment show reasonably good collapse on this basis over a wide range of flight speed and jet velocity (NPR) for an ejector of fixed geometry. Theoretical results, using simplified global theory but with representative frictional losses, show that the optimum diffuser area ratio decreases with increasing forward speed. A typical result is shown in Figure 4. Experimental results have been obtained at DHC on a forward speed simulator rig, shown in Figure 5. Normally, of course, a wind tunnel model test would be used to determine forward speed effects but in practice the close integration of ejector with air frame makes the isolation of thrust lapse rate from other aerodynamic forces very difficult. The simulator rig reproduces the primary and secondary flows through the ejector only and hence isolates it from external aero-dynamic effects. It consists of the primary nozzle assembly (actually an old wind tunnel model) mounted within a pressurized box or plenum chamber, the air flow through which provides the secondary ejector flow at a stag-nation pressure equivalent to the simulated flight speed. The primary and secondary flow rates are both accurately measured. The whole rig is on a balance and the ejector exit gross thrust is accurately measured. Net thrust is obtained by difference between gross thrust and calculated inlet momentum drag, $\dot{m}_{SEC} V_\infty$. With the test rig as shown, ingestion of main foil boundary layers is not simulated and the diffuser exit pressure is ambient.

Figure 6 shows some typical test data obtained with a simple ejector having a plain, horizontal slot nozzle. The results follow the theoretical trend. Other data, not shown, indicate that results are rather dependent on configuration details, as might be expected, since

932

inlet losses determine performance differences to a large extent. At velocity ratios typical of STOL take-off ($V_\infty/V_J$ between, say, 0.08 and 0.12, for engine by-pass air schemes), the statically optimized augmentor is usually close to optimum at forward speed. At higher climb-out speeds, however, the diffuser area ratio will probably need to be reduced for best performance.

### (c) High Subsonic Cruise Operation

Development of the cruise augmentor at DHC has been closely linked with the development of the thick multi-foil wing (see Figure 7). As a result it becomes a quite different augmentor from that used for VTOL hovering, for example. It has evolved, so far, around a continuous, horizontal, slot nozzle in the trailing edge of the main foil giving a low drag installation. The diffuser area ratio at cruise is only about 1.10 for optimum performance and diffuser wall boundary layer control is then not a problem. The effective DAR is, in fact, noticeably lower than the geometric value due to the relaxing effects of the main foil boundary layer. At high speed, the location of the shrouds is largely dictated by external airfoil considerations and as a result the secondary/primary area ratio falls out at about 10. This compares with about 20 or more for typical hovering augmentors.

There are further direct effects of forward speed. For example, for ejectors supplied by flow from a by-pass engine, nozzle pressure ratio increases significantly between static sea level condition and cruise at high altitude and convergent/divergent nozzles might need to be considered. The diffuser exit static pressure is greater than ambient at forward speed (it increases with Mach number rather like the trailing edge stagnation pressure on an airfoil). The calculated effect is dependent on diffuser area ratio and velocity ratio and may be favourable or unfavourable (see Figure 8). Ingestion of the main foil boundary layers has a beneficial effect on the performance of the ejector at forward speed, reducing the effective drag coefficient $C_{D_{eff}}$ by about 10 or 20 drag counts, depending on flight conditions. The effective drag coefficient in this case represents the internal augmentor drag as modified by jet mixing effects. It is given by

933

$$D_{eff} = -X_{NET} + X_N$$

$$\text{so that } C_{D_{eff}} = \left(1 - \frac{X_{NET}}{X_N}\right) C_{J_N}$$

where $C_{J_N}$ $= X_N / qS$ , the jet coefficient based on nozzle thrust

## EJECTOR APPLICATIONS

### 1. Advanced STOL Transport

The augmentor wing powered lift concept has been demonstrated by the Buffalo/Spey research aircraft during some 750 hours of flying at NASA, Ames Research Center (Figure 9). Low speed performance and handling qualities have been explored with a wide variety of control systems, from manual to fully automated.

Design parameters for an advanced A-W STOL transport (Figure 10) are under active study at DHC. The aircraft incorporates ejector technology in the augmentor flap for low speed flight (Figure 11) and in the powered multi-foil section for cruise. The high by-pass ratio Rolls-Royce RB419 blowing engine (Figure 12) provides high pressure (NPR = 3) air for the ejector. It features a variable pitch geared fan (particularly useful for flight path control) and a low velocity hot exhaust for low noise.

The multi-foil wing (or cruise augmentor flap) is a supercritical wing section designed to operate at high subsonic speed with or without ejector blowing. A brief history is given in Reference 1. It is an area of new technology which arose from a desire to simplify the Augmentor-Wing STOL concept (by eliminating both the need to divert blowing flow from the wing to a separate propulsion nozzle and to close down the flap elements in cruise). At the same time, certain aerodynamic advantages were visualized, including

(a) delayed drag rise Mach number, by aft loading on the upper shroud and mid-chord control of the boundary layer,

(b) increased propulsive efficiency arising from ingestion of the wing boundary layers by the ejector,

(c) improved buffet boundary due to ejector blowing

(d) increased thickness/chord ratio compared with single foils for the same $M_D$.

These benefits were essentially demonstrated by two-dimensional,

934

high Reynolds Number tests at NAE, Ottawa. Reflection-plane, half-wing tests in the 11 x 11 foot transonic tunnel at Ames also showed a remarkably low induced drag (k close to unity)which more than compensates for the higher profile drag due to skin friction on the shrouds at typical cruise lift coefficients.

Subsequent theoretical analyses have suggested that the multi-foil concept is capable of operating at values of thickness/chord ratio as high as 30%, with a reduced drag divergence Mach number, of course. There are substantial structural weight savings even at 18% t/c, the currently tested value.

## 2. Supersonic STOVL Combat Aircraft

High thrust augmentation ejector technology has been applied to design studies of an "ejector lift/vectored thrust" combat aircraft based on the R.R. Pegasus powerplant (Figure 13). Engine fan flow is fed through a duct above the engine, forward to the ejector nozzles and rearward to a 'two-dimensional' propulsion nozzle which incorporates an after-burner system.

Vertical flight is achieved with fuselage ejector thrust plus vectored hot thrust from the Pegasus propulsion nozzle in the underside of the rear fuselage. Transition is by means of thrust transfer from ejector nozzles to 2-D nozzle and rotation of the 'hot' nozzle.

Joint research programs between DHC and NASA, Ames have included large scale static tests with a model powered by a J-97 engine (Figures 14 and 15) as well as wind tunnel tests in the 40 x 80 (Reference 2).

Some characteristics of the concept which relate to integration of the fuselage ejector are:
- Favourable ground effect, due to fuselage base pressure (see Figure 16)
- Minimal hot gas re-ingestion in ground effect
- Minimal interference of ejector efflux on wing aerodynamics in transition
- Good area distribution for low wave drag
- Cold flow afterburning.

935

Measured gross thrust augmentation ratio was 1.70 at NPR =2.5 with hot gas primary flow.

The large scale model incorporated a wing augmentor flap whereas the supersonic concept would use a simple blown flap for high lift in transition.

Transition characteristics of the fuselage ejector concept have been studied extensively in the wind tunnel (Reference 3) and by calculation methods (Reference 4). Both thrust transfer and thrust vectoring of the ejector nozzles have been shown to be possible methods of achieving satisfactory acceleration/deceleration and pitch trim.

### 3. STOVL Support Aircraft

The project design illustrated in Figure 17 represents an extrapolation of AW technology to USTOL or VTOL. A tilt-wing configuration is proposed which incorporates three main elements of technology:

- augmentor flap with choke controls and duct/nozzle system
- thick, multi-foil supercritical wing
- three-stream blowing engine with, in this case, a fixed pitch, geared fan.

The engine thrust split is about 40:40:20 for the fan, wing blowing nozzles and hot exhaust respectively. Of the blowing air, 50% is cross-ducted ahead of the front spar to vectoring propulsion nozzles at the wing tips. The remainder powers the augmentor flap across the full wing span. This arrangement assures essential balance in roll and yaw in the event of engine failure, for all angles of wing rotation. The aircraft would be capable of a fully safe take-off in the STO mode with one engine out, but would suffer a controlled crash in hover mode in the event of engine failure.

Incorporation of ejector technology requires a greater compromise in this design since hover and high speed cruise requirements are rather different for the wing ejector. The cold flow power transfer by ducting rather than shafting is an attractive feature however. The design illustrates a place for the three-stream engine in STOL and VTOL aircraft of the future.

936

## CONCLUSION

This presentation has provided a brief overview of some ejector technology and applications being studied at DHC. Despite past disappointments in the field of ejector V/STOL aircraft, it is believed that more serious attention should now be paid to this class of machine, especially in the light of emerging ejector technology.

## REFERENCES

1. Farbridge, J.E.
   Smith, R.C.
   "The Transonic Multi-Foil Augmentor Wing"
   AIAA Paper No. 77-606, June 1977.

2. Whittley, D.C.
   Koenig, D.G.
   "Large Scale Model Tests of a New Technology V/STOL Concept"
   AIAA Paper No. 80-0233

3. Garland, D.B.
   Harris, J.L.
   Whittley, D.C.
   "Phase 2 and 3 Wind Tunnel Tests of the J-97 Powered, External Augmentor V/STOL Model"
   NASA CR 152380, October 1980.

4. Garland, D.B.
   "Transition Characteristics of the External Augmentor V/STOL Aircraft Concept"
   Proc. NADC V/STOL Aircraft Aerodynamics Symposium, Naval Postgraduate School, Monterey, California. May 1979.

# LABORATORY AUGMENTOR MODEL
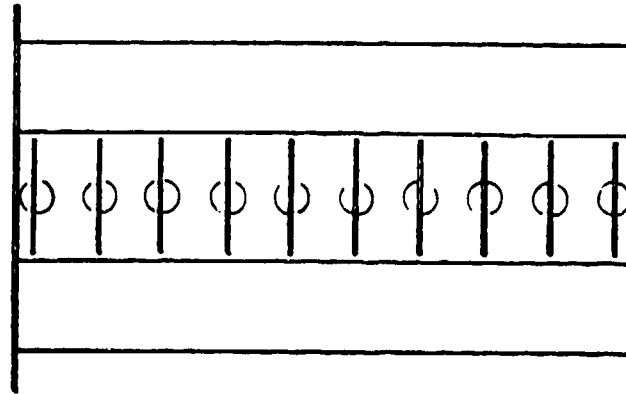


PLAN VIEW
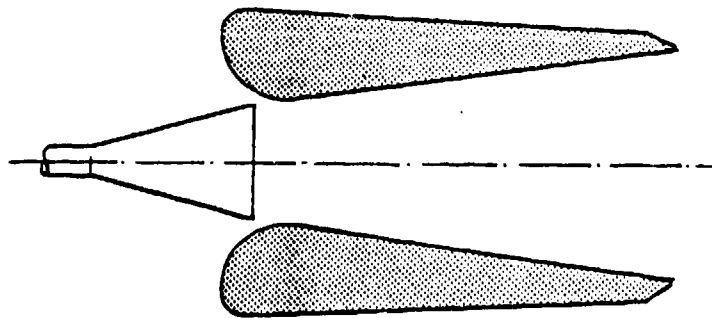
SECTION

FIG. 1

# THRUST AUGMENTOR PERFORMANCE
## SMALL SCALE MODEL RESULTS
### (NOZZLE ASPECT RATIO = 100)

THRUST AUGMENTATION — $\phi_G$

WALL MACH NUMBER — $M_W$



| SYM | NPR |
|-----|-----|
| ○ | 1.5 |
| □ | 2.0 |
| ◇ | 2.5 |
| △ | 3.0 |
| ▽ | 3.5 |

$\phi_G$

DIFFUSER AREA RATIO

OPT $\phi_G$

$M_W$

DIFFUSER AREA RATIO

FIG. 2

938
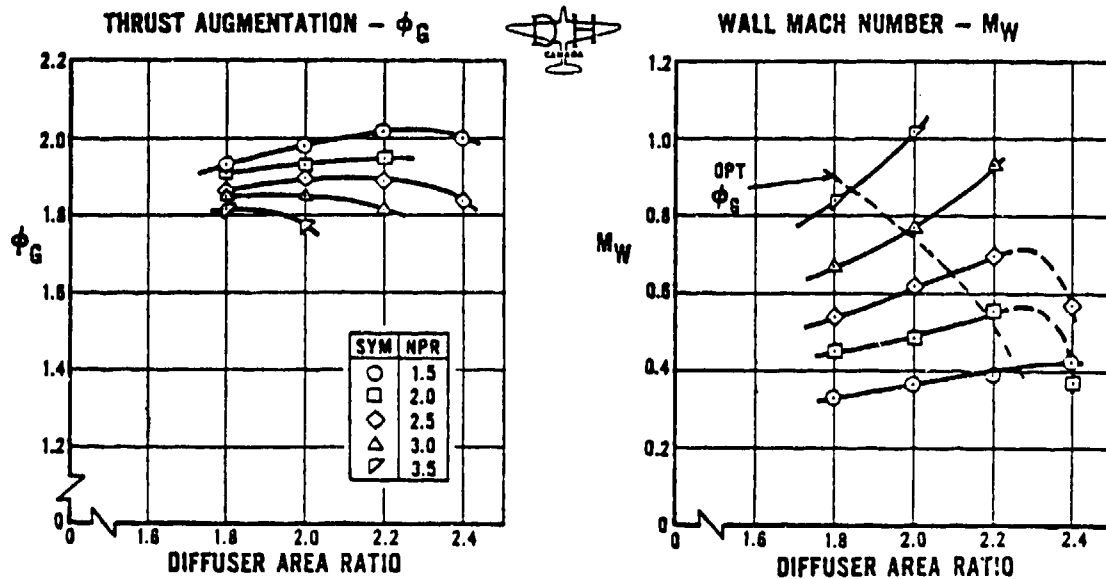
# AUGMENTOR NOZZLE WITH TRANSVERSE ENTRY



$M_{ENTRY} \geq 0.30$

JET EFFLUX DIRECTION
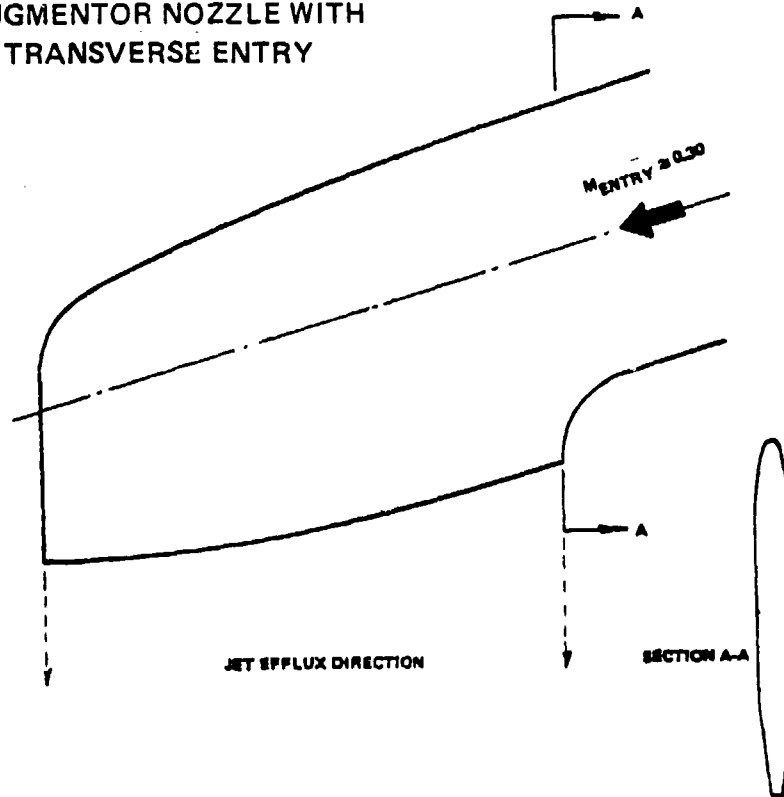
SECTION A-A

FIG. 3

## THEORETICAL EFFECT OF DIFFUSER AREA RATIO ON EJECTOR THRUST LAPSE WITH FRICTION LOSSES: NPR = 3.0 : $A_{SEC}/A_N$ = 15



NET THRUST RATIO

$X_{NET}/X_N$

DAR = 1.6

VELOCITY RATIO $\dfrac{V_\infty}{V_J}$
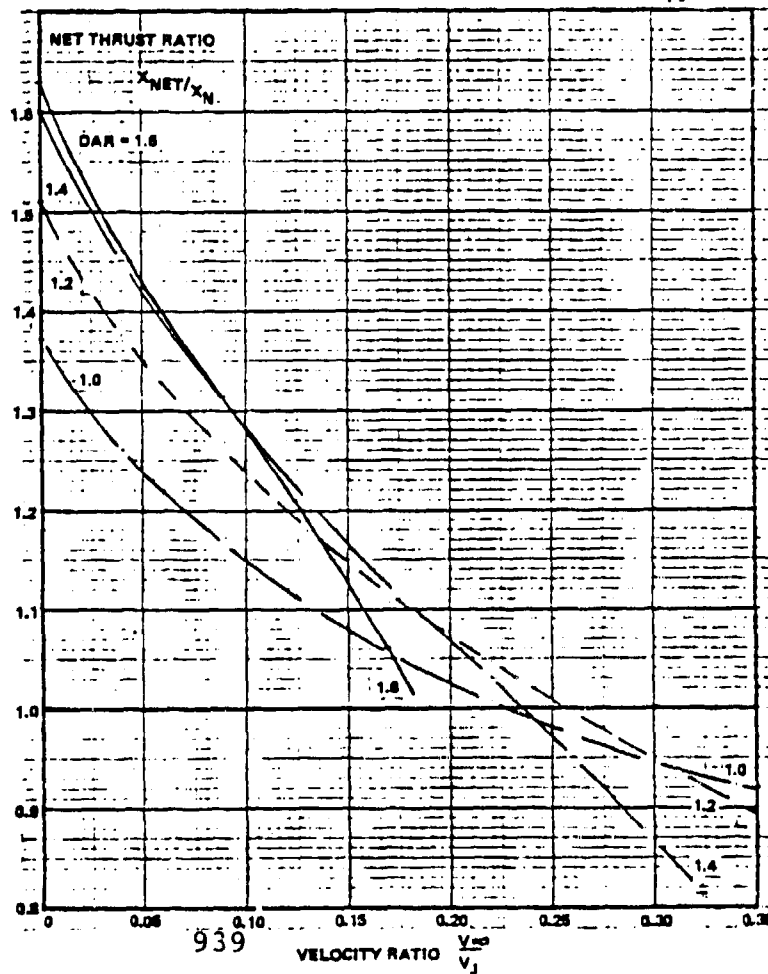
FIG. 4

# SECTION THROUGH AUGMENTOR TEST MODEL
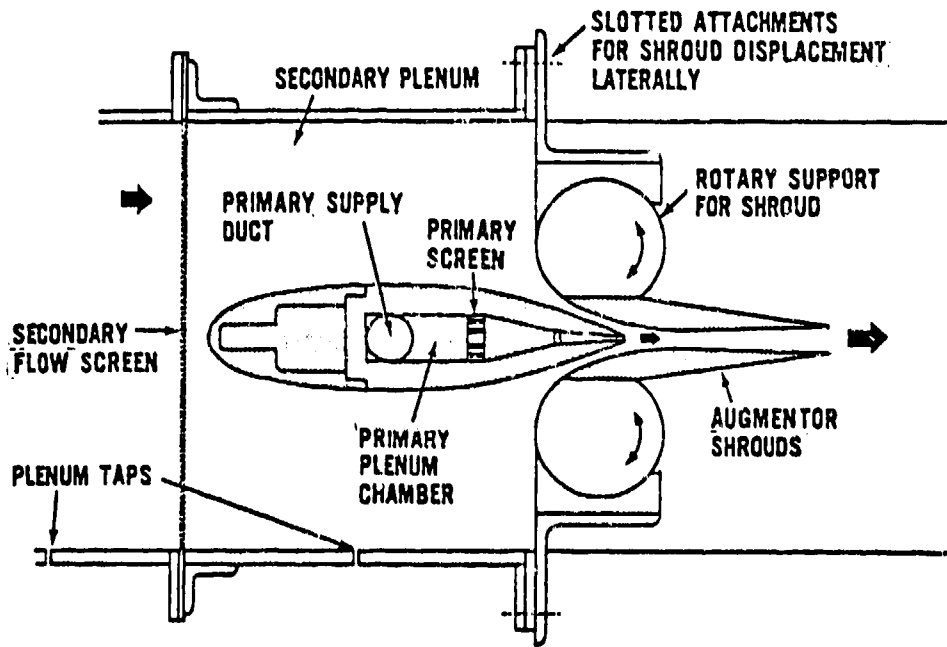


**FIG. 5**

EXPERIMENTAL EFFECT OF DIFFUSER AREA RATIO ON EJECTOR THRUST LAPSE
PLAIN NOZZLE: NPR = 3.0: $A_{SEC}/A_N$ = 12
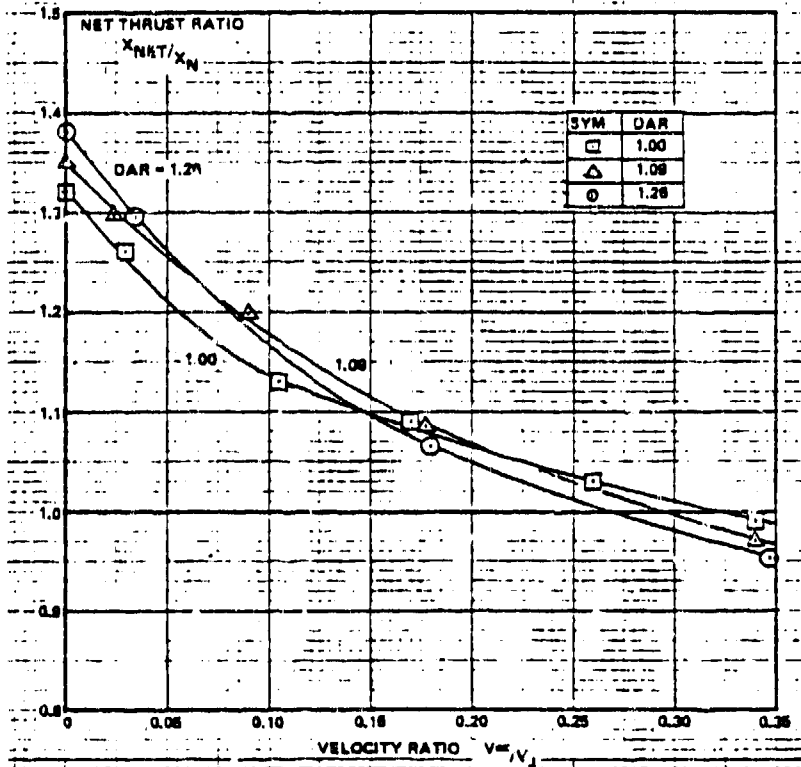


FIG. 6

# LOW DRAG, HIGH SPEED MULTI-FOIL SECTION



● t/c=0.22  ● M=0.68  ● $\alpha_{2D}$=-0.5°  ● $C_L$=0.475  ● $C_{M\frac{1}{4}C}$=-0.211
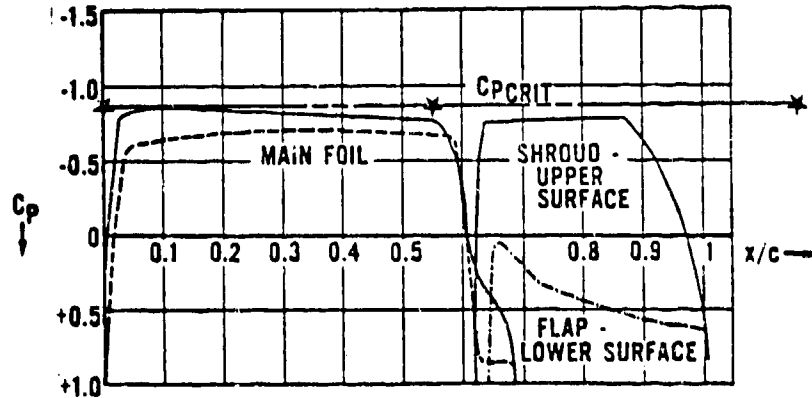


FIG. 7

## THEORETICAL EFFECT OF DIFFUSER EXIT PRESSURE
## ON EFFECTIVE DRAG COEFFICIENT



FIG. 8
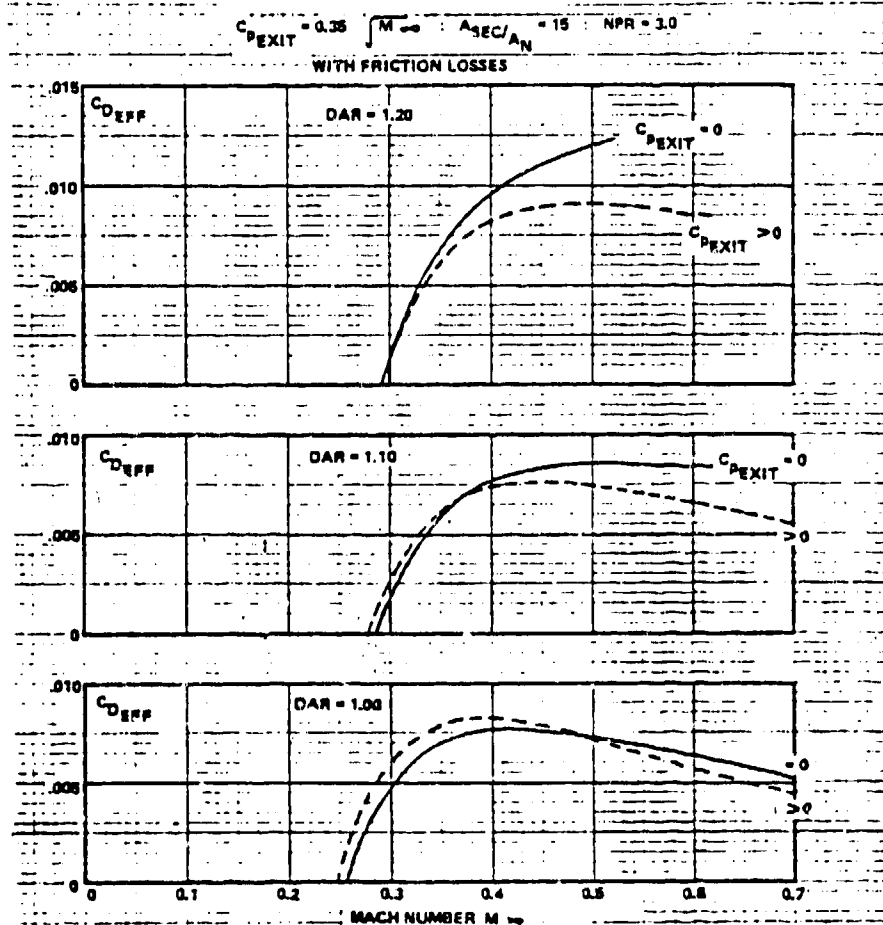
# BUFFALO/SPEY RESEARCH AIRCRAFT
## FINAL DESIGN (DHC/BOEING) 1970

| ENGINES | 2 x RR SPEY 801-SF |
| WING SPAN | 78 FT 9 IN |
| O/A LENGTH | 93 FT 10 IN |
| O/A HEIGHT | 28 FT 8 IN |
| TAIL SPAN | 32 FT 0 IN |
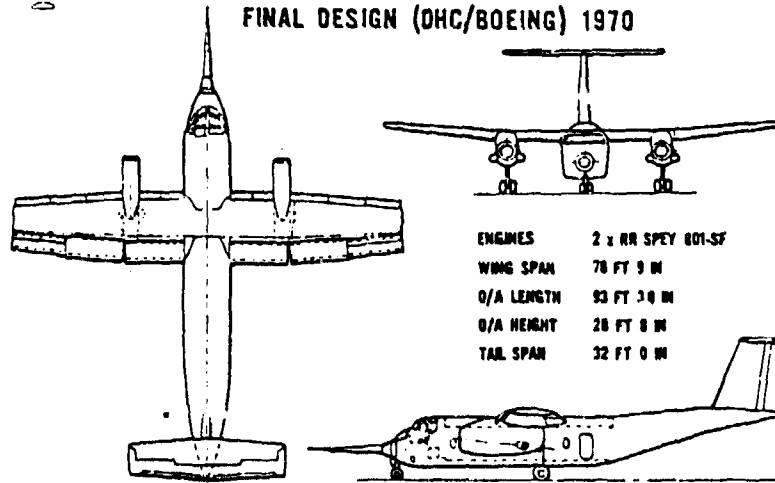
FIG. 9

# AUGMENTOR-WING TRANSPORT WITH 3-STREAM ENGINE

- POWER PLANT: ROLLS–ROYCE RB 419
- GROSS WEIGHT: 95,000 LB
- WING AREA: 11,000 SQ. FT.
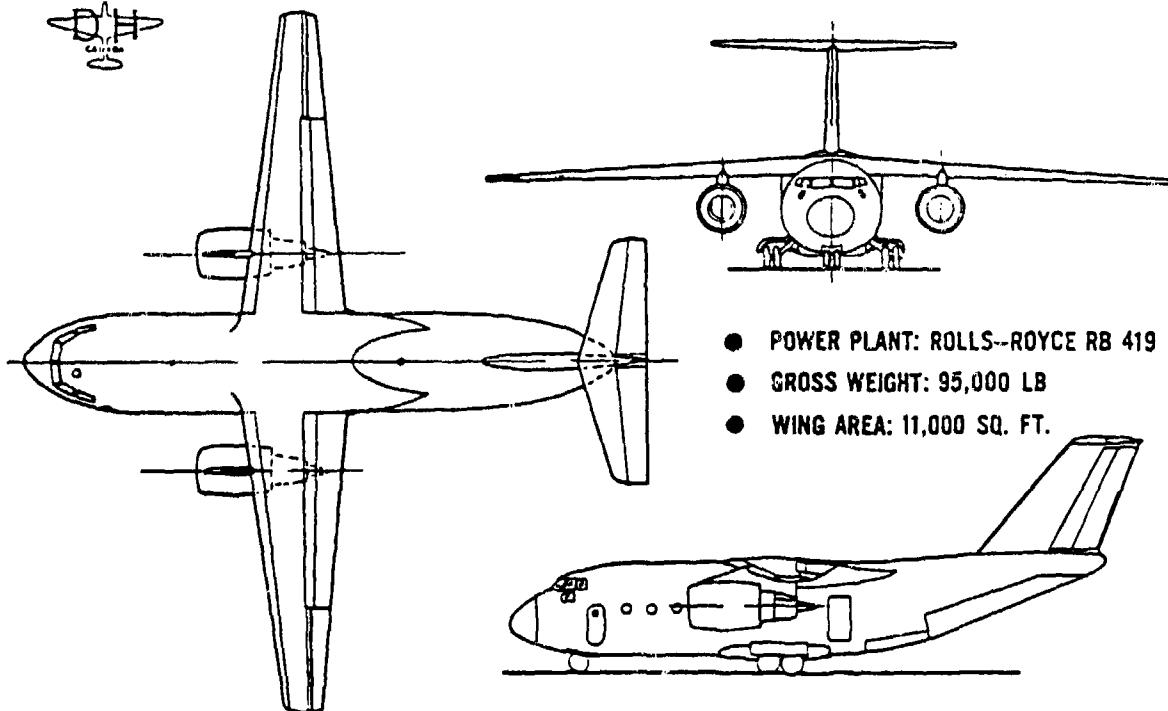
942    FIG. 10

# THE AUGMENTOR-WING CONCEPT

**CRUISE CONFIGURATION**

**LANDING CONFIGURATION**

**FLAP**

**UPPER SHROUD**
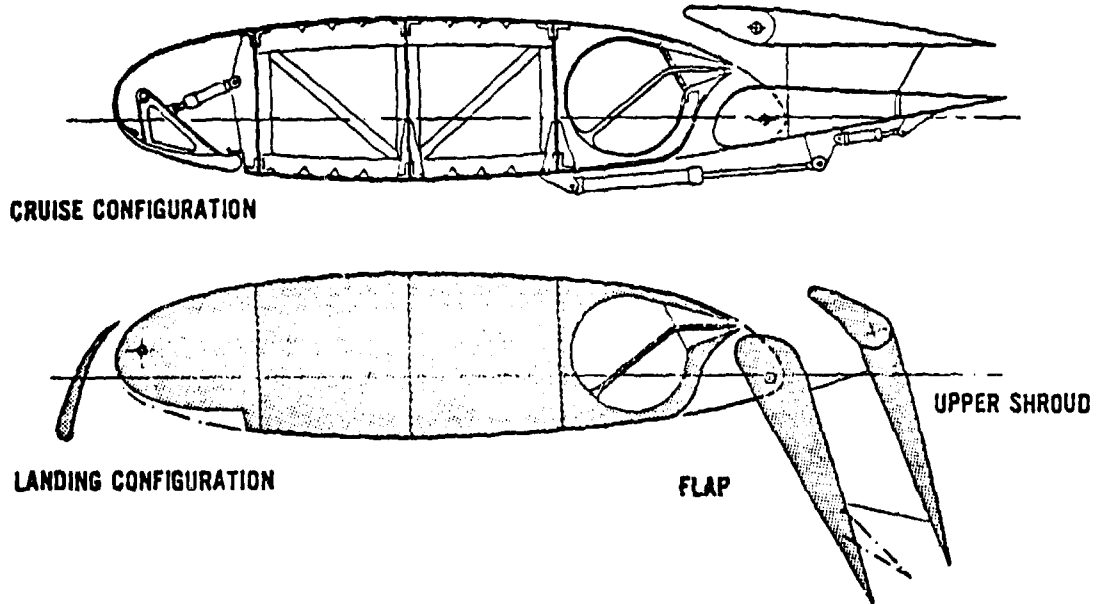
FIG. 11

# WING-BLOWING ENGINE
## BASED ON V.P. FAN AND SPEY CORE

**EXISTING TF41 FAN**
(FIRST 3 STAGES ONLY)

**EXISTING DEMONSTRATOR HUB
& REDUCTION GEAR**

**EXISTING SPEY 202
L.P. TURBINE
(RE-BLADED + NEW STAGE)**

**EXISTING SPEY 202 CORE**

**REDUCTION GEAR OIL COOLER**

**ACCESSORIES**

SCALE: 0  8  16  24  IN.

943      FIG. 12
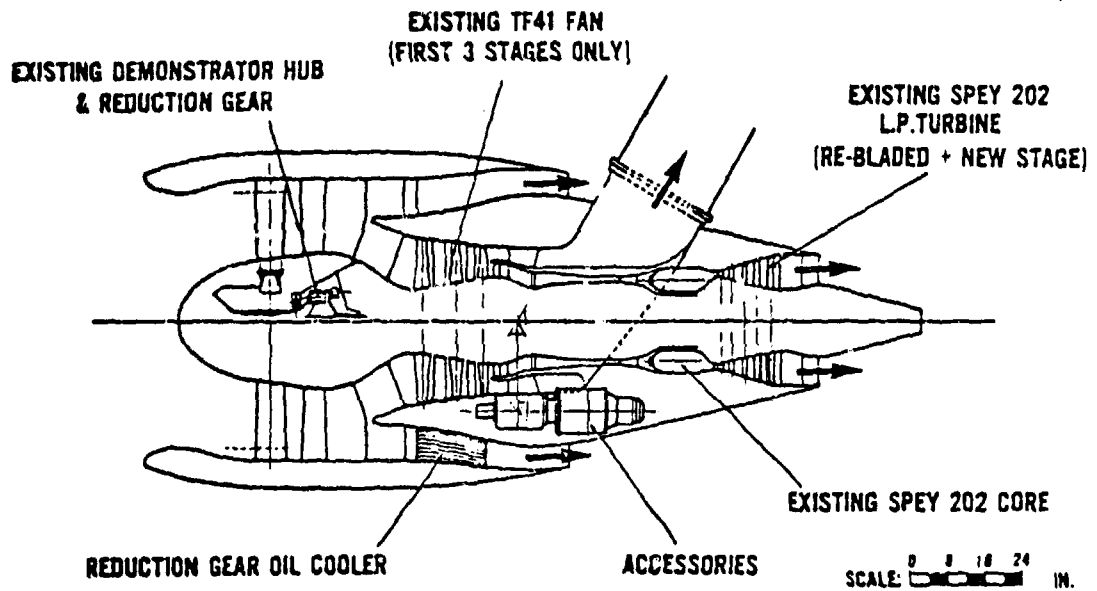
# EJECTOR LIFT/VECTORED THRUST CONCEPT

## PEGASUS POWERED STOVL COMBAT AIRCRAFT



| | |
|---|---|
| STO WEIGHT | 37,500 LB |
| VTOL WEIGHT | 29,000 LB |
| POWERPLANT: PEGASUS 'J' | 23,250 LB |
| SPAN | 31.3 FT. |
| WING SPAN | 350 SQ.FT. |
| OVERALL LENGTH | 48.3 FT. |
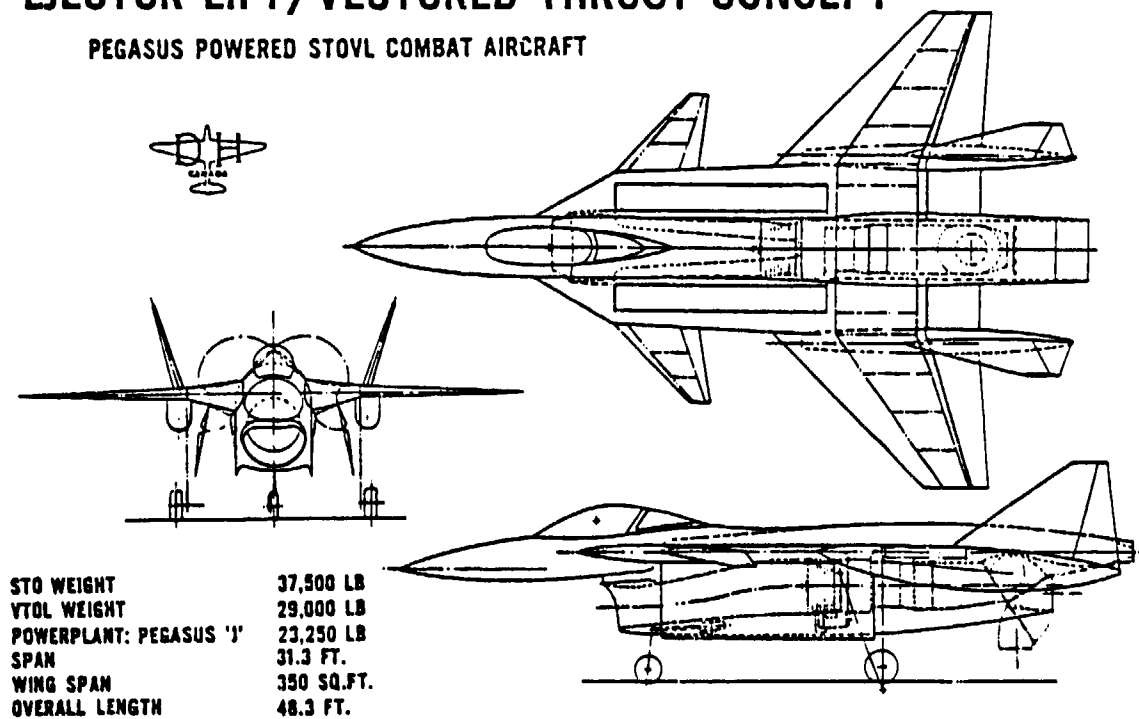
FIG. 13

# EXTERNAL AUGMENTOR V/STOL CONCEPT

## G.A. OF J-97 POWERED MODEL
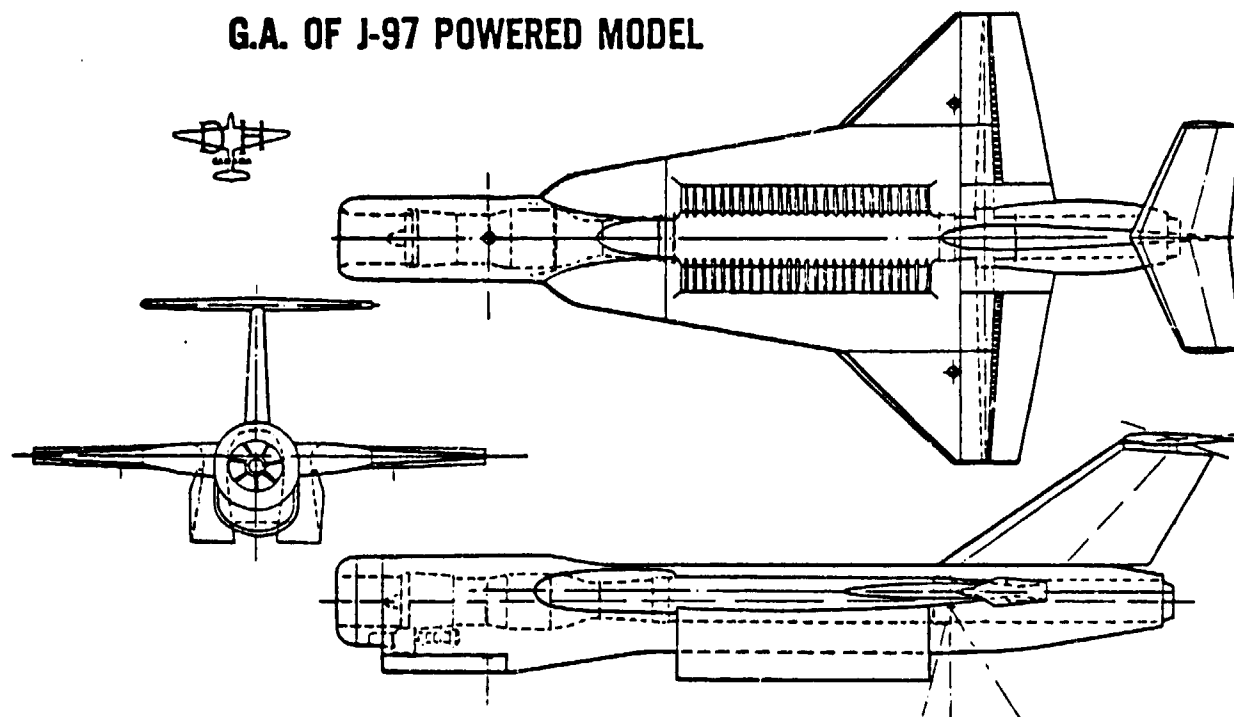


944

FIG. 14

# EXTERNAL AUGMENTOR V/STOL CONCEPT
## CROSS-SECTION OF EJECTOR SYSTEM

**VTOL CONFIGURATION**          **CRUISE CONFIGURATION**
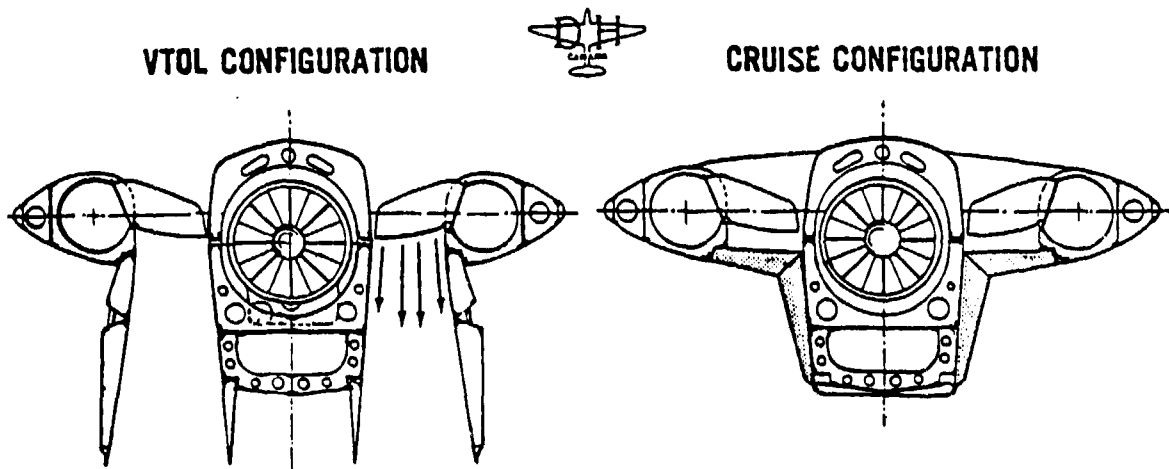
FIG. 15

# GROUND EFFECTS – J-97 POWERED MODEL

COLD AIR          INFLOW

JET          OUTFLOW

$$\phi_G= \left[ \frac{\text{MODEL LIFT}}{\text{NOZZLE THRUST}} \right]$$

FLAP ANGLE – 90°

$\phi_G$

2.5

2.0

1.5

1.0

0    10    20    30    40

(240 IN.)

GROUND CLEARANCE (IN.)
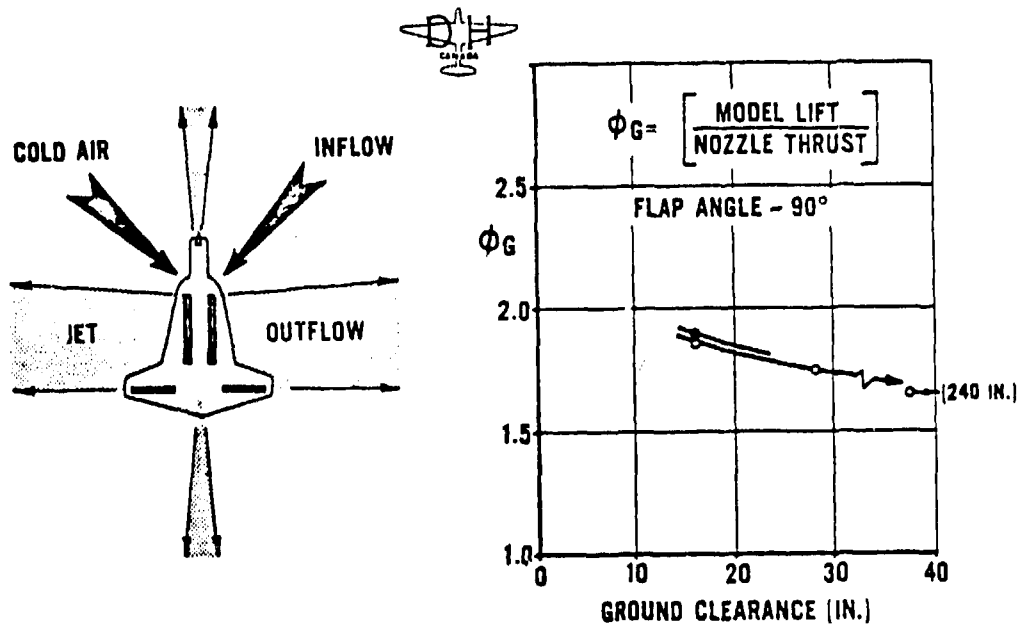
945    FIG. 16

# AUGMENTOR-WING TRANSPORT - TILT WING

WING AREA : 600 SQ.FT.
ASPECT RATIO : 6 V₂ 25%
TAPER RATIO : 0.50
POWER PLANT : R.R. V.P. FAN
3 STREAM ENGINE
S.T.O. WEIGHT : 56,000 LB.
V.L. WEIGHT : 44,000 LB.

FIG. 17

946
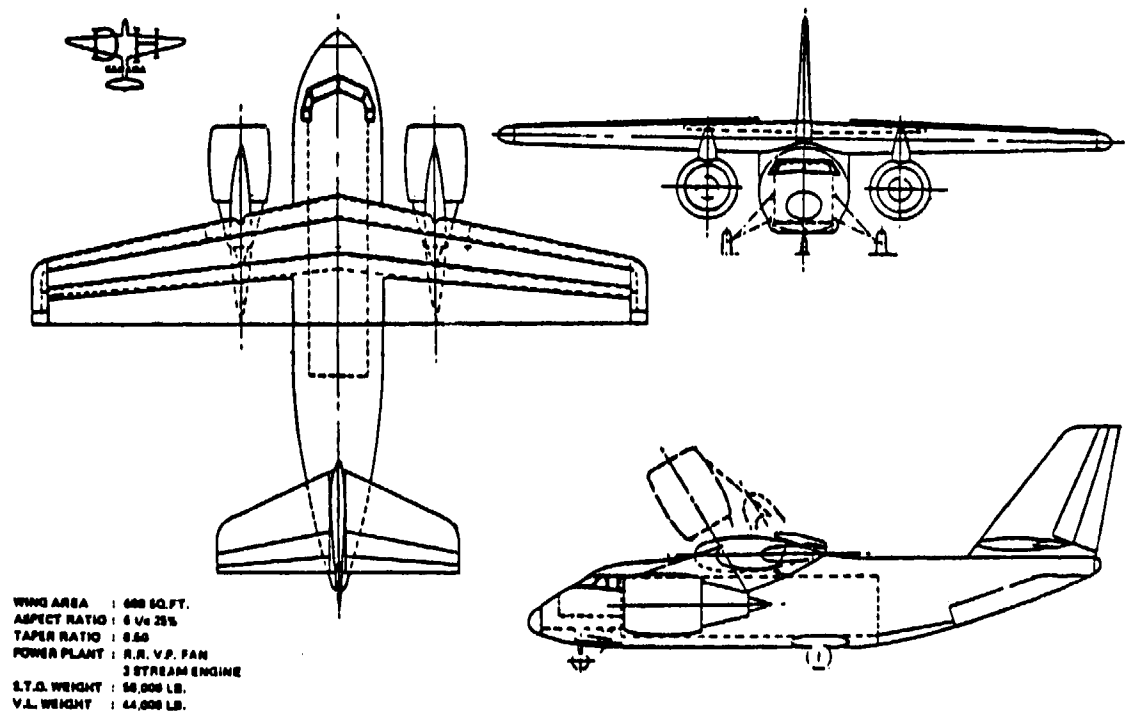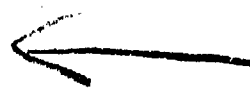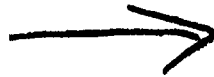
# EJECTOR RAM DRAG

## BY

### BERNARD B. BEARD

## AND

### WILLIAM H. FOLEY

### GENERAL DYNAMICS
### FORT WORTH DIVISION

ABSTRACT: Ejectors are a means of providing thrust augmentation for STOL and VTOL flight while minimizing ground impact and inlet reingestion problems. However, for some ejector configurations, experiments have indicated that axial thrust recovery is not effective in off-setting ejector ram drag so that such systems may encounter difficulties transitioning from engine-borne to wing-borne flight. This paper presents an analytical method of predicting this drag using empirical ejector performance parameters. A comparison between the theory and ram drag measurements from NASA Wind Tunnel Tests is presented.

EJECTOR RAM DRAG STUDY

√ EJECTORS CAN BE A SIMPLE WAY OF PROVIDING THRUST AUGMENTATION.

√ SOME V/STOL AIRCRAFT CONCEPTS UTILIZE VERTICALLY DIRECTED EJECTORS
TO PROVIDE TAKE-OFF THRUST. A BENIGN FOOTPRINT, AND MINIMAL
REINGESTION THRUST LOSS.

√ DURING THE TRANSITION FROM VERTICAL TO HORIZONTAL FLIGHT, THE
MOMENTUM DRAG OF THE EJECTOR SECONDARY AIRFLOW IS A SIGNIFICANT
CONTRIBUTION TO TOTAL DRAG.

√ AN ANALYTIC METHOD OF PREDICTING EJECTOR SECONDARY AIRFLOW AND RAM DRAG
FROM MEASURED EJECTOR PERFORMANCE PARAMETERS WOULD BE DESIRABLE FOR
PRELIMINARY PERFORMANCE STUDIES OF V/STOL-EJECTOR AIRCRAFT CONCEPTS.
√ METHOD SHOULD ACCOUNT FOR THE EFFECT OF THROTTLING THE EJECTOR
DURING TRANSITION TO WING-BORNE FLIGHT.

√ THUS OUR GOAL IS TO ESTIMATE EJECTOR RAM DRAG FROM
√ PRIMARY FLOW PROPERTIES, INCLUDING THROTTLING EFFECTS,
√ SYSTEM GEOMETRY,
√ AMBIENT ATMOSPHERIC CONDITIONS, AND
√ DIMENSIONLESS EJECTOR PERFORMANCE PARAMETERS.

RAM DRAG CONTROL VOLUME

AMBIENT CONDITIONS $T_A$, $P_A$



EJECTOR EXIT

$\dot{m}_E$, $T_{T_E}$, $P_{T_E}$

EXIT AREA = $A_E$

SECONDARY AIRFLOW

$\dot{m}_S$, $T_{T_S}$

SUPPLY AIRFLOW

$T_T$, $P_T$

PRIMARY AIRFLOW

$\dot{m}_P$, $T_{T_P}$, $P_{T_P}$

EJECTOR

$U_\infty$
$D$

$V_Y$  $V_X$

$F_Y$  $F_X$
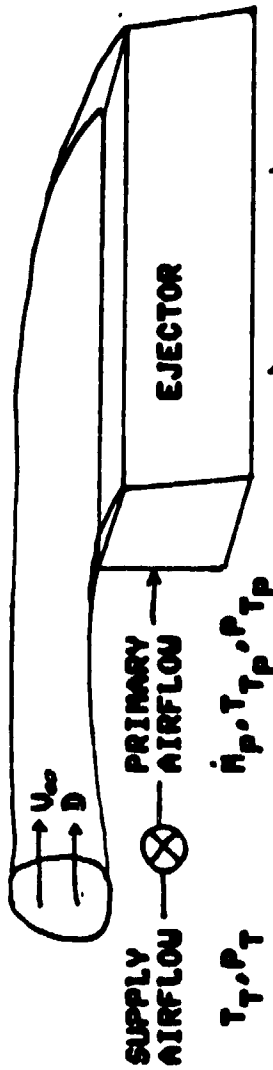
√ ASSUME PRIMARY AIRFLOW EXHAUSTS THROUGH FIXED AREA NOZZLES (AREA)=$A_P$).

√ ASSUME PRIMARY AIRFLOW INLET AXIAL MOMENTUM IS ACCOUNTED FOR ELSEWHERE.

√ IGNORE GROUND EFFECTS.

949

# MOMENTUM AND FORCE RELATIONS

✓ EJECTOR INLET MOMENTUM DRAG

$$D \equiv \frac{1}{g_c} \dot{m}_s V_o \, .$$

✓ RECOVERED AXIAL MOMENTUM THRUST

$$F_x = \frac{1}{g_c} \dot{m}_e V_x \, .$$

✓ AXIAL MOMENTUM RECOVERY FACTOR

$$\eta_A \equiv \frac{F_x}{D} = \frac{\dot{m}_e V_x}{\dot{m}_s V_o} \, . \qquad \text{(DIMENSIONLESS)}$$

✓ NET AXIAL DRAG FORCE

$$D - F_x = \frac{1}{g_c}(\dot{m}_s V_o - \dot{m}_e V_x) = \frac{1}{g_c}(1 - \eta_A)\dot{m}_s V_o \, .$$

✓ EJECTOR AUGMENTATION RATIO

$$\phi = \frac{F_{s,ACTUAL,VERTICAL}}{F_{s,IDEAL,PRIMARY}} = \frac{F_y}{F_p} \, , \qquad \text{(DIMENSIONLESS)}$$

WHERE

$$F_P = \frac{1}{g_c} \dot{m}_p \sqrt{T_p} \sqrt{\frac{2g_c R}{\gamma - 1}} \sqrt{1 - \left(\frac{P_o}{P_t}\right)^{\frac{\gamma - 1}{\gamma}}} \, ,$$

AND

$$F_y = \frac{\dot{m}_e V_y}{g_c} \, .$$

# FURTHER EQUATIONS AND DEFINITIONS

## √MASS CONSERVATION

$$\dot{m}_E = \dot{m}_P + \dot{m}_S$$

## √TOTAL TEMPERATURE RELATIONS

$$T_{T_E} = T_{S_E} + \frac{V_E^2 + V_L^2}{2 c_p g_c}$$

$$T_{T_S} = T_A + \frac{V_E^2}{2 c_p g_c}$$

## √CONSTANT ENTHALPY MIXING

$$\dot{m}_E T_{T_E} = \dot{m}_S T_{T_S} + \dot{m}_P T_{T_P}$$

## √EJECTOR EXIT MASS FLOW

$$\dot{m}_E = \rho_E V_y A_E$$

$$\rho_E = \frac{P_{S_E}}{R T_{S_E}}$$

## √PRESSURE MATCHING AT EJECTOR EXIT

$$P_{S_E} = P_A$$

# FURTHER EQUATIONS AND DEFINITIONS

## √ EJECTOR PRIMARY NOZZLE PRESSURE-MASS FLOW RELATION

$$\frac{\dot{m}_p \sqrt{T_{T_p}}}{D_1 P_A A_p} \qquad \text{FOR} \quad \dot{m}_p \geq \dot{m}_{CH,MIN}$$

$$\frac{P_{T_2}}{P_A} = \left\{ \frac{1 + \sqrt{1 + 4\left(\dfrac{\dot{m}_p^2 \, T_{T_p}}{\dfrac{2 g_c \gamma}{R(\gamma-1)} P_A^2 A_p^2}\right)}}{2} \right\}^{\frac{\gamma}{\gamma-1}} \qquad \text{FOR} \quad \dot{m}_p < \dot{m}_{CH,MIN}$$

WHERE $\dot{m}_{CH,MIN} = D_1 P_A N_{CH,MIN} A_p \sqrt{T_{T_p}}$ = MINIMUM CHOKING MASS FLOW.

AND $N_{CH,MIN} = \left(\frac{\gamma+1}{2}\right)^{\gamma/\gamma-1}$ = MINIMUM CHOKING NPR.

(NOTE $D_1 = .5317 \frac{LBM/SEC}{LBF} \frac{\sqrt{R}}{}$ = VALUE OF COMPRESSIBLE FLOW FUNCTION AT MACH NO. = 1.0)

## SOLUTION TO ABOVE SYSTEM OF EQUATIONS:

$\dot{m}_s$ WILL BE THE POSITIVE ROOT OF THE QUADRATIC EQUATION

$$(\dot{m}_s + \dot{m}_p)(\dot{m}_s + \dot{m}_p \frac{T_{pe}}{T_s}) - \dot{m}_s^2 \frac{\eta_d^2 V_o^2}{2 g_c C_p T_s} = \frac{(g_c F_y)^2}{2 g_c C_p T_s} \left( \frac{H+1}{H} \right)$$

WHERE $H = \frac{1}{2} \frac{F_y}{P_A A_e} \frac{r-1}{r}$.

THEN $\dot{m}_E = \dot{m}_s + \dot{m}_p$,

$V_y = g_c \frac{F_x}{\dot{m}_E}$,

$V_x = \frac{\dot{m}_s V_{sx}}{\dot{m}_E} \eta_A$,

AND $D - F_x = \frac{r}{g_c} (1 - \eta_A) \dot{m}_s V_{so}$.

953

# GRAPHICAL DATA

√ ACCOMPANYING CHARTS ARE FOR THE HYPOTHETICAL CASE $\dot{m}_{SUPPLY}$ 100 LBM/SEC.

$P_{T_{SUPPLY}}$ = 60 PSIA, $T_{T_{SUPPLY}}$ = 800 DEG R, AT SEA LEVEL, STANDARD DAY
CONDITIONS, WITH $\eta_\Delta$ = 0.1.

√ THROTTLING PARAMETER IS EXPRESSED AS $K = \dot{m}_p / \dot{m}_{SUPPLY}$
(K = MASS FLOW FRACTION)

√ GRAPHS ARE

√ NET AXIAL DRAG        $D - F_X$    VS   MASS FLOW FRACTION  K.

√ EJECTOR VERTICAL THRUST $F_y$    VS   MASS FLOW FRACTION  K.

√ NET AXIAL DRAG        $D - F_X$    VS   EJECTOR VERTICAL THRUST $F_y$.

√ RAM DRAG PARAMETER $(D - F_X)/\mathcal{V}_0\sqrt{F_y}$  VS  EJECTOR VERTICAL THRUST $F_y$.

√ CLEARLY THE DIMENSIONAL GROUP $(D - F_X)/\mathcal{V}_0\sqrt{F_y} \equiv \zeta_X$ IS A USEFUL ONE
FOR APPROXIMATING PERFORMANCE.

√ ALSO INCLUDED IS A GRAPHICAL COMPARISON OF TEST DATA WITH THEORY
FOR LARGE SCALE DEHAVILLAND EJECTORS TESTED AT NASA AMES'
40X80 WIND TUNNEL.
√ AGREEMENT BETWEEN THEORY AND EXPERIMENT IS GOOD FOR $\eta_\Delta$ = 0.0

954

EJECTOR RAM DRAG STUDY
EJECTOR NET AXIAL DRAG
AS A FUNCTION OF MASS FLOW FRACTION AND FLIGHT MACH NUMBER
SUPPLY FLOW RATE-100 LBM/SEC, TEMP-800 R, PRESSURE-50 PSIA
SEA LEVEL/STANDARD DAY/PHI-1.60/ETAA-0.10/AP-106.4 SQ IN

□ - MACH - 0.10
○ - MACH - 0.20
△ - MACH - 0.30

955
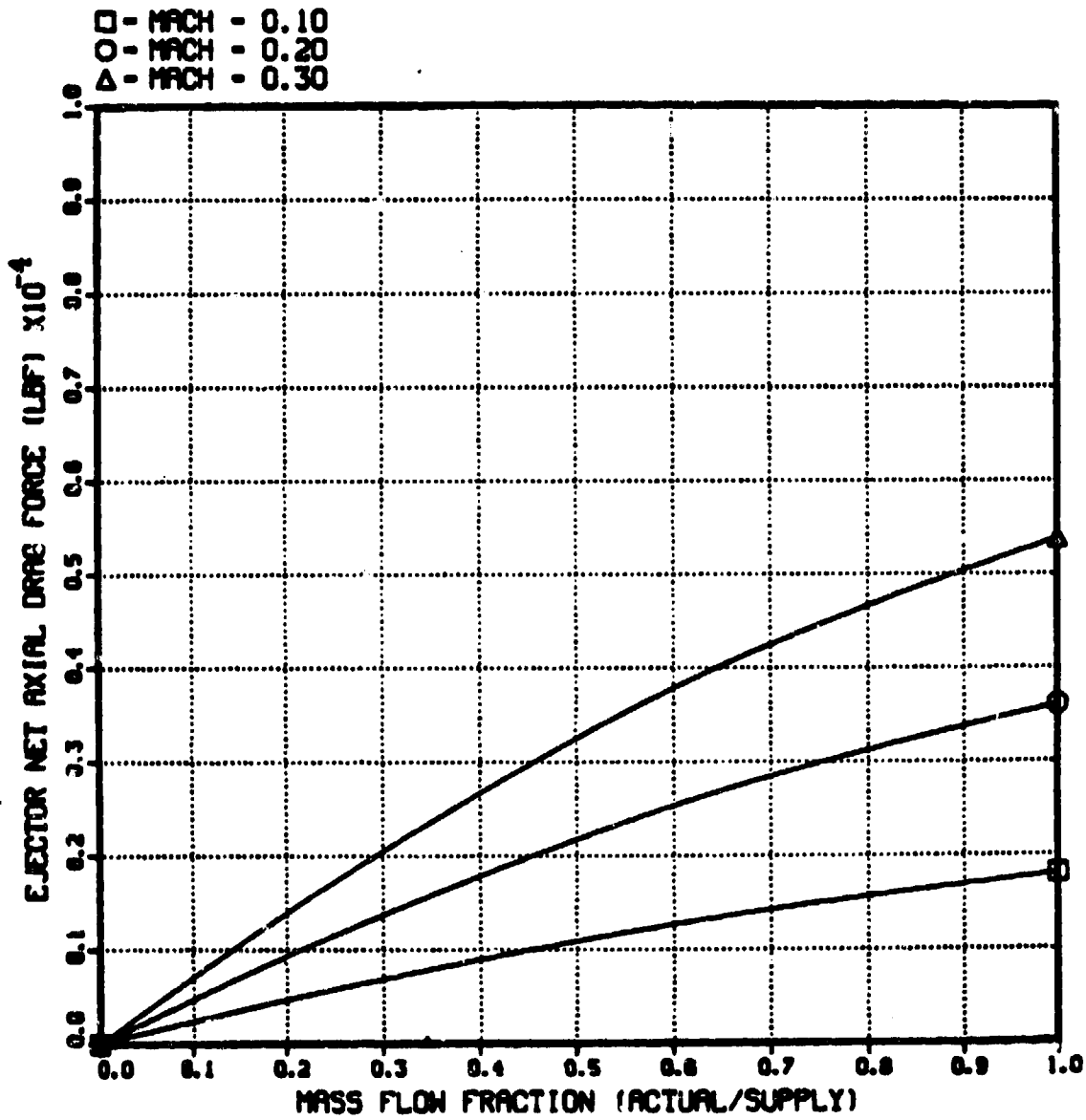
EJECTOR RAM DRAG STUDY
EJECTOR VERTICAL THRUST
AS A FUNCTION OF MASS FLOW FRACTION
SUPPLY FLOW RATE=100 LBM/SEC, TEMP=800 R, PRESSURE=50 PSIA
SEA LEVEL/STANDARD DAY/PHI=1.60/ETAA=0.10/AP=106.4 SQ IN

956
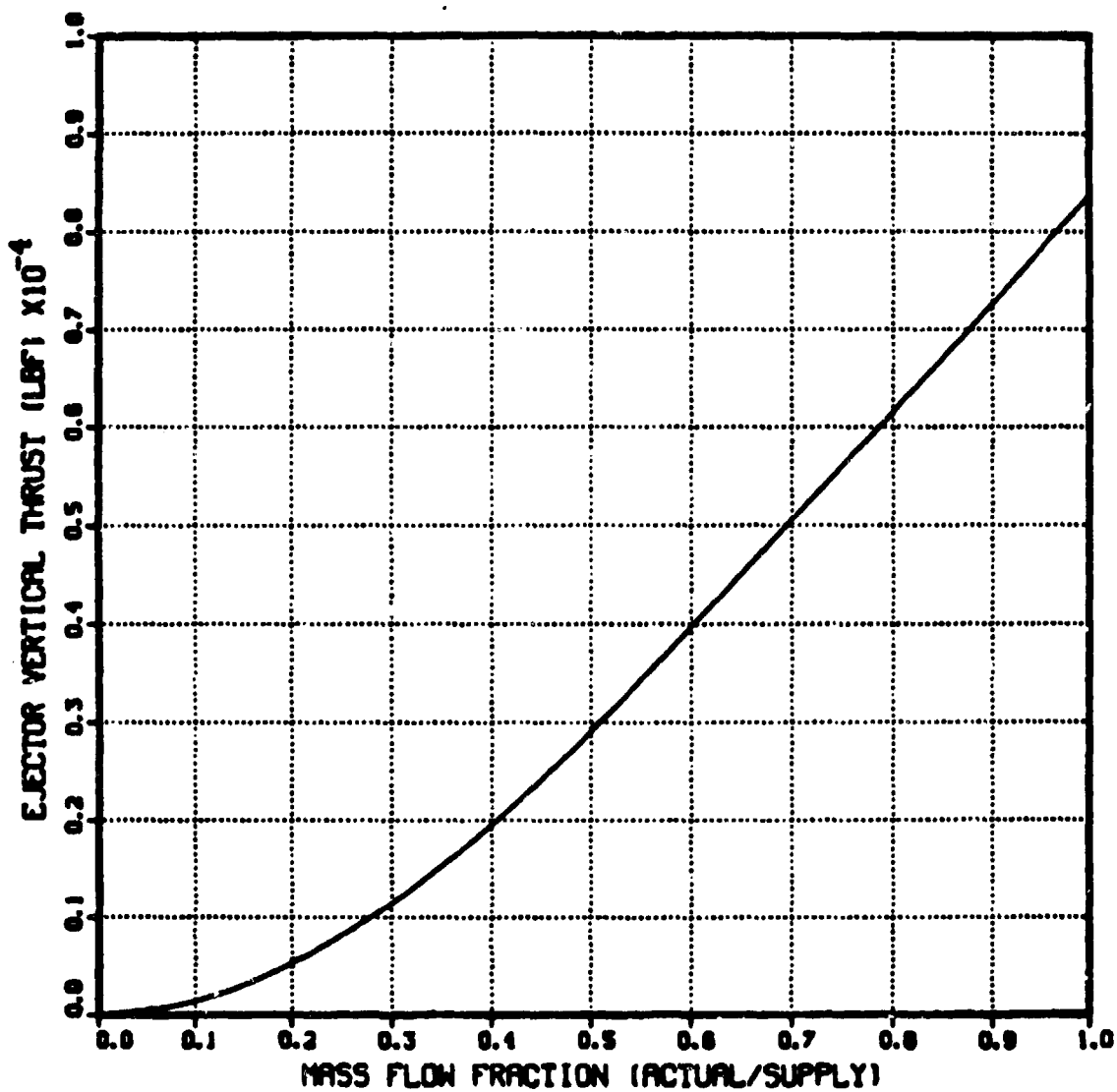
EJECTOR RAM DRAG STUDY
EJECTOR NET AXIAL DRAG VS EJECTOR VERTICAL THRUST
FOR DIFFERENT FLIGHT MACH MACH NUMBERS
SUPPLY FLOW RATE-100 LBM/SEC, TEMP-800 R, PRESSURE-50 PSIA
SEA LEVEL/STANDARD DAY/PHI-1.60/ETAA-0.10/AP-106.4 SQ IN
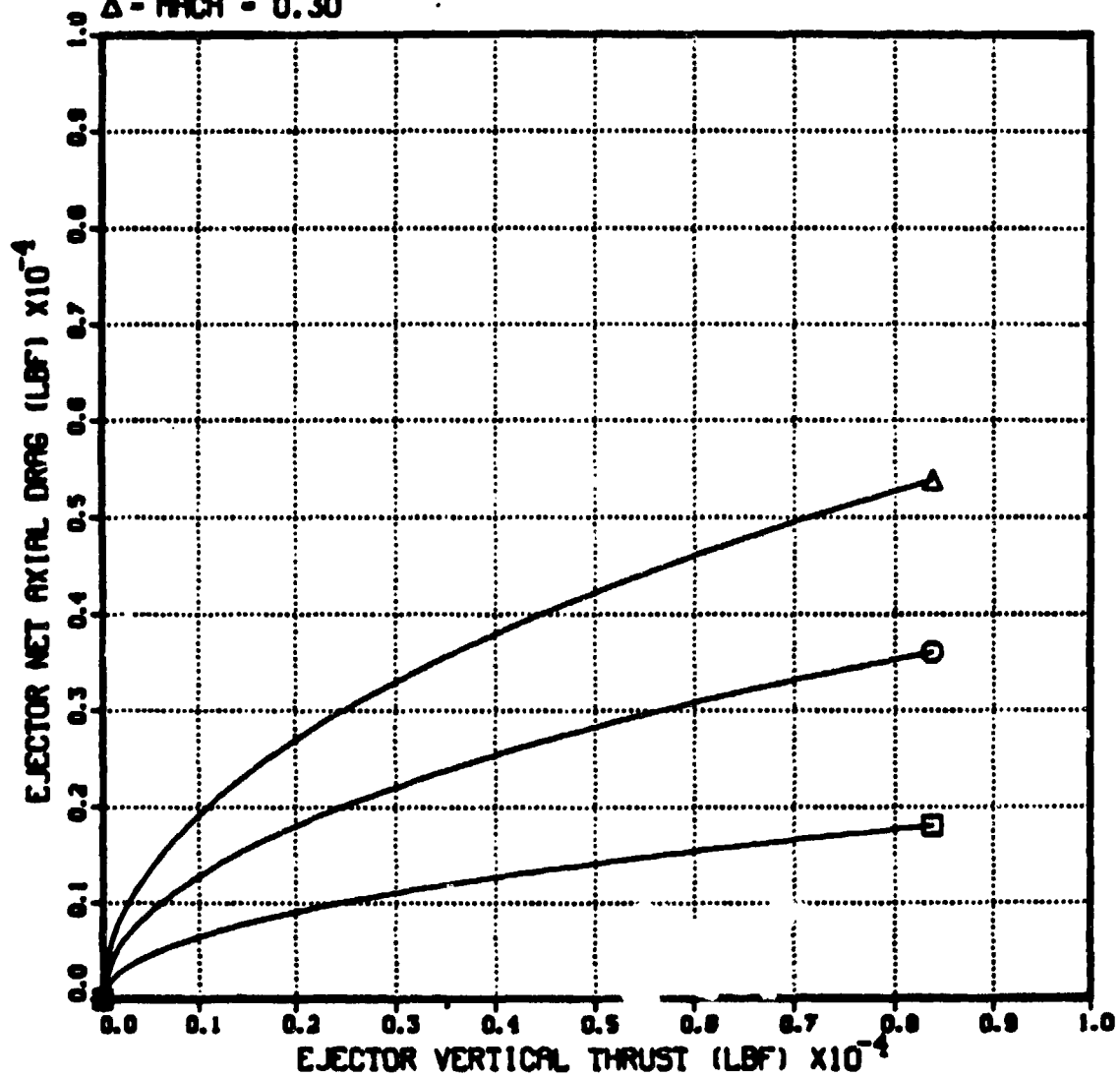
EJECTOR RAM DRAG STUDY
EJECTOR RAM DRAG PARAMETER VS EJECTOR VERTICAL THRUST
FOR DIFFERENT FLIGHT MACH MACH NUMBERS
SUPPLY FLOW RATE=100 LBM/SEC, TEMP=800 R, PRESSURE=50 PSIA
SEA LEVEL/STANDARD DAY/PHI=1.60/ETAA=0.10/AP=106.4 SQ IN

□ = MACH = 0.10
○ = MACH = 0.20
△ = MACH = 0.30
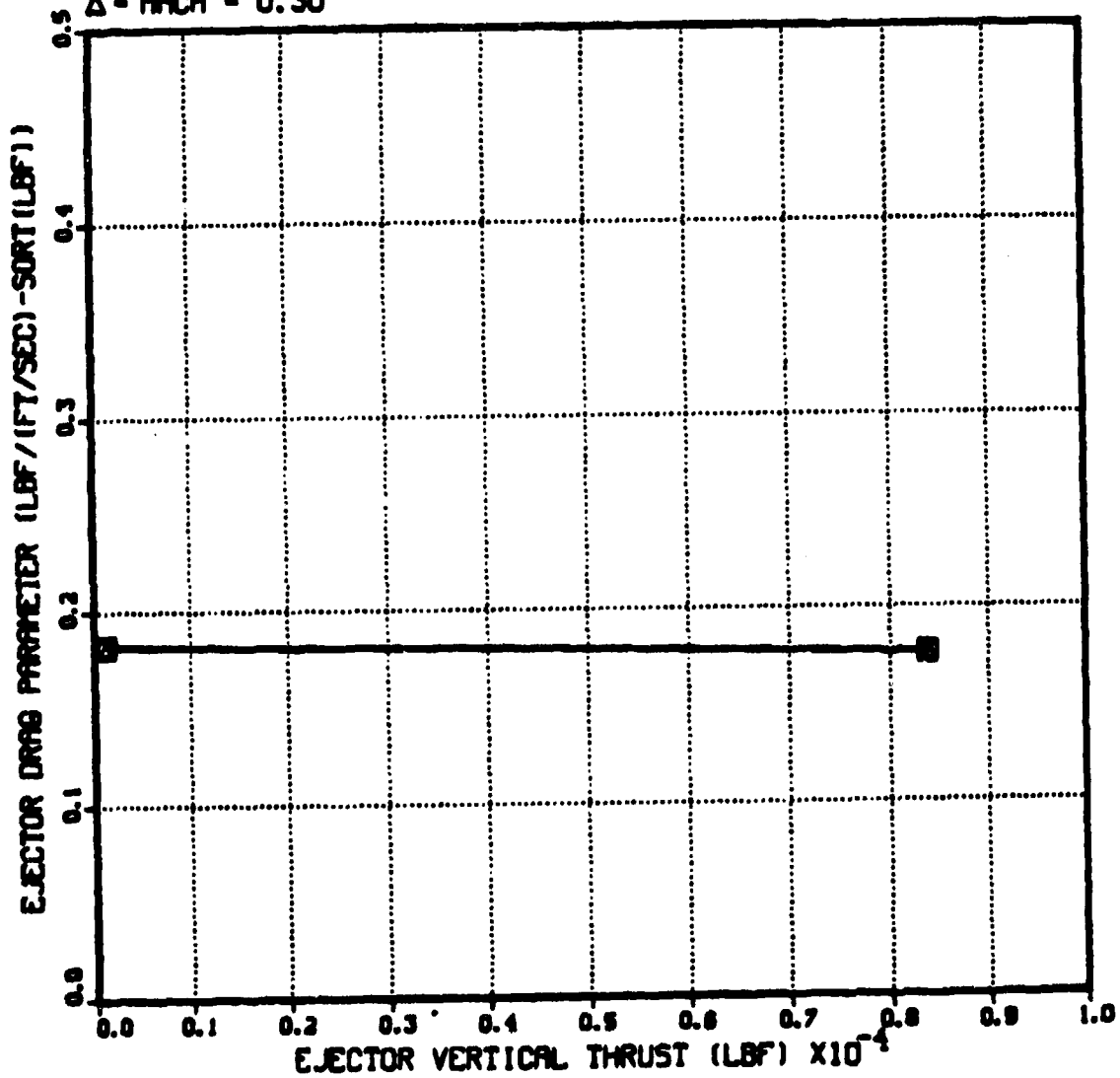
EJECTOR RAM DRAG STUDY
COMPARISON OF TEST DATA WITH THEORY
DEHAVILLAND TYPE EJECTORS TESTED AT NASA AMES

□ = NASA AMES TEST DATA
○ = THEORETICAL PREDICTION, ETAA = 0.00
△ = THEORETICAL PREDICTION, ETAA = 0.05
+ = THEORETICAL PREDICTION, ETAA = 0.10

NET AXIAL DRAG FORCE (LBF) X10$^{-3}$

FLIGHT VELOCITY (FT/SEC) X10$^{-2}$
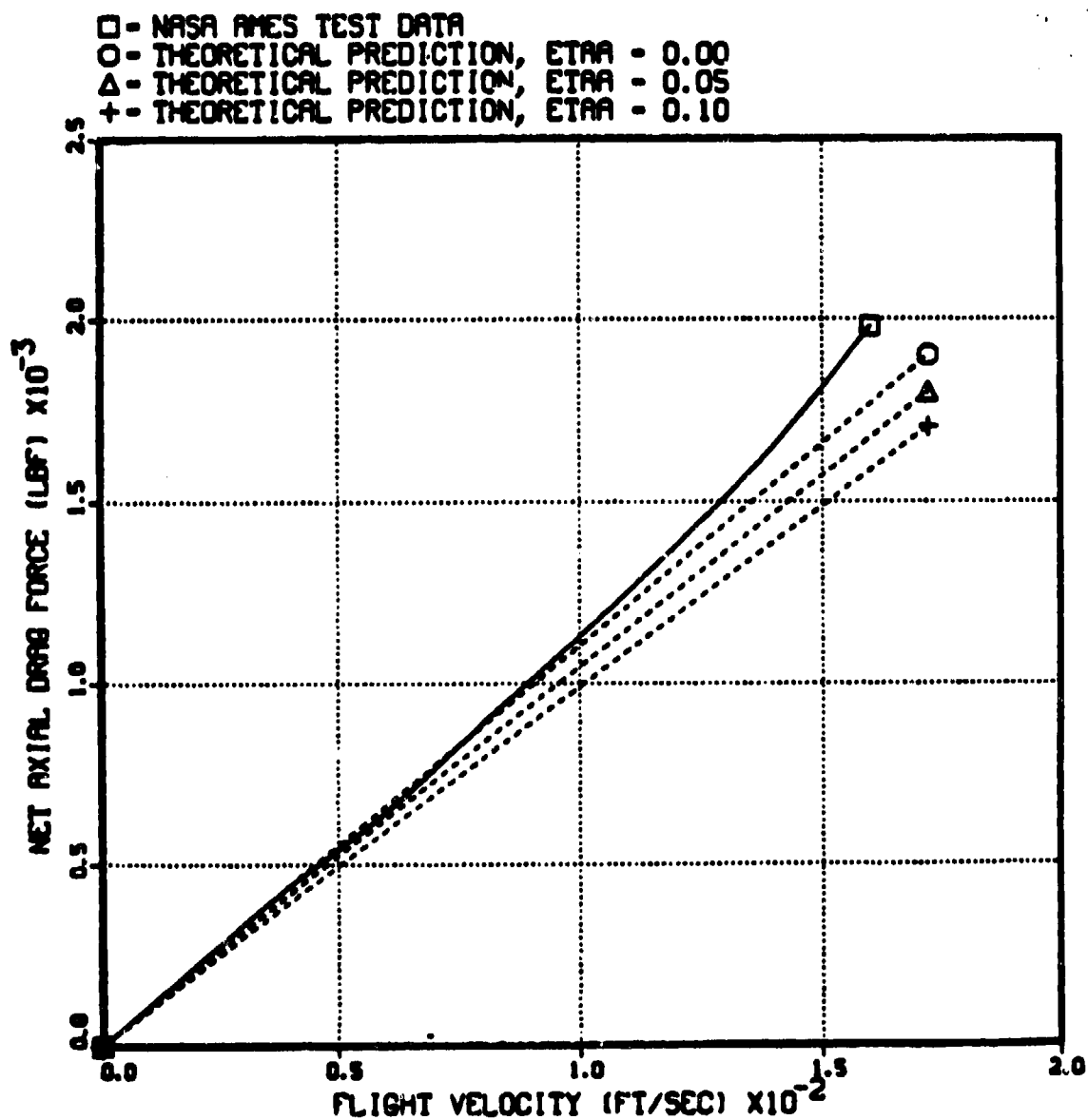
## APPROXIMATE EXPRESSION FOR RAM DRAG PARAMETER

√ MANIPULATION OF THE EXPRESSION FOR $\dot{n}_s$ GIVES

$$\alpha_R = \frac{D - F_x}{V_\infty / F_y} \doteq (1 - \eta_A) \gamma \sqrt{\frac{P_A A_E}{g_c R T_s}} - \gamma \sqrt{\frac{D_i P_2 A_P \left(1 + \frac{T_{tp}}{2 T_s}\right)^{\frac{3}{4} - 1}}{g_c \emptyset T_{tp} \gamma \frac{2 g_c R \delta}{3 \delta - 1}}} \left(\frac{T_{tp} / T_{T_s} + 1}{2}\right)$$

√ NOTE THAT $\alpha_R \cong \sqrt{A_E}$

## EJECTOR RAM DRAG STUDY — SUMMARY

√ EJECTOR DIMENSIONLESS PERFORMANCE PARAMETERS ($\phi$ AND $\eta_A$) CAN BE COMBINED WITH GEOMETRICAL AND PHYSICAL RELATIONS TO YIELD AN EXPRESSION FOR EJECTOR NET AXIAL DRAG.

√ DIRECT COMPUTATION IS FEASIBLE (NO ITERATION IS REQUIRED).

√ IN MANY CASES, EJECTOR RAM DRAG PARAMETER $q_x$ IS NEARLY CONSTANT.

√ NET DRAG IS PROPORTIONAL TO $U_\infty \sqrt{F_V} \, A_E$.

961

# SUPERSONIC EJECTOR-DIFFUSER THEORY
# AND EXPERIMENTS

A. L. Addy[†]
J. Craig Dutton[††]
C. C. Mikkelsen[†††]

August 1981

[†]  Professor and Associate Head, Department of Mechanical and Industrial
     Engineering, University of Illinois at Urbana-Champaign, Urbana,
     Illinois.

[††] Assistant Professor, Department of Mechanical Engineering, Texas A&M
     University, College Station, Texas.

[†††]Aerospace Engineer, U.S. Army MICOM, Redstone Arsenal, Alabama.

## TABLE OF CONTENTS

# LIST OF FIGURES

967

## LIST OF TABLES

NOMENCLATURE

Symbols

A          Area

$C_1, C_2, C_3$          Constants defined in text

$C_p$          Specific heat at constant pressure

D          Diameter

f( )          Function

$f_1( ), \ldots, f_5( )$          Gas dynamic functions defined in text

g, g( )          Gravitational acceleration or function

h          Specific enthalpy

L          Length

M          Mach number

Mw          Molecular weight

P          Pressure

R          Gas constant

$r_d$          Diffuser compression coefficient

t          Time

V          Magnitude of velocity

w          Mass flowrate

$W_{ss}$          Work, shaft and shear

X          Longitudinal coordinate or flow direction coordinate

Y, Z          Coordinates

$\gamma$          Ratio of specific heats

$\rho$          Density

$\mu$          Secondary-to-primary mass flowrate ratio, $w_s/w_p$

## Subscripts

| | |
|---|---|
| 0 | Stagnation state or location |
| 1,2,3,4 | System locations |
| ATM | Atmosphere |
| B | Back |
| BO | Break-off conditions |
| CS | Control surface |
| M | Mixed |
| MAX | Maximum |
| P | Primary |
| S | Secondary |
| T | Total |
| X,Y | Upstream and downstream normal shock locations |

# 1.0 INTRODUCTION

Supersonic ejector-diffuser systems have many applications both in industrial and advanced, high technology settings. These applications include jet pump compression, thrust augmentation, extraction of a secondary fluid, mixing of two streams, ventilation and air conditioning, etc. Another possible application is to the high energy chemical laser. In chemical laser systems, the flow and lasing zones within the laser cavity are established by the interaction, mixing, and reaction of multiple, two-dimensional, supersonic streams at relatively low absolute static pressure levels. Accompanying the mixing and chemical reactions between these streams, considerable energy is released to the flow which tends, qualitatively, to increase the static pressure, to decrease the stagnation pressure, and to decrease the Mach number of the "mixed" supersonic flow within the laser cavity. At the cavity exit this stream must then be pumped to ambient conditions so that the lasing process can be started and sustained. A supersonic ejector-diffuser system is a prime candidate for the pressure recovery required in this corrosive environment.

The objective of this report[t] is to present the results of an integrated theoretical and experimental investigation of supersonic ejector-diffuser systems. In all cases, consideration is limited to configurations for which the primary stream enters the mixing tube supersonically

975

while the secondary enters subsonically or sonically.  The theoretical phase of the investigation emphasizes the development of simplified flow models and computer programs to describe the performance of constant-pressure, constant-area, and staged ejectors.  In the experimental investigation, small-scale, cold-flow studies were carried out to obtain quantitative performance data for potential ejector-diffuser configurations.  These configurations included various nozzle, mixing-tube, and diffuser geometries which were operated over a range of flow variables. These data serve as a basis for comparison with the theoretical flow models.

The results of this investigation are treated in detail in subsequent sections.

## 2.0 THEORETICAL INVESTIGATION

Four areas are considered in this section; they are:

(1) Supersonic ejector system characteristics;

(2) The constant-pressure ejector;

(3) The constant-area ejector;

(4) The staged ejector.

The discussion of ejector characteristics is qualitative in nature while detailed analyses and discussions are included for each of the last three areas. In addition, the computer programs developed for making the calculations are described; detailed program listings and sample input/output data are included; and representative cases are presented and discussed. The representative cases are not intended to be comprehensive in nature but rather are presented to demonstrate the capabilities, limitations, and the various facets of the simplified theoretical models.

The computer programs have been written with both straightforward subsystems calculations and overall systems studies in mind. It is therefore felt that they can be effectively incorporated into codes developed for preliminary overall systems studies.

### 2.1 SUPERSONIC EJECTOR SYSTEM CHARACTERISTICS

To establish a basis for the detailed modeling and performance analysis of supersonic ejector systems, a qualitative discussion of the performance and nature of such systems is given in this section. Emphasis has been placed on defining the general functional relationships

describing the performance of these systems and how their form is dependent on the internal flow phenomena.

A representative ejector configuration and the associated notation are shown in Fig. 2.1-1. The primary stream is assumed to be supplied from the stagnation state $(P_{PO}, T_{PO})$ through a supersonic nozzle and the secondary stream is supplied from the stagnation state $(P_{SO}, T_{SO})$. The secondary and primary streams begin their mutual interaction at their point of confluence at the primary nozzle exit. This interaction, as well as the mixing between the streams, continues to the shroud exit where they are discharged to the ambient pressure level $P_{ATM}$.

### 2.1.1 Performance characteristics

The objective of any ejector analysis is to establish, for a given configuration and working media, the performance characteristics of the system. In general, the mass flow characteristics can be represented functionally by:

$$w_S/w_P = f(P_{SO}/P_{PO}, P_{ATM}/P_{PO}) \quad , \tag{2.1-1}$$

i.e., they are dependent on the stagnation pressure and back pressure ratios.

An alternate formulation of the pumping characteristics in terms of the initial secondary stream Mach number, $M_{S1}$, the static pressure ratio $P_{S1}/P_{PO}$ of the secondary stream at the point of confluence of the two streams, and the ambient pressure ratio, $P_{ATM}/P_{PO}$, is given in functional form by:

$$M_{S1} = f(P_{S1}/P_{PO}, P_{ATM}/P_{PO}) \quad . \tag{2.1-2}$$
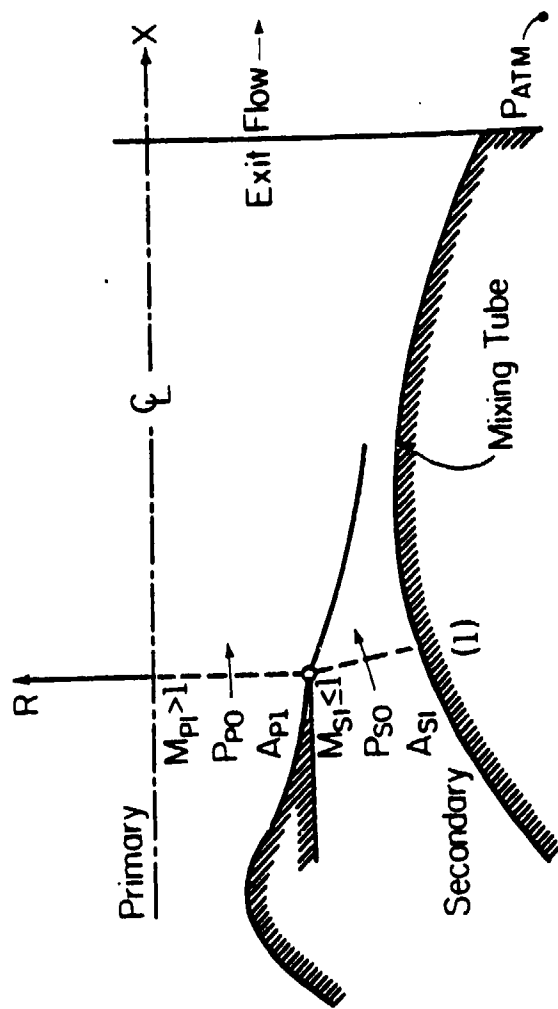
Figure 2.1-1  Ejector configuration and notation

This selection of variables, although less obvious, is convenient for performing the numerical calculations involved in many theoretical ejector analyses.

In addition to establishing the functional form of the pumping characteristics, another quantity of interest is the shroud wall pressure distribution given functionally by:

$$P_w/P_{PO} = f(w_s/w_p, P_{SO}/P_{PO}, P_{ATM}/P_{PO}, x) \qquad (2.1\text{-}3)$$

where $x$ is the axial coordinate.

After establishing the above functional relationships, the thrust characteristics of a system can then be determined in the thrust augmentation application. In practice, this is accomplished by considering the contributions in the axial direction of the entering momentum fluxes of the primary and secondary streams and the integrated shroud wall pressure distribution.

### 2.1.1.1 Three-dimensional performance surfaces

The functional relations, (2.1-1) and (2.1-2), characterize the "pumping" characteristics of an ejector system and represent surfaces in the spaces described by the coordinates $(w_s/w_p, P_{SO}/P_{PO},$ $P_{ATM}/P_{PO})$ and $(M_{S1}, P_{S1}/P_{PO}, P_{ATM}/P_{PO})$, respectively.

The pumping characteristics of a typical ejector system in terms of the first set of variables are shown in Fig. 2.1-2. This surface clearly delineates the flow regimes where'n the mass flow characteristics are independent or dependent on the ambient pressure level. These flow regimes merge together along the "break-off curve" and, in principle, this condition serves to uniquely define this curve.
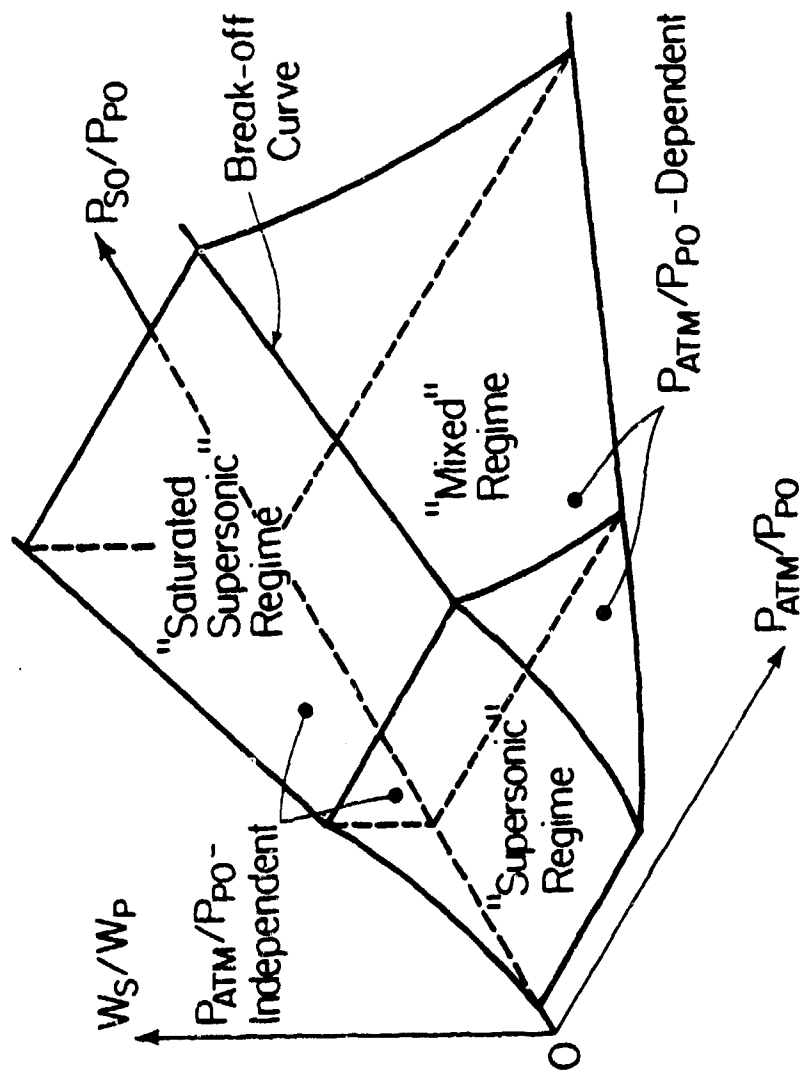
Figure 2.1-2 Ejector mass flow characteristic surface $w_S/w_P = f(P_{SO}/P_{PO}, P_{ATM}/P_{PO})$

To the left of the "break-off curve" ("supersonic" and "saturated supersonic" regimes), the mass flow characteristics are independent of $P_{ATM}/P_{PO}$ and the surface is cylindrical with its generator parallel to the $P_{ATM}/P_{PO}$ axis. For these regimes, the mass flow characteristics can be represented by:

$$w_S/w_P = f(P_{SO}/P_{PO}) \qquad (2.1\text{-}4)$$

when $P_{ATM}/P_{PO} \leq (P_{ATM}/P_{PO})_{BO}$. To the right of the "break-off curve" ("mixed" regime), the surface is three-dimensional in nature and extends from the spatial "break-off curve" to the plane where $w_S/w_P = 0$ (base pressure plane); hence,

$$w_S/w_P = f(P_{SO}/P_{PO}, P_{ATM}/P_{PO}) \qquad (2.1\text{-}5)$$

when $P_{ATM}/P_{PO} \quad (P_{ATM}/P_{PO})_{BO}$.

In principle, the "break-off curve" represents a simultaneous solution of the functional relationships (2.1-4) and (2.1-5). However, the "break-off curve" also has a phenomenological interpretation based on the flowfield interactions occurring within the ejector shroud. Points on the "break-off curve" are determined by the condition that transition from dependence to independence of the mass flow characteristics on the ambient pressure level will occur when the secondary stream just attains sonic conditions either inside the mixing tube or at its entrance. This point will be further amplified in the discussion of the constant-area ejector.

An alternative representation of the pumping characteristics in terms of the variables $(M_{S1}, P_{S1}/P_{PO}, P_{ATM}/P_{PO})$ is given in Fig. 2.1-3.
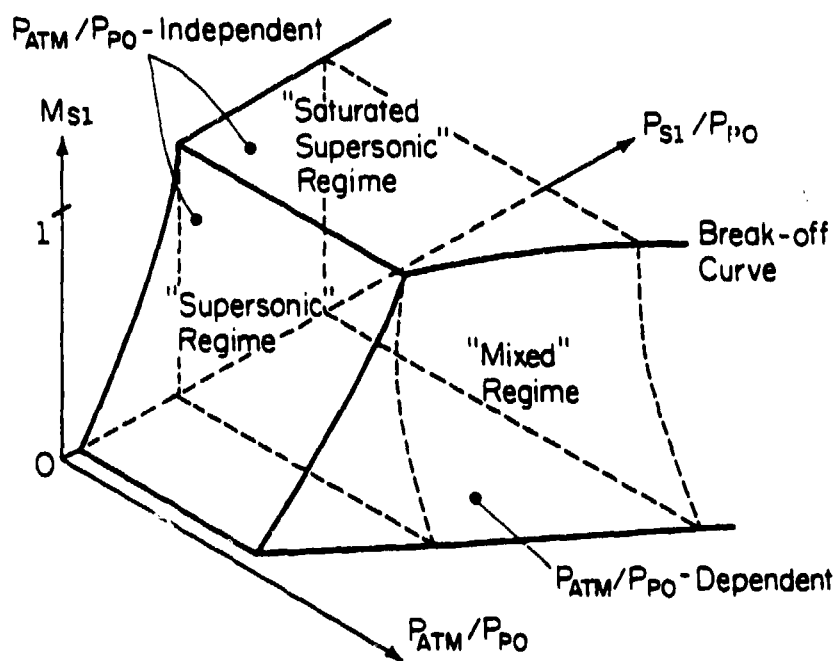
Figure 2.1-3 Ejector characteristic surface $M_{S1} = f(P_{S1}/P_{PO}, P_{ATM}/P_{PO})$

For this surface, there are direct counterparts to the $P_{ATM}/P_{PO}$-independent and $P_{ATM}/P_{PO}$-dependent regimes of the $w_s/w_p$ surface.

### 2.1.1.2 Two-dimensional parametric curves

The three-dimensional performance surfaces of Figures 2.1-2 and 2.1-3 generally have their principal value in presenting an overview of the performance characteristics of typical ejector systems. In theoretical analyses or experimental programs, it is often more convenient to consider two-dimensional parametric representations of these operating surfaces. These parametric curves usually represent nothing more than intersections of the performance surfaces with various planes corresponding to constant values of the respective variables.

Two of the more useful parametric representations of the mass flow characteristics are obtained by intersecting the $w_s/w_p$ surface by planes of constant $P_{ATM}/P_{PO}$, Fig. 2.1-4, and planes of constant $P_{SO}/P_{PO}$, Fig. 2.1-5. Another interesting and useful parametric curve can be obtained by intersecting the $w_s/w_p$ surface by a plane for which $P_{SO}/P_{PO} = P_{ATM}/P_{PU}$, Fig. 2.1-6. The latter situation corresponds to inducting the secondary fluid at ambient conditions and then discharging the ejector to the same ambient conditions as occurs in thrust augmentation applications.

Also convenient, from the standpoint of theoretical analyses, are intersections of the $M_{S1}$-surface by planes of constant $P_{ATM}/P_{PO}$, Fig. 2.1-7, and planes of constant $P_{S1}/P_{PO}$, Fig. 2.1-8.

It will be of great utility to refer to these three-dimensional solution surfaces and the two-dimensional parametric curves in succeeding discussions of the theoretical models and experimental results.
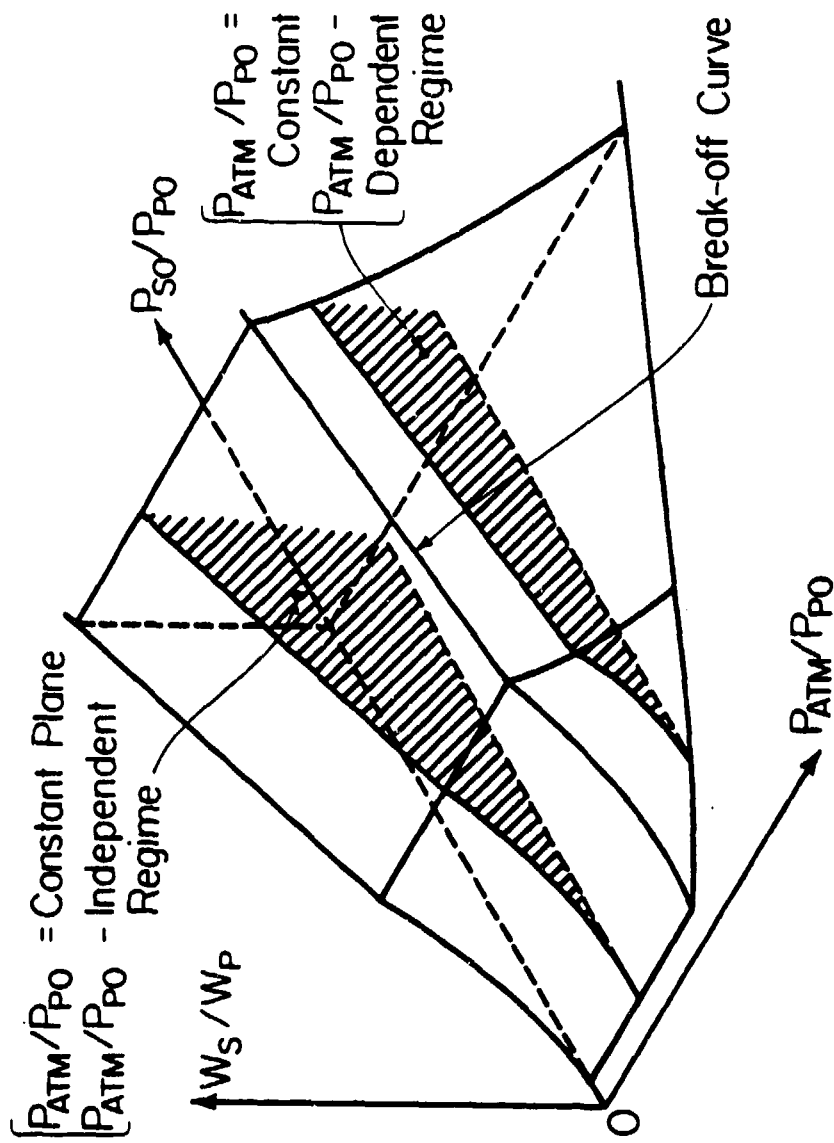
Figure 2.1-4 Intersection of the $w_S/w_P$ surface with planes of constant $P_{ATM}/P_{PO}$
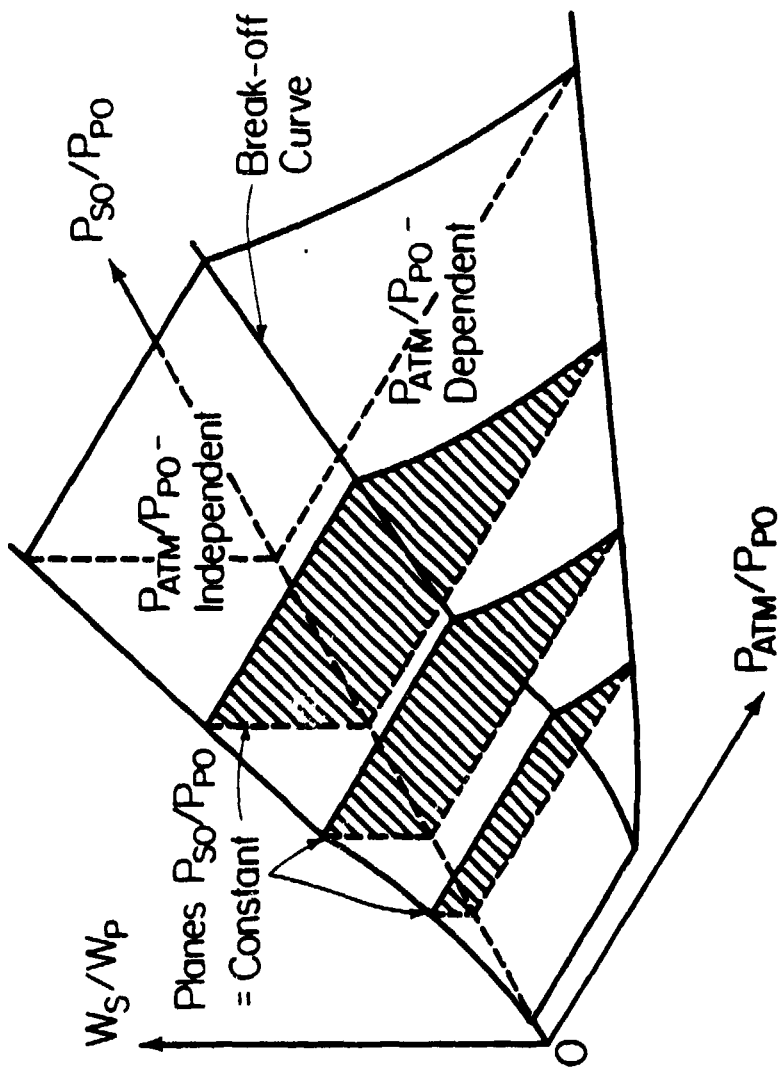
Figure 2.1-5   Intersection of the $w_s/w_p$ surface with planes of constant $P_{so}/P_{po}$
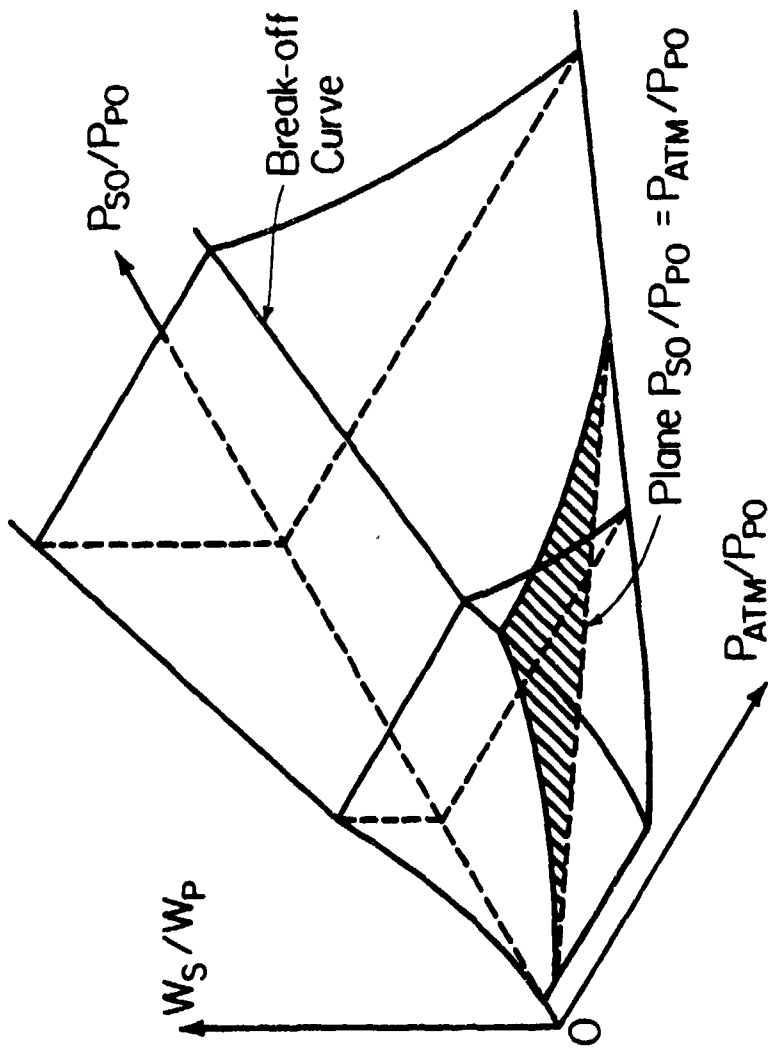
Figure 2.1-6  Intersection of the $w_s/w_p$ surface with a plane $P_{ATM}/P_{PO} = P_{SO}/P_{PO}$

Labels within figure:
- $P_{SO}/P_{PO}$
- Break-off Curve
- Plane $P_{SO}/P_{PO} = P_{ATM}/P_{PO}$
- $P_{ATM}/P_{PO}$
- $W_S/W_P$
- O
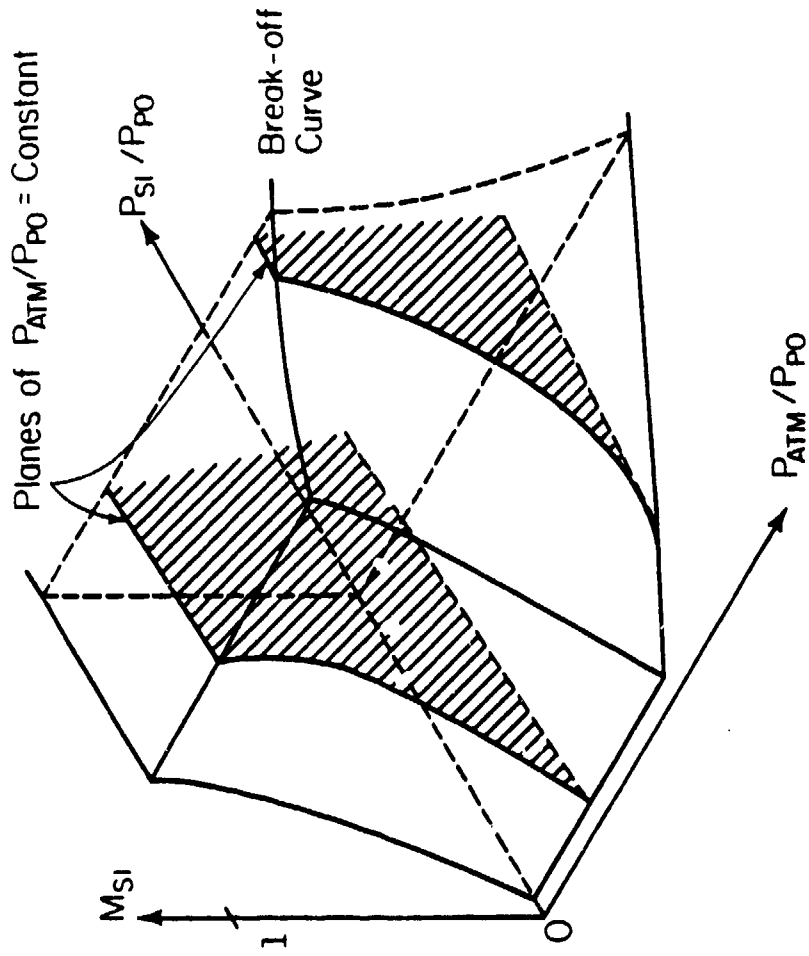
Figure 2.1-7 Intersection of the $M_{SI}$ surface with planes of constant $P_{ATM}/P_{PO}$

Figure 2.1-8  Intersection of the $M_{S1}$ surface with planes of constant $P_{S1}/P_{PO}$

989

## 2.2 CONSTANT-PRESSURE EJECTOR

A schematic of a constant-pressure ejector is shown in Fig. 2.2-1. This ejector consists of (1) a variable-area mixing section wherein the primary and secondary flows are assumed to mix to form a uniform super-sonic flow and (2) a downstream diffuser section. The analysis of this ejector is based on analyzing separately the operating characteristics of the mixing and diffuser subsystems, and then matching these characteristics to determine the operation of the overall ejector.

The analysis of the flow in the mixing section is based on the principal assumption that the area of the mixing section varies such that the summation of the integrated static pressure-area forces acting on the flow within the mixing section is zero. Of the conceivable geometry-flow combinations that could satisfy the above requirement, the assumption is made that the area of the mixing section varies such that the primary and secondary streams mix at constant static pressure to form a uniform mixed flow. Thus, to satisfy the requirement of constant static pressure in the mixing section, the mixing section area distribution must be different for each operating point of the ejector. While this requirement presents no problems from a theoretical standpoint, it does present several prob-lems from a practical hardware standpoint. The first problem is that the analysis does not provide any information on the mixing section area dis-tribution between the entrance and uniform flow sections, Sections 1 and 2, respectively, in Fig. 2.2-1. The second problem is off-design opera-tion of this ejector. Assuming that an area distribution can be found for which the static pressure is constant for a given ejector geometry and
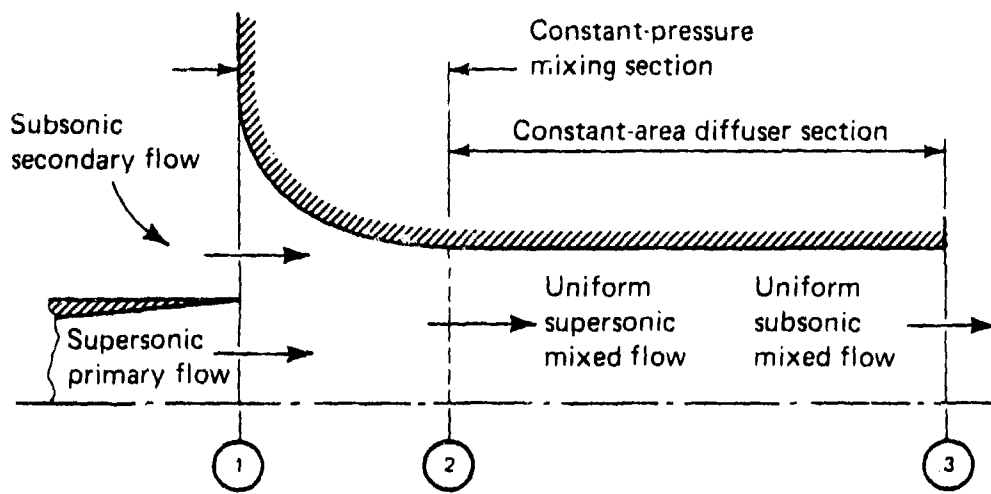
Figure 2.2-1 Constant-pressure ejector configuration

operating point, the operation of this ejector at any point other than the design point would, most probably, result in a significant mismatch of the system and operating conditions, thus causing poor ejector performance.

Downstream of the mixing section, the uniform mixed flow is diffused and discharged to ambient conditions. To analyze the overall ejector performance, a flow model must be adopted for the diffuser section. A simple but adequate approach to this part of the ejector analysis is to assume a constant-area diffuser whose pressure-rise performance can be expressed in terms of the normal-shock pressure rise and an empirical pressure-rise coefficient both of which are determined by the supersonic entrance Mach number to the diffuser.

### 2.2.1  Constant-pressure ejector analysis

#### 2.2.1.1  <u>Constant-pressure mixing section</u>

The flow in the mixing section is analyzed by applying the conservation equations and numerous assumptions to the control volume shown in Fig. 2.2-2. These assumptions are:

(1)  Steady flow, $\frac{\partial(\ )}{\partial t} \equiv 0$.

(2)  Piecewise uniform flows at Section 1 and uniform flow at Section 2.

(3)  The primary and secondary gases obey the perfect gas relationships.

(4)  The primary and secondary streams mix ideally to form a supersonic mixed stream at Section 2.

(5)  Negligible shear stresses at the wall.

(6)  Adiabatic flow between Sections 1 and 2.

992
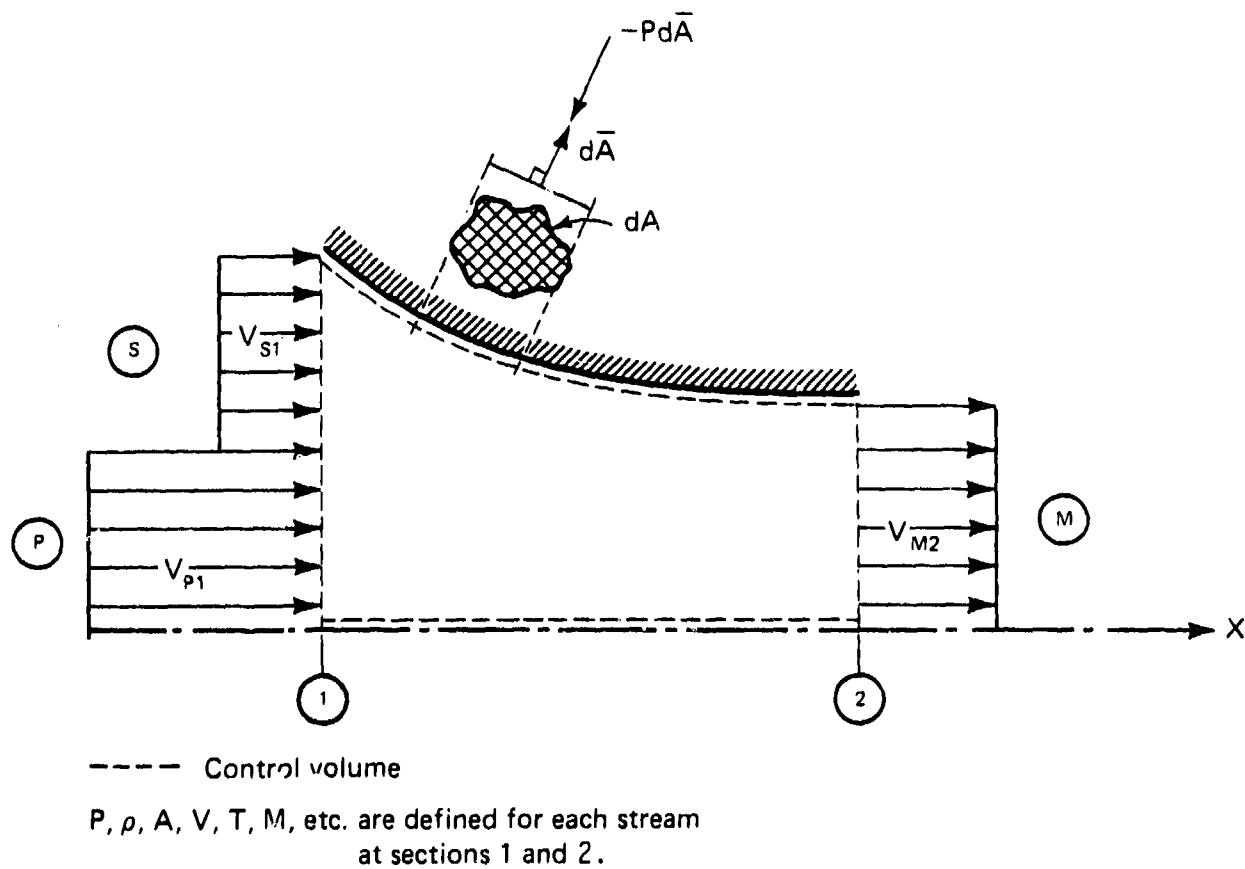
Figure 2.2-2   Constant-pressure mixing section control volume

(7) No shaft or shear work between Sections 1 and 2.

(8) A negligible change in potential energy due to variations in elevation in the mixing section.

(9) The summation of the integrated pressure-area surface forces acting in the flow direction is zero. As a special case satisfying this assumption, the area variation of the mixing tube is assumed to be always such that the static pressure of the flow is constant throughout the mixing section.

(10) The primary and secondary flows are assumed to be isentropic from their respective stagnation states to the states at Section 1.

For steady flow, the continuity equation is

$$\int_{cs} \rho \overline{V} \cdot d\overline{A} = 0 \quad . \tag{2.2-1}$$

For the control volume of Fig. 2.2-2 and with assumption (2), Eq. (2.2-1) becomes

$$\rho_{P1} V_{P1} A_{P1} + \rho_{S1} V_{S1} A_{S1} = \rho_{M2} V_{M2} A_{M2} \quad . \tag{2.2-2}$$

In terms of the mass flowrates, $w \equiv \rho A V$, the continuity equation is simply

$$w_P + w_S = w_M \quad . \tag{2.2-3}$$

The mass flowrate, $w$, can be expressed in terms of the mass flow function, $f_1(\gamma, M)$, by

$$\frac{\left[ w \frac{R}{Mw} T_0 \right]^{1/2}}{PA} = M \left[ \gamma \{ 1 + \frac{(\gamma-1)}{2} M^2 \} \right]^{1/2} \equiv f_1(\gamma, M) \quad . \tag{2.2-4}$$

994

The secondary-to-primary mass flowrate ratio, $\mu \equiv w_S/w_P$, can be expressed in terms of the mass flow function by

$$\mu = \frac{A_{S1}}{A_{P1}} \left[ \frac{Mw_S}{Mw_P} \cdot \frac{T_{PO}}{T_{SO}} \right]^{1/2} \frac{f_1(\gamma_S, M_{S1})}{f_1(\gamma_P, M_{P1})} \qquad (2.2\text{-}5)$$

where assumption (9), $P_{P1} = P_{S1}$, was used. Equation (2.2-3) can also be expressed in terms of the mass flow function by

$$\frac{A_{M2}}{A_{P1}} \left[ \frac{Mw_M}{Mw_P} \cdot \frac{T_{PO}}{T_{MO}} \right]^{1/2} \frac{f_1(\gamma_M, M_{M2})}{f_1(\gamma_P, M_{P1})} = (1+\mu) \qquad (2.2\text{-}6)$$

where $P_{P1} = P_{M2}$ was assumed.

For steady flow, the momentum equation for the flow direction is

$$\leftrightarrow \sum F_X = \oint_{cs} V_X(\rho \overline{V} \cdot d\overline{A}) \qquad . \qquad (2.2\text{-}7)$$

Neglecting wall shear stresses, the summation of forces acting on the control volume in the flow direction is

$$\leftrightarrow \sum F_X = P_{P1} A_{P1} + P_{S1} A_{S1} - P_{M2} A_{M2} - \hat{\imath}_X \cdot \int_{A_W} P d\overline{A} \qquad (2.2\text{-}8)$$

or simplifying

$$\leftrightarrow \sum F_X = P_{P1} A_{P1} + P_{S1} A_{S1} - P_{M2} A_{M2} - \int_{A_{M2}}^{A_1} P dA_X \qquad (2.2\text{-}9)$$

where $A_1 \equiv A_{P1} + A_{S1}$. According to assumption (9), the mixing section area distribution in the flow direction is assumed always to be such that the static pressure along the wall is constant; as a consequence, $\sum F_X = 0$ in Eqs. (2.2-7) to (2.2-9). Hence with assumption (2), Eq. (2.2-7) simplifies to

$$\rho_{P1} V_{P1}^2 A_{P1} + \rho_{S1} V_{S1}^2 A_{S1} = \rho_{M2} V_{M2}^2 A_{M2} \quad . \tag{2.2-10}$$

With assumption (9), $P_{P1} = P_{S1} = P_{M2}$, Eq. (2.2-10) can be expressed in the more convenient form

$$\gamma_P M_{P1}^2 + \frac{A_{S1}}{A_{P1}} \gamma_S M_{S1}^2 = \frac{A_{M2}}{A_{P1}} \gamma_M M_{M2}^2 \quad . \tag{2.2-11}$$

For steady flow, the energy equation is

$$\frac{\not{D}Q}{\not{D}t} - \frac{\not{D}W_{ss}}{\not{D}t} = \oint_{cs} \left( h + \frac{V^2}{2} + gz \right) \rho \bar{V} \cdot d\bar{A} \quad . \tag{2.2-12}$$

As a consequence of assumptions (6,7,8), the energy equation can be simplified to

$$\oint_{cs} (h_0) \rho \bar{V} \cdot d\bar{A} = 0 \tag{2.2-13}$$

where $h_0 \equiv h + \frac{V^2}{2}$ . For the piecewise uniform and uniform flows at Sections (1) and (2), respectively, the energy equation becomes

$$w_P h_{P0} + w_S h_{S0} = w_M h_{M0} \quad . \tag{2.2-14}$$

Using $h_0 = C_P T_0$ and $\mu = w_S/w_P$ , Eq. (2.2-14) can be combined with Eq. (2.2-3) and the result rewritten as

$$\frac{T_{M0}}{T_{P0}} = \frac{1}{(1+\mu)} \left[ \frac{(C_P)_P}{(C_P)_M} \right] \left[ 1 + \mu \frac{(C_P)_S}{(C_P)_P} \cdot \frac{T_{S0}}{T_{P0}} \right] \quad . \tag{2.2-15}$$

The relationships between the stagnation and static pressures for the primary and secondary flows are determined in the following way. According to assumption (10), the flows between the primary and secondary stagnation states and Section (1) are assumed to be isentropic. Thus, with $P_{S1} = P_{P1}$ , the primary-to-secondary stagnation pressure ratio is given by

996

$$\frac{P_{P0}}{P_{S0}} = \frac{f_2(\gamma_S, M_{S1})}{f_2(\gamma_P, M_{P1})} \tag{2.2-16}$$

where the isentropic pressure ratio function $f_2(\gamma, M)$ is defined by

$$\frac{P}{P_0} = \left[1 + \frac{\gamma-1}{2}M^2\right]^{-\gamma/(\gamma-1)} \equiv f_2(\gamma, M) \quad . \tag{2.2-17}$$

The static pressure, $P_{M2}$, at the entrance to the diffuser can be expressed, according to assumption (9), in terms of the secondary stagnation pressure, $P_{S0}$, by

$$\frac{P_{M2}}{P_{S0}} = \frac{P_{S1}}{P_{S0}} = f_2(\gamma_S, M_{S1}) \quad . \tag{2.2-18}$$

The preceding equations are the basis for determining the operating characteristics of the constant-pressure mixing section. However, before these characteristics can be determined, the properties of the mixed gas at Section 2 must be determined and an overall approach to defining and presenting the mixing-tube characteristics must be adopted.

A mixed perfect gas is assumed to exist at Section 2 as a consequence of the mixing of the primary and secondary gases within the mixing section. The properties of the mixed gas are determined by applying Dalton's law of partial pressures to a hypothetical mixing process at constant volume of the respective mass fractions of the primary and secondary perfect gases. From this analysis, the properties of the mixed gas can be expressed by the following relationships in terms of the secondary-to-primary mass flowrate ratio, $\mu$, and the primary and secondary gas properties.

The ratio of specific heats at constant pressure of the primary and mixed gases is

997

$$\frac{(C_p)_P}{(C_p)_M} = \frac{[1+\mu]}{\left[1 + \mu \frac{(C_p)_S}{(C_p)_P}\right]} \qquad \text{(2.2-19)}$$

In Eq. (2.2-19), the ratio of specific heats at constant pressure for the secondary and primary gases can be expressed alternatively in terms of other gas properties by

$$\frac{(C_p)_S}{(C_p)_P} = \frac{\gamma_S}{\gamma_P} \cdot \frac{(\gamma_P-1)}{(\gamma_S-1)} \cdot \frac{Mw_P}{Mw_S} \qquad \text{(2.2-20)}$$

The ratio of molecular weights of the primary and mixed gases is given by

$$\frac{Mw_M}{Mw_P} = \frac{(1+\mu)}{\left[1 + \mu \frac{Mw_P}{Mw_S}\right]} \qquad \text{(2.2-21)}$$

The ratio of the specific heat at constant pressure to the specific heat at constant volume for the mixed gas is

$$\gamma_M = \left[1 - \left\{\frac{\gamma_P-1}{\gamma_P}\right\} \frac{\{1 + \mu \frac{Mw_P}{Mw_S}\}}{\{1 + \mu \frac{\gamma_S}{\gamma_P} \cdot \frac{(\gamma_P-1)}{(\gamma_S-1)} \cdot \frac{Mw_P}{Mw_S}\}}\right]^{-1} \qquad \text{(2.2-22)}$$

Equations (2.2-19) to (2.2-22) define the mixed gas properties completely in terms of the properties of the primary and secondary gases and the mass flowrate ratio, $\mu$. Thus, any calculational approach is greatly simplified and more straightforward if $\mu$ is assumed to be known, at least parametrically, at the outset. This approach will now be discussed.

There is considerable latitude in determining and presenting the operating characteristics of an ejector. Since the ejector characteristics

998

are, of course, unique, the preference of one approach or set of variables over another is one of convenience. The basic approach adopted herein is to specify parametrically the secondary-to-primary mass flow-rate ratio, $\mu$, and then to determine the corresponding values of the ejector driving stagnation pressure ratio, $P_{PO}/P_{SO}$, and the overall ejector compression ratio, $P_{M3}/P_{SO}$. Since the operating characteristics of an ejector system can be represented by a three-dimensional surface [1],[†] the foregoing approach simply represents the intersection of this ejector operating surface in $\left( \mu, \dfrac{P_{PO}}{P_{SO}}, \dfrac{P_{M3}}{P_{SO}} \right)$ space with planes of $\mu = $ constant.[††]

At the outset, the following data are assumed to be known:

$$\left[ \gamma_S, \gamma_P, \frac{Mw_S}{Mw_P}, \frac{T_{SO}}{T_{PO}}, \frac{A_{M2}}{A_{P1}}, M_{P1} > 1 \right] \quad .$$

The specification of $A_{M2}/A_{P1}$ instead of $A_{S1}/A_{P1}$ is a convenience for later comparisons between constant-pressure and constant-area ejectors. Utilizing the foregoing data and a parametric value of $\mu$, the mixed gas properties

$$\left[ \frac{(C_P)_P}{(C_P)_M}, \frac{Mw_M}{Mw_P}, \gamma_M \right]$$

can be determined from Eqs. (2.2-19), (2.2-21), and (2.2-22), respectively. The mixed-to-primary stagnation temperature ratio, $T_{MO}/T_{PO}$, can then be

---

[†] Numbers in brackets refer to entries in REFERENCES.
[††] Unfortunately, the constant-pressure ejector model is incapable of dealing with this reality of ejector operation. This point will be considered in detail in Section 2.3 wherein the constant-area ejector is analyzed. Note that this selection of variables is somewhat different than those used in Section 2.1.

determined from Eq. (2.2-15). Using these data, the solution value of $M_{M2}$ is determined from Eq. (2.2-6) by solving

$$f_1 \left( \gamma_M, M_{M2} \right) = \frac{(1+\mu) f_1 \left( \gamma_P, M_{P1} \right)}{\dfrac{A_{M2}}{A_{P1}} \left[ \dfrac{Mw_M}{Mw_P} \cdot \dfrac{T_{P0}}{T_{M0}} \right]^{1/2}} \equiv C_1 \qquad . \tag{2.2-23}$$

The solution value for $M_{M2}$ (supersonic root) is

$$M_{M2} = \left[ \frac{\left\{ \gamma_M^2 + 2\gamma_M (\gamma_M - 1) C_1^2 \right\}^{1/2} - \gamma_M}{\gamma_M (\gamma_M - 1)} \right]^{1/2} \qquad . \tag{2.2-24}$$

The next steps in the solution procedure are to determine $A_{S1}/A_{P1}$ and $M_{S1} < 1$. To do this, Eqs. (2.2-5) and (2.2-11) are combined to eliminate the unknown area ratio, $A_{S1}/A_{P1}$, from the resulting equation. The resulting relationship to be solved for $M_{S1} < 1$ is

$$\frac{f_1 \left( \gamma_S, M_{S1} \right)}{\gamma_S M_{S1}^2} = \frac{\mu f_1 \left( \gamma_P, M_{P1} \right)}{\left[ \dfrac{A_{M2}}{A_{P1}} \gamma_M M_{M2}^2 - \gamma_P M_{P1}^2 \right] \left[ \dfrac{Mw_S}{Mw_P} \cdot \dfrac{T_{P0}}{T_{S0}} \right]^{1/2}} \equiv C_2 \tag{2.2-25}$$

where a finite value with $C_2 > 0$ is required for a meaningful solution. The solution value for $M_{S1}$ is

$$M_{S1} = \left( \frac{2}{1 + (2C_2^2 - 1)\gamma_S} \right)^{1/2} \qquad . \tag{2.2-26}$$

After determining $M_{S1} < 1$ from Eq. (2.2-26), the area ratio can then be found by rearranging Eq. (2.2-11)

$$\frac{A_{S1}}{A_{P1}} = \frac{\left[ \dfrac{A_{M2}}{A_{P1}} \gamma_M M_{M2}^2 - \gamma_P M_{P1}^2 \right]}{\gamma_S M_{S1}^2} \qquad . \tag{2.2-27}$$

The flow through the mixing section is determined by the preceding computational sequence and is characterized by the variables $[M_{S1}, A_{S1}/A_{P1}, M_{M2}]$. A constant-pressure solution will exist only if

$$\frac{A_{M2}}{A_{P1}} < \left\{ \frac{b^2}{\gamma_P M_{P1}^2} - \frac{(\gamma_M - 1)}{2\gamma_M} \gamma_P M_{P1}^2 \right\} \qquad (2.2\text{-}28)$$

where

$$b = (1+\mu) f_1(\gamma_P, M_{P1}) / \left[ \frac{Mw_M}{Mw_P} \cdot \frac{T_{PO}}{T_{MO}} \right]^{1/2} \qquad (2.2\text{-}29)$$

If a solution exists, the mixing-section pressure ratios, $P_{PO}/P_{SO}$ and $P_{M2}/P_{SO}$, can then be determined from Eqs. (2.2-16) and (2.2-17), respectively.

To complete the analysis of the constant-pressure ejector, a diffuser must be specified that will diffuse the flow at Section 2 to ambient conditions at the diffuser exit. The simple diffuser model used in this study will be discussed briefly in the next section.

### 2.2.1.2 Constant-area supersonic diffuser

Supersonic flow entering a constant-area duct is recompressed within the duct by an extended series of shock waves resulting from shock wave-boundary layer interactions. The pressure level to which the flow is recompressed depends on the entering supersonic Mach number and the length-to-diameter ratio of the diffuser duct. Experimental studies have established for various duct cross-sectional area geometries the minimum length-to-diameter ratio of the duct required for the extended shock structure. These data and an empirical correlation based on these data are shown in Fig. 2.2-3; these results are taken from [2].
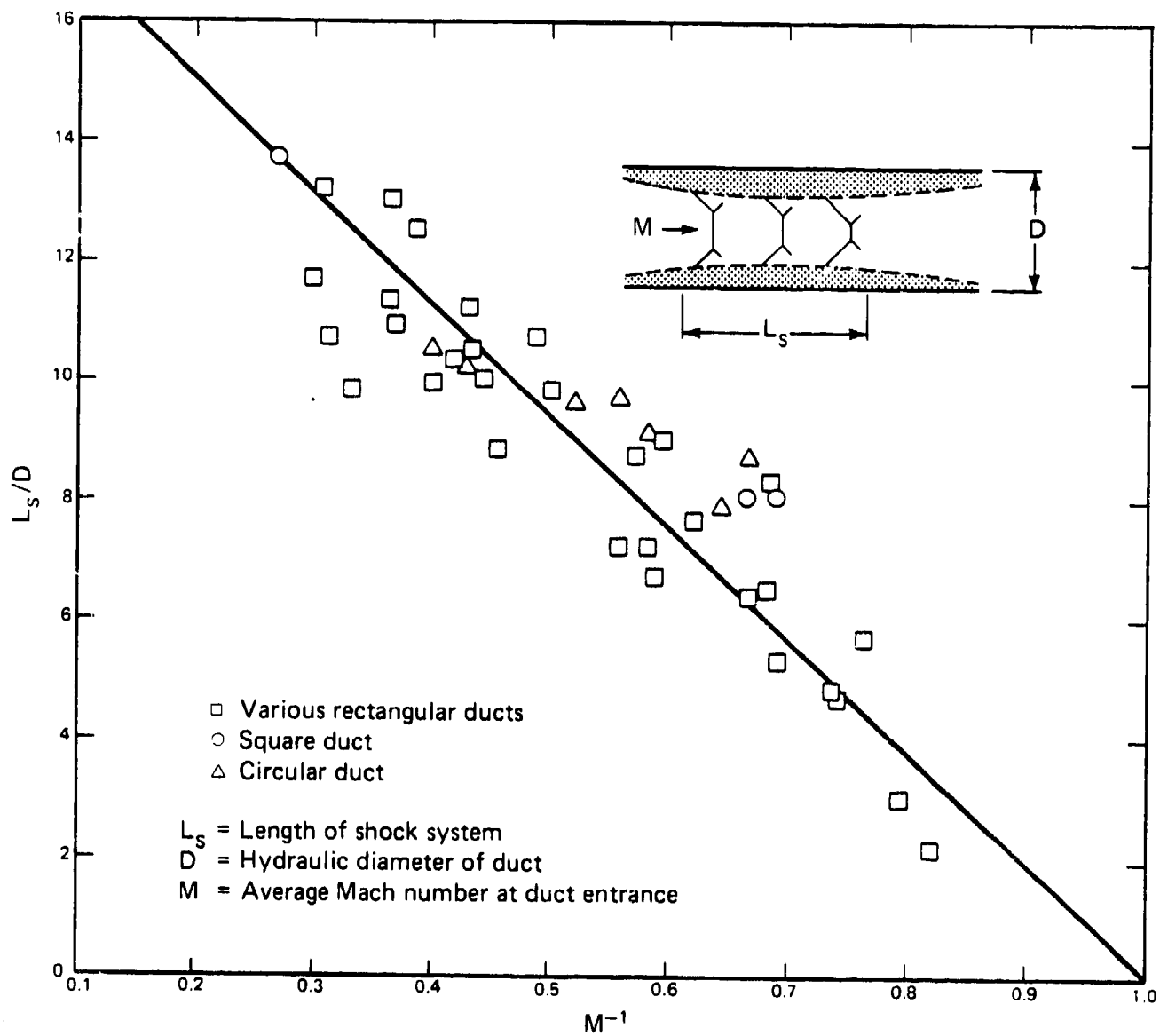
Figure 2.2-3  Empirical correlation for length-to-diameter ratio of
constant-area supersonic diffusers (from Reference [2])

Thus, for a duct of sufficient length, the recompression shock system is complete. The pressure rise across this shock system is usually expressed in terms of the pressure rise that would exist across a corresponding normal shock wave of negligible thickness occurring at the duct entrance supersonic Mach number. For the constant-area diffuser of Fig. 2.2-4, the static pressure rise across the duct is expressed by

$$\frac{P_{M3}}{P_{M2}} = r_d f_5 (\gamma_M, M_{M2}) \tag{2.2-30}$$

where $r_d$ is an empirical pressure rise coefficient and $f_5 (\gamma_M, M_{M2})$ is the normal shock static pressure ratio function. This function is defined by

$$f_5 (\gamma, M) = \frac{2\gamma}{(\gamma+1)} M^2 - \frac{(\gamma-1)}{(\gamma+1)} \quad . \tag{2.2-31}$$

The empirical coefficient, $r_d$, accounts for possible incompleteness in the shock recompression system, losses in the diffuser system, etc. For system calculations, the functional behavior of this coefficient must be determined from experiments. Another approach is to vary parametrically the value of $r_d$ to assess the influence of diffuser performance on ejector system operation. As a consequence, the value of $r_d$ is left as an input value to the computer program for estimating constant-pressure ejector performance.[†]

---

[†] Values of $r_d$ in the range, $0.75 < r_d < 1.25$, are commonly used for parametric studies.

1003

$V_{M2}$, $P_{M2}$, $\cdots$       $V_{M3}$, $P_{M3}$, $\cdots$

Multiple-shock region

D

2       3

$M_{M2} > 1$      L      $M_{M3} < 1$

$L/D >$ Minimum required value from Fig. 2.2-3
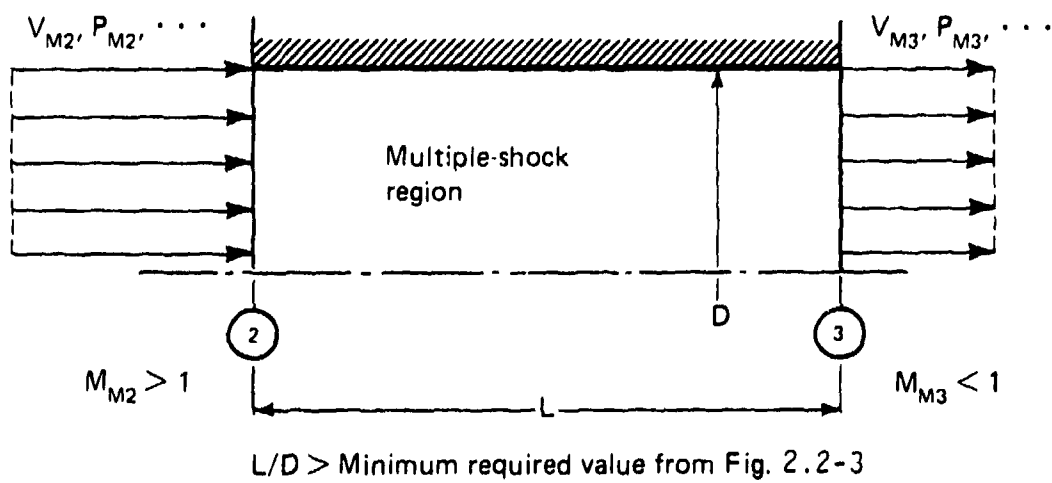
Figure 2.2-4   Constant-area supersonic diffuser notation

1004

### 2.2.1.3 Overall ejector analysis

The operating characteristics of the constant-pressure mixing section can be determined as outlined in Section 2.2.1.1. For given values of

$$[\gamma_S, \gamma_P, Mw_S/Mw_P, T_{SO}/T_{PO}, A_{M2}/A_{P1}, M_{P1} > 1]$$

and a parametric value of $\mu$, the values of

$$[M_{M2}, M_{S1}, A_{S1}/A_{P1}]$$

can be determined. Utilizing these values, the mixing section pressure ratios

$$[P_{PO}/P_{SO}, P_{M2}/P_{SO}]$$

can then be found.

For a given value of the diffuser pressure-rise coefficient, the diffuser static-pressure rise ratio, $P_{M3}/P_{M2}$, can then be determined. The overall ejector compression ratio is determined from

$$\frac{P_{M3}}{P_{SO}} = \frac{P_{M2}}{P_{SO}} \cdot \frac{P_{M3}}{P_{M2}} \qquad (2.2\text{-}32)$$

where $P_{M2}/P_{SO}$ and $P_{M3}/P_{M2}$ are from Eqs. (2.2-18) and (2.2-30), respectively.

The operation of the constant-pressure ejector is then established in terms of the variables $[\mu, P_{PO}/P_{SO}, P_{M3}/P_{SO}]$.

### 2.2.2 Constant-pressure ejector computer program (CPE)

A computer program was written, based on the analysis of Section 2.2.1, to determine the operating characteristics of constant-pressure ejectors. A complete listing of this program is given in Appendix 6.1.

The input variables, their symbols, and their default values are summarized in Table 2.2-1. The output variables and symbols are summarized in Table 2.2-2.

| Table 2.2-1 Input variables for program CPE | | |
|---|---|---|
| Variable | Symbol | Default value |
| $\gamma_S$ | GS | 1.405 |
| $\gamma_P$ | GP | 1.405 |
| $Mw_S/Mw_P$ | MWSP | 1.0 |
| $T_{so}/T_{po}$ | TSØPØ | 1.0 |
| $A_{M2}/A_{P1}$ | AM2P1 | --- |
| $M_{P1}$ | MP1 | --- (>1.0) |
| $r_d$ | RD | 1.0 |
| $\mu = w_S/w_P$ | WSPI | --- |
| --- | CASE | "NEW" |

| Table 2.2-2 Output variables for program CPE | |
|---|---|
| Variable | Symbol |
| $\gamma_M$ | GM |
| $Mw_M/Mw_P$ | MWMP |
| --- | NCASE |
| $M_{M2}$ | MM2 |
| $M_{S1}$ | MS1 |
| $A_{S1}/A_{P1}$ | AS1P1 |
| $P_{po}/P_{so}$ | PPØSØ |
| $P_{M3}/P_{so}$ | PM3SØ |

1006

## 2.2.3 Representative results

To demonstrate typical operating characteristics of a constant-pressure ejector, the ejector configuration summarized in Table 2.2-3 was selected.

| Table 2.2-3 Representative constant-pressure ejector configuration | |
|---|---|
| Variable | Value |
| $\gamma_S$ | 1.4 |
| $\gamma_P$ | 1.4 |
| $Mw_S / Mw_P$ | 1.0 |
| $T_{S0} / T_{P0}$ | 1.0 |
| $A_{M2} / A_{P1}$ | 3.0, 4.0 |
| $M_{P1}$ | 4.0 |
| $r_d$ | 1.0 |
| $\mu$ | Varied |

The operating characteristics of this ejector system are summarized in Fig. 2.2-5. From this figure, it is clear that the constant-pressure ejector solution exists for each area ratio over only a relatively small range of mass flowrate ratios. Corresponding to this range, the value of $M_{S1}$ varies throughout its possible range, $0 < M_{S1} \leq 1$. The compression ratio for this ejector is highest for relatively small values of $M_{S1}$; this is the reason that $M_{S1} = 0.20$ is often chosen in discussions of the theoretical performance of this type of ejector. In the neighborhood of small values of $M_{S1}$, it is seen that $A_{S1}/A_{P1}$ varies significantly.
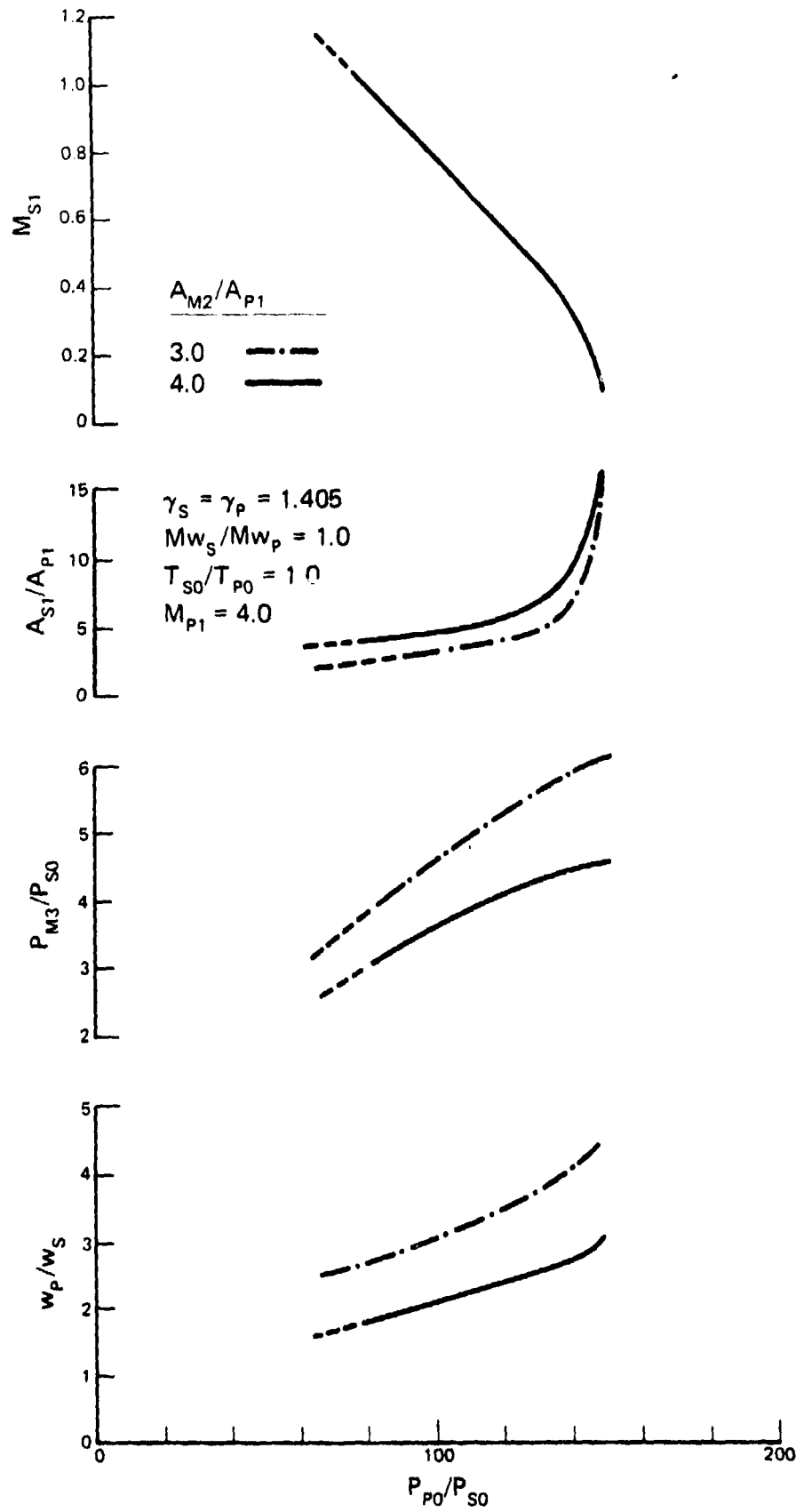
Figure 2.2-5 Representative characteristics for a constant-pressure ejector

This constant-pressure ejector configuration was chosen for comparison with a constant-area ejector with a similar configuration, Section 2.3.3.

A comparison of the compression pressure ratio characteristics of the constant-pressure ejector (Fig. 2.2-5) and constant-area ejectors (Figs. 2.3-4b,d) with the same values of $A_{M2}/A_{P1}$ and $M_{P1}$, shows that both ejectors have approximately the same maximum compression pressure ratios. However, the constant-area ejector is seen to have a much broader range of possible solutions.

Due to the large number or variables involved, no attempt was made to present herein a comprehensive parametric study of the constant-pressure ejector or expected trends as a consequence of variations in these variables. Rather, it is recommended that the computer program be used to make these studies only after a baseline configuration has been established.

## 2.3 CONSTANT-AREA EJECTOR

A schematic of a constant-area ejector is shown in Fig. 2.3-1. The ejector consists of a constant-area mixing section wherein the primary and secondary flows interact and mix to form a uniform mixed flow at the ejector exit. The constant-area ejector has two distinct operating regimes which are identified according to whether the mass flowrate characteristics of the ejector are dependent or independent of the back-pressure level imposed at the ejector exit. In the literature [3,4], the back-pressure dependent regime is referred to as the "mixed" regime and the back-pressure independent regime as the "supersonic" and

1009
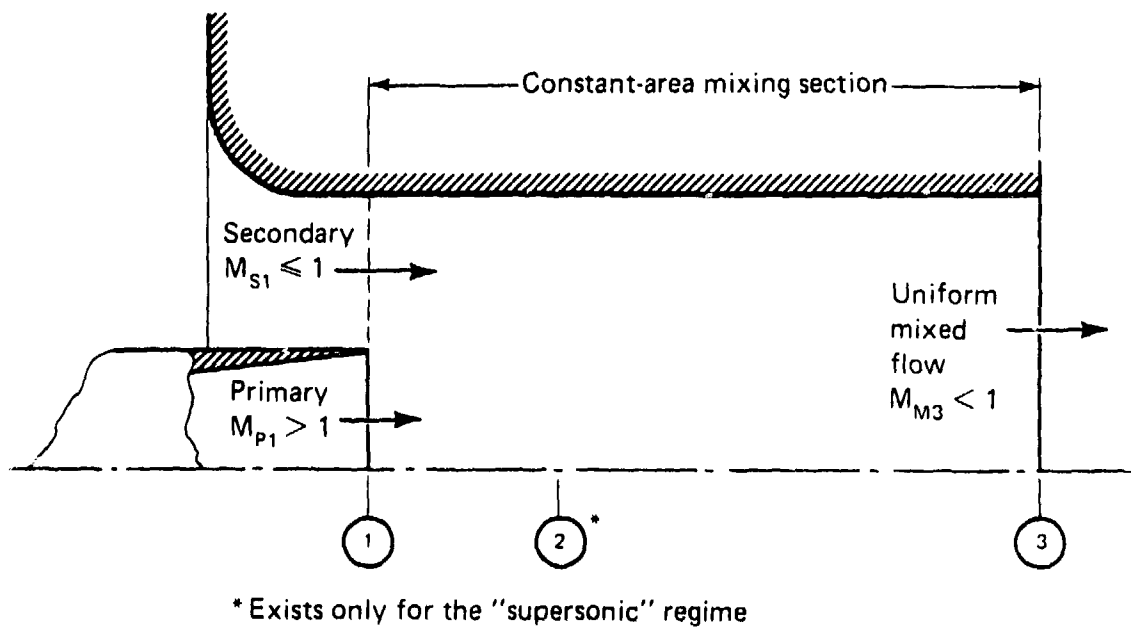
Figure 2.3-1   Constant-area ejector configuration

"saturated-supersonic" regimes. While these designations are somewhat misnomers, they do, however, describe the operating regimes of an ejector in analogy to a conventional converging-diverging nozzle [1].

The performance of an ejector system can only be analyzed by establishing both the conditions for these flow regimes to exist and the conditions for transition between these regimes. The transition conditions between the "mixed" and "supersonic" or "saturated-supersonic" regimes are referred to as the "break-off" conditions.

The "supersonic" regime of an ejector is the result of the nearly inviscid interaction between the primary and secondary streams downstream of their confluence, Section 1, Fig. 2.3-1. The static pressures at the confluence of the flows must be such that the supersonic primary flow expands and interacts with the subsonic secondary flow causing it to reach sonic flow conditions at the aerodynamically formed minimum secondary flow area. As a consequence of this secondary flow choking phenomenon, the secondary mass flowrate is determined independent of back-pressure conditions. While the ejector mass flowrate characteristics are independent of the back-pressure level, the complex shock, mixing, and interaction flow structure that governs the pressure recovery is dependent on the back-pressure level.

The "saturated-supersonic" regime is a limiting case of the "supersonic" regime. The ejector conditions are such that the secondary flow reaches sonic flow conditions at the geometric minimum area at the confluence of the primary and secondary flows (Section 1). Again, the mass flowrate characteristics of the ejector are independent of the back-pressure conditions while the recompression flow process is not.

The "mixed" regime includes all ejector operating conditions for which the secondary mass flowrate is dependent on the back-pressure level. This dependency is the result of the secondary flow not attaining sonic flow conditions at either the confluence of the streams or within the downstream interaction region. Consequently, both the secondary mass flowrate and the ejector recompression process are dependent on the back-pressure level.

The criteria for determining the "break-off" conditions are derived from the requirement that a continuous transition between the "supersonic" or "saturated-supersonic" regimes and the "mixed" regime must exist. These criteria and the determination of the "break-off" conditions are important factors in analyzing and understanding ejector operation.

The constant-area ejector has been analyzed by a detailed interaction model [1,5] which has been generalized to include variable-area mixing section ejectors [6]. While the operational characteristics predicted with this model are in good agreement with experiment, the computational time requirements and complexities eliminate this technique as an effective method for making broad-band parametric studies of ejector operation. As a consequence, the study herein is restricted to the constant-area ejector which exhibits all of the operational characteristics of more complex geometries but yet can still be analyzed by simplified one-dimensional methods. The one-dimensional analysis provides results that are generally in good agreement with experiment except at small secondary flowrates when $P_{s1} < P_{p1}$. The reason for this breakdown in the flow model is well-known [1,5]; essentially, the reason is that the flowfield shifts from being one-dimensional in nature to a flowfield that is two-dimensional in nature. This change in flowfield character is the direct

1012

result of the expanding supersonic primary flow interacting with the mix-
ing-section wall. Thus, the one-dimensional analysis would be expected
to yield poor results for this flow regime. This deficiency in the flow
model should not cause significant problems as long as there is an aware-
ness of the existence and causes of the problem.

The components of the constant-area ejector model, their analyses,
and the computational approach will now be discussed.

2.3.1 Constant-area ejector analysis

The ejector flow model consists of essentially two components.
One component is the overall analysis of the constant-area mixing section,
Sections 1 to 3. The other component is the analysis of the nearly
inviscid interaction region just downstream of the confluence of the pri-
mary and secondary flows. These components are incorporated into an
analysis from which the "break-off" conditions, the mass flowrate char-
acteristics, and the compression characteristics can be determined.

This analysis is based on the work of Fabri, et al., [3,4].

2.3.1.1 One-dimensional overall mixing-section analysis

The control volume used in the overall mixing section
analysis is shown in Fig. 2.3-2. The piecewise uniform primary and
secondary flows at Section 1 are assumed to interact and to mix within
the mixing section to form a uniform mixed flow at Section 3. As a con-
sequence of the existence of the "mixed" and "supersonic" or "saturated-
supersonic" regimes, the application of the conservation relations to
this control volume does not, in general, result in a unique solution for
the flow in the mixing section. As a consequence, additional conditions
must be imposed to find a unique solution for the "supersonic" and

1013
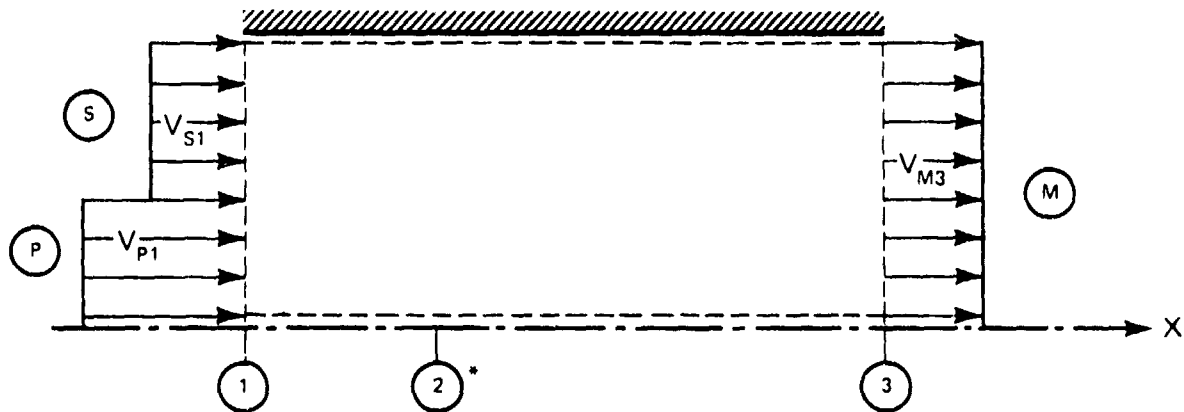
--- Control volume

P, ρ, A, V, T, M, etc. are defined for each stream
at sections 1 and 3.

* If "choking" exists

Figure 2.3-2   Constant-area mixing section control volume

"saturated-supersonic" regimes since the secondary mass flowrate charac-
teristics are independent of the back-pressure level at Section 3 for
these regimes. The additional conditions required for a unique solution
are provided by the secondary flow choking phenomenon which is the result
of the interaction of the primary and secondary flows downstream of their
confluence. No additional conditions are required for the "mixed" regime
other than satisfying the boundary condition at the ejector exit plane
that the exit-plane pressure is equal to the ambient pressure level.
The transition between these regimes defines the "break-off" conditions,
i.e., the conditions for which a unique solution can be found that
simultaneously satisfies the "supersonic" or "saturated-supersonic"
regimes and the "mixed" regime.

The analysis of the overall mixing section is based on the applica-
tion of the conservation equations and the following assumptions to the
control volume of Fig. 2.3-2. The assumptions are:

(1) Steady flow, $\frac{\partial(\ )}{\partial t} \equiv 0$.

(2) Piecewise uniform flows at Section 1 and uniform flow at
    Section 3.

(3) The primary and secondary gases obey the perfect gas
    relationships.

(4) The primary and secondary streams mix ideally to form a
    mixed stream at Section 3.

(5) Negligible shear stresses at the wall.

(6) Adiabatic flow between Sections 1 and 3.

(7) No shaft or shear work between Sections 1 and 3.

1015

(8) A negligible change in potential energy due to variations in elevation in the mixing section.

(9) The primary and secondary flows are assumed to be isentropic from their respective stagnation states to the states at Section 1.

The continuity equation is

$$\oint_{cs} \rho \overline{V} \cdot d\overline{A} = 0 \qquad (2.3\text{-}1)$$

and with assumption (2) becomes

$$\rho_{P1} V_{P1} A_{P1} + \rho_{S1} V_{S1} A_{S1} = \rho_{M3} V_{M3} A_{M3} \qquad . \qquad (2.3\text{-}2)$$

In terms of the mass flowrates, $w = \rho AV$, the continuity equation is

$$w_S + w_P = w_M \qquad . \qquad (2.3\text{-}3)$$

The mass flowrate, $w$, is expressed in terms of the mass flow function by

$$\frac{w}{PA} \left[ \frac{R}{Mw} \cdot T_0 \right]^{1/2} = M \left[ \gamma \left\{ 1 + \frac{(\gamma-1)}{2} M^2 \right\} \right]^{1/2} \equiv f_1(\gamma, M) \qquad . \qquad (2.3\text{-}4)$$

Introducing the secondary-to-primary mass flowrate ratio, $\mu \equiv w_S / w_P$, and Eq. (2.3-4) into Eq. (2.3-3) results in an expression for the static pressure ratio $P_{M3}/P_{P1}$. The result is

$$\frac{P_{M3}}{P_{P1}} = \left[ \frac{Mw_P}{Mw_M} \cdot \frac{T_{M0}}{T_{P0}} \right]^{1/2} \left[ \frac{A_{P1}}{A_{M3}} \right] \frac{f_1(\gamma_P, M_{P1})}{f_1(\gamma_M, M_{M3})} (1+\mu) \qquad (2.3\text{-}5)$$

In terms of the mass flow function, the mass flowrate ratio, $\mu$, is

$$\mu = \frac{P_{S1}}{P_{P1}} \cdot \frac{A_{S1}}{A_{P1}} \left[ \frac{Mw_S}{Mw_P} \cdot \frac{T_{P0}}{T_{S0}} \right]^{1/2} \frac{f_1(\gamma_S, M_{S1})}{f_1(\gamma_P, M_{P1})} \qquad . \qquad (2.3\text{-}6)$$

The static pressure ratio, $P_{S1}/P_{P1}$, can be expressed from Eq. (2.3-6) as

1016

$$\frac{P_{S1}}{P_{P1}} = \frac{A_{P1}}{A_{S1}} \left[\frac{Mw_P}{Mw_S} \cdot \frac{T_{S0}}{T_{P0}}\right]^{1/2} \frac{f_1(\gamma_P, M_{P1})}{f_1(\gamma_S, M_{S1})} \mu \qquad . \tag{2.3-7}$$

The momentum equation in the flow direction is

$$\mapsto \sum F_x = \oint_{CS} V_x (\rho \overline{V} \cdot d\overline{A}) \qquad . \tag{2.3-8}$$

With the foregoing assumptions, the momentum equation becomes

$$P_{P1}A_{P1} + P_{S1}A_{S1} - P_{M3}A_{M3} = \rho_{M3}A_{M3}V_{M3}^2 - (\rho_{P1}A_{P1}V_{P1}^2 + \rho_{S1}A_{S1}V_{S1}^2) \qquad . \tag{2.3-9}$$

Equation (2.3-9) can be expressed in a more convenient form by

$$\frac{P_{S1}}{P_{P1}} \cdot \frac{A_{S1}}{A_{P1}} \left(1 + \gamma_S M_{S1}^2\right) + \left(1 + \gamma_P M_{P1}^2\right) = \frac{P_{M3}}{P_{P1}} \cdot \frac{A_{M3}}{A_{P1}} \left(1 + \gamma_M M_{M3}^2\right) \tag{2.3-10}$$

Equations (2.3-5). (2.3-7), and (2.3-10) can be combined and rearranged into a form that is particularly convenient for computation; the result is

$$f_3(\gamma_M, M_{M3}) = \frac{f_3(\gamma_P, M_{P1}) + f_3(\gamma_S, M_{S1})\left[\frac{Mw_P}{Mw_S} \cdot \frac{T_{S0}}{T_{P0}}\right]^{1/2} \mu}{\left[\frac{Mw_P}{Mw_M} \cdot \frac{T_{M0}}{T_{P0}}\right]^{1/2} (1+\mu)} \tag{2.3-11}$$

where the function $f_3(\gamma, M)$ is defined as

$$f_3(\gamma, M) = \frac{(1 + \gamma M^2)}{M\left[\gamma\{1 + \frac{\gamma-1}{2} M^2\}\right]^{1/2}} \tag{2.3-12}$$

The relationship, $f_3(\gamma, M) = $ constant, can be solved for the Mach number, M, as

$$M = \left\{ \frac{-\left[f_3^2 - 2\right] \pm \left[\left[f_3^2 - 2\right]^2 + 2\left(\frac{\gamma-1}{\gamma}\right)\left(f_3^2 - \frac{2\gamma}{(\gamma-1)}\right)\right]^{1/2}}{(\gamma-1)\left[f_3^2 - \frac{2\gamma}{(\gamma-1)}\right]} \right\}^{1/2} \tag{2.3-13}$$

The energy equation is

$$\frac{\partial Q}{\partial t} - \frac{DW_{ss}}{Dt} = \oint_{cs} \left[ h + \frac{V^2}{2} + gZ \right] (\rho \overline{V} \cdot d\overline{A}) \quad . \tag{2.3-14}$$

With simplifying assumptions (6,7,8), the energy equation becomes

$$\oint_{cs} h_0 (\rho \overline{V} \cdot d\overline{A}) = 0 \tag{2.3-15}$$

where $h_0 = h + V^2/2$. For the overall mixing section control volume, the energy equation becomes

$$w_P h_{P0} + w_S h_{S0} = w_M h_{M0} \quad . \tag{2.3-16}$$

The continuity and energy equations can be combined along with $h_0 = C_P T_0$ and $\mu = w_S/w_P$ to develop an expression for the mixed-to-primary stagnation temperature ratio. The result is

$$\frac{T_{M0}}{T_{P0}} = \frac{1}{(1+\mu)} \left[ \frac{(C_P)_P}{(C_P)_M} \right] \left[ 1 + \mu \frac{(C_P)_S}{(C_P)_P} \cdot \frac{T_{S0}}{T_{P0}} \right] \quad . \tag{2.3-17}$$

The secondary-to-primary stagnation pressure ratio can be expressed by

$$\frac{P_{S0}}{P_{P0}} = \frac{P_{S1}}{P_{P1}} \cdot \frac{(P_{P1}/P_{P0})}{(P_{S1}/P_{S0})} \tag{2.3-18}$$

where the pressure ratios $P_{P1}/P_{P0}$ and $P_{S1}/P_{S0}$ are by assumption (9) determined for isentropic flow. For isentropic flow, the pressure ratio function is defined by

$$\frac{P}{P_0} (\gamma, M) = \left[ 1 + \frac{\gamma-1}{2} M^2 \right]^{-\gamma/(\gamma-1)} \equiv f_2(\gamma, M) \quad . \tag{2.3-19}$$

Thus, Eq. (2.3-18) becomes

$$\frac{P_{S0}}{P_{P0}} = \frac{P_{S1}}{P_{P1}} \cdot \frac{f_2(\gamma_P, M_{P1})}{f_2(\gamma_S, M_{S1})} \quad . \tag{2.3-20}$$

In the preceding equations, the gas properties of the mixed flow at Section 3 must be known. These properties are determined for the mixed gas by applying Dalton's law of partial pressures to a hypothetical mixing process at constant volume for the respective mass fractions of the primary and secondary perfect gases. The mixed gas properties are expressed in terms of the secondary-to-primary mass flowrate ratio and the primary and secondary gas properties by

$$\frac{(C_P)_P}{(C_P)_M} = \frac{(1+\mu)}{\left[1 + \mu \frac{(C_P)_S}{(C_P)_P}\right]} \quad , \tag{2.3-21}$$

$$\frac{Mw_M}{Mw_P} = \frac{(1+\mu)}{\left[1 + \mu \frac{Mw_P}{Mw_S}\right]} \quad , \tag{2.3-22}$$

and

$$\gamma_M = \left( 1 - \{\frac{\gamma_P - 1}{\gamma_P}\} \frac{\{1 + \mu \frac{Mw_P}{Mw_S}\}}{\{1 + \mu \frac{\gamma_S}{\gamma_P} \frac{(\gamma_P - 1)}{(\gamma_S - 1)} \frac{Mw_P}{Mw_S}\}} \right)^{-1} \quad . \tag{2.3-23}$$

The ratio of specific heats at constant pressure can be expressed in terms of other properties by

$$\frac{(C_P)_S}{(C_P)_P} = \frac{\gamma_S}{\gamma_P} \cdot \frac{(\gamma_P - 1)}{(\gamma_S - 1)} \cdot \frac{Mw_P}{Mw_S} \quad . \tag{2.3-24}$$

1019

Equations (2.3-21) to (2.3-24) define the mixed gas properties completely in terms of the properties of the primary and secondary gases and the mass flowrate ratio, $\mu$.

The computational procedure adopted herein will now be discussed. At the outset, the following data are assumed to be known

$$\left[ \gamma_S, \ \gamma_P, \ \frac{Mw_S}{Mw_P}, \ \frac{T_{S0}}{T_{P0}}, \ \frac{A_{M3}}{A_{P1}}, \ M_{P1} > 1 \right] \quad .$$

If the primary nozzle base area is assumed to be negligible, the constant-area mixing section requirement is

$$\frac{A_{S1}}{A_{P1}} = \left( \frac{A_{M3}}{A_{P1}} - 1 \right) \quad . \tag{2.3-25}$$

Using these data and a parametric value of $\mu$, the mixed gas properties at Section 3 can be determined from Eqs. (2.3-21) to (2.3-23); the results are

$$\left[ \frac{(C_P)_P}{(C_P)_M}, \ \frac{Mw_M}{Mw_P}, \ \gamma_M \right] \quad .$$

The mixed-to-primary flow stagnation temperature ratio, $T_{M0}/T_{P0}$, can then be found from Eq. (2.3-17)

An examination of Eqs. (2.3-5), (2.3-7), and (2.3-11) shows that the following variables are still to be determined; they are

$$\left[ M_{S1} \leq 1, \ \frac{P_{S1}}{P_{P1}}, \ M_{M3}, \ \frac{P_{M3}}{P_{P1}} \right] \quad .$$

Thus, this set of equations must be supplemented, as discussed in the foregoing sections, with an additional relationship before unique ejector solutions can be determined. The needed relationship is between the

1020

variables $M_{S1}$ and $P_{S1}/P_{P1}$ for a parametric value of $\mu$. The form of this relationship, as will be discussed in the following sections, is determined by the operating regime.

Thus, with the aforementioned input data, a parametric value of $\mu$, and a presumed relationship between ($M_{S1}$, $P_{S1}/P_{P1}$), all values at Section 3 can be determined by the foregoing analysis.

The subroutine, CAEOCV(...), has been written, based on the foregoing analysis for the overall control volume, to carry out the computations as just described. The subroutine has the form

CAEOCV (GP, MP1, GS, MS1, MWSP, TSØPØ, PS1P1, AP1M3, NERROR,
        MM3, PPØSØ, PM3SØ, PMØSØ).

For input values of (GP, MP1, GS, MS1, MWSP, TSØPØ, PS1P1, AP1M3), the subroutine either returns a set of solution values for (MM3, PM3SØ, PM3S1, PPØSØ, PMØSØ) or a no-solution error indicator NERROR.

A listing of this subroutine is included in Appendix 6.2.

### 2.3.1.2 Ejector flow regimes and their criteria

The relationship between the static pressures, $P_{S1}$ and $P_{P1}$, determines the operating regime of an ejector.

If $P_{S1} \geq P_{P1}$, the ejector operates in either the "saturated-supersonic" or the "mixed" regime because (1) the minimum secondary flow area is equal to the geometric secondary flow area at Section 1, and (2) the secondary flow is subsonic upstream of Section 1 thus limiting $M_{S1}$ to the range, $0 < M_{S1} \leq 1$. For the "saturated-supersonic" regime, the secondary flow is sonic at Section 1, $M_{S1} = 1$, and the secondary mass flowrate is determined solely by the upstream conditions. For the "mixed"

1021

regime, the secondary flow at Section 1 is subsonic, $M_{S1} < 1$, and the secondary mass flowrate is dependent on both the upstream and downstream conditions.

If $P_{S1} < P_{P1}$, the ejector operates in either the "supersonic" or the "mixed" regime. In both regimes, the primary flow expands and interacts with the secondary flow to form a minimum secondary flow area, i.e., an "aerodynamic" throat, in the primary-secondary interaction region, Section 2, Figs. 2.3-2, 2.3-3. Since the secondary flow is subsonic upstream of this minimum-area location, specifically $M_{S1} < 1$, the secondary flow Mach number at the minimum-area location is limited to $M_{S2} \leq 1$. For the "supersonic" regime, the secondary flow is sonic at the minimum-area location, $M_{S2} = 1$, and the secondary mass flowrate is determined solely by the conditions at and upstream of the minimum-area location. For the "mixed" regime, the secondary flow is subsonic at the minimum-area location, $M_{S2} < 1$, and the secondary mass flowrate is dependent on both the conditions upstream and downstream of the minimum-area location.

The determination of the break-off conditions for transition from one operating regime to another is an important consideration in the analysis of an ejector system. The possible transitions are between:

(1) The "saturated-supersonic" and "supersonic" regimes,

(2) The "saturated-supersonic" and "mixed" regimes, and

(3) The "supersonic" and "mixed" regimes.

The criteria for determining each transition are based on the relationship between the pressures, $P_{S1}$ and $P_{P1}$, and the Mach number at the minimum flow area, either Section 1 or 2 as the case may be. If the Mach number

1022
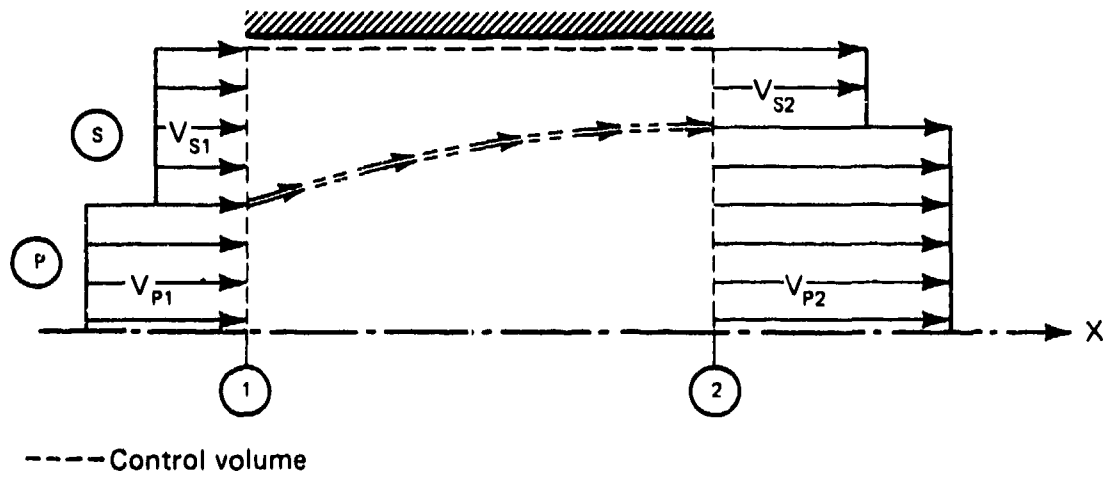
Figure 2.3-3  Control volume for Fabri "choking" analysis

1023

at the minimum flow area is unity, the ejector operates in either the "saturated-supersonic" or the "supersonic" regime; while if this Mach number is less than unity, the ejector operates in the "mixed" regime.

The break-off conditions for transition between the various regimes must satisfy the following conditions. They are:

(1) For the juncture of the "saturated-supersonic" and "supersonic" regimes: $(M_{S1})_{BO} = 1$ and $(P_{S1}/P_{P1})_{BO} = 1$;

(2) For the "saturated-supersonic" and "mixed" regimes:
$(M_{S1})_{BO} = 1$ and $(P_{S1}/P_{P1})_{BO} \geq 1$; and

(3) For the "supersonic" and "mixed" regimes: $(M_{S1})_{BO} < 1$,
$(P_{S1}/P_{P1})_{BO} \leq 1$, and $(M_{S2})_{BO} = 1$.

For case (3), the transition requirements are special since the value of $(M_{S1})_{BO} < 1$ must be determined based on the requirements that $(P_{S1}/P_{P1})_{BO} < 1$ and $(M_{S2})_{BO} = 1$. The flow model and analysis due to Fabri, et al. [3,4], for analyzing the "supersonic" regime will now be discussed.

The control volume for this analysis extends between Sections 1 and 2, Fig. 2.3-3. In addition to the assumptions listed in Section 2.3.1.1, the following additional assumptions are made:

(1) The streams remain distinct and do not mix between Sections 1 and 2.

(2) The flow is isentropic for each stream between Sections 1 and 2.

(3) The average pressures of the streams can be different at each cross-section.

1024

(4) The Mach number of the secondary flow at Section 2 is $M_{S2} = 1$.

(5) The static pressures at the mixing tube inlet are such that $P_{P1} > P_{S1}$.

For an assumed value of $M_{S1}$, and since $M_{S2} = 1$, the secondary flow area at Section 2 can be expressed in terms of the secondary flow area at Section 1 by the isentropic area-ratio function

$$\frac{A_{S1}}{A_{S2}} = \frac{A}{A^\star} (\gamma_S, M_{S1}) = f_4 (\gamma_S, M_{S1}) \qquad (2.3\text{-}26)$$

where

$$\frac{A}{A^\star} (\gamma, M) = M^{-1} \left[ \frac{2}{(\gamma+1)} \cdot \left\{ 1 + \frac{\gamma-1}{2} M^2 \right\} \right]^{(\gamma+1)/2(\gamma-1)} \qquad (2.3\text{-}27)$$

The primary flow Mach number $M_{P2}$ is determined from the available flow area at Section 2 and the assumption of isentropic flow between Sections 1 and 2. Since $A_{MS} = (A_{S1} + A_{P1}) = (A_{S2} + A_{P2}) = $ constant, the isentropic area-ratio function to be solved for $M_{P2}$ is

$$\frac{A}{A^\star} (\gamma_P, M_{P2}) = f_4 (\gamma_P, M_{P2}) = \frac{\left[ 1 - \frac{(1 - A_{P1}/A_{MS})}{(A_{S1}/A_{S2})} \right]}{(A_{P1}/A_{MS})} \cdot \frac{A}{A^\star} (\gamma_P, M_{P1}) \quad (2.3\text{-}28)$$

where $f_4 (\gamma_P, M_{P2}) \geq 1$ is necessary and the supersonic branch of the A/A* function is used.

The momentum equation for this flow and the control volume shown in Fig. 2.3-3 is

$$P_{S1} A_{S1} (1 + \gamma_S M_{S1}^2) + P_{P1} A_{P1} (1 + \gamma_P M_{P1}^2) = P_{S2} A_{S2} (1 + \gamma_S) + P_{P2} A_{P2} (1 + \gamma_P M_{P2}^2) \qquad .$$

$$(2.3\text{-}29)$$

1025

This expression can be rearranged into a more convenient form to determine $P_{S1}/P_{P1}$; the relationship is

$$\frac{P_{S1}}{P_{P1}} = \frac{\left[\frac{(P_{P2}/P_{P0})}{(P_{P1}/P_{P0})} \cdot \frac{(A_{P2}/A_P^*)}{(A_{P1}/A_P^*)}\left(1+\gamma_P M_{P2}^2\right) - \left(1+\gamma_P M_{P1}^2\right)\right]}{\left[\frac{1-(A_{P1}/A_{M3})}{A_{P1}/A_{M3}}\right]\left[\left(1+\gamma_S M_{S1}^2\right) - \frac{(P_{S2}/P_{S0})}{(P_{S1}/P_{S0})} \cdot \frac{(1+\gamma_S)}{(A_{S1}/A_S^*)}\right]} \qquad (2.3\text{-}30)$$

In Eq. (2.3-30), the functions $(P_{P2}/P_{P0}, P_{P1}/P_{P0}, P_{S2}/P_{S0}, P_{S1}/P_{S0})$ and $(A_{P1}/A_P^*, A_{P2}/A_P^*, A_{S1}/A_S^*)$ are determined from the isentropic pressure-ratio and area-ratio functions, Eqs. (2.3-19) and (2.3-27), respectively.

Thus, for the "supersonic" regime, a value of $P_{S1}/P_{P1}$ can be determined for an assumed value of $M_{S1}$ and given values of $(\gamma_S, \gamma_P, M_{P1}, A_{P1}/A_{M3})$. This then provides the necessary additional relationship between the variables to determine the "supersonic" ejector operating characteristics and the transition between the "supersonic" and "mixed" regimes.

A computer subroutine, CAEFC(...), has been written based on the foregoing analysis of the Fabri criterion for "choking" in a constant-area ejector. This subroutine has the form

CAEFC(GP, MP1, GS, MS1, AP1M3, PS1P1, NERROR, NTYPE)

where for input values of (GP, MP1>1, GS, MS1<1, AP1M3) the subroutine will return a value of PS1P1 and a value of the iteration control variable NTYPE or an error indicator NERROR.

A listing of this subroutine is included in Appendix 6.2.

Assume for the moment that the break-off values are known for each of the three transition cases; then with the analysis of Section 2.3.1.1, the break-off values at Section 3, i.e., $\{(M_{M3})_{BO}, (P_{M3}/P_{P1})_{BO}, \text{etc.})\}$ can

1026

be determined for each case. Thus, ranges of these variables can be determined for operation within the various ejector operating regimes.

For the actual operation of an ejector, the operating regime is determined by the relationship between the externally imposed pressure boundary condition, $P_{ATM}$, at Section 3 and the break-off values. The usual operation of an ejector is with $M_{M3} < 1$ and thus $P_{M3} = P_{ATM}$ required. Consequently, the ejector operating regime is determined by the relationship between $P_{ATM}$ and the break-off values $(P_{M3})_{BU}$.

### 2.3.1.3 Computational procedure

As is the case in many compressible flow problems, it is more convenient to establish the overall operating characteristics of the ejector rather than to determine the operating characteristics for a specific set of conditions. This is the approach taken herein.

The operational characteristics of the constant-area ejector are investigated and presented in terms of the variables $(\mu, P_{P0}/P_{S0}, P_{M3}/P_{S0})^{\dagger}$. For given values of $(\gamma_S, \gamma_P, Mw_S/Mw_P, A_{P1}/A_{M3}, T_{S0}/T_{P0}, M_{P1} > 1)$, the mass flowrate ratio, $\mu = $ constant, is specified parametrically and the range and solution values of $(P_{P0}/P_{S0}, P_{M3}/P_{S0})$ are to be determined.

The first step in this procedure is to determine, for the parametric value of $\mu$, whether the ejector would operate in the "saturated-supersonic" or "supersonic" regime for a very low back pressure. This determination is made in the following way. At the juncture between the "saturated-supersonic" and "supersonic" regimes, $(M_{S1})_{B0} = 1$ and

---

$\dagger$Note that this choice of variables is somewhat different than those used in Section 2.1.

1027

$(P_{S1}/P_{P1})_{BO} = 1$. For these conditions, the value of $\mu$ at the juncture of these regimes, $\mu_J$, is calculated from Eq. (2.3-6). If $\mu > \mu_J$, then the ejector would operate in the "saturated-supersonic" regime and the break-off would be between the "saturated-supersonic" and "mixed" regimes. However, if $\mu < \mu_J$, then the ejector would operate in the "supersonic" regime and the break-off would be between the "supersonic" and "mixed" regimes.

For the "saturated-supersonic" regime, $\{(M_{S1})_{BO} = 1, (P_{S1}/P_{P1}) \geq 1\}$, the corresponding break-off values of $(P_{M3}/P_{S0})_{BO}$ and $(P_{P0}/P_{S0})_{BO}$ are determined from the analysis presented in Section 2.3.1.1. The remainder of the ejector operating characteristics in the "mixed" regime are determined by arbitrarily varying $M_{S1}$ in the range $(M_{S1})_{Min} < M_{S1} < 1$ and then determining the flow conditions at Section 3 for this flow to exist. For an assumed value of $M_{S1}$ in this range, the value of $P_{S1}/P_{P1}$ is determined for the parametric value of $\mu$ from Eq. (2.3-7); the lower limit for $M_{S1}$ in this analysis is set by arbitrarily limiting $P_{S1}/P_{P1}$ to the range

$$(P_{S1}/P_{P1})_{BO} < P_{S1}/P_{P1} < (P_{S1}/P_{P1})_{MAX}$$

where $(P_{S1}/P_{P1})_{MAX}$ is the static-pressure ratio at which a normal shock wave would stand at the nozzle exit plane, i.e.,

$$\left(\frac{P_{S1}}{P_{P1}}\right)_{MAX} = \frac{P_Y}{P_X}\,(\gamma_P, M_{P1}) = f_5(\gamma_P, M_{P1}) \quad . \tag{2.3-31}$$

The values of the variables $(P_{M3}/P_{S0}, P_{P0}/P_{S0})$ for this flow to exist are then determined according to the analysis of Section 2.3.1.1 for the "mixed" regime.

1028

For the "supersonic" regime and the parametric value of $0 < \mu < \mu_J$, the values of $\{(M_{S1})_{BO} < 1, (P_{S1}/P_{P1})_{BO} < 1\}$ must be determined by an iterative procedure. The procedure followed is to assume a value of $(M_{S1})_i$ in the range $0 < (M_{S1})_i < 1$; from Section 2.3.1.2, a value of $(P_{S1}$   can be determined. With these values of $\{(M_{S1})_i, (P_{S1}/P_{P1})_i\}$ $\mu_i$ can be determined from Eq. (2.3-6). The iteration proceeds until a value of $(M_{S1})_i$ is found that satisfies the convergence requirement

$$\varepsilon > \left| 1 - \frac{\mu_i}{\mu} \right| > 0$$

where $\varepsilon$ is nominally taken as $10^{-4}$. This procedure establishes the break-off values of $\{(M_{S1})_{BO}, (P_{S1}/P_{P1})_{BO}\}$ for the "supersonic" regime. The remainder of the break-off values $\{(P_{M3}/P_{SO})_{BO}, (P_{PO}/P_{SO})_{BO}\}$ for the "supersonic" regime are determined according to the analysis of Section 2.3.1.1

The remainder of the ejector operating characteristics in the "mixed" regime are determined by arbitrarily varying $M_{S1}$ in the range $(M_{S1})_{MIN} < M_{S1} < (M_{S1})_{BO}$. For the assumed value of $M_{S1}$ in this range, the value of $P_{S1}/P_{P1} > (P_{S1}/P_{P1})_{BO}$ is determined for the parametric value of $\mu$ from Eq. (2.3-7); again, the lower limit for $M_{S1}$ in this analysis is set by arbitrarily limiting $P_{S1}/P_{P1}$ to the range

$$(P_{S1}/P_{P1})_{BO} < P_{S1}/P_{P1} < \frac{P_Y}{P_X} (\gamma_P, M_{P1}) \quad .$$

For each set of values $(\mu, M_{S1}, P_{S1}/P_{P1})$, the values of the variables $(P_{M3}/P_{SO}, P_{PO}/P_{SO})$ for this flow to exist are then determined according to the analysis of Section 2.3.1.1 for the "mixed" regime.

1029

These analyses have been incorporated into a computer program for convenience of calculation. This program will now be briefly discussed.

2.3.2 Constant-area ejector computer program (CAE)

The constant-area ejector program, CAE(...), is based on the analyses presented in the preceding sections. The program is written in FORTRAN IV and is listed in Appendix 6.2.

The program is organized from the following constant-area ejector (CAE...) and miscellaneous subroutines. They are:

(1) CAE:           Main program.

(2) CAENZF(...):   Non-zero flow ejector characteristics.

(3) CAEOCV(...):   Overall control volume analysis for the mixing section.

(4) CAEFC(...):    Fabri criterion for "choked" flow.

(5) MSAR(...):     $M^* = f(\gamma, A/A^*)$ for isentropic flow.

(6) ITER(...):     Iteration control subroutine.

The input variables and their computer symbols, default values, and input format are given in Table 2.3-1.

The output from CAE can be selected in either of two forms depending on the value of PRINT. For the default value, PRINT = 'ALL', the ejector break-off conditions, operating regime for low back pressure, and operating and compression characteristics are determined for the input values of the system variables and the parametric value of $\mu$, WSPI. Then the operating characteristics are determined within the "mixed" regime at a number of discrete points, or until the maximum value of $P_{S1}/P_{P1}$ is reached. Thus, a cut is made through the ejector operating

1030

| Table 2.3-1 | | |
| --- | --- | --- |
| Input for program CAE | | |
| Variable | Symbol | Default value |
| $\gamma_S$ | GS | 1.405 |
| $\gamma_P$ | GP | 1.405 |
| $Mw_S / Mw_P$ | MWSP | 1.0 |
| $A_{P1} / A_{M3}$ | AP1M3 | $- .. -$[†] |
| $M_{P1}$ | MP1 | $- - -$[†] |
| $T_{SO} / T_{PO}$ | TSØPØ | 1.0 |
| $\mu = w_S / w_P$ | WSPI | $- - -$[†] |
| $- - -$ | CASE | "NEW" |
| $- - -$ | PRINT | "ALL" |

[†]These data values must be input for at least the first case in a series of cases.

Notes: (1) The input format is by NAMELIST: $ICAE ... $END.

(2) See main program comments for CAE, Section 6.2.1.

surface at a value of $\mu$ = constant. In this way, the overall ejector operating characteristics can be established. These data ($\mu$, $P_{PO}/P_{SO}$, $P_{M3}/P_{SO}$), are suitable for three-dimensional graphical presentations or as a step in an iteration procedure to determine a specific ejector operating point for a specified set of conditions.

For the input value, PRINT = 'BO', only the ejector break-off conditions, operating regime for low back pressure, and operating and compression characteristics are determined for the input values of the system variables and the parametric value of $\mu$, WSPI.

1031

The output variables and their computer symbols are summarized in
Table 2.3-2.

| Table 2.3-2 Output for program CAE | |
|---|---|
| Variable | Symbol |
| $M_{S1}$ | MS1 |
| $P_{S1}/P_{P1}$ | PS1P1 |
| $M_{M3}$ | MM3 |
| --- | NCASE |
| $P_{P0}/P_{S0}$ | PPØPSØ |
| $P_{M3}/P_{S0}$ | PM3SØ |
| $P_{M0}/P_{S0}$ | PMØSØ |

Notes: (1) The regimes are identified by: "saturated-supersonic"
regime ≡ SSR; "supersonic" regime ≡ SR; and "mixed"
regime ≡ MR.

(2) The input variables and current values are printed for
each case.

2.3.3 Representative results

To demonstrate typical operating characteristics of a
constant-area ejector, the ejector configuration summarized in
Table 2.3-3 was selected.

The mass flowrate ratio characteristics for the back-pressure inde-
pendent regime are shown in Fig. 2.3-4(a) for $M_{P1}$ = 4.0 and

$A_{P1}/A_{M3} = 0.25$, 0.333 and Fig. 2.3-4(e) for $M_{P1} = 5$ and $A_{P1}/A_{M3} = 0.25$. The compression pressure ratio characteristics are given in Figs. 2.3-4 (b,c,d).

| Table 2.3-3 Representative constant-area ejector configuration | |
|---|---|
| Variable | Value |
| $\gamma_S$ | 1.405 |
| $\gamma_P$ | 1.405 |
| $Mw_S/Mw_P$ | 0.5, 1.0, 2.0 |
| $T_{So}/T_{Po}$ | 1.0 |
| $A_{P1}/A_{M3}$ | 0.25, 0.333 |
| $M_{P1}$ | 4.0, 5.0 |
| $w_P/w_S$ | 2.0-20.0 |

The compression pressure ratio characteristics are a convenient aid in understanding the operational characteristics of an ejector system. Referring to Fig. 2.3-4(b), the lower-left to upper-right band of curves represents the "mixed" regime and forms the break-off curve as the locus of "break-off" points. For any given $w_P/w_S$, the "mixed" regime follows one of these curves up to the "break-off" point where the compression curve becomes a vertical line for either the "SR" or "SSR" corresponding to the value of $w_P/w_S$. The back-pressure independent regimes are on or below the "break-off" curve. The "MR," "SSR," and "SR" are also shown in the figure.

1033
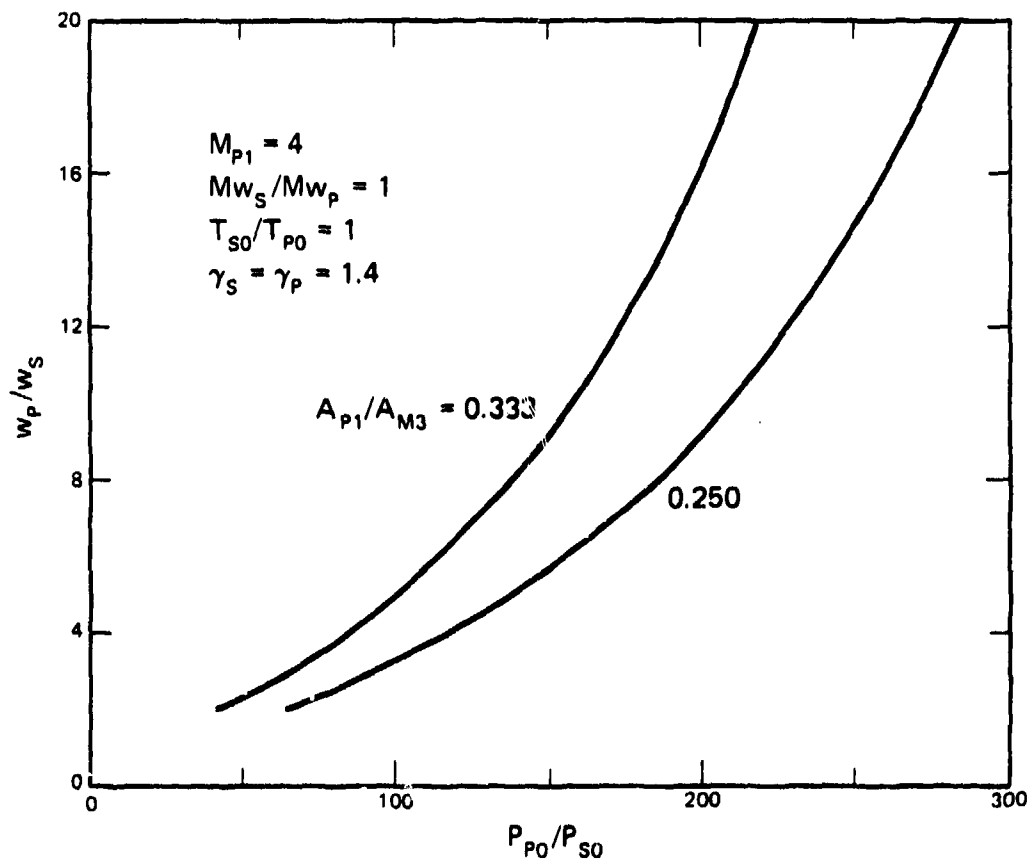
(a) Mass flowrate characteristics

Figure 2.3-4 Constant-area ejector characteristics
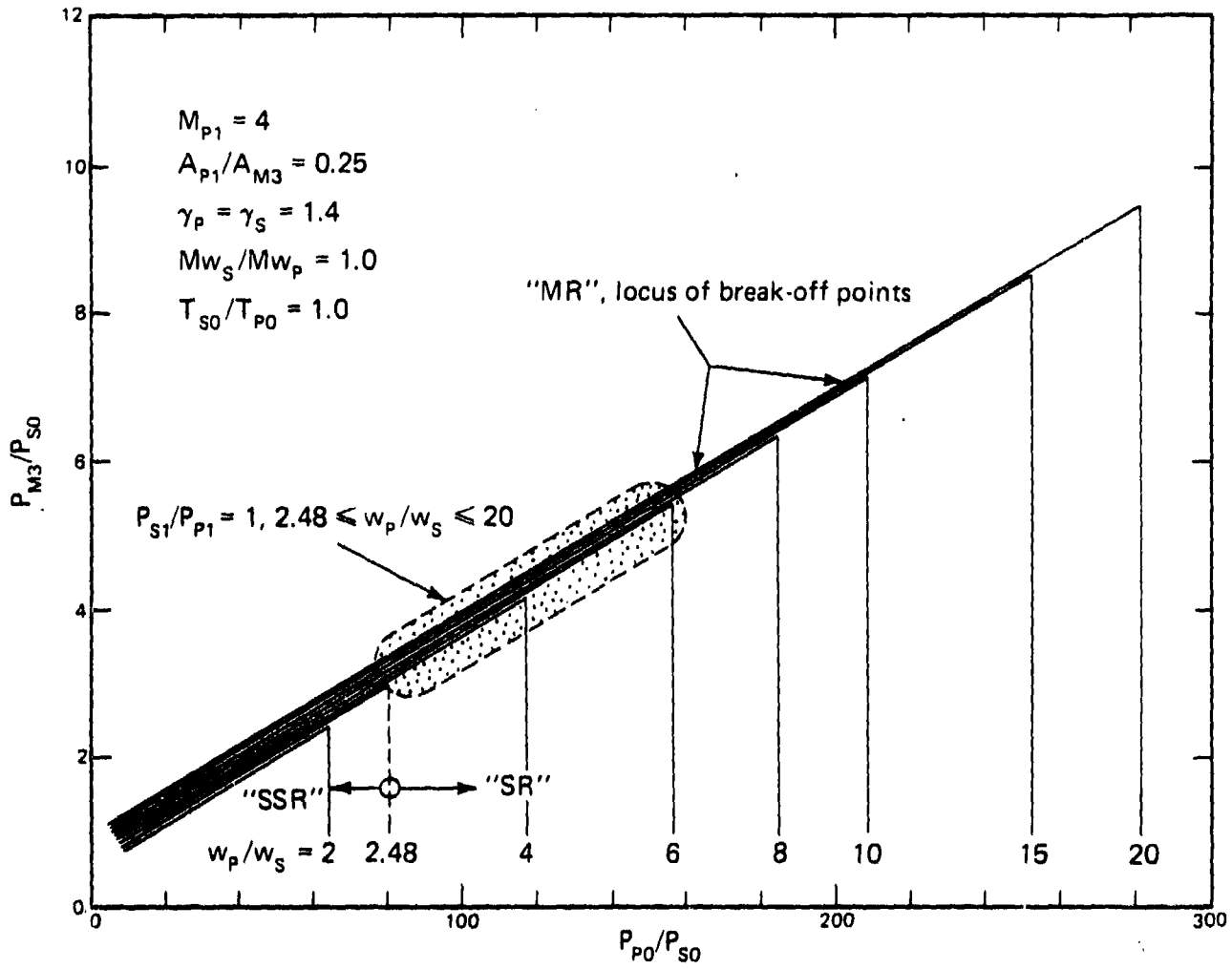
(b) Compression characteristics

Figure 2.3-4 Continued

1035
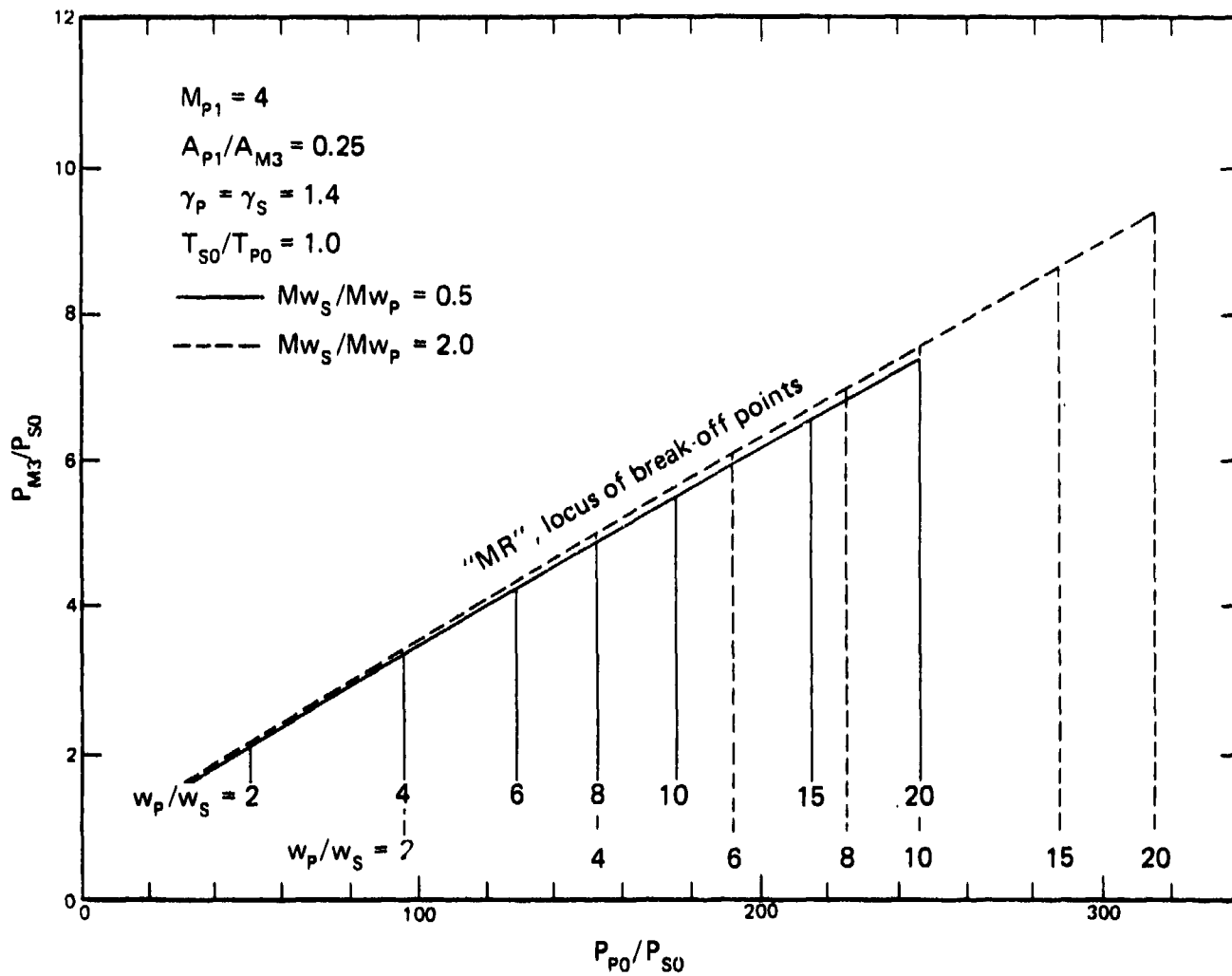
(c)  Compression characteristics for parametric
     variations in $Mw_S/Mw_P$

Figure 2.3-4 Continued

1036
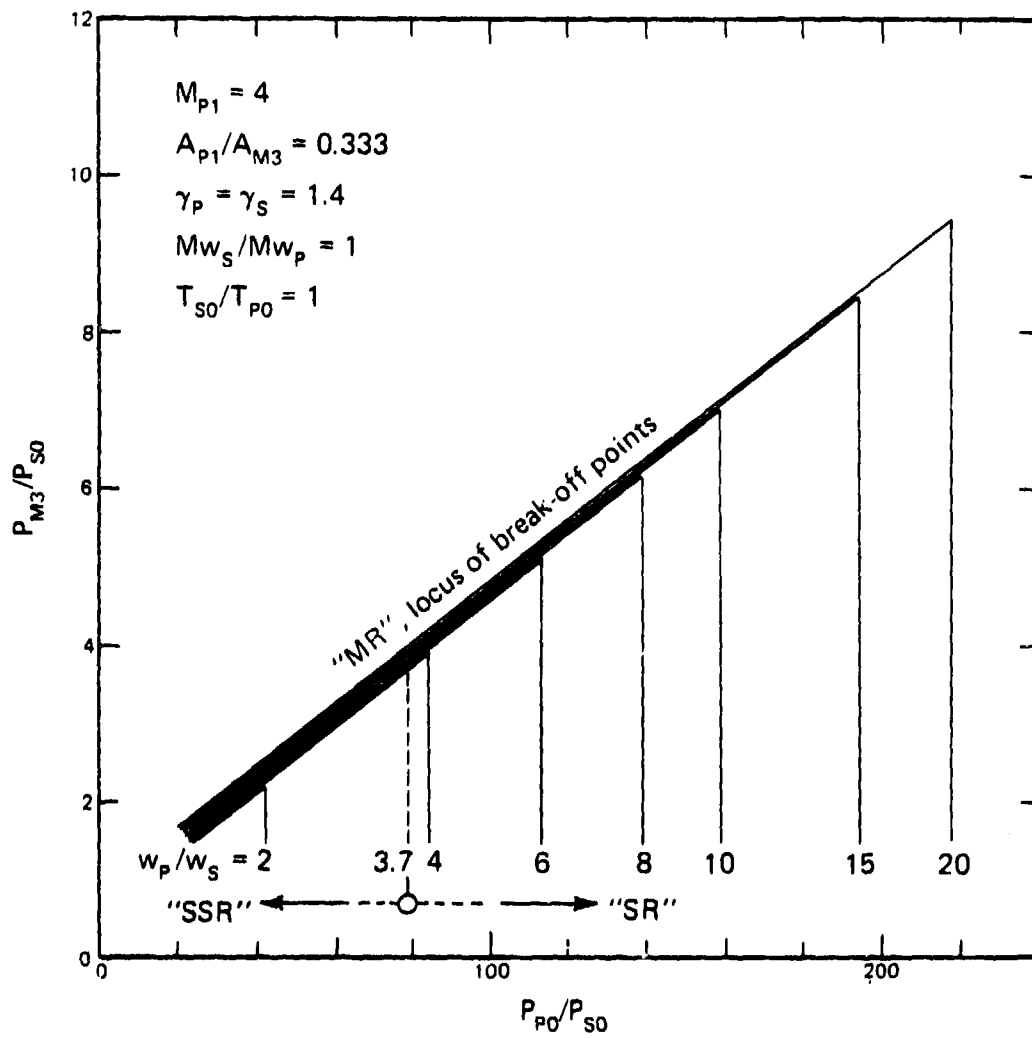
(d) Compression characteristics for a variation in $A_{P1}/A_{M3}$

Figure 2.3-4 Continued

1037
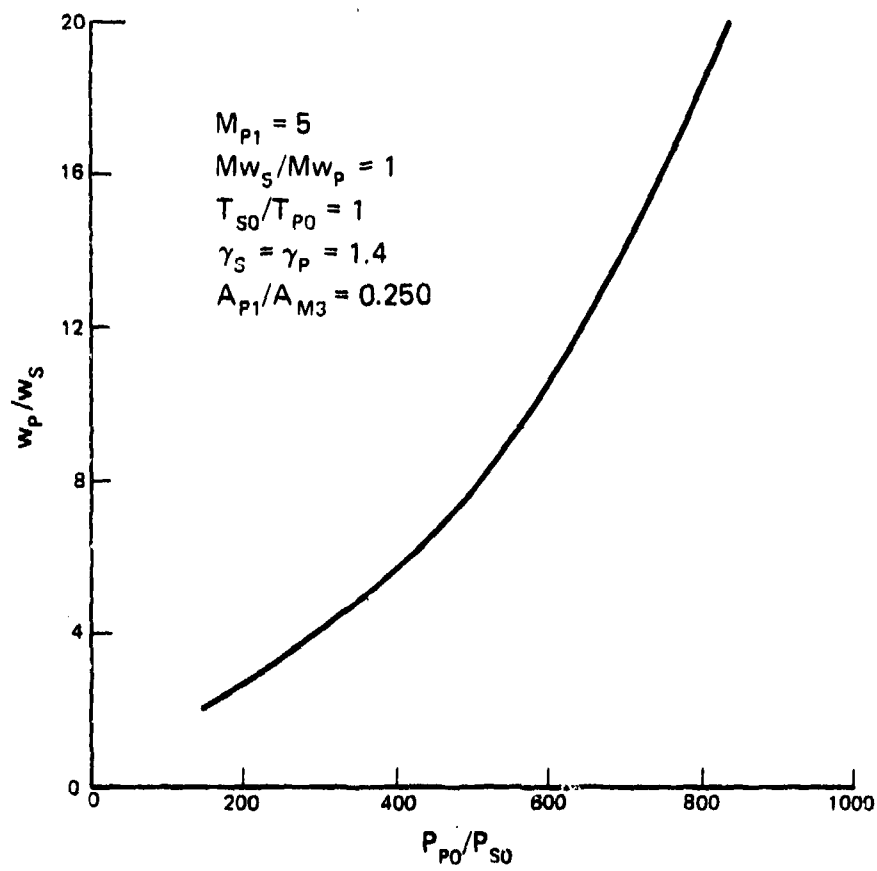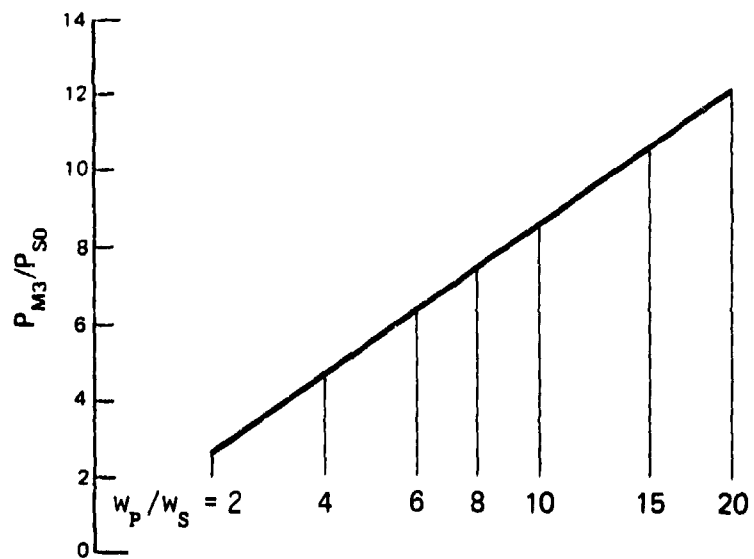
(e)  Mass flow and compression characteristics for
     a variation in $M_{P1}$

Figure 2.3-4  Concluded

1038

Some of the even more simplified analyses of constant area ejectors assume matched static pressures at the confluence of the secondary and primary streams, i.e., $P_{S1} = P_{P1}$. For the configuration analyzed in Fig. 2.3-4(b), the portion of the operating characteristics where this is true is indicated by the dotted band. The range is seen to be rather limited and thus does not present a complete picture of the overall ejector operating characteristics. As a consequence, one must conclude that this assumption is overly restrictive and not that useful.

Figures 2.3-4(c,d,e) show the effects of variations in $Mw_S/Mw_P$, $A_{P1}/A_{M3}$, and $M_{P1}$, respectively, on the compression characteristics of these constant-area ejectors.

## 2.4 STAGED CONSTANT-AREA EJECTOR SYSTEM

When an application requires an ejector system to have an overall compression-pressure ratio greater than 7-10, considerations of optimization, operating pressure levels, mass flowrate ratio, etc., indicate that a multi-staged ejector system should be used. In staged ejector systems. each stage must pump all of the mass flow through the preceding stages unless interstage condensation is used. If interstage condensation is not practical, the size and total primary mass flowrate requirements effectively limit, except in very special cases, the number of ejector stages to two. For purposes of demonstration, a two-stage ejector system based on the constant-area ejector will be discussed.

### 2.4.1 System configuration

A block diagram of a staged ejector system is shown in Fig. 2.4-1. The overall compression ratio and mass flowrate ratio are
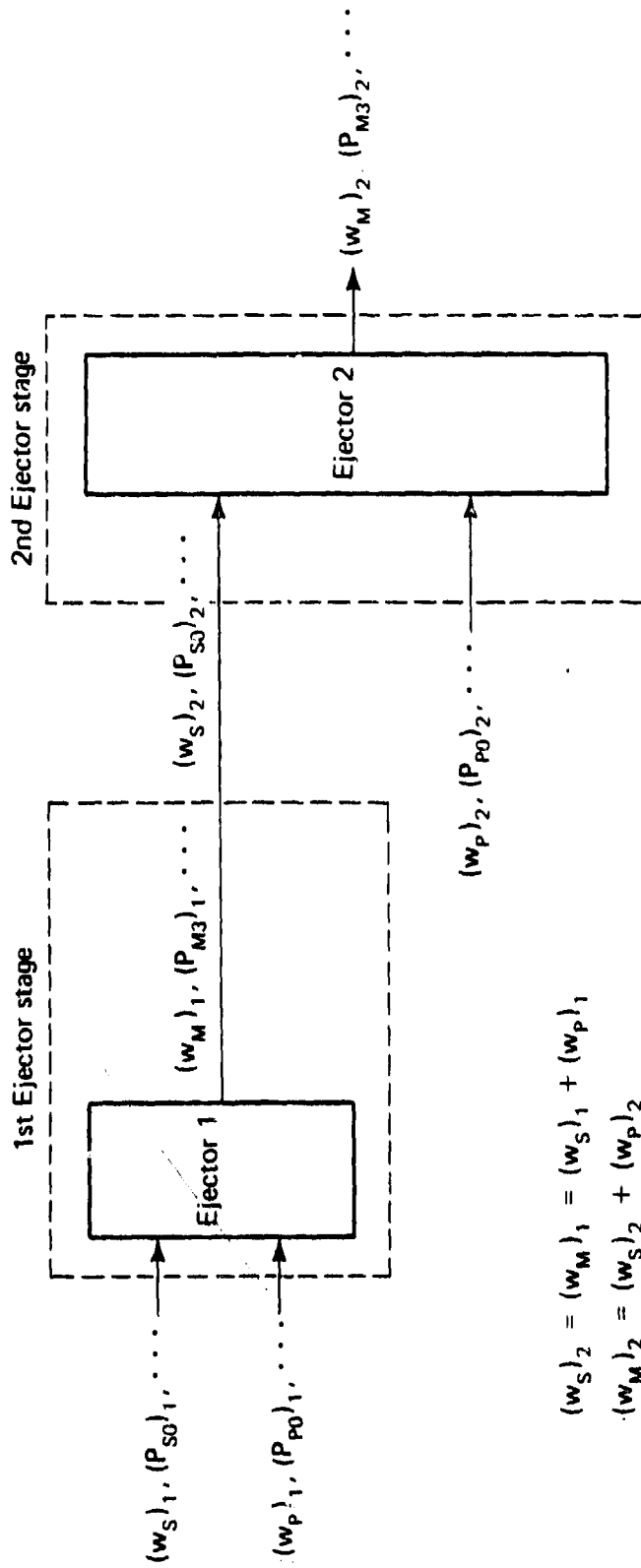
Figure 2.4-1 Staged ejector configuration and notation

The diagram shows a staged ejector configuration:

**1st Ejector stage** contains **Ejector 1** with inputs:
- $(w_S)_1, (P_{S0})_1, \ldots$
- $(w_P)_1, (P_{P0})_1, \ldots$

and output $(w_M)_1, (P_{M3})_1, \ldots$

**2nd Ejector stage** contains **Ejector 2** with inputs:
- $(w_S)_2, (P_{S0})_2, \ldots$
- $(w_P)_2, (P_{P0})_2, \ldots$

and output $(w_M)_2, (P_{M3})_2, \ldots$

$$(w_S)_2 = (w_M)_1 = (w_S)_1 + (w_P)_1$$

$$(w_M)_2 = (w_S)_2 + (w_P)_2$$

of principal concern; for each stage, the primary-to-secondary pressure ratio is also of interest. These system characteristics, referring to Fig. 2.4-1, can be expressed in terms of the individual stages by the following equations.

$$\frac{(w_S)_1}{(w_P)_T} = \frac{(w_S/w_P)_1}{\{1 + [1 + (w_S/w_P)_1]/(w_S/w_P)_2\}} \tag{2.4-1}$$

where $(w_P)_T = (w_P)_1 + (w_P)_2$. The overall compression ratio is

$$\frac{(P_{MS})_2}{(P_{SO})_1} = \left(\frac{P_{MS}}{P_{SO}}\right)_2 \cdot \frac{(P_{SO})_2}{(P_{MS})_1} \cdot \left(\frac{P_{MS}}{P_{SO}}\right)_1 \tag{2.4-2}$$

The pressures, $(P_{SO})_2$ and $(P_{MS})_1$, are related by the diffuser linking the first-stage exit and the second-stage stagnation chamber; for the purposes of this example, a value of 90% of the isentropic pressure rise, $r_d = 0.90$, will be assumed. That is,

$$\frac{(P_{SO})_2}{(P_{MS})_1} = r_d \left(\frac{P_{MO}}{P_{MS}}\right)_1 \tag{2.4-3}$$

The individual stage operating pressure ratios are $(P_{PO}/P_{SO})_1$ and $(P_{PO}/P_{SO})_2$; the second-stage pressure ratio can be expressed in terms of the first-stage pressure ratio by

$$\frac{(P_{PO})_2}{(P_{SO})_1} = \left(\frac{P_{PO}}{P_{SO}}\right)_2 \cdot r_d \left(\frac{P_{MO}}{P_{MS}}\right)_1 \cdot \left(\frac{P_{MS}}{P_{SO}}\right)_1 \tag{2.4-4}$$

The next step in the process is to select the operating points of the ejector stages. Loth [7,8] has discussed optimization of staged ejector systems; a relative optimum can be achieved by operating each stage at the same compression ratio and at its break-off point for the given compression ratio. With this stipulation, the individual-stage compression ratio, from Eqs. (2.4-2) and (2.4-3),

1041

$$\left(\frac{P_{M3}}{P_{so}}\right)_{1,2} = \left[\frac{(P_{M3})_2/(P_{so})_1}{r_d\,(P_{M0}/P_{M3})_1}\right]^{1/2} \quad . \tag{2.4-5}$$

For this example, the specifications for each stage are identical in non-dimensional form. These specifications are summarized in Table 2.4-1; also, note that an overall compression ratio of 7.6 was assumed for this system.

| Table 2.4-1 Ejector specifications | |
|---|---|
| Variable | Value |
| $(\gamma_s)_{1,2}$ | 1.405 |
| $(\gamma_p)_{1,2}$ | 1.405 |
| $(Mw_s/Mw_p)_{1,2}$ | 1.0 |
| $(T_{so}/T_{po})_{1,2}$ | 1.0 |
| $(A_{P1}/A_{M3})_{1,2}$ | 0.25 |
| $(P_{M3})_2/(P_{so})_1$ | 7.6 |
| $(M_{P1})_{1,2}$ | 4.0 |

Using program CAE, the individual stage compression ratio is found from Eq. (2.4-5) to be approximately

$$\left(\frac{P_{M3}}{P_{so}}\right)_{1,2} = 2.68 \;;$$

the remainder of the operating characteristics for the staged ejector are given in Table 2.4-2.

Thus, a comparison of the values in Table 2.4-2 shows that some gains can be made by staging. The two-stage ejector in the above example requires approximately 39% less primary mass flow and about 16% less

maximum primary pressure. However, in a broader view these gains might not be significant when consideration is given to the additional hardware required. Also, a more nearly optimum single-stage ejector could, in all probability, be found for this application.

| Table 2.4-2 Single and staged ejector performance comparison | |
|---|---|
| Variable | Value |
| (1) Two-staged ejector | |
| $(w_S/w_P)_{1,2}$ | 0.47 |
| $(P_{M3}/P_{S0})_{1,2}$ | 2.67 |
| $M_{M3}$ | 0.497 |
| $(P_{P0}/P_{S0})_{1,2}$ | 68 |
| $(P_{P0})_2/(P_{S0})_1$ | 194 |
| $(P_{M3})_2/(P_{S0})_1$ | 7.6 |
| $(w_S)_1/(w_P)_T$ | 0.114 |
| (2) Single-stage ejector | |
| $(w_S/w_P)$ | 0.082 |
| $(P_{M3}/P_{S0})$ | ~7.6 |
| $M_{M3}$ | 0.43 |
| $(P_{P0}/P_{S0})$ | 231 |

The result of this simple example indicates the need for further and broader parametric studies of the two-stage versus one-stage ejector system.

# 3.0 EXPERIMENTAL INVESTIGATION

A series of cold-flow, air-to-air experiments has been conducted with small scale axisymmetric ejectors. The configurations investigated include:

(1) constant-area ejectors,

(2) variable-area ejectors, and

(3) slotted-nozzle ejectors.

The experiments provide a data base for comparison with the theory developed in the preceding section and they also provide information on the details of the ejector flowfields which cannot be predicted with the simplified models.

Descriptions of the experimental apparatus and procedure and discussions of the results are contained in the following sections.

## 3.1 COLD-FLOW, AIR-TO-AIR, EJECTOR EXPERIMENTS

### 3.1.1 Experimental apparatus and procedure

The small-scale ejector apparatus is illustrated in Figs. 3.1-1 through 3.1-6. Figure 3.1-1 is a photograph of the continuous flow facility with the axisymmetric ejector and secondary, mass flow measurement section installed. Also visible are the test stands, control panel, and manometer bank. A second photograph of the axisymmetric ejector is presented in Fig. 3.1-2 with the three mixing tubes used in the experimental investigation. An additional schematic view of the axisymmetric ejector design is given in Fig. 3.1-3.

The cold-flow, small-scale experiments were conducted with each of the interchangeable, primary nozzles (M = 2 conical nozzle, M = 2.5

Figure 3.1-1 Continuous flow facility with axisymmetric ejector and secondary, mass flow measurement section installed.

1046

Figure 3.1-2  Axisymmetric ejector with (left to right) variable-area
mixing tube with diffuser; 1.245 in. I.D. constant-area
mixing tube installed; and 0.995 in. I.D. constant-area
mixing tube
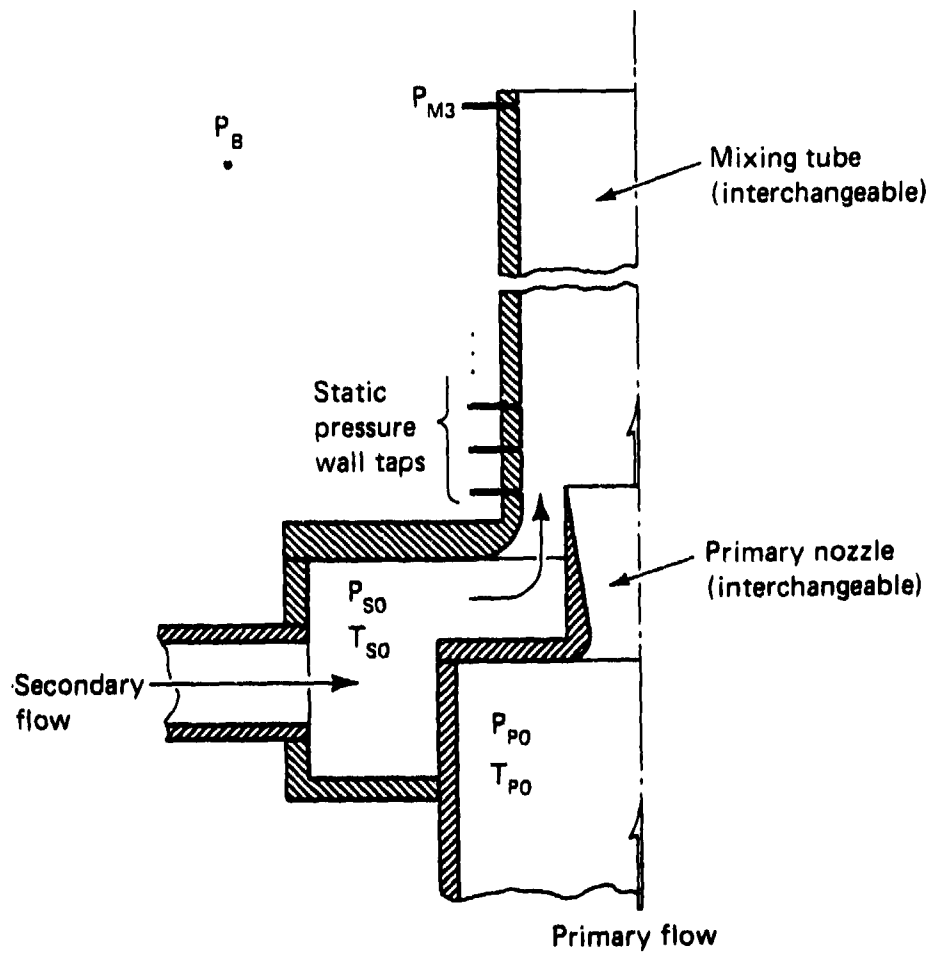
Figure 3.1-3   Schematic of axisymmetric ejector configuration

1048

(a) *Basic conical nozzle.*

(b) *Slotted extension for nozzle.*
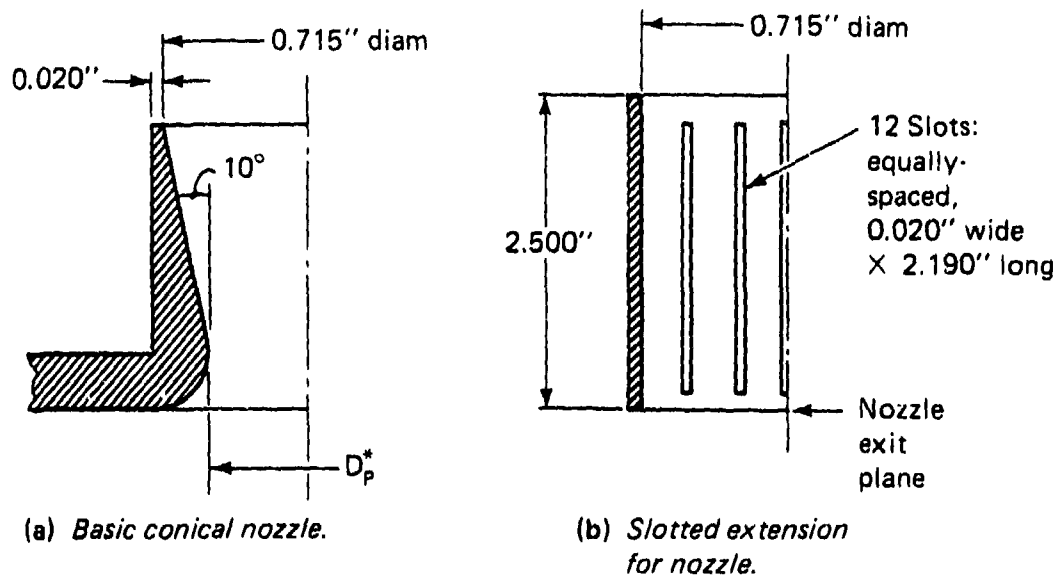
| Nozzle | $M_{P_1}$ | $D_P^*$ in. |
|--------|-----------|-------------|
| 1 | 2.0 | 0.550 |
| 2 | 2.5 | 0.440 |
| 3* | 2.5 | 0.440 |
| *Slotted nozzle | | |

(c) *Nozzle specifications.*

Figure 3.1-4 Schematics and specifications of ejector primary nozzles
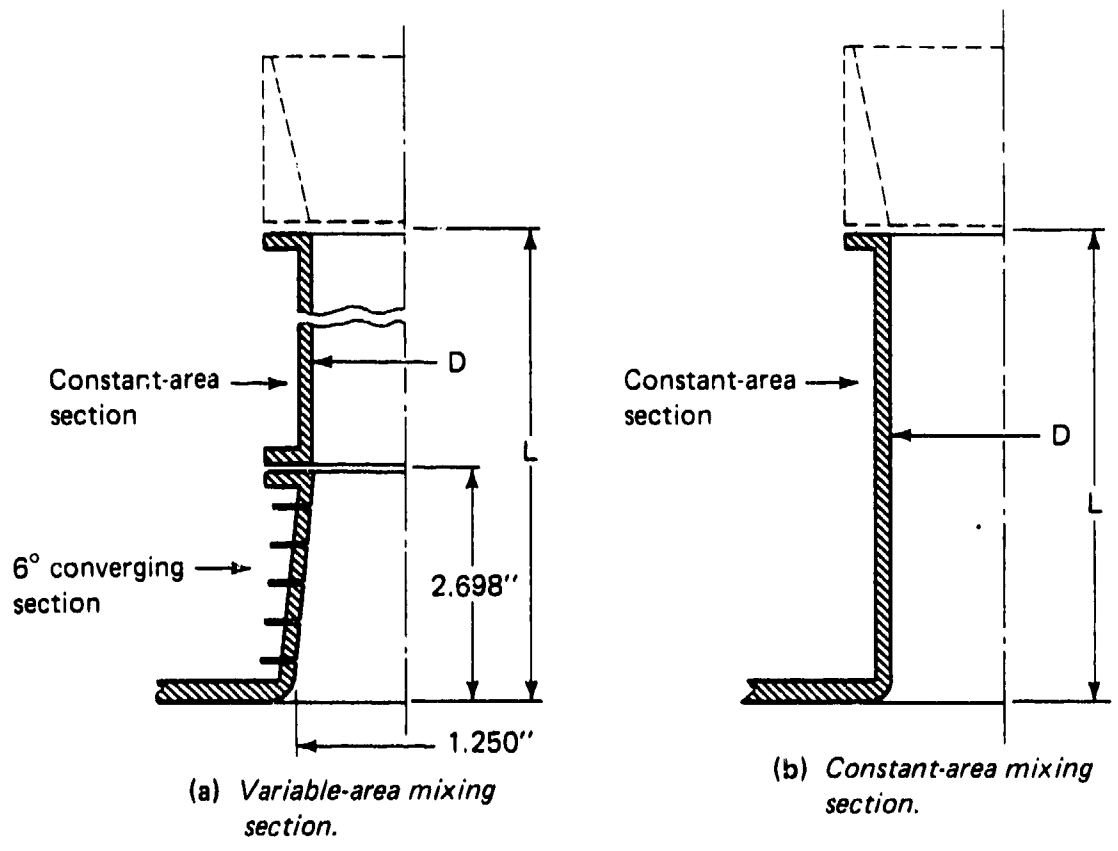
Constant-area section ← D

(a) *Variable-area mixing section.*

Constant-area section ← D

(b) *Constant-area mixing section.*

6° converging section

2.698"

1.250"

| Mixing tube | D in. | L in. |
|-------------|-------|--------|
| 1 | 0.995 | 12.500 |
| 2 | 1.245 | 13.000 |
| 3* | 0.995 | 12.882 |
| *With 6° converging section | | |

(c) *Mixing section specifications.*

1.939"

5°

5.382"

0.995"

(d) *Subsonic diffuser section.*

Figure 3.1-5 Schematics and specifications of ejector mixing sections

Figure 3.1-6  Experimental ejector set-up and notation

1051

conical nozzle, and $M = 2.5$ slotted nozzle of Fig. 3.1-4) in combination
with each of the interchangeable mixing tubes (1.245 inch I.D. constant-
area tube, 0.995 inch I.D. constant-area tube, and variable-area tube
of Fig. 3.1-5). The exit area of the primary nozzles was constant pro-
viding for identical area ratios $A_{P_1}/A_{MS}$ with each mixing tube.

The variable-area mixing tube was constructed such that the entrance
diameter was equal to the diameter of the larger 1.245 inch I.D. constant-
area tube while the exit diameter was equivalent to the diameter of the
smaller 0.995 inch I.D. constant-area tube. Pressure taps were added on
a 0.5 inch spacing through the tapered section of the tube for obtaining
the wall pressure distribution. The subsonic diffuser of Fig. 3.1-5 was
added to the variable-area tube in all cases and to the 0.995 inch I.D.
tube in selected tests.

Figure 3.1-6 is a schematic of the test set-up with notation for the
ejector and the primary and secondary mass flow measurement sections.
Air was used for both the primary and secondary gases in each experiment
while $P_{PO}$ was held constant and $P_B = P_{ATM}$; thus, the ratio $P_{PO}/P_B$ or
$P_{PO}/P_{ATM}$ was constant. In addition, $w_p$ was constant for each run since
the primary flow was choked in the supersonic nozzle and $P_{PO}$ was
constant. The secondary stream was drawn from atmosphere; a valve in the
secondary flow line was used to change $w_s$ and $P_{SO}$. Hence, $w_s/w_p$ and
$P_{SO}/P_{PO}$ were the variables in each experiment. Since the experiments
were performed with constant values of $P_{ATM}/P_{PO}$, the experimental results
may be thought of as intersections of the three-dimensional operating
surfaces, Figs. 2.1-2 and 2.1-3, with planes of $P_{ATM}/P_{PO}$ = constant.
Examples of the resulting two-dimensional parametric curves are sketched
in Figs. 2.1-4 and 2.1-7.

### 3.1.2 Experimental results

The experimental results for the $M = 2$ conical primary nozzle in the 1.245 inch I.D. $(A_{P1}/A_{M3} = 0.333)$ and 0.995 inch I.D. $(A_{P1}/A_{M3} = 0.516)$ constant-area mixing tubes are presented in Figs. 3.1-7 and 3.1-8. Figure 3.1-7 is a plot of $w_s/w_p$ vs $P_{so}/P_{Fo}$. The experimental values lie very close to the theoretical break-off curves[†] except at very small values of $w_s/w_p$ where, as previously discussed, the flowfield becomes two-dimensional in nature. The compression ratio $P_{ATM}/P_{so}$ is plotted against $P_{po}/P_{so}$ in Fig. 3.1-8. The experimental data points lie below the theoretical break-off curves which simply indicates that the ejector was operating in the $P_{po}/P_{ATM}$ independent regime.[††]

Due to the somewhat congested nature of the theoretical $P_{ATM}/P_{so}$ vs $P_{po}/P_{so}$ curves, similar to those shown in Figs. 2.3-4(a-d), the theoretical curves were not completed in the $P_{po}/P_{ATM}$ independent region of Fig. 3.1-8 except for $w_s/w_p = 0.316$, 0.108, 0.074, and 0.043 at $A_{P1}/A_{M3} = 0.330$. Comparisons between the theoretical and experimental results serve to validate the one-dimensional flow model.

From Fig. 3.1-8 it would appear that the ejector was operating closer to the theoretical break-off curve for $A_{P1}/A_{M3} = 0.330$; however, a vertical line drawn through the experimental data and the theoretical break-off curve to determine the break-off points, indicates different

---

[†] Recall that the theoretical $w_s/w_p$ vs $P_{so}/P_{po}$ curve is invariant and identical to the break-off curve in the $P_{po}/P_{ATM}$ independent regime.

[††] Refer back to Section 2.3 and Fig. 2.3-4 for a more complete presentation of the typical operating characteristics of an ejector system as determined from the theoretical constant-area ejector model.
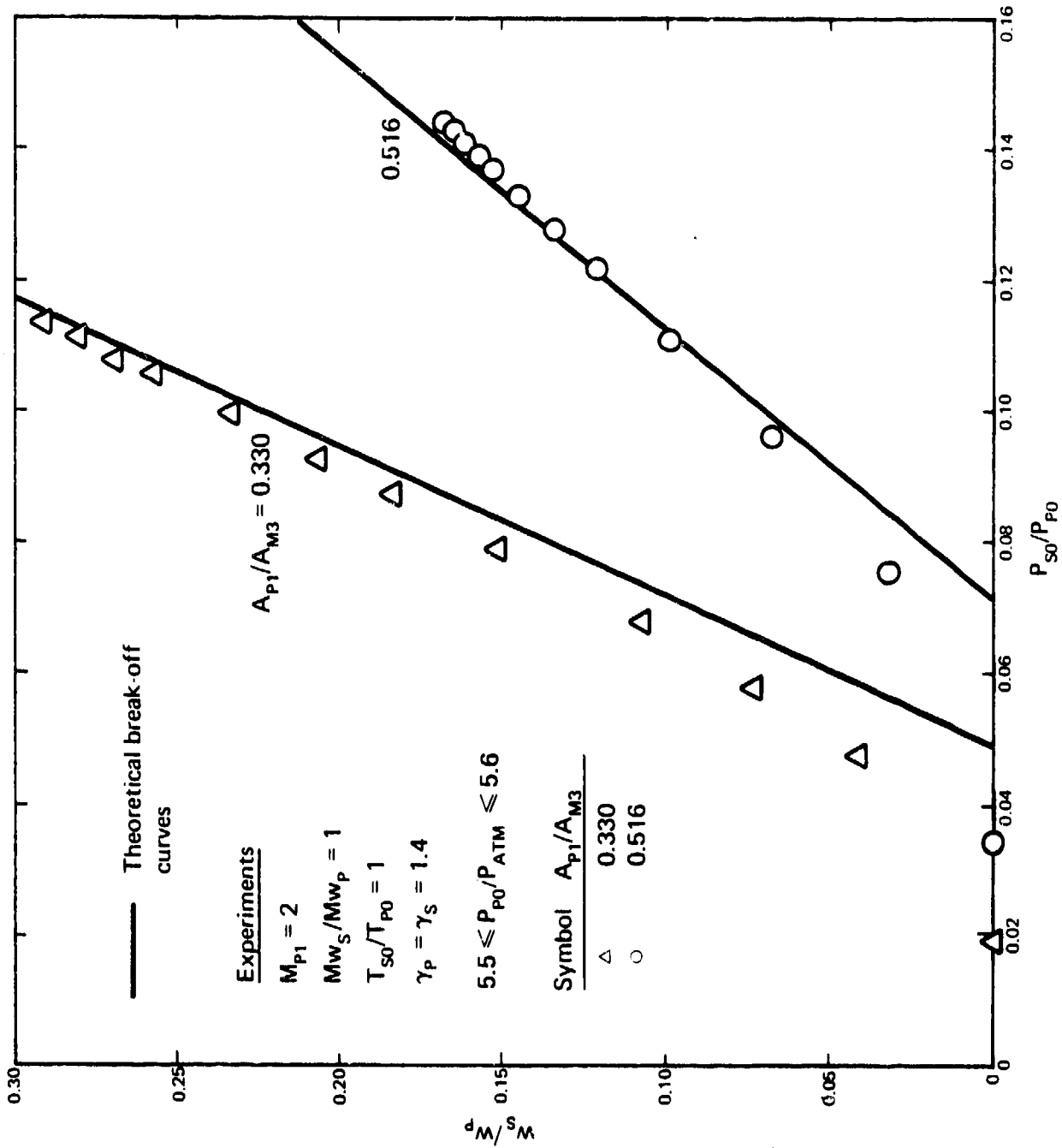
Figure 3.1-7  Constant-area ejector mass flow characteristics
($A_{P1}/A_{M3}$ = 0.330, 0.516 and $M_{P1}$ = 2.0)
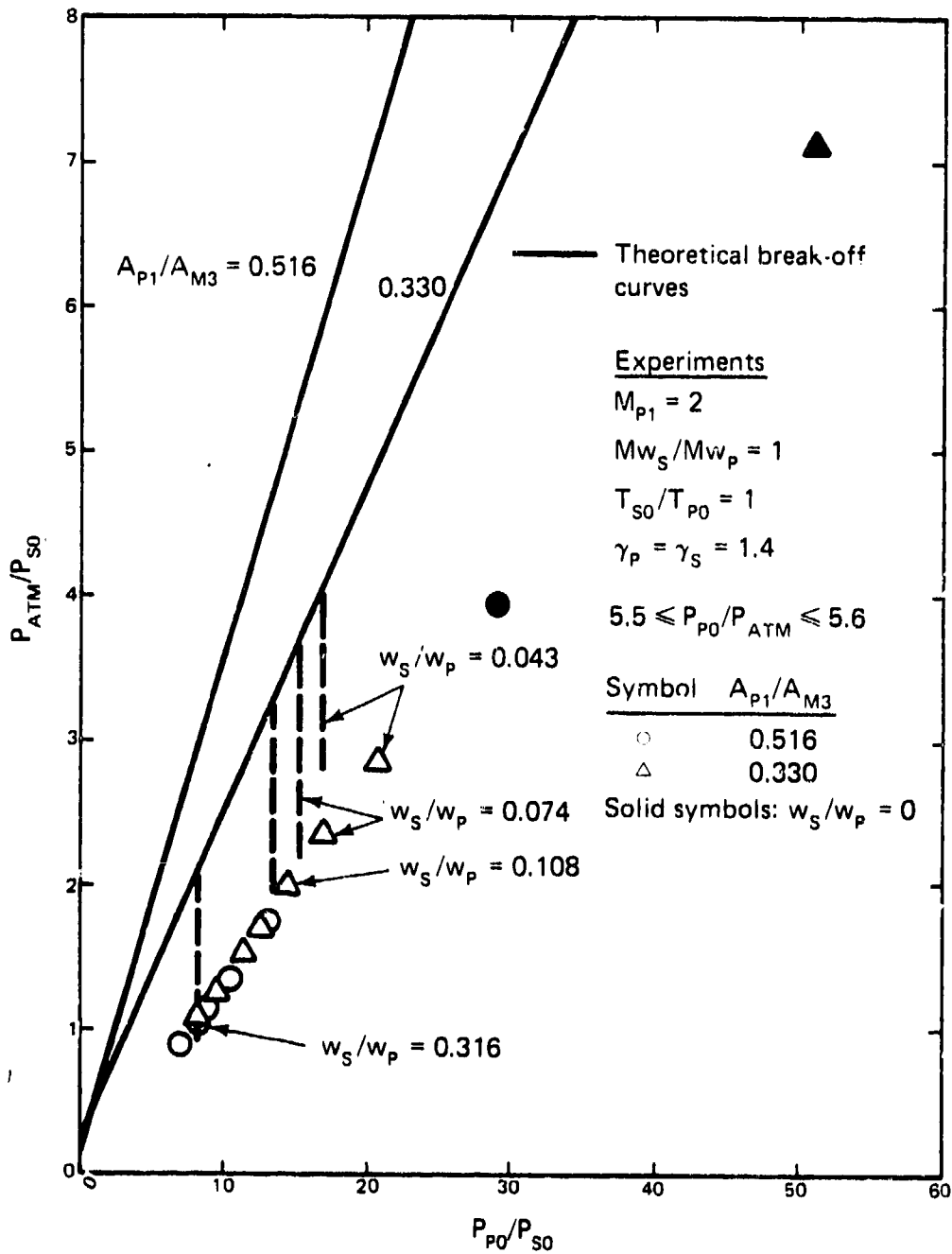
Figure 3.1-8 Constant-area ejector compression characteristics
$(A_{P1}/A_{M3} = 0.330, 0.516$ and $M_{P1} = 2.0)$

values of $w_s/w_p$ for each area ratio. This fact is borne out by the data points for $w_s/w_p = 0$ at $A_{P1}/A_{M3} = 0.330$ and $0.516$; these points indicate that the ejectors were operated significantly below the applicable break-off curve at lower values of $w_s/w_p$.

The experimental results for the $M = 2.5$ conical primary nozzle in the 1.245 inch I.D. ($A_{P1}/A_{M3} = 0.330$) and 0.995 inch I.D. ($A_{P1}/A_{M3} = 0.516$) constant-area mixing tubes as given in Figs. 3.1-9 and 3.1-10 follow the same trends as for the $M = 2$ conical nozzle. Again, the experimental values of $w_s/w_p$ vs $P_{SO}/P_{PO}$ are in good agreement with the one-dimensional flow model except at low values of $w_s/w_p$. Since the experimental data points for $P_{ATM}/P_{SO}$ vs $P_{PO}/P_{SO}$ lie below the theoretical break-off curves, ejector operation in the $P_{PO}/P_{ATM}$ independent regime is indicated. Addition of the subsonic diffuser to the 0.995 inch I.D. constant-area tube did not alter the mass flow characteristics of Fig. 3.1-9 since the diffuser affects only the recompression shock structure within the ejector in the $P_{PO}/P_{ATM}$ independent regime. From Fig. 3.1-10 it is apparent that the ejector was operating closer to the theoretical break-off curve with the diffuser; however, the experiment with the diffuser installed was conducted at $P_{PO}/P_{ATM} = 5.5$; whereas, the experiment without the diffuser was performed with $P_{PO}/P_{ATM} = 6.2$. The difference in $P_{PO}/P_{ATM}$, as will be demonstrated below, should have been responsible for the differences in $P_{ATM}/P_{SO}$ values with and without the subsonic diffuser.

The experimental results for the $M = 2.5$ slotted primary nozzle in the 1.245 inch I.D. ($A_{P1}/A_{M3} = 0.330$) and 0.995 inch I.D. ($A_{P1}/A_{M3} = 0.516$) constant-area mixing tubes are presented in Figs. 3.1-11 and 3.1-12. From Fig. 3.1-11 the experimental data for $w_s/w_p$ vs $P_{SO}/P_{PO}$
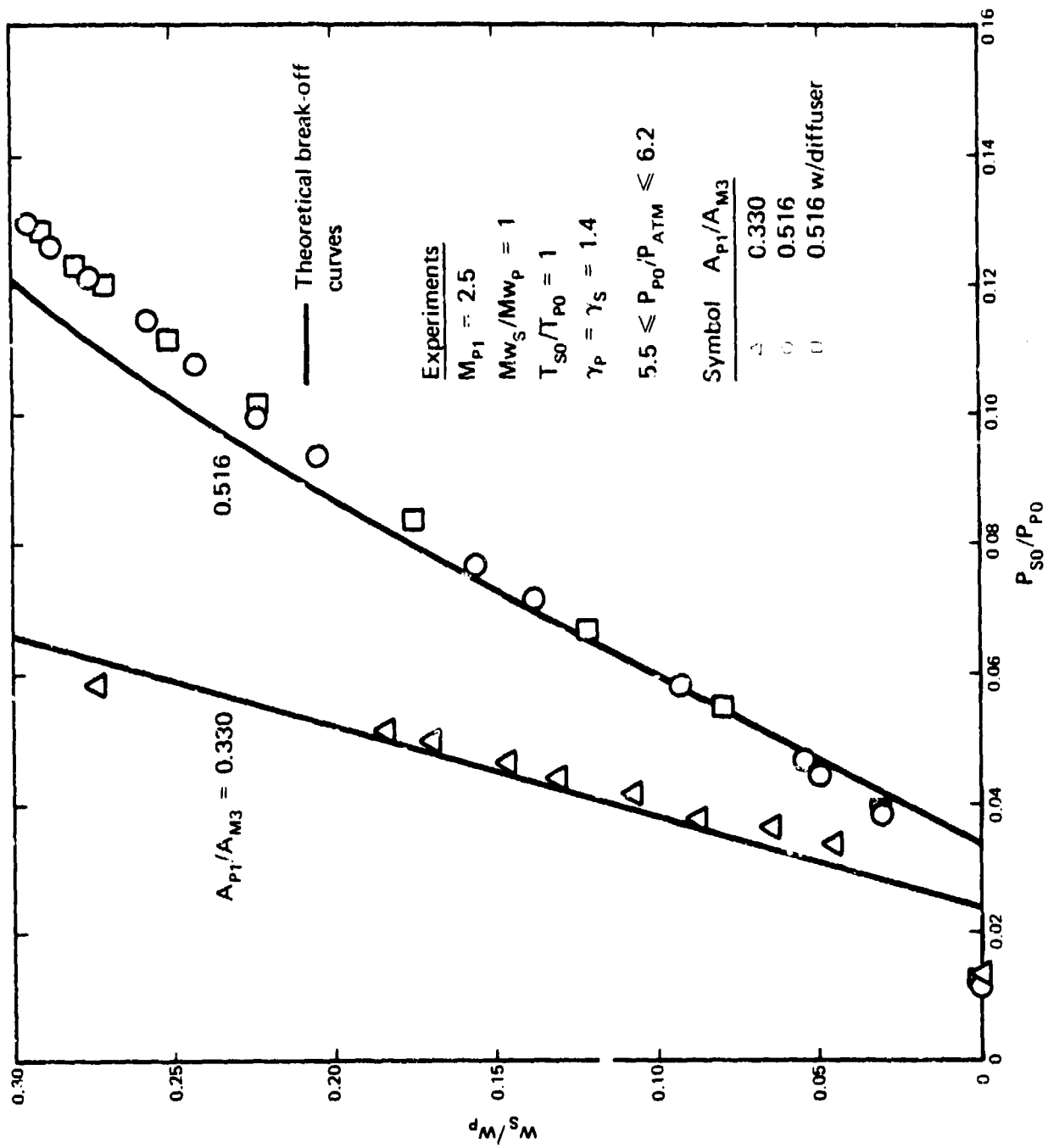
Figure 3.1-9 Constant-area ejector mass flow characteristics
$(A_{P_1}/A_{M_3} = 0.330, 0.516$ and $M_{P_1} = 2.5)$
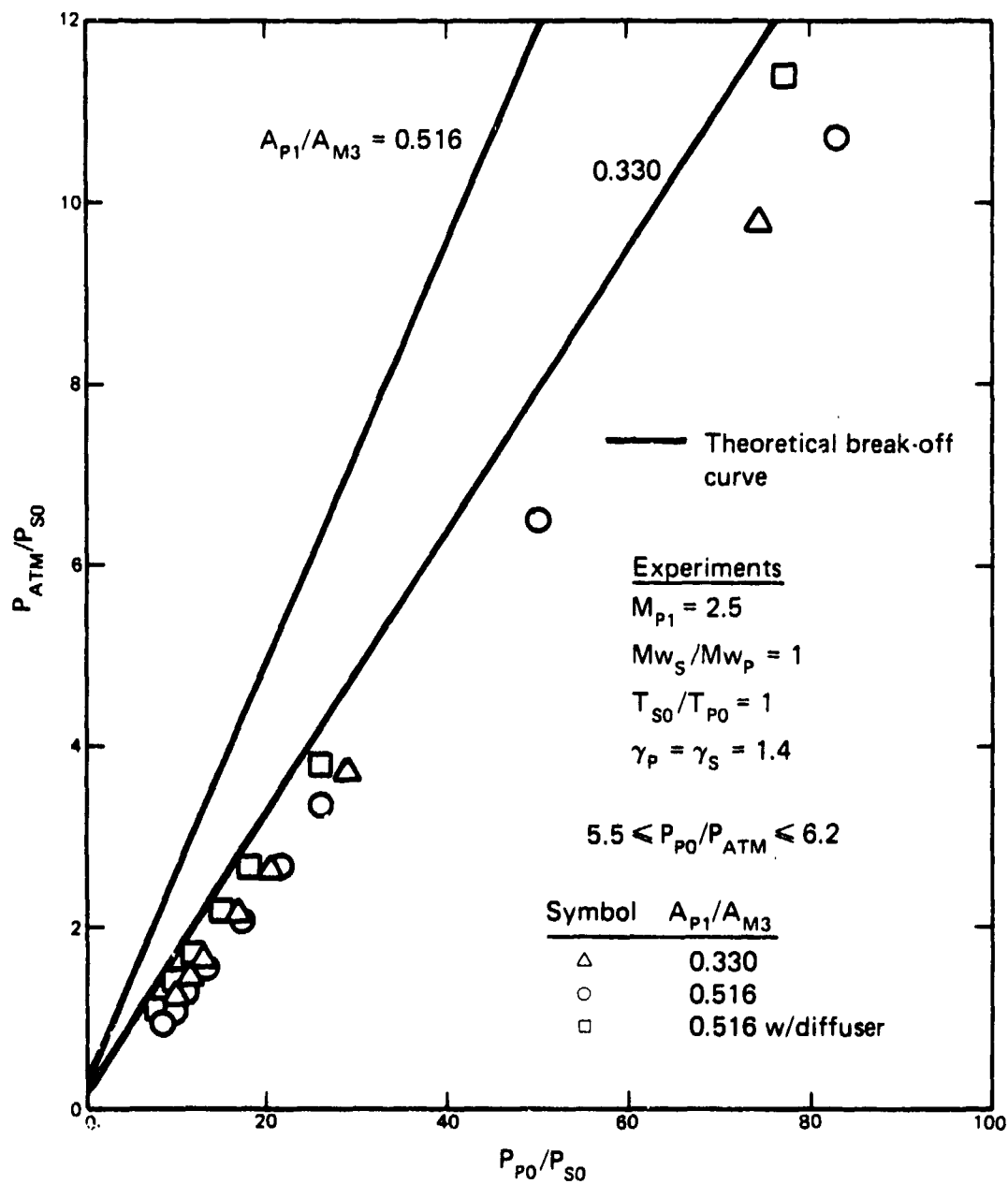
Figure 1-10 Constant-area ejector compression characteristics ($A_{P1}/A_{M3}$ = 0.330, 0.516 and $M_{P1}$ = 2.5)

1058
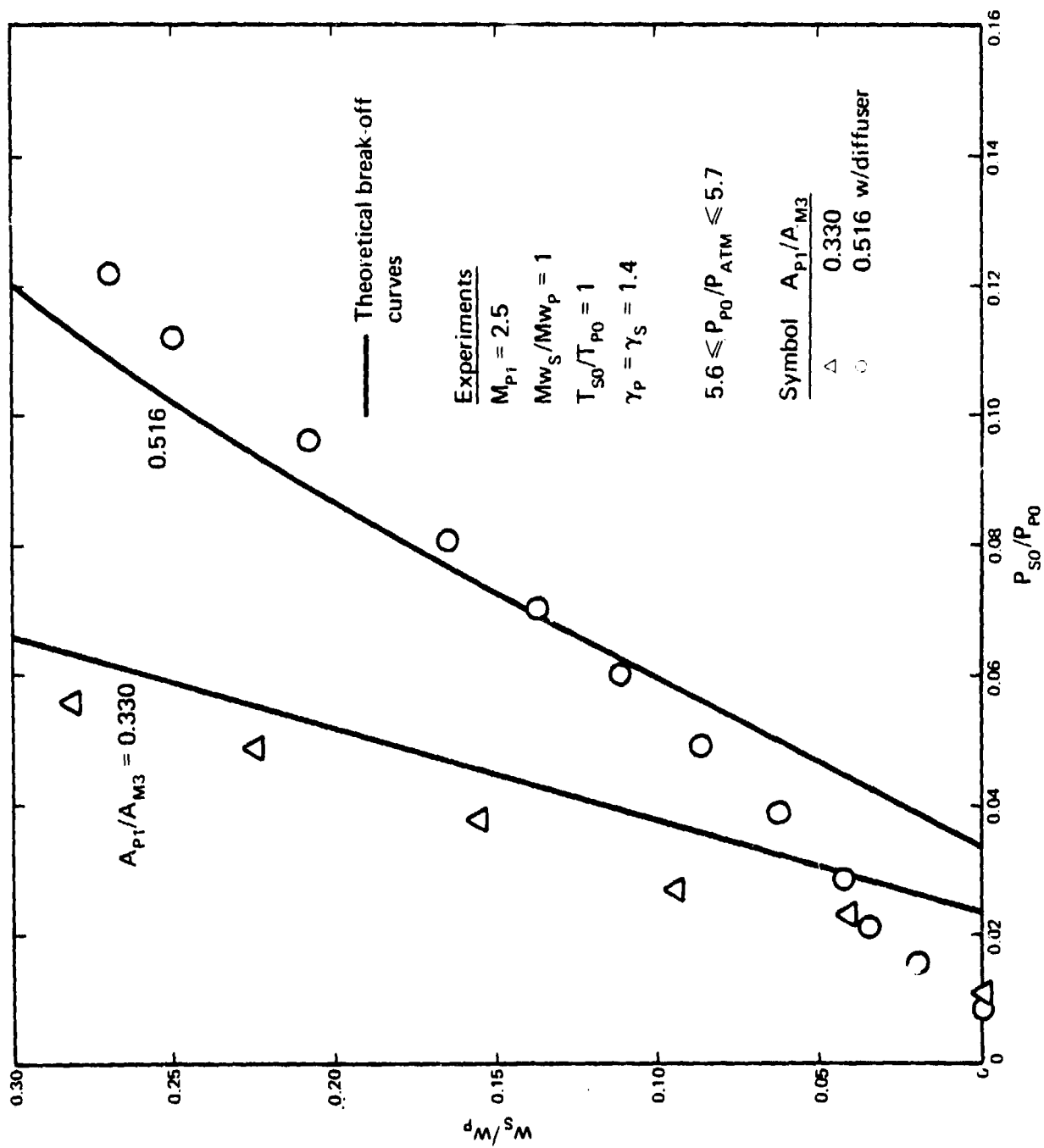
Figure 3.1-1  Constant-area, slotted-nozzle ejector mass flow characteristics ($A_{P1}/A_{M3}$ = 0.330, 0.516 and $M_{P1}$ = 2.5)
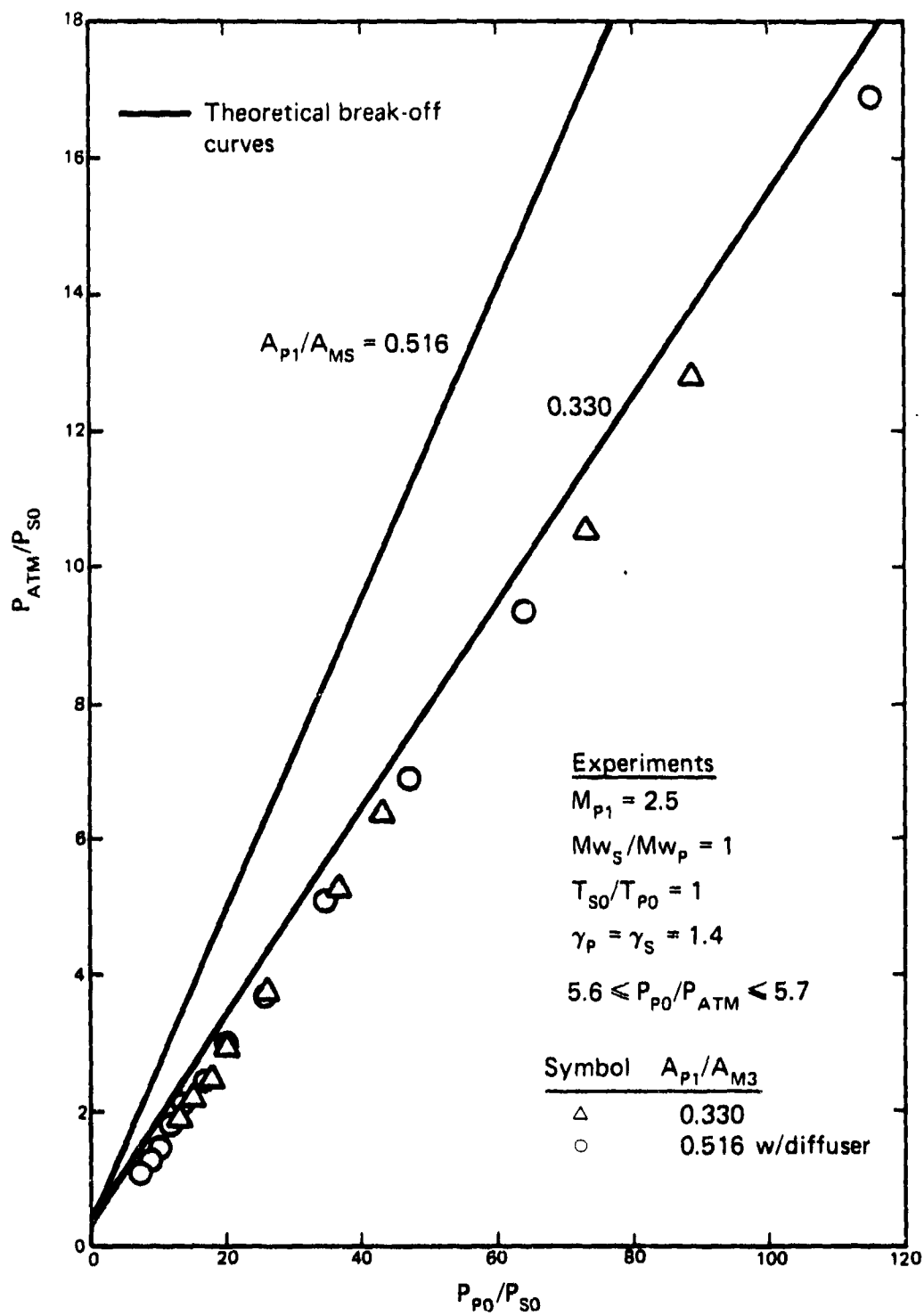
Figure 3.1-12  Constant-area, slotted-nozzle ejector compression characteristics ($A_{P1}/A_{MS}$ = 0.330, 0.516 and $M_{P1}$ = 2.5)

generally follows the theoretical break-off curves. However, deviations from the one-dimensional theory occur at larger values of $w_s/w_p$ than for the M = 2.5 conical nozzle of Fig. 3.1-9, which is not unexpected considering the geometry of the slotted nozzle. The compression ratio data of Fig. 3.1-12 is quite similar to that of Fig. 3.1-10 and indicates that the ejector was operating in the $P_{PO}/P_{ATM}$ independent regime.

The experimental results for the M = 2 and M = 2.5 conical primary nozzles in the variable-area mixing tube[†] are given in Figs. 3.1-13 through 3.1-18. The theoretical break-off curves are those for an ejector operating under the same conditions but with a constant-area mixing tube of $A_{P1}/A_{M3}$ = 0.516. Although the mass flow data of Fig. 3.1-13 deviates from the theoretical break-off curves, the one-dimensional analysis for an area ratio based on the minimum mixing tube area provides a fair representation of variable-area ejector performance, particularly at higher values of $w_s/w_p$. The variation in $P_{PO}/P_{ATM}$ did not alter the mass flow characteristics of Fig. 3.1-13 since the ejector, as shown in Fig. 3.1-14, was always operated in the $P_{PO}/P_{ATM}$ independent regime. Comparison of the compression ratio data of Fig. 3.1-14 shows that the ejector operated closer to the theoretical break-off curves at the lower values of $P_{PO}/P_{ATM}$; this demonstrates the desirability of operating at $P_{PO}/P_B$ values that are near the break-off curve in the independent regime. Note that the dimensionless mass flow characteristics remain unchanged even though the primary stagnation pressure is smaller. Figure 3.1-14

---

[†]Figure 3.1-5(a) shows this mixing section. The initial entrance diameter is 1.250 inches converging at a wall angle of 6° to a minimum mixing tube diameter of 0.995 inches.
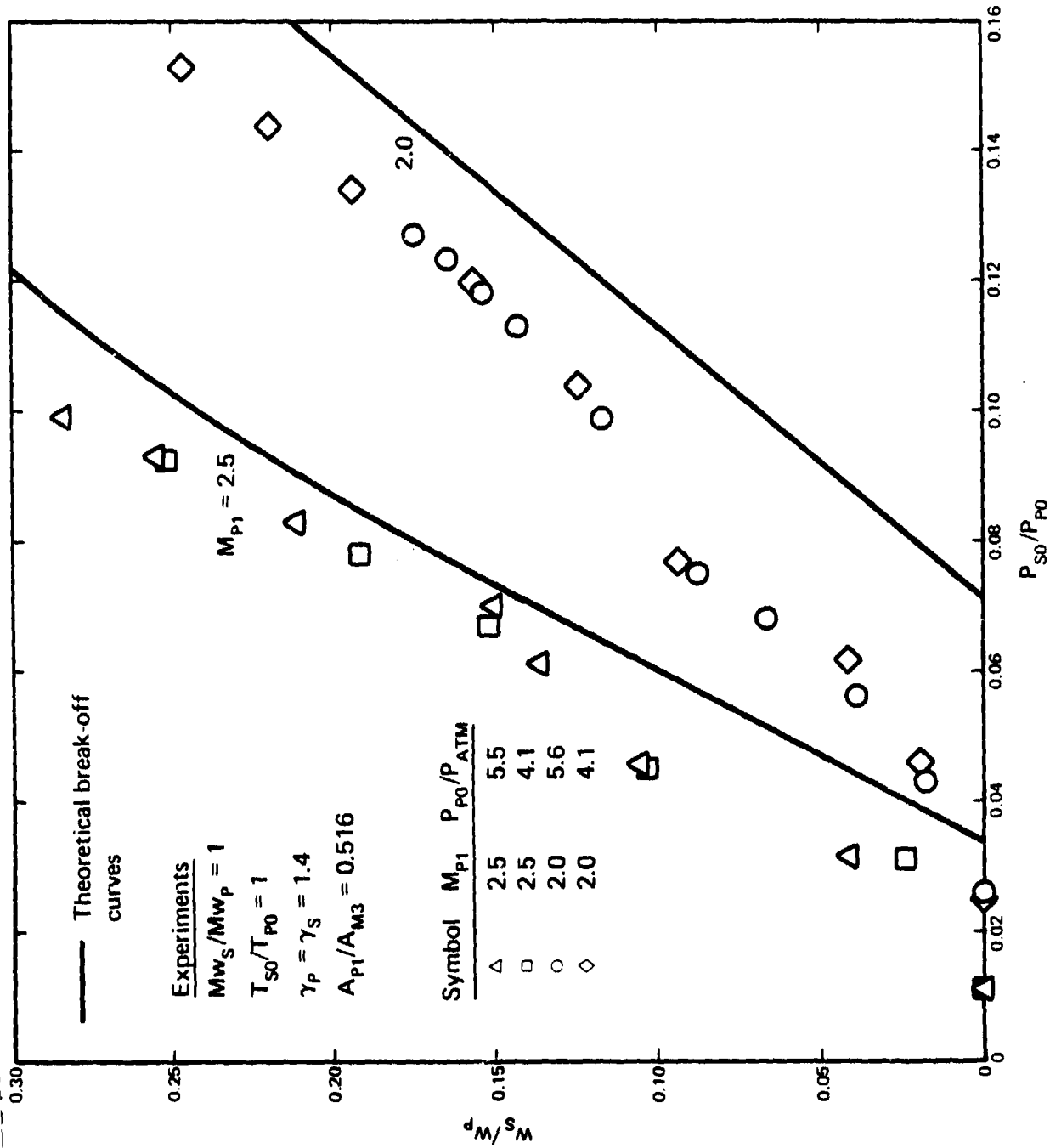
Figure 3.1-13 Variable-area ejector mass flow characteristics
($A_{P1}/A_{M3}$ = 0.516 and $M_{P1}$ = 2.0, 2.5)
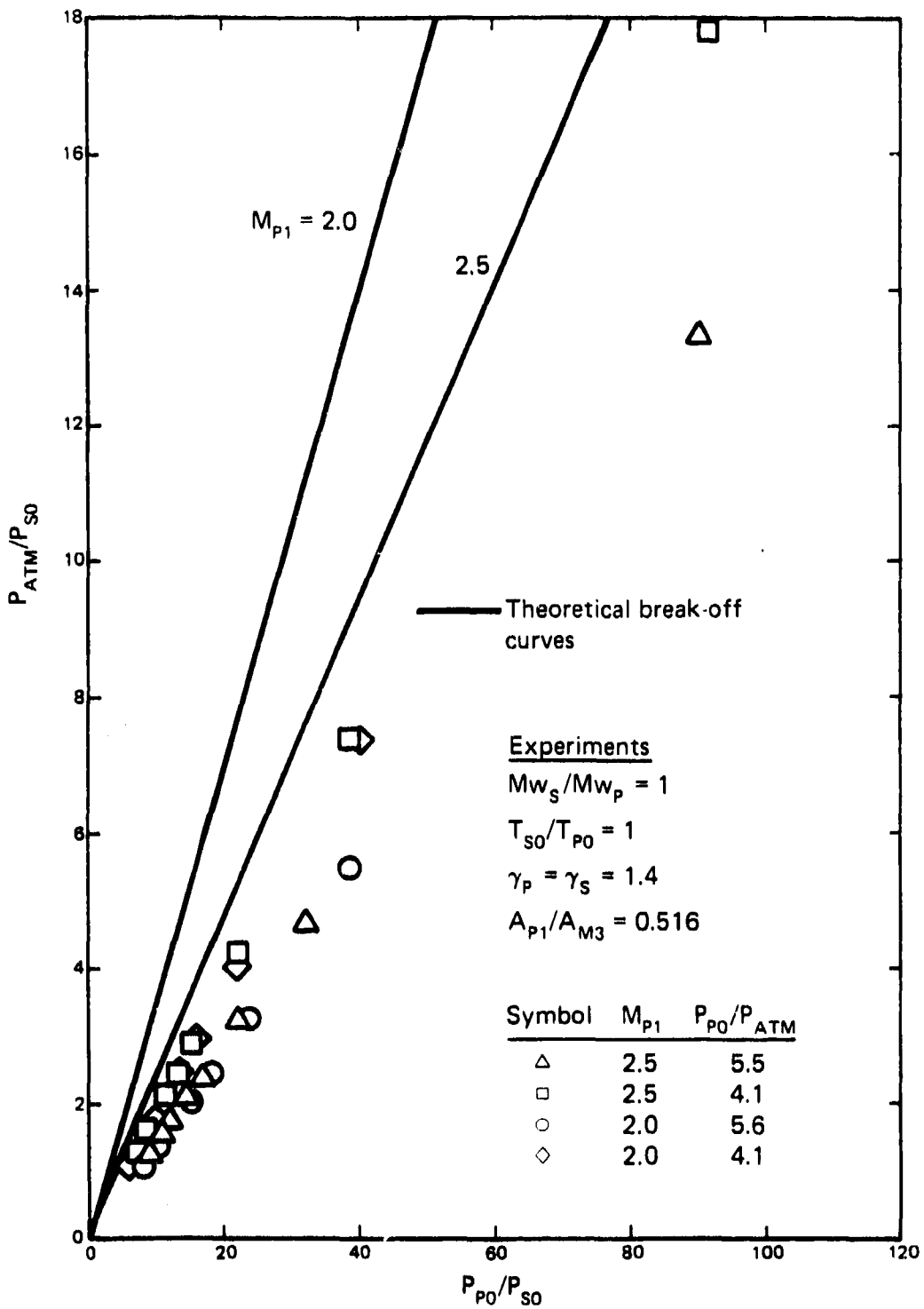
Figure 3.1-14   Variable-area ejector compression characteristics
$(A_{P1}/A_{M3} = 0.516$ and $M_{P1} = 2.0, 2.5)$
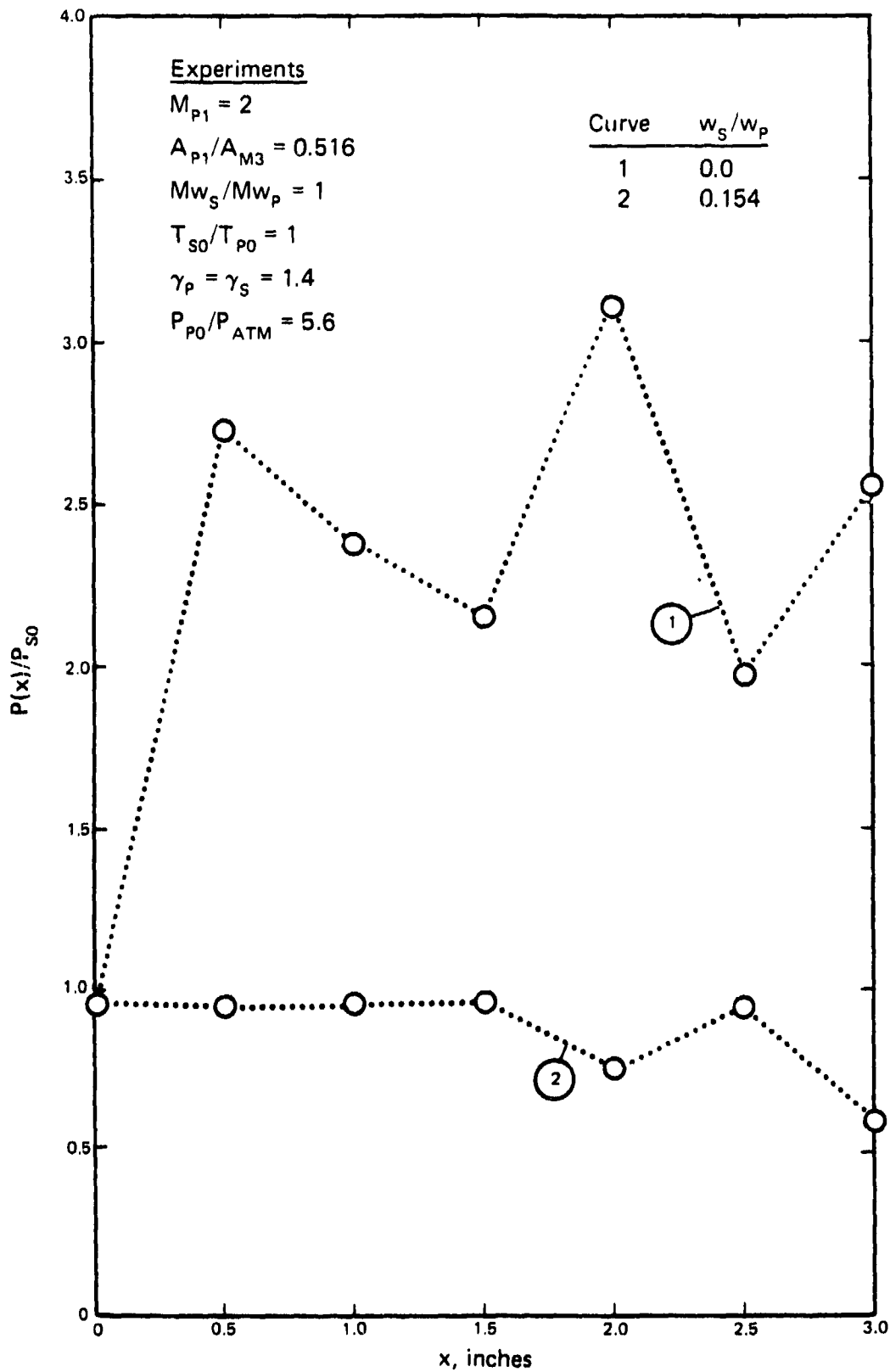
Figure 3.1-15   Variable-area ejector wall pressure distributions
$(A_{P1}/A_{M3} = 0.516,\ M_{P1} = 2.0,\ \text{and}\ P_{P0}/P_{ATM} = 5.6)$

1064
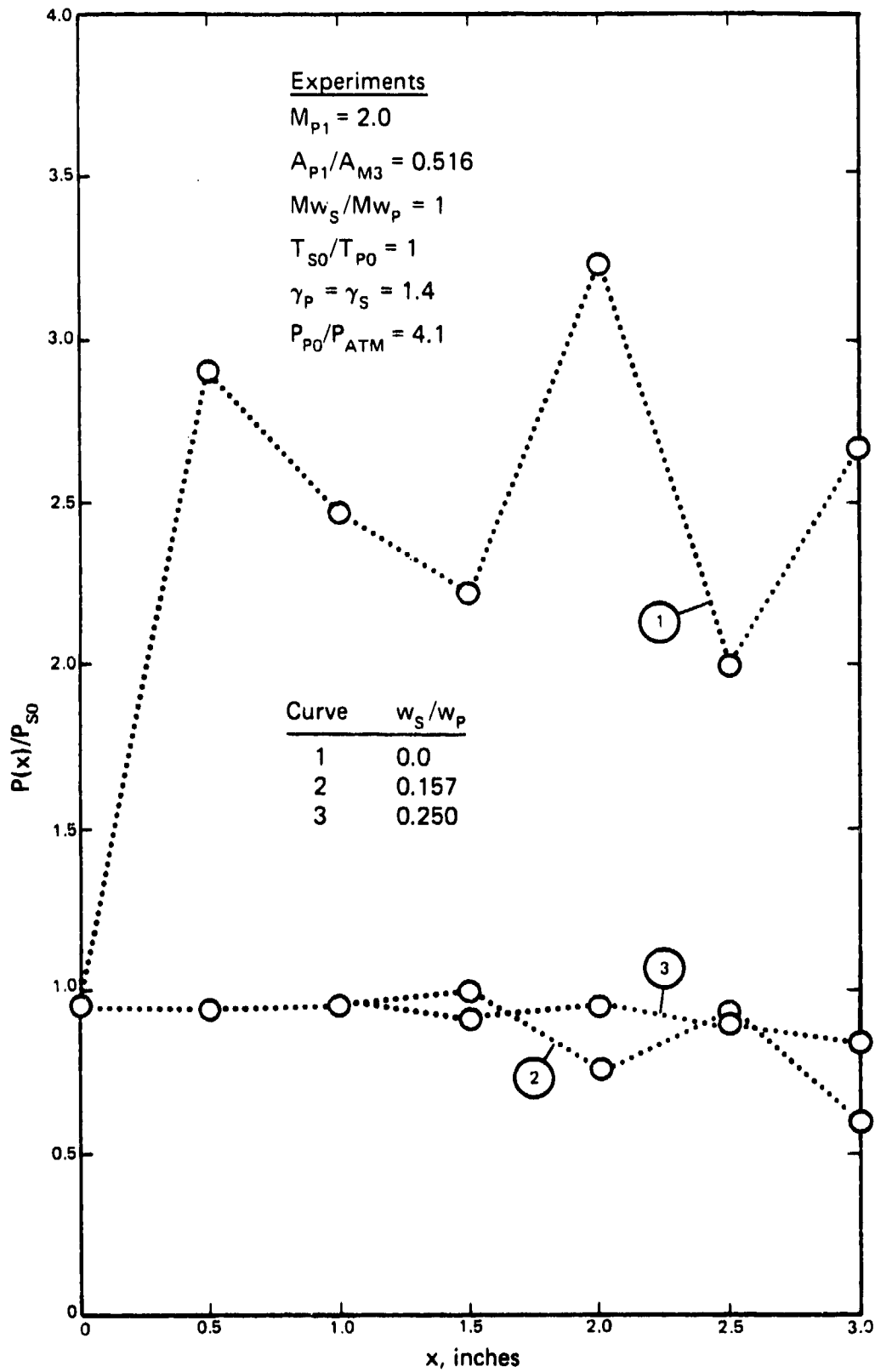
Figure 3.1-16  Variable-area ejector wall pressure distributions
$(A_{P1}/A_{M3} = 0.516, M_{P1} = 2.0, \text{ and } P_{PO}/P_{ATM} = 4.1)$

1065
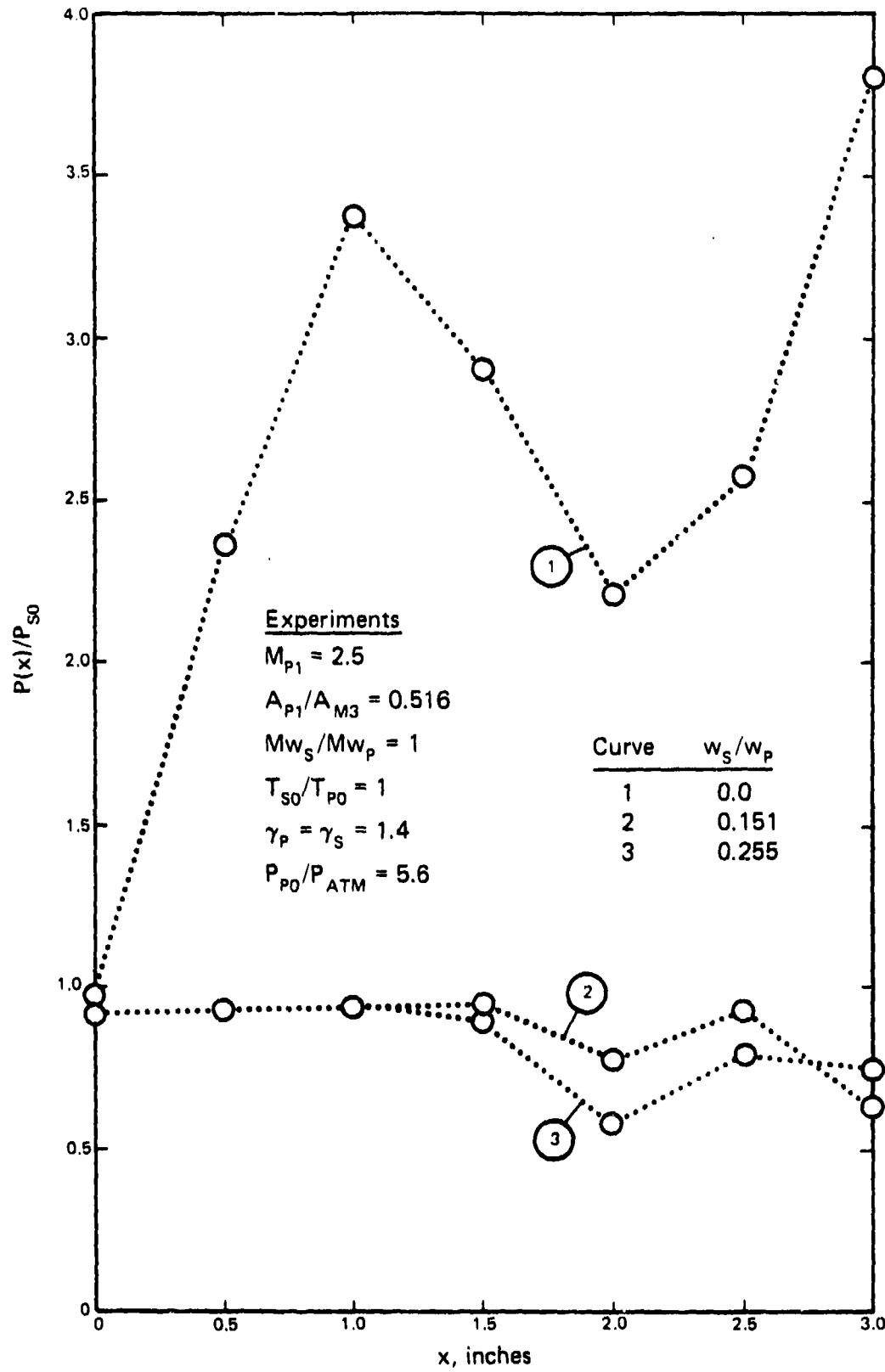
Figure 3.1-17  Variable-area ejector wall pressure distributions
$(A_{P1}/A_{M3} = 0.516, M_{P1} = 2.5, P_{PO}/P_{ATM} = 5.6)$

1066
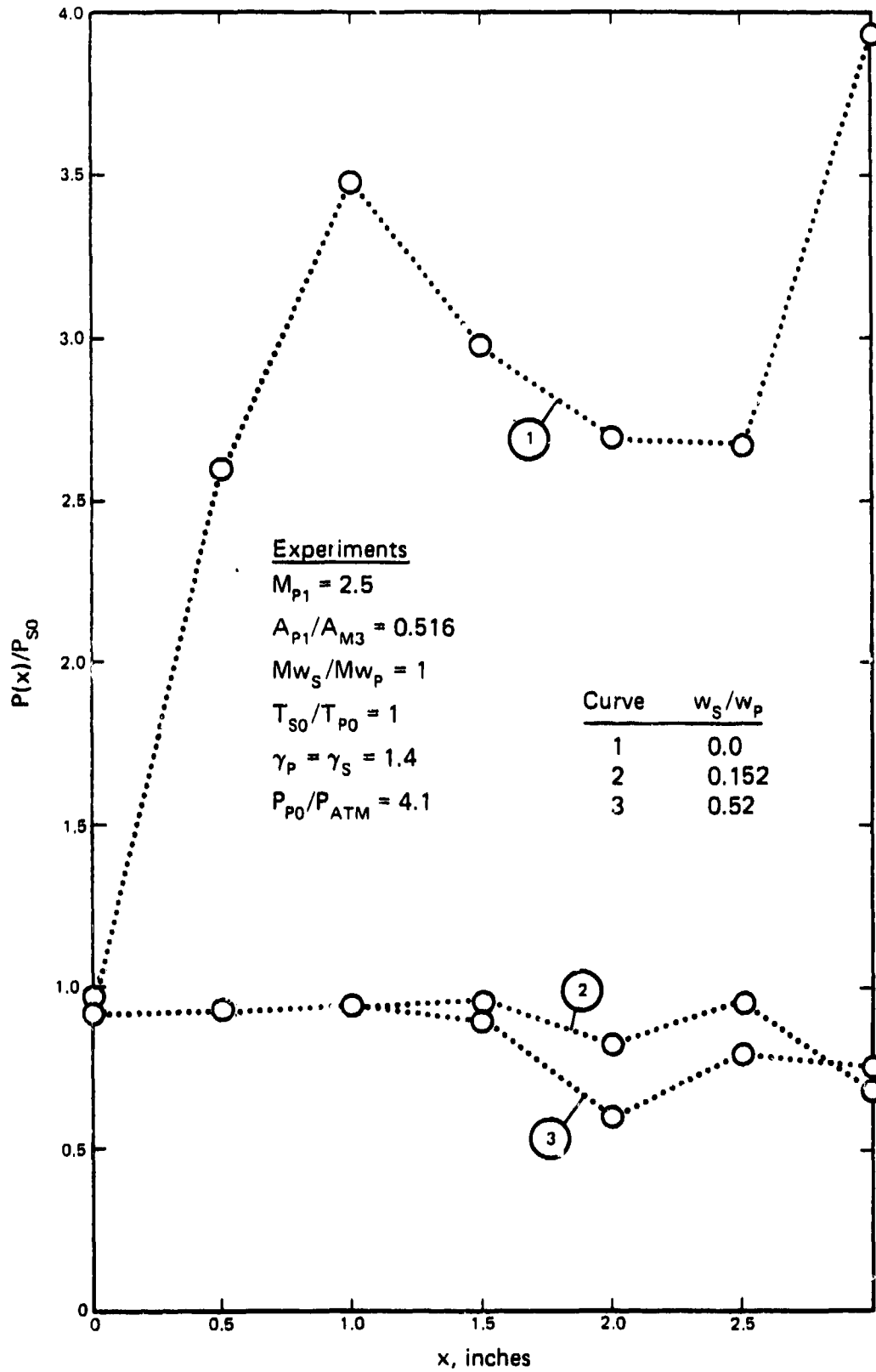
Figure 3.1-18  Variable-area ejector wall pressure distributions
$(A_{P1}/A_{M3} = 0.516, M_{P1} = 2.5, P_{P0}/P_{ATM} = 4.1)$

1067

also shows that the ejector operated closer to the appropriate theoretical break-off curve with the M = 2.5 conical primary nozzle; however, this is due to the fact that for constant $A_{P1}/A_{MS}$, an M = 2.5 nozzle requires a higher value of $P_{PO}/P_{ATM}$ than an M = 2 nozzle for $P_{PO}/P_B$ independent operation. The wall pressure distributions of Figs. 3.1-15 through 3.1-18 show that approximately constant pressure mixing occurred only at higher values of $w_S/w_P$ and, consequently, at lower values of $P_{ATM}/P_{SO}$ with $P_{PO}/P_{ATM}$ differences having little effect. In each of Figs. 3.1-15 through 3.1-18 note that only the initial part of the wall pressure distributions near the primary/secondary confluence are shown and that the final compression is to much higher levels of $P_{ATM}/P_{SO}$.

The experimental results for the M = 2.5 slotted primary nozzle in the variable-area mixing tube are presented in Figs. 3.1-19 through 3.1-22. The theoretical break-off curves are, again, those for an ejector operating under the same conditions but with a constant-area mixing tube of $A_{P1}/A_{MS}$ = 0.516, the area ratio corresponding to the constant-area section of the variable-area tube. As seen in Fig. 3.1-19, the experimental values for $w_S/w_P$ vs $P_{SO}/P_{PO}$ lie very close to the theoretical break-off curve even at low values of $w_S/w_P$. The experimental data for $P_{ATM}/P_{SO}$ vs $P_{PO}/P_{SO}$ as shown in Fig. 3.1-20 indicate that the ejector was operated in the $P_{PO}/P_{ATM}$ independent regime and re-emphasize the undesirability of operation at higher values of $P_{PO}/P_{ATM}$ than required since the mass flow characteristics of Fig. 3.1-19 were identical at each value of $P_{PO}/P_{ATM}$. Figures 3.1-21 and 3.1-22 show that wall pressure variations at low $w_S/w_P$ values were less drastic with the slotted primary

1068
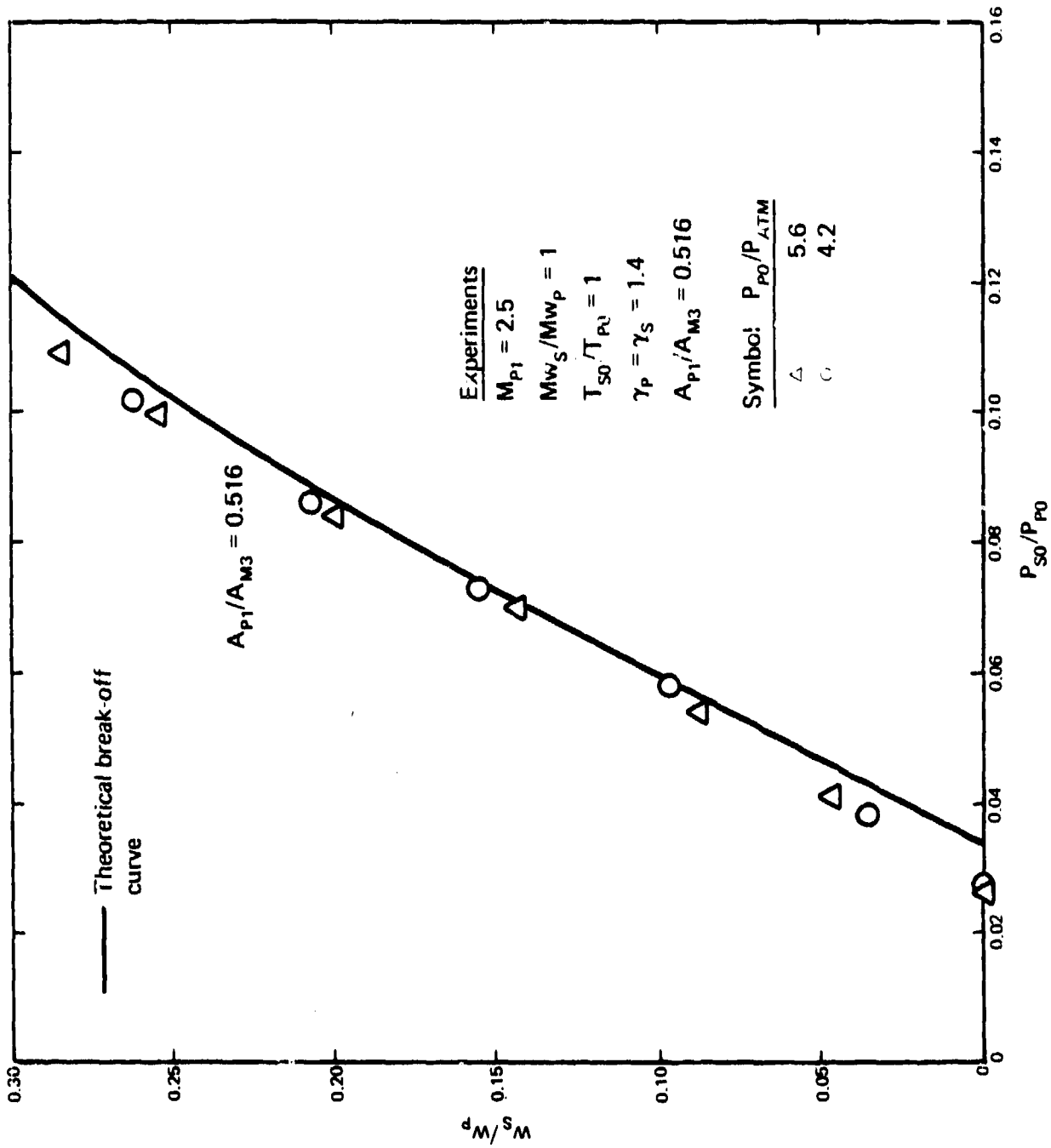
Figure 3.1-19  Variable-area, slotted-nozzle ejector mass flow characteristics
$(A_{P1}/A_{M3} = 0.516$ and $M_{P1} = 2.5)$
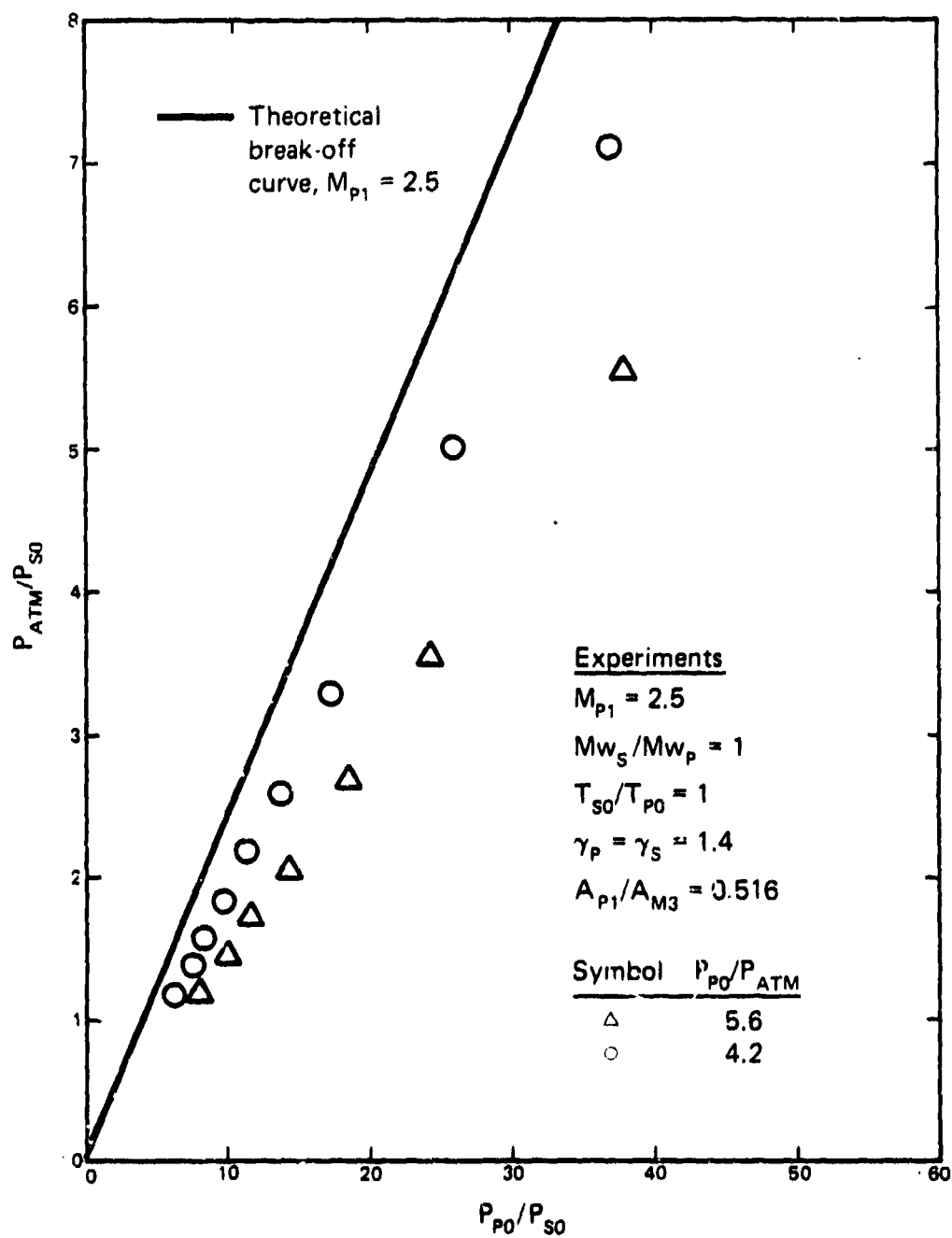
Figure 3.1-20 Variable-area, slotted-nozzle ejector compression characteristics ($A_{P1}/A_{M3}$ = 0.515 and $M_{P1}$ = 2.5)

1070
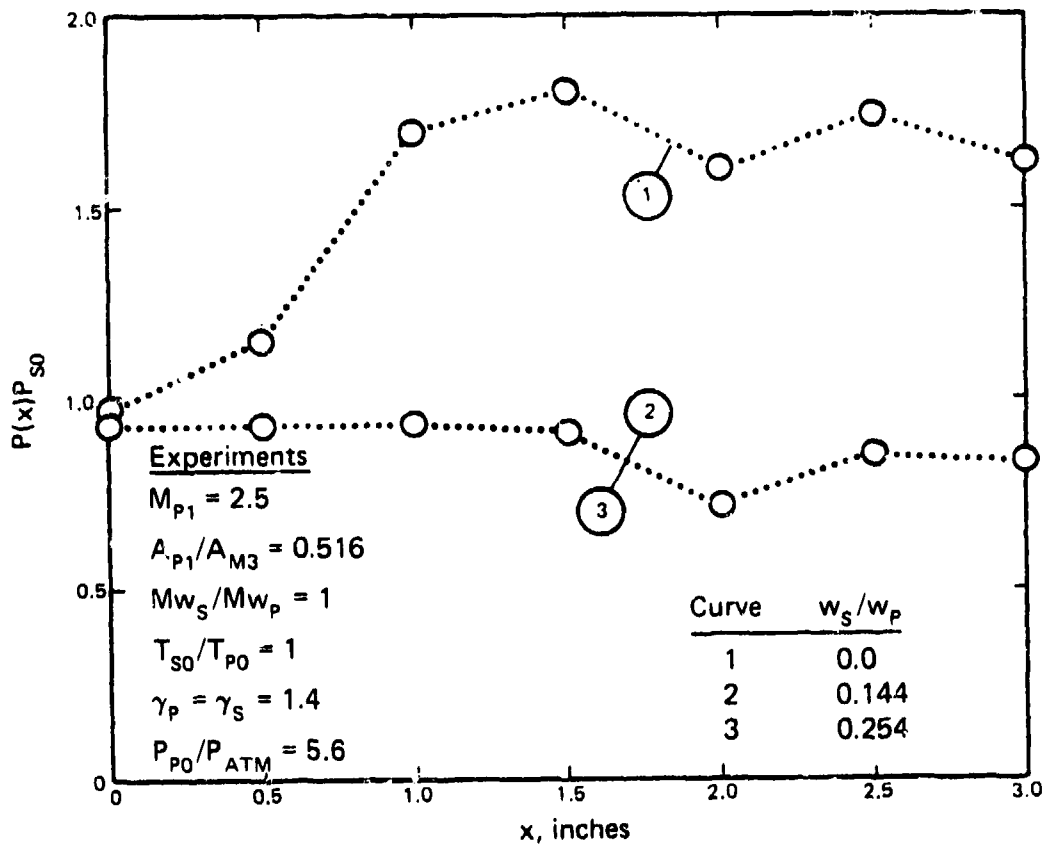
Figure 3.1-21   Variable-area, slotted-nozzle ejector wall pressure
distributions ($A_{P1}/A_{M3}$ = 0.516, $M_{P1}$ = 2.5, and
$P_{PO}/P_{ATM}$ = 5.6)

P(x)/P_{S0}

Experiments

$M_{P1} = 2.5$

$A_{P1}/A_{M3} = 0.516$

$Mw_S/Mw_P = 1$

$T_{S0}/T_{P0} = 1$

$\gamma_P = \gamma_S = 1.4$

$P_{P0}/P_{ATM} = 4.2$

| Curve | $w_S/w_P$ |
|-------|-----------|
| 1 | 0.0 |
| 2 | 0.155 |
| 3 | 0.262 |

x, inches
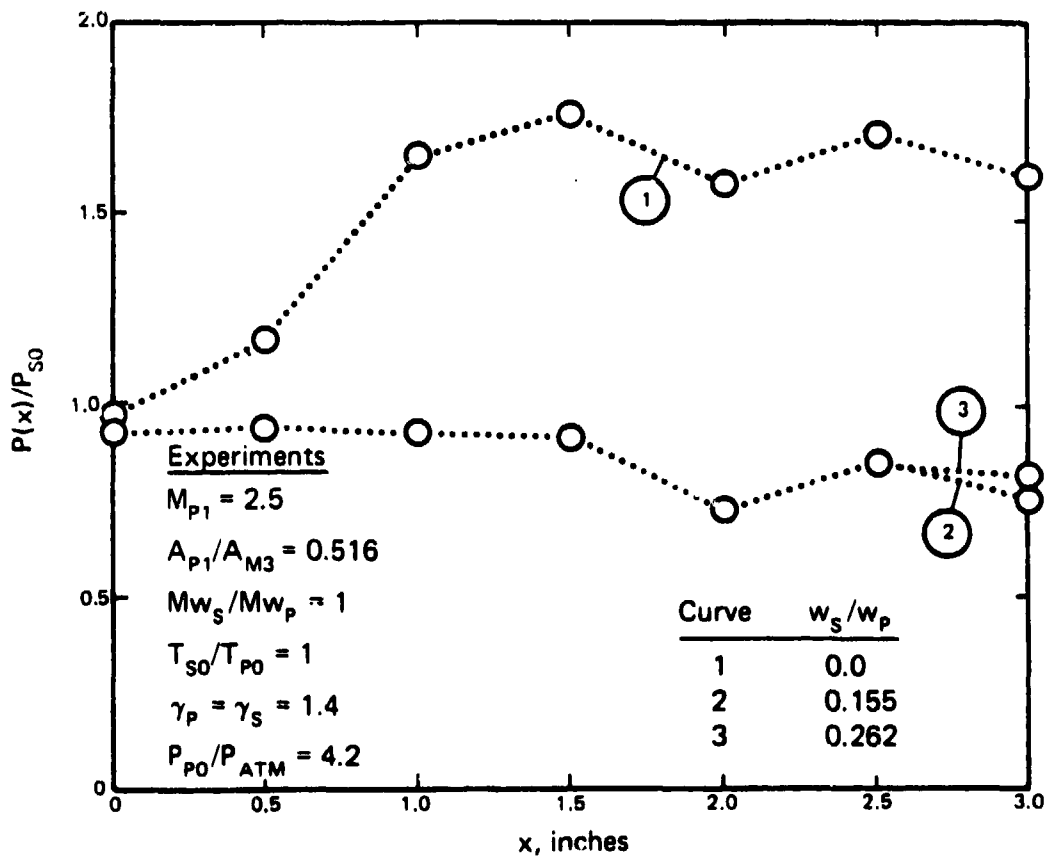
Figure 3.1-22   Variable area, slotted-nozzle ejector wall pressure distributions ($A_{P1}/A_{M3}$ = 0.516, $M_{P1}$ = 2.5, and $P_{P0}/P_{ATM}$ = 4.2)

1072

nozzle as opposed to the conical primary nozzles of Figs. 3.1-15 through 3.1-18 and may account for the excellent agreement of the $w_s/w_p$ vs $P_{so}/P_{po}$ data with the theoretical break-off curve of Fig. 3.1-19, although the constant-area mixing tube data of Fig. 3.1-11 would prejudice any conclusions based on primary nozzle design alone. Again, note that only the initial portions of the wall pressure distributions are presented in Figs. 3.1-21 and 3.1-22.

## 4.0 CONCLUSIONS

Only some general conclusions will be drawn in this section since specific conclusions were included in the foregoing sections. The conclusions are:

(1) The constant-area ejector flow model and computer program should be adopted as the basis for design and system studies. This model most realistically predicts the operational characteristics of ejector systems. The relationship and correspondence between variable-area and constant-area mixing tube ejectors should be established by both experiment and analysis.

(2) The analysis of variable-area mixing-tube ejectors should be continued.

(3) The design of potential high-performance ejectors must improve mixing and momentum transfer; some designs with potential are: unsteady flow, periodic pulsating flow, resonance phenomena, and/or various nozzle and mixing-tube geometries.

(4) The computer models developed in this study should be augmented and incorporated into an overall system program and further improvement of sub-system models should be continued.

# 5.0 REFERENCES

1. Addy, A. L., "The Analysis of Supersonic Ejector Systems," <u>Supersonic Ejectors</u>, AGARDograph No. 163, pp. 31-101 (1972).

2. <u>Handbook of Supersonic Aerodynamics</u>, Vol. 6, Section 17, NAVWEPS Report 1488.

3. Fabri, J. and Paulon, J., "Theory and Experiments on Supersonic Air-to-Air Ejectors," NACA TM 1410 (1958).

4. Fabri, J. and Siestrunck, R., "Supersonic Air Ejectors," <u>Advances in Applied Mechanics</u>, New York, New York, Academic Press, Vol. V, pp. 1-34 (1958).

5. Chow, W. L. and Addy, A. L., "Interaction between Primary and Secondary Streams of Supersonic Ejector Systems and their Performance Characteristics," AIAA Journal, 2(4):686-695 (1964).

6. Chow, W. L. and Yeh, P. S., "Characteristics of Supersonic Ejector Systems with Non-Constant Area Shroud," AIAA Journal, 3(3):525-527 (1965).

7. Loth, J. L., "Theoretical Optimization of Staged Ejector Systems," Part I, Arnold Engineering Development Center Report No. AEDC-TR-66-2 (1966).

8. Loth, J. L., "Theoretical Optimization of Staged Ejector Systems," Part II, Arnold Engineering Development Center Report No. AEDC-TR-68-80 (1968).

# A REDUCED EJECTOR EQUATION

S.H. Hasinger

Air Force Wright Aeronautical Laboratories

Wright-Patterson Air Force Base, Dayton, Ohio

In this presentation, I would like to show the features of a "Reduced Ejector Equation." If one applies the three pertinent conservation laws to the mixing section of an ejector arrangement ~~as shown in Figure 1~~, one arrives, after some algebraic manipulation, at a relation which, for a given mixing section layout, contains the inlet conditions on one side and exit conditions on the other side.* Since the treatment accounts for wall pressure forces, mixing is not restricted to constant area or constant pressure.

The separation of the variables, in respect to inlet and exit conditions, leads to a reduced ejector equation, which is plotted ~~in Figure 2~~ for two different mixing section layouts. The magnitude E on the ordinate stands for an expression containing all the inlet conditions as given by mass flow ratio, inlet area ratio, inlet Mach numbers, and thermodynamic properties of primary and secondary operating medium. The abscissa gives the mixing section exit Mach number. This plot shows that for small E values there is no supersonic solution. Only if E is sufficiently large, a supersonic solution is possible. The upper curve is based on a layout typical for thrust augmenters: constant area mixing and very low wall friction. The lower curve pertaining to ejector pumps is calculated for a tapered mixing section with wall friction corresponding to a section length of a few average section diameters. The nature of the application restricts the actual operating ranges, marked in Figure 2 by shading, to only small portions of the respective curves.

---

*The relation, which was not shown at the presentation, is attached as Figure 3 to this write-up. For reference, see: Hasinger, S., "Performance Characteristics of Ejector Devices," Aerospace Research Laboratories, Wright-Patterson AFB, Technical Report ARL TR-75-0205, June 1975.

The essential point to make here is that this plot allows one to recognize the conditions for transition to supersonic mixing. Experimental experience shows that transition occurs where mixing takes place under constant pressure. Apparently, under this condition the supersonic shock system is pushed out of the mixing section into the diffuser. Constant pressure mixing conditions can be derived from the analysis and marked on the curves. They are given by the numbers indicated as $B_t$ values. $B_t$ stands for the expression shown in the plot. The plot shows that the value of $B_t$ must be near two or larger to allow transition to supersonic mixing. $B_t$ can be made a part of the inlet conditions, i.e. an ejector can be predesigned to operate with supersonic mixing.
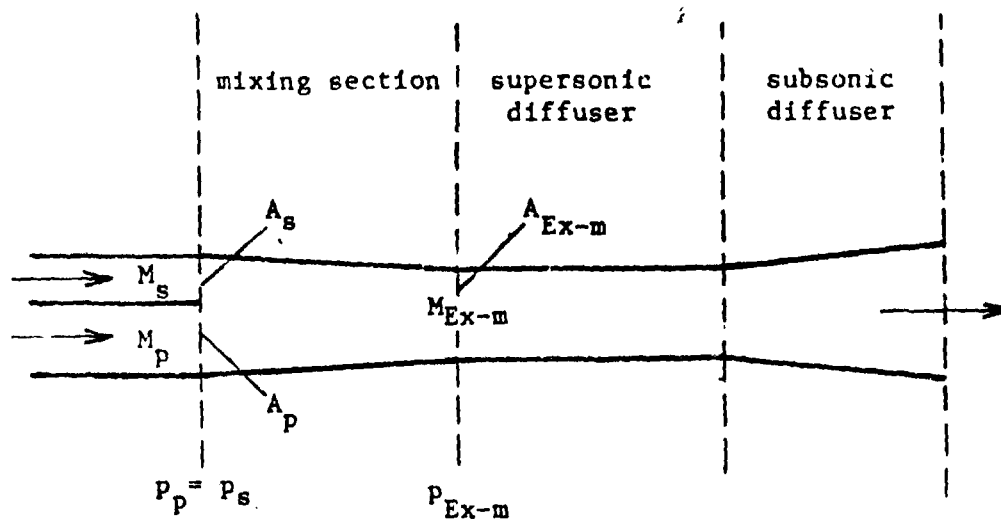


| M | Mach number | Indices: | p | refers to primary flow |
| p | static pressure | | s | " " secondary flow |
| A | flow cross section | | Ex-m | " " mixing section exit |

Figure 1.  Ejector Flow Scheme

**Figure 2 plot:**

Table in figure:

| $\gamma$ | $\tau$ | $\dfrac{C_f L}{2D}$ |
|---|---|---|
| 1.4 | 1.0 | 0 |
| 1.4 | 1.171 | 0.04 |

EJECTOR PUMP

THRUST AUGMENTER

$B_t = 10$

$M_{Ex-m} \to \infty$

$$B_t = \frac{\gamma_p M_p^2}{t\left(1 + \frac{A_s}{A_p}\right)} + \frac{\gamma_s M_s^2}{t\left(1 + \frac{A_p}{A_s}\right)}$$

(vertical axis: $E$; horizontal axis: $M_{Ex-m}$)
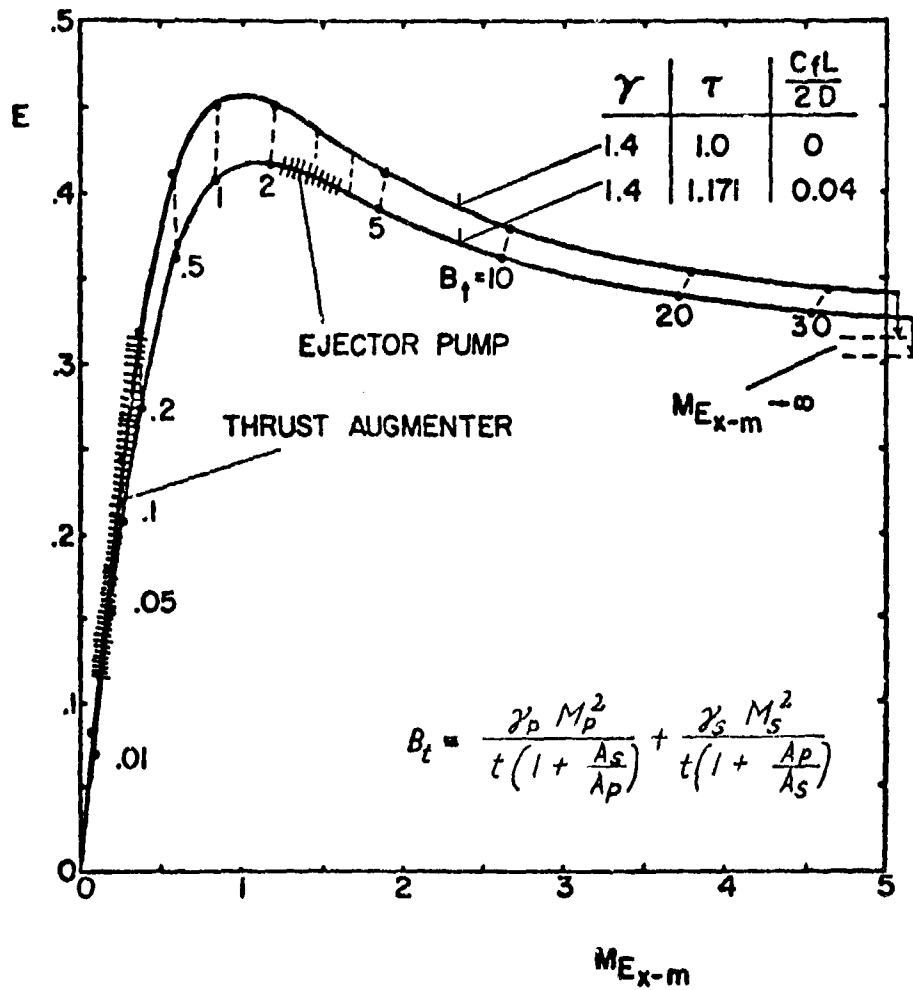
Figure 2.  Plot of Reduced Ejector Equation.

$$\frac{M_{Ex-m}\left(1 + \frac{\gamma_{Ex}-1}{2} M_{Ex-m}^2\right)^{\frac{1}{2}}}{\gamma_{Ex} M_{Ex-m}^2 c_m + \tau} = E \equiv \frac{M_s\left(\frac{m_p}{m_s}+1\right)}{B_m \cdot t\left(\frac{A_p}{A_s}+1\right)} \sqrt{\frac{\left(1 + \frac{m_p R_p}{m_s R_s}\right)\left(\frac{c_{p\cdot p}}{c_{p\cdot s}} \frac{m_p (T_p)_0}{m_s (T_s)_0}+1\right)(T_s)_0}{\left(1 + \frac{m_p \gamma_p}{m_s \gamma_s}\right)\left(\frac{c_{p\cdot p}}{c_{p\cdot s}} \frac{m_p}{m_s}+1\right) T_s}}$$

where   T   abs. temperature
      R   gas constant

$\gamma$   ratio of spec. heats
$c_p$   spec. heat at const. pressure
$\tau$   wall force parameter

$$B_m \equiv \frac{\gamma_p M_p^2}{t\left(1 + \frac{A_s}{A_p}\right)} + \frac{\gamma_s M_s^2}{t\left(1 + \frac{A_p}{A_s}\right)} + \tau$$

$c_m = 1 + c_f L/(2D)$
$c_f$   pipe friction coefficient

Figure 3.  Reduced Ejector Equation.